



University of Belgrade  
Technical Faculty in Bor,  
Mining and Metallurgy  
Institute Bor

**54<sup>th</sup> International  
October Conference  
on Mining and Metallurgy**

# PROCEEDINGS

**Editors:**

**Ljubiša Balanović**

**Dejan Tanikić**



**18-21 October 2023, Bor Lake, Serbia**

**PROCEEDINGS,  
54<sup>th</sup> INTERNATIONAL OCTOBER CONFERENCE  
on Mining and Metallurgy**

**Editors:**

**Prof. dr Ljubiša Balanović**

**Prof. dr Dejan Tanikić**

*University of Belgrade, Technical Faculty in Bor*

**Technical Editor:**

**M. Sc. Miljan Marković**

*University of Belgrade, Technical Faculty in Bor*

**Publisher:** University of Belgrade, Technical Faculty in Bor

**For the publisher:** Dean Prof. dr Dejan Tanikić

**Circulation:** 200 copies

CIP - Каталогизacija у публикацији Народна библиотека Србије, Београд

622(082)(0.034.2)

669(082)(0.034.2)

INTERNATIONAL October Conference on Mining and Metallurgy (54 ; 2023  
; Borsko jezero)

Proceedings [Elektronski izvor] / 54th International October Conference on Mining  
and Metallurgy - IOC 2023, 18-21 October 2023, Bor Lake, Serbia ; [organized by]  
University of Belgrade, Technical Faculty in Bor and Mining and Metallurgy Institute  
Bor ; editors Ljubiša Balanović, Dejan Tanikić. - Bor : University of Belgrade,  
Technical Faculty, 2023 (Niš : Grafika Galeb). - 1 USB fleš memorija ; 1 x 1 x 5 cm

Sistemska zahtevi: Nisu navedeni. - Nasl. sa naslovne strane dokumenta. - Tiraž 200. -  
Preface / Ljubiša Balanović. - Bibliografija uz svaki rad.

ISBN 978-86-6305-140-9

a) Рударство -- Зборници b) Металургија -- Зборници

COBISS.SR-ID 126659849

-----  
Bor Lake, Serbia, October 18-21, 2023





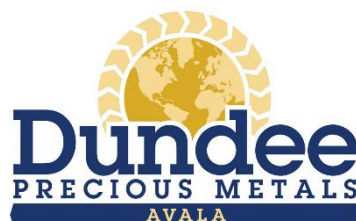
Conference is financially supported by  
The Ministry of Science, Technological  
Development and Innovation  
of the Republic of Serbia



## Platinum Donors



## Gold Donors



## Silver Donor



## Exhibitions



## Friends of the Conference



THE FOUNDATION 'B.SC. ENG. BOŠKO INJAC'



**SCIENTIFIC COMMITTEE**

Prof. Dr Dejan Tanikić (Serbia) - president  
Prof. Dr Nada Štrbac (Serbia) - vice-president  
Prof. Dr Radoje Pantović (Serbia) - vice-president

Dr Ana Kostov (Serbia)  
Prof. Dr Adam Grajcar (Poland)  
Prof. Dr Adina Negrea (Romania)  
Dr Andrei Rotaru (Romania)  
Prof. Dr Batrić Pešić (USA)  
Dr Biserka Trumić (Serbia)  
Prof. Dr Boštjan Markoli (Slovenia)  
Dr Branislav Marković (Serbia)  
Prof. Dr Cornelia Muntean (Romania)  
Prof. Dr Daniela Grigorova (Bulgaria)  
Prof. Dr Dejan Ivezić (Serbia)  
Prof. Dr Desimir Marković (Serbia)  
Prof. Dr Dimitris Pnias (Greece)  
Prof. Dr Dimitriu Sorin (Romania)  
Prof. Dr Dmitry Vasilyev (Russia)  
Dr Dragan Komljenović (Canada)  
Prof. Dr Dragan Manasijević (Serbia)  
Dr Dragan Milanović (Serbia)  
Prof. Dr Dragan Milovanović (Serbia)  
Prof. Dr Dragoslav Gusković (Serbia)  
Prof. Dr Dušan Orać (Slovakia)  
Prof. Dr Duško Minić (Serbia)  
Prof. Dr Endre Romhanji (Serbia)  
Prof. Dr Essen Suleimenov (Kazakhstan)  
Prof. Dr Farzet Bikić (Bosnia and Herzegovina)  
Prof. Emeritus Fathi Habashi (Canada)  
Prof. Dr Grozdanka Bogdanović (Serbia)  
Prof. Dr György Kaptay (Hungary)  
Prof. Dr Ivan Mihajlović (Serbia)  
Prof. Dr Iveta Vaskova (Slovakia)  
Prof. Dr Jakob Lamut (Slovenia)  
Prof. Dr Jasmin Suljagić (Bosnia and Herzegovina)  
Dr Jasmina Stevanović (Serbia)  
Dr Jasna Stajić Trošić (Serbia)  
Prof. Dr Jovica Sokolović (Serbia)  
Prof. Dr Jožef Medved (Slovenia)  
Prof. Dr Kaikun Wang (China)  
Prof. Dr Karl Heinz Spitzer (Germany)  
Prof. Emeritus Karlo Raić (Serbia)  
Prof. Dr Kemal Delijić (Montenegro)  
Prof. Dr Komnitsas Konstantinos (Greece)  
Prof. Dr Kostas Matis (Greece)  
Prof. Dr Krzysztof Fitzner (Poland)  
Prof. Dr Luis Filipe Malheiros (Portugal)  
Prof. Dr Milan Antonijević (Serbia)  
Prof. Dr Milan Trumić (Serbia)  
Dr Mile Bugarin (Serbia)

Dr Milenko Ljubojev (Serbia)  
Prof. Dr Milovan Vuković (Serbia)  
Prof. Dr Mira Cocić (Serbia)  
Mirjam Jan-Blažič (Slovenia)  
Prof. Dr Mirjana Rajčić Vujasinović (Serbia)  
Prof. Dr Mirko Gojić (Croatia)  
Dr Miroslav Sokić (Serbia)  
Prof. Dr Mirsada Oruč (Bosnia and Herzegovina)  
Dr Nadežda Talijan (Serbia)  
Prof. Dr Natalija Dolić (Croatia)  
Prof. Dr Nedeljko Magdalinović (Serbia)  
Prof. Dr Nenad Radović (Serbia)  
Prof. Dr Nenad Vušović (Serbia)  
Prof. Dr Nicanor Cimpoesu (Romania)  
Prof. Dr Nobuyuki Masuda (Japan)  
Prof. Dr Onuralp Yucel (Turkey)  
Prof. Dr Pavel Broz (Czech Republic)  
Prof. Dr Petr Solozhenkin (Russia)  
Prof. Dr Petrica Vizureanu (Romania)  
Dr Sun Zhongmei (China)  
Prof. Dr Ridvan Yamanoglu (Turkey)  
Prof. Dr Rodoljub Stanojlović (Serbia)  
Prof. Dr Rositsa Paunova (Bulgaria)  
Prof. Dr Sead Čatić (Bosnia and Herzegovina)  
Prof. Dr Sergey Krasikov (Russia)  
Dr Slavomír Hredzák (Slovakia)  
Prof. Dr Snežana Milić (Serbia)  
Prof. Dr Snežana Šerbula (Serbia)  
Prof. Dr Srba Mladenović (Serbia)  
Dr Srećko Stopić (Germany)  
Prof. Dr Stojan Groudev (Bulgaria)  
Prof. Dr Sulejman Muhamedagić (Bosnia and Herzegovina)  
Prof. Dr Svetlana Ivanov (Serbia)  
Prof. Dr Tatjana Volkov-Husović (Serbia)  
Prof. Dr Tomáš Havlik (Slovakia)  
Prof. Dr Velimir Radmilović (Serbia)  
Prof. Dr Velizar Stanković (Serbia)  
Prof. Dr Vesna Grekulović (Serbia)  
Dr Vladan Ćosović (Serbia)  
Vladan Mihailović (Serbia)  
Dr Vladan Kašić (Serbia)  
Prof. Dr Vladimir Krstić (Canada)  
Prof. Dr Vladislav Kecojević (USA)  
Dr Walter Valery (Australia)  
Prof. Dr Xuewei Lv (China)  
Prof. Dr Yong Du (China)  
Prof. Dr Žarko Radović (Montenegro)  
Prof. Dr Zdenka Zovko Brodarac (Croatia)  
Dr Zoran Stevanović (Serbia)  
Prof. Dr Željko Kamberović (Serbia)



**ORGANIZING COMMITTEE**

**Prof. dr Ljubiša Balanović, Full Professor (UB TF Bor) - president**  
**Prof. dr Saša Stojadinović, Full Professor (UB TF Bor) - vice-president**  
**Prof. dr Srba Mladenović, Full Professor (UB TF Bor) - vice-president**  
**Dr Ana Kostov, Principal Research Fellow (MMI Bor) - vice-president**

**Prof. dr Nada Štrbac, Full Professor (UB TF Bor)**  
**Prof. dr Dragan Manasijević, Full Professor (UB TF Bor)**  
**Prof. dr Vesna Grekulović, Full Professor (UB TF Bor)**  
**Prof. dr Đorđe Nikolić, Full Professor (UB TF Bor)**  
**Prof. dr Milan Radovanović, Full Professor (UB TF Bor)**  
**Prof. dr Marija Petrović Mihajlović, Full Professor (UB TF Bor)**  
**Prof. dr Zoran Štirbanović, Associate Professor (UB TF Bor)**  
**Prof. dr Milan Gorgievski, Associate Professor (UB TF Bor)**  
**Prof. dr Saša Marjanović, Associate Professor (UB TF Bor)**  
**Prof. dr Ivana Marković, Associate Professor (UB TF Bor)**  
**Prof. dr Žaklina Tasić, Associate Professor (UB TF Bor)**  
**Doc. dr Dejan Petrović, Assistant Professor (UB TF Bor)**  
**Doc. dr Anđelka Stojanović, Assistant Professor (UB TF Bor)**  
**Doc. dr Uroš Stamenković, Assistant Professor (UB TF Bor)**  
**Dr Jasmina Petrović, Assistant with PhD (UB TF Bor)**  
**Vladimir Nikolić, Assistant (UB TF Bor)**  
**Milica Zdravković, Assistant (UB TF Bor)**  
**Miljan Marković, Assistant (UB TF Bor)**  
**Milijana Mitrović, Assistant (UB TF Bor)**  
**Milan Nedeljković, Assistant (UB TF Bor)**  
**Avram Kovačević, Teaching Assistant (UB TF Bor)**  
**Sandra Vasković, English Lecturer (UB TF Bor)**  
**Oliver Marković, IT service (UB TF Bor)**  
**Violeta Aleksić, Liquidator (UB TF Bor)**





## PREFACE

On behalf of the Organizing Committee, it is a great honor and pleasure to welcome all esteemed participants of the 54<sup>th</sup> International October Conference on Mining and Metallurgy (IOC 2023), scheduled to take place at the picturesque Bor Lake, Serbia, from October 18<sup>th</sup> to 21<sup>st</sup> 2023.

The collaborative efforts of the University of Belgrade, the Technical Faculty in Bor, and the Mining and Metallurgy Institute Bor have meticulously organized this year's IOC. Our focus remains unwavering on showcasing the latest research findings and advancements in geology, mining, metallurgy, materials science, technology, environmental protection, and other engineering disciplines. Our primary objective is to foster a dynamic environment where academics, researchers, and industry professionals can come together to share their knowledge, experiences, and innovative ideas while exploring opportunities for collaborative research endeavors.

Our conference agenda is rich and diverse, encompassing plenary sessions, engaging invited lectures, technical presentations, enlightening oral and poster sessions, informative technical tours, a diverse exhibition, and memorable social gatherings. At the heart of this event lies our strong commitment to sustainable development within the mining and metallurgy sector. We are dedicated to exploring ecologically conscious methodologies, responsible resource extraction practices, and cutting-edge technologies that reduce the industry's environmental impact and enhance the well-being of local communities.

The conference proceedings comprise 129 papers authored by individuals from universities, research institutes, and industries in 22 countries. We are proud to welcome participants from Bosnia and Herzegovina, Bulgaria, Canada, China, Croatia, Germany, Greece, India, Iran, Kazakhstan, Libya, North Macedonia, Montenegro, Morocco, Romania, Russia, Slovakia, South Africa, Spain, Turkey, United States, and, of course, Serbia.

We are excited to host the 8<sup>th</sup> International Student Conference on Technical Sciences (ISC 2023) as part of IOC 2023. This event offers students from Serbia and the wider region a unique chance to showcase their research and discuss the future of their fields with experts.

We sincerely thank the Ministry of Science, Technological Development, and Innovation of the Republic of Serbia for their generous financial support. In addition, we express our profound gratitude to all our sponsors, exhibitors, and friends of the Conference for their contributions and unwavering support for playing a pivotal role in ensuring the success of IOC 2023.

We would like to express our heartfelt thanks to all authors, committees, reviewers, speakers, and chairpersons for their invaluable contributions in shaping IOC 2023.

We look forward to welcoming you to the 55<sup>th</sup> International October Conference on Mining and Metallurgy (IOC 2024), which will be held in October 2024.

On behalf of the 54<sup>th</sup> IOC Organizing Committee,

Prof. dr Ljubiša Balanović

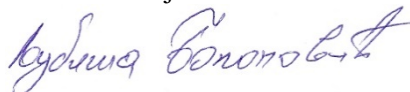




## TABLE OF CONTENTS

### Plenary Lectures

**Velimir R. Radmilović** (SERBIA)

*Energy: One of the biggest challenges in 21<sup>st</sup> century* 3-3

**Jing Yu, Mingshui Luo, Junyi Xiang, Yang You, Zhixiong You, Xuewei Ly** (CHINA)

*Efficient extraction of vanadium from vanadium slag* 4-8

### Invited Lectures

**Batrić Pešić** (UNITED STATES)

*The ongoing restructuring of universities to adopt the sophistication offered by internet* 11-19

**Yaima Filiberto, Alberto Montenegro, Eugenio Alvarez** (SPAIN)

*Machine learning applied to improving the scrap recycling and melting process in all types of ferrous alloys and steel* 20-22

**Slobodan Kostić, Qi Fenglai, Savo Pirgić, Nenad Botić, Dobrica Milovanović, Čedomir Sušić, Igor Zlatković** (SERBIA)

*Construction of a new sintering plant 180 m<sup>2</sup> within the HBIS Group Serbia Iron & Steel* 23-26

**Satyananda Patra** (INDIA)

*Acid activation of bentonite: Physico-Chemical characterization and application in goethitic iron ore green pelletization* 27-35

**Ridvan Yamanoglu** (TURKEY)

*Production of metal-based powders by atomization techniques* 36-45

**Yong Du, Rainer Schmid-Fetzer, Jincheng Wang, Shuhong Liu, Jianchuan Wang, Qiang Lu, Yuhui Zhang, Kai Li** (CHINA, GERMANY)

*Computational design of engineering materials: case studies for a cemented carbide and a heat resistant Al alloy* 46-46

### Conference Papers

**Ordinartsev Denis, Nadezhda Pechischeva, Svetlana Estemirova, Andrey Rempel** (RUSSIA)

*Cr(VI) photosorption on composite sorbent of montmorillonite with amorphous TiO<sub>2</sub>* 49-52

**Mikhail Korovkin, Ludmila Ananyeva, Andrey Zherlitsyn, Sergey Kondratyev, Olesya Savinova** (RUSSIA)

*Electro-pulse crushing in high-purity quartz production* 53-55

**Žarko Radović, Nebojša Tadić** (MONTENEGRO)

*Analytical simulation of EAF dust enrichment* 56-59

<b>Nebojša Tadić, Žarko Radović (MONTENEGRO)</b> <i>Thermal and mechanical relaxation of residual stresses in cold rolled aluminium alloy strips</i>	60-63
<b>Dragan Šabaz, Miloš Stojanović, Dejan Petrović (SERBIA)</b> <i>Selection of anchor type using AHP method</i>	64-67
<b>Miloš Stojanović, Veljko Lapčević, Ivica Vojinović (SERBIA)</b> <i>Blast fragmentation analysis in Jama Bor by using WipFrag software</i>	68-71
<b>Veljko Lapčević, Toma Jovičić, Slavko Torbica (SERBIA)</b> <i>Mine ventilation model validation by PQ survey</i>	72-75
<b>Jelena Đorđević, Jelena Stefanović, Sandra Guševac, Ivan Jelić, Stefan Trujić (SERBIA)</b> <i>Life cycle analysis (LCA) of asphalt layers containing recycled asphalt pavement</i>	76-79
<b>Jelena Ivaz, Dejan Petrović, Predrag Stolić, Mladen Radovanović, Dragan Zlatanović, Saša Stojadinović, Pavle Stojković (SERBIA)</b> <i>Occupational injuries in underground coal mining: statistical analysis of data</i>	80-83
<b>Jelena Ivaz, Dejan Petrović, Mladen Radovanović, Dragan Zlatanović, Saša Stojadinović, Pavle Stojković (SERBIA)</b> <i>Prediction of methane emissions in coalmine - Soko</i>	84-87
<b>C. Prochaska, E. Kokkinos, D. Merachtsaki, A. Lampou, E. Peleka, K. Simeonidis, G. Vourlias, A. Zouboulis (GREECE)</b> <i>Recovery of metallic fractions from medical products labelled for single use</i>	88-91
<b>Nataša Sarap, Marija Janković, Vojislav Stanić, Ivana Jelić, Marija Šljivić-Ivanović (SERBIA)</b> <i>Analysis of gross alpha and gross beta activity in samples around former uranium mine Gabrovnica</i>	92-95
<b>Dragan Manasijević, Ljubiša Balanović, Ivana Marković, Uroš Stamenković (SERBIA)</b> <i>Latent heat of some aluminium based phase change alloys for thermal energy storage</i>	96-99
<b>Andelka Stojanović, Ivica Nikolić, Isidora Milošević (SERBIA)</b> <i>Position of European countries in sustainable resource management</i>	100-103
<b>Aleksandar Đorđević, Duško Minić, Milena Zečević, Dragan Manasijević (SERBIA)</b> <i>Mechanical and electrical properties of the ternary Ag-Ge-Sn alloys</i>	104-107
<b>Milena Zečević, Duško Minić, Aleksandar Đorđević, Dragan Manasijević (SERBIA)</b> <i>Effect of chemical composition on the corrosion resistance of the ternary Ag-Ge-Sn alloys</i>	108-111
<b>Tatiana Aleksandrova, Nadezhda Nikolaeva (RUSSIA)</b> <i>Extraction of low-dimensional structures of nonferrous and noble metals from refractory raw materials</i>	112-115
<b>Viša Tasić, Tatjana Apostolovski-Trujić, Bojan Radović, Nevena Ristić, Tamara Urošević, Vladan Kamenović, Zvonko Damjanović (SERBIA)</b> <i>Air quality measurements in the Bor city during the reconstruction of the copper smelter Bor in 2022</i>	116-119

<b><u>Slavica Miletić, Biserka Trumić, Suzana Stanković</u> (SERBIA)</b> <i>Application of control charts in the laboratory for testing the metallic materials</i>	120-123
<b><u>Alexey M. Amdur, Sergei A. Fedorov, Andrey A. Forshev, Nikolay V. Grevtsev, Vera V. Yurak</u> (RUSSIA)</b> <i>Technological aspects of the use of peat as a component of pulverated coal fuel for blast furnaces</i>	124-127
<b><u>Ljiljana Avramović, Zoran Stevanović, Vanja Trifunović, Radmila Marković, Dragana Božić, Daniela Urošević, Silvana Dimitrijević</u> (SERBIA)</b> <i>Hydrometallurgical treatment of mining waste from Bor - Serbia in aim of copper recovery</i>	128-131
<b><u>Daniel Kržanović, Radmilo Rajković, Ivana Jovanović, Milenko Jovanović, Miomir Mikić</u> (SERBIA)</b> <i>Determination the final contour of the open pit Veliki Krivelj for the mining capacity 23.1 million tons of ore</i>	132-135
<b><u>Vladan Marinković, Miroslava Maksimović, Milenko Jovanović, Goran Pačkovski</u> (SERBIA)</b> <i>The use of unmanned aerial vehicles for making the precise 3D topo models and orthophoto images</i>	136-140
<b><u>Dejan Tanikić, Anđela Stojić, Jelena Đoković, Miloš Stoljiljković</u> (SERBIA)</b> <i>Mechanical characteristics of the shape memory alloy Cu-Zn-Al</i>	141-144
<b><u>Ljiljana Avramović, Vanja Trifunović, Zoran Stevanović, Radmila Marković, Dragana Božić, Dejan Bugarin, Silvana Dimitrijević</u> (SERBIA)</b> <i>Copper recovery from RE-flotation tailings by combined process</i>	145-148
<b><u>Milenko Jovanović, Daniel Kržanović, Radmilo Rajković, Vladan Marinković, Miroslava Maksimović, Miomir Mikić</u> (SERBIA)</b> <i>Application of hybrid geogrids in mining</i>	149-153
<b><u>Stefan Trujić, Miroslava Maksimović, Vladan Marinković, Ljiljana Avramović, Vanja Trifunović, Dragana Božić</u> (SERBIA)</b> <i>Geological exploration of the technogenic deposit - old flotation tailing pit - Bor with the possibility of leaching</i>	154-157
<b><u>Zoran Stevanović, Radmila Marković, Ljiljana Avramović, Vojka Gardić, Jelena Petrović, Dragana Božić</u> (SERBIA)</b> <i>Sustainable and smart mining</i>	158-161
<b><u>Snežana Ignjatović, Ivana Vasiljević, Branisav Sretković, Milanka Negovanović</u> (SERBIA)</b> <i>Using gravity data to define structural correlation affecting the formation of Neogene basins</i>	162-165
<b><u>Deniz Eylül Akpınar, Batuhan Turgut, Ugur Gurol, Savas Dilibal</u> (TURKEY)</b> <i>Characterization of wire arc additively manufactured wear-resistant bimetallic component</i>	166-169
<b><u>Mistreanu Sebastian, Ramona Cimpoesu, Dragoş Achiţei, Mihai Popa, Daniela Lucia Chicet, Vasile Manole, Ana-Maria Scripcariu, Nicanor Cimpoesu</u> (ROMANIA)</b> <i>Sandblasting process influence on stainless steel cutting element properties</i>	170-174

<b><u>Dorđe Petrović, Katarina Stanković, Latinka Slavković Beškoski, Ksenija Kumrić</u></b> (SERBIA) <i>Removal of Cu(II) from aqueous solutions using adsorbent based on chitosan hydrogel beads</i>	175-178
<b><u>Jovan P. Šetrajčić, Siniša M. Vučenović</u></b> (BOSNIA AND HERZEGOVINA) <i>Modified basic properties of electrons in layered nanocrystals with a complex lattice</i>	179-182
<b><u>Irena Nikolić, Milena Tadić, Dijana Đurović, Nevena Cupara, Ivana Milašević</u></b> (MONTENEGRO) <i>Kinetic and thermodynamic aspects of strontium adsorption by steelmaking slag</i>	183-186
<b><u>Miomir Mikić, Milenko Jovanović, Sandra Milutinović, Daniel Kržanović, Radmilo Rajković</u></b> (SERBIA) <i>New flotation plant Veliki Krivelj monitoring plan</i>	187-190
<b><u>Miomir Mikić, Radmilo Rajković, Daniel Kržanović, Sandra Milutinović</u></b> (SERBIA) <i>Recultivation of open pit Veliki Krivelj</i>	191-194
<b><u>Farzet Bikić, Khaola Awad, Halim Prčanović, Mirnes Duraković</u></b> (BOSNIA AND HERZEGOVINA) <i>Analysis of influenced factors on tropospheric ozone content in the city of Zenica during 2020</i>	195-198
<b><u>Sandra Milutinović, Ljubiša Obradović, Daniel Kržanović, Miomir Mikić, Radmilo Rajković</u></b> (SERBIA) <i>Flotation tail storage methods</i>	199-202
<b><u>Sandra Milutinović, Milena Kostović, Ljubiša Obradović, Srđana Magdalinović, Sanja Petrović</u></b> (SERBIA) <i>Methods of transportation and discharge of tails to flotation tailings pond</i>	203-206
<b><u>Uğur Gürol, Ceren Çelik, Müesser Göçmen, Mustafa Koçak</u></b> (TURKEY) <i>Microstructural and mechanical characterization of armor steel joint welded with sandwich design</i>	207-210
<b><u>Branka Pešovski, Milan Radovanović, Vesna Krstić, Danijela Simonović, Silvana Dimitrijević</u></b> (SERBIA) <i>Electrochemical characteristics of the anodized titanium oxide films in sulfuric acid</i>	211-215
<b><u>Duško Đukanović, Nemanja Đokić, Zoran Aksentijević, Daniel Radivojević, Branisl Stakić</u></b> (SERBIA) <i>Methane as an untapped energy potential of the "Soko" brown coal mine</i>	216-220
<b><u>Žaklina Tasić, Marija Petrović Mihajlović, Ana Simonović, Milan Radovanović, Maja Nujkić, Milan Antonijević</u></b> (SERBIA) <i>Electrochemical methods for the determination of tryptophan and caffeine</i>	221-224
<b><u>Isidora Milošević, Anđelka Stojanović, Sanela Arsić, Ivica Nikolić, Ana Rakić</u></b> (SERBIA) <i>Circular economy in the era of Industry 5.0</i>	225-228

<b><u>Almaida Gigović-Gekić, Elvis Agović, Belma Fakić, Hasan Avdušinović</u></b> (BOSNIA AND HERZEGOVINA) <i>Effect of delta ferrite on microstructure and hardness welded joints of steel S21800</i>	229-232
<b><u>Radmila Marković, Dragana Bozić, Zoran Stevanović, Tatjana Apostolovski Trujić, Vojka Gardić, Ljiljana Avramović, Vesna Marjanović</u></b> (SERBIA) <i>Combining neutralization and adsorption methods for metals removal from Saraka stream</i>	233-236
<b><u>Ana Petrović, Radmila Marković, Emina Požega</u></b> (SERBIA) <i>CNTs as potential material for wastewater purification: a review</i>	237-240
<b><u>Zdenka Stanojević Šimšić, Ana Kostov, Aleksandra Milosavljević, Slavica Miletić</u></b> (SERBIA) <i>Experimental investigations of CuAlNi alloys with 70 at%Cu</i>	241-244
<b><u>Ana Kostov, Aleksandra Milosavljević, Zdenka Stanojević Šimšić, Ivan Jovanović</u></b> (SERBIA) <i>Determination of melt properties in Cu-Fe alloys</i>	245-248
<b><u>Vladimir Nikolić, Milan Trumić</u></b> (SERBIA) <i>A simple method of determining of bond work index for finer samples</i>	249-252
<b><u>Ivan Jovanović, Novica Staletović</u></b> (SERBIA) <i>Management of risk assessment in environmental protection in surface copper mine</i>	253-256
<b><u>Jovan P. Šetrajić, Stevo K. Jaćimovski, Siniša M. Vučenović</u></b> (BOSNIA AND HERZEGOVINA) <i>Possibility of localized electron states appearance in ultrathin layered crystalline structures</i>	257-260
<b><u>Jovica Sokolović, Ivana Ilić, Dragiša Stanujkić, Zoran Štirbanović</u></b> (SERBIA) <i>Application of VIKOR method for comparison of the washability of coals</i>	261-264
<b><u>Vladimir Jovanović, Dejan Todorović, Branislav Ivošević, Dragan Radulović, Sonja Milićević, Marija Ercegović, Slavica Mihajlović</u></b> (SERBIA) <i>The process of obtaining biochar and the development of the products thus obtained</i>	265-269
<b><u>Jelena Petrović, Marija Ercegović, Marija Simić, Marija Koprivica, Jelena Dimitrijević, Marija Marković</u></b> (SERBIA) <i>Mg/Fe-modified hydrochar with promoted adsorption performances</i>	270-273
<b><u>Esra Dokumaci Alkan, Nurdan Ari, Murat Alkan</u></b> (TURKEY) <i>A coating application of IN718 via self-propagating high-temperature synthesis method</i>	274-277
<b><u>Murat Alkan, Esra Dokumaci Alkan, Dilan Ugurluer, Aslihan Karakanat</u></b> (TURKEY) <i>Production of AlCoCrCuXFeNi alloys via self-propagating high-temperature synthesis method</i>	278-281
<b><u>Jarmila Trpčevská, Iveta Vasková, Katarína Pauerová, Martina Laubertová, Dušan Oráč</u></b> (SLOVAKIA) <i>Zinc volatilization in the primary and the secondary zinc production</i>	282-286

<b><u>Dragan Ignjatović, Lidija Đurđevac Ignjatović, Vanja Đurđevac, Katarina Milivojević, Ivan Jovanović (SERBIA)</u></b> <i>Application of the numerical method in the definition of a substrate of circular cross section</i>	287-291
<b><u>Dragan Ignjatović, Lidija Đurđevac Ignjatović, Vanja Đurđevac, Mladen Supić, Dušan Tašić (SERBIA)</u></b> <i>Influence of the subsoil bearing capacity during formation of high landfills</i>	292-296
<b><u>Bojana Živković, Jelisaveta Marjanović, Jelena Đokić, Maja Petrović (SERBIA)</u></b> <i>Soil and rock properties as a basis for the sanitary landfill settings</i>	297-300
<b><u>Milan Gorgievski, Miljan Marković, Nada Štrbac, Vesna Grekulović, Kristina Božinović, Milica Zdravković, Marina Marković (SERBIA)</u></b> <i>Adsorption kinetics for copper ions adsorption onto onion peels</i>	301-304
<b><u>Saba Nourozi, Fatemeh Pourasgharian, Ahmad Khodadadi Darban (IRAN)</u></b> <i>Recovery of copper from low-grade copper ore using organic acid</i>	305-308
<b><u>Maria Krasteva (BULGARIA)</u></b> <i>Methodology and equipment for researching corrosion cracking processes in steel 3H14L (BDS 3692-78)</i>	309-312
<b><u>Jasmina Nešković, Pavle Stjepanović, Nenad Milojković, Dejan Lazić, Klara Konc Janković, Svetlana Polavder, Ivana Jovanović (SERBIA)</u></b> <i>Testing the Bond work index on limestone from flue gas desulphurization plant in TPP Ugljevik</i>	313-317
<b><u>Biljana Zlatičanin, Sandra Kovačević (MONTENEGRO)</u></b> <i>Impact of titanium addition on microstructure and properties of as-cast Al-Cu15 alloys</i>	318-321
<b><u>Biljana Zlatičanin, Sandra Kovačević (MONTENEGRO)</u></b> <i>Effect of cooling rate on mechanical properties of binary Al-Cu23 alloys</i>	322-324
<b><u>Desislav Ivanov, Irena Peytcheva, Marko Holma (BULGARIA)</u></b> <i>Horizon Europe AGEMERA project - Agile Exploration and Geo-modelling for European Critical Raw Materials: The potential of Assarel porphyry copper deposit for critical raw materials</i>	325-328
<b><u>Shehret Tilvaldyev, Uzziel Caldiño Herrera, Jose Omar Davalos, Manuel Alejandro Lira Martinez, Marlenne Alejandra Hernandez Lira, Diego Adan Villordo Melendez (CANADA)</u></b> <i>Problems of anthropogenic pollution of space</i>	329-334
<b><u>Mohammed Derqaoui, Abdelmoughit Abidi, Abdelrani Yaacoubi, Khalid El Amari, Omar Oabi, Abdelaziz Bacaoui (MOROCCO)</u></b> <i>Apatite flotation from low-grade sedimentary phosphate ore</i>	335-338
<b><u>Nadezhda Kazakova, Alexandar Popov, Georgi Chernev (BULGARIA)</u></b> <i>Influence of the distribution and content of limestone particles on the properties of blended cements</i>	339-342



<b><u>Daniel Ogochukwu Okanigbe, Shade Rouxzeta Van Der Merwe</u> (SOUTH AFRICA)</b> <i>Rocks of Obafemi Awolowo University and Environ, Nigeria: structural analysis of geological contact</i>	343-347
<b><u>Vladan Kašić, Ana Radosavljević Mihajlović, Jovica Stojanović, Slavica Mihajlović, Melina Vukadinović, Nataša Đorđević, Ivana Jelić</u> (SERBIA)</b> <i>Study of thermally treated zeolitic tuffs of Serbia, deposits "Zlatokop" and "Općište"-Beočin</i>	348-352
<b><u>Vesna Grekulović, Aleksandra Mitovski, Milica Zdravković, Nada Štrbac, Milan Gorgievski, Milovan Vuković, Miljan Marković</u> (SERBIA)</b> <i>Electrochemical behavior of copper in chloride medium in the presence of nettle extract</i>	353-356
<b><u>Marko Pavlović, Marina Dojčinović, Muhamed Harbinja, Atif Hodić, Dragan Radulović, Mirjana Stojanović, Zagorka Aćimović</u> (SERBIA, BOSNIA AND HERZEGOVINA)</b> <i>Effects of the application of pyrophyllite in the composition of protective coatings</i>	357-360
<b><u>Tamara Ristić, Nenad Milosavljević, Dobrica Milovanović</u> (SERBIA)</b> <i>Measures for the processing of iron with a higher incoming phosphorus content at the steel shop</i>	361-365
<b><u>Ivana Mikavica, Dragana Randelović, Milena Obradović, Jovica Stojanović, Jelena Mutić</u> (SERBIA)</b> <i>Microplastic textile fibers in urban soils of Serbia</i>	366-369
<b><u>Jianbo Zhao, Xinnan Zhao, Donglai Ma, Yang You, Zhixiong You, Xuewei Lv</u> (CHINA)</b> <i>Preparation of ferronickel by semi-molten smelting a mixture of two types of laterite ore</i>	370-374
<b><u>Mladen Radovanović, Dejan Petrović, Jelena Ivaz, Dragan Zlatanović</u> (SERBIA)</b> <i>Possibility of copper ores exploitation using in situ leaching method</i>	375-378
<b><u>Ivan Jelić, Nikola Lekić, Nikola Stanić, Miomir Mikić</u> (SERBIA)</b> <i>Selection of an optimal route for relocation of the Čehotina river bed</i>	379-382
<b><u>Milica Zdravković, Vesna Grekulović, Bojan Zdravković, Nada Štrbac, Milan Gorgievski, Miljan Marković</u> (SERBIA)</b> <i>Electrochemical behavior of steel in 0.1 mol/dm<sup>3</sup> HCl in the presence of potato peel juice</i>	383-386
<b><u>Ivana Marković, Dalibor Jović, Uroš Stamenković, Dragan Manasijević, Ljubiša Balanović, Milan Gorgievski</u> (SERBIA)</b> <i>Microstructure and thermal properties of leaded brass after quenching</i>	387-390
<b><u>Mehmet Ali Yildiz</u> (SERBIA)</b> <i>Hot strip mill walking beam slab reheating project</i>	391-394
<b><u>Peter Polyak</u> (SERBIA)</b> <i>Finishing mill automation upgrade at hot strip mill</i>	395-400
<b><u>Branislav Potić, Ana Arifović</u> (SERBIA)</b> <i>The metallurgical testing results of the boron mineralized material from Valjevo-Mionica basin</i>	401-406

<b>Uroš Stamenković, Ivana Marković, Srba Mladenović, Saša Marjanović, Avram Kovačević, Milijana Mitrović, Filip Basarabić (SERBIA)</b> <i>The influence of quenching media on different properties of C45 carbon steel</i>	407-413
<b>Yang You, Jiabao Guo, Zhixiong You, Xuewei Lv (CHINA)</b> <i>Investigation of the mixing and granulation behavior of iron ore fines in horizontal high-shear granulator</i>	414-417
<b>Jovica Sokolović, Grozdanka Bogdanović, Velizar Stanković, Gracijan Strainović, Ivana Ilić, Milan Gorgievski, Miljan Marković (SERBIA)</b> <i>Investigation on beneficiation of iron from copper ore of Mauritania Copper Mine (MCM) by magnetic separation</i>	418-421
<b>Essen Suleimenov, Rustam Sharipov, Galymzhan Maldybayev, Zhibek Orazaliyeva (KAZAKHSTAN)</b> <i>Investigation of the influence of pulsed electric current on the efficiency of decomposition of aluminate solution</i>	422-423
<b>Lovro Liverić, Tamara Holjevac Grgurić, Sunčana Smokvina Hanza, Wojciech Sitek, Vedrana Špada, Marko Kršulja (CROATIA)</b> <i>Influence of silver content on martensitic transformation of Cu-Al-Ag alloy</i>	424-427
<b>Hasan Ali Taner, Vildan Onen (TURKEY)</b> <i>Evaluation of the efficiency of different collectors in the chalcopyrite flotation</i>	428-434
<b>Vesna Conić, Dragana Božić, Miloš Janošević, Ljiljana Avramović, Vanja Trifunović, Dejan Bugarin, Ivana Jovanović (SERBIA)</b> <i>A pyro-hydrometallurgical process for the recovery of zinc from jarosite waste</i>	435-438
<b>Maria Krasteva, Rumen Petkov (BULGARIA)</b> <i>Research the rate of chemical corrosion of steel 3X14H2 (BDS 3692-78)</i>	439-442
<b>Srba Mladenović, Bojan Novaković, Ivana Marković, Uroš Stamenković (SERBIA)</b> <i>Effect of casting speed and water flow on tensile strength, elongation and microstructure of continuous cast copper wire</i>	443-447
<b>Nadira Bušatlić, Ilhan Bušatlić, Dženana Smajić-Terzić (BOSNIA AND HERZEGOVINA)</b> <i>Dependence of compressive strength of geopolymer based on fly ash and alkaline activator ratio</i>	448-451
<b>Gergana Meracheva, Efrosima Zaneva-Dobranova, Nikolay Hristov (BULGARIA)</b> <i>Hydrocarbon potential of the Lower Paleozoic sediments in NE Bulgaria by geochemistry and well-logging</i>	452-455
<b>Dragana Marilović, Grozdanka Bogdanović, Sanja Petrović (SERBIA)</b> <i>Leaching of flotation tailings with a solution of sulfuric acid and ionic liquid</i>	456-459
<b>Ivana Jovanović, Vesna Conić, Dragan Milanović, Daniel Kržanović, Tanja Stanković, Daniela Urošević, Miloš Janošević (SERBIA)</b> <i>Determination of Bond rod mill work index of a very low-grade copper ore</i>	460-463

<b><u>Hasan Ali Taner, Ali Aras, Muhammad Hashim Rasa (TURKEY)</u></b> <i>Investigation of the effect of depressant and collector conditioning times on cobalt recovery by flotation</i>	464-467
<b><u>Aleksandar Cvetković, Žaklina Tasić, Marija Petrović Mihajlović, Maja Nujkić, Milan Radovanović, Ana Simonović (SERBIA)</u></b> <i>Microplastics</i>	468-471
<b><u>Sanja Petrović, Srđana Magdalinović, Ljubiša Obradović, Sandra Milutinović, Bojan Drobnjaković, Slađana Krstić (SERBIA)</u></b> <i>Tailing management: tailings filtering equipment</i>	472-475
<b><u>Jelena Stefanović, Jelena Đorđević, Sandra Guševac (SERBIA)</u></b> <i>XRD analysis of corrosion product formed in industrial aggressive environment</i>	476-480
<b><u>Muhamad Ghulam Isaq Khan, Filip Rajković, Miljana Popović, Dejan Prelević, Aleksandar Ćitić, Tamara Radetić (SERBIA)</u></b> <i>Initiation of abnormal grain growth in cold-rolled sheet of AA5182 Al-Mg alloy: role of texture</i>	481-484
<b><u>Danijela Voza, Hesam Dehghani, Milica Veličković (SERBIA)</u></b> <i>The dissolved oxygen prediction based on the machine learning techniques</i>	485-488
<b><u>Hasan Acan, Hasan Ergin (TURKEY)</u></b> <i>A novel model for minimizing mine closure costs and the optimum final quarry boundry</i>	489-492
<b><u>Ivana Jovanović, Dragan Milanović, Oliver Dimitrijević, Vesna Conić, Igor Svrkota (SERBIA)</u></b> <i>Role of wing tank in DMS process. Suspension velocity through the seal leg orifice – case study</i>	493-496
<b><u>Dejan Petrović, Jelena Ivaz, Saša Stojadinović, Predrag Stolić, Dragan Zlatanović (SERBIA)</u></b> <i>Risk management and mining machines maintenance – a brief review</i>	497-500
<b><u>Stefan Đorđievski, Dragana Adamović (SERBIA)</u></b> <i>History of surface water pollution by mining and metallurgical activities in Bor, Serbia</i>	501-504
<b><u>Olivera Dragutinović, Vaso Manojlović, Đorđe Veljović, Stefan Dikić, Marko Simić (SERBIA)</u></b> <i>Investigation of the properties of Co-Cr-W and Co-Cr-Mo alloys coated with hydroxyapatite for use in dental implants</i>	505-509
<b><u>Zoran Karastojković, Dragoslav Gusković, Ognjen Ristić, Zorica Kovačević (SERBIA)</u></b> <i>About the “relative plasticity” between steel matrix and non-metallic inclusions</i>	510-513
<b><u>Aleksandar Jovanović, Mladen Bugarčić, Milena Milošević, Marija Vuksanović, Muna Abdualatif Abdurahman, Miroslav Sokić, Aleksandar Marinković (SERBIA, LIBYA)</u></b> <i>Modified hybrid cellulose membrane for Nickel(II) ions removal from industrial wastewater</i>	514-517
<b><u>Elena Todorova, Nadezhda Kazakova, Georgi Chernev (BULGARIA)</u></b> <i>Structural investigation via SEM analysis of silica hybrid materials</i>	518-521

<b><u>Tanja Kalinović, Jelena Kalinović, Jelena Milosavljević, Ana Radojević, Snežana Šerbula (SERBIA)</u></b> <i>Atmospheric bulk deposition as environmental quality indicator</i>	522-526
<b><u>Gordana Marković, Vaso Manojlović, Miroslav Sokić, Jovana Ružić, Dušan Milojkov (SERBIA)</u></b> <i>Designing biocompatible high entropy alloys using Monte Carlo simulations</i>	527-530
<b><u>Tatjana Volkov-Husović, Sanja Martinović, Ana Alil, Milica Vlahović (SERBIA)</u></b> <i>Application of image analysis for cavitation erosion resistance monitoring of some engineering materials</i>	531-534
<b><u>Milan Nedeljković, Srba Mladenović, Jasmina Petrović, Milijana Mitrović (SERBIA)</u></b> <i>Changes in the structure and density of copper during the refining smelting process</i>	535-538
<b><u>Jasmina Petrović, Srba Mladenović, Ivana Marković, Milan Nedeljković, Milijana Mitrović (SERBIA)</u></b> <i>Microstructure analysis of EN AW 6061 alloy using a SEM microscope after artificial aging</i>	539-542
<b><u>Milijana Mitrović, Saša Marjanović, Biserka Trumić, Jasmina Petrović, Milan Nedeljković (SERBIA)</u></b> <i>Effects of cold rolling and annealing processes on the microstructure and properties of micro-alloyed copper</i>	543-546
<b><u>Makedonka Dimitrova, Jasminka Dimitrova Kapac (NORTH MACEDONIA)</u></b> <i>Unlocking energy efficiency: financing preferences for SMEs in the Republic of North Macedonia</i>	547-555
<b><u>Zoran Štirbanović, Vesna Vojinović, Jovica Sokolović, Maja Trumić (SERBIA)</u></b> <i>Analysis of the effectiveness of different methods for cutting samples</i>	556-559
<b><u>Ivica Nikolić, Isidola Milošević, Anđelka Stojanović (SERBIA)</u></b> <i>Land turnover increases due to mining: An empirical analysis of Bor, Serbia, 2013-2022.</i>	560-563
<b>DONORS</b>	565-590
<b>AUTHOR INDEX</b>	591-596

\*\*\*



The 54<sup>th</sup> International October Conference on Mining and Metallurgy  
18-21 October 2023, Bor Lake, Serbia  
[www.ioc.tfbor.bg.ac.rs](http://www.ioc.tfbor.bg.ac.rs)

---

# PLENARY LECTURES



**PLENARY LECTURE**

**ENERGY: ONE OF THE BIGGEST CHALLENGES IN 21ST CENTURY**

**Velimir R. Radmilović**

*Serbian Academy of Sciences and Arts, Knez Mihailova 35, 11000, Belgrade, Serbia*

It is not sustainable for human kind to produce close to 80% of energy needs by burning fossile fuels (dominant in global primary energy production) mainly due to the detrimental effect of increasing CO<sub>2</sub> emission into atmosphere, causing global warming and catastrophic climate changes on one hand (global temperature rise, warming oceans, shrinking ice sheets, glacial retreat, sea level rise,...) as well as adverse effects on human health on the other. In order to solve many problems we are facing as humanity, such as poverty, infectious diseases, drinking water, etc., a reliable, affordable and more equally and fairly distributed energy supply is needed. An ever-increasing demand for energy (mostly for heat, electricity, and transport fuels) by a growing population, which will approach the 10 billion mark by the middle of 21<sup>st</sup> century, out of which 80% will live in urban areas, requires building more than double of the existing installed capacities for energy production, currently at 19 terawatts. All of this indicates that meeting the demands for sufficient supply of affordable and reliable energy that has a minimal impact on the environment, will be one of the biggest challenges facing humanity in 21st century. This requires opening and exploring many different avenues of research and development, including scavenging of heat, lost during energy production and conversion processes. One of such avenues is the field of thermoelectric materials, which demonstrate energy harvesting based on Seebeck effect i.e. the conversion of the temperature gradient into electric power, with potential applications in sensors, consumer electronics, medical devices, etc. Thermoelectric M<sub>2</sub>O<sub>3</sub>(ZnO)<sub>n</sub> nanowires, where M could be In, Ga, Fe, synthesized using facile solid-state diffusion, enabled us to control their defect structure at atomic level. Two kinds of defects, planar, parallel to basal wurtzite planes, and zigzag, parallel to pyramidal planes, facilitate decoupling of electrical and thermal properties through quantum confinement effects and control of phonon scattering. Both of these factors facilitate achieving a high figure of merit,  $ZT$  ( $ZT = \sigma \cdot S^2 \cdot T / k$ , where  $\sigma$ ,  $S$ ,  $T$ , and  $k$  represent electrical conductivity, the Seebeck coefficient, absolute temperature and thermal conductivity, respectively), used to rank thermoelectric materials. High angle annular dark field (HAADF) imaging of these nanowires revealed the presence of planar defects - monoatomic layers of indium perpendicular to the [001] direction, separated by wurtzite MZn<sub>n</sub>O<sub>(n+1)</sub><sup>+</sup> slabs of various thicknesses at nanoscale. Incomplete In/Ga monoatomic layers were observed as well. The ends of these incomplete layers are associated with edge dislocations, providing fast diffusion paths for large indium and gallium atoms. In summary, M<sub>2</sub>O<sub>3</sub>(ZnO)<sub>n</sub> polytypoid nanowires were converted from pure ZnO nanowires using a simple preferential diffusion process along line defects, which can be used to produce a wide range of ZnO alloys with controllable alloy concentration and layer density. From this study it is apparent that better control of atomic scale features could be the key in developing next-generation thermoelectric materials.

## **PLENARY LECTURE**

### **EFFICIENT EXTRACTION OF VANADIUM FROM VANADIUM SLAG**

**Jing Yu<sup>1</sup>, Mingshui Luo<sup>1</sup>, Junyi Xiang<sup>1</sup>, Yang You<sup>2</sup>, Zhixiong You<sup>2</sup>, Xuewei Lv<sup>2</sup>**

<sup>1</sup>College of Metallurgy and Materials Engineering, Chongqing University of Science and Technology, Chongqing 401331, China

<sup>2</sup>College of Materials Science and Engineering, Chongqing University, Chongqing 400044, China

#### **Abstract**

*The high roasting temperature and low leaching efficiency of vanadium from vanadium-bearing converter slag are regarded as the main factors significantly influencing the application of roasting–leaching processes in the cleaner production of vanadium. Composite salt roasting with CaO/MgO and subsequent acid leaching were conducted to improve the recovery rate of vanadium from vanadium-bearing converter vanadium slag. It has been shown that the leaching efficiency of vanadium can be improved by roasting it with a composite salt of CaO/MgO. The maximum vanadium leaching efficiency of 94% was achieved under the optimum MgO/(CaO+MgO) mole ratio of 0.5. A mechanical activation treatment was also performed to enhance the extraction of vanadium from the vanadium-bearing converter slag. The results demonstrated that the mechanical activation significantly decreased the optimum roasting temperature from 900 °C to 800 °C and increased the leaching efficiency from 86.0% to 90.9%.*

**Keywords:** Vanadium slag, Roasting, Leaching, Mechanical activation, Vanadium.

#### **1. INTRODUCTION**

Vanadium is considered a very significant metal in materials production. It is also known as “industrial monosodium glutamate” in many manufacturing fields, typically in carbon steels, tool steels, and Ti-Al-V alloys [1]. Vanadium is almost always extracted from vanadium slag in the form of vanadium pentoxide by salt roasting and water or acid leaching, followed by precipitation and calcination [2]. Calcification roasting–acid leaching, compared with sodium roasting process, appears to be a clean production method for the extraction of vanadium from vanadium slag, without the emission of corrosive gas, less harmful wastewater, and little noxious solid waste, but with low vanadium recovery [3].

The key factors for the extraction process are the extent of conversion of soluble vanadates in the roasting step and their rates of dissolution in the leaching step. Over the past decades, extensive work has been carried out on the improvement of the recovery of vanadium in the extraction process by new methods, such as microwave roasting [4], liquid oxidation technologies [5], and electro-oxidation [6].

However, for the calcification vanadium extraction process, part of vanadium spinel failed to form soluble vanadate during the roasting process, resulting in insufficient vanadium conversion and affecting the subsequent leaching process. In our previous study, we proposed the method of mechanical activation pre-treatment to enhance the effectiveness of calcification roasting for vanadium recovery from converter vanadium slag [7]. The feasibility of this process was investigated, and a systematic analysis was conducted on the mechanisms underlying mechanical



activation, oxidation roasting, and leaching behaviour [8]. Roasting with a composite additive (CaO+MgO), followed by acid leaching, was also employed to enhance the recovery of vanadium. The effect of composite additive (CaO+MgO) on the roasting and leaching behaviour of vanadium slag was investigated. The phase evolution and microstructure of the vanadium slag during roasting - leaching were also examined [9,10].

## 2. EXPERIMENTAL

### 2.1 Materials

The vanadium slag used in the study was obtained from Panzhihua Iron and Steel Corporation, Sichuan Province, China. The chemical composition of the vanadium slag is shown in Table 1. The CaO and MgO powder used as the additive in the roasting experiments was analytically pure, with a purity greater than 99.9%. Sulfuric acid used in the leaching experiments was obtained from Chongqing Chuandong Chemical Co. Ltd, with a purity of 96-98%. All aqueous solution was prepared with deionized water.

Table 1 - Chemical composition of the vanadium slag (wt.%)

V	Cr	Ti	Fe	Mn	Ca	Mg	Al	Si	P	O
8.57	0.98	8.63	31.00	5.67	1.84	1.76	1.84	6.77	0.06	32.80

### 2.2 Experimental procedure

For the composite salt roasting process, the vanadium slag was firstly mixed with a determined amount of CaO and MgO, and then roasted in an open muffle furnace at 850°C for 2 h in air. After roasting, the samples were removed from the furnace and cooled to room temperature in air. The roasted samples were milled to a particle size smaller than 75 µm, and then leached in a sulphuric acid solution with a constant pH value of 2.5, 50°C leaching temperature, 150 rpm stirring speed, and 1:10 solid to liquid ratio. A three-necked round-bottomed flask equipped with a water condenser, thermometer, pH meter, thermostatic water bath, and magnetic stirrer was used for leaching. Sulfuric acid with a concentration of 15% was used to maintain the acidity of the leaching solution throughout the leaching process. After a specific leaching time, the slurry was filtered and the leaching residue was dried at 100°C for 24 h.

For the mechanical activation process, the vanadium slag was firstly mixed with a determined amount of CaO, and then introduced into a planetary ball mill (Retsch PM 100, Germany) for mechanical activation. The mole ratio of vanadium-to-calcium in the mixture was maintained at 1.5. The mechanical activation experiments were conducted at a ball to ore weight ratio of 5:1, rotation rate of 400 rpm, and lasting 80 minutes. The activated samples were then roasted in a muffle furnace at 750 °C, 800 °C, 850 °C, and 900 °C for 2 h in the separate experiments. The roasted samples were subjected to leaching in sulfuric acid, as previously described.

The chemical compositions of the samples were established with the help of inductively coupled plasma-optical emission spectrometry (ICP-OES), using an Optima 8000 Instrument (PerkinElmer, USA).

## 3. RESULTS AND DISCUSSION

### 3.1 Effect of composite salt roasting with CaO/MgO on vanadium extraction

The effect of composite additive (CaO+MgO) on the leaching of vanadium slag was studied using roasted vanadium slag with four different MgO/(CaO+MgO) molar ratio: 0, 1/3, 2/3, and 1, at

roasting temperature of 850°C for 2 h. After roasting, the samples were ground into a powder with particle sizes < 75 μm and then leached in sulfuric acid with a constant pH of 2.5, leaching temperature of 50°C, liquid/solid ratio of 20:1 (ml/g), and reaction time of 60 min. The effect of MgO/(CaO+MgO) molar ratio on the leaching efficiency of vanadium and impurities was shown in Figure 1.

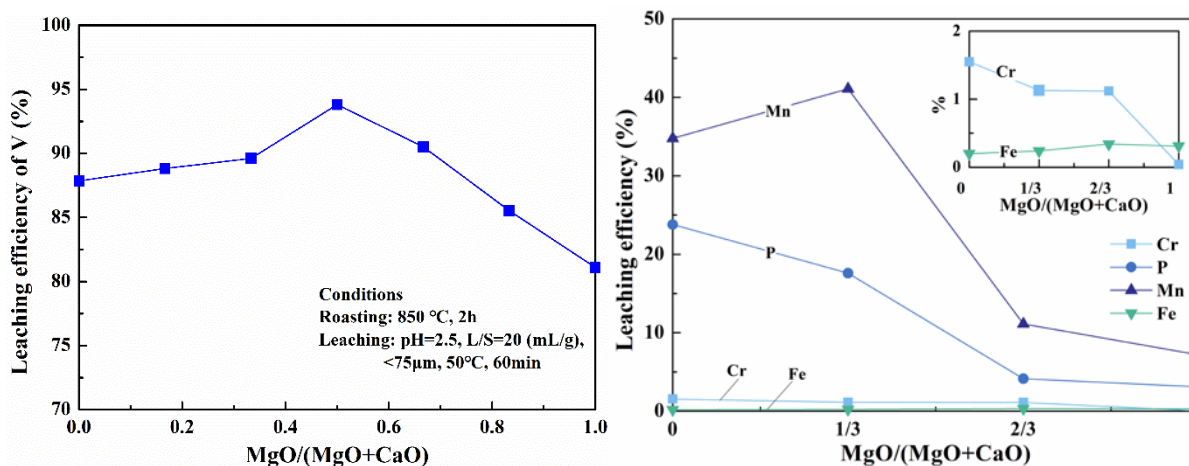


Figure 1 - Effect of MgO/(CaO+MgO) molar ratio on the leaching efficiency of vanadium and impurities

As shown in Figure 1, the leaching efficiency of vanadium increased from 87.3 to approximately 94% with the increase of MgO/(CaO+MgO) molar ratio to 0.5, then sharply decreased to approximately 80% as MgO/(CaO+MgO) continued to increase to 1. The leaching efficiency of manganese shows similar trends with vanadium, increased from 34.8 to 41.1% then significantly decreased to 7.2%. The increase of MgO/(CaO+MgO) molar ratio has little influence on the leaching of iron and chromium, and the leaching efficiency of iron and chromium is always lower than 0.5 and 1.6%, respectively. However, the leaching of phosphorus is significantly influenced by the MgO/(CaO+MgO) molar ratio. As the MgO/(CaO+MgO) molar ratio increased to 1, the leaching efficiency of phosphorus gradually decreased from 23.8 to 3.1%. The phosphate ions would combine with vanadate ions in the leach liquor to produce heteropolyacid anions, which inhibits precipitation of ammonium vanadate and thus decreases the recovery of vanadium. Therefore, the decrease in the rate of phosphorus leaching is highly beneficial for the subsequent vanadium precipitation.

### 3.2 Effect of mechanical activation pretreatment on vanadium extraction

Figure 2 shows the effect of mechanical activation and roasting temperature on the leaching of vanadium. The insufficient calcification roasting of unmilled vanadium slag at 750°C resulted in a vanadium leaching rate of less than 40%, as depicted in Figure 2. Upon increasing the roasting temperature to 800°C, the vanadium leaching rate sharply increased to 73%. Subsequently, with further increases in the roasting temperature to 850°C and 900°C, the vanadium leaching rate gradually rose to reach 85.4%. The vanadium leaching rate for the mechanically activated vanadium slag initially increased and then decreased with increasing roasting temperature. The optimal roasting effect was achieved at 800°C, resulting in a vanadium leaching rate of 90.9%. However, when the roasting temperature was further elevated to 850°C or higher, the vanadium leaching rate declined. On one hand, elevating the roasting temperature can facilitate the formation of acid-soluble calcium vanadate; on the other hand, it enhances the coating effect of silicate glass in relation to the vanadate phase. When the roasting temperature exceeds a certain threshold, the prominence of glass phase coating gradually intensifies, leading to a decrease in vanadium leaching rate due to increased diffusion resistance.

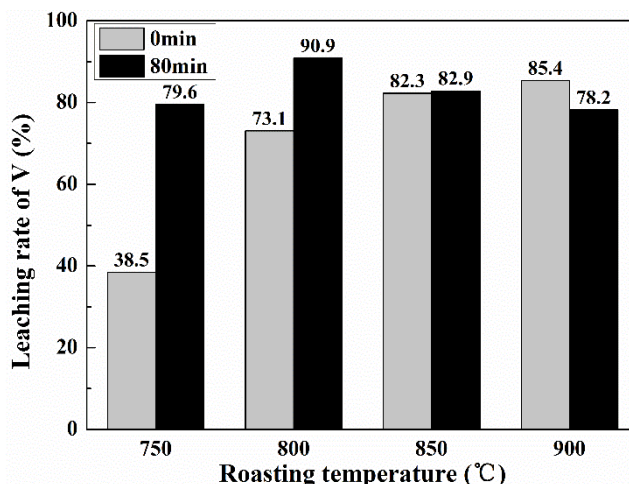


Figure 2 - The effect of mechanical activation and roasting temperature on the leaching of vanadium

The influence of mechanical activation time on the leaching rate of vanadium is illustrated in Figure 3. It can be observed that the leaching rate of vanadium gradually increases as the activation time prolongs. At a leaching time of 20 minutes, the leaching rate of un-activated vanadium slag reaches approximately 76%, whereas that of activated vanadium slag for 80 minutes approaches 87%. The leaching rate of vanadium for un-activated and activated 20-minute vanadium slag exhibits a gradual increase within the leaching time range of 20 to 60 minutes. However, the leaching rate of vanadium for activated 40-minute and 80-minute vanadium slag shows a very slow increase after 20 minutes. After reaching the activation time of 40 minutes, the leaching rate of vanadium remains relatively stable. The most significant contribution to the enhancement in vanadium leaching rate is observed when increasing the activation time from 20 to 40 minutes, while further extending it from 40 to 80 minutes has less pronounced impact. It can be seen that prolonging activation time can not only improve the leaching rate of vanadium, but also shorten the leaching time.

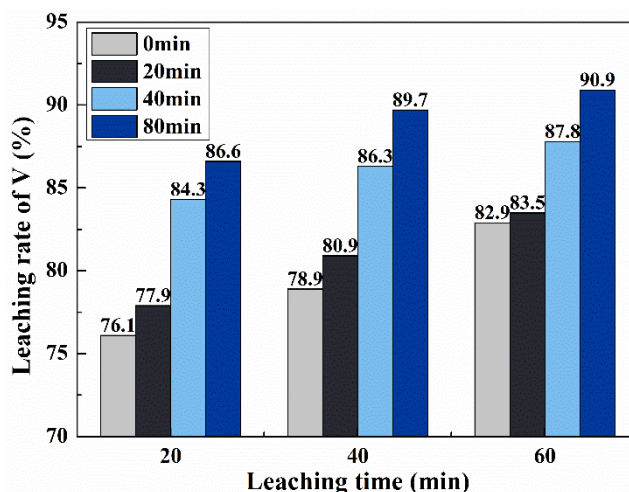


Figure 3 - The effect of activation time on the leaching efficiency of vanadium

#### 4. CONCLUSION

The effects of composite salt roasting and mechanical activation on the recovery of vanadium from the vanadium-bearing converter slag were studied and the following conclusions can be drawn:

- (1) The leaching efficiency of vanadium can be improved by roasting it with a composite salt of CaO/MgO. The maximum vanadium leaching efficiency of 94% was achieved under the optimum MgO/(CaO+MgO) mole ratio of 0.5.

(2) The mechanical activation significantly decreased the optimum roasting temperature from 900 °C to 800 °C and increased the leaching efficiency from 86.0% to 90.9%.

## ACKNOWLEDGEMENTS

*This work was financially supported by the National Natural Science Foundation of China (No.52004044), the Natural Science Foundation of Chongqing (No. CSTB2022NSCQ-MSX0801), the Foundation of Chongqing University of Science and Technology (No. ckrc2022030), and the National Undergraduate Training Program for Innovation and Entrepreneurship (No. 202311551007).*

## REFERENCES

- [1] P. R. Taylor, S. A. Shuey, E. E. Vidal, J. C. Gomez, *Mining, Metall. Explor.*, 23(2) (2006) 80-86.
- [2] C K. Gupta, [J]. *Int. Mater. Rev.*, 29(1) (1984) 405-444.
- [3] J. H. Zhang, W. Zhang, L. Zhang, S. Q. Gu, *Int. J. Miner. Process.*, 138 (2015) 20-29.
- [4] H. Y. Gao, T. Jiang, Y. Z. Xu, J. Wen, X. X. Xue, *Miner. Proc. Ext. Met. Rev.*, 41(1) (2020) 22-31.
- [5] K. H. Wu, Y. R. Wang, X. R. Wang, S. N. Wang, B. Liu, Y. Zhang, H. Du, *J. Clean. Prod.*, 203 (2018) 873-884.
- [6] Z. H. Liu, Y. Li, M. L. Chen, A. Nueraihemaiti, J. Du, X. Fan, C. Y. Tao, *Hydrometallurgy*, 159 (2016) 1-5.
- [7] J. Y. Xiang, Q. Y. Huang, X. W. Lv, C. G. Bai, *ISIJ Int.*, 57(6) (2017) 970-977.
- [8] J. Y. Xiang, Q. Y. Huang, X. W. Lv, C. G. Bai, *Metall. Mater. Trans. B.*, 48(5) (2017) 2759-2767.
- [9] J. Y. Xiang, X. Wang, G. S. Pei, Q. Y. Huang, X. W. Lv, *T. Nonferr. Metal. Soc.*, 30(11) (2020) 3114-3123.
- [10] Q. Y. Huang, J. Y. Xiang, X. Wang, G. S. Pei, X. W. Lv, *J. Chem. Technol. Biot.*, 95(6) (2020) 1773-1780.

# INVITED LECTURES



## **INVITED LECTURE**

# **THE ONGOING RESTRUCTURING OF UNIVERSITIES TO ADOPT THE SOPHISTICATION OFFERED BY INTERNET**

**Batric Pesic**

University of Idaho, College of Engineering, Moscow, ID 83843, USA

### **Abstract**

*This paper, although it does not address the technical context of the conference, does instigate the need for planning future methodology of academics engaging in passing their knowledge (teaching) to students and other audiences. Due to advancement of the internet, almost instantaneous communication with anyone, anywhere, in the world is enforcing the new methods of knowledge transfer, referred as the online teaching. Although very effective and advantageous, it does affect the key parameter, the enrollment as the revenue generator, of traditional “brick and mortar” universities. The prediction is that many colleges and universities must close the programs and/or go bankrupt. The most vulnerable university entities will be the so-called satellite colleges, those at a distance from the main university campus. In this paper key trigger issues for discussion, invoked by the power of digital communications, are: is there a need for so many universities, reduce the number of online courses and share the same among universities, libraries became mainly digitized thus merge them with university IT service, etc.? These are the key topics discussed in-person at the conference. After the material for in-person presentation was completed, the same issues are queried to get the “second opinion” from the artificial intelligence (AI). The results are presented in the body of this paper below. Considerable agreement was revealed.*

**Keywords:** *Online teaching, University restructuring, IT and library merging, Online courses sharing*

### **1. INTRODUCTION**

The advancement of communication via the internet in the last two decades has produced significant impact in all spheres of life including education. Education has always been based on the source of information (knowledge) and until the development of internet that source was “brick and mortar” university. Anyone interested in higher education, a student, had to travel and reside at the university as the source of information. For obvious reasons an adequate number of universities had to be established throughout geographic regions to enable access and space for all. The arrival of the internet has changed the direction, this time from the source, a university, to students. Travel to the source of information is no longer needed.

The invention of the internet allowing instant communication throughout the world (world wide web) is on the par with significance of Gutenberg’s printing press, developed in 15<sup>th</sup> century, the invention that eliminated the need to travel to a reader, as the only source of information. Unrestricted dissemination of books, for the first time, enabled mass communication resulting in the permanent change of society structure. About five centuries later, the information circulated by printed books and in-class teaching is surpassed by online communication and online teaching. The structure of society must change again, as it did in the post-Gutenberg era. Within the context of the conference presentation, one important component of societal structure is the institutions of higher learning, the universities. To keep up with the ongoing changes, they must adapt accordingly.

The aim of this presentation is to show via some actual data how the progress of online teaching at “brick and mortar” USA universities beside benefits also causes some structural, financial,

stresses. The sources of university revenue categorize the universities as public, private, and for-profit universities. The in-class student enrollment as the key revenue generator for public universities is now eroded by the demand for online teaching and competition from other peer universities. Lower enough enrollment evokes financial viability, with the prediction that many colleges will go bankrupt. Besides the effect on enrollment, the next discussion examines the multiplication of online courses on the exact same subject. Are they all needed? A few best-prepared online courses, for the same subject, would suffice. Consequently, with time, the university administrators will be forced to opt for reducing the number of teaching faculty, even closing the programs. It appears that time has arrived.

Upon accepting the invitation to the IOC 2023 Conference the initial plan was to talk about the importance of recycling, one of environmental sustainability necessities, how to grow the culture that nothing should be thrown away. The University of Idaho (UI) campus, and the recycling program of the city of Moscow would have served as case examples, where on the campus's 340 hectares, and about 12,000 students, not a single piece of trash (paper, soda cans, etc.) can be found lying around. Everything is pristine and clean.

However, the suddenly released, on the level of shocking, news that the University of Idaho is purchasing the University of Phoenix for about \$550 million, and several townhall meetings, thereafter, were convincing enough to change the subject of presentation. The University of Phoenix is the 100% online teaching, for-profit, university, an obvious mismatch (not only geographic) with the University of Idaho. Nobody on campus, not even remotely, expected this kind of news. The news was a catalyst to swap the attention to the importance of online teaching theme with the intention to alert the conference audience that the ongoing changes at American universities should not be casually recorded. Instead, they should be taken as the warning signal of "things to come" elsewhere, including own world, particularly at those so-called satellite-campuses.

The presentation only observes the influence of *online teaching* on the need for traditional universities to restructure. Due to space limitations, none of the prepared slides will be discussed in the written form here. The role of *artificial intelligence (AI)*, ability of computers to interact with people, is not even mentioned in the "live" discussion.

However, the AI was given the role to "judge" and present its "opinion" on the key issues discussed in the presentation.

## 2. EXPERIMENTAL

The experimental approach was to first prepare the entire presentation then to extract five key issues and post the same, in a provocative way, to the AI. Not even once was the AI consulted during the preparation. Microsoft Bing (it has embedded Chat GPT4) and Open AI (Chat GPT 3.5), were chosen. The first-round results produced were so convincing that it was decided not to go to another iteration, i.e., to debate the AI. The first runs were simply copied as asked and answered.

Once everything was completed the very last query posted was the title of the paper to test its relevance to the subjects (queries) elaborated in the paper.

## 3. RESULTS

The comments to the first three queries, posted with purple heading, are by Microsoft Bing (Chat), while the last three queries, green heading, are from the Open AI.



All universities are for profit



That is an interesting statement, but it is not entirely accurate. There are different types of universities, and they have different sources of funding and different goals. Some universities are for-profit, which means they are owned by a company or investors who seek to make money from the tuition and fees they charge. Other universities are nonprofit, which means they are not owned by anyone and they reinvest their revenues back into the institution and educational operations. Nonprofit universities may receive funding from the government, endowments, donations, research grants, and other sources. Nonprofit universities are usually more affordable and offer more financial aid than for-profit universities.

Nonprofit universities are also more likely to have higher academic standards, more qualified faculty, more diverse programs, and more accreditation than for-profit universities. Nonprofit universities tend to focus on providing quality education and research that benefit society, while for-profit universities tend to focus on maximizing profits and enrollment. Therefore, it is not correct to say that all universities are for profit, as there are significant differences between nonprofit and for-profit universities.

**It is for profit if the enrollment is the key for survival of universities**

I understand your point of view, but I think it is too simplistic to say that enrollment is the only factor that determines whether a university is for-profit or not. There are many other aspects of a university's mission, vision, values, governance, quality, and impact that differentiate it from a for-profit entity. For example:

- A for-profit university is owned by a private company or investors who seek to maximize their profits and returns. A nonprofit university is not owned by anyone and operates as a public trust or a charitable organization. A nonprofit university has a board of trustees or regents who oversee its strategic direction and fiduciary responsibility.
- A for-profit university relies heavily on tuition and fees as its main source of revenue. A nonprofit university receives funding from various sources, such as government grants, endowments, donations, research contracts, and auxiliary services. A nonprofit university can use its surplus revenue to reinvest in its academic programs, student services, faculty development, research activities, and community engagement.
- A for-profit university may have lower admission standards and less rigorous academic requirements than a nonprofit university. A for-profit university may also have less qualified faculty and less diverse curricula than a nonprofit university. A nonprofit university strives to maintain high standards of academic excellence and accreditation. A nonprofit university also offers a wide range of programs and disciplines that reflect its educational mission and goals.
- A for-profit university may have less accountability and transparency than a nonprofit university. A for-profit university may not disclose its financial information, student outcomes, or accreditation status to the public. A for-profit university may also engage in unethical or fraudulent practices, such as misleading advertising, predatory lending, or inflating graduation rates. A nonprofit university is subject to public scrutiny and regulation. A nonprofit university must report its financial data, student performance, and accreditation status to the government and accrediting agencies. A nonprofit university must also adhere to ethical and legal standards in its operations.
- A for-profit university may have less social responsibility and civic engagement than a nonprofit university. A for-profit university may not care about the welfare of its students, faculty, staff, alumni, or society at large. A for-profit university may not contribute to the advancement of knowledge, culture, or democracy. A nonprofit university has a social mission and a public purpose. A nonprofit university cares about the well-being of its stakeholders and the common good. A nonprofit university seeks to create positive change in the world through teaching, research, and service.

These are some of the major differences between for-profit and nonprofit universities that go beyond enrollment numbers. Of course, there may be exceptions and variations among individual institutions, but these are the general trends and characteristics that distinguish them.

## university libraries should transfer to IT

Thank you for sharing your opinion on university libraries and IT. I assume you mean that university libraries should be integrated with or managed by the IT department of the university. This is an interesting idea, but it may not be feasible or desirable for several reasons.

First, university libraries and IT have different missions and goals. University libraries are not just repositories of books and journals, but also centers of learning, research, and scholarship. University libraries provide access to a variety of information resources, such as databases, archives, special collections, digital repositories, and more. University libraries also offer services and programs that support the academic needs and interests of students, faculty, and staff, such as instruction, reference, consultation, outreach, and collaboration. University libraries aim to advance the educational mission and vision of the university and contribute to the creation and dissemination of knowledge.

IT, on the other hand, is responsible for providing and maintaining the technological infrastructure and systems that enable the university to function effectively and efficiently. IT provides services such as network administration, hardware and software support, security, web development, data management, and more. IT aims to ensure the reliability, availability, and performance of the university's information technology resources and systems.

While both university libraries and IT use technology to support their operations and users, they have different purposes and priorities. Merging them into one unit may create conflicts and confusion over their roles and responsibilities. It may also compromise the quality and diversity of their services and programs.

Second, university libraries and IT have different cultures and values. University libraries are rooted in the traditions and principles of librarianship, such as intellectual freedom, information literacy, user privacy, service excellence, collaboration, diversity, and innovation. University libraries are guided by professional standards and ethical codes that reflect their commitment to serving the information needs of their communities.

IT is driven by the demands and challenges of technology, such as functionality, efficiency, security, scalability, usability, and innovation. IT is governed by technical standards and best practices that ensure the optimal performance of their systems and solutions.

While both university libraries and IT value innovation and excellence, they may have different perspectives and approaches on how to achieve them. Combining them into one unit may create tensions and misunderstandings over their cultures and values. It may also undermine their identity and autonomy.

Third, university libraries and IT have different skills and expertise. University libraries employ librarians and staff who have specialized knowledge and skills in various aspects of information science, such as collection development, cataloging, metadata, preservation, reference, instruction, research support, digital scholarship, data curation, scholarly communication, copyright law and more. University libraries also require staff who have expertise in specific disciplines or fields that match the needs and interests of their users.

IT employs professionals who have specialized knowledge and skills in various aspects of information technology such as network engineering software development database administration system administration web design cybersecurity and more. IT also requires staff who have expertise in specific technologies or platforms that match the needs and preferences of their clients.

While both university libraries and IT need staff who are proficient in technology, they have different skill sets and competencies that are essential for their functions and services. Merging them into one unit may create gaps and overlaps in their skills and expertise. It may also reduce their opportunities for professional development and career advancement.

These are some of the reasons why I think university libraries should not transfer to IT. I hope this helps you understand why they are distinct and valuable units in the university.

### **YouTube should be converted into the World's University**

#### **ChatGPT**

Converting YouTube into the world's university is an interesting idea that has both potential benefits and challenges. Let's explore some of the advantages and considerations associated with this concept:

#### **Advantages:**

1. **Accessibility:** YouTube is already a widely accessible platform, making educational content available to a global audience. Converting it into a university could enhance access to education for people who may not have had the opportunity otherwise.
2. **Diverse Content:** YouTube hosts a vast array of content across different subjects, which could provide a diverse range of educational offerings. This diversity could cater to various learning styles and interests.
3. **Cost-Effective:** Traditional universities often come with high tuition fees and other costs. Converting YouTube into a university could potentially reduce financial barriers for learners, making education more affordable and inclusive.
4. **Global Reach:** YouTube's reach is truly global, allowing learners from different countries and cultures to connect and learn from one another. This could foster cross-cultural understanding and collaboration.
5. **Flexibility:** Online platforms like YouTube offer flexibility in terms of when and where learners access content, which could accommodate different schedules and lifestyles.

#### **Considerations and Challenges:**

1. **Quality Control:** Maintaining the quality and accuracy of educational content on YouTube could be challenging. Without proper oversight, misinformation and low-quality content might proliferate, leading to potential negative consequences for learners.
2. **Credibility:** Traditional universities often provide recognized degrees and certifications. Converting YouTube into a university would require a mechanism for awarding credentials that hold value in the job market and academia.
3. **Lack of Interaction:** Traditional universities offer in-person interactions with professors and peers, fostering critical thinking, debate, and discussion. Converting YouTube into a university would need to address this lack of direct interaction.
4. **Assessment and Feedback:** A robust educational system requires effective assessment methods and timely feedback. Designing these elements into a YouTube-based educational model could be complex.
5. **Regulation and Accreditation:** The education sector is heavily regulated in many countries to ensure quality and protect learners. Adapting YouTube to a university model would need to address regulatory and accreditation requirements.
6. **Monetization and Sustainability:** YouTube relies on advertising revenue and creator monetization. Converting it into a university might require rethinking its revenue model to sustainably support educational initiatives.

7. **Content Ownership:** YouTube content is often created by individuals and organizations, each with their own intentions and rights. The transition to a university model would require addressing ownership, permissions, and copyright issues.

In conclusion, while the idea of converting YouTube into the world's university has exciting potential, it also poses significant challenges that need to be carefully considered. A successful transition would likely require a comprehensive strategy involving educators, regulators, content creators, and technology experts to ensure quality, credibility, and accessibility in this new educational landscape.

## B

### A well prepared online course should be shared among universities

#### ChatGPT

Sharing a well-prepared online course among universities can have several benefits, but it also comes with certain challenges that need to be considered. Here are some advantages and considerations:

#### Advantages:

1. **Cost-Efficiency:** Developing high-quality online courses can be resource-intensive. Sharing courses among universities can help distribute the development costs, making it more cost-effective for each institution involved.
2. **Expertise Pooling:** Different universities might have expertise in various subjects. Sharing courses can allow students to access the best instructors and resources from different institutions, enhancing the overall learning experience.
3. **Wider Access:** Online courses can reach a global audience, benefiting students who might not have had the opportunity to take the course otherwise due to geographical constraints.
4. **Variety and Diversity:** Sharing courses can lead to a wider variety of courses being available to students, increasing the range of subjects they can study and potentially fostering interdisciplinary learning.
5. **Quality Improvement:** Collaboration among universities can lead to a continuous improvement cycle for the course content, as feedback and insights from multiple institutions can lead to refinements and updates.

#### Considerations:

1. **Quality Control:** Maintaining consistent quality across different institutions can be challenging. Standards for content, assessments, and interaction need to be clearly defined and enforced.
2. **Institutional Autonomy:** Each university might have its own teaching style, academic calendar, and policies. Harmonizing these differences when sharing courses can be complex.
3. **Technology and Infrastructure:** Universities may have varying levels of technological infrastructure, and not all institutions might have the necessary resources to deliver an online course effectively.
4. **Intellectual Property:** Ownership and licensing of course content need to be well-defined to avoid disputes over intellectual property rights.
5. **Cultural and Language Differences:** Courses might need to be adapted to suit different cultural contexts and languages to ensure inclusivity and effectiveness.
6. **Faculty Involvement:** Faculty members might be hesitant to adopt or adapt shared courses if they feel it diminishes their role in curriculum development.

7. **Student Engagement:** Online courses require active student engagement. If students are not accustomed to online learning or lack the necessary digital literacy skills, it could impact the effectiveness of the course.
8. **Support and Interaction:** Online courses often require technical support and opportunities for interaction with instructors and peers. Ensuring these aspects are maintained in a shared course is important for student success.

In conclusion, sharing well-prepared online courses among universities can offer numerous benefits in terms of cost-efficiency, expertise pooling, and wider access. However, careful planning is required to address challenges related to quality control, institutional autonomy, technology, and cultural considerations. Collaboration and open communication among the participating universities are crucial to successfully implementing a shared online course model.

## B

### The Ongoing Restructuring of Universities to Adopt the Sophistication Offered by Internet ChatGPT

The ongoing restructuring of universities to adopt the sophistication offered by the internet is a significant and evolving trend in higher education. This restructuring is often referred to as "digital transformation" or "online education revolution." It involves leveraging the capabilities of the internet and digital technologies to enhance various aspects of university operations, teaching, learning, and research. Here are some key areas where universities are adopting the sophistication offered by the internet:

1. **Online Learning Platforms:** Universities are increasingly offering online courses and degree programs, allowing students to access high-quality education regardless of their geographical location. These platforms provide a range of interactive tools, such as video lectures, discussion forums, quizzes, and assignments, to facilitate effective learning.
2. **Blended Learning:** Many universities are adopting a blended learning approach, which combines traditional classroom instruction with online components. This approach allows for greater flexibility and customization of learning experiences.
3. **Massive Open Online Courses (MOOCs):** MOOCs are large-scale online courses designed to accommodate a large number of participants. They often feature video lectures, interactive quizzes, and peer-to-peer interactions. MOOCs provide access to educational content from prestigious universities around the world.
4. **Digital Resources and Libraries:** Universities are digitizing their libraries and academic resources, making them accessible to students and researchers remotely. Digital libraries offer vast collections of e-books, research papers, journals, and other scholarly materials.
5. **Virtual Laboratories and Simulations:** Fields that traditionally require physical laboratories are exploring virtual alternatives. Virtual labs and simulations enable students to conduct experiments and simulations in a controlled digital environment.
6. **Collaborative Tools:** The internet offers a wide range of collaborative tools that allow students and researchers to work together remotely. Video conferencing, document sharing, and collaborative editing tools facilitate teamwork and communication.
7. **Personalized Learning:** Adaptive learning technologies use data analytics to tailor educational content to individual students' learning styles and progress. This personalization enhances the learning experience and outcomes.
8. **Global Outreach and Engagement:** Universities can now reach a global audience through online platforms, expanding their reach and influence. Virtual guest lectures, webinars, and international collaborations are easier to facilitate.



9. **Flexible Scheduling:** Online courses and resources allow students to learn at their own pace and fit education into their busy schedules, making higher education more accessible to working professionals and non-traditional students.
10. **Assessment and Feedback:** Digital tools can provide automated assessments and instant feedback to students. This allows instructors to identify learning gaps and provide timely support.
11. **Research Collaboration:** Internet-based collaboration tools enable researchers to collaborate across geographical boundaries. They can share data, findings, and resources, fostering interdisciplinary research.
12. **Administrative Efficiency:** Universities are using digital systems for administrative tasks such as registration, fee payment, and communication. This streamlines processes and improves efficiency.

However, it's important to note that while the sophistication offered by the internet has numerous benefits, challenges also exist. Ensuring the quality of online education, addressing issues of equity and access, maintaining student engagement, and safeguarding data privacy are some of the concerns that universities need to address during this restructuring process.

In conclusion, the ongoing restructuring of universities to adopt the sophistication offered by the internet is transforming the landscape of higher education. This transformation has the potential to make education more accessible, flexible, and innovative, but it also requires careful planning and adaptation to ensure its effectiveness and inclusivity.

#### 4. DISCUSSION

I disagree with the first three answers, particularly with the first two. If the students must pay for tuition a university is for profit regardless of language manipulation. Only the universities that do not charge (except minor application fees) for enrollment are genuine not-for-profit universities. Therefore, education is an industry, and in the USA trillions of dollars in size.

For public universities the student enrollment is the most watched, by the administration, parameter. If the enrollment is increasing the statements are issued that the university has recorded the growth. This kind of terminology is appropriate for stock market analysts where the revenue growth of a corporation is tied to volume of units sold, but inappropriate for the universities. Besides, education cannot grow it can only improve in quality. Private universities with limited acceptance can claim that the quality of education is the primary objective. True, they do select the brightest available students but at the same time they do evaluate the probability of each individual applicant becoming most influential in business, politics, etc. upon graduation. Reason? Because well-established alumni do contribute sizeable endowments. Thus, we are back to the money and industrial, for-profit, behavior,

Next subject of disagreement is the query regarding libraries. As explained in the presentation most, if not all, of readers of this text have not been to a university library for months. That is because information in research journals and books is digitized and can be readily retrieved at the personal desk computer. The obligation of a university library is to assure full subscription to the appropriate research digital databases eliminating the need for people resources. Therefore, the university libraries should be reorganized and downsized. Historic and special collection values should be curated under safeguarded conditions with supervised access. The rest of the library (digital form) should merge with IT sector of the university. The need for having the university library as an academic unit (dean, department chair, full, associate, and assistant professor) will be eliminated freeing the money for increased digital subscription. Perhaps in time there will only be one digital library per country, of similar model as is the CAS (Chemical Abstract Service) data centers. The very last query, the appropriateness of the paper title, did recognize the importance, and the role, of digital libraries.

As stated in the introduction the theme of the presentation is the impact of online teaching on the number of students enrolled at traditional universities. At many public universities the impact is

negative as expected. The major argument here is that not every university should teach the same subject if these are digitized. In other words, they can be shared. Just like hundreds of universities adopt the same textbooks to teach courses in math, chemistry, physics, etc., the same principle can be applied to the prepared and selected for adoption of online courses. A few best prepared (topics, narration, visual animation, homework problems and solutions, etc.) online courses, per subject of teaching, could serve worldwide university systems.

## 5. CONCLUSIONS

The evolution of online teaching is imposing universities to restructure; merging among institutions is one of the pathways. The driving force for the process in progress is the reduction of costs of education. The online teaching here is nothing more than an effective delivery of lectures, from adopted book(s) to enrolled students, to/from anywhere in the world. The lectures are exact, i.e., unbiased. Some lectures are fully online, the others hybrid (also called blended), in-class + online. The conference presentation is strictly focused on the cause/effect of online teaching on traditionally structured universities.

Although used, for curiosity, to produce the so called “second opinion”, the conference presentation is not addressing the use of artificial intelligence (computers provide the reasoning) in education. Artificial Intelligence, i.e., “the educational technology” as called by the US Department of Education, is uncharted territory. It is not unbiased as the online lectures prepared by the in-class professors. Time is required to express itself fully, according to advantages and disadvantages, before its intrinsic value in education can be fully judged.

## FURTHER READING

1. Artificial Intelligence and the Future of Teaching and Learning, U.S. Department of Education, Office of Educational Technology, May 2023.  
<https://www2.ed.gov/documents/ai-report/ai-report.pdf>
2. OpenAI, <https://en.wikipedia.org/wiki/OpenAI>
3. The purchase of University of Phoenix University, Idaho Statesman, August 22, 2023.: U of I isn't the first to buy a for-profit college. What happened when 3 other schools did (msn.com),
4. University of West Virginia closes the entire programs, August 11, 2023:  
<https://www.insidehighered.com/news/faculty-issues/tenure/2023/08/11/west-virginia-university-unprecedented-proposed-cuts-become>
5. Enrollment decline at University of Pennsylvania system, July 12, 2023:  
<https://www.insidehighered.com/news/admissions/traditional-age/2023/07/12/pa-public-colleges-battle-students-and-funding>

## INVITED LECTURE

# MACHINE LEARNING APPLIED TO IMPROVING THE SCRAP RECYCLING AND MELTING PROCESS IN ALL TYPES OF FERROUS ALLOYS AND STEEL

**Yaima Filiberto, Alberto Montenegro Correa, Eugenio Álvarez**

AMV Solutions, Vigo, Spain

### **Abstract**

*Reusing scrap in the foundry sector is critical to manufacturing metals with the quality the industry requires sustainably and efficiently. The state of the art of optimization systems for foundry raw materials is based on a characterization and classification of the different families of materials (scrap, internal returns, etc.), with the information provided by the supplier itself, in the best of cases verified with a more or less representative sample of the material received, which is melted and analyzed in small furnaces.*

*The reliability of the results given by the optimization system depends directly on the representativeness of this information. And this is where the problem arises: when the scrap is of good quality, the final results agree reasonably well with those expected; On the contrary, when the scrap is more heterogeneous or its logistical control is more complex, there is a significant risk of chemical deviations in the final metal that would mean the rejection of a substantial part of the molten castings, with the consequent negative impact on costs and productivity.*

*Consequently, low-quality scrap, which is very abundant and low-cost, is underutilized in favor of much more expensive virgin raw material and hardly sustainable production.*

**Keywords:** Machine learning, Scrap, Load optimization

## **1. INTRODUCTION**

The systems that are currently being implemented already offer Operations Research algorithms that, together, collect almost all the variables that influence the casting process: complete traceability of materials, environmental variables, preparation of furnace charges, additives, fusion parameters (times, temperatures, electrical variables), by-products, final metal, chemical composition or yields. The push towards the fourth industrial revolution, what has come to be called Industry 4.0, has come hand in hand with the application of artificial intelligence (AI) techniques to factories and production systems. There are various industry sectors where we can find Machine Learning applications, covering all those computing systems that can perceive their environment, think, learn, and act. These sectors include predictive maintenance, production quality, job planning, image recognition, and logistics [1, 2].

The principle in machine learning is that the machine generates a model from examples and uses it to solve the problem. The set of examples is used as the training set. Learning is inductive or lazy depending on when the data is operated on to generate the model. One of the most studied learning models is inductive learning, which encompasses all those techniques that apply inductive inferences on a data set to acquire knowledge inherent to them [3]. In the other case, each time an instance of the problem needs to be solved, the data is accessed to build the solution. Examples of inductive methods are the multilayer Perceptron [4] and the C4.5 algorithm [5], while the k-Nearest Neighbors (k-NN) [6] is a typical lazy learning method.

This paper presents the results of the practical application of Machine Learning techniques to know as precisely as possible the behavior of the different scrap metals according to operating conditions and inform decision-making systems in real-time. This represents a before and after in the



parameters of efficiency and quality in the manufacture of metals. Strategic products such as steel can reduce their manufacturing costs by 2% - 3%, improving their sustainability by increasing the use of low-quality scrap by more than 10%. A steel plant with a production of 1 million tons/year would mean a cost reduction of more than 10 million euros per year. This technology is also applicable to cast iron (grey/nodular) in sectors as important as automotive or wind power.

## 2. CASE STUDY

For the correct application of intelligent technology in the scrap characterization process and the real-time prediction of the chemical composition of the main elements, we must start with the importance of building the knowledge base. This is undoubtedly one of the most critical stages of the knowledge discovery process. The complete process of extracting knowledge from databases is known as KDD (Knowledge Discovery in Databases). This process comprises various stages, from obtaining the data to applying the knowledge acquired in decision-making. [7, 3].

In the case of the application, it is necessary to consider a set of variables that directly affect the chemical contribution of the materials used. Among these variables, we can find the updated chemical specifications of the final products, quality restrictions, expected returns by type of product, performance, chemistry, and residual elements, based not only on certificates issued by the supplier or on samples analyzed upon receipt, if not on the actual results obtained in production castings. Constituting these the input variables and as the output variables, the chemical composition of the elements to be analyzed. The Smart module was developed for the ALEA system, where the entire knowledge discovery process is considered, starting from the construction of the knowledge base until the visualization of the results. The figures below show the configuration and creation windows of the knowledge base.

Among the stages of the KDD, there is one that can be considered as the core of the process, and that consists of the extraction of knowledge from the data. This phase is crucial for obtaining relevant results and depends on the applied machine learning algorithm. For the proper selection of the ML model to be used in solving the problem, tests were carried out with different ML methods implemented in Weka, R, and Python, and the ones with the best results were used. These algorithms were included in the ALEA Smart module.

Once the knowledge base has been built, and the ML algorithms have been implemented, the training and model creation is carried out. The results of the evolution of the chemistry of the evaluated elements are evaluated, as well as the results of the prediction of the final chemistry of the casting, considering this characterization. This process is dynamic and based on real-time knowledge built from production data. Figure 1 shows an example of adjusting the Cu content of scrap based on its production history. Figure 2 shows an example of the results of comparing the actual chemistry and that expected by castings for the element *Cu* from the estimated chemistry for each of the scraps used in the castings.



Figure 1 - Cu characterization of scrap using ML



Figure 2 - Results of the actual vs expected chemistry (element *Cu*) using ML

To illustrate the results of the application of ML techniques for the characterization of scrap, as well as its impact on the prediction of casting chemistry, we compared the estimates before applying the model and once it was used.

Figures 3a and 3b compare the expected and real chemistry before and after applying the model, respectively. The metrics for evaluating the results are highlighted in a red box.

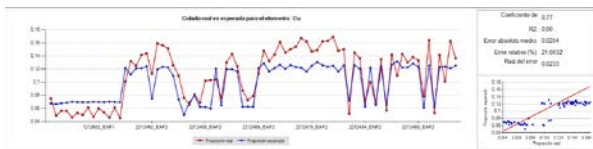


Figure 3a - Actual vs expected chemistry results (element Cu) before using the ML model

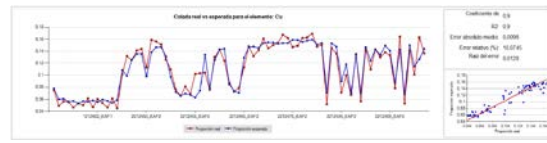


Figure 3b - Actual vs expected chemistry results (element Cu) after using the ML model

As we can be seen in the highlighted boxes, taking into account the different metrics, a significant improvement in the chemistry estimate is obtained.

Another advantage offered by the Smart module is the possibility of analyzing outliers taking into account the actual and expected chemical content for each element figure 4 and outliers in terms of the error between the expected and actual value for each element figure 5.



Figure 4 - Outliers for actual and expected chemical content (Cu element)

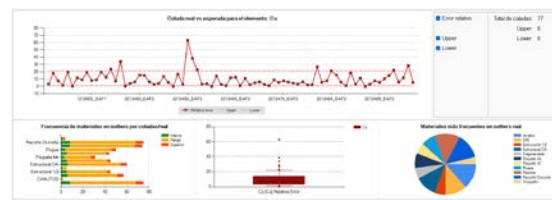


Figure 5 - Outliers regarding the error expected vs actual value (Cu element)

Although the values of the metrics selected to evaluate the accuracy of the predictions are very good, it was possible to detect that these are affected by inaccuracies in the manual entry of data and the discontinuity in the calculation of the recipes. This was possible with the help of the detection of outliers allowing us to identify these cases and evaluate the possible solutions.

### 3. CONCLUSIONS

The results of the application of the ML models allowed: - Detect anomalies, improvements in load optimization, better characterization of scrap and improve the estimates of the chemistry of the castings, reaching values of R2 above 90% higher than the values reached before the proposed solution. A solution is implemented that significantly supports decision-making, contributing to production cost savings.

### REFERENCES

- [1] J. Nieves, I. Santos, P. G. Bringas., *Rev. Metal.*, 47(4) (2011) 341-354.
- [2] E. A. Saravia Riffo., & Pradenas, L. *Predicción de la temperatura fuera del rango de control, de la caldera de gases en horno de fusión flash de concentrado de cobre*, Universidad de Concepción, Facultad de Ingeniería, Departamento de Ingeniería Industrial, 2022.
- [3] J. Ruiz., *Reconocimiento lógico combinatorio de patrones: teoría y aplicaciones*, Editorial Universitaria, Santa Clara, 2006.
- [4] F. Rosemblatt, *Principles of Neurodynamics*, New York, 1962.
- [5] J. R. Quinlan., *C-4.5: Programs for machine learning*. San Mateo, California, 1993.
- [6] T. M. Cover, P. E. Hart., *Nearest neighbour pattern classification*. *Transactions on Information Theory*. Institute of Electrical and Electronics Engineers, 1967, 13: 21-27.
- [7] Y. Filiberto Cabrera., *Métodos de aprendizaje para dominios con datos mezclados basados en la teoría de los conjuntos aproximados extendida*, Editorial Universitaria, Santa Clara, 2012.

## **INVITED LECTURE**

### **CONSTRUCTION OF A NEW SINTERING PLANT 180 m<sup>2</sup> WITHIN THE HBIS GROUP SERBIA IRON & STEEL**

**Slobodan Kostić, Qi Fenglai, Savo Pirgić, Nenad Botić, Dobrica Milovanović,  
Čedomir Sušić, Igor Zlatković**

HBIS GROUP SERBIA IRON & STEEL Srbija

#### **Abstract:**

*The construction of the new sintering plant (New Sinter Plant) had two primary goals:*

- 1. production - technological goal, which meant increasing the production of sinter, improving the quality of the produced sinter, rationalizing production as well as reducing costs per unit of product*
- 2. improvement of environmental protection, where the project solution would meet the requirements of the standard for emissions of polluting exhaust gases "Best Available Techniques (BAT) Reference Document for Iron and Steel Production 2013" ("Reference document for the best available technique (BAT) for iron production I of steel 2013").*

**Keywords:** *sinter, environmental protection, construction*

#### **1. INTRODUCTION**

The construction of the new sinter line 180 m<sup>2</sup> Sinter Plant within the HBIS GROUP SERBIA IRON & STEEL began in June 2019 when the foundation stone for the New Sinter Plant was laid, the installation of equipment began at the end of 2020, while the cold test period began in December 2021. The warm test period of the new sinter line began in February 2022, and the start of production began in April 2022. The construction of the new plant for sintering (Sinter Plant) included the construction of new facilities and the reconstruction of facilities that are part of the existing plants, with the aim of increasing the annual capacity from 1.37 million tons to 1.782 million tons of sinter, with better sinter quality. In order to rationalize the sinter production system, aiming to reduce costs per product unit. The foreseen technology reduces the consumption of all energy sources and additional materials, and the most of all coke and electricity. In order to protect the air as well as to improve the quality of the air, by reducing its pollution trough reducing polluting substances below the prescribed limit values, a dust removal system was installed. The amount of flue gases and gas containing dust in the production process of metallurgical plants is large. The dust concentration and smoke dispersion is high. Aspiration hoods and air purification devices are installed at all production workplaces where dust and flue gases occur. Projected concentration of dust when using cloth dusting bags from sintering plant must be less than 15 mg/Nm<sup>3</sup>, that from Electro Static Precipitator (ESP filter) less than 40 mg/Nm<sup>3</sup>. For the adopted semi-dry process for desulfurization, the emission of sulfur dioxide must be less than 180 mg/Nm<sup>3</sup>.

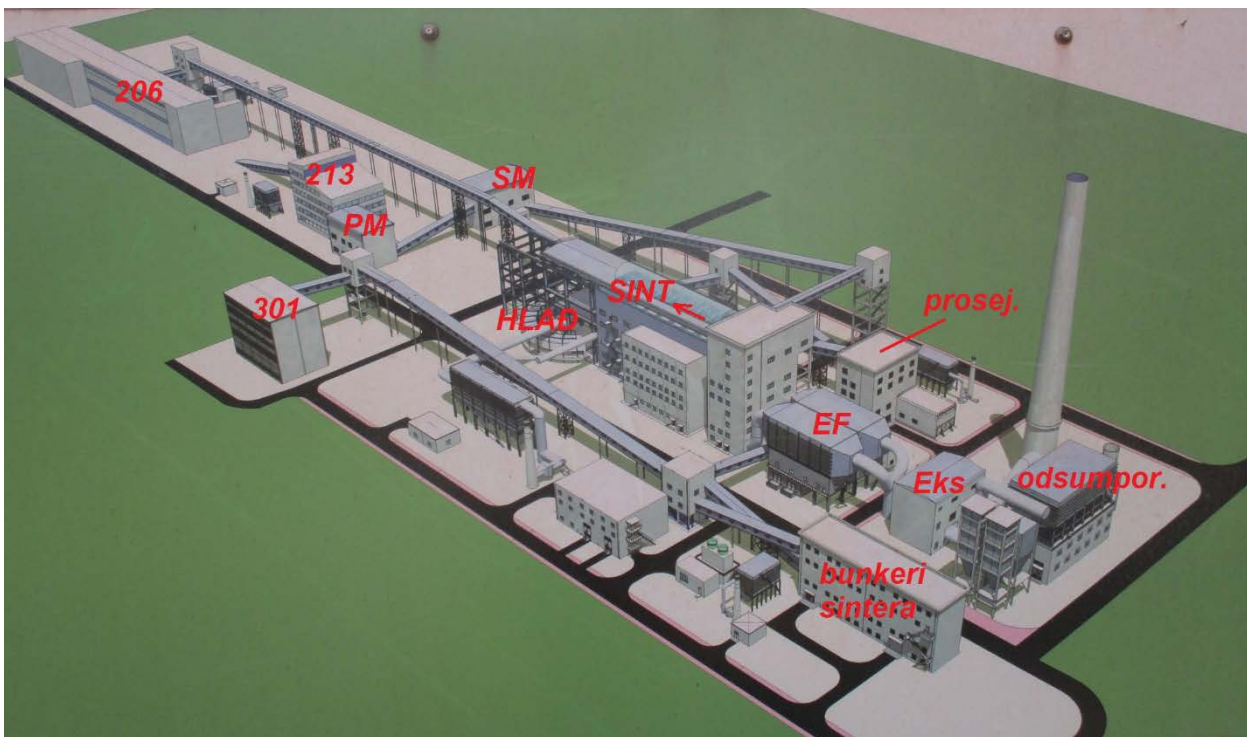
#### **2. EXPERIMENTAL**

Within HBIS GROUP Serbia Iron & Steel d.o.o. Belgrade - Smederevo branch, there are a total of 4 sintering machines in the existing sinter plant, namely sintering machines 1 and 2 of 75 m<sup>2</sup> and sintering machines 3 and 4 of 90 m<sup>2</sup>. The existing, largest annual production of 4 sintering machines in the Smederevo ironworks is 1.37 million tons, and the largest monthly production was 131 thousand tons (2006). Coke consumption is high, so production is irrational. The sintering equipment is old, the technology is outdated, the thickness of the sinter layer is only 300 mm, the

quality of the sinter is poor, so in order to reduce production costs in the blast furnace, it is necessary to optimize the production of sinter material. Therefore, the construction of a new sintering plant of 180 m<sup>2</sup> (New Sinter Plant) is planned, which includes the construction of new and reconstruction of existing plant facilities, with the aim of obtaining better quality sinter, increasing the annual capacity (current 1.37 million tons to 1.782 million tons of sinter) and rationalizing the sinter production system. Rationalization includes the reduction of costs per product unit, i.e. reduction of consumption of all energy sources and additional materials (mostly coke and electricity) per product unit.

### 3. RESULTS AND DISCUSSION

The New Sinter Plant consists of a dosing facility with a fuel crushing system, a primary mixing facility, a pelletizing facility, a sintering facility, a screening facility, a main exhaust fan facility (Exhauster) and a dedusting and desulfurization system. The complete process at the New Sinter Plant is set up in the automatic monitoring and management system in such a way that it realizes all the monitoring functions that are necessary for the control and management of the production process.



The amount of flue gases and gas containing dust in the production process of metallurgical plants is large. The dust concentration and smoke dispersion is high. The factory renovation project envisages the installation of hoods for aspiration and air purification devices at all production workplaces where dust and flue gases occur. The project solution will satisfy the requirements of the standard for emissions of polluting exhaust gases "Best Available Techniques (BAT) Reference Document for Iron and Steel Production 2013". The concentration of dust when using cloth dusting bags from the sintering plant must be less than 15 mg/Nm<sup>3</sup>, that from the Electro Static Precipitator (ESP filter) less than 40 mg/Nm<sup>3</sup>. For the adopted dry desulfurization process, the emission of sulfur dioxide must be less than 180 mg/Nm<sup>3</sup>.

It is necessary to emphasize that in addition to the installation of equipment, there was also the introduction of new technological systems that greatly contributed to the production of higher quality sinter as well as energy savings. Unlike the old technology, where a mixture of natural and blast furnace gas was used, the new Sinter Plant uses exclusively blast furnace gas, which led to a reduction in the price of sinter. The use of lime was also introduced into the technological process,



which was not used in the earlier technological process. By introducing lime into the technological process, better palletization of the sintering mixture was achieved, as well as preheating of the sintering mixture, which reduced the use of steam. In addition, by using the bottom layer that is obtained after sieving the sinter, it was possible to protect the barns on the trolley and better sucking trough sinter ore material. Through these two elements, the sintering process was improved and temperature control in the sintering process was easier.

The new technical solution for dedusting the main technological process, which is reflected in the fact that the Electro Static Precipitator (ESP filter) is placed between the sinter line and the exhauster compare to the work system of the old sinter lines where the scrubber system was located between the sinter lines and the exhauster, a dry dedusting system was introduced instead wet dedusting system, which contributed to better preservation of equipment, reduction of dust emissions, reduction of technical water consumption and better utilization of recyclable materials. With new technical solutions and the installation of adequate dedusting equipment, by which we mean the dedusting of all overflow areas, the installation of bag filters and Electro Static Precipitator (ESP filter), the emission of suspended particles has been reduced to the lowest possible minimum. All the material that are collected from the plant is returned to the production process again, through the pneumatic transport of dust, which achieves a partial saving of material through this recycling system. The newly built Desulfurization plant, which aims to purify the gases produced in the production process, as well as to remove suspended substances from those gases, giving purified air. The current efficiency of the desulfurization system is over 98% in terms of suspended particulate matter and SO<sub>2</sub> emissions. By installing the new sinter line of 180 m<sup>2</sup>, the production capacity of the Sinter Plant was increased, and accordingly, with an average daily production of 4,500 t of sinter, there is an obvious saving of electricity and fuel (Table 1). It is also necessary to mention that with the new sinter line, the quality of sinter has been greatly improved for less than 20% (Table 2), which contributed to an increase in the share of sinter in the backfill of the blast furnace by 7.5%.

Table 1

Period / Unit	SINTER PRODUCTION	BF GAS		NATURAL GAS		EL.ENERGY	
	t	Nm <sup>3</sup>	Nm <sup>3</sup> /t	Nm <sup>3</sup>	Nm <sup>3</sup> /t	KWh	KWh/t
2020	1,011,079	18,785,759	19	7,339,127	7	122,230,002	121
2021	1,153,480	5,316,382	7	11,255,478	10	127,013,941	110
2022	1,131,827	52,098,773	45	2,642,842	2	102,368,728	90
Jan-Jun 2023	682,216	44,338,401	65	0	0	47,876,712	70

Table 2

	QUALITY		
	I klass	II klass	I+II klass
2020	54	23	76
2021	41	24	65
2022	42	23	65
Jan-Jun 2023	58	24	82

Table 3

HBIS Serbia Iron & Steel d.o.o. KALKULACIJA CENE KOSTANJA						
SINTER			Mix 2021_22	2Q act 2023 usd		
Production (t)						
1						
Name	%	T/T	\$/t sintera	%	T/T	\$/t sintera
Sinter ore Zaporozje	9%	0.064				
Sinter ore Turkey 62	7%	0.044		1%	0.010	
Sinter ore KUMBA STANDARD	27%	0.183		35%	0.272	
Sinter ore Krivbas 64%						
Sinter ore Krivbas 61%	13%	0.090		7%	0.053	
Sinter ore Rudomine	11%	0.074		9%	0.072	
Sinter ore KRIVBAS 57 % Fe	11%	0.076		4%	0.029	
Sinter ore Mauritanija				21.8%	0.168	
Sinter ore Suha Balka 60%	12%	0.084		22%	0.168	
Turkish fines 58%						
Turkish fines 55%		0.020				
RUDA SITNA ROY HILL						
Sinter ore Turkey Siderite	5%	0.037				
<b>Total Sinter Ores</b>		<b>0.672</b>			<b>0.772</b>	
Purchased Scale		0.037			0.010	
<b>Total Sinter ores &amp; purchased scale</b>		<b>0.709</b>			<b>0.782</b>	
<b>Total ores &amp; purch scale &amp; concent</b>		<b>0.742</b>	<b>95.12</b>		<b>0.782</b>	<b>102.78</b>
<b>C &amp; B Scrap Total</b>		<b>0.113</b>			<b>0.087</b>	
<b>Internal Recycled Material</b>		<b>0.085</b>			<b>0.058</b>	
<b>Raw Materials</b>		<b>1.252</b>	<b>105.99</b>		<b>1.170</b>	<b>112.75</b>
<b>Total Coke Breeze</b>		<b>0.036</b>	<b>18.07</b>		<b>0.027</b>	<b>13.58</b>
<b>Fuels</b>		<b>0.060</b>	<b>25.10</b>		<b>0.059</b>	<b>22.76</b>
<b>Subtotal Energy</b>			<b>15.72</b>			<b>6.94</b>
<b>CONVERSION COST</b>			<b>157.94</b>			<b>155.80</b>

Table 4

	Fe	\$/t		\$/t
SINTER Mix 2021 / 2022	49.60	157.9397	IRON	513.45
SINTER Q2 2023	51.39	155.7985	IRON	504.69

Table 5

	Fe	\$/t		\$/t
SINTER Mix 2021 / 2022	49.60	157.9397	IRON	513.45
SINTER	51.39	160.4800	IRON	513.45

In support of the fact that the savings greatly contribute to the lower price of sinter can be seen in Table 3. Where it can be seen that with a similar composite of materials in the period of work 2021/2022 as well as the second quarter of Q2 -2023 that the price of sinter in 2023 is lower by \$2.14 /t in relation to the price of sinter in 2021/2022 when the old sinter lines 2, 3 and 4 were operating. And that the price of sinter was directly affected by the reduction in fuel and electricity consumption, even though the price of raw materials increased.

Analyzing Table 4, we can see that the price of produced sinter directly affected the production price of iron through two factors, i.e. by increasing the percentage share of sinter in Blast Furnace backfill due to the stable and high quality of sinter, as well as through the lower price of sinter as a product due to the reduction of fuel and electrical energy consumption. Therefore, due to the lower price of sinter by \$2.14/t, the price of iron is also lower by \$8.76/t.

#### 4. CONCLUSION

If we were to equate the price of produced iron in the model, Table 5, we would get that the price of sinter should be \$160.48 \$/t, which is higher than the price of sinter in the period 2021/2022 and by 1.6% with a higher share of Fe, which leads to the conclusion that the price of sinter would increase with the percentage share of Fe. However, the price of sinter produced at the new Sinter Plant is lower by 3% compared to the model, which leads to savings of \$4.68/t.

Bearing in mind the above arguments, it can be concluded that the investment in the new Agglomeration has successfully achieved both goals set by the HBIS Serbia Company.

## **INVITED LECTURE**

# **ACID ACTIVATION OF BENTONITE: PHYSICO-CHEMICAL CHARACTERIZATION AND APPLICATION IN GOETHITIC IRON ORE GREEN PELLETIZATION**

**Satyananda Patra**

Research & Development, ArcelorMittal Nippon Steel India Ltd., Surat, India-394270

### **Abstract**

*Utilization of natural bentonite in pelletization leads to contamination and degradation in metal production and high slag rate in blast furnace process due to additional gangue addition in the form of SiO<sub>2</sub> and Al<sub>2</sub>O<sub>3</sub>. Acid activation of bentonite by HCl or H<sub>2</sub>SO<sub>4</sub> can enhance the adsorption properties and reduce the alumina content in natural bentonite, which may improve metal production and reduce contamination as well. In this paper both the acid activation process has been carried out. A detailed characterization studies were conducted to know the physico-chemical variations in the activated bentonite as well as raw bentonite, which includes SEM with EDS, XRF elemental analysis, XRD, BET surface area analysis with pore volume determination, FTIR analysis and DT/TG Analysis. Besides all the detailed characterization work, all the binders were applied in iron ore pelletization to know their effect on pellet size, strength, and microstructure. Also, find out the relationship between CCS and porosity of the optimized pellets.*

**Keywords:** Natural Bentonites, Acid Activation, Characterization, Pelletization

## **1. INTRODUCTION**

Natural clays are used as a binding agent in iron ore Pelletization. The wastewater treatment process is applied for the removal of chemical pollutants such as kaolin, bentonite, and zeolite [1–6]. Among these clays, bentonite is one of the most widely used adsorbents as it possesses a net negative surface charge [6, 7]. Bentonite clays primarily consist of montmorillonite as the basic mineral. Montmorillonite Al<sub>2</sub>[(OH)<sub>2</sub>Si<sub>4</sub>O<sub>10</sub>].nH<sub>2</sub>O is belongs to a group of layered silicates. Basic structure is composed of tetrahedral layers, formed by inter-binding of tetrahedral sheets with Si<sup>4+</sup> ion in the center and four O<sup>2-</sup> ions on the tops, and octahedral layers. It is formed by binding of octahedral sheets with Al<sup>3+</sup> ion or Mg<sup>2+</sup> ion in the center and six OH<sup>-</sup> ions in the corners [8, 9]. Adsorption capability and swelling property of natural bentonites can be improved by various methods of activation, modification with various metals, pillaring, etc. [10-19].

Binders, during agglomeration, are added to the iron ore fines to improve the pellet properties and impart strength to the pellets during wet, dried, and indurated conditions [20-29]. The present study highlights the changes in bentonite after acid activation in view of physico-chemical aspects which includes specific surface area, chemical, mineralogical and morphology structures. It also focuses on comparative analysis of microstructure, porosity, CCS, and composition of green pellets formed by using both raw bentonite and acid activated bentonite as binders.

## **2. MATERIALS, METHODS AND EXPERIMENTAL SETUP**

The -3 Mesh run of mines (ROM) iron ore sample, collected from Thakurani (Eastern India) iron ore mines of Odisha, was crushed in a dodge type jaw crusher. The crushed product was passed through a roll crusher, which was then ground to 100% passing 150µm in a ball mill. The sample was then beneficiated by gravity and magnetic separation process to obtain pellet grade concentrate. The sample prepared, for the pelletization study, contains 100% passing 75micron with approximately 85% below 45µm. Bentonite sample was collected from Ashapura Minerals,

Gujarat, India approximately 2 kg of -8 mesh size. It was sampled and ground to below 200 mesh for acid activation process. H<sub>2</sub>SO<sub>4</sub>, HCl and Acrylic Acid were collected from Central Lab, AMNS India. Limestone and anthracite coal were collected from ESSAR steel India limited having size fraction of - 150 micron.

### Characterization of raw (RBt) and activated bentonites

Acid activation of raw bentonite by both HCL and H<sub>2</sub>SO<sub>4</sub> were performed, and the activated samples were characterized using various methods to analyze the variations in physico-chemical properties. The detailed chemical composition of the sample was determined through XRF, using ThermoFisher X-ray Fluorescence spectrometer operated at 30 kV voltage and 100 mA current with counting time 5 sec, except LOI which was determined by heating the sample at 950°C for 1 h in a muffle furnace. The sample was examined by Scanning Electron Microscopy-Energy dispersive spectroscopy (SEM-EDS) technique. SEM analysis was performed using a FEI 430 Nova Nano-scanning electron microscope equipped with a tungsten filament coated with zirconium oxide. The micro analyzer was a JEOL maker model JXA 8230. The acceleration tension was kept at 15 kV for all the measurements. Chemical composition of nanoparticles bentonite samples was analyzed by Energy Dispersive X- ray analyzer (EDX). The mineralogical composition of the sample was evaluated by X-ray diffraction (XRD) analysis using Rigaku Tabletop Model. Copper was used as anode material and the generator settings were maintained at 30 mA and 40 kV. The X-ray patterns were acquired in the 2θ range of 10 - 90 ° with a step size of 0.001°/s. The room temperature was maintained at 25 °C during the measurements.

The nitrogen adsorption–desorption isotherm of the sample was measured at liquid nitrogen temperature with a Quanta-chrome Nova-3200e. Pre-treatment of the sample was carried out at 230°C for 5 hours under a high vacuum. Qualitative mineral identification for the sample was done by Fourier Transform Infrared Spectroscopy (FTIR) using Thermo Scientific Nicolet 6700 series (iS10) FTIR Spectrophotometer over the range 4000 - 400 cm<sup>-1</sup> at room temperature, with an accuracy of 0.01 cm<sup>-1</sup> and resolution of ±4 cm<sup>-1</sup>.

### Experimental Setup for Pelletization Process

Pelletization experiments were carried out in a disc pelletizer having a diameter of 40 cm and a rim height of 15cm. The disc is driven by a 1hp engine through reduction gears and provided with a variable speed drive mechanism to regulate the disc speed. The disc is provided with a facility to change the disc inclination. Iron ore sample of 1kg each was mixed with binder at different proportions prior to the pelletization study. Moisture was added slowly and continuously. Pelletization time and disc inclination were fixed at 20 min and 42°, after preliminary studies. The quality of pellets was tested for size analysis (d<sub>50</sub>), % yield of +9mm pellets, mean drop number (MDN), green compressive strength (GCS), cold compressive strength (CCS) and Porosity.

## 3. RESULTS AND DISCUSSION

### XRF analysis of the raw bentonite

Chemical analysis of Raw bentonite (RBt), bentonite activated by HCL (BtHCl) and bentonite activated by H<sub>2</sub>SO<sub>4</sub> (BtH<sub>2</sub>SO<sub>4</sub>) bentonites and activated bentonites were measured by XRF analysis. Table 1 shows the details results of major and minor oxide concentrations by weight percentage (%).

Table 1 - Detailed elemental analysis of the raw as well as activated bentonite

Compound	Al <sub>2</sub> O <sub>3</sub> , %	SiO <sub>2</sub> , %	Fe <sub>2</sub> O <sub>3</sub> , %	SO <sub>3</sub> , %	K <sub>2</sub> O, %	CaO, %	NaO, %	Cr <sub>2</sub> O <sub>3</sub> , %	MnO, %	NiO, %	CuO, %	ZnO, %	Trace, %
RBt, %	19.3	55.9	19.78	0.13	0.27	1.63	2.35	0.03	0.096	0.006	0.0591	0.033	0.415
BtHCl, %	18.89	58.24	19.45	0.07	0.29	0.95	1.68	0.026	0.097	0.002	0.052	0.04	0.208
BtH <sub>2</sub> SO <sub>4</sub>	19.16	57.73	19.57	0.11	0.24	0.98	1.85	0.019	0.099	0.003	0.05	0.035	0.153



### SEM analysis of RBt, BtHCl and BtH<sub>2</sub>SO<sub>4</sub>

The SEM examination was carried out to assess the effect of the activation protocols on the surface morphology of the bentonites. It shows the aggregate mass of irregularly shaped particles that appeared to have been formed by several flaky particles stacked together in the form of agglomerates. The surface of the raw bentonite (Fig. 1(a-c)) appears to be smooth due to closely packed flakes in contrast to the ragged appearance of the acid activated bentonite (Fig. 1(a-c) for BtHCl and Fig. 1(a-c) for BtH<sub>2</sub>SO<sub>4</sub>).

Bentonite activation by H<sub>2</sub>SO<sub>4</sub> can make the bentonite more porous structured compared to raw bentonite (Fig. 1(a-c) BtH<sub>2</sub>SO<sub>4</sub>). The SEM image of the BtH<sub>2</sub>SO<sub>4</sub> indicates that the interlayer spaces may have collapsed, resulting in more tightly bound structure with reduction in porous structure. The surface morphology of the acid activated bentonite i.e., BtHCl, as shown in Fig. 1a–c BtHCl, indicates that the acid activation by HCl results in leaching of cations, making the clay surface more porous. After acid activation by HCl the uneven surface becomes highly porous, (Fig. 1a-c, BtHCl). Fig. 1a-c, BtHCl show that the surface morphology of the raw bentonite has undergone significant changes under the acid activation by HCl. The edges of the platelets were the first to be exposed to acid attack. The formation of smaller pores takes place as the impurities are removed and the exchangeable cations are replaced by H<sup>+</sup> ions. These physico-chemical reactions alter the morphology as the pores open. Thus, the bentonite surface became more porous and homogeneous. This was also evident from the increase in surface area. Comparing the SEM images for all three cases the result shows that acid activation by BtH<sub>2</sub>SO<sub>4</sub> forms more pores on bentonite surface than the acid activation by BtHCl. It is obvious that the dimension of the particles decreases markedly due to activation and cation exchange process. The increase in the porous nature of activated bentonite indicates that it can be more adsorptive in case of green pelletization, which leads to better strength and size of the pellet and porosity as well.

### BET surface area analysis of RBt, BtHCl and BtH<sub>2</sub>SO<sub>4</sub>

The BET surface areas of the samples are presented in Table 2. There is a good relationship between the BET surface area and average pore volume of the solid particles. Due to the formation of smaller pores in solid particles, surface area of particle increases which subsequently results in higher adsorption property. So, from the above study, it is understood that BtH<sub>2</sub>SO<sub>4</sub> because of its maximum surface area is the most effective binder among the three for green pelletization. XRD analysis of raw and activated bentonites is given in Fig. 2.

Table 2 - BET surface area and volumes of the micropores were clearly shown in the table.

Sample Name	Surface Area, m <sup>2</sup> /gm	Microporous volume, cm <sup>3</sup> /gm
RBt	93.233	0.011504
BtHCl	274.41	0.006574
BtH <sub>2</sub> SO <sub>4</sub>	322.81	0.003454

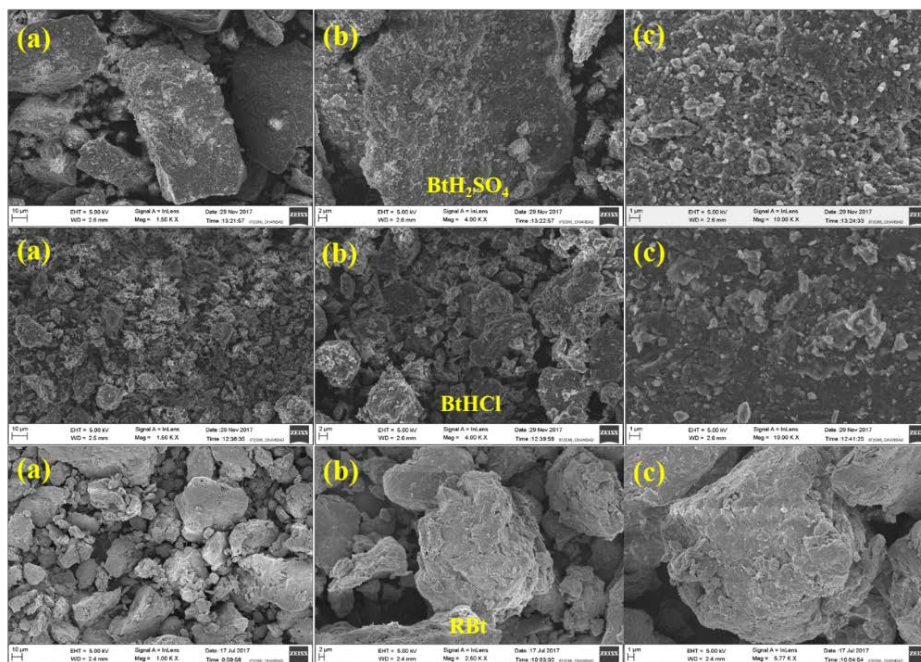


Figure 1 - SEM backscatter images of raw and activated bentonites

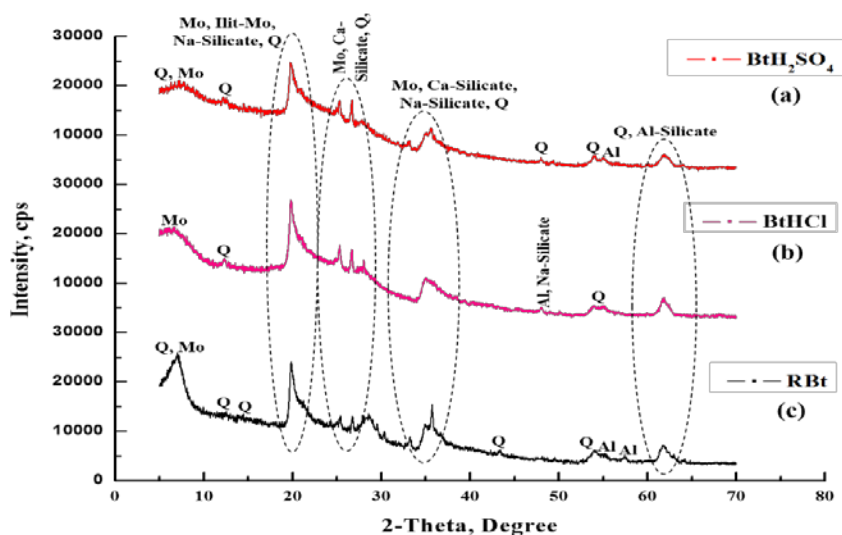


Figure 2 - XRD analysis of raw and activated bentonite

### FTIR analysis of RBt, BtHCl and Bt H<sub>2</sub>SO<sub>4</sub>

The effects of the acid-activation process on the FTIR spectra of the bentonite sample are shown in Fig. 3 a-c. The band at 3678-3359 $\text{cm}^{-1}$  (absorption by the interlayer water) becomes more diffused with increasing severity of activation. The OH stretching band occurs at 3678 $\text{cm}^{-1}$  which is shifted to 3620.84  $\text{cm}^{-1}$  for BtHCl and 3620.05  $\text{cm}^{-1}$  for BtH<sub>2</sub>SO<sub>4</sub>. OH, vibrational bending can be found at 2939 $\text{cm}^{-1}$  for RBt which is shifted to 2930.132 $\text{cm}^{-1}$  for BtHCl and 2929.795 $\text{cm}^{-1}$  for BtH<sub>2</sub>SO<sub>4</sub>. Similarly, OH vibrational bending was found at 2350 and 1761  $\text{cm}^{-1}$  for RBt, which is shifted to 2332.45 and 1733.95  $\text{cm}^{-1}$  during BtHCl activation and 2320.05 and 1731.949  $\text{cm}^{-1}$  during BtH<sub>2</sub>SO<sub>4</sub> activation. The intensity of the stretching bands of RBt at 991 $\text{cm}^{-1}$  was not affected by the acid activation. Si-O-Si stretching bands at 1203 $\text{cm}^{-1}$  for RBt shifted to 1291.595 and 1230.795  $\text{cm}^{-1}$  for BtHCl and BtH<sub>2</sub>SO<sub>4</sub>. Al-Mg-OH vibrations at 815 $\text{cm}^{-1}$  for RBt, 796.075  $\text{cm}^{-1}$  for BtHCl and 795.638  $\text{cm}^{-1}$  for BtH<sub>2</sub>SO<sub>4</sub> decrease with increasing intensity of activation. The intensity of the band at 740  $\text{cm}^{-1}$  increases significantly with increasing concentration of acid. The peak at 740  $\text{cm}^{-1}$  corresponds to the highest free SiO<sub>2</sub> content depending on decomposition by

acid adsorption. A more intensive band was found in the activated sample by H<sub>2</sub>SO<sub>4</sub> and HCl addition. Disintegration of the octahedral sheets by acid activation is shown in FTIR spectra in the 1100–450 cm<sup>-1</sup> region. The intensity of the band at 540 cm<sup>-1</sup> (Si-O-Al and Si-O-Mg coupled by OH bending or Si-O bending vibrations) is shifted to 561 cm<sup>-1</sup> for BtHCl and 556 cm<sup>-1</sup> for BtH<sub>2</sub>SO<sub>4</sub>.

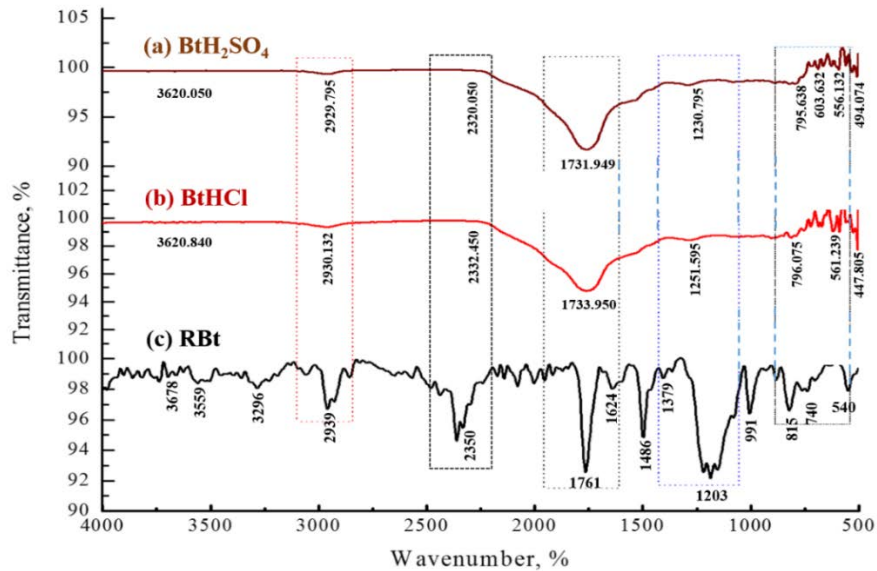


Figure 3 - IR Spectrum of raw and activated bentonite showing adsorption properties.

### Experimental Analysis and Properties of Pellets

Three binders, three moistures percentage and three discs speeds, total 45 experiments were carried out using 3 different binders (RBt, BtHCl and BtH<sub>2</sub>SO<sub>4</sub>). Green pellet testing was carried out to know the size and strength of the green pellet. The growth of pellet was represented by the mean pellet diameter (d<sub>50</sub>) and the proportion of product pellets (% yield of +9mm pellets). The weighted MDN (an average of the impact resistance capability of pellets) and green compression strength (resistance to compression load) were used to assess the strength of the product pellets. The individual influence on MDN of moisture > binder > rotation (Table 6) indicates the mobility of water through the interstitial space that may influence the size enlargement and a plastic surface resistance to impact. However, where solidity and stronger bridging is necessitated, the binder's ability to swell and move in presence of water and the extent of water immobilization bring about stronger bonding. The binder content and its relationship with the moisture content assumes significance. This is evidenced by the main and interactional effects of variables on MDN and GCS.

The main and interactional effect of variables on every response are given in Tables 6-8.

Table 3 - Represents the main and interactional effect of variables on responses for raw bentonite.

Response	Main effect	Interactional effect
d <sub>50</sub>	M>RBt>R	(M×R)>(R×RBt)>(M×RBt)
% Yield of +9 mm pellets	M>RBt>R	(M×R)>(M×RBt)>(R×RBt)
MDN	M>RBt>R	(M×RBt)>(M×R)>(R×RBt)
GCS	M>RBt>R	(M×RBt)>(M×R)>(R×RBt)
Where, M = Moisture content, R = Disc Speed and RBt = Raw bentonite		

Table 4 - Represents the main and interactional effect of variables on responses for BtHCl.

Response	Main effect	Interactional effect
d <sub>50</sub>	M>BtHCl>R	(M×BtHCl)>(M×R)>(BtHCl×R)
% Yield of +9 mm pellets	M>R>BtHCl	(M×BtHCl)>(M×R)>(BtHCl×R)
MDN	M>BtHCl>R	(M×BtHCl)>(BtHCl×R)>(M×R)
GCS	BtHCl>M>R	(M×BtHCl)>(BtHCl×R)>(M×R)
Where, M = Moisture content, R = Disc Speed and BtHCl=Activated Bentonite content		

Table 5 - Represents the main and interactional effect of variables on responses for Bt.H<sub>2</sub>SO<sub>4</sub>

Response	Main effect	Interactional effect
d <sub>50</sub>	M>BtH <sub>2</sub> SO <sub>4</sub> >R	(M×R)>(M×BtH <sub>2</sub> SO <sub>4</sub> )>(BtH <sub>2</sub> SO <sub>4</sub> ×R)
% Yield of +9 mm pellets	M>R>BtH <sub>2</sub> SO <sub>4</sub>	(M×BtH <sub>2</sub> SO <sub>4</sub> )>(M×R)>(BtH <sub>2</sub> SO <sub>4</sub> ×R)
MDN	M>BtH <sub>2</sub> SO <sub>4</sub> >R	(M×BtH <sub>2</sub> SO <sub>4</sub> )>(R×BtH <sub>2</sub> SO <sub>4</sub> )>(M×R)
GCS	M>BtH <sub>2</sub> SO <sub>4</sub> >R	(M×BtH <sub>2</sub> SO <sub>4</sub> )>(R×BtH <sub>2</sub> SO <sub>4</sub> )>(M×R)
Where, M = Moisture content, R = Disc Speed and Bt.H <sub>2</sub> SO <sub>4</sub> =Activated Bentonite content		

### Ion exchange phenomenon in bentonite

Bentonite can be categorized into two types i.e., Na type and Ca type. During water-bentonite interaction, ion exchange occurs in both cases. Na<sup>+</sup> ion is exchanged for both Na<sup>+</sup> and Ca<sup>2+</sup> ion in Na type bentonite. Besides this, its cross-linked polymeric network of hydrophilic monomers and swelling property help in adsorbing water molecules, which are responsible for establishing strong bond between these two components. Also due to the presence of exchangeable cation Na<sup>+</sup>, Na bentonite provides greater clay sheet layer extension and macroscopic swelling while encounters water [35, 36] but in case of Ca-bentonite, swelling clay properties is relatively low as compared to Na type bentonite due to presence of Ca<sup>2+</sup> cations in its interstitial space. As it is well known that Na forms stronger bond than Ca, Na activated Ca- bentonite is formed to achieve high swelling property. All Na-activated Ca bentonites are within close values range, expressing better swelling properties than the natural Ca bentonites [35] Recent research on surface phenomenon of pellets by Kawatra, Ripke and Railey suggested that the mineral surface charge causes a distinct concentration gradient of ions in the water, at proximity to the solid. In this situation, a large excess of positive ions ensues over surface negative ions. Multivalent ions are more strongly influenced due to this behaviour than monovalent ions, and consequently, the concentration factors are significantly higher for Ca<sup>+2</sup> and Mg<sup>+2</sup> than for K<sup>+</sup> and Na<sup>+</sup>, but when it comes to swelling factor Na<sup>+</sup> always having better swelling than Ca<sup>+2</sup> [26-36].

### Intra-water molecule behaviour/physical orientation of water molecule

Higher moisture content gives better GCS, MDN as well as size of the pellets. This can be explained through water molecules orientation where the V-shaped arrangement of water molecule has an atomic nucleus of the oxygen nucleolus with the two hydrogen protons at an angle of 105 degrees [37]. During the approach of two liquid water molecules towards each other, an electrostatic attraction takes place between the oxygen atom (of negative charge) which is present at the base of the 'v' of one water molecule with a hydrogen atom (of positive charge) at one corner or the other [37]. This force of attraction is called hydrogen bonding which is only 0.005-0.1times

of normal covalent bond strength. Most significant feature of this bond is that molecules can be easily oriented at certain circumstances. This physical alignment of the water molecules eases their ordered absorption onto the surface of the bentonite platelet [35, 36]. Fig. 4a-c represents the microstructure of green pellets for the binder RBt, BtHCl and BtH<sub>2</sub>SO<sub>4</sub> respectively. Fig. 4(a (4, 8 & 12)) represents the effect of acid activated bentonite by H<sub>2</sub>SO<sub>4</sub> on the microstructure of the green pellets. From Fig. 4a, it has been concluded that, bigger pellet has more plasticity than a smaller pellet. In other words, it can be proved plasticity of binder is quite important than other parameters, Here the plasticity of pellet expressed as a difference between the binder percentage variation fraction. At higher moisture bentonite gets sufficient water to swell and creates helical structure which results in close packing of particles. Contrariety in bentonite behaviour is clearly visible in Fig. 4(a<sub>8</sub>) Where moisture content is fixed, and bentonite dosage is varying. This variation in bentonite dosage is the primary factor behind the formation of multi-layered pellets. So, it is quite evident that 100% yield of +9mm pellets is achieved at both high moisture content and BtH<sub>2</sub>SO<sub>4</sub> dosage (0.75%), As layer upon the pellet increases, plasticity of bentonite expands due to which high MDN value is achieved but obtained GCS value is not as high as expected.

### **Water-bentonite interaction with BtHCl**

Fig. 4(b) establishes the effect of HCl activated bentonite on the pellet surface at high moisture content. From Fig. 4(b<sub>4</sub> & b<sub>8</sub>), it can be concluded that increased moisture content boosts the swelling property of binder with respect to moisture, which resulted in significant increase in +9mm pellet. But due to high moisture and low BtHCl dosages, porosity increases which reduces the GCS of pellet. So, to achieve pellets with desired strength, additional bentonite dosage is required. Fig. 4(b<sub>12</sub>) shows that high BtHCl dosage at high moisture content causes the formation of multiple layers on pellet surface. Though this layering enhances the GCS and MDN of pellet, an irregularity in pellet shape is observed after multiple drop numbers where round shaped pellet tends to bend and gradually changes to an elliptical shape. It can also be observed that at higher moisture content, variations in bentonite are not having effect on the green pellet MDN but influences the d<sub>50</sub> and wet compression strength as long as the rotation and moisture content are kept constant. Higher moisture content gives high swelling properties of the binder at higher dosage which could help to maximize the pellet strength but could possibly reduce the porosity of the pellet. The moisture content giving rise to plasticity formation during balling, which is specified as a material specific parameter and the major factor for creating plasticity and porosity depends on the variation in moisture and BtHCl contents.

Results in Fig. 4(c (7, 8 & 12)) show that moisture and RBt have negligible effect on pellet microstructure. Fig. 4(c<sub>7</sub>) shows porous structure associated with swollen bentonite, at higher moisture, closely packed with iron ore particles. Comparing Fig. 4(c<sub>7</sub> & c<sub>8</sub>), it is distinguished that although pellet size is acceptable in both the cases, the porosity is higher in case of low RBt dosage. At low RBt the exchange of Na<sup>+</sup> and Ca<sup>+</sup> ion is less due to low moisture and binder dosages. High porosity filling up of the interstitial spaces with water which subsequently causes weak bonding, hence pellet with moderate strength is obtained. Meanwhile in case of high bentonite dosage, pellets with good strength are produced due to less porosity and Na<sup>+</sup> ion exchange, high swelling and strong bonding between bentonite and water.

Fig. 4(c<sub>9</sub>) shows that the difference in bentonite content influences the GCS. It is clearly seen that at lower RBt content, compaction is less as compared to higher RBt dosage. This is because the isomorphous substitution of cations within the octahedral lattice results in the presence of excess electrons on the bentonite surface. These electrons enable the formation of hydrogen bonds of partially covalent character between the water molecules and the bentonite surface. The effect of excess electrons is therefore to not only strengthen the water-bentonite bonding but also to enhance the bonding of additional layers of water. It is believed that these strong bentonite-water bonds alter the electron distribution of the first layer of water molecules and facilitate the formation of another water layer. Those bonds in the next layer allow the formation of a subsequent layer to the



extent that 3 or 4 similarly oriented water layers are formed. Acceptable quality of pellets was obtained at an RBt dosage of more than 0.50% by weight of iron ore concentrate, maintaining the moisture content of 12%. This implies that the strength of green iron ore concentrate pellets is the most critical measure of binder quantity. There is a trade-off moisture: bentonite ratio for producing pellets of certain desired size and strength depending on the material characteristics (fineness, mineralogy, etc.).

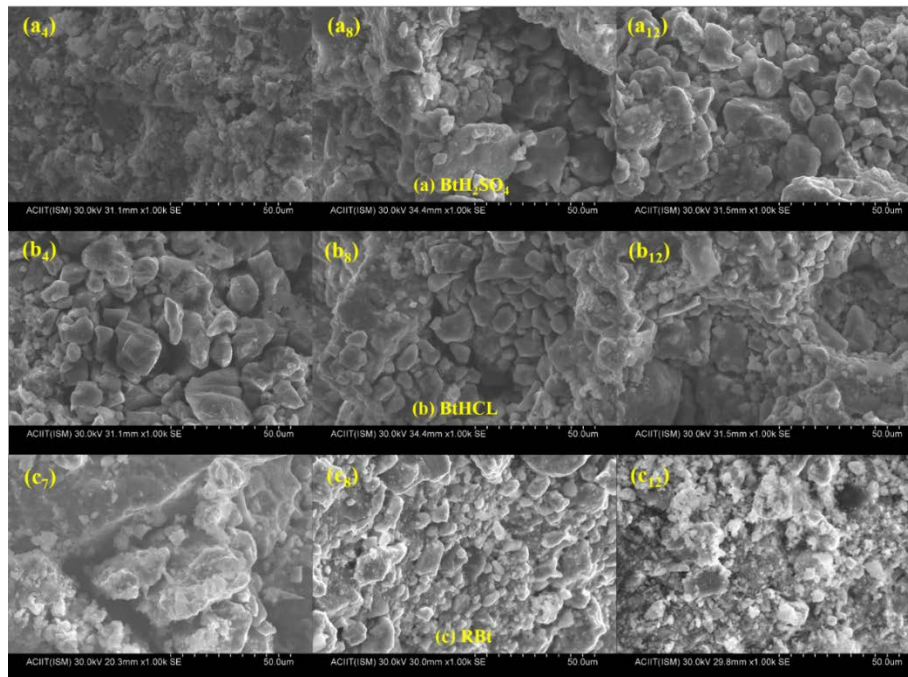


Figure 4 - The microstructure of dried pellets analyzed by SEM shows the water-bentonite interaction, properties of adsorption and morphology of the green pellets.

#### 4. CONCLUSIONS

The acid-activation of natural bentonite has led to new materials with properties different than those of raw bentonite. The dissolution of cations from the clay mineral layers and significant destruction of the clay mineral structure occurred at different acid/clay mineral ratios, accompanied by a decrease of the cation exchange capacity of the starting clay mineral. It can be concluded that the surface area of activated bentonite by  $H_2SO_4$  is 4 times higher than raw bentonite and 2 times higher than activated bentonite by BtHCl. A deeper in-sight into green pelletization is increasingly mandated due to significant variations in the feed to pelletizing. The geological setting influences the mineralogy of the ore, dictates the liberation and upgradation process (es) which results in the need to develop a well-defined and specific pelletization framework for each.

The individual and interactional effect of the materials characteristics, equipment parameters, operating conditions, monitoring & maintenance of key factors become imperative to sustain the production capacity and pellet quality & quantity. The paper outlines the significance of different operating parameters on the green pellet characteristics. The predominant role of bentonite interaction with the moisture content added in producing pellets of desired size and requisite strength is established. There is a specific moisture-bentonite ratio that needs to be identified for a particular ore material system and the methodology for such identification has been provided.

#### ACKNOWLEDGEMENTS

The authors are thankful to the Head of R&D, AMNS India for the facilities. The authors gratefully acknowledge Central lab AMNS India for the facilities like XRF, chemical analysis and TG/DTA.

## REFERENCES

- [1] C.H. Zhou, J. Keeling, *Appl. Clay Sci.* 74 (2013) 3.
- [2] V. Vimonses, B. Jin, C.W.K. Chow, C. Saint, *Appl. Clay Sci.* 43 (2009) 465.
- [3] M.N. Chong, B. Jin, C.W.K. Chow, C. Saint, *Water Res.* 44 (2010) 2997.
- [4] A. Özcan, B. Erdem, A. Özcan, *Colloids Surf., A: Physicochem Eng. Aspects* 266 (2006) 73.
- [5] G. Rytwo, Y. Gonen, *Colloid Polym. Sci.* 284 (2006) 817.
- [6] V. Vimonses, S. Lei, B. Jin, C.W.K. Chow, *Chem. Eng. J.* 148 (2009) 354.
- [7] G. Christidis, P. Scott, A. Dunham, *Appl. Clay Sci.* 12 (1997) 329.
- [8] Zoran Petrović, Pero Dugić, Vojislav Aleksić, Sabina Begić, Jasminka Sadadinović, Vladan Mičić, Nevena Kljajić, V-1 (2014) Page 133 of 139, doi: 10.7251/COMEN1401133P.
- [9] R. E. Grim, *Applied Clay Mineralogy*, McGraw-Hill Book Company, New York 1962.
- [10] F. R. Valenzuela Dias, P. S. Santos, *Quim. Nova*, Vol. 24 (2001) 345-353.
- [11] M. Önal, Y. Sarikaya, T. Alemdarogly, I. Bosdogan, *Turk J Chem*, Vol. 26 (2002) 409-416.
- [12] S. Brezovska, B. Marina, D. Burevski, B. Angusheva, V. Boseska and L. Stojanovska, *J. Serb. Chem Soc.*, Vol. 70-1 (2005) 33-40.
- [13] M. J. Žunić, A. D. Milutinović-Nikolić, N. P. Jović-Jovičić, P. T. Banković, Z. D. Mojović, D. Z. Manojlović, D. M. Jovanović, *Hem. Ind.*, Vol. 645-3 (2012) 193-199.
- [14] Z. Petrović, P. Dugić, V. Aleksić, Lj. Vasiljević, T. Botić, *Journal of Engineering & Processing management an international journal*, Vol. 1-1 (2009) 63-72.
- [15] Lj. Rožić, T. Novaković, S. Petrović, Z. Vuković, Ž. Čupić, *Chemical Industry & Chemical Engineering Quarterly (CI&CEQ)*, Vol. 4 (2008) 227-229.
- [16] S. Kaufhold, R. Dobrmann, M. Klinkerberg, S. Siegesmund and K. Ufer, *J. Colloid Interface Sci.*, Vol. 349 (2010) 275-282.
- [17] N. Yildiz, A. Calimli, *Turk J. Chem.*, Vol. 26 (2002) 393-401.
- [18] G. Josefciuk, G. Bowanko, *Clays and Clay*, Vol. 50-6 (2002) 771-783.
- [19] S. Sređić, T. Čajkovski, M. Davidović, V. Likar-Smiljanić, M. Marinović-Cincović, U. B. Mioč, Z. Nedić, R. Biljić, *Material Science Forum*, Vol. 453-454 (2004) 157-162.
- [20] Sivrikaya and Arol, 2014
- [21] Sivrikaya and Arol, 2012
- [22] Sivrikaya and Arol, 2010
- [23] Sastry et al., 2003
- [24] Kawatra and Ripke, 2003
- [25] Iveson, 2001a
- [26] Iveson, 2001b
- [27] Bhuiyan et al., 2011
- [28] Qui, 2003
- [29] Kurt Meyer, 1980
- [30] Estupinan et al., 2017
- [31] Eisele and Kawatra, 2003
- [32] Kawatra and Ripke, 2002
- [33] Kawatra and Ripke, 2001
- [34] Bergaya et al., 2001
- [35] Barast et al., 2016
- [36] Railey, 2001
- [37] Cetco, 2013

## **INVITED LECTURE**

# **PRODUCTION OF METAL-BASED POWDERS BY ATOMIZATION TECHNIQUES**

**Ridvan YAMANOGLU**

Kocaeli University, Umuttepe Campus, Engineering Faculty, Metallurgical and Materials Engineering Department, 41001, Kocaeli, Turkiye

### **Abstract**

*Today, with the introduction of additive manufacturing into our lives, the importance of powder metallurgy has increased. The properties of the products produced by powder metallurgical processes directly depend on the used raw material. Powder metallurgy needs different raw materials as particles for various production processes. While water and gas atomization methods are generally preferred for conventional powder metallurgical production technologies, different gas or plasma atomization techniques are preferred for additive manufacturing. Each atomization technique offers different powder properties. In this study, different atomization techniques such as water, gas, plasma, PREP and ultrasonic atomization were examined, and the characterization of the powders was presented. Titanium, nickel, copper, silver and aluminium-based powders produced within the scope of this study were also selected for characterization. These materials were examined by revealing the information in the literature. The effects of atomization techniques on the particle shape, size, size distribution and purity were studied. It has been concluded that gas atomization techniques have the ideal cost and quality combination method, especially for additive manufacturing methods.*

**Keywords:** Powder Metallurgy, Atomization, Additive Manufacturing, Metal Powders

### **1. INTRODUCTION**

Human beings have had to produce to meet their needs. Therefore, production techniques have always been vital. The production techniques emerge and develop according to the technology of the time. Due to people's opportunities in ancient times, the first production technology was powder metallurgy (PM) [1]. Minerals and fine particles from nature are shaped with water and then fired [2]. In the following period, the casting method developed. Until today, casting techniques have always been at the forefront regarding their economy, experience and applicability [3]. However, especially in the last 20 years, the perception has changed in terms of material production technologies. Additive manufacturing technologies have left their mark on today. The production of parts that cannot be produced with traditional powder metallurgy and casting techniques becomes possible with additive manufacturing [4]. Powder is primarily at the origin of additive manufacturing of metals. Therefore, it can be said that the age of powder metallurgy is coming again as a production technology [5]. For powder metallurgy and additive manufacturing, the most critical point, as well as the processes, is the used raw material. Different powder raw materials are required depending on the type of production process. Sometimes, expensive and sometimes cheap powders meet expectations. One of the biggest obstacles to the development and preference of additive manufacturing is the difficulties in accessing raw materials [6-8]. This study was put forward to examine the powders produced by atomization techniques. Techniques that will meet the needs of different powder metallurgical processes have been examined, and powders



have been characterized. Details about the powder requirements of different powder metallurgical processes are shared below.

Traditional powder metallurgical processes use relatively coarse powder. The powders are first mixed with a binder and then cold-shaped. The compact with raw density is then sintered. Lower-cost powders are usually used since so many parts will be produced simultaneously [9-10].

### **1.1 Powder Injection Molding**

Powder injection molding (PIM) is a technology that uses the finest powder in powder metallurgy (for industrial metallic parts). Much finer powders are used as smaller and more complex shaped parts are produced than other traditional powder metallurgical processes [11-12]. Since the powder sizes are quite fine, it is necessary to use a high amount of binder to transport the powders into the mold [13]. A large amount of binder must be removed from the structure after shaping and before or during sintering. For this reason, a structure with a high amount of porosities emerges. Therefore, much more energy is required in sintering. This energy is provided by the fine sizes of the particles [14].

### **1.2 Additive Manufacturing**

Additive manufacturing has made a name for itself, especially in the last 20 years. It is a method based on the principle of modelling very complex shaped parts in a computer environment and then building the part layer by layer with the data transferred to the printer [15]. In this method, raw materials in powder form are generally used. Since the powders must be laid in a thin layer, very fine powders are not preferred as in powder injection molding. The powders preferred in these methods are in the range of 15-63 microns [16-17]. These sizes may vary in different additive manufacturing techniques. The powders must have good flow properties when it comes to powder laying in the additive manufacturing method [18]. The powders are expected to be spherical and their surfaces to be smooth. Therefore, the production conditions require specific powder characters in the powder metallurgical methods. [19]. This characteristic feature is directly related to the production method of the powder. Generally, powders for powder metallurgy are produced by atomization techniques [20]. The following sections discuss the properties of powders obtained with different atomization techniques.

### **1.3 Raw Material for Powder Metallurgy**

In powder metallurgy, metal powders are generally characterized by four properties: particle size, particle shape, particle size distribution and purity [21]. There are many different powder shapes. The powder form can be grouped under two headings: spherical shape and irregular shape. The expression irregular shape is very broad. It is grouped under the name of an unlimited group of irregular shapes with flaky, prismatic, round and similar shapes [22]. The targeted powder shape is mainly spherical. Spherical-shaped powders move faster. Flow characteristics are good. A spherical shape is especially desired for additive manufacturing and powder injection molding methods [23]. In traditional PM, where pressing is required, powders with complex shapes may provide an advantage in packing density. Fine powders generally offer a significant advantage in terms of particle size. Fine powders have higher energies. Therefore, they offer higher density within the same temperature and time parameters during sintering. However, the thin size can sometimes be a disadvantage. The increased surface energy of fine powders causes agglomerations and negatively affects flow properties. Therefore, powders in the range of 15-63 microns, which is an optimum size range for additive manufacturing methods involving the laying process, are preferred [24-26]. Size distribution is also an essential concept. It is challenging to meet this criterion in terms of powder production methods. Generally, powders of the desired composition are blended. Purity is as effective as other properties [27]. The purity of powders directly affects production processes. The impurity of powders is characterized on their surface. It wasn't easy to

sinter powders with oxidized surfaces [28]. Although the mechanical density is high, the metallurgical density is low. In addition, the mobility of powders with oxidized surfaces is limited. Flow properties are not good. For this reason, high-purity powders are preferred. Different atomization techniques provide various powder properties. Therefore, the atomization technique chosen according to the method is critical. Below, the powder properties produced by different atomization techniques are investigated [29,30].

#### 1.4 Atomization Techniques

It is possible to produce powders with three different alternative routes in powder metallurgy. Chemical, mechanical and atomization techniques. Metals and ceramics with high melting points are produced by chemical techniques. High-purity powder is obtained by chemical techniques. Powders produced by chemical methods are generally in dendritic and spongy form due to a chemical reaction. Sizes can be fine or coarse [21,31]. Powder of high-hardness materials can also be combined with mechanical methods. By taking advantage of the brittleness properties of the material, its dimensions are reduced by mechanical forces. Mechanical methods are largely based on further refining the size of an already coarse powder. Sometimes, mechanical powder production methods are preferred to make alloys or compounds of different powders with mechanical effects. Powders obtained by mechanical methods generally present sharp-cornered shapes caused by mechanical size reduction. For this reason, the shapes of powders produced by mechanical and chemical processes are usually described as irregular [32]. Apart from these two techniques, atomization techniques are more preferred in powder metallurgy. In atomization, which is the disintegration of molten metal by different factors, the liquid metal tries to solidify by becoming spherical after being fragmented. However, the spherical shape can sometimes not be achieved due to different disintegrating environments. Again, the size and purity of the powders vary due to various disintegrating media. Below, different atomization techniques and the resulting powders are characterized and examined [33].

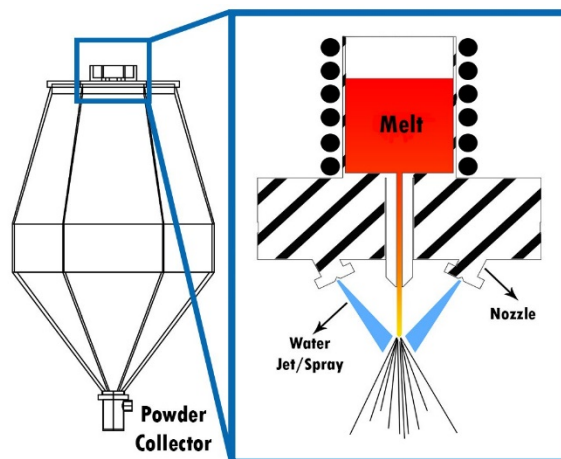


Figure 1 - Schematic representation of water atomization

#### 1.5 Water Atomization

Among atomization techniques, water atomization gives the lowest quality in terms of powder properties. Generally, water-atomized powders are used for traditional powder metallurgical processes for cost reasons. Since the powders are shaped with high pressure by a press, there is no need for the spherical shape required for other methods [34,35]. The schematic representation of water atomization is shown in Figure 1.

SEM images of pure iron powders produced by water atomization are given in Figure 2. As can be seen from the figure, the powders are relatively coarse in size and irregular in shape. Such water-atomized powders also have low purity. They are not suitable for critical applications in

production processes. Since additive manufacturing techniques are preferred for more critical applications, water-atomised powders are not recommended. In addition, the most crucial feature of water-atomized powders is their irregular shapes. The flow properties of the powders are relatively poor. These poor flow properties also make them unsuitable for additive manufacturing [36]. In PIM technology, water-atomized powders remain coarse. For this reason, just like additive manufacturing, water-atomized powders are not preferred in PIM technology.

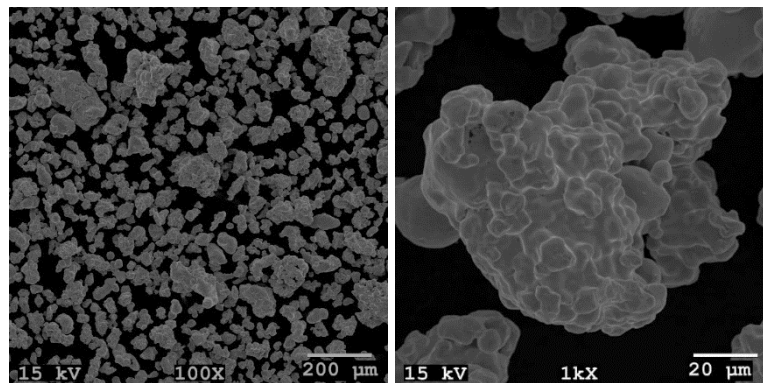


Figure 2 - Pure iron powder produced by water atomization

## 1.6 Gas Atomization

Gas atomization is the most preferred technology in the market for the breakdown of a melt. Unlike water atomization, powders are clean due to the use of different gases in the disintegration of liquid metal [37]. In addition, while the interaction with water causes rapid solidification in water atomization, gas atomization has relatively slower cooling rates. For this reason, the shapes of gas-atomized powders are quite close to spherical [38]. In gas atomization, the molten metal flows through a nozzle and is fragmented by different types of gases (Figure 3). Air, argon, nitrogen and helium are commonly used gases. The relationship between the liquid metal and the nozzle transmitting the gas directly affects the properties of the powders in gas atomization. There are many different nozzle types in the literature. Therefore, the powders on the market produced by gas atomization may sometimes be completely different from each other.

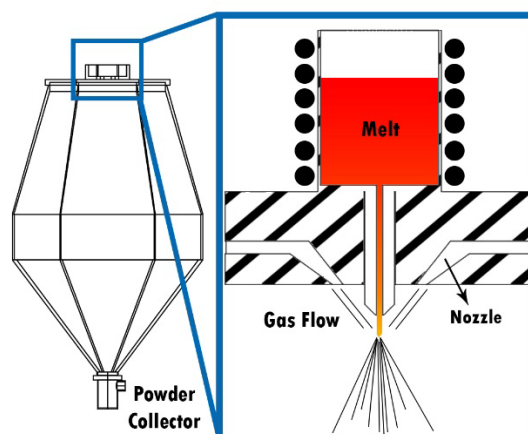


Figure 3 - Schematic representation of gas atomization

Figure 4 shows different powders produced by gas atomization. As mentioned above, different gas atomization parameters create powders with very different characteristics. Figure 4a shows CuCrZr alloy powder, widely used in additive manufacturing. Powders are far from spherical and have a rounded and elongated shape. Although these powders are produced by gas atomization, such powders are not suitable for additive manufacturing. AlSi10Mg powder, also frequently used in the additive manufacturing industry, is shown in Figure 4b. This powder was also produced by

gas atomization. Even though the powder is predominantly spherical, much satellite formation is observed. Due to the nature of gas atomization, such satellite formations can be seen. Such formations, which have a negative impact on the spherical shape, negatively affect the mobility of powder. Therefore, it is not preferred in many applications. In Figure 4c, pure copper powder is given. Copper powder has also been produced by gas atomization. As can be seen, the powder is mainly spherical, and no satellite formation is observed.

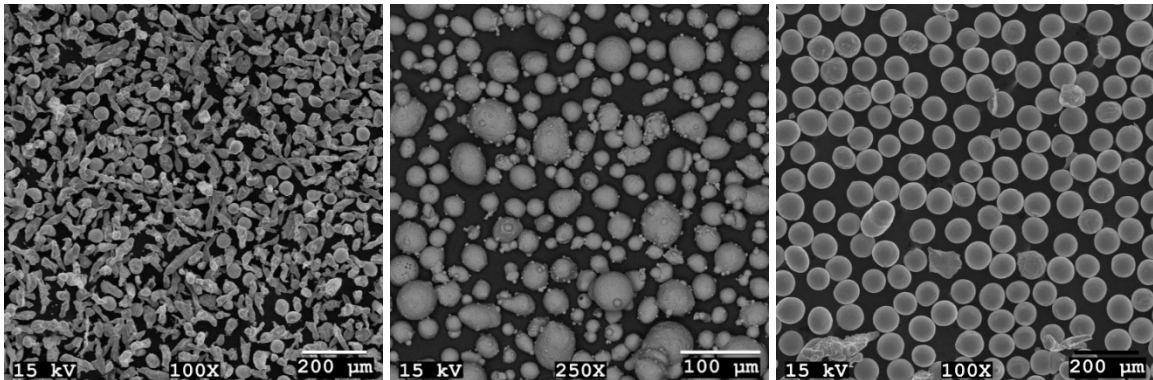


Figure 4 - Different powders produced by gas atomization. A) CuCrZr, b) AlSi10Mg, c) Pure Cu

### 1.7 Plasma Atomization

Plasma atomization is one of the most modern atomization techniques developed in recent years. It is based on melting and simultaneously disintegrating the material with high-power plasma torches (Figure 5). A furnace is not required for melting as in water and gas atomization. There is also no tundish or crucible for liquid metal [39]. For this reason, higher purity powder is obtained compared to water and gas atomization. Again, since there is no mechanical contact like water and gas, the sphericity of the powders obtained by plasma atomization is higher. However, many materials are not formed into wire form. This is a disadvantage.

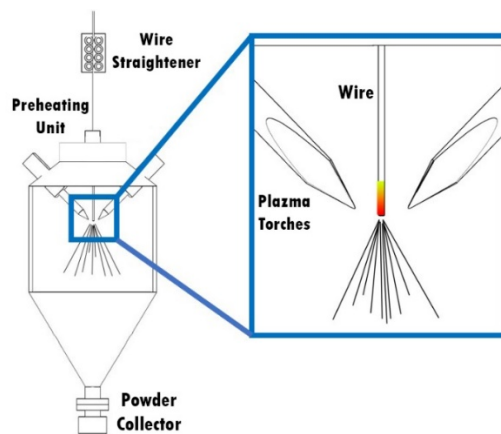


Figure 5 - Schematic representation of plasma atomization

In plasma atomization, the wire is melted by the plasma and solidifies by becoming spherical within the system under the effect of its own surface tension. More spherical powders are obtained than gas atomization. Figure 6 shows the Ti-6Al-4V alloy powder produced by plasma atomization [40]. As can be seen, the powder has a spherical character. The system includes fine and coarse particles in terms of size distribution. Satellite formations are observed, albeit in small amounts, due to solidification and spherization distances.

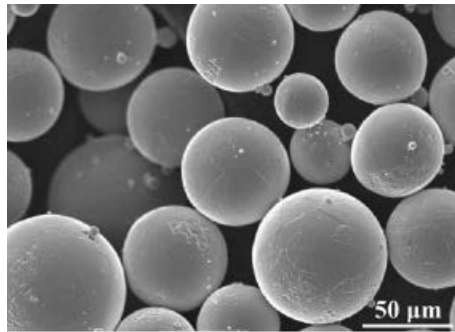


Figure 6 - Ti6Al4V powder produced by plasma atomization [40]

### 1.8 PREP Atomization

PREP (Plasma Rotating Electrode Process) is the technique that provides the most spherical powder among atomization techniques. It is based on the principle of melting the rod-shaped raw material from its face surface with a plasma. While the horizontally positioned rod rotates rapidly, the molten liquid from the face surface is scattered in the chamber by centrifugal force. Liquid droplets become spherical and solidify. The rotation speed of the rod is the most crucial parameter of the PREP method. As the speed increases, the size of the particles obtained becomes smaller. The viscosity of the metal is also important. Atomization of viscous metals is a disadvantage in this method. Viscous metals are difficult to break down. The PREP method is mainly used to produce powders of reactive metals. Titanium and aluminum are produced in large quantities by this method. The PREP chamber is first evacuated and then filled with argon or helium. The resulting powders have very high sphericity and relatively high purity. The satellite problem seen in other methods is not seen in PREP. Due to the low production amount, the PREP method is preferred for producing high-value-added materials and reactive material powders [41].

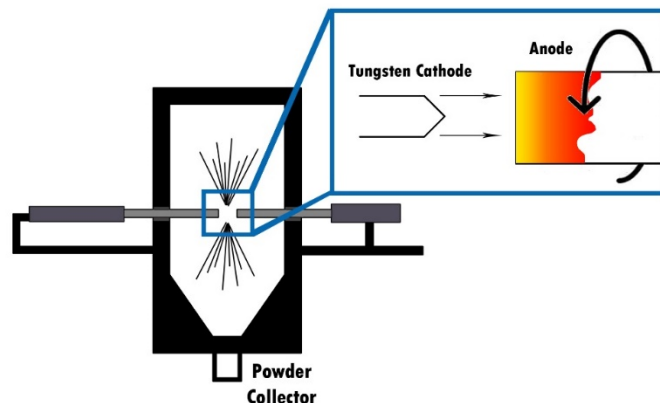


Figure 7 - Schematic representation of PREP atomization

Figure 8 shows the Ti6Al4V alloy powder produced by PREP atomization. In the PREP method, powders are mainly spherical. Since the powders are produced in a vacuum environment, they are very clean. Traces of solidification can be clearly seen on the surfaces of the powders. Figure 8 shows the grain boundaries of Ti alloy powders. It is also possible to see amorphous powders in titanium alloys due to rapid cooling with decreasing particle size. The viscosity of the material is also effective in forming an amorphous structure. Due to its relatively high viscosity, titanium has more amorphous solidification characteristics than other materials.



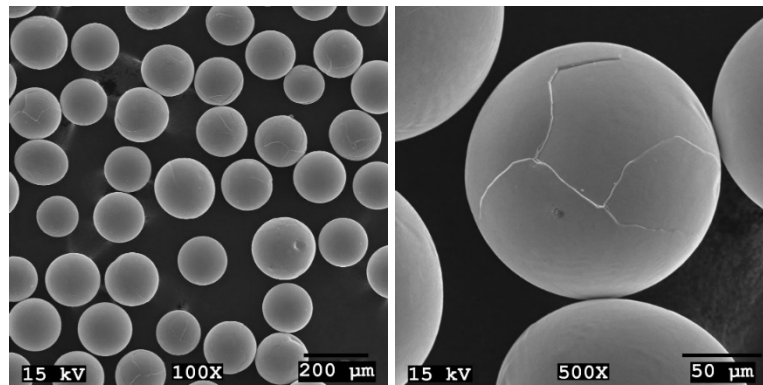


Figure 8 - Ti6Al4V alloy powder produced by PREP atomization

### 1.9 Ultrasonic Atomization

New atomization techniques began to develop, especially with the development of additive manufacturing. In fact, while ultrasonic atomization was available before, it has entered the market in a more advanced form in recent years. A schematic drawing of the ultrasonic atomization is given in Figure 9. In the process, the material is generally melted with the help of an arc and the molten metal is scattered and solidified by ultrasonic vibration at a specific frequency. Varying frequency ranges result in different sizes of powder [42].

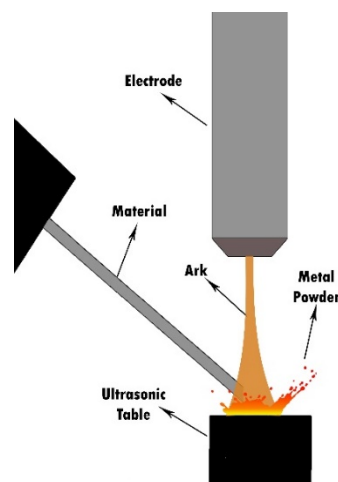


Figure 9 - Schematic representation of ultrasonic atomization

In ultrasonic atomization, the raw material can be in the form of wire or rod. The molten material is flowed onto an ultrasonic table. The ultrasonic frequency in the table causes the vibration to spread to the molten metal in the form of droplets, depending on its surface tension and viscosity. There is an inverse relationship between the frequency size in the ultrasonic stage and the powder size. The particles produced due to a frequency-dependent production have a predominantly narrow size distribution [43]. Figure 10 shows the SEM image of powders produced by ultrasonic atomization of a non alloyed steel. The shape of the powder is quite spherical. Another point that draws attention from the image is that the particle sizes are close to each other. If you pay attention, satellite formation is not observed in powder [44].

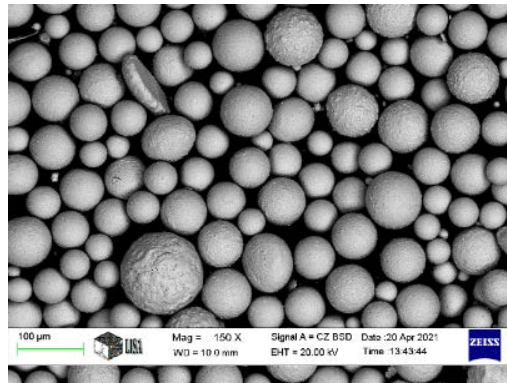


Figure 10 - Non-alloyed steel powder produced by ultrasonic atomization [44]

## 2. CONCLUSION

Different quality powders are needed for powder metallurgical applications. Powder consists of a mass of particles. Therefore, the particle's individual properties determine the powder's general properties. Each atomization method causes different powder formations. Traditionally, water atomization is preferred in powder metallurgy when cost is a priority due to mass production. The shapes of water-atomized powders are irregular. Their purity is low. The economic value of the powder is low. High density is generally not expected from parts produced with water-atomized powders. For example, many automotive parts are made from water-atomized steel powder and full density is not expected in these parts. When purity and sphericity are demanded, gas atomization comes to mind first in the market. Gas atomization offers cleaner powder due to using gas instead of water. Again, particle shapes close to spherical are obtained compared to water atomization due to the slower cooling of liquid metal. But gas atomization also has some disadvantages. The cost increases further as the liquid metal breaks apart with gas. It is also essential to evacuate the gas from the system. Satellite formations are seen in the powder produced by many gas atomizations. These satellite formations affect the final properties of the powder. PREP is another technique among traditional atomization techniques, such as water and gas atomization. PREP is a very old technique. The purity of the powders obtained with PREP, which offers crucible-free production in a closed system, is very high. In addition, the sphericity of the powders is perfect, thanks to the disintegration without using water or gas because the particles are fragmented and sphericalized by centrifugal force in a chamber of calculated size. However, low production volumes are possible in this method since the raw material size is limited. In other words, it is a low-efficiency method. For this reason, it is preferred for powders of more value-added products. The plasma atomization technique developed recently, has also begun to be widely used. The material to be pulverized must be in wire form. This is a barrier to the production of different materials. The powders produced are spherical, as in PREP atomization. However, satellite formations can be seen as in gas atomization. Ultrasound atomization has become noteworthy in recent years. As a result of production at a particular frequency, a powder with a narrow size distribution is obtained. Due to the system's design, this atomization can be preferred for low-volume production.

## REFERENCES

- [1] Upadhyaya. G. S., Powder metallurgy technology, Science Publishing, Cambridge, 1997, p.1-25.
- [2] Shanefield. D. J., Organic additives and ceramic processing: with applications in powder metallurgy, Springer Science & Business Media, New York, 2013, p.95-100.
- [3] Abdul Wadood., Titanium and Titanium Alloys, Higher Education Commission, (2018) 1-50.

- [4] Gökhan. Ö., Eklemeli Üretim Teknolojileri Üzerine Bir Derleme, Niğde Ömer Halisdemir Üniversitesi Mühendislik Bilimleri Dergisi, 9 (1) (2020) 606-621.
- [5] Wong. K. V, Hernandez, A., A Review of Additive Manufacturing, International scholarly research notices, (2012).
- [6] Popovich. A, Sufiiarov, V., Metal powder additive manufacturing, In New trends in 3D printing, IntechOpen, Rijeka, 2016, p.30-135.
- [7] Im. T, Gurung. K, Meyers. S, Cutolo. A, Oh. H, Lee. J. S, Lee. C. S., J. Mater. Process. Technol., 308 (2022) 1-9.
- [8] Kunovjanek. M, Reiner, G., Int. J. Prod. Res., 58(5) (2020) 1540-1554.
- [9] Novák, P, Moravec. H, Salvetr. P, Průša. F, Drahekoupil. J, Kopeček. J, Kubatík. T. F., Mater. Sci. Technol., 31(15) (2015) 1886-1893.
- [10] Monteiro. W. A, Carrió. J. A. G, Da Silveira. C. R, Vitor. E, Buso. S. J., MSF, 660 (2010) 41-45.
- [11] Heaney. D. F., Powders for metal injection molding (MIM), Elsevier, Amsterdam, 2019, 45-56.
- [12] Wen. G, Cao. P, Gabbitas. B, Zhang. D, Edmonds. N., Metall. Mater. Trans. A, 44 (2013) 1530-1547.
- [13] Enneti. R. K, Onbattuvelli. V. P, Gulsoy. O, Kate. K. H, Atre. S. V., Powder-binder formulation and compound manufacture in metal injection molding (MIM), Amsterdam, 2019, p.57-88.
- [14] Horn. T. J, Harrysson, O. L, Sci. Prog., 95(3) (2012) 255-282.
- [15] Chuang. A, Baris. J, Ott. C, McCue. I, Erlebacher. J. Acta Mater., 238 (2022).
- [16] Krzysztow. G, Marcin. B, Janusz. K, Ireneusz. S, Lucjan. S, Janusz. J, Jakub. L, Łukasz. S, Marcin. W, Zenon. K., Materials, 15(14) (2022) 4938.
- [17] Markusson. L., Powder characterization for additive manufacturing processes, Degree Project, Lulea, 2017, 1-120
- [18] Slotwinsk. J. A, Garboczi. E. J, Stutzman. P. E, Ferraris. C. F, Watson. S. S, Peltz. M. A., J. Res. Natl. Inst. Stand. Technol., 119 (2014) 460.
- [19] Chen. G, Zhao. S. Y, Tan. P, Wang. J, Xiang. C. S, Tang. H. P., Powder Technol., 333 (2018) 38-46.
- [20] Popov. V. V, Grilli. M. L, Koptyug. A, Jaworska. L, Katz-Demyanetz. A, Klobčar. D, Goel. S. Materials, 14(4) (2021) 909.
- [21] Angelo. P. C, Subramanian. R, Ravisankar. B., Powder metallurgy: science, technology and applications, PHI Learning Pvt. Ltd, Delhi, 2022, 1-30.
- [22] Shenoy. P, Viau. M, Tammel. K, Innings. F, Fitzpatrick. J, Ahrné. L, Powder Technol., 272 (2015) 165-172.
- [23] Sun. P, Fang. Z. Z, Xia. Y, Zhang. Y, Zhou. C., Powder Technol., 301 (2016) 331-335.
- [24] Atkinson. H. V, Davies. S., Metal. Mater. Trans. A, 31 (2000) 2981-3000.
- [25] Lei. H. Y, Li. J. R, Wang. Q. H, Xu. Z. J, Zhou. W, Yu. C. L, Zheng. T. Q., Int. J. Hydrog., 44(45) (2019) 24782-24791.



- [26] Penny. R. W, Praegla. P. M, Ochsenius. M, Oropeza. D, Weissbach., R, Meier. C, Hart. A. J., *Addit. Manuf.*, 46 (2021) 102197.
- [27] Hlosta. J, Žurovec. D, Jezerská. L, Zegzulka. J, Nečas. J., Effect of particle shape and size on the compressibility and bulk properties of powders in powder metallurgy, *Metall. Mater. Conf*, May 25-27, Brno, Czech Republic, p.1394-1399.
- [28] Mostafaei. A, Ghiaasiaan. R, Ho. I. T, Strayer. S, Chang. K. C, Shamsaei. N, To. A. C., *Prog. Mater. Sci.*, (2023) 101-108.
- [29] Newkirk. J. W, Kohser. R. A., *Designing with powder metallurgy alloys*, Handbook of Mechanical Alloy Design, CRC Press, Florida 2003, p.641-650.
- [30] Yamanoglu. R, Bahador. A, Kondoh. K., *J. Mater. Eng. Perform.*, 30 (2021) 3203- 3212.
- [31] German. R. M., *Powder metallurgy and particulate materials processing: the processes, materials, products, properties and applications*, Metal powder industries federation, New Jersey, 2005, p.150-175.
- [32] Lagutkin. S, Achelis. L, Sheikhaliev. S, Uhlenwinkel. V, Srivastava. V., Atomization process for metal powder, *Mater. Sci. Eng.: A*, 383(1) (2004) 1-6.
- [33] Mandal. S, Sadeghianjahromi. A, Wang. C. C., *Adv. Powder Technol.*, 33(11) (2022) 103809.
- [34] Fedina. T, Sundqvist. J, Powell. J, Kaplan. A. F., *Addit. Manuf.*, 36 (2020) 101675.
- [35] Yenwiset. S, Yenwiset, T. J. *Met. Mater. Miner.*, 21(1) (2011).
- [36] Hoeges. S, Zwiren. A, Schade. C., *Met. Powder Rep.*, 72(2) (2017) 111-117.
- [37] Ouyang. H. W., Xin. C., Huang. B. Y., *Trans. Nonferrous Met. Soc.*, 17(5) (2007) 967-973.
- [38] Zheng. B, Lavernia. E. J., *Melt atomization*, Handbook of Atomization and Sprays: Theory and Applications, (2011) 837-848.
- [39] Kassym. K, Perveen. A., *Mater. Today: Proc.*, 26 (2020) 1727-1733.
- [40] Chen. G, Zhao. S.Y, Tan. P, Wang. J, Xiang. C.S., Tang. H.P., *Powder Technol.*, 333 (2018) 38-46.
- [41] Yamanoglu. R, German. R.M., Karagoz. S, Bradbury. W.L, Zeren. M, Li. W, Olevsky. E.A., *Powder Metall.*, 54 (2011) 604-607.
- [42] Źrodowski. L, Wróblewski. R, Choma. T, Morończyk. B, Ostrowski. M, Leonowicz. M, Łacisz. W, Błyskun. P, Wróbel. J.S, Cieślak. G, Wysocki. B., *Materials*, 14(10) (2021) 2541.
- [43] Akyildiz. Y, Sari. S, Kaya. O.F., Yamanoglu. R, *Manuf. Technol.*, 4(2) (2023) 81-91.
- [44] Halapi. D, Varga. L., *Int. J. Manag. Sci.*, 8(2) (2023) 69-75.

**INVITED LECTURE**

**COMPUTATIONAL DESIGN OF ENGINEERING MATERIALS: CASE STUDIES FOR A CEMENTED CARBIDE AND A HEAT RESISTANT ALLOY**

**Yong Du<sup>1</sup>, Rainer Schmid-Fetzer<sup>2</sup>, Jincheng Wang<sup>3</sup>, Shuhong Liu<sup>1</sup>, Jianchuan Wang<sup>1</sup>,  
Qiang Lu<sup>1</sup>, Yuhui Zhang<sup>4</sup>, and Kai Li<sup>1</sup>**

<sup>1</sup> State Key Laboratory of Powder Metallurgy, Central South University, Changsha, Hunan 410083, China

<sup>2</sup> Institute of Metallurgy, Clausthal University of Technology, Robert-Koch-Str.42, D-38678 Clausthal-Zellerfeld, Germany

<sup>3</sup> State Key Laboratory of Solidification Processing, Northwestern Polytechnical University, Xi'an, Shanxi 710072, China

<sup>4</sup> Key Laboratory of Functional Materials and Applications of Fujian Province, Xiamen University of Technology, Xiamen 361024, PR China

**Abstract**

*A brief overview of state-of-the-art in the field of computational design of materials is given. It comprises multi-scale computational methods such as CALPHAD, atomistic simulations, phase-field and cellular automaton, and crystal plasticity finite element analysis. In the second part of this presentation, case studies for design of a gradient cemented carbide [1] and a heat resistant high-strength Al alloy [2] are presented. They are considered from the point of view of a step-by-step application of the basic methods. It is suggested that disseminating [2] this approach among professionals and students will enhance accelerated design of materials and their processing.*

**REFERENCES**

- [1] Yong Du, R. Schmid-Fetzer, Jincheng Wang, Shuhong Liu, Jianchuan Wang, and Zhanpeng Jin, Computational Design of Engineering Materials: Fundamentals and Case Studies, Cambridge University Press, 2023.
- [2] Qiang Lu, Jianchuan Wang, Hongcheng Li, Shenbao Jin, Gang Sha, Jiangbo Lu, Li Wang, Bo Jin, Xinyue Lan, Liya Li, Kai Li, and Yong Du, Nat. Commun., 14(1) (2023) 2959-2971.



# PAPERS



## Cr(VI) PHOTOSORPTION ON COMPOSITE SORBENT OF MONTMORILLONITE WITH AMORPHOUS TiO<sub>2</sub>

Denis Ordinartsev, Nadezhda Pechischeva, Svetlana Estemirova, Andrey Rempel

Institute of Metallurgy, Ural Branch, Russian Academy of Sciences, 620016, Yekaterinburg, Russia

### Abstract

*Titanium dioxide, in addition to its sorption properties, is well known as a photocatalyst, used in particular for the reduction of Cr(VI) and its conversion to less toxic Cr(III) under the influence of ultraviolet light. This work is devoted to study the effect of illumination on the sorption characteristics of a composite sorbent - montmorillonite intercalated with amorphous titanium dioxide and to compare the new sorbent with well-known TiO<sub>2</sub> nanopowder.*

**Keywords:** chromium(VI), photosorption, montmorillonite, titanium dioxide, composite sorbent

### 1. INTRODUCTION

Titanium dioxide, in addition to its sorption properties, is well known as a photocatalyst, used in particular for the reduction of Cr(VI) and its conversion to less toxic Cr(III). Not so long ago it was noticed that the conversion process of Cr(VI) to Cr(III) can be accelerated under the influence of ultraviolet light [1,2,3]. The efficiency of titanium dioxide under UV illumination increases considerably, however for photosorption application in real conditions the values of specific capacity per specific surface area or mass of material are considerably inferior to the currently existing sorbents for chromium extraction [4,5]. Besides, photosorption is an irreversible process and this means that saturated sorbent has to be utilised after all its capacity is exhausted. Despite the availability of titanium dioxide it is not economically expedient to use it in pure form for single-use adsorption of ecotoxicants, the more so that there are sorbents and reagents that allow to achieve the same effect and cost much less. Thus, there is a need to create a composite sorbent in which titanium dioxide will perform a function of active sorption centres, and a substrate will be a carrier of these centres and a storehouse of adsorbed ions. Options for synthesis of MM sorbents with titanium dioxide [6] are already known and their properties are studied [7]. However, their photosorption activity towards to chromium(VI) compounds is poorly studied and the joint contributions to photosorption and conventional sorption are not separated.

### 2. EXPERIMENTAL

#### 2.1 Synthesis of MM:CS:TiO<sub>2</sub>

The reagents used were montmorillonite grade BP-183-FJ 98% basic substance, titanium butoxide (Ti(BuO)<sub>4</sub>), distilled water, dodecyldimethyl benzylammonium chloride (CPAV) 50% CAS 8001-54-5. 20 g of BP@-183-FJ montmorillonite (MM) was added to 200 ml distilled water, stirred for 60 minutes at 1200 rpm. 4 g of 50% dodecyl dimethyl benzylammonium chloride (CS) solution was added. Stirring was carried out for 30 minutes (1200 rpm) to form a monomolecular layer of CS. The inner surface of the MM acquired a neutral charge and the ability to swell in non-polar liquids and draw non-polar liquids into the interlayer space due to hydrophobic interaction. The solution and precipitate were then separated on a vacuum filter. The CS monomolecular layer composite (MM:mCS) was dried at 75°C for 3 hours. With an accuracy of 0.001 g, 20 g of MM:mCS composite was weighed, transferred into a 100 ml beaker, stirred 500 rpm, on a screw

type stirrer, so that the blades provide uniform stirring of the powder. 10 g  $\text{Ti}(\text{BuO})_4$  was weighed to the nearest 0.001 g, and added in a thin stream with constant stirring to the beaker with MM. Stirring was done for 60 minutes. As a result, a composite of MM:mCS: $\text{Ti}(\text{BuO})_4$  was formed. In a 500 mL glass beaker 170 mL of distilled water was poured and stirred at 1200 rpm. Slowly over 10 minutes, 30 g of MM:mCS:  $\text{Ti}(\text{BuO})_4$  composite was get in. Stirring for 120 minutes, dividing the solution and the precipitate on a Schott filter 3, washing the precipitate with two portions of 100 ml water and one portion of 100 ml ethanol. Washing is necessary to remove unhydrolyzed  $\text{Ti}(\text{BuO})_4$ , butyl alcohol, unbound CS molecules. The hydrolysis results in a MM:CS: $\text{TiO}_2$  composite. The MM:CS: $\text{TiO}_2$  composite was dried at 75°C for 3 hours. The sorbent is a light, white powder.

## 2.2 Analysis of MM:CS: $\text{TiO}_2$

X-ray diffraction analysis of the MM:CS: $\text{TiO}_2$  sorbent was performed to confirm the introduction of  $\text{TiO}_2$  particles into the interlayer space of MM. The measurements were made using Shimadzu XRD-7000 diffractometer. Imaging conditions: radiation - Cu  $K\alpha$ , graphite monochromator, angular range  $2\Theta=2-80^\circ$ , imaging type - step-by-step, scanning step  $0.03^\circ$ , exposure - 7 sec. Chemical analysis of the basic elements of the sorbent was performed on a Spectra Blue(Spectra) inductively coupled plasma atomic emission instrument. Carbon content was measured by IR-adsorbition on CS-230 analyser (Leco).

## 3. RESULTS AND DISCUSSION

### 3.1 Structure analysis of MM:CS: $\text{TiO}_2$

Chemical analysis of the main elements of the MM:CS: $\text{TiO}_2$  sorbent showed that it contains, wt%:  $\text{TiO}_2$  – 9.40 %,  $\text{SiO}_2$  – 40.2 %,  $\text{Al}_2\text{O}_3$  - 13.1 %, Cl –0,7 %, C – 14.7 %.

X-ray phase analysis of the source material (Figure 1), showed that it contains MM as the main phase, monoclinic syngony, space group  $C2/m$ ; parameters of the unit cell:  $a=5.2843 \text{ \AA}$ ,  $b=9.2064 \text{ \AA}$ ,  $c=13.5099 \text{ \AA}$ ,  $\Theta =86.407^\circ$ ,  $V=655.958 \text{ \AA}^3$ .

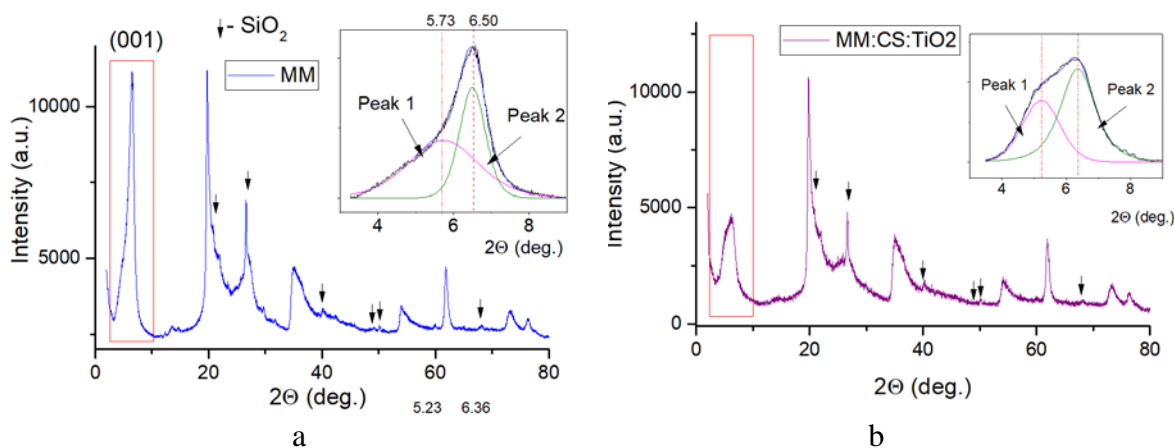


Figure 1 - X-ray diffraction patterns of initial montmorillonite (a), and after  $\text{TiO}_2$  intercalation(b); insets show enlarged fragment of peak (001).

In addition to the main phase MM contains  $\text{SiO}_2$  (polymorphic modification - quartz). The phase composition of MM with titanium compounds deposited on it has not changed (Fig. 1). However, the shape of Bragg peak (001) of MM changed significantly. Let's conditionally decompose this maximum into two peaks (peak 1 and peak 2 in the inset in Fig. 1), assuming that the MM contains 2 fractions with different dispersity and different lattice period. Peak 2 refers to a fraction with

high dispersion and a large lattice period, peak 2 contains larger crystallites and a smaller lattice parameter. In MM, after TiO<sub>2</sub> sorption, both peaks shift towards small angles, which corresponds to an increase in the interplanar distance in both fractions. The proportion of the more dispersed fraction (wide maximum 1) increases by 10%. The interplanar distances in both fractions after sorption increased by 1.4458 Å for fraction 1 and by 0.2943 Å for fraction 2. The X-ray diffraction pattern of MM:CS:TiO<sub>2</sub> does not contain peaks of the new compound because TiO<sub>2</sub> is in an X-ray amorphous state.

### 3.2 Chromium sorption on MM:CS:TiO<sub>2</sub>

The adsorption efficiency of MM:CS:TiO<sub>2</sub> is considerably higher than that of the native MM, and this difference increases considerably when UV light of Hg-vapour lamp is applied and photosorption takes place (Figure 2). Chromium content was 10 mg/l, the source was K<sub>2</sub>Cr<sub>2</sub>O<sub>7</sub>, sorption time – 2 hours.

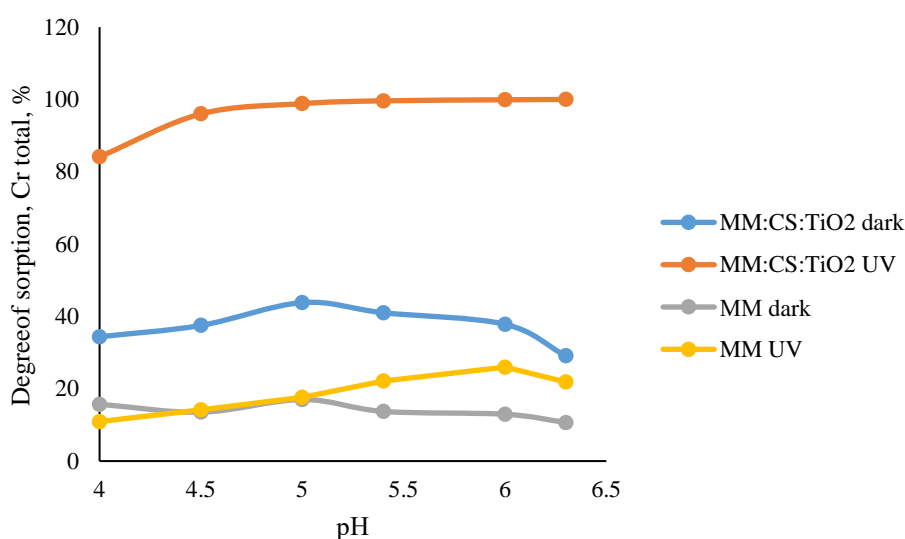


Figure 2 - Adsorption of chromium from the 15 ml of 10 mg/l solution on 0.05 g of MM:CS:TiO<sub>2</sub> compared with adsorption on pure MM under UV-radiation and without it. Acetate buffer medium.

The comparative characteristics of the sorbents with photosorption contribution separation (Table 1) show that photosorption is inherent in the MM:CS:TiO<sub>2</sub> composite as well as the highly dispersed TiO<sub>2</sub>[8], but completely absent in MM.

Table 1 - Comparative characteristics of the sorbents

Sample	Sorption degree without UV, %	Sorption degree with UV, %	Photosorption, %	q <sub>e</sub> , mg/g
MM:CS:TiO <sub>2</sub>	43.8	98.8	55	3.75
MM	17.0	17.6	0.6	0.51
Hombifine [8]	82.1	99.8	17.7	3.0

Note: By photosorption we mean the difference between UV-activated and non-UV-activated sorption. Adsorption values are given at pH=5.

The synthesis of MM:CS:TiO<sub>2</sub> composite sorbent by successive modification of CS and TiO<sub>2</sub> improves its ability to sorb chromium. The improvement of adsorption in the absence of irradiation seems to be connected with the modification of CS, whereas the increase of adsorption under irradiation is connected with amorphous TiO<sub>2</sub> particles.



#### 4. CONCLUSION

A new method of synthesis of composite sorbent based on montmorillonite and amorphous titanium dioxide is described. The hydrophobic titanium butoxide precursor is introduced into the sorbent interlayer space using the material property to adsorb cationic surfactants, resulting in the formation of a hydrophobic surface. The hydrophobic interlayer space is easily accessible to hydrophobic organic precursors. This makes it possible to form a uniform distribution of amorphous titanium dioxide particles in the interlayer space. After introduction of titanium dioxide into the matrix of montmorillonite an increase in the interlayer space of the matrix was recorded. The synthesis resulted in a composite sorbent with photosorption activity towards Cr(VI) compounds surpassing the sorption properties of commercial material Hombifine.

#### ACKNOWLEDGEMENTS (optional)

*This work was performed on equipment at the Ural-M shared resource center. This work was supported by the Russian Science Foundation, project no. 21-73-20039.*

#### REFERENCES

- [1] N. Pechishcheva, A. Korobitsyna, D. Ordinartsev, P. Zaitceva, O. Melchakova, S. Estemirova, Sep. Sci. Technol., 57(2) (2022), 180-191.
- [2] Z. Luan, E. Maes, P. Van der Heide, D. Zhao, R. Czernuszewicz, L. Kevan, Chem. Mater., 11(12) (1999), 3680-3686.
- [3] V. Kaichev, Y. Chesalov, A. Saraev, A. Klyushin, A. Knop-Gericke, T. Andrushkevich, V. Bukhtiyarov, J. Catal., 338, (2016)82-93.
- [4] A. Eliwa, A. Mubark, G. Dakroury, E. El-Shazly, K. El-Azony, J. Environ. Chem. Eng., 10(6) (2022), 108886.
- [5] N. Pechishcheva, D. Ordinartsev, A. Valeeva, A., P.Zaitseva, A. Korobitsyna, A. Sushnikova, A. Rempel', Russ. J. Phys. Chem. A, 97(2) (2023), 392-396.
- [6] B. Dou, V. Dupont, W. Pan, B. Chen, J. Chem. Eng., 166(2), (2011), 631-638.
- [7] Y. Li, J. Liu, R. Jia, Y. Guo, W., J. Zhuo, P. Na, J. Chem. Eng., 191 (2012), 66-74.
- [8] D. Ordinartsev, N. Pechishcheva, A. Valeeva, P. Zaitseva, , A. Korobitsyna, A. Belozeroва, A. Rempel', Russ. J. Phys. Chem. A, 96(11) (2022), 2408-2416.

## ELECTRO-PULSE CRUSHING IN HIGH-PURITY QUARTZ PRODUCTION

Mikhail Korovkin<sup>1,2</sup>, Ludmila Ananyeva<sup>2</sup>, Andrey Zherlitsyn<sup>3</sup>, Sergey Kondratyev<sup>3</sup>, Olesya Savinova

<sup>1</sup> National Research Tomsk Polytechnic University, 30, Lenin Ave., Tomsk, 634050, Russia

<sup>2</sup> National Research Tomsk State University, 36, Lenin Ave., Tomsk, 634050, Russia,

<sup>3</sup> The Institute of High Current Electronics SB RAS, 2/3, Academichesky Ave., Tomsk, 634055, Russia

### Abstract

*The paper focuses on micron-sized quartz concentrate obtained by electropulse disintegration of high-purity quartzite. Research results concern the composition of the obtained quartz concentrate and its machine contamination during electropulse disintegration.*

*Keywords: high-purity quartzite, electropulse disintegration*

### 1. INTRODUCTION

Although the mechanical grinding is conventionally used for rock disintegration, the electro-pulse crushing technique suggested and experimentally verified by researchers from Tomsk Polytechnic University, has been employed for over 60 years [1, 2]. This technique is used to improve metallurgical results and disintegration of strong quartz rocks, especially due to increasing consumption of high-purity quartz concentrates [3–5]. Taking the depletion of conventional rock crystal deposits into consideration, attention is paid to quartzites, quartz-rich rocks from West Siberia. Quartzites contain 97 to 99 % of SiO<sub>2</sub> and higher, the high purity of which is provided by unique conditions of their formation [6, 7]. However, production of high-purity SiO<sub>2</sub> without foreign contaminating inclusions, is currently a global technological problem, and very few publications address this issue [8, 9].

Current research is focused on the structure of micron-sized quartz concentrate prepared by electro-pulse crushing and material and elemental compositions of impurities.

### 2. EXPERIMENTAL

Electro-pulse disintegration of quartzites was performed on an original grinding unit at the Institute of High Current Electronics SB RAS, Tomsk, Russia. The absence of multistage pulse voltage generators and the use of a high-voltage energy storage provided by a single element, significantly reduced the size of the grinding unit. A 300 kV pulse transformer originally designed for quartzite disintegration, possessed high-voltage windings with turn-to-turn insulation of condenser type. The electropulse grinding generator was based on pulsed charging of the high-voltage storage capacitor from a low-voltage primary storage *via* a setup transformer. The electric discharge power was controlled by varying the high-voltage storage capacity. High-voltage electrodes operating in the core region of the crushing chamber, were made of different materials such as commercially pure iron, stainless steel, and magnetic iron alloy. Quartzites were disintegrated on a repetitively pulsed generator capable of producing a pulse train of 1000 pulses at a pulse frequency of 5 to 10 Hz, 500 J energy stored in the high-voltage storage capacitor, and 300 kV voltage. The crushing chamber operated at the drastically nonuniform electric field of the tip-plane type and positive

polarity of voltage pulses. Main ( $\rho \sim 10^4 \Omega \cdot \text{cm}$ ) and deionized ( $\rho \sim 10^7 \Omega \cdot \text{cm}$ ) water was used as operating medium [4].

### 3. RESULTS AND DISCUSSION

In the described conditions of electro-pulse disintegration of quartzites, the obtained quartz crystals were rather homogeneous and ranged in size from 0.01 to 0.5 mm. Quartz crystals were characterized by a conchoidal fracture, some of them were fused, without and with pure iron particles adhered to their surface.

As can be seen in Fig. 1, there are many foreign magnetic and nonmagnetic contaminating inclusions with complex compositions Fe-Cr-Ni-Cu-Al, most often Fe-Ni-Cr, and also Mn impurities in the form of separate grains of various shape. The magnetic fraction represents separate grains and quartz grains covered with iron hydroxide film. The grain shape of this fraction is dendritic, lamellar, acicular, round, etc.

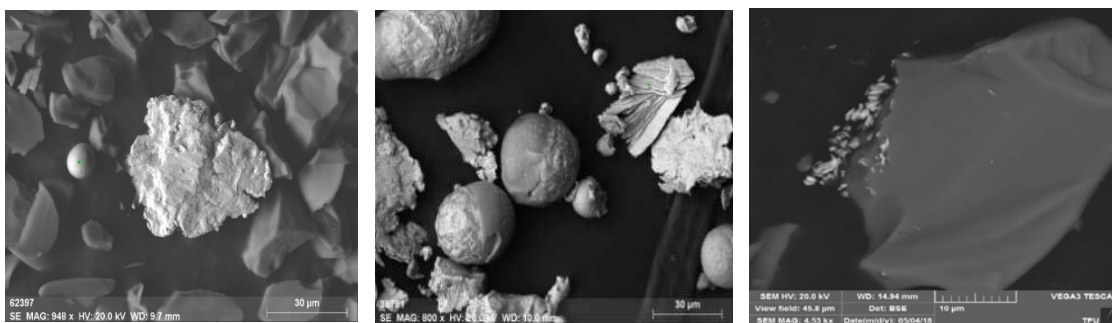


Figure 1 - SEM images of magnetic and nonmagnetic iron fractions and separate quartz grains with adhered metal particles after electropulse disintegration

A thermobaric effect observed during the high-voltage electric discharge, promotes cracking of quartz grains, formation of etch holes and channels propagating from them deep into the grain, as in the case with the microwave treatment [10]. The high temperature in the discharge channel causes not only fusion of quartz grains, but also opening of gas-liquid inclusions, thereby facilitating additional cleaning of quartz concentrate (Fig. 2).



Figure 2 - Fused particles of quartz concentrate with traces of gas-liquid inclusion opening

### 4. CONCLUSIONS

Electro-pulse disintegration of durable quartz rocks – quartzites – provided the formation of micron-sized quartz concentrate with the size ranging from 0.01 to 0.5 mm, which can then be used in industries. Changes in experimental conditions of the quartzite disintegration had a significant effect on the formation of foreign contaminating inclusions in the initial material. In order to obtain high-purity micron-sized quartz concentrate, selected were the best grinding conditions, electric discharge parameters, materials, and configuration of the crushing chamber.

All that minimized the machine contamination of quartz concentrate and removed the magnetic fraction from the grinded material by using the additional cleaning.

This work was financially supported by Grant No. 22-27-00371 from the Russian Science.

## REFERENCES

- [1] A.M. Adam, Bull. of the Tomsk Polytech. Univ., 322 (2) B (2013) 191–196.
- [2] A.F. Usov, Vestnik Kol'skogo nauchnogo centra RAN, 4. B (2012) 165–192.
- [3] S.R. Korzhenevsky, V.A. Bessonova, A.A. Komarsky, V.A. Motovilov, A.S. Chepusov, J. Mining Sci., 52 (3), B (2016) 493–496.
- [4] L. Ananyeva, S. Ilenok, M. Korovkin, E. Kumpyak, A. Zherlitsyn, Proceedings 20th International Symposium on High-Current Electronics, 17 -21 September 2018, Tomsk, Russia, p.209.
- [5] Xiaodong Pan, Suqin Li, Yongkui Li, Penghui Guo, Xin Zhao, Yinshi Cai. Miner. Eng. 183 [B](#) (2022) 107600.
- [6] A.I. Nepomnyashchikh, A.P. Zhaboedov, M.G. Volkova, A.M. Fedorov, V.N. Yashin, J. Mining Sci., 55 (3) B (2019) 444–451.
- [7] L.G. Anan'eva, M.V. Korovkin, Bull. of the Tomsk Polytech. Univ, 306 (3) B (2003),50–55.
- [8] G. Mueller, W. An, Th. Berghofer, M. DelGiaccio, Ch. Eing, R. Fetzter, B. Flickinger, W. Frey, H. Giese, M. Gottel, Ch. Gusbeth, A. Heinzl, P. Hoppe, A. Jianu, F. Lang, K. Leber, M. Sack, G. Schuhmacher, J. Singer, R. Straessner, L. Wegner, A. Weisenburger, F. Zimmermann, V. Engelko, J. Korean Phys. Soc., 59 (6) B (2011) 3588–3593.
- [9] E. Dal Martello, S. Bernardis, R.B. Larsen, G. Tranell, M. Di Sabatino, L. Arnberg, Powder Technology, 224 B (2012) 209–216.
- [10] A.J. Buttress, J.M. Rodriguez, A. Ure, R.S. Ferrari, C. Dodds, S.W. Kingman, Miner. Eng., 131 B (2019) 407-419.

## ANALYTICAL SIMULATION OF EAF DUST ENRICHMENT

Žarko Radović, Nebojša Tadić

University of Montenegro, Faculty of Metallurgy and Technology,  
Cetinjski put, bb, 81000 Podgorica, Montenegro

### Abstract

*EAF dust causes economical and environmental problems due to Zn and Pb contents. Recycling of EAF dust helps to avoid disposal of wastes, conserves resources and minimizes its environmental impact. In this paper the analytical simulation of return dust injection into EAF was analyzed. The mass of return dust varied from 6 to 10 kg/t, and its influence on the Zn content was presented. On the basis of empirical data, three different masses of primary EAF dust were analyzed: 10, 15, and 20 kg/t of produced steel.*

**Keywords:** EAF dust, Zn content, enrichment.

### 1. INTRODUCTION

Due to its physical and chemical characteristics, the world Environmental Protection Agency (EPA) classified electrical arc furnace dust as hazardous waste. This type of dust is in the form of spherical particles whose granulation is below 1 $\mu$ m. The chemical composition of EAFD depends on the quality of scrap steel, the type of steel produced and the technological parameters of the furnace operation. According to Jensen and Wolf<sup>[1]</sup> recycling the filter dust by injecting it into the electric arc furnace considerably reduces the total amount of dust.

One of the most important procedures for the valorization of electric arc furnace dust (EAFD) is the reduction melting of return dust in the furnace, whereby its enrichment with Zn is achieved in several steps<sup>[2]</sup>.

Depending on the quality of the scrap, EAFD can have a very low % of Zn (5-7%) or significantly higher (15-20%). Enrichment of EAFD, which initially has a high Zn content, is a much easier process. However, in the production of alloy steel, Zn is often < 10%, so the enrichment process is more difficult. The goal of this paper is precisely the analytical simulation of the enrichment of depleted EAFD.

### 2. EXPERIMENTAL

The mass of the primary EAFD, depending on the quality of the initial scrap is 10-20 kg/t of produced steel, and, therefore, three cases were considered in this simulation: 10, 15 and 20 kg/t. In general, practical experience from steel production shows that, in the case of using a high-quality scrap, the primary EAFD mass does not exceed 11 kg/t.

This means that in this analytical calculation, the value of 10 kg/t is closest to the real process parameters. The impact of changing the mass of return EAFD in the range of 6-10 kg/t was analyzed as an effective way to speed up the enrichment process.

Based both on practical experience and empirical data, it was observed that 97% of Zn from the return EAFD goes back to dust, which has an increasing % of Zn in each subsequent step. A very small part of Zn passes into slag and 1% of the total Zn remains in steel<sup>[1]</sup>.

As already stated, EAFD reduction enrichment is a multiple return process, which is repeated in  $n$ - steps, until reaching  $Zn_{(min)}=25\%$ , which is necessary for further economical valorization.

The Zn content after each step can be represented by the expression:

$$Zn_{(n)} = Zn_{(0)} + a_1 Zn_{(0)} + a_2 Zn_{(1)} + \dots + a_{(n)} Zn_{(n-1)}$$

where: -  $Zn_{(0)}$  – initial content of Zn in EAFD

-  $n$  – number of steps

-  $a_{1,2,\dots}$  – empirical coefficients.

The data used in the calculation are given in Table 1.

Table 1 - Parameters for calculation

Material balance	Mass of primary EAFD, (kg/ t)	Mass of returned EAFD, (kg/ t )
Mass of steel – 60 t	10,15, 20	6,7,8,9,10
Mass of slag – 200 kg/t		
Initial % Zn – 7%		

### 3. RESULTS AND DISCUSSION

As a starting case, the enrichment of the primary EAFD mass of 10 kg/t with a change in the return dust mass of 6-10 kg/t was analyzed (Figure 1).

It is observed that achieving  $Zn_{(min)}$  is possible if  $m_{(EAFD)} > 7\text{kg/t}$  after 5 return steps. According to the previously determined distribution of Zn between phases: dust-metal-slag, the content of Zn in the slag was calculated and shown in Figure 2.

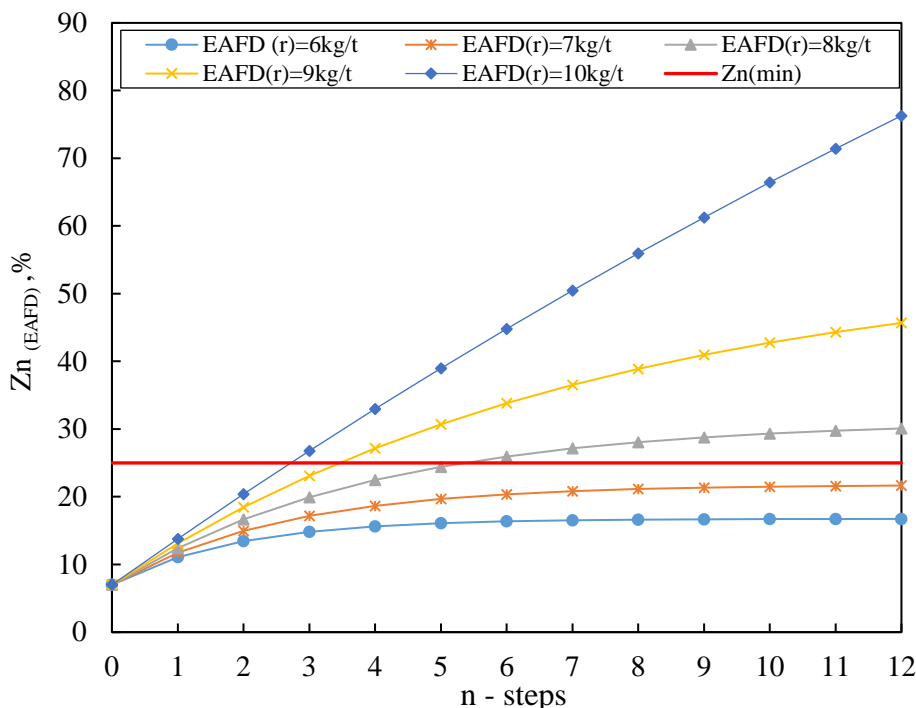


Figure 1 -  $Zn_{(EAFD)}$  as a function of returned EAFD mass (10 kg/t)

It can be seen on the graph that  $\%Zn_{(slag)}$  in all considered cases is significantly below 0,1%, which is the treshhold value in terms of not exerting a negative impact on the further valorization of the slag, acording to more recennt data by Malecki<sup>[3]</sup>.

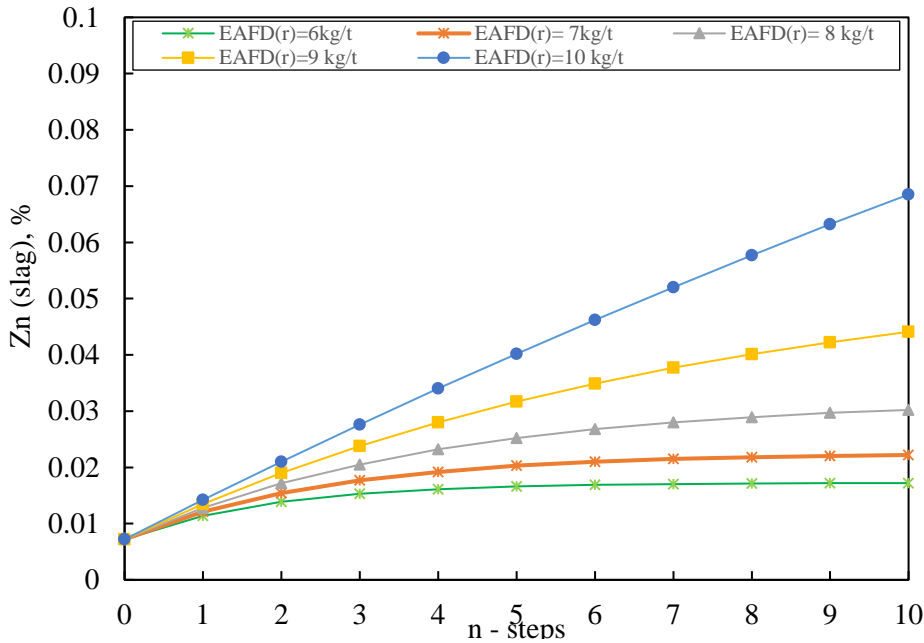


Figure 2 -  $Zn_{(slag)}$  as a function of returned EAFD mass (10 kg/t)

If larger quantities of primary EAFD (15 and 20 kg/t) are taken into consideration, it is then practically impossible to reach  $Zn_{(min)}$  regardless of the increase in the mass of return EAFD (Figures 3 and 4). From the simulation results presented, it can be seen that with the increase in the mass of the primary EAFD, this process becomes more difficult. The reason for this tendency lies in the fact that in the case of an increased mass of the primary EAFD, the return dust loses its relatively dominant influence on the enrichment process.

Due to the increased mass of depleted primary dust, its role in the overall process is also greater. Although the analytical calculation shows that at  $m_{(EAFD)} > 10\text{kg/t}$  the desired  $\%Zn_{(min)}$  cannot be achieved, it should be kept in mind that all of the above refers to depleted EAFD (7%Zn). In practice, it has been proven that, in the case of low starting  $\%Zn$ , the mass of EAFD is relatively small (<11kg/t) due to massive pieces of quality scrap.

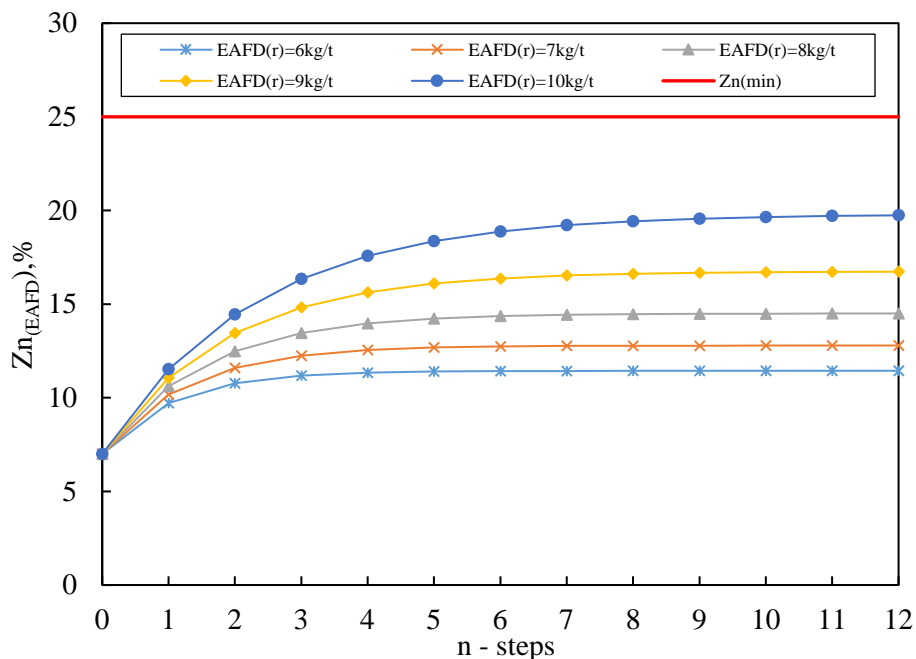


Figure 3 -  $Zn_{(EAFD)}$  as a function of returned EAFD mass (15 kg/t)



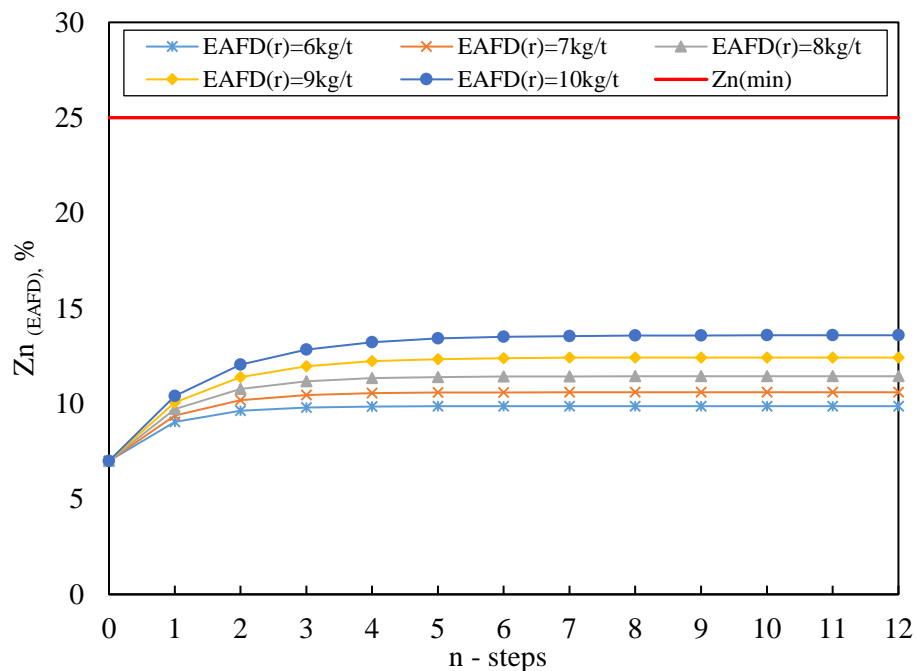


Figure 4 -  $Zn_{(EAFD)}$  as a function of returned EAFD mass (20 kg/t)

Accordingly, it has been empirically proven that with an increase in the proportion of sheets in the scrap, the mass of primary dust and the initial Zn content increase, which leads to the transition to the "rich" EAFD zone ( $> 15\%Zn$ ). Therefore, in practical conditions, it is realistic to consider the combination of 10kg/t of primary EAFD and  $Zn_{(0)} = 7\%$ , which proved to be easily feasible in the simulation. In contrast, the combination of a large starting mass of EAFD (15 and 20 kg/t) and a low Zn content (7%) is hardly possible in practice and belongs to the domain of theoretical considerations. Therefore, unfavourable simulation results for this case have no negative consequences on possible practical solutions. As opposed to the findings regarding the content Zn in EAFD, it was shown that its content in the slag is nowhere near the critical value of 0,1%, which represents the contamination threshold.

#### 4. CONCLUSION

Analytical simulation of multiple return injection of EAFD into the furnace, with the aim of reduction melting and enrichment, showed that it is necessary to change the mass of return dust. If depleted dust with  $<10\%$  Zn is treated, which is the case in the production of alloy steels, then it is necessary to increase the mass of return dust  $> 7$  kg/t. The amount of Zn that passes into slag is significantly lower than the critical value  $Zn_{(slag)} < 0.1\%$ , which is a necessary condition in the "leaching" test. The combination of low mass of primary EAFD and low content of starting  $Zn_0$  is the most realistic option in practical conditions. Cases in which the simulation proved that the procedure is unfeasible (large mass of primary EAFD and low Zn content) are virtually impossible in metallurgy and, therefore, they should not be considered outside of theoretical analyses.

#### REFERENCES

- [1] Jensen, J.; Wolf, K., MPT, 3 (1997) p.60.
- [2] Derda, W. , Metalurgija, 48 (2) (2009) p.29.
- [3] Malecki, S.; Gargul, K.; Warzecha, M., MDPI, Materials, 14 (20) (2021) p.6061.
- [4] Zhang, M.;Li, J.; Zeng, Q.; Q. Mou, Q, MDPI, Appl. Sci. , 9 (17) (2019) p.3604.

## THERMAL AND MECHANICAL RELAXATION OF RESIDUAL STRESSES IN COLD-ROLLED ALUMINIUM ALLOY STRIPS

Nebojša Tadić, Žarko Radović

Faculty of Metallurgy and Technology, University of Montenegro, Podgorica, Montenegro

### Abstract

*In this paper, the relaxation of residual stresses in cold-rolled strips made of alloys AW5083 and AW2024 was investigated, depending on the influencing parameters of the thermal and mechanical processes. In the case of thermal procedure, the desired level of stress relaxation can be achieved with sufficient precision by optimally choosing the annealing temperature and time to activate the thermally active processes. In the mechanical procedure with axial tensioning, the complete relaxation of residual stresses occurs at values of plastic deformation up to 1%. The performed analyzes and dependencies enable efficient planning and reliable control of the stress relaxation process.*

**Keywords:** cold rolling, residual stresses, thermal relaxation, mechanical relaxation.

### 1. INTRODUCTION

In cold rolling processes, as a consequence of inhomogeneous deformation, there is an inevitable occurrence of residual stresses which are permanently retained in sheets and strips [1]. The induced residual stresses are spatially balanced but also latently unstable. If their balance is disrupted during subsequent processing operations and exploitation, permanent changes in the shape and dimensions of the rolled products can occur [2,3]. Additionally, when construction elements are exposed to external loads, due to the superimposed of the stresses, the total stress can reach the critical value and cause damage or reduce the reliability of the construction elements [4]. Consequently, it is crucial to relax the residual stresses by either completely removing them or transforming them into a more favourable form that cannot cause permanent consequences. To perform and control relaxation procedures, it is necessary to know the stress values, their distribution within the element, and the changes that occur during the relaxation process [5].

This paper presents the research findings on the thermal and mechanical relaxation of longitudinal residual stresses in cold-rolled strips composed of alloys AW5083 and AW2024.

### 2. EXPERIMENTAL

For this research, commercial aluminum alloys AW5083 and AW2024 were chosen. The initial materials used were sheets in a soft annealed state, from which strips were subsequently cut for cold rolling and residual stress and relaxation testing. Table 1 provides details regarding the widths ( $b_0$ ), thicknesses ( $h_0$ ) and reduction ratio ( $\epsilon$ ) applied during the cold rolling process. The selection of these dimensions and reduction ratios was made to ensure conditions aligned with plane strain [1]. The rolling process was conducted on a laboratory duo-rolling stand using rolls with a diameter of 125 mm and a speed of 0.17 m/s.

The measurement of longitudinal residual stresses was conducted using the deflection method, which relies on disturbing the stress balance and measuring the resulting elastic lines. To disrupt the stress balance in the flat-rolled strips, metal layers were removed from one side through etching in a 20% NaOH solution at room temperature, while the remaining part of the sample was protected. As a result of this stress imbalance, the strip elastically bends symmetrically with respect to the transverse axis. Figure 1 illustrates the appearance of the strip after the rolling process and the removal of the metal layer. The complete procedure for measuring elastic lines and determining of longitudinal residual stresses is shown in paper [6].

Table 1. The dimensions of the tested strips and the reduction ratios applied during the rolling process

Alloy	$b_0$ , [mm]	$h_0$ , [mm]	$h_l$ , [mm]	$\epsilon$ , [%]
2024	40	4	3.2	20
			2.8	30
	20	2	1.6	20
			1.2	40
		1.28	1.024	20
			0.640	50
5083	20	1.28	1.024	20
			0.640	50

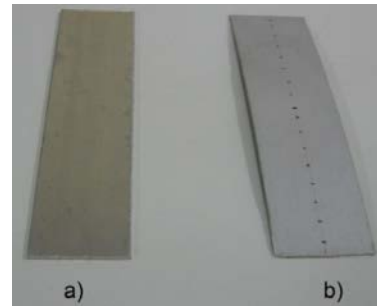


Figure 1 - The appearance of rolled strip: a) initial state, b) after the removal of layer

The thermal relaxation of the stress was conducted by annealing the original samples following the cold rolling process and removal of the metal layer from one side. The elastically bent strips were placed on a 5 mm thick metal plate and securely fixed to straighten them. Subsequently, the samples underwent thermal treatment. Upon completion of the annealing process, the samples were debonded, and the elastic line was measured. If annealing continues the procedure is repeated in the same way. The annealing temperature was selected to be  $0.25 \cdot t_m$  ( $t_m$  - melting temperature) [7]. Accordingly, for 5083 strips, the annealing temperature was set at 140°C for a duration of 1÷10 minutes, while for 2024 strips, annealing was conducted at 125°C for 1÷26 minutes. The annealing process took place in a laboratory furnace with a temperature regulation accuracy of  $\pm 2^\circ\text{C}$ . The mechanical relaxation of residual stresses was achieved through axial tensioning, applying a degree of permanent deformation of 0.5÷1%. The axial tensioning process was carried out using a Heckert FP100 universal machine.

### 3. RESULTS AND DISCUSSION

Thermal removal of residual stresses involves initiating thermal processes to relax the accumulated elastic energy. The annealing parameters (temperature and time), are adjusted based on the material state, the stress state, and the dominant mechanism of the process. The mechanism of the processes leading to the relaxation of residual stresses can be performed by utilizing the Zener-Wert-Avrami function (equation 1). In this equation, numerous coefficient values can indicate known structural changes (vacancy creep, dislocation creep and dislocation climb). In low-temperature tempering, the thermal climb of dislocations is the limiting process. However, determining the activation energy of thermal processes does not always provide a precise separation of the dominant mechanism [5,7]. Therefore, this study focuses on selecting of the temperature and time to achieve the projected reduction in residual stress values, according to the equation:

$$\sigma_{t,T}/\sigma_0 = \exp[-(A \cdot t)^m], \quad (1)$$

where:  $\sigma_0$ ,  $\sigma_{t,T}$  - the values of residual stresses for the initial and post-annealing conditions in a given t-T state, respectively;  $m$  - the numerical value indicating the dominant mechanism;  $A$  - the parameter that depends on temperature, activation energy, and Boltzmann's constant.

The results presented in Figure 2 demonstrate that the relaxation of residual stresses initiates even at the shortest annealing times and continues to progress with increasing duration. This observation suggests a high degree of instability in the residual stresses under the conditions of thermal treatment. However, within the range of short annealing times (1 min to 3 min), the relaxation of stresses is only partial, exhibiting changes that are not pronounced and that are characteristic of an incubation period. The results of multiple heating indicate that each new phase starts with the incubation period, therefore the changes are small. The intensive changes in residual stresses in 5083 alloy strips are observed only after 5 minutes of annealing, leading to a 75% reduction in

stresses. Subsequent annealing cycles exhibit significantly less intense changes in residual stresses (Figure 2a). The relaxation effects observed in the 2024 alloy are notably less pronounced. For 2024 strips with an initial thickness of 4 mm the maximum relaxation percentage is limited to 41%, whereas for strips with initial thicknesses of 2 and 1.28 mm, the relaxation percentages are limited to 25%, achieved at annealing times of 13, 8 and 5 minutes, respectively (Figure 2b,c,d). These differences compared to 5083 alloy strips can be attributed not only to the lower annealing temperature but also to the chemical and phase composition, and the structural mechanisms that contribute to stress relaxation at specific temperatures. Additionally, the stress values initiate the relaxation intensity in accordance with the energy effect and the stability of accumulated elastic energy. The varying intensity of relaxation observed for the same annealing times in both alloys is a consequence of the different sample thicknesses and through heating conditions. It is evident that stress relaxation in all investigated cases is sensitive to the influencing factors defined by the Zener-Wert-Avrami function, as well as the initial stress values.

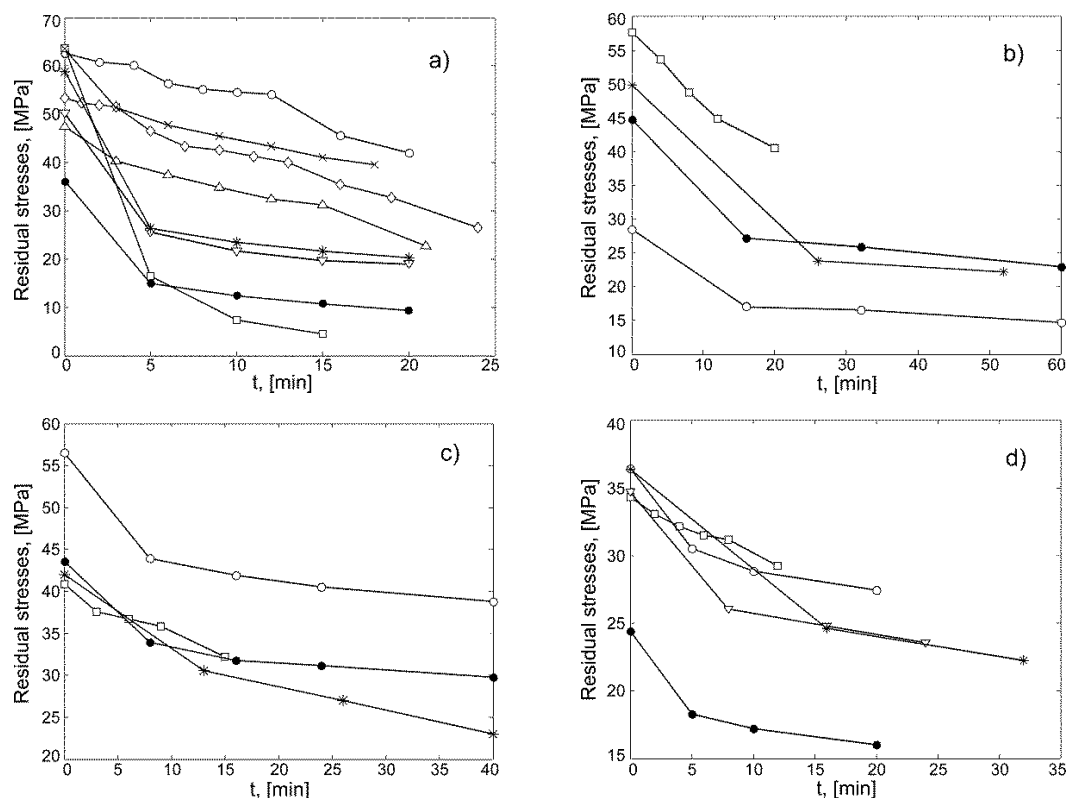


Figure 2 - Change of residual stresses depending on the annealing time in multilevel relaxation (different curves in the diagrams correspond to different samples): a) 5083,  $h_0 = 1.28$  mm; b) 2024,  $h_0 = 4$  mm; c) 2024,  $h_0 = 2$  mm; d) 2024,  $h_0 = 1.28$  mm

The basic shape of the stress change curve with annealing time is depicted in Figure 3, aligning with existing literature data [5,7]. The curve exhibits distinct regions: an initial incubation period at short annealing times, followed by an intense relaxation phase in the middle part of the curve, and concluding with another slower relaxation phase. Therefore, the relaxation of residual stresses can be achieved within a relatively short time, which should be adapted based on the chosen recovery temperature and time of through heating of the piece.

The mechanical relaxation of residual stresses was conducted on a series of samples with varying thicknesses from both alloys which were cold rolled with degrees of reduction ranging from 15% to 50% and had residual stress values ranging within the interval of 40÷70 MPa. Axial tension was then applied to these samples, inducing a permanent deformation of 0,5÷1%. Subsequent employing the deflection method, no residual stresses were detected in the samples. Furthermore, additional testing was conducted on four strips of 5083 alloy that were cold rolled with a reduction

ratio of 30%. After removing the metal layer, the elastic line and residual stresses were measured within the range of 45 MPa to 60 MPa. Subsequent tensioning of these samples, with a degree of permanent deformation of  $0.8\div 1\%$ , resulted in the complete relaxation of residual stresses since the elastic line disappeared, that is, the samples became flat. These tests provided evidence supporting the anticipated complete relaxation of residual stresses occurring at the onset of the plastic flow interval of the metal.

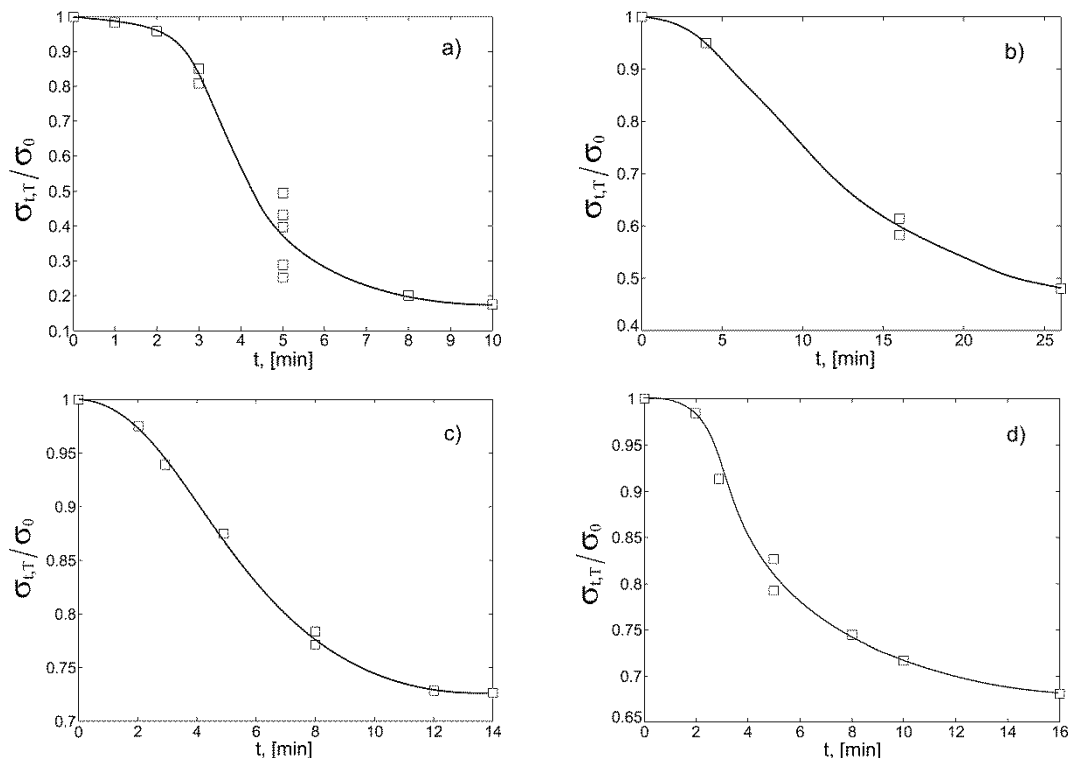


Figure 3 - The change in the ratio  $\sigma_{t,T}/\sigma_0$  depending on the annealing time:  
a) 5083,  $h_0 = 1.28$  mm; b) 2024,  $h_0 = 4$  mm; c) 2024,  $h_0 = 2$  mm; d) 2024,  $h_0 = 1.28$  mm

#### 4. CONCLUSION

The tests conducted on the relaxation of residual stresses in cold-rolled strips using thermal and mechanical procedures led to the following conclusions: High instability of residual stresses during both thermal and mechanical procedures; In the thermal procedure, by optimally selecting the appropriate temperature and annealing time, based on the function that describes the kinetics of thermal processes, it is possible to achieve the desired level of relaxation of residual stresses with sufficient precision; In the mechanical process, the complete relaxation of residual stresses occurs at a low value of permanent deformation, at the initial stages of the plastic flow of the metal.

#### REFERENCES

- [1] V.B. Ginzburg, R. Ballas, Cold Rolling Fundamentals, Marcel Dekker, New York, 2000.
- [2] DC, Tran, N. Tardif, A. Limam, Int J Solids Struct., 69-70 (2015), 343-349.
- [3] FD. Fischer, FG. Rammerstorfer, N. Friedl, J Appl Mech., 70(1) (2003), 84-90.
- [4] E. Macherauch, V. Hauk, Symposiums der Deutschen Gesellschaft für Metallkunde. Band 1; Karlsruhe: 1983. p. 2-36.
- [5] G. Totten, M. Howes, T. Inoue, Handbook of Residual Stress and Deformation of Steel, ASM International, 2002.
- [6] N. Tadić, M. Mišović, JOM, 13(4) (2007), 251-257
- [7] W.C. Leslie, The Physical Metallurgy of Steels, McGraw-Hill Book Co., New York, 1981.

## SELECTION OF ANCHOR TYPE USING AHP METHOD

Dragan Šabaz<sup>1</sup>, Miloš Stojanović<sup>1</sup>, Dejan Petrović<sup>2</sup>

<sup>1</sup>Mining and Metallurgy Institute Bor, Zeleni Bulevar 35, 19210 Bor, Serbia

<sup>2</sup> University of Belgrade Technical Faculty in Bor, Vojske Jugoslavije 12, 19210 Bor, Serbia

### Abstract

*Underground drift construction in underground mines affects the disturbance of the balance that prevails in the primary rock mass. In such an environment, there is a redistribution of stress in the rock medium and the formation of a secondary field stress around the underground drift. Importance of the supporting underground drifts is reflected in the fact that only by installing an optimal support structure, safe conditions can be ensured for the continuation of work. Total installation costs and required installation time can be highly rationalized by choosing the right type of support. Comparison and ranking of anchors in this paper was carried out according to different criteria: stability of the drift, required installation time and costs of support installing. In order to evaluate the precision of the obtained results and to ascertain whether the prescribed support structures imparted requisite safety to the subterranean enclosure, stability analysis was created utilizing Rocscience Phase software. Selection of the optimal type of anchor according to the above criteria was carried out using the Analytic Hierarchy Process (AHP) method. The analysis and evaluation of the obtained results according to the specified criteria was performed using the Expert choice software.*

**Keywords:** *underground mining, drift support, anchor type, AHP method*

### 1. INTRODUCTION

The natural balance that prevails in the rock mass is disturbed by the construction of underground mining objects. It is necessary to mitigate the resulting changes and establish a state of equilibrium similar to the one that existed before [1]. By installing an appropriate support structure, conditions are created for uninterrupted and safe utilization of the underground objects.

Application of modern techniques and technology in the support installation process, the reliability, stability and speed of constructing of underground objects are increased. In mines around the world, the implementation of anchoring system has proven to be a highly effective method of support. Anchoring system represent a network of embedded anchors within the rock mass, designed to increase the load-bearing capacity of the surrounding portion of the rock mass around the excavated underground object [2].

A universal procedure for selecting elements of anchoring system does not exist yet. For this reason, this paper presents a methodology for selecting the optimal anchor type that can be used in the construction of different shapes and dimensions of the underground objects. The methodology involves comparing and ranking anchors according to several important criteria: stability of the drift, required installation time and costs of support installing.

The adopted shape and size of the cross-section of the drift (dimension 5,3×5,3 m) and the technical characteristics of different anchor types (Swellex, Split Set and SN) were used to define parameters of anchoring system. A stability analysis of underground drift was conducted using the Rocscience Phase 2 software, considering the different anchor type. The time required for installation supporting elements was calculated, after considering all the individual operations involved in the support process.

Additionally, the total installation costs for supporting of 1 m of the underground drift were determined by considering the individual prices of the supporting elements. The results obtained according to the given criteria are shown in Table 1.

Table 1 – The input data for AHP method is defined in accordance with the criteria

Criteria	Parameters	Swellex	Split Set	SN
Supporting system	Anchor diameter (cm)	4,10	3,90	2,00
	Anchor length (m)	3,00	2,80	2,80
	Load-bearing capacity (t)	9,00	7,00	13,00
	Number of anchors in a row (com)	12	16	8
	Wire mesh	100×100×8		
	Thickness of shotcrete (cm)	5	4	6
Stability of the drift	Minimum displacements (mm)	3,00	3,30	2,60
	Maximum displacements (mm)	7,70	8,00	7,40
Installation time	Total installation time (min)	83,51	101,61	124,23
Costs of support	Anchor (din)	12.461,54	10.467,69	14.030,80
	Wire mesh (din)	7.959,69	7.959,69	7.959,69
	Shotcrete (din)	6.242,76	4.995,50	7.498,51
	Total costs (din)	26.663,99	23.422,88	29.489,00

The selection of the optimal type anchor based on the mentioned criteria was performed using the Analytical Hierarchy Process (AHP) method. Method involves evaluating the weight of the criteria and evaluating the types of anchors according to the criteria. The analysis and evaluation of the obtained results according to the mentioned criteria were performed using the Expert Choice software.

## 2. APPLICATION OF THE AHP METHOD IN THE PROCESS OF SELECTING SUPPORTING ELEMENTS

The AHP method is multi-criteria decision-making method that is used to solve complex problem, which consist of goals, criteria and alternatives. This method enables the interactive creation of a problem hierarchy, which serves as preparation for decision making. Pairs of criteria and alternatives are compared, a synthesis of all comparisons is made and the weight coefficients of all in the hierarchy are determined. The sum of weight coefficients for elements at each level of the hierarchy is 1. For the comparison of individual criteria or alternatives, the Saaty's scale is used, which consists of nine numerical ratings [3]. Decision maker uses ratings to distinguish the intensity of the relationship between the two elements. A hierarchical structure of the multi-criteria decision-making model was created based on the given criteria and alternatives (Figure 1).

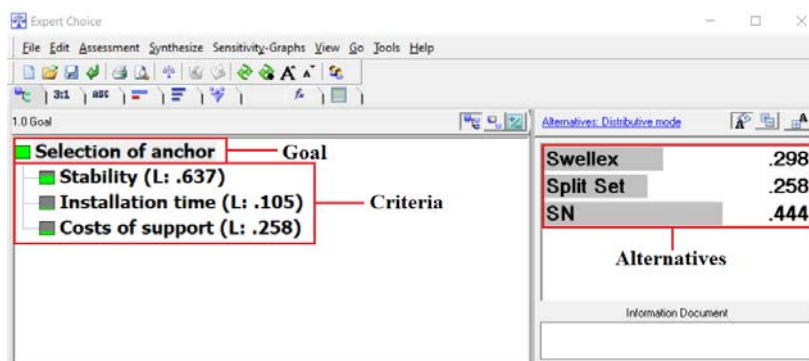


Figure 1 – The hierarchical structure of the multi-criteria decision-making model



The criteria are evaluated by importance and then compared in pairs based on Saaty's scale. After that, the weight of the criteria is determined and consistency is checked (Figure 2).

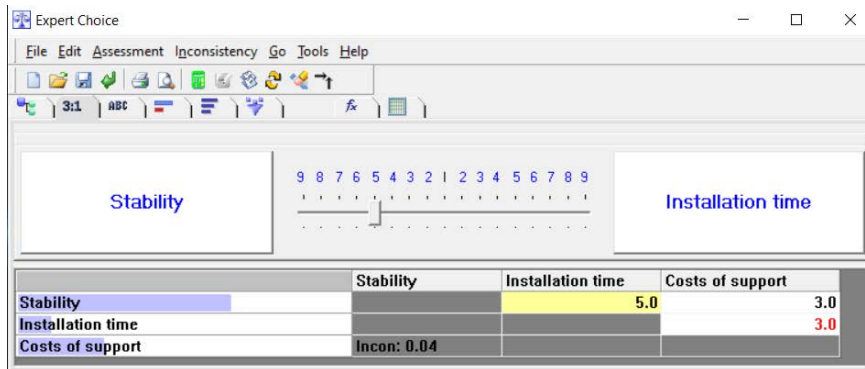


Figure 2 – Pairwise comparison of criteria

Value for pairwise comparisons of criteria is entered into the software, a consistency ratio is obtained ( $CR \leq 0,10$ ). This achieves a more objective assessment of the importance of criteria. In this case, the stability criterion is the most important, followed by cost of support, and finally installation time. The consistency level is below the threshold value, which means that the evaluation is correct.

After defining the weight coefficients of the criteria, it is necessary to define the final hierarchical level of alternatives. The formation of alternatives is carried out by selection in the main Expert Choice window, under the Alternative distributive mode (Figures 3,4,5). By comparing pairs of alternatives based on specified criterion, the weight coefficient of the alternative is determined, based on the data presented in Table 1.

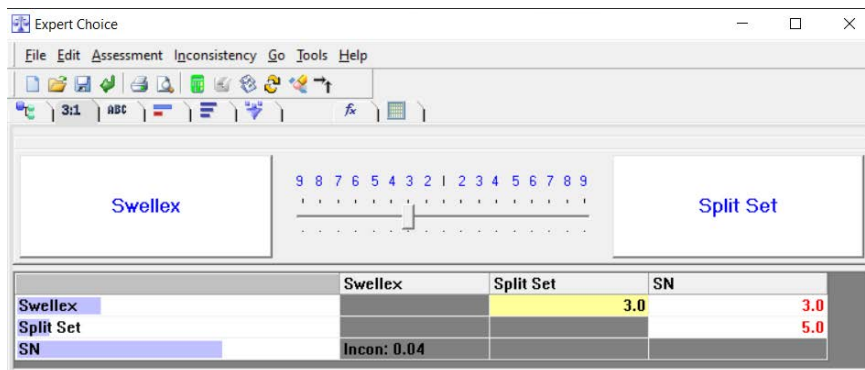


Figure 3 – Pairwise comparison of alternative based on the criterion of stability

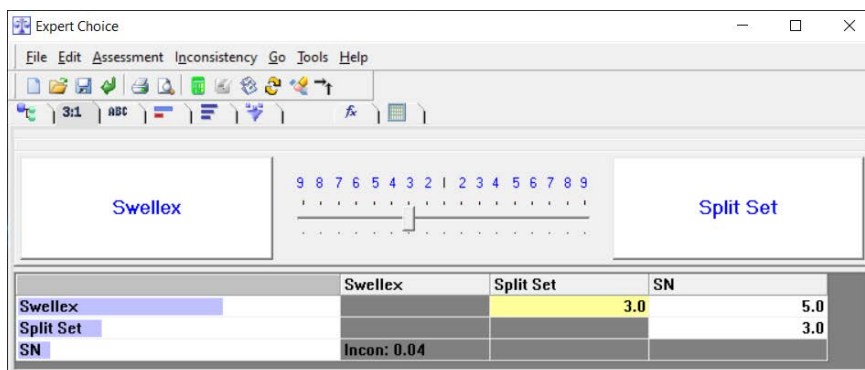


Figure 4 - Pairwise comparison of alternative based on the criterion of installation time

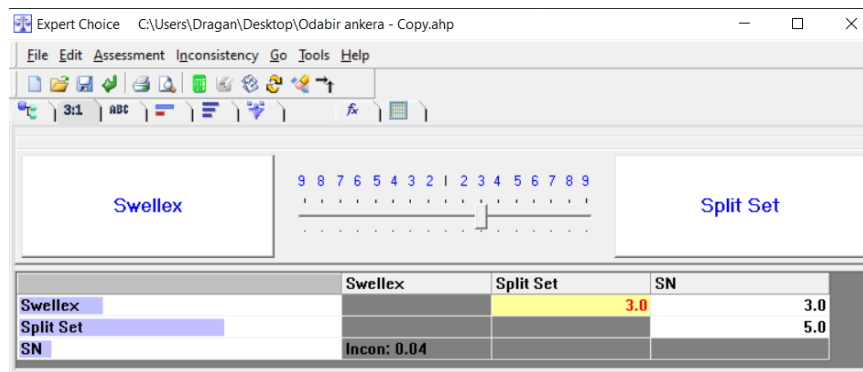


Figure 5 - Pairwise comparison of alternative based on the criterion of costs of support

Based on the previous figures, it is evident that the consistency coefficient is satisfactory in all cases ( $0,04 \leq 0,1$ ). According to the stability criterion SN anchors have proven to be the best choice, while for the installation time criterion Swellex anchors are preferred. The lowest costs were achieved using Split Set anchors.

Considering the obtained results of the relationship between alternatives and criteria, it can be conducted that SN anchors have proven to be the best solution for supporting (Figure 6).

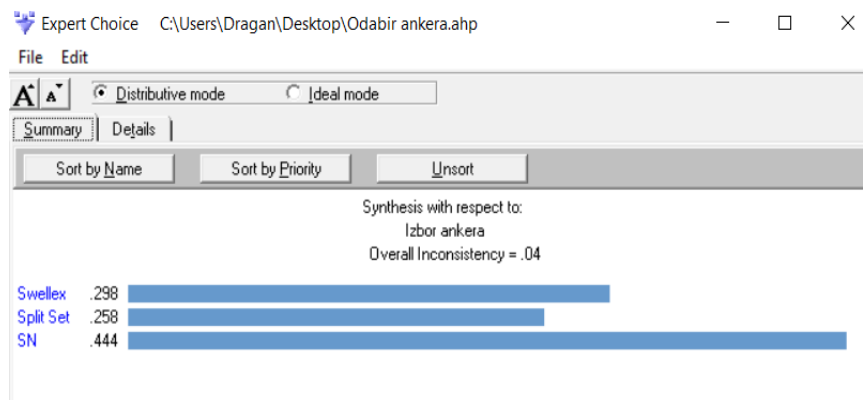


Figure 6 – Comparison of anchors based on three criteria

### 3. DISCUSION AND CONCLUSION

The selection of the optimal type of anchor for support is complex process. In order to facilitate this decision, the paper presents the application of the analytic hierarchy process (AHP) method. The weight of the criteria has been evaluated and the types of anchors have been evaluated according to these criteria. Based on the results obtained through this method, it has been concluded in the specific case, that using SN anchors achieves the best results for support an underground drift. Therefore, by applying the presented methodology for anchors selection, it significantly influences cost reduction, construction time, and achieves the necessary stability.

### REFERENCES

- [1] Kovačević J., Savremeno građenje u podzemlju, AGM knjiga, Beograd, 2014, p.467.
- [2] Milisavljević B., Primena AT višeće podgrade u rudnici Srbije, University of Belgrade – Faculty of Mining and Geology, Beograd, 2015, p.3.
- [3] T.L.Saaty, EJOR, 48(1990) 9-26.

## BLAST FRAGMENTATION ANALYSIS IN JAMA BOR BY USING WIPFRAG SOFTWARE

Miloš Stojanović<sup>1</sup>, Veljko Lapčević<sup>2</sup>, Ivica Vojinović<sup>1</sup>

<sup>1</sup>Mining and Metallurgy Institute Bor, Zeleni Bulevar 35, 19210 Bor, Serbia

<sup>2</sup>Faculty of Mining and Geology, University of Belgrade, Đušina 7, 11000 Belgrade, Serbia

### Abstract

*Blast fragmentation is a special aspect of underground mining operations, as it directly influences productivity, cost efficiency, and overall safety. It refers to the process fracturing rock mass into smaller, manageable pieces through the controlled use of explosives. Properly executed blast fragmentation allows for seamless material handling, reduced wear on equipment, and optimized energy consumption. Blast fragmentation measurement is an essential step in optimizing and controlling the overall performance of a blasting operation. By accurately measuring the size distribution of fragmented material, mining operators can identify areas for improvement and adjust their blast design. Various methods and technologies are available for measuring blast fragmentation, each with its benefits and limitations. In this paper we will discuss the use of WipFrag which is a commercially available image analysis software. This software is designed to measure and analyze blast fragmentation by processing digital images of fragmented material. In the previous period, a series of pictures of ore fragmentation in the stopes of the Jama Bor mine were taken, where the open stoping mining method is applied. Analysis of the mentioned images with this software can significantly contribute to the development in the mining industry to optimize blasting operations, improve productivity and reduce costs.*

**Keywords:** *underground mining, blasting, fragmentation, WipFrag*

### 1. INTRODUCTION

Inefficient blasting in underground mining may induce myriad inefficiencies in subsequent processes, necessitating consistent evaluation and optimization of blast outcomes. As compared to crushing and grinding, effective blasting presents a cost-effective alternative, notwithstanding its intensive initial cost due to its overwhelming technical and economic benefits. These advantages are primarily predicated on the fragments size distribution and the extent of induced microcracks. The assessment of size distribution can be either qualitatively, visually as good or poor, or quantitatively, via screening or various image analysis techniques. However, screening, while being the most accurate method, may not be suitable for large projects. On the other hand, the extent of microcracks, visible through specialized microscopes, can be systematically assessed via a study of energy consumption and production output. This document aims to address the benefits and uncertainties surrounding blast fragmentation evaluation.

The measurement of blasted rock fragment size is considerably significant in assessing the efficacy of production blasting operations. It is also a crucial factor in evaluating blasting outcomes and impacting subsequent mining and processing operations in underground mines. Fragment size distribution measurement methods fall into two overarching categories: direct and indirect methods. Despite being the most accurate among other techniques, sieve analysis, a direct method, is not practical for large-scale projects due to cost and time limitations.

The sieving analysis method involves passing a representative sample of blasted material through sieves with varying mesh sizes. The weight of the material retained on each sieve is measured, and the fraction of material in each size is calculated, which indicates fragmentation characteristics. Manual measurement methods involve physical measurement of individual rock fragments using

rulers, providing useful information in certain situations despite being less accurate and time-consuming. Indirect methods such as observational, empirical, and digital methods have been developed. Visual observations of post-blasting rock material form part of the observational methods widely utilized by blasting engineers for approximate evaluations. Recent advancements in fragmentation evaluation techniques utilizing digital image processing programs have enabled rapid, precise assessments of blast fragmentation size distribution. High-resolution cameras or scanners capture images of the blasted material in image analysis, with specialized software analysing the images to identify particle sizes. Laser scanning systems scan the surface of fragmented material using laser beams, enabling an accurate measurement of fragment size and shape for detailed analysis. The photographic analysis involves analysing photographs of the blasted material, captured via standard cameras or specialized devices, to measure fragment size distribution. Developed through the end of 20 century, digital image software has been universally accepted in the mining and mineral processing industries, providing continuous evaluations without hampering the production cycle. However, errors associated with digital image analysis can complicate accurate fragmentation estimations post-blasting. Several commercially available software such as Split-Desktop, GoldSize, WipFrag, FragScan, IPACS, can be used to quantify size distribution. However, these systems' accuracy can fluctuate between 5% and 15%. [1]

This paper will focus on the usage of WipFrag, a commercially available image analysis software, designed to measure and analyse blast fragmentation via digital image processing of fragmented material.

## **2. CONDITIONS FOR MEASUREMENT OF SIZE DISTRIBUTION**

Rock fragmentation through blasting, pivotal in the mining industry, bears substantial impacts on the facets of productivity, economic performance, and worker safety. A crucial tool in ameliorating drilling and mining operations lies in the accurate measurement of fragmented material's size distribution. Employing varying technologies and methodologies for fragmentation measurement, each comes with inherent strengths and weaknesses. The main focus here dwells on the application of WipFrag, a commercial image analysis software designed for the measurement and analysis of fragmentation through processing digital images. In a recent research, images of ore fragmentation were collected from the underground mine Zijin Copper of Serbia, which is mining according to the Supplementary mining project of changing mining method in the Borska Reka ore deposit (MMI Bor, 2022). This strategy aimed at employing the open stoping mining method in the excavation zone -170/-210 m. [2]

This research emphasized the photographic documentation of rock mass in the excavation, where fragmentation was a result of previous drilling and mining undertakings. The research primary aim was to enhance the quality of photographs by establishing numerous standards during the image capture process. Operator numbers played a crucial role, as reducing this number curtailed the potential for bias in the samples or the resultant image to be processed by WipFrag software. As Maerz highlighted in his study “Some photographers will be drawn to the largest particles; others will select areas of uniform distribution”. [3]

Consistency in camera quality was maintained throughout the study to circumvent variations in image attributes such as resolution, colour, and contrast. The standardization of the camera's position, height, and distance from the rock material was also crucial. [4]

Given the underground conditions devoid of natural lighting, two reflectors were positioned on either side of the camera lens to provide sufficient illumination. To fine-tune fragmentation estimations, WipFrag necessitates the inclusion of benchmarks or reference lines in its analysis for the differentiation and dimensioning of rock fragments. A pocket tape measure, adjustable to 0.5 m or 1 m based on the fragmentation, served this purpose. WipFrag recommends such positioning

of reference objects as an effective method, as shown in Figure 1. Considering image sharpness, the intensity is crucial, particularly when operating the camera by hand. A tripod is recommended to overcome any camera movement during exposure that could reduce sharpness. Regarding lighting, uniform illumination is essential. A single light source may result in intensity falloff towards the edges of a large area, possibly leading to underexposed material at the edges, obstructing analysis. The farther the light source, the more uniform the illumination. Hence, placing lights in proximity may lead to substantial intensity variance, with distant objects receiving significantly less illumination. The farther the light source, the more uniform the illumination. Placing lights in proximity may lead to substantial intensity variance, with distant objects receiving significantly less illumination. In sum, capturing high-quality, accurate images for fragmentation analysis in underground mines involves multiple considerations, from camera and operator consistency to lighting setup and positioning of reference objects. [4]

In sum, capturing high-quality, accurate images for fragmentation analysis in underground mines involves multiple considerations, from camera and operator consistency to lighting setup and positioning of reference objects. Such methodical approaches to imaging enable a more precise understanding of fragmentation in mining operations, which can significantly contribute to the industry's overall productivity and safety.

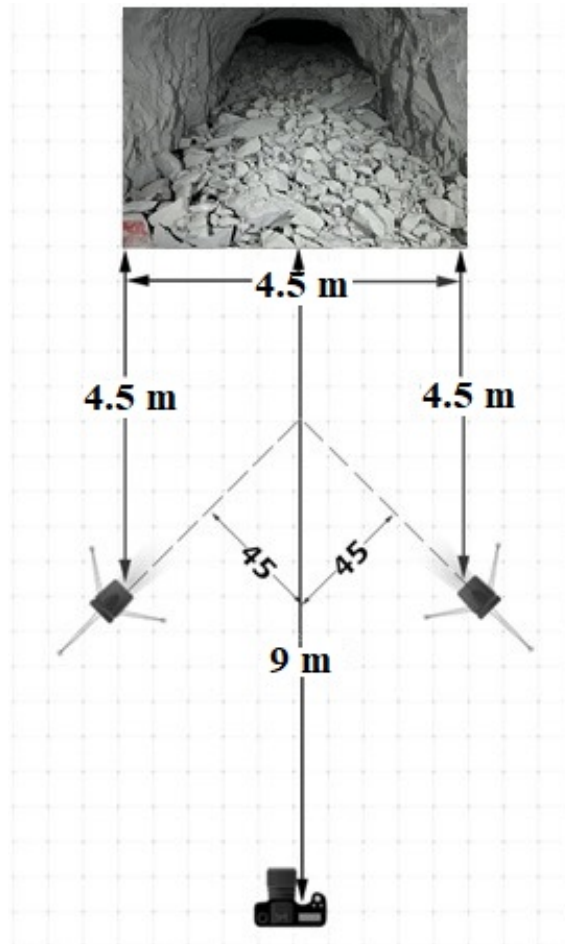


Figure 1 - Lighting Placement Diagram

### 3. RESULTS AND DISCUSSION

By digitally processing the image and separating its elements in WipFrag, the obtained ore fragmentation is categorized based on the cumulative distribution curve of size classes (Figure 2). Analysing such images with the WipFrag software can significantly contribute to the development

of the mining industry by optimizing blasting operations, improving productivity, and reducing costs.

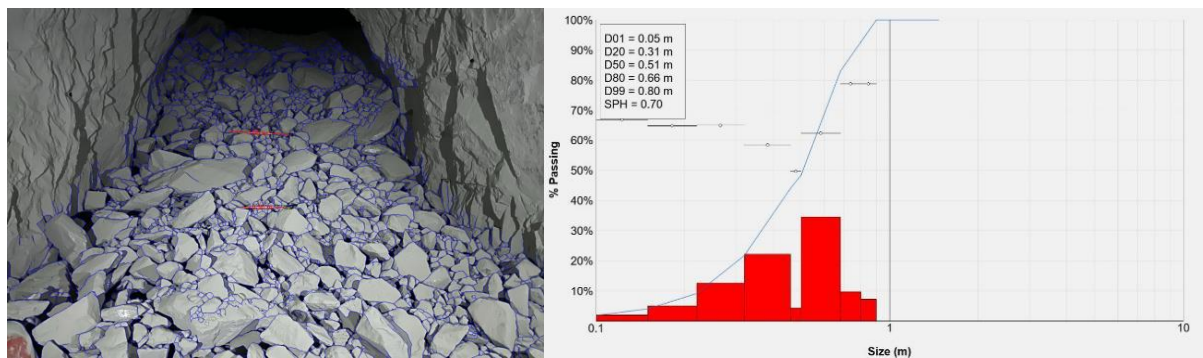


Figure 2 - Captured picture and Wipfrag cumulative distribution curve of size classes

Understanding key aspect that requires careful consideration is its particle size distribution of rock material. The particle size distribution plays a significant role in various aspects, such as the strength and load-bearing properties of rocks and soils.

Determining material density relies on the accurate assessment of particle size distribution, and numerous industrial applications necessitate stringent control over this distribution. Like any other digital image, this analysis may have errors due the difference in maximum sizes caused by captures which use only part of the available ore for photography.

#### 4. CONCLUSION

The measurement of blast fragmentation is essential for optimizing and controlling blasting operations. Various methods and technologies, including image analysis software such as WipFrag, are available for measuring blast fragmentation. Digital image analysis programs offer rapid and precise assessments of fragmentation size distribution, providing continuous evaluations without disrupting the production cycle. The study discussed in the text focused on the usage of WipFrag software for measuring and analysing blast fragmentation through the processing of digital images. The research emphasized the importance of standardization in the image capture process, including camera quality, lighting setup, and the inclusion of reference objects. Overall, the utilization of image analysis software like WipFrag can significantly contribute to the development of the mining industry by improving blasting operations, optimizing productivity, and reducing costs.

#### REFERENCES

- [1] F.I. Siddiqui, S.M. Ali Shah, JKAU: Eng. Sci., Vol. 20 No. 2, 2009.
- [2] Mining and Metallurgy Institute Bor, Supplementary mining project of changing mining method in the Borska Reka ore deposit, Serbia, Bor, 2022.
- [3] Norbert Maerz, Image Sampling Techniques and Requirements for Automated Image Analysis of Rock Fragmentation, 1996.
- [4] WipFrag, WipWare, Sampling and Analysis Guide, WipWare Technical Services, Canada



## MINE VENTILATION MODEL VALIDATION BY PQ SURVEY

Veljko Lapčević<sup>1</sup>, Toma Jovičić<sup>1</sup>, Slavko Torbica<sup>2</sup>

<sup>1</sup>University of Belgrade - Faculty of Mining and Geology, Đušina 7, 11000 Belgrade, Serbia

<sup>2</sup>Owl and Fox – Mining Consultants, Cara Dušana 67/3, 11000, Belgrade, Serbia

### Abstract

*Underground mine requires sufficient fresh air to be distributed to dilute exhaust fumes from diesel equipment and explosive detonation products. To do so, main mine fans are installed at one end of the ventilation system to provide sufficient pressure to initiate desired air movement. The installed fan is a massive power consumer, and its selection is based on the required air quantity and resistance of the ventilation network. Resistance of the network depends on the size of underground openings and their walls' friction, and the resistance's overall influence may impact fan power significantly. Underestimated resistance may result in a fan with insufficient power to provide desired air capacity for the mine, while the opposite case results in expensive fan operation. Besides this, during the operation of the fan, undesired vibrations may occur. During the design process, friction coefficients are determined by experience and designed type of underground openings, while operating mines are different cases. Such a case is analyzed within this paper, where a pressure and quantity survey was performed to determine the friction factors of the ventilation model. A study explained herein was conducted inside the concrete supported adit with regular shape along the opening. Results showed that measured resistance is within the expected range of literature-suggested values.*

**Keywords:** *underground mining, ventilation, PQ survey*

### 1. INTRODUCTION

Ventilation is an essential service in every underground mine, and the design of the air supply network must be done reliably to provide enough fresh air for safe operation. The main goal is to define the required power of the main fan that will provide enough pressure for air movement and proper air distribution. The air distribution within the network is defined with the mine design, and the end ventilation model will validate the mine design from this aspect. On the other hand, fan power depends on the required air quantity and resistance of the ventilation network. Resistance of the mine network is critical for proper fan selection and relies on the estimate or measurements of the friction factors of underground openings. Measuring wall friction factors is only possible if the mine is already operational, while in the design of the new mines, engineers must rely on empirical friction factor values suggested in the literature [1, 2]. Overestimated mine resistance leads to overestimated fan power and therefore increased energy consumption, while in the opposite situation, insufficient fan power may result in low pressure and air velocities below desired. A quantity survey has been done inside the concrete-lined adit to validate the commonly used friction factors pressure. The main idea is to increase the reliability of the ventilation model created with Ventsim [3] software and to define the main mine fan at the end of the process.

### 2. Methodology and survey results

Determination of the air resistance in certain underground openings is derived from the fundamental expression for pressure drop within that same opening [4]:



$$\Delta h = R \cdot Q^2 \quad (1)$$

where:

$\Delta h$  - pressure loss (Pa),  
 $R$  - airway resistance (Ns<sup>2</sup>/m<sup>8</sup>),  
 $Q$  - airflow (m<sup>3</sup>/s).

Airway resistance depends on the friction factor of its wall, length, perimeter, and the air's cross-sectional area. Therefore, equation 1 becomes:

$$\Delta h = k \cdot \frac{L \cdot O}{A^3} \cdot Q^2 \quad (2)$$

where:

$k$  - friction factor (kg/m<sup>3</sup>),  
 $L$  - airway length (m),  
 $O$  - perimeter (m).  
 $A$  - cross-section area of the airway (m<sup>2</sup>).

Airflow quantity is derived by measuring air velocity and adit cross sections at the exact location:

$$Q = w \cdot A \quad (3)$$

Where:

$w$  – Air velocity (m/s)

To confirm the friction factor, it is necessary to determine airflow and pressure loss within the airway and compare in-situ data with the model. Anemometer is used to determine air velocity, which determines airflow quantity within the airway. Along with this parameter, pressure loss is determined by a micromanometer. The measuring setup is illustrated in Figure 1 and consists of 2 Pitot tubes connected to the manometer using a PP tube of 6mm diameter. The Pitot tube is connected to measure total (static + dynamic) pressure. The length of the underground adit is approximately 980m, where two measurements were made at each 490m. Figure 2. illustrates measuring installation within the underground opening.

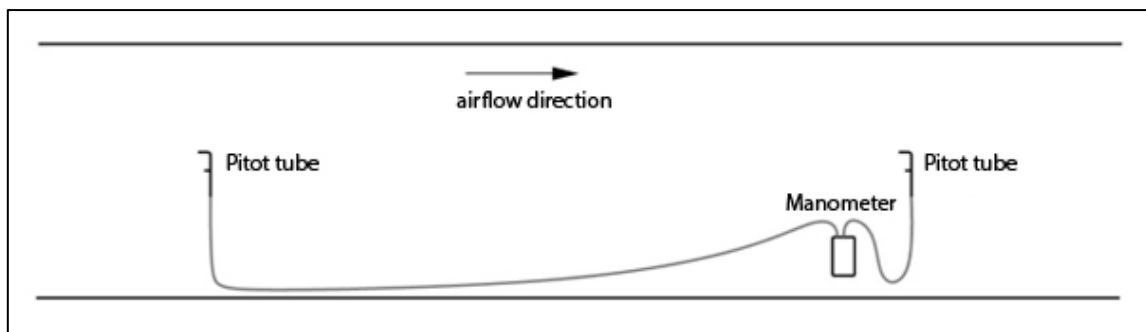


Figure 1 - Pressure loss measurement scheme



Figure 2 - Pitot's tube and tubing installation inside of the underground opening

Table 1 presents measurement results, and as can be seen, airflow velocity is constant in the adit. In contrast, the results air quantity has a slight difference due to the difference in the opening size at different locations. Total pressure loss is 5Pa for the entire length of the underground opening of 980m, resulting in airway resistance of  $0.19169 \text{ N s}^2/\text{m}^8$ . In Figure 3 Ventsim model of the same underground opening is presented with the results from the model. The model is created from the geodetic survey of the adit and has a constant cross-section with an area of  $5.1\text{m}^2$ . Therefore, constant airflow within the adit is modeled using the friction factor value suggested by literature for the concrete-lined underground openings. Results from the model show that total pressure loss is 5.8 Pa while total adit resistance is  $0.22150 \text{ N s}^2/\text{m}^8$ .

Table 1 - PQ survey results

No.	L (m)	$\Delta h$ (Pa)	W (m)	H (m)	A (m <sup>2</sup> )	Q (m <sup>3</sup> /s)	R (Ns <sup>2</sup> /m <sup>8</sup> )	V (m/s)													
1.00	490	3	2.28	2.31	<b>5.15</b>	<b>5.15</b>	0.112962	<b>1.00</b>													
			2.10	2.40					2.00	490	2	2.10	2.40	<b>5.04</b>	<b>5.04</b>	0.078735	<b>1.00</b>	2.10	2.40	<b>Total</b>	
2.00	490	2	2.10	2.40	<b>5.04</b>	<b>5.04</b>	0.078735	<b>1.00</b>													
			2.10	2.40					<b>Total</b>							0.191697					
<b>Total</b>							0.191697														

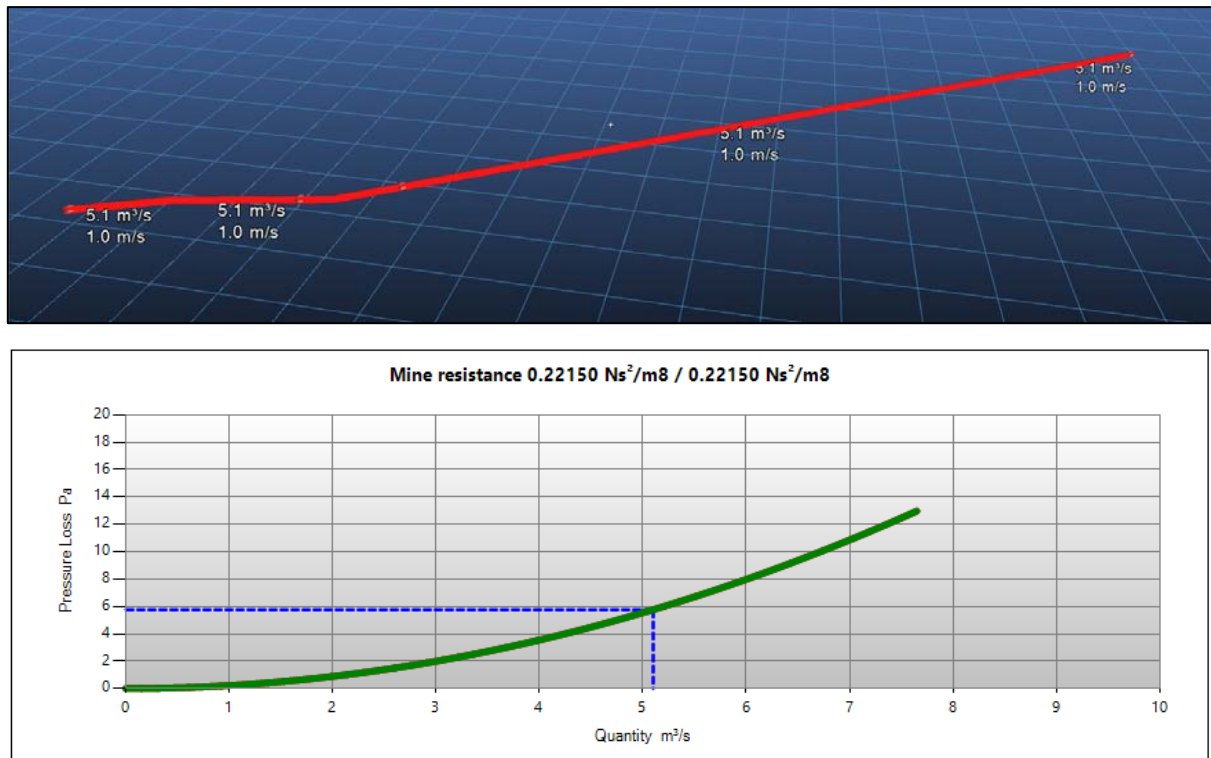


Figure 3 - Mine adit model in Ventsim and its results

### 3. CONCLUSION

Modeling mine ventilation is an essential task for mining engineers due to the health and safety impact of the fresh air supply and its distribution on the working environment. The work presented herein describes a simple and cost-effective procedure used to validate the ventilation motor to obtain results as reliably as possible. In-situ PQ measurements showed that literature-suggested values for the friction factors of the concrete-lined openings could be trusted since there is a 15% error between measured and estimated airway resistance. A reliable estimate of pressure loss in the ventilation network remains crucial for both newly designed and existing ventilation networks.

### REFERENCES

- [1] McPherson, M. J. Springer Science & Business Media, 2012, pp. 134-140.
- [2] Hartman, H.L., editor, "SME Mining Engineering Handbook," Published by The Society for Mining, Metallurgy, and Exploration, Inc., 1992, pp. 1052-1092.
- [3] Howden, Ventsim User Guide, Howden, undated.
- [4] AMC Consultants, Basic Mine Ventilation, AMC Consultants Pty Ltd, 2005, p. 62.

## LIFE CYCLE ANALYSIS (LCA) OF THE ASPHALT LAYERS CONTAINING THE RECYCLED ASPHALT PAVEMENT

Jelena Dorđević, Jelena Stefanović, Sandra Guševac, Ivan Jelić, Stefan Trujić

Mining and Metallurgy Institute Bor, Zelene bulevar 35, 19210 Bor, Serbia

### Abstract

*Rapid industrial development has led to an excessive consumption of natural resources and major environmental pollution. Every industrial sector has contributed to the increase in greenhouse gas emissions, leading to the accelerated global warming, which has become one of the leading problems in the world. Through an analysis of the life cycle, many researchers have come to the conclusion that the construction of road infrastructure is one of the main factors that contribute to the global warming in the field of construction, because during the production of raw materials, transportation, preparation and installation of mixtures, and later also during the exploitation of roads, maintenance, reconstruction and end of their life cycle, emits a significant amount of greenhouse gases. In this paper, the use of recycled asphalt pavement as a partial replacement of natural materials in asphalt mixtures was discussed and the life cycle of road constructions made of the aforementioned mixtures was analyzed. The results show that the extraction and production of natural materials have a great impact in the life cycle of the road construction. Due to this reason, the production of asphalt using recycled asphalt can be one of the ways of sustainable design of road constructions in terms of the environment improvement.*

**Keywords:** recycled asphalt pavement, LCA, asphalt mixture, environmental protection

### 1. INTRODUCTION

The Life Cycle Analysis (LCA) is one of the key tools used to develop the new and improve the characteristics of existing products. The LCA studies the aspects of the environmental protection and possible impacts on the environment during the entire life cycle of the products from the extraction of raw materials, through production, use and treatment at the end of the life cycle, recycling and final disposal, i.e., "from the cradle to the grave".

Using the LCA method, the researchers came to the result that each meter of built road annually causes the emission of greenhouse gases in the amount of 14.7 kg CO<sub>2</sub>eq, where the extraction phase and material production are the main processes that contribute to the total carbon emission and energy consumption [1].

This is the reason why the choice of materials for the road construction directly affects the local pollution and environmental degradation.

Aggregates are the main material used for the road construction. Asphalt concrete contains on average about 90% aggregates, 3% fillers, 2% additives and 5% binders, which means that the construction of one kilometer of a new road requires the consumption of about 30,000 tons of aggregates [1]. The production of asphalt binder is a complex process that involves the extraction, transportation and processing of crude oil. Each of the mentioned production stages involves the consumption of energy and burning of fossil fuels, which should not be ignored due to the emission the large amounts of harmful gases. These facts are another reason why the possibility of using alternative materials as a partial replacement of natural materials in the asphalt mixtures should be studied.

## **2. LIFE CYCLE ANALYSIS (LCA) OF THE ASPHALT ROADS CONTAINING THE RECYCLED ASPHALT**

Many researchers have investigated the possibility of using the recycled asphalt in asphalt mixtures and analyzed the life cycle of roads with recycled asphalt content. One of them is Joke Anthonissen [1], who, in his study, investigated the possibility of reducing the negative impact of bituminous roads on the environment in Flanders (Belgium).

The research was carried out in three directions: the possibility of using the recycled asphalt as a partial replacement of natural materials, lower energy consumption as a result of reducing the temperature of asphalt mixture production, and extending the life of road construction optimizing the mechanical properties of asphalt mixtures. In addition to these three basic aspects, the other impacts on the environment were also considered, such as: transport distances, moisture content in aggregates, energy consumption when making asphalt, etc.

The authors of this research came to the conclusion that the use of recycled asphalt in asphalt mixtures provides the significant environmental benefits due to the energy savings during material extraction and reduced transport distance. Recycled asphalt can be environmentally friendly if it is proven by the preliminary testing that it is not contaminated with tar [2].

The research has shown that the most favorable way of making asphalt mixtures in terms of energy saving is the production of asphalt mixture using the warm process (Warm Mix Asphalt - WMA) at temperature of 100°C to 150°C. This process can be accomplished in three ways: using the organic additives, chemical additives or water-based additives. The effect of all three types of technologies is to reduce the viscosity of bitumen in order to improve the workability of the asphalt mixture at lower temperatures [2].

The longer the service life of materials in pavement constructions, the less maintenance interventions are required, which means less consumption of materials and energy, less transport, and therefore less gas emissions. Therefore, the authors of the study paid attention to materials that are more sustainable and extend the life of road constructions. Polymer-modified bitumen, as a known type of binding material, has better properties compared to road bitumen, i.e., higher softening point, higher viscosity, higher cohesive strength or higher ductility, which results in higher resistance to rutting, fatigue and thermal cracks, and therefore the extended road life [2].

The addition of fibers is another technique to improve the mechanical properties of the asphalt mixture. Field and laboratory studies indicated that the bituminous mixture with polypropylene and aramid fibers had better properties in terms of resistance to permanent deformation, fatigue cracking and thermal cracking compared to the control mixture without fibers. The use of fibers is the subject of many research because it can contribute to a significant improvement in the mechanical characteristics of the asphalt roads [2].

Martina Irene Giani with a group of authors [3] also studied the impact of asphalt roads on the environment. The asphalt mixtures that are the subject of their study contain a certain percentage of recycled asphalt, as a partial replacement of natural material, and were made according to the method of production the warm asphalt mixtures (WMA). The aim of the study was to research whether the rehabilitation of the road base layer using the CIR technology (cold asphalt recycling in situ) can reduce the energy consumption and gas emissions and preserve natural resources [3].

In their research, the authors of the study included three types of road constructions RP1, RP2 and RP3 (Figures 1, 2 and 3) without the content of additives, but only with the content of bituminous emulsion consisting of about 45% water and 55% bitumen. The content of recycled asphalt, used instead of the new aggregate and bitumen, was between 10% and 30%.

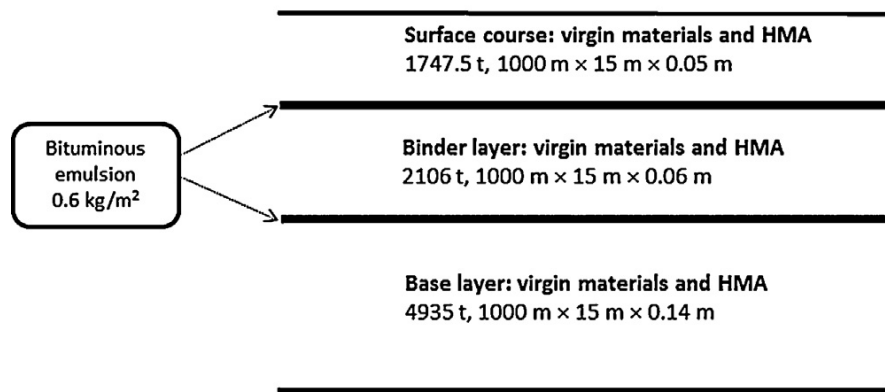


Figure 1 - Road constructions RP1 [3]

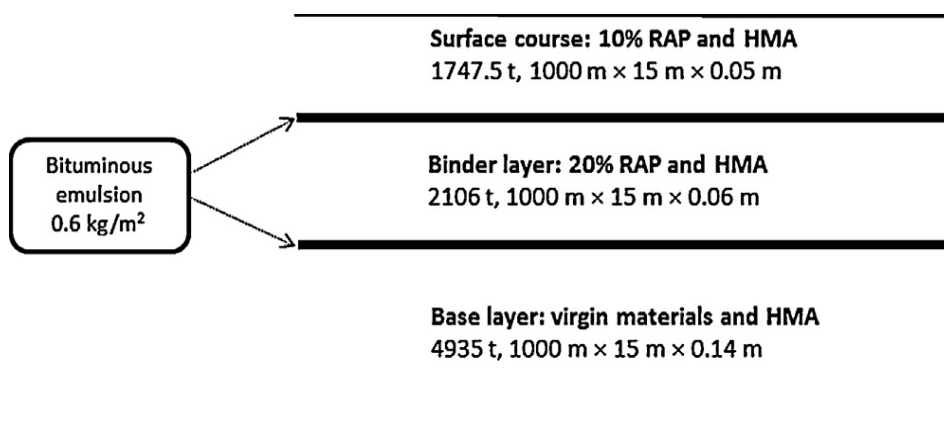


Figure 2 - Road constructions RP2 [3]

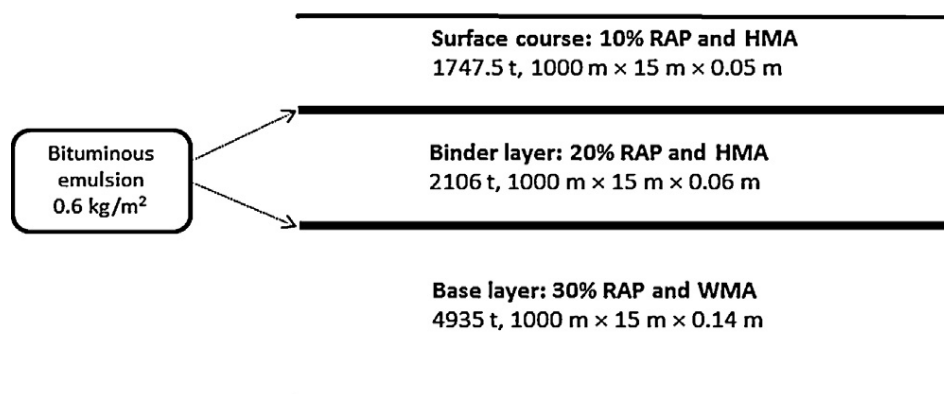


Figure 3 - Road constructions RP3 [3]

The analysis of life cycle of the road constructions RP1, RP2 and RP3 was carried out for a working life of 15 years, where the phases of extraction the raw materials, production of mixtures, installation of mixtures and transport were considered. The software used to perform the analysis was SimaPro 7.3. The impact of global warming is expressed in tons of CO<sub>2</sub> equivalent (CO<sub>2</sub>eq) and is shown in Figure 4. The results showed that the RP3 road construction is the most favorable in terms of environmental impact, so the authors devoted a part of the study to the life cycle analysis of the RP3 road construction for working life of 30 years, where they also included the reconstruction phase using the method of cold asphalt recycling in-situ and at the plant (Figure 4).



The road reconstruction, using the method of cold asphalt recycling in-situ, gave better results in terms of lower greenhouse gas emissions [3].

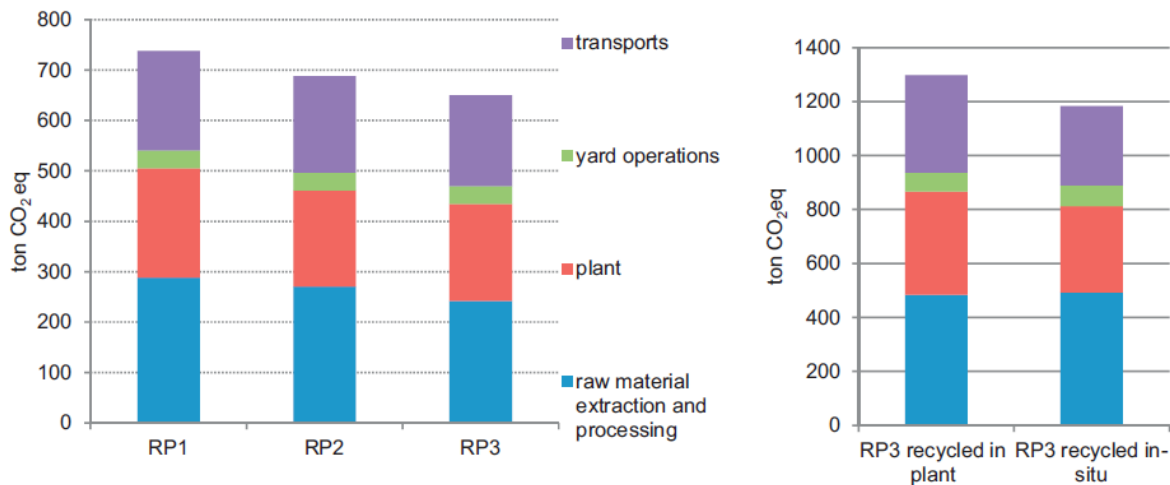


Figure 4 - CO<sub>2</sub> emission results for pavement structures RP1, RP2 and RP3 [3]

### 3. CONCLUSION

The results of studies show that the extraction and production of raw materials have a great impact on the life cycle of road construction. Due to this reason, the production of asphalt using recycled asphalt (which conserves the natural materials), together with greater savings in the production of the WMA mixtures, is the key to the sustainable design of the road constructions in terms of the environmental improvement.

### ACKNOWLEDGEMENTS

*The paper presents a part of research that was supported by the Ministry of Science, Technological Development and Innovation of the Republic of Serbia, registration number of the Contract 451-03-47/2023-01/ 200052.*

### REFERENCES

- [1] M. Díaz-Piloneta, M. Terrados-Cristos, J.V. Álvarez-Cabal, E. Vergara-González, *Materials*, 14 (13) (2003) 3587.
- [2] J. Anthonissen, W. V. D. Bergh, J. Braet, *Environ. Impact Assess. Rev.*, 60 (2016) 139-147.
- [3] M. I. Giani, G. Dotelli, N. Brandini, L. Zampori, *Resour. Conserv. Recycl.*, 104 A (2015) 224-238.
- [4] PRé Sustainability (2023) SimaPro. Available at: <https://simapro.com/> (Accessed 2 December 2022).



## OCCUPATIONAL INJURIES IN UNDERGROUND COAL MINING: STATISTICAL ANALYSIS OF DATA

**Jelena Ivaz, Dejan Petrović, Predrag Stolić, Mladen Radovanović,**

**Dragan Zlatanović, Saša Stojadinović, Pavle Stojković**

Technical Faculty Bor, University of Belgrade, V.J. 12, 19210 Bor, Serbia

### **Abstract**

*For employers, occupational accidents are the biggest problem in occupational safety and health. In underground coal mines, where a large number of injuries occur, this problem is even more significant. In order to find a suitable model for the analysis and prediction of occupational accidents, data collection research was conducted in underground coal mines in Serbia. This research took the form of statistical data collection and data collection using a questionnaire. A total of 1051 correctly completed questions were collected from the population of production workers. The descriptive statistics used to process the collected data revealed a central problem related to the safety and health of workers.*

**Keywords:** injury, coal mine, statistics

### **1. INTRODUCTION**

One of the biggest problems related to occupational safety and health in the mining industry is workplace accidents. This industry, along with construction, is known as the one with the highest number of injuries. There are several models that describe the problem of injuries and the actions that need to be taken to reduce the number of injuries. However, the factors that influence occupational injuries are not clearly defined.

Considering the multidisciplinary nature of the research conducted, the empirical research method was selected as the most appropriate method for data collection using a questionnaire. The proposed method of analysis is based on the collection of data on workers and injuries that occurred in underground coal mines. The data in the observed sample are collected using a questionnaire. The questionnaire contains all the questions that the author considers relevant to the injury of workers in the mines of Serbia, as well as the questions available in the literature [1, 2, 3, 4]. The procedure consists in interviewing the workers in a given mine. Then, the data obtained from the interviews are statistically processed and sorted by categories.

In order to better understand the collected data and its structure, and to discover regularities in the tendencies of the observed variables, descriptive statistics was applied. The basic statistical indicators of descriptive statistics were calculated: Measures of central tendency (mean, mode and median) and measures of dispersion (standard deviation, variance), as well as the display of frequencies and percentages of the collected data.

After collecting, processing and classifying the data obtained by interviewing the workers, descriptive statistics methods were applied. Based on descriptive statistics, basic statistical indicators were calculated, which were used to determine the dependencies between subjects (frequencies and percentages, arithmetic mean, standard deviation, etc.) in order to create a preliminary picture of the data collected.

The Statistical Package for the Social Sciences (SPSS) software package, version 17.00, was used for data processing. SPSS is a very powerful package that many researchers use to process a large amount of data.

## 2. EXPERIMENTAL

Data collected at the Resavica Underground Coal Mining Public Company (JP PEU Resavica) were used for this study. In addition to the downloaded data on workplace injuries, a survey was conducted among workers to determine the factors influencing the occurrence of workplace injuries. A total of 1051 correctly completed questionnaires were analysed.

Table 2 shows (in percentage and numerical terms) the demographic characteristics of the entire sample in the following categories: Sex, age, total calendar work experience, total work experience at current job, and worker qualification or occupational skill.

Table 1 – Demographic characteristics of the tested sample

Demographic parameter	Category	Frequency	Percentage %
Paul	Male	981	93,3
	Female	70	6,70
Age	18–25	82	7,80
	26 –35	278	26,5
	36 –45	307	29,2
	46–55	265	25,2
	56–65	119	11,30
Total calendar work experience	≤ 10	450	42,8
	11–15	160	15,2
	16–20	105	10,0
	21–25	124	11,8
	26–35	212	20,2
Total work experience in the current workplace	≤ 10	720	68,5
	11–15	111	10,6
	16–20	66	6,30
	21–25	55	5,20
	26–35	99	9,40
Qualification/professional qualifications	Unqualified	308	29,3
	Qualified	473	45,0
	High school diploma	225	21,4
	University degree	39	3,70
	Master's degree and	6	0,60
	doctorate		

If we look at the data on the gender of the respondents, shown in Table 1, we can see that 93.3% of the respondents are male, while only 6.7% are female. This is certainly to be expected in mining companies, where even at the global level, the percentage of women employed does not exceed 10%.

The following demographic parameter of the respondents - age - shows that the largest number of respondents is found in the 36-45 years category (29.2%), while the lowest percentage is in the youngest category 18-25 years (7.8%). The oldest employees are also represented by a very low percentage of 11.3%.

The data on total years of service show that the highest percentage of workers belongs to the group of workers with the least work experience (≤ 10 years) - 42.8%, followed by the group of workers with the most years of service (26-35) - 20.2%. A similar distribution is found in the category of total seniority in the current workplace, where 68.5% of workers have been working in the current workplace for less than 10 years. The population of the younger generation that should have the least work experience is represented by a small percentage. The data that 40% of workers have

less than 10 years of work experience indicate that mines employ older groups of workers with little or no experience, suggesting that miners are hired in their later years rather than immediately after graduation from high school.

The data on the categories of qualifications or professional degrees show that most respondents belonged to the second category, i.e. qualified is 45.00%, followed by those with the lowest education - unqualified (29.3%), followed by secondary education (21.4%), a university degree (3.7%) and a master's or doctorate (0.60%). Since most mining technology in Serbia is not mechanised, skilled and unskilled workers are the labour force that drives production itself. The selected representative sample describes very well the actual qualification structure in JP PEU Resavica, in 2019. PEU Resavica, has the following qualification structure of employees: KV - qualified (48.21%), NK - unqualified (29.37%), SSS - secondary school degree (17.22%), VSS - university degree and Ms/Phd - master degree and doctorate have in total (5.17%).

### 3. RESULTS AND DISCUSSION

For variables within each group of questions, Table 2 shows the basic indicators of descriptive statistics: measures of central tendency (mean, mode and median) and dispersion measures (standard deviation, variance).

Table 2 - Descriptive response statistics of respondents

Encrypted Question Name	Median	Modus	Mean	Standard deviation	Variance
PPE_1	5	5	4,75	0,743	0,552
PPE_2	4	4	4,01	1,169	1,367
PPE_3	4	4	3,83	1,499	2,247
PPE_4	5	5	4,32	1,087	1,181
PPE_5	5	5	4,66	0,761	0,580
WEM_1	5	4	4,23	1,217	1,482
WEM_2	5	4	4,28	1,121	1,258
WEM_3	5	5	4,21	1,176	1,383
WEM_4	4	4	3,43	1,428	2,040
WE_1	5	4	4,32	1,087	1,181
WE_2	5	5	4,50	0,886	0,785
WE_3	5	5	4,32	1,087	1,181
WE_4	5	5	4,29	1,106	1,223
WE_5	4	3	3,66	1,494	2,231
M_1	5	4	4,27	1,148	1,318
M_2	5	4	4,21	1,234	1,522
M_3	5	4	4,20	1,195	1,429
M_4	5	4	4,43	0,986	0,973
M_5	5	4	4,24	1,212	1,470
OR_1	5	4	4,29	1,055	1,114
OR_2	5	5	4,38	1,039	1,079
OR_4	4	4	4,04	1,165	1,358
T_1	5	5	4,61	0,895	0,800
T_2	5	4	4,34	1,034	1,069
T_3	5	5	4,58	0,924	0,853

The data presented in Table 2 show that the workers studied gave the highest score to the question PPE\_1 - I believe that personal protective equipment is necessary for work at my workplace (4.75). Workers recognized the importance of PPE and have a positive attitude towards it. Personal protective equipment plays an important role in the event of an injury - this refers to both preventing injury and providing protection when the injury occurs - with personal protective equipment influencing the severity of the injury. In addition to its role in preventing injury, personal protective equipment also has an impact on reducing occupational illness, chronic disease, and work comfort. The lowest rated question was WEM\_4 - The conditions of the work environment (temperature, humidity, dust...) are satisfactory (I feel comfortable at work) (3.43). It is obvious that the conditions of the working environment in mines are not satisfactory, while the negative conditions of the working environment in underground mines are even more pronounced. Confined spaces, working underground, artificial ventilation, etc. contribute to a poor rating of this issue.

#### **4. CONCLUSION**

The conducted analysis of the collected data in the population of productive workers in underground coal mining in Serbia has highlighted certain indicators of safety and health at work as those to which workers attach the greatest importance. Among the workers with the highest rating, i.e. as positively most important, was the issue of the use of personal protective equipment, indicating a high level of awareness among workers regarding the use of personal protective equipment at work. The issue of working conditions was also rated among the lowest, indicating that workers are aware of poor working conditions and the resulting hazards. Working conditions are in fact a factor created not by workers but by mine management, which should be considered another weakness of the OHS system in mines.

#### **REFERENCES**

- [1] B. Kunar, A. Bhattacharjee, N. Chau, J. South. Afr. Inst. Min. Metall., 110, 2010, 1–9.
- [2] Y. Lu, L. Taksa, H. Jia, Saf. Sci. , 132, 2020, 104947.
- [3] M. Elenge, Leveque, A. Brower, 2013. Int. J. Occup. Med. Environ. Health , 26, 2013, 267-274
- [4] M. Ajith, A.K. Ghosh, 2019. Saf. Sci., 118, 2019, 212–220.

## PREDICTION OF METHANE EMISSIONS IN COALMINE – SOKO

**Jelena Ivaz, Dejan Petrović, Mladen Radovanović, Dragan Zlatanović**

**Saša Stojadinović, Pavle Stojković**

Technical Faculty Bor, University of Belgrade, V.J. 12, 19210 Bor, Serbia

### **Abstract**

*Methane in underground mines represents a high level of risk from the aspect of safety and health at work, namely the explosion of this gas is one of the most common causes of major disasters in coal underground mines. The consequences of these accidents are a large number of injured workers as well as material damage, and very often the shutdown of the mines themselves. Methane also has a negative effect on the atmosphere because it creates a greenhouse effect. However, methane, in addition to its negative effects, is also used in the chemical industry as an energy source for mass consumption. The paper presents a method for predicting methane emissions based on an artificial neural network (ANN). The model was created for ten years of data on the amount of methane in the exhaust air for ventilation in the underground coal mine - Soko. This method can very accurately predict methane emissions in coal mines. Data on methane emissions have multiple benefits for mines because they enable the prevention of major disasters in mines, as well as the potential exploitation of methane, which would reduce the negative impact on the environment.*

**Keywords:** neural network, methane, coal mine, prediction.

### **1. INTRODUCTION**

Globally, the largest amounts of methane are produced in countries with leading coal exploitation such as China, India, Russia, etc., [1]. Underground coal mines in Serbia do not have methane drainage systems from deposits, so methane is released into a free atmosphere exclusively through a ventilation network. The amount of methane released into the atmosphere poses a serious threat to the environment. Methane is known to take far less time to decompose in the atmosphere, but compared to carbon dioxide, it can accumulate 84 times more heat, making it a potentially more dangerous greenhouse gas. The underground exploitation of coal releases most of the methane through the ventilation network, and these parameters must be checked daily,[3]. This gas poses a special danger to the safety of miners primarily because of its propensity to explode, and is the cause of the biggest accidents that have occurred in underground coal mines in Serbia in the last 50 years.

The Artificial Neural Network (ANN) or shorter neural networks are often used as a substitute for statistical data processing methods, primarily because they do not require extensive calculations and large databases, [5]. They are most commonly used to solve and quickly process problems that have an uncertain result and when there are a large number of variable sizes that affect the end outcome. They successfully solve problems of prediction, classification, recognition, approximation, optimization, etc. An artificial neural network is a system of connected neurons that communicate with each other through their connections. Neurons are very simple processing elements and their role is to process the signal they receive from the environment or other neurons. The signals exchanged by neurons extend along connections that have their numerical weights (weight coefficients). Numerical weights change during the learning process and, based on them, the network builds its ability to independently learn and generalize the nature of a phenomenon, [6].

## 2. EXPERIMENTAL

The Soko brown coal mine is located in the Eastern part of Serbia and operates within the company for underground coal mining JP PEU Resavica. The average ten-year production of the mine is 89,300.00 tons of commercial coal. Coal mining in this pit dates back to 1898 to the present day. The cave survived several disasters where a large number of workers were killed, the last recorded occurred on 01.04.2022., when as a result of methane choking, eight workers were killed and nineteen were injured. The pit is characterized as a high-risk pit i.e. the one that works in a special protection regime, however, despite all the measures carried out accidents resulting from the ever-present methane are still happening.

For obtaining data, the adroit computer application is used as part of the ADK (automatic remote control) system of gas-ventilation parameters (for data processing). Within the ADK system, in addition to measuring devices for the control of other gas ventilation parameters, measuring devices for continuous monitoring of methane concentrations in the characteristic locations in the pit have been installed. One of the measuring devices is placed on the path of the total main output of the air current at the V.O. shaft on k+240 (detector SN4-25). The measurement of the amount of methane released into the atmosphere via the output air current is carried out daily and the data are published in the form of reports on a monthly and annual basis. For the purpose of this paper, twenty-year data on the released amount of methane are attached, the same are shown in Table 1.

Table 1 – Average annual absolute methane emission rate (m<sup>3</sup>/min) Soko

Years	Average annual absolute methane emission rate (m <sup>3</sup> /min)
2001	4,39
2002	4,2
2003	3,6
2004	3,6
2005	1,86
2006	5,04
2007	4,29
2008	5,19
2009	2,59
2010	6,46
2011	6,59
2012	6,59
2013	4,39
2014	2,72
2015	2,71
2016	5,71
2017	5,71
2018	0,53
2019	1,88
2020	1,28
2021	1,76
Average of 20-year absolute methane emission rate (m <sup>3</sup> /min)	<b>4,05</b>

Data from the table indicate that the highest absolute absolute methane emission rate in the observed period was recorded in 2011, while the minimum value of this parameter was recorded in 2018, it is also noted that the mean value in the last twenty years was 4.05m<sup>3</sup>/min.

### 3. RESULTS AND DISCUSSION

For the purpose of modeling the problem of predicting absolute methane emission rate, feed forward back propagation neural network was created, the architecture of which is shown in Figure 1. The created network involves an architecture consisting of two layers, has 10 neurons in its hidden layer, while in the output it uses only 2. ANN uses the most commonly used learning rule for the created ANN Levenberg -Marquardt backpropagation procedure (LMBP).

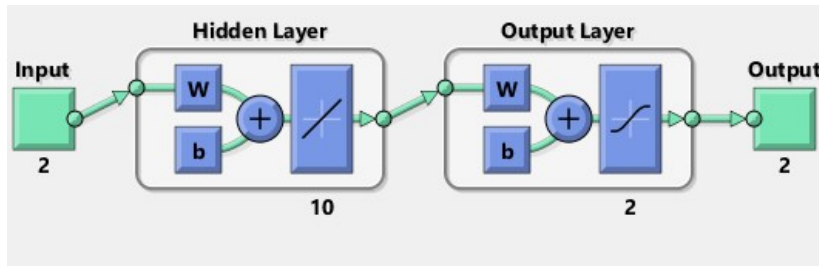


Figure 1 - Schematic representation of feed forward back propagation neural network

The previously collected data, a set of a total of 20 measured absolute CH<sub>4</sub> values, were processed in the network described above. According to predefined parameters, 75% of the data was used for network training, while 15% was used for validation and testing. After network was trained, the regression results shown in Figure 2 were obtained.

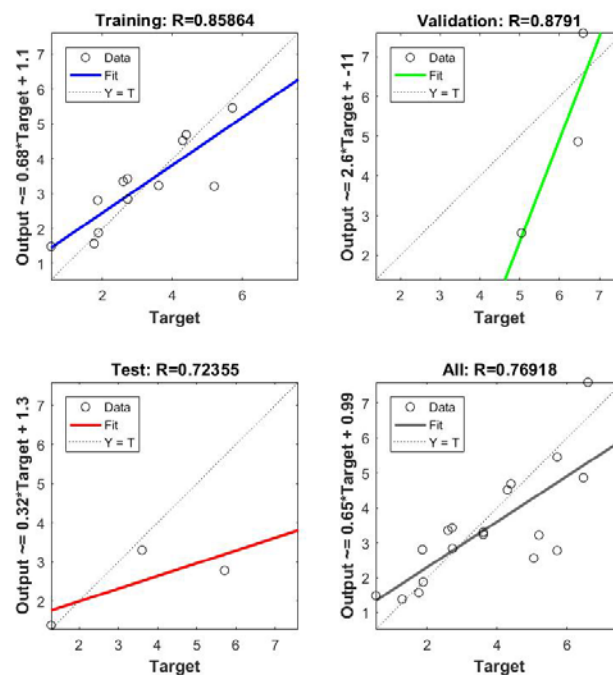


Figure 2 - Results of the regression analysis for feed forward back propagation neural network

Figure 2 shows the results of each phase of the network. From the figure, it can be seen that R is very close to unity, indicating good network performance.

The quality of the prediction of a given network implies how accurate it is, i.e., how large is the absolute difference between the values of the predicted quantities and those actually measured. Figure 3 shows the measured and predicted values for a period of 20 years.



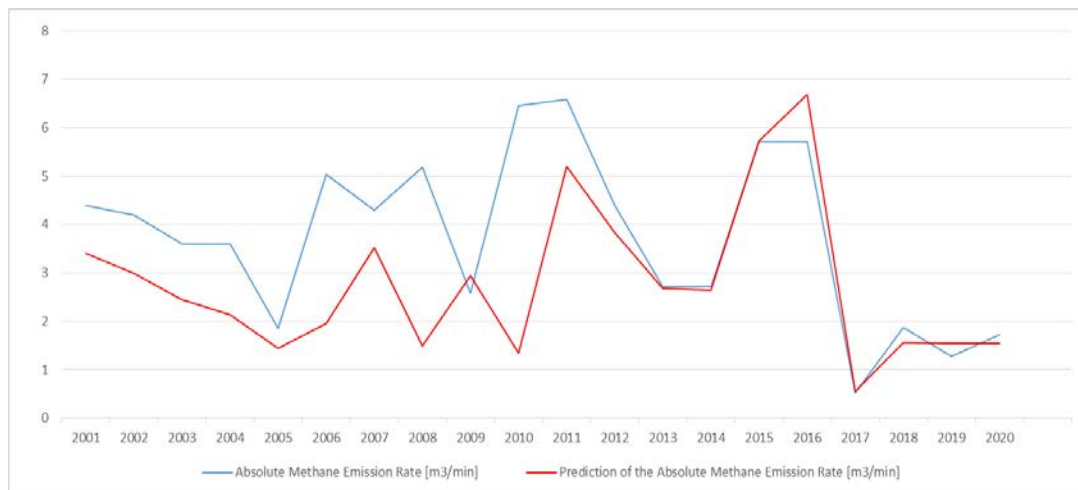


Figure 3 - Comparison of measured and predicted value of absolute methane emission rate

The graphs show that the network predicted significantly lower values of absolute methane mobility for certain parameters that faithfully describe the trend of movement of certain quantities. The largest error was shown for the year 2010, where the measured value was 6.46 m<sup>3</sup>/min, while the network predicted a value of 1.35 m<sup>3</sup>/min. The network predicted the value of absolute methane emission rate for 2015, for which the absolute error is only 0.02.

#### 4. CONCLUSION

The model is based on data measured in the value of the absolute methane emission rate over the period from 2001 to 2021 at the Soko mine. The mine itself emits significant amounts of methane, which can have a negative impact on the ecology, but most importantly, methane poses a major risk to mine workers. For these reasons, it is important to predict methane emissions so that the occupational safety and health system in underground coal mines can be improved and disasters can be prevented. The presented model based on artificial neural networks can be used to predict the value of absolute methane emission rate because it describes this phenomenon with satisfactory accuracy. To make the model even more accurate, it is necessary to include a larger number of input variables, i.e. to use data obtained on a monthly or daily basis.

#### REFERENCES

- [1] J. Swolkień, *Int. J. Greenh. Gas Control*, 94 (2020) 102921.
- [2] UN Climate Change Conference UK 2021, <https://ukcop26.org/uk-at-cop27/>.
- [3] M. Tutak, J. Brodny, *Energies* 2019, 12, 3840.
- [4] J. Ivaz, S. Stojadinović, D. Petrović, P. Stojković, *Int. J. Inj. Contr. Saf. Promot.*, 27(3), (2020) 362 – 377.
- [5] I. Ćirić, 2015. *Inteligentno upravljanje mobilnim robotima na osnovu neuro-fazi-genetskog prepoznavanja objekata i praćenja ljudi u robotskoj viziji*. Doktorska disertacija. Niš: Univerzitet u Nišu, Mašinski fakultet.
- [5] M. Vuković, Z. Miljković, 2014. *Mašinsko učenje veštačke neuronske mreže sa radikalnom aktivacionom funkcijom Gausovog tipa na bazi Kalmanovog filtera – Teorijske osnove*. *Tehnika – Mašinstvo*, 63, pp. 613–622.

---

## RECOVERY OF METALLIC FRACTIONS FROM MEDICAL PRODUCTS LABELLED FOR SINGLE USE

C. Prochaska<sup>1</sup>, E. Kokkinos<sup>1</sup>, D. Merachtsaki<sup>1</sup>, A. Lampou<sup>1</sup>, E. Peleka<sup>1</sup>,  
K. Simeonidis<sup>3</sup>, G. Vourlias<sup>3</sup>, A. Zouboulis<sup>1</sup>

<sup>1</sup>Laboratory of Chemical and Environmental Technology, Department of Chemistry, Faculty of Sciences, Aristotle University of Thessaloniki, Thessaloniki, 54124, Greece

<sup>3</sup>Department of Physics, Aristotle University of Thessaloniki, Thessaloniki, 54124, Greece

### Abstract

*Limited research has been made so far regarding technological approaches for the recovery of precious metals such as Pt and Ir from single-use medical products such as electrophysiology catheters, with most, if not all, of their quantity being discarded as medical waste. In this study, we investigate a commercial diagnostic electrode catheter which is widely used in medical practice, for its metallic fraction recovery. The process under investigation involves pyrolysis at a temperature of 550°C for 60 min. The recovery of the precious metals is determined through Scanning Electron Microscopy with Energy Dispersive Spectroscopy (SEM/EDS) and X-ray photoelectron spectroscopy (XPS) analyses of the samples before and after treatment. It was found that the transfer of precious metals (Pt and Ir) was >90 % in the metal fraction, without significant changes in the structure of the metals. It is within the aims of this study, conducted under the framework of a granted research project, co-funded by Greece and the European Regional Development Fund, that brings together a research consortium consisting of a business, a hospital, and university, to serve as the basis for providing a solution for efficient management of such medical wastes and metallic fraction recovery and provide motivation towards sustainable practices in a field that so far lacks engagement and demands changes at the local, institutional, regulatory, and industry level, before sustainable practices can be established.*

**Keywords:** (metal recovery, pyrolysis, single use medical products).

### 1. INTRODUCTION

Among various single-use medical products, an alloy of Pt and Ir, is contained in cardiac electrophysiology catheters. Up to now the prevailing culture with respect to such single-use medical products is to discard them to medical wastes directly after the medical procedure is over. Considering that the number of such procedures is raising worldwide, metal recovery from such medical wastes provides an opportunity to conserve precious metals and ease the burden on ore mining. Therefore, the development of an eco-friendly approach for the recovery of such metallic fractions is a necessity.

As these single-use products translate not only into the precious metals of interest but also into plastics, chemical-free pyrolysis of such wastes, carried out at temperatures of 500–600°C, which is a relatively low-temperature range, provides an environmentally attractive option that can also help in enhancing the separation of the metallic fractions of interest. The additional economic benefit of recovering precious metals from medical waste may mitigate the higher initial economic cost of investment in a pyrolysis unit (30-50% higher than an incineration unit) [1] which is still one of the main obstacles to its promotion.

To the best of our knowledge, no integrated study has been reported so far, for both pyrolysis of plastic materials and recovery of metallic fractions from medical products. However, results from Jadhao et al. (2020) [2] studying the recovery of Au and Pt (among other metals) from electronic wastes and specifically from printed circuit boards, which are major parts of electronic and electrical equipment, applied slow pyrolysis in a temperature range of 200–600°C, for 10–60

minutes. In their experiments, they used fragments of the waste weighing 5 g and 1 mm in size. Under optimized operating conditions, at a pyrolysis temperature of 400°C and a pyrolysis time of 20 min, 35 wt% gas, and 60 wt% solid product were obtained. The solid product was a mixture of metals and other solid residues. The transfer of the metals of interest to the present research project, i.e. Pt, to the solid residue, after pyrolysis, was approximately 100%. Su et al. (2021) [1] also reported that the basic materials of medical wastes undergo pyrolysis sequentially with increasing pyrolysis temperature as follows: rubbers, plastics, proteins, cellulose, and synthetic fibers. The maximum pyrolysis temperature of all samples was in the range of 370 – 520°C. Keeping the samples in the reactor for 60 minutes after reaching the maximum pyrolysis temperature ensures the complete decomposition of the plastic items, since after 60 min no other gaseous products are recovered, corresponding pyrolysis times are also noted in previous studies [3]. Given that the weight loss of most samples reached 80%, it becomes clear that pyrolysis technology can also drastically reduce the volume of medical waste.

Combining the above data, it is therefore interesting, in the context of this research, to study the effect of pyrolysis on the recovery of the metals of interest, from a selected type of medical material which is typically used and in considerable quantities in hospitals, as it appears that, on the one hand, pyrolysis is an attractive alternative to incineration/sterilization for the management of medical wastes, and on the other hand, that with pyrolysis it may be possible to transfer valuable metals from the original medical wastes to the solid pyrolytic residue at a high rate. It is within the aims of this study, conducted with the participation of a public Greek hospital, under the framework of a granted research project, co-funded by Greece and the European Regional Development Fund, to serve as the basis for providing a solution for efficient management of such medical wastes and metallic fraction recovery and provide motivation towards sustainable practices.

## **2. EXPERIMENTAL**

For the pyrolysis, a digital laboratory muffle furnace FHX-05, 1670 W WITEG with a capacity of 4.5 l, with ceramic insulation, maximum temperature up to 1200°C, with a temperature rise rate of 30/min, and with gas extraction was used. The experiments were carried out by placing the samples to be pyrolyzed in porcelain capsules, with a capacity of 30 ml, and covering the capsules with corresponding porcelain lids. The porcelain lids ensure the minimization of the amount of oxygen inside the capsule, in order to escape the gases produced during pyrolysis, capsule and lid do not close hermetically and airtight, but there are small escape points. The process under investigation involved pyrolysis at a temperature of 550°C, for 60 min. Fragments of the following medical product was used for pyrolysis experiments: Diagnostic catheter Boston Scientific Viking catheter, M00440000406Fr, metals of interest: Pt/Ir (Figure 1 a, b). The JEOL JSM-7610F Plus Scanning Electron Microscope (SEM), with integrated X-ray Energy Dispersive Spectrometer and Oxford Instruments AZTEC analytical system was used in the present study to acquire SEM images of the sample before and after pyrolysis. X-ray photoelectron spectroscopy (XPS) measurements were performed before and after pyrolysis experiments. Measurements were performed on an Axis Ultra DLD system from KRATOS. Monochromatic Al Ka radiation was used as an X-ray source. The pass energy was kept constant at 40 eV. It was calibrated for charge-induced shifts, considering the C1s peak (originating from surface contamination of carbon) to be at 284.6 eV.

## **3. RESULTS AND DISCUSSION**

As seen from Figure 1 c, pyrolysis removed the purple plastic cover, 53.63% mass loss (Table 1) and revealed the supporting stainless steel grid, leaving few plastic residuals on the grid. The ring containing the Pt/Ir alloy of interest was macroscopically unaffected.

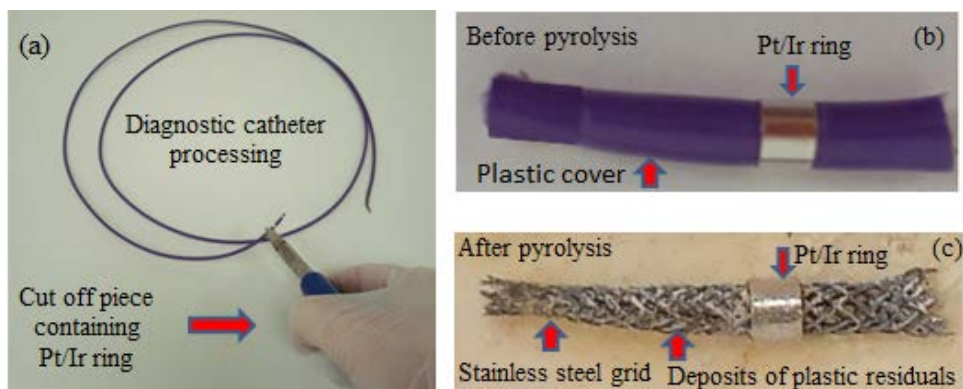


Figure 1 - (a) Cut off catheter fragment, (b) Catheter fragment before pyrolysis (c) Catheter fragment after pyrolysis

Table 1 – Results from pyrolysis experiment (550°C, for 60 min).

Medical product	Solid residual (%)	Mass loss (%)
Diagnostic catheter, metals of interest: Pt/Ir	46.36	53.63

SEM images of Pt/Ir alloy on the catheter ring, before and after pyrolysis are presented in Table 2.

Table 2 – SEM images of Pt/Ir ring before and after pyrolysis experiment

Before pyrolysis	After pyrolysis

SEM images of the surface of the Pt/Ir alloy rings revealed a quite smooth morphology with few surface scratches attributed to the metallurgical production process before and after pyrolysis. The percentage of Ir in the alloy was estimated by EDS spectroscopy close to 14% before and after pyrolysis, while Pt content was measured higher after pyrolysis, due to the removal of the outer polymeric layer of the material after pyrolysis.

Results from XPS measurements for Pt/Ir alloy of the catheter ring, before and after the pyrolysis experiment are presented in Figure 2. Pt showed the smallest percentage increase of oxidized forms of Pt(II) 1.7-4.4% (Figure 2 a-b), compared to the non-pyrolyzed material, while peaks at 73.012 and 76.495 eV, attributed to Pt(IV), appeared after pyrolysis. For Ir the percentage content was measured at 14%, while an increase of the oxidized forms of Ir (II) was higher 13-13.3% (Figure 2 c-d). It is clarified that oxidized forms of the metals were identified during the characterization of the starting, commercially available, material, while the manufacturer labels the product as a Pt/Ir alloy, containing 10% of Ir.

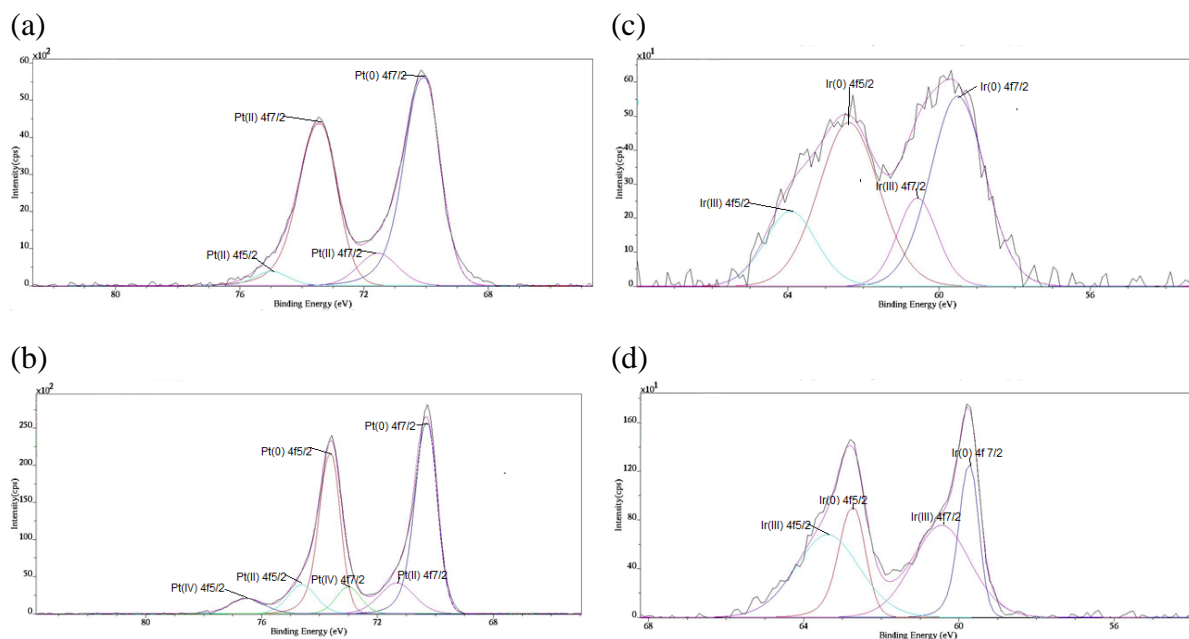


Figure 2 – XPS measurements for Pt and Ir on the catheter Pt/Ir ring. (a)-(b) Pt before and after pyrolysis, (c)-(d) Ir before and after the pyrolysis.

#### 4. CONCLUSIONS

In the field of technological approaches that can be applied to the management of the specific medical wastes, the results of the preliminary pyrolysis experiments presented here, are encouraging, as after pyrolysis the Pt/Ir alloy was separated from its outer polymeric layer of the material, otherwise difficult to be accomplished, and the transfer of the Pt/Ir alloy in the metal fraction was >90 %, without significant changes in the structure of the metals. The recovery of metals from medical products considered in this research, stands as a basis to enhance knowledge of the effective perspectives for the utilization of such wastes as a resource, as the recovered metallic fractions can act as the feedstock for the efficient recovery of individual metals using e.g. different leaching processes. Nevertheless, much more research is needed to realize the valorisation of pyrolysis for the particular medical wastes.

#### ACKNOWLEDGEMENTS

*The project «Collection, processing and metallurgical recovery of critical raw materials (Au, Pt, Ir, Ta) from discarded medical material» (Project code: KMP6-0084436) was implemented under the framework of the Action «Investment Plans of Innovation» of the Operational Program «Central Macedonia 2014 2020», that is co-funded by the European Regional Development Fund and Greece.*

#### REFERENCES

- [1] G. Su, H. C. Ong, S. Ibrahim, I. M. R. Fattah, M. Mofijur, and C. T. Chong, *Environ. Pollut.*, 279, 2021 1-13.
- [2] P. R. Jadhao, E. Ahmad, K. K. Pant, and K. D. P. Nigam, *Waste Manag.*, 118, 2020 150–160.
- [3] S. K. Tulashie, E. K. Boadu, and S. Dapaah, *Therm. Sci. Eng. Prog.*, 11, 2019 417-424.

## ANALYSIS OF GROSS ALPHA AND GROSS BETA ACTIVITY IN SAMPLES AROUND FORMER URANIUM MINE GABROVNICA

Nataša Sarap, Marija Janković, Vojislav Stanić, Ivana Jelić, Marija Šljivić-Ivanović

Vinča Institute of Nuclear Sciences, National Institute of the Republic of Serbia, University of Belgrade, Radiation and Environmental Protection Department, Mike Petrovića Alasa 12-14, 11001 Belgrade, Serbia

### Abstract

*Gabrovnica, uranium mine near Kalna in the Eastern Serbia was a natural ore with uranium content. Exploitation of the uranium ore in this region was started in the 1960s and it was terminated in 1996. The aim of this work was to analyze radiological characterization of environmental samples around uranium mine Gabrovnica. Soil samples were taken in the autumn of 2022 and spring 2023, while surface soil samples (Gabrovnicka River) were taken continuously for six month (July-December 2022 and January-June 2023). All samples were analyzed in order to determine gross alpha and gross beta activities and measured on ultra low level gas proportional counter Thermo-Eberline FHT 770T.*

**Keywords:** *Gabrovnica; environmental samples; gross alpha and gross beta activity*

### 1. INTRODUCTION

Exploitation of the uranium ore was started in the 1960s in the region of Stara Planina Mountain (Eastern Serbia) in the vicinity of the Bulgarian border. The first investigated location was Aldina reka, while in 1951 uranium ore occurrences were discovered in Mezdreja. Uranium ore exploitation was carried out in three uranium mines: Mezdreja, Srneći Do and Gabrovnica. The area surrounding the town of Kalna on Stara Planina Mountain represents a location characterized by the increased content of natural radionuclides. Gabrovnica is situated north from Mezdreja, on the left side of the Gabrovnicka River at about 1.5 km from its running into the Timok River [1]. Gabrovnicka River is the right tributary of the Trgoviški Timok [2]. The Gabrovnica mine had a plant processing about 200 t/day of ore [1].

Knowledge of impacts on the natural environment from uranium mining in general, is essential. An assessment of impact in terms of contaminated soil, surface water, groundwater, lake sediments, etc. or activity levels and doses are very important and directly linked to potential uptake of radionuclides by humans, principally from soils and water. Radionuclides could be taken up and concentrated by plants in the vicinity, thereby posing a potential risk to vegetation as well as to animals higher in the food chain, including humans [3].

Various methodological procedures were applied in order to determine the contamination of waters in the area of the abandoned mines (geoecological, radiological, geochemical and hydro chemical investigations were carried out in the study area). In order to analyze radioactivity contents of natural radionuclides, gamma spectrometry were applied [4-6]. In that case, it is possible to determine the concentrations of individual radionuclides present in environmental samples. It is not known whether gross alpha and gross beta activity was analyzed in soil and water samples in the vicinity of Gabrovnica mine, which is the aim of this paper.

### 2. EXPERIMENTAL

Soil sampling was carried out in the immediate vicinity of former mine Gabrovnica (Hydrometallurgical plant) (43° 26' 25" N and 22° 25' 30" E) using the method of representative



samples, from three depths: surface layer 0-5 cm, 5-10 cm and 10-15 cm during October 2022 and April 2023.

Surface water samples from Gabrovnická River were sampling once a month and the analysis was done in a composite six-month sample. Sampling were done upstream of the Hydrometallurgical plant (43° 26' 32" N and 22° 25' 40" E) and downstream of the Hydrometallurgical plant (43° 26' 24" N and 22° 25' 29" E) during the period July-December 2022 and January-July 2023.

Soil sample preparation includes cleaning from grass and stones, and samples were dried in the oven at the temperature of 105°C to constant mass, and sifted through the 2 mm sieve. A certain mass of homogeneous sample was weight in a Aluminium planchet and fixated with -alcohol [7]. For water samples method EPA was applied [8]. An aliquot of a preserved water sample is evaporated to dryness and ashed at 450 °C. Samples were placed in a Aluminium planchet and fixated with alcohol.

For the gross alpha and gross beta activity measurements, the gas low-level proportional counter Thermo-Eberline FHT 770T was used. The counting gas is a mixture of 90 % Ar and 10 % methane. Efficiencies were determined using the certified radioactive calibration standards <sup>241</sup>Am and <sup>90</sup>Sr (9031-OL-334/11 and 9031-OL-335/11, respectively, Czech Metrology Institute), traceable to the Bureau International des Poids et Mesures (BIPM). The counting efficiency was 26 % for alpha and 35% for beta radiation. Measurement time was 14400 s, by 4 independent detectors simultaneously. Measurement uncertainty was expressed as an expanded measurement uncertainty at the confidence level of 95% (k=2).

### 3. RESULTS AND DISCUSSION

Results for gross alpha and gross beta activity for water samples are presented in Table 1. In six-months composite samples, lower values for gross alpha activity was obtained for samples taken upstream of the Hydrometallurgical plant for both investigated period. The same trend was observed also for gross beta activity. A greater difference between the results was obtained for those taken in the second half of 2022 for the samples downstream of the Hydrometallurgical plant, compared to those taken in the first half of 2023. For the samples taken upstream, that difference is smaller.

Table 1 - Gross alpha and gross beta activity in surface water samples

Surface water sample Gabrovnická River	Gross alpha activity (Bq/l)	Gross beta activity (Bq/l)
Upstream of the Hydrometallurgical plant July-December 2022	0.022 ± 0.005	0.057 ± 0.009
Downstream of the Hydrometallurgical plant July-December 2022	0.279 ± 0.017	0.454 ± 0.022
Upstream of the Hydrometallurgical plant January-July 2023	0.032 ± 0.006	0.073 ± 0.006
Downstream of the Hydrometallurgical plant January-July 2023	0.072 ± 0.009	0.116 ± 0.008

In Serbian Legislation, the allowed values for gross alpha and gross beta activity are defined only for drinking water (0.1 Bq/l for gross alpha and 1 Bq/l for gross beta) [9]. The gross beta activity is mainly due to the presence of <sup>40</sup>K but also <sup>137</sup>Cs, while the gross alpha activity in samples originates from the decay chains of <sup>238</sup>U and <sup>232</sup>Th.

The obtained results for gross alpha and gross beta activity in soil samples from different depths for autumn 2022 and spring 2023 are presented at Figures 1 and 2. Samples are marked with S1: 0-5 cm; S2: 5-10 cm; S3: 10-15 cm. Gross alpha activity is higher for samples taken in autumn, with the fact that this difference is the largest for the sample S1 (0-5 cm depth). For gross beta



activity, for the soil samples S1 and S3 higher values were obtained for samples taken in autumn, while for sample S2 gross beta activity is higher for sample taken in spring. Gross alpha and gross beta activity for samples taken in spring increase with depth increasing, which indicates the fact that there was a migration of radionuclides in depth. The situation is slightly different with the samples taken in autumn, where there was a decrease in activity at a depth of 5-10 cm, and then an increase again at a depth of 10-15 cm.

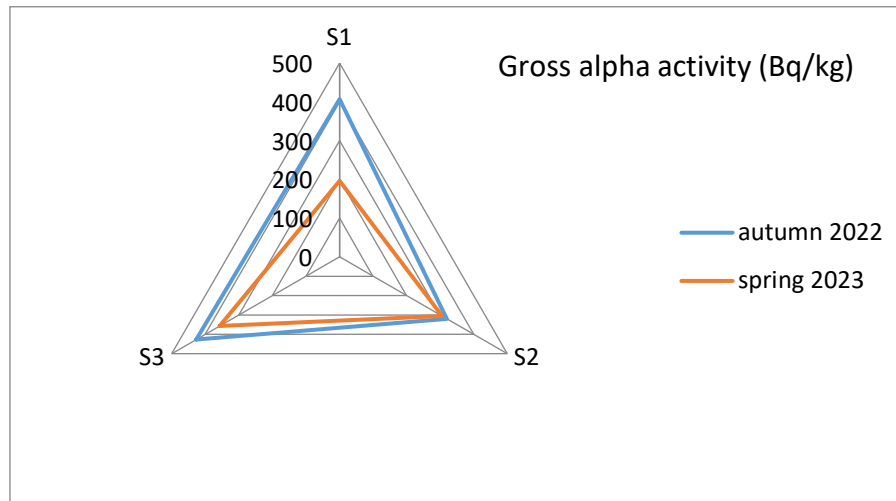


Figure 1 - Gross alpha activity in soil samples

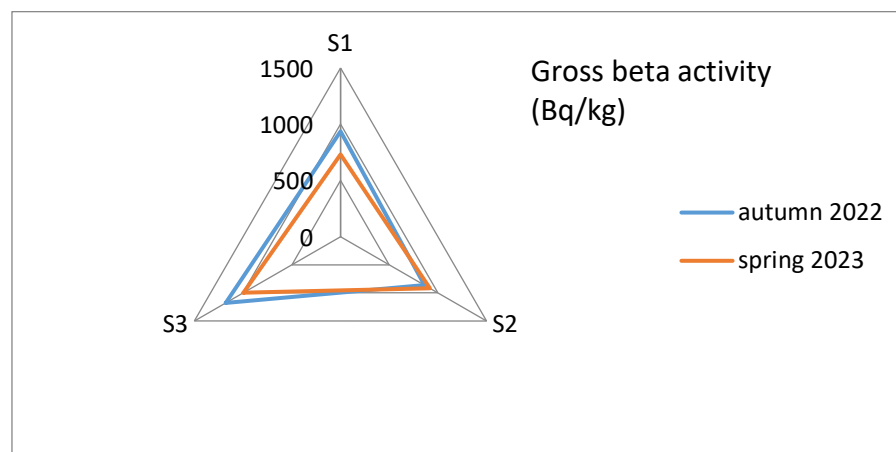


Figure 2 - Gross beta activity in soil samples

The impacts on the environment from uranium mining are not all related to the radionuclide content alone. The presence of other contaminants may also have an influence on the environment. The other effects may include: the chemical toxicity of the radionuclides, including uranium; the chemical toxicity of heavy metals and metallic compounds; the chemical toxicity of non-metallic minerals and compounds in the ore or introduced during processing (e.g. sulphuric acid, kerosene); acidity, resulting from sulphidic (ore) minerals; increased turbidity in surface waters; increased salinity [3]. In order to assess the radiological impact on the environment in the vicinity of abandoned mines, constant monitoring is necessary.

#### 4. CONCLUSION

Soil samples in the vicinity of former mine Gabrovnica and surface water samples from Gabrovnička River were analyzed using screening method gross alpha/beta activity, in order to assess the radiological impact on the environment. Results show that gross alpha and gross beta activity in water are higher for the samples taken downstream of the Hydrometallurgical plant. Given the fact that there are no prescribed limits for the permitted values for gross alpha and gross

beta activity in rivers, the comparison can only be made in relation to the values defined for drinking water. The gross beta activity is mainly due to the presence of natural radionuclide  $^{40}\text{K}$  but can also contain artificial radionuclide  $^{137}\text{Cs}$  or  $^{90}\text{Sr}$ , while the gross alpha activity originates from the decay chains of  $^{238}\text{U}$  and  $^{232}\text{Th}$ . In this regard, in soil samples, greater activity is observed with increasing depth, which means that radionuclides have migrated from the surface layer.

**Acknowledgments:** The research was done with financial support of the Ministry of Science, Technological Development and Innovation of the Republic of Serbia, within the funding of scientific research work at the University of Belgrade, Vinča Institute of Nuclear Sciences (Contract No. 451-03-47/2023-01/ 200017)

## REFERENCES

- [1] D. Milenic, V. Dragisic, N. Savic, A. Vranjes., Environmental impact of uranium mine waters in Eastern Serbia, *Mine Water and the Environment*, Proceedings, (2008) 495-498.
- [2] Z. Nikic, Lj. Letic, J. Kovacevic, V. Nikolic., *Herald of the Faculty of Forestry*, 107 (2013) 163-174.
- [3] Environmental Contamination from Uranium Production Facilities and their Remediation, Proceedings of an International Workshop Lisbon, 11–13 February 2004, International Atomic Energy Agency, Vienna, 2005, ISBN: 92–0–104305–8
- [4] J. Nikolov, S. Forkapic, J. Hansman, I. Bikit, M. Veskovic, N. Todorovic, D. Mrdja, K. Bikit., *J. Radioanal. Nucl. Chem.* 302 (2014) 477–482.
- [5] S. M. Abdulqader, B. Vakanjac, J. Kovacevic, Z. Naunovic, N. Zdjelarevic., *Minerals*, 8 (2018) 6.
- [6] J. Nikolov, S. Forkapic, J. Hansman, U. Koymidis-Luburic, I. Bikit, M. Veskovic, M. Krmar, N. Todorovic, D. Mrdja, K. Bikit., Natural radioactivity around former uranium mine, *Gabrovnica XXVII Symposium Radiation Protection Association of Serbia and Montenegro*, Proceedings, Vrnjačka Banja 02.-04.10.2013. Eds.: O. Ciraj-Bjelac, G. Pantelic, 92-96, ISBN: 978-86-7306-115-3.
- [7] Multi-Agency Radiological Laboratory Analytical Protocols Manual (MARLAP); Volume II, Appendix F, Part II; United States Environmental Protection Agency: Washington, DC, USA, 2004; pp. 12-1–12-44.
- [8] 900.0 Prescribed Procedures for Measurement of Radioactivity in Drinking Water EPA-600/4-80-032, 1980.
- [9] Rulebook on Limits of Radionuclides Content in Drinking Water, Foodstuffs, Feeding Stuffs, Medicines, Product for General Use, Construction Materials and Other Goods to be placed on Market (Official Gazette RS 36/18)

## LATENT HEAT OF SOME ALUMINIUM BASED PHASE CHANGE ALLOYS FOR THERMAL ENERGY STORAGE

Dragan Manasijević, Ljubiša Balanović, Ivana Marković, Uroš Stamenković

Technical Faculty in Bor, University of Belgrade, V.J. 12, 19210 Bor, Serbia

### Abstract

*Latent heat energy storage (LHES) is one of the most effective methods of thermal energy storage (TES). The knowledge of the thermal properties such as melting point, latent heat of melting, specific heat, thermal diffusivity and thermal conductivity is crucial for the development of the phase change materials (PCMs) for LHES applications. Due to their good properties, aluminium based eutectic alloys have become the most widely studied metal-based PCMs. In the present study, latent heat of melting for Al-12.6% Si, Al-33.3% Cu, and Al-27.8% Cu-5.2% Si (mass %) eutectic alloys were calculated using the CALPHAD (CALculation of PHase Diagram) method and the optimized thermodynamic parameters from the literature. The results of calculations were compared with the experimental results from the literature and good mutual agreement was noticed. The obtained results indicate that the applied calculation approach can be successfully used to predict the latent heat of eutectic alloys.*

**Keywords:** aluminium alloys, phase change material, eutectic, latent heat

### 1. INTRODUCTION

In terms of the global energy and resource crisis, the development of phase-change energy storage technologies has an increasing role in industrial conditions as well as in daily life [1]. Therefore, in recent years new phase-change materials (PCMs) for thermal energy storage are being investigated, with the ability to accumulate (storage) and release a large amount of thermal energy in the form of latent heat of a reverse phase transformation at a constant temperature. A variety of different materials have been studied so far and commercially implemented in the field of PCMs for heat storage [1,2]. The disadvantage of commercial PCMs such as inorganic salts, is their low thermal conductivity, which significantly limits the heat transfer in the material [1,2]. In order to improve the thermal conductivity, intensive research is being carried out on a variety of metals and eutectic alloys as potential PCMs for heat storage [3-5]. Based on a review of current literature [1-3], it is evident that a large number of eutectic alloys, which have the potential for application in the field of PCMs, are not yet fully investigated and many important physicochemical properties such as eutectic concentration, latent heat of melting, thermal conductivity, specific heat etc. are not determined. The eutectic Al-based alloys have significant potential application in the field of high-temperature PCMs ( $T_m > 300$  °C) [3-5]. In the present work, CALPHAD (CALculation of PHase Diagram) method was used for the calculation of phase diagrams of Al-Si, Al-Cu, and Al-Cu-Si systems, identification of eutectic compositions, and determination of latent heat for three eutectic Al based alloys: Al-12.6% Si, Al-33.3% Cu, and Al-27.8% Cu-5.2% Si. The results of calculation were compared with the literature data.

### 2. THEORETICAL BASIS

The enthalpy of melting (fusion) of a substance, also known as latent heat of melting, is the change in its enthalpy resulting from providing energy, typically heat, to a specific quantity of the substance to change its state from a solid to a liquid, at constant pressure. The knowledge of this thermophysical property of material is very important in determining the possibility of its use in the LHES field. The CALPHAD method [6] is based on the minimization of total Gibbs energy of the system. It employs a variety of thermodynamic models to describe Gibbs energy function

dependencies on composition and temperature of all the phases in the system. The models are tailored to describe the Gibbs energy of a specific phase using thermodynamic parameters. These parameters need to be optimized so that the model can fit the available experimental data for the particular phase. After entering the models together with their fitted parameters into specialized thermodynamic software it is possible to calculate thermodynamic functions (specific heat capacity, enthalpy, Gibbs energy, etc.) and phase equilibria of the system of interest. The accuracy of the calculation largely depends on the quality of thermodynamic assessments included in the database. In the present study, thermodynamic calculations according to the CALPHAD method was done using PANDAT software [7] and COST MP0602 thermodynamic database [8].

### 3. RESULTS AND DISCUSSION

The literature values of thermophysical properties for pure Al, Cu, and Si are presented in Table 1.

Table 1 - Thermophysical properties of pure Al, Cu, and Si [9]

Metal	Melting point /°C	Latent heat of melting/ Jg <sup>-1</sup>	Density/gcm <sup>-3</sup>	Specific heat capacity/Jg <sup>-1</sup> K <sup>-1</sup>	Thermal conductivity /Wm <sup>-1</sup> K <sup>-1</sup>
Al	660.4	397	2.6989 at 20 °C	0.9 at 25 °C	247 at 25 °C
Cu	1084.9	205	8.93 at 20 °C	0.386 at 20 °C	398 at 27 °C
Si	1414.0	1807.9	2.329 at 25 °C	0.713 at 27 °C	156 at 27 °C

Phase diagrams of the Al-Si and Al-Cu binary systems, calculated using optimized thermodynamic parameters from [8], are shown in Fig. 1.

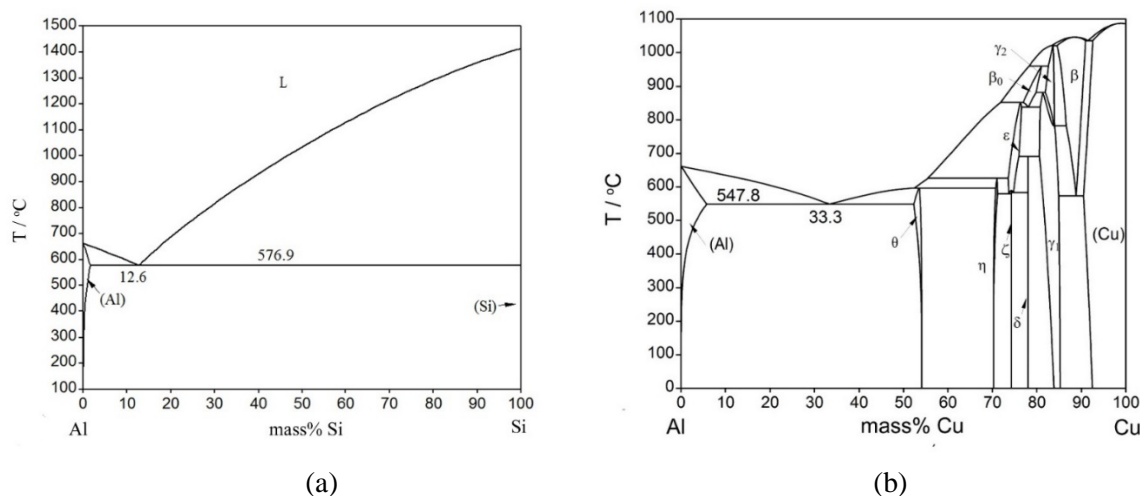


Figure 1 - Phase diagram: (a) Al-Si binary system; (b) Al-Cu binary system

The calculated liquidus projection of the Al-Cu-Si ternary system is presented in Fig. 2. The ternary eutectic composition corresponds to the point marked with the letter E.

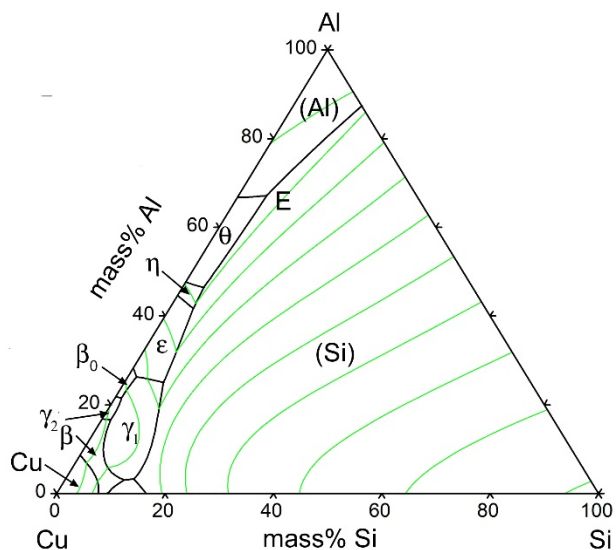


Figure 2 - Calculated liquidus projection of the Al-Cu-Si ternary system

The obtained eutectic reaction, eutectic composition and corresponding eutectic temperature for the Al-Si system are:  $L \leftrightarrow (Al) + (Si)$ , 12.6% Si, and 576.9 °C. For the Al-Cu system:  $L \leftrightarrow (Al) + \theta(Al_2Cu)$ , 33.3% Cu, and 547.8 °C. For the ternary Al-Cu-Si system:  $L \leftrightarrow (Al) + \theta(Al_2Cu) + (Si)$ , 27.8% Cu, 5.2% Si, and 523.4 °C. In the next step, enthalpy variations with temperature for the studied alloys were calculated. Fig. 3 shows the calculated dependence of enthalpy vs. temperature for the investigated Al–12.6% Si alloy with the characteristic jump at the eutectic temperature corresponding to the enthalpy of melting (latent heat of melting- LHM).

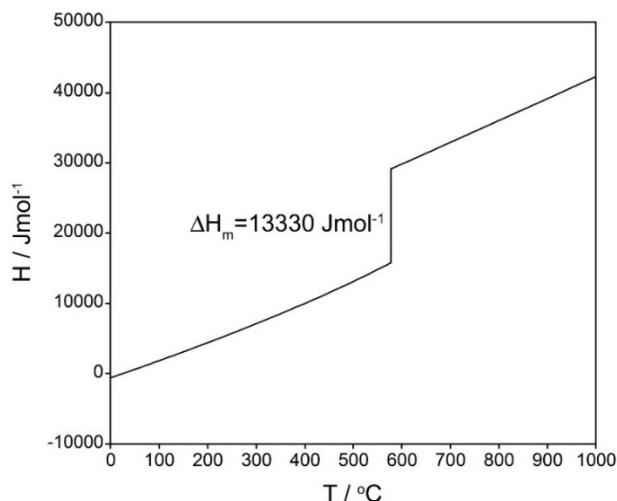


Figure 3 - Temperature dependence of enthalpy for the Al–12.6% Si alloy calculated using optimized thermodynamic parameters from [8]

Table 2 shows the calculated latent heat values for the studied eutectic alloys with the literature data.

Table 2 - Comparison of the calculated and literature values of LHMs for the studied Al based eutectic alloys (Jg<sup>-1</sup>)

Alloy composition /mass%	Calculation – this work	Literature values	Reference
Al-12.6% Si	491.6	499.2	[3]
Al-33.3% Cu	376.4	331-372	[2]
Al-27.8% Cu-5.2% Si	393.4	361.0	[5]

#### 4. CONCLUSION

Al based eutectic alloys have the potential to be used for thermal energy storage. In the present study, the eutectic temperatures, eutectic compositions, and latent heat of melting of Al-12.6% Si, Al-33.3% Cu, and Al-27.8% Cu-5.2% Si eutectic alloys were calculated using the CALPHAD method and the optimized thermodynamic parameters from literature. The obtained results were compared with the existing literature data. Among the investigated alloys, the Al-12.6% Si alloy has the largest value of latent heat (491.6 Jg<sup>-1</sup>). Thermodynamic calculation according to the CALPHAD method is a valuable tool in seeking new potential thermal storage materials.

#### ACKNOWLEDGEMENTS

*The research presented in this paper was done with the financial support of the Ministry of Science, Technological Development and Innovations of the Republic of Serbia, with the funding of the scientific research work at the University of Belgrade, Technical Faculty in Bor, according to the contract with registration number 451-03-47/2023-01/200131.*

#### REFERENCES

- [1] A. Sharma, V.V. Tyagi, C.R. Chen, D. Buddhi, *Renew. Sust. Energ. Rev.*, 13 (2) (2009) 318-345.
- [2] S. C. Costa, M. Kenisarin, *Renew. Sust. Energ. Rev.*, 154 (2022) 111812.
- [3] Z. Wang, H. Wang, X. Li, D. Wang, Q. Zhang, G. Chen, Z. Ren, *Appl. Therm. Eng.*, 89 (2015) 204-208.
- [4] J. Zhao, Y. Yuan, F. Cui, *J. Therm. Anal. Calorim.* 129 (2017) 109-115.
- [5] Y. Kageyama, K. Morita, *High Temp. Mater. Process.*, 42(1) (2023) 20220269.
- [6] H. Lukas, S. Fries, B. Sundman, *Computational Thermodynamics: the Calphad Method*, Cambridge University Press, Cambridge, 2007.
- [7] W. Cao, S.L. Chen, F. Zhang, K. Wu, Y. Yang, Y.A. Chang, R. Schmid-Fetzer, W.A. Oates, *Calphad*, 33 (2) (2009) 328-342.
- [8] A. Kroupa, A. Dinsdale, A. Watson, J. Vřešťál, A. Zemanova, P. Broz, *J. Min. Metall. B: Metallurgy*, 48(3) (2012) 339-346.
- [9] ASM, *Handbook Volume 2: Properties and Selection: Nonferrous Alloys and Special- Purpose Materials*, ASM International, 1990.

## POSITION OF EUROPEAN COUNTRIES IN SUSTAINABLE RESOURCE MANAGEMENT

Andelka Stojanović, Ivica Nikolić, Isidora Milošević

Technical Faculty Bor, University of Belgrade, V.J. 12, 19210 Bor, Serbia

### Abstract

*The emergence of new crises, along with old global trends in production and consumption, impose serious challenges on planetary boundaries regarding pollution, climate change, and severe depletion of natural resources. With the further development of industry in recent decades, the problems relating to the environment became pronounced and provoked global interest. As a result, the United Nations proposed Sustainable Development Goals to promote practices and targets for reducing adverse effects caused by socio-economic development. This paper presents an approach to assessing sustainable resource management practices measured through indicators of responsible consumption and production available in the Eurostat database. The Evaluation Based on Distance from Average Solution (EDAS) method has been used to evaluate the efforts of 27 European countries according to indicators that are part of sustainable development goals. The results indicate the spatial division of EU countries in implementing environmentally oriented sustainable practices. This research can imply that more developed European countries should promote successful practices and help the rest to the whole of Europe reach sustainability until targeted 2030.*

**Keywords:** *sustainable resource management, EU countries, EDAS*

### 1. INTRODUCTION

Globalization, innovations, and the development of information and communication technologies, as well as recent economic, pandemic, and war crises, have shaped the world's society and economy and significantly impacted production and consumption. Growing production and consumption undoubtedly deplete natural resources reaching and overcoming planetary boundaries [1]. With more climate changes, land degradation, and biodiversity losses, environmental issues have become more prominent and critical challenges for sustainability [1,2]. Along with the world, the European economies have passed turbulent times recently. After a constant annual increase in the value of sold production from 2014-2018, the outbreak caused by COVID-19 significantly impacted production and consumption in European Union (EU). The value of sold production in 2020 decreased by 7%, while in 2021 increased again by 8% compared with the previous year [3]. In addition, the newest war crisis in European territories will undoubtedly have an influence that will need analysis in the future.

On the other hand, governments and world organizations are trying to find appropriate strategies to deal with emerging issues and to reach long-term prosperity. To help the world become more sustainable, United Nations proposed Sustainable Development Goals to promote practices and targets for reducing adverse effects caused by socio-economic development and, among them, environmental issues [4]. Under Goal 12, Ensure sustainable consumption and production patterns of 2030 Agenda for Sustainable Development, it is defined the developed countries leading role in implementing the programs for sustainable management and efficient use of natural resources. Certainly, the critical part in achieving sustainability goals belongs to developing countries and their abilities to change towards sustainable production and consumption.

The industries also seek the appropriate business strategies to balance constant pressures to reduce environmental impact and economic performance. Therefore, sustainable resource management



(SRM) has been defined as the way of using natural resources to maximize people's well-being and minimize environmental impact [5]. SRM includes a set of practices that effectively and efficiently improve environmental performance and sustainability. Therefore, in literature, SRM is often described with multidimensional models and measurable parameters. This study aims to determine the positions of European countries in implementing SRM practices using the multi-criteria decision analysis tool The Evaluation Based on Distance from Average Solution (EDAS). The ranking of 27 EU countries will be computed based on six indicators that are part of SDG12 targets. Quantitative values for each indicator were retrieved from the Eurostat database. The study contributes to identifying the current position of EU countries in SRM to establish benchmarking and guide lower-ranking countries to make effective improvements toward sustainable practices.

## 2. DATA AND METHODS

### 2.1 Data

This quantitative research uses data from the Eurostat database over the six sustainable production and consumption (SPC) indicators explained in the Table 1.

Table 1 – SPC indicators

Label	Indicator	Description	Unit
SPC1	Energy productivity	The indicator measures the amount of economic output that is produced per unit of gross available energy. The gross available energy represents the quantity of energy product necessary to satisfy all demands of entities in the geographical area under consideration.	Euro per kilogram of oil equivalent
SPC2	Raw material consumption	The material footprint represents the global demand for the extraction of materials (minerals, metal ore, biomass, fossil energy materials) induced by the consumption of goods and services within a geographical reference area.	Tonnes per capita
SPC3	Average CO2 emissions per km from new passenger cars	Average carbon dioxide (CO2) emissions per km by new passenger cars in a given year. The reported emissions are based on type approval and can deviate from the actual CO2 emissions of new cars.	
SPC4	Circular material use rate	Measures the share of material recovered and fed back into the economy in overall material use. The CMU is defined as the ratio of the circular use of material to the overall material use.	Percentage
SPC5	Generation of waste, excluding major mineral wastes by hazardousness	Measures all waste generated in a country. Due to the strong fluctuations in waste generation in the mining and construction sectors and their limited data quality and comparability, major mineral wastes, dredging spoils, and soils are excluded.	Kilograms per capita
SPC6	Gross value added in environmental goods and services sector	The gross value added in EGSS represents the contribution of the environmental goods and services sector to GDP. It is defined as the difference between the value of the sector's output and intermediate consumption.	Percentage of gross domestic product (GDP)

### 2.2 Methodology

EDAS method belongs to the outranking group of methods proposed by Keshavarz and associates [6]. One benefit of the EDAS method, as compared to other MCDA techniques, is its simplicity and ease of understanding. Additionally, there is no requirement for the normalization of the initial matrix. As a result, EDAS has been widely used in several engineering and decision-making problems [7]. The main approach offered by EDAS presupposes the assessment of alternatives in terms of distance from an average solution. An appraisal score (AS) can be calculated for each alternative by determining the positive and negative distances from averages and their weighted sums to rank alternatives. The detailed procedure is presented in [6].

As described previously, the SRM is measured with six indicators used as criteria in the proposed model. The criteria weights are equally distributed. The type of criteria and the summary statistics are presented in the Table 2. The 27 EU countries were used as alternatives.

Table 2 – Data summary statistics and initial data for EDAS method

	SPC1	SPC2	SPC3	SPC4	SPC5	SPC6
	max	min	min	max	min	max
criteria weights	0.17	0.17	0.17	0.17	0.17	0.17
min	2.48	7.75	85.70	1.50	962.00	0.98
max	22.41	33.62	125.10	30.00	6291.00	6.24
mean	7.91	17.97	110.57	9.79	1833.50	2.65
std. deviation	4.18	6.82	10.07	6.71	1053.85	1.12

### 3. RESULTS AND DISCUSSION

Using the obtained data and the EDAS methodology, the rank of 27 EU countries according to the effectiveness of sustainable resource management was obtained (Table 3). According to the results, the Netherlands represents the leader in SRM implementation. The reason for these results lies in the commitment of the Dutch government to establish an innovation infrastructure that facilitates companies to move toward sustainability goals. That means permanent striving for innovation and sustainability across all sectors and close collaboration between business, science, and government [8].

Table 3 - Rank of 27 EU countries according to SRM indicators

Rank	Country	AS	Rank	Country	AS	Rank	Country	AS
1	Netherlands	0.932	10	Sweden	0.539	19	Croatia	0.461
2	Italy	0.812	11	Greece	0.532	20	Portugal	0.457
3	France	0.782	12	Czechia	0.522	21	Latvia	0.426
4	Ireland	0.714	13	Luxembourg	0.514	22	Cyprus	0.406
5	Denmark	0.676	14	Finland	0.508	23	Poland	0.387
6	Austria	0.644	15	Malta	0.501	24	Lithuania	0.368
7	Spain	0.633	16	Slovakia	0.480	25	Romania	0.315
8	Germany	0.616	17	Slovenia	0.479	26	Estonia	0.250
9	Belgium	0.550	18	Hungary	0.474	27	Bulgaria	0.239

Also, the results indicate regional divides within EU countries. First, two of the first three economies in the EU are at the top of the ranking: Italy at the second place (third contributor to EU GDP) and France at the third place (second contributor to the EU GDP). At the end of the ranking string relating to SRM are the countries with less than 1% contribution to EU GDP [9]. From a geographical standpoint, there seems to be a west-east pattern in the variation of SRM practices across Europe (Figure 1).

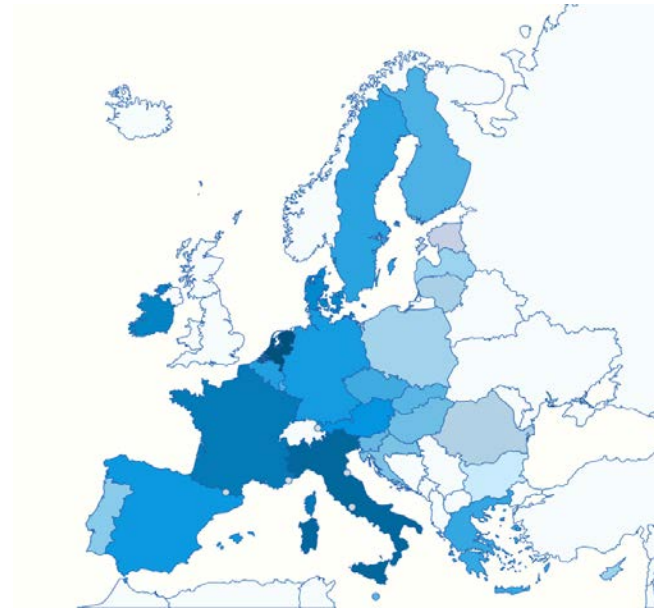


Figure 2 – Map of the SRM variation across the EU

#### 4. CONCLUSION

After analyzing the results, it is clear that there are significant implications to consider. As outlined in SDG12, it is recommended that developed countries take a leadership role in implementing the proposed framework to achieve sustainable consumption of natural resources, reduce waste generation, and promote sustainable resource management practices among companies. These targets should remain a top priority. It is crucial to assist developing countries in enhancing their capabilities across various domains, including institutional, technological, and scientific aspects. Furthermore, promoting positive attitudes and sustainable production and consumption patterns are of great importance.

#### REFERENCES

- [1] L. Persson, B.M. Carney Almroth, C.D. Collins, S. Cornell, C.A. de Wit, M.L. Diamond, P. Fantke, M. Hassellöv, M. MacLeod, M.W. Ryberg, P.S. Jørgensen, P. Villarrubia-Gómez, Z. Wang, M.Z. Hauschild, *Environ. Sci. Technol.*, 56 (3) (2022) 1510-1521.
- [2] Y. Geng, P. Rao, *A. Resour. Policy*, 79 (2022) 103050.
- [3] Eurostat, <https://ec.europa.eu/eurostat/>, 2022.
- [4] United Nations, <https://sdgs.un.org/goals>, 2023, April.
- [5] S. Bringezu, R. Bleischwitz, Routledge, UK, 2017.
- [6] M. Keshavarz Ghorabae, E.K. Zavadskas, L. Olfat, Turskis, *Z. Informatica*, 26(3) (2015) 435–451.
- [7] D. Stanujkic, E.K. Zavadskas, M.K. Ghorabae, Z. Turskis, *Stud. Inform. Control.*, 26(1) (2017) 5–12.
- [8] Invest in Holand, Sustainable Future. <https://investinholland.com/> 2023, April.
- [9] Eurostat, <https://ec.europa.eu/eurostat/web/products-eurostat-news/-/ddn-20211220-1>, 2021.

## MECHANICAL AND ELECTRICAL PROPERTIES OF THE TERNARY Ag-Ge-Sn ALLOYS

Aleksandar Đorđević<sup>1</sup>, Milena Zečević<sup>1</sup>, Duško Minić<sup>1</sup>, Dragan Manasijević<sup>2</sup>

<sup>1</sup>Faculty of Technical Science, University of Prishtina in Kosovska Mitrovica, Department of Technological engineering, Knjaza Miloša 7, 38220 Kosovska Mitrovica, Serbia

<sup>2</sup>Technical Faculty Bor, University of Belgrade, V.J. 12, 19210 Bor, Serbia

### Abstract

*This study presents the results of experimental and analytical tests. Experimental part includes results of the hardness and electrical properties of the selected ternary Ag-Ge-Sn alloys. In the experimental part of the study, alloys of selected compositions were prepared and then examined using scanning electron microscopy (SEM) and energy dispersive spectrometry (EDS), X-ray powder diffraction (XRD), hardness measurements by Brinell method and electrical conductivity measurements. Analytical part includes, calculations of equilibrium phase diagram of the Ag-Ge-Sn ternary system by using the Calphad method and the corresponding thermodynamic program (Pandata ver. 8.1). The results include calculated characteristic isothermal sections. Isothermal section of the ternary Ag-Ge-Sn system at 25 °C have been extrapolated using optimized thermodynamic parameters from literature. Experimentally obtained results were compared with the results of thermodynamic calculation of phase diagrams. Good overall agreement between experimental and calculated values was obtained. Hardness and electrical conductivity of selected alloys were measured and by using appropriated mathematical model these properties were predicted in the whole composition range.*

**Keywords:** Ag-Ge-Sn system; hardness; electrical conductivity; mathematical model.

### 1. INTRODUCTION

The study of ternary systems based on Ge-Sn attracts a lot of attention. Increased attention to the research of these alloys can be attributed to the specific properties of the Ge and Sn elements, such as good insulating properties, easy machinability, forging and many others. The ternary Ag-Ge-Sn system has been investigated previously by our group [1]. In our previous study reliable thermodynamic data set has been proposed and experimentally confirmed with experimental investigation alloys from three vertical sections (Ag-GeSn, Ge-AgSn and Sn-AgGe) and two isothermal sections at 200 and 300 °C. Since reliable thermodynamic data set has been obtained by previous study [1], in the current study same thermodynamic parameters has been used for calculation of the isothermal section at 25 °C. Thermodynamic calculation of the isothermal section were performed by using Pandat software [2]. Calculated phase diagram of the isothermal section were compared with experimental results done in current study. The following experimental techniques were used for experimental trials of this ternary system: scanning electron microscopy (SEM) and energy dispersive spectrometry (EDS), X-ray powder diffraction (XRD), hardness measurements by Brinell method and electrical conductivity measurements. In addition to the experimental test, the thermodynamic calculation of equilibrium diagrams of the state of ternary system was performed using the CALPHAD method. For each phase present in the examined system, the thermodynamic model and the values of thermodynamic parameters that occur in it were determined. For better insight into the properties of the Ag-Ge-Sn alloys, hardness and electrical conductivity were investigated in the current study. Based on experimental results and by using appropriated mathematical model these properties were predicted along whole composition range.

## 2. EXPERIMENTAL PROCEDURE

High-purity Ag, Ge and Sn produced by Alfa Aesar (Germany) were used for preparation of investigated binary and ternary alloys. Used elements were carefully measured in different molar ratio. Total mass of sample were 3 g. Such samples were melted and re-melted five times in an induction furnace under high purity Ar atmosphere. The average weight loss of the sample during melting was about 1 mass %. Samples were used for SEM-EDS, XRD, hardness tests and electrical conductivity measurements. Samples are prepared by classical experimental procedure as it is deskripcion in our previous paper [3].

## 3. RESULTS AND DISCUSSIONS

### 3.1 Microstructural analysis

Twelve ternary samples were selected to SEM-EDS test. Overall compositions of samples were situated along three vertical sections (samples 1 to 4, along Ag-GeSn vertical section, samples 5-8 along Ge-AgSn vertical section and samples from 9-12 along Sn-AgGe vertical section). As a result, it shown that in ten samples same three phases are detected. Detected phases are marked as (Ge), ( $\beta$ Sn) and  $\epsilon$ . Two SEM microstructures of samples 1 and 5 are presented as an illustration in Figure 1a) and 1b). In microstructure of sample 3, three phase are detected. By EDS composition of phases, it is determined that detected phases are (Ge),  $\epsilon$  and  $\zeta$ . Microstructure of sample 3 is given on Figure 1c). Sample 4, have two phases in microstructure. Presented phases are determined to be (Ge) and  $\zeta$ . Microstructure of sample 4 is given on Figure 1d).

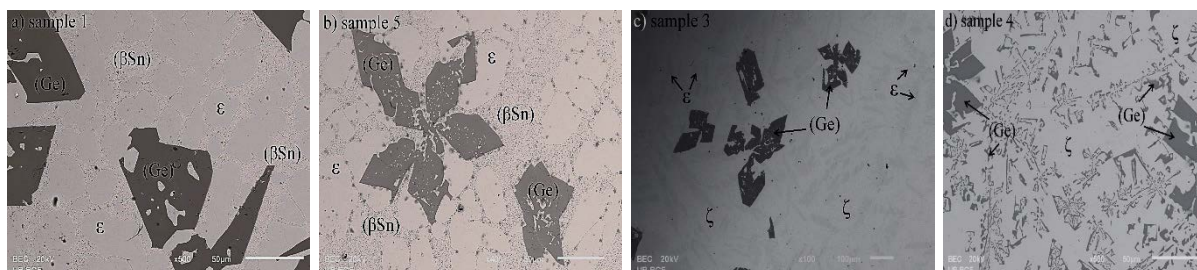


Figure 1 - SEM micrographs of the a) sample 1, b) sample 5, c) sample 3 and d) sample 4.

### 3.2 Brinell hardness measurements

Twelve ternary samples were subjected to the Brinell hardness measurements. Brinell hardness measurements for all tested alloy samples were performed at room conditions. Relation between mean value of Brinell hardness and alloy composition are presented grafically on Figure 2.

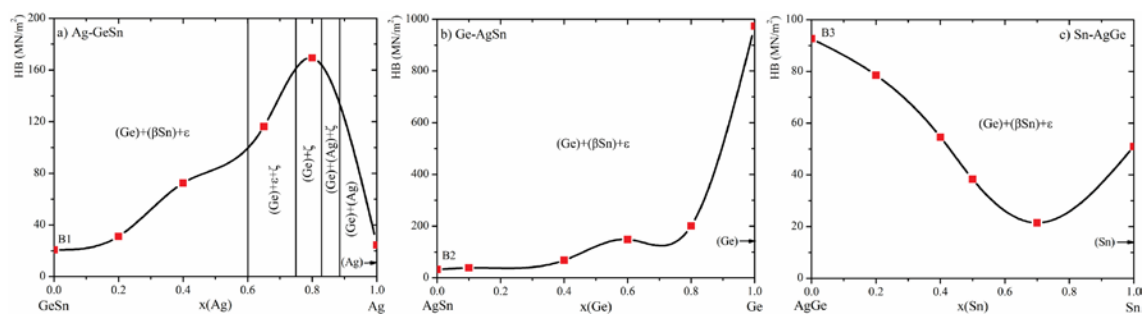


Figure 2 - Graphical presentation of Brinell hardness depending on the composition vertical section: a) Ag-GeSn, b) Ge-AgSn and c) Sn-AgGe.

Experimental results shows that ternary alloy Ag<sub>10</sub>Ge<sub>80</sub>Sn<sub>10</sub>, sample 8 have highest hardness in comparison with other ternary alloys. Detected hardness is 201 MN/m<sup>2</sup>. High percent of (Ge) phase inside sample 8 is responsible for high value of Brinell hardness. In microstructures of samples 1,2, 5-12, the same three phases are present as in sample 8. The hardness value determined in these samples have a decreasing trend in comparison with hardness of sample 8. Reason for this

trend can be related to the dominant presence of ( $\beta$ Sn) and  $\epsilon$  phase. In microstructure of samples 3 and 4, different phases are detected in comparison with all other ternary samples. Sample 3, have (Ge)+ $\epsilon$ + $\zeta$  three phase structure. Sample 4, have two phase structure. In general, can be concluded that percent of (Ge) phase influence on hardness values and that sample 8, have the highest hardness in comparison with other ternary samples. Also it is clear that phase  $\zeta$  is responsible for high hardness, since this phase is dominant in sample 4. Based on the obtained results, and appropriate mathematical model it can be predicted behavior of Brinell hardness allong all composition range. The final equation of the predictive model in terms of real components is:

$$\ln(\text{HB}) = 3.94623547x(\text{Ag}) + 6.70578429x(\text{Ge}) + 3.7583475x(\text{Sn}) - 7.8742816x(\text{Ge})x(\text{Sn}) \quad (1)$$

Iso-lines contour plot for Brinell hardness of alloys defined by equation 1 is shown in Figure 3.

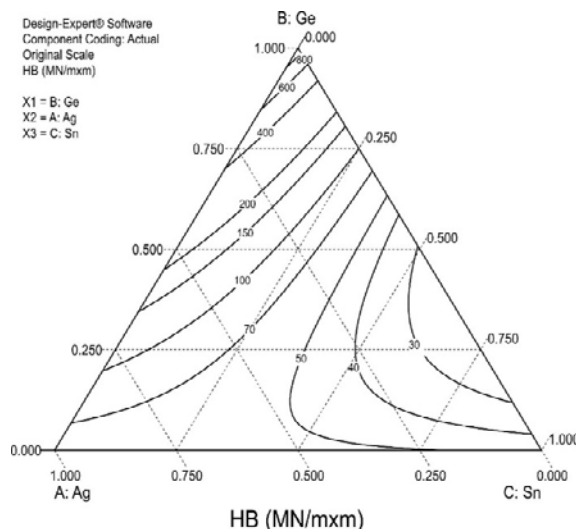


Figure 3 - Calculated iso-lines of Brinell hardness in ternary Ag-Ge-Sn system.

### 3.3 Electrical conductivity measurements

Electrical conductivity was measured in the same samples as Brinell test. The obtained results of electrical conductivity are also presented graphically. Figure 4 shows a graphical representation of the relationship between electrical conductivity of the tested alloys and the composition of the alloys.

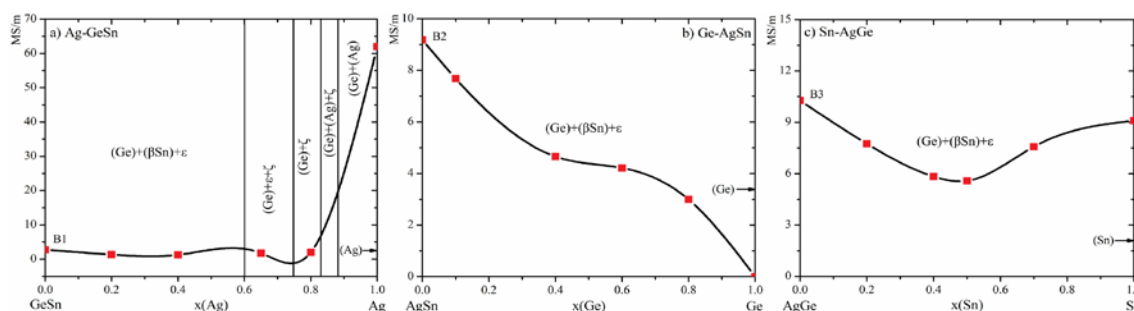


Figure 4 - Graphical presentation of electrical conductivity dependence of composition and phase fraction vertical section a) Ag-GeSn, b) Ge-AgSn and c) Sn-AgGe.

From results shown in Figure 4a), it can be seen that the values for electrical conductivity are very small and quite uniform. While value of electrical conductivity of samples 5 to 12 are higher than for samples 1 to 4. In the microstructure of samples 5 to 12 same three phases are presented ( $\beta$ Sn)+(Ge)+ $\epsilon$ . Different phase fraction in responsible for slight changes in electrical conductivity. It can be concluded that high percent of  $\epsilon$  is mostly responsible for high value of electrical conductivity in ternary alloys. On the other hand beside  $\epsilon$  phase, ( $\beta$ Sn) phase is also responsible for high value of electrical conductivity.



The final equation of the predictive model in terms of Real components is:

$$\begin{aligned} \ln(EP+1.00) = & 4.036388638x(\text{Ag}) + 0.137064739x(\text{Ge}) + 2.175797172x(\text{Sn}) + 0.463525434x(\text{Ag}) \\ & x(\text{Ge}) - 4.099509193x(\text{Ag})x(\text{Sn}) - 16.81004221x(\text{Ag})x(\text{Ge})x(\text{Ag-Ge}) - 11.38241626x(\text{Ag}) \\ & x(\text{Sn})x(\text{Ag-Sn}) \end{aligned} \quad (2)$$

Iso-lines contour plot for Electrical conductivity of Ag-Ge-Sn alloys defined by equation 2 is shown in Figure 5.

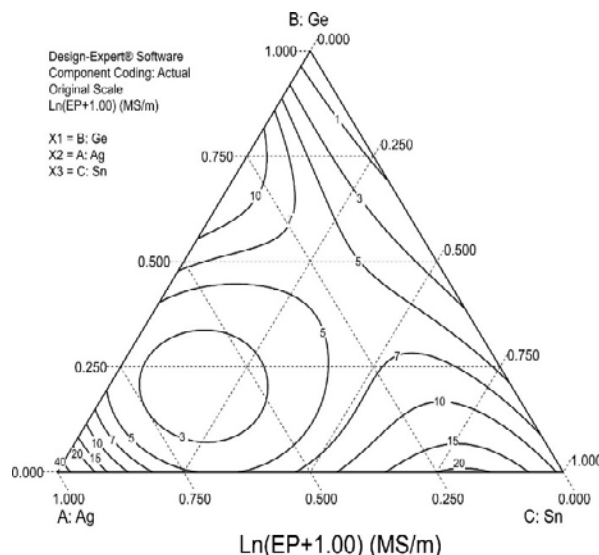


Figure 5 - Calculated iso-lines of Electrical conductivity in ternary Ag-Ge-Sn system.

#### 4. CONCLUSION

The ternary Ag-Ge-Sn system has been experimentally investigated by using several experimental techniques: SEM-EDS, XRD, hardness measurements by Brinell method and electrical conductivity measurements. Experimentally determined phases by XRD analysis were compared with calculated isothermal section at 25 °C and agreement between the results was reached. Experimentally determined compositions of coexisting phases were in good agreement with related calculated compositions. Conducted experiments did not indicate any new ternary phases or large solubility of third element in binary phases. Microstructural, hardness, electrical conductivity tests were performed on twelve ternary alloys. Results of Brinell hardness and electrical conductivity measurements were presented and discussed with respect to alloys compositions and phase constituents. By using appropriated mathematical model these properties were predicted in the whole composition range.

#### ACKNOWLEDGEMENTS

*This work has been supported by the National Nature Science Foundation of China (project No.51950410600) and the Ministry of Education, Science and Technological Development of the Republic of Serbia (Grant No. OI172037).*

#### REFERENCES

- [1] N. Toskovic, M. Premovic, M. Tomic, D. Minic, D. Manasijevic, M. Gorgievski, J. Chem. Thermodynamics, 131 (2019) 563–571.
- [2] W. Cao, S.L. Chen, F. Zhang, K.Wu, Y. Yang, Y.A. Chang, R. Schmid-Fetzer and W.A. Oates, Calphad, 33 (2) (2009) 328–342.
- [3] A. Marković, D. Minić, M. Premović, D. Manasijević, D. Guresić, M. Kolarevic, Alloys Mater. Res., 22 (6) (2019) e20190372.



## EFFECT OF CHEMICAL COMPOSITION ON THE CORROSION RESISTANCE OF THE TERNARY Ag-Ge-Sn ALLOYS

Milena Zečević<sup>1</sup>, Duško Minić<sup>1</sup>, Alekandar Đorđević<sup>1</sup>, Dragan Manasijević<sup>2</sup>

<sup>1</sup>Faculty of Technical Science, University of Prishtina in Kosovska Mitrovica, Department of Technological engineering, Knjaza Miloša 7, 38220 Kosovska Mitrovica, Serbia

<sup>2</sup>Technical Faculty Bor, University of Belgrade, V.J. 12, 19210 Bor, Serbia

### Abstract

*In this paper selected system is Ag-Ge-Sn. This system was previously studied by our group. In this paper results are focused on corrosion resistance. Experimental part includes results of the corrosion resistance of the binary alloys Ge<sub>50</sub>Sn<sub>50</sub>, Ag<sub>50</sub>Sn<sub>50</sub>, Ag<sub>50</sub>Ge<sub>50</sub> and ternary (Ag-Ge-Sn) alloys in 3% NaCl, of the selected ternary Ag-Ge-Sn alloys. The corrosion resistance of these alloys was examined in 3% NaCl solution using the potentiodynamically polarization method (Tafel plots) and electrochemical impedance spectroscopy (EIS). Tafel plots were fitted using the DC Corrosion Technique software. The results of electrochemical impedance spectroscopy (EIS) were fitted using the Gamry Echem Analyst program and the corresponding equivalent circuit. The value of the exponent  $n$  was used to determine the degree that controls the rate of the electrochemical reaction. It was investigated how the chemical composition affects corrosion.*

**Keywords:** Metals and alloys, Ag-Ge-Sn system, corrosion resistance

### 1. INTRODUCTION

Knowledge of corrosion properties of ternary systems based on Ag, Ge and Sn are of great importance due to different applications in the field of energy and electronics and further practical use [1]. Also, Ge-based alloys are necessary for the development of memory materials [2], for the production of optical discs, DVDs, Blue-Ray discs, flash memory, etc. The corrosion resistance of these alloys was examined in 3% NaCl solution using the potentiodynamically polarization method (Tafel plots) and electrochemical impedance spectroscopy (EIS). Tafel plots were fitted using the DC Corrosion Technique software. This paper presents representative results of performed electrochemical measurements. The results of electrochemical corrosion parameters provide the possibility of a clearer understanding of the potential application of the tested alloys. They provide better understanding of practical application of the tested alloys of the ternary Ag-Ge-Sn system.

### 2. EXPERIMENTAL PROCEDURE

All tested samples were prepared from high purity elements: silver, germanium and tin. Samples were melted in an induction furnace under high-purity argon atmosphere and slowly cooled to the room temperature. Total mass of sample were 7 g and the dimension were (15x15x1) mm for corrosion resistance. Such prepared samples are subjected to experimental tests.

Three binary Ge<sub>50</sub>Sn<sub>50</sub>, Ag<sub>50</sub>Sn<sub>50</sub>, Ag<sub>50</sub>Ge<sub>50</sub> and six ternary Ag<sub>45</sub>Ge<sub>10</sub>Sn<sub>45</sub>, Ag<sub>30</sub>Ge<sub>40</sub>Sn<sub>30</sub>, Ag<sub>65</sub>Ge<sub>17.5</sub>Sn<sub>17.5</sub>, Ag<sub>80</sub>Ge<sub>10</sub>Sn<sub>10</sub>, Ag<sub>25</sub>Ge<sub>25</sub>Sn<sub>50</sub>, Ag<sub>15</sub>Ge<sub>15</sub>Sn<sub>70</sub> alloys were selected for measurement of corrosion resistance. The corrosion resistance of these materials was examined in 3% NaCl solution using the potentiodynamic polarization method and electrochemical impedance spectroscopy (EIS). Tafel polarizing plots were fitted using the DC Corrosion Technique software. The results of electrochemical impedance spectroscopy (EIS) were fitted using the Gamry Echem Analyst program and the appropriate equivalent circuit.

Electrochemical tests of the corrosion resistance of the alloys in 3% NaCl solution were conducted using potentiodynamic polarization measurements (Tafel diagrams) and measurements of

electrochemical impedance spectroscopy (Nyquist diagrams), on a potentiostat/gavanostat /ZRA Gamry Series GTM 750 with an appropriate software.

Electrochemical methods for corrosion resistance testing are described in detail in the relevant literature [3,4].

### 3. RESULTS AND DISCUSSIONS

Three binary ( $Ge_{50}Sn_{50}$ ,  $Ag_{50}Sn_{50}$ ,  $Ag_{50}Ge_{50}$ ) and six ternary alloys (sample 1  $Ag_{65}Ge_{17.5}Sn_{17.5}$ , sample 2  $Ag_{80}Ge_{10}Sn_{10}$ , sample 3  $Ag_{45}Ge_{10}Sn_{45}$ , sample 4  $Ag_{30}Ge_{40}Sn_{30}$ , sample 5  $Ag_{25}Ge_{25}Sn_{50}$  and sample 6  $Ag_{15}Ge_{15}Sn_{70}$ ) were selected for the corrosion resistance test. Tafel plots are given in Figures 1 and 2, while the corresponding Nyquist diagrams are given in Figures 3 and 4. Tables 1 and 2 show the obtained electrochemical polarization parameters for corrosion. The results for electrochemical impedance corrosion parameters are shown in Tables 4 and 4.

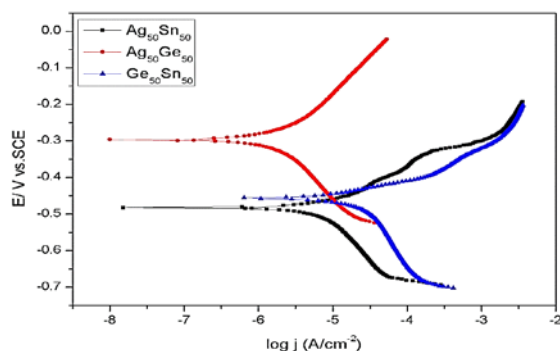


Figure 1 - Tafel plots for tested binary alloys  $Ge_{50}Sn_{50}$ ,  $Ag_{50}Ge_{50}$  and  $Ag_{50}Sn_{50}$

Table 1 - Electrochemical polarization parameters of corrosion for tested binary alloys  $Ge_{50}Sn_{50}$ ,  $Ag_{50}Ge_{50}$  and  $Ag_{50}Sn_{50}$

Alloy	Predicted percent of the phase at 25 °C	$-E_{corr}$ (mV)	$j_{corr}$ ( $\mu A/cm^2$ )	$v_{corr}$ (mm/year)	$\beta_a$ (mV/dec)	$\beta_k$ (mV/dec)
B1, $Ge_{50}Sn_{50}$	50%(Ge)+50%(βSn)	456	16,10	0,54	73,40	105,8
B2, $Ag_{50}Sn_{50}$	33%(βSn)+67%ε	482	2,940	0,098	37,40	57,90
B3, $Ag_{50}Ge_{50}$	50%(Ag)+50%(Ge)	296	1,060	0,035	84,40	114,3

From the presented data (Figure 1 and Table 1) for the tested samples of three binary alloys B1  $Ge_{50}Sn_{50}$ , B2  $Ag_{50}Sn_{50}$  and B3  $Ag_{50}Ge_{50}$  it is evident that the corrosion potentials of  $E_{corr}$  range from -296 mV for B3  $Ag_{50}Ge_{50}$  to -482 mV for B2  $Ag_{50}Sn_{50}$ . The  $j_{corr}$  corrosion current densities range from 1,060  $\mu A/cm^2$  for B3  $Ag_{50}Ge_{50}$  to 16.10  $\mu A/cm^2$  for B1  $Ge_{50}Sn_{50}$ . The lowest value of corrosion rate  $v_{corr}=0.035$  mm/year is for the binary alloy B3  $Ag_{50}Ge_{50}$ , which is more corrosion resistant than the binary alloy B1  $Ge_{50}Sn_{50}$  ( $v_{corr}=0.54$  mm/year) and the binary alloy B2  $Ag_{50}Sn_{50}$  ( $v_{corr}=0.098$  mm/year), which has the highest value of the corrosion rate of the three binary alloys tested.

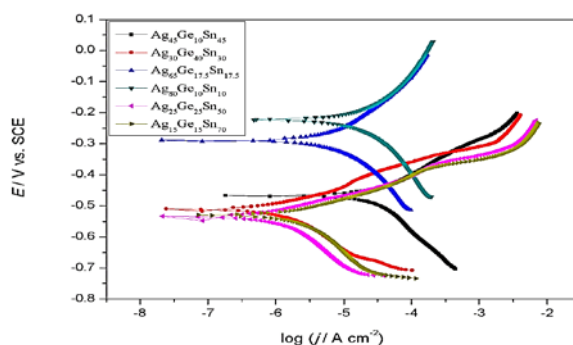


Figure 2 - Tafel plots for tested ternary alloys Ag-Ge-Sn

Table 2 - Electrochemical polarization parameters of corrosion for tested ternary alloys Ag-Ge-Sn

Alloy	Predicted percent of the phase at 25 °C	-E <sub>corr</sub> (mV)	j <sub>corr</sub> (μA/cm <sup>2</sup> )	v <sub>corr</sub> (mm/year)	β <sub>a</sub> (mV/dec)	β <sub>k</sub> (mV/dec)
1 - Ag <sub>65</sub> Ge <sub>17,5</sub> Sn <sub>17,5</sub>	17%(Ge)+53%ε+30%ζ	289	0,94	0,031	32,66	67,76
2 - Ag <sub>80</sub> Ge <sub>10</sub> Sn <sub>10</sub>	10%(Ge)+90%ζ	224	2,67	0,089	33,66	68,61
3 - Ag <sub>45</sub> Ge <sub>10</sub> Sn <sub>45</sub>	30%(βSn)+10%(Ge)+60%ε	466	3,859	0,129	25,33	67,22
4 - Ag <sub>30</sub> Ge <sub>40</sub> Sn <sub>30</sub>	20%(βSn)+40%(Ge)+40%ε	509	0,16	0,005	24,39	49,77
5 - Ag <sub>25</sub> Ge <sub>25</sub> Sn <sub>50</sub>	42%(βSn)+25%(Ge)+33%ε	533	0,22	0,007	38,58	53,59
6 - Ag <sub>15</sub> Ge <sub>15</sub> Sn <sub>70</sub>	65%(βSn)+15%(Ge)+20%ε	529	0,42	0,013	37,12	51,33

Based on the presented data (Figure 2 and Table 2) of the tested alloys of the ternary Ag-Ge-Sn system, the highest corrosion resistance was shown by sample 4 (Ag<sub>30</sub>Ge<sub>40</sub>Sn<sub>30</sub>), with corrosion potential  $E_{corr} = -509 \text{ mV}$ , the lowest corrosion density  $j_{corr} = 0,16 \text{ } \mu\text{A}/\text{cm}^2$  and the lowest corrosion rate  $v_{corr} = 0,005 \text{ mm/year}$ . This can be related to high percent of (Ge) phase inside this sample. Compared with other samples percent of (Ge) phase is highest in sample 4 and then decreases. Sample 5 (Ag<sub>25</sub>Ge<sub>25</sub>Sn<sub>50</sub>) also show very high corrosion resistance, where the corrosion current densities are  $j_{corr} = 0,22 \text{ } \mu\text{A}/\text{cm}^2$  and corrosion rate  $v_{corr} = 0,007 \text{ mm/year}$ . Based on the corrosion current density and the calculated depth indicator of corrosion-corrosion rate  $v_{corr}$ , all tested alloys are very resistant to corrosion ( $v_{corr} = 0.005-0.129 \text{ mm/year}$ ) in 3% NaCl solution. The corrosion resistance of the tested alloys decreases in the following order: sample 4 (Ag<sub>30</sub>Ge<sub>40</sub>Sn<sub>30</sub>), 5 (Ag<sub>25</sub>Ge<sub>25</sub>Sn<sub>50</sub>), 6 (Ag<sub>15</sub>Ge<sub>15</sub>Sn<sub>70</sub>) 1 (Ag<sub>65</sub>Ge<sub>17,5</sub>Sn<sub>17,5</sub>), 2 (Ag<sub>80</sub>Ge<sub>10</sub>Sn<sub>10</sub>) and 3 (Ag<sub>45</sub>Ge<sub>10</sub>Sn<sub>45</sub>). Similar trend is relating to reduction of (Ge) phase: 4, 5, 1, 6, 2 and 3.

Nyquist diagrams for three samples of binary alloys and six samples of ternary alloys were recorded by electrochemical impedance spectroscopy (EIS) (Figures 3 and 4). The fitting of the experimental data was done using an equivalent circuit (Figure 5) and the results (electrochemical impedance corrosion parameters) are shown in Tables 3 and 4.

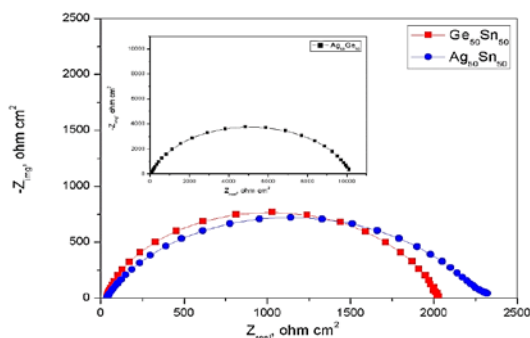


Figure 3 - Nyquist diagrams for tested binary alloys B1-Ge<sub>50</sub>Sn<sub>50</sub>, B2-Ag<sub>50</sub>Sn<sub>50</sub> and B3-Ag<sub>50</sub>Ge<sub>50</sub>.

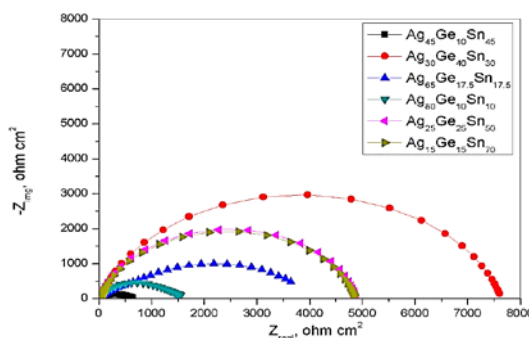


Figure 4 - Nyquist diagrams for tested ternary alloys of the Ag-Ge-Sn system.

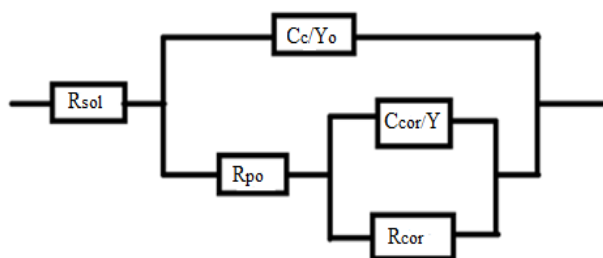


Figure 5 - Equivalent circuit

Table 3. Electrochemical impedance corrosion parameters for tested binary alloys B1-Ge<sub>50</sub>Sn<sub>50</sub>, B2-Ag<sub>50</sub>Sn<sub>50</sub> and B3-Ag<sub>50</sub>Ge<sub>50</sub>.

Alloy	$R_{soln}, (\Omega)$	$R_{cor}, (\Omega)$	$R_{po}, (\Omega)$	$R_{tot}, (\Omega)$	$C_{cor}, (F)$	$n$	$C_c, (F)$	$m$	Fitting error
B1-Ge <sub>50</sub> Sn <sub>50</sub>	65,15	635,3	1672	2307,3	$9,70 \cdot 10^{-4}$	0,846	$2,10 \cdot 10^{-5}$	0,773	$2,985 \cdot 10^{-4}$
B2-Ag <sub>50</sub> Sn <sub>50</sub>	35,41	3233	1870	5103,0	$1,52 \cdot 10^{-2}$	0,525	$6,34 \cdot 10^{-6}$	0,743	$1,598 \cdot 10^{-4}$
B3-Ag <sub>50</sub> Ge <sub>50</sub>	34,94	10050	142,4	10 192,4	$1,16 \cdot 10^{-5}$	0,745	$6,06 \cdot 10^{-6}$	0,901	$1,090 \cdot 10^{-3}$

Table 4. Electrochemical impedance corrosion parameters for tested ternary alloys of the Ag-Ge-Sn sytem.

Alloy	$R_{soln}, (\Omega)$	$R_{cor}, (\Omega)$	$R_{po}, (\Omega)$	$R_{tot}, (\Omega)$	$C_{cor}, (F)$	$n$	$C_c, (F)$	$m$	Fitting error
3-Ag <sub>65</sub> Ge <sub>17,5</sub> Sn <sub>17,5</sub>	25,42	3263	770,5	4033,5	$2,93 \cdot 10^{-4}$	0,6159	$2,39 \cdot 10^{-5}$	0,7286	$366,8 \cdot 10^{-6}$
4-Ag <sub>80</sub> Ge <sub>10</sub> Sn <sub>10</sub>	24,29	1672	25,56	1697,56	$2,51 \cdot 10^{-5}$	0,3477	$2,94 \cdot 10^{-5}$	0,8922	$150,2 \cdot 10^{-6}$
5-Ag <sub>45</sub> Ge <sub>10</sub> Sn <sub>45</sub>	32,45	642,7	171,4	814,1	$1,41 \cdot 10^{-5}$	0,4133	$4,55 \cdot 10^{-6}$	0,9635	$1,521 \cdot 10^{-3}$
6-Ag <sub>30</sub> Ge <sub>40</sub> Sn <sub>30</sub>	27,53	6567	943	7510	$3,79 \cdot 10^{-6}$	0,8792	$1,13 \cdot 10^{-5}$	0,8765	$2,541 \cdot 10^{-3}$
11-Ag <sub>25</sub> Ge <sub>25</sub> Sn <sub>50</sub>	26,88	398,3	4457	4855,3	$1,22 \cdot 10^{-4}$	0,9899	$1,30 \cdot 10^{-6}$	0,8835	$3,269 \cdot 10^{-4}$
12-Ag <sub>15</sub> Ge <sub>15</sub> Sn <sub>70</sub>	26,32	3234	1605	4839	$1,54 \cdot 10^{-6}$	0,9613	$2,38 \cdot 10^{-5}$	0,8531	$4,245 \cdot 10^{-3}$

For the analyzed data using the equivalent circuit of Figure 5, a low value of the error estimation of the fitting procedure was obtained (Tables 3 and 4). It can be concluded that the selected equivalent circuit is sufficiently precise to describe the tested alloys.

#### 4. CONCLUSION

The corrosion resistance of six ternary and three binary alloys was examined in 3% NaCl solution using the potentiodynamically polarization method (Tafel plots) and electrochemical impedance spectroscopy (EIS). The highest corrosion resistance is for sample 6 (Ag<sub>30</sub>Ge<sub>40</sub>Sn<sub>30</sub>).

#### ACKNOWLEDGEMENTS

*This work has been supported by the National Nature Science Foundation of China (project No.51950410600) and the Ministry of Education, Science and Technological Development of the Republic of Serbia (Grant No. OI172037).*

#### REFERENCES

- [1] V. Ponnambalam, D.T. Morelli, A Novel, J. Alloys Compd., 740 (2018) 42-46.
- [2] D. Ielmini, A.L. Lacaíta, Mater. Today, 14 (2011) 600-607.
- [3] Y. Tan, Heterogeneous Electrode Processes and Localized Corrosion, John Wiley & Sons, Inc., Hoboken, New Jersey, 2013, p.120-131.
- [4] D. Landolt, Corrosion and Surface Chemistry of Metals . EPFL Press, 2007, p.206-224.

## EXTRACTION OF LOW-DIMENSIONAL STRUCTURES OF NOBLE AND NONFERROUS METALS FROM REFRACTORY RAW MATERIALS

Tatiana Aleksandrova, Nadezhda Nikolaeva

Saint Petersburg mining University, 199106, 21 line, 2, Saint – Petersburg, Russia

### Abstract

*In connection with the depletion of legacy reserves of non-ferrous and noble metals, the search for and involvement in the processing of non-traditional minerals is a rather urgent task. The use of physical and chemical impacts at different stages of beneficiation allows to make the processing of such raw materials cost-effective. The object of the study in this work was a refractory gold-bearing ore. This object is characterized by the presence of organic carbon and low-dimensional structures of noble and nonferrous metals in the form of inclusions in sulfide minerals - concentrators. The work presents the results of studying the effect of physical effects (cryo- and microwave impacts) on mineral raw materials at different stages of beneficiation. It was found that because of cryo-action at the stage of grinding increases the destruction of raw materials, and microwave impacts to flotation concentrates leads to the enlargement of valuable components. Based on experimental and theoretical studies, the methods of intensification of ore preparation and beneficiation processes through the use of controlled physical and chemical effects at the successive stages of transformation of minerals, which allow to accelerate by thousands (sometimes by millions) times the natural processes occurring in the Earth's crust for thousands of years, are substantiated in the work.*

**Keywords:** non-ferrous and precious metals, disintegration, flotation, intensification

### 1. INTRODUCTION

Engaging in the processing of unpayable, refractory mineral raw materials which contain low-dimension structures of non-ferrous and noble metals, is due to the depletion of rich and easily recoverable deposits [1]. There are some of serious problems in the processing of deposits of complex unpayable raw materials with characteristic features: what valuable components to extract first, the optimal depth of enrichment, which enrichment and processing technologies will be the most effective and economically justified, and in some cases the inability to extract valuable metals and, therefore, large losses during concentrating. Extraction of low-dimension structures of non-ferrous and noble metals from refractory minerals requires a deeper structural restructuring of the enriched minerals than the processing of ores with finely dispersed valuable metals [2]. It is possible to intensify the enrichment and processing processes by physical-mechanical and chemical effects (defragmentation, change in structure, etc.) at consecutive steps of raw material reorganization. Thus, the extraction of low-dimension structures ("invisible" particles) of metals from difficult to concentrate carbonaceous raw materials using various physical and chemical effects at the main stages of concentration allows to create new technological solutions for cost-effective processing and replicate them to other types of minerals.

### 2. MATERIALS AND METHODS

The object of the study in this work was a refractory gold-bearing ore. This object is characterized by the presence of organic carbon and low-dimensional structures of noble and nonferrous metals in the form of inclusions in sulfide minerals - concentrators. The main valuable component is gold, which content in the ore is approximately 5 g/t. The mineralogical composition of the ore was established using advanced equipment (Fig. 1). The work was conducted in various directions:

research of the effect of cryogenic impact on the disintegration stages; flotation enrichment; research of the effect of microwave impact for enlargement of low-sized structures of valuable components. Experimental studies were carried out on the facilities of the Saint Petersburg Mining University (jaw crusher, roller crusher, ball mill, Laarmann Flotation Bench Test Machine, laser diffractometer "Mastersaizer", laboratory microwave oven with the ability to adjust the power to 1000 W, etc.). The elemental composition was analyzed using an EDX 7000 X-ray fluorescence analyzer (Shimadzu).

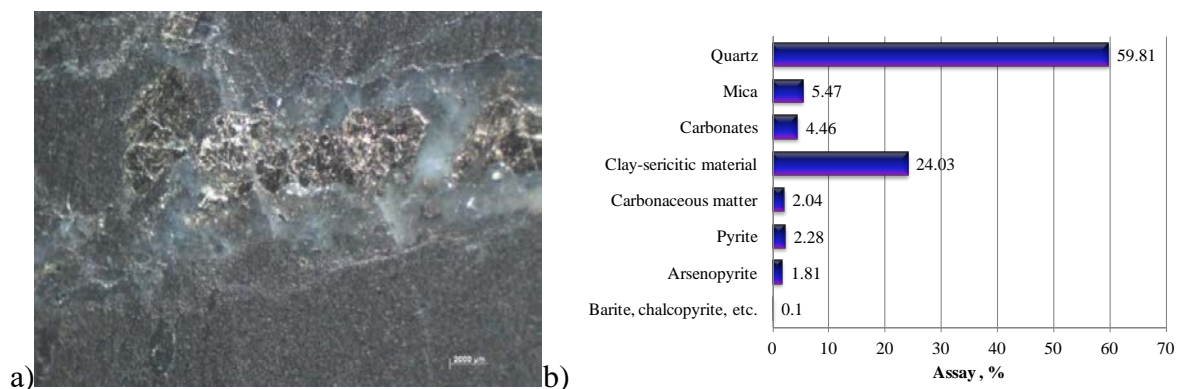


Figure 1 - The object of the study: a - microphotograph of the sample, b - mineralogical composition

### 3. RESULTS AND DISCUSSION

#### 3.1 Influence of cryogenic impacts on the disintegration of minerals to intensify the extraction of precious and non-ferrous metals

One of the variants of intensification of disintegration processes is the use of cryogenic impact. Especially, it is relevant for the deposits of the Arctic zone, which are now actively involved in the processing. The research was conducted to obtain the maximum yield of the prepared class (-0.14 mm) with a minimum consumption of energy and time. The effect of cryogenic impact was studied for a prefrozen sample (down to -50 °C) and with the use of refrigerants and cryoagents (CO<sub>2</sub> and N<sub>2</sub>) directly during grinding. The use of low and ultralow temperatures during grinding leads to the development of existing defects, nucleation, and development of microcracks, including in the volume of minerals.

As a result of the studies, a series of characteristic features was established. To evaluate the efficiency of cryogenic impact on the fracture process, the efficiency coefficient of obtaining the prepared class  $K_{ef}$  was used. The results are visualized in Figure 2.

$K_{ef}$  were calculated according to the formula:

$$K_{ef} = \frac{\gamma_1 - \gamma_0}{100 - \gamma_0},$$

where  $\gamma_i$  is the yield of the desired class after grinding, % (i – method of impact);  $\gamma_0$  is the yield of the desired class in the sample, %.

It was found that the use of cryogenic impacts allows to achieve an increase in the efficiency of refractory minerals grinding ( $K_{ef}$  has been increased from 0.45 to 0.98), which is achieved due to the development of hydration and cryohydration processes occurring both on the surface and in the volume of minerals.

It was also found that grinding in liquid nitrogen medium is the most effective, as the maximum yield of the prepared class is achieved under equal conditions.



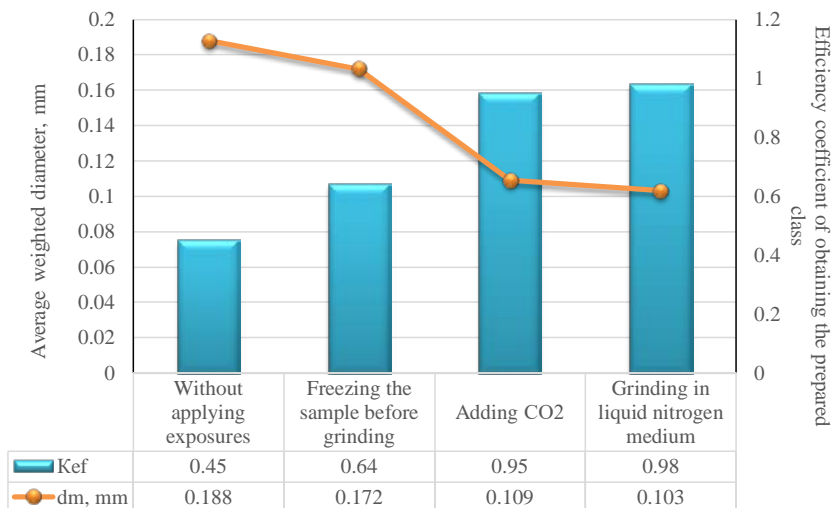


Figure 2 - Visualization of the results of assessing the effect of the type of cryogenic impact on the grinding efficiency

Nitrogen freezing provides a high rate of temperature reduction, and the inert atmosphere prevents self-oxidation, and the destruction of organic carbon occurs. It can be assumed that the use of ultralow temperatures will reduce the refractoriness of carbon-bearing ores due to the high content of carbonaceous matter.

### 3.2 Application of microwave impact to increase the efficiency of refractory minerals processing

To evaluate the efficiency of physical and energy methods of impact to activate the raw materials, the effect of microwave impact on sulfide flotation concentrates obtained after flotation beneficiation was investigated. After flotation beneficiation the concentrates were filtered and dried. Representative samples were taken from the obtained sulfide flotation concentrates to estimate the activation energy of the samples before impact. The sulfide flotation concentrates were treated with Microwave impact for 5 minutes at a power of 1 kW. Thermal examination was performed at three sample heating rates (5, 10 and 20 °C/min). The results of thermal investigation of samples in air with heating rate of 20 degrees per minute crushed ore and ore after microwave impact are shown in Figures 3 and 4, respectively.

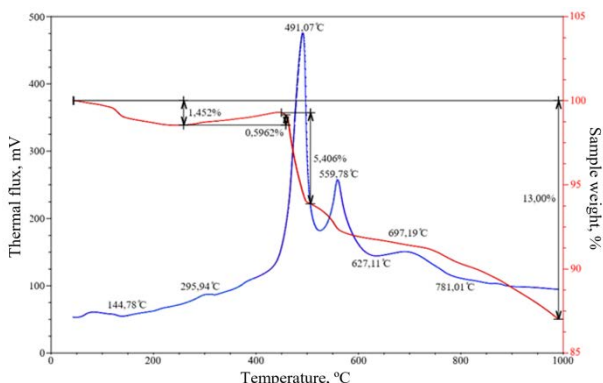


Figure 3 - Activation energy calculation results for samples before microwave impact

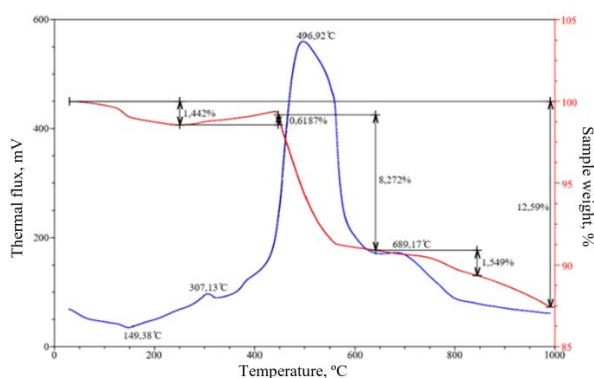


Figure 4 - Results of calculation of activation energy for samples after microwave impact

Calculation of energy of activation for samples at degrees of transformation from 0.02 to 0.98 with a step of 0.08 was carried out with application of the developed program for a computer [3]. The analysis of the received data has allowed to establish, that average value of energy of activation for samples of flotation sulphide concentrates before impact makes at calculation by a differential



method 215.79 kJ/mol, on an integral-kinetic method 210.95 kJ/mol. Additionally, the pre-exponential multiplier for these samples was calculated to be 23.495 s<sup>-1</sup>. The average value of activation energy for sulfide flotation concentrate samples after microwave action is 323.16 kJ/mol by the differential method and 313.91 kJ/mol by the integral-kinetic method. Additionally, the pre-exponential multiplier for these samples was calculated, which is 34.865 s<sup>-1</sup>. To evaluate the efficiency of microwave impact to minerals the calculation of the developed complex criterion was conducted by the formula:

$$K_a = \frac{\sum_{i=1}^n \frac{E_{a_i}^{after}}{n} \cdot \sum_{i=1}^n \frac{E_{a_i}^{after}}{n} \cdot \sum_{i=1}^n \frac{\ln A_i^{after}}{n}}{\sum_{i=1}^n \frac{E_{a_i}^{before}}{n} \cdot \sum_{i=1}^n \frac{E_{a_i}^{before}}{n} \cdot \sum_{i=1}^n \frac{\ln A_i^{before}}{n}}$$

which was  $K_a = 0.302$ . These values correspond to activation of raw materials at application of various types of physical-energetic impacts. Grinding

Based on the conducted research the basic scheme of extraction of low-dimensional structures of noble and nonferrous metals from refractory raw materials (fig. 5) was substantiated.

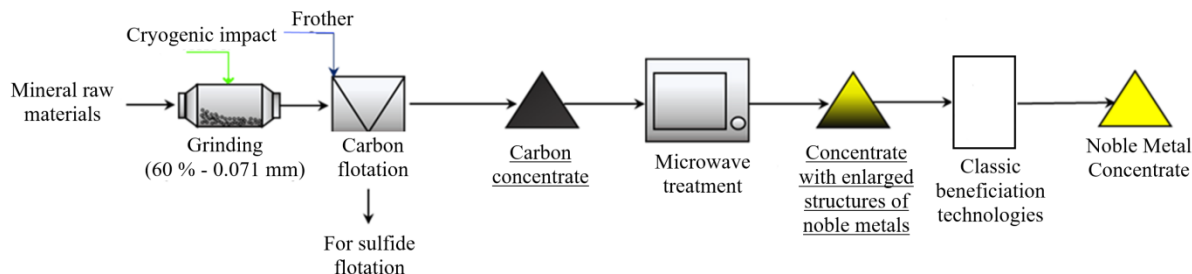


Figure 5 - Schematic scheme of the nature-like technology for the extraction of noble and nonferrous metals using cryo- and microwave impacts

#### 4. CONCLUSIONS

In the work research on extraction of low-dimension structures of noble and non-ferrous metals from refractory raw materials were conducted. Experimental and theoretical studies substantiated methods of intensification of ore preparation and beneficiation processes through the use of directed physical impacts at the consecutive steps of mineral raw material transformation, which allow to intensify by thousands (sometimes by millions) times the natural processes that occur in the Earth's crust for thousands of years, have been substantiated.

#### ACKNOWLEDGEMENTS

*This work was carried out within the grant of the Russian Science Foundation (Project N 19-17-00096).*

#### REFERENCES

- [1] H.Y. Sohn. Nonferrous Metals: Production and History, Reference Module in Materials Science and Materials Engineering. Elsevier, 2017, ISBN 9780128035818.
- [2] V.A. Chanturiya, I.Z. Bunin. Minerals, 2022, 12, 1177.
- [3] T.N. Aleksandrova, A.V. Afanasova, E.A. Ivanov. Program for calculating the energy of mechanoactivation of raw materials by interpreting thermograms. Registration certificate for computer program RU 2019666779, 13.12.2019.

## AIR QUALITY MEASUREMENTS IN THE BOR CITY DURING THE RECONSTRUCTION OF THE COPPER SMELTER BOR IN 2022

Viša Tasić<sup>1</sup>, Tatjana Apostolovski-Trujić<sup>1</sup>, Bojan Radović<sup>1</sup>, Nevena Ristić<sup>1</sup>, Tamara Urošević<sup>1</sup>, Vladan Kamenović<sup>1</sup>, Zvonko Damnjanović<sup>2</sup>

<sup>1</sup>Mining and Metallurgy Institute Bor, Zeleni bulevar 35, 19210 Bor, Serbia

<sup>2</sup>Kompjuter centar Bor, Trg Oslobođenja 8, 19210 Bor, Serbia

### Abstract

*Industrial activities in Bor, especially those related to the operation of the copper smelter, have caused a number of negative impacts on the environment in the region (including air, water, and soil) and have caused serious concern about the effects they have on human health. The Government of the Republic of Serbia invested significant funds in the construction of a new copper smelter in Bor which began operating in 2016. The new copper smelter uses flash-smelting technology, so the emissions of waste gases from metallurgical plants are of different intensities and compositions than before. In the meantime, the mining and smelting basin of Bor goes through an ownership transformation in 2018. ZiJin, one of the world's leading mining companies in the production of copper and precious metals, became a strategic partner. The Serbia ZiJin Bor Copper launched a number of projects to increase mining and metallurgical production in Bor. The capacities of the copper smelter in Bor are being expanded during 2022-2023 by about 2.5 times and a new sulfuric acid factory and a new electrolysis plant is being built. The start of operation of the expanded facilities in the copper smelter is expected in the middle of 2023. This paper presents the results of air quality measurements in the city of Bor in the time period when the copper smelter in Bor is not working, due to reconstruction (June - December 2022). These measurements aimed to determine the level of air pollution at locations not part of the state or local air quality monitoring network. These measurements are of great importance because many people live in those areas. The obtained results will serve as a basis for future air quality monitoring when the copper smelter in Bor starts to operate again.*

**Keywords:** copper smelter, air pollution, suspended particles, arsenic

### 1. INTRODUCTION

The copper ore has been mined and processed on the territory of the city of Bor (Serbia) for more than a century. The operations of the copper ore excavation and processing have caused a number of negative impacts on the environment in the region (including air, water, and soil) and have caused serious concern about the effects they have on human health [1,2,3]. Air quality monitoring in the city of Bor has been systematically carried out since the seventies of the last century. Since 2005, automatic methods of measuring sulfur dioxide concentrations have been applied at several measuring points in the city [4,5,6]. The smelting technology in the copper smelter in Bor was changed in 2016, so the concentrations of sulfur dioxide that have been recorded since then are significantly lower than during the period of operation of the copper smelter with the old smelting technology. Despite the changed copper smelting technology, the concentration of SO<sub>2</sub> and carcinogenic elements, especially arsenic, in the suspended particles of the PM<sub>10</sub> fraction is still higher than prescribed by law at certain measuring points in the city [7,8,9].

ZiJin, one of the world's leading mining companies in the production of copper and precious metals, became the majority owner of the copper smelter and mine in Bor in 2018 [10]. The Serbia ZiJin Bor Copper company launched a number of projects to increase mining and metallurgical production in Bor. The capacities of the copper smelter in Bor are being expanded during 2022-2023 by about 2.5 times and a new sulfuric acid factory and a new electrolysis plant are being

built. The start of operation of the expanded facilities in the copper smelter is expected in the middle of 2023. During the reconstruction period (from June 2022 to March 2023), the copper smelter in Bor was not operated, so this period was used for air pollution monitoring with an aim to better understand the impact of the smelter's operation on air pollution in Bor.

## 2. EXPERIMENTAL

Based on the analysis of the concentrations of air pollutants measured at the existing measuring points in the city of Bor from 2016 up to 2022, as well as the possible impact of the new mining and metallurgical facilities on the air quality, additional measurement locations were selected. So, those locations are not part of the national or local air quality monitoring network. This was done in order to better assess the impact of the operation of the Bor copper smelter on air quality and human health at those locations too.



Figure 1 - Map of the agglomeration of Bor with measurement points marked (1. Bor Lake, 2. Brestovacka Spa, 3. Metovnica, 4. Brestovac, 5. Oštrelj, 6. Industrial zone, 7. Slatinsko naselje, 8. Police headquarters, 9. Slatina, 10. Gornjane, KR- Krivelj, BR- Brezonik, TP - Town Park, IN- Institute MMI, SL- Slatina) [11]

At each of additional measuring point (marked with numbers 1-10 in Figure 1), sampling of suspended particles ( $PM_{10}$ ) was carried out for 10 consecutive days (June 2022 - December 2022). Daily  $PM_{10}$  samples were collected with reference sampler Sven/Leckel LVS3[12] on Whatman QM-A quartz filters with a diameter of 47 mm. Sampling and determination of the mass concentration of suspended particles  $PM_{10}$  were performed in accordance with the standard SRPS EN12341:2015 [13]. Further preparation of samples for chemical analysis was carried out in accordance with the SRPS EN14902:2008 [14]. The content of chemical elements in the  $PM_{10}$  samples was determined using ICP MS (Agilent model 7700) [15]. The detection limits of this device for As, Pb, Cd, and Ni were 0.1, 0.5, 0.02, and 0.7  $ng/m^3$ , respectively. The control of the applied procedures was carried out using the reference material [16]. Simultaneously with gravimetric measurements, continuous measurements of mass concentrations of gaseous pollutants  $SO_2$ ,  $NO_x$ ,  $NO_2$ ,  $NO$ ,  $CO$ , and  $O_3$  were carried out using Teledyne automatic gas analyzers [17] installed in a mobile measuring station.

## 3. RESULTS AND DISCUSSION

The measurement results presented in Table 1 show that there was no exceedance of the daily limit values for gaseous pollutants, nor was there an exceedance of the limit value for the average daily concentration of lead in suspended particles of the  $PM_{10}$  fraction. There was no overshooting of

target values for annual concentrations of cadmium and nickel in PM<sub>10</sub>. The concentration of arsenic in PM<sub>10</sub> at measuring point 8 (PU Bor) was above the target annual value for 3 out of 10 measurement days. The maximum measured mean daily value of arsenic concentration in PM<sub>10</sub> at this measuring point was 11.3 ng/m<sup>3</sup>. We believe that surface emissions of suspended particles inside the copper smelter Bor (road dust, construction works) are the dominant source of As detected in PM<sub>10</sub> at this measuring point.

Table 1 - Results of air quality monitoring (measuring points marked from 1-10 in Figure 1). Mean daily concentrations of PM<sub>10</sub>, chemical elements in PM<sub>10</sub>, SO<sub>2</sub>, NO<sub>x</sub>, NO<sub>2</sub>, NO, CO, and O<sub>3</sub> (AMS -Automatic Monitoring Station)

	Unit	Measuring point									
		1	2	3	4	5	6	7	8	9	10
PM <sub>10</sub>	µg/m <sup>3</sup>	12.8	19.4	26.3	19.1	20.9	44.2	25.7	35.9	23.3	34.8
As	ng/m <sup>3</sup>	0.3	0.5	1.2	1.8	0.7	4.2	3.5	6.1	3.5	0.5
Cd	ng/m <sup>3</sup>	0.0	0.1	0.0	0.1	0.1	0.4	0.1	0.2	0.1	0.1
Pb	ng/m <sup>3</sup>	0.5	1.7	3.9	4.2	2.6	19.6	47.6	10.9	4.2	3.5
Ni	ng/m <sup>3</sup>	1.9	1.3	2.9	3.5	2.4	4.2	3.9	0.9	3.8	0.8
Al	ng/m <sup>3</sup>	2.4	38.8	289.2	230.0	306.6	565.2	582.2	268.2	244.0	237.7
Sb	ng/m <sup>3</sup>	0.0	0.1	0.1	0.3	0.1	0.7	1.0	0.5	1.1	0.4
Zn	ng/m <sup>3</sup>	10.0	29.7	3.8	18.1	24.0	47.8	23.5	11.8	45.1	10.5
Cu	ng/m <sup>3</sup>	1.2	5.8	8.2	33.5	41.4	73.1	106.1	5.4	27.3	4.6
Co	ng/m <sup>3</sup>	0.0	0.1	0.3	0.1	0.1	0.3	0.3	0.1	0.2	0.1
Mn	ng/m <sup>3</sup>	0.4	2.2	6.2	6.1	6.1	21.5	11.8	6.8	6.4	6.0
Cr	ng/m <sup>3</sup>	5.0	1.8	7.0	4.6	6.2	8.1	6.5	0.2	7.6	0.2
Fe	ng/m <sup>3</sup>	4.4	65.3	241.2	156.2	253.5	706.9	440.5	209.6	212.1	186.0
Se	ng/m <sup>3</sup>	1.8	2.3	2.0	2.2	2.0	1.8	16.5	2.2	2.3	2.0
Sr	ng/m <sup>3</sup>	0.5	1.2	1.3	1.9	2.4	4.6	5.2	0.7	1.7	0.6
Mo	ng/m <sup>3</sup>	0.5	0.6	1.2	1.1	1.0	0.5	1.3	0.6	1.0	0.5
Ag	ng/m <sup>3</sup>	0.5	0.6	1.8	2.0	1.8	0.4	5.1	2.0	1.8	1.8
Sn	ng/m <sup>3</sup>	0.5	0.6	0.6	4.2	1.7	0.6	1.2	0.5	0.6	0.5
Ba	ng/m <sup>3</sup>	1.5	2.6	2.8	2.0	14.9	11.8	11.8	2.7	5.8	2.3
Ca	ng/m <sup>3</sup>	158.0	289.9	403.4	348.3	785.8	1177.2	1302.1	90.1	565.4	82.7
K	ng/m <sup>3</sup>	71.7	168.6	133.5	108.3	151.7	271.6	273.0	317.5	149.6	284.1
Mg	ng/m <sup>3</sup>	36.3	37.1	80.8	69.7	110.5	146.5	158.3	22.5	76.5	20.9
Na	ng/m <sup>3</sup>	248.2	258.4	48.1	136.2	274.8	231.3	712.7	11.3	146.5	10.3
S	ng/m <sup>3</sup>	181.3	520.3	1112.2	344.6	569.4	1358.0	659.1	579.9	867.6	520.7
AMS SO <sub>2</sub>	µg/m <sup>3</sup>	9.3	7.3	21.0	4.4	6.1	8.0	8.0	15.9	21.4	5.3
AMS NO <sub>x</sub>	µg/m <sup>3</sup>	8.0	6.5	7.9	10.0	9.9	19.6	16.5	25.7	14.2	12.2
AMS NO <sub>2</sub>	µg/m <sup>3</sup>	4.6	3.6	4.1	6.7	6.4	12.8	12.9	11.0	8.7	8.0
AMS NO	µg/m <sup>3</sup>	3.0	1.8	2.4	2.4	2.3	4.4	2.5	9.7	3.5	2.9
AMS CO	mg/m <sup>3</sup>	0.2	0.3	0.2	0.2	0.2	0.7	0.2	0.6	0.4	0.5
AMS O <sub>3</sub>	µg/m <sup>3</sup>	66.1	72.6	94.7	93.0	91.8	57.6	87.1	68.0	88.0	67.6

#### 4. CONCLUSION

This paper presents the results of air quality measurements at an additional 10 locations in the Bor agglomeration in the period June - December 2022, at a time when the copper smelter in Bor was not operating. Based on a complete insight into the results of air quality measurements in the Bor agglomeration in 2022 [11,18], it can be concluded that, in the period when the copper smelter was in operation, a dominant share in the levels of SO<sub>2</sub>, as well as the concentrations of As, Cd, and Pb in PM<sub>10</sub> originates from emissions of gaseous pollutants from a copper smelter Bor.

## ACKNOWLEDGEMENTS

*This work was financially supported by the Ministry of Science, Technological Development, and Innovation of the Republic of Serbia, Grant No. 451-03-47/2023-01/ 200052*

## REFERENCES

- [1] Kovačević, R., Jovašević-Stojanović, M., Tasić, V., Milošević, N., Petrović, N., Stanković, S., Matić-Besarabić, S., Chem. Ind. Chem. Eng. Q., 16 (3) (2010) 269–279.
- [2] Pope, C.A., Burnett, R.T., Thun, M.J., Calle, E.E., Krewski, D., Kazuhiko, I., et al., J. Am. Med. Assoc., 287 (9) (2002) 1132–1141.
- [3] Razos, P., Christides, A., Int. J. Environ. Res., 4 (4) (2010) 785-794.
- [4] Serbula, S., Ilic, A., Kalinovic, J., Kalinovic, T., Petrović, N., Environ. Earth Sci., 71 (4) (2014) 1651–1661.
- [5] Serbula, S., Kalinovic, T., Kalinovic, J., Ilic, A., Environ. Earth Sci. 68 (7) (2013) 1989–1998.
- [6] Tasić, V., Kovačević, R., Maluckov B., Apostolovski-Trujić T., Cocić M., Matić, B., Štearnik M., Water Air and Soil Pollut., 228 (2017) 230.
- [7] State of Environment in the Republic of Serbia during 2019 (in Serbian) [http://www.sepa.gov.rs/download/izv/Vazduh\\_2019.pdf](http://www.sepa.gov.rs/download/izv/Vazduh_2019.pdf) Accessed in April 2023
- [8] State of Environment in the Republic of Serbia during 2020 (in Serbian) [http://www.sepa.gov.rs/download/izv/Vazduh\\_2020.pdf](http://www.sepa.gov.rs/download/izv/Vazduh_2020.pdf) Accessed in April 2023
- [9] Serbula, S. Milosavljevic, J. Kalinovic, J., Kalinovic, T., Radojevic, A., Apostolovski- Trujic, T., Tasic, V., Sci. Total Environ., 777 (2021) 145981
- [10] ZiJin (2022). <https://www.zijinmining.com/> Accessed in April 2023
- [11] Tasić, V., Apostolovski-Trujić, T., Radović, B., Kovačević, R., Ristić, N., Urošević, T., Kamenović, V., Copper, 48 (1) (2023) 53-62.
- [12] <https://www.et.co.uk/assets/resources/datasheets/lvs3mvs6e.pdf> Accessed in April 2023
- [13] SRPS EN 12341:2015 Ambient air - Standard gravimetric measurement method for the determination of the PM<sub>10</sub> or PM<sub>2.5</sub> mass concentration of suspended particulate matter <https://iss.rs/en/project/show/iss:proj:49389> (in Serbian) Accessed in April 2023
- [14] SRPS EN 14902:2008 Ambient air quality - Standard method for the measurement of Pb, Cd, As and Ni in the PM<sub>10</sub> fraction of suspended particulate matter <https://iss.rs/en/project/show/iss:proj:18667> (in Serbian) Accessed in April 2023
- [15] <https://www.agilent.com/Library/brochures/5990-4025EN.pdf> Accessed in April 2023
- [16] Standard Reference Material 1648a - Urban Particulate Matter [https://www-s.nist.gov/srmors/view\\_detail.cfm?srm=1648A](https://www-s.nist.gov/srmors/view_detail.cfm?srm=1648A) Accessed in April 2023
- [17] <https://www.teledyne-api.com/products> Accessed in April 2023
- [18] Ambient Air Quality Testing in Bor (annual report for 2022), MMI Bor, 2022 (in Serbian) Accessed in April 2023

## APPLICATION OF CONTROL CHARTS IN THE LABORATORY FOR TESTING THE METALLIC MATERIALS

Slavica Miletć, Biserka Trumić, Suzana Stanković

Mining and Metallurgy Institute Bor, Zelene bulevar 35, 19210 Bor, Serbia

### *Abstract*

*Control charts are methods for collecting, processing, analyzing and displaying data to ensure the product and process quality. Control charts as tools belong to the statistical process control (SPC). The accuracy of the results is ensured by application the control charts for accreditation the tensile testing methods. This paper presents the application of control charts for validation the testing method of steel wires by tension. Control charts show that the analyzed method is under control. The main goal of control charts is to quickly detect errors during testing and prove that the processes are under control.*

**Keywords:** application, control charts, testing, metal materials

### 1. INTRODUCTION

Control charts are the statistical process control (SPC) techniques. The SPC is an online quality control system, defined as a philosophy, strategy and methods for improving systems, outcomes and processes. [1]. The static process monitoring methods have an irreplaceable position in a smart process control [2]. The static methods began to be successfully applied in the twenties of the last century. The use of control charts has grown significantly in recent times. Various forms of control charts have been developed for the process monitoring. The classic parametric control charts represent the presence of normal data, constant mean and variance, and data independence [3,4,5]. In a practical sense and smart manufacturing processes with a complex structure, such prerequisites are often not met. Therefore, an incorrect application of the parametric control charts can lead to the wrong conclusions about the static stability of process. More reliable non-parametric control charts have been designed for these types of processes [6,7]. The non-parametric control charts to overcome the shortcomings of classical parametric control charts have shown a great role in a smart manufacturing process monitoring due to their ability [8,9,10,11].

The control charts are considered as the most important tool for the process quality control. They are presented as graphs where the vertical line represents the order of control and the horizontal value of the parameter that is controlled on the certain size samples. The graph shows the process quality variation in relation to certain control limits. The control limits are given by the standard or calculated depending on the process or method. When the process variation occurs within given limits, that process is said to be in a state of static control. Otherwise, if the process variation is outside the control limits, the process is said to be out of static control.

The control charts are the simplest form of process control providing a detailed insight into the state. Also, they provide enough visibility to conclude whether the process is under control or not. They clearly show where the measured individual quantities are in relation to the tolerance field. This means that the control charts accurately show the range of individual measured quantities [12].

This paper provides an example of control charts for the testing method of tension the metallic materials at room temperature, method B, SRPS EN ISO 6892-1:2020.



## 2. EXPERIMENTAL

This paper deals with demonstration the application of control charts in the Laboratory for Materials Testing (LIM) on the method: tensile testing of metallic materials at room temperature, method B, SRPS EN ISO 6892-1:2020. The control chart is the primary tool in technique of the static method of process control. The creator of the control charts is Dr. Suhart.

According to Dr. Suharo, a task of control charts is to:

1. maintain the production process in a state of control
2. bring the production process under control
3. with an indication of whether the state of control has been achieved.

A control chart is a diagram that shows exactly where the process being controlled is located. The values of quality characteristic, whose variation is studying, are written on the vertical axis, The tensile strength  $R_m$  is written in the work. The control chart is characterized by the central lines (processes) and control limits (lower and upper limits).

This paper presents the 8 tests of steel wires (Table 1).

X-Mean value of tensile strength  $R_m$ , upper and lower limits of  $R_m$  are given in Table 1.

Nominal tensile strength of a steel wire, test tube  $R_m=1570 \text{ N/mm}^2$ .

Table 1 - Test tube test results

Ord. No.	Measured wire diameter, mm	Tensile strength $R_m$ , $\text{N/mm}^2$	X-Mean value $R_m$	Lower limit $R_m$	Upper limit $R_m$
1	0,9	1700	1677.85	1570	1920
2	0,9	1659	1677.85	1570	1920
3	0,9	1654	1677.85	1570	1920
4	0,9	1627	1677.85	1570	1920
5	0,89	1739	1677.85	1570	1920
6	0,89	1689	1677.85	1570	1920
7	0,91	1677	1677.85	1570	1920

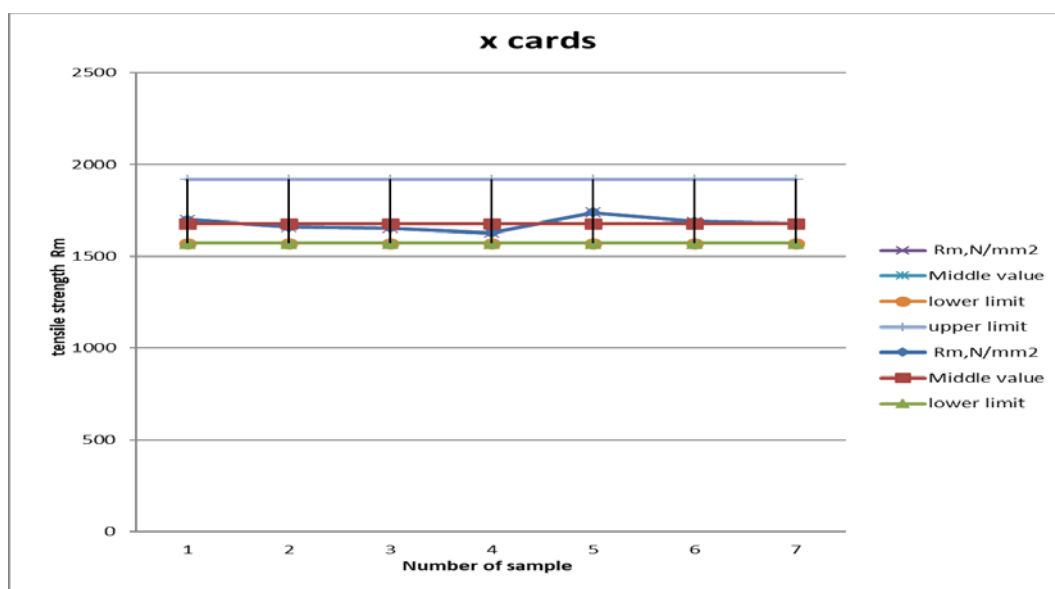


Figure 1 - Control chart



Methods of a control chart: Metallic materials - Tensile testing at room temperature, Method B, Determination of tensile strength (SRPS EN ISO 6892-1 2020) (Figure 1).

Criteria that determine the upper and lower limit values are: Nominal tensile strength  $R_m$  and nominal wire diameter  $d$ .

Nominal value  $R_m=1570 \text{ N/mm}^2$  represents the lower limit value.

The upper limit value is equal to the lower limit values, plus the tolerances given in Table 2, and they are taken from the SRPS ISO 3154:2014 Standard.

For this example, the lower limit value is  $R_m=1570 \text{ N/mm}^2$ , and for the upper limit value  $350 \text{ N/mm}^2$  (Table 2) is added so that it amounts  $R_m=1920 \text{ N/mm}^2$ .

Table 2 - Upper tolerance limits for nominal tensile strength  $R_m=1570 \text{ N/mm}^2$

Nominal wire diameter, $d$ mm	Upper tolerance limits for nominal strength $\text{N/mm}^2$
$0.8 \leq d < 1$	350

Source: [13]

### 3. RESULTS AND DISCUSSION

The control charts are most commonly used in various laboratories for the process control. The control charts have proven to be an excellent tool to improve the quality of testing the metallic materials, steel wires in the LIM.

In this work, the 8 samples were tested (Table 1) according to the method: Metal materials - Tensile testing at room temperature, Method B, Determination of tensile strength (SRPS EN ISO 6892-1 2020) with the following characteristics:

- Nominal wire diameter  $d$  value  $0.8 \leq d < 1$
- Nominal tensile strength  $R_m=1570 \text{ N/mm}^2$
- Calculated mean values  $X= 1677.85 \text{ N/mm}^2$
- Lower limit value is the nominal tensile strength and is  $R_m=1570 \text{ N/mm}^2$
- Upper limit value is  $R_m=1920 \text{ N/mm}^2$

The upper and lower limit values determine whether the process is in control or out of control. From the experimental part of the work, Figure 1 shows that the process is under control. This means that the variation in quality is normal and room temperature tensile testing process, method B, is stable.

Control charts in this work have the role of intermediate checks of operators involved in the process of testing and checking the device on which the test is performed.

### 4. CONCLUSION

This paper presents the role of control charts in the LIM on the method: tensile testing of metallic materials at room temperature, Method B, SRPS EN ISO 6892-1:2020.

The graphic display of the control charts shows that during the testing process of 8 samples, the tensile strength does not exceed the control limit, the lower and upper limit. The room temperature tensile test method for metallic materials is controlled.

Application of control charts in the laboratory for material testing (steel wire) by tensioning leads to the process improvement and reduction of errors.

The control charts provide the opportunity for laboratory managers to have the objective information about the state of quality of processes, personnel and devices.

### **ACKNOWLEDGEMENTS**

*The research presented in this paper was carried out with the financial support of the Ministry of Education, Science and Technological Development of the Republic of Serbia, as a part of funding the scientific research work in the Mining and Metallurgy Institute Bor, according to the contract with registration number 451-03-47/2023-01/ 200052.*

### **REFERENCES**

- [1] Suman, G. and D. Prajapati, D., Control Chart Applications in Healthcare: A Literature Review. *Int. J. Metrol. Qual. Eng.* 9, 5 (2018). <https://doi.org/10.1051/ijmqe/2018003A>.
- [2] Smajdorová, T., Noskievičová, D., Analysis and Application of Selected Control Charts Suitable for Smart Manufacturing Processes, *Appl. Sci.* 2022, 12(11), 5410; <https://doi.org/10.3390/app12115410>.
- [3] Jarošová, E.; Noskievičová, D. *Pokročilejší metody statistické regulace procesů (Advanced Methods of Statistical Process Control)*, 1st ed.; Grada Publishing: Praha, Czech Republic, 2015; pp. 139–144. [Google Scholar]
- [4] Qiu, P. *Introduction to Statistical Process Control*, 1st ed.; Chapman and Hall/CRC: Boca Raton, FL, USA, 2014; pp. 73–254. [Google Scholar]
- [5] Shewhart, W.A. *Statistical Methods from the View-Points of Quality Control*, 1st ed.; Dover Publication: New York, NY, USA, 1986. [Google Scholar]
- [6] Bakir, S.T. Classification Of Distribution-Free Quality Control Charts. In *Proceedings of the Annual Meeting of the American Statistical Association*, Atlanta, GA, USA, 5–9 August 2001. [Google Scholar]
- [7] Hollander, M.; Wolfe, D.A.; Chicken, E. *Nonparametric Statistical Methods*, 3rd ed.; John Wiley & Sons: Hoboken, NJ, USA, 2014; pp. 744–759. [Google Scholar]
- [8] Dempír, J.; Dohnal, L. Některé robustní postupy určení střední hodnoty a rozptýlení souboru výsledků a jejich použití (Some Robust Methods for Determination of Mean and Variance and Their Application). *Klin. Biochem. Metab.* 2005, 13, 139–144. [Google Scholar]
- [9] Woodall, W.H.; Montgomery, D.C. Research Issues and Ideas in Statistical Process Control. *J. Qual. Technol.* 1999, 3, 376–386. [Google Scholar] [CrossRef]
- [10] Figueiredo, F.; Gomes, M.I. Monitoring Industrial Processes with Robust Control Charts. *REVSTAT Stat. J.* 2009, 7, 151–170. [Google Scholar]
- [11] Koutras, M.V.; Triantafyllou, I.S. A General Class of Nonparametric Control Charts. *Qual. Reliab. Eng. Int.* 2018, 34, 427–435. [Google Scholar] [CrossRef]
- [12] Drenovac, Ž. A., Drenovac, Ž. B & Drenovac, M. D., Kontrolne karte kao sredstvo statističke kontrole kvaliteta, *Vojnotehnički glasnik*, Vol. LXI, No.1, 2013 pp,101-122. DOI: 10.5937/vojtehg61-2292.
- [13] Standard SRPS ISO 3154:2014

## TECHNOLOGICAL ASPECTS OF THE USE OF PEAT AS A COMPONENT OF PULVERATED COAL FUEL FOR BLAST FURNACES

Alexey M. Amdur<sup>1</sup>, Sergei A. Fedorov<sup>1,2</sup>, Andrey A. Forshev<sup>3</sup>,  
Nikolay V. Grevtsev<sup>1</sup>, Vera V. Yurak<sup>1</sup>

<sup>1</sup>Research Laboratory of Disturbed Lands' and Technogenic Objects' Reclamation, Ural State Mining University, Kuibysheva str. 30, 620144 Yekaterinburg, Russian Federation

<sup>2</sup>Laboratory of Pyrometallurgy of Non-Ferrous Metals, Institute of Metallurgy of Ural Branch of Russian Academy of Science, Amundsena str. 101, 620016, Yekaterinburg, Russian Federation

<sup>3</sup>JSC "EVRAZ NTMK", Metallurgov str. 1, 622025, Nizhny Tagil, Russian Federation

### Abstract

*Pulverized coal fuel (PCF) for blast furnaces was produced from peat and coal. The composition of PCF with peat is close to average values, %: ash – 6.48; volatile – 22.08; sulfur – 0.37; moisture – 1.63. Pulverized coal fuel containing 5-10 wt.% peat was blown into a blast furnace. There were no deviations in the operation of the blast furnace. Due to the introduction of peat, the consumption of lean coal was reduced, considering the carbon content in them. The consumption of PCF and natural gas remained virtually unchanged. The productivity of the blast furnace, the basicity of the slag and the composition of the pig iron correspond to the work in the base period.*

**Keywords:** blast furnace, pulverized coal fuel, calorific value, composition of pulverized coal fuel, peat

### 1. INTRODUCTION

There is a global trend in the development of technologies related to saving energy costs per unit of output in blast furnace production by pulverized coal fuel instead of a part of coke. In addition to economic aspects, it must be considered that coke production is one of the most harmful in the ferrous metallurgy. PCF is considered as a source of energy through the combustion of carbon. The composition of PCF is selected experimentally, based on the technological conditions of the blast furnace process and the cost of the coals included in it. When choosing components, they are guided by a high carbon content and corresponding calorific value, low ash content and its composition, the minimum amount of alkali metal oxides, the composition and number of volatile components.

Purpose of the work is study of an affordable and low-cost fuel resource – milled peat as a component of PCF and the possibility of its use in blast-furnace production to expand the raw material base.

### 2. EXPERIMENTAL

The peat structure was studied on a TESCAN VEGA LMS scanning electron microscope equipped with an Xplore30 energy dispersive attachment. The processes occurring during the heating of peat and coals were analyzed on a synchronous thermal analysis device (further thermal analyzer) model STA 449 F5 Jupiter. The experiments were carried out in an argon atmosphere with different oxygen content in the measuring chamber of the instrument. Furnace heating rate is 10°C/min. The higher calorific value was experimentally determined by increasing the temperature of water in a calorimetric vessel, in which a metal container is placed for burning a sample of solid fuel in a compressed oxygen atmosphere.

Industrial experiments were carried out at the operating metallurgical plant. The standard composition of PCF used in the blast furnace shop where the studies were carried out: 70% lean coal (further grade T) and 30% long-flame coal (further grade D). Peat was partially replaced by lean coal. The main replacement condition is to maintain the average carbon content of the PCF.

### 3. RESULTS AND DISCUSSION

Studies on a scanning electron microscope showed that peat particles have an elongated shape of "fibers" ranging in size from 50 to 400 microns. The predominant grain structure is cellular, less often fibrous and layered. The cell size is on average 10-30 microns. Peat carbon is a constituent of cellulose, humic acids and other compounds [1]. This carbon is in a finely dispersed state and it is distributed throughout the volume of peat fibers. The size of individual particles containing carbon is several microns. Oxide components (ash) are concentrated mainly in the cell walls (oxides of silicon, aluminum, iron, calcium, potassium and sodium). Sulfur is also present in the cell walls.

According to the technology adopted at most metallurgical plants, raw coal is fed into a vertical roller mill with controlled oxygen partial pressure. In the mill, coal is crushed, dried and classified for supply with a given particle size distribution to the blast furnace. To select the operating modes of the mill, it is necessary to know what processes occur in peat, including at the drying temperature, and their difference from processes in coal.

As studies on a thermal analyzer at various partial pressures of oxygen  $P_{O_2}$  showed, thermal destruction and combustion in peat occur at a much lower temperature than in long-flame and lean coal. The second peak on the curves of the DTG weight change rate belongs to destruction. The first peak is associated with the evaporation of moisture from peat. In an inert atmosphere, the temperature of the beginning of destruction (2nd DTG peak) is 220°C. It remains approximately constant in the presence of oxygen up to the composition of synthetic air. The destruction products in an argon atmosphere contain the same gases as in the destruction of long-flame coal:  $H_2O$ ,  $CO_2$ ,  $CO$ ,  $CH_4$ ,  $H_2$ ,  $SO_2$ ,  $NO_2$ ,  $NO$ . In [2], small emissions of hydrogen sulfide and light hydrocarbons were also recorded. The temperatures of the beginning of the 3rd peak (combustion region) little depend on the oxygen content in the gas (leaving about 340°C). The maximum rate of the process in the region of the 2nd peak is observed at 300°C. The maximum rate in the region of the 3rd peak is 380°C. These temperatures are much lower than for long-flame and lean coals. The temperature of the end of the chemical reaction in the area of the 2nd peak varies in the range of 320-350°C. It does not depend on the concentration of oxygen in the atmosphere. However, the temperature of the end of the chemical reaction in the region of the 3rd peak decreases with an increase of oxygen in the furnace atmosphere from 540 (6.7%  $O_2$ ) to 460–470°C (20.9%  $O_2$ ). The maximum burning rate of peat is higher than that of long-flame coal, since the carbon particles in peat are micron in size. It increases in proportion to  $P_{O_2}$  in the device atmosphere from 2.25%/min to 4.5%/min versus 1.75–3.5%/min for coal. The temperature of the maximum  $CO_2$  content in the combustion products also decreases with an increase in  $P_{O_2}$ . This is consistent with a decrease in the temperatures of the peak rates of chemical reactions. The results are close to the data of [2, 3-5]. However, the temperature of the beginning of the destruction of peat from other deposits is below 200°C [2, 3-5].

The thermal destruction of peat in an inert atmosphere accounts for 59% of the mass loss, which is somewhat higher than a few published data [2, 4]. The maximum destruction rate is 2.69%/min versus 2.0%/min for long-flame coal. It has been established that the rate of thermal destruction of coals and peat decreases with an increase in the degree of metamorphism: for peat it is 2.69%/min, for brown coal 1.48%/min, for lean coal 0.55%/min, and for anthracite 0.30%/min. The release of volatile components begins later (at 425°C for lean, against 300°C for brown coal and 220°C for

peat). The mass loss during combustion does not depend on the oxygen content in the gas and is 85-88%. About 27% of the total mass loss of peat belongs to combustion itself. While for long-flame coal this value is 57%. This is due to the low mass fraction of nonvolatile carbon in the analytical sample, which is 26.3%.

The heating time of individual particles of peat and coals was estimated using the example of long-flame coal with a diameter of 80  $\mu\text{m}$  to the temperature at which the drying and grinding of PCF is carried out (250°C). To do this, numerical methods in the Matlab package were used to solve the parabolic differential equation of heat conduction (non-stationary case) under the Dirichlet boundary conditions. Peat (on average) has a higher thermal conductivity and heat capacity and a lower density than coal. The heating time of peat particles is of the order of  $(4\div 6)\cdot 10^{-2}$  s, for coal it is longer ( $10^{-1}$  s). Probably, at such heating rates in industrial conditions for the production and use of pulverized coal, the processes of destruction and combustion will overlap.

The determination of the total specific surface area was carried out on a device for measuring the specific surface area and porosity of dispersed materials SORBI MS. Heat treatment of the samples before measurement was carried out at a temperature of 150°C and a holding time of 60 min. The specific surface varies in the range  $(1.75\div 3.2)\cdot 10^3$   $\text{m}^2/\text{kg}$  at 10% peat content in PCF.

Figure 1 shows the experimental data on the higher calorific value of PCF in the presence of peat in its composition.

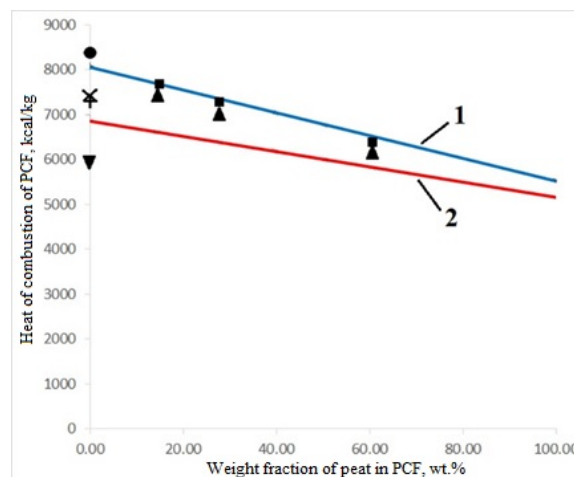


Figure 1 - Dependence of the calorific value of PCF on the content of dry ashless peat in it: 1 is higher calorific value (calculation by additivity); 2 is lower calorific value (calculation by additivity); ▲ is experimental data on the highest calorific value; ■ is experimental data on the lower calorific value; ● is higher calorific value of coal grade T; × is the highest calorific value of coal grade D; + is lower calorific value of coal grade T; ▼ is lower calorific value of coal grade D; the points of intersection of the straight lines with the y-axis are the heat of combustion of the used PCF by additivity (70% T – 30% D).

The use of peat with significantly different characteristics from coals will lead to a change in the properties of PCF. This is especially noticeable in the yield of volatiles, which reaches 51% with a peat content of 60.5%. The mass fraction of total carbon in this case drops to 61.56%. The mass fraction of oxygen increases to 22.71%. The mass fraction of hydrogen (a product of the thermal destruction of coals and peat) is at the level of 5.80–5.95%. The role of this hydrogen in the processes taking place in the blast furnace has not been fully studied. Due to the high moisture content of peat, the mass fraction of analytical moisture becomes 5.1%. The content of total sulfur, the ash content of the material, the mass fraction of hydrogen, considering the determination errors, change within acceptable limits.

Calculations based on our experimental data showed that even with 10% peat, the decrease in the higher calorific value of PCF will be 3.7%, and the total carbon content will be 2.8%. The maximum content of peat in the mixture of PCF should be established according to the indicators of the blast furnace process: the temperature of the iron, the composition of the iron and slag.

#### **4. CONCLUSION**

Samples of mixtures of peat and coals used as PCF components for blast furnaces in various proportions were produced. For each composition, tests were carried out to determine the moisture content; ash content; chemical composition of ash; ash deformation temperature; sulfur content; release of volatiles; content of carbon, oxygen, hydrogen, nitrogen, sulfur, calorific value. The indicators of PCF with peat are close to the average values, %: ash is 6.48; volatile is 22.08; sulfur is 0.37; moisture is 1.63. It has been established that the properties of mixtures depend on the peat content according to a linear law.

PCF containing 5-10% wt. peat blown into a blast furnace. The equipment of the PCF supply path worked stably without changing the operating parameters. There were no deviations in the operation of the blast furnace. Due to the introduction of peat, the consumption of lean coal was reduced, considering the carbon content in them. The consumption of PCF and natural gas remained virtually unchanged. The productivity of the blast furnace, the basicity of the slag and the composition of the pig iron correspond to the work in the base period.

#### **ACKNOWLEDGEMENTS**

*The research was funded by the Ministry of Science and Higher Education in accordance with the state assignment on science for Ural State Mining University №075-03-2023-219 dated 16.01.2023.*

#### **REFERENCES**

- [1] A.A. Terentev, V.I. Suvorov., Research of peat structure, Science and Technology, Minsk, 1980, p. 94.
- [2] A.S. Mikhailov, S.A. Piralishvili, E.G. Stepanov et al., J. Eng. Phys. Thermophy., 90 (2017) 491–496.
- [3] Zhao W., Chen H., Liu N. et al., J. Therm. Anal. Calorim., 117 (2014) 489–497.
- [4] D.V. Ermolaev, S.S. Timofeeva, S.I. Islamova, K.S. Bulygina, M.F. Gilfanov., Biomass Conversion and Biorefinery, 9 (2019) 767–774.
- [5] G.C. Krieger Filho, P. Bufacchi, F. Costa, E.V. Cortez, J.C. Andrade, K. Ribeiro, F. Souza., Proceedings of the Combustion Institute, 38 (3) (2021) 5053-5062.

## HYDROMETALLURGICAL TREATMENT OF MINING WASTE FROM BOR - SERBIA IN AIM OF COPPER RECOVERY

**Ljiljana Avramović, Zoran Stevanović, Vanja Trifunović, Radmila Marković,  
 Dragana Božić, Daniela Urošević, Silvana Dimitrijević**

Mining and Metallurgy Institute Bor, Zelene bulevar 35, 19210 Bor, Serbia

### Abstract

*Flotation tailings deposited on the Old Flotation Tailing Dump in Bor contains 0.2-0.4% Cu and represents a significant resource for recovery of copper and other useful components. The results of experimental laboratory tests of the copper recovery process from the flotation tailings using the beaker leaching (BL) and high pressure leaching (HPL) are given in this paper. By the use of beaker leaching, the degree of copper recovery of 70% and iron of 12% at temperature of 60°C, time of 24 hours and concentration of sulfuric acid of 15 g/l was achieved. A high degree of copper recovery of 99% was achieved by the high pressure leaching using water as an leaching reagent at a temperature of 180°C and pressure of 1.5 MPa.*

**Keywords:** *flotation tailings, beaker leaching, high pressure leaching, copper recovery*

### 1. INTRODUCTION

Pyrometallurgical process for copper production from sulphide minerals has existed in Bor for many years. During the processing of such type of ore, there is a formation of tailings generated during the flotation processes and containing the metal sulphides and under the effect of atmospheric conditions, the self-leaching process of tailings is developed resulting in a significant degradation the quality of surrounding water and soil [1,2].

It is estimated that more than 2000 ha of the most fertile coastal area of the Bor River, Bela River, and downstream Timok and Danube have been degraded by the flotation tailings. In addition to the physical contamination of the coastal area, the Bor River is constantly contaminated with wastewater generated by a drainage through the flotation tailing dumps and landfills.

This work presents the results of experimental laboratory test of copper recovery from the flotation tailings by the acid leaching process of tailings at the atmospheric pressure (BL) and high pressure leaching with the addition of oxidant (HPL). The highest level of copper leaching of 99% was achieved using the HPL method.

### 2. EXPERIMENTAL

For the experimental tests of the leaching process: BL and HPL, the flotation tailings from the Old Flotation Tailing Dump in Bor was used with a particle size of 72% -75 µm. The chemical composition of the initial flotation tailings sample is given in Table 1.

Table 1 - Chemical composition of flotation tailings

Element	Cu	Fe	S-total	S-sulphide	Ag	Au	As
Unit	%	%	%	%	g/t	g/t	%
Content	0.29	9.51	10.10	7.32	1.10	0.50	0.013



The BL experiments were carried out in order to investigate the effect of the following parameters: temperature (20-80°C), sulfuric acid concentration (2-40 g/l H<sub>2</sub>SO<sub>4</sub>) and process time (2-48 h). The pulp density of 25% and stirring rate of 700 rpm were constant in all experiments. After completion of the leaching process, the filtered leaching solutions were analyzed to determine the leaching degree of Cu and Fe.

The HPL experiments were carried out on the same samples of flotation tailings in the Nitto Koastu autoclave, Japan, with a volume of 2 L of reaction vessel. The effect of sulfuric acid concentration (0-50 g/l), pulp density in the range of 10-40% and temperature (140-180°C) with the oxygen introduction at total pressure of 0.8 to 2.0 MPa was tested. The reaction time in all experiments is 60 minutes and stirring rate is 700 rpm.

The ICP-OES Spectro Vision device was used to analyze the concentration of tested elements.

### 3. DISCUSSION OF RESULTS

#### 3.1. Beaker Leaching

The leaching degrees of copper and iron, depending on the process temperature, concentration of H<sub>2</sub>SO<sub>4</sub> in the leaching solution and leaching time are shown in Figures 1, 2 and 3, respectively.

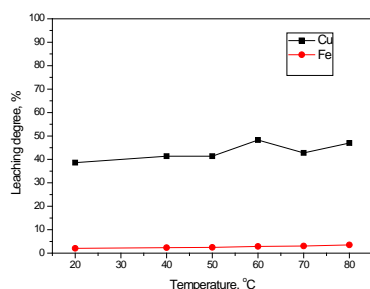


Figure 1 - The temperature effect on a leaching degree of Cu and Fe ( $\tau=2$  h, 2g/l H<sub>2</sub>SO<sub>4</sub>)

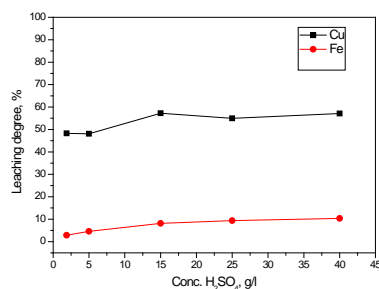


Figure 2 - The concentration effect of H<sub>2</sub>SO<sub>4</sub> on a leaching degree of Cu and Fe ( $\tau=2$  h,  $t=60^\circ\text{C}$ )

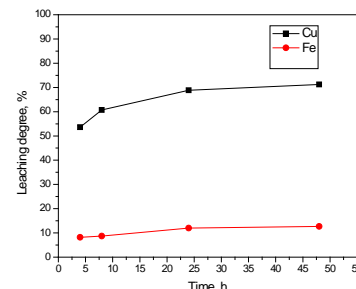


Figure 3 - The time effect on a leaching degree of Cu and Fe (15g/l H<sub>2</sub>SO<sub>4</sub>,  $t=60^\circ\text{C}$ )

Based on the obtained testing results of the temperature effect (Figure 1), the leaching degree of copper ranges from 38% (20°C) - 48% (80°C). Considering that the similar values for the leaching degree of copper were obtained at temperatures of 60°C and 80°C (48% and 47%, respectively), it was decided that the further tests of the flotation tailings leaching process should be carried out at 60°C. With an increase in H<sub>2</sub>SO<sub>4</sub> concentration in the leaching solution (Figure 2), an increase in the leaching degree of copper to 15 g/l was observed. Further increase in the concentration of H<sub>2</sub>SO<sub>4</sub> to 40 g/l did not have a significant effect on a leaching degree of Cu. Maximum copper leaching degree of 71% was achieved at a leaching time 48 hours, temperature 60°C and 15g/l H<sub>2</sub>SO<sub>4</sub> (Figure 3).

The most influential parameters for the leaching degree of iron is the concentration of H<sub>2</sub>SO<sub>4</sub> in leaching solution (Figure 2) and ranges from 2% (2 g/l H<sub>2</sub>SO<sub>4</sub>) to 10% (40 g/l H<sub>2</sub>SO<sub>4</sub>). With an increase in the leaching time of 48 h, an increase in the leaching degree of iron at 12.7% was observed (Figure 3).

Having in mind the fact that copper from the leaching solutions is recovered by the solvent extraction processes and electro-winning SX-EW, and that the increased iron concentration has a negative impact on the electrochemical copper extraction, in a selection the optimal parameter BL, the time was adopted of 24 h, temperature 60°C and concentration H<sub>2</sub>SO<sub>4</sub> of 15 g/l.

### 3.2. High Pressure Leaching

The results of a high pressure leaching (HPL) are presented in Table 2.

Table 2 - Experimental conditions and results of the HPL process

Exp. No.	Pulp density (%)	Reagent	P <sub>total</sub> (MPa)	Temperature (°C)	Time (h)	Stirring rate (rpm)	Leaching degree (%)	
							Cu	Fe
1	10	H <sub>2</sub> O	2	180	1	700	95	24
2	20	H <sub>2</sub> O	2	180	1	700	98	43
3	30	H <sub>2</sub> O	2	180	1	700	92	60
4	40	H <sub>2</sub> O	2	180	1	700	94	61
5	10	20 g/l H <sub>2</sub> SO <sub>4</sub>	2	180	1	700	97	66
6	10	50 g/l H <sub>2</sub> SO <sub>4</sub>	2	180	1	700	98	95
7	10	H <sub>2</sub> O	0.8	180	1	700	21	2,35
8	10	H <sub>2</sub> O	1.5	180	1	700	99	49
9	10	H <sub>2</sub> O	2	140	1	700	89	40
10	10	H <sub>2</sub> O	2	160	1	700	90	37

Water and sulfuric acid were used as a leaching reagent for the HPL process (Table 2). Leaching with water is based on the fact that the high content of pyrite (FeS<sub>2</sub>) in the flotation tailings sample can be the source of H<sub>2</sub>SO<sub>4</sub> (Equation 1) [3], which leads to a decrease in the pH (from 3.79 to 0.35) and thus increases copper dissolution (chalcopyrite as the main copper minerals).



By leaching with water, the realized degree of copper leaching was 99%, iron 49%, at 180°C, pressure of 2 MPa, pulp density 10%, time 1 h, stirring rate 700 rpm. With an increase in the H<sub>2</sub>SO<sub>4</sub> concentration from 20 g/l to 50 g/l, the percentage of copper leaching has been slightly increased from 97% to 98%, while the degree of iron leaching increases from 67% to 95%. From an economic point of view, H<sub>2</sub>O has been selected as a copper leaching medium from the flotation tailings.

The effect of total pressure on copper dissolution from the flotation tailings has been tested in the range of 0.8 to 2.0 MPa, with water as a dissolving medium, temperature of 180°C, pulp density of 10% and time of 60 min (Table 2). The degree of copper leaching was 21% and iron 2.35% at pressure of 0.8 MPa (without the introduction of oxygen). It can be concluded that after the initial dissolution of copper, a passive layer of elemental sulfur [4] was formed on chalcopyrite, which had a negative effect on kinetics of copper dissolution. With an increase in the pressure of 0.8 to 2.0 MPa with the oxygen supply, the degree of copper and iron leaching increased to 99%, i.e. 49%, respectively. The present oxygen allows oxidation and prevents the formation of passivation layer (Equation 2) [3,5].



With a temperature increase of 140 to 160°C, the degree of copper and iron leaching increased from 89 to 99% and from 37 to 49%, respectively. Based on the literature data [5], the chalcopyrite leaching controls the kinetics of chemical reaction on the grain surface with activation energy of about 70-90 kJ/mol. This implies that the leaching degree is highly dependent on temperature. An optimum condition for the next experiments was chosen to be the temperature of 180°C with a copper leaching degree of 99%.

As shown in Table 2, the first degree of copper leaching has not changed much with an increase of pulp density from 10 to 40%, i.e. no effect on the copper leaching degree [6,7]. As an optimal, the pulp density of 40% is chosen, since in this case the copper concentration in leaching solution is four times higher than the copper concentration in 10% pulp, which is a significant parameter for the copper extraction process from leaching solutions.

#### 4. CONCLUSION

On the basis of the results obtained for the BL process of flotation tailings leaching, it can be concluded that the maximum degree of copper recovery is 71% and iron 12%, while in the HPL process, with the application of water as the leaching reagent, a significantly higher degree of copper recovery of 99% and iron recovery of 61% was realized.

A high concentration of iron in the solution after leaching in the HPL process is a serious problem in further copper recovery processes (SX-EW process) as a commercial product. Due to this reason, a consideration should be given to the possibility of introducing an additional phase of iron removal from the pregnant leaching solutions before the SX-EW process.

In order to select the method of copper leaching from the flotation tailings will largely be a decisive economic aspect of the tested BL and HPL processes what will be the subject of future research.

#### ACKNOWLEDGEMENTS (optional)

*The authors are grateful for funding by the Minister of Science, Technological Development and Innovation of the Republic Serbia, the Grant No. 451-03-47/2023-01/200052. Also, this work was financially supported by the EU under Interreg – IPA CBC Romania-Serbia Programme and co-financed by the partner states in the Programme. Project Romania Serbia NETWORK for assessing and disseminating the impact of copper mining activities on water quality in the cross-border area (RoS-NET2) eMS code RORS - 337. Also, this work was financially supported by the EU under Program 2nd EIT-HEI call: Building Ecosystem Integration Labs at HEI to foster Smart Specialization and Innovation on Sustainable Raw Materials - HEI4S3-RM.*

#### REFERENCES

References should be listed at the end of the paper as they appear in the text. If a publication is referred in the text, use [1] for one reference, or [1,2,3] for more than one. Use the following styles for journals, proceedings and books, respectively:

- [1] R. Jonović, Lj. Avramović, Z. Stevanović, M. Jonović, Mining and Metallurgy Engineering Bor 3 (2014) 153-160.
- [2] L. L. Godirilwe, K. Haga, B. Altansukh, Y. Takasaki, D. Ishiyama, V. Trifunovic, Lj. Avramovic, R. Jonovic, Z. Stevanovic, A. Shibayama, Metals 11 (9) (2021) 1335.
- [3] B. Han, B. Altansukh, K. Haga, Y. Takasaki, A. Shibayama, Z. Stevanovic, R. Jonović, Lj. Avramovic, D. Urosevic, Y. Takasaki, N. Masuda, D. Ishiyama, A. Shibayama, J. Hazard. Mater., vol. 352 (2018), 192-203.
- [4] A.A. Baba, K.I. Ayinla, F.A. Adekola, M.K. Ghosh, O.S. Ayanda, R.B. Bale, S.R. Pradhan, Int. J. Min. Eng. Miner. Process. 1.1 (2012) 1–16.
- [5] A. Muszer, J. Wodka, T. Chmielewski, S. Matuska, Hydrometallurgy 137 (2013) 1-7.
- [6] R. Padilla, P. Pavez, M.C. Ruiz, Hydrometallurgy 91 (2008) 113-120.
- [7] Lj. Avramović, R. Jonović, M. Bugarin, A. Shibayama, K. Haga, H. Baisui, R. Marković, M. Jovanović, XI International Symposium on Recycling Technologies and Sustainable Development (2016), 240-247.

## **DETERMINATION THE FINAL CONTOUR OF THE OPEN PIT VELIKI KRIVELJ FOR THE MINING CAPACITY 23.1 MILLION TONS OF ORE**

**Daniel Kržanović, Radmilo Rajković, Ivana Jovanović, Milenko Jovanović, Miomir Mikić**

Mining and Metallurgy Institute Bor, Zelene bulevar 35, 19210 Bor, Serbia

### **Abstract**

*This paper presents determination of the final contour of the Open Pit Veliki Krivelj, which operates within the Copper Mine Bor, from the aspect of achieving the maximum net present value of the project. The final contour was defined in the optimization process of the mine boundary using the modern Whittle strategic production planning software.*

**Keywords:** *final open pit contour, optimization, open pit Veliki Krivelj.*

### **1. INTRODUCTION**

Determination of the final open pit contour is carried out through the optimization process. Optimization of the pit boundary involves the geological and operational modeling, which is realized through the application of optimization software that uses some of the mathematical algorithms. The process involves identifying the combination of controlled variables that maximize the project value in the context of a given set or range of assumptions [1].

An optimal contour of the pit is that contour of the pit that gives the maximum net present value (NPV), which implies taking into account the time factor of the value of money in defining the blocks that should be excavated, and which blocks should be left for duration of the project.

Strategic mine planning seeks to answer how best to develop an ore body in support of the objective of maximizing the NPV. Development of a strategic plan may represent the totality of planning at the conceptual or scoping stage of mine planning [2].

The Open Pit Veliki Krivelj is located about 3 km by the airline north of the town of Bor and has the primary role in the copper production in the company Copper Mine Bor, which is a part of the company Serbia Zijin Bor doo.

Determination of the final contour of the Open Pit Veliki Krivelj was performed using the Whittle Four-XTM algorithms (LG 3D), whereby a series of the open pit shells was determined on the basis of different Revenue factors with an iterative step of changing the metal price in relation to the base price. Each shell generated represents an incremental increase in the amount of reserves according to an incremental increase in the selling metal price. The optimization criterion is based on determination the maximum NPV, i.e., the discounted difference between the income from metal sales and total operating costs.

### **2. INPUT DATA FOR OPTIMIZATION**

Mining processes are complex and complicated, with many different economic, technical, environmental and other parameters that must be planned before the project gets its practical value. Many of these parameters are evaluated independently of the other, due to the expediency and difficulty in predicting the values of variables under consideration. The costs, prices, reserves, ore mining and processing, as well as many aspects of society, such as the issuance for implementation of works are absolutely essential for the project evaluation.

The basic, primary input in the planning and design process of the open pit is a geological block model of the ore body. It is very important to accurately calculate the block value in optimization, because the wrong calculation leads to the wrong optimal contour of the open pit [3].

### 3. METHODOLOGY

Optimization of the open pit boundary is a process based on the implementation of the Lerchs-Grossmann (LG) algorithm. The LG algorithm gives a mathematically optimal final boundary of the open pit, when the criterion for optimization is the maximum undiscounted cash flow [4]. The only optimization criterion is the maximization of the net present value (NPV) of the cash flows resulting from the sale of metal or concentrate.

The process selects the optimal final open pit boundary for the Best, Worst and Specified case of the mining plans of excavation for which the NPV curves are obtained. In this way, a wide range of possible pits is generated from which the engineer chooses the optimal pit, which once again confirms that the engineer still has an irreplaceable role in designing despite the strong development of software and computer equipment.

### 4. OPTIMIZATION RESULTS - ANALYSIS OF DISCOUNTED CASH FLOWS

The result of optimization is a series of the open pit contours that are generated with different metal sales prices, which are expressed as a Revenue Factor. The cash flow for each contour is calculated using the Metal Sales Price input parameter and Revenue Factor. Cash flow provides an indication of how economic parameters are changed for various contours.

The results of the Open Pit Veliki Krivelj boundary optimization are shown in Figure 1.

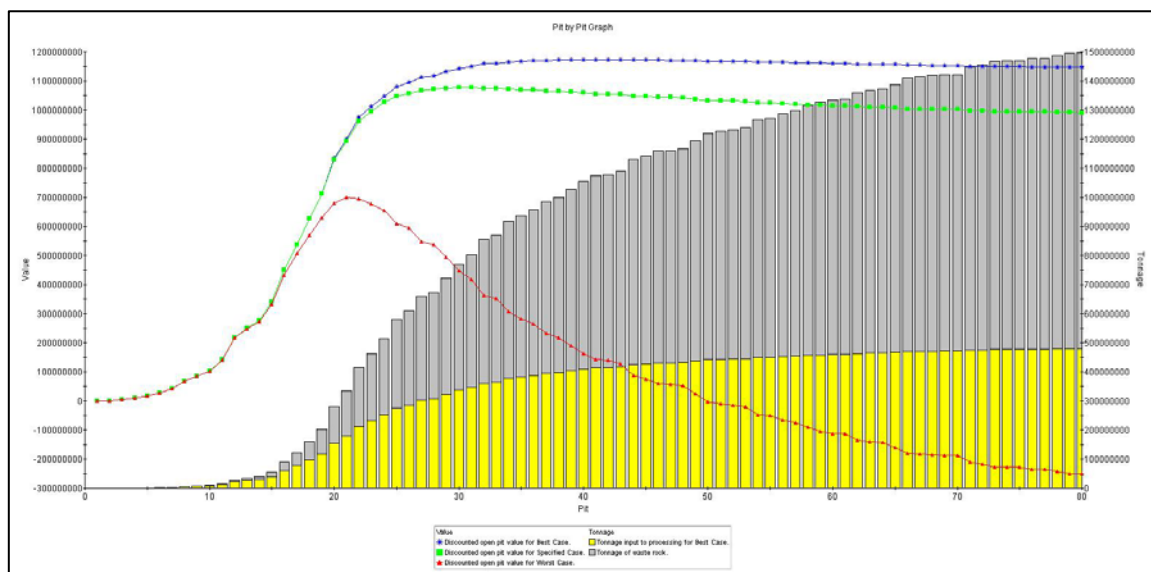


Figure 1 - Pit by Pit Graph

The analysis of discounted cash flows was performed with the aim of determining the final contour of the Open Pit Veliki Krivelj. During the optimization, the base price of metal was varied in the Revenue Factor range from 0.32 to 2.0 with a step of 0.03, and in this way the 57 potential surface open pit contours were generated. The amounts of waste, ore and metal are determined for each open pit contour individually with the operational NPV discounted by 10%.

### 5. SELECTION OF THE FINAL (OPTIMAL) OPEN PIT CONTOUR

Figure 1 shows the resulting graph with the economic optimization parameters, formed on the basis of annual production of the Open Pit Veliki Krivelj of 23.1 million tons of ore.

As it can be seen from figure, the limit shell of the pit number 24 (Revenue Factor 1.01) was chosen as the optimal final contour of the open pit. This open pit contour has a maximum discounted value for the Best case and a significant positive value for the Worst case, while the Specified case is respectable. The chosen final contour of the open pit enables the optimal utilization of the deposits during the exploitation life of the open pit of 19-24 years.

The parameters of the optimal open pit contour are listed in Table 1.

Table 1 - Techno-economic parameters of the optimal open pit

Parameter	Unit	Value
Ore	ton	426,397,362
Waste	ton	648,315,385
Stripping ratio	t/t	1.52
Average copper grade	%	0.318
Average gold grade	g/t	0.053
Average silver grade	g/t	0.24
Best case NPV	\$	1,239,209,132
Specified case NPV	\$	935,489,223
Worst case NPV	\$	132 152 423

A graphic representation of the Whittle shell of the final contour of pit number 24 is given in Figure 2.

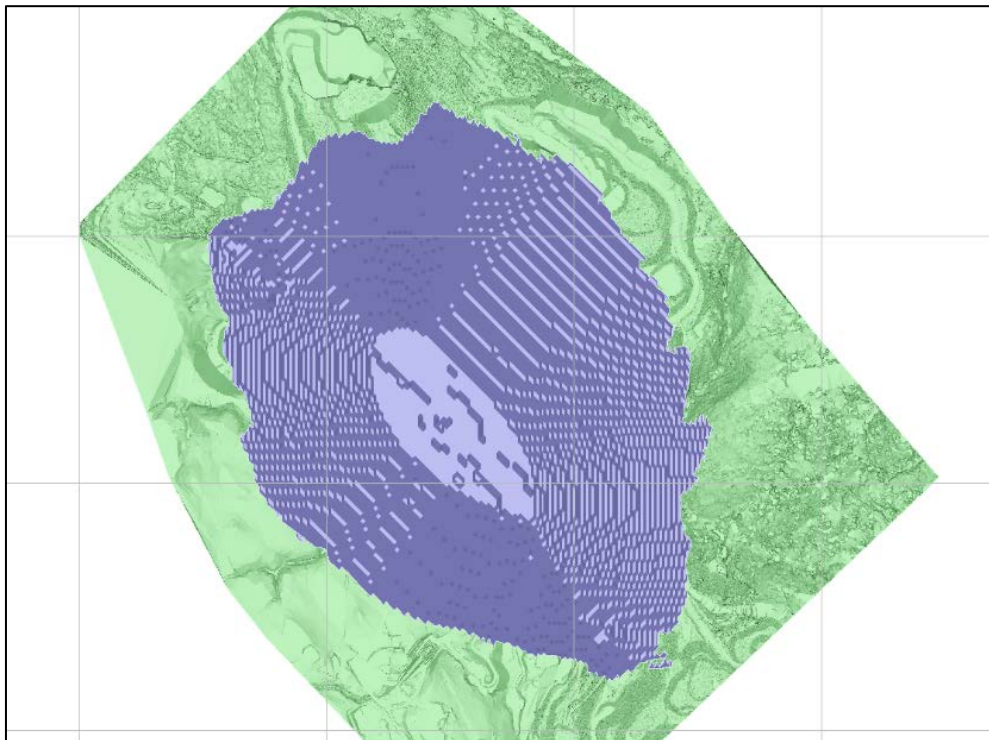


Figure 2 - Whittle 3D view of the optimal pit number 24

## 6. CONCLUSION

On the basis of the block model of the deposit and defined input techno-economic parameters in the software Whittle, for the change of Revenue Factor from 0.32 to 2.0, the 57 shells of the open pits were generated. The mine shell number 24 was selected as the final mine contour. Within this contour, 426,397,362 t of ore will be mined, with the average copper content of 0.318%, and the maximum NPV for the Best case is \$1,239,209,132.

## ACKNOWLEDGEMENTS

*This work was financially supported by the Ministry of Education, Science and Technological Development of the Republic of Serbia, Grant No. 451-03-47/2023-01/200052.*

## REFERENCES

- [1] Daniel Kržanović, Radmilo Rajković, Miomir Mikić, Milenko Ljubojev, Effect of Stage Development of Mining Operations on Maximization the Net Present Value in Long-Term Planning of Open Pits, Mining and Metallurgy Engineering Bor, 4/2014, Mining and Metallurgy Institute Bor, pp. 33-40.
- [2] Daniel Kržanović, Miroslav Grujić, Dejan Stevanović, Nenad Vušović, Milenko Ljubojev, Strategic Mine Planning Phases of the Copper Ore Open Pits - A Case Study: The Open Pit Veliki Krivelj, Serbia, 50<sup>th</sup> International October Conference on Mining and Metallurgy, Proceedings, 30<sup>th</sup> September – 3<sup>rd</sup> October 2018, Hotel “Jezero” Bor Lake, Serbia, pp. 43-46.
- [3] D. Kržanović, N. Vušović, M. Ljubojev, R. Rajković, Importance of Planning the Open Pits in the Conditions of Contemporary Mining - A Case Study: The Open Pit South Mining District Majdanpek, Mining & Metallurgy Engineering Bor, No. 1-2 2017, pp. 15-22.
- [4] D. Kržanović, M. Ljubojev, I. Jovanović, N. Vušović, An Analysis the Effects of Changes in Price of Metal and Operating Costs to the Profit in Exploitation the Copper Ore Deposits, A Case Study: Copper Mine Majdanpek, Serbia, Mining & Metallurgy Engineering Bor, No. 3-4 2017, pp. 51-58.



## THE USE OF UNMANNED AERIAL VEHICLES FOR MAKING THE PRECISE 3D TOPO MODELS AND ORTHOPHOTO IMAGES

Vladan Marinković, Miroslava Maksimović, Milenko Jovanović,  
Goran Pačkovski, Stefan Trujić

*Mining and Metallurgy Institute Bor, Alberta Ajnštajna 1, 19210 Bor, Serbia,*

### **Abstract**

*The idea of unmanned aerial vehicle is not new; Nikola Tesla was the first who presented this idea in 1915 in his dissertation. In geodesy, an unmanned aerial vehicle was first used in 1980. To make a precise and quality 3D topo model and orthophoto image, in addition to the equipment, the certain software tools and materials are also required. The program that is often used to make the 3D topo models and orthophoto images is the AgisoftPhotoScan. Surfaces that can be shot by the unmanned aerial vehicles vary from several hectares to several tens of hectares, and even hundreds of hectares. In this way, it is possible to get up to many thousands of photos that need to be further processed. Processing of recorded photographs and making the 3D topo models, depending on the number of photos and computer quality on which the processing is done, can take several weeks, why besides the unmanned aerial vehicle and other necessary equipment, the access to the quality computer equipment is also necessary.*

**Keywords:** *unmanned aerial vehicle, high precision GPS device, AgisoftPhotoScan, point cloud*

### **1. INTRODUCTION**

The idea of unmanned aerial vehicle is not new; Nikola Tesla was the first who presented this idea in 1915 in his dissertation. On that occasion, he described a non-pilot airplane that would be used to protect the sky above the United States [1].

In geodesy, an unmanned aerial vehicle was first used in 1980 when the professor Wester-Ebbinhaus used an aircraft in the form of a helicopter for the photogrammetric purposes [1].

In the beginning, the unmanned aerial vehicles were used exclusively for the military purposes: for reconnaissance and espionage. The reason for this were the exceptionally high prices of aircrafts, as well as the technology that was available only to the army.

By entering the market of large manufacturers from Asia, the unmanned aerial vehicle technology has become available to a wider market, so the aircrafts have found application in various industry branches:

- In civil engineering, the unmanned aerial vehicle is used to monitor and control the condition of structures having heavy, such as: high dams and pillars of bridges.
- In mining, the unmanned aerial vehicles are used to monitor the state of operations at the open pits, and it is possible to make the calculation of excavated material volume by a combination of several shots from different periods of time.
- In geology, it is possible to use the unmanned aerial vehicle to monitor the landslide phenomenon and their spreading.
- In forestry and agriculture, the unmanned aerial vehicles are used to monitor the state of forests and crops, monitoring the spread of naked (untreated areas), illegal logging, and in a combination with a camera that captures the NIR (near infrared) spectrum, it is possible to monitor the development of disease in plants.
- In ecology, the unmanned aerial vehicles can monitor spreading of pollution, or coverage of a certain area with different waste (municipal, industrial or mining).

- In film industry, marketing and television, the unmanned aerial vehicles are used to record various movie sequences from the air as well as for production the advertisements and transmission of various sports, cultural or political events.

## 2. MAKING THE ORTHOPHOTO IMAGES AND PRECISE TOPO MODELS

To make a precise and quality 3D topo model and orthophoto image, in addition to the equipment, the certain software tools and materials are also required

The required equipment includes an unmanned aerial vehicle (Figure 1) and high precision GPS device (Figure 2).



Figure 1 - The unmanned aerial vehicle Phantom 3 Professional (manufacturer DJI)



Figure 2 - The high precision GPS device (manufacturer Trimble, model R4)

The unmanned aerial vehicles are equipped with GPS chips, however, these chips do not have a satisfactory precision. The field level is determined by this technology on the basis of a focal length, that is, the distance between the camera lens on the aircraft (Figure 3) and field to be recorded [2].

Also, the camera lens has a certain curvature which is responsible for the so-called effect of a "bowl", that is, there are elevations in the field where they are not present. All these negative effects can be fixed by using the high accuracy GPS devices in a combination with the field markers (Figures 4) that fall into materials needed to make the 3D topo model and orthophotos.



Figure 3 - Camera on the aircraft Phantom 3 (manufacturer Sony, model FC300X ).



Figure 4 - View of ta field marker

Markers are black-white plates that are placed in the field being recorded. These markers must be large enough to be visible from the air, and placed in the field by tapping on the wooden wedges. It is very important that the markers in the field are fixed. The number and schedule of markers depends on the size of field being recorded. After placement of markers, the position of their center is measured by a high precision GPS device, which gives the exact position of markers in the space in all three axes (X, Y and Z axis).

In addition to the aforementioned equipment and materials for making the 3D topo models and orthophoto images, the certain software tools are also needed. The two required programs are a program that controls the flight of an unmanned aerial vehicle and program that further processes the photos taken by the aircraft.

For the aircraft control, the most commonly used programs are: Pix4d, Altizure and Drone Deploy. The Drone Deploy program was used to make the orthophoto images and 3D models presented in this paper. It is possible to control with this program: the flight speed of the aircraft, flight height, the camera operation and route by which the aircraft flies (Figures 5, 6 and 7). All these flight parameters are very important in overlapping the images, on which the quality of orthophoto image and 3D model depends. To create a high-quality orthophoto image and 3D model, it is necessary to have a frontal and lateral overlapping of recorded images of at least 60% [3].

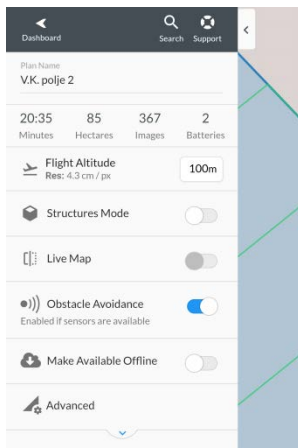


Figure 5 - Command window in which the flight height is adjusted

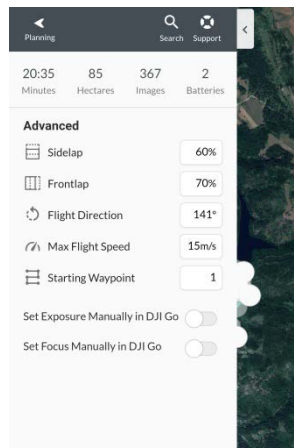


Figure 6 - Command window in which the overlapping of images is adjusted



Figure 7 - Command window in which the flight route is adjusted

The program that is the most commonly used to make the 3D topo models and orthophoto images is the AgisoftPhotoScan (Figure 8).

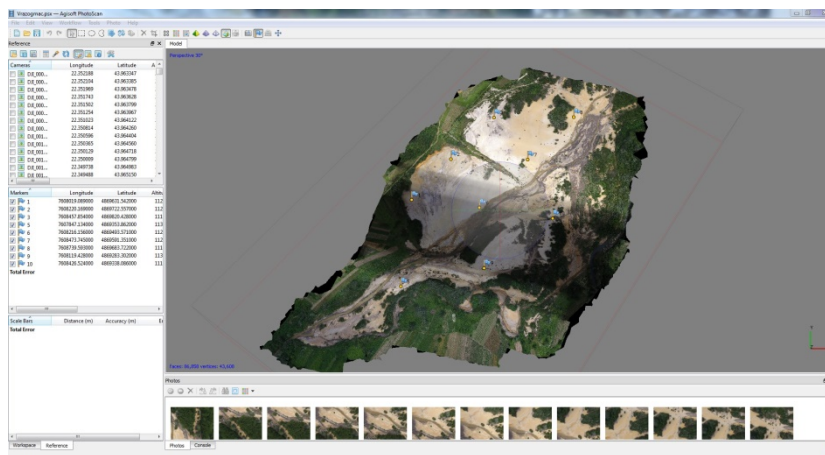


Figure 8 - Program AgisoftPhotoScan (the mouth of the Bela River into the river Timok)

All recorded photos are loaded into this program. In addition to photos, the information about the marker positions are also loaded for the purpose of georeferencing and image equalization.

After loading the basic data, the creation of a point cloud is made, depending on the field size, the point cloud can consist of several tens to several hundreds of thousands of points (Figure 9) [4]. The next step in creating a 3D topo model is to create a dense point cloud. The program uses an

already created point cloud to perform a multiple interpolation of each point in order to result in a dense point cloud that can comprise more than hundreds of millions of points (Figure 10) [4].

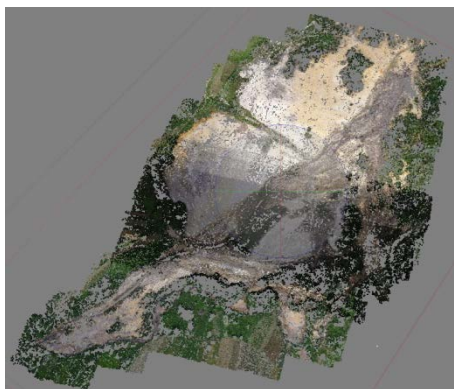


Figure 9 - A point cloud made in the program AgisoftPhotoScan (the mouth of the Bela River into the river Timok)



Figure 10 - A dense point cloud made in the program AgisoftPhotoScan (the mouth of the Bela River into the river Timok)

A dense point cloud is the basis for creation a 3D topo model, from which it is possible later to make a DEM (digital elevation model) (Figure 11) [4]. This model can be loaded into various GIS programs and further processed; it is also possible to execute a contouring, thus obtaining the field isolines that can be further exported to Dxf or Dwg format (Figure 12) [4].

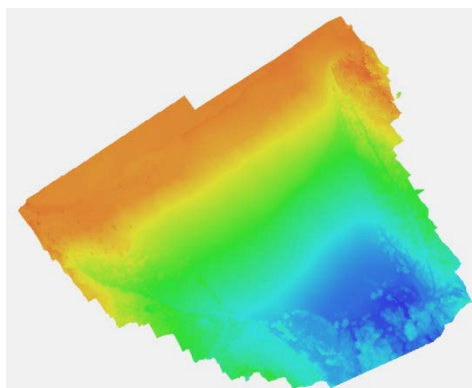


Figure 11 - DEM model made in the program AgisoftPhotoScan (Dam 3 of the flotation tailing dump Veliki Krivelj)

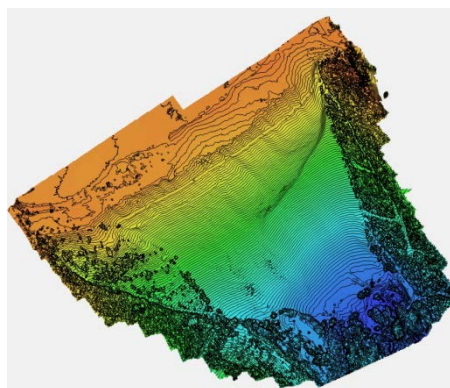


Figure 12 - Field isoline made in the program AgisoftPhotoScan (Dam 3 of the flotation tailing dump Veliki Krivelj)

### 3. CONCLUSION

The technology behind the unmanned aerial vehicle is progressing from day to day so that in the near future these aircrafts will be increasingly used in all spheres of life.

Despite the great possibilities that the aircrafts have to offer, there are a number of restrictions in their use, both technical and legal.

One of the biggest technical constraint are certainly the cameras that these aircrafts carry. The best results are achieved above the naked and non-afforested field.

It also needs to be aware of legal restrictions. In the Republic of Serbia, the law stipulates that each aircraft is registered and that each pilot has a license. A flight height is limited for the second category of unmanned aerial vehicle to maximum of 150m, and it is necessary to report each flights in advance to the army of the Republic of Serbia and to get a permit for it. Also, in the Republic of Serbia, there are the air traffic control zones such as: airports, military barracks, military and police polygons and public administration buildings [5].

## **ACKNOWLEDGEMENT**

*The authors are grateful for funding by the Minister of Science, Technological Development and Innovation of the Republic Serbia, the Grant No. 451-03-47/2023-01/200052. Also, this work was financially supported by the EU under Interreg – IPA CBC Romania-Serbia Programme and co-financed by the partner states in the Programme. Project Romania Serbia NETwork for assessing and disseminating the impact of copper mining activities on water quality in the cross-border area (RoS-NET2) eMS code RORS - 337. Also, this work was financially supported by the EU under Program 2nd EIT-HEI call: Building Ecosystem Integration Labs at HEI to foster Smart Specialization and Innovation on Sustainable Raw Materials - HEI4S3-RM.*

## **REFERENCES**

- [1] Amel Žilić, Geodetski Glasnik, No. 46 (2015).
- [2] DJI Phantom 3 user manual, V1.8, 2017.07.
- [3] DroneDeploy on line manual, <https://www.dronedeploy.com/product/get-started/>.
- [4] AgisoftPhotoScan manuals, <http://www.agisoft.com/support/tutorials/intermediate-level/>.
- [5] Official Gazetter RS, Nos73/10, 57/11, 93/12, 45/15 and 66/15.



## MECHANICAL CHARACTERISTICS OF THE SHAPE MEMORY ALLOY Cu-Zn-Al

Dejan Tanikić\*, Anđela Stojić, Jelena Đoković, Miloš Stoljiljković

Technical Faculty Bor, University of Belgrade, V.J. 12, 19210 Bor, Serbia

### Abstract

*Shape memory alloys – SMA are specific alloys which possess unusual characteristic called shape memory effect. This effect enables them to change their own shape and return to some memorized state, according to the environment temperature. The area of usage of shape memory alloys is very large and heterogeneous. There are two main groups of SMAs in commercial usage: Ni-Ti alloys and copper based alloys. This paper will present some of the experimentally obtained mechanical characteristics of the shape memory alloy Cu-Zn-Al.*

**Keywords:** SMA, mechanical characteristics, Cu-Zn-Al alloy

### 1. INTRODUCTION

The term Shape Memory Alloy (SMA) is used for the group of metallic materials that shows the ability to return to some previously defined shape when subjected to the adequate temperature. For example, these materials can be plastically deformed at some relatively low temperature, and exposure to higher temperature will return their original shape, prior to the deformation.

A wide variety of alloys exhibits the shape memory effect, but only those that can recover substantial amounts of strain or which can generate significant force upon changing shape are of commercial interest. The most common are the nickel-titanium alloys and copper-base alloys, such as Cu-Al-Ni and Cu-Zn-Al. The shape memory effect has been firstly noticed on the copper based alloys (Cu-Zn and Cu-Sn) in 30's years of the past century [1]. Nitinol (alloy on the basis of nickel and titanium), one of the most frequently used shape memory alloy was revealed in the 60's years of the past century in Naval Ordnance Laboratory in USA. This is commonly assigned as the origin of the investigation in the field of shape memory alloys. The first reported and documented large usage of SMA was in 1971 for a coupling which was used to connect titanium hydraulic tubing installations in the Grumman F-14 air-craft [2]. The significant usage of the shape memory alloys for manufacturing the valves for air-condition devices was reported in Japan in the 80's of the past century. Approximately at the same time started the large usage of the shape memory alloys primarily in dental, and after that, for all other medical applications. Among many materials including metals, alloys, ceramics etc. available commercially, only a limited number are currently being used as prostheses or biomaterials in medicine and dentistry. The reason for this is that prostheses need to satisfy two important demands: biofunctionability and biocompatibility [3].

The mechanical properties of shape memory alloys vary greatly over the temperature range spanning their transformation. In this paper, some of the mechanical characteristics of Cu-Zn-Al, one of the mostly commercially used SMA, are presented.

### 2. THE SHAPE MEMORY EFFECT

The main characteristic of the SMA is their shape transformation, caused by changes in the environment temperature. Depending on the environment temperature and amount of the applied load, shape memory alloys can be present in two different crystal structures, i.e. phases [4]. The low temperature phase is martensite, while the high temperature phase is austenite. Solid state phase transition from martensite to austenite, and vice versa, is a key process which enables shape

changing of the SMAs. This effect is called martensitic thermoelastic transformation [5]. Starting and finishing temperatures of the martensite transformation, as well as starting and finishing temperatures of the austenite transformation depends on the physical and chemical characteristic of the alloy. The copper-aluminium binary alloy (Cu-Zn-Al alloy) displays shape memory effect and has a transformation temperature which is generally too high for practical use. But, the addition of zinc to this system produces a new alloy, Cu-Zn-Al, which is of commercial importance.

The specimens used in this study were made from Cu-Zn-Al alloy, in the form of wire, with diameter of 2.9 mm. Before testing, the specimens were thermally prepared on three different ways: 1. Annealed on 800 °C for 15 minutes, then water cooled; 2. Cold deformed; 3. Thermally processed on the following way: annealed on 450 °C for 15 minutes, then water cooled, after that annealed on 550 °C for 2 hours, then cooled in the furnace to 450 °C and finally cooled on air.

**Tensile strength testing:** The specimens in the form of wire were used for determination of the tensile strength. The examinations were performed on the Universal Testing Machine, Figure 1. Each specimen was preliminary measured, marked and mounted in the machine. The tensile force is then applied, which causes elastic, then plastic elongation and finally tearing of the wire. The tensile force is then noticed, together with the values of the elongations.



Figure 1 - Universal Testing Machine with specimen.

Three independent tests were performed for each group of thermally prepared specimens. The values of the obtained tensile strengths are:

$$R_{m1} = \frac{445.23 + 427.42 + 440.78}{3} = 437.81 [\text{MPa}], R_{m2} = \frac{749.48 + 791.03 + 802.91}{3} = 781.14 [\text{MPa}]$$

$$\text{and } R_{m3} = \frac{406.65 + 425.94 + 424.46}{3} = 419.02 [\text{MPa}].$$

**Hardness testing:** The hardness of the material was determined by the Vickers hardness test. The specimen was a cylinder made from shape memory alloy, Figure 2, with chemical composition: Cu-68.16%, Zn-27.33%, Al-4.09%. In order to obtain accurate results, one side of the specimen must be flat, so it was machined on the surface grinder. Specimen is then mounted in the Vickers testing machine, Figure 2 and a diamond in the form of a square-based pyramid, with the angle of the opposite sides of 136° is applied. In this particular case injection was performed at 5 different points of the specimen. Injection force was 49.05 [N]. After unloading, area of the square which remains on the specimen surface is calculating by measuring its diagonals.



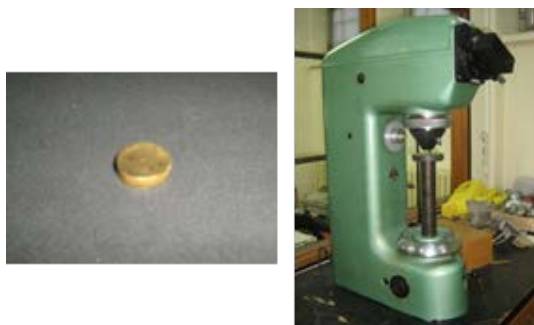


Figure 2 - Specimen and machine for Vickers hardness testing.

The mean value of the hardness is calculated on the following way:

$$HV_{sr} = \frac{86.7 + 71.6 + 99.7 + 99.7 + 102}{5} = 91.94 \text{ [N/mm}^2\text{]} .$$

**Metallographic testing:** The preparing phase for the metallographic examinations includes the following operations: 1. Sampling operation – very important step which must provide the real crystal state of the alloy block; 2. Grinding process is the second phase of the specimen preparing. This is necessary operation which is performed on the grinding machine using row and fine grindstones. The final quality of the machined surface is obtained using grinding paper; 3. Polishing is third preparing phase which includes polishing of the specimen with felt panel and polishing pastes which usually contains metal oxide powders; 4. Abrasion is the final phase in the specimen preparing. Abrasion substances are usually acid or salt solutions, with water, alcohol, glycerine or some other solvent. The reagents which are used depend on the material type and the goal is to obtain shineless surfaces. In this case ferric chloride was used (20 g of ferric chloride, 6 cm<sup>3</sup> of hydrochloric acid and 100 cm<sup>3</sup> of water).

Metallographic testing was performed by analysing of the structure of the prepared specimen, using metallographic microscope which operates with reflected light “EPY type 2”, Figure 3. The structures which were obtained by examination with magnifications of 200x and 500x are presented at Figure 3 (a) and (b), respectively.

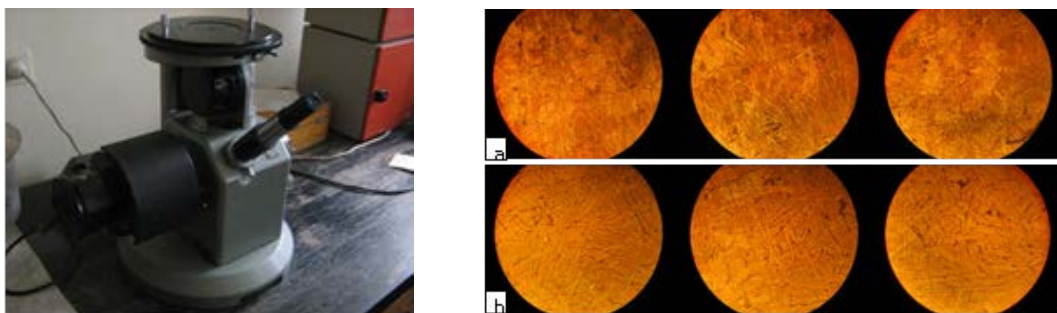


Figure 3 - Microscope “EPY type 2” and structures obtained by metallographic examinations with magnification of: (a) 200x and (b) 500x.

**Microhardness testing:** The values of the microhardness were measured on the device for microhardness measuring “PMT-3”, Figure 4(a). The procedure is similar as the procedure for hardness measuring and the main difference is in the amount of the load which is applied. In this case a load of 100 g during 10 s was applied on 5 different points on the specimen.

The mean value of the microhardness obtained by this method is:

$$HV_{\mu sr} = \frac{14.3 + 14.8 + 13.8 + 14 + 12.9}{5} = 13.96 \text{ [kgf/mm}^2\text{]} = 136.915 \text{ [N/mm}^2\text{]} .$$

**Electrical conductivity testing:** Electrical conductivity was measured at 5 different points on specimen using the device for electrical conductivity measuring “Sigmatest”, Figure 4(b).



(a)



(b)

Figure 4 - (a) Device for microhardness measuring “PMT-3” and (b) Device for electrical conductivity measuring “Sigmatest”.

The mean value of the measured electrical conductivity is:

$$\sigma_{sr} = \frac{10.9 + 10.8 + 10.7 + 10.8 + 10.8}{5} = 10.8 \left[ \frac{MS}{m} \right].$$

### 3. CONCLUSION

Mechanical characteristics of Cu-Zn-Al shape memory alloy are presented in this paper. Some studies have shown that the mechanical properties of SMAs mainly depend on the wire form, or the relationship between the microstructure and thermally induced phase transitions. The investigation shows that thermal treatment of the specimen has a big impact on its mechanical properties. However, SMAs generally have good mechanical and physical characteristics and their ability to remember some previous shape is widely used in almost all fields of science and engineering.

### 4. ACKNOWLEDGEMENT

The authors are grateful to the Ministry of Education, Science and Technological development of the Republic of Serbia for financial support (451-03-47/2023-01/ 200131).

### REFERENCES

- [1] D. Mantovani, JOM – J. Min. Met. Mat. S.; 52 (10) (2000) 36–44.
- [2] D. Tanikić, R. Pantović, V. Despotović, M. Žikić, Proceedings of the XXIII International Conference „Ecological Truth“ ECO-IST ‘15, 17-20 June, Kopaonik, Serbia (2015) 274–280.
- [3] K. Otsuka, C. M. Wayman, Shape Memory Materials, Cambridge University Press, (1998), ISBN: 0 52 1 44487 X hardback.
- [4] T. Kanada, M. Enokizono, J. Magn. Magn. Mater.; 196-197 (1999) 349-350
- [5] W. Ochoński, Ind. Lubr. Tribol.; 62 (2) (2010) 99-110.

## COPPER RECOVERY FROM RE-FLOTATION TAILINGS BY COMBINED PROCESS

Ljiljana Avramović, Vanja Trifunović, Zoran Stevanović, Radmila Marković,  
Dragana Božić, Dejan Bugarin, Silvana Dimitrijević

Mining and Metallurgy Institute Bor, Zeleni bulevar 35, 19210 Bor, Serbia

### Abstract

*An efficient method has been proposed to recovering substantial amounts of copper from re-flotation tailings and reducing the environmental impact of flotation tailings by a combined hydrometallurgical process which includes High Pressure Leaching (HPL)-Solvent extraction (SX)-Electrowinning (EW) processes. As a result of HPL using water or sulfuric acid as leaching solution, high copper leaching rate (>95%) was obtained even with water. Then, the copper concentration in the stripped solution reached 44.8 g/L and the iron concentration was 1.4 g/L by the SX tests using LIX-84I as extractant. Moreover, it was confirmed that as lower iron concentration in the electrolyte for the copper electrowinning process, the better the current efficiency of copper electrodeposition.*

**Keywords:** copper recovery, flotation tailings, HPL, SX, EW

### 1. INTRODUCTION

In the process of copper ore processing, more precisely in the flotation process, which is carried out in order to obtain copper concentrate, flotation tailings are generated as an intermediate product of the process. These tailings are disposed of in a dump, while the copper concentrate is used in the smelting process, after which pure metallic copper is obtained. In the course of long-term mining activities, a large amount of flotation tailings was deposited at the Old Flotation Tailings Dump in Bor, Serbia. Given that the copper content in these tailings is about 0.2-0.4%, there is a possibility that the tailings can be used as a secondary raw material for copper recovery. In order to increase the concentration of copper in the flotation tailings, re-flotation process of the tailings was carried out as a pre-treatment, after which a re-flotation tailings was obtained. In this paper, experimental investigations were carried out on the copper recovery from re-flotation tailings by a combined hydrometallurgical process that includes the three following processes: High Pressure Leaching (HPL) process, Solvent Extraction (SX) process, and Electrowinning (EW) process.

### 2. EXPERIMENTAL

In order to achieve a high level of copper leaching rate from the re-flotation tailings, which consists of chalcopyrite as the main component of copper, leaching was carried out under high pressure in an autoclave [1]. Then, the solvent extraction of copper from the pregnant leaching solution (PLS) that was obtained by HPL was carried out for obtaining the Cu-rich solution. Finally, a copper electrowinning experiment was carried out in relation to the composition of the solution obtained by applying the optimal process parameters of solvent extraction. In order to perform tests for obtaining copper, it is desirable that the concentration of copper in the electrolyte is high (45 g/L) and the iron concentration is low (under 2 g/L). Therefore, the influence of iron ions on the current efficiency of copper electrodeposition was confirmed. Current copper electrodeposition efficiency is described in Khouraijbchia et al. [2].

#### 2.1 High pressure leaching process

The chemical compositions of re-flotation tailings sample used for HPL tests was as following: Cu 0.34 wt.%, Fe 8.96 wt.%, Al 8.12 wt.%, S 11.2 wt.% and SiO<sub>2</sub> 57.8 wt.%. The content of the

investigated elements was determined using Inductively Coupled Plasma Optical Emission Spectroscopy (ICP-OES) and X-ray Fluorescence Spectrometry (XRF). An autoclave device (Nitto Koatsu, Japan) containing a teflon reaction cell with a volume of 2 L was used for the High Pressure Leaching experiments of re-flotation tailings.

The investigated experimental conditions of HPL process were as following: leaching reagents – water or 0.2-0.5 mol/L H<sub>2</sub>SO<sub>4</sub>, total pressure of O<sub>2</sub> gas 0.8-2.0 MPa, pulp density 100-400 g/L, temperature 140-180 °C and leaching time 60 min.

## 2.2 Solvent extraction process

In the SX process, the influence of the pH value of PLS obtained after the HPL process on the degree of Cu extraction was investigated. Correction of the pH value was done with a 1.0 M NaOH solution. The following parameters of the SX process were constant: extractant LIX-84I diluted in kerosene in the ratio 1:1, ratio of organic and aqueous phase O/A=0.2, process time 15 min. After the SX process was completed, the solution was centrifuged for 5 min at 4000 rpm in order to rapidly separate the phases.

After determining the optimal conditions of the SX process, the influence of sulfuric acid concentration of 0.5, 1.0 and 1.5 M on the degree of Cu re-extraction process from Cu-rich phase was examined. Other constant parameters of the re-extraction process were as follows: ratio of organic and aqueous phase O/A = 5, duration of the process 15 min.

The concentrations of copper in the aqueous solutions after the extraction and re-extraction processes were determined using ICP-OES, after which the processes efficiencies were calculated.

## 2.3 Electrowinning process

Conditions of electrowinning process of copper are presented in Table 1. For the EW process, platinum anode and steel cathode with an area of 10x10 mm<sup>2</sup> were used. Before and after the EW process, electrodes were measured and based on the difference in weight, the amount of deposited Cu was recalculated, and also the efficiency of the process.

Table 1 - Experimental conditions of EW process

Volume of electrolyte (L)	Cu concentration (g/L)	Fe concentration (g/L)	Current density (A/m <sup>2</sup> )	Temperature (°C)	Free H <sub>2</sub> SO <sub>4</sub> (g/L)	Process time (4)
0.5	44.8	1.4	250	40	170	4

## 3. RESULTS AND DISCUSSION

### 3.1 High pressure leaching process

Figure 1 presents the influence of H<sub>2</sub>SO<sub>4</sub> concentration (0 (water)-0.5 mol/L) on copper recovery from the re-flotation tailings. The copper approximately completely dissolved, while the iron leaching rate reached 95.5%. Even though the sulfuric acid concentration is zero, as leaching reagent water was used, a high degree of copper leaching was achieved. This is due of the generation of sulfuric acid by the oxidation of pyrite as shown in equation (1) [4]. As a result of the formation of sulfuric acid, there was a decrease in the pH value of the slurry from 3.79 to 0.35 after the HPL process using water as leaching reagent.



After experimental investigations of the HPL process, it can be concluded that the optimal process parameters are as follows: water as leaching reagents, total pressure of O<sub>2</sub> gas: 2.0 MPa, pulp density: 100 g/L, temperature: 180 °C and leaching time: 60 min.

From an economic point of view, water is selected to be the leaching reagent for copper leaching from the re-flotation tailings. Under the optimal HPL conditions, leaching rate of Cu is 94.4% and the Cu concentration in the obtained PLS is 2.9 g/L.

To further recovery of copper from PLS, a solvent extraction process was carried out using the leaching solution obtained under the optimal HPL conditions.

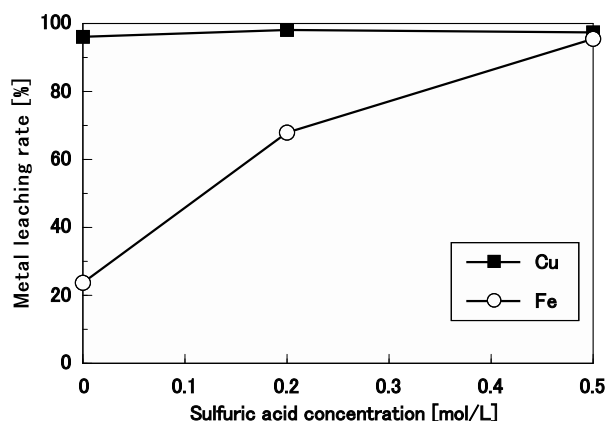


Figure 1 - Leaching rate of copper and iron as a function of sulfuric acid concentration (Total pressure: 2.0 MPa, temperature: 180 °C, pulp density: 100 g/L, leaching time: 60 min)

### 3.2 Solvent extraction process

The results of the study of the influence of the pH value of the PLS on the EX process show that the degree of copper extraction depends on the equilibrium pH values that minimize the extraction of other metal ions such as iron [1]. For the EW process, for the selective extraction of copper, the pH of the PLS of 2 was determined as the optimal value.

As for the re-extraction process, the degree of copper recovery from the Cu-rich organic phase increases linearly from 24.7 to 97.4% with increasing H<sub>2</sub>SO<sub>4</sub> concentration from 0.5 to 1.5 M. A 1.5 M solution of H<sub>2</sub>SO<sub>4</sub> was chosen as the optimal parameter for the copper re-extraction process from the Cu-rich organic phase. The concentration of copper and iron in the solution obtained after re-extraction contains approximately 44.8 g/L Cu and 1.4 g/L Fe.

### 3.3 Electrowinning process

The results obtained for the process of electrochemical extraction of copper from the solution - EW process, indicated a high level of current efficiency, over 98%, with the following parameters: copper concentration in the electrolyte 44.8 g/L, H<sub>2</sub>SO<sub>4</sub> concentration 170 g/L, current density 250 A/m<sup>2</sup>, electrolyte temperature 40°C and time 4 h. The concentration of iron in the electrolyte is limited to a value below 2 g/L. Based on the examination of the influence of the presence of Fe ions in the electrolyte, it was determined that the best current efficiency was achieved in the presence of only ferrous (Fe<sup>2+</sup>) ions in the electrolyte. The presence of ferric (Fe<sup>3+</sup>) ions in the electrolyte leads to reduced current efficiency.

## 4. CONCLUSION

An effective method for copper recovery from re-flotation tailings and reducing the negative impact that flotation tailings have on the environment is investigated. The process consists of a combination of the following processes: high pressure leaching (HPL) - solvent extraction (SX) – electrowinning (EW) process.

After the HPL process using water as a leaching reagent under optimal conditions (total pressure of O<sub>2</sub> gas: 2.0 MPa, pulp density: 100 g/L, temperature: 180°C and leaching time: 60 min) a copper leaching rate of >95% was achieved. In the SX process, which had an aim to concentrate Cu and

purify the pregnant leaching solution from Fe under optimal conditions (extraction process: pH of the solution 2, extractant LIX-84I diluted in kerosene in the ratio 1:1, O/A=0.2, time 15 min; re-extraction process: concentration of H<sub>2</sub>SO<sub>4</sub> 1.5 M, O/A = 5, time 15 min), the concentration of Cu is 44.8 g/L, and Fe 1.4 g/L. The current efficiency of copper electrodeposition in the EW process decreases with increasing iron ion concentration.

## ACKNOWLEDGEMENTS

*The authors are grateful for funding by the Minister of Science, Technological Development and Innovation of the Republic Serbia, the Grant No. 451-03-47/2023-01/200052. Also, this work was financially supported by the EU under Interreg – IPA CBC Romania-Serbia Programme and co-financed by the partner states in the Programme. Project Romania Serbia NETwork for assessing and disseminating the impact of copper mining activities on water quality in the cross-border area (RoS-NET2) eMS code RORS - 337. Also, this work was financially supported by the EU under Program 2nd EIT-HEI call: Building Ecosystem Integration Labs at HEI to foster Smart Specialization and Innovation on Sustainable Raw Materials - HEI4S3-RM.*

## REFERENCES

- [1] B. Han, B. Altansukh, K. Haga, Z. Stevanovic, R. Jonovic, L. Avramovic, D. Urosevic, Y. Takasaki, N. Masuda, D. Ishiyama, A. Shibayama, J. Hazard. Mater. 352, (2018) 192-203.
- [2] Y. Khouribchia, M. Moats, Minerals and Metallurgical Processing, 26, (2009) 176-190.
- [3] M.E. Schlesinger, M.J. King, K.C. Sole, W.G. Davenport, Extractive Metallurgy of Copper, fifth ed., Elsevier, (2011) 358-362.
- [4] B. Han, B. Altansukh, K. Haga, Y. Takasaki, A. Shibayama, Resour. Process. 64, (1), (2017) 3–14.

## APPLICATION OF HYBRID GEOGRIDS IN MINING

**Milenko Jovanovic, Daniel Krzanovic, Radmilo Rajkovic,  
Vladan Marinkovic, Miroslava Maksimovic, Miomir Mikic**

Mining and Metallurgy Institute Bor, Zeleni bulevar 35, 19210 Bor, Serbia

### Abstract

*Geogrids have a special place in the field of application of geosynthetics. There are geogrids made of synthetic materials, geogrids made of natural materials, and a hybrid type of geogrid, which combines the features of the first two types. A special part of this field refers to geogrids and geotextiles made of natural materials (organic), which, with some variations in the use of building materials, is the main topic of this paper. Organic geogrids have unique characteristics, they consist of biologically and chemically degradable natural fibers. They are designed to hold the soil in place until natural vegetation is established. On the other hand, geogrids and geotextiles made of synthetic materials have much greater strength, elasticity and durability. By combining these types (materials) of geogrids and geotextiles in the form of a kind of hybrid technology for the production of these products, we obtain useful parameters suitable for the preservation of the natural environment and the required mechanical and temporal usability. Seemingly contradictory requirements, by applying these hybrid geomaterials, can be effectively fulfilled.*

**Keywords:** *Geosynthetics, hybrid geogrids, hybrid geomaterials, natural environment*

### 1. INTRODUCTION

Pollution of the surface layers of the earth easily leads to pollution underground (in deeper layers). In order to prevent this, man began to strive for the most effective solution to this global problem.

Geosynthetics play a major role in soil protection, whether it is a landfill, some other surface pollution or degradation.

Mining and construction works are carried out in accordance with the laws on mining and construction of the Republic of Serbia. The laws are explicit and binding, and presented with the necessary technical documentation.

In accordance with the technical documentation of the Law on Mining, the obligation to recultivate the land is determined, according to the current Project. By amending the Law and harmonizing it with international standards (EN ISO 10318-1:2015 CEN/TC 189) and articles (ISO 10318-1:2015 ISO/TC 221) related to ecology and work safety, the introduction of "new" security and protection measures is foreseen mining facilities and surroundings. One of them is the application of geosynthetics, as a (future) mandatory measure for securing mining and construction facilities (dumping sites, securing slopes, embankments, canals, etc.). The aforementioned standards (ISO 10318-1:2015 ISO/TC 221) define terms related to functions, products, properties and other terms, as well as symbols used in geosynthetics.

A special part of this field refers to geogrids and geotextiles made of organic material (from nature). Organic geogrids have unique characteristics, they consist of biologically and chemically degradable natural fibers. They are designed to hold the soil in place until natural vegetation is established. On the other hand, geogrids and geotextiles made of synthetic materials have much greater strength, elasticity and durability.

By combining these types (materials) of geogrids and geotextiles in the form of a kind of hybrid technology for the production of these products, we obtain useful parameters suitable for the preservation of the natural environment and the required mechanical and temporal usability.



Seemingly contradictory requirements, by applying these hybrid geomaterials, can be effectively fulfilled. [1, 3, 4, 7]

### **1.1 Geogrids – materials, differences and types**

Geogrids are made of polymer materials such as polyethylene, polyester and polypropylene and are characterized by high tensile strength. The original geogrids were made by drilling holes in a sheet of material. Today, such geogrids are made by the so-called extrusion process. Now we have geogrids made of polyester fibers coated with polyethylene. Many unbroken fibers are combined into a thread, which is then woven in longitudinal and transverse directions with a certain distance between the ribs, and the folds are additionally strengthened and then the fibers are coated.

Geogrids are most often used to strengthen and stabilize weak soil. The geogrid absorbs the forces and prevents the formation of cracks on the newly installed asphalt layer. The third important purpose of geogrids is to protect against soil erosion. For this purpose, there are two-dimensional geogrids that have small mesh openings and three-dimensional geogrids. Depending on the manufacturer, geogrids may differ, but their primary function and mode of operation is the same.

- absorb the kinetic energy of erosive elements (rain, wind) and stabilize the soil surface, creating numerous micro-dams over it,
- keeps seeds and hydroseeding material in place, even on steep soil slopes, leading to successful seed germination
- helps the penetration of water through the soil and moisture retention, which leads to better seed germination and good grass growth.

The application of anti-erosion geotextiles can increase and support the effect of erosion control in areas with particularly steep slopes or in areas subject to erosion. [1, 2, 3, 4, 5]

## **2. EXPERIMENTAL**

### **2.1 Application of geogrids in measures of recultivation of degraded land**

New materials and technologies make it possible to achieve significant improvements in many areas of mining and construction in the field of faster, safer, more efficient construction, insurance, maintenance and rehabilitation of mining and construction facilities, primarily civil engineering, although some materials have wide application in the field of environmental protection and high-rise buildings.

Generally speaking, within the recultivation of degraded areas, it is necessary to apply technical, bio-technical and biological measures.

Technical measures contribute to the improvement of the resistant and deformable characteristics of the landfill, which directly affect the increase in erosion stability of the slopes.

Bio-technical measures, together with technical measures, contribute to faster achievement and maintenance of permanent landfill stability.

Bio-technical measures imply proper selection and application of vegetation which, together with technical measures, will lead to permanent stability, both in horizontal and vertical direction. On almost horizontal locations, after the completion of technical measures, biological measures of landfill reclamation can be applied.

Biological measures are applied in the final phase of recultivation. Biological recultivation implies the raising of arable and fruit crops, afforestation... [1, 2, 3, 7, 8]

### 3. RESULTS AND DISCUSSION

#### 3.1 Control of erosion processes

The emergence of erosion processes depends on the degree of implementation of technical measures and the possibility of unexpected excessive natural or anthropogenic phenomena.

Analysis of erosion stability should be performed taking into account: physical and mechanical characteristics of natural soil and landfill, indicators of filtration current flow, probability of high water occurrence, landfill geometry, as well as other specific indicators that can affect erosion stability.



Figure 1 - Setting up a geogrid

At landfills, there are conditions for the emergence of surface and internal forms of erosion. Some of the surface forms of erosion arise as a consequence of the existence of internal erosion. Locations sensitive to the emergence of surface forms of erosion are slopes (Fig. 1 and Fig. 2) and depressions, created as a result of internal erosion processes.



Figure 2 – Jute geogrid

Prevention of surface erosion is done by reducing the water that reaches the slope, a system of drainage channels with a mandatory perimeter channel and drainage or geosynthetics. By using geogrids, the surface layer of the soil can be protected from erosion. They are placed and secured with wedges, and then covered with a substrate mixed with grass seed or weeding is done by hydroseeding.

Another way to control erosion processes is the installation of geomembranes. Geomembranes produced from natural fibers of jute or hemp, consist of natural cellulose veils as a supporting layer, grass seeds and additives for accelerated growth. [1, 3, 9, 10]

#### 4. CONCLUSION

The primary function of geomembranes and geodrains on landslides is drainage, while geotextile performs multiple functions: filtering, draining, reinforcement and separation.

Geogrids have a reinforcing function, while the function of geocomposites is different, depending on the combination of constituent materials.

Materials that are very effective in the rehabilitation of landfills and degraded areas are almost never used in our country, is it because we hardly accept newspapers or because of their price? Price cannot be the answer and justification, because what we keep with them actually has no price.

Geosynthetics has proven to be the most effective material for wide application. Its building elements ensure high quality and multi-purpose use in civil engineering, high-rise construction, mining, environmental protection... Regardless of the high price of these materials, their use is necessary and fully justified.

Geogrids and geotextiles made of organic material (coconut, jute) are a natural and 100% biodegradable solution for erosion control using geogrids or coir geotextile mats. Organic geogrids have unique characteristics, they consist of biologically and chemically photo-degradable natural fibers. They are designed to hold the soil in place until vegetation is established. A geogrid or permeable geotextile provides a natural support system (improvement of characteristics) to the soil (soil, landfill...) and vegetation.

A hybrid approach to the use of construction materials exists as a possible life-saving solution in many cases, where an effective result is sought both in terms of ecology and construction, safety, and terrain security. Namely, by using (combined - hybrid) different types of materials when making geogrids or geotextiles, we can solve seemingly contradictory requirements in their application.

Such hybrid materials, which would contain crossed bundles of organic and synthetic origin, can, depending on the purpose and their mutual relationship, be an "ideal compromise", that is, a saving solution. Material of organic origin would have a positive effect on the development and preservation of vegetation and the entire ecosystem, while geosynthetic materials would have a primary application of a mechanically stabilizing nature, as many times stronger and more time-stable materials. In addition to the above, organic geogrids act as "mulch" and thereby improve the establishment of vegetation. After degradation, they do not leave any toxic material.

It is necessary to point out that such materials have a very wide application in the field of environmental protection, especially in the prevention of groundwater and surface water pollution through infiltration control, and also in the treatment and immobilization of various types of waste, especially hazardous waste.

## **ACKNOWLEDGEMENT**

Note: This work was financially supported by the Ministry of Education, Science and Technological Development of the Republic of Serbia, Grant no. 451-03-47/2023-01/ 200052.

## **REFERENCES**

- [1] Nonweiler, E. Slope sliding and stabilization, Školska knjiga, Zagreb, (1987)
- [2] Veinović, Ž., Kvasnička, P. Surface landfills, Internal script, Faculty of Mining, Geology and Petroleum Engineering, University of Zagreb, Zagreb, (2007)
- [3] Zidar, M. Landslide remediation methods, Faculty of Geotechnics, University of Zagreb, Varaždin, (2009)
- [4] Mladen Bogičević - Gradjevinarstvo.rs/ Construction.rs/ (03.12.2008.year)
- [5] Dragan M. Đorđić, Research of deformation characteristics of nonwoven geotextile materials made of polyester and polypropylene fibers - Doctoral Dissertation, (2016)
- [6] SRPS EN ISO 10318:2015- Geosintetika/ Geosintetics - Terms and definitions (ISO 10318:2015)

- [7] Sandra Lenče, Final paper (work): Application of geosynthetics in landscaping – k 3 6.
- [8] Lukavečki Iva, Final paper (work), About geosynthetics and applications in landfill remediation; (p.1821), (2010./2011.)
- [9] Milenko Jovanović, Study research II (Doctoral dissertation): eoGeosynthetics - purpose and application (in mining), University of Belgrade, Technical Faculty in Bor, (2019)
- [10] Milenko Jovanović, Study research III (Doctoral dissertation): "Organic geogrids", University of Belgrade, Technical Faculty in Bor, (2019)

## **GEOLOGICAL EXPLORATION OF THE TECHNOGENIC DEPOSIT - OLD FLOTATION TAILING PIT - BOR WITH THE POSSIBILITY OF LEACHING**

**Stefan Trujić, Miroslava Maksimović, Vladan Marinković,  
Ljiljana Avramović, Vanja Trifunović, Dragana Božić**

Technical Faculty Bor, University of Belgrade, V.J. 12, 19210 Bor, Serbia

### **Abstract**

*Technogenic deposit of copper from the old flotation tailings pit - Bor was created by the deposition of flotation tailings that was created by processing ore from several ore bodies of the Bor copper deposits. The deposit of copper was explored with drilling from the surface. Research has established relatively low, evenly distributed contents of copper and gold. An experimental study of the leaching process of flotation tailings is done in the aim of valorization the present copper. The degree of copper leaching was about 60%, which is exactly the participation of oxide copper forms regarding to the total copper content of the flotation tailings.*

**Keywords:** Flotation tailings, Bor, copper, leaching

### **1. INTRODUCTION**

Technogenic deposit of copper from the old flotation tailings pit in Bor was created by depositing material that remained after the flotation processing of the ore from the old Bor open pit and from the ore bodies that were excavated underground. Tailings were formed over a long period of time, since the beginning of the exploitation and processing of copper and gold ore, using different technological procedures, with different utilization of useful components, which means that a significant amount of copper and gold remained in them, which is probably possible to valorize.

### **2. GEOLOGICAL EXPLORATION OF THE TECHNOGENIC DEPOSIT - OLD FLOTATION TAILING PIT - BOR**

The largest part of the material in the tailings was created by the exploitation of porphyry and massive sulphide deposits and ore bodies of copper and gold from the Bor, Veliki Krivelj, Cerovo and Majdanpek ore fields. Figure 1 shows the contours of the approved investigation area.

The tailings deposit is divided into two fields - Field 1 and Field 2. Based on geological documentation and made profiles, the thickness of material ranges from 25 m to 65 m. The entire area (Field 1 and Field 2) has an elliptical shape, and its area is about 0.6 km<sup>2</sup> (Figure 2) [1].

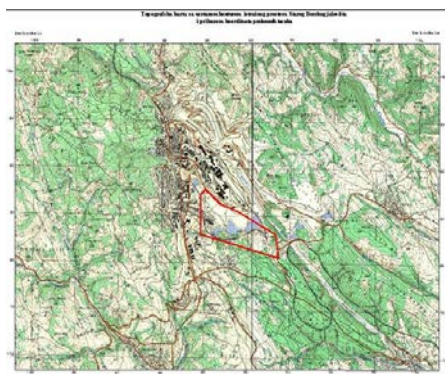


Figure 1 - Location of the research area Old flotation tailings pond Bor (red polygon).

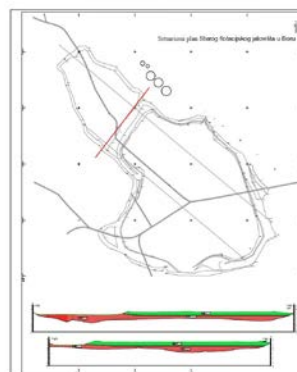


Figure 2 - Situational plan of the old tailings pit with longitudinal profiles.

### 3. APPLIED METHODS AND PROCEDURES OF MODERN GEOLOGICAL RESEARCH OF THE TECHNOGENIC DEPOSIT OLD FLOTATION PIT- BOR

For the subject of this work, the geological research conducted in the period 2018-2021 is particularly important. In addition, research was also carried out in order to obtain the necessary data for the recultivation of the area in question.

Sixteen drill holes were designed, in Field 2, with a total length of 500.7 m. The smallest depth of the drill hole is 10.0 m, and the largest is 63.5 m. The obtained results on the content and distribution of useful components obtained by chemical analysis were the basis for the spatial contouring of technogenic raw material deposits, as well as the determination of the quality and the calculation of the amount of technogenic raw mineral material.

Geological logging and photographing of the core was carried out by MMI Bor (Figure 3). The samples were analyzed in the MMI Bor laboratory. The sample for chemical tests was formed in this way, by taking the entire material of the core, 1 m long, for the sample. The preparation of the samples involved dividing one meter of the previously logged core into two equal halves.

The technological tests gave good results regarding the utilization of copper from the flotation tailings.

Individual chemical analyzes of the samples included determination of the content of basic ore elements - Cu, Au and Ag.



Figure 3 - Core of technogenic raw material from the old flotation tailing pit - Bor

The distribution of copper and gold, as well as mercury and arsenic by samples are shown in the vertical profile of the characteristic drill hole B-14/2 (Figure 4).



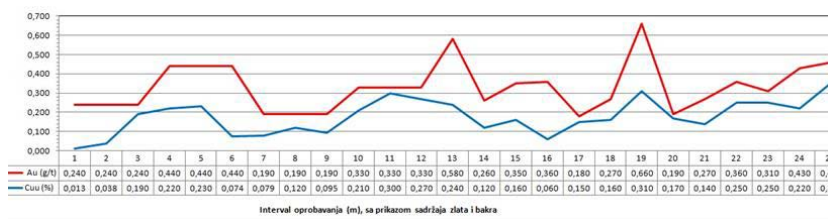


Figure 4 - The distribution of copper and gold

From Figure 4, it is possible to see that the distribution of copper and gold in the vertical profile of the analyzed drill hole is uneven with increases and decreases. It is important to know that elevated gold contents follow elevated copper contents, as well as that the gold contents are more unevenly distributed with more pronounced peaks. [1]

#### 4. POSSIBILITY OF LEACHING

This study deals with the physico-chemical and mineralogical characterization of the flotation tailing pit and chemical characterization of the mine waste water from the accumulation ‘Robule’. Technological composite samples (Table 1) are formed for laboratory testing of the leaching process of copper (Figure 5). The parameters of agitation leaching of flotation tailings with the mine waste water from the accumulation of ‘Robule’ were defined.

Table 1 - Chemical content of a composite sample of tailings

Element	Content, %	Element	Content. %
Cu	0.43	Au, g/t	<0.05
Cu, ox	0.18	Ag, g/t	0.8
Fe	16.56	Hg, g/t	0.2



Figure 5 - Composite sample of flotation tailings prepared for experimental testing

Leaching test and TCLP (Toxicity Characteristic Leaching Procedure) test were carried out on a composite sample of flotation tailings. Experimental testing the leaching process of flotation tailings in order to determine the optimal parameters of copper extraction were performed on a laboratory scale. Samples from flotation tailing dump were treated by the agitation leaching method. The mine water from the accumulation Robule (mine waste water) was used as leaching solution, The highest degree of copper leaching of 56.21% was achieved at temperature of 80°C. Based on the results of leaching, it can be stated that the time of development the leaching process has no significant effect on degree of copper. The highest degree of copper leaching of 56% was achieved in the following process parameters: temperature of 80°C, time 4 h and ratio S:L = 1:2.5. Solutions after leaching with copper content up to 1.5 g/dm<sup>3</sup> are suitable for the SX-EW process.

#### 5. CONCLUSION

Results of experimental laboratory testing of copper leaching from flotation tailings indicate that the highest degree of copper leaching was achieved in the following process parameters: time: 4



h, temperature: 80°C, ratio of solid: liquid is 1:2.5, pH of leaching solution: 1. The mine water from the accumulation Robule with correction of pH value was used as leaching solution, what presents a special contribution to solving the problems of use the integrated treatment of waste mine water and flotation tailings. This would be result both into economic and ecological effect by collecting the mine water, their recirculation in the controlled leaching process of mine waste.

#### **ACKNOWLEDGEMENT**

*This work was financially supported by the Ministry of Education, Science and Technological Development of the Republic of Serbia, contract no. 451-03-47/2023-01/ 200052.*

#### **REFERENCES**

- [1] Završni izveštaj o izvršenim primenjenim, detaljnim geološkim istraživanjima tehnogene mineralne sirovine na prostoru starog flotacijskog jalovišta Bor ( Polje 1 i Polje 2).
- [2] Lj. Avramović, R.Jonović, M.Bugarin, R. Marković. Leaching of flotation tailings 2014.
- [3] M.Bugarin, R. Jonović, Lj.Avramović, M.Ljubojev, Z.Stevanović, V. Marinković, Integrated Treatment od Waste Water and Solid Mining Waste.
- [4] Pregledna topografska karta razmere 1:25 000 sa ucrtanom granicom i koordinatama istražnog prostora Starog borskog flotacijskog jalovišta (polje 1 i 2).

## SUSTAINABLE AND SMART MINING

**Zoran Stevanović, Radmila Markovic, Ljiljana Avramovic,  
Vojka Gardić, Jelena Petrović, Dragana Božić**

Mining and Metallurgy Institute Bor, Zelene bulevar 35, 19210 Bor, Serbia

### **Abstract**

*This paper describes a general view of mining and impacts of mineral resources on countries economy. It presents the importance of mineral resources in the development of the country's economy, and the requirements for their sustainable development. Requirements are explained through possible principles, instruments and responsibilities. The main fact considered in this paper is that sustainable and smart mining during transition to low-carbon emissions will be most important issue that will significantly shape the development of mining in the future.*

**Keywords:** mining, mineral resources, sustainability, responsibilities, BDP, low-carbon emissions

### **1. INTRODUCTION**

In more than 100 countries around the world, mining companies exploit minerals and metals out of the ground, satisfying continuously increasing demand from industrial production, agriculture, high-tech sectors, etc. Among those countries are more than 50 that can be considered as “mining countries,” well known for the sector's contribution to export earnings. Mining countries also include those where the sector is highly relevant domestically, either because it primarily serves large domestic markets, as in the United States, or because it employs millions of workers, such as in China or India. About 3.9 billion people live in today's 56 “mining countries,” 90 percent of them in the 51 developing and transition countries. Among the people in these countries, about 1.5 billion live on less than \$2 a day, making up nearly two thirds of the world's poorest population. Their countries have potential mineral wealth, and thus one of the key questions for them is how they can turn this endowment into an economic asset that will help them find ways out of persistent poverty. There is practically no doubt that mining as an industry will continue to expand over the next 20 to 30 years. This especially if the World Bank “The Climate Smart Mining Initiative” for transition to low-carbon emission is taken in consideration.

### **2. MINING AT A GLANCE**

A vibrant mining sector, just as any other sector, should provide significant opportunities for a country's growth (*Mining in Developing Countries – treasure or Trouble*. Mining Department World Bank and IFC, 2002) [1]. Yet there are a number of features that distinguish mining from sectors such as manufacturing or tourism. Mainly this is four most important issues:

- What's under the ground is a national asset. Extractive natural resources have been treated differently from other natural endowments. Many countries consider minerals to be assets belonging to the “public” as a whole. This has resulted either in state ownership of mining companies or in more-than-usual involvement of the state in the licensing of mining companies, the mining regulation, and financial matters including investments in supporting infrastructure.
- A “footprint industry.” By its very nature, the mining leaves an environmental, social, and economic impact. However, even when only local or regional in nature, badly managed impacts on the environment or the social fabric of society can reflect negatively on economic parameters countrywide. It is thus important to weigh the benefits against the risks and costs surrounding the industry's operations, and to mitigate any negative impacts.

- A priority area for foreign direct investment. Many developing countries pose high risks for foreign investors. Mining operations, with their export orientation and dollar-based cost and revenues, are often the first ones to present an acceptable risk reward formula to investors.
- A large source of government revenues. A vibrant mining sector tends to generate large fiscal incomes, relative to other sectors. Since in most developing countries large parts of fiscal incomes are export-based, export sectors such as minerals and ores gain more-than proportionate weight for government incomes. In some mining countries, up to 25 or 30 percent of fiscal revenues rely directly on the mining sector.

By registered mineral resources, leading countries worldwide are [2]:

1. Russia – 75 trillion US dollars (coal, natural gas, oil, gold, timber, rare earth metals);
2. United States of America – 45 trillion US dollars (coal, timber, natural gas, gold, copper);
3. Saudi Arabia – 34,4 trillion US dollars (oil, timber);
4. Canada – 33,2 trillion US dollars (oil, uranium, timber, natural gas, phosphate);
5. Iran – 27,3 trillion US dollars (oil, natural gas);
6. China – 23 trillion US dollars (coal, rare earth metals, timber);
7. Brazil – 21,8 trillion US dollars (gold, uranium, iron, timber, oil);
8. Australia – 19,9 trillion US dollars (coal, timber, copper, iron ore, gold, uranium);
9. Iraq – 15,9 trillion US dollars (oil, phosphate rock);
10. Venezuela – 14,3 trillion US dollars (iron, natural gas, oil).

### **3. MINING CONTRIBUTION INDEX (MCI) TO COUNTRY ECONOMIES**

International Council on Mining and Metals (ICMM's) Mining Contribution Index (MCI) synthesizes into a single number – and an associated ranking – the significance of the mining sector's contribution to national economies.

This provides an indication of the relative importance of mining to the economic life of a country based on four indicators:

1. Exports of minerals including coal as a share of total merchandise exports;
2. The total production value at mine stage of metallic minerals, industrial minerals, and coal, expressed as a percentage of GDP;
3. Mineral rents as a percentage of GDP;
4. Exploration expenditure.

Higher value of MCI shows higher importance of mining to the economic life of a country. Figure 1 shows the Mining Contribution Index Map [3]. As it can be seen on Figure 1, MCI is significantly higher for Russia, Australia and Chile as a countries recognized as “mining developed countries”, reach with mineral resources. One of the main indicators of the mining developed countries is a significantly higher royalties and taxes and consequently higher contribution of the mining sector in GDP.

However, MCI is also very high for lot of developing countries and Africa countries as well. In these cases, even there are not huge, currently registered mineral resources, high MCI indicate dominant impact of mining on country economy, probably due to not developed other industries and presence of foreign investment in mining as explained in Chapter 2. Having on mind that mining will have to develop in the future in strict environmental limits, for the developing Countries is crucial to start sustainable mining development regarding higher mining benefits to the global country economy.

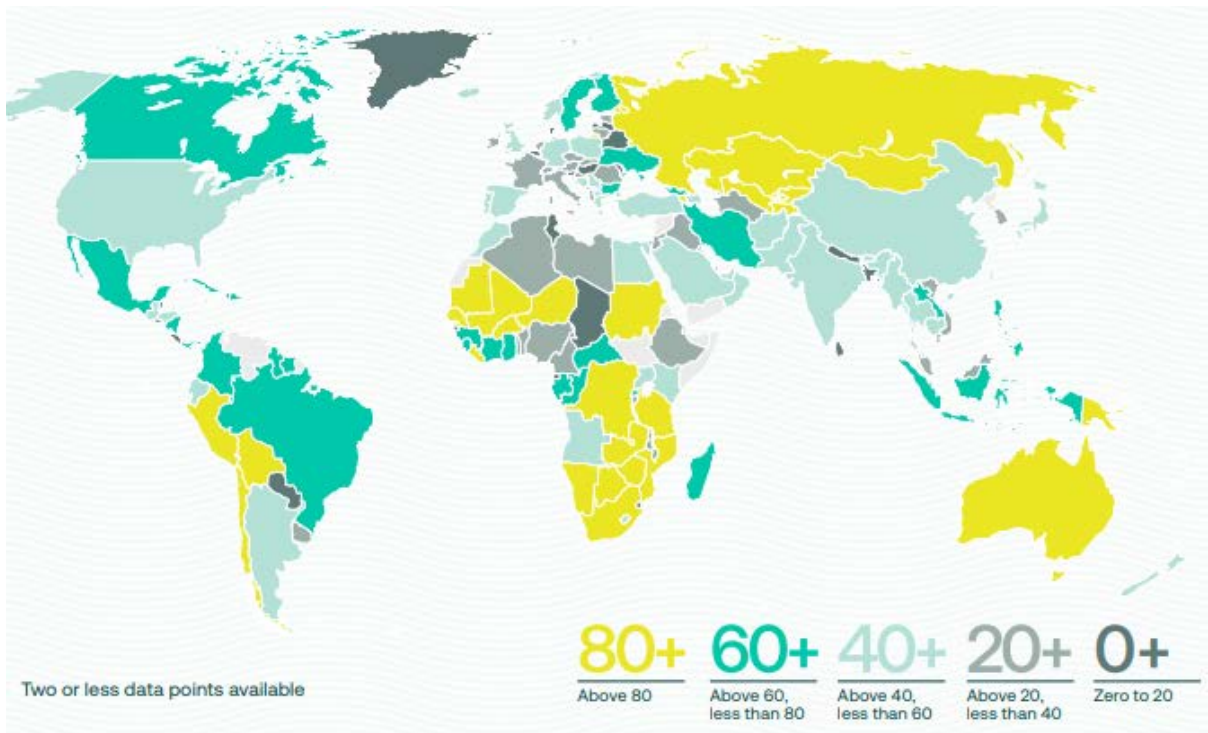


Figure 1 - Mining Contribution Index Map

#### 4. SUSTAINABLE MINING

One of the most used definition of sustainable development linking economic development and environmental stability is “development that meets the needs of the present without compromising the ability of future generations to meet their own needs” [4]. Albeit somewhat vague, this concept of sustainable development aims to maintain economic advancement and progress while protecting the long-term value of the environment, it “provides a framework for the integration of environment policies and development strategies” (United Nations General Assembly, 1987).

According to above general definition, mining sustainability could be considered on the same way, development of current mining operations without compromising the ability of future generations to develop same operations and live in same conditions as we live now. Principles of mining sustainability are based on integrated development of economic mining activity with environmental integrity and social concerns. The instruments required for environmental integrity are: environments laws, advanced mining technologies, advanced monitoring system and strong bond between mining Companies and State. From the other side, the instruments necessary for social concerns are: effective government systems, royalties and development funds. Objected on effective development on mining integrated sustainability, those instruments must be divided as responsibilities of all stakeholders influential on mining development which are State, Mining Companies, Mining Consulting Companies, Institutes and Certified Laboratories. Above principles, instruments and responsibilities are of the most importance for the development of mining integrated sustainability for developing Countries.

#### 5. WORLD BANK “THE CLIMATE SMART MINING INITIATIVE”

Beside Sustainable mining principles and having on mind climate changes, nowadays is of the crucial importance transition to low-carbon emission industry. A World Bank Group report, "Minerals for Climate Action: "The Mineral Intensity of the Clean Energy Transition," finds that the production of minerals, such as graphite, lithium and cobalt, could increase by nearly 500% by

2050, to meet the growing demand for clean energy technologies [5]. It estimates that over 3 billion tons of minerals and metals will be needed to deploy wind, solar and geothermal power, as well as energy storage, required for achieving a below 2°C future. While the growing demand for minerals and metals provides economic opportunities for resource-rich developing countries and private sector entities alike, significant challenges will likely emerge if the climate-driven clean energy transition is not managed responsibly and sustainably.

Considering this status World Bank launched “The Climate Smart Mining (CSM) Initiative” which will help resource-rich developing countries benefit from the increasing demand for minerals and metals, while ensuring the mining sector is managed in a way that minimizes the environmental and climate footprint. CSM supports the sustainable extraction, processing and recycling of minerals and metals needed to secure supply for low-carbon technologies and other critical sectors by creating shared value, delivering social, economic and environmental benefits throughout their value chain in developing and emerging economies. CSM is a public-private partnership led by the World Bank and IFC with the aim of achieving more sustainable mineral supply chains by providing technical and policy advice, direct investment financing, leveraging private sector financing, providing risk mitigation instruments, and helping countries define and craft tangible solutions for decarbonizing and improving ESG standards for climate action minerals.

## **ACKNOWLEDGEMENTS**

*The authors are grateful for funding by the Minister of Science, Technological Development and Innovation of the Republic Serbia, the Grant No. 451-03-47/2023-01/ 200052. Also, this work was financially supported by the EU under Interreg – IPA CBC Romania-Serbia Programme and co-financed by the partner states in the Programme. Project Romania Serbia NETWORK for assessing and disseminating the impact of copper mining activities on water quality in the cross-border area (RoS-NET2) eMS code RORS - 337. Also, this work was financially supported by the EU under Program 2nd EIT-HEI call: Building Ecosystem Integration Labs at HEI to foster Smart Specialization and Innovation on Sustainable Raw Materials - HEI4S3-RM.*

## **REFERENCES**

- [1] M. Weber-Fahr, Mining in Developing Countries – Treasure or Trouble. Mining Department World Bank and IFC Report, Washington, 2002.
- [2] D. Elis, Top 10 countries based on natural resources, Mining, Editor: Lanre-Peter Elufisan, January 31, 2022.
- [3] Mining Contribution Index (MCI) (6th Edition), International Council on Mining & Metals (ICMM), London, December 2022, p.6.
- [4] Bruntland Commission Report, Our Common Future, (United Nations General Assembly, New York, 1987, p. 43.
- [5] K. Hund, D. La Porta, T. P. Fabregas, T. Laing, J. Drexhage, Minerals for Climate Action: The Mineral Intensity of the Clean Energy Transition, The World Bank Group Publications, Washington DC, USA, 2020, p. 11,12.

## USING GRAVITY DATA TO DEFINE STRUCTURAL CORRELATION AFFECTING THE FORMATION OF NEOGENE BASINS

Snežana Ignjatović, Ivana Vasiljević, Branisav Sretković, Milanka Negovanović

Faculty of Mining and Geology, University of Belgrade, Đušina 7, 11000 Beograd, Serbia

### Abstract

*A gravity survey can help to define the structural correlation in the study area. The structures that have influenced the development of Neogene basins can be defined using gravity data. By applying mathematical transformations to gravity data, the geological structures (faults, nappes, etc.) that impacted the formation of Neogene basins can be defined. We have taken the part of the Dinarides as the test region. The paper presents the results obtained using the procedure residual, vertical gradient, and total horizontal gradient on gravity data. The obtained results are in correlation with the known geological data, which indicates that the application of mathematical transformations to gravity data can detect structural correlation that affected the formation of Neogene basins.*

**Keywords:** gravity survey, mathematical transformation, basin

### 1. INTRODUCTION

The geological structures (faults, nappes, etc.) that impacted the formation of Neogene basins today on the site are hard to observe due to the coverage. Gravity data can be used to define the geological structures that influenced the formation of the basin. By applying certain procedures of mathematical transformations to gravity data, structural correlation can be identified. The mathematical transformations that give satisfactory results are the procedure residual, vertical gradient, and total horizontal gradient, which is applied to the Bouguer anomaly data.

This paper presents the theoretical basis of the procedure residual, vertical and total horizontal gradient, and its practical application. As a practical example, we used data from gravity measurements in part of the Dinarides. Gravity survey data from the former Yugoslavia were used to create the Bouguer anomaly map [1].

The Golden Software Surfer geophysical software package was applied during the processing and analysis of gravity data.

### 2. THEORETICAL BACKGROUND

The procedure residual enables to extract the residual component from the total anomaly, by reducing the regional component of the field. A map of local anomalies is obtained in this way.

To detect the boundaries of near-surface sources of gravity anomalies, as well as to identify the position of contacts with a large dip angle (the fault, the front of thrust, etc.) we can use the procedure vertical gradient (first vertical gradient) and total horizontal gradient.

The first vertical gradient (VDR) can be expressed as [2]:

$$\text{VDR} = - \partial f / \partial z, \quad (1)$$

where  $f$  – gravity field (in paper Bouguer anomaly),  $\partial f / \partial z$  is the first-order derivative of the gravity field in the vertical direction  $z$ .

For vertical gradient is characteristic that he is positive over the source, has zero over the edges and is negative outside of a vertical side source [2, 3].

The total horizontal gradient (THDR) is defined as [2]:

$$\text{THDR} = \sqrt{\left(\frac{\partial f}{\partial x}\right)^2 + \left(\frac{\partial f}{\partial y}\right)^2} \quad (2)$$

where  $f$  – gravity field (in paper Bouguer anomaly),  $\frac{\partial f}{\partial x}$ ,  $\frac{\partial f}{\partial y}$  - are first-order derivative of the gravity field in x and y directions.

The maximum values of THDR are above the edge of the source of the anomaly, and the zero value is above the center of gravity of the body, which is the source of the anomaly. On the map of the total horizontal gradient, the contacts are detected as the elongated maximum [2,3].

### 3. FIELD EXAMPLE

As a test we took the part of the Dinarides. The boundaries of the survey area in UTM system [600000 m - 710000 m] and [4810000 m - 4900000 m]. The geological structures (faults, nappes, etc.) in Dinarides have a main direction NW-SE [4,5].

To create the Bouguer anomaly (gravity anomaly) map, which is the basis for further processing, gravity survey data from the former Yugoslavia were used [1]. The Bouguer anomaly map was done using a density value of 2.60 t/m<sup>3</sup>. To eliminate or reduce errors and disturbances in the measured signal, data filtering was performed. The filtered map of the Bouguer anomaly is shown in Figure 1. In the central part of the map (Fig. 1), the minimum values of anomalies are detected. These anomalies indicate the possible presence of a basin in this part of the terrain. On the map of the Bouguer anomaly (Fig.1) sudden changes in anomaly values indicate the possible existence of vertical or sub-vertical contacts between two environments of different densities, which can be interpreted as faults.

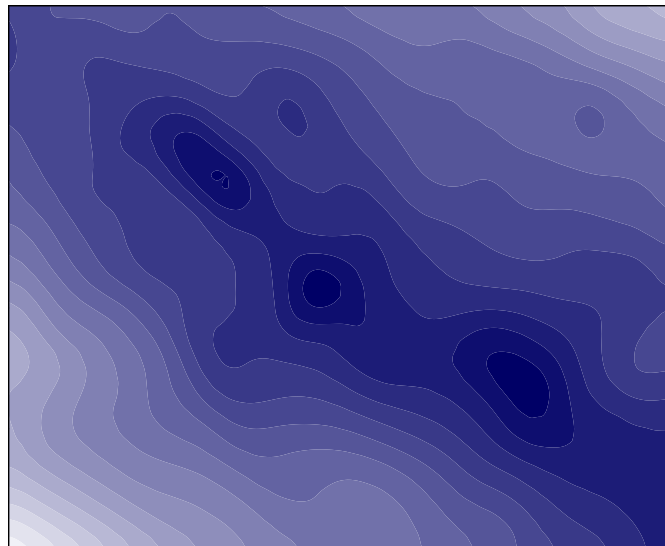


Figure 1 - Filtered map of Bouguer anomaly

To locate the geological structures that influenced the formation of Neogene basins, it was necessary to remove the regional influence of the primary anomaly sources (the Dinarides) and distinguishing local effects produced by smaller dimensions sources, such as the Neogene basins



in the Dinarides. By removing the regional influence of the Dinarides from gravity anomalies, the procedure residual was applied. The result of this procedure was a local gravity anomalies map (Figure 2). The shape and position of the minimum values in the central part of the map (Fig.2.) indicate the existence of three basins.

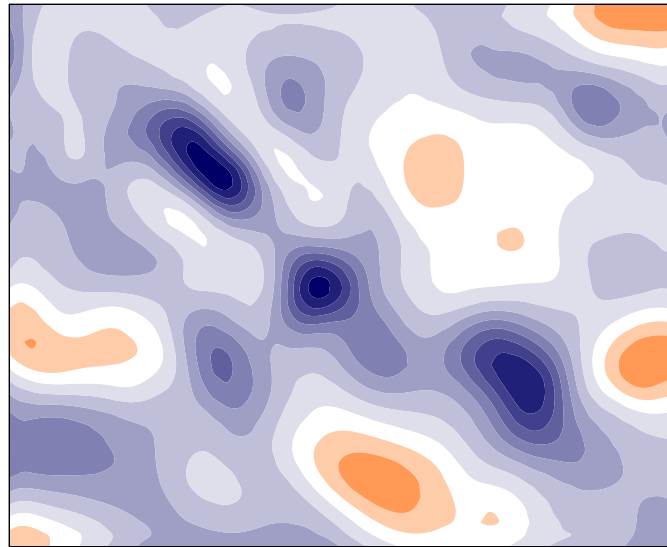


Figure 2 - Local gravity anomalies map

Next step in detect geological structures (faults, nappes, etc.) was applied mathematical transformations vertical and total horizontal gradient on local gravity anomalies map. The results obtained by the application of these two transformations correlate well with each other and can assist in locating the lateral (mainly vertical or subvertical) contacts between geological units of different density. The results of VDR are shown in Figure 3. In the central part of the map, structures that indicate the contacts that affected the formation of Neogene basins are marked with black dashed lines.

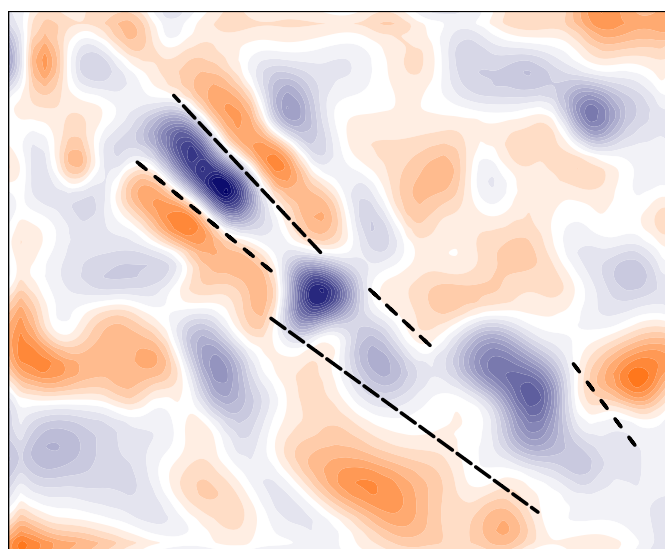


Figure 3 - The map of vertical gradient (black dashed lines - interpretation contacts)

The results of THDR are shown in Figure 4. The structures that indicate the contacts that affected the formation of Neogene basins are marked with red lines in the central part of the map.

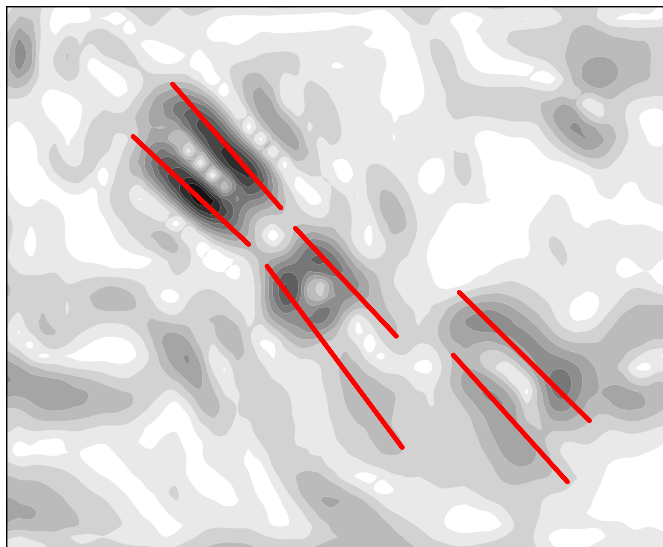


Figure 4 - The map of total horizontal gradient (red lines - interpretation contacts)

The analysis of Fig. 3 and Fig. 4 shows that contacts have general direction NW-SE. This direction corresponds to the main direction of structures (faults, nappes, etc.) in Dinarides [4,5].

#### 4. CONCLUSION

By applying certain procedures of mathematical transformations (such as residual, vertical gradient, and total horizontal gradient) to gravity data, structural correlation affecting the formation of Neogene basins can be identified. The obtained results are in correlation with the known geological data. The detected contacts have a typical Dinaric direction (NW-SE) corresponding to the faults and nappes.

#### REFERENCES

- [1] P. Bilibajkić, M. Mladenović, S. Mujagić, L. Rimac., Tumač za gravimetrijsku kartu SFR Jugoslavije – Bugeove anomalije 1:500 000, Savezni geološki zavod, Beograd, 1979.
- [2] GETECH., Advanced Processing and Interpretation of Gravity and Magnetic Data, Getech Kitson House Elmete Hall Leeds, UK, 2007.
- [3] G.H. Miller, V. Singh., Appl. Geophys. 32, 1994, p. 213-217.
- [4] M. D. Dimitrijević., Geology of Yugoslavia, 2nd edition, Geoinstitut, Belgrade, 1997.
- [5] S. Schmid, D. Bernoulli, B. Fügenschuh, L. Matenco, S. Schefer, R. Schuster, M. Tischler, K. Ustaszewski., Swiss J. Geosci. 101, 2008, p.139-183.

## CHARACTERIZATION OF WIRE ARC ADDITIVELY MANUFACTURED WEAR-RESISTANT BIMETALLIC COMPONENT

Deniz Eylül Akpınar<sup>1</sup>, Batuhan Turgut<sup>2</sup>, Uğur Gürol<sup>3,4</sup>, Savaş Dilibal<sup>5,6</sup>

<sup>1</sup>Department of Mechanical Engineering, Istanbul Gedik University, Türkiye

<sup>2</sup>Research and Development Center, Gedik Welding Company, Türkiye

<sup>3</sup>Department of Metallurgical and Materials Engineering, Türkiye

<sup>4</sup>Welding Technology Research and Application Center, Istanbul Gedik University, Türkiye

<sup>5</sup>Department of Mechatronics Engineering, Istanbul Gedik University, Türkiye

<sup>6</sup>Robot Technology Research & Application Center, Istanbul Gedik University, Türkiye

### Abstract

Wire Arc Additive Manufacturing (WAAM) with robotic systems enables the production of complex and large-scale metallic parts in various industrial fields such as automotive, maritime, defense, and aerospace. Functional bimetallic parts can also be manufactured using the WAAM process. The manufacturing process of wear-resistant components involves cladding hard-facing material onto the base metal as a conventional method. This process is often complicated, expensive, and time-consuming. This study proposes using the WAAM process to fabricate bimetallic parts with hard-facing solid welding wire for high wear resistance. In the WAAM process, a 6-axis OTC Daihen FD-B6L welding robot was used for manufacturing the bimetallic part. A synergic GeKa-Mac GMAW WB P500L welding machine with a water-cooled torch was used as the power source of the WAAM cell. The low spatter mode is used in the welding machine to prevent poor weld seams caused by unstable arc and spattering. The WAAMed bimetallic component was produced by depositing hard-facing welding wire on the top of the 316L austenitic stainless steel layers. The produced bimetallic component was first subjected to visual inspection and digital radiographic examination. Then macrostructure analysis, microstructure characterization, and hardness were performed on the samples extracted from the manufactured component. The interface region of the bimetal structure was also detailed examined. As a result, this study offered a more efficient and cost-effective new route for manufacturing wear-resistant bimetallic components. It also widened the design opportunities of monolithic components with site-specific properties.

**Keywords:** Wire Arc Additive Manufacturing, Gas Metal Arc Welding, Bimetallic Component, Interface Characterization

### 1. INTRODUCTION

Additive manufacturing has revolutionized traditional manufacturing techniques by enabling the layer-by-layer fabrication of three-dimensional components [1]. One of the prominent additive manufacturing (AM) methods is Wire Arc Additive Manufacturing (WAAM), which leverages wire as a feedstock and an arc heat source to fabricate intricate 3D shapes [2-3]. WAAM encompasses several well-established welding processes, including gas tungsten arc welding, gas metal arc welding, and plasma arc welding [4]. Utilizing an electric arc as an energy source, the WAAM process melts the welding wire (solid or metal-cored) to build up the desired component structure. A shielding gas environment is employed to ensure optimal conditions, preventing the molten metal layers from the atmospheric air. Additionally, the welding consumables in the market can be seamlessly integrated into WAAM technologies [5].

In the WAAMed structure, the macroscopic characteristics and microstructure of the deposited layers are significantly influenced by welding parameters such as the direction of the temperature gradient, welding current mode, cooling time, and interlayer temperature [6]. Critical parameters

in the WAAM method include heat input, speed, wire feeding rate, solidification rate, deposition current, inter-pass temperature, and torch movement speed [7]. Researchers have been actively exploring the application of WAAM in joining diverse metal structures required in various industries, such as aviation, automotive, and shipbuilding [8-9]. The ability to fabricate bimetallic parts using WAAM brings new possibilities for designing lightweight, high-strength, and corrosion-resistant structures [10-11]. This technology enables the integration of dissimilar metals, optimizing material properties and enhancing overall performance in critical applications [12]. Moreover, WAAM-based bimetallic component manufacturing offers cost-effective solutions by reducing material waste and minimizing assembly processes. This study proposes a new route for manufacturing wear-resistant bimetallic components using robotic WAAM technology. The manufactured WAAMed wall was examined via microstructure characterization.

## 2. EXPERIMENTAL PROCEDURE

An experimental study was carried out in a robot welding cell which includes a 6-axis OTC Daihen FD-B6L industrial welding robot, GeKaMac Power MIG GPS WB P500L synergistic welding machine, OPTRIS CT 3M pyrometer, and OPTRIS Xi 400 thermal camera. The low spatter mode is used in the welding machine to prevent poor weld seams caused by unstable arc and spattering. Two different welding wires having a diameter of 1.2 mm were used as feed material, namely GeKa ELOX SG 316 L Si (ER 316 LSi, according to AWS A5.9) and GeKaTec 600 G (MSG 6 GZ-60) (according to DIN 8555) to build bimetallic WAAMed component. The base plate was used in SS316 quality with the dimensions of 350 mm x 150 mm x 12 mm. The chemical composition of the welding wires and the substrate are given in detail in Table 1.

Table 1 - Typical chemical analysis values of welding wires and substrate (wt.%)

	C	Si	Mo	Cr	Ni
ELOX SG 316L Si	0.02	0.80	1.98	18.5	11.50
GeKaTec 600G	0.4	3	-	9	0.5
SS 316L (substrate)	0.022	0.003	-	16.70	-

To produce a thick section WAAMed wall, a total of 60 layers were deposited, consisting of 3 passes overlapped by 1/3 of each other. In the experimental context, 30 layers were deposited on the SS316 substrate using ER 316 LSi welding wire. Then, another 30 layers were deposited on the ER 316 LSi side using hard-facing welding wire. Optris CT 3M pyrometer was used to observe the temperature changes of the substrate during the deposition process. The thermal images were taken every 5 passes during deposition and for 5 seconds before starting the deposition process using the Optris Xi 400 thermal camera. The welding parameters used for both welding wires within the scope of the experiment are listed in Table 2.

Table 2 - Process parameters used during the manufacturing of bimetallic components.

	Unit	ELOX SG 316L Si	Hardcor 600 G
Current	A	130-160	150-180
Voltage	V	17-19	18-21
Torch angle	°	90	90
Welding speed	mm/min	35-45	35-45
Shielding gas flow rate	l/min	15	15

Two different shielding gases classified as M21 and M12 gases were used for ELOX SG 316L Si and Hardcor 600 G, respectively. In the WAAM process, heat accumulation occurs during layer-by-layer deposition. This heat build-up changes the pattern of heat transfer across the part. This effect causes the emergence of different mechanical and microstructure properties of the material from place to place [11]. To minimize the heat accumulation that may occur within the scope of the experiment, a dwell time of 180 seconds between layers was programmed, and the WAAM part was allowed to cool. As a result, the bimetallic component was first subjected to visual

inspection and digital radiographic examination to reveal any indication that occurred during the deposition process. The mechanical properties of various locations were evaluated with Vickers hardness and flat tensile test results.

### 3. EXPERIMENTAL RESULTS

The front view and macro section of the thick WAAM wall produced in this study are illustrated in Figure 1a-b. The wall comprises stainless steel (at the bottom) and hard-facing wire (Hardcor 600G) sides, which can be distinguished. To determine the dimensions of the wall, measurements were taken at five different locations and subsequently averaged, resulting in dimensions of 330 mm x 150 mm x 18 mm.

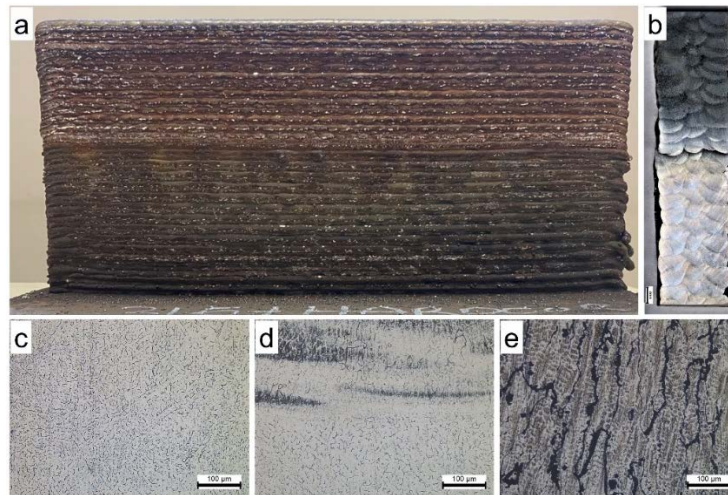


Figure 3.1 - The as-built WAAMed bimetal wall

Visual inspection and X-Ray test results confirmed that a stable burning arc consistently melted both wires during the deposition process. Consequently, no surface or internal defects, such as porosity, solidification cracks, or lack of fusion, exceeded the tolerances specified in ISO 5817-B. In the microstructure investigations, it is observed that various types of delta ferrites are formed within the austenite matrix in the region of the 316L austenitic stainless wire, as shown in Figure 1c. The interface was free of microcracks or defects, confirming the excellent bonding. In the hard-facing region, the presence of metal carbides predominantly precipitated along the grain boundaries in the martensite matrix was evident.

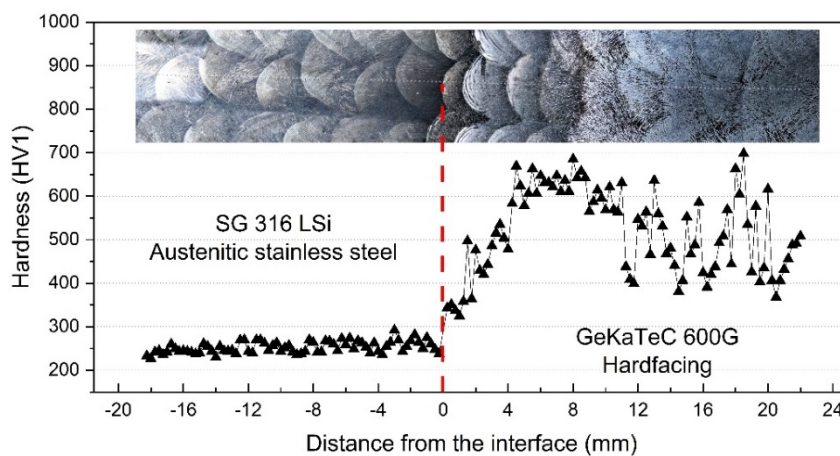


Figure 3.2 - Hardness distribution along the deposition direction

As depicted in Figure 3.2, the hardness remains consistent from the stainless zone to the interface; however, a gradual increase was observed at the interface and beyond and reached over 700 HV.

This increase can be attributed to the higher carbon content, leading to martensite and chrome carbides forming on the hard-facing wire side. According to the DIN 8555 standard, MSG 6 alloys reveal hardness values above 500 HB due to their high carbon content, which agrees with the experimental results. Moreover, the variations in hardness on the hard-facing side can be explained by the temperature fluctuations during the process, resulting in diverse microstructures.

Table 3 - The mechanical properties of the WAAMed bimetallic wall

	Yield strength, MPa	Tensile strength, MPa	Elongation, %
<b>Hard-facing side</b>	815	1337	1.52
<b>Interface</b>	326	463	3.52
<b>Stainless steel side</b>	337	579	33.75

On the other hand, the highest yield and tensile strength, 815 MPa and 1335 %, respectively, and the lowest elongation values were obtained at the hard-facing side, which had metal carbides in the martensitic matrix as expected. In contrast, the stainless zone demonstrated the highest percentage of elongation, about %33.75. Notably, the lowest yield and tensile strength were found at interface regions, 326 MPa, and 463 MPa, respectively.

#### 4. CONCLUSIONS

In this study, a bimetal wall was built using ELOX SG 316L Si and Hardcor 600 G welding wires. In conclusion, the visual and X-Ray test results demonstrated that a successful wear-resistant bimetallic component has been built using WAAM technology. On the other hand, the lowest hardness value was found to be 204 HV on the 316L side, while the highest hardness value was measured as 711 HV on the 600G side in the as-built WAAM part. These results indicated that the WAAM technology was an efficient alternative to the conventional cladding part as a wear-resistant bimetallic component.

#### FUNDING

This study has been supported by the Scientific and Technological Research Council of Turkiye (TUBITAK) under the University-Industry Cooperation Support Program scope with project number 5220023.

#### REFERENCES

- [1] ASTM International. F2792-12a-Standard Terminology for Additive Manufacturing Technologies. Rapid Manuf Assoc 2013:10–2.
- [2] T. Artaza, T. Bhujangrao, A. Suarez, F. Veiga, A. Lamikiz, *Metals* 10 (6) (2020) 771.
- [3] T. Bhujangrao, F. Veiga, A. Suarez, E. Iriando, F.G. Mata, *Crystals* 10 (8) (2020) 689.
- [4] T. DebRoy, H.L. Wei, J.S. Zuback, T. Mukherjee, J.W. Elmer, J.O. Milewski, A. M. Beese, A. Wilson-Heid, A. De, W. Zhang, *Prog. Mater. Sci.* 92 (2018) 112–224.
- [5] J. Mehnen, J. Ding, Lockett, H., Kazanas, P. *Int J. Product Development* 19 (2) (2014) 2-20.
- [6] A. Kumar, K. Maji, *J. Mater. Eng. Perform.* 30 (7) (2021) 5413–5425.
- [7] B. Wu, Z. Qiu, Z. Pan, K. Carpenter, T. Wang, D. Ding, S.V. Duin, H. Li, *J. Mater. Sci. Technol.* 52 (2020) 226–234.
- [8] A. Vahedi Nemani, M. Ghaffari, A. Nasiri, *Addit. Manuf.* 32 (2020) 101086.
- [9] U. Gurol, M. Tumer, S. Dilibal *Trans Indian Inst Met.* 76 (5) (2023) 1371-1379.
- [10] U. Gurol, S. Dilibal, B. Turgut, M. Koçak 64(6) (2022) *Mater. Testing* 755–767.
- [11] U. Gurol, S. Dilibal, B. Turgut, et al. *Int. J. 3D Printing Technologies and Digital Industry* 6 (2022) 548–555.
- [12] M.R.U. Ahsan, A.N.M. Tanvir, T. Ross, A. Elsayy, M.-S. Oh, D.B. Kim, *Rapid Prototype. J.* 26 (3) (2019) 519–530.



## SANDBLASTING PROCESS INFLUENCE ON STAINLESS STEEL CUTTING MATERIAL

**Mistreanu Sebastian, Ramona Cimpoeșu, Dragoș Achiței, Mihai Popa, Daniela Lucia Chicet, Vasile Manole, Ana-Maria Scripcariu, Nicanor Cimpoesu**

Technical University Gheorghe Asachi from Iasi , Materials Science Department , Blv.  
Mangeron no. 44, Romania

### **Abstract**

*Paper deals with stainless steel behavior analysis at sandblast operation. Sandblasting is a method utilized to enhance the surface quality of materials by bombarding them with abrasive particles at high speeds. The outcome is a hardened surface layer that delivers long-lasting durability while maintaining the corrosion-resistant properties of stainless steel. This hardening process is desired in many applications like cutting tools, pump shafts, and valves, where wear resistance is a crucial factor for the material's longevity. Using sandblasting hardening, stainless steel increases its wear resistance without altering the chemical composition of the base material, thereby maintaining its fundamental mechanical, chemical, and esthetic properties. In this paper a wood working stainless steel cutting tool was investigated by usage defects point of view, surface modification through sandblasting for different time periods: 5,10, 15 ... 60 seconds and corrosion resistance through immersion in a cooling liquid used during the wood peeling. Surface profile was investigated through 3D profile images made with SEM and by determining the surface profile using a portable profilometer. Hardness of the stainless steel was investigated before and after the sandblast operation.*

**Keywords:** sandblasting, stainless steel, hardness.

### **1. INTRODUCTION**

Sandblasting is a mechanical surface preparation technique widely employed in diverse industries to enhance material properties and prepare surfaces for various applications. This paper focuses on investigating the profound influence of sandblasting on stainless steel cutting material. The study aims to comprehensively analyze how sandblasting affects the material's properties and performance, evaluating the multitude of advantages and limitations this technique presents in various industrial applications. When an abrasive material is blasted onto the metal surface, it causes a plastic deformation that compresses the top layer of the surface, resulting in the increase of hardness and wear resistance [1].

Stainless steels are iron alloys enriched with a significant chromium content (minimum 10.5%), forming a protective chromium oxide passive layer on the material's surface, rendering it highly resistant to corrosion. These exceptional materials are renowned for their corrosion resistance, durability, and ability to withstand high temperatures. As a result, stainless steels find application across a wide spectrum of industrial sectors, including the oil and gas industry, chemical processing, food processing, construction, and many more[2-4].

The sandblasting process entails propelling fine particles, such as sand, glass beads, or metal grit, onto the material's surface through a forceful jet of air or pressurized water. This technique serves a myriad of purposes and offers an array of advantages [5-7]:

a) Surface Preparation: Sandblasting excels at removing deposits, rust, impurities, and contaminants from the material's surface, ensuring an immaculate base for subsequent processes.



- b) **Enhanced Adhesion:** By creating a roughened surface, sandblasting significantly improves the adhesion between the stainless steel cutting material and other materials it interfaces with during application.
- c) **Aesthetic Appeal:** Employed in architectural and industrial designs, sandblasting imparts stainless steel with a refined matte or satin finish, enhancing its visual allure.
- d) **Surface Remodeling:** In specialized cases, sandblasting facilitates reshaping and molding the stainless steel cutting material to meet precise project requirements.

The sandblasting process elicits various effects on stainless steel cutting material, yielding substantial implications for its properties and performance. Notable effects include [8]:

- a) **Altered Surface Profile:** Sandblasting modifies the topography of the stainless steel cutting material, transitioning it from a smooth surface to a textured one. This transformation may impact the material's mechanical strength and adhesion characteristics.
- b) **Residual Stresses:** Residual stresses may arise in the stainless steel cutting material as a result of sandblasting, influencing its structural integrity and stability. Proper management and elimination of such stresses are crucial for optimal material performance, especially in critical applications.
- c) **Passive Layer Thickness:** The sandblasting process can impact the thickness of the naturally formed chromium oxide passive layer on the stainless steel surface, consequently affecting its corrosion resistance.
- d) **Surface Deformations and Defects:** Sandblasting may lead to surface deformities and defects in the stainless steel cutting material, potentially influencing both its functional performance and aesthetic appeal.

The versatility of sandblasting renders it applicable in a broad spectrum of industries, including metallurgy, construction, food processing, chemical processing, and more. Nevertheless, certain limitations accompany this technique [9]:

- a) **Impact on Mechanical Properties:** The sandblasting process may cause a reduction in the mechanical strength of the stainless steel cutting material, particularly in regions with increased surface roughness.
- b) **Contamination Concerns:** Sandblasting can introduce foreign particles or contaminants to the material's surface, posing potential challenges to its overall quality and performance.
- c) **Cost-Effectiveness:** Due to its sophisticated nature, sandblasting can prove costly and necessitates adequate preparation and equipment to ensure process efficiency and precision.

A comprehensive understanding of its impact on material properties is essential to optimize the utilization of stainless steels across diverse industrial applications. Combining sandblasting with other structural and chemical modification techniques will pave the way for superior, durable, and economically viable outcomes in the future. Further research and development in this domain will undoubtedly enhance our understanding of the potential applications and limitations of sandblasting, contributing to the advancement of materials engineering and industrial practices [10].

## **2. EXPERIMENTAL**

In this paper, we propose a process of hardening through shot blasting for stainless steel. Shot blasting is a method utilized to enhance the surface quality of materials by bombarding them with abrasive particles at high speeds. When an abrasive material is blasted onto the metal

surface, it causes a plastic deformation that compresses the top layer of the surface, resulting in the increase of hardness and wear resistance.

The outcome is a hardened surface layer that delivers long-lasting durability while maintaining the corrosion-resistant properties of stainless steel. This hardening process is desired in many applications like cutting tools, pump shafts, and valves, where wear resistance is a crucial factor for the material's longevity. Using shot blasting hardening, stainless steel increases its wear resistance without altering the chemical composition of the base material, thereby maintaining its fundamental mechanical, chemical, and esthetic properties.

An electro-erosion cutting machine used to cut the pieces of woodworking blades into 10 mm pieces. The next step was grinding and polishing the samples, after this, the samples were sandblasted (fig 1). After completion of the blasting process, the ultrasonic cleaning of the samples was continued.

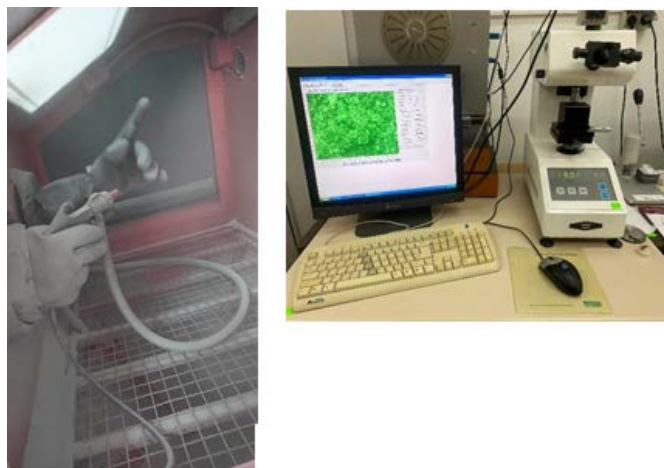


Figure 1 - Sandblasting equipment used in the project and micro-hardness equipment

In table 1 the mean values from three determinations for each sample are given and an increase is observed with the sandblasting time period. After a certain sandblasting period the hardness decrease (for example after 25 seconds) and increase again with the exposure time. The microhardness characteristics are strictly connected to the surface roughness.

Table 1 - Average values of micro-hardness

Time of sandblasting [s]	Vickers hardness results (average value from 3 determinations)
Initial (0 s)	758.89
10	1006.76
15	1007.6
20	852.49
25	783.7

30	738.9
35	792.9
40	791.9
45	803.2
50	860.2
55	849.8
60	926.9

The result was variable hardening depending on the blasting time of the samples, from 0 to 60s. From the table 1 see that the highest hardness is for the 15 s sample, and the result is from the average of 3 tests.

Table 2 - The roughness result of 3- test average

Time /Roughness parameters	R <sub>a</sub> (μm)	R <sub>z</sub> (μm)	R <sub>max</sub> (μm)
Initial sample (0 sec)	0.54	3.83	4.67
10 sec	0.97	6.41	8.17
15 sec	0.98	7.52	9.97
20 sec	1.00	6.44	9.95
25 sec	0.92	7.52	9.21
30 sec	0.74	6	7.32
35 sec	0.91	6.62	8.94
40 sec	1.22	9.38	9.88
45 sec	1.15	8.43	9.41
50 sec	1.28	8.6	10.92
55 sec	1.20	8.81	10.91
60 sec	1.16	8.03	11.47

And before the test, the samples are cleaned again at the ultrasonic machine. The roughness test was carried out using an M1 profilometer and the result is shown in the table 2 (3-test average)

### 3. CONCLUSIONS

In the conclusions about the hardening of stainless steel for knife blades used in the wood industry through sandblasting:

1 Sandblasting hardening is an effective method of improving the mechanical properties of the knife blade.

2 The use of special stainless steel powder in the sandblasting process can improve the adhesion of abrasive particles to the workpiece surface, thereby reducing material loss and increasing process efficiency.

3 Sandblasting hardening can increase the hardness of the knife blade and improve resistance to wear and abrasion.

4 The sandblasting hardening process can help improve the performance of the knife blade in the wood industry by increasing durability and the blade's lifespan. It is important to use the special stainless steel powder in the sandblasting process to ensure that the blade surface remains smooth and free of cracks or imperfections that could affect the blade's performance over time.

**ACKNOWLEDGEMENTS** *A part of this research was funded by TUIASI, grant number 3281/01.02.2023.*

## **REFERENCES**

- [1] M. Iqbal, D. Prasetya, The effect of sandblasting on AISI 316L stainless steels, Industrial Research Workshop and National Seminar, 2011.
- [2] O. Rusu, I. Rusu, IOP Conf. Series: Materials Science and Engineering 916 (2020) 012096
- [3] G.W. Critchlow, D.M. Brewis., Int J Adhes Adhes 16 (1996) 255-275.
- [4] L.F.M. da Silva et al. Int J Adhes Adhes 29 (6), (2009) 621-632
- [5] S.G. Prolongo et al Int J Adhes Adhes 29(1): (2009) 23-31.
- [6] N. Brack et al. Int J Adhes Adhes 48: (2014) 20–27
- [7] J. Aakkula et al. Int J Adhes Adhes 127 (2014) 149-157.
- [8] R. G. Chelariu, M. Benchea, R. Cimpoesu, O. Rusu, V. Manole, D. P. BurduhoS-Negris, N. Cimpoesu, C. Bejinariu, Materials Today Proceedings, 1 – 6, (2022)
- [9] L. Dobreci, O. Rusu, D. Vasincu, M. Jarcău, C. M. Rusu, S. Gurlui, V. Ghizdovat, A. Gavrilit and M. Agop, Entropy, 24, (2022) 484.
- [10] L.F.M. da Silva et al. Int J Adhes Adhes 30(8) (2010) 735-743.

## REMOVAL OF Cu(II) FROM AQUEOUS SOLUTIONS USING ADSORBENT BASED ON CHITOSAN HYDROGEL BEADS

Dorđe Petrović<sup>1</sup>, Katarina Stanković<sup>1</sup>, Latinka Slavković Beškoski<sup>2</sup>, Ksenija Kumrić<sup>1</sup>

<sup>1</sup>University of Belgrade, "Vinča" Institute of Nuclear Sciences – National Institute of the Republic of Serbia, Mike Petrovića Alasa 12-14, 11001 Belgrade, Serbia

<sup>2</sup>Anahem Laboratory, Mocartova 10, 11160 Belgrade, Serbia

### Abstract

Mine waters and tailings resulting from mining and mineral processing often have a harmful effect on the local environment. Copper has a strong biocidal activity that greatly affects ecosystems. Therefore, the removal of copper from wastewater is of great importance to the environment. Chitosan, a natural biopolymer, obtained from chitin, the most abundant natural fiber, often has better properties than much more expensive synthetic polymers. This paper investigates the application of chitosan-based sorbents for removing copper from aqueous solutions. A novel adsorbent, chitosan hydrogel beads (CHBs), was synthesized from chitosan flakes (medium molecular weight), via ionic/covalent cross-linking. Batch experiments were carried out to optimize the process conditions for efficient removal of Cu(II) and to determine the adsorption capacity of prepared CHBs. The results showed that the maximum Cu(II) adsorption capacity estimated with Langmuir isotherm modeling was 103.6 mg/g which was three times higher than chitosan flakes (33.7 mg/g).

**Keywords:** Copper, chitosan, adsorption.

### 1. INTRODUCTION

Wastewaters containing heavy metals as pollutants originate from a large number of metal-related industries and mines [1]. Unfortunately, heavy metals are not biodegradable and tend to accumulate in living organisms, causing several diseases and disorders. Copper is one of the most common heavy metals observed in the aquatic environment [2]. Excess of Cu(II) in human blood system can create reactive oxygen species and damage important compounds such as: proteins, lipids and DNA and can cause various diseases such as Wilson and Alzheimer's disease [3]. Technologies used for metal ion removal from the wastewaters include chemical precipitation, reverse osmosis, membrane separation, flocculation, electrolysis, ion exchange mechanism and adsorption [4].

Various types of adsorbents have been investigated aimed at the adsorption of heavy metal ions. Favorable features of chitosan, such as resource abundance, non-toxicity, biodegradability and existence of sufficiently active sites (-NH<sub>2</sub> and -OH) for adsorption of various pollutants, make chitosan-based hydrogels the promising adsorbents for the removal of heavy metal ions from aqueous solutions [5].

In the present work, a method for synthesis of citric acid (CA)/ glutaraldehyde (Glu) co-cross-linked chitosan hydrogel beads (CHBs) was developed. The obtained CHBs were used as adsorbents in further batch adsorption experiments designed to investigate their potential application for the removal of Cu(II) ions from aqueous solutions. The effects of the initial solution pH and initial concentration of Cu(II) were evaluated with respect to the removal efficiency of Cu(II) from aqueous solution. For analyzing the equilibrium adsorption data Langmuir and Freundlich isotherms were employed.

## 2. EXPERIMENTAL

Chitosan flakes (CF) of medium molecular weight, glacial acetic acid (AA), Glu solution, CA and copper(II) nitrate hepta hydrate were purchased from Sigma-Aldrich (USA). All the chemicals were analytical reagent grade and used without further purification.

Preparation of CHBs was carried out by dissolving 1 g of chitosan flakes in 40 cm<sup>3</sup> of (1) 2 wt% of AA, (2) 1 wt% AA and 1 wt% CA and (3) 2 wt% of CA. 5% (v/v) Glu solution was added into the obtained suspension and the mixtures were magnetically stirred for 2 h at room temperature. In order to get the uniform CHBs, obtained solutions, separately, were dropped into 1 mol dm<sup>-3</sup> NaOH. After 24 hours of aging in the NaOH solution, CHBs were neutralized by rinsing with deionized water.

The experiments were conducted in a batch mode by mixing approximately 0.5 g wet CHBs and 10 cm<sup>3</sup> of the Cu(II) solution of different concentrations. The effect of pH was studied by adjusting pH with either 0.1 M NaOH or 0.1 M HNO<sub>3</sub> from 3 to 7.

The mixtures were shaken at a speed of 150 rpm for 24 h. Aliquots above the adsorbent were taken and concentrations of Cu(II) ions were determined by polarography system 797 VA Computrace analyser (Metrohm, Herisau, Switzerland) applying differential pulse anodic stripping voltammetry (DPASV) at a hanging mercury drop electrode. All experiments were performed at room temperature.

The effect of the initial Cu(II) concentration was investigated in the range from 10 to 250 mg dm<sup>-3</sup>. The obtained results were discussed in terms of removal efficiency,  $E$  (%), and adsorption capacity,  $q_e$  (mg g<sup>-1</sup>), at equilibrium defined by the equations:

$$E = \left( \frac{C_i - C_e}{C_i} \right) 100$$
$$q_e = \left( \frac{C_i - C_t}{m} \right) V$$

where  $C_i$  and  $C_e$  (mg dm<sup>-3</sup>) are the initial and equilibrium concentrations of Cu(II) ions in the solution, respectively,  $V$  (dm<sup>3</sup>) is the volume of the solution, and  $m$  (g) is the mass of the dried adsorbent.

## 3. RESULTS AND DISCUSSION

Approximately spherically shaped CA/Glu co-cross-linked CHBs had diameters of about 3.0 mm. The three tested CHBs samples (non-cross-linked (CHB), cross-linked with 1% CA (CHB-1% CA) and 2% CA (CHB-2% CA)) contained water in the range of 97.0-97.5%. The surface charge of the adsorbent largely depends on the initial pH of solution influencing the removal efficiency of the adsorbent. pH of initial solutions was studied from 3 to 7 in order to find the value at which adsorption is the highest. In our experiments, the highest removal efficiency (98-99%) of Cu(II) for the three tested adsorbents was achieved in the pH range of 4-6. According to the literature data [6], at low pH (acidic solution), amine groups in the beads became protonated which induced an electrostatic repulsion of Cu(II) ions. On the other hand, solutions with pH values higher than 6 should be avoided due to the possibility of Cu(II) hydroxide formation which will affect the adsorption by the beads. The increase in the adsorption capacity at pH > 4 of CA/Glu co-cross-linked CHBs compared to non-cross-linked CHBs can be explained by the presence of additional carboxylic groups on the surface of the adsorbent. It can be assumed that improved removal of Cu(II) ions by CA/Glu co-cross-linked CHBs comes from deprotonated carboxylic groups which attracts positively charged Cu(II) ions and, hence, improve their adsorption capacity.

There are several isotherm models to investigate the equilibrium of the system and to define the capacity of the adsorbent. Usually, Langmuir or Freundlich model describe accurately the system in the case of two parameters. The Langmuir model assumes monolayer adsorption onto homogenous surface where the binding sites have equal affinity and energy, and there is no transmigration or interaction between the molecules. The Langmuir equation is given by:

$$q_e = \frac{q_m K_L C_e}{1 + K_L C_e}$$

where  $q_e$  is the amount of adsorbed mg per g of adsorbent at equilibrium (mg/g),  $q_m$  is the maximum capacity of the system (mg/g),  $C_e$  is the adsorbate concentration in solution at equilibrium (mg/dm<sup>3</sup>),  $K_L$  is the constant of the Langmuir Isotherm model (dm<sup>3</sup>/mg).

The Freundlich adsorption isotherm, however, is an empirical model and can be used in the case of a heterogeneous surface energy system.

$$q_e = K_F \cdot C_e^{1/n_F}$$

where  $C_e$  is the equilibrium concentration of metal ion (mg/L),  $q_e$  is the amount of metal ion adsorbed on adsorbent mass unit (mg/g),  $K_F$  is the maximum adsorption capacity of metal ions (mg/g) and  $n_F$  is a constant present in non-linear Freundlich isotherm which indicated the adsorption intensity [7].

The Langmuir and Freundlich plots are presented in Figure 1, while the obtained fitting parameters are reported in Table 1.

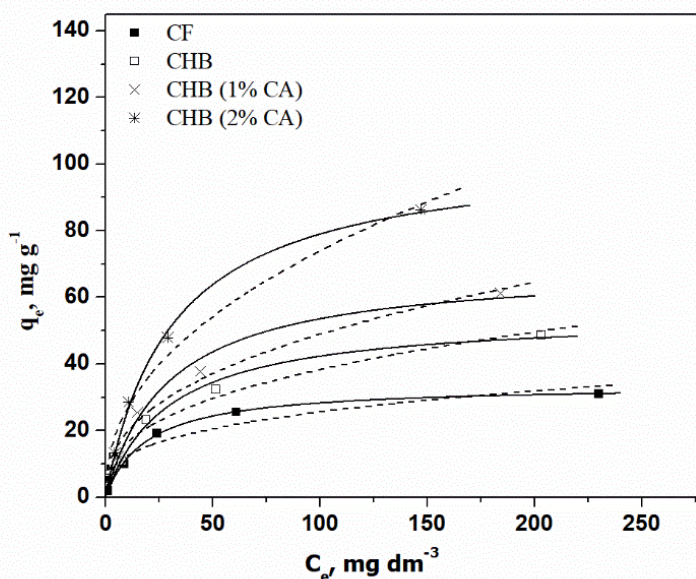


Figure 1 - Fitting of experimentally obtained data for adsorption equilibrium of Cu(II) onto: CF, CHB, CHB (1% CA) and CHB (2% CA). Solid and dash lines represent Langmuir and Freundlich curve, respectively

The equilibrium adsorption data on the effect of the initial concentration of Cu(II) were fitted using the non-linear Langmuir and Freundlich isotherm models in order to determine the surface properties and the affinity of the adsorbent. The corresponding isotherm parameters and the determination coefficients of these two models are reported in Table 1. Based on the values of the  $R^2$ , it is evident that adsorption of Cu(II) by CA/Glu co-cross-linked CHBs can be better described by the Langmuir isotherm. CA/Glu co-cross-linked CHBs with the higher content of CA showed



better  $q_m$  value compared to other samples, probably due to incorporation of additional carboxylic groups that have positive impact on the features of CHBs.

Table 1 - Langmuir and Freundlich parameters for the adsorption of Cu(II) ions onto CA/Glu co-cross-linked CHBs

Adsorbent	Langmuir isotherm			Freundlich isotherm		
	$q_m$ , mg g <sup>-1</sup>	* $K_L$	$R^2$	$n_F$	** $K_F$	$R^2$
CF	33.7	0.052	0.999	3.15	5.93	0.911
CHB	54.7	0.034	0.993	2.68	6.90	0.988
CHB - 1% CA	69.2	0.034	0.994	2.51	7.78	0.992
CHB - 2% CA	103.6	0.032	0.996	2.23	9.40	0.983

\* $K_L$ , dm<sup>3</sup>/mg; \*\* $K_F$ , (mg/g)(dm<sup>3</sup>/mg)<sup>1/n</sup>

#### 4. CONCLUSION

The adsorption of Cu(II) ions from aqueous solutions onto CA/Glu co-cross-linked CHBs was investigated in the present study. The obtained results showed that the maximum removal efficiency of Cu(II) was achieved in the pH range 4-6. Equilibrium isotherm data were fitted using Langmuir and Freundlich models. The Langmuir model provided the best fit of the experimental data. The maximum adsorption capacity for Cu(II) ions was exhibited by CHB - 2% CA (103.6 mg/g).

It can be concluded that investigated chitosan-based hydrogels could potentially contribute to the environmental friendly method for the treatment of Cu(II) contaminated waters.

#### ACKNOWLEDGEMENTS

*This research was funded by the Ministry of Science and Technological Development of the Republic of Serbia (contract number: 451-03-47/2023-01/ 200017).*

#### REFERENCES

- [1] T. Vengris, R. Binkien, A. Sveikauskait., *Appl. Clay Sci.*, 3-4 (2001) 183-190.
- [2] H. Gupta, P. R. Gogate., *Ultrason. Sonochem.*, 30 (2016) 113-122.
- [3] G.J. Brewer, *Clin. Neurophysiol.*, 121 (4) (2010) 459-460.
- [4] M. Ahmad, B. Zhang, J. Wang, J. Xu , K. Manzoor, S. Ahmad, S. Ikram, *Int. J. Biol. Macromol.*, 136 (2019) 189–198.
- [5] L. Chiappisi, S. Prévost, I. Grillo, M., *Langmuir*, 30 (2014) 10608–10616.
- [6] W.S. Wan Ngah, C.S. Endud, R. Mayanar, *React. Funct. Polym.*, 50 (2002) 181–190.
- [7] S. A. Akolo, A. S. Kovo, *J. Encap. Adsorpt. Sci.*, 5 (2015) 21-37.

## MODIFIED BASIC PROPERTIES OF ELECTRONS IN LAYERED NANOCRYSTAL FILMS WITH A COMPLEX LATTICE

Jovan P. Šetrajčić<sup>1</sup>, Siniša M. Vučenović<sup>2</sup>

<sup>1</sup>Academy of Sciences and Arts of the Republic of Srpska, Banja Luka, B&H

<sup>2</sup>University of Banja Luka, Faculty of Sciences and Mathematics, Republic of Srpska, B&H

### Abstract

*Using the method of two-time temperature Green's functions, in this paper we determined the electron spectra in perturbed crystal ultrathin film-structures with a complex lattice (NaCl type). The presence of boundaries as well as the energy change of the boundary parameters at the boundaries of these structures leads to new properties and a specific effect in relation to the bulk, significant for clarification, e.g. mechanisms of high-temperature superconductivity. One of the basic results is the appearance of energy gaps and localized electronic.*

**Keywords:** *electrons, ultrathin films, discretization of spectra, energy gaps, state localization*

### 1. INTRODUCTION

Research into low-dimensional layered systems (nanostructures: ultrathin films, superlattices, nanotubes, ...) and quantum confinement effects has become intense, especially in this century, due to their increasingly wide application in optoelectronics, nanomedicine, energy, ecology, ... [1]. Thin films are used as coatings (to protect against corrosion) which are already widely used in the automotive and aviation, especially in the military industry [2]. The development and improvement of technological procedures (evaporation, spraying, doping, etc.) enables the production of completely new materials, i.e. materials with changed properties. On the other hand, this innovative technology requires the synthesis of materials with predefined properties. This is exactly the interest in modern research in the physics of condensed matter, and it is based on finding the possibility that by adequately changing the characteristic parameters of the lattice, especially at the boundaries of the nanostructure, the physical properties of the sample can be manipulated [3]. The nature and mechanism of drastic and diverse changes in the fundamental physical properties of nanostructured materials in relation to bulk samples has not been deciphered, and therefore considerable attention is paid to theoretical modeling that should explain the relationship between the required characteristics of materials, their nanostructure and manufacturing technology.

Phenomena related to the basic properties of charge carriers (in general: electrons) in low-dimensional structures lead to the creation of completely new or changed physical characteristics of materials. This is very interesting because electrons with phonons are carriers of all transport processes in materials [4]. By microtheoretical analysis - the method of two-time temperature Green's functions (GFs) [5], here we will determine the electron dispersion law in the model of an ultrathin crystal film with a complex crystal structure (with two sublattices). We will analyze the influence of the change in the boundary parameters of the film on the electronic spectra and states numerically.

### 2. MODEL OF ELECTRONS IN ULTRATHIN FILM NANOSTRUCTURES

Unlike ideal unbounded (bulk) structures, real crystals do not have the property of translational invariance. The existence of boundaries is certainly the cause of breaking this symmetry, but it has significant repercussions only in the case of nanostructures [1]. Here, we form a model of a crystalline nanofilm with a complex lattice. In the XY planes, the film is unbounded, while in the

$z$ -direction it has a finite thickness ( $L$ ). This means that this film has two infinite boundary - surface planes parallel to the  $XY$  planes for  $z = 0$  and  $z = L$  (Fig. 1, where the two different types of atoms  $a$  and  $b$  are shown by white and black circles).

The boundary surfaces of the film are normal to the  $z$ -direction, so the layer index  $n_z$  takes the values:  $n_z = 0, 1, 2, \dots, N_f$ , where  $N_f \in [4, 12]$  for ultrathin films. The indices  $n_x$  and  $n_y$ , which determine the position of atoms in each crystallographic plane, have arbitrary integer values. Due to the influence of the boundaries, i.e. the environments with which the film borders, we assume that the basic electronic parameters  $\Delta$  and  $W$  are perturbed along the  $z$ -direction of the film in the boundary - surface planes (for  $n_z = 0$  and  $N_f$ ) and boundary layers (between  $n_z = 0$  and 1 and between  $n_z = N_f - 1$  and  $N_f$ ). It follows:

$$\Delta_z^{a/b} = \Delta^{a/b} \left( 1 + \gamma_0^{a/b} \delta_{0,n_z}^{a/b} + \gamma_{N_z}^{b/a} \delta_{N_z,n_z}^{b/a} \right);$$

$$W_{n_z,n_z-1} \equiv W_x^{a/b} = W_z \left( 1 + w_0^{a/b} \delta_{1,n_z}^{b/a} + w_{N_z}^{b/a} \delta_{N_z,n_z}^{b/a} \right); \quad (1)$$

$$W_{n_z,n_z+1} \equiv W_z^{a/b} = W_z \left( 1 + w_0^{a/b} \delta_{0,n_z}^{a/b} + w_{N_z}^{b/a} \delta_{N_z-1,n_z}^{b/a} \right).$$

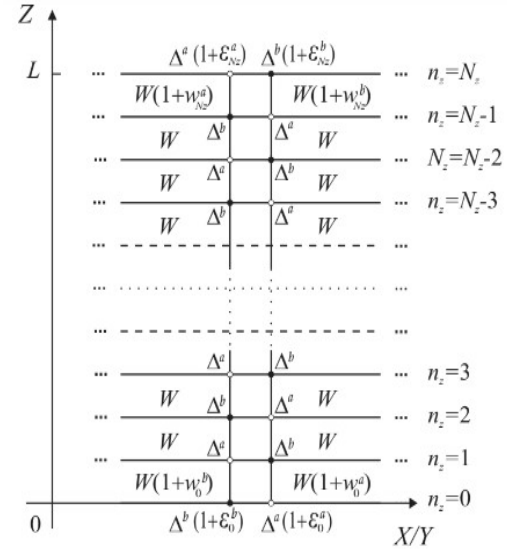


Figure 1 - Cross section of our model of crystal film with two sublattices in  $X/Y-Z$  planes

Based on the electronic Hamiltonian of the beam within the Hubbard model and the derived Hamiltonian of a simple film [4–6], the electron Hamiltonian of this model has the form:

$$H = \sum_{m_x, m_y, m_z} \sum_{n_z}^+ a_{m_x, m_y, m_z}^+ \left[ \Delta_z^{a/b} a_{m_x, m_y, m_z} - W_z^{a/b} (a_{m_x+1, m_y, m_z} + a_{m_x-1, m_y, m_z}) - W_y^{a/b} (a_{m_x, m_y+1, m_z} + a_{m_x, m_y-1, m_z}) - W_z \left( 1 + w_0^{a/b} \delta_{1, n_z}^{b/a} + w_{N_z}^{b/a} \delta_{N_z, n_z}^{b/a} \right) a_{m_x, m_y, m_z-1} - W_z \left( 1 + w_0^{a/b} \delta_{0, n_z}^{a/b} + w_{N_z}^{b/a} \delta_{N_z-1, n_z}^{b/a} \right) a_{m_x, m_y, m_z+1} \right]. \quad (2)$$

Due to the confinement of the system, only a partial spatial Fourier transformation - along the  $x$  and  $y$  directions, can be performed (more details in [6–9]). After that we get two sets of equations for  $2(N_z + 1)$  GFs. The first set:  $G_0^a, G_1^b, G_2^a, \dots, G_{N_z-1}^a, G_{N_z}^b$  corresponds to atomic line (along  $z$ -direction) with atom  $a$  at the first  $XY$ -layer (for  $n_z = 0$ ), while the second set:  $G_0^b, G_1^a, G_2^b, \dots, G_{N_z-1}^b, G_{N_z}^a$  corresponds to atomic line with atom  $b$  at the first layer. Also, the boundary conditions must apply:  $G_{n_z}^{a/b} = 0$  for  $n_z < 0$  and for  $n_z > N_f$ .

The general form of the first set of equations is then:

$$G_{2j-1; m_z}^a + \left( \rho - \frac{\Delta^a}{W_z} \gamma_0^a \delta_{0, n_z}^a \right) G_{2j; m_z}^a + \left( 1 + w_0^a \delta_{0, n_z}^a + w_{N_z}^b \delta_{N_z-1, n_z}^a \right) G_{2j+1; m_z}^b + R G_{2j; m_z}^b = K_{2j; m_z}^a \quad (3)$$

$$\left( 1 + w_0^a \delta_{1, n_z}^b + w_{N_z}^b \delta_{N_z, n_z}^b \right) G_{2j; m_z}^a + \left[ \rho + \frac{\Delta^a}{W_z} (1 - \theta - \epsilon_{N_z}^b \delta_{N_z, n_z}^b) \right] G_{2j+1; m_z}^b + G_{2j+2; m_z}^a + R G_{2j+1; m_z}^a = K_{2j+1; m_z}^b$$

The second set of equations is of the form:

$$G_{2j-1; m_z}^a + \left[ \rho + \frac{\Delta^a}{W_z} (1 - \theta - \theta \gamma_0^b \delta_{0, n_z}^b) \right] G_{2j; m_z}^b + \left( 1 + w_0^b \delta_{0, n_z}^b + w_{N_z}^a \delta_{N_z-1, n_z}^b \right) G_{2j+1; m_z}^a + R G_{2j; m_z}^a = K_{2j; m_z}^b$$

$$\left( 1 + w_0^b \delta_{1, n_z}^a + w_{N_z}^a \delta_{N_z, n_z}^a \right) G_{2j; m_z}^b + \left( \rho - \frac{\Delta^a}{W_z} \epsilon_{N_z}^a \delta_{N_z, n_z}^a \right) G_{2j+1; m_z}^a + G_{2j+2; m_z}^b + R G_{2j+1; m_z}^b = K_{2j+1; m_z}^a \quad (4)$$

where abbreviated markings are introduced:

$$\rho = \frac{\hbar\omega - \Delta_a}{W_z}; \quad R = \frac{2F_{x/y}}{W_z}; \quad F_{x/y} = W_x \cos a_x k_x + W_y \cos a_y k_y; \quad \theta = \frac{\Delta_b}{\Delta_a}; \quad K_{n_z; m_z}^{a/b} = \frac{i\hbar \delta_{n_z; m_z}^{a/b}}{2\pi W_z}.$$

In order to determine the dispersion law (energy spectrum) of electrons, it is sufficient to calculate the poles of GFs [4,6], i.e. to determine the roots of determinants ( $D$ ) of system equations (3) and (4), which comes down to the condition:  $D = 0$ . In general, this condition is not analytically solvable, and numerical methods must be used. As an example, we will study the following case,  $\theta = 0.5$ , i.e.  $\Delta_b = 0.5 \Delta_a$ ,  $W_x = W_y = W_z \equiv W$ , for various film widths:  $N_z + 1 \in [5, 13]$ . Here we assume that the parameters  $w$  and  $\varepsilon$  on the same surface should be similar to each other:  $w_0^a \approx w_0^b \equiv w_0$ ;  $w_{N_z}^a \approx w_{N_z}^b \equiv w_{N_z}$ ;  $\varepsilon_0^a \approx \varepsilon_0^b \equiv \varepsilon_0$ ;  $\varepsilon_{N_z}^a \approx \varepsilon_{N_z}^b \equiv \varepsilon_{N_z}$ .

The obtained results of the analysis of the boundary effects (film thickness and parameter changes) on the electronic spectra are shown graphically in Figs. 2 and 3.

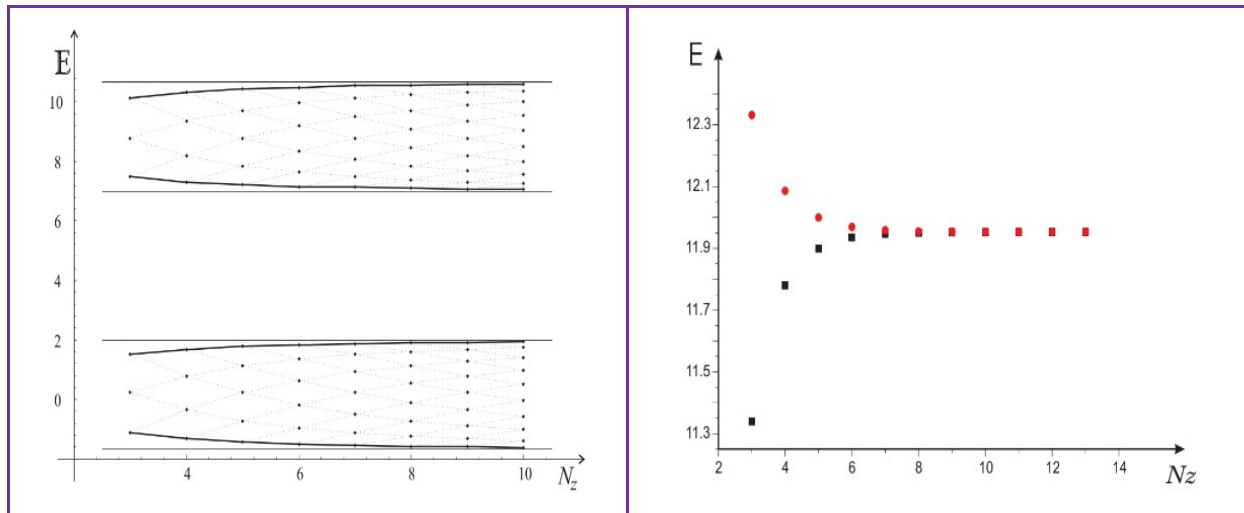


Figure 2 - The electron energy spectra dependence on film thickness

Figure 3 - Distribution of localized electron states though film thickness

Due to the close boundaries and altered boundary parameters, the electron energy spectra in an ultrathin film with a complex lattice are discrete (as in a film with a simple lattice [6,7]). The number of possible energy levels is equal to twice the number of crystal planes of the film along the  $z$ -direction, which is shown in Fig. 2. It can be seen that the discrete energy zone is divided into two allowed energy zones, between which is a forbidden zone. Unlike the allowed energy ranges in bulk crystal, the energy zones in the film are narrower, so two energy gaps appear (at the top and bottom of the allowed zones). The energy gaps decrease with increasing film thickness and the gap width is larger for thinner films.

The energy spectra of electrons depend on the value of the perturbation parameters, similar to the case of a simple thin film: increasing the electron energy at the boundary surfaces shifts the spectrum to higher energies (with an increase in the lower and a decrease in the upper gap), while for an increase in the electron transfer energy in the boundary layers, the spectrum broadens (while reducing the lower and upper gap). Depending on the values of surface interaction parameters, certain energy levels can lie outside the allowed energy ranges, even in the forbidden energy zone, so localized electron states appear.

### 3. CONCLUSION

This paper presents the results of studying the energy states of electrons in ultrathin films with a complex lattice. The consequence of the violation of translational invariance in the boundary layers of the film is the appearance of energy gaps in the electron spectra. The appearance of the lower energy gap has a special physical significance, because it (re)defines the energy of the basic state of the system [3–5]). Since electrons with the lowest energies are responsible for superconductivity [6], we can conclude that resistance less transfer cannot be expected in the direction orthogonal to the boundary surfaces of the film structures, but in plane parallel surfaces this movement is enabled. This is in agreement with the fact that the superconducting properties of films are better than bulk samples, especially for high-temperature Cu-O ceramics [8]. The occurrence of localized states are well known as Tam's states [4] and have a huge influence on the transport characteristics and other altered physical properties of the material.

### ACKNOWLEDGEMENTS

*The research presented in this paper was financially supported by the Ministry of Scientific and Technological Development, Higher Education and Information Society of the Republic of Srpska (Projects No. 19.032/961-36/19 and 19.032/961-42/19).*

### REFERENCES

- [1] C.I. Idumah, et al., Surf. Interfaces 21 (2020) 100734.
- [2] Y. Ahmadi, S. Ahmad, in: Micro and Nano Technologies, Corrosion Protection at the Nanoscale (S. Rajendran, et. al. Eds.), Elsevier, London, 2020, Ch. 19.
- [3] V. D. Sajfert, B. S. Tošić, J. Comput. Theor. Nanosci. 7(1) (2010) 15–84.
- [4] Ch. Kittel, Introduction to Solid State Physics, Wiley, New York 2004.
- [5] J.P. Šetrajić, S.K. Jaćimovski, S.M. Vučenović, Green's Functions in Quantum Statistical Physics – Condensed Matter Physics, Accepted in Materials Today 2023.
- [6] J.P. Šetrajić, S.M. Vučenović, S.K. Jaćimovski, Zaštita Materijala 57(2) (2016) 239-243.
- [7] B. Markoski, et al. Mod.Phys.Lett. 23 (2) B (2009) 129-135.
- [8] J.P. Šetrajić, et al. in Thermodynamics (Ed. M. Tadashi), InTech, Vienna, 2011, Ch.15.

## KINETIC AND THERMODYNAMIC ASPECTS OF STRONTIUM ADSORPTION BY STEELMAKING SLAG

Irena Nikolić<sup>1</sup>, Milena Tadić<sup>1</sup>, Dijana Đurović<sup>2</sup>, Nevena Cupara<sup>2</sup>, Ivana Milašević<sup>2</sup>

<sup>1</sup>Faculty of Metallurgy and Technology, University of Montenegro, Džordža Vašingtona bb, 81000 Podgorica, Montenegro

<sup>2</sup>Institute of Public Health of Montenegro, Džona Džeksona bb, 81000 Podgorica, Montenegro

### Abstract

*This paper aimed to investigate kinetic and thermodynamic of Sr<sup>2+</sup> adsorption from aquatic solution using electric arc furnace slag (EAFS). Adsorption experiments were carried out in a batch conditions for 35 min at adsorbent dosage of 1.5 g/l, initial concentrations of 150 mg/L, pH value of 5 and temperatures of 20 °C, 30 °C and 45 °C. Kinetic of Sr<sup>2+</sup> adsorption onto EAF slag was evaluated using pseudo-first and pseudo-second order models and results have shown that experimental data better fit the pseudo-second order model. Thermodynamic investigation indicated that adsorption of Sr<sup>2+</sup> onto EAFS is endothermic in nature, spontaneous and more favorable at higher temperature.*

**Keywords:** Strontium, Adsorption, Slag, Kinetic, Thermodynamic

### 1. INTRODUCTION

Electric arc furnace slag (EAFS) is a by-product of steel making production in a electric arc furnaces. This slag is mainly utilized in a civil engineering in a road construction [1], as a supplement for cement production [2], as an adsorbent for heavy metal removal from wastewaters [3] and in pass decade this slag is considered as a precursor for a production of alkali activated binders (green cements) [4].

One of the biggest problems of nuclear waste management is the disposal of radioactive wastewater which mainly contains isotopes such as strontium, cesium, plutonium, americium and technetium [5]. Strontium is a persistent radionuclide in the environment [6]. It is also present in high level liquid waste generated by the reprocessing of spent nuclear fuel [7]. Thus, separation of strontium from waste solutions requires special attention. Different adsorbents have been proposed for this purpose but to the best of our knowledge there is no data regards the usage of EAF slag for the treatment of wastewaters loaded with Sr<sup>2+</sup> by means of kinetics, and thermodynamic analysis of Sr<sup>2+</sup> adsorption process.

### 2. EXPERIMENTAL

Sorbent (EAFS) used in this research was supplied from the Still Mill in Montenegro. Chemical composition of slag is given in Table 1. Prior the adsorption test EAFS was powdered washed and dried.

Adsorption experiments were carried out in a batch conditions for 35 min at the sorbent dosage 1.5g/L, initial concentrations of 150 mg/L, pH value of 5 and temperatures of 20 °C, 30 °C and 45°C. Solution containing Sr<sup>2+</sup> ions was prepared from analytical grade chemicals, SrCl<sub>2</sub> in deionized water. During the adsorption experiments, an aliquot of the suspension was taken at certain intervals of time, filtered and tested for the concentrations of metal ions using inductively coupled plasma optical emission spectrometry (ICP-OES).

Removal efficiency of Sr<sup>2+</sup> ions (*RE*) and adsorption capacity (*q<sub>t</sub>*) at any given time were calculated according Eq 1. and 2.

$$RE = \frac{C_0 - C_t}{C_0} \cdot 100\%. \quad (1\text{Error!})$$

Bookmark not defined.)

$$q_t = \frac{(C_0 - C_t)}{m} V. \quad (2\text{Error!})$$

Bookmark not defined.)

where  $C_0$  and  $C_t$  are the initial and final concentrations of  $\text{Sr}^{2+}$  ions in solution,  $V$  is the volume of  $\text{Sr}^{2+}$  ions solution and  $m$  is the dry mass of adsorbent.

Adsorption kinetic was evaluated using the pseudo-first-order (PFO) and pseudo-second-order (PSO) kinetics model which integrated forms are expressed by Eq. (3) and (4), respectively:

$$\log(q_e - q_t) = \log q_e - \left(\frac{k_1}{2.303}\right) t \quad (3)$$

$$\frac{t}{q_t} = \frac{t}{q_e} + \frac{1}{k_2 q_e^2} \quad (4)$$

Where  $q_e$  ( $\text{mg g}^{-1}$ ), denotes adsorption capacity in equilibrium,  $k_1$ , ( $\text{min}^{-1}$ ) and  $k_2$ , ( $\text{g mg}^{-1} \text{min}^{-1}$ ) are rate constants of the pseudo first-order sorption and pseudo second-order sorption, respectively. When PFO model was applied, values of  $k_1$  and  $q_e$  were calculated from the slope and intercept of straight line plot  $\log(q_e - q_t)$  versus  $t$ . In case of PSO model,  $k_2$  and  $q_e$  were calculated from the intercept of and slope of the plot of  $t/q_t$  versus time.

Thermodynamic of  $\text{Sr}^{2+}$  adsorption onto EAF slag was evaluated using following equations:

$$\Delta G^\circ = \Delta H^\circ - T \Delta S^\circ \quad (5)$$

$$\Delta G^\circ = -RT \ln K \quad (6)$$

$$\ln K_d = \frac{\Delta S^\circ}{R} - \frac{\Delta H^\circ}{RT} \quad (7)$$

$$K_d = \frac{(C_0 - C_e) \cdot V}{C_e \cdot m} \quad (8)$$

Where,  $\Delta G^\circ$ ,  $\Delta H^\circ$ ,  $\Delta S^\circ$  and  $K_d$  present standard free energy, enthalpy, entropy and equilibrium distribution coefficient, respectively. The straight-line plots  $\ln K_d$  vs  $1000/T$  enables determination the values of  $\Delta H^\circ$  and  $\Delta S^\circ$  from the slope ( $\Delta H^\circ/R$ ) and intercept ( $\Delta S^\circ/R$ ), respectively.

Table 1 - Chemical composition of EAFS

Component	%
CaO	46.5
FeO	23.5
SiO <sub>2</sub>	12.2
Al <sub>2</sub> O <sub>3</sub>	7.2
MgO	6.5
MnO	1.3
TiO <sub>2</sub>	1.06
Fe <sub>2</sub> O <sub>3</sub>	0.9
Cr <sub>2</sub> O <sub>3</sub>	0.8
L.O.I*	4.2

\*Loss on ignition

### 3. RESULTS AND DISCUSSION

The results of  $\text{Sr}^{2+}$  removal from aquatic solution using EAFS was are given in the Fig 1. The achieved removal efficiencies of  $\text{Sr}^{2+}$  within 35 min of adsorption at 20 °C were 68.75% and the



major fraction of  $\text{Sr}^{2+}$  was removed from solution by EAF slag within the first 15 min. Further prolongation of adsorption process practically had no influence on the  $\text{Sr}^{2+}$  adsorption indicating that after 15 min equilibrium was reached. Increase of temperature of adsorption to 35 °C and 45 °C was favorable for the adsorption of  $\text{Sr}^{2+}$  onto EAFS. The rise of temperature from to 35 °C and 45 °C increases the removal efficiency of  $\text{Sr}^{2+}$  onto EAF slag to 75.93% and 88.40%, respectively.

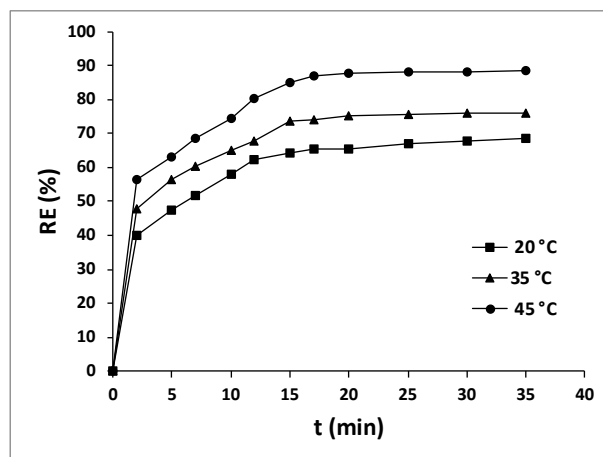


Figure 1 - Removal efficiency of  $\text{Sr}^{2+}$  ions by EAFS

The results of investigation of adsorption kinetic of  $\text{Sr}^{2+}$  ions onto EAF slag are given in Fig.2(a) and Table 2. Analysis of adsorption kinetic has shown that PSO kinetic model better fit with experimental data since high regression coefficients ( $R^2$ ) were obtained and calculated values of  $q_e$  were in good agreement with the experimental values for  $q_e$  (Table 1).

Table 2 - Kinetics and thermodynamic parameters for  $\text{Sr}^{2+}$  adsorption onto EAFS

Pseudo-first-order kinetic model				
Temperature, (°C)	$q_e$ , experimental	$q_e$ , calculated	$k_1$	$R^2$
20	64.2	57.72	0.26	0.9357
35	75.3	51.70	0.22	0.9531
45	87.73	63.80	0.20	0.9322
Pseudo-second-order kinetic model				
Temperature, (°C)	$q_e$ , experimental	$q_e$ , calculated	$k_2 \times 10^{-3}$	$R^2$
20	64.2	71.43	10.152	0.9963
35	75.3	79.37	10.332	0.9969
45	87.73	90.91	10.827	0.9972

The results of thermodynamic investigation (Table 3) and (Fig.2(b)) indicated that adsorption of  $\text{Sr}^{2+}$  onto EAF slag is endothermic in nature since positive value of enthalpy (44.89  $\text{KJ mol}^{-1}$ ). Moreover this value fall in the range 40–200  $\text{kJ mol}^{-1}$  which means that the  $\text{Sr}^{2+}$  adsorption onto EAFS involves chemisorption. Negative values of free energy ( $\Delta G^\circ$ ) obtained at all investigated temperatures indicate that  $\text{Sr}^{2+}$  adsorption onto EAF slag occurs spontaneously. The rise of temperature lead to the decrease of  $\Delta G$  which indicates that the adsorption process is more favorable at higher temperatures.

Table 3 - Thermodynamic parameters of  $\text{Sr}^{2+}$  adsorption onto EAFS

Temperature (°C)	$K_d$	$-\Delta G^\circ$ , ( $\text{KJ mol}^{-1}$ )	$\Delta H^\circ$ , ( $\text{KJ mol}^{-1}$ )	$\Delta S^\circ$ , ( $\text{J mol}^{-1}\text{K}^{-1}$ )
20	1.25	0.55	44.89	156.30

35	2.76	2.59		
45	5.51	4.51		

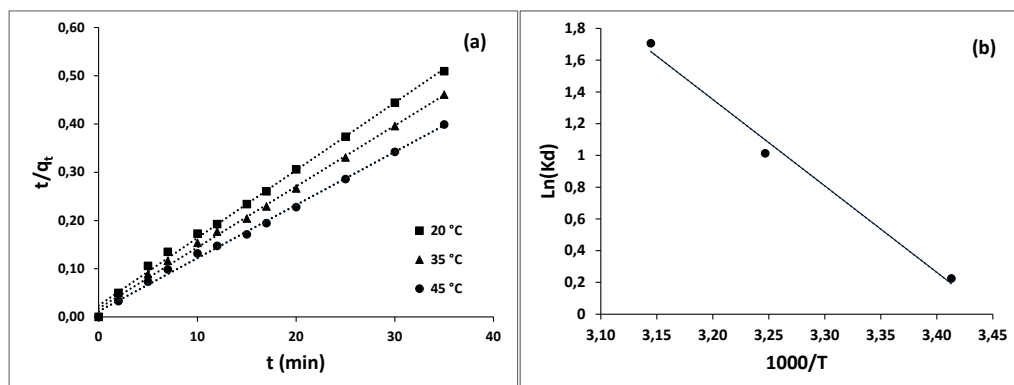


Figure 2 - The PSO kinetics plots (a) and plot  $\ln K_d$  vs.  $1000/T$  (b) for the adsorption of  $\text{Sr}^{2+}$  onto EAFS

#### 4. CONCLUSIONS

The results of investigation of  $\text{Sr}^{2+}$  adsorption onto EAFS have shown that this slag can be used an effective adsorbent. The high removal efficiency (68.75%) at 20°C was achieved in relatively short time. The increase of temperature lead to the increase of removal efficiency and 88.40% of  $\text{Sr}^{2+}$  ions can be removed from aquatic solution at 45 °C. The results of kinetic analysis suggested that adsorption of  $\text{Sr}^{2+}$  onto EAF slag proceeds according to the pseudo second-order and thermodynamic investigations have indicated that  $\text{Sr}^{2+}$  is endothermic in nature and spontaneous. Increase of temperature favors adsorption process.

#### REFERENCES

- [1] P.Sukmak, G. Sukmak, P. De Silva, S. Horpibulsuk. S. Kassawat, A. Suddepong., Constr. Build. Mater. 368 (2023) 130393.
- [2] Y. Jiang, T.C. Ling, C.Shi, S.Y. Pan., Resour. Conserv. Recycl, 136 (2018) 187-197.
- [3] I. Nikolić, D. Đurović, M. Tadić, V.V. Radmilović, V.R., Radmilović. Chem. Eng. Commun., 207(9), 1278-1297.
- [4] J.J. Chang, W. Yeih, T.J. Chung, R. Huang., Constr. Build. Mater. 109 (2016) 34- 40.
- [5] A. Ahmadpour, M. Zabihi, M. Tahmasbi, T.R. Bastami, J. Hazard. Mater. 182 (2010) 552–556.
- [6] R. Apak, G. Atun, K. Güçlü, E. Tütem., J. Nucl. Sci. Technol. 33 (1996) 396–402.
- [7] T. Kawamura, T. Ito, S.Y. Kim,,J. Radioanal. Nucl. Chem. 320 (2019) 9–14.

## NEW FLOTATION PLANT VELIKI KRIVELJ MONITORING PLAN

**Miomir Mikić, Milenko Jovanović, Sandra Milutinović,  
Daniel Kržanović, Radmilo Rajković**

Mining and Metallurgy Institute Bor, Zeleni bulevar 35, 19210 Bor, Serbia

### Abstract

*The ore from the deposit is exploited from the open pit "Veliki Krivelj", from where it is further subjected to the technological processes of crushing, grinding, classification, then flotation concentration of the mineral raw material and finally the process of dewatering, filtering and thickening, the output products of flotation concentration (concentrate and tailings), as and their transport to their final destinations. Veliki Krivelj mine's New Flotation Plant was built, which will operate with a capacity of 13.2 Mt, alongside and independently of the existing one, which has a capacity of 9.9 Mt. Based on this, it is necessary to establish adequate monitoring for monitoring the quality of air, water and surrounding land, in order to monitor the quality of the living environment.*

**Keywords:** *monitoring, open pit, flotation, environmental.*

### 1. INTRODUCTION

The primary purpose of the monitoring plan is to define the criteria and details for the environmental monitoring plan and implementation in order to quantify the environmental impact of the facility and provide a basis for the decision-making process.

The monitoring plan and the results obtained from its implementation should lead to the achievement of the following specific goals:

- evaluations of compliance of the operator's emissions with the emission limit values defined by the respective laws and by-laws;
- assessments of compliance with the conditions of the integrated permit;
- assessments of the implementation of the best available techniques;
- provision of data confirming the implementation of the measures required by the permit;
- provision of data necessary for assessing the impact of the operator's activities on the environment;
- provision of preventive measures to prevent possible environmental pollution that may occur as a result of the operator's activities.

According to the law on environmental protection, monitoring is carried out by systematic measurement, examination and evaluation of indicators of the state and pollution of the environment, which includes the monitoring of natural factors, i.e. changes in the state and characteristics of the environment, including: air, water, soil, forests, biodiversity, noise, waste as well as assumed obligations from international agreements.

The monitoring system should consist of: identification of pollution sources and parameters, selection of environmental parameters for which measurements are made, determination of critical areas and data collection, analysis and assessment.

### 2. FLOTATION PLANT LOCATION VELIKI KRIVELJ

The open pit "Veliki Krivelj" is located northeast of Bor at a distance of 3 km. Near the open pit is the village of the same name, after which the deposit got its name. A flotation facility with a

flotation tailings and other supporting facilities (a workshop for heavy and light vehicles and a pumping station for liquid fuels) necessary for the exploitation and preparation of ore was built near the open pit.

Figure 1 shows a satellite image of the location of the new Veliki Krivelj copper ore processing plant, where you can see all the infrastructure facilities of the corresponding technological units for crushing, transport, grinding and classification, flotation concentration, thickening and filtering of copper concentrate and tailings disposal within flotation plant V. Krivelj, as well as other accompanying facilities, which enable its smooth functioning:

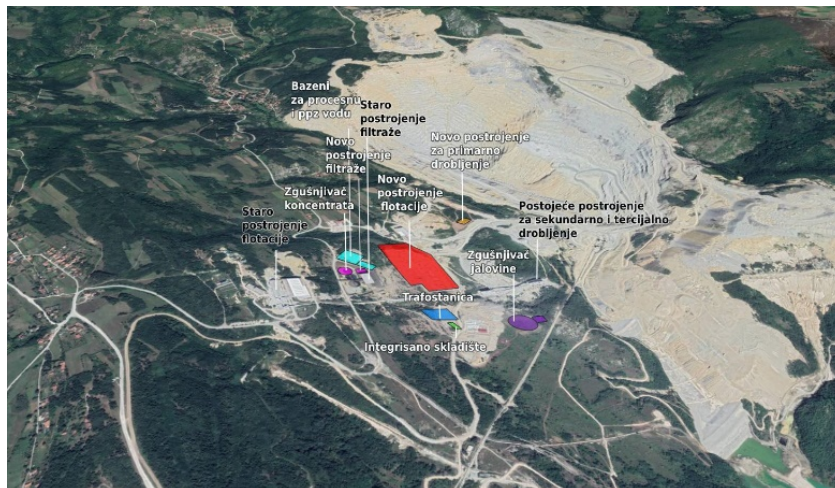


Figure 1 - Satellite image of the location of the new copper ore processing plant in Veliki Krivelj

### 3. PARAMETERS ON THE BASIS OF WHICH HARMFUL EFFECTS ON THE ENVIRONMENT CAN BE DETERMINED

Taking into account the technological processes that have been designed within the new flotation plant, it can be stated that at the location in question the largest emitter of polluting substances is the primary crushing and the transport routes along which the mechanization will move. Also, it should be noted that the project envisages a conveyor belt from the primary crushing to the flotation hall, however this system will be placed in a tunnel, so there will be no harmful impact on the air in the environment.

Surface water, as the largest transport medium, should be monitored diligently, in terms of monitoring the water quality of nearby watercourses.

Taking into account the projected technological process, it can be safely asserted that the project has no impact on groundwater. In the vicinity of the subject location, there is a well in the yard of a private house. As a preventive measure, the quality of this water will be monitored.

Monitoring soil quality will mean monitoring the distribution of heavy metals in the soil in accordance with the wind rose.

The designed machines and devices in the new flotation plant do not represent sources that can contribute to an increase in noise. However, the primary crusher plant and the machinery that moves around the plant are potential sources that can lead to excessive noise. The measurement of noise emissions into the environment will be monitored, with an emphasis on the area where the concentration of the surrounding population is closest to the mining facilities.

The parameters to be monitored on the mentioned entities are shown in table 1. Disposition of measuring points are shown on figure 2. Label for each measure point are: PV-for surface waters, PD – for underground waters, MB - for noise level, PMV – for PM (Particulate matter), V- for sedimentation matter, SMM – for wastewaters, Z – for soil.

Table 1 - Monitoring parameters

Location	Frequency of monitoring	Parameters
<b>Waters:</b> 1. surface waters : <ul style="list-style-type: none"> <li>Kriveljska reka</li> <li>Borska reka</li> <li>Saraka potok</li> </ul> 2. underground <ul style="list-style-type: none"> <li>wells</li> </ul>	<ul style="list-style-type: none"> <li>4 time per year</li> </ul>	<ul style="list-style-type: none"> <li>Water temperature, colour, smell, pH, electrical conductivity, sedimentary matter, suspended matter, HPK, BPK5, soluble oxygen, oxygen saturation;</li> <li>Metals, metalloids and their compounds: Cr, As, Cd,Pb, Zn,Hg,Ni,Fe,Cu,Mn</li> <li>Sulfates; Cyanides; Nitrates, nitrites; Mineral oils and hydrocarbons; Total fats and oils.</li> </ul>
<b>Air</b> <ul style="list-style-type: none"> <li>Measuring points are placed near private houses in the southeast, northwest and west of the proposed location</li> </ul>	<ul style="list-style-type: none"> <li>Sedimentation matter - monthly</li> <li>Suspended particles - daily samples, twice a year (summer and winter period, 30 days each);</li> <li>Exhaust gases</li> </ul>	<ul style="list-style-type: none"> <li>Total sediments: amount of sediments,</li> <li>Suspended particles: PM10, PM2.5</li> <li>content of heavy metals (Cr, As, Cd,Pb, Zn,Hg,Ni,Fe,Cu,Mn)</li> <li>Exhaust gases: sulfur dioxide, nitrogen oxides, carbon monoxide</li> </ul>
<b>Noise:</b> Measuring points in the vicinity of the nearest private buildings (northwest and west)	1 per year	<ul style="list-style-type: none"> <li>Equivalent intensity level, daily measurements</li> <li>Equivalent level-intensity, night measurements</li> </ul>
<b>Soil:</b> The measuring points are located on the surrounding areas to the southeast, northwest and west of the subject location	1 per year	<ul style="list-style-type: none"> <li>humus content</li> <li>Soil pH</li> <li>calcium carbonate, nitrogen, electrical conductivity; phosphorus;</li> <li>Metals: As, Cd, Pb, Zn, Hg, Ni, Fe, Cu</li> <li>Sulfates; Fluorides; Chlorides; Nitrites, nitrates, Cyanides. Aromatic organic compounds</li> </ul>



Figure 2 - Disposition of measuring points



#### **4. CONCLUSION**

Mining activity has increased significantly due to significant population growth and worldwide demand for mineral resources [1]. This increase coincides with a new awareness in which environmental issues have become an increasing challenge for all actors in the sector[2,3]. There is an increased social demand for sustainable development of all activities related to mining, especially adequate management of waste products during each phase of the mining process, including prospecting and research, development, extraction, transportation and treatment of the obtained products, etc. [4]. Energy requirements, environmental and human health risks, water resource requirements and required technology must be taken into account [5].

Taking these arguments into account, the monitoring system gains great importance. The monitoring system collects and interprets the information necessary to determine whether the environmental protection management plan and related systems have been effectively implemented, and whether the environmental goals set by the company, the authorities and the community have been properly met.

The monitoring system should consist of: identification of pollution sources and parameters, selection of environmental parameters for which measurements are made, determination of critical areas and data collection, analysis and assessment.

The goal of the environmental monitoring system is to analyze the sources of pollution while considering the effectiveness of the applied environmental protection measures.

#### **ACKNOWLEDGEMENTS**

*This work was financially supported by the Ministry of Education, Science and Technological Development of the Republic of Serbia, contract no. 451-03-47/2023-01/ 200052*

#### **REFERENCES**

- [1] Reichl, C.; Schatz, M.; Zsak, G. World-Mining-Data. In Minerals Production; International Organizing Committee for the World Mining Congresses: Vienna, Austria, 2016; Volume 31.
- [2] Dold, B. Rev. Environ. Sci. Bio/Technol. 2008, 7, 275–285.
- [3] Gómez Ros, J.M.; García, G.; Peñas, J.M. Union. Ecol. Eng. 2013, 57, 393–402.
- [4] Bakken, G.M. Montana, Anaconda, and the Price of Pollution. Historian 2007, 69, 36–48. Available online: <http://www.jstor.org/stable/24453910> (accessed on 14 April 2018).
- [5] Durucan, S.; Korre, A.; Muñoz-Melendez, G. J. Clean. Prod. 2006, 14, 1057–1070.

## RECUltIVATION OF OPEN PIT VELIKI KRIVELJ

Miomir Mikić, Radmilo Rajković, Daniel Kržanović,  
Milenko Jovanović, Sandra Milutinović

Mining and Metallurgy Institute Bor., Zeleni bulevar 35, 19210 Bor, Serbia

### Abstract

*Exploitation of copper ore at the "Veliki Krivelj" open pit means the degradation of the surrounding soil during the formation of the projected contours of the open pit. In this case, the Veliki Krivelj open pit will be expanded, to the greatest extent in the northern northwestern part (in the direction of the Veliki Krivelj village). For the reclamation of the Veliki Krivelj open pit, recultivation will be consist of technical and biological stages.*

**Keywords:** *recultivation, open pit, degradation*

### 1. INTRODUCTION

The "Veliki Krivelj" copper deposit is located, about 3 km northeast (azimuth about 10) from the town of Bor, and 0.5 km northeast (azimuth about 125) from the nearest village of Veliki Krivelj, in the Krivelj river basin. Within the "Veliki Krivelj" copper deposit, there is the "Veliki Krivelj" open pit, where exploitation began in 1982. Regional road 393 passes in the immediate vicinity of this open pit, and connects it with Bor and the village of Veliki Krivelj.

Exploitation of copper ore at the "Veliki Krivelj" open pit means the degradation of the surrounding soil during the formation of the projected contours of the open pit as (figure 1). In this case, the Veliki Krivelj open pit will be expanded, to the greatest extent in the northern northwestern part (in the direction of the Veliki Krivelj village).



Figure 1 - Spatial layout of facilities: open pit (1), waste landfill Saraka (2)



## 2. DEGRADED SURFACES

The final contour of the open pit Veliki Krivelj, Figure 2, was designed with the lowest bench - the bottom of the mine, at an elevation of K-85m, and the highest bench at an elevation of K+530. This projected contour includes a total area of 2,412,230 m<sup>2</sup>. Degraded areas that are intended for reclamation by this project are flats, whose total area for reclamation is 1,252,620 m<sup>2</sup>.

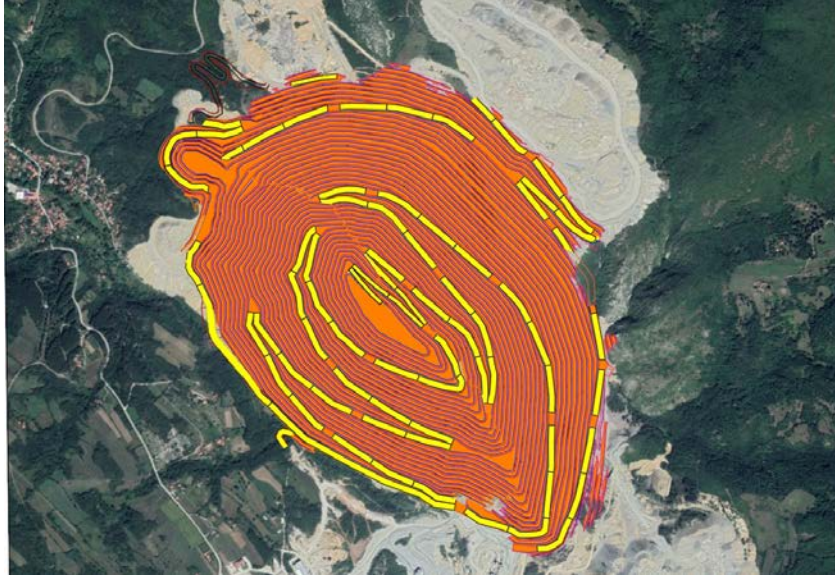


Figure 2 - The final contour of the designed surface mine Veliki Krivelj

## 3. CHOICE OF RECULTIVATION METHOD

The analysis of the state of the landscape after the formation of the final contour of the open pit in Veliki Krivelje indicates that the conditions created at the end of the exploitation period will be such that the concept of biological reclamation should be adapted to the function of achieving visual harmony of the disturbed environment with the surrounding undisturbed environment, using species adapted to the ecological conditions that prevail on newly formed degraded surfaces.

In accordance with the set functional requirements, the goals of reclamation are: creation of new, anthropogenic forest ecosystems, revitalization of degraded areas and return to the cycle of natural biological flows, provision of a healthy environment, protection and improvement of biodiversity, ensuring terrain stability, prevention of erosion processes, regulation of surface water runoff as and improving soil quality. [1]

For the reclamation of the Veliki Krivelj open pit, reclamation with the following stages will be applied:

- Technical reclamation
- Biological reclamation

## 4. TECHNICAL PHASE OF RECULTIVATION

Technical reclamation includes the degraded surface of the surface mine, i.e. the storey level. The technical phase of reclamation represents the stage of preparatory works, which enable the execution of biological reclamation. As part of the technical reclamation, in order to ensure the execution of the works, several operations will be carried out, namely:

- leveling the bench levels of the open pit;
- drilling and mining works in order to form pits for seedlings;

- spreading earthen material on benches.

Within the framework of technical recultivation, works on digging pits for seedlings are also included. Excavation of pits will be performed mechanically.

## 5. BIOLOGICAL PHASE OF RECULTIVATION

The biological phase of optimal recultivation is the application of phytomelioration measures on previously prepared soil substrate (degraded surface) in order to establish and survive vegetation for the later formation of a stable ecosystem. The greening of the degraded surface has primarily the role of environmental protection, and at the same time contributes to a better appearance of the environment and a better microclimate of the area.

On a flat surface (benches), afforestation will be applied according to a square scheme.

For the recultivation of the Veliki Krivelj open pit, the selection of plant species for afforestation was carried out, namely:

- *Betula alba* L. (birch) - A pioneer species that sometimes occurs as a wild plant on the surfaces of the landfill and tailings of the "Veliki Krivelj" surface mine. It grows quickly and quickly covers the bare surface of the substrate. It is easily regenerated naturally, it tolerates poor soils with an acidic reaction, which it repairs with its fallen leaves and twigs, creating humus. It is resistant to low and high temperatures and wind. It creates a very faint shade that does not disturb the grasses. Intended for planting on plateaus and terraced levels of external landfills and tailings, as well as on landfills where, due to improper deposition, processes of reduction and lowering of the pH value have begun.
- *Acer campestre* L. (chub) – A lower tree, a species with a wide ecological amplitude. It is included in the composition of the natural potential vegetation of this area, and it also inhabits much drier forest communities than nature, which indicates the potential for good growth on the desolation of the surface mine.

Selected sedges in nature are found in stands mixed with each other. Due to the unfavorable basic substrate and the possibility of reception, as well as the geometric shape of the benches and the slope of the open pit, planting is carried out:

- on level benches in four rows at a distance of 3 m between seedlings.

Arrangement of seedlings, i.e. of woody and shrubby crops is given in Figure 3.

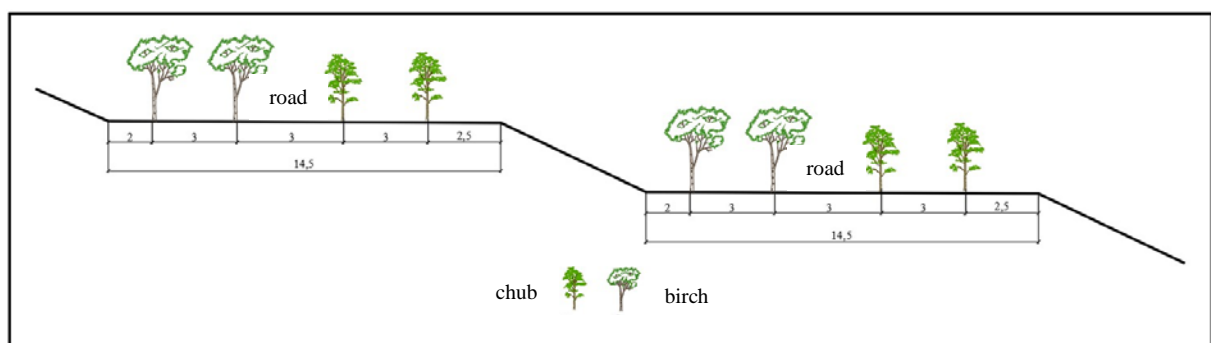


Figure 3 - Transversal profile of benches showing the arrangement of cultures

The total number of birch saplings is 64,884, while the total number of chub saplings is 61,672. The number of seedlings to be purchased is increased by 5%, which is taken as a reserve, because it is possible that a certain number of seedlings may be damaged during transport, dry, etc. Based on that, the total number of birch saplings is 68,129, and chub 64,756. Classic planting material is chosen for afforestation. The age of the seedlings should be 2+1.

## **6. CONCLUSION**

The recultivation of degraded areas at the Veliki Krivelj open pit at the location in question is aimed at preserving the environment, and with the application of the foreseen technical and biological measures, good results can be expected despite the unfavorable underlying base. In this case, no economic profit is expected from the plantations, but only the protection of damaged soil from erosion and the improvement of the microclimate. In addition, the root system of seedlings and leaves that fall and rot on degraded surfaces will initiate pedological processes in the direction of humus creation.

The effects of recultivation of degraded areas are reflected in the fact that:

- Forest plantings enable better binding of the soil, stimulate the development of ground flora, activate pedological processes in the substrate with the root system, prevent insolation and drying of the soil, blowing of strong winds and raising of dust.
- Afforestation of degraded areas contributes to environmental protection, improving the microclimate and the aesthetic appearance of the environment.

## **ACKNOWLEDGEMENTS**

*This work was financially supported by the Ministry of Education, Science and Technological Development of the Republic of Serbia, contract no. 451-03-47/2023-01/200052*

## **REFERENCES**

[1] Studija izvodljivosti eksploatacije ležišta mineralnih sirovina "Veliki Krivelj" za godišnji kapacitet rude od 23,1 mt – RGF Beograd, 2020.god.

## ANALYSIS OF INFLUENCED FACTORS ON TROPOSPHERIC OZONE CONTENT IN THE CITY OF ZENICA DURING 2020

Farzet Bikić, Khaola Awad, Halim Prcanović, Mirnes Duraković,

Faculty of Engineering and Natural Sciences, University in Zenica, Travnička cesta 1, 72 000  
Zenica, Bosnia and Herzegovina

### Abstract

*Tropospheric ozone is a pollutant that is created mainly by photochemical reactions in the lower layers of the atmosphere. Nitrogen oxides and volatile organic compounds are needed for the formation of tropospheric ozone by photochemical reactions. This paper presents and analyzes data on average monthly concentrations of NO<sub>x</sub> and O<sub>3</sub> recorded at three automatic pollutant measuring stations in the air, located in the center of the city of Zenica, Radakovo and Tetovo. Data were analyzed for the entire year 2020. The research results show that the key factors in increasing the concentration of tropospheric ozone from photochemical reactions in the city of Zenica are the increased intensity of car traffic, the burning of fossil fuels in thermal power plants and the intensity of solar radiation.*

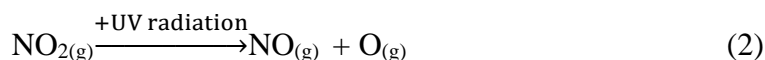
**Keywords:** ozone, nitrogen oxides, troposphere, photochemical smog

### 1. INTRODUCTION

Certain pollutants that are formed from primarily emitted pollutants by photochemical processes in the atmosphere are known as photochemical oxidants. They can oxidize compounds in the atmosphere that under normal conditions cannot be oxidized by oxygen [1]. One of the most important photochemical oxidants is ozone (O<sub>3</sub>). Ozone is an allotropic modification of oxygen whose molecule consists of 3 oxygen atoms. Ozone is a blue gas with a strong smell. Soluble in water, 50 times better than oxygen. It is very unstable in high concentrations. The formation of ozone in the troposphere is caused by other pollutants present in the atmosphere, especially nitrogen oxides and hydrocarbons [1, 2, 3]. The formation of tropospheric ozone by photochemical reactions describes the mechanism shown in a simplified manner by reactions 1, 4 and 5. With the increase in car traffic, the concentration of hydrocarbons, which are the fuel used in cars, and nitrogen oxides in the air increases. Nitrogen oxides are formed in car engines, where nitrogen and oxygen from the atmosphere react at high temperatures. The product of this reaction is nitrogen monoxide (NO):



Nitrogen monoxide, a colorless gas, goes into the atmosphere together with other exhaust gases. Through complex reactions, in which participate oxidized hydrocarbons, nitrogen monoxide produces a red-brown gas, nitrogen dioxide, NO<sub>2</sub>. Under the action of the sun's ultraviolet radiation, nitrogen oxide molecules break down into nitrogen monoxide and atomic oxygen [4]:



Atomic oxygen is very reactive, so it combines with oxygen molecules to form ozone:



Ozone and nitrogen oxides, collectively known as photochemical smog, react with hydrocarbons in the polluted atmosphere to create highly toxic organic compounds. The described processes take

place in the lower layers of the atmosphere and are a major environmental problem. The formation of tropospheric ozone by photochemical reactions can also be shown schematically, Figure 1.

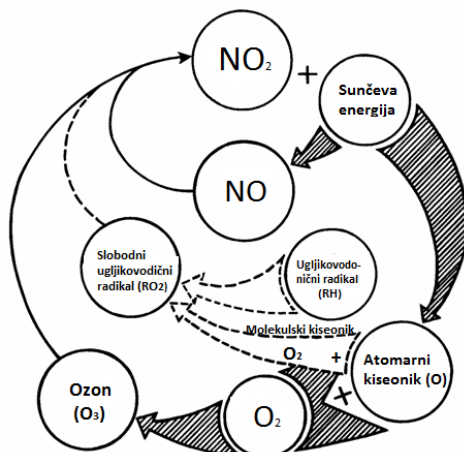


Figure 1. Photolytic cycle in which hydrocarbon radicals participate [5]

Although life on Earth is not possible without ozone in the stratosphere, in the lower parts of the atmosphere this gas is harmful to health. Inhaling ozone causes a feeling of lack of air, coughing, irritation of the nose and throat, and chronic diseases such as asthma and bronchitis.

The aim of the research carried out in this paper is to analyze the data on the average monthly concentrations of NO<sub>x</sub> and O<sub>3</sub> for the year 2020, recorded at three automatic measuring stations for pollutants in the air, located in the area of the city of Zenica. After analyzing the data on the content of NO<sub>x</sub> and O<sub>3</sub>, the goal is to determine the influencing factors on the appearance of tropospheric ozone at the mentioned locations. The mission of the research is to try to give recommendations on how tropospheric ozone emissions created by photochemical reactions can be reduced.

## 2. EXPERIMENTAL

The goal of the conducted research is to determine the dependence of the existence of tropospheric ozone depending on the location of the measuring station, the content of nitrogen oxides NO<sub>x</sub> in the troposphere, and the season (month). Data on the average monthly concentrations of NO<sub>x</sub> and O<sub>3</sub> recorded at three automatic air pollutant measuring stations, located in the center of the city of Zenica, Zenica city zone name Radakovo, and the village of Tetovo near the Industrial Zone in Zenica. The measurement of NO<sub>x</sub> and O<sub>3</sub> concentrations in the air is carried out using standard methods that are in accordance with EN and ISO standards and the Rulebook on the manner of monitoring air quality and defining the types of pollutants, limit values and other air quality standards of FBiH. Measurement methods and standards are shown in table 1.

Table 1 - Overview of methods and standards for NO<sub>x</sub> and O<sub>3</sub> monitoring

Polutanti	Korištena metoda
NO <sub>x</sub>	BAS EN 14211 - Hemiluminiscentna metoda
O <sub>3</sub>	BAS EN 14625 - Metoda nedisperzivne ultravioletne apsorpcije

## 3. RESULTS AND DISCUSSION

Diagrams 1, 2 and 3 show the average monthly concentrations of nitrogen oxides and ozone for the year 2020 measured at stationary automatic measuring stations AMS-1- Zenica-Centar, AMS-2- Zenica-Radakovo and AMS-3- Zenica-Tetovo.

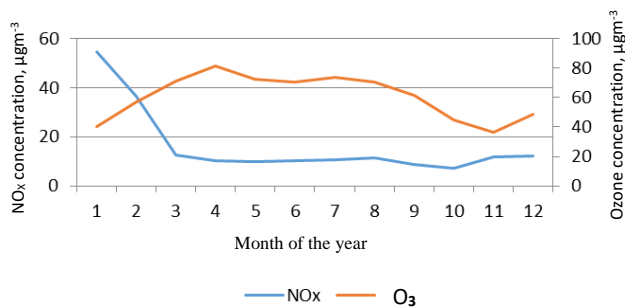


Diagram 1 - Average monthly concentrations of nitrogen oxides and ozone for AMS-1-Zenica-Centar for the year 2020.

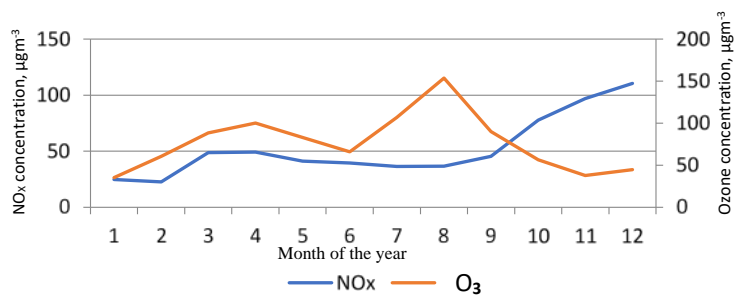


Diagram 2 - Average monthly concentrations of nitrogen oxides and ozone for AMS-2-Zenica-Radakovo for the year 2020.

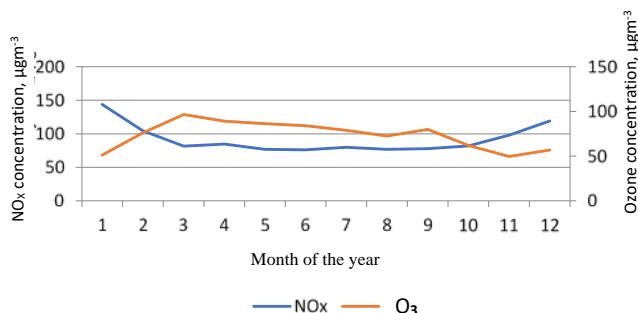


Diagram 3 - Average monthly concentrations of nitrogen oxides and ozone for AMS-3-Zenica-Tetovo for the year 2020.

Diagrams 1, 2 and 3 show an indirect dependence between NO<sub>x</sub> and O<sub>3</sub> concentrations, which was to be expected. Namely, ozone is formed by the degradation of NO<sub>2</sub> photochemically, with the effect of UV rays. This dependence also proves the formation of photochemical smog, reactions 1, 2 and 3. The highest average concentration of ozone was recorded at AMS-2-Radakovo, in the month of August, and was 153.72 µg/m<sup>3</sup>. As the automatic measuring station AMS-2 in Radakovo is near the main road M 17, this could be the key reason why the ozone concentration is higher in Radakovo compared to the ozone concentrations in Zenica City Center and Tetovo. The lowest average monthly ozone concentrations for 2020 were recorded at the automatic measuring station AMS-1 in the center of the city of Zenica. The reason for this may be that the measuring station is located far from the M-17 highway as well as from the Zenica industrial zone, where nitrogen oxides are also emitted by the burning of fossil fuels.

The lowest ozone concentrations at all three measuring stations were recorded in the first, eleventh and twelfth months of 2020. This is also to be expected, because in the mentioned months there is the least amount of sunlight in the Zenica basin, which means that there is the least possibility of more intense photochemical reactions of ozone formation. The highest concentrations of nitrogen oxides NO<sub>x</sub> diagrams 1, 2 and 3 were recorded in the mentioned three months, which directly confirms the deficiency of photochemical reactions of ozone formation through NO<sub>2</sub> degradation. In the mentioned three months, analyzing the average NO<sub>x</sub> concentrations depending on the



location, the city center of Zenica, Tetovo and Radakovo, the highest average monthly NO<sub>x</sub> concentration was recorded in Tetovo, AMS-2, which for the month of January 2020 is 143.13 µg/m<sup>3</sup>, diagram 2. The reason for this is the burning of fossil fuels in thermal power plants in the industrial zone of Zenica.

#### 4. CONCLUSION

The results presented in this paper prove the formation of photochemical ozone in the troposphere of the city of Zenica. This is confirmed by the indirect dependence between NO<sub>x</sub> and O<sub>3</sub> concentrations, that is, the areas on the diagrams where the NO<sub>x</sub> concentration is lower than the O<sub>3</sub> concentration, diagrams 1-3.

The key factors in increasing the concentration of photochemical ozone in the troposphere of the city of Zenica are:

- Increased intensity of car traffic. By comparing data on ozone concentrations measured at stationary automatic measuring stations AMS-1-Zenica-Centar, AMS-2-Zenica-Radakovo and AMS-3-Zenica-Tetovo in 2020, it was found that the highest average ozone concentration was recorded at AMS-2-Radakovo located near the main road M 17;
- Combustion of fossil fuels in thermal power plants. Analyzing the average NO<sub>x</sub> concentration depending on the location, Zenica City Center, Tetovo and Radakovo in the first, eleventh and twelfth months of 2020, the highest average monthly NO<sub>x</sub> concentrations were recorded in Tetovo, AMS-2;
- Intensity of solar radiation. The lowest ozone concentrations at all three measuring stations were recorded in the first, eleventh and twelfth months of 2020, i.e. in the months with reduced intensity of solar radiation. In the mentioned three months, the concentrations of nitrogen oxides NO<sub>x</sub> are the highest at all three measuring stations, which directly confirms the deficiency of the photochemical reactions of ozone formation through the degradation of NO<sub>2</sub>.

Reducing the intensity of traffic of motor vehicles with internal combustion engines, and the reduced intensity of burning fossil fuels in thermal power plants are the key factors leading to the reduction of photochemical ozone emissions in the city of Zenica.

#### REFERENCES

- [1] Dr. Jovan Đuković, Hemija atmosfere, Rudarski institut Beograd, Beograd, 2001. p.36, 59.
- [2] D.H. Nguyen, C. Lin, C.T. Vu, N. K. Cheruiyot, M.K. Nguyen, T.H. Le, W. Lukkhasorn, T.D.H. Vo, X.T. Bui, Environ. Technol. Innov. 28 (2022) 102809.
- [3] Y. Zhao, Y. Li, A. Kumar, Q. Ying, F. Vandenberghe, M.J. Kleeman, Atmos. Environ. 285 (2022) 119224.
- [4] M. Tomljanović, Anorganska kemija, Hijatus, Zenica, 2004. p.194.
- [5] Prof.dr. Jovan Đuković, Aerozagađenje, D.P. Institut zaštite i ekologije, Banja Luka, 2000. p.61.
- [6] Izvještaj o rezultatima kontinuiranih mjerenja zagađenosti zraka u Zenici za 2020. godinu, Institut „Kemal Kapetanović, 2020.



## METHODS FOR THE DISPOSAL AND STORAGE OF FLOTATION TAILINGS

Sandra Milutinović, Ljubiša Obradović, Daniel Kržanović,  
Miomir Mikić, Radmilo Rajković

Mining and Metallurgy Institute Bor., Zeleni bulevar 35, 19210 Bor, Serbia

### Abstract

*Flotation tailings ponds vary significantly in size, design, complexity, and method of operation. In some countries, companies neglect the storage of tailings, which is why various accidents happen to them. Lousy design and inadequate operational management are the two main causes of almost all accident situations that occur at tailings ponds. The method by which the tailings will be stored depends on the mining company, their way of preparing mineral raw materials, the characteristics of the tailings, as well as the location where the tailings are stored. This paper describes in detail the methods of tailings storage. It discusses the different options a mining company has for tailings storage as well as the complexity of their design and operation.*

**Keywords:** Tailings, storage methods,

### 1. INTRODUCTION

A tailings pit is a mining facility that forms a fenced area (natural or artificial) and is used for the permanent deposit of waste material. After extraction of useful components, from consumption for the preparation of mineral raw materials, from metallurgical plants, etc. a large amount of waste material is obtained - tailings, which, if not adequately deposited, can endanger the environment and cause an ecological disaster. This problem imposes the need for the construction and operation of such an object to be safe in terms of safety, to prevent even the smallest mistake that would endanger the living and working environment.

Each tailings storage facility is unique and must be designed according to the conditions specific to its location. The method of operation at one particular tailings pit may not apply to another tailings pit, even though for example the raw material that has undergone preparation is the same. Considering the requirements and policies of the mining company, the designers and operators of the tailings pit must overcome many challenges to meet the goals and objectives storage of tailings in a certain place. The various tailings storage methods discussed in this paper help meet site-specific requirements and reduce the risk of catastrophic accident situations. Strict regulations will ensure that environmental protection comes first and that adequate design and application of modern technology reduce the risks associated with tailings storage. Izbor metode skladištenja jalovine na jalovištima je podeljeno u nekoliko faza. Prva faza je da se sagledaju različite alternativne opcije za rukovanje jalovinom pre razmatranja njenog skladištenja na jalovištima. Alternativne opcije za skladištenje ili utrošak jalovine bez njenog deponovanja na jalovištu su [1]:

- disposal in abandoned mine pits, underground burial, and/or disposal at sea;
- practical use of tailings (eg construction material).

Tailings toxicity has a dramatic impact on the environment and should be taken into account when designing a tailings storage facility. The storage of process water in tailings ponds is a particular challenge for water management and, in the event of a tailings dam breach, water can act as a transport mechanism for tailings leaving the tailings pond [2].

The tailings are either pumped or gravitated through pipelines or open channels, from the plant for the preparation of mineral raw materials to their final location at the tailings pond.

## 2. TAILINGS STORAGE AT TAILINGS PONDS

The method of tailings storage depends on both the soil's natural forms and the tailings' characteristics as a waste material. The three main methods for tailings disposal are [3]:

- Storage in cassettes or cells,
- Storage in valley reservoirs – cross valley, side hill, and valley bottom;
- And on old surface mines pit.

### 2.1 Storage of tailings in cassettes or cells

To reduce the negative impact on the environment and minimize the risks that always come with large objects filled with water and sludge, such as flotation tailings, it is possible that all mining waste generated during the exploitation and processing of ore in surface mines and flotation, using the new Integral Waste Management Facility (IMWF), they dispose together at the exact location. In this way, the construction of a classic flotation tailings pond is eliminated, that is, the permanent risk that can be caused to the environment, facilities, and population located downstream from the tailings pond due to damage to the dam caused by an earthquake or some other weather event is eliminated.

The method of storing mining wastes generated during the exploitation and processing of ore in surface mines and flotation was applied in the Ada Tepe Gold Mine in Kumovgrad (Bulgaria). The concept of the IMWF in Kumovgrad is that the thickened tailings, which have been dried to a paste consistency, are placed in cells-cassettes built from mine tailings. The IMWF is made in two small valleys, functioning as two separate facilities at the beginning of the project, and will later be merged into one facility, Figure 1 [4].

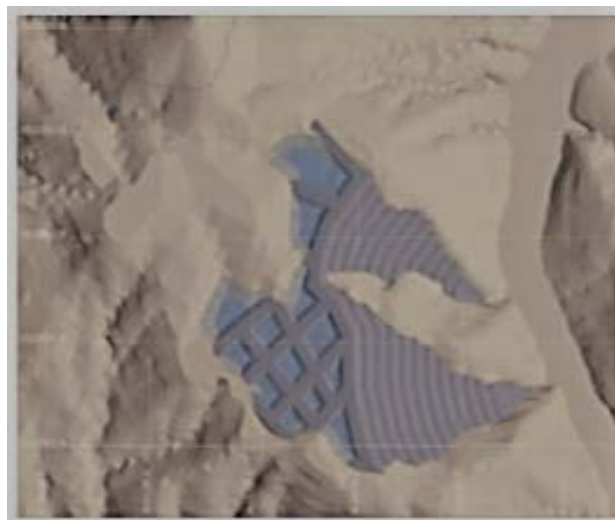


Figure 1 - IMWF conceptual layout

### 2.2 Storage in valley accumulations

Storage in valley reservoirs is usually used to take advantage of the natural topography of the land. The three main types of such storage are cross-valley, side-hill, and valley-bottom designs. The cross-valley design is similar to a conventional storage arrangement, where an embankment is placed across the valley to enclose the drainage space. Figure 2 shows one such tailings dump in Majdanpek.



Figure 2 - Tailings pond Šaški Potok in Majdanpek, Google Earth, 2023.

The design of the side hill tailings pond relies on containment by embankments on three sides [5]. This type of tailings pond design is shown in Figure 3, where it can be seen that dams have been built on two sides and embankments on the third. The side hill design is best suited for slopes less than 10%, because the steeper the slope, the greater the fill volume required in the embankments relative to the achievable storage volume [6].



Figure 3 - Field 1 - Veliki Krivelj, Google Earth, 2023.

Valley floor reservoirs are considered where the valley span is too large and high water runoff is a challenge for cross-valley storage. Valley floor reservoirs are actually a compromise between cross valley and side hill designs and are usually built in multiple formations similar to side hill facilities.

### 2.3 Storage in old surface mines pit

Tailings storage at old open pits is simply the process of backfilling abandoned open pits with tailings. Figure 4 shows this storage design, showing the RTH tailing pit in Bor, which was created on the surface of the old ore body H. This method is very popular for mining companies because the costs are lower due to the developed areas that can be filled with tailings. Another advantage of storage in old surface mines is that such tailings do not require the construction of dams and levees, thereby eliminating the risks associated with levee instability.





Figure 4 - Tailings on the surface of the ore body H - Bor, Serbia, Google Earth, 2023.

### 3. CONCLUSION

Each tailings storage facility is unique and must be designed according to site-specific conditions. The method of designing the operation of one particular tailings pond does not necessarily have to be applied to another tailings pond. Considering regulations, requirements and policies of mining companies, tailings designers must overcome many challenges in order to meet the goals and objectives of tailings storage at a particular site. The various methods of tailings storage discussed in this paper provide an overview of how tailings are stored and help meet site-specific requirements for the construction of a tailings facility. Strict regulations and laws will ensure that environmental protection comes first and that adequate design and application of modern technology reduce the risks associated with tailings storage. This particularly applies to countries where tailings landfills have failed with catastrophic consequences, or where abandoned closed tailings storage facilities cause significant environmental pollution.

### ACKNOWLEDGEMENTS

*This work was financially supported by the Ministry of Education, Science and Technological Development of the Republic of Serbia, contract no. 451-03-47/2023-01/200052.*

### REFERENCES

- [1] G.M. Ritcey, Tailings Management: Problems and Solutions in the Mining Industry (Vol. 6), Elsevier, Amsterdam, New York. ISBN: 0444873740,1989
- [2] G.E. Blight, Destructive mudflows as a consequence of tailings dyke failures. Proceedings of the Institution of Civil Engineers, Geotechnical Engineering, 125 (1),1997, p.9–18
- [3] W. Darron, M. Dixon-HardyJon, Land Contamination & Reclamation 15(3),2007, 301-317
- [4] T.E. Golder, B. Wickland, A. Goldstone, M. Kissiova, Integrated mine waste storage concept, Krumovgrad Gold Project, Bulgaria,2011., <https://doi.org/10.14288/1.0107692>,
- [5] D. Norman, Innovations and trends in reclamation of metal mine tailings in Washington. Washington Geology, 26 (2/3),1998, p.29–42
- [6] S.G. Vick, Planning, Design and Analysis of Tailings Dams. 2nd ed. BiTech, Vancouver,1990, ISBN: 0921095120

## METHODS OF TRANSPORTATION AND DISCHARGE OF TAILS TO FLOTATION TAILINGS POND

Sandra Milutinović<sup>1</sup>, Milena Kostović<sup>2</sup>, Ljubiša Obradović<sup>1</sup>,  
Srđana Magdalinović<sup>1</sup>, Sanja Petrović<sup>1</sup>

<sup>1</sup> Mining and Metallurgy Institute Bor., Zeleni bulevar 35, 19210 Bor, Serbia

<sup>2</sup> Faculty of Mining and Geology, University of Belgrade, Đušina 7, 11120 Beograd, Serbia

### Abstract

*There are different ways of transporting tailings to flotation tailings, this paper presents all of them that are in use in Europe. For conventional storage, tailings are generally discharged from outfalls located along the embankments (dams) of the facility. For surface thickened disposal and paste storage, the tailings are generally discharged from a central location - either through risers or from point sources that are raised during the life of the plant. There is also dry stacking of tailings, which is usually done using conveyors or trucks.*

**Keywords:** *Tailings, transportation, discharge, methods*

### 1. INTRODUCTION

In order for a tailings pit to be safe for use, tailings engineers must study the characteristics of the tailings, the cycle of deposition, the climate, etc. The characteristics of the tailings can greatly influence the behavior of the tailings during transport and after their discharge into the tailings dumps. Also, the appearance of the tailings pond and the characteristics of the embankment should be considered. In general, tailings are transported from the plant for the preparation of mineral aggregates to the tailings dump via pipelines.

As tailings are disposed of, they flow out of the outlet and natural segregation occurs. The degree of this segregation essentially depends on the size range of the tailings particles and the density of the slurry pulp [1]. As the degree of tailings densification increases, there is less suspension to carry the coarse fraction, and the tailings begin to settle closer to the point of discharge where they lead to an unsegregated suspension. When this stage is reached, the voids in the coarse suspension fraction are filled with fine ones, resulting in a homogeneous mixture.

If the pulp density is low, the coarse tailings fraction is deposited closest to the discharge point, while the finer material is carried farthest. In the work of the author Vick [1], he notes that for most types of tailings, the expected beach slope is 0.5–2.0 % in the first few hundred meters and that the higher the density of the pulp and/or the coarser the gradation of the overburden, the steeper the beach and the greater the slope.

### 2. METHODS OF TRANSPORTATION AND DISCHARGE OF TAILS TO FLOTATION TAILINGS POND

There are three general methods of settling tailings:

- single point discharge,
- spigot and
- cyclonication.

There are variations on all of these methods and the methods can be used in combination to meet design criteria set by tailings engineers.

## 2.1 Single point discharge

Single-point discharge is the technique of discharging tailings through a pipeline from one side of the tailings pit. This method is often used with reservoirs that discharge tailings upstream of the lake and dam (ie, not from the top of the dam). Single-point discharge can also be used for tailings that are at lower elevations than the treatment plant, so the tailings are gravity stored in the tailings via pipelines. One such example is the "Šaški Potok" accidental tailings pond, which is located near Majdanpek and is used for accidental situations in case of unforeseen stoppages and breakdowns in the flotation concentration plant, Figure 1.



Figure 1 - Flotation tailings pond Šaški Potok

## 2.2 Spigotting

Spigotting is a technique of discharging tailings through small pipes originating from multiple points at regular intervals along the tailings weir line [2]. The method is used to achieve a uniform flow of tailings, which in theory will create uniform beaches. However, attention should be paid to leveling the beach on all sides of the tailings pond, which is why these spigots must be moved. The spigots form a gently sloping beach where the coarsest fraction is deposited near the discharge point, and the fine fraction (sludge) is deposited progressively further away from the discharge point. As a result of this, the density, stability, and permeability of deposited solids decrease with increasing distance from the point of discharge, which gives greater stability to the dams and embankments themselves. Figure 2 shows the "Valja Fundata" flotation tailings pond located in Majdanpek, where this method was applied to Dams 1 and 5.



Figure 2 - Tailings pond Valja Fundata in Majdanpek

## 2.3 Cycloning

Hydrocyclone sand (coarse tailings fraction) can be used to build tailings dams during active deposition. Mining companies usually see cost savings as the main advantage of using coarse fractions in this way. Since the sand is produced from the material that is deposited, all costs associated with the acquisition of materials for the construction of the embankment are eliminated



or significantly reduced, Figure 3. This practice also reduces the total volume of tailings deposited in the reservoir, since at least part of the coarse fraction is used in construction. dams.



Figure 3. - Using a hydrocyclone to build a dam

The method used to separate the fine from the coarse fraction in the total tailings is cyclonication. Cyclones are simple mechanical devices used to separate coarse and fine particles from suspension by centrifugal action. As the tailings, moving under pressure, enter the cyclone, the fine particles and most of the water rises to the upper outlet. Large particles spiral down through the conical part and exit at the bottom. The separated fine fraction is called dressing, and the coarse fraction is called sand. The sand is used to build dams and embankments on tailings, while the overflow is discharged through a special pipeline to the reservoir itself.

The overflow and sand should be monitored regularly to measure pulp densities, gradation, and cyclone inlet pressure. Cyclone adjustments are required to maintain pulp density and grain size goals. Certain criteria should be taken into account when assessing whether cyclones can be an effective tool in the construction of embankments on tailings.

Cyclone sand should have a permeability that is sufficiently higher than the tailings deposited in the reservoir, also the sand should allow rapid drainage after discharge to facilitate the handling and spreading of the sand. The amount of cycloned sand must be large enough to allow the dam to be raised if necessary to maintain adequate volume.

If it happened that the amount of sand decreased, the costs could increase because it would be necessary to use some other materials for the construction of the dam. Tailings containing less than 60 percent of particles passing a No. 200 sieve are considered to contain sand of acceptable quality for use in cyclones. During the sampling campaigns, the work of the hydrocyclone on the dams is checked, in order to determine the granular composition of the sand of the hydrocyclone in order to define the content of the class -0.074 mm (reference class). The content of this class for tailings in Eastern Serbia is limited to a maximum of 15% in hydrocyclone sand, and this should be adhered to, because embankments and dams are stable only when they are dry and when high-quality sand is incorporated into them, as few fine silty particles as a possible tendency to retain water

Two basic methods of cyclones that are common in tailings ponds:

- central cyclone (or stationary cyclone) i
- cyclones on the dam.

The third method, hydraulic cyclone, is a more sophisticated method that is used less often. A central cyclone method in which a single permanent or semi-permanent high-capacity cyclone is placed at a strategic location, often at a dam abutment that is larger than the designed crest of the dam. Excavation machinery moves tailings sand from the landfill to the embankment where it is



deposited and compacted. Construction machinery lays and compacts the sand where it acquires a high relative density. Therefore, the method is suitable for use in areas subject to seismic activity.

A dam cyclone system consists of several cyclone units mounted on towers, skids, trucks, scaffolds, or suspended from cranes placed along the top of the dam. The number of cyclones is determined by the size of the cyclone. The cyclones move as the sandbanks raise the height of the dam. The cyclone system on the dam is cost-effective because the sand is placed hydraulically in its final place, no mechanical action is required. One disadvantage of this method is that non-mechanical placement results in lower relative densities, which generally range from 30 to 68 percent, as reported in the work by Lighthall [2].

Using the hydraulic cell method, diluted cyclone sand is deposited in cells with a berm on the embankment. The tailings are cycloned in a central cyclone and water is added to facilitate pipeline transport to the tailings cells. The solids in the cells are then allowed to settle before the excess water is decanted from the end of the cell opposite the discharge point.

### **3. CONCLUSION**

Each tailings storage facility is unique and must be designed according to site-specific conditions. Each of these methods of transporting tailings to the tailings dump has its pros and cons, you just need to choose the best one, based on the characteristics of the material being replenished and based on the location and type of terrain on which the tailings dump is located.

### **ACKNOWLEDGEMENTS**

*This work was financially supported by the Ministry of Education, Science and Technological Development of the Republic of Serbia, contract no. 451-03-47/2023-01/ 200052.*

### **REFERENCES**

- [1] Vick, S.G., Planning, Design and Analysis of Tailings Dams. 2nd ed. BiTech, Vancouver, 1990, ISBN: 0921095120
- [2] Lighthall, P.C., B.D. Watts and S. Rice. 1989. "Deposition Methods for Construction of Hydraulic Fill Tailings Dams." In: Geotechnical Aspects of Tailings Disposal and Acid Mine Drainage. The Vancouver Geotechnical Society, Vancouver, British Columbia, May 26, 1989.

## MICROSTRUCTURAL AND MECHANICAL CHARACTERIZATION OF ARMOR STEEL JOINT WELDED WITH SANDWICH DESIGN

Uğur Gürol<sup>1,2</sup>, Ceren Çelik<sup>3</sup>, Müesser Göçmen<sup>2</sup>, Mustafa Koçak<sup>4</sup>

<sup>1</sup>Welding Technology Research and Application Center, Istanbul Gedik University, Türkiye

<sup>2</sup>Department of Metallurgical and Materials Engineering, Istanbul Gedik University, Türkiye

<sup>3</sup>Department of Mechanical Engineering, Istanbul Gedik University, Türkiye

<sup>4</sup>Department of Mechatronics Engineering, Istanbul Gedik University, Türkiye

### Abstract

*The armor steel plates are well known for their superior mechanical and ballistic performances and hence used in the fabrication of armor vehicles. These steels are traditionally welded by austenitic stainless steel (ASS) welding wires to prevent hydrogen-induced cracking. However, the armor steel plates show poor ballistic performance when using such strength under-matching stainless-steel wires. The present study aims to investigate the effect of the sandwich butt joints using low hydrogen ferritic (LHF) wires between the soft ASS weld layers on the mechanical performance of robotic gas metal arc welded armor steel plates. Mechanical properties of such multi-material but-joints were evaluated using hardness, tensile, and Charpy V-notch impact tests. Results were correlated with microstructural characterizations at various locations across the joint using stereo, optical, and scanning electron microscopes. As a result, the sandwich joint showed increased hardness values between the ASS layers and met the base metal's minimum Charpy impact requirement. These findings suggested that a new joint design using multiple welding wires will increase the strength of the joint and hence better impact toughness and ballistic performance of the welded armor steel plates.*

**Keywords:** Armor steel, Gas metal arc welding, Sandwich joints, Microstructure, Mechanical properties

### 1. INTRODUCTION

Armor steels are used in the fabrication of special high-performance and safety-related vehicles because of their high hardness, strength, and impact energy absorbing properties [1]. Improving the impact penetration resistance of such steels by layering them with materials having different properties was started to be performed in the late 1800s. [2]. Most of the studies in the literature mainly focused on improving the ballistic performance of armor plates using hard-facing process with arc welding [3]. The weld regions are commonly considered the weakest region of the armored steel structures since they are usually welded at lower strength (which creates undermatching joints susceptible to a plastic strain concentration during impact loading) welding consumables. However, the improved mechanical performance of such weld joints could be achieved through careful selection of welding parameters, filler materials, and weld joint design. [4,5]. On the other hand, these steels are prone to hydrogen-related delayed cracking (Hydrogen induced cracking, HIC) and/or restraint cracking during the service and fabrication due to hard martensitic phase formations at heat-affected zone (HAZ) regions. Therefore, lower strength (than armor steel) austenitic welding consumables having a high tolerance for dilution are commonly used in the joining of armor steel plates due to the low diffusibility of hydrogen in the weld metal to HAZ in the austenitic phase [6]. However, the armor steel joints welded with austenitic stainless-steel wires show poor ballistic performance compared to base metal due to the inherently lower strength weld metal region. Madhusudhan et al. [7] reported that the ballistic performance could be improved by depositing a hard-facing alloy material as the middle layer in the welds to build ballistic-resistant structures. The weld joints of the armor plates with high fracture toughness

materials at the top face and root regions of the butt-joint while utilizing weld material with high hardness and tensile properties in the middle layers of the weld joint would be an alternative and new joint design to increase ballistic performance without sacrificing the overall toughness properties. Based on this new design approach, the current project has started to examine various combinations of joint designs. This study is reporting only a part of this large research project. The results of the investigations on the multi-material joint with the low-alloyed high-strength ferritic wire (ER 110S-G) used for depositing the middle layer of the austenitic weld will be presented in this paper. The aim was to study the effect of the higher strength mid-section weld layer on microstructural features and mechanical properties of the armor steel joint.

## 2. EXPERIMENTAL PROCEDURE

Milux-OY Company manufactured high-strength armor steel plates (MIL-A 46100, Protection 500) with dimensions of 15 mm x 150 mm x 350 mm were machined to have a bevel angle of 30°. A ceramic backing was utilized to smooth the back/root bead formation, and a 2 mm root opening was kept forming a 60° V-groove butt joint. Armor steel plates were welded with 5 straight stringer passes (no oscillation) using the robotic GMAW method. The new joint design, which has an austenitic stainless steel capping face layer, ferritic welding wire in the interlayer, and austenitic stainless steel root layer, is termed the "sandwich" joint. The commercially available austenitic solid wire of ER 307 and low-alloyed high-strength ferritic wire (ER 110S-G) having a 1.2 mm diameter were used as filler metal to obtain sandwich joints. The purpose of using high-strength ferritic wire in the middle passes of the joint was to allow a comparative study of different combinations of armor steel welds with respect to hardness, tensile, Charpy impact tests and microstructural evolutions. The certified chemical composition of base metal and the filler metals are listed in Table 1.

Table 1 - Chemical composition of the base metal and filler materials used (wt.%)

Materials	C	Mn	Si	Cr	Ni	Mo
Base metal (Protection 500)	0.21	1.02	0.49	0.62	0.42	0.29
Welding wire SG 307	0.06	6.41	0.54	17.71	8.52	0.02
Welding wire ER 110S-G	0.09	1.75	0.54	0.26	1.45	0.25

The following welding parameters with low spatter welding mode were used for welding armor plates: Arc current of 205-220 A, Arc voltage of 18-20 V, and welding speed of 26-27 cm/min. A mixture of 97.5% Argon and 2.5% CO<sub>2</sub> and a mixture of 82% Argon and 18% CO<sub>2</sub> gases were utilized as the shielding gases with a flow rate of 15 L/min for austenitic and ferritic wires, respectively. The heat input was kept between 0.88 – 0.97 kJ/mm to obtain a narrow softened region at heat affected zone. A preheating procedure (135-165°C) was performed before the ferritic pass to prevent hydrogen embrittlement and solidification cracking.

The soundness of the sandwich joint was checked using liquid penetrant testing and X-ray testing to check for any embedded cracking or interlayer defects. Mechanical characterizations were realized by Vickers hardness, tensile, and Charpy V- impact tests. The macrostructures and microstructures at various locations were analyzed through stereo microscope (SM), optical microscope (OM), and scanning electron microscopy (SEM).

## 3. RESULTS AND DISCUSSION

Figure 1a shows the macro-section of the sandwich butt joint where the root and top regions are made of austenitic welding wire. No significant defects were found in the weld seam, such as pores, cracks, or others. The liquid penetrant and X-ray inspections also confirmed the soundness of this multi-material welded joint. The microstructures of various locations of the sandwich joint, including the capping layer, mid-layer and root pass are shown in Figure 1b-d. The microstructure

of the undiluted stainless steel capping layer and root pass (Fig. 1b and d) clearly showed the presence of  $\delta$  ferrite structures (dark regions) in an austenitic matrix (bright regions). In contrast, the mid-layer welded using low hydrogen ferritic filler material exhibited a martensitic matrix with metal carbides precipitated along the grain boundaries (Fig. 1c) due to mix of ASS and LHF weld regions.

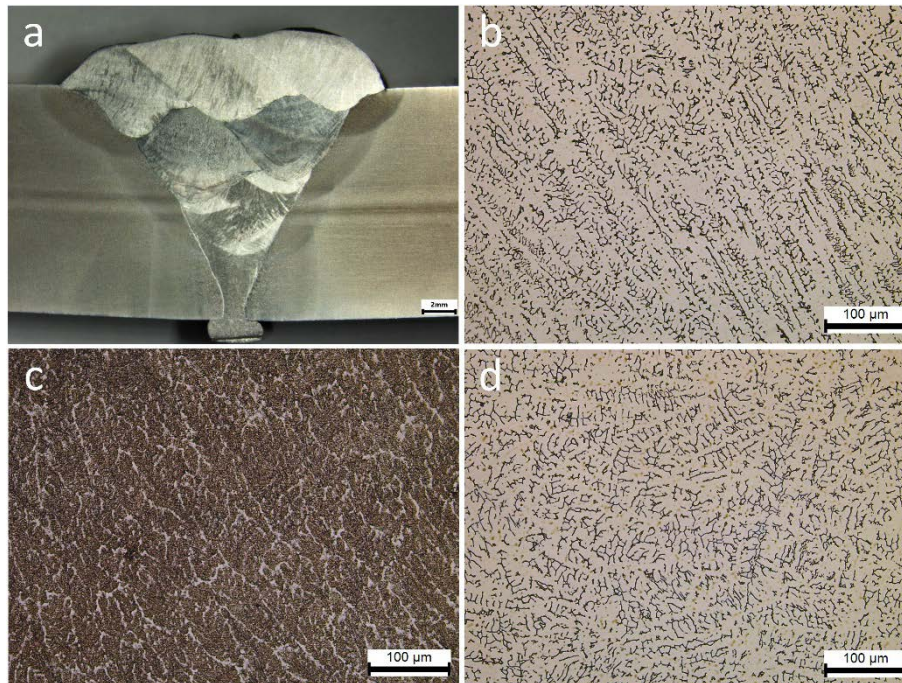


Figure 1 - Macroscopic appearance of the sandwich joint (a) and optical micrographs taken from the (b) capping layer, (c) middle layer and (d) root pass.

Vickers hardness tests were performed across the weld joint, including base metal, HAZ, and weld metal, with 0.5 mm intervals. The summary of the results is listed in Table 2. The lowest hardness in the weld region was obtained at about  $212 \pm 15$  HV at capping layers (5<sup>th</sup> layer), depending on the mechanical properties of the austenitic filler material. However, due to dilution and faster cooling rates, the austenitic weld regions tended to increase hardness values from the cap region to the root. The higher hardness values exceeding 400 HV were obtained in mid regions (where LHF wire was used) due to forming a martensitic matrix with metal carbides. On the other hand, the minimum hardness value of 477 HB permitted, according to the related MIL-A-46100 standard, for the base material (equivalent to 509 HV) must be achieved at a maximum of 15.9 mm measured from the toe of the weld on any ballistic surfaces [8]. In this study, the hardness values obtained 15.9 mm from the weld toe were found to be higher than the minimum hardness of 509 HV permitted by MIL-A-46100, confirming that the HAZ width of the sandwich joint met the minimum requirements of MIL-STAN-1185 standard. Additionally, the tensile strength of base metal was measured at  $1756 \pm 15$  MPa, while the transverse tensile of the sandwich joint was found to be  $837 \pm 5$  MPa, indicating a reduction of ~52 % in tensile properties, which is much higher than the conventionally fabricated 100% austenitic weld joint.

Table 2 - Hardness test results (HV) from the root (1<sup>st</sup> layer) to the capping (5<sup>th</sup> layer) layer

1 <sup>st</sup> layer	2 <sup>nd</sup> layer	3 <sup>rd</sup> layer	4 <sup>th</sup> layer	5 <sup>th</sup> layer
$265 \pm 7$	$248 \pm 9$	$239 \pm 18$	$432 \pm 26$	$212 \pm 15$

The Charpy impact test results of base metal were found at  $20 \pm 3.4$  J, while weld and HAZ regions of the sandwich joint were found at  $31.4 \pm 1.8$  and  $65 \pm 16.7$ , respectively, as listed in Table 3. The weld regions showed 57 % higher ductility than base metal because of using austenitic stainless

steel filler metal at capping and root layers. The results indicated that impact toughness tests in both weld and HAZ regions met the minimum requirements of MIL-A-46100 (16.27 J in transverse and 18.98 J in longitudinal direction).

Table 3 - Charpy impact test results (at -40°C)

Weld region	HAZ	Base metal
31.4±1.8	65±16.7	20±3.4

#### 4. CONCLUSIONS

This study investigated the microstructural and mechanical properties of the sandwich armor steel butt joints. The austenitic (SG307) wire was used for the capping and root layer, while the low-hydrogen ferritic wire (ER 110S-G) was used after root passes for the mid-layer of the butt joint. The main conclusive results are listed below.

1. The Protection 500 armor steel plates were successfully welded using a sandwich joint design with the robotic GMAW process at low heat input (0.88 – 0.97 kJ/mm). No defects, such as cracks and porosity, were found in the weld metal.
2. The use of low-hydrogen ferritic wire at the mid-section of the joint increased hardness values over the 400 HV at the mid-layer, which suggests a new design creates the opportunity for increased ballistic performance of the armor steel plate joints.
3. The width of the HAZ was obtained within the range accepted in the military standard MIL-STAN-1185 (max. 15.9 mm from the toe of the weld).
4. The impact values of the weld zone were found to be 57 % higher than the base material, confirming that the reported sandwich type of joint design is suitable for obtaining better impact properties for the welded joints of the armor steel plates. These results strongly indicate that the ballistic test results will also show better and improved performance for the joint with mid-section with higher strength weld material.

#### ACKNOWLEDGEMENTS

*This study has been supported by the Scientific and Technological Research Council of Turkey (TUBITAK) with project number 5210029. The authors also wish to thank Miilux OY Steel Company and Mr. Mert Basmacı for the steel plates' provisions and the preparations for welding.*

#### REFERENCES

- [1] M. Balakrishnan, V. Balasubramanian, G. Madhusudhan Reddy, P. Parameswaran, Metall. Mater. Trans. A, 44 (2013), 4218-4229.
- [2] M. Balakrishnan, V. Balasubramanian, G.M. Reddy, Def. Technol., 9 (4), (2013) 249-258.
- [3] S.H. Choo, E.R. Baek, S. Lee, Metall. Mater. Trans. A, 27 (1996) 3335–3340.
- [4] O. Coban, U. Gürol, S. Erdöl, M. Koçak, 6th International Conference on Welding Technologies and Exhibition (ICWET'21), 13-15 October 2021, Hatay-Turkey, Paper ID-46.
- [5] C. Çelik, RM. Kurt, O. Çoban, H. Baykal, HK. Akben, U. Gürol, Proceedings of 21st International Metallurgy and Materials Congress, 6-8 October 2022, İstanbul, Turkey, 589-593.
- [6] U. Gürol, T. Karahan, S. Erdöl, O. Çoban, H. Baykal, M. Koçak, Trans. Indian Inst. Met., 75 (2022) 757–770
- [7] M. Balakrishnan, V. Balasubramanian, GM. Reddy, Mater. Des., 44 (2013) 59-68.
- [8] SJ. Alkemade, Defence Science and Technology Organisation, 1996



## ELECTROCHEMICAL CHARACTERISTICS OF THE ANODIZED TITANIUM OXIDE FILMS IN SULFURIC ACID

Branka Pešovski<sup>1</sup>, Milan Radovanović<sup>2</sup>, Vesna Krstić<sup>1,2</sup>,  
Danijela Simonović<sup>1</sup>, Silvana Dimitrijević<sup>1</sup>

<sup>1</sup>Mining and Metallurgy Institute Bor, Zeleni Bulevar 35, 19210 Bor, Serbia

<sup>2</sup>Technical Faculty in Bor, VJ 12, 19210 Bor, Serbia

### Abstract

We presented some research into titanium electrode anodizing in  $H_2SO_4$  solutions in the potential range – 1 to 5 V at different scan rates (10, 50, 100  $mV s^{-1}$ ) by cyclic voltammetry measurements. Linear potentiodynamic measurements had used before and after the oxide layer formed on the Ti- surface. Three characteristic oxide peaks appeared at 0.2 V, 2.3 V, and 3.5 V on CV curves at all scan rates for all  $H_2SO_4$  concentrations. Voltammetric tests showed the passivation of the Ti-surface in all cases. XRD and SEM-EDS measurements confirmed the existence of  $TiO_2$  species in a crystalline form on the Ti surface after anodizing in 3M  $H_2SO_4$  and annealing the anodized Ti electrode at 400 °C in the airflow.

**Keywords:** titanium oxides, cyclic voltammetry, XRD, linear voltammetry, polarization

### 1. INTRODUCTION

The exact nature of formed oxide films on the Ti surface during the anodization process is still not well known, even though, in the study of surface modifications, many of the latest techniques for the investigating properties of such films have been used. A series of different oxides of low-valent titanium is present in the oxide film. Electrochemical dissolution of the passive film occurs at the boundary of the oxide-solution phase, according to eq. (1), where the dissolution is not localized [1]



The quantities of non-stoichiometric oxides obtained within the electrochemically formed oxide film depend on the potential and pH solution. This anodization can be represented according to the reaction (2): [2]



for  $1.5 \leq n \leq 2$

The XRD obtained data indicates the presence of  $Ti_3O_5$  in a dominant  $TiO_2$  matrix. The following reactions of  $TiO_2$  film dissolution in  $H_2SO_4$  solutions occur: [3]



### 2. EXPERIMENTAL

The concentrations of  $H_2SO_4$ : 1.5 M, 1 M, 0.5 M, 0.1 M, and 0.05 M were used. The following measurements into the electrochemical behavior of Ti electrodes were done:

- Scanning of the Ti electrode cyclic voltammograms in  $H_2SO_4$  solutions at different scan rates (10, 50, and 100  $mV s^{-1}$ ); Scans were carried out for five cycles in the potential range of –1 to 5 V; Linear potentiodynamic measurements had taken after measuring the open circuit potential in various concentrations of  $H_2SO_4$  solutions; Passivizing  $TiO_2$  layer is applied by cyclic voltammetry at a scan rate of 50  $mV s^{-1}$ ;



Linear potentiodynamic measurements were performed on a Ti electrode on which a passive TiO<sub>2</sub> film has previously been applied at a scan rate of 1 mV s<sup>-1</sup>; Anodic oxidation of a Ti electrode has performed in a 3 M H<sub>2</sub>SO<sub>4</sub> solution before XRD and SEM-EDS measurements in a CV range of –1 to 5 V at a scan rate of 100 mV s<sup>-1</sup> during five cycles. The working electrode was a Ti plate, the reference electrode was a saturated calomel electrode (SCE), and the auxiliary electrode was a Pt electrode. The working electrode was polished with grinding paper from 280 to 2000 grit and washed with distilled water. The IVIUMSTAT.xRe instrument provided hardware and software support. X-ray analysis had performed on the instrument „Rigaku MiniFlex 600”. The surface appearance and mineralogical composition investigation of the samples SEM (JEOL, JSM IT 300LV) and EDS (OXFORD Instruments) analyses were applied.

## 2.1 Materials and Solutions

The working electrode was made of a titanium plate Grade II, like a spatula shape in the lower part, and dimensions of 1.5 × 1.5 × 0.2 cm, with a handle length of 15.0 cm. The working solution was sulphuric acid, 96 % H<sub>2</sub>SO<sub>4</sub> p.a. quality.

## 3. RESULTS & DISCUSSION

### 3.1 Cyclic Voltammetry

Based on the CV measurements, the growth of the oxide film was usually in the form of a TiO<sub>2</sub> structure. The first peak may occur due to the formation of the Ti oxides with the lower Ti-valence. These would probably be Ti<sup>2+</sup> and Ti<sup>3+</sup> (TiO and Ti<sub>2</sub>O<sub>3</sub>), while the second and third peaks correspond to the forming of TiO<sub>2</sub> films [4]. Unstable Ti<sub>2</sub>O<sub>3</sub> oxide rapidly oxidizes to TiO<sub>2</sub> in contact with water.

### 3.2 Open circuit potential

Open circuit measurements of Ti- and (Ti+TiO<sub>2</sub>)-electrodes had performed for 60 min in different concentrations of H<sub>2</sub>SO<sub>4</sub> solutions and the results obtained are presented in Fig. 3, and Table 1. In Figure 1 it can see that in the H<sub>2</sub>SO<sub>4</sub> solutions, immediately after the electrode immersion, there is a sudden drop in the value of the open circuit potential, which most likely indicates titanium oxide dissolution on the electrode surface.

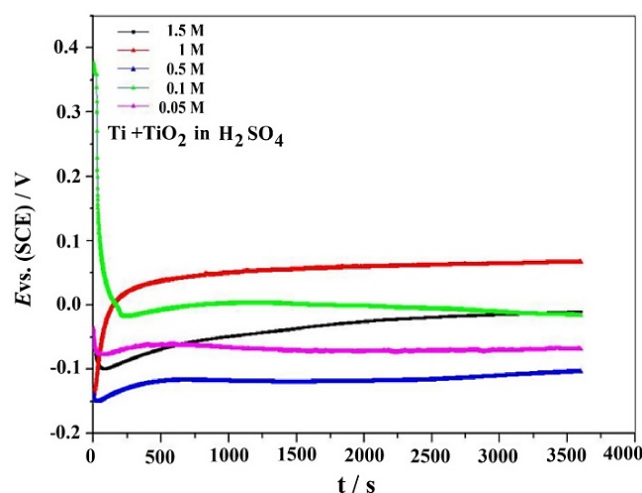


Figure 1 - The plot of the open circuit potential of (Ti+TiO<sub>2</sub>)-electrode in different concentrations of H<sub>2</sub>SO<sub>4</sub> solutions.

Table 1 - The potential values for a Ti-electrode on OCP in different H<sub>2</sub>SO<sub>4</sub> concentrations

Potential on $t = 3600$ s	H <sub>2</sub> SO <sub>4</sub> concentration				
	1.5 M	1 M	0.5 M	0.1 M	0.05 M
$E / V_{SCE}$	-0.0636	-0.0926	0.0166	-0.0205	-0.0363

### 3.3 Linear potentiodynamic measurements

Figure 2 shows polarization curves in the various concentrations of H<sub>2</sub>SO<sub>4</sub> solutions of the Ti- and (Ti+TiO<sub>2</sub>)-electrodes. A rapid formation of the oxide film observes at the beginning of the polarization process. On potentials higher than 1.5 V, there is an increase in the current density that undoubtedly indicates further oxidation of titanium.

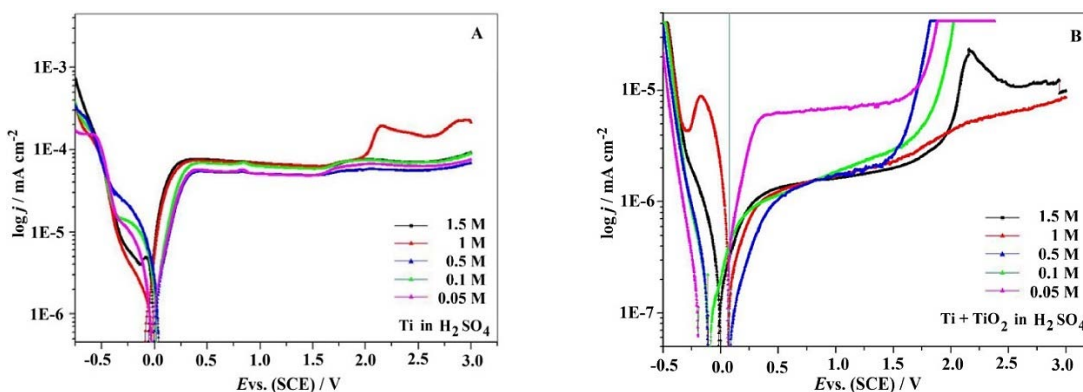


Figure 2 - The potentiodynamic polarization curves in H<sub>2</sub>SO<sub>4</sub> solutions: A) Ti electrodes, and B) (Ti+TiO<sub>2</sub>)-electrode. The scan rate is 1 mV s<sup>-1</sup>.

The kinetic parameters of electrochemical processes have been determined: the corrosion potential ( $E_{corr}$ ), corrosion current density ( $i_{corr}$ ), anodic ( $b_a$ ), and cathodic ( $b_c$ ) Tafel's slopes are presented in Table 2.

 Table 2 - Electrochemical parameters of (Ti+TiO<sub>2</sub>)-electrode.

H <sub>2</sub> SO <sub>4</sub>	$E_{corr}/mV$	$i_{corr}/mA\ cm^{-2}$	$b_a$	$b_c$
1.5 M	$-0.44 \cdot 10^{-2}$	$1.74 \cdot 10^{-4}$	545.26	-283.53
1 M	$7.84 \cdot 10^{-2}$	$1.57 \cdot 10^{-4}$	359.59	-106.90
0.5 M	$-8.86 \cdot 10^{-2}$	$1.18 \cdot 10^{-4}$	597.20	-332.40
0.1 M	$-1.44 \cdot 10^{-2}$	$3.29 \cdot 10^{-5}$	111.98	-671.43
0.05 M	$-7.32 \cdot 10^{-2}$	$2.70 \cdot 10^{-5}$	357.21	-428.33

The influence of the H<sub>2</sub>SO<sub>4</sub> concentration on the coverage degree of the titanium surface with Ti-oxide was presented in Table 3.

 Table 3 - Coverage degree of titanium electrode surfaces with oxide in various concentrations of H<sub>2</sub>SO<sub>4</sub> solutions on constant potentials

H <sub>2</sub> SO <sub>4</sub> concentration	Coverage degree, $\theta$ (%)		
	$E=0.5$ V	$E=1.0$ V	$E=1.5$ V
1.5 M	98.24	97.62	96.78
1 M	98.32	97.43	96.32
0.5 M	98.32	97.04	94.95
0.1 M	98.04	96.54	94.58
0.05 M	88.60	86.11	83.44

#### 4. XRD and EDS analyses of anodized and annealed Ti substrates in H<sub>2</sub>SO<sub>4</sub>

Figure 3 shows the XRD image of the Ti substrate after anodization in 3 M H<sub>2</sub>SO<sub>4</sub> and after annealing the sample at 400 °C in the airflow, previously prepared in the same way. The intensity of peaks for the anatase type of crystals also suggests a thin TiO<sub>2</sub> film formation. The height of the same peaks increases after the annealing titanium electrode at 400 °C, which indicates that the oxide film of anatase becomes thicker after heat treatment.

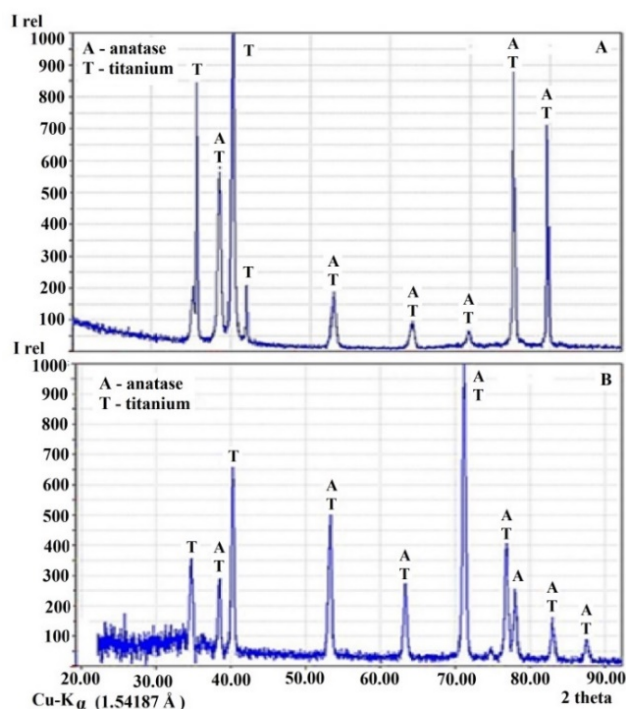


Figure 3 - XRD patterns of Ti electrode: A) after anodizing in 3M H<sub>2</sub>SO<sub>4</sub>, B) after annealing anodized Ti electrode, at 400 °C in the the airflow.

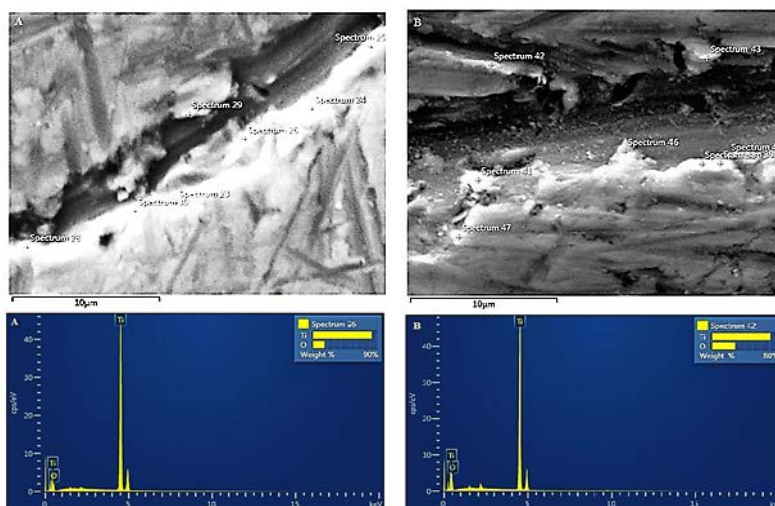


Figure 4 - SEM-EDS images of A) Ti electrode after anodizing in 3M H<sub>2</sub>SO<sub>4</sub>, B) annealed Ti electrode at 400 °C 1 h after anodizing in 3M H<sub>2</sub>SO<sub>4</sub>

SEM-EDS analyses confirm the results obtained by XRD measurements. It can also observe that after anodization on the titanium surface Ti and O<sub>2</sub> species exist. According to chemical analysis, after annealing of titanium, the content of O<sub>2</sub> species increase indicating thicker TiO<sub>2</sub> oxide films (Table 4).

Table 4 - Chemical composition of titanium surface after anodization in 3 M H<sub>2</sub>SO<sub>4</sub> and after annealing at 400 °C at a time of 1 h.

Atomic species	O %	Ti %	Total %
after anodization	17.30	82.70	100.00
after thermal treat.	28.40	71.60	100.00

## 5. CONCLUSIONS

It was observed that TiO<sub>2</sub> is the most stable oxide formed, besides TiO and Ti<sub>2</sub>O<sub>3</sub> oxides. CV measurements indicate the rapid formation of an oxide layer with variations in stoichiometry and morphology. After thermal treatment of the electrode, XRD patterns showed a higher intensity of anatase peaks in the anodized oxide films. SEM-EDS images also confirmed the higher presence of oxides in the heat-treated titanium electrode.

## ACKNOWLEDGEMENTS

*This work was financially supported by the Ministry of Education, Science and Technological Development of the Republic of Serbia, Grant No. 451-03-47/2023-01/ 200052 and No. 451-03-47/2023-01/ 200131.*

## REFERENCES

- [1] T. Ohtsuka, M. Masuda, N. Sato, J Electrochem Soc, 134(10) (1987) 2406-2410.
- [2] O.R. Camara, C.P. De Pauli, M.C Giordano, Electrochim. Acta, 29(8) (1984) 1111.
- [3] D.J. Blackwood, L.M. Peter, D.E. Williams, Electrochim. Acta, 33(8) (1988) 1143.
- [4] G. Blondeau, M. Froelicher, M. Froment, A.H. Le Goff, J. less-common met, 5(2) (1977) 215-222.

## METHANE AS AN UNTAPPED ENERGY POTENTIAL OF THE "SOKO" BROWN COAL MINE

Dusko Djukanovic<sup>1</sup>, Nemanja Djokic<sup>2</sup>, Zoran Aksentijevic<sup>2</sup>,  
Daniel Radivojevic<sup>2</sup>, Branislav Stakic<sup>2</sup>

<sup>1</sup>Technical Faculty Bor, University of Belgrade, V.J. 12, 19210 Bor, Serbia

<sup>2</sup>"JP PEU RESAVICA", P.Ž. 2, 35237 Resavica, Serbia

### Abstract

*Active coal mines in Serbia are not significant sources of methane, except for the "Soko" mine, which has a high methane content. The methane content in the "Soko" mine is so pronounced that it poses a threat to safe coal exploitation. Through mining operations and from old workings, significant amounts of methane are released into the atmosphere from the "Soko" coal deposit. The potential of the "Soko" mine lies in the possibility of exploiting the methane from the deposit and utilizing it for electricity and heat production. On average, over 2 million m<sup>3</sup> of CH<sub>4</sub> are released into the atmosphere from the mine annually, which is enough to operate a 2 MW gas power plant, supplying electricity and heat to 66% of households or 8,800 citizens of Sokobanja. With an initial investment of 3 million euros, the investment would be recovered within 2.5 years.*

**Keywords:** methane, exploitation, green energy, coal

### 1. INTRODUCTION

In the world, coal remains the most significant source of electricity production. According to projections, the largest industrialized economies, emerging economies, and economies in transition will continue to rely on coal as an energy source in the foreseeable future. Currently, coal accounts for 25% of global primary energy, 40% of global electricity, and nearly 70% of the world's steel and aluminum industries. The International Energy Agency (IEA) predicts that new economies will experience a staggering 93% increase in demand for electricity by 2030, largely driven by China and India, with coal expected to be the leading "fuel" to meet the growing needs. Methane (CH<sub>4</sub>) released during coal exploitation creates hazardous working conditions in many underground mines worldwide. Efficient gas (methane) management, however, is not limited to safety concerns alone. Methane released into the atmosphere, particularly from the drainage system, represents a permanent loss of energy source. The resulting emissions also contribute to climate change. Coal mines are significant sources of methane emissions, with methane being the most prevalent greenhouse gas, exceeding carbon dioxide by more than 20 times (IPCC, 2007). [4] Methane accounts for 14% of global anthropogenic greenhouse gas emissions, while coal mines are estimated to contribute 6% of the total anthropogenic methane emissions, equivalent to 400 million tons of carbon dioxide (MtCO<sub>2</sub>e) annually. Future coal mining faces increasing challenges as shallow deposits are depleted and excavated, while deeper deposits become dominant with significant gas content and tectonic disturbances. [5] Some countries aim for complete closure of coal mines and a transition to electricity generation from renewable-green energy sources, while others see an opportunity in exploiting methane from coal deposits during their transition to green energy. Although methane extraction from coal deposits has been ongoing worldwide for some time, significant projects have not yet been implemented in our domestic coal mines. Following the accident at the "Soko" lignite mine in April 2022, operations at the mine were suspended until measures for operational safety and collective protection of workers during mining operations and construction of mining facilities are implemented. One of these measures is methane degasification from deposits through drainage boreholes. This would provide a dual

benefit, as it would not only generate electrical energy but also create safer and better conditions for underground mining. Large amounts of methane are released into the atmosphere from the "Soko" coal deposit through mining operations and old workings, under the influence of the main fan. Releasing methane into the atmosphere brings no economic benefit. The potential of the "Soko" mine lies in the possibility of extracting methane from the deposit and utilizing it for electricity production through methane cogeneration ("Green Energy"), which also yields heat energy that can be used for heating infrastructure facilities, among other things. Coal excavation in the "Soko" mine is carried out using the longwall mining method with cross cuts, roof coal caving, and roof collapse, due to complex geological conditions. This method has been applied in the mine since 1985. It belongs to mechanized excavation methods, where only coal transport from the excavation is mechanized. The mine is ventilated depressurized, using the main mine axial fan type "TURMAG GVhv15-160", located in the surface fan station and connected to the ventilation shaft through an airway. The air distribution system in the mine is diagonal, with one inlet and one outlet air stream. All working areas in the mine are ventilated separately using axial fans and compression flexible pipelines. Control of gas-ventilation parameters is carried out automatically and operationally.

## 2. QUANTITIES OF METHANE FROM THE PERSPECTIVE OF RELATIVE AND ABSOLUTE METHANE EMISSIONS

Quantities of methane in terms of absolute and relative methane emission were obtained from the methane balance report of the "Soko" mine for the period 2000-2020. A part of the Automatic Remote Control system for gas-ventilation parameters was used to obtain this data.

In addition to measuring devices for monitoring other gas-ventilation parameters, the ADK system includes measuring devices for continuous monitoring of methane concentration at characteristic locations in the mine. One of the measuring devices is placed on the path of the total main outgoing air stream in PH-170 (CH<sub>4</sub> meter - 1). Table 1 shows the absolute and relative methane emissions for the observed period.

Table 1 - Presentation of absolute and relative methane emissions for the period 2000-2020

Time period (years)	Absolute methane emission (m <sup>3</sup> CH <sub>4</sub> /min.)	Relative methane emission (m <sup>3</sup> CH <sub>4</sub> /t.)	CH <sub>4</sub> Quantity m <sup>3</sup> CH <sub>4</sub> /year
2000	5.16	21.3	2,719,526
2001	3.69	20.4	1,939,464
2002	4.39	24.3	2,307,384
2003	4.20	20.6	2,207,520
2004	3.60	23.6	1,897,344
2005	2.76	15.5	1,450,656
2006	1.86	14.2	977,616
2007	5.04	33.3	2,649,024
2008	4.29	19.7	2,261,002
2009	5.19	22.9	2,727,864
2010	4.39	17.8	2,307,384
2011	6.59	25.8	3,463,704
2012	5.14	21.6	2,708,986



2013	2.94	13.6	1,545,264
2014	2.71	11.7	1,424,376
2015	5.98	29.9	3,143,088
2016	5.71	34.7	3,009,398
2017	3.54	23.9	1,860,624
2018	0.54	5.8	283,824
2019	1.87	11.9	982,872
2020	1.28	8.9	674,611
Average	3.85	20.07	2,025,787

Analyzing the above-mentioned values, it can be determined that the average annual methane emissions from the RMU "Soko" mine amount to approximately 2,025,787 m<sup>3</sup>. Although the quantities of methane are significant, the extraction of methane from the RMU "Soko" mine has not been purposefully carried out, except through the regular removal of methane from the working areas and ventilation practices aimed at creating normal operating conditions where methane concentrations are reduced to permissible limits. In this case, methane is discharged through the exit air stream and expelled outside through the ventilation shaft. [2]

### 3. METANE DEGASIFICATION METHODS AND COGENERATION

Metane degasification methods used worldwide allow for the drainage (collection) of methane before, during, and after coal mining operations. Degasification is achieved through the use of vertical, horizontal, and inclined boreholes. The construction of degasification boreholes enables additional exploration of the coal seam, identification of geological anomalies, and potential increase in coal reserves. By reducing the methane concentration in the mine air, the safety level of the mine operation is improved, and ergonomic working conditions are enhanced. Vertical degasification boreholes from the surface are designed for pre-drainage of one or more coal seams and/or subsequent degasification of methane from collapsed mined-out areas. Pre-drainage boreholes are constructed 2-7 years before mining a specific part of the coal seam. This method allows for the degasification of 50-90% of methane from the coal seam. Horizontal degasification boreholes are primarily used for pre-drainage of coal seams. Boreholes constructed from preparatory headings enable the drainage of methane from a portion of the coal seam immediately before mining. Since the drainage period is relatively short, approximately 10-20% of CH<sub>4</sub> is drained from the coal seam. Inclined degasification boreholes are constructed from preparatory mine openings, sloping upward into the roof strata or downward into the floor strata. Due to mixing with the mine air, the gas quality in these boreholes is low (below 25-50% CH<sub>4</sub>). [6]

Cogeneration represents the process of producing electrical energy while simultaneously generating thermal energy that would otherwise be lost in condensation processes. The fuel efficiency in condensing power plants is typically around 30-40%, while in cogeneration plants it reaches even more than 85%, precisely because the thermal energy in the form of steam or hot water is simultaneously used for heating or industrial processes. This enables significant savings in primary energy consumption for the same amount of electricity and heat production, leading to lower operational and overall costs, as well as a reduction in the emission of pollutants into the atmosphere that contribute to the greenhouse effect and global warming.

#### **4. EKONOMIC FEASIBILITY**

Based on the monitoring of methane emissions and its release into the atmosphere through the ventilation system from 2000 to 2020, it has been determined that approximately 5,550 m<sup>3</sup> of CH<sub>4</sub>/day is emitted into the atmosphere. According to data obtained from the company "GreenGas DPB," which exploits methane in the Czech Republic, it can be concluded that the potential of the "Soko" mine deposit allows for the construction of a gas power plant with a capacity of 2-3 MW. Information from manufacturers of such systems indicates that the investment for building gas power plants is around 1 million euros per MW. In the case of the "Soko" mine, this would amount to an investment of 2-3 million euros for the construction of the gas facility. Based on the required equipment for implementing degassing operations in the "Soko" mine, the cost structure is as follows: equipment for underground exploration drilling with accompanying tools amounts to 600,000 euros, while the equipment for the pipeline and associated tools costs 108,800 euros. Additional costs are estimated at 50,000 euros, resulting in a total cost of methane degassing of 758,800 euros. The average annual electricity consumption per household in Serbia is a total of 5,048 kWh (Republic Statistical Office, 2020). When all these data are considered and analyzed, a 2,000 kWh gas power plant could generate 17.52 GWh of electricity per year, which is sufficient for approximately 3,470 households. According to the 2022 census, the municipality of Sokobanja has a total population of 13,325 people in 5,209 households. By exploiting methane from the "Soko" coal deposit and constructing a 2 MW gas power plant, electricity could be provided to 66% of households in Sokobanja, equivalent to 8,800 residents. Heat energy could also be provided to a large number of households, which is not included in the calculation. With an investment of approximately 800,000 euros for installing the drainage system in the mine and around 2,200,000 euros for installing a 2 MW gas power plant, by selling only electricity without thermal energy at an average price of 5.2 RSD per kW or 0.0443 euros per kW to households, the investment would be recovered in approximately 28 months, or 2 years and 4 months. The monthly revenue from selling electricity to households would amount to 110,000 euros. [1]

#### **5. CONCLUSION**

The "Soko" coal mine, with its confirmed reserves of high-quality brown coal amounting to 52,000,000 tons, represents a significant asset within the JP PEU Resavica mining complex and holds great potential in the energy sector in the Republic of Serbia. [3] In addition to coal extraction, methane exploitation can contribute to the production of a certain amount of electrical energy through methane cogeneration ("Green Energy"), where the heat energy extracted can be used for district heating purposes. Currently, coal extraction in the Soko mine is on hold due to an accident that occurred in April 2022. To resume operations, measures for operational safety and collective protection of workers during mining and construction activities need to be implemented. One of these measures includes methane degassing from the coal seams. This is where the potential of the "Soko" mine lies, as methane can be collected and utilized for the production of electrical and thermal energy in a gas power plant instead of being released into the atmosphere, resulting in a permanent loss of potential. This approach would provide a dual benefit, both in terms of electricity generation and improved safety and conditions for underground mining. Based on the analysis of investment costs for degassing equipment and the construction and installation of a 2 MW gas power plant, approximately 3,000,000 euros would be required. Such a gas power plant of this capacity could supply around 3,470 households, which is equivalent to 66% of households in the municipality of Sokobanja. In addition to its global ecological significance in reducing methane emissions into the atmosphere, methane degassing, collection, and utilization contribute to increased safety and capacity in underground coal mines, while also offering significant economic benefits through the use of methane as an energy source.

## REFERENCES

- [5] D. Đukanović, N. Đokić, Z. Aksantijević, D. Radivojević, B. Stakić, The possibility methane exploitation from the bmc “Soko” deposit in Sokobanja, Proceedings Mining 2023, May 30-June 2, Zlatibor, Serbia, 2023, p. 75.
- [6] D. Milinković, D. Đukanović, M. Ignjatović, “Mogućnost eksploatacije metana sa aspekta metanoobilnosti jame RMU “Soko” Sokobanja, Proceedings Mining, June 24, Vrnjačka Banja, Serbia, 2006, p. 163.
- [7] R. Pantović, V. Milić, N. Vidanović, R. Tokalić, „Studija istraživanja primenjenih metoda miniranja u rudnicima uglja sa podzemnom eksploatacijom“, Technical Faculty in Bor and Faculty of Mining and geology, 2006.
- [8] Kelafant J. R., A Workshop - New Trends in Coal Mine Methane Recovery and Utilization, "Current Developments in Methane Degasification", A Workshop - New Trends in Coal Mine Methane Recovery and Utilization, Szczyrk, Poland, 2008.
- [9] Mattus R., A Workshop - New Trends in Coal Mine Methane Recovery and Utilization, Megtec Systems, Converting VAM to Energy, Szczyrk, Poland, 2008.
- [10] Kathleen C. Araújo, Journal of Environmental Management, Methane Capture: Options for Greenhouse Gas Emission Reduction.

## ELECTROCHEMICAL METHODS FOR THE DETERMINATION OF TRYPTOPHAN AND CAFFEINE

Žaklina Tasić, Marija Petrović Mihajlović, Ana Simonović,  
Milan Radovanović, Maja Nujkić, Milan Antonijević

Technical Faculty in Bor, University of Belgrade, V.J. 12, 19210 Bor, Serbia

### Abstract

*Electrochemical methods are widely used for the determination of various chemical compounds due to their simplicity and short time for analysis, as well as enabling low detection limits. Various electrodes have been developed over the years, including those made from carbon materials, gold, mercury, as well as various modified electrodes for detection of analytes. Carbon electrodes are particularly favored as they possess low background current and high electrical conductivity. Also, they are relatively inexpensive, easy to prepare, and generally non-toxic. In this study, the sensor characteristics of a graphite electrode prepared from spent zinc-carbon batteries for the determination of tryptophan and caffeine have been investigated. Britton-Robinson and acetate buffers were used as electrolytes. The obtained results demonstrated that this electrode is a good electrochemical sensor for detecting tryptophan alone as well as in the presence of caffeine. Additionally, the modified graphite electrode is resulting in improved sensor characteristics for the determination of tryptophan in Britton-Robinson buffer. The results obtained by differential pulse and cyclic voltammetry highlight the potential of graphite electrodes as effective electrochemical sensors for the detection of analytes.*

**Keywords:** *electrochemical sensor, zinc-carbon batteries, caffeine, tryptophan, modified graphite electrode*

### 1. INTRODUCTION

Electrochemical methods used for the analysis and detection of chemical compounds have significant advantages over other analytical methods, such as simplicity in operation, short time for analysis, and achieving low detection and low quantification limits. Over the past decades, there has been a growing trend in the development of various electrodes, such as electrodes prepared from carbon materials, as well as gold, mercury, and modified electrodes for the determination of different analytes [1,2]. Carbon electrodes possess favorable electrochemical properties, including low background current and high electrical conductivity, which make them a suitable choice for sensors. Moreover, they are relatively inexpensive, easy to prepare, and typically non-toxic. However, in light of increasing waste generation due to technological advancements, some researchers [3,4] have recommended using graphite rods from discarded batteries instead of commercial electrodes. Zinc-carbon batteries, for example, are a source of such waste. Improper disposal of such batteries can result in heavy metal pollution in the environment, which can lead to severe adverse effects on living organisms. Recycling these batteries would be an environmentally responsible measure, with significant economic benefits [5]. Considering the high electrical conductivity and large surface area of graphite rods, they have the potential to be utilized as effective electrochemical sensors [3].

The aim of this study was to investigate the sensor characteristics of a graphite electrode prepared from spent zinc-carbon batteries for the determination of tryptophan without and with the addition of caffeine in Britton-Robinson and acetate buffers using electrochemical methods, cyclic voltammetry and differential pulse voltammetry.

## 2. EXPERIMENTAL

For the experimental investigations, a three-electrode system consisting of a graphite electrode as the working electrode, a saturated calomel electrode (SCE) as the reference electrode, and platinum wires as auxiliary electrodes was used. The graphite electrode was rinsed with distilled water, polished with Al<sub>2</sub>O<sub>3</sub>, rinsed again with distilled water, and dried before each measurement.

The concentrations of the analyzed solutions of tryptophan (TRP) were  $4 \cdot 10^{-4}$  M and  $1 \cdot 10^{-4}$  M while for caffeine (CAF) was  $1 \cdot 10^{-4}$  M. Britton-Robinson buffer (BR), with a concentration of 0.04 M, was prepared by mixing solutions of 0.04 M H<sub>3</sub>BO<sub>3</sub>, 0.04 M H<sub>3</sub>PO<sub>4</sub>, and 0.04 M CH<sub>3</sub>COOH, while the acetate buffer with a concentration of 0.2 M was prepared by mixing solutions of 0.2 M CH<sub>3</sub>COOH and 0.2 M CH<sub>3</sub>COONa. The solution of 1M NaOH was used to adjust the pH value of the solutions.

Electrochemical methods used for the analysis of tryptophan and caffeine, were cyclic voltammetry (CV) and differential pulse voltammetry (DPV). The CV and DPV curves were recorded in the potential range of 0.0 to 1.2 V (vs. SCE), with a scan rate of 50 mV/s.

## 3. RESULTS AND DISCUSSION

Since it has been shown that a graphite electrode can be used to determine TRP in BR buffer solution at pH 4 [6], further experiments were performed in BR at pH 1.8 and acetate buffer at pH 4.35 using electrochemical methods. Figures 1a and 1b illustrate the obtained DPV curves in BR buffer (pH 1.8) and acetate buffer (pH 4.35) without and with the addition of  $1 \cdot 10^{-4}$  M TRP as well as  $1 \cdot 10^{-4}$  M TRP +  $1 \cdot 10^{-4}$  M CAF on graphite surface.

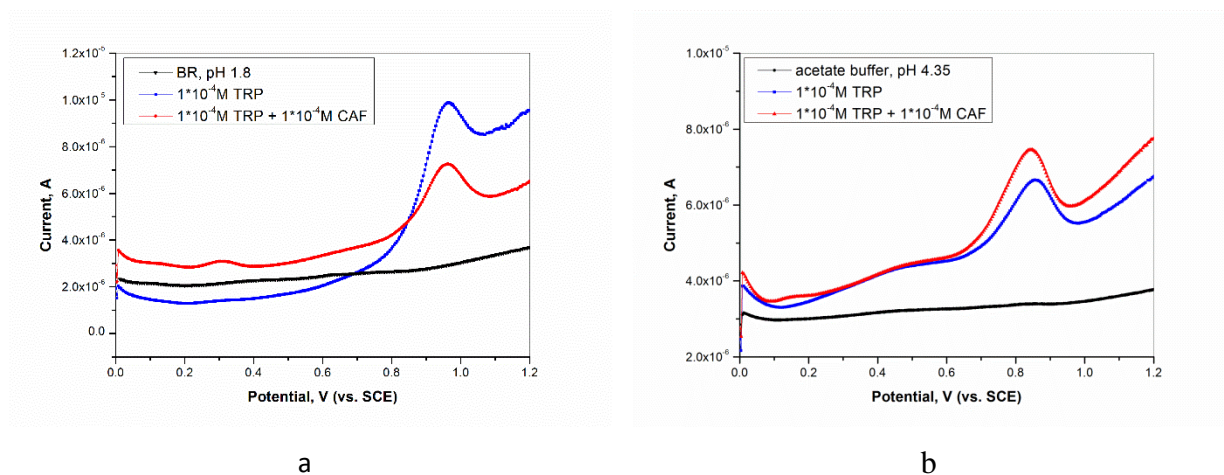


Figure 1 - (a) Differential pulse voltammetry curves on graphite electrode in Britton-Robinson buffer solution (pH 1.8) and (b) acetate buffer solution in the absence and in the presence of  $1 \cdot 10^{-4}$  M of tryptophan as well as  $1 \cdot 10^{-4}$  M of tryptophan +  $1 \cdot 10^{-4}$  M of caffeine, scan rate 50.0 mV/s

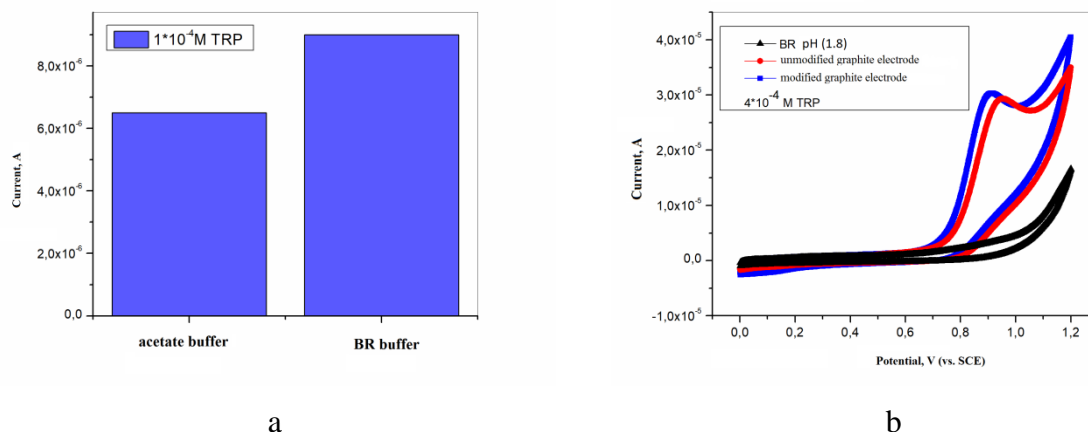


Figure 2 - (a) dependence of the intensity of the tryptophan current peak on type of buffer solution; (b) cyclic voltammetry curves of TRP on unmodified and modified graphite electrode in Britton-Robinson buffer solution (pH 1.8)

From Figure 1a, it can be observed that there are no current peaks in the basic solution, while in the presence of TRP, a peak is observed at a potential of 0.93 V, which can be observed in the solution containing both TRP and CAF. Figure 1b shows the differential pulse voltammogram of  $1 \cdot 10^{-4}$  M TRP, as well as  $1 \cdot 10^{-4}$  M TRP +  $1 \cdot 10^{-4}$  M CAF in acetate buffer solution. Based on the voltammogram in Figure 1b, it can be seen that there are no current peaks in the basic solution, while a peak is observed at a potential of 0.82V in the presence of TRP. Additionally, the current peak is observed at a potential of 0.83V in the solution containing both CAF and TRP at a concentration of  $1 \cdot 10^{-4}$  M. It can be concluded that the graphite electrode in the acetate buffer (pH 4.35) is able to detect tryptophan. In addition, in the acetate buffer, in the presence of both tryptophan and caffeine, the intensity of the current peak was higher than the current peak of tryptophan alone. These results indicate that the graphite electrode has high sensitivity for determining TRP in both BR and acetate buffer. Additionally, it can be observed that when CAF and TRP are present in the BR solution simultaneously, the intensity of the tryptophan peak is reduced.

Based on the voltammograms (Figure 1a) and the paper by Tasic et al. [6], it can be concluded that changing the pH of the solution results in a shift in the potential of the tryptophan current peak. Decreasing the pH value leads to the appearance of an oxidation peak of TRP at higher potential values. It was also observed that caffeine leads to a decrease in the current peak of TRP in BR solution. Figure 2a shows the influence of the buffer on the intensity of the current peak of tryptophan analyzed using the graphite electrode and DPV. It can be observed that the intensity of the current peak of tryptophan in the Britton-Robinson buffer reaches a value of  $9.0 \cdot 10^{-6}$  A, while in the acetate buffer, it reaches a value of  $6.5 \cdot 10^{-6}$  A. Therefore, the type of buffer is an important parameter for determining the desired analytes. For improving the sensitivity of the sensor, a modification of the graphite electrode in a 0.5 M solution of  $H_2SO_4$  was performed. The modification was carried out using cyclic voltammetry, in the potential range from 0V to 2V. The prepared electrode surface was then used for the determination of tryptophan. The behavior of the unmodified and modified graphite electrode in the Britton-Robinson solution in the presence of tryptophan is shown in Figure 2b. From the cyclic voltammogram (Figure 2b), it is evident that the TRP oxidation peak at the unmodified graphite electrode occurred at a potential of about 0.95V, while the TRP oxidation peak at the modified graphite electrode was observed at a potential of about 0.90V. The current density value was higher on the modified graphite electrode than on the



unmodified graphite electrode. It is assumed that the electrode modification has developed a larger specific surface area, which affects the intensity of the current response of tryptophan.

According to the literature data [6,7] and the results obtained in this investigation, the mechanism of TRP oxidation at the graphite electrode was proposed and shown in Figure 3.

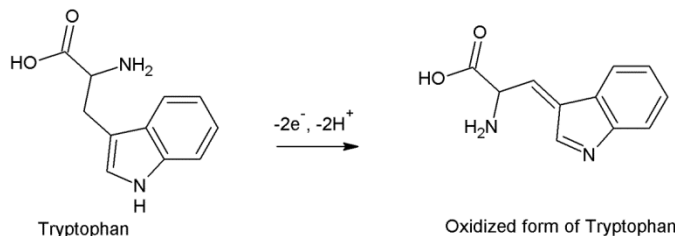


Figure 3 - The proposed mechanism of TRP oxidation on the graphite electrode

#### 4. CONCLUSION

Based on the experimental data presented in the paper, it can be concluded that the graphite electrode has shown to be a good electrochemical sensor for the detection of tryptophan without and with the addition of caffeine. The results indicate that the graphite electrode can be successfully used for tryptophan determination at pH values of 1.8 in Britton-Robinson buffer and 4.35 in acetate buffer solutions. Additionally, it has been shown that the choice of buffer also effects the potential and intensity of the oxidation peaks of the analyzed compounds. In order to improve the sensor characteristics, the surface of the graphite electrode was modified in a simple way and it proved to be successful in determining tryptophan.

#### ACKNOWLEDGEMENTS

*The authors are grateful to the Ministry of Science, Technological Development and Innovation of the Republic of Serbia for financial support according to the contract with the registration number (451-03-47/2023-01/200131).*

#### REFERENCES

- [1] Y. Liu, L. Wang, L. Yang, L., Int. J. Electrochem. Sci. 16 (2021) Article ID: 210534.
- [2] Z. Wang, R. An, Y. Dai, H. Luo., Int. J. Electrochem. Sci. 16 (2021) Article ID: 210450.
- [3] J.W. Zhang, X. Zhang., J. Alloy Compd., 842 (2020) 155934.
- [4] S.T. Palisoc, E.J.F. Cansino, I.M.O. Dy, C.F.A. Razal, K.C.N. Reyes, L.R. Racines, M.T. Natividad., Sens. Bio-Sens. Res., 28 (2020) 100326.
- [5] Y. Wang, N. An, L. Wen, L. Wang, X. Jiang, F. Hou, Y. Yin, J. Liang., J. Alloy Compd. 842 (2020) 155934.
- [6] Ž.Z. Tasić, M.B. Petrović Mihajlović, M.B. Radovanović, A.T. Simonović, D.V. Medić, M.M. Antonijević., Sci. Rep. 12 (2022) 5469.
- [7] C. Yıldız, D.E. Bayraktepe, Z. Yazan., Monatshefte für Chemie - Chemical Monthly 151 (2020) 871-879.

## CIRCULAR ECONOMY IN THE ERA OF INDUSTRY 5.0

Isidora Milošević<sup>1</sup>, Anđelka Stojanović<sup>1</sup>, Sanela Arsić<sup>1</sup>, Ivica Nikolić<sup>1</sup>, Ana Rakić<sup>2</sup>

<sup>1</sup>University of Belgrade, Technical Faculty Bor, V.J. 12, 19210 Bor, Serbia

<sup>2</sup>University of Belgrade, Faculty of Organizational Sciences, Jove Ilića 154,  
11000 Belgrade, Serbia

### Abstract

*The circular economy is an emerging concept based on the circulation of materials in the economy, in which waste is recycled, reused, or repaired. By recycling waste, new raw materials are obtained from which products or certain materials can be made, and devices can have alternative uses. A circular economy is needed to change outdated business practices based on a linear production-consumer paradigm into creative, innovative semi and final products. Industry 5.0 puts people at the center of the production process and uses innovative technical advances to ensure a sustainable and resilient path to smart manufacturing. Therefore, the circular economy and Industry 5.0 lay the foundations of intelligent and sustainable production based on real-time data collection, contributing to society's smart industry. This paper examines whether companies need to transform from a linear production-consumer paradigm to a circular economy to achieve sustainable development in the era of the new industrial revolution known as Industry 5.0.*

**Keywords:** *Circular economy, Industry 5.0, Sustainable development, Transform*

### 1. INTRODUCTION

Traditional business practice based on a linear production-consumption paradigm is a concept that remains behind us [1]. As an alternative to this traditional model, an approach that transforms the use of resources, known as the Circular Economy (CE), appears [2]. Therefore, the Circular Economy is a concept based on the circulation of materials in economics. It refers to the production and consumption of goods in a closed material flow cycle [3] in order to achieve the maximum efficiency of the use of limited resources with a gradual transition to renewable resources and the reuse of materials and products at the end of their life cycle [1]. The basic principles of the circular economy are efficient use of material resources, waste collection, recycling, and reuse in production. By applying these principles, organizations can manage their resources more effectively through cost savings, finding new income streams, becoming more resistant to external disturbances, etc. [4]

With the transformation of the production-consumption paradigm into a circular economy, a parallel transformation of the industrial paradigm into a socio-technological one is imposed [5]. This phenomenon, known as Industry 5.0, could be described as a "humanized vision of technological transformations in the industry" [6], which supports the circulation of materials in the economy, balancing the needs of society with the sustainable optimization of energy consumption and the extension of the product lifecycles. In that manner, Industry 5.0 puts people at the center of the production process and uses innovative technical advances to ensure a sustainable and resilient path to smart manufacturing [7, 8]. Therefore, Circular Economy and Industry 5.0 lays the foundations of intelligent and sustainable production based on real-time data collection, contributing to society's smart industry [4, 9].

Although many studies have dealt with the Circular Economy in the fourth industrial revolution era [10, 11, 12, 13], this relationship in the context of the Circular Economy and Industry 5.0 is almost unexplored in the literature. This paper step further with the existing academic literature in

order to fill this gap. Hence, the research examines whether companies need to transform from a linear production-consumer paradigm to a circular economy to achieve sustainable development in the era of the new industrial revolution known as Industry 5.0.

## 2. METHODOLOGY

### 2.1 Sample and collection of data

This study investigated whether companies need to transform from a linear production-consumer paradigm to a circular economy to achieve sustainable development in the era of the new industrial revolution known as Industry 5.0. Therefore, the online questionnaire was utilized and distributed to companies through LinkedIn in the second half of 2022. A total of 205 respondents participated in the research. The target group of respondents consisted of all employees of companies in Serbia. The need for a transition from a linear to a Circular Economy was measured, consisting of seven indicators displayed in Table 1.

Table 1 - Defined variables

Measurement	Variables	Label
Circular Economy	The company should provide an active response to environmental challenges	CE1
	The resources necessary for the functioning of the economy are constantly decreasing	CE2
	The electricity sources available to the economy are constantly decreasing	CE3
	The company has an increasing need for energy	CE4
	The waste generated by the economy is constantly increasing	CE5
	The emission of green gases generated by the economy is constantly increasing	CE6
	Customers increasingly choose products from ecological companies	CE7

### 2.2 Analysis and research results

Exploratory factor analysis (EFA) is a statistical method used to describe the variability among observed, correlated variables. For this research, EFA was employed to summarize the information contained in a more significant number of observable variables into a smaller number of latent variables, i.e., to define the items of the factor determining the measurement scale for Circular Economy. The summary statistic of the examined variables was implemented on 205 respondents, and obtained values are shown in Table 2.

Table 2 - Statistics of the examined variables

Measurement	Label	Mean	Std. Deviation	Factor loadings
Circular economy	CE1	3.849	1.010	0.920
	CE2	3.817	0.883	0.898
	CE3	3.892	0.902	0.851

	CE4	3.913	0.880	0.787
	CE5	3.784	0.942	0.908
	CE6	3.978	0.820	0.767
	CE7	3.871	0.862	0.798

The results of PCA, the reliability of measurement scales, and convergent validity (AVE) are depicted in Table 3. The presented results indicate that the data collected are adequate for carrying out the factor analysis, given that Kaiser-Meyer-Olkin Measure of Sampling Adequacy (KMO test) values are above the recommended threshold value of 0.6 [14]. The obtained values of factor loadings are very high and give substantial weight to the selected factor. Also, the reliability of the measurement scale was applied to establish internal consistency and confirmed by Cronbach's Alpha coefficient [15]. The recommended values the internal consistency are above 0.7 [16]. The obtained value of Cronbach Alfa coefficient is 0.935, which is a very satisfying value, and the internal consistency is confirmed. Also, convergent validity is proved, indicated by AVE values greater than recommended values above 0.5 [14]. Finally, correlation analysis was utilized to examine whether there is a relationship between two variables or two data sets (Table 3). Correlation analysis was used to determine whether there is a relationship between two variables or two data sets (Table 3). The results of the correlation analyze was discovered that there is a significant correlation among variables.

Table 3 - Measurement scales and Correlation Matrix

Measurement	KMO Test		% of variance explained*	Cronbach's Alpha		The average variance extracted (AVE)	
Circular economy	0.884		72.086	0.935		0.721	
CE1	1						
CE2	0.857	1					
CE3	0.757	0.793	1				
CE4	0.609	0.650	0.631	1			
CE5	0.868	0.813	0.765	0.633	1		
CE6	0.665	0.579	0.452	0.614	0.626	1	
CE7	0.664	0.596	0.624	0.572	0.647	0.672	1

### 3. CONCLUSION

Until a few decades ago, the concept of Circular Economy was not applicable since the existing technology could not support its application. However, with the development of a new industrial revolution known as Industry 5.0, the importance of research and innovation to support the industry in its long-term service to humanity is emphasized. Considering that the existing economic model imposed a disposable lifestyle, which needs to be stopped, this paper has established a nuanced link between Circular Economy and Industry 5.0.

With the idea to analyze the companies' need to transition from a linear to a Circular Economy, this paper suggests a set of indicators that could be used for reliable assessment applicable to the

Circular Economy. Furthermore, these indicators could serve managers and other decision-makers in companies to develop a roadmap for implementing the circular economic business model in its operations to achieve sustained economic growth.

This study has some limitations. The main limitation is the measurement scale which was not cover all research questions that reflect the need to transform from a linear to a circular economy. Therefore, future investigations will be focused on expanding the listed questions. Also, it would be useful to study the relationships between Industry 5.0 and the Circular economy in specific industry sectors to study circularity within their sphere of operation.

## ACKNOWLEDGEMENTS

*The research presented in this paper was done with the financial support of the Ministry of Education, Science and Technological Development of the Republic of Serbia, within the funding of the scientific research work at the University of Belgrade, Technical Faculty in Bor, according to the contract with registration number 451-03-47/2023-01/ 200131.*

## REFERENCES

- [1] D. Ubavin. *Man. Sys. and Techn. for the N. Fron.*, (2018) 537-542.
- [2] S. Sauvé, S. Bernard, P. Sloan, *Environ. Dev.* 17 (2016) 48-56.
- [3] M. Haradhan. *J. of Ec. Dev. Environ. and Peop.* 9 (3) 2020 38-62.
- [4] K. Voulgaridis, T. Lagkas, C.M. Angelopoulos, S.E. Nikolettseas. *Comp. Net.* (2022) 219.
- [5] Barataa, J., & Kayser, I., *Proc. Comp. Sci.* 219 (2023) 778–788.
- [6] J. Lindström, E. Lejon, P. Kyösti, M. Mecella, D. Heutelbeck, M. Hemmje, M. Sjö Dahl, W. Birk, B. Gunnarsson. *Proc. CIRP.* (2019) 880–885.
- [7] P.K.R. Maddikunta, Q.V. Pham. *J. of Ind. Infor. Integ.* 26 (2022) 100257.
- [8] X. Xu, Y. Lu, B. Vogel-Heuser. *J. of Man. Sys.* 61 (2021) 530–535.
- [9] European Commission. (2021) [https://ec.europa.eu/info/research-and-innovation/researcharea/industrial-research-and-innovation/industry-50\\_en](https://ec.europa.eu/info/research-and-innovation/researcharea/industrial-research-and-innovation/industry-50_en).
- [10] D. Findik, A. Tirgil, F.C. Özbuğday. *J. of Clean. Prod.* (2021) 410.
- [11] Y. Ren, R. Li, K. Wu, M. Tseng, *Clean. and Respons. Consump.* 9 (2023) 100123.
- [12] A. Behl, R. Singh, V. Pereira, B. Laker. *Technol. Forecast. Soc.* 189 (2023) 122363.
- [13] A. Upadhyay, K. C. Balodi, F. Naz, M. Di Nardo, L. Jraisat. (2023). *Comput. Ind. Eng.* 177 (2023) 109072.
- [14] A. Upadhyay, K. C. Balodi, F. Naz, M. Di Nardo, L. Jraisat. (2023). *Comput. Ind. Eng.* 177 (2023) 109072.
- [15] J.F. Hair, W.C.Black, B.J. Babin, R.E. Anderson, Pearson Education Limited, Harlow, England and Associated Companies throughout the world 2014.
- [16] L.J. Cronbach. *Psychom.* 16 (1951) 297-334.
- [17] J.C. Nunnally, I. Bernstein, J.T. Berge, New York: McGraw-Hill 1967

## EFFECT OF DELTA FERRITE ON MICROSTRUCTURE AND HARDNESS WELDED JOINTS OF STEEL S21800

Almaida Gigović-Gekić<sup>1</sup>, Elvis Agović<sup>1</sup>, Belma Fakić<sup>2</sup>, Hasan Avdušinić<sup>1</sup>

<sup>1</sup> Faculty of Engineering and Natural Sciences, University in Zenica, Travnička cesta 1, 72 000 Zenica, Bosnia and Herzegovina

<sup>2</sup> Institute “Kemal Kapetanović”, University of Zenica, Travnička cesta 7, 72 000 Zenica, Bosnia and Herzegovina

### Abstract

*Welding is one of the most important processes in the metal industry. In order for the weldability of a material to be satisfactory, it is necessary to find the most adequate type of welding and the conditions in which welding will be performed. Weldability of a steel depends about an initial materials (chemical composition, microstructure...) and from a filler material too. Austenitic stainless steel S21800 was used for testing influence of the delta ferrite on microstructure a welded joint. Steel rods with different content of the delta ferrite (0.12 and 1.95 %) used for welding. As a filler metal in this experiment austenitic stainless steel 316L is used. The TIG method is most commonly used for welding stainless steels, and is therefore considered adequate for this experiment. Analysis of microstructure showed increases of the delta ferrite content in a weld metal for both case. Presence of a sigma phase on the delta ferrite islands noticed too.*

**Keywords:** *welding, delta ferrite, microstructure, stainless steel*

### 1. INTRODUCTION

The weldability of a material is consider to be good if, after welding process of the structural part, the properties of the weld (WM) and the heat affected zone (HAZ) meet the structural requirements and the level of safety of the structural part. If the requirements are not met, the weldability is considered limited or unsatisfactory [1-3]. The most common problems in welding austenitic stainless steels (ASS) are corrosion-induced cracking, hot cracking and sigma phase formation [4,5]. When ASS are exposed heating in the temperatures range from 450 to 850 °C, there is possibility precipitation the chromium carbides along the grain boundaries. This reduces the chromium content in the vicinity of the boundary and a potential difference occurs, which causes intercrystalline corrosion. Segregation of sulfur and phosphorus compounds also negatively affects on the weldability of these steels, because these compounds in the last stage of solidification can initiate the appearance of intercrystalline hot cracks. It has been proven that optimal amounts of the delta ferrite in HAZ reduce the appearance of hot cracks. However, with a higher content of the delta ferrite, there are greater possibilities for the formation of the sigma phase, because the delta ferrite is the basis for the formation of the sigma phase. The sigma phase is hard and brittle, most often formed in the temperature range from 600 to 950 °C [6-9]. The aim of testing was investigate the influence of delta ferrite on a microstructure and hardness of the weld metal after welding of the steel S21800. The samples with different content of the delta ferrite used for welding.

### 2. EXPERIMENTAL PART

The welding process was performed on steel samples that have different content of delta ferrite in the initial microstructure. Chemical composition and the content of the delta ferrite is given in Table 1. The chemical composition is in accordance to standard ASTM A276.



Table 1 - Chemical composition and the content of delta ferrite for the steel S21800

Standard/ Melts	Chemical composition (wt.%)								Content of delta ferrite (%)
	C	Si	Mn	Cr	Ni	P	S	N	
<b>ASTM A276</b>	$\leq 0.10$	3.4-4.5	7-9	16-18	8-9	$\leq 0.006$	$\leq 0.03$	0.08- 0.18	
<b>No.1</b>	0.05	4.5	8.6	16	8	0.007	0.016	0.147	1.95
<b>No.2</b>	0.05	3.8	8.9	17	9	0.007	0.005	0.161	0.12

The standard electric arc process - TIG in a protective argon atmosphere is used for welding. The welding conditions for all samples were the same (Current strength -70 - 80 A, wire feed rate - 0.5 m/min, gas flow rate- 10 l/min) and steel 316 L AISI used as a filler metal. The magnetic method (a ferritoscope) was used to determine the delta ferrite content and a optical microscope with a magnification max. 1000x used for analysing microstructure. Analysis of hardness of welded joint was done according to standard BAS EN ISO 6507-1:2018 (Vickers method HV10 at room temperature).

### 3. RESULTS AND ANALYSIS

#### 3.1. Analysis microstructure and content of the delta ferrite

Analysis of microstructure as well as the content of delta ferrite was done before and after welding process. Results of the microstructure analysis for the samples before welding are presented in Figure 1. The samples are in rolling state.

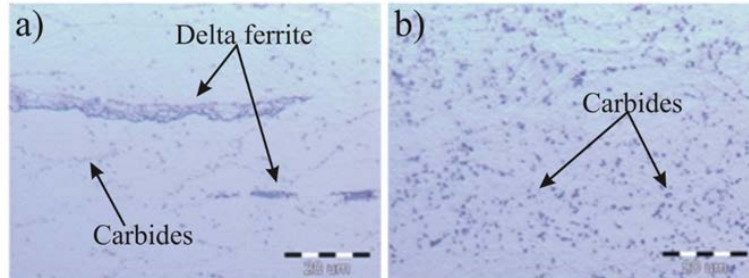


Figure 1 - Microstructure of initial state for the melts a) No.1 and b) No.2

From the Figure 1 it can be seen the presence of the chromium carbides and the delta ferrite in the austenite matrix. Figure 2 and 3 present microstructure welded joints for samples with higher (Figure 2. No.1.) and lower (Figure 3 -No.2) content of the delta ferrite.

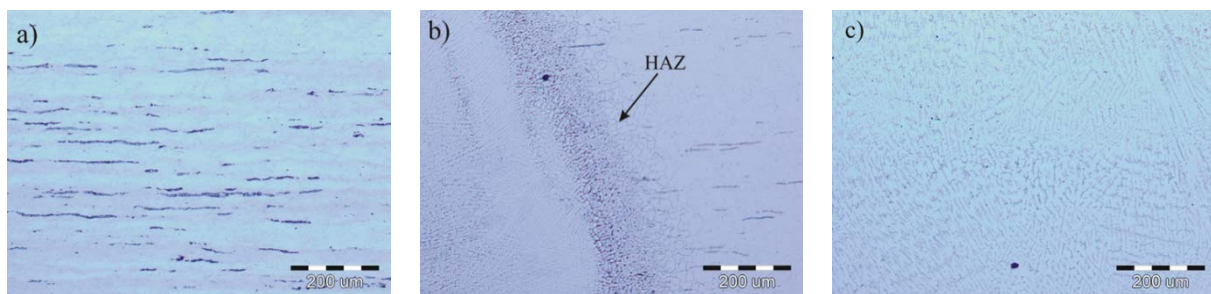


Figure 2 - Microstructure welded joint for sample No.1: a) base material, b) heat affected zone and c) weld metal, Kalling #2, 100x

The microstructure of the base material is austenitic with the particles of chromium carbides and delta ferrite. The presence of the sigma phase on delta ferrite islands is visible in the base material as well as in the heat affected zone and weld metal. An increase in grain size can be noticed in the heat affected zone. The microstructure of the weld metal is a cast microstructure. The weld metal has an austenitic microstructure with interdendritic and/or intercellular ferrite (AF model). That is, during solidification, austenite first forms, and delta ferrite is formed by eutectic reaction from the remaining melt between the austenite dendrites [10,11].

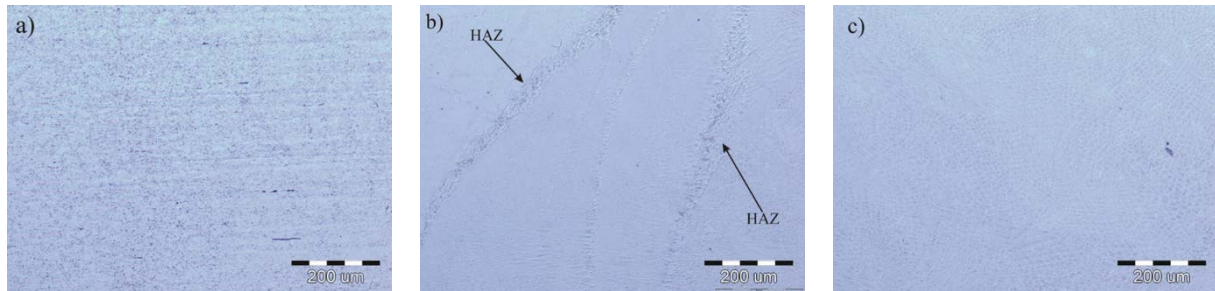


Figure 3 - Microstructure welded joint for sample No.2: a) base material, b) heat affected zone and c) weld metal, Kalling #2, 100x

It is evident from the Figure 3 that the base material has an austenite microstructure with precipitates (the chromium carbides). An increase in grains was observed in the heat affected zone. This zone, as in the previous case, is characterized by a small width. The precipitates were separated along the grain boundaries. Weld metal is characterized by the AF model of solidification. The presence of the sigma phase on the delta ferrite in the weld metal and the heat affected zone can be seen.

After welding, the content of delta ferrite in the heat affected zone and the weld metal was measured, Table 2.

Table 2 - The content of the delta ferrite

Melts	Number of sample	Content of delta ferrite			Content of delta ferrite				
		Heat affected zone			Average	Weld metal			Average
No.1	1	2.1	1.9	1.4	<b>1.8</b>	5.6	6.1	5.4	<b>5.7</b>
	2	1.9	1.6	1.8	<b>1.8</b>	5.8	4.8	5.2	<b>5.3</b>
	3	1.9	1.2	1.8	<b>1.6</b>	6.3	5.3	5.1	<b>5.6</b>
No.2	1	0.70	1.10	0.69	<b>0.8</b>	2.4	2.6	2.0	<b>2.3</b>
	2	0.69	0.61	0.88	<b>0.7</b>	2.6	2.1	2.8	<b>2.5</b>
	3	0.60	0.72	1.10	<b>0.8</b>	2.7	2.3	2.0	<b>2.3</b>

From the Table 2 it can be seen that the delta ferrite content is higher in the weld metal than in the heat-affected zone.

### 3.2. Analysis of the welded joints hardness

Analysis of hardness of welded joint was done according to standard BAS EN ISO 6507-1:2018 (Vickers methods). The results of the hardness testing are presented in Figure 4. From the results it could be seen that the weld metal has the lowest hardness for both cases. Higher values of the hardness of the base materials and the heat affected zone are the result of the precipitation of chromium carbides and the sigma phase.

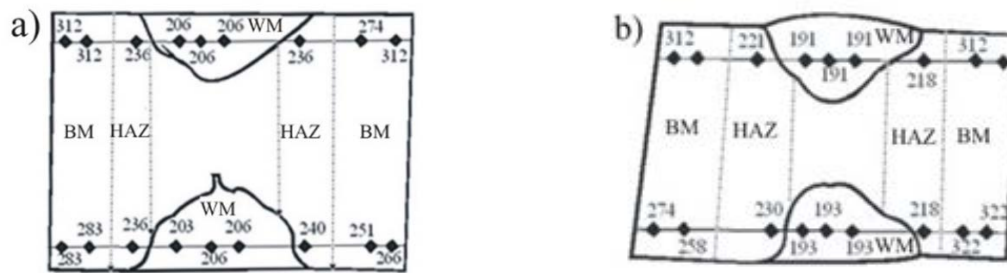


Figure 4 - Results of the hardness measuring for a) melt No.1 and b) melt No.2

#### 4. CONCLUSION

Metallographic analysis of the base material revealed that the microstructure is the austenitic with a certain amount of the delta ferrite and chromium carbides. The precipitated carbides form strings along the grain boundaries and are precipitated at the austenite/delta ferrite phase boundary. The analysis of the microstructure of the welded joints showed that the microstructure of the weld metal is austenitic - ferritic (AF solidification model) and that the sigma phase was precipitated on the delta ferrite. Chromium carbides are also present. Analysis of the content of delta ferrite using a ferritoscope after the TIG welding process revealed an increase in the content of delta ferrite in the weld metal compared to the base metal. This increase is characteristic of samples from both melts. For a melt with a higher content of delta ferrite in the base material, there is also a higher content of delta ferrite in the weld metal. The measurement of the hardness of the welded joint showed a lower hardness in the weld metal compared to the heat affected zone and base materials. The reason for the increase in hardness is the precipitation of chromium carbides and the sigma phase.

#### REFERENCES

- [1] I. Hrivnjak, Teorija zavarivosti metala i legura, Slovačka akademija nauka, Bratislava, 1989, p. 15
- [2] I. Samardžić, D. Bogovac, T. Jorgić, K. Kovačić, Tech. J., 9 (2) (2015), p. 202-208.
- [3] B. Fakić, Uticaj postupka zavarivanja na fiziko-metalurške karakteristike čelika: S355J2G3, 16Mo3 i 13CrMo4-5 u zoni uticaja toplote, Univerzitet u Zenici, Fakultet za metalurgiju i materijale, Zenica, 2010, p.2
- [4] J. Pavić, J. Majić, D. Marić, I. Samardžić, 7. Međunarodno znanstveno-stručno savjetovanje SBZ 2013, 23-25.10.2013, Slavonski Brod, Hrvatska, 2013, p.287-293
- [5] A. Hodžić, Utjecaj sigma faze na svojstva austenitnog nehrđajućeg čelika Nitronic 60, Univerzitet u Zenici, Metalurško-tehnološki fakultet, Zenica, 2019, p.9
- [6] G. E. Totten, Steel Heat Treatment Handbook Metallurgy and Technologies, Taylor & Francis Group, New York, 2006, p.695-735.
- [7] A.F. Padilha, P.R. Rios, ISIJ International, 42 (4) (2002), p. 325-337.
- [8] K. Guan, X. Xu, H. Xu, Z. Wang, Nucl. Eng. Des. 235 (2005), p.2485-2494.
- [9] K.H. Lo, C.H.Shek, J.K.L. Lai, Mater. Sci. Eng. R, 65 (2009), p.39-104.
- [10] G. George, H. Shaikh, in Corrosion of Austenitic Stainless Steels Mechanism, Mitigation and Monitoring (H.S. Khatak, B. Raj Editor), Narosa Publishing House, Delhi, 2002, p.1-36.
- [11] F.Tehovnik, F.Vodopivec, L.Kosec, M.Godec, Mater. Tehnol. 40 (2006), p.129-137.

## COMBINING NEUTRALIZATION AND ADSORPTION METHODS FOR METALS REMOVAL FROM SARAKA STREAM

**Radmila Marković, Dragana Bozić, Zoran Stevanović, Tatjana Apostolovski Trujić, Vojka Gardić, Ljiljana Avramović, Vesna Marjanović**

Mining and Metallurgy Institute Bor, Zeleni bulevar 35, 19210 Bor, Serbia

### Abstract

*The possibility of metals removal from real acid mine drainage from the Saraka stream, that flow near the plant for copper ore mine treatment in Serbia, was investigated by combination of neutralization and adsorption methods. A new approach of metals removal from acid mine drainage is in a two-step neutralization method by controlling the pH value aiming to obtain a different type of sludge during each step of neutralization process. The results are confirmed that the concentration of Cu and Fe is maximally reduced during the first neutralization step on pH 7. Values for the concentration of the other elements on pH 7 is as following: Mg>Mn>Ni>Cd>Co. On pH 10 (second neutralization step) removal mass percentage is the same for all elements (more than 99 mass%). As an alternative to metal removal at pH values above 7, a method of adsorption with the crosslinked hydrogel obtained by crosslinking the Type B gelatin and chitosan with glutaraldehyde is used. Studies have shown that the highest adsorption removal rate of 81.43% is achieved for Co.*

**Keywords:** real acid mine drainage, metal, removal, neutralization, adsorption

### 1. INTRODUCTION

Active and passive treatment methods are the common methods for purification of acid mine drainage (AMD) that causes water and soil systems pollution around the mine. Mine waters originating from active or closed copper mines contain copper ions sometimes in a considerable concentration usually associated with an equivalent or even a two times higher concentration of Fe<sup>2+</sup>/Fe<sup>3+</sup> ions. The presence of the other heavy metal ions such as Mn, Cd, Zn, Pb, Ni, etc. in mine water depends on the mineralization of an ore body but their concentration is much lower than the concentration of copper or iron. Mine waters are acidic with pH value mostly between 2.5 and 4. The most environmentally effective techniques available for AMD are internal neutralization methods, water-covers and biological/natural degradation processes [1].

The aim of this paper is to investigate the multistep neutralization process of acid mine drainage from Saraka stream aim to precipitate the present metal ions in a different sludge type. First neutralization step was realized on pH 7 and second neutralization step was realized on pH 11. According to the literature data [2,3], the pH value for Mn recovery is greater than 7, and for the above reason, the second step of neutralization process (pH 10) is applied. Crosslinked hydrogels were used aim to investigate the possibility of removal the metal ions after the first neutralization step [4].

### 2. EXPERIMENTAL

#### 2.1. Neutralization process procedure

- Laboratory tests

Neutralization process is carried out with 1000 ml of real Saraka samples to reached pH 7; 7.5 and 8. As a neutralizing agent is used lime milk, concentration 25 g/L. After reached the pH 7, 7.5 and 8, solution is filtered by vacuum filtration with aim to separate solid from liquid phase. Dewatered sludge was dried on 40°C to constant mass. AMD neutralized on pH 7; 7.5 and 8 was used as start samples for neutralization on pH 9 and 10. As in the first neutralization stage, liquid and solid

phase are separated by vacuum filtration. Liquid phase is used for the chemical analyses and solid phase is dried on 40°C and measured after reaching the constant mass value.

- Two-stage pH control on pilot plant

Approximately 1800 l of AMD was feed to the pilot plant and pH was set: for a first step on pH 7 and for a second step on pH 10. Waste water pump with constant flow rate of 5 l/min is used for waste water transport to pH control tank A. In the same time, in pH control tank A is continually added 2.5 mass% lime milk from lime slurry tank by lime slurry pump. In pH control tank A is immersed pH meter aim to control first neutralization step pH value. Suspension from pH control tank A overflows in flocculation tank A. Flocculant, type Accoflock A-95 (0.05 mass %) is pumped by flocculant pump A with constant flow rate of 0.025 l min<sup>-1</sup> to flocculation tank A. The solid-liquid separation is followed in thickener A. Supernatant that overflows from thickener A is going to pH control tank B for second neutralization step pH control (according to the second set pH value of 10). Flocculation is followed in flocculation tank B thereafter, and then solid-liquid separation is occurrence in thickener B. Supernatant that overflows from thickener B is taken for the chemical analysis and discharged continuously by gravity as treated water. Thickener A/B are discharged one by one aim to dewater the sludge on a filter press.

## 2.2. Adsorption tests with cross-linked hydrogels

Adsorption tests for a metal removal using crosslinked hydrogels prepared from gelatin Type B and chitosan, which are crosslinked with glutaraldehyde, were performed with next type of real waste water: 1. original AMD sample (saraka stream sample), 2. AMD sample after first neutralization step and 3. AMD sample after second neutralization step. Cross-linked hydrogel sheets (8 cm-square shape) were used as adsorbent. Incubation time of each adsorption test was (h): 0.5; 1; 2; 4; 6; 24; 48. Mass of the gelatin hydrogel sample was measured on the start and on the end of each test.

## 3. RESULTS AND DISCUSION

### 3.1. Neutralization process

- *Laboratory experiments*

Saraka stream is the branch of the Krivelj River located down-stream of over burden damp site. The over burden contains oxidized copper minerals as well as pyrite. It suggests that the seepage water from the dump contains copper. It is confirmed by chemical composition of the sample from Saraka stream: Al – 71.005 mg/l; Ca – 529.715 mg/l; Fe – 46.169; Mg – 250.295 mg/l; Mn – 16.145 mg/l; Zn – 1.782 mg/l; Cu – 88.237 mg/l; Co – 1.178 mg/l; Ni – 248.3 µg/l; As – 4.1 µg/l; Se – 29.1 µg/l; Sr – 591.8 µg/l and Cd – 17.9 µg/l. Concentration of Pb, Cr and Cs was below the sensitivity limit of used analytical method. In the Table 1 are presented the results of the first and second neutralization steps.

Table 1 - Concentration of the elements in the AMD after first and second neutralization step

From pH start value: 3.8	Concentration of elements, mg/l						
	Ca	Cd	Co	Cu	Fe	Mn	Ni
to pH 7	626.2	0.0123	0.471	0.842	<0.1	12.500	0.075
to pH 7.5	638.3	0.0071	0.215	0.521	<0.1	11.300	<0.01
to pH 8	646.6	0.0030	0.03	0.1	<0.1	7.600	<0.01
Neutralization from pH 7 to	Concentration of elements, mg/l						
	Ca	Cd	Co	Cu	Fe	Mn	Ni
pH 9	638.2	0.004	0.138	0.28	<0.1	5.8	<0.01
pH 10	845.2	0.0038	0.007	<0.1	<0.1	0.193	<0.01

Neutralization from pH 7.5 to:	Concentration of elements, mg/l						
	Ca	Cd	Co	Cu	Fe	Mn	Ni
pH 9	701.6	0.007	0.0025	<0.1	<0.1	5.8	<0.01
pH 10	782.1	<0.0001	0.0001	<0.1	<0.1	0.006	<0.01
Neutralization from pH 8 to:	Concentration of elements, mg/l						
	Ca	Cd	Co	Cu	Fe	Mn	Ni
pH 9	653.9	<0.0001	0.0015	<0.1	<0.1	0.9	<0.01
pH 10	800.7	<0.0001	<0.0001	<0.1	<0.1	0.006	<0.01

- *Two-stage pH control on pilot plant*

According to the obtained laboratory data for chemical composition and lime milk consumption, test on pilot plant is carried out as following: first neutralization step: on pH 7 and second neutralization step: on pH 10 (Table 2).

Table 2 - Content of the elements after two neutralization steps

From pH start value of 4.3 to:	Concentration of elements, mg/l						
	Ca	Cd	Co	Cu	Fe	Mn	Ni
pH 7	626.2	0.0123	0.471	0.842	<0.1	12.500	0.075
pH 10	701.7	0.00014	0.0052	0.036	< 0.007	0.18	0.018

## 2.2. Adsorption tests with cross-linked hydrogels

In the Table 3 are presented the results of metals adsorption degree from different AMD samples.

Table 3 - Adsorption degree of Cu, Co, Cd and Mn

Adsorption time, h	0.5	1	2	4	6	24	48
Cu, mass %							
Real Saraka water	-	5.53	8.6	15.89	17.11	31.26	30.06
Co, mass %							
Neutralized on pH 7	7.78		13.2	14.64	16.89	21.56	27.9
Neutralized on pH 10	51.43	57.14	58.57	62.86	67.14	68.57	81.43
Cd, mass %							
Real Saraka water			4.81	7.21	11.54		
Neutralized on pH 7	13.56		30.51	33.9	47.46	64.41	71.19
Mn, mass %							
Real Saraka water	7.81	6.52	15.69	10.18	12.23	12.95	15.07
Neutralized on pH 7		5.89	7.12	11.64	15.26	21.88	21.39
Neutralized on pH 10	10.17	9.75	16.1	15.68	18.22	13.98	17.8

## 4. CONCLUSION

A new approach of metals recovery from acid mine drainage in combination with adsorption method gives the satisfactory results regarding to reduce the metals concentration. Using two-step neutralization method is obtained a different type of sludge during each step of neutralization process. Concentration of the elements on pH 7 is as follows: Mg > Mn > Ni > Cd > Co > Cu > Fe. On pH 10 (second neutralization step) recovery mass percentage is the same for all elements (more than 99 mass %). Based on data for lime consumption at pH values above 7, method of adsorption with the crosslinked hydrogel obtained by crosslinking the Type B gelatin and chitosan with glutaraldehyde is used. Studies have shown that the highest recovery rate of 81.43% is achieved for Co.



## **ACKNOWLEDGEMENTS**

*The authors are grateful for funding by the Minister of Science, Technological Development and Innovation of the Republic Serbia, the Grant No. 451-03-47/2023-01/200052. Also, this work is financially supported by the EU under Program 2<sup>nd</sup> EIT-HEI call: Building Ecosystem Integration Labs at HEI to foster Smart Specialization and Innovation on Sustainable Raw Materials - HEI4S3-RM.*

## **REFERENCES**

- [1] Z. Stevanović, Lj. Obradović, R. Marković, R. Jonović, Lj. Avramović, M. Bugarin, J. Stevanović, Waste Water - Treatment Technologies and Recent Analytical Developments, InTech, Rijeka, 2013, p.41.
- [2] Z. Štirbanović, V. Gardić, D. Stanujkić, R. Marković, J. Sokolović, Z. Stevanović, Water Resour. Manag, 35 (2021) 3737–3753.
- [3] E.Y. Seo, Y.W. Cheong, G.J. Yim, K.W. Min, J.N. Geroni, Catena 148 (2017) 11–16.
- [4] R. Markovic, M. Bessho, N. Masuda, Z. Stevanovic, T. Apostolovski-Trujic, V.Gardic, Appl. Sci., 10 (17) (2020) 5925.

## CNTs AS POTENTIAL MATERIAL FOR WASTEWATER PURIFICATION: A REVIEW

Ana Petrović, Radmila Marković, Emina Požega

Mining and Metallurgy Institute Bor, Zeleni bulevar 35, 19210 Bor, Serbia

### Abstract

*Water purification has been identified as a key global concern, due to fast developing of economy which is result of crude oil exploration and production, as well as pharmaceuticals manufacturing. Comparing to other adsorbents carbon nanotubes have proven to be good choice for wastewater treatment of organic pollutants because of their high adsorption capacity. This paper presents a review of literature data on the use of carbon nanotubes to the purification of wastewater, which has been one of the most prominent and major areas for their application since their creation and commercial usage.*

**Keywords:** carbon nanotubes, organic pollutants, wastewater treatment

### 1. INTRODUCTION

Pharmaceuticals, personal care products, organic dyes, pesticides, detergents and a typical industrial organic wastes such as phenols, halogens and aromatics are examples of organic pollutants. Worryingly, they are unremitting and persistent in the environment. They are growing more prevalent as industrialization progresses. In comparison to the limited varieties of heavy metals in water, organic contaminants are increasing in number as industrial growth continues. The international environmental accord imposed restrictions on the manufacture, use, and discharge of twelve important persistent organic pollutants [1].

The worldwide distribution of oil and its derivatives generates a significant danger to the environment. There are multiple traditional methods for removing oil from water, but due to several defects and disadvantages, research efforts have centered on identifying such adsorbents that may boost oil adsorption capacities. Oil spills in oceans, seas, lakes, and rivers make up a significant environmental catastrophe [2].

Adsorption is a simple, inexpensive, and efficient method of eliminating hydrocarbons from water. Carbon-based adsorbents, particularly carbon nanotubes (CNTs), are frequently used to separate water and oil. In comparison with other adsorbents, they satisfy all of the requirements for effective oil adsorption [3].

### 2. REMOVAL OF ORGANIC POLLUTANTS FROM WASTEWATER

Chemical oxidation, adsorption and photocatalytic degradation are the most often used ways for cleaning water from organic contaminants. Most organic pollutants may be successfully oxidized into inorganic carbon (CO<sub>2</sub>) via the oxidation process (using O<sub>2</sub>, O<sub>3</sub>, Cl<sub>2</sub>, ClO<sub>2</sub> and H<sub>2</sub>O<sub>2</sub>), but the potential drawback of this procedure is health risk of incomplete degradation of side products [4]. Compared to oxidation process, with adsorption process doesn't exist risk of secondary potential contamination and it has shown to be the most successful and vital approach for removing contaminants from water at an affordable cost. This process has been applied for wastewater purification for many years owing to its speed, effectiveness and economic benefits. Its efficacy is mostly determined by the type of adsorbent and operating conditions. Active carbons, zeolites, clays and carbon nanomaterials (graphene, graphene oxide, and carbon nanotubes) are the most often utilized adsorbents for the adsorption of organic contaminants in water [5]. Photocatalytic degradation is one of the methods for removing organic contaminants from water that uses the

Fenton process to degrade organic pollutants.  $\text{TiO}_2$ ,  $\text{TiO}_2$  and  $\text{ZnO}$  can be utilized in this method since they have the capacity to break down organic contaminants into little molecules without being hazardous [6].

## 2.1 Removal of organic pollutants from water using CNTs

Oil products are the most widespread sources of water pollution, coming into contact with water through the release of oil and fuel from land-based plants, tanker spills and accidental leaks during transport. Removal of unleaded gasoline from water is possible using multi-walled carbon nanotubes (MWCNTs) due to a number of favorable properties they possess as adsorbents, such as good hydrophobicity and oleophilicity, capacity and speed of uptake and retention of hydrocarbons. During the experiments, the conditions of actual polluted water were simulated. Dispersions of commercial unleaded gasoline (20 ml) in water (30 ml) were used, which were exposed to varying amounts of MWCNTs (0.2–0.8 g) at room temperature. Obtained results are shown graphically in Figure 1. The highest percentage of unleaded gasoline removed was obtained by using small amounts (0.7 g) of MWCNTs during a very short mixing time (5 min), larger amounts of adsorbent did not improve the efficiency of the process. Small amounts used in the presented experiments, simple regeneration after each application and low costs of the raw materials used for the production of MWCNTs, make this process economical [7].

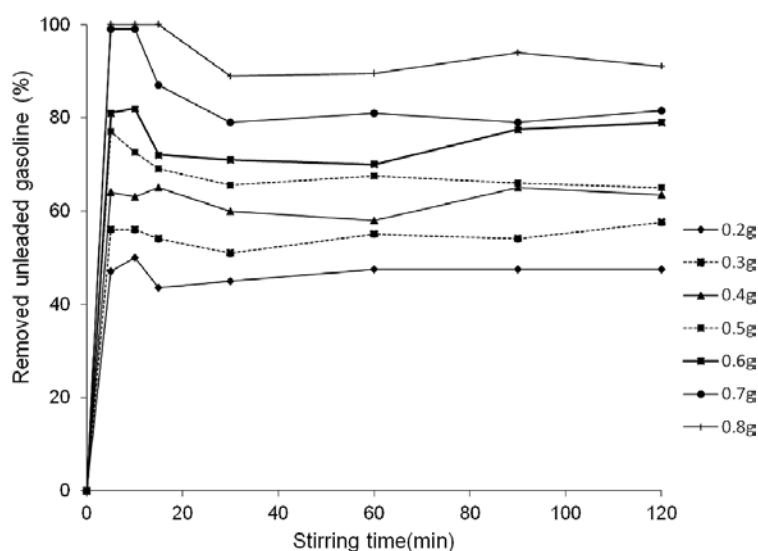


Figure 1 - Removed unleaded gasoline (%) from hydrocarbon / water dispersion as function of mixing time [7]

In order to produce a hydrophobic adsorbent, the MWCNTs surface can be modified using the microemulsion method (MEMWCNT) without changing their structure. The results of UV spectrophotometric analysis showed that MEMWCNTs are more effective for adsorbing toluene from the toluene-water mixture (90%) compared to untreated MWCNTs (77%). Using kerosene as a model hydrocarbon, the efficiency of its adsorption from water in the presence of MWCNTs was compared with MEMWCNTs. From 35%, which was adsorbed by MWCNT, using MEMWCNT this value increased to 96%. The adsorption capacities of MEMWCNTs are higher than those of MWCNTs for all hydrocarbon models and range from 6.07 to 5.68 g/g, while the adsorption capacity of MWCNTs is in the range of 2.48–4.64 g/g. The experimental results proved that MEMWCNTs are good hydrocarbon adsorbents, and that the surface modification of MWCNTs by the microemulsion method had a beneficial effect on the hydrophobic properties of MWCNTs [8].

Aromatic amines and phenols are considered the most common pollutants found in water bodies. Their presence in the aquatic ecosystem causes an imbalance, because the food chain is disrupted, which further causes the death of many aquatic organisms. The removal of aniline by MWCNTs is performed in two steps. First, aniline molecules diffuse from the aqueous solution to the outer surface of the MWCNTs, and then the aniline molecules diffuse through the MWCNTs. The highest removal efficiency of toluene, ethylbenzene and xylene isomers was observed with MWCNTs oxidized by 3% NaOCl. The presence of oxygen-containing groups caused less pore damage. The removal increased with longer contact time, while it decreased with increasing reaction temperature [9].

Various pharmaceutical and personal care products (PPCPs) have been detected in groundwater, rivers and lakes. For the removal of ibuprofen and triclosan from synthetic water, single-walled CNTs (SWCNTs) showed the highest efficiency compared to MWCNTs and oxidized MWCNTs. Due to their large specific surface area (~1020 m<sup>2</sup>/g) SWCNTs are often used to remove pharmaceuticals from water. Adsorption of diclofenac on MWCNTs was 41.4 mg/g in clean water and 22.3 mg/g in wastewater. According to the research results, oxidized MWCNTs can improve tetracycline adsorption due to the introduction of COOH and C–O groups on the MWCNTs surface. Oxidized MWCNTs show a greater ability to adsorb other drugs, such as ciprofloxacin, due to improved hydrophilicity and dispersibility. Pore size is the rate-determining step, and the introduction of ionic liquid into CNTs resulted in an improvement in the hydrophobicity of CNTs, which allows for more interactions between the adsorbent and the adsorbate [9].

CNTs have the ability for successful adsorption of dye molecules from wastewater. Methylene blue was removed from wastewater using carpet-like vertical arrays of CNTs connected to porous carbon foam surfaces by coating with a silicon dioxide buffer layer. The amount of CNTs on the foam and adsorption capacity of hybrid CNTs are directly related. The maximum adsorption capacity for methylene blue using CNT arrays is around 43.5 mg/g, which is more than what can be accomplished with a variety of other methylene blue adsorbents [10].

### 3. CONCLUSION

The contamination of the planet by countless harmful compounds, both from manufactured and natural sources is continual. Numerous harmful substances have been released into the environment as a result of rapid industrial development and population increase. Without properly evaluating the threats to the environment and impacts on human health, many new compounds are utilized. Based on previous experiments, CNTs have proven to be excellent adsorbents for organic dyes, oil, pharmaceutical products and pesticides. Before implementing on a large-scale, a risk evaluation for the environment and human health should be made, since nanomaterials frequently have hazardous effects on aquatic creatures when used in large amounts.

### ACKNOWLEDGEMENTS

*The authors are grateful for funding by the Minister of Science, Technological Development and Innovation of the Republic Serbia, the Grant No. 451-03-47/2023-01/ 200052. Also, this work is financially supported by the EU under Program 2nd EIT-HEI call: Building Ecosystem Integration Labs at HEI to foster Smart Specialization and Innovation on Sustainable Raw Materials - HEI4S3-RM.*

### REFERENCES

- [1] A. Ojha, D. Tiwary, Contamination of Water, Academic Press, Cambridge, 2021, p.237-250.
- [2] B. Zhang, E. Matchinski, B. Chen, X. Ye, L. Jing, K. Lee, World Seas: an Environmental Evaluation (Second Edition) Volume III: Ecological Issues and Environmental Impacts, Elsevier Ltd., Amsterdam, 2019, p.391-406.

- [1] T. A. Abdullah, T. Juzsakova, S. A. Hafad, R. T. Rasheed, N. Al-Jammal, M. A. Mallah, A. D. Salman, P. C. Le, E. Domokos, M. Aldulaimi, *Clean Technol. Environ. Policy*, 24 (2) (2022) 519-541.
- [2] M. Panizza, G. Cerisola, *Chem. Rev.*, 109 (12) (2009) 6541-6569.
- [3] M. N. Rashed, *Org. Pollut.- Monit. Risk Treat.*, IntechOpen, London, 2013, p.167–194.
- [4] P. K. Pandis, C. Kalogirou, E. Kanellou, C. Vaitsis, M. G. Savvidou, G. Sourkouni, A. A. Zorpas, C. Argirusis, *ChemEngineering*, 6 (1) 8 (2022).
- [5] D. Lico, D. Vuono, C. Siciliano, J. B. Nagy, P. De Luca, *J. Environ. Manage.*, 237 (5) (2019) 636-643.
- [6] N. Al-Jammal, T. A. Abdullah, T. Juzsakova, B. Zsirka, I. Cretescu, V. Vágvölgyi, V. Sebestyén, C. Le Phuoc, R. T. Rasheed, E. Domokos, Functionalized carbon nanotubes for hydrocarbon removal from water, *J. Environ. Chem. Eng.*, 8 (2) (2020) 103570.
- [7] K. M. Lee, C. P. P. Wong, T. L. Tan, C. W. Lai, *Mater. Sci. Eng.*, 236-237 B (2018) 61-69.
- [8] H. Vijwani, M. N. Nadagouda, V. Namboodiri, S. M. Mukhopadhyay, *Chem. Eng. J.*, 268 (2015) 197-207.

## EXPERIMENTAL INVESTIGATIONS OF CuAlAg ALLOYS WITH 70 at%Cu

Zdenka Stanojević Šimšić, Ana Kostov, Aleksandra Milosavljević, Slavica Miletić

Mining and Metallurgy Institute Bor, Zeleni bulevar 35, 19210 Bor, Serbia

### Abstract

Represented results in this paper are obtained from the experimental investigations of the selected as-cast alloys with Cu content of 70 at% in the ternary Cu-Al-Ag system. These investigations included microstructural characterization and experimental determination of hardness, microhardness and electrical conductivity. Microstructure of the investigated alloys has been done by light optical microscopy. In the frame of investigations of some mechanical properties, hardness and microhardness were determined by Vickers standard method. Electrical conductivity was determined too.

**Keywords:** Copper-rich alloys, Microstructure, Mechanical properties, Electroconductivity

### 1. INTRODUCTION

Smart materials and shape memory materials, as part of this large group of materials, have been studied very well and in detail for decades [1,2]. A huge number of shape memory alloys of various binary, ternary and multicomponent systems, such as Ag-Cd, Au-Cd, Cu-Sn, Cu-Al-Ag, Cu-Al-Ag-Mg, Cu-Al-Au, Cu-Ag- Au, Cu-Au-Zn, Cu-Zn-Ga, Ni-Al, Ti-Ni-Cu, Ni-Ti-Nb, Ti-Pd-Ni, In-Ti, In-Cd and others, have been obtained and investigated due to the fact that their properties make them convenient for different purposes. Alloys of the Cu-Al-Ag ternary system have also, been studied for a long time but the shape memory effect which is characteristic for these alloys and their good properties are the reason for further research by scientists [3,4,5].

This paper represents the results of the experimental investigations of the CuAlAg alloys chosen along vertical section with constant copper content of 70 at% as an addition to the previous published in ref. [5].

### 2. EXPERIMENTAL

All alloy samples were cast using induction melting and the purities of the constituent metals, Cu, Al and Ag, were 99,99%. Samples preparation was done under argon atmosphere with total metal losses of the samples less than 1%. All alloys were melted and cooled repeatedly due to improvement of the compositional homogeneity.

A study of the microstructure of the investigated alloys has been done by light optical microscopy using Reichert MeF2 microscope. Hardness and microhardness measurements were carried out using Vickers standard method at a load of 10N and 100g. Electrical conductivity measurements were carried out on "Institute dr. Förster SIGMATEST 2.06" device.

Composition and mass of selected as-cast alloys are shown in Table 1.

Table 1 - Composition and mass of investigated alloys

Sample	$X_{Cu}$	$X_{Al}$	$X_{Ag}$	$m_{Cu}$	$m_{Al}$	$m_{Ag}$
C1	0,7	0,06	0,24	3,0894	0,1124	1,7982
C2	0,7	0,12	0,18	3,3127	0,2411	1,4461
C3	0,7	0,18	0,12	3,5709	0,3899	1,0392
C4	0,7	0,24	0,06	3,8727	0,5638	0,5635



### 3. RESULTS AND DISCUSSION

All investigated as – cast alloys, C1, C2, C3 and C4, with compositions given in Table 1., are located in the area with 70 at% of copper, based to their chemical compositions and calculated phase diagram [5].

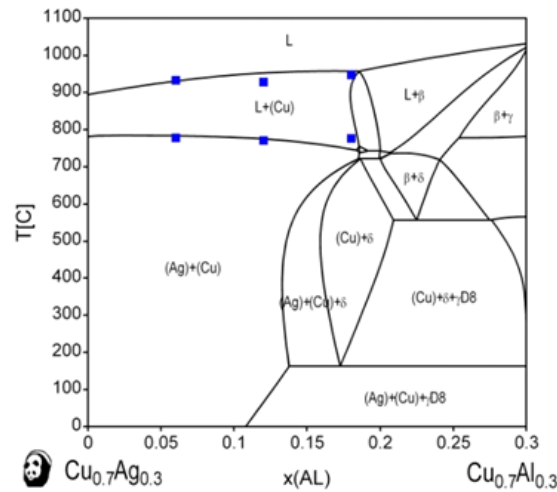


Figure 1 - Calculated vertical sections of the Cu-Al-Ag ternary system with constant copper content of 70at% compared with DTA results [5]

Phase diagram of the calculated vertical section with 70 at% of copper, presented in the Figure 1, shows that the tested alloys mainly belong in the area of primary crystallization - Liquid + (Cu) - copper-based solid solution.

The results of microstructural characterization are presented in the following Figures:

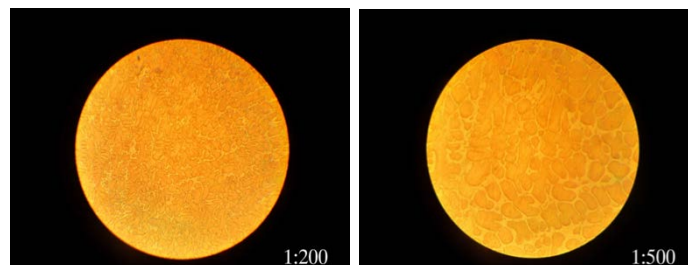


Figure 2 - Sample alloy C1 (Cu<sub>70</sub>Al<sub>6</sub>Ag<sub>24</sub>)

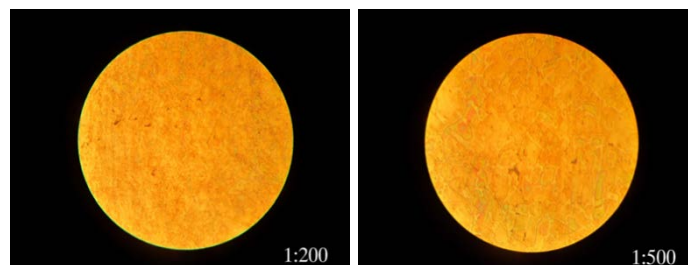


Figure 3 - Sample alloy C2 (Cu<sub>70</sub>Al<sub>12</sub>Ag<sub>18</sub>)

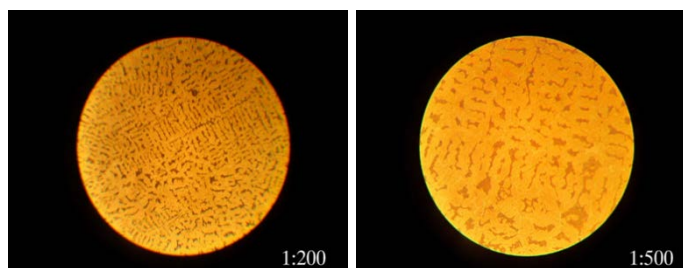


Figure 4 - Sample alloy C3 ( $\text{Cu}_{70}\text{Al}_{18}\text{Ag}_{12}$ )

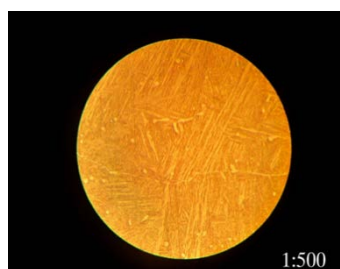


Figure 5 - Sample alloy C4 ( $\text{Cu}_{70}\text{Al}_{24}\text{Ag}_6$ )

The microstructure of the investigated copper-rich samples with 70 % at Cu, which are presented in Figures 2-4, consists of primary crystals of copper based solid solution (Cu) and silver based solid solution (Ag), in the form of precipitates on the edges of copper crystals. Sample C3 in Figure 4 is characterized by a dendritic structure, while in the alloy C4 (Figure 5), exists martensitic structure.

### 3.1 Hardness and microhardness measurements

The results of the hardness measurements of the alloys samples along the vertical cross-section of 70 at% Cu are presented in Table 2. It is noticeable that with the increase of aluminum content, the hardness values of the tested alloys increase.

Table 2 - Results of the hardness measurements for selected as-cast alloy samples

Sample label	Sample	HV10
C1	$\text{Cu}_{70}\text{Al}_6\text{Ag}_{24}$	95
C2	$\text{Cu}_{70}\text{Al}_{12}\text{Ag}_{18}$	102
C3	$\text{Cu}_{70}\text{Al}_{18}\text{Ag}_{12}$	111
C4	$\text{Cu}_{70}\text{Al}_{24}\text{Ag}_6$	164

Table 3 - Results of the microhardness measurements for selected as-cast alloy samples

Sample label	Sample	HV0.1		
		Measuring point 1	Measuring point 2	Measuring point 3
C1	$\text{Cu}_{70}\text{Al}_6\text{Ag}_{24}$	83	93	78
C2	$\text{Cu}_{70}\text{Al}_{12}\text{Ag}_{18}$	91	128	86
C3	$\text{Cu}_{70}\text{Al}_{18}\text{Ag}_{12}$	166	151	190
C4	$\text{Cu}_{70}\text{Al}_{24}\text{Ag}_6$	309	211	323

As it can be seen in Table 3, microhardness values of the tested alloys increase with the increase in aluminum content

### 3.2 Electrical conductivity

The results of the electroconductivity measurements are presented in Table 4. Measured values of the electroconductivity of the tested alloys decrease with increase of the aluminum content.

Table 4. Results of the electrical conductivity measurements for selected as-cast alloy samples

Sample label	Sample	Electrical conductivity (MS/m)		
C1	Cu <sub>70</sub> Al <sub>6</sub> Ag <sub>24</sub>	8,4	8,9	8,9
C2	Cu <sub>70</sub> Al <sub>12</sub> Ag <sub>18</sub>	5,8	5,8	5,4
C3	Cu <sub>70</sub> Al <sub>18</sub> Ag <sub>12</sub>	5,4	5,9	5,8
C4	Cu <sub>70</sub> Al <sub>24</sub> Ag <sub>6</sub>	5,6	5,6	5,7

## 4. CONCLUSION

This paper represents the obtained results from the experimental investigations of the selected as-cast alloys with Cu content of 70 at% in the ternary Cu-Al-Ag system. The investigations included microstructural characterization and experimental determination of hardness, micro-hardness and electrical conductivity. Microstructure of the investigated alloys has been done by light optical microscopy. Hardness and micro-hardness values of the tested alloys increase with the increase in aluminum content. With increase of the aluminum content, the values of the electro-conductivity of the tested alloys decrease.

## ACKNOWLEDGEMENTS

*This work was financially supported by the Ministry of Science, Technological Development and Innovation of the Republic of Serbia, within the financing of scientific research work at the Mining and Metallurgy Institute Bor, according to contract no. 451-03-47/2023-01/ 200052.*

## REFERENCES

- [1] I. N. Qader, M. Kök, F. Dagdelen, Y. Aydogdu, El-Cezerî J. Pet. Sci. Eng. 6 (3) (2019) 755-788.
- [2] K. Otsuka, K. Shimizu, Y. Suzuki, Y. Sekiguchi, C. Taki, T. Homma, S. Miyazaki, Splavi s Effektom Pamjati Form, Metallurgija, Moskva, 1990, p. 123.
- [3] M. F. Ijaz, M. S. Soliman, A. S. Alasmari, A.T. Abbas, F. H. Hashmi, Crystals, 11 (11), (2021) 1330.
- [4] U. Büyük, N. Marasli, E. Çadırlı, H. Kaya, K. Keslioglu., Curr. Appl. Phys., 12 (2012) 7-10.
- [5] Z. Stanojević Šimšić, D. Živković, D. Manasijević, T. Holjevac Grgurić, Yong Du, M. Gojić, S. Kožuh, A. Kostov, R.Todorović, J. Alloys Compd. 612 (2014) 486-492.

## DETERMINATION OF MELT PROPERTIES IN Cu-Fe ALLOYS

Ana Kostov, Aleksandra Milosavljević, Zdenka Stanojević Šimšić, Ivan Jovanović

Mining and Metallurgy Institute Bor, Zeleni bulevar 35, 19210 Bor, Serbia

### Abstract

*The goal of the paper is to find a copper alloys with iron content that would have practical application in electronics as an electronic functional material. The melt properties of the special alloys in system Cu-Fe are given in this paper.*

*Keywords: Cu-Fe alloys, melt, Gibbs free energy*

### 1. INTRODUCTION

Considering the fact that the world economy has changed in recent years, that there is a recession in world and European industrial countries, and especially in the post-covid period, there was a need for some materials that are used for everyday use to be produced in own country and at that way to avoid their import.

This especially applies to the use of classic metal materials in electronics and electronic industry, where there is the greatest demand.

A lot of attention was given to investigation of special copper alloys with iron in the best laboratory conditions in the world [1-5]. However, these alloys offer remarkable electrical conductivity, thermal conductivity, magnetism, and wear resistance characteristics, making them ideal for applications across a wide range of fields, including 5G/6G communication systems, AI/IoT, medicine/antibacterial uses, and vehicle-mounted equipment. Characteristics can be adjusted by varying the copper and iron content, allowing to offer solutions to suit particular applications.

### 2. EXPERIMENTAL

Alloys of the Cu-Fe system on the copper side are usually two-component or multi-component copper alloys with iron in the amount of up to 3%. Alloys of copper with iron can also contain some usual amounts of phosphorus and zinc, which are introduced primarily as agents for the deoxidation of copper before the introduction of iron, or they can be additionally alloyed with these components, which significantly improves the mechanical properties without fear that under their influence they can more significantly reduced the electrical conductivity.

Copper alloys with iron belong to the group of alloys with medium electrical conductivity and medium hardness.

The alloys are obtained by classical melting of copper and reduced iron powder in an electric induction furnace and the addition of phosphorus and zinc for the deoxidation of the copper melt.

It is emphasized that the melting of special copper alloys with iron is very important and related to the concept of melting alloys of the Cu-Fe system, according to phase diagram of the Cu-Fe system. The role of phosphorus and zinc in the alloys are also important, given the fact that they are present in amounts of up to 0.15% and 0.20%, respectively.

The chemical composition of the obtained set of the special copper alloys with iron is shown in the Table 1.

Table 1 – Chemical composition of the Cu-Fe alloys

Alloys	Content, %				
	Cu	Fe	P	Zn	Pb
Cu-Fe	balance up to 100%	2.10-2.60	0.03		
Cu-Fe-P	balance up to 100%	2.10-2.60	0.015-0.15	0.20	0.03

### 3. RESULTS AND DISCUSSION

In order to determine the melt properties of the investigated alloys, the basis of the quasi-chemical theory and the principle of quasi-regular melts, where the averageness of the micro-range is taken into account, are used for calculation of the thermodynamic properties of the investigated alloys of the Cu-Fe system, such as enthalpy of mixing and Gibbs free energy.

The system Cu-Fe belongs to the group of the eutectic alloys in which there is a tendency towards layering or non-mixing in the liquid state, immediately near the liquidus line.

Enthalpy of mixing liquid copper with iron is calculated at two temperatures: 1773K and 1873K. The results are shown in the Table 2.

Table 2 – Enthalpy of mixing in Cu-Fe alloys

Alloys	Temperature, K	Enthalpy, kJ/mol
Cu-Fe	1773	8.37
	1873	8.63
Cu-Fe-P	1773	8.14
	1873	8.19

The change of the Gibbs free energy is calculated at different temperatures: 1473K, 1673K, 1773K and 1873K. The results are shown in Table 3.

Table 3 – Gibbs free energy of Cu-Fe alloys

Alloys	Temperature, K	$\Delta G$ kJ/mol
Cu-Fe	1473	-15.84
	1673	-25.38
	1773	-30.16
	1873	-34.94
Cu-Fe-P	1473	-9.52
	1673	-17.67
	1773	-21.75
	1873	-25.82

According to the obtained data, the process of mixing liquid copper with iron is characterized by an endothermic heat effect and the changing of the Gibbs free energy is negative in the investigated temperature range. The thermal effect of mixing the melt is relatively small. The obtained data showed the melt of alloys belong to the group of quasi-regular melts.

Results of surface tension measurement at temperature 1473K, 1673K and 1773K are shown in Figure 1.

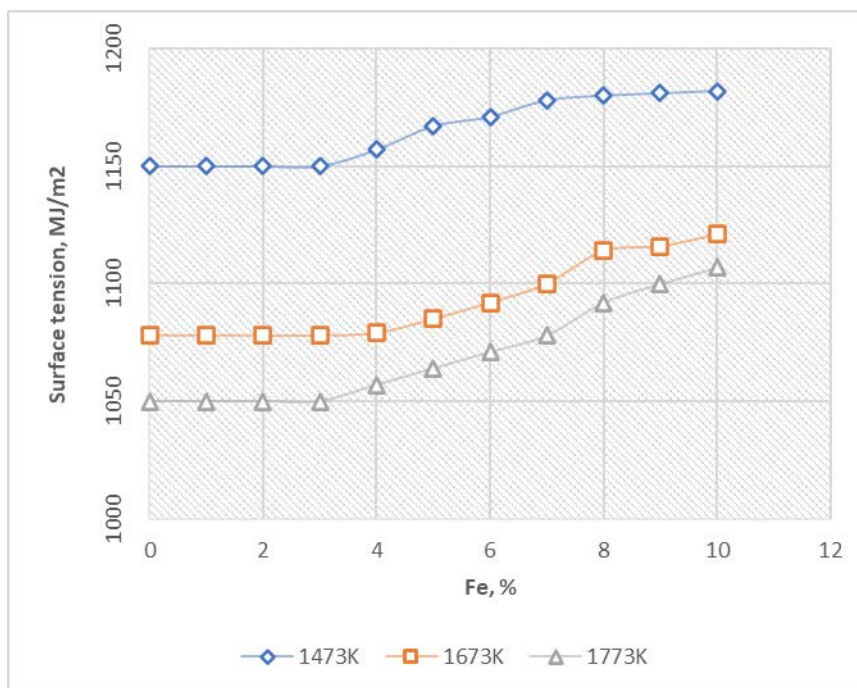


Figure 1 - Surface tension of Cu-Fe alloys at 1473K, 1673K and 1773K

According to the obtained results, isotherms of the surface tension of the Cu-Fe alloys at a content of up to 10 mass% show the surface tension practically does not change at a content of up to 4 mass% of iron, and then begins to increase slowly. In this connection, the best practical application in electronics and for electronic materials is taken alloys with iron content up to 3 mass%.

The specific volume of the alloys is determined for alloys with a higher copper content till 10 mass% of iron and at 1773K. The obtained results are shown in Figure 2.

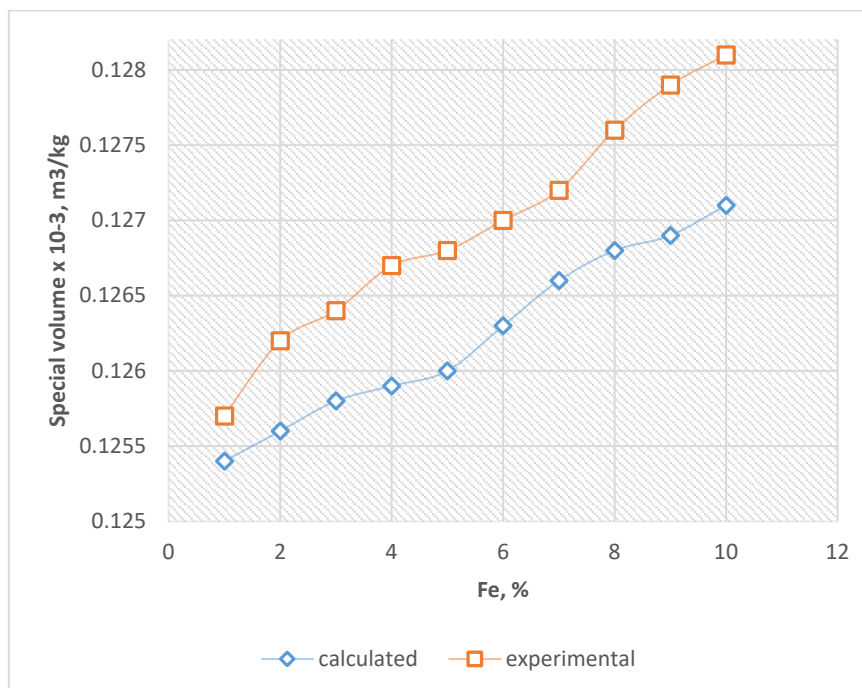


Figure 2 - Specific volume of Cu-Fe alloys at 1773K calculated and experimental values



The obtained results show that in melts rich in copper, even at high overheating for copper alloys up to the order of 1773K-1873K, it is possible to layer the melt by forming iron-enriched groups, that is, emulsion-like melts are obtained.

Based on the Cu-P and Fe-P phase diagrams, it can be seen that copper forms a eutectic with phosphorus. Therefore, the addition of insignificant amounts of phosphorus to the alloy melt in the Cu-Fe system will affect the fact that phosphorus binds more to iron due to its greater affinity compared to the affinity to copper. Due to the stronger mutual bonds of phosphorus with iron in the melt with copper, i.e. the greater affinity between these two elements compared to copper and phosphorus, layering of the alloy will not occur, which will enable obtaining a liquid cast during melting and forming alloys with a satisfactory composition without segregations.

All that mention above should be kept in mind when overcoming the technology of making alloys of this system.

#### **4. CONCLUSION**

Obtaining special alloys of copper with iron, which will be used as an electronic material implies obtaining alloys with precisely defined compositions.

The structural properties of alloys in the system Cu-Fe depend first of all on the chemical composition, but also on the solidification conditions of the melt and then on the plastic treatment and thermal treatment.

Therefore, knowing and determining the properties of the melt greatly contributes to obtaining quality alloys with properties that are suitable for wide application in electronics and the electrical industry.

Based on the obtained results, it can be concluded that iron is completely dissolved during melting. The phosphorus content guarantees the complete deoxidation of copper in the process of melting and making alloys.

#### **ACKNOWLEDGEMENTS**

*The research presented in this paper was carried out with the financial support of the Ministry of Science, Technological Development and Innovation of the Republic of Serbia, as a part funding the scientific research work in the Mining and Metallurgy Institute Bor, according to the Contract with registration no. 451-03-47/2023-01/ 200052.*

#### **REFERENCES**

- [1] Z. M. Rdzawski, J. Stobrawa, W. Głuchowski, J. Achiev. Mater. Manuf. Eng., Vol. 33, 1 (2009) 7-18.
- [2] K. Sugioka, Y. Tsutsui, H. Kobatake, Int. J. Microgravity Sci. Appl., 39 (2022) 4.
- [3] J. Vít, Proceedings of 31<sup>st</sup> International Conference on Metallurgy and Materials, May 18 - 19, Brno, Czech Republic, 2022, pp. 669-674.
- [4] A. Lukyanov, A. Churakova, D. Gunderov, A. Filatov, E. Antipov, V. Sitdikov, A. Ganeev, R. Valiev, V. Pushin, Rev. Adv. Mater. Sci., 45 (2016) 20-27.
- [5] G.-C. Zhao, Y. Qiu, C.-G. Liu, ACS Omega, 7 (2022) 41586 - 41593.

## A SIMPLE METHOD OF DETERMINING OF BOND WORK INDEX FOR FINER SAMPLES

Vladimir Nikolić, Milan Trumić

Technical Faculty Bor, University of Belgrade, V.J. 12, 19210 Bor, Serbia

### Abstract

The Bond's method is based on the experimental determination of the Bond work index which represents a measure of ore resistance to grinding and its denotation is  $W_i$ . The conditions for performing the test and initial sample size are precisely defined within Bond's standard test. The procedure for the determination of the Bond work index for finer samples was presented in this paper. These finer samples are usually seen as a problem for practitioners who work on the design and optimization of a plant.

**Keywords:** (Finer Samples, Bond Work Index, Grindability)

### 1. INTRODUCTION

The ball mill grindability test sometimes referred to as “the Bond test” was developed in the 1930s by the Allis Chalmers company to help them perform ore hardness characterisation testing to assist in industrial mill sizing [1]. It was extended by Bond (1952) [2] to provide a ‘work index’ result that was empirically calibrated to make a laboratory work index match the corresponding work index measured in an industrial grinding mill. The fitted equation, in metric form, is given as Equation (1).

$$W_i = 1.1 \cdot \frac{44.5}{P_c^{0.23} \cdot G^{0.82} \cdot \left( \frac{10}{\sqrt{P_{80}}} - \frac{10}{\sqrt{F_{80}}} \right)} \quad (1)$$

where in:

$P_c$  - closing screen size ( $\mu\text{m}$ ),

$G$  - net mass (grams) of undersize product per unit revolution of the mill, in g/rev,

$P_{80}$  - the 80 % passing product particle size ( $\mu\text{m}$ ),

$F_{80}$  - the 80 % passing feed particle size ( $\mu\text{m}$ ).

The Bond method consists in the experimental determination of the Bond work index, which expresses the resistance of the raw material to comminution and is denoted by  $W_i$ . In Bond's standard test, the test performance conditions are precisely defined. The starting size of the sample is also defined. Due to the sheer scope of the test, many researchers have conducted research with the aim of shortening the test and finding alternative methods of determining Bond work index [3-12]. However, very few researchers have dealt with the determination of Bond work index obtained from the test based on finer samples.

Levin (1989) [13] proposed a method for determining the grindability of fine material that included the estimation of energy necessary for the grinding. Magdalinovic et al. (2012) [14] determined the Bond work index on samples of non-standard size. Nikolić and Trumić (2021) [15] provided the procedure for determination of Bond work index for finer samples. This paper represents a continuation of the research published by Nikolić and Trumić (2021) [15].

## 2. EXPERIMENTAL

The samples used in the study were prepared by crushing in a jaw crusher and then sieved through a sieve with an opening size of -3.35 mm. Two monomineralic types of raw material, zeolite and dacite, were used in the study. Five 10 kg samples with different initial sizes (- 3.35 + 0 mm; - 2.36 + 0 mm; - 1.70 + 0 mm; - 1.18 + 0 mm; - 0.850 + 0 mm) were formed for each individual type of raw material for grinding test based on the standard Bond procedure. The dry grinding was used, simulating a closed grinding cycle, until a circulating load of 250 % was established [17]. A 75 µm closing screen size was used. The Bond work index was calculated by Equation (1).

## 3. RESULTS AND DISCUSSION

The obtained results for the Bond work index for samples of zeolite and dacite, on fine size classes are shown in Table 1.

Table 1 - Parameters  $F_{80}$ ,  $P_{80}$ ,  $G$  and value of  $W_i$  for samples of zeolite and dacit used on fine material

Sample	Class size (mm)	$P_c = 75 \mu m$			
		$F_{80}$ (µm)	$P_{80}$ (µm)	$G$ (g/rev)	$W_i$ (kWh/t)
Zeolite	- 3.35 + 0	2440	65.72	2.03	9.834
	- 2.36 + 0	1652	66.40	2.13	10.010
	- 1.70 + 0	1090	66.48	2.20	10.197
	- 1.18 + 0	727	66.84	2.35	10.371
	- 0.850 + 0	544	67.12	2.57	10.572
Dacite	- 3.35 + 0	2646	64.70	0.96	17.800
	- 2.36 + 0	1729	64.76	1.00	18.130
	- 1.70 + 0	1253	65.76	1.05	18.333
	- 1.18 + 0	807	65.20	1.10	18.827
	- 0.850 + 0	609	65.64	1.12	19.196

The authors Nikolić and Trumić (2021) [15] provided the equation for the determination of the Bond work index for fine materials, and it is presented by Equation (2). The Equation (2) was tested on a zeolite sample, and further research was conducted on sample dacite.

$$W_{Fm} = k \cdot \frac{W_i}{F_{Fm}^{0.05}} \quad (2)$$

where in:

$W_{Fm}$  - BWI for fine materials, (kWh/t);

$W_i$  - BWI for a standard size sample (- 3.35 + 0) mm, (kWh/t);

$F_{Fm}$  - the 80 % passing fine material particle size, (µm),

$k$  - value of coefficient  $k$  was given in table 2.

Table 2 - Value of coefficient  $k$

Value of coefficient $k$	$k = 1.47$	$k = 1.48$	$k = 1.49$
<b>BWI (kWh/t)</b>	10 - 17	18 - 20	> 21

The comparative results of the Bond work index for finer materials obtained experimentally by ( $W_i$ ) and Equation (2) ( $W_{Fm}$ ), as well as the results found in literature, are shown in Table 3.

Table 3 - Results obtained with experiments and equation (2)

Sample	References	Class size (mm)	$F_{80}$ ( $\mu\text{m}$ )	$P_c = 75 \mu\text{m}$		$W_{Fm}$ (kWh/t)	Error $\Delta$ (%)
				$W_i$ (kWh/t)	$k$		
Zeolite	[15]	- 3.35 + 0	2440	9.834	1.47	-	-
		- 2.36 + 0	1652	10.010		9.980	+ 0.30
		- 1.70 + 0	1090	10.197		10.190	+ 0.07
		- 1.18 + 0	727	10.371		10.399	- 0.27
		- 0.850 + 0	544	10.572		10.550	+ 0.21
Dolomite	[14]	- 3.327 + 0	2468	12.70		-	-
		- 2.356 + 0	1662	12.91		12.89	+ 0.15
		- 1.651 + 0	1090	13.16		13.16	0.00
		- 1.168 + 0	727	13.38		13.43	- 0.37
		- 0.833 + 0	544	13.69		13.63	+ 0.44
Commercial aggregate	[17]	- 3.35 + 0	2134	15.0	-	-	
		- 2.36 + 0	1492	15.3	15.3	0.00	
Copper ore	[14]	- 3.327 + 0	2646	15.67	-	-	
		- 2.356 + 0	1729	15.70	15.97	- 1.72	
		- 1.651 + 0	1253	15.84	16.24	- 2.53	
		- 1.168 + 0	807	16.19	16.54	- 2.16	
		- 0.833 + 0	609	16.79	16.84	- 0.30	
Dacite		- 3.35 + 0	2646	17.800	1.48	-	-
		- 2.36 + 0	1729	18.130		18.146	- 0.88
		- 1.70 + 0	1253	18.333		18.441	- 0.60
		- 1.18 + 0	807	18.827		18.851	- 0.13
		- 0.850 + 0	609	19.196		19.118	+ 0.41
Quartzite	[14]	- 3.327 + 0	2650	22.63	1.49	-	-
		- 2.356 + 0	1790	23.17		23.19	- 0.09
		- 1.651 + 0	1240	23.52		23.62	- 0.43
		- 1.168 + 0	870	24.14		24.04	+ 0.41
		- 0.833 + 0	610	24.72		24.47	+ 1.01

Based on the obtained results presented in Table 3, it can be concluded that when the Bond work index for finer samples is calculated by Equation (2), the reliable results are obtained and the error is not greater than 2.50 %. This fact confirms the accuracy and validity of Equation (2).

#### 4. CONCLUSION

The determination of Bond work index for finer samples is possible if the value of Bond work index for the standard size sample is known and using the Equation (2). This procedure offered the maximum error of -2.53 % for  $W_i$ . Such a small error obtained this way confirms the accuracy and validity of the suggested procedure for the determination of Bond work index for finer samples.

#### ACKNOWLEDGEMENTS

*"The research presented in this paper was done with the financial support of the Ministry of Education, Science and Technological Development of the Republic of Serbia, within the funding*

*of the scientific research work at the University of Belgrade, Technical Faculty in Bor, according to the contract with registration number 451-03-47/2023-01/200131".*

## REFERENCES

- [1] W.L. Maxson, F. Cadena, F.C. Bond, *Trans. Metallur. Soc. AIME*, 112 (1933) 130-145.
- [2] F.C. Bond, *Trans AIME*, 193 (1952) 484-494.
- [3] T.F. Berry, R.W. Bruce, *Can. Min. J.*, 87 (1966) 63-65.
- [4] R.W. Smith, K.H. Lee, *Trans. Metallur. Soc. AIME*, 241 (1968) 91-99.
- [5] P.C. Kapur, *Trans. Inst. Min. Metallur.*, 79 (1970) 103-107.
- [6] W.E. Horst, J.H. Bassarear, *Trans. Metallur. Soc. AIME*, 260 (1977) 348-351.
- [7] V.K. Karra, *CIM Bull.*, 74 (827) (1981) 195-199.
- [8] N. Magdalinović, *Int. J. Miner. Process.*, 27 (1-2) (1989) 125-132.
- [9] N. Magdalinović, *J. Min. Metallur.*, 39 (1-4) A (2003) 1-10.
- [10] R. Ahmadi, S. Shahsavari, *Miner. Eng.*, 22 (1) (2009) 104-106.
- [11] E. Ford, V. Sithole, *Copper Cobalt Africa*, incorporating the 8<sup>th</sup> Southern African Base Metals Conference, Livingstone, Zambia, 6-8 July, 2015, 65-68.
- [12] D. Todorovic, M. Trumic, Lj. Andric, V. Milosevic, M. Trumic, *Physicochem. Probl. Miner. Process.*, 53 (1) (2017) 321-332.
- [13] J. Levin, *J. S. Afr. Inst. Min. Metall.*, 89 (1) (1989) 13-21.
- [14] N. Magdalinovic, M. Trumic, G. Trumic, S. Magdalinovic, M. Trumic, *Int. J. Miner. Process.*, 114-117 (2012) 48-50.
- [15] V. Nikolić, M. Trumić, *Miner. Eng.*, 165 (2021) 106858.
- [16] F.C. Bond, *Br. Chem. Eng.*, 6 (6 and 8) (1961) 378-385 & 543-548.
- [17] A. Jankovic, S. Suthers, T. Wills, W. Valery, *Miner. Eng.*, 71 (2015) 133-138.

## MANAGEMENT OF RISK ASSESSMENT IN ENVIRONMENTAL PROTECTION IN SURFACE COPPER MINE

Ivan Jovanović<sup>1</sup>, Novica Staletović<sup>2</sup>

<sup>1</sup>Mining and Metallurgy Institute Bor, Zeleni bulevar 35, 19210 Bor, Serbia

<sup>2</sup>University Union “Nikola Tesla”, Faculty of Ecology and Environmental Protection, Cara Dušana 62-64, 11158 Belgrade, Serbia

### Abstract

*Successful environmental protection is largely based on a quality assessment of possible and present risks. Environmental risk management is a complex process that includes: risk identification, risk assessment and risk control, which taking measures to reduce that risk to an acceptable level. The focus of this work is on the application of the methodology of environmental risk assessment and analysis, as the most important aspect of successful management of environmental protection. The paper presented the analysis of the risk analysis that was carried out for one copper surface mine in Serbia.*

**Keywords:** risk assessment, environmental protection, surface copper mine

### 1. INTRODUCTION

Due to the destructive impact of human economic activities on the environment for the purpose of a sustainable global economy, the intensity and duration of exploitation in all areas of industry also means major disturbances in the integrity of the terrain, air and eco-system.

Therefore, investing in the protection and restoration of the natural environment is one of the priorities of all of us. Reasonable environmental management should include adequate measures to minimize environmental damage.

Management of environmental protection in mines for the exploitation of metal mineral raw materials enables to identify and control the impact of exploitation activities, products and services on the environment, to improve the attitude towards the environment, to implement a systematic approach that will achieve the goals related to environmental protection and provide evidence that the set goals have been achieved. [1]

The introduction and functioning of the environmental protection management system is influenced by several factors, the most important of which are: constant environmental pollution, fear of complete exhaustion of natural resources, lack of organized and systematic monitoring of the consequences of pollution, increased interest of public opinion in environmental protection, legal solutions and special working conditions in endangered areas. [2]

Management of environmental protection requires a multidisciplinary perspective and the involvement of all members of society. This is due to the fact that health, the environment and social conditions are in constant interaction, so the disturbance of the environment leads to ecological disturbances and disturbances of social relations, which are interconnected and conditioned. By evolving the very understanding of environmental problems, the main focus of current environmental management is centered on the integration of social and ecological systems. In this context, environmental decision-making must deal with the complexity of both ecological systems and interdependent human organizational and institutional systems. [3]

Proper management of environmental protection can reduce negative impacts on the environment, reduce the risks of environmental disasters, increase the ability to quickly and effectively



intervene, improve reputation and build trust with the community, increase legal certainty due to compliance with environmental protection laws, easier to obtain authorizations and permits from local and state authorities, increase energy efficiency and water protection, carefully select raw materials and control waste recycling, contribute to cost reduction and raise competitiveness, improve the quality of workplaces and employee morale, and open new employment opportunities in mining industry markets where ecological production is important. [4]

## **2. EXPERIMENTAL**

Risk assessment is an integral part of risk management and contributes to minimizing the possibility that the environment and employees in that environment are exposed to danger during the performance of work activities, some scientific and research activities were carried out, which had as their subject the analysis of the process of preventing the potential risk that the activities in copper surface mining production could lead to in technical and technological systems, in order to prevent them.

The analysis and evaluation of the existing state of the environment, as well as the assessment of possible risks to the environment and human health that are a consequence of the operation of the copper surface mine, show that the quantification of possible consequences can be achieved through the analysis of the impact of surface exploitation and preparation of copper ore on the environment.

The identification of environmental aspects and their possible impacts represents an analysis of the relationship between surface mining, flotation, tailings - the environment, where, on the basis of knowledge of the basic ecological potential of the analyzed space and the basic relationships in the system of emissions - transmission - immission - impact, all relevant facts are defined for the selection of adequate technologies of surface exploitation and preparation of copper ore.

## **3. RESULTS AND DISCUSSION**

The analysis of possible causes of environmental pollution and degradation within the risk and impact assessment of surface exploitation and preparation of copper ore includes the following processes:

- surface mine with ore dump,
- transport of ore to flotation,
- flotation: crushing, grinding and flotation of ore,
- transport of concentrate and tailings, and
- flotation tailings pond.

The following possible sources of environmental pollution can be registered in the mine.

### **a) Air pollution**

By analyzing air pollution with suspended particles (mineral dust), the following potential sources of pollution were identified:

- dry surfaces on active floors and surfaces (surface mine and ore dump),
- road routes for truck transport on the surface mine,
- crushing plant for ore and tailings at the surface mine,
- conveyor route with tailings belt,
- operational activities of mining machines and technological equipment at the surface mine (drilling rigs, excavators, bulldozers, graders),
- machines and technological equipment for the preparation of copper ore (crushing, grinding, flotation),
- conveyor route with ore belt,
- road routes for truck transport of concentrate,

- dry areas on the flotation tailings.

Air pollution with exhaust gases (CO, NO<sub>x</sub>, SO<sub>2</sub>) from the engines of mining loading, transport and auxiliary machines was caused by the following possible sources: trucks and bulldozers.

The blasting process in surface mine can represent a potential source of air quality threats because, under the influence of the wind, dust and gaseous blasting products (CO, NO, NO<sub>2</sub>, etc.) are distributed in the area of mining operations.

#### b) Noise

By analyzing the process of working noise sources in the mine, the following potential sources of noise emissions and threats were identified:

- mining mechanization, machines and technological equipment at the surface mine (drilling rigs and compressors, excavators, bulldozers, graders),
- machines and technological equipment for the preparation of copper ore (crushers, mills, flotation machines),
- transport machines (trucks, conveyors),
- auxiliary machines (bulldozers, loaders).

#### c) Water pollution

The registered threat sources were:

- water drainage systems from the mine area,
- impact on the hydrological regime of the exploitation area, lowering of the groundwater level,
- atmospheric waters that reach the contour of the mine and landfill,
- potential contamination of local rivers with process water from flotation and tailings,
- potential contamination of local groundwater in the tailings area,
- potential change in the hydraulic regime of local groundwater,
- influence on the hydrological regime of the area,
- atmospheric waters that wash away material from the slopes of the dams, creating torrents that pollute the surrounding area.

#### d) Land degradation

The identified sources of land endangerment are:

- surface mine - mining waste,
- ore deposit at the surface mine,
- flotation facilities - ore waste, concentrate waste, and
- flotation tailings pond - waste flotation sludge.

The purpose of the analysis of the situation and management of environmental protection based on risk analysis in the copper surface mine is to act productively and proactively in order to timely establish risk control mechanisms and take measures to realize opportunities and thus achieve the necessary balance between creating opportunities for profit and minimizing production loss.

From the context of global and local problems due to the increasing and faster technical-technological progress of society as a whole, the constant advancement of technology means that it is very difficult to determine the level of technological risk. That is why it is necessary to constantly develop and improve methods and principles as well as criteria for risk assessment and management.

Finally, the obtained results of this work were reflected in the identification of risks and the prevention of negative impacts of mining works and processes not only on the environment but

also on the context of the economic and financial effects that the mine can cause with its irresponsible operations, both on its the environment as well as the social community as a whole.

#### **4. CONCLUSION**

Technical-technological systems, which include surface copper mines, can threaten the safety of people, the economic stability of the organization and the environment in a wider sense. Therefore, the analysis of the risks to the environment in mines are becoming not only a subject of increasing interest, but also an increasingly subject of legislative regulation.

Environmental risks in mines must be assessed, quantified, in order to predict and prevent potential damages, both for the business entity itself and for the wider social community. The purpose of the activities carried out was to analyze the process of prevention of potential risks caused by mining activities and processes in mines, in order to prevent them.

It can be concluded that the process of prevention of potentially dangerous events that lead to technical-technological accidents with as many possible aspects as possible, from definition, strategy, goals, legal regulation, risk assessment methods, to their impact on financial effects and sustainable development, is important.

#### **ACKNOWLEDGEMENTS**

*The research presented in this paper was carried out with the financial support of the Ministry of Science, Technological Development and Innovation of the Republic of Serbia, as a part funding the scientific research work in the Mining and Metallurgy Institute Bor, according to the Contract with registration no. 451-03-47/2023-01/ 200052.*

#### **REFERENCES**

- [1] Project Environmental and Social Impact Management Framework (ESMF), Project P176770, Ministry of Mining and Energy, Belgrade, February 2022.
- [2] Environmental Protection Agency, Ministry of Environmental Protection, Republic of Serbia, <http://www.sepa.gov.rs>
- [3] S. Živković, S. Milutinović, Environmental Protection Management, University of Niš, Faculty of Occupational Safety in Niš, Niš, 2021.
- [4] M. Drenovak-Ivanović, Environmental protection in legislation and practice, OSCE Mission in Serbia, Belgrade, 2015.

## POSSIBILITY OF LOCALIZED ELECTRON STATES APPEARANCE IN ULTRATHIN LAYERED CRYSTALLINE STRUCTURES

Jovan P. Šetrajčić<sup>1</sup>, Stevo K. Jaćimovski<sup>2</sup>, Siniša M. Vučenović<sup>3</sup>

<sup>1</sup>Academy of Sciences and Arts of the Republic of Srpska, Banja Luka, B&H

<sup>2</sup>University of Criminalistics and Police Studies, Zemun – Belgrade, Serbia

<sup>3</sup>University of Banja Luka, Faculty of Sciences and Mathematics, Republic of Srpska, B&H

### Abstract

The dispersion law of electrons in film-structures was evaluated by the method of two-time temperature dependent Green's functions. In variance from unbounded structures, the electron energy spectra in film posses the top and bottom gap and the band of electron energies is narrower and strictly discrete. The conditions for the appearance and existence of the localized electron states were found and analyzed as the function of boundary parameters.

**Keywords:** electrons, ultrathin films, dispersion law, energy gaps, localization states

### 1. INTRODUCTION

Fundamental physical properties of quasi-twodimensional electronic systems arise primarily from their spatial boundness, as well as from special perturbative conditions which appear at and within their surface layers [1,2]. The aim of this paper is the analysis of the influence of finite dimensions of the crystalline ultrathin film and boundary conditions onto the energy spectrum of the electrons with particular interest in the possibility of the appearance of the localized electron states.

We base our analysis on the standard electron Hamiltonian of the model film-structure in the nearest-neighbours approximation [3-5]:

$$H = \sum_{m_x m_y m_z} a_{m_x m_y m_z}^+ \left\{ [1 + \varepsilon(\delta_{m_z,0} + \delta_{m_z,N_z})] \Delta a_{m_x m_y m_z} - [1 + w(\delta_{m_z,1} + \delta_{m_z,N_z-1})] W (a_{m_x+1, m_y m_z} + a_{m_x-1, m_y m_z} + a_{m_x m_y+1, m_z} + a_{m_x m_y-1, m_z} + a_{m_x m_y m_z+1} + a_{m_x m_y m_z-1}) \right\} \quad (1)$$

where  $\Delta \equiv \Delta_{\vec{n}_x \vec{n}_y \vec{n}_z}$  is the energy of an electron localized at the site  $\vec{n} \equiv (\vec{n}_x, \vec{n}_y, \vec{n}_z)$ , and  $W \equiv W_{\vec{n}_x \vec{n}_y \vec{n}_z, \vec{m}_x \vec{m}_y \vec{m}_z}$  is the energy of the electron transfer from the site  $\vec{n}$  to the site  $\vec{m}$ . The parameter  $\varepsilon$  defines the change of the electron energy at the surface layers of the film, while  $w$  defines the change of the transfer energy within the surface layers. The fact that the film is of finite dimension along all  $\mathbf{z}$ -directions (orthogonal to the film boundary surfaces) is expressed in terms of the conditions:  $n_z = 0, 1, 2, \dots, N_z$ ,  $N_z \sim 10$ ;  $n_\alpha \in [-\frac{N_\alpha}{2}, +\frac{N_\alpha}{2}]$ ,  $N_\alpha \sim 10^8$ ,  $\alpha = (x, y)$ .

### 2. ELECTRON DISPERSION LAW

The dispersion law for the electrons will be looked for by one of the most suitable theoretical treatments of the quantum solid state physics - Green's functions method [6-8]. For that purpose, we study single-electron, two-time anticommutator Green's function:

$$G_{n_x n_y n_z; m_x m_y m_z}(t) = \Theta(t) \left\{ a_{n_x n_y n_z}(t), a_{m_x m_y m_z}^+(0) \right\} \quad (2)$$

Following the standard procedure [6–8], using equations of motion for the Green's function and performing the temporal and partial spatial ( $XY$ ) Fourier-transformation we obtain the system of  $N_z + 1$  nonhomogeneous algebraic-difference equations:

$$\begin{aligned} & [1 + w(\delta_{n_z,1} + \delta_{n_z,N_z})]G_{n_z-1} + [\varrho - \varepsilon(\delta_{n_z,0} + \delta_{n_z,N_z})]G_{n_z} + \\ & + [1 + w(\delta_{n_z,0} + \delta_{m_z,N_z-1})]G_{n_z+1} = K_{n_z}, \end{aligned} \quad (3)$$

where:  $G_{n_z} \equiv G_{n_z;m_z}(k_x k_y, \omega)$  ;  $K_{n_z} \equiv \frac{i\hbar}{2\pi W} \delta_{n_z,m_z}$  and

$$\varrho = \hbar \frac{\omega}{W} - \frac{\Delta}{W} + 2(\cos ak_x + \cos ak_y). \quad (4)$$

The determination of Green's function poles, which define the spectrum of possible electron energies, turns into the calculation of the roots of the determinant of the system of equations (3), i.e. to condition:

$$D_{N_z+1}(\varrho) \equiv \varrho - \frac{\Delta}{W} \varepsilon)^2 C_{N_z-1} - 2(1+w)^2 (\varrho - \frac{\Delta}{W} \varepsilon) C_{N_z-2}(\varrho) + (1+w)^4 C_{N_z-3}(\varrho) = 0, \quad (5)$$

where  $C_n$  are the characteristic Chebishev's polynomials:  $C_{n-1} = \varrho C_n - C_{n+1}$ .

In the general case, this equation is not analytically solvable (analytically solvable case arises for  $\varepsilon = w = 0$  [9,10]), so numerical methods must be applied. For given numerical values of the parameters  $N_z$ ,  $\varepsilon$  and  $w$ , one can obtain the numerical values for  $\varrho_\nu$ ,  $\nu = 1, 2, 3, \dots, N_z + 1$  from the equation (5). Their substitution into (4) leads to the electron dispersion law in the following form:

$$E_{xy}(\nu) \equiv \frac{\hbar \omega_{xy}(\nu)}{4W} = F_{xy} + G_\nu; \quad F_{xy} \equiv \sin^2 \frac{a_x k_x}{2} + \sin^2 \frac{a_y k_y}{2}; \quad G_\nu \equiv \frac{\varrho_\nu + 2}{4}. \quad (6)$$

The study of the influence of the surface parameters of the studied film onto the energy spectrum was performed for  $N_z \in \{3, 5, 10, 20\}$  and  $(\varepsilon, w) \in \{-1.0, -0.8, -0.5, -0.2, 0.0, 0.2, 0.5, 0.8, 1.0\}$ . Similar to the case of ideal crystalline film [5], one concludes that the energy spectra of electrons are discrete with the finite number of energy levels ( $N_z + 1$ ) and that they possess a top and a bottom energy gap:

$$b \equiv G_\nu^{\min} = G_{\nu=1}(\varepsilon, w) ; \quad t \equiv 1 - G_\nu^{\max} = 1 - G_{\nu=N_z+1}(\varepsilon, w) . \quad (7)$$

Analyzing the energy gap dependence on the film thickness and boundary parameters  $\varepsilon$  and  $w$  [5], one can register the appearance of the surface localized states of electrons for some values of parameters:  $b < 0$ ,  $t < 0$ , i.e.  $E_{\min}^F < E_{\min}^B = 0$ ,  $E_{\max}^F > E_{\max}^B = 1$  for  $k_x = k_y = 0$ .<sup>1</sup>

Energy levels out of the continuum band of the allowed energies of an infinite crystal correspond to the complex values of quasimomentum, i.e. there arise the localized electron states at the surface film layers (Fig. 1). The conditions for the appearance of the localized states are determined from the equation (5) by substituting:  $\omega_{\min} < 0$ , where  $\varrho < -2$  and  $D_n = (-1)^n(n+1)$  or  $\omega_{\max} > \frac{4W}{\hbar}$ , with  $\varrho > 2$  and  $D_n = n+1$  and in both cases for  $k_x = k_y = 0$ . It is interesting to note that in this case we obtain the conditions:<sup>2</sup>

$$\begin{aligned} & \frac{\Delta}{W} \varepsilon < (1+w)^2 - 2; \quad \omega_{\min} < 0, \\ & \frac{\Delta}{W} \varepsilon > 2 - (1+w)^2; \quad \omega_{\max} > \frac{4W}{\hbar}. \end{aligned}$$

Increasing the film width, the energies of the localized states approach to the bulk band boundaries, so in the limiting case ( $N_z \rightarrow \infty$ ) they coincide with them.

<sup>1</sup> Indices F and B correspond to film and bulk, respectively.

<sup>2</sup> Which do not include the dependence on the number of layers, i.e. on the film width.

Bottom energy gap dependence on boundary parameters in the case of the appearance of localized states is studied, because low energy states have the main influence onto the thermodynamics and transport properties of thin films (Fig. 2). The boundary electron localization increases with the increase of the parameter  $w$  and the decrease of the parameter  $\varepsilon$ . These results have physical explanation. With decreasing  $\varepsilon$ , the electron localization for crystal sites becomes smaller, and for greater  $w$ , the electron transport from inner sites to boundaries increases. The electron energies can become negative (for imaginary values of quasimomentum), so the Fermi level in the crystalline film has to be redefined.

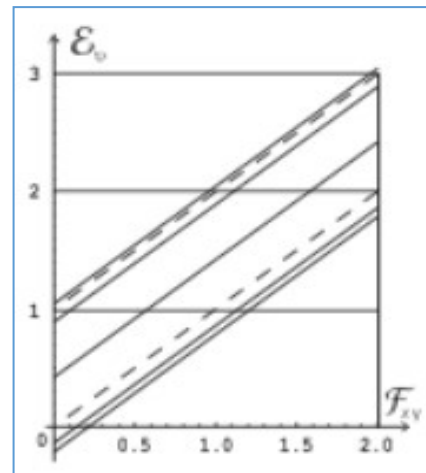


Figure 1 - Energy spectrum of the electrons of ultrathin film (the appearance of the localized subbands outside bulk boundaries)

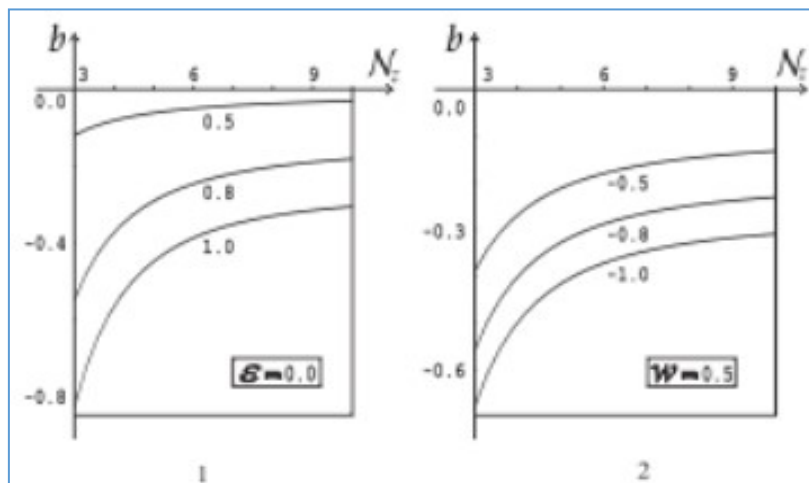


Figure 2 - Bottom energy gap dependence on film thickness and the boundary parameters:  
 1)  $\varepsilon = 0.0$ ,  $w = +0.5, +0.8, +1.0$ ; 2)  $w = 0.5$ ,  $\frac{\Delta}{w} \varepsilon = -0.5, -0.8, -1.0$

### 3. CONCLUSION

Results of these analyses confirm the essential differences in dispersion law of electrons in film structures in comparison with unbounded ones, which is as an exclusive consequence of boundaries existence.

- 1) Energy spectrum of electrons in the crystalline film is a discrete one with the finite number of possible energy levels equal to the number of atomic planes in the film along  $z$  - direction.
- 2) The consequence of the spectrum discreteness is the existence of the top and bottom energy gap which decrease with the increase of the film width.
- 3) Increase of the electron energy at the boundary surfaces induces the shift of the spectrum towards higher energies (the increase of the bottom gap and the decrease of the top gap), while for the increase of the transfer energy of electrons at the surfaces, the spectrum broadens (the decrease of both bottom and top gap).
- 4) Depending on the values of the parameters of surface interactions, certain energy levels can lie outside the energy band of the ideal crystal, so there appear the surface localized states of electrons.
- 5) Increasing the film width, the energy of the localized states shifts towards the bulk band

boundaries, coinciding with them for  $N_z \rightarrow \infty$ . In this limit the localized states, as well as the energy gaps vanish, while the spectrum turns in the quasicontinual spectrum of the ideal infinite crystal.

- 6) The position of the Fermi level in the film differs from its bulk position and depends strongly on the boundary parameters and the film thickness.

## ACKNOWLEDGEMENTS

*The research presented in this paper was financially supported by the Ministry of Scientific and Technological Development, Higher Education and Information Society of the Republic of Srpska (Projects No. 19.032/961-36/19 and 19.032/961-42/19).*

## REFERENCES

- [1] M.G. Cottam and D.R. Tilley, Introduction to Surface and Superlattice Excitations, Univ. Press, Cambridge 1989.
- [2] L.L. Chang and L. Esaki, Phys.Today, Oct. 36 (1992).
- [3] Ch. Kittel, Introduction to Solid State Physics, Wiley, New York 2004.
- [4] J.P. Šetrajčić, S.K. Jaćimovski, Elementary Excitations in Nanostructured Superconductors, Criminal and Police Academy, Belgrade 2014. – in Serbian
- [5] J.P. Šetrajčić, S.M. Vučenović, S.K. Jaćimovski, Materials Protection 57(2) (2016) 239-243.
- [6] G. Mahan, Many-Particle Physics, 3<sup>rd</sup> ed. in: Physics of Solids and Liquids, Springer, New York 2000, pp. 247-250.
- [7] V.D. Sajfert and J.P. Šetrajčić, Application of Green's Functions and Difference Equations in Theoretical Analyses of Nanostructures, in: Monograph Series on the Foundations of Natural Science and Technology, Vol. 15: Topics in Nanoscience, Part I: Basic Views, Complex Nanosystems: Typical Results and Future, Ed. Schomers W., Ch. 7, pp. 311-412, World Scientific, Singapore 2022.
- [8] J.P. Šetrajčić, S.K. Jaćimovski, S.M. Vučenović, Green's Functions in Quantum Statistical Physics – Condensed Matter Physics, Accepted in Materials Today 2023.
- [9] S.M. Stojković, et al. Surface Science 477 (2001) 235-242.
- [10] J.P. Šetrajčić, et al. Mod. Phys. Lett. B 28(4) (2014) 1450023.



## APPLICATION OF VIKOR METHOD FOR COMPARISON OF THE WASHABILITY OF COALS

Jovica Sokolović, Ivana Ilić, Dragiša Stanujkić, Zoran Štirbanović  
Technical Faculty Bor, University of Belgrade, V.J. 12, 19210 Bor, Serbia

### Abstract

*This paper summarizes the results of the comparison of the washability characteristics of three coals (anthracite, brown, and lignite) by the VIKOR method. Based on the float-sink test results, the theoretical values of the coal yield and the quality of the clean coal product were calculated. Two washability parameters, the Index of Washability (IW) and the Near Gravity Material Index (NGMI), as well as the Separability Coefficient (K), were computed, and the results were compared. The results presented in this study indicate that the washability of the anthracite coal is relatively easy at a specific density of 1650 kg/m<sup>3</sup>.*

**Keywords:** coal, washability, VIKOR, method.

### 1. INTRODUCTION

Gravity separation of coal, also known as coal washing or coal beneficiation, is a process for separating coal based on the difference in density between the coal and the impurities (mineral matter) typically associated with the coal.

Washability curves based on laboratory float-sink tests are used to evaluate the coal's washability. This test is used to distribute the coal by density fraction to determine the optimum separation density. The theoretical values of the coal yield and the quality of the clean coal product, i.e. the ash content in the separated coal product, thus depend on the separation density. Washability of coal is affected by a variety of factors, including grain size, ash content, floating and sinking products, and the amount of near-gravity materials [1]. The “index of washability” [2] and “near-gravity material index” [3] have been proposed for comparative analyses of washability characteristics of different coals. The “separability coefficient” [4] is very useful parameter for interpreting separability data in the study of coal washability.

MCDM methods present very efficient tool which can simplify compare coals when large number of criteria is involved. Therefore, in this paper are presented the results of comparison of the washability of three coals (antracihte, brown coal, and lignite) by the VIKOR method. [5]

### 2. EXPERIMENTAL

#### 2.1. Materials

Raw coal samples were collected from the Vrska Cuka Anthracite Coal Mine, the Bogovina Brown Coal Mine, and the Lubnica Lignite Coal Mine, located in Eastern Serbia. Representative samples were obtained after coning and quartering the collected samples, and afterward they were sieved in order to prepare samples needed for further laboratory float sink tests.

#### 2.2. Float–Sink Test

Float-sink tests were carried out on different coals, and the washability characteristics of coals were investigated. The float-sink tests were performed using zinc-chloride as heavy media at different specific densities ranging from 1300 to 1850 kg/m<sup>3</sup>.

All products were analyzed for ash content. Based on the obtained results, the cumulative yield and ash values were computed. According to methodologies by Govindarajan and Rao (1994) [2] and Majumder and Barnwal (2004) [3], the values of the index of washability (IW) and near-gravity material index (NGMI) were calculated. The washability data obtained in the study were used for the comparison of the washability of coals. The comparison was performed between three coals with different washability characteristics. The results of the float-sink analysis of raw coals are shown in Table 1 [3].

Table 1 – Results of the float-sink tests of raw coals

Specific gravity kg/m <sup>3</sup>	Vrska Cuka		Bogovina		Lubnica	
	Mass %	Ash %	Mass %	Ash %	Mass %	Ash %
-1300	3.52	1.99	3.93	10.86	20.39	9.85
-1400	54.43	5.90	18.79	12.42	33.55	13.49
-1500	12.91	11.75	20.15	13.55	14.58	27.18
-1600	4.08	22.19	7.95	15.41	7.39	37.61
-1700	2.09	29.28	2.15	27.19	5.01	54.09
-1800	1.49	39.55	1.44	43.51	4.10	68.16
-1850	0.69	47.42	1.24	48.68	2.22	76.67
+1850	20.79	72.65	44.36	55.31	12.75	86.02
Σ	100.00	22.34	100.00	33.06	100.00	31.45

Based on the float-sink test results and washability data, it can be noticed that depending on the quality, in the range of separation densities between 1400 and 1800 kg/m<sup>3</sup>, the best separation of raw coals was achieved at a separation density of 1650 kg/m<sup>3</sup>. At this density, a comparison of coal separability, i.e., washability, and theoretical values of yield and quality of a clean coal product was made using the VIKOR method.

### 2.3. Methodology

Three alternatives, shown in Table 2, were evaluated based on the six criteria shown in Table 3. Table 4 also shows the weights of the criteria.

Table 2 - Alternatives for the selection of flotation collector

Alternative	Coal Rank	Coal Mine
A <sub>1</sub>	Anthracite	Vrska Cuka
A <sub>2</sub>	Brown	Bogovina
A <sub>3</sub>	Lignite	Lubnica

Criteria that were used for selection and their weights are given in Table 3.

Table 3 - The weights of selection criteria

Criteria	Weight
C <sub>1</sub> – Index of washability (IW)	0.15
C <sub>2</sub> – Near-Gravity Material Index (NGMI)	0.15
C <sub>3</sub> – Separability coefficient (K)	0.15
C <sub>4</sub> – Theoretical value of the mass yield of clean coal (%)	0.20
C <sub>5</sub> – Quality (ash content) of clean coal (%)	0.20
C <sub>6</sub> – Price of clean coal product (EUR/t)	0.15

The ratings of alternatives in relation to the selected criteria are shown in Table 4.

Table 4 - The ratings of alternatives in relation to the selected criteria

	<b>C<sub>1</sub></b>	<b>C<sub>2</sub></b>	<b>C<sub>3</sub></b>	<b>C<sub>4</sub></b>	<b>C<sub>5</sub></b>	<b>C<sub>6</sub></b>
	max	min	max	max	min	max
<b>A<sub>1</sub></b>	33.23	0.07	2.82	75.99	7.91	114.62
<b>A<sub>2</sub></b>	33.78	0.06	2.45	51.88	13.50	81.10
<b>A<sub>3</sub></b>	40.39	0.12	1.16	78.42	18.66	59.78

The comparison was made by using VIKOR method. The VIKOR method was proposed by Opricovic and Tzeng in 2004 [5], and it can be also mentioned as a prominent and often used MCDM method. VIKOR means Multicriteria Optimization and Compromise Solution (visekriterijumska optimizacija i kompromisno rešenje, in Serbian). The procedure for evaluating alternatives using the VIKOR method was explained in the following steps by Opricovic and Tzeng [5].

### 3. RESULTS AND DISCUSSIONS

The ratings of the alternatives in relation to the criteria are shown in Table 4. The optimization directions of the criteria are also shown in Table 4. The best and worst values for each criterion are shown in Table 5.

Table 5 - The best and worst value for each criterion

	<b>C<sub>1</sub></b>	<b>C<sub>2</sub></b>	<b>C<sub>3</sub></b>	<b>C<sub>4</sub></b>	<b>C<sub>5</sub></b>	<b>C<sub>6</sub></b>
	max	max	min	max	min	max
$x_j^*$	40.39	0.06	2.82	78.42	7.91	114.62
$x_j^-$	33.23	0.12	1.16	51.88	18.66	59.78

Based on the data from Table 4 and Table 5, the average  $S_i$  and group  $R_i$  score for each alternative were determined. The calculated values are shown in Table 6. Table 6 also shows the overall ranking index  $Q_i$ , and  $\nu = 0.5$ , as well as the ranks of each considered alternatives.

Table 6 - The overall ranking index and rank of considered alternatives

	<b><math>S_i</math></b>	<b><math>R_i</math></b>	<b><math>Q_i</math></b>	<b>Rank</b>
<b>A<sub>1</sub></b>	0.21	0.150	0.00	1
<b>A<sub>2</sub></b>	0.57	0.200	0.91	2
<b>A<sub>3</sub></b>	0.65	0.200	1.00	3

From Table 6, it can be seen that the alternative denoted as  $A_1$  was selected as the most acceptable alternative. Alternative  $A_1$  represents anthracite coal. As it can be seen from Table 5, the coal yield ( $C_4$ ) was the highest at 78.42%. Clean coal grade ( $C_5$ ) was 7.91%, which were the lowest obtained values of ash content. The "index of washability" was the lowest, indicating lower washability, but since the weight of this criterion was not very high, it did not influence the overall ranking of alternative  $A_1$ . The "near-gravity material index" has been proposed for comparative analyses of washability characteristics of different coals, and the lowest value was obtained for alternative  $A_2$ , which represents brown coal. The "separability coefficient" was the highest for alternative  $A_1$ , indicating better separability of the anthracite coal. Considering all this, it can be concluded that the criteria  $C_4$  and  $C_5$ , i.e., mass yield ash content of clean coal products, had the most influence during the comparison of coal washability by application of the VIKOR method, which was expected since they were assigned the highest weight.

#### 4. CONCLUSION

Washability of coal plays a very important role in the gravity process of coal, so it is important to select a separation density that will provide good washability and separability of coal from associate minerals. The washability of coal is affected by a variety of factors, including grain size, ash content, floating and sinking products, and the amount of near-gravity materials. The "index of washability", the "near-gravity material index," and the "separability coefficient" are very useful parameters for interpreting separability data in the study of coal washability.

During the comparison, a large number of criteria should be taken into consideration, making the comparison process difficult. Therefore, the solution to the problem can be the application of MCDM methods, which can simplify the selection process when a large number of criteria are involved.

The comparison of coals from the Vrska Cuka Anthracite Coal Mine, the Bogovina Brown Coal Mine, and the Lubnica Lignite Coal Mine by the VIKOR method was the aim of the study, presented in this paper. The criteria for comparison were:  $C_1$  – Index of washability (IW),  $C_2$  – Near-Gravity Material Index (NGMI),  $C_3$  – Separability coefficient (K),  $C_4$  – Theoretical values of the mass yield of clean coal (%),  $C_5$  – Quality (ash content) of clean coal (%), and  $C_6$  – Price of clean coal product (EUR/t). Based on the float-sink test results, and the results of the MCDM analysis the anthracite coal was selected as the coal with the best washability.

#### ACKNOWLEDGEMENTS

*The authors would like to acknowledge the Ministry of Science, Technological Development and Innovation of the Republic of Serbia for the financial support of scientific research at the University of Belgrade, Technical Faculty in Bor according to the contract with registration number 451-03-47/2023-01/200131.*

#### REFERENCES

- [1] D.S. Rao, T. Gouricharan, Coal processing and utilization. London, UK: CRC Press/Taylor & Francis Group, 2016.
- [2] B. Govindarajan, T. C. Rao, Int. J. Miner. Process., 42 (3–4) (1994) 285–93.
- [3] A. K., Majumder, J. P. Barnwal, Miner. Eng., 17 (1) (2004) 93–96.
- [4] R. Ignjatović, Physical methods of concentration, Textbook, Technical Faculty in Bor, Bor, 1983.
- [5] S. Opricovic, G.H. Tzeng, Eur. J. Oper. Res., 156 (2) (2004) 445-455.

## THE PROCESS OF OBTAINING BIOCHAR AND THE DEVELOPMENT OF THE PRODUCTS THUS OBTAINED

Vladimir Jovanović, Dejan Todorović, Branislav Ivošević, Dragan Radulović,  
Sonja Milićević, Marija Ercegović, Slavica Mihajlović

Institute for technology of nuclear and other mineral raw materials, 86 Franchet d'Esperey St,  
11000 Belgrade, Serbia, v.jovanovic@itnms.ac.rs

### Abstract

*Biochar continues to strengthen its presence in many new industries with its new applications, which are full of scientific and business news. A flurry of activity has sprung up around this carbon-based material, produced from biomass, following its use in water treatment, energy production and animal husbandry. In any new industry, process and product development, as well as feasibility studies, are very important for the product to come to market. This is especially true when it comes to biochar. Besides being in its infancy as an industry, biochar itself presents a number of challenges that make various tests necessary. Many properties affect the quality and performance of biochar products (pore size, cation exchange, electro-conductivity...) and will most likely vary depending on the starting material and the method of obtaining. Biochar can be made from a very long list of biomass materials. Although the above creates opportunities for industries that abound with highly adaptable products, it can still make biochar unpredictable, given that each starting material affects the characteristics of the final products differently.*

**Keywords:** biochar, biomass, pyrolysis, development, processes.

### 1. INTRODUCTION

Wood chips, sawdust, corn stover, sugarcane bagasse, and coconut husks represent just a few of the biomass materials that can be transformed into a biochar product. Similarly, even the same material can vary significantly across different sources, with factors such as moisture content, particle size distribution, bulk density, and more all requiring consideration [1].

Biochar is a solid, carbon-rich material generally obtained from thermochemical conversion of biomass and respective carbonization in oxygen-limited environments and has been proposed as a potential solution to climate change, energy security, degradation of natural resources, food security and catastrophic forest fires worldwide. Biochar production implies a complex chemical reaction process where biomass undergoes decomposition, depolymerization and condensation in anoxic high temperature conditions [2].

Biochar is produced by heating biomass in the total or partial absence of oxygen (Figure 1). Pyrolysis is the most common technology employed to produce biochar, and also occurs in the early stages of the combustion and gasification processes. Besides biochar, bio-oil and gas can be collected from modern pyrolysers. These could be refined to a range of chemicals and/or used as sources of renewable energy if derived from sustainably produced biomass [3].



Figure 1 - Biochar

## 2. THE PRODUCTS

**Biomass:** living or once-living material, which is the feedstock (starting material) for making biochar. Nearly all organic materials, such as bark, nutshells, crop residues, and manures can be used as feedstock in appropriate devices [4].

**Charcoal:** the solid, carbon-rich residue left when biomass is heated in an environment with limited oxygen. Generally, charcoal is made from wood, and is intended for use as fuel. Charcoal can be further processed to produce “activated carbon”.

**Biochar:** a charcoal-like material made under suitable conditions from non-contaminated starting material, and crushed into small pieces for mixing in the soil. It is often enhanced with nutrients and microorganisms, intended to improve soil properties and plant growth [5].

**Char:** a general term for the solid product arising from thermal decomposition (pyrolysis) of any organic material.

**Pyrogas (or Pyrolysis gas):** The gas and aerosols from pyrolysis or gasification comprising primarily combustible gases CO, H<sub>2</sub> and CH<sub>4</sub> along with CO<sub>2</sub>, steam and N<sub>2</sub>; also known as wood gas and syngas.

**Ash:** Inorganic compounds in the biochar. (Also refers to material remaining after combustion, which includes a small percentage of carbon.) [6]

## 3. THE PROCESSES

**Pyrolysis (from Greek roots pyr“fire” and lysis “loosening”)** is the thermal decomposition (breakdown under heat), in a limited oxygen environment, of biomass into a carbon-rich solid residue (char), gases, and liquids. [7]

**Carbonisation** emphasizes the carbon enrichment, as opposed to the “breakdown”, aspect of pyrolysis. “Carbonization” is often used interchangeably with “pyrolysis.”

**Conditioning** refers to changes in chemical and physical properties of biomass at temperatures of approx. 110-180oC, where biomass starts to soften and chemically-bound water starts to be driven off.

**Torrefaction** is a chemical process that takes place at a temperature of approx. 180-300oC which produces a more energy dense, stable, sterile feedstock or soil amendment [5].

**Activation** refers to further enhancement of charcoal via chemical processes and/or higher temperature oxidation to produce activated carbon with high microporosity and surface area.

**Gasification** is the conversion of biomass into a gas commonly referred to as “producer gas”, using a limited amount of air or steam. A gas rich in CO, CH<sub>4</sub>, CO<sub>2</sub> and H<sub>2</sub> is produced. [6]

### 3.1 Processing Conditions

In addition to the characteristics of the source material influencing the end product, the processing conditions also have an impact on the characteristics of the end product.

Biochar is produced from biomass through a process called pyrolysis, in which dried biomass is processed in an oxygen-free atmosphere at temperatures between 250 – 430°C . This is typically carried out in an indirect-fired rotary kiln (Figure 2), or pyrolysis kiln.

A variety of process parameters such as retention time, temperature, and more will all play a role in shaping the characteristics of the end product and in turn, how it performs. [8]



Figure 2 - Drying of various materials in indirect kiln[1]

### 3.2 Biochar Testing Facilities

As a developing industry, the supply of testing facilities hasn't quite caught up with the demand. We have definitely seen an influx of inquiries around testing biochar lately, People are coming to develop biochar for use in all sorts of applications and to test each part of the process – agglomeration, drying, and high temp thermal processing. This allows them to zero-in on exactly what's working and what needs improvement.

### 3.3 Types of Testing Available

While pyrolysis is a major focus of the process development stage, it is also necessary to test the drying and agglomeration steps. In each scenario, testing helps to define process data and provide the information necessary for scale-up to commercial production capacities. Testing will also help to determine if any sort of pre-treatment (such as grinding or mixing) will be required. [9]



### 3.4 Drying

Few materials can boast such significant variation in characteristics as biomass. Before biomass can be pyrolyzed in a rotary kiln, it must first be dried. The variation in moisture content, particle size distribution, and more require a biomass drying system to be designed around the unique source at hand to produce the most efficient drying solution. Drying is also necessary as a downstream step to agglomeration.

Drying parameters such as temperatures, retention time, flight design and pattern can all be worked out through testing.

### 3.5 Pyrolysis

The pyrolysis process also requires testing to work out process variables and design a commercial scale unit.

Testing for pyrolysis is typically carried out first at batch scale, then at pilot scale. Testing around pyrolysis helps to determine the rotary kiln design parameters that will best suit the material at hand to produce the desired results.

### 3.6 Agglomeration

Biochar leaving the rotary kiln is in the form of a powder. Although biochar can be used in powder form, it is often desirable to agglomerate it, particularly in the case of soil amendments [10]. Some biochars may be difficult to pelletize alone and as such, may be included as part of a blend to assist in enabling successful agglomeration [11].

Soil amendment producers are often looking to combine biochar with other materials such as compost in order to create a specialized product [12].

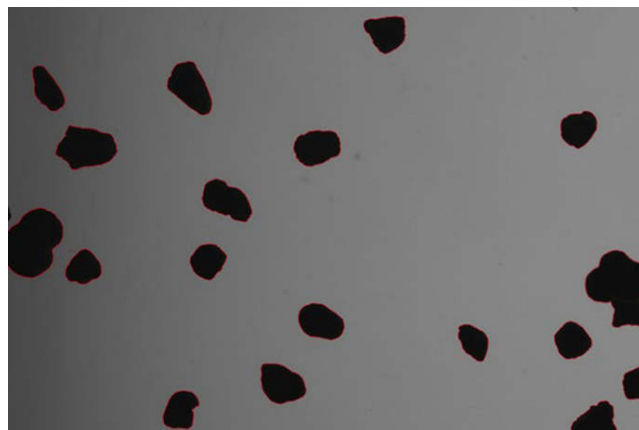


Figure 3 - Particle Analysis

## 4. PARTICLE ANALYSIS

Throughout biochar testing, it is necessary to analyze particles for a variety of parameters.

A 3D Dynamic Image Analysis tool can provide real-time particle analysis during testing to measure density, thickness, surface roughness, size, shape, and more (Figure 3).

Furthermore, particles can be analyzed to determine attrition, compression, crush strength, green/wet strength, moisture content, and more to ensure particles will perform exactly as desired. [1]

## 5. AUTOMATION

A variety of data points can be tracked, trended, and even adjusted in real-time to create a seamless and highly intuitive testing experience.

## 6. CONCLUSION

Various characteristics, including pore size, cation exchange, electrical conductivity, and more will influence the performance of a biochar product and are all likely to differ based on the source material and the processing conditions. Biochar can be created from a nearly endless list of biomass materials.

Testing is a critical part of any new industry, but may be especially important with biochar, due to its significant variability and the challenges it can present. As new applications for biochar are constantly developing, the need for testing facilities is in high demand.

## ACKNOWLEDGEMENTS

*The research presented in this paper was done with the financial support of the Ministry of Education, Science and Technological Development of the Republic of Serbia, within the funding of the scientific research work, according to the contracts with registration numbers 451-03-47/2023-01/200023.*

## REFERENCES

- [1] <https://feeco.com/biochar-process-product-development-in-the-innovation-center/>
- [2] Processes 2022, 10, 2684. <https://doi.org/10.3390/pr10122684>  
<https://www.mdpi.com/journal/processes>
- [3] <https://biochar.international/the-biochar-opportunity/biochar-production-and-by-products/>
- [4] Zhao, L.; Cao, X.; Mašek, O.; Zimmerman, A. J. Hazard. Mater. 2013, 256–257, 1–9.
- [5] Biochar Is a Valuable Soil Amendment. WOKA Foundation. Available online: <https://biochar-international.org/biochar/> (accessed on 7 September 2022).
- [6] <https://biochar.international/guides/basic-principles-of-biochar-production/>
- [7] Leng, L.; Huang, H. Bioresour. Technol. 2018, 270, 627–642.
- [8] Xie, Y.; Wang, L.; Li, H.; Westholm, L.J.; Carvalho, L.; Thorin, E.; Yu, Z.; Yu, X.; Skreiberg, Ø. J. Anal. Appl. Pyrolysis 2022, 161, 105405. [CrossRef]
- [9] Payam Danesh, Parsa Niaparast, Payam Ghorbannezhad, Imtiaz Ali, Biochar Production: Recent Developments, Applications, and challenges, Fuel, Elsevier, 337, 1. April 2023., 126889
- [10] Feeco international, Agglomeration handbook, <https://feeco.com/literature/>
- [11] Petrović M.; Mineral Processing – Fundamentals of Agglomeration, Faculty of Mining, Geology and Civil Engineering: Tuzla, Bosnia and Herzegovina; 2008; p. 288.
- [12] Wang, D.; Jiang, P.; Zhang, H.; Yuan, W. Sci. Total Environ. 2020, 723, 137775.

## Mg/Fe-MODIFIED HYDROCHAR WITH PROMOTED ADSORPTION PERFORMANCES

Jelena Petrović, Marija Ercegović, Marija Simić,  
Marija Koprivica, Jelena Dimitrijević, Marija Marković

Institute for Technology of Nuclear and Other Mineral Raw Materials, Belgrade, Serbia

### Abstract

*This study examined Mg/Fe-pyro-hydrochar produced from grape pomace as potential sorbent for Cu<sup>2+</sup> ions. Obtained results show that the Mg/Fe-modification increases the adsorption capacity for five times. To evaluate the effectiveness of produced sorbent, Langmuir, Freundlich, Sips and Redlich-Peterson isotherm models were applied to batch adsorption results. According to applied models Cu<sup>2+</sup> adsorption at equilibrium fitted the Sips isotherm model, with a maximum achieved capacity of 75 mg/g. Spectroscopic analysis reveal that oxygenated active sites and aromatic groups on pyro-hydrochar surface participate in Cu<sup>2+</sup> ions binding. In general, preliminary findings from this paper offers perspective to effective utilization of waste biomass as an efficient adsorbents for Cu<sup>2+</sup> ions removal.*

**Keywords:** waste biomass, pyro-hydrochar, heavy metal removal, adsorption mechanism.

### 1. INTRODUCTION

Over the years, rapid development of industrial activities caused accelerated production of industrial effluents contaminated with heavy metals. The inadequate management of polluted wastewater and its release into water bodies poses a serious threat to the environment and human health [1,2]. Besides other heavy metals, copper (Cu<sup>2+</sup>) is classified as an essential micronutrient, however numerous anthropogenic activities are the significant contributors to the detrimental levels of Cu<sup>2+</sup> in the environment, thus its concentration exceeds the permissible limits [3]. For this reason, removal or reduction of Cu<sup>2+</sup> ions to standards defined acceptable quantity from the various industrial effluents become essential. Until now, various physical and chemical strategies (chemical precipitation, ion exchange, coagulation, oxidation, membrane filtration, adsorption, etc.) have been widely used for this purpose [4]. Among aforementioned techniques, adsorption is currently considered as a simple, efficient, low energy demand, and cost-effective method for wastewater purification. Along with adsorption, the development of novel adsorbents is on the rise. A movement toward greener methods proposes utilization of waste agricultural biomass as a chip, renewable and highly available as adsorbent material in adsorption technique. Furthermore, conversion of agricultural waste to carbonaceous materials has made their practical application even more attractive. Carbon-rich adsorbents can be produced from various waste biomasses by gasification, pyrolysis or hydrothermal carbonization (HTC).

The latter conversion process offers significant advantages over dry pyrolysis, such as milder reaction conditions (180-260°C) and high conversion efficiency of wet waste biomass into a carbon-rich product, hydrochar [2]. Although produced material exhibit smaller active surface and porosity compared to activated carbon, hydrochars shows significant potential for application in wastewater treatment due to a large number of functional groups on their surface [5]. Regarding improvement of adsorption potential, numerous studies have examined various physical and chemical modifications or functionalization of hydrochars. Previous experiences have shown that the treatment with hydrogen peroxide, different alkalis or metal salts can significantly increase their adsorption efficiency [2,5].

Within this study, the potential application of Mg/Fe doped grape pomace hydrochar as a potential adsorbent of Cu<sup>2+</sup> ions from aqueous solutions will be investigated for the first time. In order to detail examine the binding mechanism and the metal adsorption process, characterization of hydrochar before and after Cu<sup>2+</sup> removal, as well as isothermal study was performed.

## 2. EXPERIMENTAL

### 2.1 Preparation and modification of hydrochar

Waste pomace was collected from an open landfill site after processing of grapes into confectionery products. Pomace was air-dried, ground, and hydrothermally carbonized in an autoclave (Carl Roth, model II), in water as a reaction medium (1:15 m/v ratio) at 220°C, for one hour. The resulting hydrochar (GPHC) was filtered and dried at 105°C. The impregnation of the obtained hydrochar with MgO and FeO was carried out by a two-step co-precipitation procedure during which 1g of the HC-GP was stirred with Mg and Fe salts for 4 h at 60°C. Thereafter, the material was subjected to pyrolysis (Nabertherm 30-3000°C, Germany) at 300°C, within 1h, in an inert atmosphere. Obtained Mg/Fe-activated pyro-hydrochar was labeled as Mg/FeGPHC.

### 2.2 Characterization of obtained Mg/Fe-pyro-hydrochar and adsorption test

To gain insight into the influence of modification process onto adsorbent surface, and to reveal participation of functional groups in the binding of Cu<sup>2+</sup> ions, the spectroscopic analyses using Thermo Scientific Nicolet iS50 FT-IR spectrometer were performed. The KBr pastilles that include 0.8 mg of powdered Mg/Fe-HC and 80 mg of KBr have been recorded in transmission mode under spectral range from 4000 to 400 cm<sup>-1</sup>.

The influence of the initial Cu<sup>2+</sup> concentration on the removal efficiency and the evaluation of the equilibrium adsorption capacity were examined under batch adsorption test. For this reason, 25 mL of Cu<sup>2+</sup> solutions (pH 5.0) of different concentrations (100-500 mg/L) were stirred with 0.5 g/L of the Mg/FeGPHC during 24 h at room temperature (298±0.5 K), and 250 rpm. The content of Cu<sup>2+</sup> in the resultant filtrates was measured using Atomic Absorption Spectrophotometer (AAS) (Analytic Jena Spekol 900T). The amounts of Cu<sup>2+</sup> removed by tested Mg/FeGPHC were calculated by following equation:

$$q_{eq} = \left( \frac{C_0 - C_{eq}}{m} \right) \times V \quad (1)$$

where C<sub>0</sub> and C<sub>eq</sub> are the initial and equilibrium concentrations of the Cu<sup>2+</sup> solution (mg/L); V represents the volume of the Cu<sup>2+</sup> solution (L), m is the amount of adsorbent (Mg/FeGPHC) (g), respectively.

## 3. RESULTS AND DISCUSSION

### 3.1 Spectroscopic assay

In order to gain insight into the involvement of functional groups on the Mg/FeGPHC surface, and therefore the reveal potential mechanism of Cu<sup>2+</sup> ion removal, a spectroscopic analysis of the adsorbent material before and after adsorption was performed. The obtained results (Figure 1a.) reveal that Mg/FeGPHC showed the peaks common to hydrochars, which indicate an aromatic structure rich in oxygen functional groups. Thus, the FTIR diagrams of modified GP hydrochar display a broad peak at around 3300 cm<sup>-1</sup>, attributed to stretching vibrations of hydroxyl and carboxyl groups, aromatic C=C at around 1590 cm<sup>-1</sup>, band at around 1380 cm<sup>-1</sup> corresponding to stretching vibrations of carboxylate -CH<sub>2</sub> or C-O, as well as correlated bands (1200 to 1000 cm<sup>-1</sup>) attributed to stretching vibrations of aromatic and aliphatic C-O groups [2]. The peaks notable in spectral range from 750 to 500 cm<sup>-1</sup> indicating the presence of MgO and FeO incorporated onto

the hydrochar surface during the modification process [6]. Obtained findings suggest that the Mg/FeGPHC display surface abundant with functional groups, which contribute to heavy metal removal.

As a result of Cu<sup>2+</sup> ions adsorption, certain changes are notable through all spectral range. A broad intense peak that occurs at about 3300 cm<sup>-1</sup> after adsorption shows a significant decrease in intensity. Similarly, the other bands notable on the FTIR spectrum become less pronounced and shifted to lower wavenumbers after the adsorption of Cu<sup>2+</sup> ions. This observation indicates that the potential mechanisms responsible for metal ions binding include Cu-π reaction between aromatic groups of Mg/FeGPHC (C=C) and Cu<sup>2+</sup> ions, surface complexation with oxygen-containing functional groups (-OH, C=O), as well as exchange with Mg and Fe ions.

### 3.2 Preliminary adsorption test

#### 3.3 Isothermal study

Preliminary adsorption test reveal that modified hydrochar exhibited significantly higher adsorption capacity (71 mg/g) towards Cu<sup>2+</sup> ions in comparison to unmodified (14 mg/g). In order to gain insight into the nature of the interaction between Cu<sup>2+</sup> ions and modified Mg/FeGPHC surface, and to determine a theoretical maximum adsorption capacity, four isotherm models were applied to the experimental results [2,7].

The Langmuir isotherm model:

$$q_e = \frac{q_m K_L C_e}{1 + K_L C_e} \quad (2)$$

The Freundlich isotherm model:

$$q_e = K_F C_e^{1/n} \quad (3)$$

The Sips isotherm model:

$$q_e = q_m \frac{K_S C_e^{n_s}}{1 + K_S C_e^{n_s}} \quad (4)$$

and Redlich-Peterson (R-P) isotherm model:

$$q_e = \frac{K_{RP} C_e}{1 + a_{RP} C_e^\beta} \quad (5)$$

Where C<sub>e</sub> represents the equilibrium concentration (mg/L), q<sub>m</sub> is the maximum quantity of adsorbed Cu<sup>2+</sup> ions (mg/g), K<sub>L</sub>, K<sub>F</sub>, K<sub>S</sub>, and K<sub>RP</sub> are model constants, 1/n adsorption intensity, n<sub>s</sub> is the Sips model exponent, and a<sub>RP</sub> (L/mg) represents the R-P equilibrium constant.

The obtained results are presented and summarized in Figure 1b, and Table 1.

Table 1- Parameters and determination coefficients of the isotherm models for Cu<sup>2+</sup> removal

Models	Parameters	Value	Models	Parameters	Value
Langmuir	q <sub>m</sub> (mg g <sup>-1</sup> )	83.28	Freundlich	K <sub>F</sub> (mg g <sup>-1</sup> )(L mg <sup>-1</sup> ) <sup>1/n</sup>	17.95
	K <sub>L</sub> (L mg <sup>-1</sup> )	0.14		1/n	0.41
	R <sup>2</sup>	0.9755		R <sup>2</sup>	0.9828
Sips	q <sub>m</sub> (mg g <sup>-1</sup> )	75.0	R-P	K <sub>RP</sub> (L g <sup>-1</sup> )	35.54
	K <sub>S</sub> (L mg <sup>-1</sup> )	0.14		a <sub>RP</sub> (L mg <sup>-1</sup> )	1.23
	n <sub>s</sub>	0.62		β	0.72
	R <sup>2</sup>	0.9930		R <sup>2</sup>	0.9900

Based on results of correlation coefficients ( $R^2$ ) displayed in Table 1 can be concluded that the Sips isotherm model best described nature of the interaction. Thus, adsorption occurs as multi-layered adsorption on a heterogeneous surface. Furthermore, according to Sips isotherm model the maximum adsorption capacity ( $q_m$ ) was 75 mg/g. In addition, summarized parameters from applied isothermal models ( $K_L < 1$ ,  $K_F > 1$ , the  $1/n$ , and  $n_s$  values are in range from 0 to 1, and  $\beta < 1$ ) suggesting that the removal of  $\text{Cu}^{2+}$  ions onto investigated material are favorable.

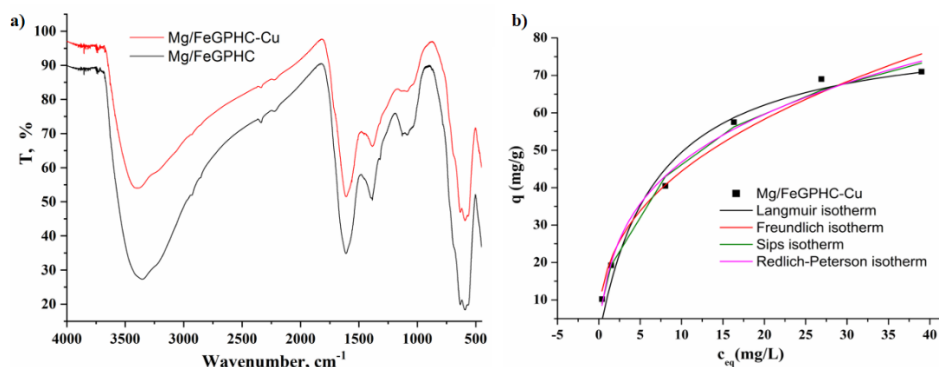


Figure 1- FTIR spectra (a) before and after adsorption onto Mg/FeGPHC, and applied isotherm models (b)

#### 4. CONCLUSION

In this study, Mg/Fe doped grape pomace hydrochar was investigated as potential adsorbent of  $\text{Cu}^{2+}$  ions from aqueous solution. The prepared Mg/FeGPHC was subjected to spectroscopic analysis before and after adsorption, as well as isothermal study tests. Based on the results, oxygen-containing functional groups and aromatic functional groups from Mg/FeGPHC surface participate in the binding of  $\text{Cu}^{2+}$  ions from aqueous solutions, with maximum adsorption capacity of 75 mg/g. Moreover, removal of  $\text{Cu}^{2+}$  ions onto investigated material is favorable process.

#### Acknowledgement

The authors are grateful to the Ministry of Science, Technological Development and Innovation of the Republic of Serbia for the financial support (contract no. 451-03-47/2023-01/200023).

#### REFERENCES

- [1] X. Hu, L. Dai, Q. Ma, J. Xu, J. Ma, X. Liu., *Ind. Crops Prod*, 187 (2022) 115396.
- [2] J. Petrović, M. Ercegović, M. Simić, D. Kalderis, M. Koprivica, J. Milojković, D. Radulović *J. Mol. Liq.* 376 (2023) 121424.
- [3] W-C. Chen, H-M. Saad, K-S. Sim, V-S. Lee, K-W. Tan., *J. Mol. Struct.* 1254 (2022) 132337.
- [4] K. Majhi, M. Let, U. Halder, A. Chitikineni, R-K. Varshney, R. Bandyopadhyay., *Environ. Res.* 223 (2023) 1185431.
- [5] B. Li, J-Q. Lv, J-Z. Guo, S-Y. Fu, M. Guo, P. Yang., *Bioresour. Technol.* 275 (2019) 360-367.
- [6] S-W. Hwang, A. Umar, G-N. Dar, S-H. Kim, R-I. Badran., *Sensor Letters*, 12 (2014) 1-5.
- [7] M. Simić, J. Petrović, T. Šoštarić, M. Ercegović, J. Milojković, Z. Lopičić, M. Kojić., *Processes*,10 (2022) 1957.

## A COATING APPLICATION OF IN718 VIA SELF-PROPAGATING HIGH-TEMPERATURE SYNTHESIS METHOD

Esra Dokumaci Alkan<sup>1</sup>, Nurdan Ari<sup>2</sup>, Murat Alkan<sup>1</sup>

<sup>1</sup>Dokuz Eylul University, Faculty of Engineering, Department of Metallurgical and Materials Engineering, 35390 Izmir, Turkey

<sup>2</sup>Dokuz Eylul University, The Graduate School of Natural and Applied Sciences, Department of Metallurgical and Materials Engineering, 35390 Izmir, Turkey

### Abstract

*This study aims to produce a coating layer of Inconel 718 superalloys on a steel substrate. The production of this alloy was realized by a self-propagating high-temperature synthesis (SHS) method, which is a fast and low-energy required process. A mixture of metal oxide powders with reducing Al metal powder was used as raw material to produce the alloy having the targeted composition. The exothermic reactions were realized by initiation, and the obtained molten alloys were simultaneously poured on the substrates to form the coating layers. The substrates were made of AISI 1050 alloys having 20 mm diameter. During the coating application, the plate on which the substrates were placed was also rotated at 200 rpm speed.*

**Keywords:** Inconel 718, Self-propagating High-temperature Synthesis, Coating

### 1. INTRODUCTION

Nickel-based superalloys, owing to their superior mechanical and chemical properties, find wide applications in the aerospace, marine, nuclear reactor, and chemical industries. These superalloys contain at least 50 mass % Ni. Many of these superalloys contain different alloying elements, including high amounts of Cr (10–20 mass %), Al and Ti (up to 8 mass % combined), and Co (5–15 mass %) together with small amounts of Mo, W, and C. One of the essential alloys for aerospace applications, mainly used in jet engines, is Inconel 718. It is a high-strength, corrosion-resistant alloy used at temperatures up to 750 °C [1]. Despite many superior properties of Inconel 718, the machinability of the alloy is very low due to its thermo-mechanical properties, low thermal conductivity, and high hardness [2]. Self-propagating high-temperature synthesis (SHS) process is based on some principles: the ignition of the starting reagents by an external effect, the initiation of a highly exothermic reaction, and the propagation of the combustion wave spontaneously on the reaction mixture. It is also called by names such as combustion synthesis, gasless combustion, self-propagating combustion, and self-propagating exothermic reactions [3]. The method is straightforward and has low energy requirements. By this method, complex phases can be acquired, and the products are high purity [4]. There are two types of SHS products: the intermediate products (which are synthesized to be used in later processes) and the final products (produced directly, and the reaction is carried out in a single step). The coating processes can be done in both product types. Factors such as particle size, the stoichiometry of reactants, green density, gas pressure, pellets size, and ignition mode play a vital role in SHS reactions [5]. The advantages of the SHS process are the fast processing time with low operating and processing costs [6]. With the SHS process, advanced ceramics, intermetallic and refractory materials can be produced, as well as coatings. As a result of recent research, various SHS-composite products have been developed and synthesized for hard tribological and heat-resistant coatings. Without cracks and pores, synthesis can produce a variety of metal substrates and intermetallic layers [3, 7, 8].



## 2. EXPERIMENTAL

In the SHS experiments, a mixture of technical grade (min. 98.0 % purity) metal oxide powders (NiO, Cr<sub>2</sub>O<sub>3</sub>, Nb<sub>2</sub>O<sub>5</sub>, MoO<sub>3</sub>, TiO<sub>2</sub>, Co<sub>3</sub>O<sub>4</sub>, and Fe<sub>2</sub>O<sub>3</sub>) with metallic Al powder as reducing agent was used as raw material. All raw materials have similar particle sizes (100-150 μm). Low alloy steel (AISI 1050) having 20 mm diameter was selected as the substrate material. The starting mixtures were prepared to produce a targeted alloy composition of 52.0 % Ni, 21.0 % Cr, 12.0 % Fe, 6.0 % Nb, 4.0 % Mo, 3.0 % Ti, and 2.0 % Co by mass. This selected alloy composition falls within the composition ranges of the IN718 superalloy. The raw material powders were dried in an oven at 105 °C for 2 h. The starting mixtures were weighed to 50 g, then mixed for 30 min in a plastic container. The mixtures were charged into a copper crucible, and the exothermic reactions were initiated using a resistance wire (Cr25Al5). Different setups were studied to obtain a coating layer on the steel substrates. In the first series, the steel substrate was placed at the bottom of a crucible, and the starting mixtures were charged onto the substrate at the same crucible. In the second series of experiments, the starting mixture and the steel substrate were placed in separate crucibles. These crucibles were placed on each other. An aluminum foil, which kept the starting mixture in the upper crucible without spilling, was used as a separator. The molten alloy obtained from the exothermic reaction was poured onto the substrate through the hole in the foil and formed the coating layer. In the last series, a rotor was used to rotate the lower crucible at different speeds where the substrate was placed. The schematic views of the experimental setups are given in Figure 1.

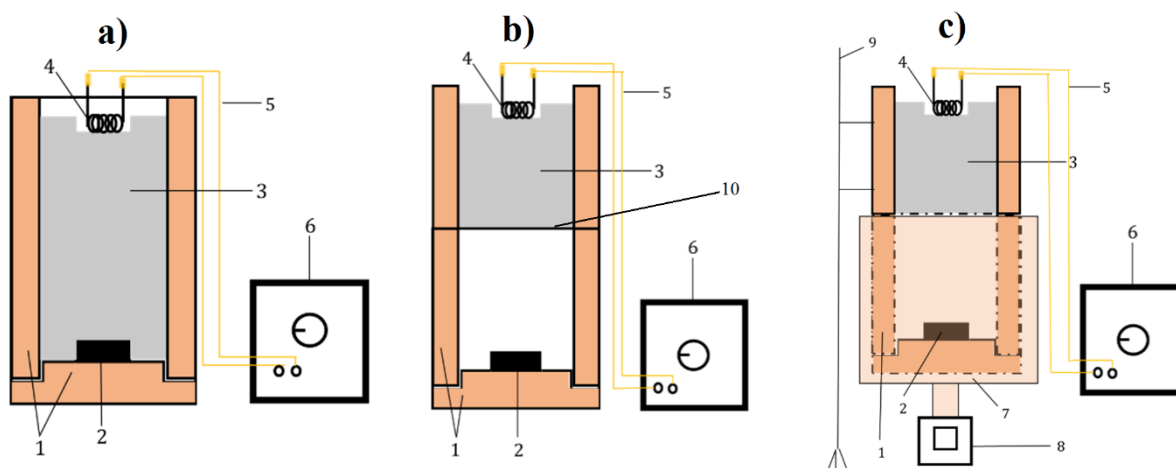


Figure 1 - The schematic view of a) the first, b) the second, and c) the last experimental setups. (1. Crucible, 2. Substrate, 3. Raw mixtures, 4. Resistance wire, 5. Cu cable, 6. Power supply, 7. Rotary head, 8. Rotor, 9. Stand, and 10. Al foil)

The chemical compositions of the products were calculated by using X-ray fluorescence (XRF) equipment. The morphologies of the products were characterized by scanning electron microscope (SEM) with EDS (Energy Dispersive Spectrometer). Also, microhardness tests of substrates and coating layers were performed.

## 3. RESULTS AND DISCUSSION

As a result of the SHS reaction, a strong bonding was formed between the steel substrate and superalloy coating. According to the results of the XRF analysis on the produced coatings, the average composition of the alloy was as follows: 55.3 % Ni, 17.8 % Cr, 11.3 % Fe, 5.6 % Nb, 4.0 % Mo, 0.5 % Ti, 2.2 % Co, and 2.7 % Al by mass. The weights of the coatings were measured as 23.32, 16.98, and 10.34 g in the first, second, and last experimental setups, respectively. Metal recoveries were 82.4, 60.0, and 36.5 %, respectively. The microstructure images of the substrate

and coating regions obtained in three separate setups are given in Figure 2. It is seen that the obtained superalloys were also diffused into the substrate.

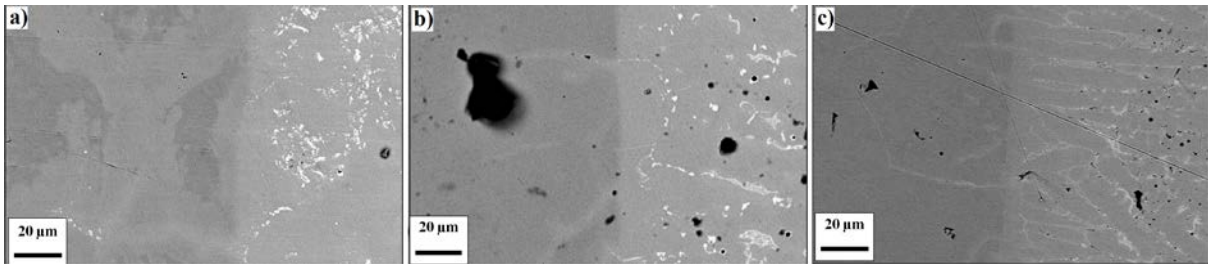


Figure 2 - SEM images of the cross-sections of the products were obtained in a) first, b) second, and c) last experimental setup (left side: substrate, right side: coatings).

X-ray mapping and EDS results of the obtained product from the second experimental setup are given in Figure 3. It is seen in the X-ray maps that there were Ni, Cr, Nb, Mo, and Al transitions toward the steel substrate. It is also seen that the matrix of the coating alloy consisted of a nickel-rich ( $\gamma$ ) phase. There were also some Nb-rich phases in the microstructure. It is thought that this Nb-rich structure may belong to the  $\gamma''$  phase. Even a tiny amount of eutectic formations were observed in the coating.

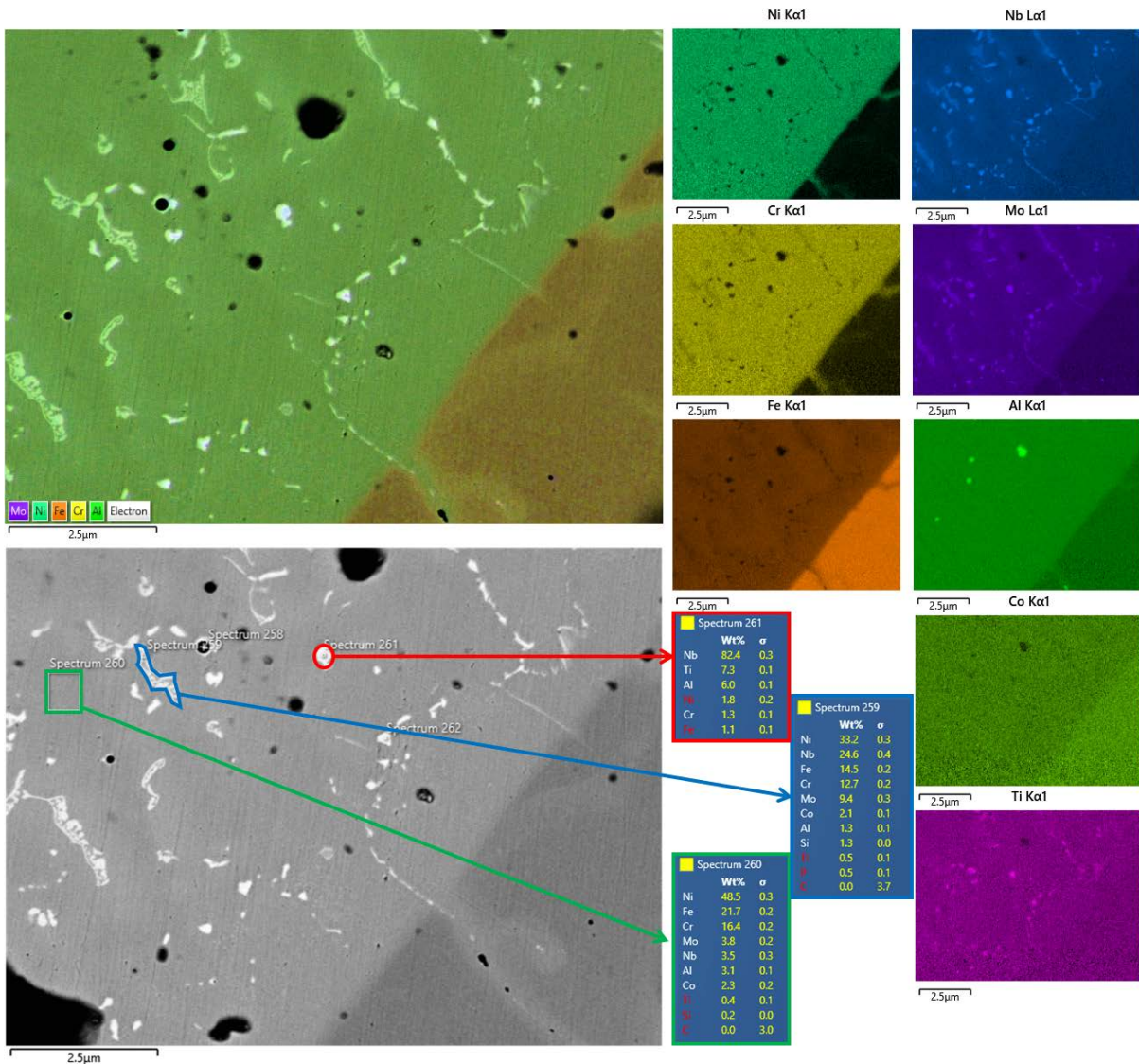


Figure 3 - X-ray mapping and EDS results of the products obtained in the second experimental setup.

Figure 4 shows the microhardness measured at the coating portion, the interface, and the steel substrate. A load of 50 g was applied to the samples. It was observed that the hardness value increased from the steel substrate to the superalloy coating. When the interface close to the steel substrate is examined, the surface properties of the low alloy steel material are improved.

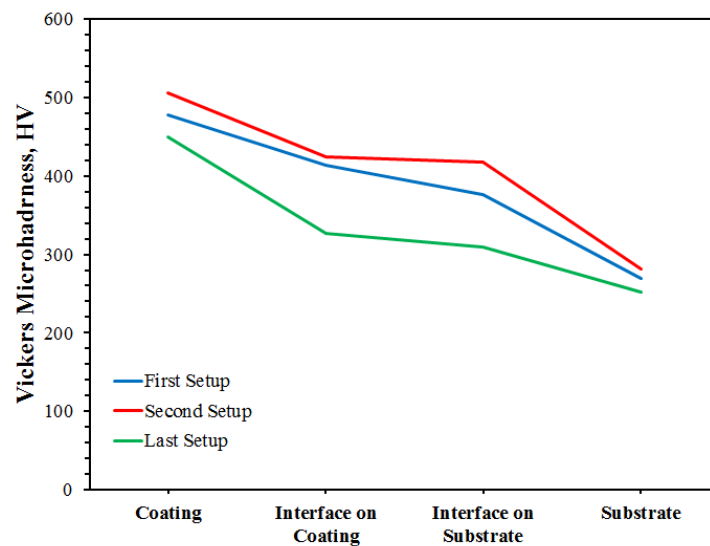


Figure 4 - The microhardness values of the obtained products.

#### 4. CONCLUSION

In this study, the production of IN718 alloy as a coating on a steel substrate was carried out. The self-propagating high-temperature synthesis method, which uses low-cost raw materials and allows fast production, was chosen as the production process. Production was carried out using different experimental setups. Similar structures were obtained in each setup, and the highest metal recovery was achieved in the first experimental setup. Excellent bonding occurs at the interfaces within the coated area. It is thought that this study will shed light on the following studies to improve the surface properties of metallic materials.

#### ACKNOWLEDGEMENTS

*The authors would like to thank Research Assistant Mr. Özgür Yasin Keskin for helping with the analyses.*

#### REFERENCES

- [1] A. Mouritz., Introduction to Aerospace Materials, Woodhead Publishing Limited, Cambridge, 2012, pp. 251-267.
- [2] F. Pusavec, A. Deshpande, S. Yang, R. M'Saoubi, J. Kopac, O.W. Dillon Jr, and I.S. Jawahir., J. Clean. Prod., 81 (2014) 255-269.
- [3] J. Subrahmanyam and M. Vijayakumar., J. Mater. Sci., 27 (1992) 6249-6273.
- [4] Z.A. Munir and U. Anselmi-Tamburini., Mater. Sci. R., 3 (7-8) (1989) 277-365.
- [5] P. Mossino., Ceram. Int., 30 (3) (2004) 311-332.
- [6] X. Yangtao, X. Tiandong, and H. Yanling., Rare. Metal. Mat. Eng., 38 (8) (2009) 1333-1337.
- [7] E.A. Levashov, A.S. Mukasyan, A.S. Rogachev, and D.V. Shtansky., Int. Mater. Rev., 62 (4) (2017) 203-239.
- [8] A.E. Sytshev, S.G. Vadchenko, O.D. Boyarchenko, D. Vrel, and N.V. Sachkova., Int. J. Self-Propagating High-Temp. Synth., 20 (3) (2011) 183-188.

## PRODUCTION OF AlCoCrCu<sub>x</sub>FeNi ALLOYS VIA SELF-PROPAGATING HIGH-TEMPERATURE SYNTHESIS METHOD

Murat Alkan<sup>1</sup>, Esra Dokumaci Alkan<sup>1</sup>, Dilan Ugurluer<sup>2</sup>, Aslihan Karakanat<sup>2</sup>

<sup>1</sup>Dokuz Eylul University, Faculty of Engineering, Department of Metallurgical and Materials Engineering, 35390 Izmir, Turkey

<sup>2</sup>Dokuz Eylul University, The Graduate School of Natural and Applied Sciences, Department of Metallurgical and Materials Engineering, 35390 Izmir, Turkey

### Abstract

*This study aims to produce high-entropy alloys (HEA) having AlCoCrCu<sub>x</sub>FeNi stoichiometry ( $X = 0.0 - 1.0$ ) by a self-propagating high-temperature synthesis process. A mixture of metal oxide powders with reducing Al metal powder was used as raw material to produce the alloy having the targeted composition. The effects of the weight ratios of the metal oxides on metal recovery values and properties of the final alloys were investigated. The final products were characterized by using XRD, optic microscope and SEM/EDS techniques.*

**Keywords:** High-Entropy Alloys, Self-propagating High-temperature Synthesis, Cu ratio

### 1. INTRODUCTION

Recently, high-entropy alloys (HEAs) have been produced as an alternative to traditional alloys. Unlike conventional alloys, HEAs comprise at least five principle elements with a 5 to 35 % molar ratio. HEAs must have high configurational entropy, higher than  $1.51 R$  ( $R$  is the gas constant,  $8.314 \text{ J/K mol}$ ). The microstructure is simpler because of its higher configurational entropy and the number of phases in alloys is lower than expected. The high-entropy effect decreases the Gibbs free energy and forms solid solution phases. This is why many reported high entropy alloys included only one or two solid solutions in their microstructures [1-4]. HEAs are also known as multi-element alloys. According to the components and microstructure of alloys and production methods mechanical properties of HEAs and their application areas can be varied. HEAs can have great mechanical properties like better hardness, strength, ductility with oxidation, and wear resistance. Therefore, HEAs were used in coatings, biomedical applications, tools, and engine materials [5-7]. The first study on the production of high entropy alloys by the self-propagating high-temperature synthesis (SHS) method was published in 2016. In that study, NiCrCoFeMnAl<sub>x</sub> alloy systems were produced. The mole amount of the Al element was changed from 0 to 2. Researchers investigated the effects of Al addition on the phases, density, and hardness values of alloy [8].

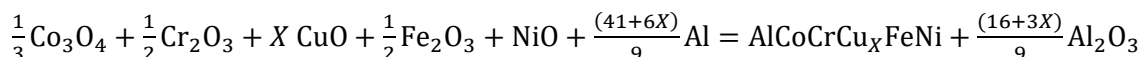
In this study, AlCoCrCu<sub>x</sub>FeNi-based high-entropy alloys were produced by a self-propagating high-temperature synthesis method. The different molar ratios of the starting mixture were selected, and their effects on the microstructure, phases, and properties of the final alloys were investigated.

### 2. EXPERIMENTAL

In the SHS experiments, a mixture of technical grade (min. 98.0 % purity) metal oxide powders (Co<sub>3</sub>O<sub>4</sub>, Cr<sub>2</sub>O<sub>3</sub>, CuO, Fe<sub>2</sub>O<sub>3</sub>, and NiO) with metallic Al powder as reducing agent was used as raw material. All raw materials have similar particle sizes (100-150  $\mu\text{m}$ ). The amount of components in initial mixtures prepared from dried powders were calculated to produce HEAs as targeted compositions (AlCoCrCu<sub>x</sub>FeNi where  $X = 0.0, 0.2, 0.4, 0.6, 0.8$  and  $1.0$ ). The raw material



powders were dried in an oven at 105 °C for 2 h. The starting mixtures were weighed to 200 g, then mixed for 30 min in a plastic container. The mixtures were charged into a copper crucible, and the exothermic reactions were initiated using a resistance wire (Cr25Al5). The reaction realized by passing current through the wire. The obtained SHS products were discharged from the crucible after cooling. The reaction follows as:



Thermodynamic investigations were also performed before and during the experimental studies. A thermochemical simulation was performed to calculate the standard enthalpy of formation, the released energy per gram product and the adiabatic temperature of the reduction reactions by using HSC Chemistry software. The released energy per gram product value of the reaction should be in the range of 2250-4500 J/g so that metal and slag can be easily separated from each other. The theoretical adiabatic temperature value must be higher than 1527°C in order to self-propagate of the combustion wave [9]. Thermo-Calc software and TCHEA4 (High Entropy Alloys v4.0) database were also used to make thermodynamic predictions about phase stabilities and phase compositions under both equilibrium and non-equilibrium cooling conditions.

The chemical compositions of the products were calculated by using X-ray fluorescence (XRF) equipment. The morphologies of the products were characterized by scanning electron microscope (SEM) with EDS (Energy Dispersive Spectrometer). Also, microhardness tests of substrates and coating layers were performed.

### 3. RESULTS AND DISCUSSION

According to the results of the thermochemical simulation of HSC Chemistry software, the adiabatic temperature of the reactions are measured between 2691 (where X=0.0) – 2917 (where X=1.0) °C, while the released energy per gram product changes between 3359.1 – 3500.9 J/g. So, due to the thermochemical calculations, all of the reactions could be realized in self-sustaining.

The weights and the chemical compositions of all products were calculated. The distribution ratios of metals among the alloy, slag and scattered part were calculated by using this equation:

$$[D_{Me}] \text{ or } (D_{Me}) = \frac{[\% \text{ Me}] \times \text{weight of alloy} \text{ or } (\% \text{ Me}) \times \text{weight of alloy}}{\text{wt.}\% \text{ Me in initial mix} \times \text{weight of initial mix}}$$

where  $[D_{Me}]$  is the distribution ratio of a metal in alloy,  $(D_{Me})$  is the distribution ratio of a metal in slag.

The distribution of metals into the products obtained with usage of different ratios of raw materials was given in Figure 1. The highest metal recovery values were obtained where X = 0.4. With the increasing in the ratio of CuO in the initial mixtures, the reduction reaction were realized highly explosive and the amount of the lost part (due to the scattered and vaporizing) were also increased. One of the reason of that is the moisture content in CuO. The theoretical energy calculations, measured by using HSC Chemistry software, depend on the assumption of the HEAs are the ideal solutions. If the formation of AlCoCrCu<sub>x</sub>FeNi alloys is exothermic (negatively deviate from ideal solution) the released energy per gram product will be increased. The calculated configurational entropies of the alloys were measured between 1.56R – 1.76R.

The results of SEM micrographs of HEAs were given in Figure 2 and their XRD results were given in Figure 3, relatively. Due to the back scattered electron images of HEAs, there are two phases can be seen in AlCoCrFeNi alloy, while there are three phases can be seen in AlCoCrCu<sub>x</sub>FeNi alloys. With the increasing in Cu content in HEAs, the matrix phase was changed from body centered cubic to face centered cubic structure (Figure 3).

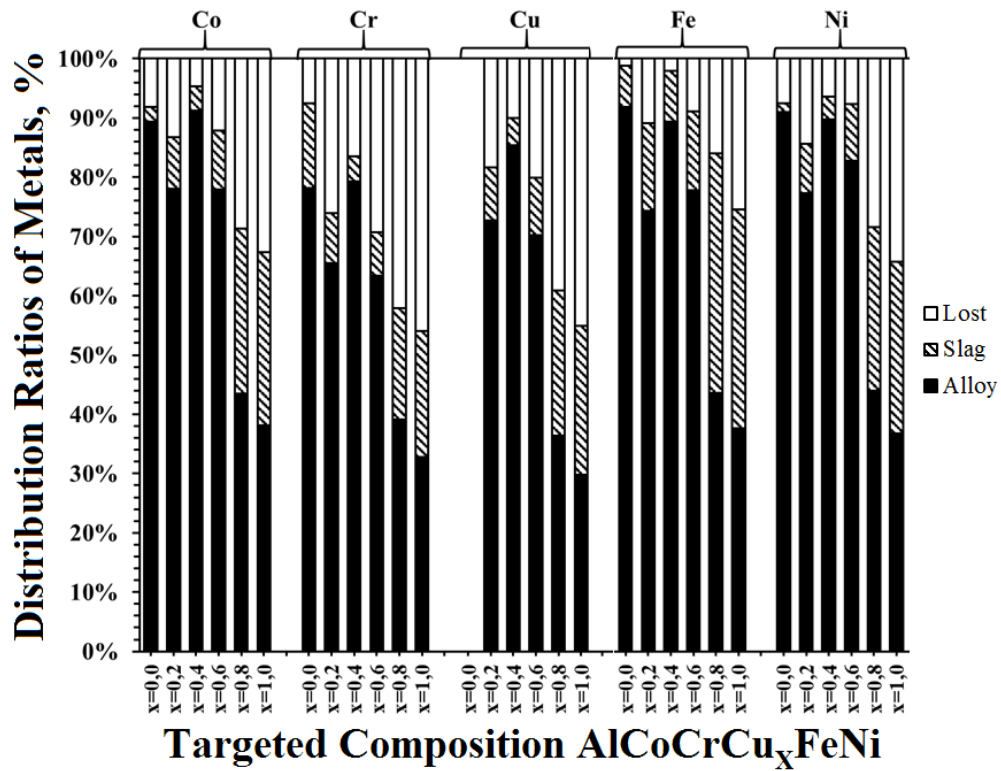


Figure 1 - The distribution ratios of metals among alloy, slag and scattered parts.

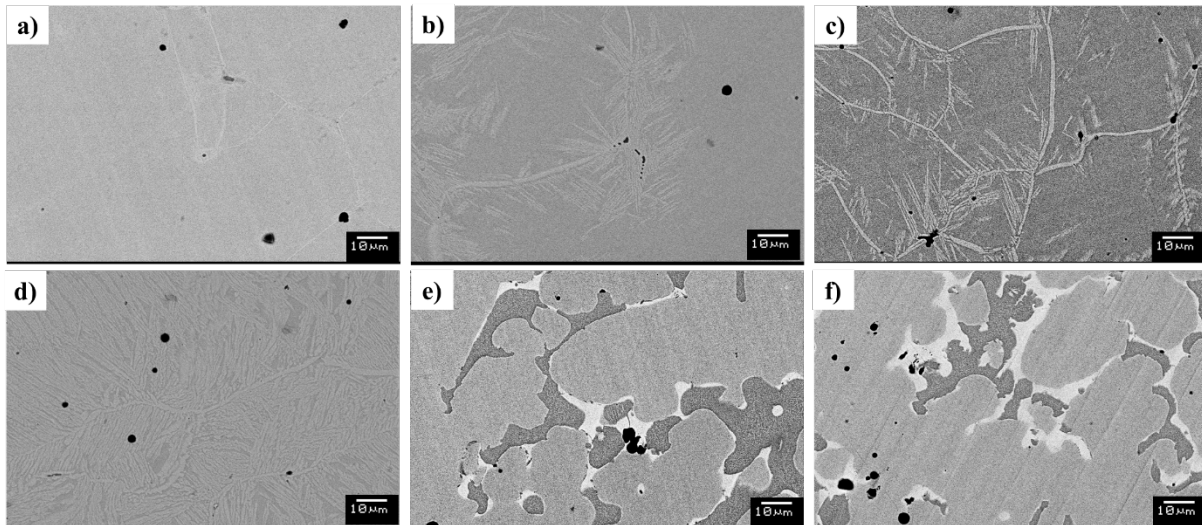


Figure 2 - The microstructures of obtained AlCoCrCu<sub>x</sub>FeNi alloys where X = a) 0.0, b) 0.2, c) 0.4, d) 0.6, e) 0.8 and f) 1.0.

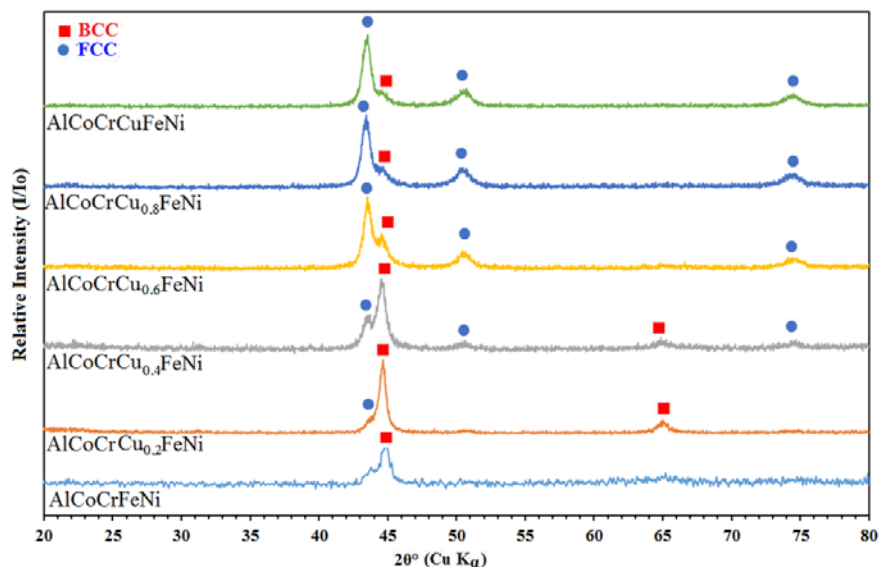


Figure 3 - The comparative XRD results of HEAs.

#### 4. CONCLUSION

In this study, AlCoCrCu<sub>x</sub>FeNi based high-entropy alloys were produced by SHS method. With the increasing in CuO content in the initial mixture, the enthalpy values of the reduction reactions were also increased, and the amount of the scattered material were also increased. The microstructure of HEAs transformed from BCC structure to FCC structure with increasing in Cu content in final alloy.

#### ACKNOWLEDGEMENTS

The authors are pleased to acknowledge the financial support for this research from TUBITAK (The Scientific and Technological Research Council of Turkey, Project No. 118M204). The authors would like to thank Assistant Professor Dr. Nuri SOLAK for his support with the usage of the Thermo-Calc software.

#### REFERENCES

- [1] J.W. Yeh., in High Entropy Alloys (M.C. Gao, J.W. Yeh, P.K. Liaw and Y. Zhang), Springer, Switzerland, 2016, pp.1-19.
- [2] Y.Y. Chen, T. Duval, U.D. Hung, J.W. Yeh, and H.C. Shih., Corros. Sci. 47 (2005) 2257-2279.
- [3] J. Chen, X. Zhou, W. Wang, B. Liu, Y. Lv, W. Yang, D. Xu, and Y. Liu., Y. J. Alloy. Compd. 760 (2018) 15-30.
- [4] E.J. Pickering, R. Munoz-Moreno, H.J. Stone, and N.G. Jones., Scripta. Mater. 113 (2016) 106-109.
- [5] J.W. Yeh., Ann. Chim.-Sci. Mat. 31(6) (2006) 633- 648.
- [6] Z.D. Han, H.W. Luan, X. Liu, N. Chen, X.Y. Li, Y. Shao, K.F. Yao., Mat. Sci. Eng. A, 712 (2018) 380–385.
- [7] E.P. George, W.A. Curtin, and C.C. Tasan. Acta. Mater. 188 (2020) 435–474.
- [8] V.N. Sanin, V.I. Yukhvid, D.M. Ikornikov, D.E. Andreev, N.V. Sachkova, and M.I. Alymov., M. I. “SHS metallurgy of high-entropy transition metal alloys”, Dokl. Phys. Chem. 470 (2) (2016) 145-149.
- [9] Z.A. Munir, and U. Anselmi-Tamburini., U. (1989). Mater. Sci. Rep. 3 (7-8) (1989) 277-365.



## ZINC VOLATILIZATION IN THE PRIMARY AND THE SECONDARY ZINC PRODUCTION

Jarmila Trpčevská, Iveta Vasková, Katarína Pauerová, Martina Laubertová, Dušan Oráč

Faculty of Materials, Metallurgy and Recycling, Technical university of Kosice, Letná 9, 04200  
Košice, Slovakia

### Abstract

*Zinc is characterized by low boiling point, which is the basis for its production via pyrometallurgical processes. Zinc volatilizes immediately and reoxidizes as it meets the air. Zinc has been known for some three thousand years in the form of brass. Regular production of unalloyed zinc occurred relatively late. As a volatile metal, its production required sophisticated distillation installations. Before Europe established large scale zinc production in 18<sup>th</sup> century, only India and China produced unalloyed zinc on an industrial scale. Distillation technology can be used to refine secondary zinc to remove impurities. Research was conducted to distillation of hard zinc formed during hot dip galvanizing. The zinc refining from bottom zinc dross has been investigated in terms of zinc recovery due to the argon flow within the set temperature. Thus, different types of high purity zinc products have been produced.*

**Keywords:** zinc production, volatilization, hard zinc, zinc refining

### 1. INTRODUCTION

Zinc smelting has historically been more difficult than the smelting of other metals, e.g., iron, because in contrast, zinc has a low boiling point. The most important reason is that the reduction temperature of zinc oxide is quite close to the boiling point of metallic zinc. For obtaining pure zinc, distillation technology needed to be developed. The main existing states of zinc in nature are sulfide and oxide. Zinc oxide ores can be directly reduced and distilled by mixing with reducing agents in the retorts. Treatment of sulfide zinc ores is more complicated since they must be roasted before smelting [1].

Distillation technique began to be adopted for zinc production in medieval times in India and China. It is widely acknowledged that India was the first country in the world to smelt zinc; the earliest archaeological evidence comes from Zawar in Rajasthan and dates as early as AD 1025–1280. Ancient Chinese zinc production can be traced back to at least the early Ming Dynasty (early sixteenth century). Chinese and Indian zinc-smelting technologies are quite different in their condensing techniques, furnaces, and retorts (the condensing pots). The process in India used for the distillation of zinc in Zawar mines is unique because it is designed based on downward distillation. In contrast, the Chinese zinc smelting process was based on the principle of distillation by ascending, which seems fundamentally different from the Indian one. The principle of zinc production by distillation in Europe was first applied in Bristol, England in 1743 under leadership of William Champion using vertical retorts. In the improved Ruberg method used in Upper Silesia, Poland retorts were mounted horizontally in the furnace. The Ruberg method became an economical method for large-scale zinc production in Europe. At the end of the 1920s an advance was made in the United States by developing a continuous retort process [2,3,4,5,6,7].

The principle of condensation of zinc vapors was also used in the development of a new method of simultaneous production of zinc and lead by Imperial Smelting Process (ISP). The Imperial Smelting Process was developed in 1960s from a standard lead smelting blast furnace, but completely sealed in which rapid quenching of zinc vapors is a key principle. This process

currently works in Miasteczko Slaskie in Poland, is the only one furnace operating in Europe according to Imperial Smelting Process [6,7].

The thermal volatilization and condensation of zinc can be used in refining process of secondary zinc, such as hard zinc (bottom zinc dross) formed in hot dip galvanizing process. Hard zinc contains high amount of zinc (94-97%) and iron as impurity (2-3%). In this work distillation of hard zinc in the argon flow within the set temperature was studied. Different morphology of the final product was achieved in dependence on argon flow rate.

## 2. EXPERIMENTAL

For all experiments zinc bearing waste samples as shown in the Figure 1 were used. All the experiments have been conducted in the apparatus as shown in the Figure 2. Sample was put into quartz tube with diameter of 12 mm. This quartz tube was then inserted into a larger quartz tube with a diameter of 20 mm.

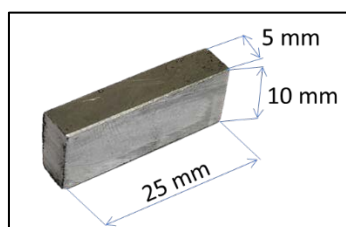


Figure 1 - Zinc sample prepared for experiments

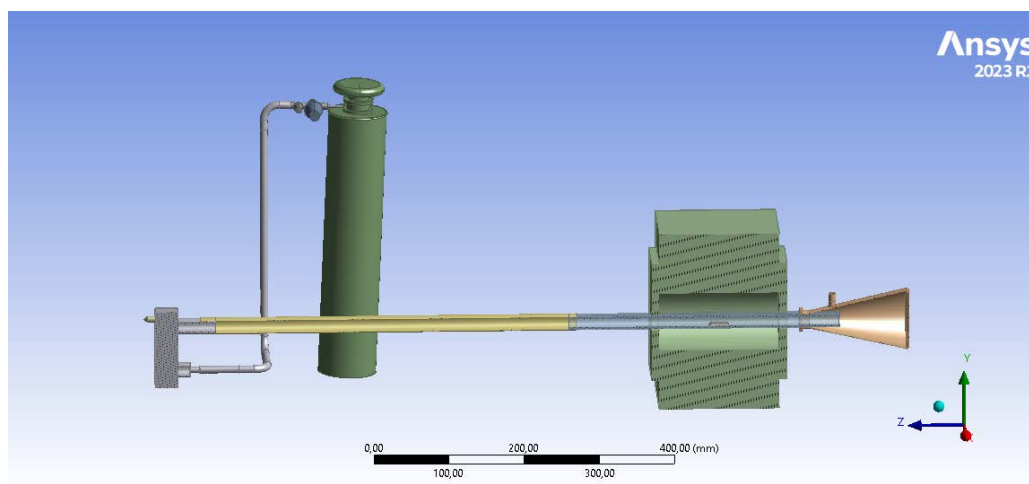


Figure 2 - Apparatus for zinc waste evaporation

The entire apparatus system was blown with argon to protect the zinc vapor from oxidation. The temperature of the evaporation system was set to 800 °C for each experiment. The choice of temperature was determined based on the previous study [8]. The observed variable was the argon flow rate in range of 100-300 mL/min.

## 3. RESULTS AND DISCUSSION

Depending on the argon flow rate different mass of final products has been formed. The dependence the final form of the products on the argon flow rate can be seen in the graph in Figure 3.

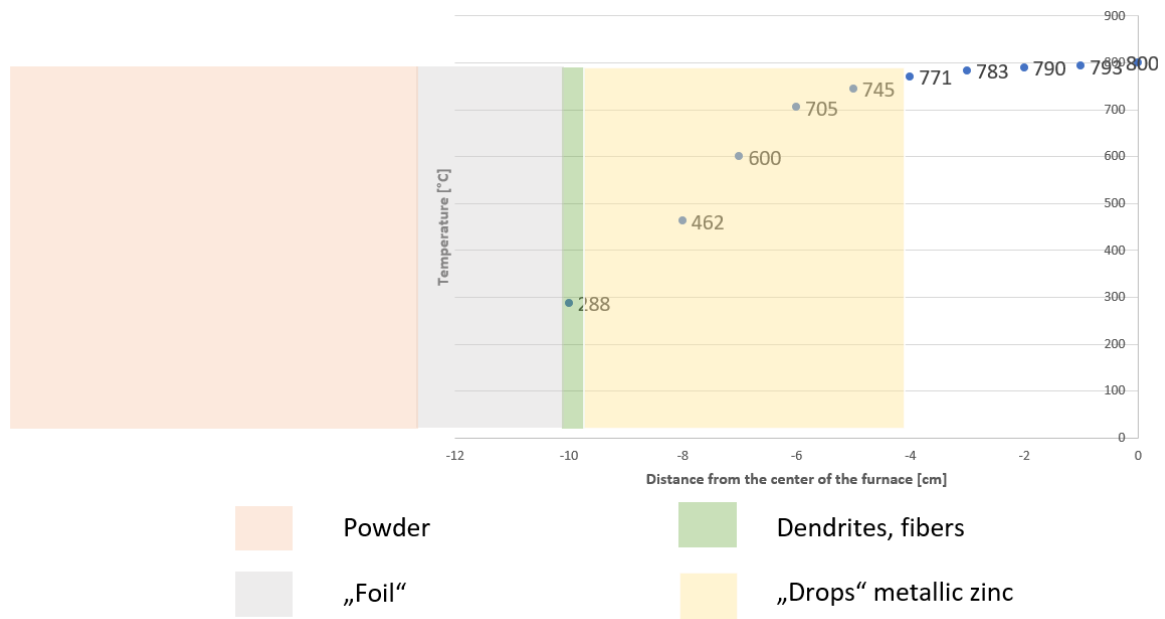


Figure 3 - Dependence of the final form of the products on the argon flow rate

The experiments carried out led to the formation of zinc nanofibers, zinc powder, zinc dendrites, and zinc metal. The final products formation is presented in Figures 4-8. Within the lower argon flow rates, the fibers (Figure 4), dendrites (Figure 5), and metallic zinc (Figure 6) have been formed. The zinc powder (Figure 7) has been formed within the higher argon flow rates.

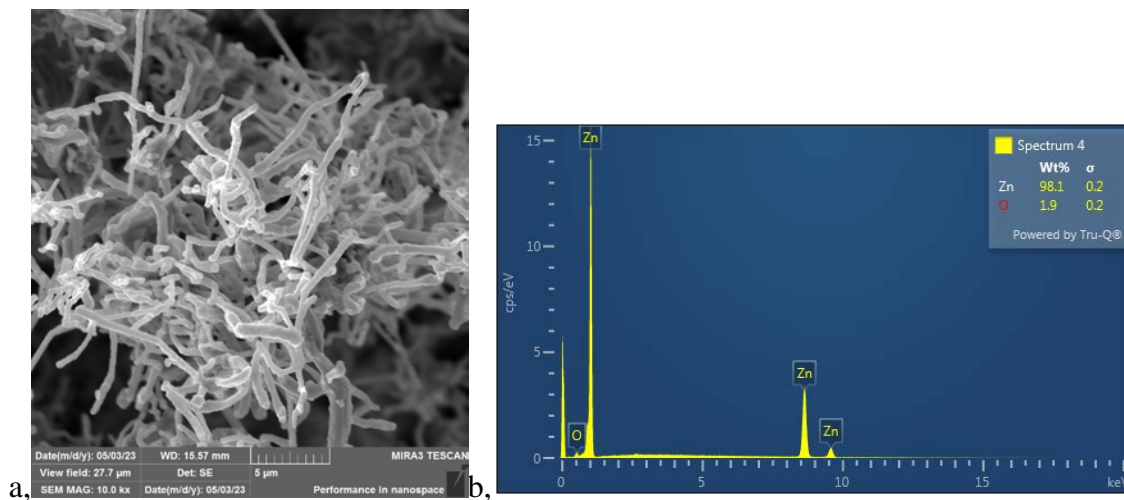


Figure 4 - a, Morphology of zinc nanofibers b, EDX analysis of zinc nanofibers

According to EDX analysis, the product had a high purity of zinc in form of nano fibers.

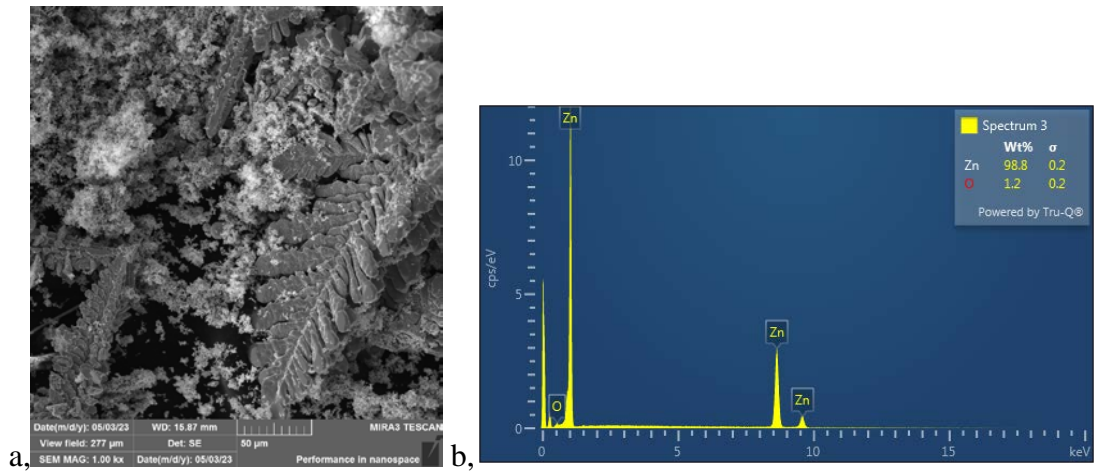


Figure 5 - a, Morphology of zinc dendrites b, EDX analysis of zinc dendrites

A high purity zinc dendrites were detected in the sample by EDX.

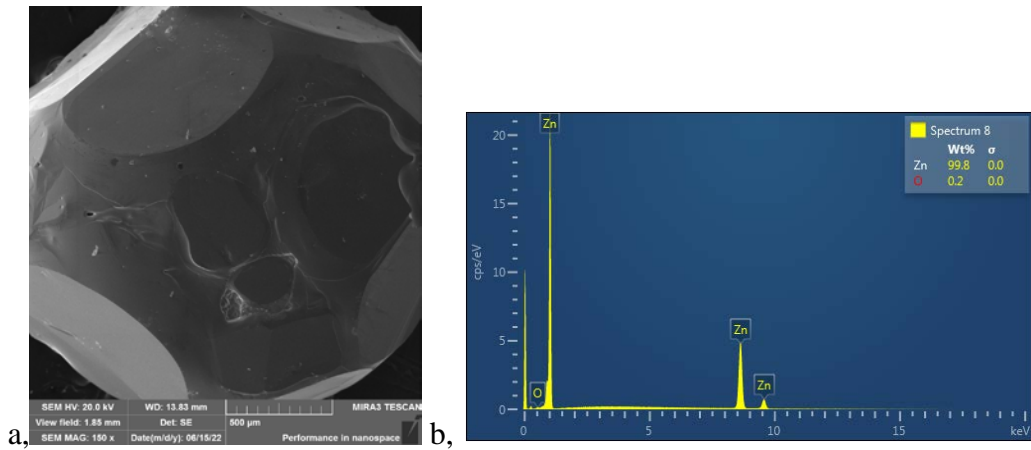


Figure 6 - a, Morphology of metallic zinc b, EDX analysis of metallic zinc

EDX analysis of metallic zinc referred to a zinc in its purest form.

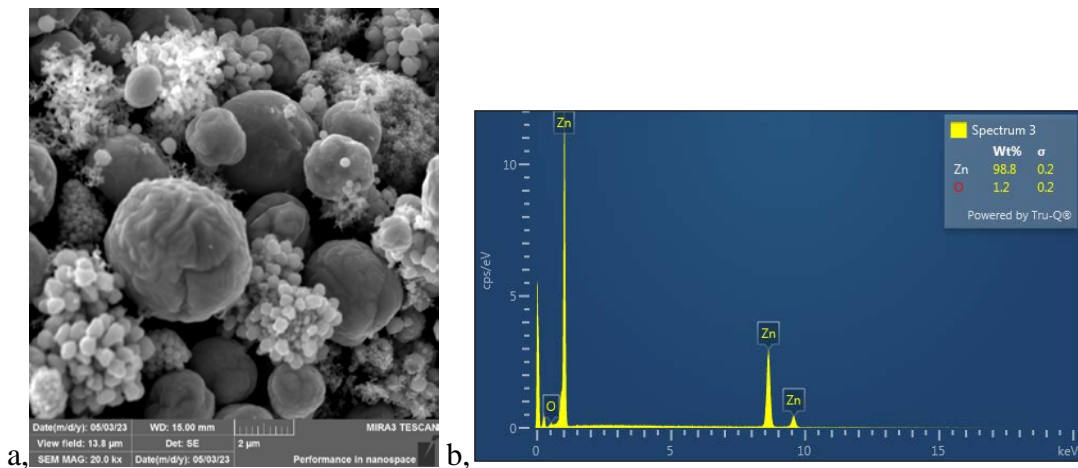


Figure 7 - a, Morphology of zinc powder b, EDX analysis of zinc powder

As all the given products above, also the zinc powder analysis proved high purity.

#### **4. CONCLUSION**

Volatilization and condensation of zinc from hard zinc formed during hot dip galvanizing process have been investigated experimentally. This process can be considered as refining process. It can be clearly observed that the morphology of the metal zinc condensation products depends on argon flow rate. Fibrous structure, zinc powder, zinc dendrites and zinc metal were obtained. Within the lower argon flow rates, the fibers, dendrites, and metallic zinc have been formed. The zinc powder has been formed within the higher argon flow rates. The purity of the products was proved by EDX analysis.

#### **ACKNOWLEDGEMENTS**

*The authors gratefully acknowledge the contribution of the Scientific Grant Agency of the Slovak Republic under the grants 1/0408/23.*

#### **REFERENCES**

- [1] Y. Xiao, et al., J. Archaeol. Sci. Rep. 32 (2020) 1-13.
- [2] Y. Li et al., T Ancient zinc smelting in the Upper and Middle Yangtze River region. Antiquity, 2020, 1-7.
- [3] W. Zhou et al., J. Archaeol. Sci., 39 (2012), p. 908-921.
- [4] W. Zhou et al., J. Archaeol. Sci., 43 (2014), p. 278-288.
- [5] AnChuan Fan et al., Quat. Geochronol., 30 (2015), p. 369-373.
- [6] H. Kania, M. Saternus, Appl. Sci., 13 (2023), p. 1-22.
- [7] R.J. Sinclair, The extractive Metallurgy of zinc, The Australian Institute of mining and metallurgy, 2005, p. 297.
- [8] K. Paureova et al., Materials, 15 (2022), p. 1-15.

## APPLICATION OF THE NUMERICAL METHOD IN THE DEFINITION OF A SUBSTRATE OF CIRCULAR CROSS SECTION

Dragan Ignjatović, Lidija Đurđevac Ignjatović, Vanja Đurđevac,  
Katarina Milivojević, Ivan Jovanović

Mining and Metallurgy Institute Bor, Zeleni Bulevar 35, 19210 Bor, Serbia

### Abstract:

Looking at the stages of development of the shape of the cross-section of the horizontal room of the pit, it can be concluded, regardless of their diversity, that at the base of all shapes, trapezoidal, vaulted and circular shapes, with appropriate combinations, appear as basic shapes.

When applying the Phase<sup>2</sup> software, a circular cross-section of the room was used. In order to define (design) the tunnel lining in the case of a circular cross-section, the geomechanical data of the example provided by the software producer Phase<sup>2</sup> was used.

**Keywords:** circular cross section, finite element method, Phase2 v 8.0

### 1. INTRODUCTION

The dependence between geometric and physical quantities in continuum mechanics is established on elements of differentially small dimensions. The very continuity of those dependencies, by expanding from that infinitesimally small hot spot to the entire observed area, gives differential equations, which define the task with appropriate boundary conditions. We know the primary state of stress  $\sigma_{ij}^0$  which depends only on the coordinates. Secondary state of stress - occurs due to the opening of the hole. We are familiar with Kirsch's solution of the state of stress in an infinite plate in the case of a circular opening [1] (Figure 1).

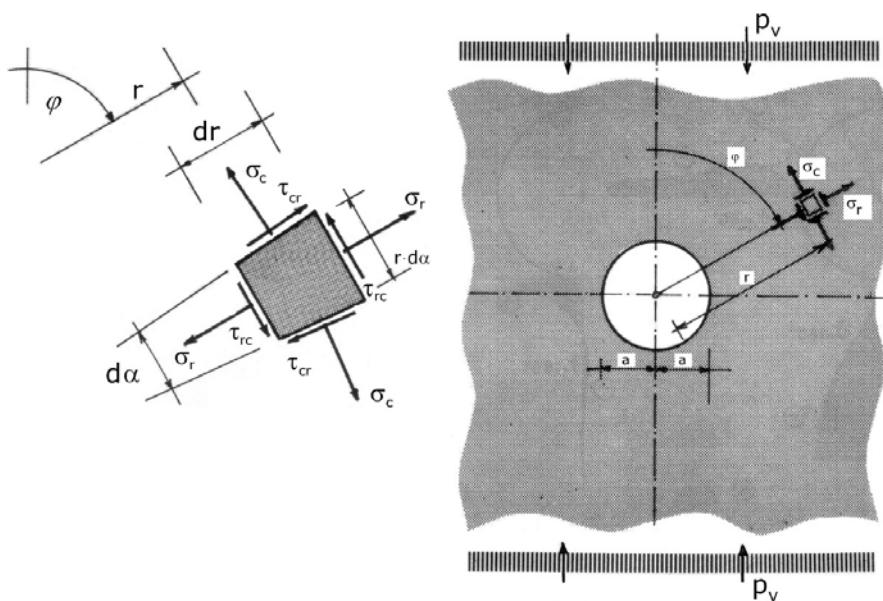


Figure 1 - The case of a circular opening in an infinite plate

Analytical solution of secondary stress or stress concentration for the case of vertical pressure only  $p_v$ , is shown by the following expression:

$$\sigma_r = \frac{p_v}{2} \left[ 1 - \frac{a^2}{r^2} + \left( 1 - \frac{4a^2}{r^2} + \frac{3a^4}{r^4} \right) \cdot \cos 2\varphi \right]$$



$$\sigma_t = \frac{p_v}{2} \left[ 1 + \frac{a^2}{r^2} + \left( 1 + \frac{3a^4}{r^4} \right) \cdot \cos 2\varphi \right]$$

$$\tau_{rt} = \frac{p_v}{2} \left[ 1 + \frac{2a^2}{r^2} - \frac{3a^4}{r^4} \right] \cdot \sin 2\varphi$$

Solving planar and spatial problems is therefore based on solving differential equations.

When solving the continuum problem with the assumed constitutive connection, it is necessary to simultaneously satisfy the conditions of the equation:

- a) equilibrium conditions
- b) continuity conditions
- c) conditions on the contour and others.

## 2. CONSTRUCTION OF UNDERGROUND SPACE OF CIRCULAR CROSS SECTION IN INFINITELY ELASTIC ENVIRONMENT

This problem considers the case of an underground room with a circular cross-section, diameter 1m, which is made in an ideally elastic medium. It is assumed that the hydrostatic pressure is applied, the value of which is 30 MPa. Figure 2 shows the configuration of the model, including the limit values [2] , while Table 1 shows the material properties and other parameters.

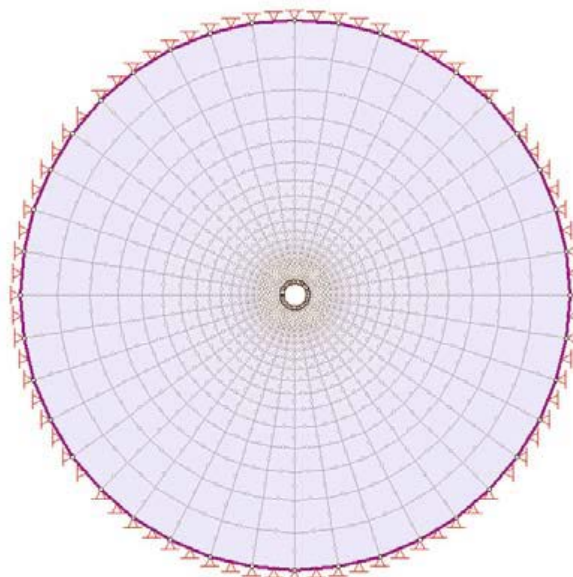


Figure 2 - Room model of a circular cross-section in an infinitely elastic medium in the **Phase<sup>2</sup> program**

Table 1 - Model parameters

Parameter	Value
Jung's modulus (E)	10000 MPa
Voltage field (p <sub>1</sub> , p <sub>2</sub> )	30 MPa
Poisson's ratio (ν)	0.2

This model in the **Phase<sup>2</sup> program** uses a radial grid with 840 8-node quadrilateral elements with a fixed outer boundary that is 21m from the center of the room. The room is divided into 40 segments.



## 2.1 Substructure of underground rooms in an elastic environment

In this example, an account is given of solving the problem of the occurrence of axial force and bending moment in the rock mass in subgrade, during the construction of mining rooms with a circular cross-section, in an ideally elastic environment. Figure 3 shows the model, which was applied in the *Phase<sup>2</sup> program*, which defines the support as an elastic thick-walled lining in both phases, during bending and peripheral deformations.

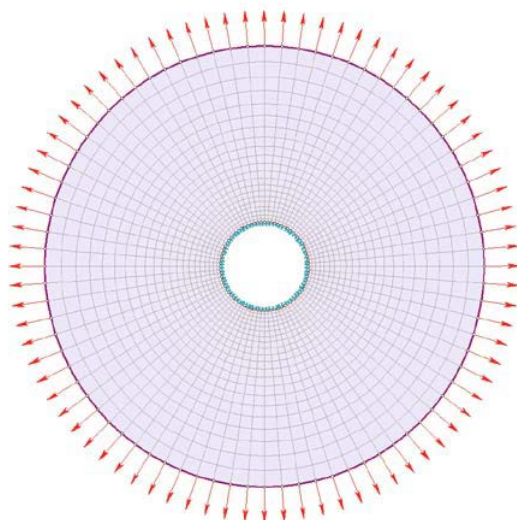


Figure 3 - Model of the finished mining room that was applied in **Phase<sup>2</sup>**. The support is shown in blue

The relevant parameters of the model are given in Table 2. The model uses a radial mesh with 1680 4-node quadrilateral elements. The underground room and support are divided into 80 segments; substructure elements are simplified using the Euler-Bernoulli equation. The finite element method is used along the outer boundary.

Table 2 - Characteristics of rock material and subgrade

Parameter	Value
Horizontal voltage ( $\sigma_{xx}^0$ )	30 MPa
Vertical stress ( $\sigma_{yy}^0$ )	15 MPa
Jung's modulus (E)	6000 MPa
Poisson's ratio ( $\nu$ )	0.2
Characteristics of the support	
Young's modulus ( $E_s$ )	20000 MPa
Poisson's ratio ( $\nu_s$ )	0.2
Thickness (h)	0.5 m
Diameter (a)	2.5 m

In order to calculate the tunnel deformations, Vlachopoulos and Diederichs met from over the numerical method of finite elements in plastic zones at total displacements [3]. The layout of the model is given in Figure 4. All calculations are made for the condition when the internal pressures in the tunnel are equal to zero.

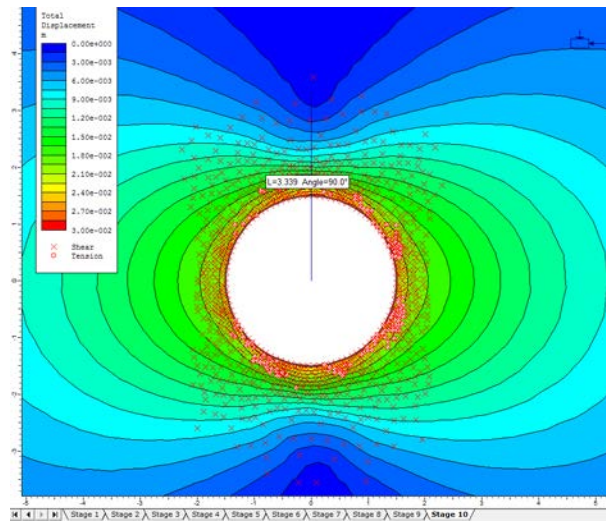


Figure 4 - Total displacements in the tenth phase at maximum media stresses with the distance to the plasticity zone where the displacement is equal to zero.  $R_p = 3,339$  m

After that, the selection of the support and concrete that will satisfy the balance system and the safety factor of 1 is approached; 1.2 and 1.4 for the given condition. The choice of substructure and concrete is given in Figure 5.

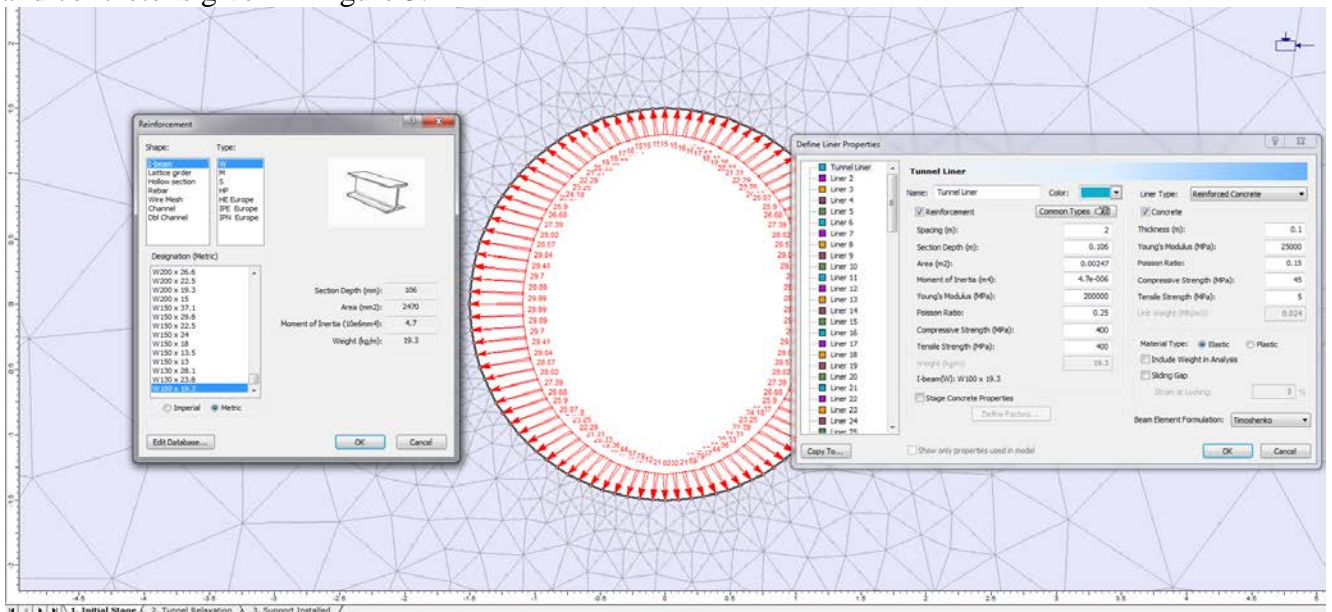


Figure 5 - Selection of standardized profiles as well as concrete with its characteristics.

After selecting the approach, the safety factor is checked, which is shown in Figure 6. In case the support, concrete or both do not meet the safety factors, the selection is made until the desired balance is reached.

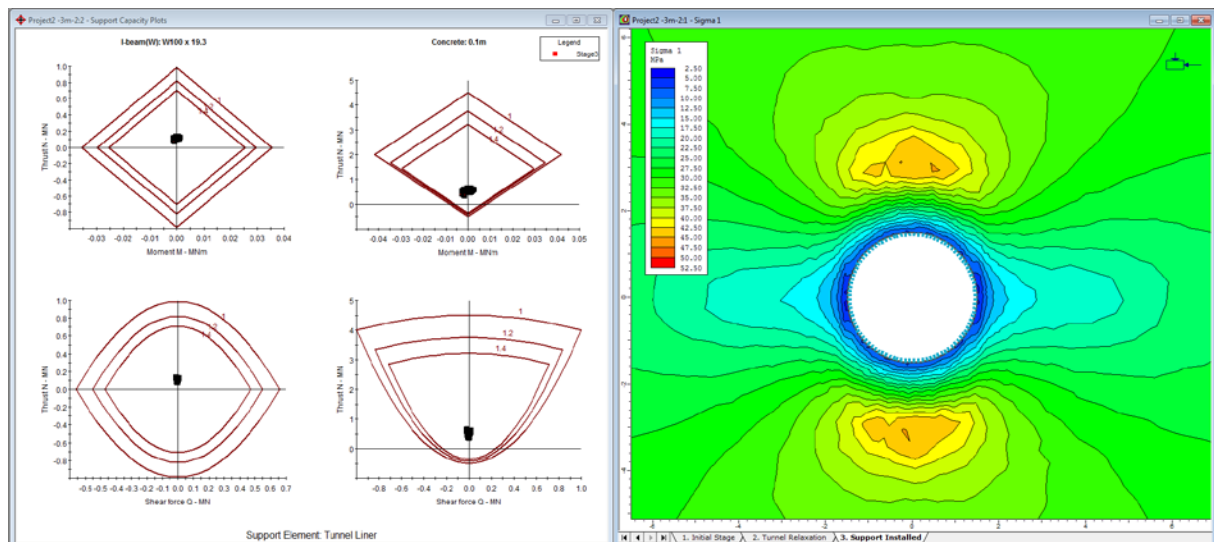


Figure 6 - Showing a good support selection

### 3. CONCLUSION

Based on all the analyses, the theory was confirmed that, if possible, it is most practical to apply a circular cross-section of the room, especially in weaker environments.

In terms of software, the standardized substructure is mainly considered. It is common in practice that for each specific case, the selection of subgrade and concrete recipe is subjected to tests. The substructure is standardized and its selection is considered by the moment of inertia and twisting as well as the force it can resist. When choosing cement, it is necessary to be guided by the conditions to which the subgrade will be exposed, as well as the function intended for it. Thus, when making a concrete lining from sprayed concrete, in solid and stable environments, it is possible to use Portland cement of standard quality. When applying sprayed concrete on the walls of the room immediately behind the front of the work site, and with weak and unstable rocks, it is necessary to use fast-setting cements or normal Portland cement with the addition of a setting accelerator.

### ACKNOWLEDGMENTS

*This study was provided by the Ministry of Education, Science and Technological Development of the Republic of Serbia with No. 451-03-47/2023-1/200052.*

### LITERATURE

- [1] EG Kirsch. (1898) Die Theorie der Elastizitat und die Bedrijfne der Festigkeitslehre. Zentralblatt Verlin Dtsch. Ingenieure, vol. 42, p. 797–807.
- [2] Tutorial from software package Phase<sup>2</sup> ver.8.0, company RocScience, [www.rocscience.com](http://www.rocscience.com).
- [3] Numerical methods in geotechnics", Authors - Lidija Frgić, Antonia Jaguljnjak-Lazarević and Krešimir Tor, Faculty of Mining, Geology and Petroleum, University of Zagreb, 2007. Zagreb.

## INFLUENCE OF THE SUBSOIL BEARING CAPACITY DURING FORMATION OF HIGH LANDSFILLS

**Dragan Ignjatović, Lidija Đurđevac Ignjatović, Vanja Đurđevac,  
Mladen Supić, Dušan Tašić**

Mining and Metallurgy Institute Bor, Zeleni Bulevar 35, 19210 Bor, Serbia

### **Abstract**

*Stability analysis and interaction of the disposed material and the surface of the soil were the main issues of this paper. Analysis was carried out with the help of the programs Slide v6.0 and Phase2 v 8.0. Test results of physical - mechanical and deformation characteristics, such as: density ( $\gamma_z$ ), compressibility module ( $M_s$ ), cohesion ( $c$ ), the angle of internal friction ( $\phi$ ), modulus of elasticity ( $E_t$ ,  $E_s$ ) and Poisson's ratio ( $\nu$ ) were used as input parameters for calculating stability and bearing capacity of the soil (clayey sand, colorfully clay and sand). These tests were carried out in the geomechanical laboratory of Mining and Metallurgy Institute Bor. By analyzing the relationship of different materials (disposed material - soil) it can be concluded that the least settlement of disposed material was when the base soil was marl. All analyzes were carried out on sandy clay and marl.*

**Keywords:** *settlement of material, physical - mechanical and deformation properties, compressibility module, safety factor, Slide v6.0, Phase2 v 8.0*

### **1. INTRODUCTION**

Increasing technical - technological development in the world has led to an increase in the amount of disposed material of different origin and type (municipal waste, industrial waste, flotation tailings, tailings obtained during the process of surface exploitation and the like). The problem with the formation of landfills is that they degrade, pollute and even change the ecosystem and microclimate of the place where they are formed. In order to correct these and similar negative effects, it was necessary to reduce the area of the landfill as much as possible and increase its height. Of course, in order to realize this, it is necessary to know the physical - mechanical and deformation characteristics of both the deposited material and the soil on which the disposal is carried out.

The first experiments in the surface exploitation of mineral raw materials in Yugoslavia for the formation of one-story landfills were carried out in 1975 at the tailings disposal site at the Šumarnica bauxite deposit, Krunići location, Vlasenica bauxite mine [1]. The maximum height of the landfill reached 55 m. The experiment showed and proved that stable, economical and safe single-level landfills can be made, which significantly affect the efficiency and economy of the surface exploitation of mineral raw materials. Until then, single-level landfills did not even exist as a concept in mining, and even less in the practice of surface exploitation of mineral raw materials. In order to prove all the advantages of this type of landfill, experiments were carried out, both in the laboratory and in the field (IN SITU), which were mentioned in the previous text. Thus, over time, the use of one-story landfills in design and construction practice began at all surface mines of Vlasenica bauxite ore. The maximum height of one-story landfills reaches 90 m already in 1980 [1].

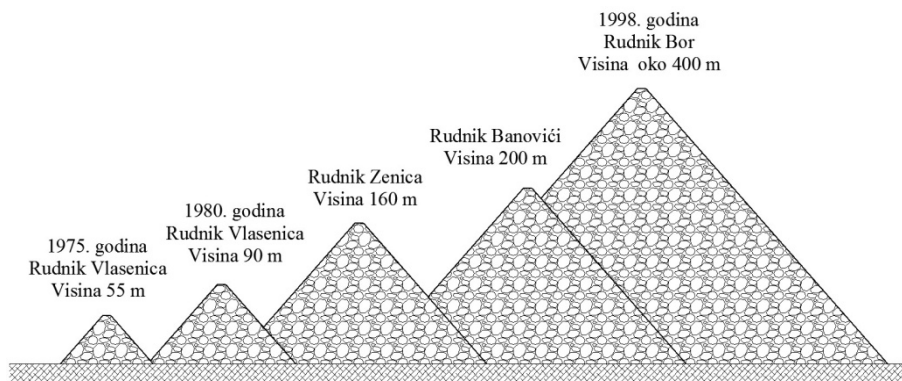


Figure 1 - Layout of the development of single-level open pit disposal sites in Bosnia and Herzegovina and Serbia

## 2. TESTING MATERIALS AND METHODS

### 2.1 Laboratory and in situ tests

Research that needs to be carried out occasion considerations problems single-level ones We were putting off what , in particular in conditions further development superficial \_ \_ operations, are listed in this chapter .

Based on the geomechanical tests, which would be conducted for the disposed material, it is necessary to create a model that would confirm the theoretical facts about the heights and angles characteristic of one-story high landfills.

Laboratory tests must be carried out in order to obtain valid geomechanical characteristics of the material that will be disposed of. The characteristics of the overburden material will be used in the calculation of the height and angle of the one-story landfill, as well as the measures to be taken in the preparation of the substrate on which the overburden will be deposited. [2], [3].

Tests that are necessary in the further analysis of the stability of the " landfill - soil" system are [4]:

- determination of the volumetric mass of the material that is disposed of in a compacted and loose state,
- angle of natural hold (  $\alpha$  ),
- natural moisture of the material,
- Proctor's experiment to determine the changes in the volumetric mass of a material with a change in water content,
- change in material shear strength with change in water content at constant normal stress,
- granulometric composition of the deposited material.

### 2.2 Software packages in landfill slope stability analysis

The analysis of the stability of the slope of the landfill and the mutual relationship between the overburden and the base of the thus formed landfills was done in the **SLIDE v6.0** and **PHASE2 v8.0 programs** of **ROCSCIENCE**. The **SLIDE** program was used to calculate the stability in limit equilibrium conditions according to the Yanbu criterion, because this criterion is the most rigorous in the calculation for this type of terrain and bulk material, and using the critical stress reduction factor (SRF).



### 2.3 Failure criteria for the analyzed materials

When considering the failure criteria for different disposal substrate materials (sandy clay, silty sand and sand), it is observed that for sandy clay and silty sand a non-linear failure criterion is obtained, while for sand the failure criterion is linear (Figure 2). These tests were performed at a humidity of 15%, [1].

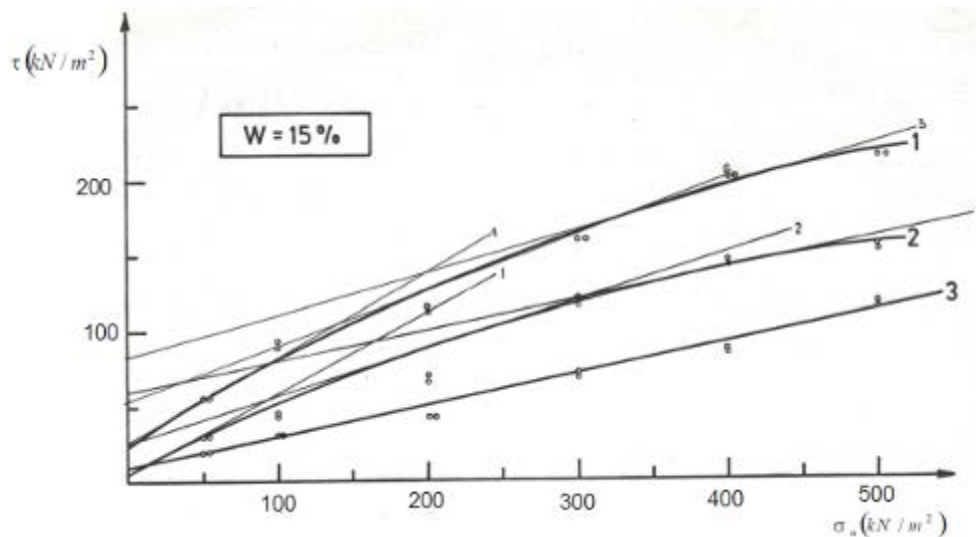


Figure 2 - Failure criterion for sandy clay (1), silty sand (2) and sand (3) at humidity  $w=15\%$

From the failure criteria obtained in this way, it can be expected that the deposited mass, in the case of a one-story landfill, will behave according to the laws of a continuous decrease in the inclination of the slope of the landfill with an increase in height.

Table 1 shows the parameters of the physical-mechanical and deformation properties of the bulk material and the soil material, on which the disposal would take place, [5].

Table 1 - Parameters of physical-mechanical and deformation properties of bulk material and soil material

The name of the material	The color	Volumetric weight (kN/m <sup>3</sup> )	Type of elasticity	Jung's modulus (kPa)	Poisson's ratio	Criterion of failure	Material type	Tensile strength (kPa)	Angle of internal friction (peak) (°)	Cohesion (peak) (kPa)	Pore pressure coefficient $R_u$
Sandy clay		23.00	Isotropic	40000	0.39	Mor-Kolumbov	Plastic	55.00	12.0	55.0	0.2
Marls		17.75	Isotropic	550000	0.38	Mor-Kolumbov	Plastic	189.00	28.0	189.0	0.2
Disposal site		16.00	Isotropic	80000	0.33	Mor-Kolumbov	Plastic	34.00	20.0	34.0	0.2

Figures 3 and 4 show analyzes of stress-deformation states and stability and slope for sandy clays and marls.

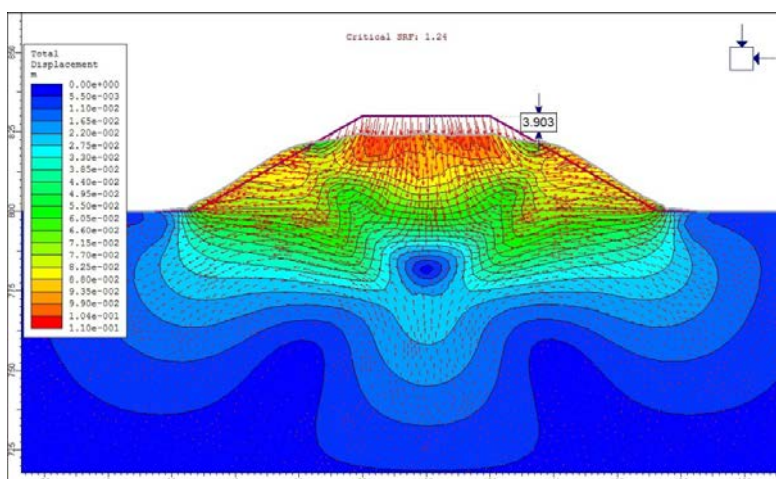


Figure 3 - Total displacements of deposited material on sandy clay soil. Coefficient SFR=1.24 while the total material settlement is 3.903m

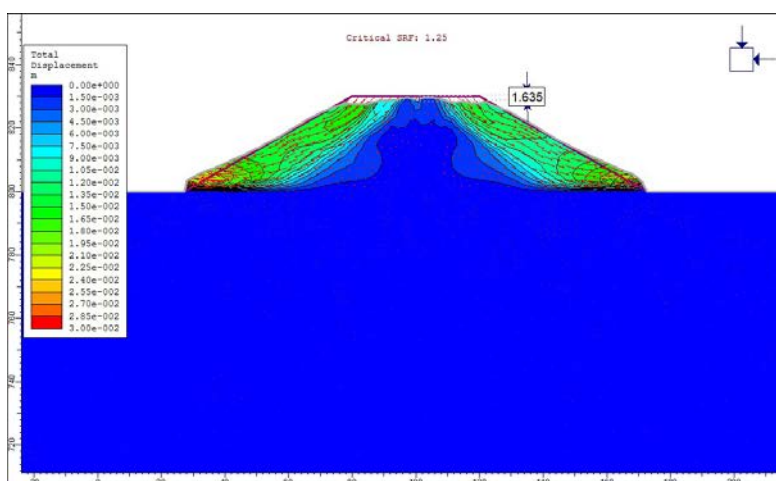


Figure 4 - Total displacements of deposited material on marl soil. The coefficient SFR=1.25, while the total settlement of the material is 1.635m

### 3. CONCLUSIONS

The design and construction of one-story landfills represents a major challenge for mining designers. Laboratory and field tests have shown on which materials is possible to create a one-story high landfill.

The stability of the slope of the deposited material is within the limits prescribed by the Law. The lowest material settlement is on the marl base (1,635m). It can also be concluded that the deposited masses have the least influence on the settlement of the marl soil, which confirms the theory that better geomechanical properties of the soil base ensure better bearing capacity and less settlement of the deposited masses.

### ACKNOWLEDGEMENTS

*This study was provided by the Ministry of Education, Science and Technological Development of the Republic of Serbia with No. 451-03-47/2023-1/200052.*



## REFERENCES

- [1] Enver Mandžić, *High one-story landfills for overburden material during surface exploitation of mineral raw materials*, Gazette of the Faculty of Mining, Geology, and Civil Engineering, ISSN:2303-5145 Vol.2014/2, pp. 05-13, paper by invitation
- [2] *Mining machines, script for students of the mining department*, University of Belgrade, RGF, Belgrade, 2009.
- [3] prof. Dr. Dragan Ignjatović, *Mining machines, script part II*, University of Belgrade, RGF, Belgrade, 2009
- [4] R. Popović, M. Ljubojev, L. Đurđevac Ignjatović, *Deformability parameters for forming a model of the stress-deformation state of the rock massif*, Mining and Metallurgy Engineering Bor, 3/2013
- [5] N. Gojković, R. Obradović, V. Čebašek, *Slope stability of open pit landfills*, University of Belgrade, RGF Belgrade, Belgrade, 2008.

## SOIL AND ROCK PROPERTIES AS A BASIS FOR THE SANITARY LANDFILL SETTINGS

Bojana Živković<sup>1</sup>, Jelisaveta Marjanović<sup>2</sup>, Jelena Đokić<sup>1</sup>, Maja Petrović<sup>3</sup>,

<sup>1</sup>University of Pristina in Kosovska Mitrovica, Faculty of Technical Sciences, Serbia

<sup>2</sup>International Business College Mitrovica-IBCM, Kosovska Mitrovica, Serbia

<sup>3</sup> University of Novi Sad, Faculty of Technical Sciences, Serbia

### Abstract

*Toxic substances from leachate have an accumulatively harmful effect on the environment, so their penetration into the soil must be prevented. The characteristics of the soil define the infiltration of leachate, its retention and availability in the soil, as well as the migration of pollutants. The paper presents the results of physico-chemical analysis and the content of mechanical fractions of the soil sample of the "Savina Stena" sanitary landfill, in order to predict the possibility of the spread of contaminating substances due to the potential leachate of the landfill reaching the environment. The coordinates of the sampling site are 42.963747 and 20.831592 and the surface sample (0-30cm) was analyzed. Physico-chemical analysis showed the values of the following parameters: moisture content 11.03% (m/m); dry matter content 88.97% (m/m); pH value (aqueous solution) 6.90; pH value (1M KCl solution) 5.83; content of organic C 0.88% (m/m); humus content 1.52% (m/m); P<sub>2</sub>O<sub>5</sub> content 0.96 mg/100g and K<sub>2</sub>O content 14.4 mg/100g. Mechanical soil analysis showed that the analyzed soil belongs to clay loam (GI) with a clay content of 30.62%. The texture class of the soil is made according to the American classification - USDA.*

**Keywords:** landfill, physico – chemical analysis, mechanical analysis, soil

### 1. INTRODUCTION (PAPER FORMAT AND MARGINS)

The importance of environmental protection cannot be overstated. It is extremely important to take care of all segments of this complex process, in accordance with legal regulations. The disposal of municipal waste in organized sanitary landfills is an important, clearly defined factor that contributes to the reduction of environmental pollution. The positive effects of this type of waste disposal are achieved only if all standards and regulations are followed, which, among other things, refer to the implementation of numerous soil analyses.

The biggest threat to the environment is leachate from the sanitary landfill. Leachates are highly concentrated complex effluents that contain organic matter, heavy metals, minerals and other hazardous substances, which, when they reach the environment, migrate to great distances [1]. Their harmfulness is assessed on the basis of waste composition, volume, temperature, age of the landfill and soil characteristics [2]. Penetration of leachate into the soil around the landfill leads to its contamination and makes it unsuitable for many purposes [3].

Physico-chemical soil characteristics define soil behavior, such as moisture content that affects the degree of soil compaction [4], while organic C content and humus content affect the reduction of soil compaction and water permeability [5]. The mechanical composition of the soil affects properties such as: water holding power, substitution, general and differential porosity, etc.

## 2. EXPERIMENTAL

### 2.1. Sample Area

The sanitary landfill "Savina Stena" is located on the territory of the municipality of Zvečan, in the village of Srbovac. It has a total area of 26.6 ha while the area allocated for the landfill, along the highway Raška-Kosovska Mitrovica. The landfill was built along the right bank of the Ibar River, at a distance of 300m. It was designed to accept municipal waste for four northern municipalities of Kosovo and Metohija (Zvečan, Leposavić, Kosovska Mitrovica and Zubin Potok), for a period of 20 years.

### 2.2 Soil analysis

The paper presents the results of the physical-chemical and mechanical analysis of the soil of the "Savina Stena" sanitary landfill. For testing, a surface sample (0-30 cm) was taken, at coordinates 42.963747 and 20.831592. The sample was air-dried and then sieved through a 2 mm sieve. From the physico-chemical parameters, the following were examined: moisture content, dry matter content, pH (aqueous solution), pH (1M KCl solution), organic C content, humus content, P<sub>2</sub>O<sub>5</sub> content and K<sub>2</sub>O content..

Moisture content and dry matter content were determined by the gravimetric method, defined by SRPS ISO 11465:2002, the measured value is shown in percent (m/m.) pH value (aqueous solution) and pH value (1M KCl solution) were determined by the experimental method with using a glass electrode and with a volume fraction of 1:5. This method is defined by the SRPS ISO 10390:2022 standard. The content of organic carbon and the content of humus are shown in percentages (m/m) and are determined by the elementary method BU.DM.01, while the content of P<sub>2</sub>O<sub>5</sub> and K<sub>2</sub>O content is expressed in mg/100g and is determined by the methods BU.DM.02 and BU .DM.03.

The mechanical composition of the sampled soil defines the textural classification of the soil based on the USDA classification (US Department of Agriculture). This is the most common type of land classification, developed in 1938 and based on the triangular classification diagram [6]. According to the USDA, the classification is based on the size of the particles in the soil, and the fractions are determined: stone (> 20mm), gravel (2-20mm), coarse sand (0.2-2mm), fine sand (0.05-0.2mm), coarse powder (0.02-0.05mm), fine powder (0.002-0.02mm) and clay (< 0.002mm).

## 3. RESULTS AND DISCUSSION

### 3.1. Physical and chemical analysis of soil

The physical and chemical analysis of the soil of the sanitary landfill "Savina Stena" gave insight into the percentage content of important soil components, as well as the pH value in water and KCl solution (Table 1).

Soil moisture content has a pronounced effect on the degree of soil compaction, shear and strength. It is necessary for the transport and accumulation of dissolved pollutants, and is of exceptional importance. The analysis gave a value of 11.03% (m/m), which is relatively low humidity. The content of dry matter in the sample is 88.97% (m/m).

According to the pH determination method, soil is classified as:

1. pH in H<sub>2</sub>O - extremely acidic (< 4.5), very acidic (4.5 - 5.0), very acidic (5.1 - 5.5), medium (moderately) acidic (5.6 - 6.0), slightly acidic (6.1 - 6.5). ), neutral (6.6 - 7.3), slightly alkaline (7.4 - 7.8), medium (moderately) alkaline (7.9 - 8.4), strongly alkaline (8.5 - 9.0) and very alkaline (> 9.1).

2. pH in KCl - very acidic (< 4.5), acidic (4.51 - 5.5), weakly acidic (5.51 - 6.5), neutral (6.51 - 7.2) and alkaline (> 7.20) [8].

The obtained pH values of the tested sample (depending on the method of determination) show that the soil of the sanitary landfill "Savina Stena" is neutral (6.90) to slightly acidic (5.83).

Table 1 - Physical - chemical analysis of soil of sanitary landfill "Savina Stena"

<b>PHYSICAL - CHEMICAL ANALYSIS OF SOIL</b>			
<b>Tested parameter</b>	<b>Unit of measure</b>	<b>Measured value</b>	<b>Method label</b>
Moisture content	% (m/m)	11.03	SRPS ISO 11465:2002
Dry matter content	% (m/m)	88.97	SRPS ISO 11465:2002
pH value (aqueous solution)	-	6.90	SRPS ISO 10390:2022
pH value (1M KCl solution)	-	5.83	SRPS ISO 10390:2022
Content of organic C	% (m/m)	0.88	BU.DM.01
Humus content	% (m/m)	1.52	BU.DM.01
P <sub>2</sub> O <sub>5</sub> content	mg/100g	0.96	BU.DM.02
K <sub>2</sub> O content	mg/100g	14.4	BU.DM.03

Humus content (%) is expressed through 4 categories: < 1 - very low humus; > 1-2 - weak humus; > 2- 4 – humus and > 4 - very humus [7]. Based on that, the tested soil is low in humus, with a humus content of 1.52% (m/m). As the humus is loose and water permeable, the obtained value is considered positive.

Soil stability, absorption, distribution and retention of water in soil increases with increasing carbon concentration [9]. The content of total organic carbon in the sample is 0.88% (m/m), which classifies the examined soil as suitable for the purpose, that is, it does not significantly contribute to the spread of pollutants.

The values of P<sub>2</sub>O<sub>5</sub> and K<sub>2</sub>O are: < 5.00 (very low); 5.01 – 10.00 (low); 10.01 - 15.00 (middle); 15.01 - 25.00 (optimal); 25.01 – 40.00 (high); 40.01 – 50.00 (very high) and >50.01 (harmful). The result of P<sub>2</sub>O<sub>5</sub> is 0.96mg/100g, that is, K<sub>2</sub>O 14.4mg/100g and they range from very low to medium content, which reduces the ability to absorb and distribute water. [9].

### 3.2. Mechanical analysis of soil

Through mechanical analysis, we define the texture of the soil, on the basis of which it is classified. This type of soil classification is significant because it provides us with information about the characteristics of the examined soil, based on its composition. The composition of the mechanical fractions of the soil of the sanitary landfill "Savina Stena" is shown in Table 2.

Table 2 - Mechanical analysis of the land of the sanitary landfill "Savina Stena"

<b>CONTENTS OF MECHANICAL FRACTIONS</b>							
Big sand	Fine sand	Total sand	Big powder	Fine powder	Total powder	Clay	Hygros-copic moisture
0.2-2mm	0.05-0.2mm	0.05-2mm	0.02-0.05mm	0.002-0.05mm	0.002-0.05mm	<0.002mm	%
<b>23.68</b>	<b>10.14</b>	<b>33.82</b>	<b>21.01</b>	<b>14.55</b>	<b>35.56</b>	<b>30.62</b>	<b>11.03</b>
<b>TEXTURAL SOIL CLASS ACCORDING TO THE AMERICAN USDA CLASSIFICATION: GI</b>							

According to the mechanical composition, the soil of the sanitary landfill "Savina Stena" belongs to clay loam (GI). Clay loam has unfavorable water characteristics, it is very plastic, which initiates weak infiltration and movement of water through it. Thanks to these characteristics, GI will be a natural barrier for contamination of the living environment with leachate, due to its eventual arrival in the environment of the landfill.

#### 4. CONCLUSION

The sanitary landfill "Savina Stena" is located on the right bank of the river Ibar. The proximity of the river dictates a special commitment to environmental protection, with an emphasis on the care of leachate. It is necessary to establish the possibility of the spread of polluting substances into the environment, due to the eventual penetration of leachate.

The paper presents a physical-chemical and mechanical analysis of the soil on which the landfill was built. They were tested for moisture content, dry matter content, pH value (aqueous solution), pH value (1M KCl solution), content of organic C, humus content, P<sub>2</sub>O<sub>5</sub> content and K<sub>2</sub>O content. The soil moisture content is 11.03% (m/m), which indicates a reduced distribution of dissolved pollutants. The dry matter in the sample is 88.97% (m/m), while the pH value ranges from neutral (6.90 with H<sub>2</sub>O) to slightly acidic (5.83 with KCl). The total C content is 0.88% (m/m), which is appropriate for the purpose of the soil, considering that water retention and distribution increase with increasing C concentration. /m), also a favorable characteristic. The values of P<sub>2</sub>O<sub>5</sub> (0.96mg/100g) and K<sub>2</sub>O (14.4mg/100g) are of very low and medium content and reduce the ability to absorb and distribute water.

The mechanical analysis classified the soil as a clay loam (GI), which, based on its characteristics, belongs to a high plasticity soil that infiltrates little water and the movement of water through the soil is minimal.

The conducted analyzes of the soil of the sanitary landfill "Savina Stena" lead to the conclusion that, based on its characteristics, the examined soil will represent additional, natural protection against potential environmental pollution by leachate from the landfill.

#### REFERENCES

- [1] B., Słomczyńska, T., Słomczyński., Pol. J. Environ., 13(6) (2004) 627-637.
- [2] B., S., Badmus, V., C., Ozebo, O., A., Idowu, S., A., Ganiyu, O., T., Olurin., Afr. Rev. Phys., 9 (2014).
- [3] R., N., Uma, R., Prem Sudha., K., Murali., Int. J. Chem. Sci, 14(4) (2016) 3265-3276.
- [4] N., G., Maphuhla, F., B., Lewu, O., O., Oyedeji. IJERPH, 18(1) (2021) 221.
- [5] M., Manojlović, R., Pivić., Uloga zemljišta u kruženju ugljenika i ublažavanju klimatskih promena, Inicijativa za šumarstvo i životnu sredinu – fea, Novi Sad, 2020.
- [6] M., S., Kovačević, D., Jurić-Kaćunić., Građevinar, 66(09) (2014) 801-810.
- [7] D., Jakšić, I., Bradić, V., Perović, M., Beader, M., Ristić, J., Ninkov, M., Živanov., Karakterizacija zemljišta Rasinskog okruga za optimalni izbor loznih podloga vinskih sorti vinove loze, Institut za ratarstvo i povrtarstvo, Novi Sad, (2022).
- [8] M., Belić, L., Nešić, V., Ćirić., Praktikum iz pedologije. Univerzitet u Novom Sadu, Poljoprivredni fakultet, Novi Sad, (2014) 1-90.
- [9] A., Grand, V., Michel., Organska materija zemljišta. (2020).

## ADSORPTION KINETICS FOR COPPER IONS ADSORPTION ONTO ONION PEELS

Milan Gorgievski, Miljan Marković, Nada Štrbac, Vesna Grekulović,  
Kristina Božinović, Milica Zdravković, Marina Marković

University of Belgrade, Technical Faculty in Bor, V.J. 12, 19210 Bor, Serbia

### Abstract

*Kinetic analysis of copper ions adsorption onto onion peels is presented in this paper. The experimental kinetic data were analyzed using two kinetic models, namely the pseudo-first order kinetic model and the pseudo-second order kinetic model. The kinetic parameters were calculated from the linearized plots of the corresponding models. The obtained results indicate that the adsorption of copper ions onto onion peels follows the pseudo second-order kinetic model, with a correlation coefficient of  $R^2 = 0.994$ . This indicates that the chemical interaction between the surface functional groups is the limiting factor of the process rate.*

**Keywords:** adsorption, onion peels, copper ions, kinetic models

### 1. INTRODUCTION

Environmental pollution, which includes water, air, and soil pollution, is a serious environmental problem. Water contaminated with heavy metals is one of the biggest environmental problems today. Water polluted with heavy metals affects flora and fauna, and through the food chain, also affects human health. After reaching the human body, heavy metals can lead to serious health problems and complications [1].

Heavy metals can be removed from wastewater by well-known industry-applied conventional methods, such as chemical precipitation, cementation, ion exchange, solvent extraction, etc. These methods don't always give satisfactory results in terms of insufficient degree of metal ions removal, formation of significant amounts of sludge that needs further processing, the need for excessive amounts of chemicals consumed in the process, and high costs. Due to the tendency of every industrial process to be more economical and efficient, adsorption using natural adsorbents - biosorption is being investigated as one of the alternatives to conventional technologies for wastewater treatment, especially those with low heavy metal ions content [2,3].

Biosorption is a new process, which, at the laboratory level, has proven to be effective in the treatment of aqueous solutions with a certain content of these metal ions [4].

The main advantages of this method compared to conventional technologies are reflected in the efficiency in removing heavy metal ions, as well as in the availability and price of such adsorbents, with very often minimal or without economic value [5].

The analysis of the experimentally obtained data and the determination of the mechanism of the adsorption process, its speed, as well as the step that determines the overall speed of the adsorption process, can be performed using kinetic models of adsorption. Some of the models used to describe the kinetics of the adsorption process and mostly found in the literature are: the pseudo-first order kinetic model and the pseudo-second order kinetic model [6, 7].

### 2. EXPERIMENTAL

The biosorption experiments were performed in batch conditions, on a magnetic stirrer. The change in the adsorption capacity of copper ions with time was determined by bringing into contact 50 mL of a solution with an initial Cu concentration of  $0.2 \text{ g dm}^{-3}$  with 0.5 g of onion peels, for



different process time. Biosorption was terminated after 90 minutes, assuming that this time was long enough to establish equilibrium in the system [3].

### 3. RESULTS AND DISCUSSION

Figure 1 shows the change in the adsorption capacity with time. It can be seen that at the beginning of the process (first 5 minutes), the adsorption capacity increases rapidly with the contact of the phases. The rapid increase in capacity at the beginning of the process is due to the large number of available active sites in the biosorbent structure where copper ions can be incorporated. Further, with process time, a slight increase in the adsorption capacity is observed, due to a decrease of available active sites, as well as a decrease in the concentration of copper ions in the solution.

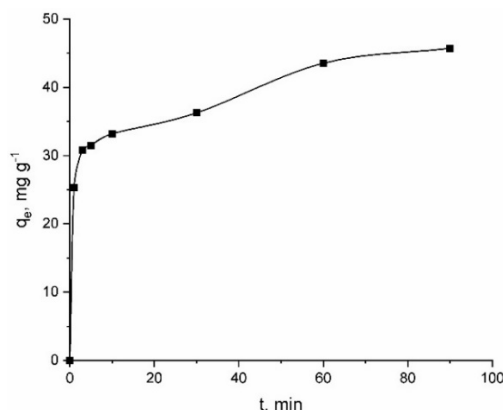


Figure 1 – Change in the adsorption capacity with time

#### 3.1 Pseudo-first order kinetic model

Lagergren showed that the rate of the adsorption of a solute onto an adsorbent is based on the adsorption capacity and follows a pseudo-first-order equation. Lagergren's pseudo-first-order kinetic model can be represented by the following equation [8]:

$$\frac{dq_{(t)}}{dt} = k_1(q_e - q_{(t)}) \quad (3)$$

where:  $q_{(t)}$  – adsorption capacity defined as the mass of adsorbed metal per unit mass of adsorbent for time  $t$  ( $\text{mg g}^{-1}$ ),  $q_e$  – adsorption capacity defined as the mass of adsorbed metal per unit mass of adsorbent at equilibrium ( $\text{mg g}^{-1}$ ),  $k_1$  – adsorption rate constant for the pseudo-first order kinetic model ( $\text{min}^{-1}$ ).

A plot of  $\log(q_e - q_{(t)})$  vs.  $t$  (Figure 2) gives a linear dependence, from which the constant  $k_1$  and the equilibrium adsorption capacity  $q_e$  can be determined from the slope and intercept, respectively. The kinetic parameters are given in Table 1, together with the correlation coefficient for this model.

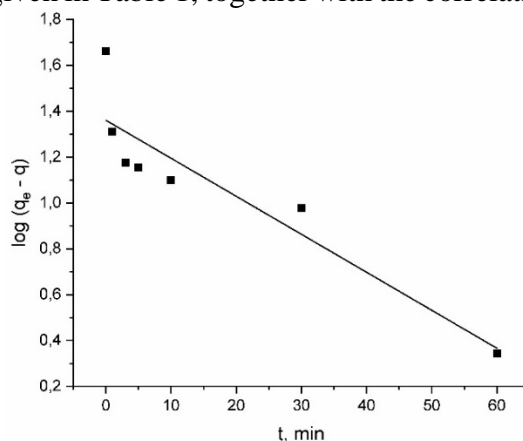


Figure 2 – Pseudo-first order kinetic model for copper ions adsorption onto onion peels

Table 1 – Pseudo-first order kinetic model parameters for copper ions biosorption onto onion peels

Parameter/ion	$k_1$ ( $\text{min}^{-1}$ )	$q_{e,\text{exp}}$ ( $\text{mg g}^{-1}$ )	$q_{e,\text{cal}}$ ( $\text{mg g}^{-1}$ )	$R^2$
$\text{Cu}^{2+}$	0.0382	45.71	22.19	0.845

Based on the value of the correlation coefficient  $R^2 = 0.845$  (Table 1), it can be concluded that the functionality of this model is not satisfactory, which it cannot be used to describe the adsorption process of copper ions on onion peels. Also, the obtained values for the parameters  $q_{e,\text{exp}}$  and  $q_{e,\text{cal}}$  differ significantly.

### 3.2 Pseudo-second order kinetic model

The pseudo-second-order kinetic model is based on the assumption that the adsorbate binds to the surface of the adsorbent by chemisorption [9]. This model can be represented by the following equation:

$$\frac{dq_{(t)}}{dt} = k_2(q_e - q_{(t)})^2 \quad (6)$$

where:  $q_{(t)}$  – adsorption capacity defined as the mass of adsorbed metal per unit mass of adsorbent for time  $t$  ( $\text{mg g}^{-1}$ ),  $q_e$  – adsorption capacity defined as the mass of adsorbed metal per unit mass of adsorbent at equilibrium ( $\text{mg g}^{-1}$ ),  $k_2$  – adsorption rate constant for the pseudo-second order kinetic model ( $\text{min}^{-1}$ ).

The plot  $t/q_{(t)}$  as a function of  $t$  (Figure 3) gives a linear dependence from which the equilibrium adsorption capacity  $q_e$  and constant  $k_2$  can be calculated from the slope and intercept, respectively. The kinetic parameters are given in Table 2, together with the correlation coefficient for this model.

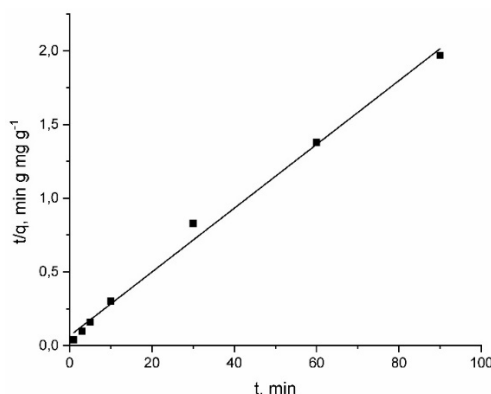


Figure 3 – Pseudo-second order kinetic model for copper ions adsorption onto onion peels

Table 2 – Pseudo-second order kinetic model parameters for copper ions biosorption onto onion peels

Parameter/Ion	$k_2$ ( $\text{min}^{-1}$ )	$q_{e,\text{exp}}$ ( $\text{mg g}^{-1}$ )	$q_{e,\text{cal}}$ ( $\text{mg g}^{-1}$ )	$R^2$
$\text{Cu}^{2+}$	0.007	45.71	46.18	0.994

The correlation coefficient from Table 2 ( $R^2 = 0.994$ ), indicates that the pseudo-second order kinetic model shows an excellent agreement with the analyzed experimental data. This means, that the adsorbate binds to the surface of the adsorbent by the chemisorption. Also, the close values of  $q_{e,\text{exp}}$  and  $q_{e,\text{cal}}$  confirm the good functionality of the proposed model.

## 4. CONCLUSIONS

The kinetic analysis of the adsorption of copper ions onto onion peels is presented in this paper. Two kinetic models, namely the pseudo-first order and the pseudo-second order kinetic model, were used to fit the experimental data. Obtained results show that the pseudo-second order kinetic

model is the best fit for the analyzed data. This leads to the conclusion that chemisorption is a possible way of binding the copper ions to the active sites on the surface of the onion peels.

## ACKNOWLEDGEMENTS

*The research presented in this paper was done with the financial support of the Ministry of Science, Technological Development and Innovation of the Republic of Serbia, within the funding of the scientific research work at the University of Belgrade, Technical Faculty in Bor, according to the contract with registration number 451-03-47/2023-01/ 200131.*

## REFERENCES

- [1] R. B. Garcia-Reyes, J. R. Rangel-Mendez, *Bioresour. Technol.* 101 (2010) 8099-8108.
- [2] F. Veglio, F. Beolchini, *Hydrometallurgy* 44 (1997) 301-316.
- [3] M. Gorgievski, D. Božić, V. Stanković, N. Štrbac, S. Šerbula, *Ecol. Eng.* 58 (2013) 113-122.
- [4] J. Febrianto, A. N. Kosasih, J. Sunarso, Y. Ju, N. Indraswati, S. Ismadji, *J. Hazard. Mater.* 162 (2009) 616- 645.
- [5] N. T. Abdel-Ghani, G. A. El-Chaghaby, *IJLRST* 3 (2014) 24-42.
- [6] U. Farooq, J. A. Kozinski, M. A. Khan, M. Athar, *Bioresour. Technol.* 101 (2010), 5043-5053.
- [7] Y. Liu, Y. J. Liu, *Sep. Purif. Technol.* 61 (2008), 229-242.
- [8] V. C. Taty-Costodes, H. Fauduet, C. Porte, A. Delacroix, *J. Hazard. Mater.* 105 (2003), 121-142.
- [9] M. Z. Momčilović, M. M. Purenović, M. N. Miljković, A. Lj. Bojić, M. S. Ranđelović, *Hem. Ind.* 65(2) (2011), 123-129.

## RECOVERY OF COPPER FROM LOW-GRADE COPPER ORE USING ORGANIC ACID

Saba Noroozi, Fatemeh Poursagharian Roudsari<sup>2</sup>, Ahmad Khodadadi Darban<sup>1</sup>

<sup>1</sup>Department of Mining and Environmental Engineering, Faculty of Engineering, Tarbiat Modares University, Tehran, Iran

<sup>2</sup>Department of Mineral Processing, Faculty of Engineering, Tarbiat Modares University, Tehran, Iran

### Abstract

This study aimed to investigate the effectiveness of organic acids, specifically citric acid and acetic acid, in extracting copper from low-grade copper ore. The experimental procedure involved leaching copper-containing samples with varying concentrations of the organic acids. Compared to acetic acid, citric acid had a better performance in copper oxide recovery. Also, the results of the experiments showed that the concentration of 1 M citric acid had the highest recovery. The recovery of copper and copper oxide using citric acid at a concentration of 1 M was 77.8% and 88.7% respectively.

**Keywords:** (Organic acid; copper; leaching)

### 1. INTRODUCTION

Copper is one of the non-ferrous metals and is naturally found in oxide and sulfide minerals. Copper is widely used in various industries. The increase in demand for copper has led to the consideration of low-grade oxide ores, as well as the common high-grade ores as commercial source of copper. On the other hand, there is an incentive to develop metal extraction processes with reduced environmental impact. Thus, in recent years, the researchers have focused on replacing the conventional copper extraction methods with environmentally friendly hydrometallurgical processes [1-4].

The commonly used leaching reagents are strong inorganic acids such as sulfuric acid, nitric acid, and hydrochloric acid. However, employing these acids can cause the release of toxic gases like Cl, SO, and NO<sub>x</sub> during the extraction process. Moreover, the remaining acid in the process tailings is a threat to the environment. Therefore, replacing the common hazardous leaching reagents with relatively safer ones sounds rational. For this purpose, utilizing organic acids as the extraction solvent is suggested since they are fully water-soluble and the tailing is easier to be processed [5-8].

The most studied organic acids in ore leaching are citric acid, acetic acid, lactic acid, formic acid, and succinic acid. All of these organic acids only partially dissociated in aqueous solutions. The weak acid behavior as well as unknown side reactions with ores are the main challenges for industrial application of organic acid in ore leaching [9-12]. Therefore, understanding the interaction of organic acids and different types of ores is required to achieve acceptable extraction yields.

This study aims to investigate copper extraction from a low-grade oxide ore using different concentrations of two organic acids including citric acid and acetic acid in order to obtain a better understanding of organic acids utilization for developing an environmentally friendly leaching process.

## 2. EXPERIMENTAL

The ore sample was milled smaller than 75 microns. Leaching procedure was carried out within 240 minutes, stirring speed of 500 rpm, solid weight percentage of 10% and temperature of 25 °C. Extraction tests were conducted using 0.5, 1, 1.5, 2 M solutions of either citric acid or acetic acid. At the end of each experiment the content of the container was filtered and the obtained cake was dried. The amount of total copper ions, CuO, and CuS in the solid feed and the dried cake were measured by atomic absorption spectrometry (AAS) and the recovery of each component was calculated.

## 3. RESULTS AND DISCUSSION

### 3.1 Copper extraction with citric acid

The results obtained for copper leaching using different concentrations of citric acid and acetic acid are reported in Table 1. Considering the results, recoveries of total copper (RCu), copper from the oxide (RCuO) and sulfide (RCuS) portions of the ore were calculated. The recoveries obtained in citric acid leaching are illustrated in Figure 1.

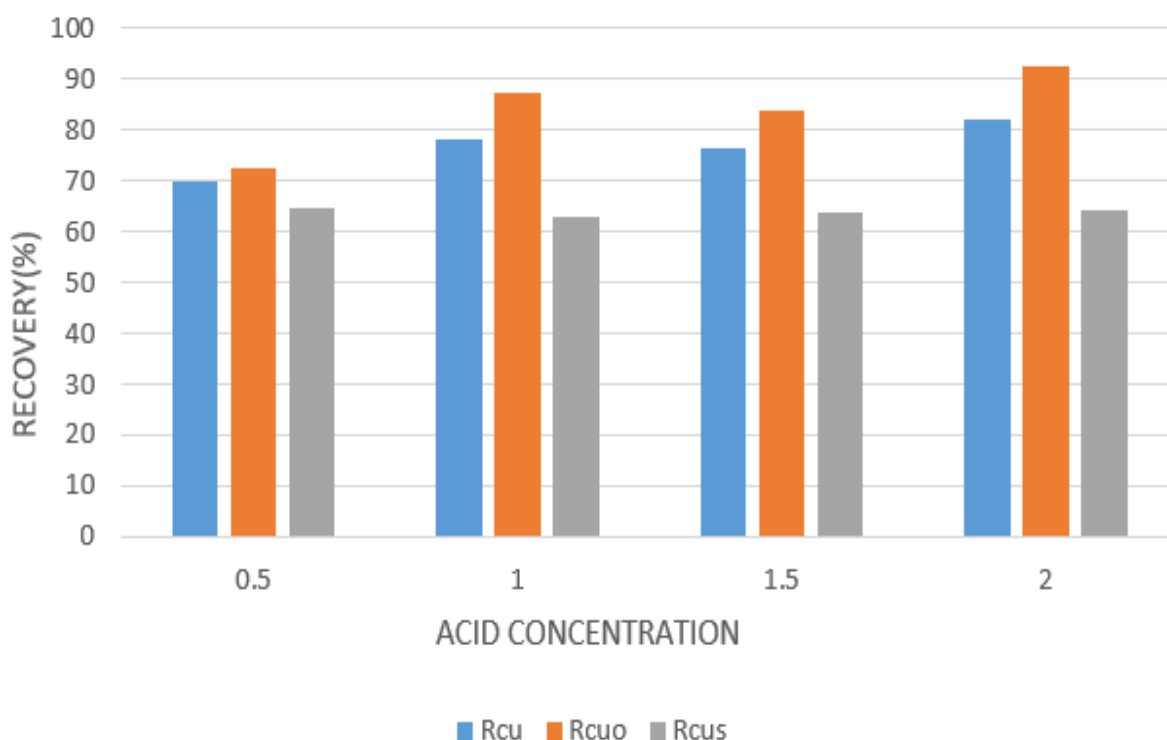


Figure 1 – Effect of citric acid concentration on the recovery of copper, CuO, and CuS

### 3.2 Copper extraction with acetic acid

According to the results of Cu, CuO, and CuS content in the tailings of acetic acid leaching process, the respective recoveries of total copper (RCu), copper from the oxide (RCuO) and sulfide (RCuS) portions of the ore were calculated. The recoveries are depicted in Figure 2. Increasing acetic acid concentration resulted in decreasing copper sulfide recovery.

In comparison with citric acid, acetic acid was less successful in leaching copper.

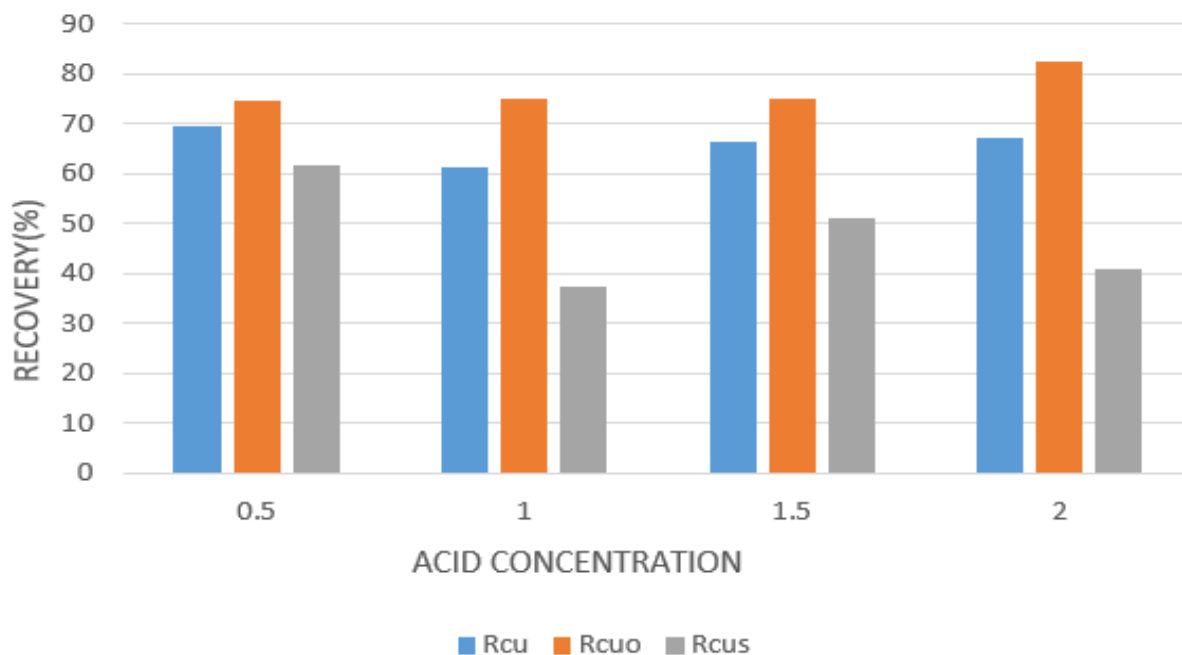


Figure 2 - The recoveries of total copper (RCu), copper from the oxide (RCuO) and sulfide (RCuS) portions of the ore

#### 4. CONCLUSION

Considering copper recovery values, it can be concluded that citric acid had a better performance. There is approximately 20% difference between citric acid and acetic acid recoveries.

Investigation and comparison of copper recovery in different concentrations of citric acid showed that 1 M concentration had the highest recovery. Despite increasing the acid concentration, there is no increase in recovery. This issue can be attributed to the inability of organic acid ions to compete with activated copper ions in the solution, which happens by increasing copper ions and covering mineral surfaces.

#### REFERENCES

- [1] Habbache N, Alane N, Djerad S, et al. *Chem Eng J.* 2009;152(2–3):503–508.
- [2] Yaras, Ali, Hasan Arslanoglu. *Canadian Metallurgical Quarterly* 57.3 (2018): 319-327.
- [3] Amiliana, R. A., et al., *IOP Conference Series: Materials Science and Engineering*. Vol. 333. No. 1. 2018. IOP Publishing.
- [4] Arzutug, M. Emin, M. Muhtar Kocakerim., *Industrial & engineering chemistry research* 43.15 (2004): 4118-4123.
- [5] M. Gharabaghi, M. Irannajad, M. Noaparast., *Hydrometallurgy* 103.1-4 (2010): 96-107.
- [6] V. Forti, et al. *The Global E-Waste Monitor 2020. Quantities, Flows, and the Circular Economy Potential* (2020), pp. 1-119.
- [7] D. Das, S. Mukherjee, M.G. Chaudhuri, *Studies on leaching characteristics of electronic waste for metal recovery using inorganic and organic acids and base Waste Manag. Res.*, 39 (2) (2021), pp. 242-249.

- [8] L. Li, et al. Recovery of cobalt and lithium from spent lithium ion batteries using organic citric acid as leachant *J. Hazard Mater.*, 176 (1–3) (2010), pp. 288-293, 10.1016/j.jhazmat.2009.11.026
- [9] U. Jadhav, et al. Acetic acid mediated leaching of metals from lead-free solders *Biores. Bioprocess.*, 4 (1) (2017), pp. 1-10, 10.1186/s40643-017-0173-5
- [10] N. Adhapure, et al. Use of large pieces of printed circuit boards for bioleaching to avoid 'precipitate contamination problem 'and to simplify overall metal recovery *Methods X*, 1 (2014), pp. 181-186.
- [11] J.W. Moffett, R.G. Zika, Reaction kinetics of hydrogen peroxide with copper and iron in seawater *Environ. Sci. Technol.*, 21 (8) (1987), pp. 804-810.
- [12] S. Wasay, S. Barrington, S. Tokunaga, Organic acids for the in situ remediation of soils polluted by heavy metals: soil flushing in columns *Water Air Soil Pollut.*, 127 (1) (2001), pp. 301-314.



## METODOLOGY AND EQUIPMENT FOR RESEARCHUNG CORROSION CRACKING PROCESSES IN STEEL 3H14L (BDS 3692-78)

**Maria Krasteva**

University of Chemical Technology and Metallurgy, Sofia, Bulgaria, St. "Kl. Ohridski" №8

### Abstract

*Stress corrosion is the least studied and systematized in terms of literature data on the impact of various aggressive environment (type, temperature and concentration), composition and structure of the material, mode of heat treatment, method of obtaining and cleaning the casting, methodology for determination of corrosion under stress, as well as equipment for carrying out similar studies. There are two kind of stress corrosion. One of them is under mechanical stress – the so called „corrosion cracking”. Corrosion cracking is the destruction of metal under static stresses and an aggressive environment. Corrosion fatigue is destruction of the metals and the alloys under the impact of cyclic mechanical pressure and aggressive environment simultaneously. The purpose of this paper is to present the methodology and equipment developed for corrosion cracking testing of cast alloys.*

**Keywords:** stress corrosion, corrosion cracking, U- figurativeness test specimen, casting alloys

### 1. INTRODUCTION

In corrosion cracking, parts and structures fail as a result of the surface cracking initiation and the subsequent growth of cracks into the material, which causes their instantaneous failure, which in turn determines the durability of metals and metal structures. [1]. The potential of metals, and in particular steels, to corrosion cracking depends significantly on the composition of the environment (medium) in which the work pieces and structures are operated. As temperature and the electrolyte concentration increase, the aggressiveness usually increases as well [2]. There are no uniform theories and methodologies in literature for determining stress corrosion, in particular stress corrosion cracking of metals and alloys.

When selecting the test specimen, the main considerations should be aimed at ensuring the convenience of the experiments and the accuracy and reproducibility of the results. From this point of view, the use of a U-shaped test specimen is the most appropriate.

The load is created by pure bending. The area of the highest stress is focused at the top of the specimen, which can be immersed in the aggressive medium during the experiments. In this particular case, a U-shaped [3, 4] specimen with a circular cross-section with a diameter of  $d=7.3\text{mm}$ , a 11.5mm radius of roundness at the tip and an arm of 38.5mm was chosen. This choice was made based on the capabilities of the available equipment (LRu-1 type strength testing apparatus).

The aim of the present task is to investigate the resistance to stress corrosion cracking under static loading of cast steels, in particular 3X14L, BDS 3692-78 in different structural states, using the methodology and equipment for laboratory stress corrosion resistance testing already developed by the author.



Photograph 1  
Test specimen

### 2. EXPERIMENTAL

**Experimental methodology.** In order to develop the required stress in the test specimens when testing their stress corrosion resistance, the relationship between the deformation and the stress inducing it must be known. This relationship must be determined experimentally. The

aggressive environment and the temperature conditions for the test are determined on a case-by-case basis, mainly depending on the type of metal (alloy), but also taking into account the specific task - service conditions of workpieces and alloy products or of experimental interest.

**Method of work.** The most suitable method for obtaining castings of the dimensions and configuration characteristic of the selected test specimen is fusion casting [6]. In order to obtain a casting of the specified dimensions and configuration, several preparatory steps must be carried out to obtain the test specimen.

**Design and manufacture of the mould.** For the implementation of the method, it is necessary to construct and manufacture the corresponding tooling - the mould for the wax patterns of the castings and for the casting system. The preparation of the master pattern and the final shaping of its workspace by casting with K-154 composition was carried out in the metal casting laboratory of the University of Chemical Technology and Metallurgy.



Photograph 2 Mould



Photograph 3 Open mould

**Fabrication of the casting mould and casting system.** The specific dimensions of the casting system, or the mould board, are tailored to the characteristics of the melting unit to be used (laboratory induction furnace) and the way the mould is poured (directly from the furnace) - diameter 25mm and height of the active part 120mm; the capacity of this casting system is 12 castings. The casting system pattern is made of aluminium alloy. The required wax layer on its surface is applied by repeated dipping in molten pattern composition [7, 8, 9]. The casting mould is made using a moulding compound. The mould is constructed from five process layers, using silica sand fraction 010 to fix the first layer and 040 for the remaining four layers.

The moulds were fired at the UCTM in a laboratory chamber furnace at 800°C in a support backfill of silica sand.

**Manufacturing test specimens.** The moulds for the casting of the test specimens were manufactured at the plant of Buser-96 OOD. When making the mould board, the casting patterns are mounted on the pattern casting system by brazing.

Removal of the patterns from the finished mould was done by melting in a water bath.

**Blending and melting the alloy, pouring the mould.** The experiments were designed to use corrosion-resistant, chromium steel grade 3X14L according to BDS 3692-78. As blending materials, 3X14L steel gates (sprues), low-carbon ferrochrome for composition adjustment and for annealing - FeSi75 and aluminium were used. Melting was carried out in a crucible high frequency induction laboratory furnace with a crucible capacity of 3kg. The casting temperature was 1570°C, and was controlled with a Pt-Rh 30/6 thermocouple and RT 384 programmable logic controller. Pouring was done directly from the furnace.



Photograph 4  
Casting mould



Photograph 5  
Wax patterns

**Displacement/stress relation.** The relation between absolute deformation of the test specimens and the stress inducing it was determined experimentally using a mechanical testing

apparatus type LRu-1. Suitable end-pieces have been designed and fabricated to clamp the test specimen to the loading unit of the apparatus. The absolute and residual strain of the specimen were read using an indicating micrometre with an accuracy of 0.01 mm. The results of this determination are available in previous work by the author [10, 12].

**Stress selection.** To perform the control test, as recommended, a stress exceeding the yield point was used, with the specific condition being that the residual strain should be around 5% - i.e. some plastic deformation is realised in the specimens. Using the results of the study of the  $\sigma=\sigma(\epsilon)$  relationship, it was determined that the set condition is satisfied by a stress of 530 MPa (54 kgf mm<sup>-2</sup>) occurring at an absolute specimen strain of 1 mm, where the residual strain is within 0.05 mm [3]. This stress was created in the specimens during the tests [12].

**Selection of aggressive medium.** Due to the lack of systematic data for 12-14% chromium, corrosion-resistant steels and in particular for 3X14L, the choice of aggressive medium was made based on literature data according to which corrosion resistant steel 1X18H9L under a load of about 50kg/mm<sup>2</sup> in boiling 45% MgCl<sub>2</sub> solution (110°-125° C) fails in about 8 hours [3, 11], for the present control study the same conditions were adopted [12].



Photograph 6  
Loaded test specimens

### 3. RESULTS AND DISCUSSION

The failure stress of the sample specimens of each group was determined at intervals through 1 hour (1÷6). The results of the test are shown graphically in Figures 1 and 2, and in Tables 1 and 2.

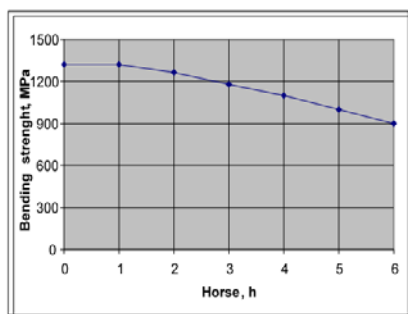


Figure 1 - Dependence of failure stress on time of treatment in the aggressive solution – 1 series test specimens

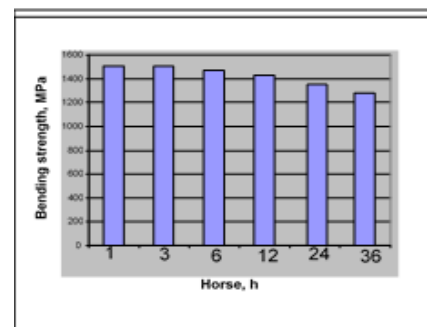


Figure 2 - Dependence of failure stress on time of treatment in the aggressive solution – 2 series test specimens

Table 1 - Failure stress of the samples of the 1 series in the test of their corrosion-mechanical resistance

Hours, h		1	2	3	4	5	6
Destructive load	kgf	133.22	118.79	117.05	111.37	101.14	92.05
	N	1306.89	1165.33	1148.26	1092.54	992.18	903.01
Failure stress	kgf/mm <sup>2</sup>	134.56	119.98	118.22	112.48	102.15	92.07
	MPa	1320.03	1177.00	1159.74	1103.43	1002.09	903.21

Table 2 - Failure stress of the samples of the 2 series in the test of their corrosion-mechanical resistance

Hours, h		0	3	6	12	24	36
Destructive load	kgf	152.34	152.27	148.15	144.11	136.51	128.88
	N	1494.44	1493.27	1413.98	1413.98	1339.12	1264.3
Failure stress	kgf/mm <sup>2</sup>	153.86	153.79	149.63	145.55	137.88	1130.17
	MPa	1509.40	1508.71	1467.88	1427.86	1352.55	1276.95

#### 4. CONCLUSION

The conclusions that can be drawn from the methodology thus established and from the study of the corrosion cracking of cast, high alloy chromium steel 3H14L (BDS 3692-78):

1. A methodology for testing the corrosion-mechanical performance of cast steels has been developed. For this purpose: a sample body with the required configuration and dimensions has been selected; - the necessary equipment for the casting of test bodies by the method of fusible models has been constructed and manufactured and the necessary additional accessories to the LRu-1 mechanical test apparatus were constructed and constructed – test body grip tips, a deformation recorder and an effort stepping system.

2. The methodology can be used to determine the corrosion-mechanical resistance of other alloys, according to the possibility of making castings according to the classic precision casting wheel.

3. A control study was carried out according to the methodology, which includes: production of wax models and casting molds for test bodies; casting of 3X14L steel test bodies; testing of the corrosion-mechanical resistance of the steel at two states on the surface of the sample bodies – in the state after casting and after surface naklep.

The positive influence of the surface naklep (surface cleaning) on the corrosion mechanical characteristics of 3X14L steel was found, resulting in the extension of the incubation period of the crack and the process of its development.

#### REFERENCES

- [1] Ml. Georgiev, Crack resistance of metals under static load, Bulvest, Sofia, 2000.
- [2] R. Dimitrova, B. Tabakova, Features of welding of corrosion-resistant clad steels used in the power industry, XIV Science Conference, Sozopol, 2009
- [3] V. Gerasimov, V. Gerasimova, Stress cracking of austenitic stainless steels, Metallurgy, Moscow, 1976.
- [4] R. Bakes, Corrosion, USA, 1970.
- [5] N. Parkins, R. Mants, G. Roils, K. Skali, Protection of Metals, Metallurgy, Moscow 1973.
- [6] <http://www.castingarea.com> > education > methods-1.
- [7] N. Stoqnov, Foundry technology, Tehnica, Sofia, 1987
- [8] Technological development for making fusible models, Buser AD, Sofia, 2000.
- [9] Technological methodology for making ceramic forms, Buser AD, Sofia, 2000.
- [10] C. A. Loto, Int. J. Adv. Manuf. Technol., 93 (9–12) (2017), 3567–3582.
- [11] H. Kohl, Werkstoffe und Korrosion, 1968.
- [12] Petkov R., M.Krasteva, A.Karadjova Investigation of corrosion-mechanical stability of castings of steel 3X14H2. Journal of Foundry bulletin, 4 (2006) 3-6.
- [13] F. Himushin, Stainless steel, Metallurgy, Moscow, 1967.

## TESTING THE BOND WORK INDEX ON LIMESTONE FROM FLUE GAS DESULPHURIZATION PLANT IN TPP UGLJEVIK

Jasmina Nešković<sup>1</sup>, Pavle Stjepanović<sup>1</sup>, Nenad Milojković<sup>1</sup>, Dejan Lazić<sup>1</sup>,  
Klara Konc Janković<sup>1</sup>, Svetlana Polavder<sup>1</sup>, Ivana Jovanović<sup>2</sup>

<sup>1</sup>Mining institute Ltd. Belgrade, Batajnički put 2, 11080 Belgrade, Serbia

<sup>2</sup>Mining and Metallurgy Institute Bor, Zeleni Bulevar 35, 19210 Bor, Serbia

### Abstract

*In order to reduce the emission of sulfur dioxide from the flue gases of thermal power plants, a desulphurization plant was introduced. The desulphurization technology is based on a wet process using limestone in the form of a suspension. Limestone as a raw material in this process needs to satisfy requirements, and the value of Bond's work index as an indicator of electricity consumption is particularly important. In this paper, the Bond work index was determined on two different samples of limestone used in the thermal power plant Ugljevik. The results obtained correspond to literature data for this type of raw material.*

**Keywords:** limestone, bond work index, desulfurization, thermal power plants

### 1. INTRODUCTION

Wet flue gas desulphurization processes at thermal power plants require preparing a limestone suspension of specific characteristics related to chemical composition, reactivity, and granulation. The required limestone size is achieved by crushing and grinding.

Ore crushing is an ongoing economic task for science and industry. In mining, ore crushing to the projected size requires the most energy, significantly more than in all other preparation and concentration processes. From this aspect, it is critical to predict energy consumption in industrial processes in a limited energy source world. The energy required for crushing and grinding is represented by the Bond work index and is determined using the Bond grindability test in the Bond ball mill. Its value is an ore property and is used in industrial crushing plant design.

The Bond work index  $W_i$  is determined by simulating a dry grinding locked cycle until achieving 250% circulating load in a special laboratory Bond ball mill. Determining the Bond work index is a complex procedure that requires a special Bond ball mill, about 10 kg sample sized  $-3.326 + 0$  mm, trained staff, and 7-10 grinding cycles to balance the process. [1,2,3,4].

### 2. EXPERIMENTAL (MATERIALS AND METHODS)

Limestone samples used in the desulphurization processes at TE Ugljevik were examined in this research. The test involved total moisture, determining the particle size distribution and then determining the Bond work index.

The moisture content was tested on the starting samples prior to their characterization, by drying in a dryer at 105°C to the constant mass. [5]

Particle size distribution was determined by the sieving method on standard laboratory sieves. Sieving was manual, on Laboratory Test Sieve Endecotts LTD London England and DIN series sieves. [6,7]

Determination of the Bond work index was performed in a standardized Bond ball mill using the empirical method. [8].

### 3. RESULTS AND DISCUSSION

Since the delivered samples from TPP Ugljevik were wet, it was necessary to dry them to constant mass. It was determined that the mean value of total moisture content in the samples from samples TPP Ugljevik is 0,3%. The samples were then homogenized to make a composite sample for further testing. Next, the composite sample was crushed to 100% - 3.35 + 0 mm, which represents the input for the Bond work index determining experiment. After crushed, the sample was homogenized, and the final sample was separated chess field method.

The particle size distribution of crushed composite limestone sample used for desulphurization in TPP Ugljevik (sample 1), with a volume of 700 cm<sup>3</sup>, is shown in Figure 1.

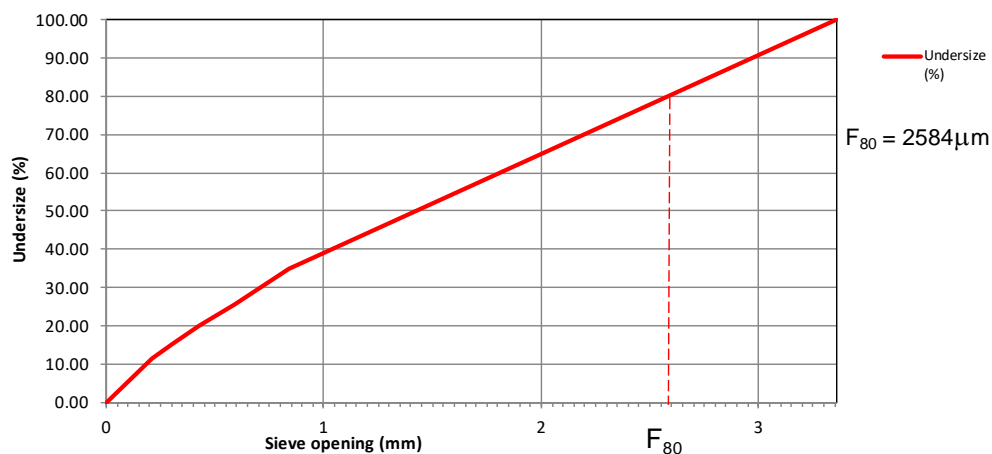


Figure 1 - Particle size distribution of crushed composite limestone sample used for desulphurization in TPP Ugljevik (sample 1)

From Figure 1 the read F<sub>80</sub> parameter is 2584μm. A total of nine grinding cycles were performed on the sample, which are shown in Table 1.

Table 1 - The Bond work index test results

Grinding cycles	ai	bi	bi - ai	Xi	Gbp
<b>I</b>	131.8	308.0	176.2	100	1.76
<b>II</b>	38.0	300.4	262.4	167	1.57
<b>III</b>	43.0	332.2	289.2	184	1.57
<b>IV</b>	38.0	353.6	315.6	187	1.68
<b>V</b>	41.2	341.2	300.0	173	1.73
<b>VI</b>	40.4	352.6	312.2	179	1.74
<b>VII</b>	40.7	336.4	295.7	167	1.77
<b>VIII</b>	40.0	334.3	294.3	165	1.78
<b>IX</b>	39.0	334.1	295.1	165	1.78

Where:

- ai: undersize product -0.212 + 0 mm in fresh feed
- bi: undersize product -0.212 + 0 mm after mill cycle
- bi – ai: particle size -0.212 + 0 mm growth in mill cycle



Xi: number of mill rotations in cycle

Gbp: Grindability index  $Gbp = (bi-ai)/Xi$

The mean Gbp index of VII, VIII, and IX grinding cycles is 1.78. The mean  $P_{80}$  parameter of VII, VIII, and IX grinding cycles was determined from the particle size distribution chart shown in Figure 2.

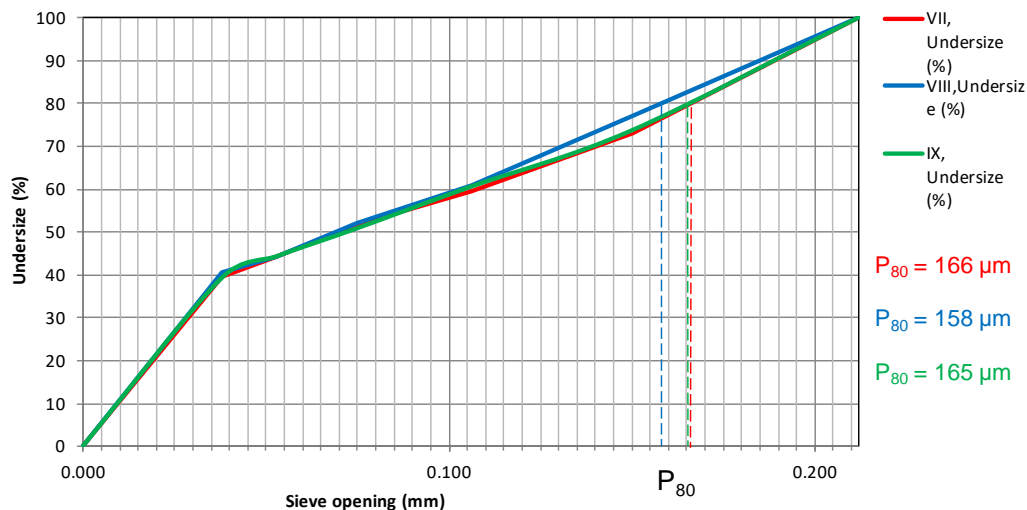


Figure 2 - Particle size distribution of ground material from VII, VIII, and IX grinding cycles

The  $P_{80}$  parameter value is 162.87 μm. The Bond work index on this sample is:

$$W_i = 13.81 \text{ kWh/st}$$

$$W_i = 1.102536 \times 13.81 = 15.22 \text{ kWh/t}$$

The particle size distribution of crushed composite limestone sample used for desulphurization in TPP Ugljevik (sample 2), with 700 cm<sup>3</sup> volume, is shown in Figure 3.

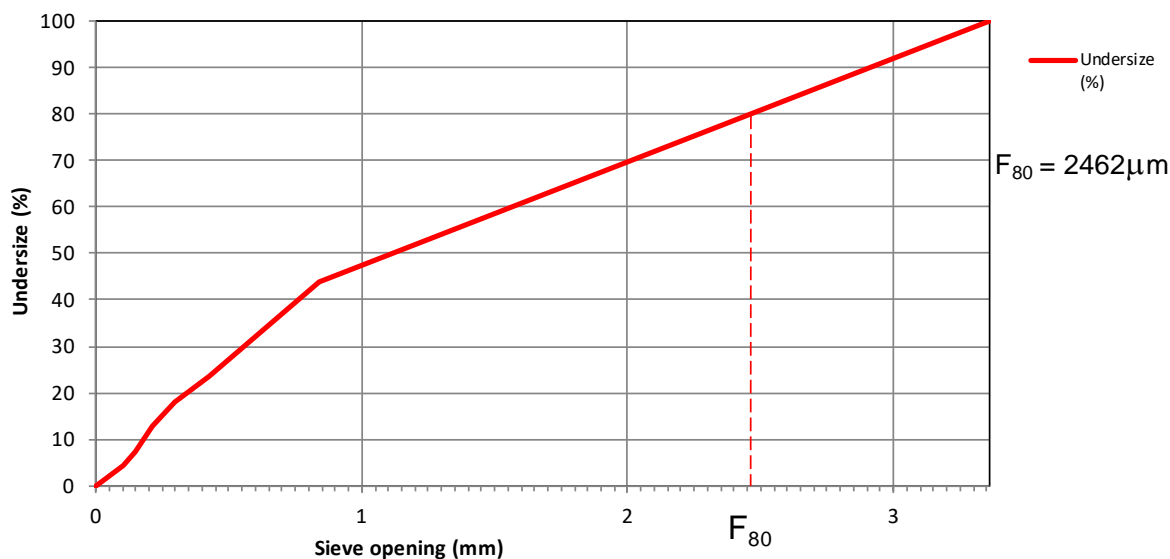


Figure 3 - Particle size distribution of crushed composite limestone sample used for desulphurization in TPP Ugljevik (sample 2)

From Figure 3 the read  $F_{80}$  parameter is 2462 μm. A total of ten grinding cycles were performed on the sample, which are shown in Table 2.



Table 2 - The Bond work index test results

Grinding cycles	ai	bi	bi - ai	Xi	Gbp
I	147.0	329.4	182.4	100	1.82
II	47.3	304.7	257.4	154	1.67
III	45.2	337.7	292.5	169	1.73
IV	46.2	346.4	300.2	162	1.85
V	51.9	335.1	283.2	149	1.90
VI	48.6	324.9	276.3	147	1.87
VII	46.5	340.6	294.1	149	1.97
VIII	58.5	325.0	266.5	136	1.95
IX	53.4	324.7	271.3	140	1.93
X	46.6	327.5	280.9	145	1.93

The mean P<sub>80</sub> parameter of VIII, IX, and X grinding cycles was determined from the particle size distribution chart shown in Figure 4. The P<sub>80</sub> parameter value is 172.3 μm.

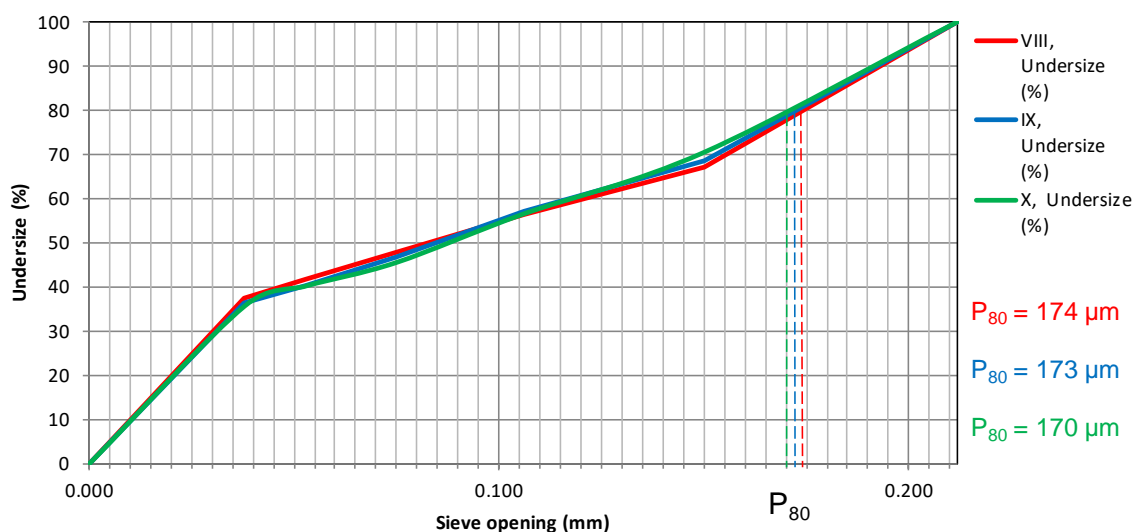


Figure 4 - Particle size distribution of ground material from VIII, IX, and X grinding cycles

The Bond work index on this sample is:

$$W_i = 13.47 \text{ kWh/st}$$

$$W_i = 1.102536 \times 13.47 = 14.86 \text{ kWh/t}$$

#### 4. CONCLUSION

The test of Bond's work index was performed on samples of limestone used in the desulphurization process of TE Ugljevik. The obtained values of Bond's work index are 13.47 kWh/t and 13.81 kWh/t, which is average to the literature data for this type of mineral raw material. The values shown refer only to the supplied samples and can serve as an indication that the hardness of the mineral raw material can only be an indicative indicator of electricity consumption.

## REFERENCES

- [1] A. McIntyre, L. R. Plitt., The interrelationship between Bond and Hardgrove grindabilities, CIM Bulletin., 73: 818 (1980) 149–155.
- [2] D. Ivanković, M. Čeh., Dry grinding of non-metallic mineral raw materials, 4 (1965) 49-62.
- [3] D. Todorović., Inhomogeneous composite material grindability study and shortened procedure testing for the determination of Bond work index - doctoral dissertation, University of Belgrade, 2016, p.122. (In Serbian)
- [4] N. Magdalinović., A contribution to a more accurate calculation of electricity consumption in a ball mill, Bulletin of Mines, 2 (27) (1988) 28-30. (In Serbian)
- [5] R. Tomanec., Methods of testing mineral resources in the preparation of mineral resources, Faculty of Mining and Geology, Belgrade, 2000, p.315. (In Serbian)
- [6] N. Čalić., Theoretical foundations of mineral preparation, Faculty of Mining and Geology, University of Belgrade, 1990, p.496. (In Serbian)
- [7] Standards: SRPS B.B1.018/2005.
- [8] N. Magdalinović., Meljivost mineralnih sirovina, monografija, Nauka, Beograd, 1997, p.103.

## IMPACT OF TITANIUM ADDITION ON MICROSTRUCTURE AND PROPERTIES OF AS-CAST Al-Cu15 ALLOYS

Biljana Zlatičanin<sup>1</sup>, Sandra Kovačević<sup>2</sup>

<sup>1</sup>Faculty of Metallurgy and Technology, 81000 Podgorica, Montenegro

<sup>2</sup>Central School of Chemical Technology Spasoje Raspopović, 81000 Podgorica, Montenegro

### Abstract

*The grain refinement of Al-Cu alloys has been extensively investigated with a view to improve their mechanical properties and castability. The addition of Al-Ti-B grain refiners such as Al-5%Ti-1%B in Al-Cu alloys has been widely used due to their higher nucleation potency and wider potential for industrial applications. In this paper, the influence of Al-5%Ti-1%B on the structure and properties of as-cast Al-Cu15 alloys are examined. Various theories regarding the mechanisms by which Al-5%Ti-1%B based grain refinement occurs have been proposed. These include the so-called particle theory, phase diagram theory, peritectic hulk theory, the free growth theory, the interdependence theory, an epitaxial model for heterogeneous nucleation on potent substrates and a new concept for growth restriction during solidification.*

**Keywords:** aluminium- copper alloys, titanium, boron

### 1. INTRODUCTION

Aluminum-copper alloys are important engineering materials used in applications requiring high tensile properties. Al-Cu alloys are extensively in use for high quality castings in industrial applications, such as aviation or automotive. The main factors that influence the structure of Al-Cu alloys are chemical composition [1], cooling rate [2], liquid treatment (melt refining, impurity control and grain refining) [3] and heat treatment [4]. A refined dendritic structure, small secondary dendrite arm spacing (DAS) and less dendrite branching leads to a homogeneous structure [5-8]. In this paper we observed the influence of grain-refining additives Al-Ti-B for the same chemical composition of the aluminium-copper alloy. Grain refinement is achieved through the addition of Al – 5%Ti – 1%B master alloys. Al-5%Ti-1%B grain refiner contain Al<sub>3</sub>Ti and TiB<sub>2</sub> particles. Al<sub>3</sub>Ti particles will go into solution of molten aluminum. TiB<sub>2</sub> particles are insoluble and act as good nucleation sites for the aluminium grains.

### 2. EXPERIMENTAL

Binary Al-Cu15 alloy with the compositions given in Table 1. was prepared in an electrical resistance furnace from 99.5% pure aluminium and 99.9 % pure copper. Within the framework of this study, five Al-Cu15 alloys were melted. The chemical composition (in wt. %) of the Al-Cu15 alloys was specified by quantometry analysis and the results are reported in Table 1. The solidification structure was modified by the addition of the Al-5%Ti-1%B to give alloys containing: 0.02%Ti, 0.08%Ti, 0.15%Ti, 0.25% titanium. The liquid metal has been heated to 760°C and then grain refiner (master alloy) was introduced to the melt. The base Al-Cu15 alloy has the following chemical composition: Cu: 13.48-14.38; Ti: 0.000-0.287; Si: 0.06-0.08; Fe: 0.12-0.14; Zn: 0.049-0.062; Al: Balance. The liquid metal was cast into molds and the pouring temperature was 760°C. The X-ray diffraction analysis was performed on the AlCu15 samples using a wide range of angles (2θ) from 5 to 100° with a step of 0,02° and a holding time of 0,50 seconds at each step. A diffractometer with a graphite monochromator and a constant divergence slit (D) of 1mm was used.

Table 1 - Chemical composition of the investigated alloy (in wt.%).

TYPE OF SAMPLE	%Fe	%Si	%Ti	%B	%Cu	%Zn	%Mg	
Al-Cu15	0%Ti	0.13	0.07	0.000	0.000	14.25	0.062	0.000
	0.02%Ti	0.12	0.06	0.020	0.018	13.48	0.049	0.000
	0.08%Ti	0.14	0.07	0.100	0.026	14.35	0.059	0.000
	0.15%Ti	0.14	0.08	0.179	0.050	14.38	0.060	0.000
	0.25%Ti	0.13	0.07	0.287	0.092	14.24	0.061	0.000

The dendrite arm spacing, the linear intercept size of eutectic cells and the grain size were calculated using standard linear intercept method. Statistical analysis of the results was performed. Hardness of the samples has been measured by use of the Brinell method. Compression strength of the samples of cast alloys has been tested on a universal electronic tensile testing machine of  $1 \times 10^4$  kg. Average size of samples was as follows: diameter  $D_0=10$ mm and height  $H_0=20$ mm. All of the tested samples have been fractured. Compression strength is measured in the moment of fracture.

### 3. RESULTS AND DISCUSSION

In this paper, the effects of titanium and boron contents on the structure of Al-Cu15 alloy were examined. It is generally accepted that the grain refinement of Al-Cu alloys can be attributed to two key factors: nucleation potency and growth restriction. Nucleation potency is believed to be dependent on the number, size and size distribution of the nucleants,  $Al_3Ti$  and  $TiB_2$  in the present investigation. Growth restriction on the other hand, is believed to depend mainly on the alloying elements themselves. Of all the alloying elements, Ti has the strongest growth restriction effect and Cu is also known to have a positive, albeit small, growth restriction effect. In alloy containing high titanium the average values of the grain size were found to decrease (Table 2). Besides, the presence of titanium causes a little change in the average values of the DAS and the medium value of the length eutectic (Le) (Table 3 and 4). From the enclosed results of the testing it can be seen that addition of the Al-5%Ti-1%B performs modification of the structure, i.e. making finer grains. It is confirmed that titanium and boron are very effective grain refiners. The number of primary grains depends on the type of nucleating agent, its usage and granulation, the overheating and modification temperatures as well as the time since the modification treatment. The benefits of modification are: better distribution of porosity, better dispersion of secondary phases, better mechanical properties, e.g. strength [2]. Through X-ray powder diffraction method it has been found out that tetragonal  $Al_2Cu$  with parameters of crystal screen:  $a = 6,076 \text{ \AA}$ ,  $c = 4,886 \text{ \AA}$ ,  $V = 180,4 \text{ \AA}^3$  is formed.

Table 2 - Grain size for different titanium contents in investigated alloys

TYPE OF SAMPLE	Average, $\mu\text{m}$	min, $\mu\text{m}$	max, $\mu\text{m}$	RSE, %	
Al-Cu15	0%Ti	810.48387	193.54839	2709.67742	5.06863
	0.02%Ti	230.63492	47.61905	777.77778	3.78064
	0.08%Ti	53.00000	9.37500	162.50000	2.94158
	0.15%Ti	49.71717	15.15152	121.21212	2.99332
	0.25%Ti	48.39966	10.10101	126.26263	2.76879

Table 3 - Dendrite arm spacing (DAS) for different titanium contents in the investigated alloys

TYPE OF SAMPLE		Average, $\mu\text{m}$	min, $\mu\text{m}$	max, $\mu\text{m}$	RSE, %
Al-Cu15	0%Ti	20.22536	1.63	123.27	2.12289
	0.02%Ti	23.13044	1.63	112.65	2.22268
	0.08%Ti	23.30254	1.22	90.61	2.32280
	0.15%Ti	20.66491	1.22	102.86	2.16452
	0.25%Ti	18.98537	1.63	92.24	2.09712

Table 4 - The linear intercept size of eutectic cells (Le) for different titanium contents in the investigated alloys

TYPE OF SAMPLE		Average, $\mu\text{m}$	min, $\mu\text{m}$	max, $\mu\text{m}$	RSE, %
Al-Cu15	0%Ti	7.05516	1.63	46.53	2.74649
	0.02%Ti	7.38373	1.63	51.43	3.24170
	0.08%Ti	8.34064	1.63	63.67	3.50108
	0.15%Ti	6.67921	1.22	42.86	3.04908
	0.25%Ti	7.30999	1.22	55.10	2.93505

We have also examined the following properties of these materials: hardness measurement and pressure strength. The hardness of the modified alloy is higher than the hardness of the alloy without any modification treatment (Table 5). By increasing the content of titanium the compression strength also increase (Table 6).

Table 5 - Hardness of the investigated alloys with different amounts titanium

TYPE OF SAMPLE		HB <sub>1</sub>	HB <sub>2</sub>	HB <sub>3</sub>	HB <sub>4</sub>	HB <sub>average</sub>
Al-Cu15	0%Ti	88.7	88.7	90.7	91.9	90.00
	0.02%Ti	90.7	88.7	92.8	92.8	98.97
	0.08%Ti	94.9	99.5	97.2	94.9	99.25
	0.15%Ti	104.0	105.0	102.0	98.6	102.40
	0.25%Ti	105.0	105.0	104.0	99.5	103.37

Table 6 - Compression strength of the investigated alloys with different amounts titanium

TYPE OF SAMPLE		F <sub>0.2 P</sub> (N)	R <sub>P0,2</sub> (N/mm <sup>2</sup> )	F <sub>PM</sub> (N)	R <sub>m</sub> (N/mm <sup>2</sup> )	$\delta_P$ (%)	$\Psi_P$ (%)
A-ICu15	0%Ti	16800	214.01	38600	491.72	27.15	31.67
	0.02%Ti	17400	221.66	38600	491.72	22.74	25.80
	0.08%Ti	18000	229.30	43800	557.96	22.06	24.92
	0.15%Ti	18120	230.83	43880	558.98	17.14	18.80
	0.25%Ti	18800	239.49	43880	558.98	15.61	16.97

#### 4. CONCLUSION

Microstructure can be influenced by addition of titanium and boron in form of Al-5%Ti-1%B containing fine insoluble crystals of TiB<sub>2</sub> phase acting as nucleants for the aluminium phase. Titanium usually, together with aluminium causes a peritectic reaction with TiAl<sub>3</sub> phase which depending on content always hardens above hardening point of pure aluminium or its phase of the  $\alpha$ -hard solution. Number of primary grains is one of the most important factors for determining the quality of castings. The final grain density in the casting depends on the nucleation process at the beginning of solidification. Each nucleus gives rise to one single grain. Consequently, it represents the nucleation potential. The following factors significantly influences the number of primary grains in the casting: chemical composition, modification, cooling rate and temperature of liquid metal. However, the measure used in practice to radically increase the number of grains is modification. The resulting dispersion of insoluble components as well as a smaller porosity and fewer non-metal inclusions improved the mechanical properties.

#### REFERENCES

- [1] M. Nabawy, A.M. Samuel, F.H. Samuel, H.W. Doty, AFS Transactions, 119 (2011) 123-139.
- [2] M. Górny, G. Sikora, J. Mater. Eng. Perform, 24(3) (2015) 1150-1156.
- [3] L. Zhixue, D. Long, C. Juqiang, China Foundry, 10(6) (2013) 355-359.
- [4] I. Wierszyłowski, S. Wieczorek, A. Stankowiak, J. Samolczyk, Obróbka Plastyczna Metali, 16(5) (2005) 31-37.
- [5] J.Y. Hwang, H.W. Doty, M.J. Kaufman, Mater. Sci. Eng. A 488 (2008) 496-504.
- [6] B. Zlaticanin, S. Đurić, B. Jordović, B. Radonjic, Mater. Sci. Tech., 20(1) (2004) 138-140.
- [7] B. Zlaticanin, B. Radonjic, M. Filipovic, Mater. Trans., 45(2) (2004) 440-446.
- [8] B. Zlaticanin, B. Radonjic, S. Đurić, B. Jordović, B. Stojanović, Mater. Technol., 36(1-2) (2002) 49-51.

## EFFECT OF COOLING RATE ON MECHANICAL PROPERTIES OF BINARY Al-Cu<sub>23</sub> ALLOYS

Biljana Zlatičanin<sup>1</sup>, Sandra Kovačević<sup>2</sup>

<sup>1</sup>Faculty of Metallurgy and Technology, 81000 Podgorica, Montenegro

<sup>2</sup>Central School of Chemical Technology Spasoje Raspopović, 81000 Podgorica, Montenegro

### Abstract

*In this study, effects of cooling rate on the solidification microstructure and mechanical properties of Al-Cu<sub>23</sub> alloys were investigated. The cooling rate has a significant effect on the morphology of primary  $\alpha$ -Al phase and  $\theta$ -Al<sub>2</sub>Cu phase. When the cooling rate increases, the microstructure is significantly refined and the mechanical properties of Al-Cu<sub>23</sub> alloys are improved.*

**Keywords:** Al-Cu alloys, growth rate

### 1. INTRODUCTION

Cooling rate is a critical factor controlling the grain size of cast metals. Generally, it is accepted that higher cooling rate leads to smaller grains due to the high undercooling achieved. During the solidification and cooling process, the cooling rate, one of the critical parameters, directly affects product performance. In recent years, numerous researchers have conducted a great amount of research in this field. S.G. Shabestari [1] reported that a higher cooling rate would significantly decrease the size of dendrite arm spacing, the recalescence undercooling temperature, and total solidification time, and increase the liquidus temperature, nucleation undercooling temperature, and solidification range. B. Benjunior et al. [2] studied the effect of different cooling rate conditions on thermal profile and microstructure of aluminum 6061, indicating that different cooling rate conditions will alter the material phase change temperatures. Furthermore, cooling rate was performed to reduce the porosity by reducing the size of dendrite arm spacing [3], which influences mechanical properties to some extent. A series of casting experiments was performed with binary Al-Cu<sub>23</sub> alloys with varying cooling rates and cooling conditions [4-6].

### 2. EXPERIMENTAL

Five samples were prepared by melting raw materials. The designed compositions were synthesized by high-purity Al (99.5%), and pure Cu. The chemical composition (in wt. %) of the AlCu<sub>23</sub> alloys was specified by quantometry analysis and the results are reported in Table 1. The solidification structure was modified by the addition of the AlTi5B1 master alloy to give alloys containing 0 to 0.3 wt.% titanium. The melting temperature was kept at 760°C. To study the variations in the mechanical properties with respect to cooling rate, the alloys were cast by conventional air-cooled and water-cooled methods. Properties of the materials have been investigated, eg.: hardness and determination of compression strength. Hardness has been measured by use of the Brinell method. Hardness measurement for AlCu<sub>23</sub> alloys samples was performed using a Brinell hardness tester with a load of 62.5 kp (1kp = 9.80665 N), 2.5 mm diameter ball and a dwell time of 30 s. Compression strength of the samples have been tested on an electronic tensile testing machine of 10t. Special attention was given to an assessment of the different structural parameters by modern quantitative microstructure analysis, using an automatic device for quantitative picture analysis and linear measuring method, which was considered as more reliable, accurate and faster than conventional manual methods of microstructure analysis.



Table 1 - Chemical composition of the investigated alloy (in wt.%).

Type of sample	%Fe	%Si	%Ti	%B	%Cu	%Zn	%Mg	
Al-Cu23	0%Ti	0.11	0.06	0.000	0.000	20.00	0.072	0.000
	0.02%Ti	0.10	0.07	0.027	0.009	20.24	0.074	0.000
	0.08%Ti	0.15	0.08	0.103	0.025	21.08	0.069	0.000
	0.15%Ti	0.10	0.06	0.198	0.054	22.95	0.078	0.000
	0.25%Ti	0.10	0.07	0.306	0.094	20.69	0.073	0.000

### 3. RESULTS AND DISCUSSION

The cooling rate affects the structure of as-cast alloys in a well-established manner, i.e. the grain size and the dendrite arm spacing (DAS) decrease with increasing the cooling rate. It is important to note that the grain size depends on the conditions of both nucleation and growth, only the latter being explicitly dependent on the cooling rate, while the nucleation is strongly affected by other factors, such as the amount of nucleation sites, undercooling. The dendrite arm spacing and the grain size were calculated using standard linear intercept method, using an image-analysis software. Statistical analysis of the results was performed. It is found that the dendrite arm spacing (DAS) were found to decrease from 17.37  $\mu\text{m}$  to 10.32  $\mu\text{m}$  for Al-Cu23 (0.08% Ti) with increasing cooling rate. Fast cooling rate condition produced smallest the grain size for the same content of titanium in the Al-Cu23 (0.08% Ti), the grain size are decreased from 57.71  $\mu\text{m}$  to 41.26  $\mu\text{m}$  and we obtain a fine, uniform grain structure.

In this study the mechanical properties like compressive strength and hardness of both air-cooled and water cooled cast specimens were tested and the results were compared (Tables 2 -5). Increases in hardness and compressive strengths of the water cooled cast specimen have been encountered from the present work. This result reveals that increase in cooling rate leads to enhancement of the mechanical properties.

Table 2 - Hardness of the investigated alloys with different amounts titanium (air-cooled samples)

Type of sample	HB <sub>1</sub>	HB <sub>2</sub>	HB <sub>3</sub>	HB <sub>4</sub>	HB <sub>average</sub>	
Al-Cu23	0%Ti	99.5	104.0	107.0	104.0	103.87
	0.02%Ti	102.0	104.0	105.0	104.0	104.50
	0.08%Ti	109.0	111.0	111.0	111.0	110.00
	0.15%Ti	130.0	130.0	125.0	130.0	127.50
	0.25%Ti	143.0	145.0	138.5	145.0	142.37

Table 3 - Hardness of the investigated alloys with different amounts titanium (water cooled samples)

Type of sample	HB <sub>1</sub>	HB <sub>2</sub>	HB <sub>3</sub>	HB <sub>4</sub>	HB <sub>average</sub>	
Al-Cu23	0%Ti	143.0	144.0	135.0	138.0	140.00
	0.02%Ti	145.0	146.0	143.0	145.0	144.75
	0.08%Ti	146.0	147.0	145.0	148.0	146.50
	0.15%Ti	148.0	147.0	145.0	148.0	147.00
	0.25%Ti	148.0	149.0	153.0	149.0	149.75

Table 4 - Compression strength of the investigated alloys (air-cooled samples)

Type of sample		F <sub>0.2P</sub> (N)	R <sub>P0.2</sub> (N/mm <sup>2</sup> )	F <sub>PM</sub> (N)	R <sub>m</sub> (N/mm <sup>2</sup> )	□ <sub>P</sub> (%)	□ <sub>P</sub> (%)
A-ICu23	0%Ti	18000	229.30	35200	448.41	25.45	29.37
	0.02%Ti	18600	236.94	37800	481.53	14.76	15.97
	0.08%Ti	23000	292.99	40000	509.55	8.82	9.24
	0.15%Ti	27200	346.49	40200	512.10	7.47	7.76
	0.25%Ti	27200	346.69	40280	513.12	7.30	7.58

Table 5 - Compression strength of the investigated alloys (water cooled samples)

Type of sample		F <sub>0.2P</sub> (N)	R <sub>P0.2</sub> (N/mm <sup>2</sup> )	F <sub>PM</sub> (N)	R <sub>m</sub> (N/mm <sup>2</sup> )	□ <sub>P</sub> (%)	□ <sub>P</sub> (%)
Al-Cu23	0%Ti	27160	345.99	40000	509.55	11.71	12.45
	0.02%Ti	28400	361.78	40080	510.57	6.11	6.30
	0.08%Ti	28800	366.88	41400	527.39	5.94	6.12
	0.15%Ti	32000	407.64	43200	550.32	3.05	3.10
	0.25%Ti	33000	420.38	45200	575.80	2.64	2.67

#### 4. CONCLUSION

The microstructure and mechanical properties of cast products are greatly influenced by the cooling rate during their solidification. It is evident that the increase in cooling rate improves the mechanical properties of the cast alloy. The measurements of the average dendrite arm spacing show the refinement of dendritic constitution with increasing cooling rate. The results show that the higher the cooling rate, the smaller the grain size of the alloy. Quantitative relationships between the average dendrite arm spacing, grain size and the cooling rate are found experimentally for Al–Cu23 alloys. The dendrite arms spacing and grain size decrease with increasing cooling rate. The hardness and compression strength of the casting alloys increased with cooling rate. The DAS decreases with increasing cooling rate, and the hardness and strength increase correspondingly. In addition, higher cooling rates produced a finer primary  $\alpha$ -phase particle. As an elemental material, the basic properties of aluminum do not change with mechanical or physical processing. This means that aluminum is intrinsically sustainable: once produced, it can be recycled repeatedly without any loss in quality and reused in the manufacture of consumer and industrial products.

#### REFERENCES

- [1] S.G. Shabestari, M. Malekan., *Can. Metall. Q.*, 44 (2005) 305–312.
- [2] B. Benjunior, A.H. Ahmad, M.M. Rashidi, M.S. Reza., *Procedia Eng.*, 184 (2017) 298–305.
- [3] W. Jatimurti, B. Alexander, A.T. Wibisono., *Mater. Sci. Forum*, 964 (2019) 124–129.
- [4] B. Zlaticanin, S. Đurić, B. Jordović, B. Radonjic., *Mater. Sci. Tech.*, 20 (2004) 138-140.
- [5] B. Zlaticanin, B. Radonjic, M. Filipovic., *Mater. Trans.*, 45 (2004) 440-446.
- [6] B. Zlaticanin, B. Radonjic, S. Đurić, B. Jordović, B. Stojanović., *Materials and Technology*, 36 (2002) 49-51.

## AGEMERA PROJECT – THE POTENTIAL OF ASAREL PORPHYRY COPPER DEPOSIT FOR CRITICAL RAW MATERIALS

Desislav Ivanov<sup>1</sup>, Irena Peytcheva<sup>2</sup>, Marko Holma<sup>3</sup>,

<sup>1</sup> Asarel-Medet JSC, 4500 Panagyurishte, Bulgaria

<sup>2</sup> Geological Institute, Bulgarian Academy of Sciences, 1000 Sofia, Bulgaria

<sup>3</sup> Muon Solutions, 90840 Oulu, Finland

### Abstract

*Horizon Europe AGEMERA project - Agile Exploration and Geo-modelling for European Critical Raw Materials: The potential of Asarel porphyry copper deposit for critical raw materials* Asarel-Medet JSC Mining and Processing Complex is the first, biggest and leading Bulgarian company for open pit mining and processing of copper and other types of ores. Asarel-Medet JSC is the only Bulgarian company that participates in the international research project AGEMERA to study the potential of Europe regarding critical raw materials for the green transition. The supply of European critical raw materials (CRMs) does not currently meet the European demand. This gap is predicted to increase, making Europe even more dependent on outside suppliers. AGEMERA is a project to help tackle this strategic problem by studying several CRM sites in Finland, Poland, Spain, the Balkans, and Zambia in different deposit types. To check the potential of the porphyry systems in Europe as a source of CRMs, the Asarel porphyry-Cu deposit was selected as a test site. Here we present preliminary geochemical and mineral chemistry data for hydrothermal ore and alteration minerals in Asarel that reveal the potential of the deposit to source some CRMs as by-products. Further studies will combine the geochemical data with innovative geophysical methods for an improved deposit model and provide enhanced knowledge about effective exploration techniques for CRMs.

**Keywords:** critical raw materials, Asarel-Medet, AGEMERA, porphyry systems

### 1. INTRODUCTION

Asarel-Medet JSC Mining and Processing Complex is the first, largest and leading Bulgarian mining company for open pit mining and processing of copper and other ores. It is located 11 km northwest of the town of Panagyurishte and 90 km east of the capital, Sofia. Asarel-Medet JSC is a joint-stock company the core activity of which is open pit mining and processing of copper and other ores, biochemical copper recovery and any engineering and trade activities associated with it. The company has been awarded with dozens of national and international prizes in the field of investment, innovation, environmental protection, management, corporate culture, occupational health and safety and corporate social responsibility. The national industry award for innovations bestowed to the company in 2021 for the successful implementation of the X-mine international project under the Horizon Europe program was among these acknowledgements. Currently, the company is facing another challenge in the innovations area and green transition technological revolution in mining: the AGEMERA project. Asarel-Medet JSC is the only Bulgarian company which is involved in AGEMERA international research project aimed at exploring the potential of Critical Raw Materials in Europe. The company integrates its resources, expertise, innovation power and new technologies with entities from 10 European countries: Finland, Germany, Netherlands, Croatia, Estonia, Hungary, Spain, Bosnia and Herzegovina, Poland and Bulgaria. The consortium includes universities, scientific institutions, technological companies and mining

companies and its coordinator is the University of Oulu in Finland. Apart from Asarel-Medet JSC, the Geological Institute at the Bulgarian Academy of Science also takes part in the project representing Bulgaria.

The global demand for critical raw materials is expanding rapidly due to the transition to environmentally friendlier technologies, electric power generation and the endeavor towards a more digitalized world. Mobilizing Europe's internal critical raw material potential is a crucial prerequisite for enabling the European Union (EU) to be more resilient and develop its strategic autonomy. The Old Continent has a long tradition of mining and recovering strategic base metals (such as Cu, Zn and Pb), but a more humble experience in critical raw materials mining. This is partly due to the fact that plenty of them were not considered valuable at an earlier stage. However, Europe has a significant potential for critical raw material mining in various ore regions. Remedying the raw material supply bottlenecks in the near future is of utmost importance for achieving a strategic autonomy of the supply chains of the European industries. The latter is particularly indispensable for critical raw materials which play an essential role in the transition to a low-carbon and digital economy. In a number of cases, the same raw materials are required by multiple technologies and sectors which are crucial to the clean energy transition and therefore they are effectively competing with each other.

AGEMERA's goal is to develop and test innovative and non-invasive geophysical exploration methods to develop a more detailed map of the critical raw materials in Europe, including cobalt, bauxite, lithium, vanadium, niobium, tantalum, etc. The new geophysical exploration technologies have been planned to cover a total area of over 4,700 square km in six European countries: Poland, Germany, Finland, Bulgaria, Spain, Bosnia and Herzegovina and in one African country, Zambia. The three-year research and development project aims at resolving some of the most topical issues of European critical raw materials supply. Its main objective is to enhance the geological understanding of the explored ore regions, improve their genetic models and acquire information about the critical raw materials as the main ore products or by-products. The project will also be focused on raising the public awareness of the critical raw material crucial role in both the green transition and the EU's strategic autonomy and sustainability.

Exploration targeting of the mineral associations, sampling, modelling and geophysical field testing have been scheduled for various study sites in order to ensure a variety of locations and mineralized systems. The pre-selected areas are located in Bosnia and Herzegovina, Bulgaria, Finland, Poland, Spain and Zambia. The targets are orogenic gold, karst bauxites, epithermal massive sulfides, porphyry Cu-Au-Mo systems, stratabound Cu-Ag and sediment-hosted stratiform Cu. The deposits to be explored are located in the Peräpohja schist belt (Finland), Iberian pyrite belt (Spain), Kupferschiefer district (Poland), Panagyurishte and Rosen districts (Bulgaria), Jajce and Posušje regions (Bosnia and Herzegovina) and the Zambian copper belt (Zambia).

The deposits of a porphyry type are the principal source for copper and molybdenum mining and may contain economic grades of Au, Ag and platinum group elements (PGE). A number of strategic and high-tech elements such as Re, W, Bi, In, Te and Se may reach economic concentration and be recovered as by-products. The Asarel copper-porphyry deposit was selected as a test site in order to explore the potential of the porphyry systems in Europe as a critical raw materials source. This paper presents preliminary geochemical and mineral chemical data of the hydrothermal mineralization and metasomatic altered minerals in the deposit. It will form the basis for their further integration with agile exploration methods and better geological modeling of the deposit.

## **2. REGIONAL LOCATION AND GEOLOGICAL SETTING OF THE ASAREL COPPER-PORPHYRY DEPOSIT**

Most of the world's magmatic-hydrothermal porphyry Cu ( $\pm$ Au $\pm$ Mo) and epithermal Au $\pm$ Ag $\pm$ Cu deposits of economic importance are genetically associated with magmatic arcs (Sillitoe, 2010 and references therein). In Southeast Europe, the Late Cretaceous Apuseni-Banat-Tymok-Srednogorie Belt (ABTS) represents the westernmost arc in the Alpine-Himalayan orogenic system associated with the Neotethys subduction (Popov et al., 2002; von Quadt et al., 2005). This magmatic arc stretches on more than 1,000 km starting from the Apuseni mountains in Romania, passing through Serbia and Bulgaria and reaching the Black Sea and then Iran.

The Bulgarian part of the ABTS belt is known as the Srednogorie zone which is an 80 to 100-kilometer-wide east-west oriented tectonic-magmatic unit located between the Balkan zone in the north and the Rhodope massif in the south. The most strongly mineralized segment of the Central Srednogorie, also called Panagyurishte ore region (Popov et al., 2002), consists of a northwest-southeast trending alignment of porphyry and epithermal Cu–Au deposits located at 60 to 90 km east of Sofia. The basement of the Central Middle Srednogorie dates back to the Variscan period. It is composed of metamorphic rocks (mainly gneisses, gneiss-schists and amphibolites) with Paleozoic and older protoliths and a high-grade metamorphic imprint of 330-340 Ma (Carrigan et al., 2005, 2006; Lazarova et al., 2015). They are intruded by Variscan granitoids and gabbro at 314–305 and  $\approx$ 290 Ma (Carrigan et al., 2006; Peycheva and von Quadt, 2004) and intruded and overlaid by Late Cretaceous calc-alkaline magmatic rocks (intrusives/shallow intrusives, volcanics and volcanoclastics/epiclastics).

More than 150 ore deposits and mineral occurrences are known in the Panagyurishte ore region consisting mainly of porphyry copper and high-sulphide Cu-Au epithermal types (Popov et al., 2012). The Asarel porphyry copper deposit is among the largest operating mines in the area of resources of 467 Mt of ore of average head grade of 0.32% Cu and 0.12 ppm Au (Milev et al., 2007). The ore formation is associated with the consequent intrusion of pre-ore, syn-ore and post-ore shallow igneous bodies and dykes of predominantly transitional composition. A number of hydrothermal mineral parageneses have been identified: early quartz-magnetite-hematite; a major quartz-pyrite-chalcopyrite Cu-mineral association, related with propylitic, sericitic and transitional sericitic-propylitic alteration occurring in the host rocks as veins, small nests and disseminations; quartz-molybdenite association associated mainly with propylitic alteration; quartz-pyrite association locally occurring in veins and streaks; quartz-sphalerite-galena (pyrite, chalcopyrite) association occurring as veins in the deposit upper and outer parts; supergene alteration assemblage containing variable amounts of chalcocite, covellite, malachite and Fe-hydroxide. Specific and rare (Cu-Au-Te and Cu-Ag-Bi-Te with Se, Pb and Zn) associations have been described by Petrunov et al. (1991).

The Asarel porphyry copper deposit poses a challenge in terms of its mineralogical and geochemical predictability. This fact is attributable to the availability of secondary overlying areas, vast alteration areas with significant argillic to advanced argillic alteration and complex structures such as pre-ore, syn-ore and post-ore faults. One of the faults (Mialski fault) displaces the eastern part of the deposit and led to the exhumation of the basement rocks with cross-cutting subvolcanic dykes exposing them at the same level as the volcanics in its western part.

## **3. SAMPLING AND ANALYSIS METHODS**

The samples for this study have been collected from the Asarel open pit mine, from the exploration structural drillholes and the flotation plant. The JEOL JSM-6610 LV scanning electron microscope at the University of Belgrade (Faculty of Mining and Geology) was used for SEM-EDS definition of the predominant elements in the minerals. LA-ICP-MS analyzes of trace elements were performed at the Geological Institute of the Bulgarian Academy of Sciences using a NW excimer

laser connected to a DRC-e PE system. SILLS (Signal Integration for Laboratory Laser Systems) software was applied for data reduction.

#### 4. RESULTS AND CONCLUSIONS

Our preliminary studies of critical raw material potential at the Asarel deposit reveal high concentrations of several critical raw material elements in some ores and hydrothermally altered minerals. The Cobalt grade is up to 1,000-1,630 ppm in the tested pyrite, while Galena contains Selenium concentrations of 2-3 wt%. Molybdenite is not uniformly distributed in the tested pyrite and is the main carrier of Mo and Re, but the grade of the latter varies from 600 to 45,790 ppm. Considering the metasomatic altered minerals, the hydrothermally altered Rutile concentrates trace elements such as V (110-6,700 ppm), Nb (2,300-4,600 ppm), Ta, W and Sc; epidotes and APS (aluminum-phosphate-sulfate) minerals contain elevated REE grades.

Along with the geochemical studies of hydrothermally ores and hydrothermally altered minerals, we also monitored the behavior of the critical raw materials in the grinding and flotation circuits under the conditions of the applied technology at Asarel-Medet JSC. Some elements follow Cu and Au to the final concentrate, while others concentrate in the tailings (for example, cobalt) or the by-products.

The innovations for state-of-the-art geophysical explorations which are to be developed and tested under genuine conditions to a technological availability level within the AGEMERA project will enable the underground depths to be characterized at different coverage, volume and time interval. Some of the innovations will support active and flexible data collection (satellite remote geophysical and drone methods), while others will passively provide valuable information at a longer time scale (muography and sensor technologies).

**Acknowledgments:** *This study was partially supported by the AGEMERA project within the Horizon Europe Research and Innovation Program, Grant No. 101058178.*

#### REFERENCES

- [1] Carrigan, C., S. Mukasa, I. Haydoutov, K. Kolcheva. *Lithos* 82 (2005) 125–147
- [2] Carrigan, C., S. Mukasa, I. Haydoutov, K. Kolcheva. *Precambrian Res.* 147 (2006) 404–416.
- [3] Cioacă, M.-E., M. Munteanu, E. Lynch, N. Arvanitidis, M. Bergqvist, G. Costin, D. Ivanov, V. Milu, R. Arvidsson, A. Iorga-Pavel, K. Högdahl, V. Stoilov. *Minerals* 10 (2020) 946.
- [4] Lazarova, A., K. Nadenov, N. Petrov, V. Grozdev. *Geol. Carpathica.*, 66 (6) (2015) 443-454.
- [5] Milev, V., N. Obretenov, V. Georgiev, A. Arizanov, Zhelev, D., Bonev, I., Baltov, I., and Ivanov, V. 2007). *Gold deposits in Bulgaria*. Sofia: Zemina'93 Publishing House. 208 p. (in Bulgarian with English abstract)
- [6] Petrunov, R., P. Dragov, H. Neykov. *Rev. Bulg. Geol. Society* 52 (1) (1991) 1-7. (in Bulgarian with English abstract)
- [7] Peytcheva, I, A. von Quadt. 2004. The Palaeozoic protoliths of Central Srednogorie, Bulgaria: records in zircons from basement rocks and Cretaceous magmatites. – *Proceed. 5<sup>th</sup> Intern. Symp. Eastern Mediterran. Geol.*, 14-20.04.2004, Thessaloniki, Greece, Vol. 1, 392-395.
- [8] Popov, P., T. Berza, A. Grubic, D. Ioane. *Geol. Balc.*, 32 (2–4) (2002) 145–163.
- [9] Popov, P., S. Strashimirov, K. Popov, M. Kanazirski, K. Bogdanov, R. Radichev, S. Dimovski, S. Stoykov. *Geology and metallogeny of the Panagyurishte ore region*. University of Mining and Geology Press, Sofia, 2012, 227 pp. (in Bulgarian, with extended English summary).
- [10] Sillitoe, R. H. *Econ. Geol.* 105 (1) (2010) 3–41.
- [11] von Quadt, A., Moritz, R., Peytcheva, I., Heinrich, C. *Ore Geol. Rev.* 27 (1–4) (2005) 95–126.

## PROBLEMS OF ANTHROPOGENIC POLLUTION OF SPACE

**Shehret Tilvaldye, Uzziel Caldiño Herrera, Jose Omar Davalos, Manuel Alejandro Lira Martinez, Marlenne Alejandra Hernandez Lira, Diego Adan Villordo Melendez**

Department of Aeronautics, Universidad Autonoma de Ciudad Juarez, Ave. Del Charro 450 N  
Cd. Juárez Chih. CP 32310, México

### **Abstract**

*Since the inception of the Space Age emerged an unprecedented technological, economic, military and social development for the humanity, although brought inevitable negative consequences due to the early exploration of space. A side effect of this development is pollution in space that is increasing over the years. In general, the term pollution is used to indicate a despoiling of the natural environment. This term applies equally when it comes to space from the moment the first artificial satellite was launched into Earth's orbit, and is known as Space Debris. This article contains the concept of «space debris» and statistical data techno-genic pollution of outer space, and describes the possible methods of dealing with space debris and justifies the need for international cooperation to solve outer space pollution problem.*

**Keywords:** (Space debris, Pollutions of outer space, Space law)

### **1. INTRODUCTION**

The Space Debris encompasses both natural micrometeoroid and artificial particles (man-made orbital debris). Meteoroids are in orbit around the sun, while most artificial debris is in orbit around the Earth. Besides the location there is a significant difference between natural and artificial debris that is the length of time that they remain in Near-Earth space, which will depend on orbital velocity and the altitude. For natural debris, such meteoroids it arrives unanticipated from the deepness of space and quickly pass through Near-Earth space and most of them will burn up in lower atmosphere or, in unusual cases fragments reach the surface of Earth. On the other side, artificial debris once the Man-made Orbital Debris (MOD) are launched from Earth into orbit, and the length of time that they remain can be thousands or even millions of years which represents danger for active spacecraft and satellite vehicles.

An investigation shows the statistic of the total number of MODs that remain in space and have listed by the automatic warning system for dangerous situations in near- Earth space until August 31,2015 and was a total of 17,250. Of this amount 1,362 space objects are active spacecraft and satellites. [1] On the other hand, 15,888 are man-made space debris (MSD), which represents a 92% of the total number of MODs in Near-Earth space. These man-made space debris are classified including: 2682 non-active spacecraft, 1907 upper-stage rockets and final stage vehicles, and 11,299 fragments of spacecraft, upper-stage rockets, final stage vehicles and other elements. [2] Other data provided by the National Aeronautics and Space Administration (NASA) shows that there are more than 20,000 pieces of debris larger than a softball orbiting the Earth. They travel at speeds up to 17,500 mph, fast enough for a relatively small piece of orbital debris to damage a satellite or a spacecraft, and there are 500,000 pieces of debris which size of a marble or larger, also there are many millions of pieces of debris that are so small they can't be tracked. [3]

### **2. SPACE SECURITY AND SPACE DEBRIS TERMS**

The primacy in the space sphere as dawn of the space age, and now means for state domination not only in the space, but throughout the world. Therefore successful participation in the



exploration of outer space has a strategic importance for modern states. The result of the realization of this fact was the resumption of in the XXI century struggle for control over the pace that led to the beginning of the "second space race".

Along with the opportunities that give practical space exploration, appeared a new problem in the sphere of global security and increasing its dependence on reliable work of space infrastructure. The cessation of the functioning of space information systems can lead to the escalation of the conflicts. One of the main problems is the clogging outer space that creates threats not only for the existence and effective operation of space vehicles, but it also affects development and security various spheres of life of the states and society, including the provision of space and, in turn, national and global security.

Today under space security understand not only the ability of one state to have military superiority in space before another, but also above all "the ability of state to control part of the cosmic space and carry out a certain activity without being subject to external pressure, threats or attack from the parties of opponents " [4]. Very important to notice that today the threat of space security no longer solely from hostile subjects and natural disturbances, but an increasing threat from pollution of outer space.

In international law there is no definition the concept of "space debris". In the legal literature there is the following definition: "This kind of pollution includes any artificial objects in orbit around Earth, which are non-functional and in respect of which one cannot expect a start or the renewal of their intended functioning, which is authorized in the future, including fragments and parts thereof. Space debris Includes inactive spacecraft, used parts of missiles, material of formations as a result of planned space operations, fragments formed satellites and upper levels as a result of explosion or collision, as well as containing on board dangerous (nuclear, toxic, etc.) materials "[3, c. 119].

We suggested the following definition: *"The artificial debris (or Space Pollution) is considerate any object send by the man which no longer serves a useful function; like inactive satellites, nonfunctional spacecraft, abandoned launch vehicle stages, mission-related debris and fragmentation debris."*

In addition to the threats that space debris be directly implemented space activities, there is a danger of it uncontrolled descent from orbit, incomplete combustion during the passage of the atmosphere and the fall on the surface of the Earth.

The term "space debris" is used for all artificial objects and their small fragments in outer space, which will never function again and can serve no useful purpose, but which are a dangerous functioning spacecraft.

The problem of pollution of near-Earth space by "space debris" it theoretically appeared immediately after the launch of the first artificial earth satellites in the 50-ies of the XX century, but at the international level received official status only after the fact, as the Secretary-General of the United Nations, on 10 December 1993, gave a presentation on the theme "Space environmental activities ", in which he indicated the international and global he pattern of clogging of the outer space of the Earth with various wastes.

### **3. STATISTICS OF SPACE DEBRIS**

In 2014, according to experts, near-Earth space was more than 200 thousand objects larger than 1 cm and over 330 million objects larger than 1 mm in size more than 5 000 tons. Only about 10% of them were detected, tracked and entered into catalogs with using ground-based radar and optical means. For example, for 2013, the US military command contained 16,600 objects (mostly larger than 10 cm) [3], and Russian catalog contained 15,800 objects of "space debris" in August 2014 [4]. All these objects was formed from launched to the orbit Space crafts. Total amount of launched spacecraft and launch failure showing on Figure1.

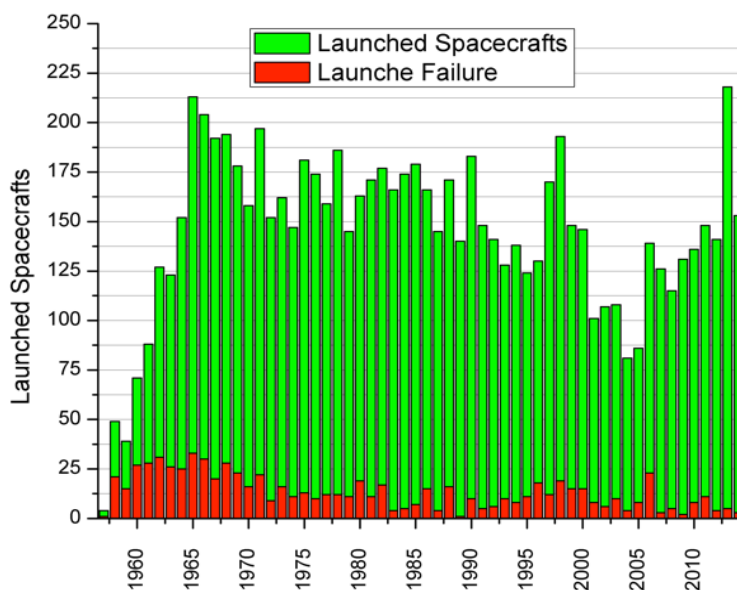


Figure 1 - Total Launched Space crafts and Launch Failure (1957 - 2015)

As we can notice, the process of launching spacecrafts to the orbit is going with high intensity. But from 1990-th to 2004-th intensity was decreasing mostly because of political situation in Soviet Union and Russian Federation. Russia still holding leading positions in space exploration: we can see it from plots on Figure 2, showing success-launched spacecraft total and by countries.

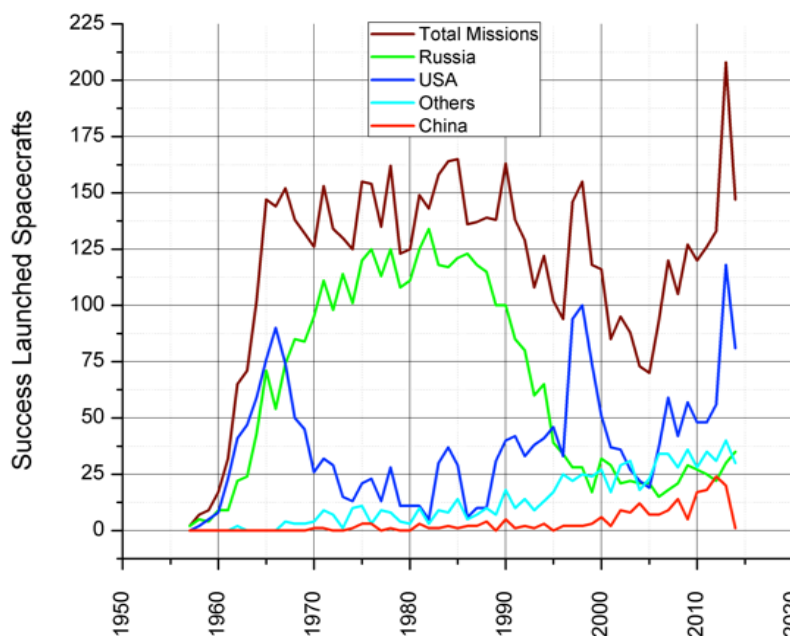


Figure 2 - Success launched spacecrafts by countries (Russia, USA, Others and China) and total (1957 - 2015)

The total number of spacecraft Launched in this period is 8,593. Number of Russian spacecraft is 3,743; number of USA spacecraft – 2,022; number of other governments (Europe, Japan, China, Canada, India and others) spacecraft is 1,162. Among them, the number of Civilian Spacecraft is

4,519, and Military spacecraft – 4,074. In Civilian Programs the number of Piloted Spaceships (+35 military) is 610; number of Planetary Probes is 248; number of Communication Satellites is 1,381; and number of Meteorology Satellites is 241. Some of mentioned statistical information presented on Figure 3.

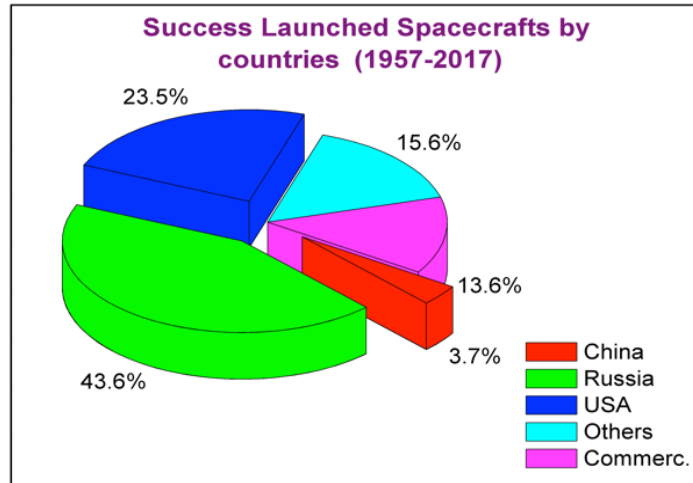


Figure 3 - Success launched spacecraft by countries (Russia, USA, Others and China)

According to some estimates, the contribution to the creation of "space debris" by country is following: China - 40%; the USA - 27,5%; Russia - 25.5%; other countries - 7% [5]. According to other estimates (for 2014): Russia -39.7%; The United States - 28.9%; China - 22.8% [6]. Our estimation of contribution Russia, USA, China, and other countries to the “forming” of space pollution presented on Figure 4.

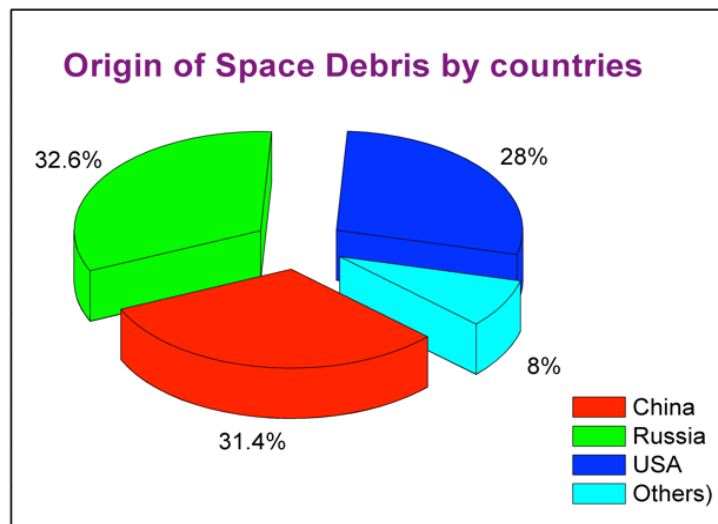


Figure 4 - Origin of Space Debris by countries (Russia, USA, Others and China)

Here important to notice that when we speak about the amount of Space Debris we are dealing with approximate number, but the top three leaders are Russia, USA and China, and the growth of space junk is the most serious in the last few years.

#### 4. PROBLEMS OF ANTHROPOGENIC POLLUTION OF SPACE

Existing intensity of investigation the space and an increase in the number of participants in space activities contribute to a significant increase quantity of Space Pollution. Explosions of waste space vehicles and an increase in the number of particles from accidental collisions of large Space objects can lead to the effect of cascading from collisions.

While increasing the rate of pollution, the use of some altitudes will be complicated or will be completely impossible. So, because of the space pollution, in future will not be possible to use geostationary orbit where located space vehicles for various purposes - from communication satellites to systems of early warning of a missile attack. Also is polluting the area of low Earth circular orbits with a altitude of up to 2 thousand km, on which orbital grouping of space vehicles of various purpose and programs are being implemented for manned space flight and in the long term it is planned to organize works on the assembly of interplanetary space complexes.

In addition, increasing the probability of termination functioning of existing spacecraft and the threat to safety launching new ones. It should be noted that the damage can made by debris particles up to 1 cm large, and avoid this type of collision practically is impossible due to lack of technology tracking particles of a given size.

Thus, in 1991, the US shuttle in order to avoid a collision with remnants of the Soviet satellite Kosmos-955 had to make a series of maneuvers. In 1996 a fragment of the third stage of the French rocket "Ariane-4" disabled French satellite "Cerise". International Space Station has repeatedly adjusted the orbit to avoid collision with Space Debris. And in 2009, the US commercial satellite collided with a non-functioning Russian military communications satellite "Cosmos-2251" [9].

Serious consequences can have cases fall of large space objects on Earth, in areas of large concentrations of people and on the territory of hazardous industrial facilities.

According to experts, in 40-50 years humanity will face the so-called "Debris rain" – unauthorized space debris, some of which because of its size cannot completely burn out when passing through dense layers of the atmosphere, from orbits to the Earth.

All this affects not only the provision of interests of national security of the states, but also to ensure global security generally, and it leads humanity to understand the need to solve this problem. However, this is possible only with joint efforts of the entire world community. The realities are such that in view of many factors (scientific, technical, legal and financial) no one countries cannot solve this problem by oneself. At the international level, work on this problem is mainly going in the two structures - Scientific and Technical Subcommittee of the Committee The United Nations Space Agency and the Inter-Agency Committee on Space Debris.

In addition, countries such as Russia, the United States, Japan, and the European Union have its near-Earth monitoring systems space for observation, cataloging and analysis of environmental conditions and prevention collisions in space. Each system uses various methods of monitoring and exchanges data with others, which allows more quickly and efficiently collision avoidance measures operating spacecraft with space debris.

Since the problem of "space debris" affects the interests of all countries involved in space exploration, its solution needs an international legal basis and close cooperation. For the adoption of agreements in this area, it is important to recognize importance of the problem by all global community.

#### REFERENCES

- [1] Burian K. "Space debris" and environmental safety // *Evoluția sistemului internațional și procesele de integrare europeană*. Chișinău, 2014. pp. 59-66.
- [2] Burian K. "Space debris" and environmental safety // *Evoluția sistemului internațional și procesele de integrare europeană*. Chișinău, 2014. pp. 59-66.

- [3] NASA Orbital Debris Program Office [website]. Access mode: <http://orbitaldebris.jsc.nasa.gov/faqs.html#3> (reference date: 5.05.2013).
- [4] Fenenko A.V. Competition in Space and International Security. International trends, 2008, vol. 6, (18), pp. 26–41.
- [5] Rubanov AA The concept of humanity in international space law / / Right: Zh. Higher education shk. economy. No 3. 2012.
- [6] H.H. Crockell, “Specialization and International Competitiveness,” in Managing the Multinational Subsidiary, H. Etemad and L. S, Sulude (eds.), Croom-Helm, London. 1986.
- [7] K. Deb, S. Agrawal, A. Pratab, T. Meyarivan, “A Fast Elitist Non-dominated Sorting Genetic Algorithms for Multiobjective Optimization: NSGA II,” KanGAL report 200001, Indian Institute of Technology, Kanpur, India, 2000.
- [8] J. Gerald, "Sega Ends Production of Dreamcast," vnunet.com, para. 2, Jan. 31, 2001. [Online]. Available: <http://nl1.vnunet.com/news/1116995>. [Accessed: Sept. 12, 2004].
- [9] Report of head of department of strategic planning and target programs of Federal space agency Yu.N. Makarov at Symposium “Space and Global Security of Humanity”. The Russian Federal Space Agency [website]. Access mode: <http://www.federspace.ru/main.php?id=2&nid=8047> (reference date: 5.05.2013). <http://www.gizmag.com/spaceport-america-hits-nags/36200/>, (accessed 30.04.16).
- [10] Space Debris Mitigation Guidelines of the Committee on the Peaceful Uses of Outer Space. Annex A/AC.105/C.1/L.260. N. Y., 2007.
- [11] Development and International Cooperation: Environment. Report of the World Commission on Environment and Development: Our Common Future. A/42/427. N.Y.,1987
- [12] US warned China of military action over space missiles [website]. StratPost, 2011. Access mode: <http://www.stratpost.com/us-warned-china-of-militaryaction-over-space-missiles> (reference date: 19.05.2013).

## APATITE FLOTATION FROM LOW-GRADE SEDIMENTARY HOSPHATE ORE

Mohammed Derqaoui<sup>1, \*</sup>, Abdelmoughit Abidi<sup>1</sup>, Abdelrani Yaacoubi<sup>1</sup>,  
Khalid El Amari<sup>2</sup>, Omar Oabi<sup>3</sup>, Abdelaziz Bacaoui<sup>1</sup>

<sup>1</sup> Laboratory of Applied Chemistry and biomass, Department of Chemistry, Faculty of Sciences  
Semplalia-Marrakech (FSSM), Cadi Ayyad University, Boulevard Prince My Abdellah, BP  
2390, 40000 Marrakech, Morocco.

<sup>2</sup> Laboratory of Georesources, Geoenvironment and Civil Engineering, Faculty of Sciences and  
Technologies – Marrakech (FSTM), Cadi Ayyad University, Boulevard Abdelkrim Al  
Khattabi, BP 549, 40000 Marrakech, Morocco.

<sup>3</sup> OCP Group SA, Morocco.

### Abstract

*Low-grade phosphate ores are becoming an alternative resource for phosphorus to meet the global demand for food production. Nevertheless, the upgrading of low-grade sedimentary phosphate ore remains a continuous challenge for the phosphate industry. In this study, a novel flotation process using two stages has been investigated at natural pH for beneficiating low-grade Moroccan phosphate ore never exploited before.*

*The effect of operating factors, such as the dosage of E.SA as a depressant in the first stage and the dosage of NaOL as a collector in the first and second stages, on flotation responses were optimized, at bench-scale, using the response surface methodology (RSM) based on the Box-Behnken design.*

*The optimum bench-scale flotation conditions at natural pH resulted in a phosphate concentrate assaying 28.08% P<sub>2</sub>O<sub>5</sub> from a feed grade of 19.24% P<sub>2</sub>O<sub>5</sub> with 65.36% P<sub>2</sub>O<sub>5</sub> recovery.*

**Keywords:** *Flotation, low-grade Phosphate ore, Fluorapatite, Depressant.*

### 1. INTRODUCTION

Sedimentary phosphate deposits account for approximately 90% of the world's phosphate rock production [1], of which 95% is used for producing phosphate fertilizer [2]. More recently, the combined effect of depleting high-grade phosphate deposits and the rapid increase in global phosphorus demand will inevitably impact the world's phosphorus shortage [3]. Therefore, the upgrading of low-grade sedimentary phosphate ores as alternative phosphorus sources becomes an urgent necessity.

Despite the fact that froth flotation is the main process used for the beneficiation of phosphate ores [4], a universal flotation process for recovering apatite from low-grade sedimentary deposits has not yet been developed to date.

For a complex flotation process involving a series of simultaneous interactions [5, 6], the use of statistical tools is an interesting and valuable alternative for conducting this type of study.

Hence, the current paper investigates, for the first time, a novel flotation process using the Box-Behnken design for the recovery of fluorapatite from a representative low-grade sedimentary Moroccan phosphate ore at its natural pH.

## 2. EXPERIMENTAL

### 2.1. Sample

The phosphate ore under investigation was provided by the Office Chérifien des Phosphates (OCP) group, Morocco. The phosphate ore was well homogenized and split to obtain a representative sample. The fine particles (- 40 μm) were eliminated through the de-sliming process. Subsequently, the de-slimed phosphate ore, with a d80 of 174 μm, was subjected to flotation tests as the feed.

The chemical analysis results reveal that the studied phosphate ore is characterized by a low-grade of 19.24% P<sub>2</sub>O<sub>5</sub>, with a relatively high CaO content of 51.27%. In terms of the other accompanying elements, SiO<sub>2</sub> and MgO stood out, with grades of 5.84% and 0.63%, respectively. Mineralogical characterization identified fluorapatite (Ca<sub>5</sub>(PO<sub>4</sub>)<sub>3</sub>F) as the phosphate mineral and calcite (CaCO<sub>3</sub>) as the main gangue mineral, classifying the studied sample as a calcareous type.

### 2.2. Reagents

The reagents used in this study were: sodium oleate (NaOL, ≥ 82%) as a collector, extracted sodium alginate (E.SA) as a depressant, and methyl isobutyl carbinol (MIBC) as a frother. The characterization of E.SA was presented in [7]. Distilled water was used in all experiments.

### 2.3. Bench-Scale flotation tests

Before conducting the flotation experiment, an attrition scrubbing test was conducted using a slurry solid content of 62% by weight for 10 min. After the de-sliming process, the scrubbed product is subjected to flotation tests.

The flotation tests were performed at the natural pH using a 750 mL laboratory flotation cell, in accordance with the flow sheet shown in Fig.1.

The flotation reagents were added sequentially, following the amounts defined by the experimental design. After adding 30 g/t of the frothing agent MIBC, the flotation process was performed at an airflow rate of 4.5 L/min.

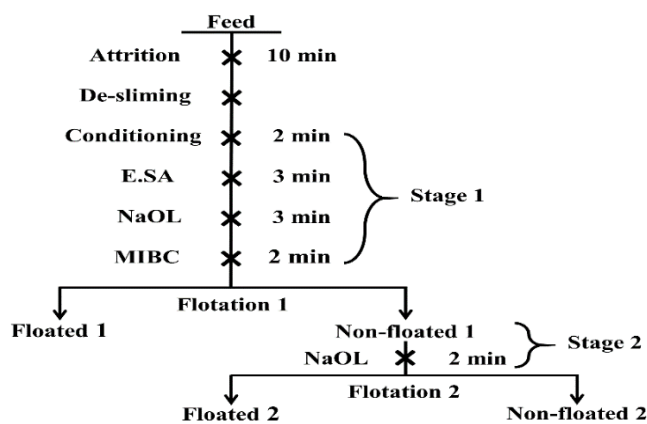


Figure 1 - The flowsheet of flotation tests for low-grade phosphate ore

The concentrates and tailings products were collected, dried and analyzed for P<sub>2</sub>O<sub>5</sub> content. The flotation recovery of P<sub>2</sub>O<sub>5</sub> was calculated using the following Eq. (1):

$$R_e = \frac{c \times C}{f \times F} \times 100 \quad (1)$$

Where Re is the flotation recovery (%); C is the dried concentrate weight (g); F is the feed weight (g); c and f are the P<sub>2</sub>O<sub>5</sub> grade of the concentrate and the feed (%), respectively.



## 2.4. Optimization of flotation process

The response surface methodology (RSM) based on the Box-Behnken design was applied in this study to optimize the main and interaction effects of operational factors on flotation responses, namely  $P_2O_5$  grade and  $P_2O_5$  recovery in the second stage. The dosage of the NaOL in the first flotation stage (X1), the dosage of the E.SA in the first flotation stage (X2), and the dosage of the NaOL in the second flotation stage (X3) were selected as the operational factors.

## 3. RESULTS AND DISCUSSION

In this study, we exercised the Box-Behnken experimental design to optimize the flotation process for a representative sedimentary low-grade phosphate ore. We assumed that the carbonate minerals will be removed in the froth of the first flotation stage, while  $P_2O_5$  will be concentrated in the floated fraction of the second flotation as the final flotation product.

The results of the ANOVA analysis confirm the validity of the mathematical models, which establish a correlation between operational factors and the studied responses, yielding a determination coefficient ( $R^2$ ) value higher than 87%.

The effect of operational factors on  $P_2O_5$  grade / recovery is shown in Fig. 2 as 3D response surfaces.

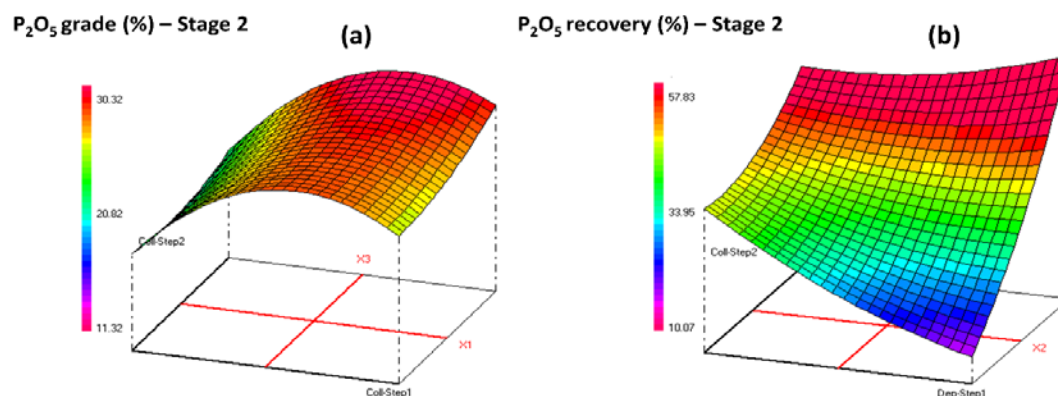


Figure 2 - 3D plot iso-response variation of  $P_2O_5$  grade (a) and  $P_2O_5$  recovery (b) in the second flotation stage (%) as a function of operational factors X1, X2 and X3

The  $P_2O_5$  grade in the second flotation stage ranged between 22.63% and 30.31%, and  $P_2O_5$  recovery varied from 20.14% to 57.83%. As shown in Fig. 2a, at the medium level of collector X1 dosage, the variation of the collector X3 dosage from 600 to 1000 g/t significantly improves the  $P_2O_5$  grade in the float product. Moreover, the operational conditions under which the  $P_2O_5$  grade was high (30.31%) involved the simultaneous use of a medium collector X1 dosage (600 g/t) with a high collector X3 dosage (1000 g/t).

Regarding  $P_2O_5$  recovery, Fig. 2b indicates that the simultaneous use of the lowest E.SA dosage (X2) with the highest collector dosage (X3) resulted in the highest values for  $P_2O_5$  recovery. However, when the collector dosage (X3) is fixed at a low level, the  $P_2O_5$  recovery slightly decreases as the E.SA dosage (X2) increases.

Following calculation through the Nemrodw software, the optimal experimental conditions that maximize both  $P_2O_5$  grade and recovery in the flotation concentrate are 507.57 g/t of NaOL collector in the first flotation stage (X1), 66.58 g/t of E.SA depressant in the first flotation stage (X2), and 1112.44 g/t of NaOL collector in the second flotation stage (X3). The flotation experiments reveal that the optimum setting of factors resulting in a phosphate product assaying 28.08%  $P_2O_5$  at 65.36% recovery. These results demonstrate a good correlation between the

experimental and predicted data, confirming the accuracy and applicability of the experimental design for modeling and optimizing the flotation process.

#### 4. CONCLUSION

This study investigates an innovative two-stage flotation process at natural pH for recovering fluorapatite from low-grade sedimentary phosphate ore. The Box-Behnken design combined with response surface methodology was applied to optimize the operational factors of the flotation process, namely E.SA depressant dosage in the first flotation stage and NaOL collector dosage in both the first and second flotation stages.

The optimization of bench-scale flotation stages reveals that the optimum setting of factors resulted in a phosphate concentrate assaying 28.08% P<sub>2</sub>O<sub>5</sub> with 65.36% recovery from a feed containing 19.24% P<sub>2</sub>O<sub>5</sub> is as follows: 507.57 g/t of NaOL collector and 66.58 g/t of E.SA depressant in the first flotation stage, and 1112.44 g/t of NaOL collector in the second flotation stage. The flotation results indicated a good correlation between the predicted and experimental values.

#### ACKNOWLEDGMENTS

The Authors would like to acknowledge the support through the R&D Initiative APPHOS projects – sponsored by OCP (OCP Foundation, R&D OCP, Mohammed VI Polytechnic University, National Center of Scientific and technical Research CNRST, Ministry of Higher Education, Scientific Research and Professional Training of Morocco MESRSFC) under the project entitled “Direct flotation of low-grade Moroccan phosphates”, project ID\*TRT-BAC-01/2017\*”. We thank our sponsors who provided insight, expertise and follow-up that greatly assisted this research.

#### REFERENCES

- [1] El Bamiki, R., Raji, O., Ouabid, M., Elghali, A., Yazami, O.K., Bodinier, J.L., *Minerals.*, 11 (2021) 1–23.
- [2] Aydin, I., Imamoglu, S., Aydin, F., Saydut, A., Hamamci, C., *Microchem. J.*, 91 (2009) 63–69.
- [3] Amar, H., Benzaazoua, M., Elghali, A., Hakkou, R., Taha, Y., *J. Clean. Prod.*, 381 (2022) 135151.
- [4] Derqaoui, M., Aarab, I., Abidi, A., Yaacoubi, A., EL Amari, K., Etahiri, A., Baçaoui, A., *Arab. J. Geosci.*, 15 (2022) 1–21.
- [5] Boujounoui, K., Abidi, A., Baçaoui, A., El Amari, K., Yaacoubi, A., *J. South. Afr. Inst. Min. Metall.*, 120 (2020) 693–700.
- [6] Aarab, I., Derqaoui, M., EL Amari, K., Yaacoubi, A., Abidi, A., Etahiri, A., Baçaoui, A., *Metall. Explor.*, 39 (2022) 1721–1741.
- [7] Derqaoui, M., Aarab, I., Abidi, A., Yaacoubi, A., El Amari, K., Etahiri, A., Baçaoui, A., *Waste Biomass Valorization.*, 13 (2022) 2623–2636.

## INFLUENCE OF THE DISTRIBUTION AND CONTENT OF LIMESTONE PARTICLES ON THE PROPERTIES OF BLENDED CEMENTS

Nadezhda Kazakova, Alexander Popov, Georgi Chernev

University of Chemical Technology and Metallurgy, bul. Kliment Ohridski 8, Sofia, Bulgaria

### Abstract

*The cement industry, like the rest of the construction industry, is facing unprecedented challenges related to energy resources, CO<sub>2</sub> emissions and the use of alternative materials. Globally, the cost of energy is rising inexorably as fuel sources are depleted. This is a clear, traceable impact on the cost of cement production and its market price. Green taxes are additional costs that arise if emissions are not limited and could potentially lead to a doubling of the price of cement by 2030. Investigating the influence of various factors on the properties of Portland cement by separately grinding limestone with high specific surface area requirements and a grain size composition to be mixed with coarser ordinary Portland cement obtained by co-grinding clinker and gypsum under industrial conditions. Expected benefits are lower clinker/cement ratio, reduced carbon footprint, electricity savings, higher early strength, lower product cost.*

**Keywords:** *blended cement, limestone, grinding, environmental*

### 1. INTRODUCTION

The Cement Initiative for Sustainable Development, developed by the World Business Council for Sustainable Development, brings together major cement producers from around the world to try and tackle this problem [1]. Due to concern for the environment and energy efficiency, there is a growing interest in the development of blended Portland cement in which the amount of clinker is reduced and partially replaced by mineral additives. There are three main motivators behind these efforts: (1) environmental benefits, as a result of lower CO<sub>2</sub> emissions into the atmosphere, (2) economic benefits, as cement with reduced clinker content is cheaper to produce, and (3) scientific / technological advantages based on improved cement and concrete qualities. There are two main types of mineral admixtures: (1) pozzolanic admixtures such as fly ash, slag, and metakaolin [2-4] and (2) materials that are not considered pozzolanic generally have low reactivity with cementitious minerals. Of the latter type, limestone is one of the most attractive additives because it is considered natural, affordable and economical. Several studies have shown that cement mixed with limestone had improved initial compressive strength with lower setting time compared to the original cement, i.e. without added limestone [5-7]. The addition of fine inert limestone powder, whose specific surface area is greater than that of clinker, increases the early age rate and generated heat of hydration [6]. The properties of cement are explained by the effect of density, which is defined as the ratio between the volume of the solid phase and the total volume of the system. The inclusion in the system of particles with an improved particle size gradation leads to an increase in density and thus reduces porosity [8].

The aim of the present work is to investigate the influence of various factors on the properties of Portland cement by separately grinding limestone with high requirements for specific surface area and grain size composition and mixing it with coarser cement obtained by co-grinding clinker and gypsum in industrial conditions. Expected benefits are: lower clinker/cement ratio, reduced carbon footprint, electricity savings, higher early strength, lower product cost.

## 2. EXPERIMENTAL

The clinker used in the industrial tests was produced in the same plant by the dry method in a rotary kiln with a heat exchange tower (Table 1). The industrial gypsum used was obtained from TPP Maritsa East (table 2).

Table 1 - Chemical composition of the clinker used in the experiment.

Oxides	
SiO <sub>2</sub>	21.49
Al <sub>2</sub> O <sub>3</sub>	4.46
Fe <sub>2</sub> O <sub>3</sub>	4.16
CaO	65.83
MgO	1.73
SO <sub>3</sub>	0.51
K <sub>2</sub> O	0.62
Na <sub>2</sub> O	0.27
C <sub>3</sub> S	62.26
C <sub>2</sub> S	14.64
C <sub>3</sub> A	4.78
C <sub>4</sub> AF	12.65
LSF	96.65
SM	2.50
AM	1.07
freeCaO	1.60

Table 2 - Indicators of gypsum used in industrial tests.

Gypsum	SO <sub>3</sub>	Humidity,%	LOI
	45.32	8,20	21.2

In table 3 are presented the receipt of studied compositions.

Table 3 - Ratios Clinker – Gypsum – Limestone

	Clinker,%	Gypsum,%	Limestone,%
	96.0	4.0	<b>0</b>
<b>Composition 1</b>	76.5	3.5	<b>20</b>
<b>Composition 2</b>	71.5	3.5	<b>25</b>
<b>Composition 3</b>	66.5	3.5	<b>30</b>
<b>Composition 4</b>	68.0	4.0	<b>28</b>

The obtained samples are subjected to the following analyses:

-Sieve analysis; -Determination of the Blaine specific surface area; - Determination of the standard consistency; - Time binding; - Compressive strength test.

## 3. RESULTS AND DISCUSSION

Results of the analysis carried out for specific surface area and sieve residue of the ground limestone and added in different dosages in the cement mixture are shown in table 4.

Table 4 - Specific surface area and sieve residue of ground limestone UFL

Parameter	Composition 1	Composition 2	Composition 3	Composition 4
Specific surface area	10787	10725	10613	10176
Sieve residue 90 $\mu\text{m}$	0	0	0	0
Sieve residue 45 $\mu\text{m}$	6.0	5.1	6.0	5.3
SO <sub>3</sub>	0.22	0.25	0.33	0.26
CaO	54.57	54.49	54.52	54.51
SiO <sub>2</sub>	0.27	0.26	0.33	0.29

Table 5 - Results of the sieve residue, specific surface area, standard consistency and binding period.

	90 $\mu\text{m}$	45 $\mu\text{m}$	Blaine	Standard consistency	Binding period	
Control	0.3	4.1	3312	27.4	210	275
Composition 1	0.5	3.4	4361	27.8	130	175
Composition 2	0.4	3.1	4669	28.2	125	170
Composition 3	0.2	2.7	5062	28.0	110	155
Composition 4	0.3	3.3	5080	27.4	110	170

The results shows that as the UFL content in the cement mixture increases, the sieve residue at 45  $\mu\text{m}$  decreases and the specific surface according to Blaine increases. The water required to reach the normal consistency also increases. Also, as the UFL content in the cement mixture increases, both the start and end setting times decrease.

Table 6 show that the addition of 20% UFL to the cement mixture (formulation 1) improves the early strengths of the cement mixture compared to the sample without added UFL but lowers the ultimate strengths at day 28 by about 5%.

Table 6 - The results of the tensile strength tests performed on all samples.

	1 day	2 day	7 day	28 day
Control	16.3	26.5	44.6	61
Composition 1	20.1	31.5	46.4	57.9
Composition 2	16.2	24.9	42.6	50.8
Composition 3	15.3	23.9	41.1	48.5
Composition 4	13.8	25.3	40.8	46.3

The table clearly shows that as the limestone content increases, the initial and ultimate strengths decrease, with (recipe 4) showing a decrease in ultimate strengths of about 24% compared to the sample without added limestone.

#### 4. CONCLUSIONS

It is clear that cement, in all its different types and forms, is a vital product which, when combined with other ingredients in the right proportion, makes it a key building material. The demand for cement is high and growing as it knows no bounds and this looks set to continue for the foreseeable future. To ensure sustainable, cost-effective, yet profitable cement production, the industry needs to change. The two most important challenges facing industry are the urgent need to reduce CO<sub>2</sub> emissions and improve energy efficiency. The most effective methods for producing green,

ecological, and economically sustainable cements of the highest quality are the use of alternative, low-carbon fuels and the development of new cement formulations and production methods.

Using limestone in cement as a replacement for clinker offers a reduction in CO<sub>2</sub> emissions by requiring less raw materials and therefore burning less fuel to produce clinker.

From the experiments carried out in this study, the following conclusions can be drawn: that the addition of 20% UVB to the cement mixture improves the early strengths of the cement mixture compared to the sample without added UVB, but lowers the ultimate strengths at day 28 by about 5%. As the limestone content increases, the initial and ultimate strengths decrease, showing a decrease in ultimate strengths of about 24% compared to the sample without added limestone.

## ACKNOWLEDGEMENTS

*This study has been supported by the project BG05M2OP001-1.001-0008: National Centre of Mechatronics and Clean Technologies, funded by Operational Programme for Science and Education for Smart Growth at EU Funds.*

## REFERENCES

- [1] OECD/IEA and the World Business Council for Sustainable Development, Cement Technology Roadmap, 2009.
- [2] Hubler M., Thomas J., Jennings H. Cem. Concr. Res. 2011;41:842–6.
- [3] Siddique R. Cem. Concr. Res. 2003;33:539–47.
- [4] Chindapasirt P., Jaturapitakkul C., Sinsiri T. Constr. Build. Mater. 2007;21:1534–41.
- [5] Vuk T., Tinta V., Gabrovsšek R., Kaučič V. Cem. Concr. Res. 2001;31:135–9.
- [6] Kadri EH, Aggoun S, De Schutterk G, Ezziane K. Mater. Struct. 2010;43:665–73.
- [7] Lv H, Jia F, Cheng Y, Yang J. Adv. Mater. Res. 2011;168:1449-54.
- [8] Stovall T, DE Larrard F, Buil M. Powder Technol. 1986;48:1–12.
- [9] Annual project for mining and primary processing of limestone and marl from "Zlatna Panega" quarry 2021.

## ROCKS OF OBAFEMI AWOLOWO UNIVERSITY AND ENVIRON, NIGERIA: STRUCTURAL ANALYSIS OF GEOLOGICAL CONTACT

Daniel Ogochukwu Okanigbe<sup>1</sup>, Shade Rouxzeta Van Der Merwe<sup>2</sup>

<sup>1</sup>Department of Chemical, Metallurgical and Materials Engineering, Faculty of Engineering and the Built Environment, Tshwane University of Technology, South Africa. 0183

<sup>2</sup>Department of Mechanical Engineering and Mechatronics, Faculty of Engineering and the Built Environment, Tshwane University of Technology, South Africa. 0183

### Abstract

*In order to ascertain the nature of deformation at the contact between the migmatite gneiss complex and rocks of the study area's schist belt, structural data were gathered during a geological mapping exercise. According to field data, the region experienced three periods of deformation known as D1, D2, and D3. When compared to the foliation (S1), which is flat-lying and marked by millimeter-scale mineralogical banding in the schist, D1 is an isoclinal fold in the migmatite gneiss complex. As part of the migmatite gneiss complex, D2 is exposed to tight folds (F2) that folded S1 and refolded F1 into folds whose axes constituted a lineation. In the schist, D2 has tight, upright folds that are isoclinal and open, affecting D1 and producing steeply dipping foliation (S2) that is often parallel to S1. D3 is a shear deformation that produced several drag folds and mylonite of a quartzite in the migmatite gneiss complex and schist. The rocks of the schist belt entirely encircle the migmatite gneisses on the Obafemi Awolowo University campus, and the structural characteristics point to a dome structure. Most likely the results of big scale fold interference.*

**Keywords:** Migmatite–gneiss, Mica schist belt, Nigerian Precambrian basement complex, structural geology

### 1. INTRODUCTION

The Nigerian Precambrian Basement Complex (NPBC) is located in the Pan-African mobile belt, which runs between the West African and Congo cratons in the regional geologic environment. The belt was classified into four major regions by Ajibade and Fitches (1988): The Pan-African mobile belt, which in the local geologic setting stretches between the West African and Congo cratons, is where the Nigerian Precambrian Basement Complex (NPBC) is found. According to Ajibade and Fitches (1988), the belt is composed of the following broad regions:

- “The frontal region, on the craton's eastern edge in West Africa”.
- “The interior region, which appears to have undergone minimal sedimentation during the Pan-African orogeny before being reactivated and invaded by granitoids”.

The NPBC, as seen on Figure 1, is situated inside the Pan-African mobile belt, according to Caby et al. (1981). According to Rahaman (1988), the NPBC contains six major kinds of rocks. Those are:

- The migmatite-gneiss quartzite complex, which also contains quartzite, quartz schist, biotite and biotite hornblende gneisses as well as small lenses of calc-silicate rocks.
- Slightly migmatized to migmatized paraschists and metaigneous rocks are referred to as younger metasediments, as well as schist belts and as newer metasediments.
- Charnokitic, gabbroic, and dioritic rocks.



- Potassic syenites, older granites, and rocks with compositions ranging from granodiorite to real granites are included in this category of rocks.
- Rocks that have completed metamorphism to their unmetamorphosed state, such as calc-alkaline volcanic and hypabyssal rocks
- Dolerite dykes, such as the oldest basic dykes and syenites dykes that have not undergone transformation.

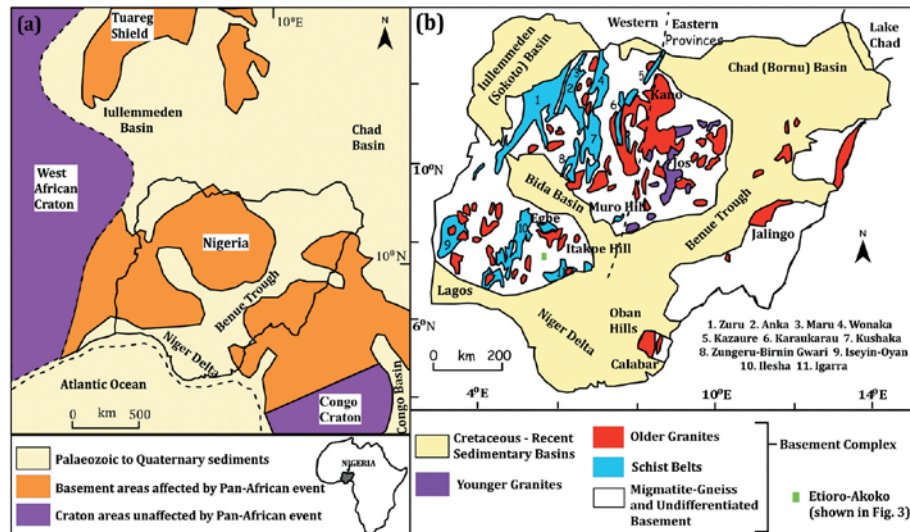


Figure 1 - (a) Regional geological map of Nigeria within the Pan-African mobile belt (b) geological map of Nigeria (Akingboye and Osazuwa, 2021)

The Ife-Ilesha Schist Belt is one of many Schist Belts, according to Turner (1983). He asserts that the initial sediments of the ife-ilescha schist belt were deposited in a synclinal basin with a trend from north-northeast to south-southwest. Although the Ife-Ilesha schist belt has been the subject of several studies, little is known about the type of deformation that took place between the schist and gneiss there. Due to this knowledge gap, this research was necessary, and it was made possible because of the exposed geological structures that were discovered after a road cut through the study area. This made it possible to gather data that would help scientists better understand the nature of deformation that took place along the contact between these two groups of rocks.

## 2. METHODOLOGY

On the research region, a thorough geological mapping exercise was conducted. Different rock types were encountered and studied during the field work. A scale of 1: 50, 000 was used for the traverse method of geological mapping, and the global positioning system (GPS) assisted with precise location of outcrops on the topographic base maps. The topographic map also includes orientation measurements and geologic connections. Samples of heads were taken in order to conduct additional study.

## 3. RESULTS

### 3.1 Structural Analysis of Mica Schist

Away from the boundary with the migmatite – gneiss complex, in the direction of Osu town (i.e. Obafemi Awolowo University's environ), S1 foliation in the schist can be seen in outcrops exposed by road cuts. It was probably produced by millimetric mineralogical banding, in which dark bands rich in biotite alternate with light bands rich in quartz and feldspar (Figure 2a). The large-scale

isoclinal folds with shallow dips of foliation observed in the inner parts of the orogeny (e.g. western side of the ife-ilesha area) are believed to be associated with the production of D1 nappes. During the beginning of the second deformation (D2), planar structures (i.e. pinch and swell) that are sub-parallel to the S1 surface with direction of 270° were produced (Figure 3). As conditions probably changed, F1 was refolded, to give varying styles from open tight to isoclinal upright folds. S1 was reoriented to a surface combination of S1 and S2 that is steeply dipping (Figure 2a). The third episode of deformation is a shear deformation as was observed in the granite gneiss. It resulted in wide spread drag folds especially in the coarse grained mica schist. Associated with this deformation is a mylonite of a quartzite (D3 deformation).

### 3.2 Structural Analysis of Migmatite-Gneiss Complex

The first episode of deformation recognized in both grey gneiss and granite gneiss designated as D1, is represented as centimetric isoclinal folds (F1) whose axial surface are parallel to the foliation. This foliation is marked by mineralogical banding in which bands rich in biotite alternate with bands rich in quartz and feldspar (Figure 2b). This is the oldest metamorphic surface recognized and it is here designated as S1. The second episode of deformation (D2) is a folding phase. The axes of this folds define a lineation L1, which plunge about 36° to the south. In the granite gneiss, F2 open folds were observed to have axes perpendicular to S1 foliation (Figure 2b). The third episode of deformation (D3) is a shearing deformation. It is seen in granite gneiss outcrops on OAU campus. It is represented by widespread drag folds due to displacement along the shear plane. The sense of motion is dextral.

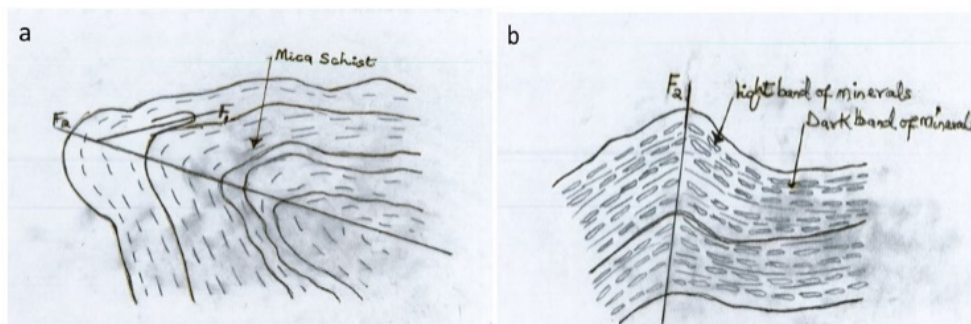


Figure 2 - a) F2 Isoclinal fold and refolded F1 folds in the schist b) F2 open fold in a granite gneiss whose axis is oblique to the foliation (S1), located behind Mozambique hall in O.A.U

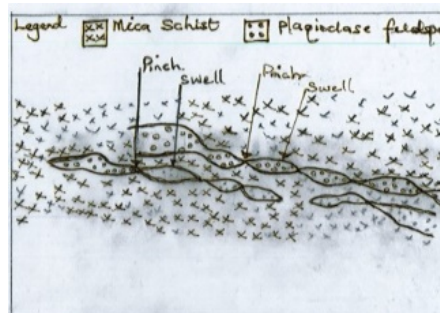


Figure 3 - D2 pinch and swell structure sub parallel to the foliation (S1) exposed along the new Ife-Ilesha by-pass.

## 4. DISCUSSION AND FINDINGS

### 4.1 Discussion on nature of geologic contact between Migmatite-Gneiss and Mica Schist

The idea of a forceful intrusion will mean the migmatite gneiss was originally a granitic body that powered its way through the overlying metasediments. The problem with this hypothesis is that the migmatite-gneiss is older than the schist of the study area that is on the basis of available geochronological data, reported by Grant (1970). Eskola (1949) described a mantle gneiss dome as a core of granitic migmatite or gneiss overlain by a layered metasedimentary or metavolcanic cover or “mantle”. He added that the core rocks in the central positions of some domes have an igneous microstructure, but near to the contact with the mantle they are foliation and this foliation, the contact and the layering in the mantle are all parallel to one another and generally dip outward away from the gneiss core, in such a way that they define a dome (Figure 4). The interaction of the migmatite gneiss with the mica schist of the study area produces an “egg box” or dome and basin pattern (Ramsay 1967).

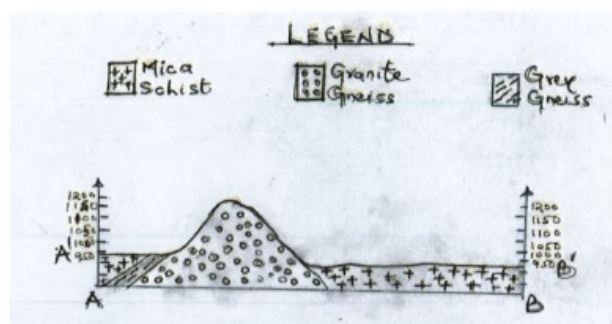


Figure 4 - Cross section of the study area's geological map

### 4.2 Findings from Structural Analysis of Contact between Migmatite-Gneiss and Mica Schist

#### Migmatite-gneiss

- D1 isoclinal folds whose axial surface are parallel to the S1 foliation (mineralogical banding).
- D2 open to tight folds (F2) that fold S1 and refolded F1. The axes of the folds define a lineation.
- D3 is a shear deformation

#### Mica Schist

- D1 isoclinal folds associated with a flat lying foliation (S1), defined by millimetric mineralogical banding.
- D2 open tight to isoclinal upright folds that affected S1 and produced steeply dipping foliation (S2), generally parallel to S1.
- D3 is a shear deformation that gave rise to wide spread drag folds and mylonite quartzite

## 5. CONCLUSIONS

This study's goal is to identify the type of deformation occurring at the contact between the migmatite gneiss and the schist belt in the studied area, afterwards infer its origin. According to field data, the region saw three periods of deformation known as D1, D2, and D3. The structural

diversity seen along the geological contact between the two rock types is better explained by the interference fold pattern theory.

### **ACKNOWLEDGEMENT**

The author appreciates department of applied geology and geophysics, Obafemi Awolowo University, Ile-Ife, Osun state, Nigeria, for allowing use of facilities to execute this study.

### **REFERENCES**

- [1] A.C. Ajibade, W.R. Fitches, Precambrian geology of Nigeria, 1 (1988) 45-53.
- [2] R. Caby, J.M. Bertrand, R. Black, Precambrian geology. 4 (1981) 407-434.
- [3] M.A. Rahaman, Precambrian geology of Nigeria, (1988) 11-41.
- [4] A.S. Akingboye, I.B. Osazuwa, J. Astron. Geophys., 10(1) (2021) 43-57.
- [5] D.C. Turner, J. Precambrian Res. 21(1-2) (1983) 55-79.
- [6] N.K. Grant, EPSL, 10 (1970) 29-38.
- [7] P.E. Eskola, Q. J. Geol. Soc., 104(1-4) (1948) 461-476.
- [8] J.G. Ramsay, Folding and fracturing of rocks. Mc Graw Hill Book Company, (1967) 568.

## STUDY OF THERMALLY TREATED ZEOLITIC TUFFS OF SERBIA , DEPOSITS "ZLATOKOP" AND "OPĆIŠTE"-BEOČIN

Vladan Kašić, Ana Radosavljević Mihajlović, Jovica Stojanović,  
Slavica Mihajlović, Melina Vukadinović, Natasa Djordjević, Ivana Jelić<sup>1</sup>  
Institute for Technology of Nuclear and Other Mineral Raw Materials, Franchet d'Esperey 86,  
Belgrade, Serbia

### Abstract

*Zeolites are a group of natural and synthetic inorganic compounds. They have specific physicochemical properties suitable for industrial application [1,2]. According to their origin, variety of chemical composition, structural characteristics and application, zeolites form a specific group of minerals within the tectosilicates. In sedimentary formations rich in zeolites, the most characteristic minerals that are present are: clinoptilolite/hailandite, chabazite, mordenite, erionite, phillipsite and analcime. The most widespread zeolite of sedimentary origin is represented by the HEU series (clinoptilolite-heylandite). Its general crystal chemical formula is  $(Na,K,Ca)_6Al_6Si_{30}O_{72}nH_2O$ . Based on chemical and X-ray powder diffraction analysis, it is not possible to separate clinoptilolite and hoylandite . This is due to their isostructural nature. To identify these two isostructural minerals, even today, the simplest so-called Mampton's test [3]. Mumpton [4]. The results of X-ray diffraction analysis of thermally treated clinoptilolitic tuffs from the Zlatokop and Beočin deposits will be presented in this paper. The interplane distance values will be shown in the characteristic temperature range from 400°C to 500°C (when the first polymorphic transition occurs). These values characterize the zeolitic tuffs of our deposits in a certain way.*

**Keywords:** zeolitic tuff, X-ray powder analysis, thermal stability

### 1. INTRODUCTION

Zeolites are tectro aluminosilicates in which  $(Si, Al)O^4$  tetrahedra build secondary building units (SBU). By connecting with each other, they form characteristic configurations of four-membered, five-membered, six-membered and eight-membered single or double rings. In doing so, they create cavities in which there are cations and water molecules, which have a significant degree of mobility. This allows cation exchange and reversible dehydration. Based on their spatial, chemical and structural characteristics, natural zeolites are systematized into 13 composite series. Within them, 82 minerals have been defined so far [5] In sedimentary formations rich in zeolites, the most characteristic minerals present are clinoptilolite/heylandite, chabazite, mordenite, erionite, phillipsite and analcime.

The main deposits of this raw material are present in all parts of the world. The largest production of this raw material is in the USA, Japan, Jordan, Iran, Korea, Slovakia and Turkey. Demand for this raw material is growing year by year, production is expected to increase by 10% per year. The most important properties of zeolite minerals are absorption capacity, ion exchange processes and catalysis. The very selectivity of the zeolite for the appropriate cations will depend on the basic crystal-chemical and structural properties of each zeolite. It can be defined as a measure of the preference that the exchanger shows for one ion in relation to another. The amount of exchangeable cations or cation exchange capacity depends on the crystal-chemical and structural composition of the zeolite itself (expressed in mmol M<sup>+</sup>/100g) [5,6].



The deposits of zeolitic tuffs in the area of the former Yugoslavia are spatially related to volcanogenic-sedimentary rocks in the area of the Serbo-Macedonian massif and the outer Dinarides. They were formed in sediments of marine or lake origin, of Senonian and Neogene age. They were created as a product of devitrification of volcanic glass. The lake environment had a great influence on the diagenesis of sediments and the formation of clinoptilolite at the expense of volcanic glass. The most important deposits in the Republic of Serbia are Beočin (Fruškogorsk basin), Zlatokop (Vranje basin), Igroš (Kopaonik slopes), Toponica and the Slanci locality (Danube key, near Belgrade) [2].

## 2. MATERIAL AND METHODS

For mineralogical and crystallographic tests, tuff samples with a grain size of  $\leq 63 \mu\text{m}$  were used. Quantitative chemical analysis was performed using the silicate analysis method [5]. The content of  $\text{SiO}_2$  and LA (loss on annealing at 105 and 1000°C) were determined gravimetrically. Diffractograms of thermally treated zeolite samples were recorded in the angle interval  $2\theta$  from 4 to 35°, with a step of 0.02. The morphology of the examined zeolites was analyzed using a scanning electron microscope JEOL 840A (Joel, Japan). Crystallinity tests of zeolitic tuff after annealing were performed in the temperature range from 300 to 750°C, in a time interval of 2 h. The annealed material was examined using the X-ray powder diffraction method on a polycrystalline sample.

Thermal analyzes were performed on the "Netzsch STA 409EP" apparatus. The samples were thermally treated in the range from 25°C to 1000°C. They were tested at a heating rate of 5°C/min, in a static air atmosphere.  $\text{Al}_2\text{O}_3$  was used as a reference sample. Previously, the samples were first weighed on an analytical balance in 100 mg increments.

## 3. DTA/DTG ANALYSIS OF ZEOLITIC TUFF

The basic structural motif of the zeolitic network of the minerals clinoptilolite and heylandite is basically identical. That is why it is very difficult to distinguish them from each other. These two minerals are isostructural. They differ in the Si/Al atomic ratio, the arrangement and content of off-lattice cations, and based on thermal stability at certain temperatures. During thermal treatment, clinoptilolite is shown to be a more stable form. The polymorphism of heylandite consists in visible lattice vibrations after minimal heating to  $230^\circ\text{C} \pm 10^\circ\text{C}$  [4].

Heylandite is present in two structural forms: Heylandite type 1 at temperatures of about 400°C and above. Then we have a polymorphic transition to phase B. Sometimes this transition is quite slow, and phase B is stable even at room temperature. Another structural form is Heylandite type 2, which represents a polymorphic transition from phase A to phase B at higher temperatures than 400°C. At the same time, phase B is not stable at room temperature and changes to phase A [4]. Based on chemical and X-ray powder diffraction analysis, it is not possible to separate clinoptilolite and hoylandite, due to their isostructural nature. To identify these two isostructural minerals, the simplest is the so-called Mumpton's test [4, 1, 2]. Mumpton defines clinoptilolite as a more stable form compared to heylandite, whose structure remains unchanged up to a temperature of 700°C. Polymorphic changes in heylandite begin already at a temperature of 350-400°C. Therefore, an experimental test is introduced to distinguish them. It is performed by X-ray examination and comparison of the powder diagram after heating to a temperature of 350-400°C. If there is no change in the interplane distances of the diffraction line (020), it is clinoptilolite, and on the contrary, hoylandite. Comparative diffractograms of thermally treated zeolitic tuff powder in the temperature range from 300 to 650°C are shown in Figure 1.

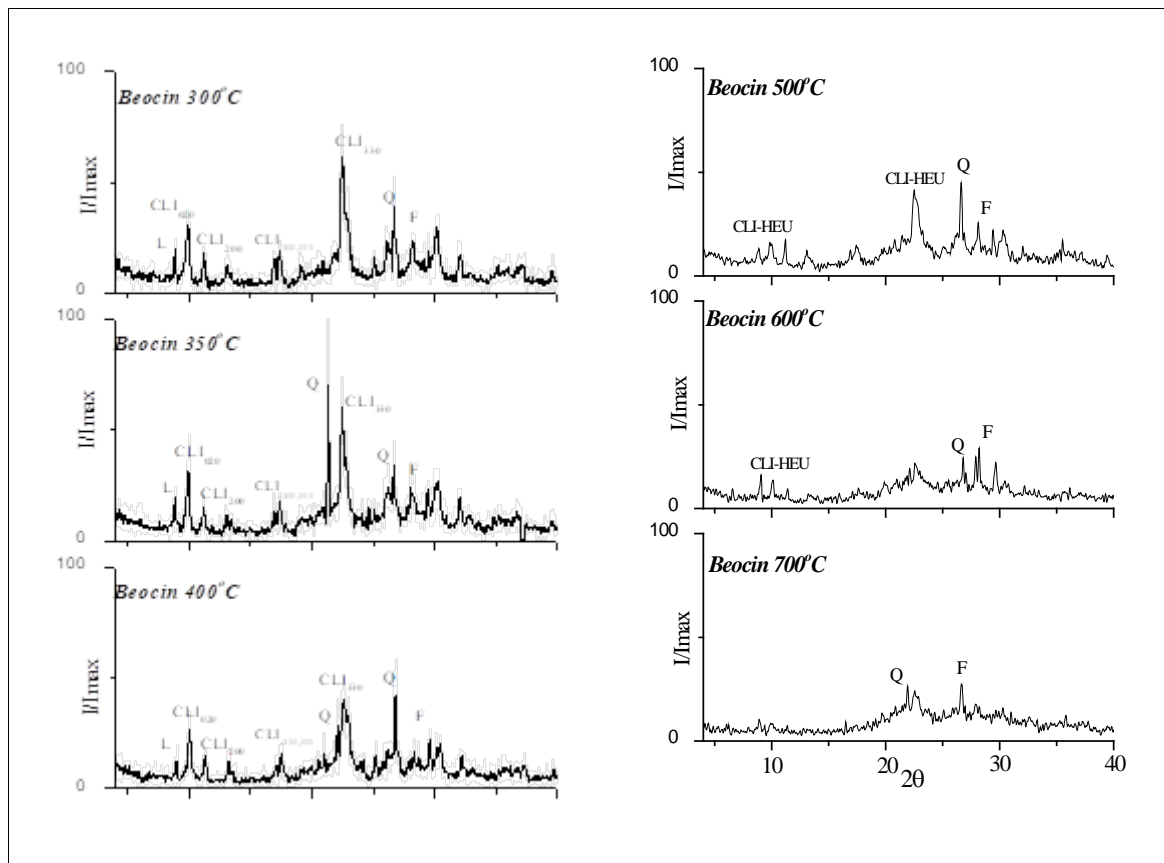


Figure 1 - Comparative X-ray diagrams of the powder of thermally treated clinoptilolite tuff of the Opčište-Beočin deposit (HEU-type zeolites, CLI-clinoptilolite, Q-quartz, F-feldspars).

Structural tests of the thermal stability of zeolitic tuffs were performed by annealing the samples in the temperature range from 300°C to 750°C, in a time interval of 2 hours. The annealed samples were examined by X-ray. The (020) reflection at the  $2\theta$  angle of about  $9.90 \text{ \AA}$  was used to determine the thermal stability field. The d-values of the 020 reflection were observed in the characteristic temperature range of 300-500°C. Comparative diagrams of X-ray powder analysis of thermally treated clinoptilolitic tuffs are shown in Figures 1 and 2. [5].

Based on the comparative diagrams (Figures 1 and 2), if the initial and thermally treated samples up to 400°C are observed, the structural stability of both zeolitic tuffs is observed. At these temperatures, dehydration processes are related to the weakest coordinated water, in channel A. At a temperature of 500°C, further dehydration was achieved related to water coordinated by cations in position M2, channel B. It could be said that the structure of the Zlatokop zeolite tuff is still stable. The structure of Beočin zeolite is disturbed. A polymorphic transition to the heulandite structure is present. At temperatures higher than 600°C, the zeolitic tuff of the Zlatokop deposit is more stable. Its structure is still present with appropriate reflections. The zeolite structure of the Beočin deposit is completely destroyed at these temperatures. At higher temperatures, due to the



presence of minerals of the tectosilicate group (feldspar and quartz), the formation of feldspathoid structures occurs.

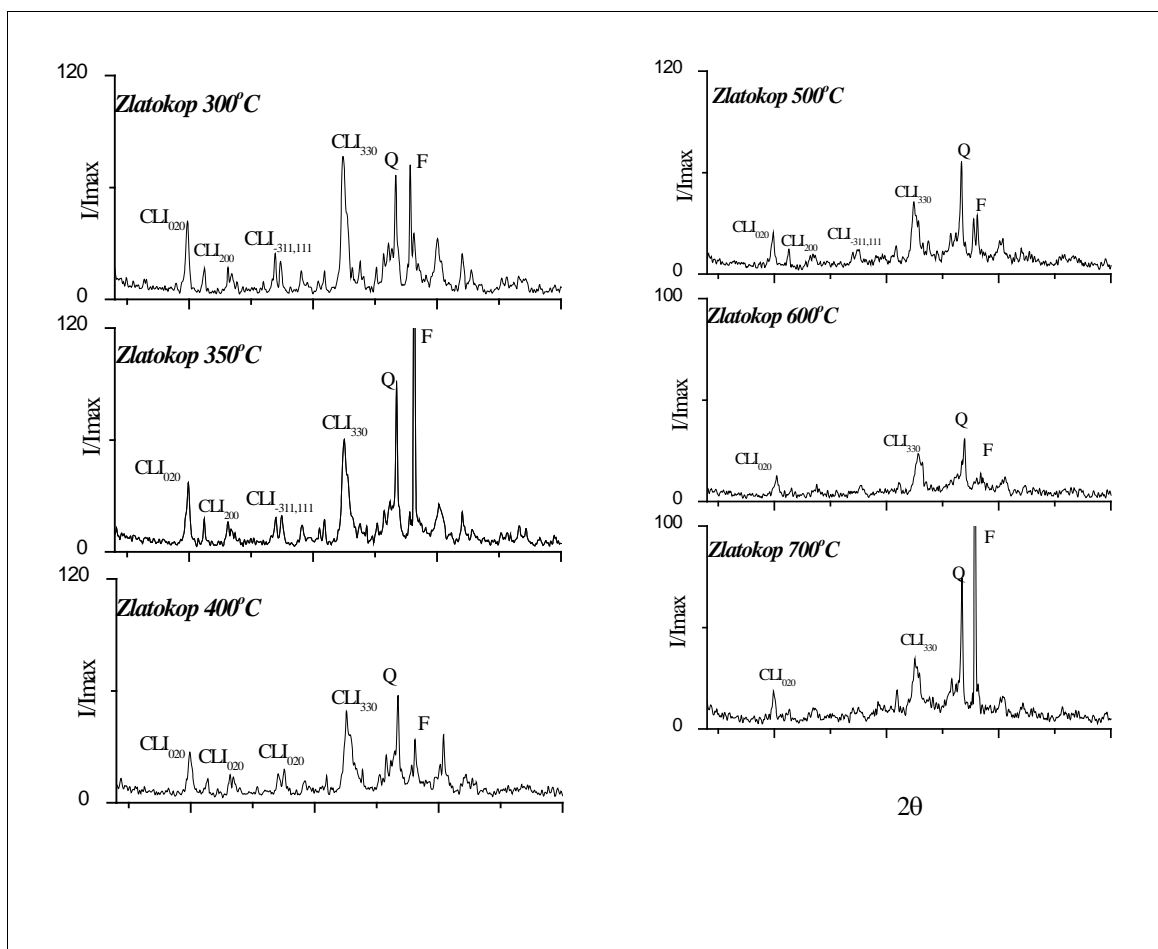


Figure 2 - Comparative X-ray diagrams of the powder of thermally treated clinoptilolitic tuff of the Zlatokop deposit (HEU-type zeolites, CLI-clinoptilolite, Q-quartz, F-feldspars)

The interplane distance values were also observed in the characteristic temperature range from 400°C to 500°C. Then the first polymorphic transition occurs. In this temperature interval, the weakest bound water is lost. This loss of water is associated with changes that are most often manifested by changes in the values of interplane distances. Values for interplane distances for both zeolitic tuffs are given in table 1.

Table 1 - Values for interplane distances of thermally treated zeolitic tuffs of the Zlatokop and Opčište-Beočin deposits [5]

Treated zeolitic tuffs	Zlatokop d-value (Å)	Beočin d-value (Å)
<i>d</i> - initial	9.91	9.90
<i>d</i> - 400 ° C	9.85	9.83
<i>d</i> -500 about C	9.88	9.78

Based on literature data [7], the following was determined: at temperatures higher than 400°C, if there is a shift in the value of the interplane distance towards values from 9.90 to 9.80, it is

characteristic of clinoptilolite; if the values range from 9.90 to 9.60, then we are talking about the transitional form of clinoptilolite-hoylandite. Values below 9.60 correspond to the hoylandite phase. These values vary depending on both the ratio of network cations and the ratio of off-network cations in the structure of zeolitic tuffs. It is observed that the values of interplane distances in the temperature range from 400°C to 500°C, for the tuff of the Zlatokop deposit, range from 9.91Å to 9.88Å. These values are characteristic of the mineral clinoptilolite. The zeolitic tuff Beočin, according to its values of interplane distances from 9.90Å to 9.78Å, corresponds to the transition between the minerals hoylandite and clinoptilolite.

#### 4. CONCLUSION

Based on the above, it can be concluded that there are differences between the minerals of zeolitic tuffs during thermal treatment. They are most likely a function of the chemical and mineral composition, that is, the type and content of both offline and network cations. Based on the results of the Mumpton test (Figures 1 and 2), it can be concluded that the mineral Ca-clinoptilolite is present in the Zlatokop zeolite tuff deposit. The zeolitic tuff of the Općište-Beočin deposit corresponds to the transition between the minerals hoylandite and clinoptilolite.

#### ACKNOWLEDGEMENT

*The authors would like to thank the Ministry of Education, Science and Technological Development of the Republic of Serbia for supporting the research presented in the paper (contract no. 451-03-47/2023-01/200023)*

#### REFERENCES

- [1] Kašić V., Simić V., Životić D., Radosavljević-Mihajlović A., Stojanović J. (2017): Mineraloška i kristalohemijska svojstva minerala HEU-tipa i ležišta zeolitskih tufova Srbije, Hemijska Industrija 71 (1), Beograd, 49-60.
- [2] Kašić, V., Minerageny of zeolite tuffs of Serbia, Doctoral dissertation, RGF, Beograd, (2017), 168.
- [3] Mason B., Sand L. B., (1960): Clinoptilolite from Patagonia, the relation ship between clinoptilolite and heulandite, Am. Mineral. 45, 341-350.
- [4] Mumpton F. A., (1960): Clinoptilolite redefined, The American Mineralogist, vol. 45, March-April, Am. Mineral. 45, 351-369.
- [5] Radosavljević-Mihajlović, A., (2004): Characterization and stability of dealuminated clinoptilolitic tuffs from different deposits. Master's thesis, Faculty of Physical Chemistry, Belgrade, 123 p.
- [6] Radosavljević-Mihajlović, A., Stojanović, J., Kašić, V., Comparative mineralogical, crystallochemical and thermal properties of deposits of zeolite tuffs of Serbia rich in HEU-type minerals, Geoinstitut papers, Vol.40., (2005), 191 -200.
- [7] Treacy, M.M. and Higgins, J.B., (2001): Collection of simulated XRPD patterns for zeolites Structure. Commission of International zeolite Association, ELSEVIER, Amsterdam-London-New York-Oxford-Paris-Shannon-Tokyo, 184-186.

## ELECTROCHEMICAL BEHAVIOR OF COPPER IN CHLORIDE MEDIUM IN THE PRESENCE OF NETTLE EXTRACT

Vesna Grekulović<sup>1</sup>, Aleksandra Mitovski<sup>2</sup>, Milica Zdravković<sup>1</sup>,  
Nada Štrbac<sup>1</sup>, Milan Gorgievski<sup>1</sup>, Milovan Vuković<sup>1</sup>, Miljan Marković<sup>1</sup>

<sup>1</sup> Technical Faculty Bor, University of Belgrade, V.J. 12, 19210 Bor, Serbia,

<sup>2</sup> Engineering Dobersek GmbH, 41169 Moenchengladbach, Germany

### Abstract

*The use of plant extracts to inhibit copper corrosion is the subject of numerous scientific studies. This paper presents the results of research the electrochemical behavior of copper during oxidation in a 0.5 mol/dm<sup>3</sup> NaCl solution in the absence and presence of nettle extract (NE) in different concentrations. The electrochemical behavior of copper was investigated using the cyclic voltammetry and the potentiostatic method. The results of cyclic voltammetry showed that three current peaks appear on the anodic polarization curves, which correspond to the formation of copper chloride and copper oxide. Potentiostatic polarization was performed at 0 mV vs. SCE during 100 s at 25 °C. The potentiostatic curves indicate that the stationary currents decrease with increasing extract concentration in the electrolyte. Microphotographs confirmed that in the presence of NE, a protective layer was formed on the copper surface, which prevents the corrosion process.*

**Keywords:** copper, electrochemical behavior, chloride medium, nettle extract

### 1. INTRODUCTION

Copper has been for decades one of the most strategically important metals in the industry, because of its physical and chemical properties, which enable its wide range usage in numerous products of modern society. Copper corrosion and its inhibition in various environments are the subject of numerous scientific investigations [1-3]. Inhibitors are substances added in different concentrations to a given solution containing aggressive ions. They can be of the organic or inorganic origin. However, many inhibitors are toxic. Plant extracts as potential environmental corrosion inhibitors have become the subject of numerous scientific investigations in the last few years. Various plant parts can be extracted and used as metal corrosion inhibitors [3].

This paper presents the results of investigation the addition of nettle extract (in following text: NE) on the copper corrosion behavior in 0.5 mol/dm<sup>3</sup> NaCl solution.

### 2. EXPERIMENTAL

The experiments were carried out in a system consisting of an electrochemical cell and a hardware interface for computerized control and data acquisition. In a standard three-electrode electrochemical cell, the working electrode was made of copper, whose potential was controlled against a reference saturated calomel electrode (SCE). Platinum foil was used as a counter electrode. The computerized control (National Instruments card, NI-6251) and data acquisition software (LabVIEW 8.2 platform), fully developed at the Technical Faculty in Bor [4], were used to run the electrochemical experiments.

Investigation of the copper electrochemical behavior in 0.5 mol/dm<sup>3</sup> NaCl solution in the absence and the presence of NE was performed by recording the anodic polarization curves. The curves were recorded in the potential range of -0.4 V vs. SCE up to 1 V vs. SCE with a scan rate of 20

mV/s. The potentiostatic curves were recorded at 0 V vs. SCE for 100 s. Optical microscopy was used for the electrode surface characterization after potentiostatic oxidation.

The substances used for the preparation of the working solutions were NaCl (p.a purity), manufactured by d.d. "Zorka Pharma" Šabac and fresh nettles harvested in the vicinity of Bor. The NE was prepared as follows: 100 g of nettle was chopped and placed in 200 mL of 96% ethanol. After standing in ethanol solution for one month, the solution was filtered and the obtained nettle extract was stored in the refrigerator.

### 3. RESULTS AND DISCUSSION

Figure 1 shows the anodic polarization curves recorded for copper in 0.5 mol/dm<sup>3</sup> NaCl without and with NE of different volumes.

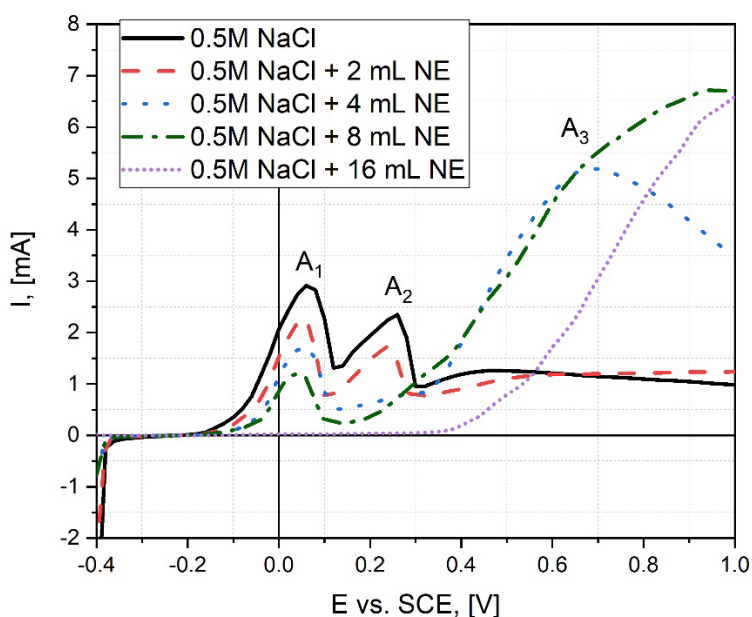


Figure 1 - Anodic polarization curves for copper with a scan rate of 20 mV/s in 0.5 mol/dm<sup>3</sup> NaCl with and without the addition of NE

On the anodic polarization curve, obtained for 0.5 mol/dm<sup>3</sup> NaCl, three current peaks appeared. They correspond to the formation of copper chloride and copper oxide [5, 6]. Comparing the anodic polarization curves for copper obtained in the presence of NE with the anodic polarization curve without the NE, it can be observed that the current values for the current peaks A1 and A2 in the presence of 2 mL, 4 mL and 8 mL NE are lower in relation to the current values without NE. The best inhibitory effect is achieved with the addition of 16 mL NE, as shown by the current values of the current peaks A1 and A2, which are approximately equal to zero. With the addition of 2 mL NE in the potential area where the current peak A3 appears, the current values are approximately equal to the current values without the addition. With the addition of 4 mL NE, a clearly defined current peak A3 appears, which represents the formation of copper oxide. In the presence of 8 mL and 16 mL NE, there is a sudden current value increase in the potential area where the current peak A3 appears, which indicates that there is a separation of oxygen and the formation of a certain amount of copper oxide.

Figure 2 shows the potentiostatic curves after the potentiostatic treatment of copper during 100 s in 0.5 mol/dm<sup>3</sup> NaCl without and with the addition of NE.

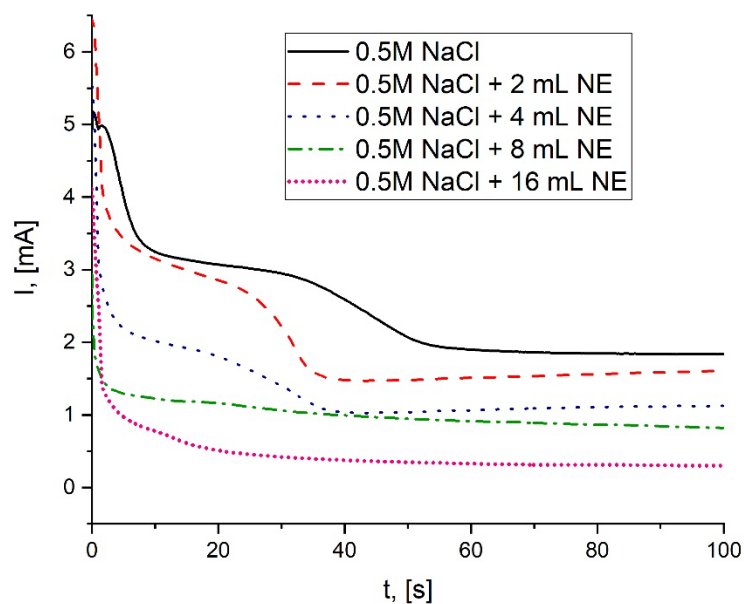


Figure 2 - Potentiostatic curves for copper in 0.5 mol/dm<sup>3</sup> NaCl without and with the addition of NE at 0 V vs. SCE

The current strength for copper in 0.5 mol/dm<sup>3</sup> NaCl without the addition of NE drops sharply in the first 8 s, then slowly decreases until about 55 s, after which it stabilizes. The value of the stationary current strength amounts to 1.838 mA. With the addition of 2 mL and 4 mL NE, there is a sudden drop in the current strength in the first 4 s, then it slowly decreases until about 40 s, after which there is a slight increase and stabilization. The value of the stationary current with the addition of 2 mL NE is 0.818 mA, and with the addition of 4 mL NE is 0.565 mA. The potentiostatic curve obtained for copper with the addition of 8 mL NE drops sharply in the first few seconds, then continues to decrease slightly and stabilizes at about 90 seconds, with the value of the stationary current strength being 0.536 mA. With the addition of 16 mL NE, the current drops sharply in the first seconds, after which it slowly decreases until about 60 s, and then it stabilizes and reaches the stationary current value of 0.499 mA. Based on the obtained results, it can be concluded that with an increase in the volume of NE, the stabilization of the current is achieved faster and the values of the stationary current are lower, which indicates that a protective layer is formed on the copper surface.

Analysis of the copper surface by optical microscopy was performed after the potentiostatic treatment of copper in the presence and in the absence of NE.

Figures 3a, 3b, 3c, 3d and 3e show microphotographs of the copper surface after potentiostatic treatment in a solution of 0.5 mol/dm<sup>3</sup> NaCl without and with the addition of NE. Figure 3a shows a microphotograph of the copper surface after potentiostatic treatment in 0.5 mol/dm<sup>3</sup> NaCl, where it is clearly seen that the surface is significantly damaged and that copper chlorides and copper oxide were formed on the surface during the oxidation process. In the presence of NE, a protective film is formed, which protects the copper surface from corrosion. As the volume of NE increases, the copper surface is less damaged and there is less presence of chlorides and oxides. With the addition of 16 mL NE only a black phase is present on the copper surface. This confirms the results obtained by the method of cyclic voltammetry, that the NE prevents the formation of copper chloride, and stimulates the process of copper oxide formation.

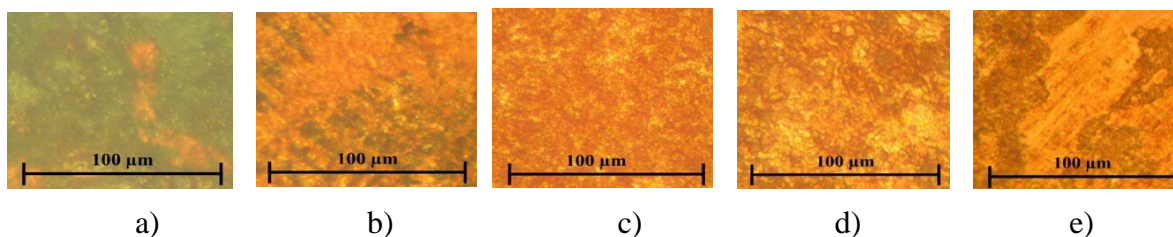


Figure 3 - Microphotographs of the copper surface after potentiostatic treatment on the potential of 0 V vs. SCE during 100 s: a) in 0,5mol/dm<sup>3</sup> NaCl; b) in 0,5mol/dm<sup>3</sup> NaCl + 2 mL NE; c) in 0,5mol/dm<sup>3</sup> NaCl + 4 mL NE; d) in 0,5mol/dm<sup>3</sup> NaCl + 8 mL NE; e) in 0,5mol/dm<sup>3</sup> NaCl + 16 mL NE

#### 4. CONCLUSION

Based on the performed experiments, the following conclusions can be drawn:

Investigation of the electrochemical behavior of copper using the cyclic voltammetry method in 0.5 mol/dm<sup>3</sup> NaCl, three current peaks appeared on the anodic polarization curve, which corresponds to the formation of copper chloride and oxide. In the presence of NE, the inhibitory effect is achieved in the area of copper chloride formation potential at all tested concentrations of NE, while in the area of copper oxide formation potential, NE acts as a corrosion activator. Potentiostatic tests show that the stationary current strength in the presence of nettle extract is significantly lower compared to the stationary current strength in 0.5 mol/dm<sup>3</sup> NaCl. Lower stationary current values in the presence of the extract indicate that a protective layer was formed on the copper surface, which prevents the corrosion process. With the increase of NE concentration, the values of the stationary current are lower. After the potentiostatic treatment of copper in 0.5 mol/dm<sup>3</sup> NaCl solution, the microphotograph of the copper surface shows that copper chloride and oxide are formed and that the copper surface is significantly damaged. In the presence of NE, damage on the copper surface is less noticeable and the copper chloride and oxide amount are decreased. As the concentration of the extract increases, the damage is less noticeable, which indicates that the NE provides good protection of copper against corrosion.

#### ACKNOWLEDGEMENTS

*The research presented in this paper was done with the financial support of the Ministry of Education, Science and Technological Development of the Republic of Serbia, within the funding of the scientific research work at the University of Belgrade, Technical Faculty in Bor, according to the contract with registration number 451-03-47/2023-01/ 200131.*

#### REFERENCES

- [1] M. Rajčić Vujasinović, V. Grekulović, Z. Stević, D. Dragulović, S. Dimitrijević, Bakar, 41 (2) (2016) 35-40.
- [2] M. Scendo, Corros. Sci., 50 (6) (2008) 1584-1592.
- [3] M. Sangeetha, S. Rajendran, T. S. Muthumegala, A. Krishnaveni, Mat. Prot., 52 (2011) 3-19.
- [4] Z. Stević, M. Rajčić Vujasinović, Hem. Ind., 61 (2007) 1-6.
- [5] T. Kosec, I. Milosev, B. Pihlar, Appl. Surf. Sci., 253 (2007) 8863-8873.
- [6] M. Pourbaix., Atlas d'équilibres électrochimiques, Gauthier-Villars et Cie, Paris, 1963.



## EFFECTS OF THE APPLICATION OF PYROPHYLLITE IN THE COMPOSITION OF PROTECTIVE COATINGS

Marko Pavlović<sup>1</sup>, Marina Dojčinović<sup>2</sup>, Muhamed Harbinja<sup>3</sup>, Atif Hodić<sup>3</sup>,  
Dragan Radulović<sup>4</sup>, Mirjana Stojanović<sup>5</sup>, Zagorka Aćimović<sup>5</sup>

<sup>1</sup> Innovation Center of Faculty of Mechanical Engineering, Belgrade, Serbia

<sup>2</sup> University of Belgrade, Faculty of Technology and Metallurgy, Belgrade, Serbia

<sup>3</sup> Innovation Scientific Development Center (INRC), AD Harbi Ltd., Sarajevo, B&H

<sup>4</sup> Institute for Technology of Nuclear and Other Raw Mineral Materials, Belgrade, Serbia

<sup>5</sup> Engineering Academy of Serbia

### Abstract

*In the paper, samples of protective coatings based on pyrophyllite were examined. The initial sample of pyrophyllite was obtained from the Parsovići deposit, Konjic, Sarajevo, AD Harbi BiH. Pyrophyllite samples were subjected to micronizing grinding to a filler grain size of 20 μm. XRD, SEM and optical microscopy methods were used to characterize the obtained fillers based on pyrophyllite. The optimal composition of protective coatings based on pyrophyllite and the manufacturing process were determined. The resistance of refractory coatings to the effect of cavitation was experimentally determined using the ultrasonic vibration method with a stationary sample according to the ASTM G32 standard. Based on the value of the cavitation rate, the analysis of the formation and development of damage to the surface of the samples, the possibility of applying a protective coating in the conditions of exploitation in which the occurrence of corrosion and cavitation is expected was assessed.*

**Keywords:** pyrophyllite, protective coatings, cavitation, cavitation resistance

### 1. INTRODUCTION

Pyrophyllite is a type of phyllosilicate mineral, from the group of layered silicates, based on a combination of two tetrahedral (T) and one octahedral (O) plates, containing no isomorphic substitution and therefore no layer charge. The basic 2:1 structure (T-O-T), with silicon in tetrahedral layer and aluminum in octahedral layer, is pyrophyllite (Al<sub>2</sub>Si<sub>4</sub>O<sub>10</sub>(OH)<sub>4</sub>). The layers are held together by weak van der Waals forces, which makes the mineral extremely soft. The hardness of pyrophyllite on the Mohs scale is 1-1.5. It is hydrophobic, electroneutral, and the pH value is between 7.5-8.5. It has the characteristic softness of phyllosilicate and crystalline structure, good grindability, low coefficient of thermal conductivity, low coefficient of linear thermal expansion. It has a great ability to stick and coat surfaces, a high melting point, high inertness, i.e. resistance to acids, alkalis and heating. The technology of processing pyrophyllite rocks is ecologically clean, and the products obtained from technological processing of pyrophyllite are not carcinogenic [3,4]. Research [5] showed the existence of a potential raw material base, which all influenced the choice of this non-metallic raw material for obtaining a wide range of products for various industrial branches [6-8]. One of the directions of research, the results of which are presented in this paper, was the application of pyrophyllite as a filler for refractory coatings. The aim of the test was to determine the quality of the coating and the



possibility of application for the protection of metal surfaces in conditions of wear, corrosion, cavitation and elevated temperatures.

## 2. EXPERIMENTAL

### 2.1 Materials

To investigate the possibility of using pyrophyllite as a filler in the composition of protective coatings, the initial sample of pyrophyllite rock from the Parsovići deposit, Konjic, Sarajevo, AD Harbi BiH, was ground to a grain size of 20  $\mu\text{m}$ . In the composition of protective coatings, the following were used (%): refractory filler based on pyrophyllite (80-85); binder based on epoxy resin (14-15); organic additives (1-1,2); organic solvent to a coating density of  $\rho=2.5\text{g/cm}^3$ . During the synthesis of the coating, all components from the composition of the coating were gradually added with constant mixing. For testing, the obtained protective coatings were applied in two layers to a metal plate, and then dried in the air for 60 min.

### 2.2 Methods

To determine the resistance properties of the obtained protective coatings based on pyrophyllite, the ultrasonic vibration method with a stationary sample according to the ASTM G32 standard [9] was applied. Testing methodology described in earlier works [5,7,8]. The aim of the test was to determine the quality of the coating and the possibility of application for the protection of metal surfaces in conditions of wear, corrosion and cavitation. Interval of exposure of samples to the effect of cavitation (min): 15; 30; 45; 60. The loss of coating mass as a function of cavitation time was monitored. The cavitation rate was determined as an indicator of the resistance of the coating under conditions of cavitation loads. The method of X-ray diffraction analysis was used to characterize the refractory filler. The morphology of the surface damage of the samples was monitored using scanning electron microscopy. Based on the value of the cavitation rate and the analysis of the morphology of the surface damage, the cavitation resistance of the tested protective coatings was determined.

## 3. RESULTS AND DISCUSSION

Figure 1 shows an XRD and SEM microphotograph of a filler based on pyrophyllite. Figure 1a shows that the mineralogical composition of the pyrophyllite-based filler sample is as follows: pyrophyllite, quartz, calcite, dolomite, with the most abundant minerals being pyrophyllite and quartz. Figure 1b shows a SEM microphotograph of the filler based on pyrophyllite, where it is clearly shown that this material occurs in irregular forms of different dimensions, with the presence of flaky aggregates.

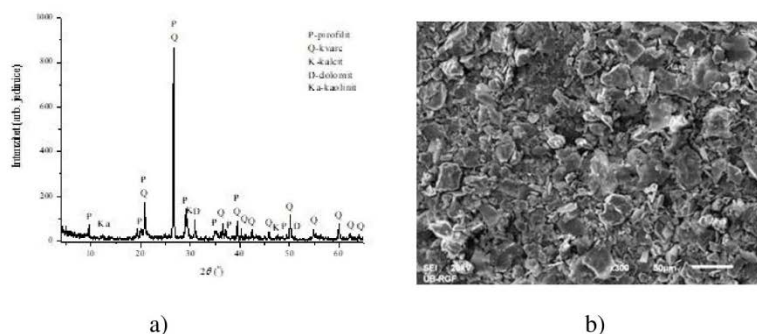


Figure 1 - Filler based on pyrophyllite: a) X-ray diffraction; b) SEM microphotograph.

Synthesized refractory coatings were applied to metal supports and tested for cavitation effects. Figure 2 shows the surfaces of the coating samples before and during the cavitation effect test. The appearance of a smaller number of dimples is observed after 30 min of exposure, which change slightly during further testing up to 60 min. The presence of shallow pits on the surface of the coating indicates minor damage to the surface of the coating, i.e. it shows satisfactory resistance of the surface of the coating to the effect of cavitation, Figure 3.

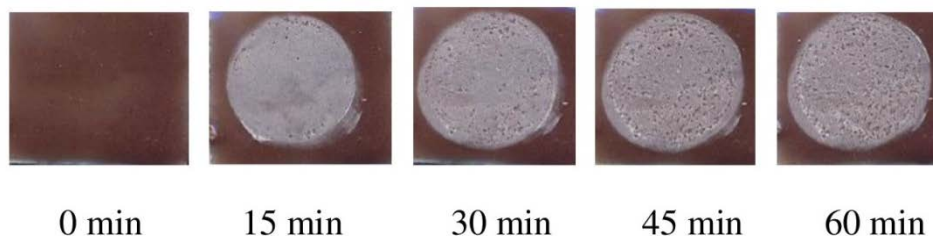


Figure 2 - Photographs of the surface of the coating samples before and during the cavitation test.

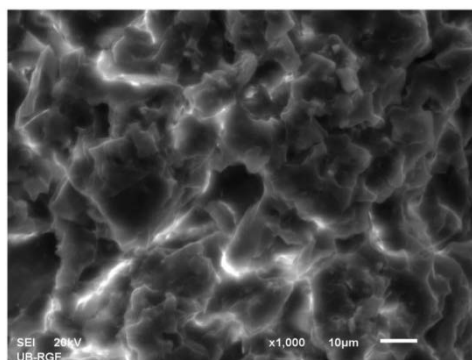


Figure 3 - SEM microphotograph of a pyrophyllite-based coating sample after 60 min of cavitation.

Figure 4 shows the cavitation rate diagram for pyrophyllite-based coatings. From the diagram it can be seen that there is no incubation period and that damage to the coating surface under the effect of cavitation begins immediately with the formation of small and shallow pits, which change slightly during exposure. Calculated cavitation rate was  $V=0.42$  mg/min.

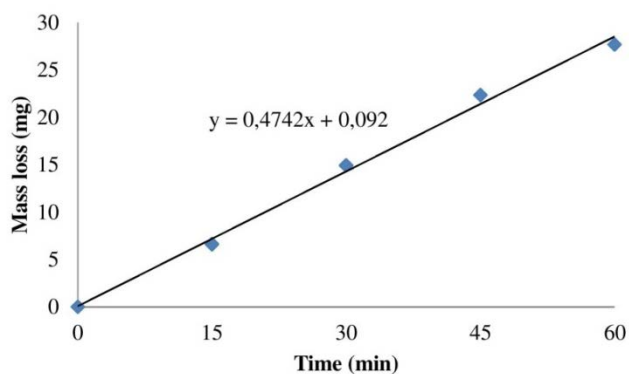


Figure 4 - Cavitation rate of pyrophyllite-based protective coating samples.

From the obtained research results, it can be estimated that the examined protective coatings based on pyrophyllite have a satisfactory resistance to cavitation.

#### **4. CONCLUSION**

These are the initial results of testing protective coatings based on pyrophyllite. Satisfactory resistance to the effect of cavitation has been demonstrated, which means that the coatings can be applied to protect metal structures in moderate cavitation conditions. In order to improve the rheological properties of the coating, to improve the stability of the coating in rigorous operating conditions, further research into the synthesis of the coating should be focused on changing the composition of the coating, applying new organic additives, and changing the procedures for making the coating.

#### **ACKNOWLEDGEMENTS**

*This work was supported by the Ministry of Science, Technological Development and Innovation of the Republic of Serbia (Contract No.451-03-47/2023-01/200135).*

#### **REFERENCES**

- [1] M.A. Ali, H.A.M. Ahmed, H.M. Ahmed, M. Hefni., Appl. Sci. 11, 2021, 11357.
- [2] P. Sanchez-Soto., Thermochim. Acta 138, 1989, 267–276.
- [3] Lj. Andrić, D. Radulović, M. Pavlović, M. Petrov, J. Stojanović., Journal of materials protection 61 (3), 2020, 210-219.
- [4] A. Terzic, D. Radulovic, M. Pezo, J. Stojanovic, L. Pezo, Z. Radojevic, L. Andric., Constr Build Mater. 258, 2020, 119721.
- [5] Elaborate on pyrophyllite research, University od Banja Luka, Faculty of Science, Banja Luka B&H (2018).
- [6] Lj. Andrić, M. Pavlović, M. Dojčinović, D. Radulović., Journal of materials protection 62 (2), 2021, 126-134.
- [7] M. Pavlović, M. Dojčinović, A. Sedmak, I. Martić, F. Vučetić, Z. Aćimović., Synthesis and characterisation of the mullite-based protective coatings, 53 IOC Bor 2022, 3-5 October 2022, Proceedings, pp. 147-150, ISBN 978-86-7827-052-9.
- [8] M. Pavlović, Z. Tanasković, M. Dojčinović, Z.Aćimović.,Quality managment of protective coating based on zirconium silicate, 13<sup>th</sup> International Scientific Conference Science and Higher Education in Function of Sustainable Development – SED 2023, VrnjačkaBanja, Serbia, Proceedings p.p. 54-58.
- [9] ASTM G32-10, Standard Test Method for Cavitation Erosion Using Vibratory Apparatus, ASTM International, West Conshohocken, PA, 2010, www.astm.org, n.d.

## MEASURES FOR THE PROCESSING OF IRON WITH A HIGHER INCOMING PHOSPHORUS CONTENT AT THE STEEL SHOP

Tamara Ristic, Nenad Milosavljevic, Dobrica Milovanovic

HBIS GROUP Serbia Iron & Steel doo Belgrade, Serbia

### Abstract

*Due to newly created conditions in the Market, which reduced the possibility of acquiring adequate raw materials, and in order to preserve the level and quality of the produced steel, our factory was forced to acquire lower quality raw materials. One of the main problems due to these conditions is the increased content of phosphorus. In accordance with production possibilities we have implemented some of the basic measures to remove phosphorus in the converter process. These measures are based on production of steel with casting of first-formed slag and formation of a new slag (double slag process), increasing the Basicity of converter slag by adding more calcite lime, increasing the FeO content in the slag by correcting the blowing height (soft blow) and achieving lower temperature at the end of the converter process with an increase in oxygen activity. This analysis is based on a period of 2 months, February and March of this Year. During the examination of the process, we came to the conclusion that we are getting optimal parameters that met our expectations.*

**Keywords:** converter, phosphorus, iron

### 1. INTRODUCTION

The content of individual elements in liquid iron, which is used for further processing at the Steel Shop, is of great importance. One of these elements is phosphorus, which belongs to harmful elements, and its content directly affects the possibility of producing some types of steel. If we know that when making steel, the target share of liquid iron is 80%, then it is clear why the phosphorus content in liquid iron must be as low as possible. Our Internal Standard for the quality of liquid iron stipulates that the maximum phosphorus content should not exceed 0.09%. This phosphorus content enables the Steel Shop to achieve the desired quality of steel in the slab through the prescribed procedures. If we start from the fact that all the phosphorus introduced in the process, with the raw materials in the blast furnace, almost all goes into liquid iron, then it is clear that the key factor for the desired phosphorus content in liquid iron is the selection of raw materials that participate in the blast furnace process. Contemporary events in the world have a great influence on many currents of social and economic life, including on events in metallurgy. Due to these newly created conditions, there was a disruption in the market, which reduced the possibility of acquiring adequate raw materials. Due to this situation on the market, our factory was forced, and in order to maintain the level of production, it acquires lower quality raw materials. One of the main problems that arose due to these conditions is the increased content of phosphorus. In order to preserve the level and quality of the produced steel, it was necessary to adjust the process technology.

For the reasons mentioned above, we have implemented some of the basic measures to remove phosphorus in the converter process.

These measures are based on:

- production of steel with casting of first-formed slag and formation of a new slag (double slag process)
- increasing the basicity of converter slag by adding more calcite lime

- increasing the FeO content in the slag by correcting the blowing height (soft blow)
- achieving lower temperature at the end of the converter process with an increase in oxygen activity

## 2. EXPERIMENTAL

In this paper, we will present the analysis of some of the achieved parameters related to the application of the measures we use to remove phosphorus in steel and at the same time we will discuss possible process improvements.

This analysis is based on a period of 2 months, February and March of this Year.

## 3. RESULTS AND DISCUSSION

According to the current state of raw materials, on Table 1 we have the following ferrous raw materials for the production of iron in blast furnace (BF).

Table 1 - Ferrous raw materials for the production of Iron in blast furnace

BF raw material	Content of P (%)
Sinter	0.050 -0.055
Pellets	0.011
Coarse ore	0.045
Metalic Add-ons	0.22
Fuel	0.04

For the controlled content of phosphorus in iron, ferrous raw materials are important because the influence of other factors of the blast furnace process is negligible or there is no choice (fuel, smelters, etc.).

After a detailed analysis of all raw materials available for the production of liquid iron and a techno-economic analysis of the process, it was concluded that the phosphorus content in liquid iron will be in the range of 0.095% to 0.110%.

Figure 1 shows the realized content of P in iron at the entrance to the converter process in the months of February and March.

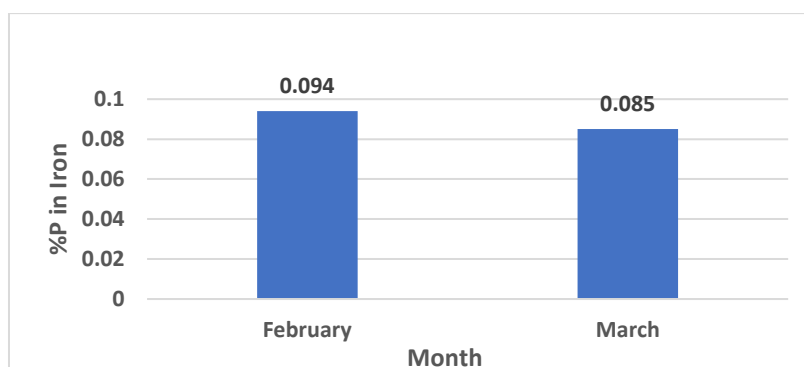


Figure 1 - Phosphorus content in Iron

One of our most effective measures is working with two slags (double slag process), which represents the casting of the first-formed slag, which is saturated with  $P_2O_5$  oxide, somewhere in the middle of the process, and the formation of a new slag with the addition of calcite lime.

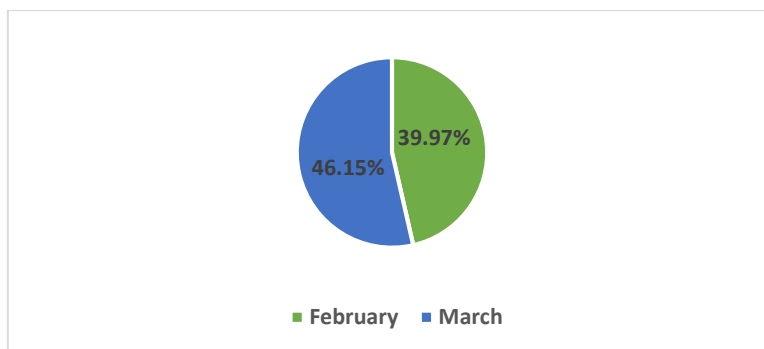


Figure 2 - Double slag process

The percentage of the heats that were made with the formation of two slags is shown at Figure 2.

The next measure is a larger targeted Basicity of slag to create a favorable environment that allows better phosphorus removal. In order to achieve this, a larger amount of calcite lime than recommended is added in the process.

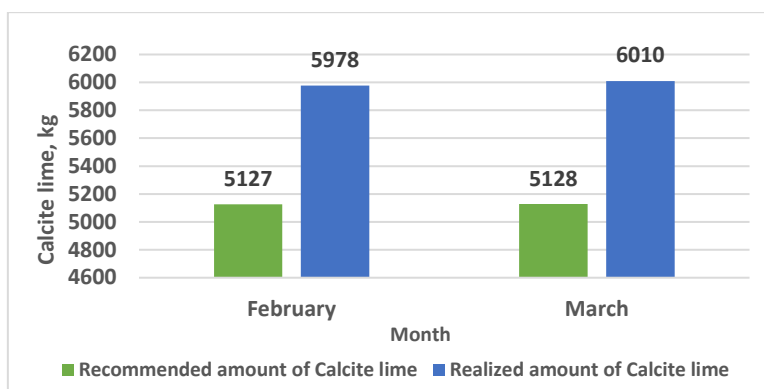


Figure 3 - Recommended and actual amount of Calcite lime added to the converter process

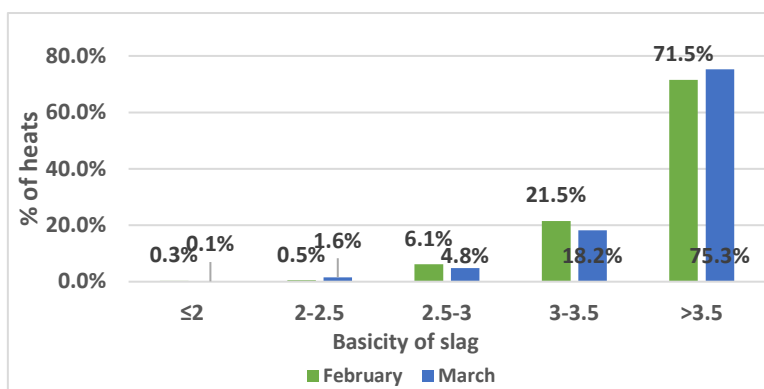


Figure 4 - Basicity of the slag

These Figures, 3 and 4, show the amount of calcite lime that we add in the converter process and the achieved Basicity of slag.

By adjusting the blowing profile, i.e. the blowing height, it is possible to achieve a better removal of phosphorus in the converter process. It is known that with a higher blowing height, the so-called softer blowing of the heats, we achieve a higher FeO in the slag, which enables the formation of more fluid slag, which favors the better removal of all impurities in the process. Accordingly, we consciously raise the blowing height in order to achieve the highest possible FeO in the slag, which is shown in the Figure 5 below.

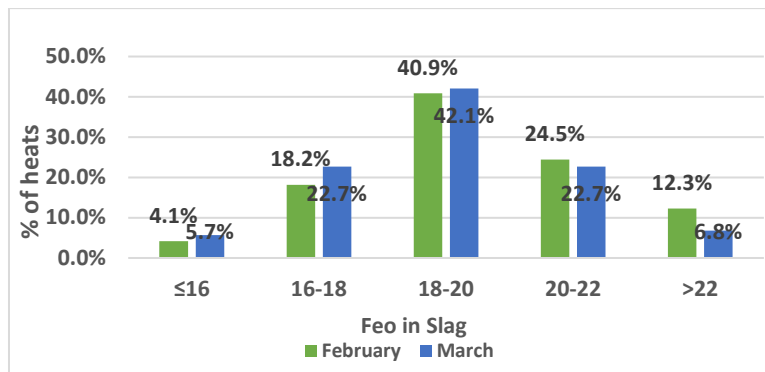


Figure 5 - FeO in the Slag

The plan is to introduce the possibility of adding mill scale pellets to the converter, which is one of the most efficient measure for increasing FeO in the slag.

Due to the lack of Ladle Furnace (LF) in our steel shop and the impossibility of reheating the heats, temperature is the most important factor. This is a big problem when removing phosphorus because it is known that phosphorus is removed better when the process itself in the converters is colder. Because of that, we try to achieve as low temperatures as possible, which are suitable for phosphorus removal, but in such a way as not to endanger the production process, Figure 6. We are also trying to aim for a lower carbon, so we can achieve a slightly higher activity ( $O_2$  ppm) of oxygen in the steel at the end of the heats, Figure 7.

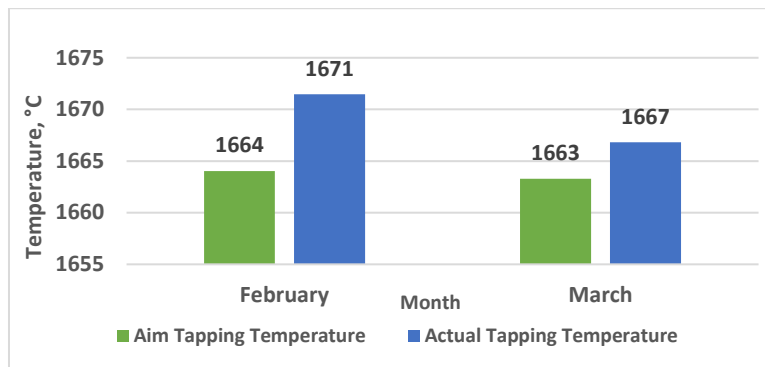


Figure 6 - Aimed and Actual Tapping Temperature

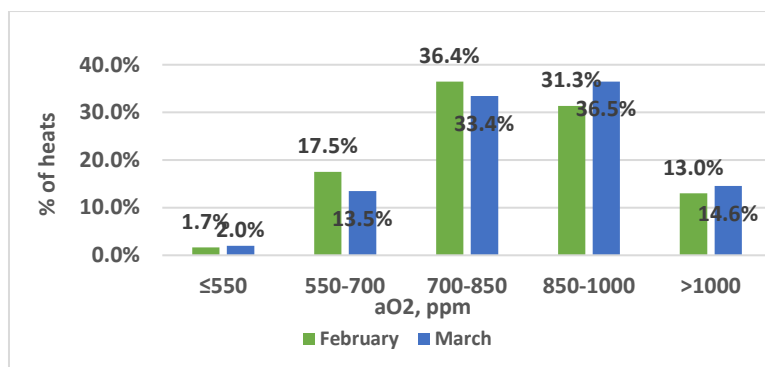


Figure 7 - aO<sub>2</sub> in Steel

The data in figure 8 are the realized phosphorus contents before the tapping in February and March of this year, as well as the realized phosphorus distribution factor ( $L_p$ ) in figure 9, where we achieve optimal results (minimal 80, targeted over 120). The realizations of P before the tapping and  $L_p$  show us that we are achieving favorable results with the application of phosphorus removal measures.



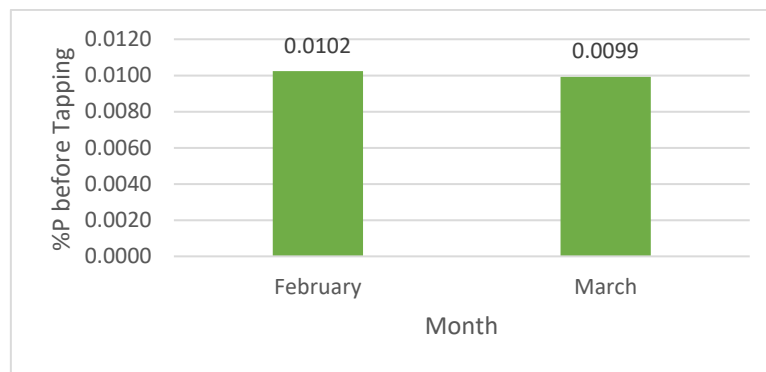


Figure 8 - Phosphorus content before Tapping

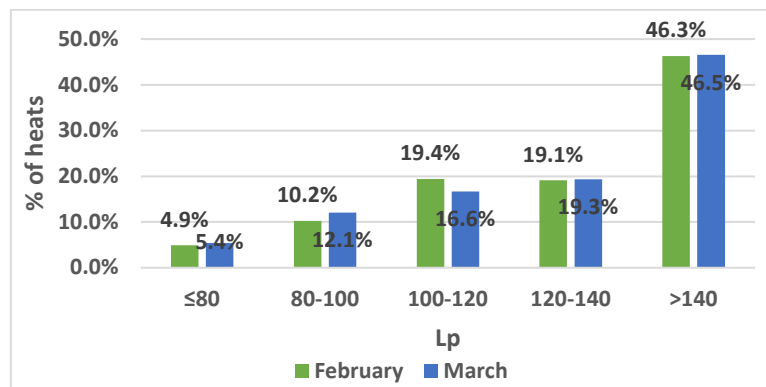


Figure 9 - %Phosphorus in Slag/% phosphorus in Steel (Lp)

#### 4. CONCLUSION

Due to economic reasons, we are forced to work with more incoming phosphorus in iron in the coming period, and for these reasons we have implemented a program with measures to remove elevated phosphorus in the converter process. This paper presents the achieved parameters, obtained by practicing the measures, as well as a possible improvement in the form of the addition of mill scale pellet.

#### REFERENCES

- [1] V. E. Laukart, B. O. Chukvulebe, A. A. Dobromilov, G. V. Kuznetsov, A. N. Shvetsov, Converter Processing of High-Phosphorus Hot Metal for Continuous Casting, Steel in Translation, 2007, p. 690–692
- [2] B. Deo, A. Overbosch, B. Snoeijer, D. Das, K. Srinivas, Control of Slag Formation, Foaming, Slopping, and Chaos in BOF, India, 2013

## MICROPLASTIC TEXTILE FIBERS IN URBAN SOILS OF SERBIA

Ivana Mikavica<sup>1</sup>, Dragana Randelović<sup>1</sup>, Milena Obradović<sup>1</sup>,  
Jovica Stojanović<sup>1</sup>, Jelena Mutić<sup>2</sup>

<sup>1</sup>Institute for Technology of Nuclear and other Minerals Raw materials, Boulevard Franchet  
d'Esperey 86, Belgrade, Serbia

<sup>2</sup>University of Belgrade, Faculty of Chemistry, Studentski trg 12 - 16, P. O. Box 51, 11158,  
Belgrade, Serbia

### Abstract

*Microfibers, as a considerable component of microplastic pollution in the environment have received notable attention during past years. Fast fashion and extensive use of synthetic and semi-synthetic outfits, aging, and discharge of used textile items are dominant sources of microfiber generation and ending up in urban soils. Herein, we examined microfibers' presence in the urban soils of Sremska Mitrovica and Bor. A flotation method based on density separation using saturated NaCl solution was utilized to assess microplastics concentration in soils. The abundance of microfibers was 200 and 600 items per kg of soil, respectively. Fiber structure was confirmed by ATR-FTIR analysis. Items isolated from soil from Sremska Mitrovica contained the natural fiber of cotton, while microfibers detected in soil from Bor referred to semi-synthetic polymer, viscose, i.e. rayon. Despite similar chemical structures based on cellulose, differences in IR spectra allowed the distinguishing of these fiber types. This paper provides insight into the current state of environmental pollution by microplastic fibers and suggests potential origin. More in-depth research on fiber content in soils, measures of prevention, and subsequent remediation should be carried out to face the challenge of microfibers presence in the ecosystem, their entering the food chain, and their impact on biota.*

**Keywords:** *microfibers, cotton, viscose, isolation, structure*

### 1. INTRODUCTION

Natural and regenerated textile fibers, a commonly used material for the manufacture of textiles, apparel, furniture, and other commonly used items, play a fundamental role in human societies. The estimated amount of plastic material produced for textile fibers in 2016 reached 65 million tons globally, while the plastic waste generation rate is approaching 400 Mt per year [1, 2]. Production, use, and end-of-life disposal of apparel, industrial, agricultural, and home textiles, and other fibrous materials cause the shedding and releasing of microfibers, a type of microplastics (MPs) found to be ubiquitous in air, terrestrial, and water environments [3]. One of the most common fiber types found in the environment is the natural fiber of cotton and viscose, a semi-synthetic fiber, both extensively used in textile production. Microplastics, defined as solid particles of polymer matrices < 5mm in size, represent ubiquitous pollutants that have become a global environmental challenge [4]. Terrestrial soil is considered a sink for microplastics (MPs). While farmland and agricultural soils have gained considerable attention regarding microplastic pollution, investigations of urban soils have been neglected to a certain extent resulting in a current dearth of knowledge. Due to the increased migration from rural to urban areas, followed by rapid urbanization, anthropogenic activities tend to concentrate in urban sites (express stations, textile mills, urban road dust, atmospheric deposition), representing a crucial source of microplastics pollution [5]. It is known that MPs in soil showed an impact on soil physicochemical properties (pH value, water holding capacity, porosity, aggregation, bulk density, electrical conductivity), and consequently, the function of the soil ecosystem, causing adverse effects on soil biota (bacteria, fungus, pathogens, and plants) [1]. Several methods for microplastic extraction from soil

have been proposed, of which the flotation method based on density separation is commonly used and found to be the most appropriate [5].

Herein, we examined the presence and content of microfibers in urban soils in Serbia, using the density separation method, followed by the characterization of isolated particles, indicating the potential pollution sources.

The aims of this study were: 1) assessment of microfiber abundance in urban soils from two cities in Serbia, 2), determination of fibers' chemical structure, i.e. polymer type 3) identification of potential sources of microfiber pollution.

## 2. EXPERIMENTAL

### 2.1 Study site description and sample collection

Samples collection was carried out in June of 2021, in Sremska Mitrovica (SM), situated at the east longitude of 19° 36' 33" and the north latitude of 44° 58' 20", at an altitude of 82 m and Bor (BO), located in the Bor District, 222 km south of Belgrade (44°04'25" N, 22°05'26" E), eastern Serbia, at 381 m of altitude (Figure 1).



Figure 1 - Sampling site map

Up to 20 cm in depth of the top-soil layer was sampled for the analysis. About 1 kg of the composite sample formed from at least 5 subsamples, was taken from each sampling site. All sample manipulations and analyses were performed omitting the contamination from the potential contact with plastic materials.

### 2.2 Isolation, quantification and characterization of microplastics

Microplastic particles were isolated from soil using the flotation method [5]. After air-drying for two weeks, soil samples were sieved. Fraction below 2mm was additionally dried at 60°C to a constant weight in the heating oven and used for further analysis. 5 g of soil was measured and covered with 60 ml of saturated NaCl solution (1.2 g cm<sup>-3</sup>), subjected to the ultrasound treatment for 15 min (energy input of 60 J ml<sup>-1</sup>), and left overnight. About 30 ml of top layers of supernatant containing MPs and SOM were extracted by a glass dropper and filtered through a 20 µm porous stainless steel filter. Filter holding microplastic and organic matter particles was left in 30% H<sub>2</sub>O<sub>2</sub> solution in an ultrasonic bath for 10 min and rinsed thoroughly afterward with prefiltered distilled water. The suspension left over was heated to 60°C and kept for 24h to digest SOM and filtered through a steel filter (20 µm). MPs observation and counting were carried out using a polarizing microscope (Carl Zeiss Jena Pol-U). Analysis was carried out in three replicates. Isolated particle characterization was done by ATR-FTIR spectroscopy using a Thermo Scientific Nicolet iS50 spectrophotometer.

### 3. RESULTS AND DISCUSSION

#### 3.1 Microfibers abundance in soils

Soils from Bor contained 600 items per kg on average. The mean concentration of 200 fibers in kg was found in soil from Sremska Mitrovica. Our finding is consistent with MPs content reported in soils from Ahvaz (Iran), Nanjing (China), and roadside dust from Victoria (Australia) [4, 5, 6] (Table 1). However, these data consider not only microfibers but microplastic particles in general, including fragments, films, pellets, etc. Particularly, soil from Nanjing contained 39.1% of fibers. Authors identified cosmetics, textile, and plastic manufacturing as the dominant sources of MPs [5]. Microfibers detected in samples from the urban area behind the Lihe River in China contributed 30.88% to the total microplastics content [7]. On the other side, microfibers were the most abundant MPs in urban soils from Ahvaz (70%).

Table 1 – Microplastics abundance reported in urban soils.

Location	Sample type	MPs abundance (items per kg)	Dominant polymer type	Reference
Victoria, Australia	Roadside dust	201 - 529	PE, PP	[6]
Abadan, Khorramshahr, Iran	Urban soil	3470	PET, PP	[2]
Lihe River watershed, China	Urban soil	1293	PP, PAN, PE, Rayon	[7]
Ahvaz metropolis, Iran	Urban soil	100 - 3135	PE, PTFE, Nylon	[4]
Nanjing, China	Urban soil	461 ± 222	PETG, PP	[5]

In general, there is a lack of literature data on microfibers content in soils from (sub)urban areas. For instance, farmland soil from Bangladesh showed MPs at a concentration of  $2.13 \times 10^4$  particles  $\text{kg}^{-1}$  [1]. Due to the application of municipal biosolids and sewage sludge containing high levels of microfibers, agricultural and farm soils have been identified as more significant sinks for microplastic fibers containing almost 90% of the total MPs detected [8].

#### 3.2 Microfibers chemical composition

Fibers chemical structure was characterized by ATR-FTIR (Figure 2). All isolated particles from soil from Bor were regenerated cellulose fibers and viscose. The only detected polymer in Sremska Mitrovica was the natural fiber of cotton.

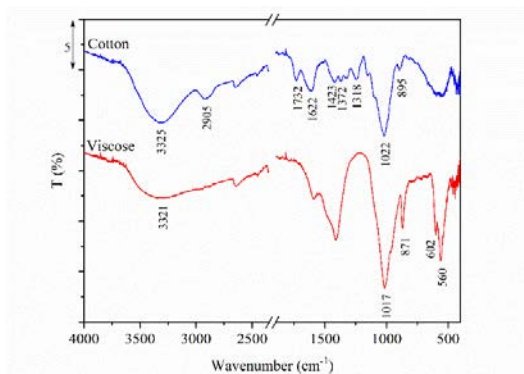


Figure 2 - ATR-FTIR spectra of isolated microplastic fibers of cotton and viscose/rayon

Chemically, viscose and cotton both represent cellulose-based fibers, with differences regarding fiber structure. Cotton is made up of natural fibers, twisted and not uniformly shaped, due to the higher degree of polymerization and crystallinity. Viscose is a man-made fabric, constituted from chemically treated regenerated cellulose. Crystallinity and a higher degree of polymerization in cotton refer to closely parallelly packed cellulose molecules held together by hydrogen bonds, resulting in higher fiber strength. Since both materials are predominantly made from cellulose, the

spectra of either group of fibers appear similar (Figure 2). However, particular differences allow the distinguishing of two fiber types. The first one is -OH stretching band profile, found featureless and broad in the spectra of man-made fibers. In natural fiber spectra, it exhibits a distinct peak near  $3330\text{ cm}^{-1}$ . Additionally, there is a band close to  $1725\text{ cm}^{-1}$ , usually not identified in semi-synthetic fiber, but appears in cotton spectra, being associated with pectine [9]. Natural fiber spectra contained an absorption peak at  $1423\text{ cm}^{-1}$  belonging to O-C-H of  $\text{CH}_2$  bending (Figure 2), that corresponds with previous reports.

### 3.3 Potential sources of microfibers in soils

Microfibers end up in the environment through different pathways. In general, wastewater released by domestic laundering and textile industries is considered a direct and prevailing source of microfibers [1]. Additionally, fibers shedding from clothes and discarded textiles aging, interior items, agricultural activities, and atmospheric and ambient deposition significantly contribute to microfiber pollution, as releasing from disposable face masks used during the COVID-19 pandemic. Fiber fragmentation from larger items may result from physical, chemical, and photodegradation and abrasion.

## 4. CONCLUSION

Microplastic fibers, omnipresent in the environment, represent a matter of global concern. This research assessed microplastic textile fiber content in urban soils from two cities in Serbia, for the first time. Microfibers abundance in soil from Sremska Mitrovica was 200 items per kg, referred to as natural fiber, cotton, as confirmed by ATR-FTIR analysis. Soil from Bor contained 600 microfibers in kg, and all of the isolated fibers were characterized as semi-synthetic material – viscose, also known as rayon. Clothes and discharged textiles shedding could be the dominant source of microfibers' presence in urban soils. Significant effort is needed to reduce microfibers generation and emission. The implementation of regulations on microplastic pollution, which is currently lacking, and adequate control are necessary to prevent and minimize microfibers' release into the ecosystems.

## REFERENCES

- [1] N. Hossain, M. Rahman, S. Afrin, A. Akbor, A.B. Siddique, G. Malafaia, *Sci. Total Environ.*, 858 (2023), 160118
- [2] Z. Mokhtarzadeh, B. Keshavarzi, F. Moore, R. Busquets, M. Rezaei, E. Padoan, F. Ajmone-Marsan, *IJEST*, 19 (2022), 10199–10210
- [3] J. Liu, Y. Yang, J. ding, B. Zhu, W. Gao, *Environ. Sci. Pollut. Res.*, 26 (2019), 29497–29501
- [4] M.J. Nematollahi, B. Keshavarzi, F. Mohit, F. Moore, R. Busquets, *Sci. Total Environ.*, 819 (2022), 152051
- [5] Y. Zhou, J. Wang, M. Zou, Q. Yin, Y. Qiu, C. Li, B. Ye, T. Guo, Z. Jia, C. Wang, S. Zhou, *Chemosphere*, 303 (2022), 134999
- [6] L. Su, B. Nan, N.J. Craig, V. Pettigrove., *Chemosphere*, 252 (2020) 126567
- [7] Y. Qiu, S. Zhou, W. Qin, C., Zhang, C. Lv, *Chemosphere*, 324 (2023), 138292
- [8] J. Yang, L. Li, L. Xu, Y. Shen, S. Li, C. Tu, L. Wu, P. Christie, Y. Luo, *Environ. Pollut.*, 289 (2021), 117943
- [9] I.R. Comnea-Stancu, K. Wieland, G. Ramer, A. Schwaighofer, B. Lendl, *Appl. Spectrosc.*, 71(5), 939-950

## PREPARATION OF FERRONICKEL BY SEMI-MOLTEN SMELTING A MIXTURE OF TWO TYPES OF LATERITE ORE

Jianbo Zhao, Xinnan Zhao, Donglai Ma, Yang You, Zhixiong You, Xuewei Lv

College of Materials Science and Engineering, Chongqing University, Chongqing 400044, China

### Abstract

*In this study, a method of smelting a mixture of two types of laterite ores (saprolitic and limonitic) was proposed for preparing ferronickel. The effect of basicity on the semi-molten smelting process was investigated. Thermodynamic analysis indicated that the melting temperature of slag can be distinctly decreased by adjusting the CaO and FeO contents in the slag. The favorable basicity of B2 (CaO/SiO<sub>2</sub>) was 0.28–0.61 which fell in the lowest melting temperature area of diopside. The softening and melting characteristics can be improved by adjusting the basicity. The softening, hemisphere and flow temperature decreased about 93 °C, 82 °C, 47 °C when B2 was increased from 0.01 to 0.5. A ferronickel product with 6.42wt% Ni, 86.99wt% Fe was prepared with basicity of 0.3, via reduction roasting at 1300 °C with C/O of 0.86 and 20 wt% limonitic laterite ore, followed by magnetic separation. The corresponding Ni and Fe recoveries reached up to 88.60wt% and 72.25wt%, respectively.*

**Keywords:** *Laterite nickel ore; Semi-molten smelting; Basicity; Magnetic separation; Ferronickel*

### 1. INTRODUCTION

The global demand for Ni has rapidly increased in recent years due to soaring stainless steel production and its wide utilization in battery field [1]. Nickel is often extracted from nickel sulfide and laterite ores. Nowadays, nickel laterite ore is considered the main resource for extracting nickel metal [2]. Saprolitic and limonitic laterite are two common nickel laterite ores. Limonitic laterite ore is typically characterized by low Ni, SiO<sub>2</sub>, and MgO content (0.5–1.5 wt%, <10 wt%, and <5 wt%, respectively) and high iron content (40–50 wt%) [3,4]. In contrast, saprolitic laterite ore has relatively higher Ni, SiO<sub>2</sub>, and MgO content (1.8–3 wt%, 30–50 wt%, and 10–25 wt%, respectively) and lower iron content (10–25 wt%) [5,6].

Up till now, the process of rotary kiln-electric furnace (RKEF) has been the preferred pyrometallurgical technology to produce ferronickel from saprolitic laterite ore. However, the RKEF process is quite energy-intensive because it involves several high-temperature steps [7,8]. An alternative route has also been put into practice for producing ferronickel by Nippon Yakin Kogyo Co. Ltd., Japan. Ferronickel alloy was obtained via direct reduction in the semi-molten state in a rotary kiln, followed by physical separation. In the direct reduction processes, partially melting the slag phase is always desirable, which promotes the growth of ferronickel and facilitates the subsequent separation process [9,10]. Therefore, various fluxing agents like Na<sub>2</sub>SO<sub>4</sub> and CaF<sub>2</sub> were added to enhance the reduction of laterite ore, as well as to decrease the melting temperature of slag in the reduced product [11,12]. These additives inevitably caused heavy environmental pollution and corrosion in the equipment.

In this study, a novel method was proposed for preparing ferronickel alloys by smelting a mixture of limonitic laterite and saprolitic laterite ores. limonitic laterite ore was used to decrease the slag melting temperature in reduced briquette by adjusting the FeO content during the carbothermic reduction process. The basicity of slag fraction was also adjusted to promote the growth of ferronickel. Thermodynamics of smelting the mixture of two types of laterite ores was calculated at first, followed by investigating the softening and melting characteristics of slag fraction. Finally, ferronickel alloy was prepared by semi-molten smelting a mixture of two types of laterite ore.

## 2. EXPERIMENTAL

### 2.1 Materials

The main chemical composition of the two types of nickel laterite ores is shown in Table 1. The Ni content and total Fe content (TFe) in the saprolitic laterite ore are 1.73 wt% and 21.09 wt%, and that of limonitic laterite ore are 0.83 wt% and 44.41 wt%, respectively. The saprolitic laterite sample has high silica and magnesia content, but their content in limonitic laterite ore are relatively low. The mineralogical analysis of the two nickel laterite ore was investigated by X-ray diffraction (XRD), and the results indicate that the saprolitic laterite sample is mainly composed of lizardite ((Mg,Fe,Ni)<sub>3</sub>Si<sub>2</sub>O<sub>5</sub>(OH)<sub>4</sub>, goethite (FeO(OH)) and silica (SiO<sub>2</sub>). The limonitic laterite ore is mainly composed of goethite (FeO(OH)) and limonite (Fe<sub>2</sub>O<sub>3</sub>·nH<sub>2</sub>O).

Bituminous coal with FC<sub>ad</sub> 74.22wt% and V<sub>daf</sub> of 9.60wt% was used as a reductant for carbothermic reduction.

Table 1 - Chemical composition of nickel laterite ore/wt%.

Ore	TNi	TFe	Co	MgO	SiO <sub>2</sub>	Al <sub>2</sub> O <sub>3</sub>	CaO	Cr <sub>2</sub> O <sub>3</sub>	MnO <sub>2</sub>	LOI
Saprolitic (A)	1.73	21.09	0.10	20.88	28.49	0.86	0.24	1.53	0.65	13.82
Limonitic (B)	0.83	44.41	0.08	3.74	7.12	3.97	0.62	4.34	/	14.26

### 2.2 Methods

The high-temperature softening and melting characteristics of the slag are tested using an ash melting point analyzer. Upon heating, the cylinder slag sample melts gradually. The temperatures when the height of the slag sample is reduced by 1/4, 1/2 and 3/4 represent the softening temperature, hemisphere temperature and flow temperature, respectively.

Before reduction roasting, nickel laterite ores were dried at 120 °C for 2 hours in an oven and ground so that 80 wt% of the particles passed 0.074 mm. The ground sample was mixed to homogeneity with bituminous coal in a certain proportion. The mixture was then briquetted into spherical pellets (Φ15 mm) by a powder tablet press machine at an absolute pressure of 10 MPa.

The reduction process was carried out in a resistance furnace in an argon atmosphere with the roasting temperature controlled within ±2 °C. Before each experiment, a graphite crucible (Φ80 mm×20 mm) was placed in the furnace as a protective crucible, and heated together with the furnace. When the temperature of the roasting zone reached 800 °C, the corundum crucible loading the pellets was introduced, post which the furnace was continuously heated in an argon atmosphere at 10 K/min. The heating schedule was chosen by simulating the heating process in a rotary hearth furnace (RHF). After reaching the given temperature, the reduction roasting was completed. The corundum crucible was taken out of the furnace and quenched rapidly to the ambient temperature (25 °C). Subsequently, the reduced sample was dried and crushed to a size lesser than 0.074 mm, and separated into magnetic and non-magnetic parts through an XCGS-50 Davies Magnetic Tube using a magnetic field intensity of 80 kA/m. The obtained product was prepared for analysis.

## 3. RESULTS AND DISCUSSION

### 3.1 Thermodynamic basis

It has been proved that FeO is beneficial for improving the high-temperature performance of the slag by reducing its melting temperature [1]. Hence, limonite laterite ore was mixed to adjust the FeO content in slag fraction. By fixing the proportion of Al<sub>2</sub>O<sub>3</sub>/(CaO+SiO<sub>2</sub>+MgO)=5%, FeO/(CaO+SiO<sub>2</sub>+MgO)=10%, the phase diagram of CaO-MgO-SiO<sub>2</sub>-5wt%Al<sub>2</sub>O<sub>3</sub>-10wt%FeO was calculated by FactSage 8.1. It can be seen from Figure 1 that, the phase with the lowest melting temperature is diopside phase (CaMgSi<sub>2</sub>O<sub>6</sub>) in the area of ABCDE. The eutectic temperature of



this area is in the range of 1223.44°C(E)–1266.17 °C (A). These temperatures were decreased distinctly compared to that of the components of saprolitic laterite ore. The corresponding CaO content and B2 (CaO/SiO<sub>2</sub>) is 16.00wt%(D)–29.59wt%(C) and 0.28(D)–0.61(C). Hence, it can be concluded that the comprehensive regulation of CaO and FeO contents was a feasible way to the semi-molten smelting process.

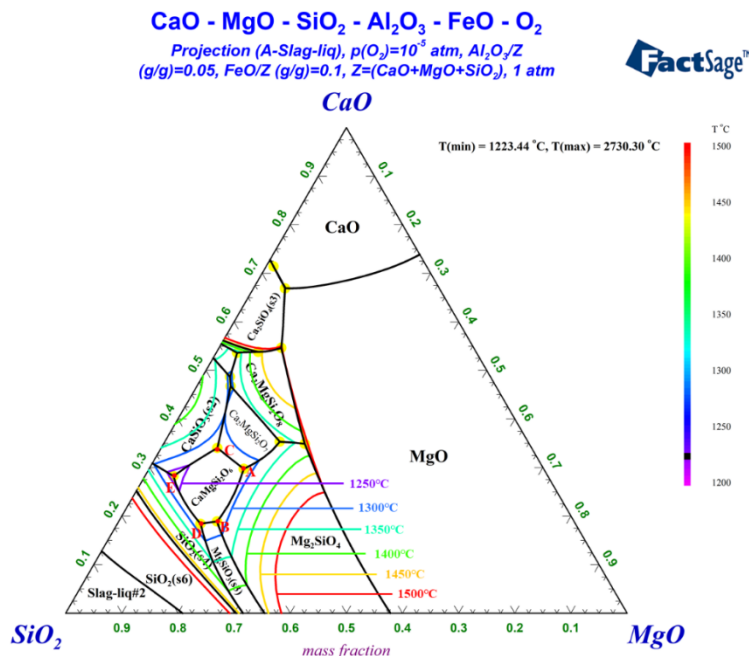


Figure 1 - The phase diagram of CaO-SiO<sub>2</sub>-MgO-5wt% Al<sub>2</sub>O<sub>3</sub>-10wt% FeO system.

### 3.2 Softening and melting characteristics

By mixing these two laterite ores in the proportion B/(B+A) at 10wt%, the component of the slag fraction is about 40.81wt% MgO, 56.11wt% SiO<sub>2</sub>, 2.49wt% Al<sub>2</sub>O<sub>3</sub> and 0.59wt% CaO assuming all the iron and nickel elements are reduced to the metallic state. The B2 of the slag is about 0.01 which is far lower than the calculated 0.28-0.61.

The effect of basicity on the softening and melting characteristics of slag is shown in Figure 2. It can be seen that all these temperatures decreased gradually with increase in basicity. The softening and hemisphere temperatures at B2 of 0.3 were 1350 °C and 1404 °C, respectively, which remained almost constant after that. According to the above thermodynamic analysis, the CaO content in the area of ABCDE is 17.76wt%-31.79wt%. The CaO content with basicity of 0.3-0.5 is 14.48wt%-22.01wt%, which is closed to the calculated area. The softening, hemisphere and flow temperature decreased about 93 °C, 82 °C, 47 °C when B2 was increased from 0.01 to 0.5. Increasing basicity of slag fraction has played a positive role in promoting slag melting and improving slag fluidity.

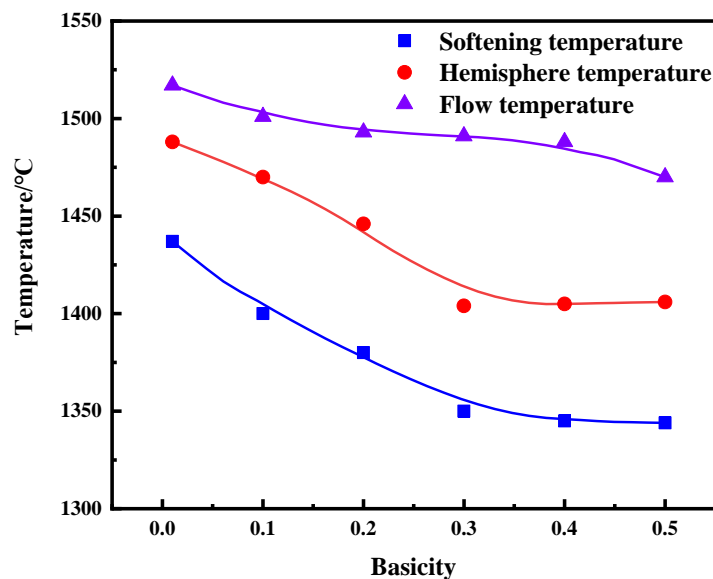


Figure 2 - Effect of basicity on melting characteristic temperature.

### 3.3 Reduction roasting followed by magnetic separation

The effect of basicity on the reduction roasting and magnetic separation for preparation of ferronickel was carried out by fixing the proportion B/(B+A) at 20wt%. The experiments were conducted at 1300 °C with C/O of 0.86. The results of Fe, Ni content and recovery are plotted in Figure 3. It can be observed that both the Ni and Fe content in the magnetic fraction first increased and then decreased with increase in basicity. The highest Ni grade is 6.42wt% at basicity of 0.3. The change of Ni recovery was the same to the Ni content. Meanwhile, the Fe recovery remained almost unchanged. It is demonstrated that increasing basicity to about 0.3 is beneficial to the reduction as well as the separation of magnetic fraction from the nonmagnetic fraction.

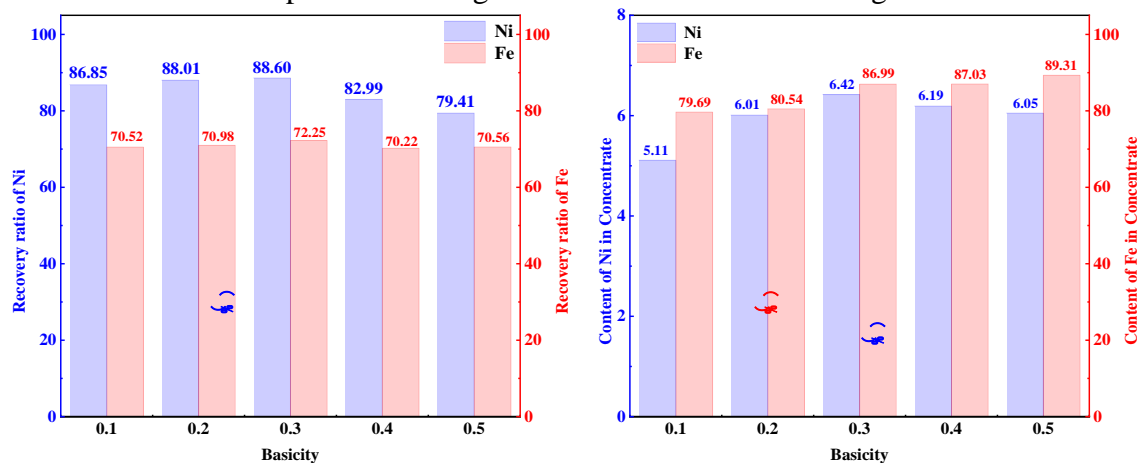


Figure 3 - Effect of basicity on the Ni, Fe content and recovery.

## 4. CONCLUSIONS

In this study, the effect of basicity on smelting a mixture of two types of laterite ores for preparing ferronickel alloy was investigated. The conclusions are drawn as follows:

- (1) Thermodynamic analysis revealed that the slag melting temperature can be distinctly decreased by adjusting the CaO content in the slag. The favorable basicity of B2 was 0.28–0.61.
- (2) The softening and melting characteristics can be improved by increasing the basicity. The softening, hemisphere and flow temperature decreased about 93 °C, 82 °C, 47 °C when B2 was increased from 0.01 to 0.5.

(3) A ferronickel product with 6.42wt% Ni, 86.99wt% Fe was prepared via reduction roasting at 1300 °C with C/O of 0.86 and 20 wt% limonitic laterite ore, followed by magnetic separation. The corresponding Ni and Fe recoveries reached up to 88.60wt% and 72.25wt%, respectively.

## ACKNOWLEDGEMENTS

*This work was financially supported by the National Natural Science Foundation of China (No.51904047), and the State Key Laboratory of Complex Nonferrous Metal Resources Clean Utilization, China.*

## REFERENCES

- [1] X.M. Lv, L.W. Wang, Z.X. You, W.Z. Yu, X.W. Lv., JOM, 71 11 (2019) 4191–4199.
- [2] D.L. Ma, J.B. Zhao, Q.Q. Hu, X.M. Lv, Y. You, Z.X. You, X.W. Lv., Trans. Nonferrous Met. Soc. China, 32 (2022) 3459–3468.
- [3] W. Liang, H. Wang, J.G. Fu, Z.X. He., J. Cent. South Univ., 42 2173 (2011) 2173–2177.
- [4] D.Q. Zhu, Y. Cui, S. Hapugoda, K. Vining., T. Nonferr. Metal. Soc., 22, 907 (2012) 907–916.
- [5] Z.C. Cao, T.C. Sun, H.F. Yang, J.J. Wang, X.D. Wu., J. Univ. Sci. Technol. Beijing, 6, 708 (2010) 708–712.
- [6] Z.H. Liu, X.B. Ma, D.Q. Zhu, Y.H. Li, Q.H. Li., J. Cent. South Univ., 10, 2905 (2011) 2905–2910.
- [7] E.N. Zevgolis, C. Zografidis, T. Perraki., J. Therm. Anal. Calorim., 100, 133 (2010) 133–139.
- [8] I. Kobayashi, Y. Tanigaki, A. Uragami., Iron Steelmaker, 28, 19 (2001) 28.
- [9] T. Watanabe, S. Ono, H. Arai, T. Matsumori., Int. J. Miner. Process., 19, 173 (1987) 173–187.
- [10] G.H. Li, T.M. Shi, M.J. Rao, T. Jiang, Y.B. Zhang., Miner. Eng., 32, 19 (2012) 19–26.
- [11] M. Rao, G. Li, T. Jiang, J. Luo, Y. Zhang., JOM, 65, 1573 (2013) 1573-1583.
- [12] B.Z. Ma, P. Xing, W.J. Yang, C.Y. Wang, Y.Q. Chen, H. Wang., Metall. Mater. Trans. B, 4, 2037 (2017) 2037–2046.

## POSSIBILITY OF COPPER ORES EXPLOITATION USING THE IN SITU LEACHING METHOD

Mladen Radovanovic, Dejan Petrovic, Jelena Ivaz, Dragan Zlatanovic

Technical Faculty Bor, University of Belgrade, V.J. 12, 19210 Bor, Serbia

### Abstract

*Underground exploitation takes place at greater depths which causes the need to reduce the operational costs of excavation. That can be achieved by choosing an appropriate mining method. Large scale mining methods are commonly used to excavate deposits with a low content of useful components that lie at greater depths. Sometimes conventional mining methods cannot produce the satisfying results. In that case application of unconventional mining methods or combination of both conventional and unconventional mining methods can be used for exploitation of metal ores. In situ leaching is one of unconventional methods that can be used for exploitation of copper deposits, and which in the near future may become one of the most favorable methods for the excavation of copper ores.*

**Keywords:** (leaching, underground mining, unconventional method)

### 1. INTRODUCTION

The main characteristic of the exploitation of copper ores over the years is the decreasing of copper content due to the fact that the richer deposits lying closer to the surface have been exploited and as a result of the change in the types of deposits that are exploited. In recent years, the main production of copper comes from porphyry deposits with a lower content of useful components [1,2]. Figure 1 shows the trend of decreasing copper content in ore for the last thirty years.

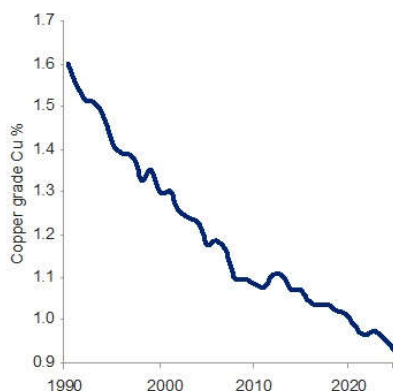


Figure 1 - Copper content in world deposits for the period 1990-2022.

The underground exploitation takes place at ever greater depths. This causes the need to reduce the operational costs of excavation, which can be achieved by choosing an adequate mining method. High mining costs, increasing depths and lower ore grades open the possibility to consider exploitation using non-conventional mining methods.

One of the most commonly used unconventional mining method is in situ leaching. In situ leaching (ISL) is most often used in the exploitation of uranium, and today over 50% of the produced uranium in the world is obtained by applying this method. In situ leaching can also be successfully applied to obtain other metals, especially copper. About 25% of the copper produced annually in the US is obtained using this mining method.

In the exploitation of copper ores, the ISL method is mainly used as a procedure for increasing the recovery of metal from the deposit, for the exploitation of inaccessible parts of the deposit, for obtaining copper from caved ore after the application of caving mining methods, etc.

In situ leaching represents the circulation of liquid through the deposit with the aim of obtaining the desired metal or mineral with the subsequent return of the liquid to the surface for further treatment [3]. In some cases, a lixiviant is used to treat the ore through a system of injection and return wells (Figure 2). In other cases, the lixiviant is flooded or sprayed over residual ore in mines, often after using explosives to fragment and comminute the ore and increase the surface area exposed to the lixiviant [4].

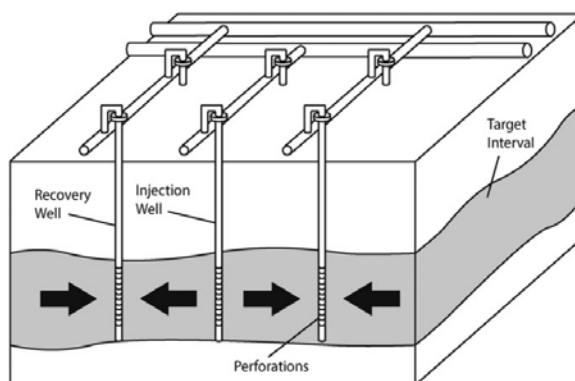


Figure 2 - A system of wells for the application of in situ leaching method

## 2. EXPERIMENTAL

To apply the ISL method, there are two critical parameters that must be satisfied:

- mineralization must be located in a permeable environment;
- the lixiviant should be suitable for the selective extraction of a certain component from the deposit.

The exploitation of copper by leaching is based on copying the natural processes of dissolution (leaching) and precipitation (precipitation) that took place over millions of years, and are still taking place. Known as supergene enrichment, this natural process has been observed in many of the world's copper deposits. This process takes place when hypogene (ie primary) ores, containing sulphide minerals such as pyrite ( $\text{FeS}_2$ ), chalcopyrite ( $\text{CuFeS}_2$ ) and bornite ( $\text{Cu}_5\text{FeS}_4$ ), oxidize over time. During the oxidation process, the iron contained in these minerals turns into red, red-brown, orange and yellow colored iron oxides, while the sulfur combined with groundwater creates a weak solution of sulfuric acid. The copper in the rock is dissolved in acidic solutions while it is filtered (filtered) down to the upper limit of the groundwater (water table), where copper is deposited in the form of chalcosine ( $\text{Cu}_2\text{S}$ ) in reduced conditions (the amount of oxygen is reduced). Over time, these processes create an oxidized zone (ie, leach cap, iron hat) above the thick copper-rich overburden zone, known as the enrichment layer. Thus, a solution rich in copper is obtained, which is collected and transported to processing plants, where copper is obtained. The presence of large covers, i.e. layers (rich in copper) for beneficiation in many of the world's porphyry copper deposits, enable the economic extraction of copper from these deposits [5].

The dissolution of oxide minerals is relatively easy and is carried out in simple reactions. The greatest practical and economic importance is the leaching of copper oxide minerals, which can be successfully dissolved in water. As solvents also can be used following compounds:  $\text{H}_2\text{SO}_4$ ,  $\text{HCl}$ ,  $\text{HNO}_3$ ,  $\text{NH}_3$ ,  $\text{Fe}_2(\text{SO}_4)_3$ ,  $\text{FeCl}_3$ ,  $\text{NaCl}$  and  $\text{NaOH}$ . Metal sulfides appear in more complex

forms, which makes it difficult to define the oxidation process that precedes the leaching process. The leaching solution must contain an oxidant and there are different leaching systems in which acids or alkali are used as reagents.

Good leaching results to a large extent, are achieved by crushing the ore as much as possible. In order to better "open" of the minerals, the material to be leached is previously subjected to appropriate preparation, when there are prerequisites for this. It consists in shredding by crushing or blasting, and also in the previous chemical processing of the mineral raw material. All this is done in order to convert the metal or its compounds from hard-to-dissolve compounds to easily-soluble ones as much as possible. For this purpose, various chemical procedures are applied: frying, oxidation or reduction, chlorination, sulphation, etc. Beside purely chemical leaching, the so-called bacterial leaching also can be applied, in which the oxidation process of the raw material being leached is improved by using special bacteria.

There are several methods of in situ leaching. Heap leaching is used to treat mineral raw materials with a low content of useful components. The essence of this procedure is the special preparation of the terrain and the disposal of poor ore or mineralized overburden from surface mining, which is then leached in one of the described ways. Underground leaching is the process of converting metal from ore into a liquid state in the deposit itself, and then, usually on the surface, the resulting solutions are processed by cementation, liquid-liquid extraction or some other processes. Underground leaching can provide greater recovery of metals from the deposits thanks to their extraction from poorer ores, which cannot be economically exploited by traditional methods. Underground leaching is based on ion exchange of metals during the directed movement of reagents through a massif with natural permeability or through previously crushed or in different ways stored ore. The basic prerequisite for the successful application of underground leaching is the presence of a useful component in compounds soluble in mineral or organic acids or alkalis, salt solutions, etc. Modern underground leaching facilities consist of an exploitation, pipeline and processing complex. The principle scheme includes a complex of rooms and facilities for carrying out the technological process of obtaining metal extraction solutions. Depending on the method of opening, there are: borehole, pit and combined method of underground leaching.

### **3. RESULTS AND DISCUSSION**

ISL can be successfully applied to increase ore recovery in caving mines. After mining has been completed using some traditional sublevel or block caving method, a significant amount of ore may remain in the caved material. Underground leaching can be used for exploitation of remain ore in caving mines. In that case the combination of traditional caving methods and leaching can be used for exploitation of copper deposits on greater depths with low grade ores. In US in situ leaching already takes important place in copper production. Experiences from mines where ISL method are applied shows that this method can be wide use in future for excavation of copper deposits.

In block caving mines exploitation by leaching takes place above in the inactive part of mine. A solution used for leaching is introduced into the deposit using perforated pipes laid on the surface of the ground above the ore body and a series of shallow injection wells. Solutions containing copper are collected in a collector in a pit below the caved part and pumped to the surface, where they undergo further treatment. When ISL is used as a main excavating method, exploitation is carried out by introducing the solution through injection wells to the copper-bearing ores, which should be characterized by intensively fractured rocks. Solution movement through the rock is controlled by pumping from adjacent return wells, which creates a hydraulic gradient that causes introduced solutions to flow from the injection wells to the adjacent return wells. After being pumped to the surface, copper-containing solutions are further processed to obtain the desired product – copper cathode.

ISL enables the exploitation with minimal impact on the environment. Unlike classic surface and underground mining methods, this time there is no degradation of large areas by mines, landfills and depots, no the need to relocate rivers or springs and other objects on the surface of the terrain, the amount of waste water generated by mining and hydrometallurgical activities is significantly lower, and there is also no environmental pollution with dust, noise and exhaust gases.

From an ecological aspect, using the ISL method, there is a risk of soil and surface and groundwater contamination from reagents and solutions used for leaching, however if the process is properly managed, the chances of contamination are minimal [6].

#### **4. CONCLUSION**

In situ leaching is one of the most effective available methods that can be used to exploitate ores in inaccessible parts of the deposit, ores remaining in the sides and mined parts of the massif, remaining metals in the caved ore after the application of caving mining methods. In addition, the in situ leaching method achieves lower production costs compared to traditional mining methods, which enables the application of this method for the exploitation of low-grade deposits or their parts.

Although ISL is auxiliary method to traditional mining benefits of ISL usage is large and they are reflected in better economic aspects (less investments for the development of the mine itself, processing plant and infrastructure, the possibility of starting production with low capital costs followed by an increase in production and flexibility of production capacities). Also ISL enables the exploitation of ore with minimal impact on the environment as long as projects are properly planned and managed.

#### **REFERENCES**

- [1] P. Crawson, *Resour. Policy* 37 (2012), 59-72.
- [2] L. Weber, *Berg- hüttenmänn. Monatsh.* 160 (2015), 71-78.
- [3] L. Sinclair, J. Thompson, *Hydrometallurgy* 157 (2015), 306-324.
- [4] J.K. Ahlness, M.G. Pojar, *In Situ Copper Leaching in the United States: Case Histories of Operations.* U. S. Bureau of Mines., 1983.
- [5] J.M. Guilbert, C.F. Park, *The Geology of Ore Deposits: W. H. Freeman and Company, New York, 1986, p. 985.*
- [6] G. Mudd, *A Research Report for Friends of the Earth (Fitzroy) with the Australian*



## SELECTION OF AN OPTIMAL ROUTE FOR RELOCATION OF THE ČEHOTINA RIVER BED

Ivan Jelić, Nikola Lekić, Nikola Stanić, Miomir Mikić  
Mining and Metallurgy Institut Bor, Zeleni bulevar 35, 19210 Bor, Serbia

### **Abstract**

*This work presents a selection of an optimal route of the Čehotina river bed in Pljevlja at the "Potrlica" location where, due to the coal exploitation, it is necessary to relocate the river via an internal landfill. Defining a new route requires balancing of the hydraulic, economic, environmental and other criteria. After consideration of five routes, the "Variant 5" was adopted, which extends from the Durutovići dam to the existing river bed near the sediment basin with a length of about 3.2 km. Also, a flexible waterproof river bed was present that can withstand the differential ground subsidence that will occur at the landfill, while maintaining the role of waterproofing.*

**Keywords:** displacement of rivers, EPDM geomembrane

### **1. INTRODUCTION**

The coal exploitation at the location "Potrlica" - Pljevlja has caused the relocation of the Čehotina river bed to the southwest side. This route was put into operation in 2009. Now, 14 years after its first relocation, the Čehotina river is again at the excavation front of works and according to the current DMP, its relocation must be done at the beginning of 2024.

### **2. DEFINING THE CRITERIA FOR SELECTION A NEW ROUTE OF THE ČEHOTINA RIVER**

In defining a new route of the river, it is important to determine an optimal solution where hydraulic, economic, ecological and other criteria will be met to the maximum extent allowed.

#### **2.1 Hydraulic criteria**

Designing the route of a new river bed is a job that precedes the transverse profile calculation, because only from the route and longitudinal profile of the new river bed can the slope of the riverbed be determined and required hydrotechnical facilities be predicted.

From the point of view of hydraulic criteria, the most favorable route would be without additional hydrotechnical structures (cascades, rapids, waterfalls, etc.), where the drop of bed would be less than the critical one, i.e., where there would be a calm flow regime. The slope of the channel bottom is limited by the maximum permissible velocities that occur in it, and are prescribed for different materials from which the channel is built.

#### **2.2 Economic criteria**

The most economically profitable route is the one with the shortest length, because the least amount of material is needed for its construction. This would mean that from the economic point of view, the most profitable route is a straight line, however, due to the terrain topography at the given location, this is not possible.

Also, in selection the route of the new bed, the attention should be paid to the excavations and embankments, because they can significantly affect the final price of the costs. In this case, a

special attention should be paid to a part of the route that cuts into the rock massif, because the excavation in material of the category V is extremely expensive.

Dimensions of the cross-section of the regulated bed are directly related to both economic and hydraulic criteria. From the economic point of view, it would be best if the river bed is as small as possible, again due to the consumption of materials. However, a river bed of smaller cross-sectional dimensions must have a greater channel drop to pass identical flow. It clearly follows from the above that it is necessary to find an optimal solution where the dimensions of cross-section of the new bed will be reduced to a minimum, while at the same time the conditions regarding the permitted speed in the bed, i.e., the bottom slope, will be met.

### 2.3 Environmental criteria

The new route of the Čehotina river must be such that it disturbs the natural regimes of the locality as little as possible. The conditions for free migration of fish and other migratory species must be met. The relocated bed must be made of natural materials, which is specially applied to a part of the route that enters the urban area.

### 3. CONSIDERING THE ROUTES OF THE NEW RIVER BED

Five variants of the route of the Čehotina river bed were considered, which are shown in Figure 1. The Variants 1 and 2 have a disadvantage because they directly exit to the landfill, which has not yet reached the required elevation of 760 meters above sea level. Also, a bend is planned at the landfill, where the channel, due to the uniform and significant subsidence, is designed from the gabion mattresses on a geosynthetic base. Behind the bend there would be a high slope. This could be a problem in the event of a maximum flow of high water.

The river bed route in the Variant 3 was made in 2020. However, the formation of the landfill did not go according to the expected dynamics. That is why it was necessary to envisage a new variant, where the route would be set aside on a part of the landfill that had already been formed. It is on the safety side to lay a route on material that has been stored for a long time, because there has been a certain amount of consolidation in that place. This avoids uneven and large settlements. It was also necessary to optimize the part of the route in the Variant 3 that passes through the rock massif. It is about the redemption of the category V material, which is possible using dynamite or a hydraulic hammer. In this case, the immediate vicinity of the arch dam does not allow the use of dynamite because it would lead to the creation of cracks in the rock massif on which the dam is built. The price of excavation using a hydraulic hammer is considerably high. With this conclusion, the need arose to find the most optimal solution that would comply with the hydraulic criteria, and from the economic side, the costs would be reduced to a minimum.

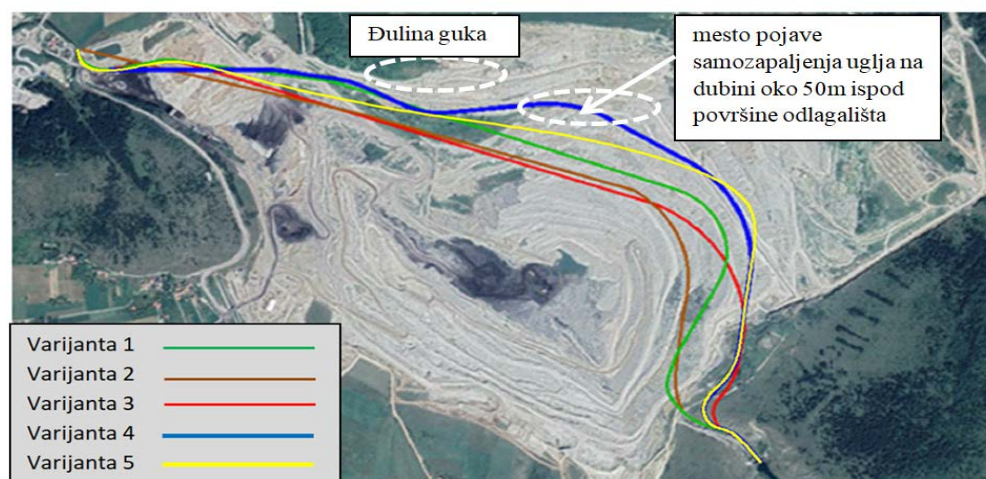


Figure 1 - Variant solutions for the new route of the Čehotina river bed

By the engineering geological mapping of the terrain at the location marked in Figure 1, an increased soil temperature was observed, as well as the appearance of smoke from drillholes. It is assumed that the coal caught fire at the bottom of embankment. The ignition of coal in this stretch can over time cause the differential subsidence, which is estimated at 2m. With this, the channel of the newly designed bed of the Čehotina river would be threatened, so the route of Variant 5 of the river in that part was moved to the edge of the landfill by approximately 120 m compared to the Variant 4. Also, the Variant 5 was conditioned by the fact that in the part of Djulana guka, the slope stabilization in the variant 4 would go outside the border of UTU. Therefore, this part of the route was also moved to the edge of the landfill.

#### 4. DESCRIPTION OF THE ADOPTED ROUTE - VARIANT 5

The section of the Čehotina river under consideration stretches from the Durutovići dam to the existing bed near the settling tank. The length of the relocated bed route is about 3.2 km and consists of the following elements, i.e., hydrotechnical facilities:

1. sound box with an overflow sill at the end
2. concrete channel with a trapezoidal cross-section, width at the bottom  $B=13\text{m}$
3. the first transition section, width of the channel at the bottom from  $B_1=13$  to  $B_2=8\text{m}$
4. concrete channel with a trapezoidal cross-section, width at the bottom  $B=8\text{m}$
5. cascade with waterfall and technical fishing path
6. the second transition section from the concrete channel with bottom width  $B=8\text{m}$  to the complex cross-section that corresponds to the dimensions of the channel at the landfill
7. gabion channel with a complex section at the landfill
8. the third transition section from the gabion channel with a complex cross-section to a rectangular cross-section with a width of  $B=12\text{m}$
9. channel made of stone in cement mortar with rectangular cross-section  $B=12\text{m}$ .

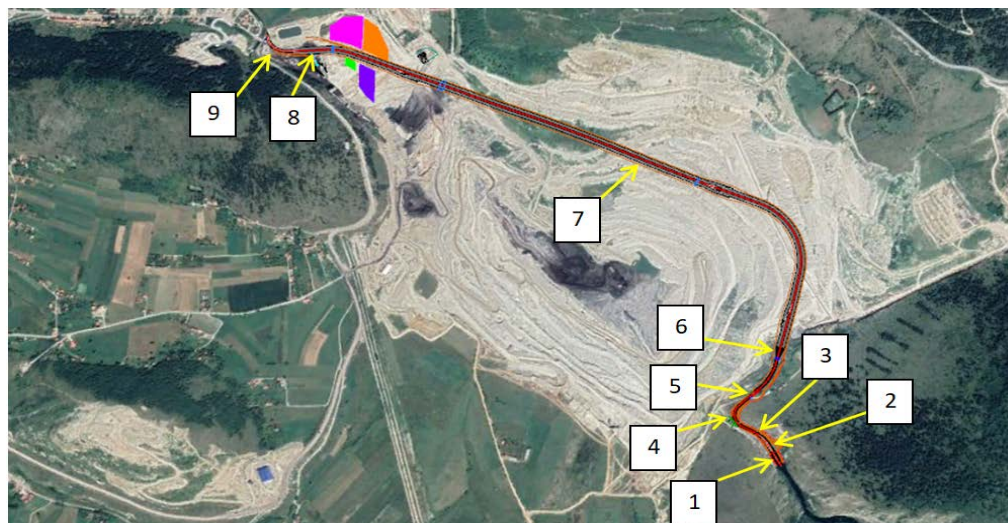


Figure 2 - Adopted route

#### 5. TYPE OF CHANNEL AT THE SITE OF EXPECTED DIFFERENTIAL GROUND SUBSIDENCE

The channel at the landfill will be constructed of flexible material. The formation of the slope is provided by gabion mattresses with a thickness of  $d=30\text{cm}$  in the upper part and  $0.5\text{m}$  in the lower part of the slope, which rest on a stone leg made of large stone. Formation of the river bottom is foreseen from a rock pile, made of large stones, the thickness of the layer is from  $0.5\text{m}$  to  $1.0\text{m}$  (Figure 3).

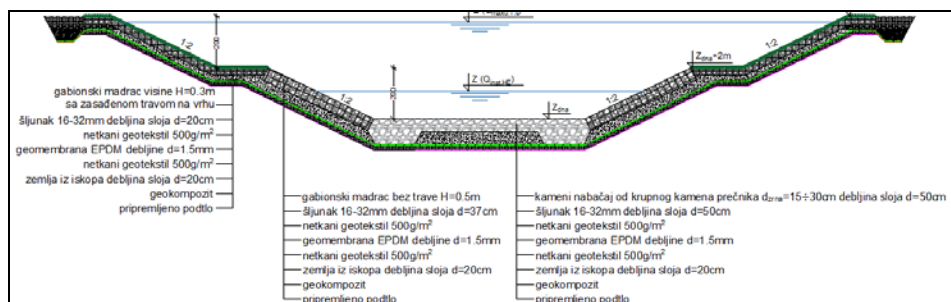


Figure 3 - Cross-section of the channel at the landfill

Ensuring the waterproofing of the channel at the landfill is achieved using a geomembrane made of EPDM, 1.5 mm thick, laid on a geotextile of min. 500 gr/m<sup>2</sup>, with the geotextile of 500 gr/m<sup>2</sup> being installed over the EPDM geomembrane.

In order to prevent the EPDM geomembrane from cracking due to differential ground subsidence, the installation of transverse and longitudinal "EPDM lyres" is planned. Transverse lyres are provided at the point of transition from limestone to the landfill and immediately before the beginning of the third transition section. Two longitudinal lyres are provided along the entire length of the bed of complex cross-section at the landfill. These lyres are made at the bottom of the river bed, at a distance of 1m each from the edges of the slopes (distance of the axis of the lyre). Their wheelbase is 6m.

It is necessary in the plan of laying the geomembrane to foresee that the part of the geomembrane with the "EPDM lyre" is installed in one piece. On the upper surface of the geomembrane, and before installing the geotextile, it is necessary to install a layer of polyethylene (PE) film with a thickness of 0.5 mm, which will allow, if necessary, the embedded EPDM in the lyre to "slide" with the help of the PE film (there will be no surface resistance of the geomembrane).

## 6. CONCLUSION

The selection of a river replacement route is a complex and important process that requires careful consideration of various factors in order to achieve an optimal result.

As a rule, the channel should be routed on stable ground, however, in this case it was not possible to avoid the internal deposit of the Potrlica surface mine, which is characterized by differential settlement. Therefore, a channel with a flexible lining was applied. The watertightness of the channel is ensured by the use of geosynthetics, more precisely the EPDM geomembrane, and uneven settlements are canceled by placing lyre (folds).

## ACKNOWLEDGMENTS

*The research presented in this paper was carried out with the financial support of the Ministry of Science, Technological Development and Innovation of the Republic of Serbia, as a part funding the scientific research work in the Mining and Metallurgy Institute Bor, according to the Contract with registration no. 451-03-47/2023-01/ 200052.*

## REFERENCES

- [1] Tehnički hidrograđevinski projekat izmeštanja reke Čehotine
- [2] Jovanović, Miodrag B. "Regulacija reka-radovi i građevine." (2022).
- [3] Mladenović, Marina Babić. Uređenje vodotoka. Institut za vodoprivredu Jaroslav Černi, 2018.



## ELECTROCHEMICAL BEHAVIOR OF STEEL IN 0.1 mol/dm<sup>3</sup> HCl IN THE PRESENCE OF POTATO PEEL JUICE

Milica Zdravković, Vesna Grekulović, Bojan Zdravković, Nada Štrbac,  
Milan Gorgievski, Miljan Marković

Technical Faculty in Bor, University of Belgrade, V.J. 12, 19210 Bor, Serbia

### Abstract

Corrosion control is possible by adding a small amount of a compound that opposes the anodic or cathodic corrosion reaction or both. This paper presents the results of investigating the electrochemical behavior of steel with 0.1 mol/dm<sup>3</sup> HCl in the absence and presence of potato peel juice (2 mL-10 mL). Electrochemical methods of open circuit potential measurement and cyclic voltammetry were applied. The results show that in the presence of potato peel juice (PPJ), there is a shift towards more positive values of the open circuit potential and that value is increasingly positive with the increase in the PPJ concentration. The results obtained by cyclic voltammetry indicate that there are no clearly expressed current peaks on the cyclic voltammogram. With all the PPJ additions the current strength values are lower compared to the current strength values without the addition. The lowest value of the current strength was obtained with the addition of 10 mL PPJ. Lower current values in the presence of PPJ indicate that the potato peel juice slows down both anodic and cathodic processes to a certain extent. Potato peel juice acts as a mixed type of steel corrosion inhibitor in 0.1 mol/dm<sup>3</sup> HCl.

**Keywords** steel, electrochemical behavior, chloride medium, potato peel

### 1. INTRODUCTION

Steel C15 belongs to the group of low-carbon steels for cementation. The carbon content in C15 steel is up to 0.2%. Steel C15 is used for making parts of small dimensions and simple shapes, exposed to wear and low loads, where high hardness of the core is not required (handles, levers, sleeves, joints) [1].

Industrial food by-products are attracting the attention of researchers as possible green corrosion inhibitors. A large amount of by-products is obtained from potato processing. Potato (*Solanum tuberosum* L.) is one of the most important foods in the world. This food originated in South America, around 500 BC. Over time, the potato has become an important food item in the human diet, which can be attributed to its nutritional value [2]. Potato processing by-products, like other food by-products, are organic materials whose disposal is very important for environmental reasons. Potato peel requires additional processing, especially if it is used for animal feed due to the high fiber content [3].

This paper presents the results of investigating the effect of potato peel juice (*Solanum tuberosum* L.) on the steel corrosion in 0.1 mol/dm<sup>3</sup> HCl.

### 2. EXPERIMENTAL

The experiments were carried out in a system consisting of a three-electrode electrochemical cell and hardware interface for computerized control and data acquisition. The steel C15 was used as working electrode, the saturated calomel electrode (SCE) as reference electrode and platinum foil as a counter electrode. The computerized control (National Instruments card, NI-6251) and data acquisition software (LabVIEW 8.2 platform), fully developed at Technical Faculty in Bor [4], was used to run the electrochemical experiments.

Investigation of the steel C15 electrochemical behavior in 0.1 mol/dm<sup>3</sup> HCl without and with the addition of PPJ was performed by measuring the open circuit potential in relation to a saturated calomel electrode for 1800 s and using the cyclic voltammetry method. Cyclic voltammograms were recorded using the cyclic voltammetry method in the potential range from -1 to 0.2 V in relation to SCE in 0.1 mol/dm<sup>3</sup> HCl.

The 37% HCl produced by "VWR Chemicals Prolabo BDH" was used to prepare a 0.1 mol/dm<sup>3</sup> HCl solution. Solutions were prepared from chemicals p.a. purity and distilled water in the amount of 1000 mL. The working solutions were obtained by adding PPJ. Before peeling, the potatoes were washed with plain water, then with distilled water to remove impurities from the potatoes surface. After peeling, the juice of the potato peel was obtained using a Philips HR1853 juicer. The resulting PPJ was filtered on a Bichner apparatus.

The working electrode was obtained from C15 steel melted in epoxy resin. The electrode working surface was wire cross-section with a diameter of 3 mm.

### 3. RESULTS AND DISCUSSION

The results of measuring the open circuit potential for steel in 0.1 mol/dm<sup>3</sup> HCl without and with the addition of PPJ are shown in Figure 1. The change in the open circuit potential was monitored during 1800 s. The open circuit potential for steel in 0.1 mol/dm<sup>3</sup> HCl without the addition drops sharply in the first 60 s, then rises sharply until about 250 s, after which it decreases, fluctuates, and stabilizes at about 1600 s. The stabilized value of the open circuit potential obtained in 0.1 mol/dm<sup>3</sup> HCl without the addition of PPJ is  $E = -0.565$  V vs. SCE.

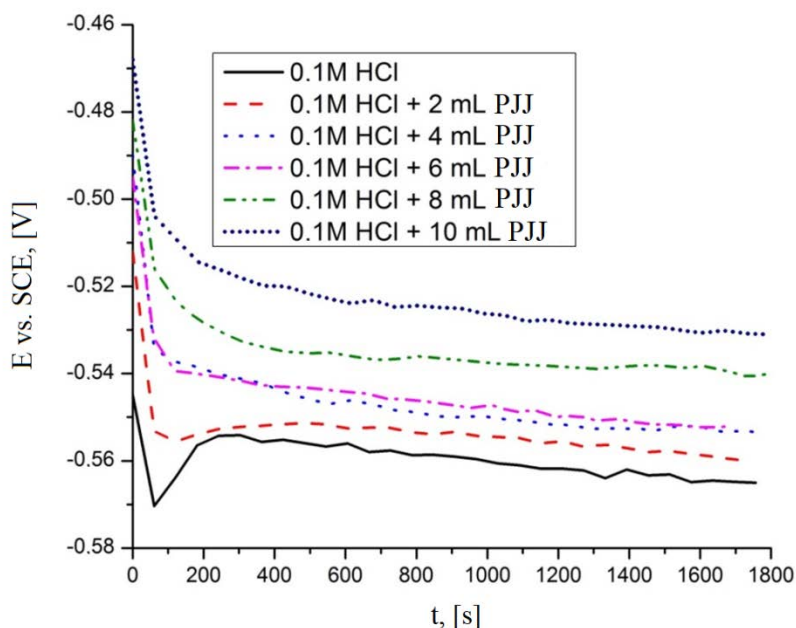


Figure 1 - Results of measuring the open circuit potential for steel in 0.1 mol/dm<sup>3</sup> HCl without and with the addition of PPJ for 1800 s

With the addition of 2 mL, 4 mL, 6 mL, 8 mL and 10 mL PPJ, there is a sudden drop in the potential in the first 50 s. With the addition of 2 mL PPJ after 50 s, the potential value begins to rise slightly until 500 s, then falls slightly, after which it stabilizes at around 1500 s and amounts to  $E = -0.560$  V vs. SCE. The open circuit potential with the addition of 4 mL and 6 mL PPJ after a sharp drop in the first 50 s, continues to decrease slightly and stabilizes at about 1400 s. The potential values are approximately equal, and after stabilization with the addition of 4 mL PPJ, it amounts to  $E = -$

0.554 V vs. SCE, and with the addition of 6 mL PPJ is  $E = -0.553$  V vs. SCE. With the addition of 8 mL and 10 mL PPJ, the potential drop after 50 s is less pronounced compared to the potential values without the addition and with the addition of 2 mL, 4 mL, and 6 mL PPJ. The open circuit potential with the addition of 8 mL and 10 mL PPJ stabilizes after 1600 s, and amounts to  $E = -0.540$  V vs. SCE and  $E = -0.531$  V vs. SCE, respectively.

At all concentrations of PPJ the values of the open circuit potential for steel in 0.1 mol/dm<sup>3</sup> HCl are more positive compared to the value of the open circuit potential without the addition. The value of the open circuit potential is increasingly positive with the increase in the PPJ concentration.

The results obtained by the cyclic voltammetry are shown in Figure 2. Cyclic voltammograms were recorded in the potential range from -1 V in relation to SCE to 0.2 V in relation to SCE at a potential change rate of 50 mV/s. There are no clearly defined current peaks on the voltammogram without the addition of PPJ, as well as on the voltammograms with the addition of juice.

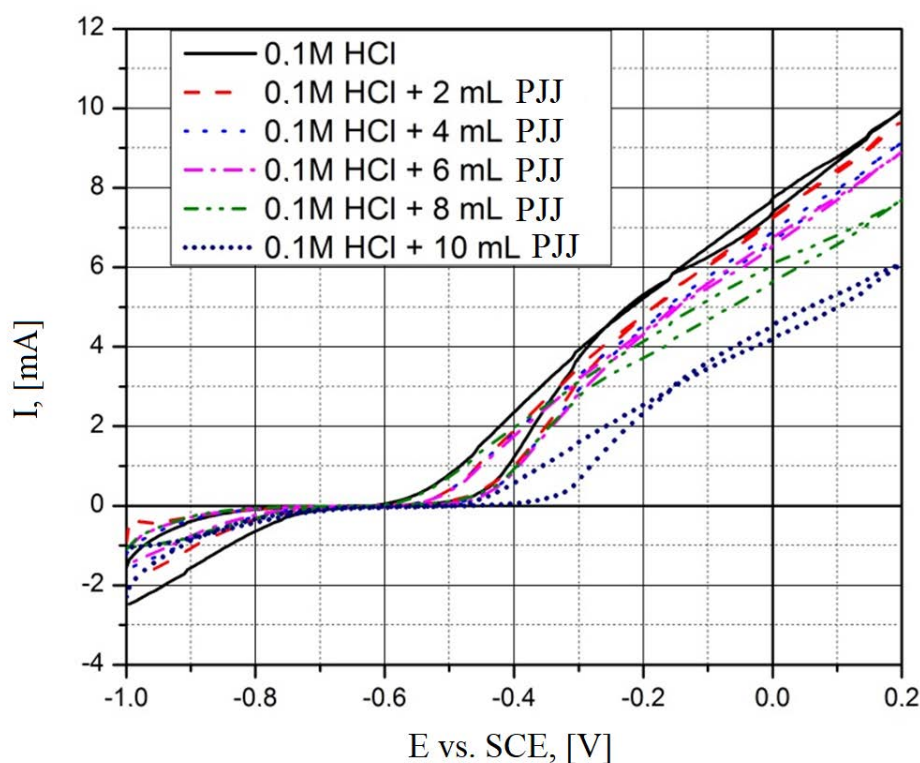


Figure 2 - Cyclic voltammograms obtained for steel in 0.1 mol/dm<sup>3</sup> HCl without addition and with the addition of PPJ at a potential change rate of 50 mV/s, surface of the working electrode 0.07 cm<sup>2</sup>

In the anodic part of the cyclic voltammogram, it can be seen that with the addition of 2 mL PPJ, the current strength values are approximately equal to the current strength values for steel in 0.1 mol/dm<sup>3</sup> HCl without the addition. At potentials more positive than -0.5 V vs. SCE leads to an increase in current strength, which means that the corrosion process is taking place. With the addition of 4 mL, 6 mL, 8 mL and 10 mL PPJ, the current strength values are lower compared to the current strength values without the addition. The lowest value of the current strength was obtained with the addition of 10 mL PPJ.

In the cathodic part of the cyclic voltammogram, it is clearly seen that in the entire potential range, the current strength values in the PPJ presence are lower compared to the current strength values



without the addition. The lowest value of the current strength was obtained with the addition of 10 mL PPJ. Lower current values in the presence of PPJ indicate that the addition slows down both anodic and cathodic processes to a certain extent. Which means that PPJ acts as a mixed type of steel corrosion inhibitor in 0.1 mol/dm<sup>3</sup> HCl.

#### 4. CONCLUSION

Based on the obtained results of measuring the open circuit potential, it can be concluded that with the addition of PPJ (*Solanum tuberosum L.*) in a 0.1 mol/dm<sup>3</sup> HCl solution, the open circuit potential of steel C15 moves towards more positive values. The value of the open circuit potential is more positive with increasing concentration of PPJ.

The results of investigating the electrochemical behavior of steel using cyclic voltammetry in 0.1 mol/dm<sup>3</sup> HCl without and in the presence PPJ (*Solanum tuberosum L.*) indicate the effect of PPJ as steel corrosion inhibitor. The value of the current strength in the presence of PPJ decreases and this decrease is more significant with the increase in the PPJ concentration. Potato peel juice acts as a mixed corrosion inhibitor C15 steel in 0.1 mol/dm<sup>3</sup> HCl. It is assumed that protection against corrosion is achieved by the protective film formation on the steel surface, which is a consequence of the adsorption of ingredients present in the juice.

#### ACKNOWLEDGEMENTS

*The research presented in this paper was done with the financial support of the Ministry of Education, Science and Technological Development of the Republic of Serbia, within the funding of the scientific research work at the University of Belgrade, Technical Faculty in Bor, according to the contract with registration number 451-03-47/2023-01/ 200131.*

#### REFERENCES

- [1] [http://afrodita.rcub.bg.ac.rs/~rzoran/6-MM\\_ho.pdf](http://afrodita.rcub.bg.ac.rs/~rzoran/6-MM_ho.pdf), 03.07.2019.
- [2] J. E. Bradshaw, G. Ramsay, S. Jaspreet, K. Lovedeep, Advances in potato chemistry and technology, Academic press, San Diego, U. S. A., 2009, p. 1-26.
- [3] G. G. Birch, N.Blakebrough, K. J. Parker, Enzymes and food processing, Applied science publishers ltd, London, UK, 1981, p. 296.
- [4] Z. Stević, M. Rajčić-Vujasinović, Chem. Ind., 61 (1) (2007) 1-6.

## MICROSTRUCTURE AND THERMAL PROPERTIES OF LEADED BRASS AFTER QUENCHING

Ivana Marković<sup>1</sup>, Dalibor Jović<sup>2</sup>, Uroš Stamenković<sup>1</sup>, Dragan Manasijević<sup>1</sup>, Ljubiša Balanović<sup>1</sup>, Milan Gorgievski<sup>1</sup>

<sup>1</sup>Technical Faculty in Bor, University of Belgrade, V.J. 12, 19210 Bor, Serbia

<sup>2</sup>Serbia Zijin Copper DOO, Đorđa Vajferta 29, 19210 Bor, Serbia

### Abstract

Rapid cooling of Cu-Zn alloys from the two-phase ( $\alpha + \beta$ ) or single-phase  $\beta$  region can reduce or even prevent the existence of the  $\alpha$  phase. In this way, by quenching, the proportion of  $\alpha$  and  $\beta'$  crystals changes compared to the initial microstructure obtained by casting, which directly affects the change in the properties of these alloys. The investigation in this paper was conducted to analyse the influence of quenching temperature on the thermal properties of CuZn40Pb2 alloy. After casting the alloy, it was heated at 500 °C, 600 °C, 700 °C, and 800 °C and cooled in ice water, to maintain the high-temperature structure. Microstructure was analysed using optical microscopy. The values of thermal diffusivity, specific heat, and thermal conductivity were determined for the alloy in the cast and quenched states. The sample that was quenched from 800 °C was subjected to continuous annealing during the DSC analysis showing two endothermic reactions characteristic for the melting of a lead phase and disordering of  $\beta'$  phase.

**Keywords:** lead bronze, thermal diffusivity, specific heat, thermal conductivity

### 1. INTRODUCTION

Cu-Zn alloys (brasses) have very high electrical and thermal conductivity, good corrosion resistance, and excellent workability. Because of these properties, they are widely used in numerous industries [1-4]. Lead is usually added to brasses to increase their machinability (due to increasing chip breakage), cutting parameters, and tool life (due to decreasing the cutting forces) [1,5,6]. Properties of  $\alpha + \beta'$  brasses depend on phase composition, i. e. contribution of two main phases:  $\alpha$  solid solution with face-centered cubic crystal lattice and  $\beta$  phase which is intermetallic compound CuZn with body-centered cubic crystal lattice with a disordered structure, that below 454 °C undergo to ordering and transformation into the ordered  $\beta'$  phase. In the structure of duplex leaded brasses, except these two phases, particles of free lead are always presented [7,8]. Lead-free or low-leaded brasses have been studied by numerous researchers [9,10]. However, the cost of these types of brasses is high and their high-temperature strength is lower [11]. Therefore,  $\alpha + \beta'$  brass with a low content of lead (2 wt.% Pb) and traces of Sn, Fe, and Ni was used as starting material, to analyse how changes in the ratio  $\alpha/\beta'$  in the structure influence the thermal properties of these alloys.

### 2. EXPERIMENTAL

After measuring the calculated amount of pure copper and alloying elements, they were melted in a flame furnace with a silicon carbide pot. The CuZn40Pb2 alloy (in wt.%) was obtained by casting the melt in a sand-clay mould, whereby a cylindrical ingot with a diameter of 20 mm was obtained. The ingot was machined on a "PA-B 30" lathe to a diameter of 12.7 mm and cut into 10 mm high samples, which were subjected to further heat treatment. The cutting was done using the "Mesotom - Struers" cutting device. The samples were solution annealed in the furnace "Vims-elektrik LPŽ-7.5S" at four temperatures: 500 °C, 600 °C, 700 °C, and 800 °C for 1 h. After heating at different temperatures, the samples were quenched. Microstructure was analysed using "Carl Zeiss Jena

EPITYP 2" optical microscope. The following thermal properties of quenched samples were measured: thermal diffusivity, thermal conductivity, and specific heat using the "Discovery Xenon Flash DXF-500" device. Differential scanning calorimeter (DSC) "TA Instruments Q600 SDT" was used to analyse the thermal behaviour of CuZn40Pb2 alloy quenched from 800 °C during heating at a constant rate of 10°C/min.

### 3. RESULTS AND DISCUSSION

The microstructure of CuZn40Pb2 alloy in cast and quenched states is shown in Fig. 1. The microstructure of cast CuZn40Pb2 alloy is two-phase  $\alpha + \beta'$ . With increasing quenching temperature amount of  $\beta'$  phase gradually increased. Sample quenched from 800 °C shows the presence of only  $\beta'$  phase.

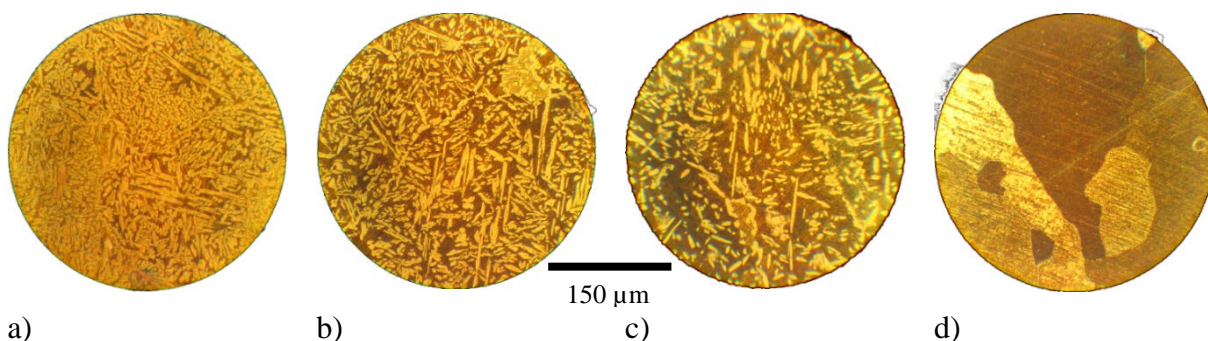


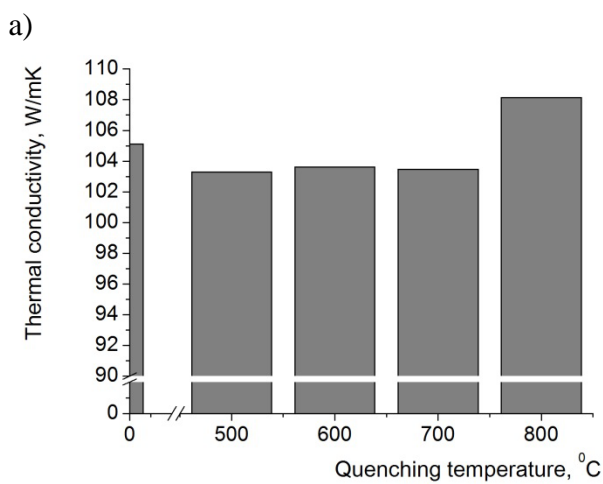
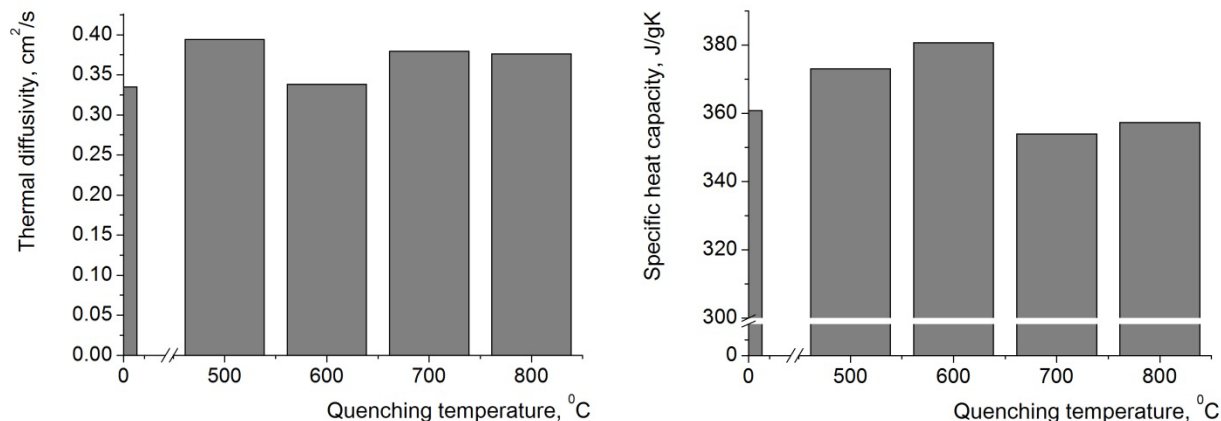
Figure 1 - Microstructure of CuZn40Pb2 alloy after (a) casting; (b) quenching from 600 °C; (c) quenching from 700 °C; (d) quenching from 800 °C

Among the thermal properties, the values of thermal diffusivity, specific heat capacity, and thermal conductivity were measured. The values of thermal properties of CuZn40Pb2 alloy after casting and quenching from different temperatures are shown in Fig 2. Copper has excellent thermal properties (thermal diffusivity 1.16 cm<sup>2</sup>/s; specific heat capacity 385 J/kgK; and thermal conductivity 397.48 W/mK [12]). It is noted that cast CuZn40Pb2 alloy has similar values of specific heat capacity (360.8 J/kgK) as copper, but a quarter of the thermal diffusivity (0.335 cm<sup>2</sup>/s) and thermal conductivity (105.1 W/mK) of pure copper. From Fig. 2, it can be seen an irregular pattern in the increase and decrease of the thermal properties of CuZn40Pb2 alloy as the quenching temperature increases. Generally, quenching causes an increase in thermal diffusivity values compared to the cast state. Quenching from 500 °C and 600 °C has led to an increase in specific heat capacity, while quenching from higher temperatures decreased it. The thermal conductivity of quenched samples was something smaller compared to the cast state except for the sample quenched from 800 °C whose thermal conductivity is the highest. This sample has a microstructure that consists only of  $\beta'$  phase, unlike the other samples with  $\alpha + \beta'$  microstructure.

The sample quenched from 800 °C was subjected to continuous heating at a constant heating rate of 10 °C/min up to 500 °C on a DSC device to analyse phase changes, and possibly detect the decomposition of the presaturated  $\beta'$  phase. Fig. 3 shows the DSC curve of CuZn40Pb2 alloy quenched from 800 °C. DSC monitors the difference in heat flux to the sample and standard when they are heated [13].

The first slight peak on the DSC curve indicates an endothermic reaction and occurs around 325 °C. This peak designates the melting of a lead phase, which is present in the CuZn40Pb2 alloy in a small amount [14]. The required heat for melting the lead phase is 0.3554 J/g. The second peak on the DSC curve also indicates an endothermic reaction and occurs around 460 °C. This endothermic peak indicates a phase change according to the phase diagram Cu-Zn-Pb, where the

$\beta'$  ordered phase becomes the disordered  $\beta$  phase. The required heat for the transition from the ordered  $\beta'$  phase to the disordered  $\beta$  phase is 0.6761 J/g.



a) b) Figure 2 - Influence of quenching temperature on thermal properties: (a) thermal diffusivity (b) specific heat capacity (c) thermal conductivity of the investigated CuZn40Pb2 alloy

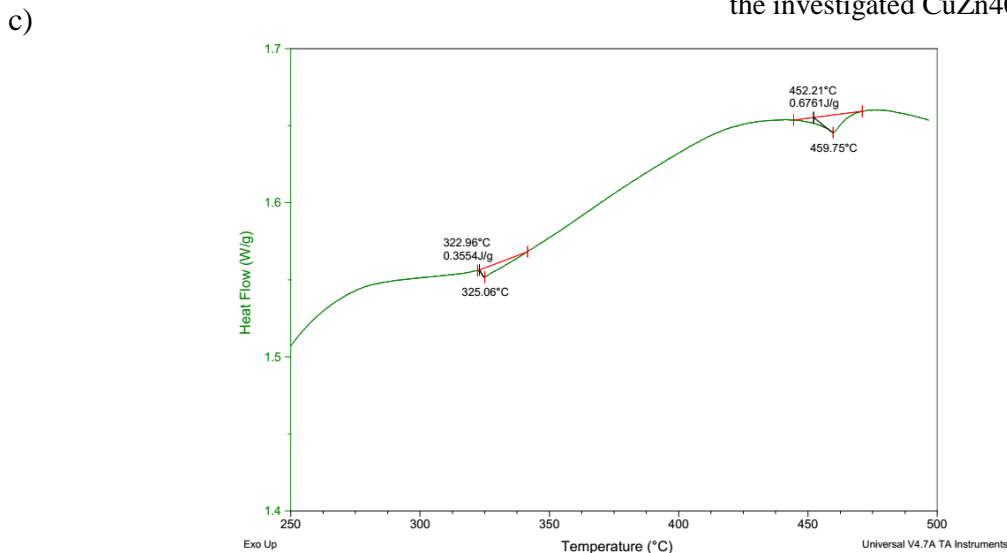


Figure 3 - DSC curve of CuZn40Pb2 alloy quenched from 800 °C

#### 4. CONCLUSION

Based on the performed experiments, the following can be concluded:

- The cast CuZn40Pb2 alloy is two-phased  $\alpha + \beta'$  brass. With an increase in quenching temperature the amount of  $\beta'$  phase gradually increased up to 800 °C where there is only  $\beta'$  phase.

- The cast CuZn40Pb2 alloy has a similar specific heat capacity as copper, but a quarter of the thermal diffusivity and thermal conductivity of pure copper. The thermal diffusivity increases slightly with quenching. The best thermal conductivity was achieved after the quenching from 800 °C.

- DSC curve of quenched brass showed two endothermic reactions indicating the melting of a lead phase (around 325 °C) and disordering of  $\beta'$  phase (around 460 °C).

## ACKNOWLEDGEMENTS

*The research presented in this paper was done with the financial support of the Ministry of Science, Technological Development and Innovations of the Republic of Serbia, with the funding of the scientific research work at the University of Belgrade, Technical Faculty in Bor, according to the contract with number 451-03-47/2023-01/200131.*

## REFERENCES

- [1] N.M. Vaxevanidisa, N.A. Fountasa, A. Koutsomichalisb, J.D. Kechagias, *Procedia Struct.*, 10 (2018) 333–341.
- [2] A. Momeni, G.R. Ebrahimi, H.R. Faridi, *Mater. Sci. Eng. A*, 626 (2015) 1–8.
- [3] A.A. Fadhil, M.S. Ghattas, B.A. Iskander, S.A. Ajeel, T.A. Enab, *Alex. Eng. J.*, 57 (2018), 1301–1311.
- [4] P. García, S. Rivera, M. Palacios, J. Belzunce, *Eng. Fail. Anal.*, 17 (2010) 771–776.
- [5] V. Buršikova, J. Buršik, V. Navratil, K. Milička, *Mater. Sci. Eng. A*, 324 (2002) 235–238.
- [6] J. Johansson, P. Alm, R. M'Saoubi, P. Malmberg, J.E. Stahl, V. Bushlya, *Int. J. Adv. Manuf. Technol.*, 120 (2022) 7263–7275.
- [7] N.B. Pugacheva, *Met. Sci. Heat Treat.*, 49 (1-2)(2007) 67–74.
- [8] N.B. Pugacheva, A.A. Pankratov, N.Y. Frolova, I.V. Kotlyarov, *Metally.*, 3 (2006) 239–248.
- [9] W. Chen, Y. Jia, J. Yi, M. Wang, Q. Derby, B. Lei, *J. Mater. Res.*, 32 (2017) 3137–3145.
- [10] P. Suksongkrm, S. Rojananan, S. Rojananan, *Mater. Trans.*, 59 (2018) 1747–1752.
- [11] K.J Chen, *Metals*, 10 (2020) 722–734.
- [12] <https://thermtest.com/thermal-resources/materials-database>
- [13] P. Gill, T.T. Moghadam, B. Ranjbar, *J. Biomol. Tech.*, 21(4) (2010) 167–193.
- [14] T. Jantzen, P.J. Spencer, *Calphad*, 22 (3)(1998) 417–434.

## HOT STRIP MILL WALKING BEAM SLAB REHEATING PROJECT

**Mehmet Ali Yildiz**

HBIS GROUP Serbia, Iron & Steel d.o.o. Beograd, 11100 Belgrade, Serbia

### **Abstract**

*HBIS had 2 pushing type of Slab Reheating Furnaces, consuming 50m<sup>3</sup> Natural Gas per ton+Blast Furnace gas around 75% of the mix. Walking beam furnace has enables HBIS to use %100 blast furnace gas for slab reheating. Walking beam furnace has state of art technologies such as Evaporative cooling, automatic double burner combustion proses, level 2 automation, self-recuperative heating.*

**Keywords:** Hot strip mill; Walking beam; Reheating; Blast furnace gas

### **1. INTRODUCTION**

Purpose of this project is to use blast furnace gas for slab reheating in HSM instead of natural gas to save energy, reduce the cost and improve heating quality. Natural gas is the purchased energy with high price, and its supply is restricted by the market. Blast furnace gas is a by-product of steel mills, with relatively low price.

### **2. EXPERIMENTAL**

#### **2.1 Technical specification**

Technical specification was defined by MCCO and WISDR according to HBIS requirement

Heating Capacity 250 ton/hour

Furnace interior dimensions, 35.000 mm length and 12.800 mm width

Main fuel: blast furnace gas

Type: Walking beam

Charging/discharging, charging by charging machine and discharging by discharging machine

Cooling mode of support beam: forced circulation and evaporative cooling

Combustion mode: air-gas double regenerative combustion

Walking beam mechanism type: double-wheel inclined rail, hydraulic drive

Cold furnace startup / maintenance and drying: natural gas is used when the furnace temperature lower than 700 °C, and blast furnace gas is used when the furnace temperature greater than 700°C

#### **2.2 Site survey and engineering**

Site survey and engineering work was done by MCCO and WISDR and Tang Steel experts

#### **2.3 Installation**

Installation was done by MCCO and WISDR using subcontractor companies

#### **2.4 Commissioning**

Commissioning was done by MCCO and WISDR, Tang steel and HBIS experts

#### **2.5 Performance test**

Main performance test criteria of WBF

Productivity, 250 ton/hour

Yield loss, maximum 1%



Fuel consumption, 1,3 GJ/t  
Furnace pressure 0-30 d Pa  
Roof temperature, maximum 120C



Figure 1 - HBIS Walking Beam Furnace

### 3. RESULTS AND DISCUSSIONS

WB Furnace has been utilizing by HBIS since September 2022 and it has provided important advantages

#### 3.1 Charging –Discharging of slabs



Figure 2a - Charging



Figure 2b - Discharging

Slab Size 750-2.050 mm wide 4.500-12.000 mm length of slabs

Single Charge 5.900- 12.000 mm

Double Charge 4.500-5.900 mm

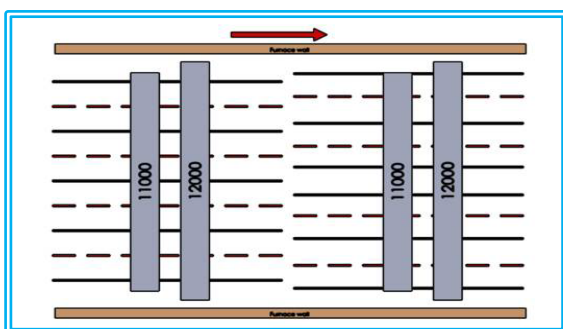


Figure 3 – Single charge

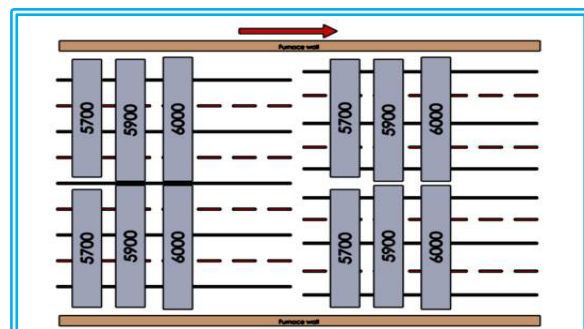


Figure4 – Double charge



### 3.2 Slab movement in the furnace

There are 4 lines of walking beams and 5 fixed on the entry, and again 4 walking beams and 6 fixed beams on the exit side to move the slabs towards exit by making a four step cycle, up, forward, down and backward.

### 3.3 Combustion system



Figure 5 – Combustion system HMI screen

There is a fully automatic combustion system with 4 modes of regenerative burners, which are upper air burners, upper gas burners, lower air burners and lower gas burners. Each mode burner has 22 pieces, and the total quantity is 88 burners. The exhaust gas and air is used to heat the inlet air and gas to save energy. Automatic combustion system uses numerous thermocouples, flow feedback and pressure feedback devices to adjust the parameters.

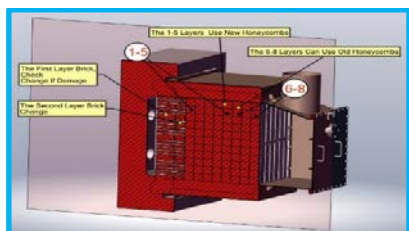


Figure 6 – Burner Block

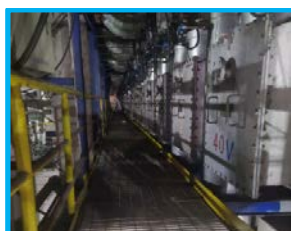


Figure 7 – Burner Blocks

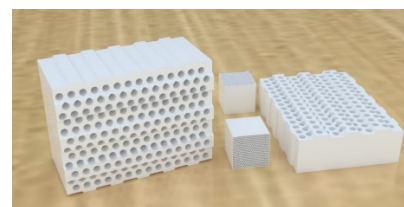


Figure 8 - Honeycomb and bricks

### 3.4 Skid beams cooling system

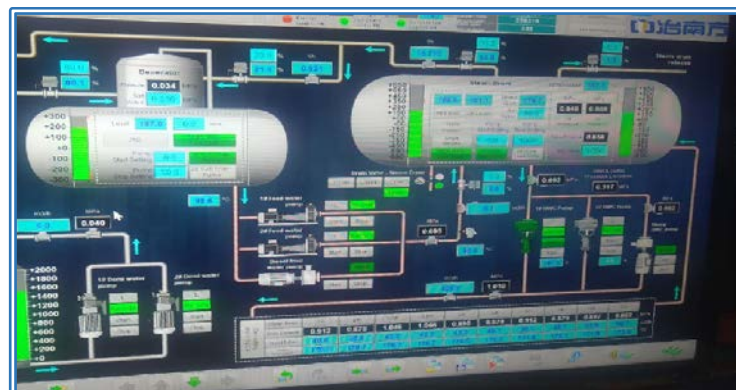


Figure 9 - Evaporative cooling HMI screen

System consist of a demi water feeding tank, a Deaerator, water pumps, cooled skid beams, return steam drum and heat exchangers. Deaerators are mechanical devices that remove dissolved gases

from boiler feed water. Deaeration protects the steam system from the effects of corrosive gases. It accomplishes this by reducing the concentration of dissolved oxygen and carbon dioxide to a level where corrosion is minimized. The water is fed into the beams by pumps and return steam goes into the steam drum. The steam goes through heat exchangers and fed back to deaerator unit.

### **3.5 Level 2 system**

Level 2 system works for

Automatic charging discharging, by utilizing telemeters, switches

Automatic movement of walking beam

Automatic combustion

Automatic temperature control for each specific heating zone of the furnace

### **3.6 Advantages of WBF**

#### **3.6.1 Environmental advantages**

Blast Furnace gas is a byproduct created in iron making process, it has to be burned and released into the air if it is not used in the production process. WBF uses 100% blast Furnace gas so that BF gas is used fully and no need to use natural gas.

#### **3.6.2 Quality Advantages**

Improve the heating quality, Avoid skid marks

Homogeneous Heating, uniform bottom and top temperatures

Charging by charging machine, avoid scratch on the lower surface during hot slab charging

No furnace hearth pile up issue

It is convenient to start and stop the furnace, and to charge, discharge, empty and stop the furnace.

Avoid accidents such as curved steel and sticking steel

The slabs heated is not limited by the shape such as conical

#### **3.6.3 Cost advantages**

Energy saving due to utilizing blast furnace gas, no need natural gas

Evaporative cooling, recover waste heat

Pushing Furnaces natural gas cost is around 20USD/ton, we save about 17 USD /ton by using 100% blast Furnace gas.

## **4. CONCLUSION**

HBIS WBF project was initiated for reducing cost by using 100% blast furnace gas in slab reheating. This created a big advantage in terms of cost. But on the other hand state of art double regenerative self-recuperative heating and evaporative cooling walking beam furnace created big environmental and quality advantages as well as cost advantage.

## FINISHING MILL AUTOMATION UPGRADE AT HOT STRIP MILL

**Peter Polyak**

HBIS GROUP Serbia, Iron & Steel d.o.o. Beograd, 11100 Belgrade, Serbia

### **Abstract**

*Finishing Mill Automation upgrade is including the Crop Shear, Descaler, 6 stand Rolling Mill, Laminar Cooling Control system replacement – Level1&2, Control Systems, HMI, Self-learning/ adapting, Reporting. The main reason were the obsolete system, not available spare parts and the product quality improvement.*

**Keywords:** *Finishing mill; Automation; Rolling mill; Laminar cooling control system*

### **1. INTRODUCTION**

Hot rolled strips rolled on semi-continuous six-stand rolling mill. On this line, hot rolled strip can be produced in the range from 720mm to 2050mm of width and from 1.5mm to 15mm of thickness. At the end of the production line hot rolled strips are wound up into coils of inner diameter 740mm and maximum outside diameter 2000mm. The Hot rolling line can produce smooth strips with mill surface and patterned strips (pattern type: diamond or tear). The Mill produces Structural steels; Low-carbon steels for cold forming or for further cold rolling; Steels for shipbuilding; Steels for boilers and high pressure vessels; Micro-alloyed, thermo-mechanically rolled, high yield strength steels for cold forming; Line-pipes steels according to API 5L standards.



Figure 1 – Photo of 6 Stand Finishing Mill

Scope of the upgrade package consist of:

- Replacement of Mill Level 1 Automation and Technological Controls.
- Replacement of Crop shear Level 1 Automation, Drive unit and Technological Controls.
- Laminar Cooling Level 2 Control system.



- Level 2 Automation, providing setups to new level 1 system. The Level 2 is a self-learning, adapting and improving system. Data collection and reporting are basic functions.
- Replacement of existing HMI systems considering the Level 1 and Level 2 HMI screens.
- Interfacing of existing and remaining plant areas, controllers and measuring gauges.



Figure 2 – Photos of Old Automation and Old Pulpit

## 2. EXPERIMENTAL

### 2.1 Technical specification

Detailed technical description of existing system, rolling process and specification of revamp scope was worked out by HBIS Serbia specialists.

### 2.2 Tender

SMS Group was selected as a supplier.

### 2.3 Site survey and Engineering

The site survey, basic / detailed engineering, software development was executed with full involvement of HBIS personal. SMS Group applied their own developed product X-Pact system.

### 2.4 Integration test

Prior to installation and commissioning on site the integrated system test was executed at supplier facility. HBIS Serbia automation engineers, operation and quality staff participated on this test.

### 2.5 Installation

Installation of equipment was performed during normal operation respectively during the planned maintenance downtimes.

### 2.6 Shadow mode

In order to properly adjust the new automation we decided to prepare a parallel / shadow mode, when while running with old automation we could test, adjust the new automation system resp. later when having issues with new automation system to be able to switch back to old automation system anytime. This solution brought us advantages, gave opportunity to pre-tune the new system and saved us a lot of downtimes when the fixes in new system took longer time.

### 2.7 Commissioning, Fine tuning and Optimization

SMS Group applied Plug and Play system. The first coil was rolled as expected. Not demanding products rolling was achieved easy. While rolling critical products as light gauge 1.5 mm, heavy gauge micro alloyed products, critical dimensions we experienced difficulties and was needed more time to adjust the Reduction plans, Automatic Gauge control, the stand speeds and interstand tensions. We had numerous switching back to old system, in order prepare the corrections and test again new settings. During first commissioning period mostly the Process, Level 1, Level 2

specialists were at site and later most of the intervention were done remotely. Remote assistance saved a lot of mutual resources. We were receiving a professional good technical support.

## 2.8 Performance test

There were 4 major key parameters to test – the Automation system availability, Thickness, Mill exit temperature, Coiling temperature.

### 2.8.1 Thickness

Nominal Thickness [mm]	± Tolerances ( $P_G=95.4\%$ ) for strip body [ $\mu\text{m}$ ] ( $P_G=95.4\%$ )			
	≤ 1200	>1200 ≤ 1500	>1500 ≤1800	> 1800
≤ 2.00	45	45	50	NA
>2.00 ≤ 2.50	45	50	50	NA
>2.50 ≤ 3.00	50	55	55	60
>3.00 ≤ 4.00	50	55	55	60
>4.00 ≤ 5.00	55	60	60	65
>5.00 ≤ 6.00	55	60	65	65
>6.00 ≤ 8.00	70	80	85	85
>8.00 ≤ 10.0	75	90	95	100
>10.0 ≤ 12.5	85	100	110	110
>12.5 ≤ 15.0	100	110	120	125

Table 1 – Thickness performance and tolerances

### 2.8.2 Mill exit temperature

Strip length	Strip definition	Lower temperature range [°C]	Aimed temperature [°C]	Upper temperature range [°C]
Body ( $P_G= 95,4 \%$ ) ( $P_G= 95,4 \%$ )	Subsequent strip	-15	Set-up	+15
	Start-up and Change over strips	-20	Set-up	+20
Head and Tail ( $P_G=95,4 \%$ )	Subsequent strip	-30	Set-up	+30
	Start-up and Change over strips	-30	Set-up	+30

Table 2 – Mill exit temperature performance and tolerances

### 2.8.3 Coiling Temperature

Strip length	Strip definition	Lower temperature range [°C]	Aimed temperature [°C]	Upper temperature range [°C]
Body PG (95,4 %)	Subsequent strip	-20	Set-up	+20
	Start-up and Change over strips	-25	Set-up	+25
Head and Tail PG (95,4 %)	Subsequent strip	-30	Set-up	+30
	Start-up and Change over strips	-30	Set-up	+30

Table 3 – Coiling temperature performance and tolerances

### 2.9 Service Contract

After Performance test we agreed Service contract, SMS group provides a global customer support service in case of faults, problems or in case of new developments. In case of faults the service is accessible via hotline 24 hours a day, 365 days a year.

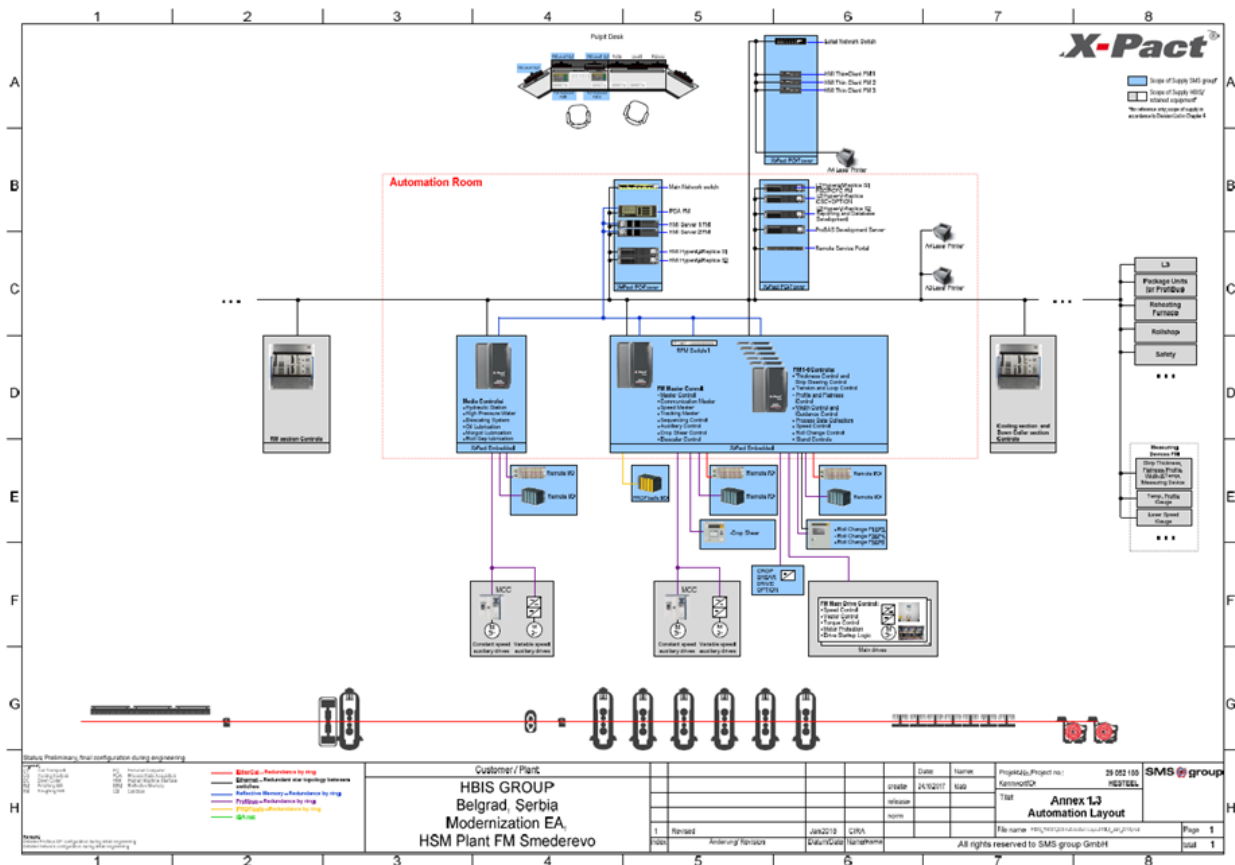


Figure 3 – Automation layout diagram

## 3. RESULTS AND DISCUSSION

### Technological controls:

- **Finishing Mill:** Mill master control; Communication Master; Speed control master; Tracking Master; Sequencing control; Auxiliary Control; Crop Shear Control; Decaler Control

- **FM stands 1 – 6 Control:** Mill stand control; Thickness and strip steering control; Tension and loop control; Profile and Flatness Control; Strip width and guidance control; Roll change control
- **Media controls:** Hydraulic Station; High Pressure Water; Descaling System; Oil Lubrication; Morgoil Lubrication; Roll Gap Lubrication

**Level 2 PSC, PCFC, CSC, REP, DEV** virtualized machines: Pass Schedule Calculation (PSC); Profile Contour and Flatness Calculation (PCFC); Cooling Section Control (CSC\*\*) Reporting (REP); Development (DEV)



Figure 5 – Photos of New Automation and New Pulpit



Figure 6 and 7 – HMI L1 Finishing Mill Overview and Pass Schedule Calculation

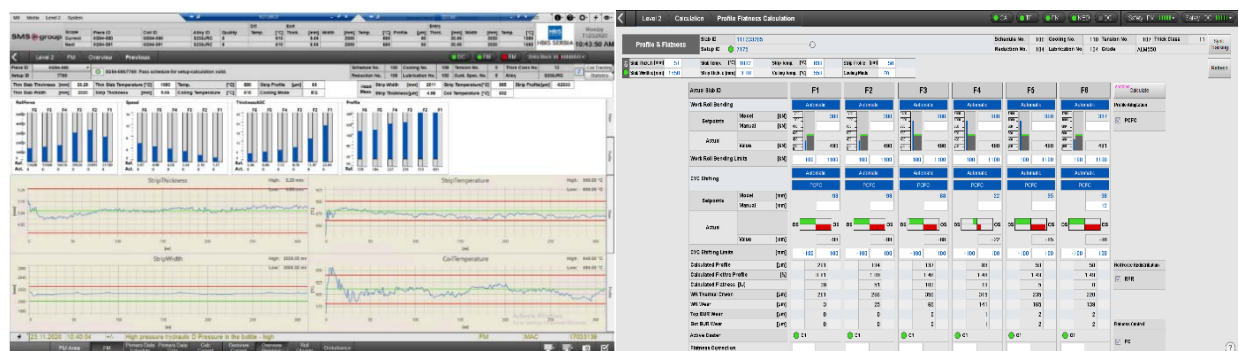


Figure 8 and 9 – HMI L2 Finishing Mill Overview and Profile Flatness Calculation



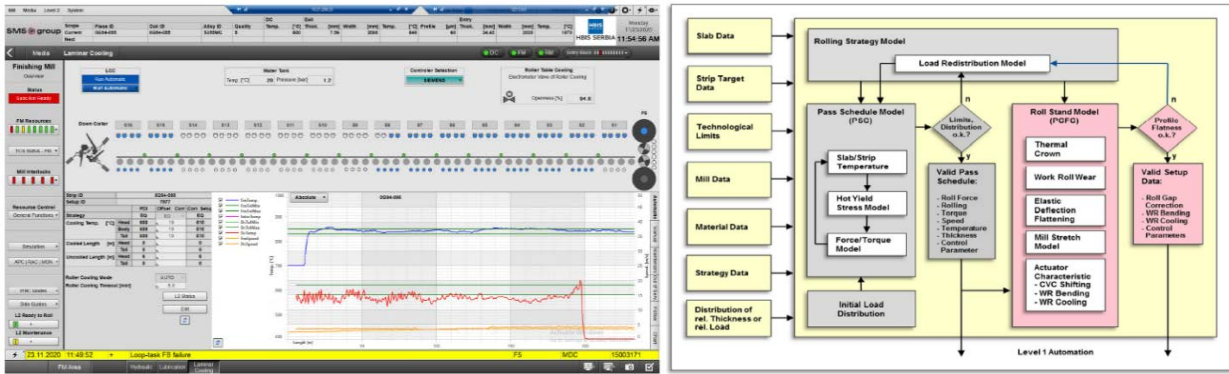


Figure 10 and 11 - Integrated setup calculation for the FM (PSC® <math>\leftrightarrow</math> PCFC®) and HMI Laminar cooling

#### 4. CONCLUSION

This modernization makes our position stronger on the challenging market and allow us further product improvement and product development. We can provide to our customers some new extras as well.

The new automation system availability/ reliability increased and there is no any more problems with spare parts.

We improved the product quality throughout the length of the strip. We achieved reduced thickness variations and tighter thickness tolerances, consistent rolling and coiling temperatures made more stable product mechanical properties, we reduced off gauge at head and tail of the strip.

The other benefits are improved reporting, very good diagnostics for troubleshooting and the alarm/ fault message system makes faster operators and maintenance actions. During operation the mechanical equipment acting more smoothly, which leads to overall better equipment performance and lifetime.

## THE METALLURGICAL TESTING RESULTS OF THE BORON MINERALIZED MATERIAL FROM VALJEVO-MIONICA BASIN

**Branislav Potić, Ana Arifović**

Euro Lithium Balkan doo, Divci, 14222 Valjevo

### **Abstract**

*Due to the assumed mineral potential, the Valjevo-Mionica Neogene basin became the subject of exploration of the expected mineralization of boron, lithium and accompanying elements at the beginning of the 21st century. Accordingly, in the previous period, complex geological research, and accompanying laboratory tests were carried out. The positive results of the early stages of exploration directed further work toward determining and proving mineral resources and mineral reserves (geological and classified reserves) as a prerequisite for exploitation. The existence of boron mineralization (B), which is represented by sodium borates (Borax, Tincalconite), sodium-calcium borates (Probertite, Ulexite), and sodium borosilicate (Searlesite), was confirmed. The grade and content indicated the economic justification of the development of the mineral project towards the expected exploitation of boron ore. As an accompanying element, lithium (Li) is present in Li-montmorillonite clays.*

*During recent geological research by Euro Lithium Balkan, the main focus was on getting knowledge of the technological properties of mineral raw materials, i.e., boron mineralization. Technological-metallurgical tests in certified laboratories were carried out both on the laboratory level (bench scale) and later on the pilot scale. These tests were performed on the material (core of the exploration drillholes) of different size fractions, using hot water and Na<sub>2</sub>CO<sub>3</sub> at different temperatures. It has been shown that hot water is an important factor in the technological process of extraction, i.e. obtaining Borax pentahydrate. The pilot scale process confirmed the bench scale testing results, proving out the concept of a low cost, environmentally responsible, and relatively simple boron extraction circuit, which can produce Borax pentahydrate, with equal chemical characteristics as the commercial product.*

**Keywords:** *Valjevo-Mionica Basin, geological research, technological-metallurgical tests, Boron, Borax pentahydrate*

### **1. INTRODUCTION**

In the western part of Serbia, the movements of Sava tectogenesis created the Valjevo Depression, which extends from the Ljig-Milanovac dislocation in the east through the middle course of Kolubara and Bela Crkva further to the river Drina. The slopes of Maljen and the Cer mountain formed W and NE borders. Towards the east and southeast, the lake was constrained by Mesozoic formations, and in the younger phase along the Ljig-Milanovac dislocation there was a descent of the mainland and the creation of a connection with the Belanovica Basin. With the appearance of faults with E-W and NE-SW strike, the original orientation was changed and Lake basins such as Valjevo-Mionica, Radjevo and Jadar were formed [1].

Due to assumed mineral potential, the Valjevo-Mionica basin became the subject of applied geological research of mineralization of boron, lithium and accompanying elements at the beginning of the XXI century.

The intention of this paper is to summarize the results of applied research mineralization of boron and supporting elements mostly created by the activities of the company Eurolithium Balkan d.o.o., Divci, (ELB+), with the emphasis on metallurgical testing and processing.

## 1.1 The summary of applied geological exploration

Valjevo-Mionica basin is one of a series of neogene basins that have been explored over the past two decades as a "lithium-boron metallogenetic zone" that can be traced from Motajica mountain (BiH), along the Sava river valley, across Lopare (BiH), Jadar and Valjevo-Mionica basin, Rekovac, Pranjani, Jarandol and Pobrdje (Figure 1). Further, it continues into its Turkish counterpart, the Izmir-Ankara-Erzincan zone, hosting the large borate deposits of Bigadiç, Sultanyaçır, Kestelek, Emet, Kırka and Göcenoluk [2].

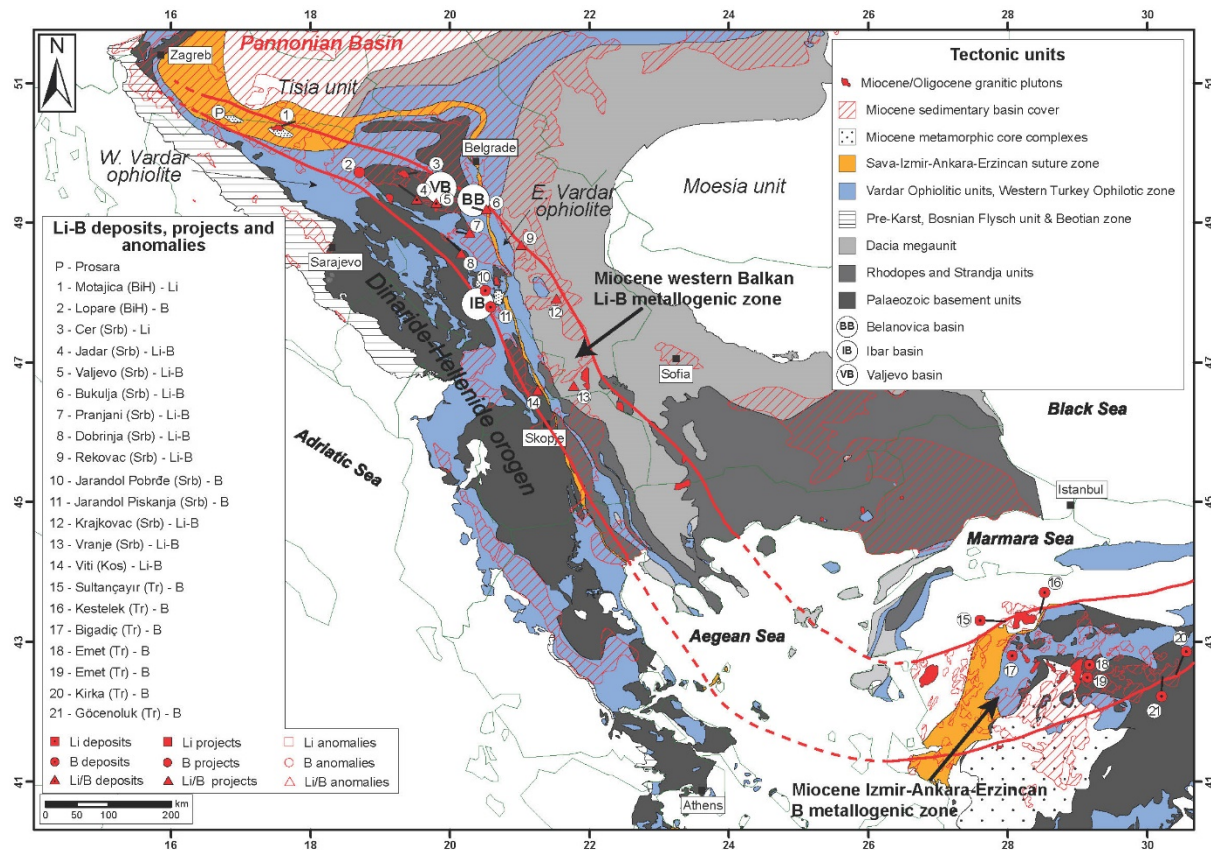


Figure 1 - Basic geological map of the Balkan Peninsula and western Turkey with Li-B deposits and projects in the region [2]

As the earliest methodology, geophysical methods were applied, within which gravimetric and MT methods were used. In addition to geophysical methods, surface testing of the soil was performed. The best insight into the geological and lithological features and mineral characteristics was given by exploration drilling.

From 2011., a total of 49 exploration drillholes were drilled. The total length of the obtained core is about 17 km, and nearly 5,000 samples were sent for chemical analysis. Mineralization of boron (Searlesite, Probertite, Ulexite, Borax and/or Tincalconite) was intersected by 38 holes, and the elevated grade of Li was detected in practically every drillhole.

Mineralization generally occurs in an approximate 30 to 75 m thick unit of tuffaceous sediments, ranging from claystone and siltstone to finegrained sandstone at a depth of 240 m to 315 m from the surface, with an average depth of approximately 275 m.

The positive results induced intensive metallurgical test work in several stages which was focused on borate products. The specific boron mineral association which consists mostly of Na and Na-Ca borates is an important characteristic of the deposit in Valjevo-Mionica basin, thus the test work led to exploration of the Borax pentahydrate flowsheet.

## 1.2 The mineralization of boron and accompanied lithium

X-ray tests detected the Na and Na-Ca borates, as well as the Na-silicoborates [3]. Elevated lithium content is related to montmorillonite clay (Swinefordite), and high boron content for borax minerals (Figures 2 and 3), probertite and ulexite.

PROBERTITE – Ca-Na borate,  $\text{NaCaB}_5\text{O}_9 \cdot 5\text{H}_2\text{O}$ , is the hallmark of the entire deposit in the Valjevo-Mionica basin, and makes the most of the borate mineralization.

ULEXITE – Ca-Na borate,  $\text{NaCaB}_5\text{O}_6 \cdot 5\text{H}_2\text{O}$ , appears on the border with the borax zone.

BORAX - Na-borate,  $\text{Na}_2\text{B}_4\text{O}_7 \cdot 10\text{H}_2\text{O}$  is located in the central part of the deposit “shell”. The Borax usually appears as the alternation of mineral layers and layers of fine-grained clastites. Sometimes it occurs as completely clear, almost vitreous, large, massive layers (Figure 2).

SEARLESITE – Na-silicate,  $\text{NaBSi}_2\text{O}_5(\text{OH})_2$ , has been identified in all drillholes performed, so far. As a silicate, it is not leachable like other borate minerals present in deposit.



Figure 2 – The massive layer of Borax in drillcore

## 2. THE RESULTS OF THE METALLURGICAL TESTING

The main focus during recent geological research was on developing knowledge on the technological properties of mineral raw materials, i.e. mineralization of boron. Most of the testing was done in the laboratories of the Canadian company Kemetco Research Inc, which was followed by the reports issued.

Performed metallurgical tests (on sampled geological mineralized material), showed that borax-pentahydrate ( $\text{Na}_2\text{B}_4\text{O}_7 \cdot 5\text{H}_2\text{O}$ ) can be obtained as a commercial product, in a economical and environmentally sustainable way. These tests were performed on material of different fraction sizes and using hot water and soda-ash ( $\text{Na}_2\text{CO}_3$ ) at different temperatures.

Over the period of two years, exploration was carried out in three phases. In the first two phases, composite samples were tested at the laboratory scale level with different boron content, from 1.58% to 3.96%. It also analyzed the amount of  $\text{Na}_2\text{CO}_3$  in hot water, in order to ensure the optimal results.



In the third phase, the mineralized material was analyzed on lab scale, but also on “pilot” scale. The material for testing (composite) was obtained from the core which was drilled in the central high-grade boron zone of the deposit.

Chemical analysis of composites showed a level of 3.6% B (B<sub>2</sub>O<sub>3</sub> equivalent of 11.58%) and an average lithium concentration of 874 mg/kg (0.0874%), which represents the average grade of the deposit. X-ray diffraction analysis (XRD) showed that boron was present mainly in the form of the probertite (19.3% mass), and the rest of boron minerals were the 7.5% of total mass.

This material has been subjected to laboratory testing using the conditions established by testing in the previous two phases (2022, Kemetco): 25% solids, 90 °C, standby time 4 hours and 20g/l Na<sub>2</sub>CO<sub>3</sub>. Single-stage lye tests, conducted on various granulation from 1.4mm to 10.8mm, showed boron extractions ranging from 74% to 66.2%. The reduction to 1.4mm increased boron extraction by more than 5% (Table 1).

Table 1 - Boron extraction as a function of grind size - test conditions and results

Test ID	Units	GT08-A	GT08-B	GT08-C	GT08-D
B	wt%	3.60	3.60	3.60	3.60
B <sub>2</sub> O <sub>3</sub>	wt%	11.59	11.59	11.59	11.59
Li	wt%	0.09	0.09	0.09	0.09
D 80	mm	10.78	5.69	1.40	3.35
<b>Test conditions</b>					
Solids mass	g	532.21	499.08	500.2	504.83
Intitial Na <sub>2</sub> CO <sub>3</sub> conc	g/L	20	20	20	20
Temperature	°C	90	90	90	90
Pulp density	%	25	25	25	25
Lixiviant (Na <sub>2</sub> CO <sub>3</sub> )	g	1597	1497	1501	1514
<b>PLS</b>					
B	mg/kg	7209	7267	8175	7939
Li	mg/kg	7	6	8	6
Na	mg/kg	11935	11557	12492	12965
CO <sub>2</sub> consumed	%	59.4	69.2	72.1	69.5
<b>Residue</b>					
Leach residue mass	g	449	421	413	399
D <sub>80</sub>	µm	24.9	22.1	21.7	24.6
Mass loss	%	15.7	15.6	17.4	21.0
B	mg/kg	13280	12226	10679	14196
<b>Extraction</b>					
B extraction	%	66.2	68.7	74.0	66.8

After completing the composite leaching test at the laboratory scale, a more detailed comprehensive plan for assembly and operation in the test process, i.e. the "pilot" scale facility, was prepared. The design included all available test results from previous stages of research, as well as calculations of water mass and balance. Based on these results, it was decided that the phases of physical separation will not be included, but that the filtration phase will be included in the cycle for solid-liquid separation in order to improve the utilization and overall balance of water consumption. To improve the allocation, the fraction of shredding raw material was selected, which at the laboratory level showed the best extraction (1.4mm), and the deposition time was increased to 8 hours. The cycle for purification of saturated solutions, crystal recycling and control of solution recycling and total water is also adjusted. The modified cycle scheme is shown in Figure 3.

The “pilot” level process for the utilization of Borax pentahydrate production was carried out over a period of five days. Material that remained, alkali residues, which are now depleted by boron, have been retained as a raw material for the technological cycle for potential lithium-carbonate producing in the next testing program, which will be performed.

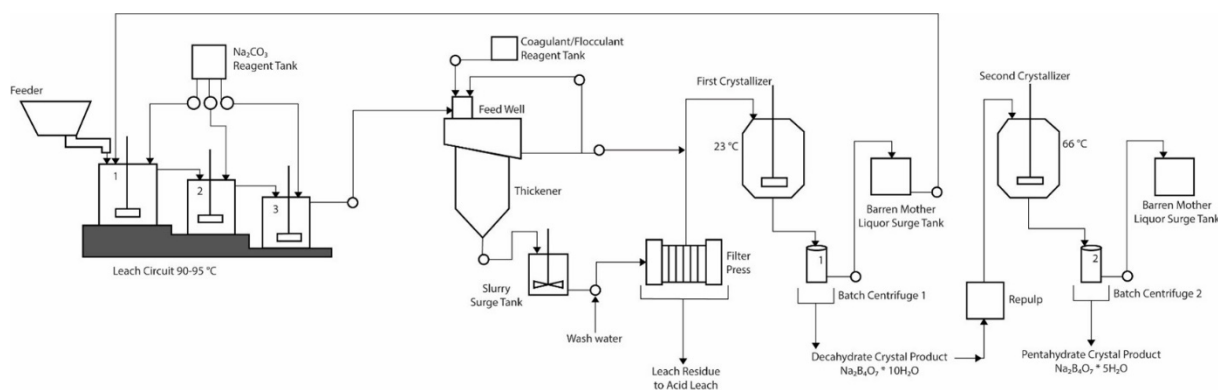


Figure 3 – The Borax pentahydrate flowsheet

During the continuous technological process ("pilot" campaign), 337 kg of input material, composites with a content of 3.6% B, were processed. 300 liters of 24g/l solution were used for starting but also during the cycle of allocation and thickening in crystallizer 1 for the first 14 hours of operation. After this point, the concentration of the solution in the alkali cycle was performed using 24g/l  $\text{Na}_2\text{CO}_3$  solution and the pulp density was maintained with fresh warm water until the recycled barren liquid residue (after centrifuge) was available from crystallizer. About 19.5 kg of diluted coagulant solution (1%) was dosed into a thickener to further thicken the raw material.

A total of 387kg of wet pulp was collected from filters with an average humidity of 29%. The content of the pulp varied significantly from a minimum of 6.47 g/kg in the initial batch before the solution was recycled, and a maximum of 20.4 g/kg in the final batch, at the end of the campaign when the pulp was not washed. Weighted, the average wrinkle content was 15g/kg. The cumulative boron remaining in the pulp, calculated based on the mass and content of boron in each pulp, was 4.13kg. The lithium content in the pulp was upgraded to a maximum of 1082 mg/kg. Additional pulp rinsing performed on pulp samples increased boron extraction and reduced the concentration of boron in the pulp by an average of 30%.

The unsaturated solution created during the process that is in crystallizer 1 is cooled to 23°C to obtain crystal borax decahydrate, weighing about 35kg after centrifuge. The resulting borax decahydrate was used to crystallize borax pentahydrate as the final product. 18.5 kg of decahydrate and 17.6 kg of barren liquid residue were used, so the resulting solution was heated to 90 °C. The solution was filtered to remove the insoluble particles and then cooled to 66 °C to successfully produce borax pentahydrate. During this process, 8 kg of final product was obtained.

Chemical analysis of the obtained crystal Borax pentahydrate showed  $\text{Na}_2\text{O}$  content from 20.97% to 21.76%, and  $\text{B}_2\text{O}_3$  from 47.82% to 48.82%, which is very similar to the product that can be found on sale and whose content is  $\text{Na}_2\text{O}$  is 21.5% and  $\text{B}_2\text{O}_3$  is 49.0%.

In addition to the fact that the tests carried out during the "pilot" process confirmed the results of the previous laboratory scale of testing, thus cancelling the concept of low cost, environmentally friendly and relatively simple boron extraction cycle – these chemical analyses of the final product confirm that borax pentahydrate produced during technological tests by ELB+, can be promptly placed on the market.

One of the reasons for the positive technological results achieved at the laboratory level, as well as during the pilot process, is the specific mineralization of boron that exists in this tray, where Na-Ca borates predominate, which can be dissolved in the manner described above. The dominant Probertite, as well as Borax located in the central part of the deposit, are very prone to dissolution (Borax is soluble in water itself), and therefore suitable for technological processing.

## **ACKNOWLEDGEMENTS**

*The paper is prepared following the results that were obtained during the applied exploration of boron and accompanied elements (Li, Na, Ca, Sr) performed by Euro Lithium Balkan doo (ELB+). The exploration work was performed within two exploration licenses “Valjevsko-mionički basen” and “Valjevo Sever”.*

## **REFERENCES**

- [1] J. Obradović, N. Vasić, Jezerski baseni u neogenu Srbije, SANU, Beograd, (2007), 37.
- [2] S. Borojević Šoštarić, T. Brenko, Miner. Deposita, 58, (2023), 639.
- [3] N. Vasić, The Study on Sedimentological Research of Miocene Units within the Part of Valjevo-Mionica Basin, ELB+ internal fund, Valjevo, (2020), 25.



## THE INFLUENCE OF QUENCHING MEDIA ON DIFFERENT PROPERTIES OF C45 CARBON STEEL

Uroš Stamenković, Ivana Marković, Srba Mladenović, Saša Marjanović,  
Avram Kovačević, Milijana Mitrović, Filip Basarabić

Technical Faculty Bor, University of Belgrade, V.J. 12, 19210 Bor, Serbia

### Abstract

*The subject of this paper was the investigation of the influence of different quenching media on the mechanical, thermal, and structural properties of C45 medium carbon steel. After normalization heat treatment, steel samples were austenitized at 880°C for 50 minutes. Austenitization was followed by quenching in different quenching media: pure water and different aqueous solutions (2–8%) of NaOH. After each heat treatment, hardness and thermal properties were determined, along with structural investigations using the optical microscope. After normalization, samples had the lowest hardness values, while thermal conductivity was the highest compared to the other tested samples. Metallographic analysis showed that the structure consists of fine-grained ferrite and perlite. Quenching in water and aqueous solutions, the values of hardness increased significantly, while the values of thermal properties decreased. Samples quenched in aqueous solutions exhibit extreme hardness. Metallographic analysis of the samples after quenching revealed fine needles of martensite.*

**Keywords:** *quenching, aqueous salt solutions, hardness, thermal conductivity*

### 1. INTRODUCTION

Carbon steels with carbon content between 0.3-0.5% are often called medium-carbon steels. These steels play an important role in the industry settings such as transportation industries, military and civil [1]. The C45 steels belong in this category as well. Machine parts made out of these steels sometimes require extremely high values of hardness and tensile strength due to the high demand for wear-resistant materials. Generally, these are steels that have martensitic structures, and often their hardness exceeds 800 HV, with tensile strength over 2500 MPa [2,3]. In order to improve properties of steels, heat treatment must be applied. Overall, most used heat treatments of steel include: normalizing heat treatment in order to obtain fine pearlite, and quenching for obtaining martensite [4,5]. Quenching heat treatment is one of the most important processes that often improves the performance and applicability of steels through martensite formation. During quenching, the metallic sample is rapidly cooled in a quenching medium (quenching solution) from the austenitization temperature, in the range of 845–900°C (for carbon steels) [6]. The two important phenomena that occur during quenching and influence the final structure and properties of steels are heat transfer and wetting [7]. The commonly used quenchant are water, oil, brine (aqueous salt solution), and synthetic solutions. All of these quenching media have their positive and negative sides. Water has low cost and is highly available, but provides high quenching rates that can lead to cracks; oils are expensive but provide slower cooling than water which is sometimes necessary, and are excellent quenchant for alloyed steels; polymer solutions provide quenching speed between water and oil, but those solutions are expensive and have varying concentrations throughout the quenching process. Brine solutions are used in cases where higher quenching severity is required [8]. During the quenching in liquid quenchant, three stages are usually observed: *vapor blanket*, *nucleate boiling*, and *convective cooling*. The second stage (nucleate boiling) is the most important stage in the quenching process. The faster the second stage starts, the faster the cooling rate will be. In order for the second stage to start, the first one has to be shortened, i.e., the vapor blanket should be eliminated [9]. One way to eliminate a vapor blanket

and obtain more uniform cooling is to add various types of salts to the water in different concentrations, creating aqueous salt solutions. It is important to note that since high cooling rates are obtained by quenching in brine, the propensity for cracking and distortion is also increased, so brine solutions are often used for the quenching of low-hardenability steels [10,11]. Some authors investigated the influence of quenching in different salt solutions. Lozano et al. gave a great deal of information on quenching in differently concentrated aqueous salt solutions. Among the investigated quenching solutions, the results of the quenching rate of aqueous solutions of NaOH at different concentrations were also given. Lozano et al. concluded that with an increase in the concentration of NaOH in the solution, the quenching rate increases [10]. The quenching power of aqueous salt solutions was investigated by L.H. Zordao et al. The authors investigated the properties of the C45 steel after quenching in differently concentrated aqueous salt solutions (NaCl, NaNO<sub>2</sub>, Na<sub>2</sub>SO<sub>4</sub>, NaHCO<sub>3</sub>). They showed that quenching in aqueous salt solutions breaks up the vapor blanket and leads to better heat dissipation during cooling. Also, in almost all tested solutions, an increase in salt concentration led to an increase in the cooling rate during quenching [9]. Sitorus et al. investigated the effect of quenching in NaOH solution on the properties of medium-carbon steel. The authors showed that an increase in the concentration of the NaOH solution leads first to an increase and then to a decrease in the tensile strength of the tested steel. The authors obtained the maximum values of mechanical properties after quenching in a 20% NaOH solution [12].

By reviewing the literature, no data were found on how quenching in aqueous salt solutions affects the change in thermal properties. Considering that items made of C45 steel are used at high temperatures after quenching, it is of great importance to know the change in thermal properties after obtaining extremely high hardness values by quenching in aqueous salt solutions. The goal of this paper was to obtain the extremely high values of hardness by quenching the samples made from C45 in the NaOH aqueous salt solution. After that, determine the influence of high quenching rate on thermal and structural properties.

## 2. EXPERIMENTAL

The experiments were performed on medium-carbon (C45) steel. Steel was obtained in the form of a round bar with a diameter of 20 mm. The chemical composition of the investigated steel is given in Table 1.

Table 1 - Chemical compositions of investigated steel (mass. %)

<i>C45 medium-carbon steel</i>				
<b>Fe</b>	<b>C</b>	<b>Mn</b>	<b>S</b>	<b>P</b>
98.51-98.98	0.42-0.5	0.6-0.9	≤0.05	≤0.04

In the first place, all the samples were normalized at 900°C for 1 hour in an electric resistance furnace, Vims elektrik LPŽ-7,5 S in order to remove the as-received structure, and then cooled in air. After normalization, samples were heated to austenitization temperature at 880°C for 50 minutes and then quenched separately in water and in 2%, 4%, 6%, and 8% NaOH solutions. After each heat treatment, samples were separated and investigated. The heat treatment process can be seen in Figure 1.

Hardness was measured on the VEB Leipzig Vickers hardness tester using a 30 kg load and a 15 s dwelling time.

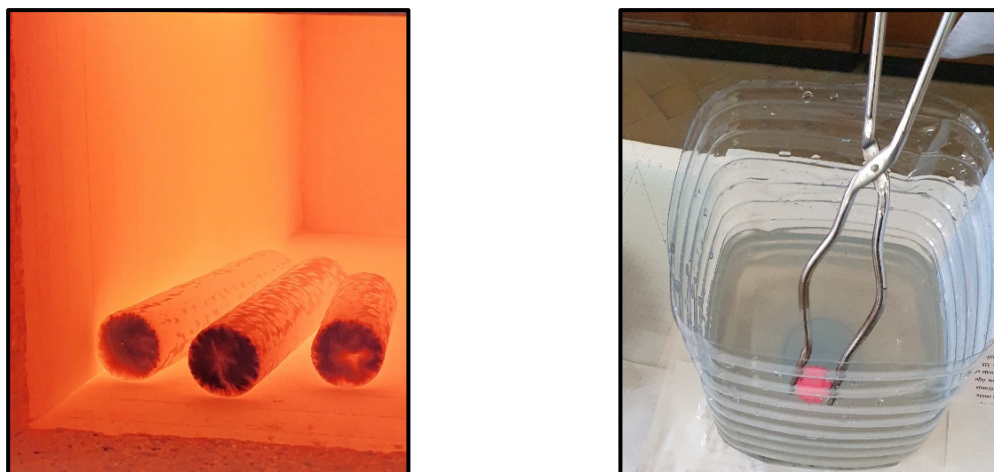


Figure 1 - Heat treatment of steel samples in an electric resistance furnace, followed by quenching

Xenon flash method was applied to determine the thermal diffusivity of the investigated samples after different heat treatments by irradiating the disc-shaped specimens with a diameter of 12.7 mm with the xenon lamp in a nitrogen atmosphere. The thermal conductivity as a function of temperature was calculated according to the equation:

$$\lambda(T) = \rho(T) \times c_p(T) \times \alpha(T) \quad (1)$$

where,  $\lambda$  - thermal conductivity; (W/m\*K),  $\rho$  - density; (kg/m<sup>3</sup>),  $c_p$  - specific heat capacity; (J/kg\*K),  $\alpha$  - thermal diffusivity; (cm<sup>2</sup>/s), T - temperature; (°C).

A Reichert MeF2 optical microscope was used for the investigation of the microstructures. The preparation of the samples for optical examinations included wet grinding on a series of SiC papers; polishing with alumina suspension; and etching in a 4% Nital solution.

### 3. RESULTS AND DISCUSSION

In figures 2 and 3, the change in hardness and thermal conductivity of the samples can be seen as a function of the applied heat treatment: normalization, quenching in water, and quenching in differently concentrated aqueous NaOH solutions, respectively.

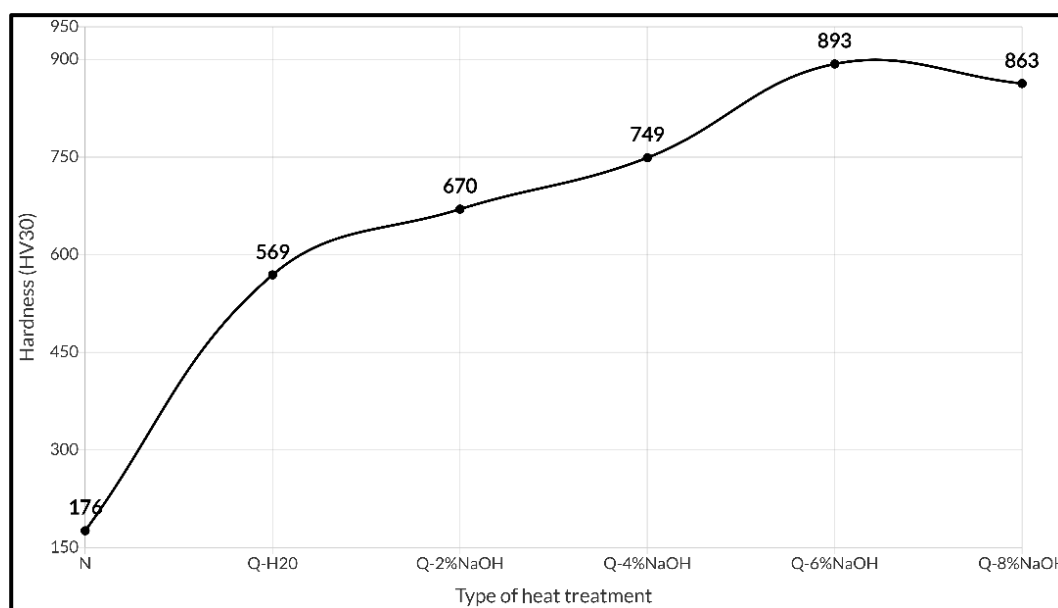


Figure 2 – Change in hardness as a function of the type of heat treatment; N- Normalized; Q-H2O- quenched in water; Q-2-8%NaOH- quenched in NaOH solutions

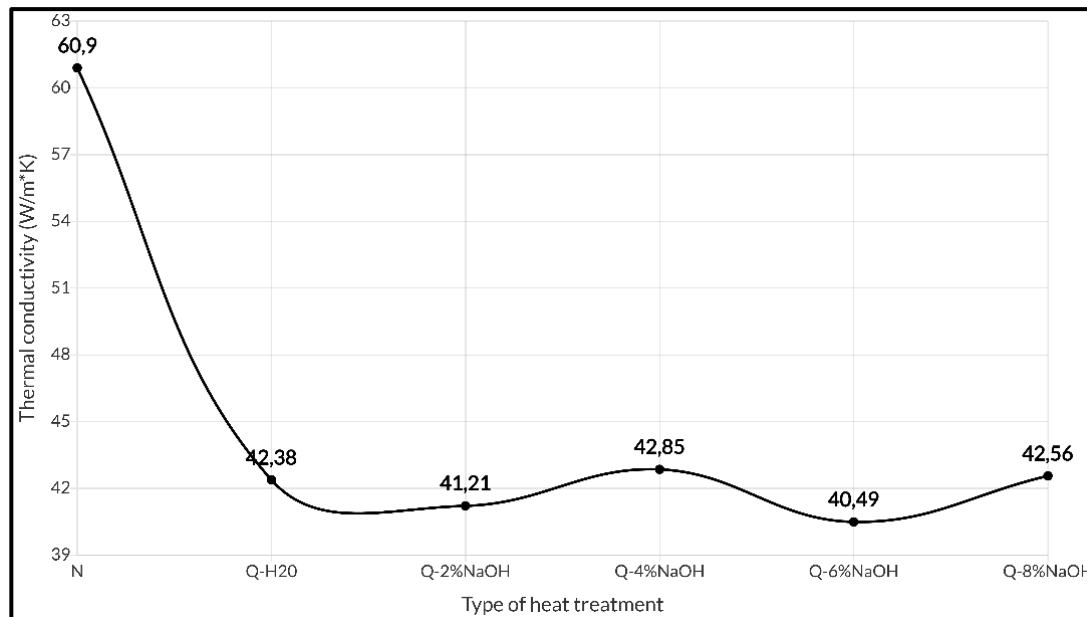


Figure 3 – Change in thermal conductivity as a function of the type of heat treatment; N- Normalized; Q-H2O- quenched in water; Q-2-8% NaOH- quenched in NaOH solutions

On analysis of the graph given in Fig. 2, it can be concluded that the hardness values increased very rapidly after quenching in water and aqueous NaOH solutions. The absolute increase in hardness of the water-quenched sample compared to the normalized one is 393 HV30. By quenching in the NaOH solutions, extremely high hardness was obtained, higher than the samples quenched in water. Quenching in a 2% NaOH solution caused an increase in hardness by 101 HV30 in comparison to the hardness of the water-quenched sample. Also, an increase in the concentration of NaOH led to an increase in the hardness after quenching. The maximum hardness of 893 HV30 was obtained after quenching in a 6% NaOH solution. A further increase in NaOH concentration (8%) led to a slight decrease in hardness.

The first thing to notice in Fig. 3 is that, in general, with quenching, the thermal conductivity values decrease. Immediately after quenching in water, the thermal conductivity decreased by 18.52 W/m<sup>2</sup>K compared to the normalized state. Thermal conductivity values fluctuate after quenching in differently concentrated NaOH solutions. During quenching in a 4% NaOH solution, slightly higher thermal conductivity values were obtained than those obtained after quenching in pure water. Similarly to the obtained hardness values, the thermal conductivity was the lowest after quenching in a 6% NaOH solution. Also, somewhat higher values of thermal conductivity were obtained after quenching in an 8% NaOH solution.

The reason for obtaining very high hardness values after quenching in differently concentrated aqueous NaOH solutions lies in the achievement of extremely high cooling rates. By adding various inorganic salts to the water, the vapor blanket is broken during quenching. After immersing the austenitized piece in an aqueous solution (in our case, a NaOH solution), salt crystals are deposited at the boundary between the red-hot piece and the coolant. At the boundary of the hot piece, due to the very high temperature and supersaturation, microexplosions occur that break the vapor blanket [8,9,13,14]. By breaking the vapor blanket, it is possible to obtain extremely high cooling rates, even up to 2-3 times higher than the cooling rate in water [15]. When such extremely high cooling rates are achieved, it is possible that a larger amount of martensite is obtained in the structure, i.e., that the hardenability suddenly rises, and with that, higher hardness values are expected. This was also shown by Zordao et al. in their work by quenching in aqueous solutions



of Na<sub>2</sub>SO<sub>4</sub> and NaCl [9]. Sitorus et al. also obtained similar results, where with increasing concentrations of NaOH in quenching solutions, hardness values gradually increased [12].

On the other hand, this type of structure hinders the movement of electrons (carriers of thermal energy), lowering the values of thermal conductivity [16,17]. Quenching in NaOH solutions caused extreme saturation of the iron matrix due to high cooling rates. Quenched-in carbon, certain other elements present in steel, and quenched-in vacancies serve as electron scattering centers. This is also the reason for the general drastic reduction of thermal properties after quenching in NaOH solutions compared to the normalized state, and later also compared to the state after quenching in water. The fluctuation of thermal conductivity after quenching in NaOH solution is explained by the fact that, by quenching in aqueous solutions, it is impossible to predict what saturation will be in the lattice after quenching and what the morphology of martensite will be. In this regard, there is a possibility that, regardless of the high values of hardness obtained with a higher proportion of martensite due to high cooling rates, the flow of electrons in such a lattice will be somewhat more pronounced. This can be seen with the sample that was quenched in an 8% NaOH solution, where a slightly lower hardness was obtained compared to the maximum (6% NaOH), but there is a significantly higher thermal conductivity.

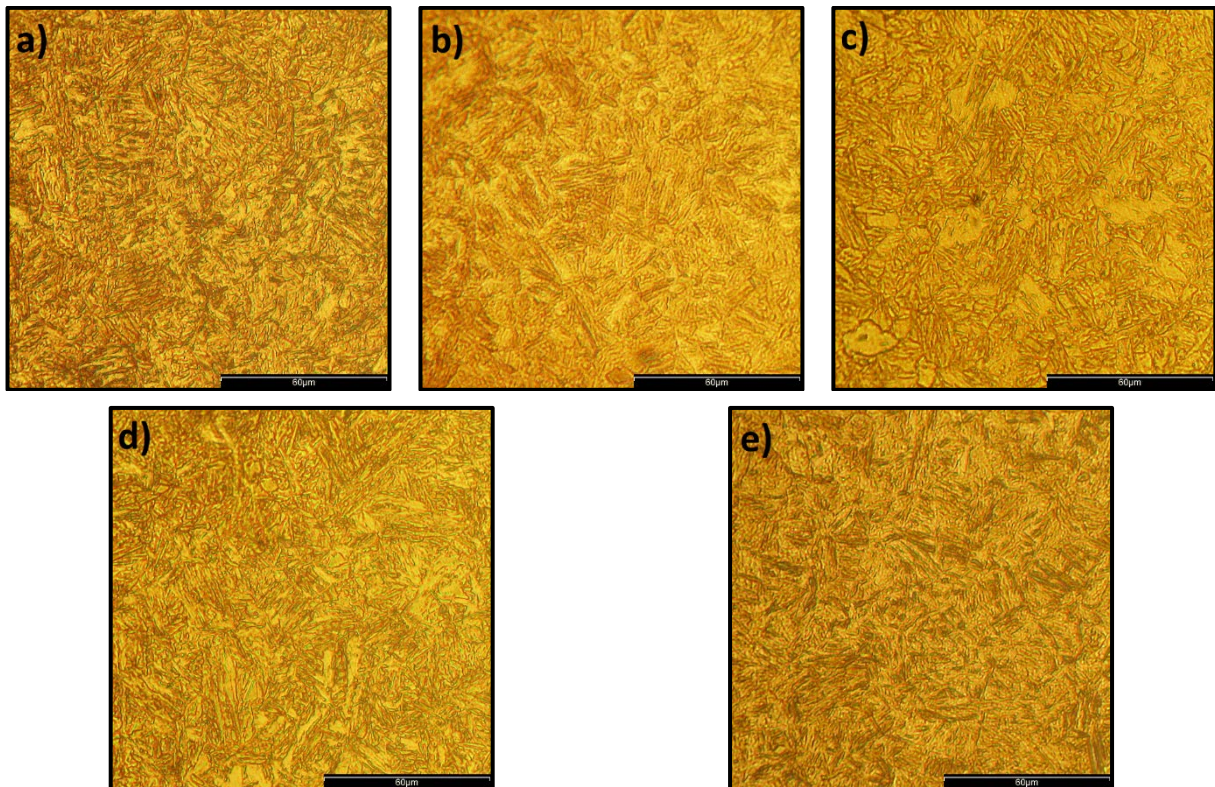


Figure 4 – Microstructure of the C45 after quenching in: a) water; b) 2%NaOH; c) 4%NaOH; d) 6%NaOH; e) 8%NaOH

T

he microstructure of the quenched samples can be seen in Figure 4. An analysis of the microstructures can confirm, to some extent, what was stated before. In all samples, the critical cooling rate was reached, so martensite was obtained. No major differences can be observed in the microstructures after quenching in water and aqueous NaOH solutions.

## ACKNOWLEDGEMENTS

*The research presented in this paper was done with the financial support of the Ministry of Education, Science and Technological Development of the Republic of Serbia, within the funding of the scientific research work at the University of Belgrade, Technical Faculty in Bor, according to the contract with registration number 451-03-47/2023-01/200131.*

## 4. CONCLUSIONS

Based on the obtained results, the following conclusions can be drawn:

- After quenching in water, the hardness increased compared to the normalized sample.
- Extremely high cooling rates were achieved by quenching in aqueous NaOH solutions. This condition resulted in extremely high values of mechanical properties but also relatively low values of thermal properties.
- A 407% increase in hardness (the maximum) was achieved after quenching in a 6% NaOH solution in comparison to the normalized sample, and a 57% increase in comparison to the sample quenched in water.
- By quenching in aqueous NaOH solutions, the thermal conductivity was significantly lower in comparison to the normalized sample and, in some cases, lower in comparison to the sample quenched in water.
- The value of thermal conductivity was the lowest after quenching in a 6% NaOH solution.

Based on the conducted experiments, it can be concluded that water and NaOH aqueous solutions are adequate for quenching C45 steel. After quenching, no distortion, cracks, or other damages were observed on the samples. The obtained hardness values are extremely high for this type of steel.

An increase in the concentration of NaOH in the quench bath led to an increase in the hardness values. With an increase in NaOH concentration, hardness increased, reaching maximum values after quenching in a 6% solution. After that, the hardness decreased slightly after quenching in an 8% solution. It is interesting that after quenching in an 8% NaOH solution, the hardness had a relative decrease of 3.3% in relation to the maximum obtained hardness value after quenching in a 6% NaOH solution. On the other hand, by quenching in an 8% NaOH solution, the thermal conductivity had a relative increase of 5.11% compared to the sample quenched in a 6% NaOH solution and even a relative increase of 0.42% compared to the sample that was water quenched.

## REFERENCES

- [1] A. Laouissi, M.M. Blaoui, H. Abderazek, M. Nouioua, A. Bouchoucha, *Met. Mater. Int.*, 28 (2022) 3087-3105.
- [2] O. Haiko, A. Kaijalainen, S. Pallaspuuro, J. Hannula, D. Porter, T. Liimatainen, J. Komi, *Appl. Sci-Basel*, 9 (2019) 4231.
- [3] G. Krauss. *Mater. Sci. Eng. A*, (273-275) (1999) 40–57.
- [4] D.R. Askeland, P.P. Fulay, *Essentials of Materials Science and Engineering Second Edition*, SI, Cengage Learning, Stamford, 2010, p.493.
- [5] W.F. Smith, H. Javad, *Foundations of Materials Science and Engineering McGraw-Hill Series in Materials Science 4th edition*, McGraw-Hill, Boston, 2006.
- [6] G. Krauss, *Principles of Heat Treatment of Steel*, American Society for Metals, Ohio, EUA, 1980.
- [7] G. Ramesh, K.N. Prabhu, *Metall. Mater. Trans. B*, (45) B (2014) 1355–1369.

- [8] B.R. Rana, K.M. Rana, V.J. Rao, *Int. J. Appl. Sci. Eng.*, 4 (10) (2020) 253-259.
- [9] L.H. Zordao, V.A. Oliveira, G.E. Totten, L.C.F. Canale, *Int. J. Heat Mass Tran.*, 140 (2019) 807-818.
- [10] D. Lozano, *Quenching: Brine and Caustic from: Encyclopedia of Iron, Steel, and Their Alloys*, CRC Press, 2016.
- [11] G.E. Totten, C.E. Bates, N.A. Clinton, *Handbook of Quenchants and Quenching Technology*, ASM International, Materials Park, OH, 1993, p. 291–338.
- [12] S. Sitorus, P. Sinuhaji, *J. Technomaterial Phys.*, 3 (2) (2021) 141 – 146.
- [13] E.T. Daiula, G.B. Nyior, R.A. Mohammed, *The Nigerian Academic Forum*, 9 (4) (2005) 98-101.
- [14] G. Ramesh, K.N. Prabhu, *Exp. Heat Transfer*, 28 (5) (2015) 464-492.
- [15] M. A. Grossman, M. Asimov, *Iron Age*, 145 (17) (1940), 25-29.
- [16] J. Wilzer, F. Ludtke S. Weber, W.Theisen, *J. Mater. Sci.*, 48 (2013) 8483-8492.
- [17] J. Wilzer, J. Kupferle, S. Weber, W. Theisen, *J. Mater. Sci.*, 49 (2014) 4833-4843.



## INVESTIGATION OF THE MIXING AND GRANULATION BEHAVIOR OF IRON ORE FINES IN HORIZONTAL HIGH-SHEAR GRANULATOR

Yang You, Jiabao Guo, Zhixiong You, Xuewei Lv

College of Materials Science and Engineering, Chongqing University, Chongqing 400044, China.

### Abstract

*Granulation is a key operation unit in preparation of iron ore raw materials. This work presented an study on the iron ore granulation and sintering using a novel horizontal high-shear granulator and a traditional drum granulator. The mixing and granulation performance and the effect of granulation on sintering indicators were analyzed. The results showed that the uniformity, bed permeability and the fracture strength of the granules from the shear granulator were significantly better than those from the drum granulator. Compared with the drum granulator, the shear granulator had better mixing ability in the axial direction, more even distributions of water and calcium and less segregation. For the thick-bed sintering with a height of 900 mm, the sintering indicators in terms of sintering speed, sinter yield, strength and flue composition showed the shear granulator was significantly better than that of the drum granulator.*

**Keywords:** Horizontal high shear granulator, Drum granulator, Iron ore, Granulation efficiency.

### 1. INTRODUCTION

In the ironmaking process, iron ore fines need to be granulated to large granules in the drum granulators. However, previous reports verified that the water is difficult to get well dispersed on the surface of the raw materials at heavy loading operation and high proportion of iron ore concentrate, which leads to serious segregation of granule size in the drum granulators [1, 2].

High-shear granulators are widely used in the pharmaceutical, food and chemical industries for particle mixing and granulation [3-5]. A high-shear granulator consists of a cylindrical container and several impellers. The high-speed rotating impellers collide and shear particles, causing forced convective mixing of the particles and promoting particle agglomeration and granule growth. Rahmanian et al. [6] investigated the effects of the parameters of the shear granulator, such as impeller speed, granulation time and binder viscosity, on granules properties. They found that granules were more consolidated at high impeller speeds, and granules produced with high binder viscosity had lower strength and wider size distributions. However, studies on high-shear granulator have been mainly focusing on pharmaceutical, food and chemical products. Reports of its use in iron ore granulation are still rare.

This work investigates the influence of granulation performance on sintering indicators and to compare the granulation performance of a drum granulator and a horizontal high-shear granulator. The findings will be useful for the optimization and application of horizontal high-shear granulators in iron ore granulation.

### 2. EXPERIMENTAL

Fig. 1 shows the shear granulator and the drum granulator used in the experiments. The shear granulator consisted of 4 impellers and a cylindrical container of 400 mm in diameter and 500 mm in length. The shear granulator could be readily converted to the drum granulator by removing the impellers.



Figure 1 - (a) High-shear granulator; and (b) drum granulator used in the experiments.

In the granulation experiments, the mixed raw materials of the total mass of 12.5 kg were fed into the granulators. The size distribution and mass fraction of raw materials are listed in Table 1. The mass fractions of the raw materials were the same as those in real sintering plants.

Table 1 - Size distributions and mass fractions of raw materials (wt-%)

Raw materials	Size distribution (mm)							Mass-based fraction
	<0.5	0.5~1	1~2	2~3	3~5	5~8	8~10	
Mixed iron ore	14.56	30.84	14.98	11.55	13.70	11.83	2.54	67.96
Dolomite	12.26	28.18	11.62	26.04	21.59	0.09	0.22	2.86
Limestone	18.76	24.67	11.61	19.06	20.52	5.10	0.28	2.67
Quicklime	51.81	30.47	10.62	4.53	2.57	0	0	3.48
Coke breeze	13.35	18.89	8.27	13.42	22.50	21.16	2.41	3.38
Return fines	0	0	20.23	28.33	46.71	4.73	0	19.65

### 3. RESULTS AND DISCUSSION

Fig. 2 shows the size distributions of the granules at different filling levels. For the shear granulator (Fig. 2a), the effect of filling level is minimal. The mass fraction of +3 mm granules increases slightly with increasing filling level, reaches a peak of 84% at the filling level of 9%, and then decreases. On the other hand, filling level has a more significant effect for the drum granulator (Fig. 2b). The mass fraction of +3 mm granules firstly increases with increasing filling level and decrease when the filling level is higher than 12%. This is because the moderate increase in filling level increases the collisions between particles and promotes the agglomeration and growth of fine particles. However an excessively high filling level causes a dead zone in the drum granulator for the movement of some mixture materials, which reduce the performance of mixing and granulating of iron ores.

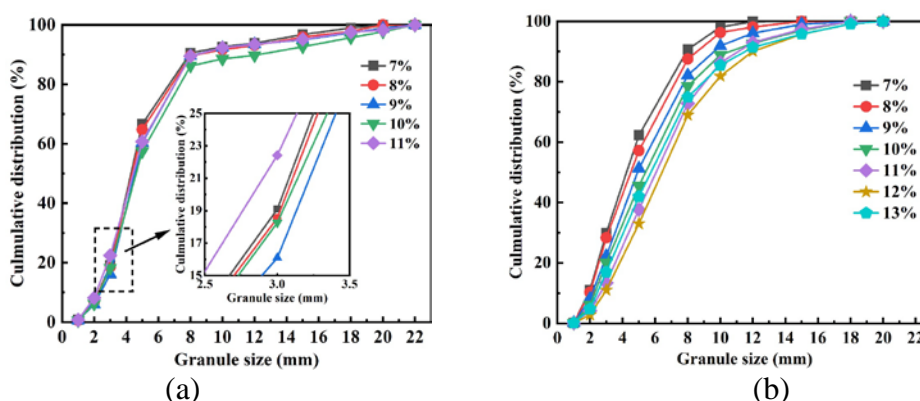


Figure 2 - Granules size distributions of shear granulator (a) and drum granulator (b).

To further compare the granulation performance of the two granulators, the mean granule size and uniformity index are also analyzed, as shown in Fig. 3(a). The variations of the mean granule size with filling level are similar for the two granulators, showing an upward and then downward trend. The effect of filling level is more pronounced for the drum granulator than for the shear granulator.

The mean granule sizes from the shear granulator are larger than those from the drum granulator when the filling level is less than 10%. The current results are consistent with our previous simulation results that the kinetic energy and collision frequency of particles in the shear granulator are significantly greater than those in the drum granulator. The frequent shear, collision and friction promote the agglomeration and growth of fine particles, a better granulation performance is thus achieved in the shear granulator despite low filling level. On the other hand, the effect of filling level on the uniformity index of granules is minimal, particularly for the drum granulator. The overall uniformity indexes of the shear granulator are higher than those of the drum granulator. It indicates that the granules in the shear granulator have more uniform size distributions as the shearing of the high-speed rotating impellers can break larger granules resulting more granules with sizes between 3 to 8 mm.

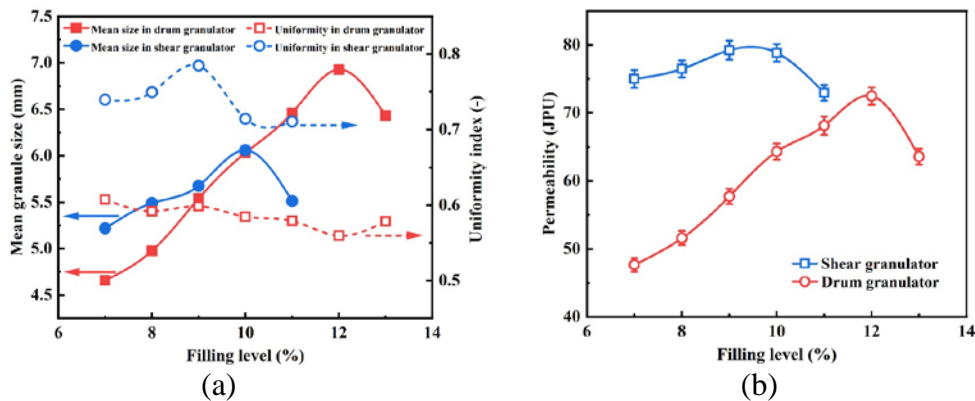


Figure 3 - Comparison of mean granule size, uniformity index (a) and permeability (b).

Fig. 3(b) shows the bed permeability of two types of granules at different filling levels. The filling level corresponding to the best permeability in the shear granulator is 9%, while that in the drum granulator is 12%. Another difference is that the bed permeability of granules from shear granulator is significantly higher than that from drum granulator with the same filling level. The highest permeability of the granules formed in the shear granulator is 79.2, which is significantly better than that of the granules in the drum granulator (70.5). This is because the granules from the shear granulator have a more uniform size distribution, resulting in a loose packing with a higher voidage. On the other hand, the granules from the drum granulator have a wide size distribution, which causes a large number of small granules embedded in the gaps between the large granules to form a close packing, and the bed permeability is lower.

Fig. 4(a) shows the comparisons of sintering indicators for the two types of granules. All the indicators suggest the granules from the shear granulator have better sintering performance than those from the drum granulator: the sintering speed increases from 19.56 mm/min to 22.50 mm/min while the yield, falling strength and tumbler index of sinter are improved by 1.76%, 3.38% and 2.67%, respectively. This is because the uniform granule size distribution in the shear granulator improves the bed permeability, thereby accelerating the sintering speed. On the other hand, the uniform distribution of fuel and chemical composition avoids the segregation of liquid phase in the sintering process, thus improving the strength of the sinter.

Fig. 4(b) shows the microstructure of product sinter of two types of granules. The upper two images are the sinter from the drum granulator while the bottom two images are those from the shear granulator. The iron-bearing minerals and the bonding phase in the sinter corresponding to the two granulation processes are combined to form the granular or phenocryst structure, which is also the reason for the higher strength of the sinter. From a partial perspective, there are more noodle-like SFCA with high strength in the sinter from the shear granulator, while some undesirable skeletal crystals exist in the sinter from the drum granulator. The microstructure of the sinter agrees well with the sintering performance of the granules. In addition, as the granule bed

from the shear granulator has better gas permeability, more pores are formed after the granule layer is sintered.

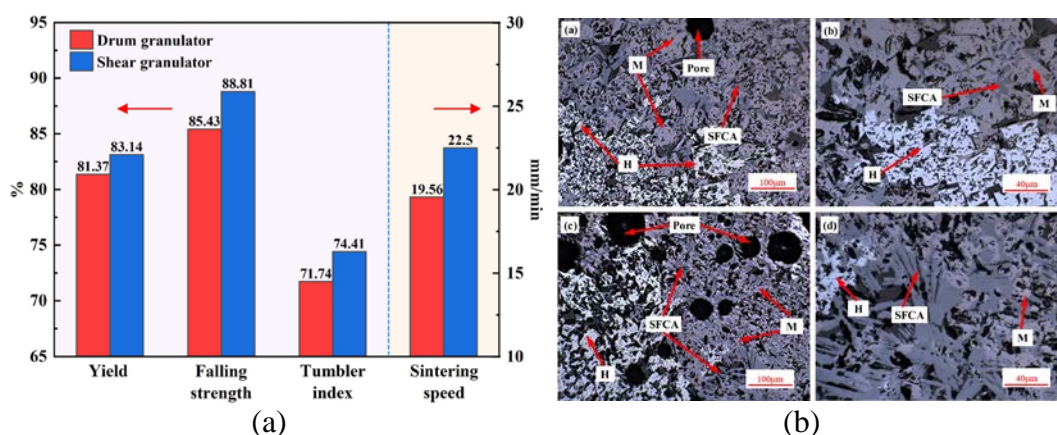


Figure 4 - Comparison of sintering indicators (a) and microstructure of product sinter (b) for different granulation processes.

#### 4. CONCLUSIONS

- (1) The shear granulator had better mixing ability in the axial direction than the drum granulator. Excellent mixing effect of the shear granulator was the key to improving granulation and sintering performance.
- (2) The optimal filling levels for the shear and drum granulators were 9% and 12%, respectively. The uniformity of granule size, bed permeability and fracture strength of granules from the shear granulator were significantly better than those from the drum granulator.
- (3) The sintering indicators including sintering speed, sinter yield, strength and flue composition corresponding to the shear granulator were significantly better than that of the drum granulator.

#### REFERENCES

- [1] Y.Z. Wang, J.L. Zhang, Z.J. Liu, C.B. Du, JOM, 2017, 69 (11) 2404-2411.
- [2] A.M. Nyembwe, R.D. Cromarty, A.M. Garbers-Craig, Powder Technol., 2016, 295 7-15.
- [3] S.A. de Koster, K. Pitt, J.D. Litster, R.M. Smith, Powder Technol. 355 (2019) 514-525.
- [4] F.M. Mahdi, M. Mehrabi, A. Hassanpour, F.L. Muller, Powder Technol. 356 (2019) 253-262.
- [5] S. Sarkar, B. Chaudhuri, Asian J. Pharm. Sci. 13 (2018) 220-228.
- [6] N. Rahmanian, A. Naji, M. Ghadiri, Chem. Eng. Res. Des. 89 (2011) 512-518.

## INVESTIGATION ON BENEFICIATION OF IRON FROM COPPER ORE OF MAURITANIA COPPER MINE (MCM) BY MAGNETIC SEPARATION

Jovica Sokolović<sup>1</sup>, Grozdanka Bogdanović<sup>1</sup>, Velizar Stanković<sup>1</sup>,  
Gracijan Strainović<sup>2</sup>, Ivana Ilić<sup>1</sup>, Milan Gorgievski<sup>1</sup>, Miljan Marković<sup>1</sup>

<sup>1</sup>Technical Faculty Bor, University of Belgrade, V.J. 12, 19210 Bor, Serbia

<sup>2</sup>Mauritania Copper Mines SA, First Quantum Minerals, Nouakchott, Mauritania

### Abstract

*In this study, magnetic separation were used to beneficiation iron from copper ore of Mauritania Copper Mine (MCM). The work aimed to maximize the recovery of iron values by upgrading to a high-grade product suitable for steelmaking industry. The received ore contains 1.30% Cu, and 49.50% Fe. Research was conducted on two size fractions: A (-3.35+0 mm) and B (-0.425+0 mm), as a product of grinding the crushed ore until to reach a size fraction of containing 60% of particles < 75 μm. Comparing the mass yields as the distribution of copper and iron by magnetic and non-magnetic fractions, the better results is achieved on the finer size fraction at the magnetic field of  $7.15 \times 10^{-4}$  T. Under that condition, the magnetic fraction, has a mass yield of 23.43 %, containing 74.86% Fe and 0.2% Cu. The magnetic fraction, with 74.86% Fe, can be used as a raw material in iron metallurgy.*

**Keywords:** copper, MCM ore, iron, magnetic, separation

## 1. INTRODUCTION

Magnetic separation is one of the most widely used processes for the upgradation of iron ore [1, 2]. The concentration of various ferrous and non-ferrous minerals has become an important application from industrial minerals [3]. This method of concentration can be used very effectively to extract and valorize iron from other ores, such as copper ore from MCM [4]. In this study, the results of the laboratory magnetic concentration analysis tests were shown.

## 2. EXPERIMENTAL

### 2.1. Materials

Research was conducted on copper ore of Mauritania Copper Mine (MCM). The results of the chemical analysis show that the received ore contains 1.30% Cu, and 49.50% Fe. The dominant iron minerals include goethite, hematite, and siderite [4].

### 2.2. Laboratory magnetic concentration

The teste of magnetic concentration were carried out on the laboratory Davis Tube magnetic analyzer at different strengths of magnetic field in the range from 1.79 to  $11.02 \times 10^{-4}$  T. The conditions under which the laboratory experiment took place in magnetic analyzer were as follows: temperature: 22 °C, solid-liquid ratio: S:L = 1:4, current: 1, 3, 5, 7 and 9 A and time: 10-15 min.

Research was conducted on two samples with different size fractions: Sample A (-3,35+0 mm) and Sample B (-0,425+0 mm), which is the product of grinding the copper ore with a content of -0.075 mm size fraction of 60%. The content of iron (Fe) and copper (Cu) were analyzed in the obtained magnetic (MF) and nonmagnetic (NMF) fractions in all carried out experiments.



### 3. RESULTS AND DISCUSSION

Results of the laboratory magnetic concentration tests of sample A (-3,35+0 mm) are shown in Table 1 – 2, and Figures 1 – 2.

Table 1 - Results of the laboratory magnetic concentration tests of sample A (-3,35+0 mm)

Current (A)	1	3	5	7	9
Magnetic induction (T) x 10 <sup>-4</sup>	1.79	4.63	7.15	9.55	11.02
Mass of Magnetic (MF) fraction (%)	5.11	27.57	33.57	34.71	34.07
Mass of Non-magnetic (NMF) fraction (%)	94.89	72.43	66.43	65.29	65.93
Σ	100.00	100.00	100.00	100.00	100.00

Table 2 - Results of Cu and Fe grade of the magnetic (MF) and nonmagnetic (NMF) fractions

Current (A)	Magnetic (MF) fraction				Non-magnetic (NMF) fraction			
	Cu (%)	RCu (%)	Fe (%)	RFe (%)	Cu (%)	RCu (%)	Fe (%)	RFe (%)
1	0.20	0.77	77.35	7.99	1.36	99.23	48.00	92.01
3	0.47	10.00	66.57	37.07	1.62	90.00	43.01	62.93
5	0.56	14.58	71.38	48.42	1.67	85.42	38.43	51.58
7	0.52	13.99	69.85	48.98	1.71	86.01	38.69	51.02
9	0.53	13.76	70.57	48.55	1.71	86.24	38.65	51.45

RCu – Distribution of copper in the magnetic (MF) and nonmagnetic (NMF) fractions

RFe – Distribution of iron in the magnetic (MF) and nonmagnetic (NMF) fractions

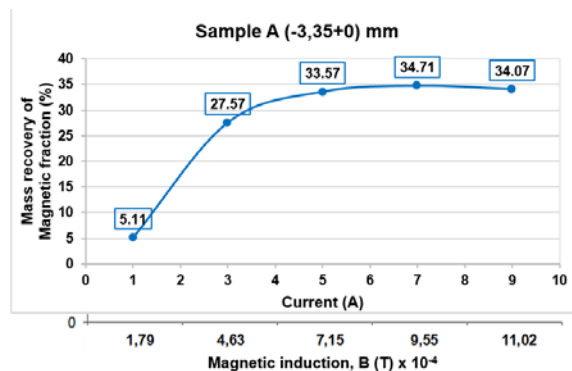


Figure 1 - Effect of intensity on mass recovery of the magnetic fraction

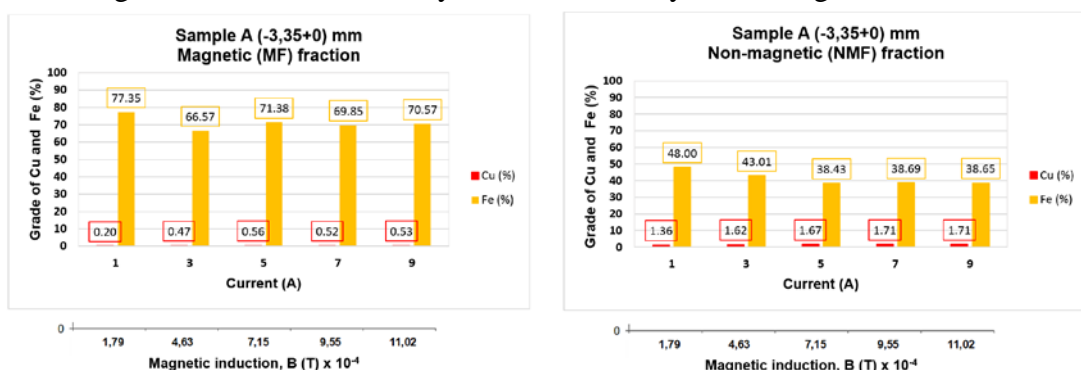


Figure 2 - Effect of intensity on Cu and Fe grade of the  
a) magnetic fraction and b) non-magnetic fraction

Based on the results of the experiments shown in Tables 1 and 2, it can be concluded that the magnetic field strength significantly influences the mass recovery and quality of the magnetic product. The best magnetic separation of the tested sample into the magnetic and non-magnetic fractions is obtained at a current intensity of **7 A** or at the induction of a magnetic field of **9.55 x 10<sup>-4</sup> T**.



The non-magnetic fraction, obtained from this magnetic field induction in the mass of **65.29%** and with copper and iron content of **1.71% Cu** and **38.65% Fe**, is useful for further leaching treatment, in order to recovery copper.

Results of the laboratory magnetic concentration tests of sample B (-0,425+0 mm) are shown in Table 3 – 4 and Figures 3 – 4.

**Table 3** - Results of the laboratory magnetic concentration tests of sample B (-0,425+0 mm)

Current (A)	1	3	5	7	9
Magnetic induction (T) x 10 <sup>-4</sup>	1.79	4.63	7.15	9.55	11.02
Mass of Magnetic (MF) fraction (%)	12.83	21.73	23.43	23.19	23.84
Mass of Non-magnetic (NMF) fraction (%)	87.17	78.27	76.57	76.81	76.16
Σ	100.00	100.00	100.00	100.00	100.00

**Table 4** - Results of Cu and Fe grade of the magnetic (MF) and nonmagnetic (NMF) fractions

Current (A)	Magnetic (MF) fraction				Non-magnetic (NMF) fraction			
	Cu (%)	RCu (%)	Fe (%)	RFe (%)	Cu (%)	RCu (%)	Fe (%)	RFe (%)
1	0.18	1.82	75.20	19.48	1.46	98.18	45.72	80.52
3	0.20	3.31	75.48	33.14	1.61	96.69	42.29	66.86
5	0.20	3.57	74.86	35.44	1.64	96.43	41.74	64.56
7	0.21	3.75	75.75	35.48	1.63	96.25	41.58	64.52
9	0.20	3.69	74.83	36.04	1.64	96.31	41.57	63.96

RCu – Distribution of copper in the magnetic (MF) and nonmagnetic (NMF) fractions

RFe – Distribution of iron in the magnetic (MF) and nonmagnetic (NMF) fractions

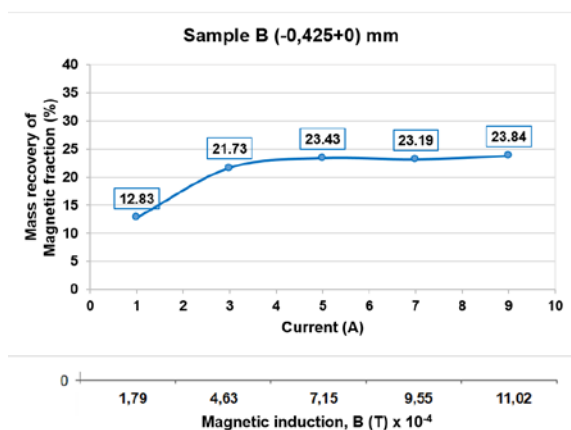


Figure 3 - Effect of intensity on mass recovery of the magnetic fraction

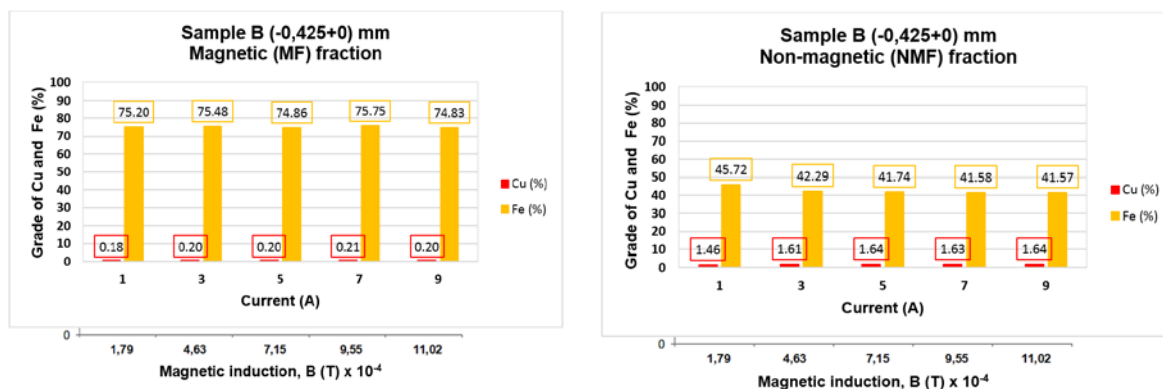


Figure 4 - Effect of intensity on Cu and Fe grade of the  
a) magnetic fraction and b) non-magnetic fraction

According to the results of the experiments shown in Tables 3 and 4, it can be concluded that at a current intensity of **5 A** or the induction of a magnetic field of  **$7.15 \cdot 10^{-4}$  T**, the best magnetic separation results of the tested sample into magnetic and non-magnetic fractions is obtained. The optimum grade that could be obtained from single-stage magnetic separation was **74.86% Fe**, in the case of sample B.

The magnetic fraction, which has a mass yield of **23.43%** with iron content of **74.86% Fe**, can be used as a raw material in iron metallurgy to obtain steel. The minimum iron content in the ore for steel production varies depending on the specific process and requirements of the steelmaking industry. However, in general, iron ore with a minimum iron content of around 50% to 55% is typically used for steel production.

The non-magnetic fraction, which has a mass yield of **76.57%** with copper and iron content of **1.64% Cu** and **41.74% Fe**, is thus appropriate for additional leaching treatment in order to recover copper. Further leaching studies of non-magnetic fraction are needed to maximize the efficiency of copper upgrading.

#### 4. CONCLUSION

Magnetic concentration analysis of the oxide ore was conducted on two size fractions: A (-3.35+0 mm) corresponding to the crushed ore and B (-0.425+0 mm), as a product of grinding the crushed ore until to reach a size fraction of containing 60% of particles < 75  $\mu$ m. Magnetic concentration tests were carried out on the laboratory Davis Tube magnetic analyser, at magnetic field strengths in a range from  $1.79 \times 10^{-4}$  to  $11.02 \times 10^{-4}$  T. Experimental results shown a better magnetic separation is achieved on the finer size fraction at the current intensity of **5 A** what corresponds to  **$7.15 \cdot 10^{-4}$  T**. Under that condition, the magnetic fraction, has a mass yield of **23.43 %**, containing **74.86% Fe and 0.2% Cu**. The non-magnetic fraction has a mass yield of **76.57 %**, with an increased copper content of **1.64 % Cu**, while an iron concentration was **41.74 % Fe**. The magnetic fraction, with 74.86% Fe, can be used as a raw material in iron metallurgy. Also, further leaching studies of non-magnetic fraction are needed to maximize the efficiency of copper upgrading.

#### ACKNOWLEDGEMENTS

*The results presented in this paper are part of the research within the study: Hydrometallurgical testing of copper oxide minerals from MCM oxide ore parties and Interim Report prepared for First Quantum Minerals - Mauritanian Copper Mines. The authors would like to acknowledge the Ministry of Science, Technological Development and Innovation of the Republic of Serbia for the financial support of scientific research at the University of Belgrade, Technical Faculty in Bor according to the contract with registration number 451-03-47/2023-01/200131.*

#### REFERENCES

- [1] S. K. Bhoja Tripathy, Y. R. Murthy, T. K. Ghosh, C. R. Kumar, D. P. Chakraborty, Minerals, 11 (2), (2021) 150.
- [2] K. O. Jang, V. R. Nunna, S. Hapugoda, A. V. Nguyen, W. J. Bruckard, Miner. Eng., 60, (2014)14-22.
- [3] J. Svoboda, Magnetic techniques for the treatment of materials. Springer Science & Business Media, 2004.
- [4] XPS Report entitled "Oxide Ores Au Department Study", First Quantum Minerals – Mauritanian Copper Mines, 2021.

## INVESTIGATION OF THE INFLUENCE OF PULSED ELECTRIC CURRENT ON THE EFFICIENCY OF DECOMPOSITION OF ALUMINATE SOLUTION

**Essen Suleimenov, Rustam Sharipov, Galymzhan Maldybayev, Zhibek Orazaliyeva**

Kazakh-British Technical University, str. Tole bi 59, 050000, Almaty, Kazakhstan

### Abstract

*This paper examines the study of the decomposition of an aluminate solution under the influence of electric current at different frequencies. It has been established that a lower current frequency makes the solution decomposition reaction more efficient. In addition to such data, it can be said that recognition of the molecular (supra-molecular) nature of liquid systems allows the creation of original and effective technical solutions. The effect of pulsed electric current on model alkaline solutions containing sodium aluminate was studied. It has been shown that a decrease in the current frequency leads to an increase in the efficiency of the solution decomposition reaction with the release of sodium hydroaluminat.*

**Keywords:** current frequency, aluminate solutions, inorganic aqueous solution

### 1. INTRODUCTION

Establishing the possibility of the influence of pulsed electric current on changing the microstructure of condensed systems, in particular, inorganic aqueous solutions, and the principle of formation of the components of their microstructure will make it possible to intensify industrial technological processes. For example, to intensify the decomposition of aluminate solutions, which is carried out in order to obtain aluminum hydroxide [1-2]. A feature of modern alumina production, in particular, is two mutually exclusive requirements. First: the aqueous solution of aluminum oxide must be sufficiently stable to ensure minimal loss of alumina when purifying the aluminate solution from solid suspensions at the limits of thickening and filtration. Second: the aluminate solution must have maximum decomposition ability to increase the rate of decomposition, reduce the volume of tank equipment and reduce energy costs for decomposition.

The process of decomposition of aluminate solutions currently continues to be quite slow, energy-consuming and requiring significant capital investments.

### 2. EXPERIMENTAL

The influence of current frequency and current intensity on the electrical conductivity of aluminate solutions (250 g/l Na<sub>2</sub>O and  $d_k = 1.7$ ) was investigated. Below is shown the change in the resistance of solutions depending on frequency with changes in current and voltage on the electrodes with a two-electrode measurement scheme shown in Table 1.

Table 1 - Change in resistance of solutions depending on current frequency

J, mA	1	2	6	10	20	40	70	100	150
R, ohm	36	36,7	37,5	33	30	21	14,6	13	11,3

With a further increase in current to 500 mA, the solution resistance decreased to 9.5 ohms. The transition of the resistance through the maximum does not speak in favor of continuum theories of the structure of the solution. To obtain more or less stable readings, at least 3-5 kHz is required. As is believed in the literature, at low frequencies, a large error in measuring electrical conductivity using a two-electrode scheme is introduced by the polarization resistance of the electrodes, which

depends on the frequency and current strength. Quantitatively, the magnitude of concentration polarization is determined by a change in potential,

$$\Delta\varphi = \frac{RTJ_0}{n^2F^2C_0\sqrt{\omega D}} \cdot \sin\left(\omega t - \frac{\pi}{4}\right), \quad (1)$$

from which it follows that the magnitude of polarization decreases with decreasing current density. However, the above data indicate an increase in polarization with decreasing current density.

### 3. RESULTS AND DISCUSSION

The decomposition of aluminate solutions was carried out depending on the frequency and strength of alternating current. Table 2 shows experimental data using current frequencies of 20 Hz and 50 Hz.

Table 2 - Decomposition of aluminate solutions depending on the frequency and strength of alternating current

mA	P, g, according to Faraday's law	P, g. total	Total percentage of decomposition	Percentage of decomposition, for aluminum from solution
For current frequency 20 Hz				
150	0,1175	0,2787	83,71	75,80
200	0,2518	0,2718	80,60	74,07
250	0,2518	0,3088	82,29	73,51
300	0,3022	0,4199	87,11	75,17
For current frequency 50 Hz				
100	0,1007	0,2390	79,14	72,34
150	0,1175	0,2770	75,62	67,75
200	0,2010	0,2801	52,48	44,50
250	0,2518	0,4234	71,44	59,42

Obviously, in this case, a lower current frequency makes the solution decomposition reaction more efficient. In addition to such data, it can be said that recognition of the molecular (supra-molecular) nature of liquid systems allows the creation of original and effective technical solutions; a more realistic view of the nature of the microstructure of liquids and the peculiarities of structure formation and structural transformations in condensed systems makes it possible to create technical solutions that are more responsive to the modern mineral resource base and the technology needs of multicomponent, complex and chemically resistant systems.

### 4. CONCLUSION

As can be seen from the table data, a low oscillation frequency causes a greater physicochemical effect for a given physicochemical system. That is, for inorganic aqueous solutions, a low frequency of pulsed energy impacts can increase the rate of both the decomposition processes of solutions and the growth of quasi-solids.

### REFERENCES

- [1] K. Rotmanov, M. Smirnov, Physical and chemical properties of aluminate solutions. Bulletin of Moscow University. Ser.2., Chemistry. T. 62. No. 3, (2021).  
 [2] T. Megyes, S. Balint, T. Grosz, T. Radnai, I. Bako, P. Sipos, *J. Chem. Phys.* 128, (2008) p.044501.

## INFLUENCE OF SILVER CONTENT ON MARTENSITIC TRANSFORMATION OF Cu-Al-Ag ALLOY

Lovro Liverić<sup>1</sup>, Tamara Holjevac Grgurić<sup>2</sup>, Sunčana Smokvina Hanza<sup>1</sup>,  
Wojciech Sitek<sup>3</sup>, Vedrana Špada<sup>4</sup>, Marko Kršulja<sup>5</sup>

<sup>1</sup> Faculty of Engineering, University of Rijeka, V. 58, 51 000, Rijeka, Croatia

<sup>2</sup> School of Medicine, Catholic University of Croatia, I. 242, 10 000, Zagreb, Croatia

<sup>3</sup> Faculty of Mechanical Engineering, Silesian University of Technology, K. 18A, 44-100 Gliwice, Poland.

<sup>4</sup> METRIS Research Centre, Istrian University of Applied Sciences, R. 6, 52100 Pula, Croatia

<sup>5</sup> Department of Engineering, Juraj Dobrila University of Pula, Z. 30, 52100 Pula, Croatia

### Abstract

SMA alloys possess unique properties, such as the shape memory effect and pseudoelasticity, which are due to the thermoelastic martensitic transformation between austenite and martensite structures. Cu-Al-Ag alloys, unlike other SMAs, exhibit higher martensite transformation temperatures, making them suitable for certain applications. The role of silver (Ag) as a microalloying component and its influence on the properties of Cu-Al-Ag alloys is still being thoroughly investigated. In this work, a Cu-10 wt%-Al-1 wt% alloy was prepared by melting pure metals in an electric arc furnace and casting the melt into a cylindrical mould. The microstructure of as-cast and quenched samples was determined by optical microscopy (OM) and scanning electron microscopy (SEM) with energy dispersive analysis (EDS). X-ray diffraction (XRD) analysis was performed to identify the crystal structure and global texture of the samples, while, the transformation temperatures were determined by differential scanning calorimetry (DSC). The results showed partially formed martensite 18R, and Cu precipitation in the cast state and fully formed martensite 18R in quenched state of Cu-10Al-1Ag alloy.

**Keywords:** Shape memory alloys, Cu-Al-Ag alloy, Microstructure, Phase transformations, Martensite

### 1. INTRODUCTION

Cu-Al-Ag shape memory alloys (SMA) differ from Cu-based SMA in their high martensitic transformation temperatures, typically ranging between 200 and 600 °C. This range depends on the aluminum and silver content [1, 2]. To date, research on the incorporation of silver in binary Cu-Al SMAs and especially in ternary Cu- SMA alloys is still sparse. In particular, the addition of silver to Cu-Al alloys improves their hardness, corrosion resistance, ageing properties and magnetic properties, as Silva [3] points out. Santos [4] attributes the increased microhardness of ternary alloys with 3%at. Ag to the formation of bainite. Limited studies [5] highlight the role of silver in the formation of martensitic phases in slowly cooled samples, while it also alters the transformation temperatures in ternary systems [1]. Manasijević [6] demonstrated that Cu-Al-Mn-Ag alloys with higher manganese content yield complete martensite, while those with less manganese exhibit  $\alpha$ -phase precipitates. Krishna [30], who studied Cu-XAl-5Mn-2Ag alloys, found that Al concentration affects martensite formation and directly influences the shape memory effect. In this study, the effects of adding 1 wt.% Ag to an as-cast Cu-10Al alloy on microstructural properties, martensitic and phase transformation were investigated using metallographic techniques, SEM and advanced XRD analyses.

## 2. EXPERIMENTAL

The study was performed on a Cu-10Al-1Ag alloy in as-cast and quenched state. The alloy was produced in an electric arc furnace under an argon atmosphere, subjected to two vacuum cycles, from raw material consisted of pure copper (Cu, 99.9% purity), aluminum (Al, 99.5% purity), and silver (Ag, 99.99% purity). The alloy was remelted four times to achieve better homogenization and subsequently cast into cylindrical molds with dimensions 12 mm x 8 mm. Heat treatment parameters for quenching were 900°C for 30min, followed by cooling in water. The sample was prepared for metallographic examinations by grinding using 600#, 800#, 1200#, and 2400# SiC abrasives. It was subsequently polished with diamond pastes of 3  $\mu\text{m}$ , 1  $\mu\text{m}$ , and 0.25  $\mu\text{m}$  on a TERGAMIN-30 grinding-polishing machine. The microstructure was exposed by etching the samples with a solution composed of 2.5 g FeCl<sub>3</sub>, 48 mL CH<sub>3</sub>OH, and 10 mL H<sub>2</sub>O. Microstructural observations were done using the Axio Vert A1 light optical microscope and the FED QUANTA 250 SEM FEI scanning electron microscope, which includes energy dispersive X-ray spectroscopy (EDS) functionality. For XRD analysis, a Bruker D8 diffractometer with CuK $\alpha$  radiation was used. Measurements were taken in a 2 $\theta$  range of 20-90°, with steps of 0.02° at a count time of 0.6 s, powered at 40 kV and 25 mA. A Mettler-Toledo 822e Differential Scanning Calorimeter was used to determine the transformation temperatures. The dynamic measurements included two heating/cooling cycles from -50 °C to 350 °C in a nitrogen atmosphere at a rate of 10 K/min.

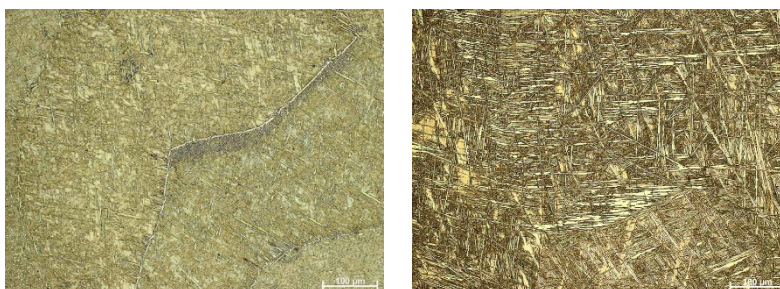
## 3. RESULTS AND DISCUSSION

The average overall composition of the prepared sample, as determined by EDS, is shown in Table 1. A negligible difference can be observed between the designed and experimental composition of the Cu-10Al-1Ag SMA alloy

Table 1 - Composition of SMA alloy determined by SEM-EDS average.

Composition (wt. %)			
Design alloy	Cu	Al	Ag
Cu-10Al-1Ag As-cast	87.53 $\pm$ 0.77	10.18 $\pm$ 0.47	0.99 $\pm$ 0.34

OM (Figure 1.) and SEM (Figure 2.) were used for microstructural analysis of the investigated Cu-Al-Ag alloy in the as-cast and quenched state. Images of OM were taken both in bright field (BF) and with polarized light (POL). Figure 1. shows the precipitates present in the  $\beta$ -parent phase of the microstructure in the as-cast state. The early stages of martensite structure formation can be seen at the grain boundaries. Within the grains, short needle-like martensite crystals form from the DO<sup>3</sup> parent phase, probably of the  $\beta_1'$  type with the monoclinic 18R structure. The polarized OM microphotographs clearly show the grain boundaries and reveal different orientations of the martensite crystals within the grains in the structure. After quenching, a fully developed martensite structure can be seen. Compared to the as-cast state, the martensite appears significantly larger. The observations show that only  $\beta_1'$ -martensite crystals are present, which predominantly exhibit the characteristic zig-zag morphology (as shown in Figures 1 and 2). These  $\beta_1'$ -variants of martensite show thermoelastic behavior due to their controlled growth in self-accommodating zig-zag groups [8].





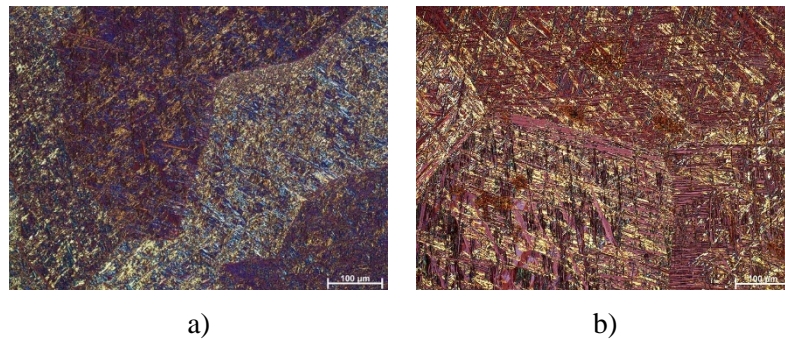


Figure 1 - OM micrographs of Cu-10Al-1Ag SMA: a) As-cast state: BF and POL, mag. 200x, b) Quenched state: BF and POL, mag. 200x

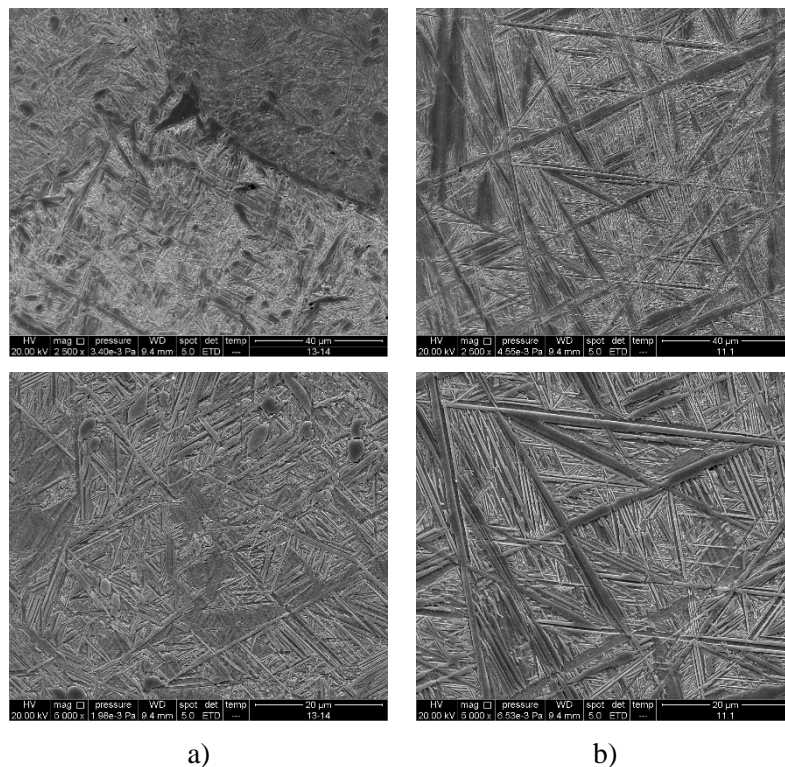


Figure 2 - SEM micrograph of Cu-10Al-1Ag SMA: a) As-cast state: mag. 2500x and 5000x, b) Quenched state: mag. 2500x and 5000x

SEM the microscopic images show the presence of a single type of martensite in both states, with no obvious coarse plates of  $\gamma_1'$ -martensite. This  $\gamma_1'$ -martensite is another thermally induced martensite typically found in Cu-Al SMAs. It is worth noting that the driving force for nucleation of  $\gamma_1'$  (2H) is greater than that of  $\beta_1'$  (18R) martensite. However, whether both 18R and 2H structures coexist depends largely on the alloy composition and the specifics of the heat treatment process. The differences in morphology between  $\beta_1'$  and  $\gamma_1'$  result from their different inhomogeneous shear methods [9]. In Figure 3., XRD analysis comprises XRD measurements between as-cast and quenched state. Diffractograms confirms the presence of 18R ( $\beta_1'$ ) martensite in both states of Cu-10Al-1Ag alloy. Additionally, two prominent peaks for the f.c.c. Cu ( $\alpha$ -Cu phase) suggest that an extremely slow cooling rate results in Cu precipitation in As-cast state, while fully formed martensite 18R ( $\beta_1'$ ) structure is formed in quenched sample. Furthermore, the DSC thermogram for cast Cu-10Al-1Ag alloy shows martensite transformation in cooling curves with start and finish temperatures of martensite transformation,  $M_s = 182$  °C and  $M_f = 154$  °C (1<sup>st</sup> cooling cycle) and 151 °C (2<sup>nd</sup> cooling cycle) (Figure 3.). After quenching, martensitic transformation shows start martensitic temperature at  $M_s = 180$  °C and finish transformation temperature  $M_f=132$ °C. Martensitic transformation temperatures didn't change significantly in the

first and second cycle. In relation to cast alloy start martensite temperature is similar, but transformation releases higher heat fusion, and finish transformation temperature is shifted to lower value. DSC results indicate that the formed  $\beta_1'$ -martensite is thermally stable, which is very important for the application of SMA.

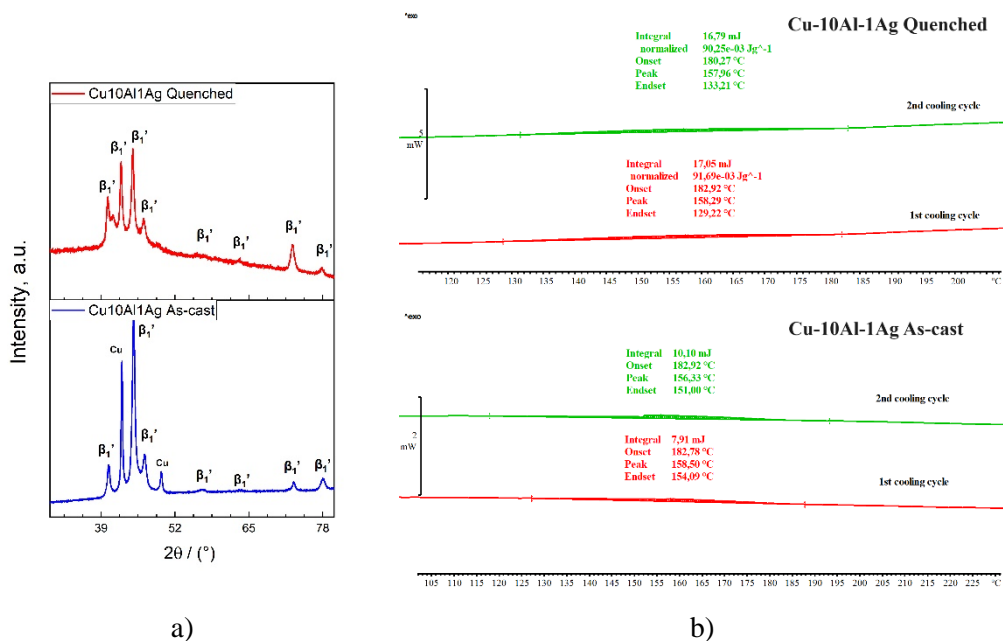


Figure 3 - Cu-10Al-1Ag SMA alloy: a) XRD diffractograms of as-cast and quenched samples, b) DSC thermogram of as-cast and quenched samples

#### 4. CONCLUSION

The Cu-10Al-1Ag alloy, produced by melting in an electric arc furnace, exhibited a distinct martensitic structure in as-cast and quenched state, particularly the monoclinic 18R ( $\beta_1'$ ) form, that is thermally stable. The 18R martensite formed in the as-cast state is partially provided with pockets of Cu precipitates, whereas in the quenched state of the Cu-10Al-1Ag alloy there is fully formed 18R martensite. In conclusion, both OM and SEM analyses, supported by DSC, show that the addition of only 1 wt.% silver to the Cu-Al-Ag alloy leads to a shift in transformation temperature and achieves shape memory properties.

#### REFERENCES

- [1] J. Fernández, A. Isalgue, R. Franch, Mater. Today: Proc., 2S (2015) S805-S808.
- [2] R.O. Ferreira, L.S. Silva, R.A.G. Silva, J. Therm. Anal. Calorim., 146 (2) (2021) 595.
- [3] R. Silva, A. Paganotti, S. Gama, A. Adorno, T. Carvalho, C. Santos, Mater. Charact., 75 (2013) 194-199.
- [4] C. Santos, A. Adorno, A. Paganotti, C. Silva, A. Oliveira, R. Silva, J. Phys. Chem. Solids., 104 (2017) 145-151.
- [5] C.M.A. Santos, A.T. Adorno, M. Stipcich, A. Cuniberti, J.S. Souza, C.V.X. Bessa, R.A.G. Silva, et al, Mater. Chem. Phys., 227 (2019) 184-190.
- [6] D. Manasijević, T. Holjevac Grgurić, L. Balanović, U. Stamenković, M. Gorgievski, M. Gojić, Met. Mater., 58(04) (2020) 293-299.
- [7] T.V. Krishna, D.S. Rao, Aust. J. Mech. Eng., 1 (2022) 17.
- [8] U. Sarı, I. Aksoy, J. Alloys Compd., 417 (2006) 138.
- [9] E. Aldırmaz, I. Aksoy, Arab. J. Sci. Eng., 39 (2014) 575.

## EVALUATION OF THE EFFICIENCY OF DIFFERENT COLLECTORS IN THE CHALCOPYRITE FLOTATION

**Hasan Ali Taner, Vildan Onen**

Department of Mining Engineering, Faculty of Engineering and Natural Sciences, Konya  
Technical University, Selcuklu/Konya, Turkey

### **Abstract**

*Determining the appropriate type/dosage of collector is a key factor in increasing flotation recovery and achieving the optimum concentrate grade. In this study, the effect of five different collectors (3418A, MX-515, HX-231, NaIPX, KAX) on the flotation of chalcopyrite ore was investigated and the results were evaluated by measuring the contact angle with the most suitable collector. In comparison to the other collectors, 3418A had the highest selectivity for chalcopyrite. The optimum collector dosage and conditioning time using 3418A were determined as 50 g/t and 3 min, respectively. In contact angle measurements with 3418A, the hydrophobicity of the chalcopyrite surface increased and the maximum contact angle was obtained as 58.4° at a collector dosage of 0.1 g/L at pH 12.*

**Keywords:** *chalcopyrite, collector, contact angle, flotation, pyrite*

### **1. INTRODUCTION**

The demand for copper, which is used in strategic sectors like energy, continues to increase due to its fundamental role in modern technologies. Chalcopyrite ( $\text{CuFeS}_2$ ) is the most copper-containing mineral and is the primary source of commercial copper metal [1,2]. One of the most important mineral processing methods for copper minerals is flotation. This method is commonly used for the enrichment of low-grade and complex ores. Flotation is a complex physicochemical process that separates minerals based on differences in surface hydrophobicity. Many researchers have worked to improve flotation recovery and selectivity by developing specific chemical reagents, flotation machines, and technologies [3,4,5,6].

The probability of bubble and particle attachment in flotation primarily depends on the hydrophobic nature of the mineral surface. Collectors are used to impart hydrophobic properties to the mineral surface or to increase hydrophobicity. The collectors need two functionalities in their molecules in order to attach to surfaces and impart hydrophobicity: a hydrophilic group that can interact chemically or electrostatically with the surfaces of mineral species, and a non-polar group made up of an aliphatic chain that extends toward the liquid phase and confers the hydrophobic property.

Due to their superior collecting capabilities and affordable production costs, traditional flotation collectors such as xanthates are still the most often used flotation collectors for the recovery of copper and other non-ferrous minerals [7]. The most common collectors for the flotation of copper sulfide ores belong to the class of hydrogen sulfide (-SH), also known as thiols, sulfhydryl group, or mercapto group (C-S). They can be grouped into families such as xanthates (X), dithiophosphates (DTP), dithiocarbamates (DTC), thionocarbamate, thiocarbamate, and mercapto benzothiazole (MBT) [8]. The appropriate use of the collector in flotation is important for flotation recovery. A proper dosage may give the best results, while an overdose may result in low recoveries owing to double-layer adsorption. Due to their complicated embedding relationships and comparable natural floatability in the ore, chalcopyrite and pyrite are typically difficult to separate by flotation [9]. One of the common problems in chalcopyrite flotation is pyrite

depression. In order to depress pyrite, the pH value is increased to around 10-12 by adding lime and copper minerals can be floated with xanthate and dithiophosphate-type collectors.

In this study, the flotation performances of various collectors were evaluated for a sulfide copper ore, and the results were assessed by measuring contact angle with the selected optimal collector type.

## 2. EXPERIMENTAL

### 2.1 Material

The sulfide ore sample used in this study was obtained from an enrichment plant located in Madenköy, a region within the Sirvan district of Siirt province in Southeastern Anatolia, Turkey. The ore's D<sub>80</sub> particle size, determined using Malvern Mastersizer 2000, is 80 µm. Based on semi-quantitative XRD analysis, the ore was found to contain kaolinite, illite, and chlorite clay minerals, as well as chalcopyrite, pyrite, and magnetite [10]. The ore contains 2.63% Cu and 38.38% Fe. The sample used for contact angle measurements was manually collected as piece ore from the plant.

Sodium silicate as depressant/dispersant, methyl isobutyl carbinol (MIBC) as frother, and lime for pH adjustment were used in the flotation experiments. Five different collectors presented in Table 1 were tested in the experiments. Collectors were prepared daily as 1% stock solutions before the experiments.

Table 1 - Reagents used in the experiments and their properties

Collector	Chemical Composition	Purity Degree (%)	Molecular Weight (g/mol)	Producer Company
Sodium isopropyl xanthate (NaIPX)	(CH <sub>3</sub> ) <sub>2</sub> CHOCSSNa	99.5	202.37	Kimsan
Potassium amyl xanthate (KAX)	CH <sub>3</sub> (CH <sub>2</sub> ) <sub>4</sub> OCS <sub>2</sub> K	99.5	202.37	Kimsan
Hostafloat HX-231	Thionocarbamate	-	-	Clariant
Aerofloat MX-515	Mixture of isopropanol, dithiophosphate and thionocarbamate	99	-	Cytec
Aerophine 3418A	Sodium diisobutyl dithiophosphinate C <sub>8</sub> H <sub>18</sub> PS <sub>2</sub> .Na	50	232	Cytec

### 2.2 Method

#### 2.2.1 Flotation experiments

The Denver model 1 L conventional laboratory device was used for the flotation experiments conducted at 10% solid ratio, 10 L/min air-flow rate, 2 cm froth height, and 1350 rpm stirring speed. Sodium silicate was used as dispersant (100 g/t), while MIBC was used as frother (80 g/ton). A mineral suspension was formed by mixing the ore with tap water. First, lime stock solution was added to the mineral suspension, the pH was raised to 11.5 and conditioned for 5 min. Then the dispersant was added and conditioned for 3 min. Following the addition of the collector and 3 min of conditioning, the frother was added to the pulp and conditioned for 1 min. The froth was then scrapped for 3 min to collect the concentrate. After the experiments, the concentrate and gangue products were collected, filtered, and dried (105 °C). Finally, Cu and Fe grades and weights of the products were determined in order to calculate the flotation recoveries. Atomic Absorption Spectrometer (AAS) instrument (GBC brand SensAA model) was used to determine the grade of products.



### 2.2.2 Contact Angle Measurements

Four pieces of samples taken from the ore were cut with a stone-cutting machine to obtain smooth surfaces (Figure 1a). Then, these surfaces were polished using a rotary polishing device (Figure 1b). Since it was not possible to obtain a sufficiently polished surface, the surfaces were rubbed in slurry on a glass plate with 600 and 800  $\mu\text{m}$  particle size aluminum oxide powder. Contact angle measurements were performed with the KSV CAM 101 model contact angle measurement device (Figure 1c). The captive bubble method was used on the polished surface of the sample for these measurements. In this method, the mineral is placed in a solution containing the necessary reagents, and bubble is formed on the surface of the sample by injecting air with a syringe (Figure 1d). By injecting air with a syringe, a bubble (0.1  $\mu\text{L}$ ) was created and made to adhere to the mineral surface. This measurement was repeated at different points on the mineral surface, and the average value of contact angle readings was taken.

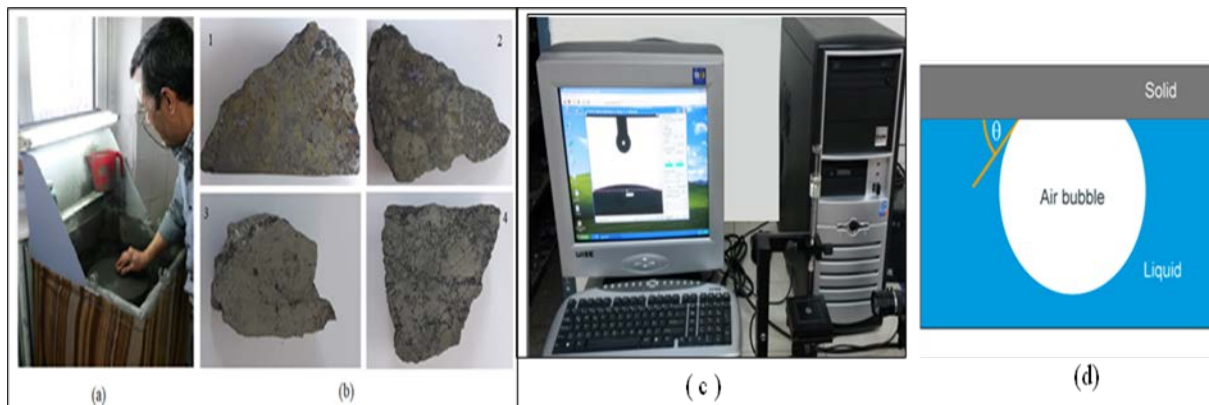


Figure 1 - Rotary polishing device (a) and polished section samples (b) goniometer (c) Captive bubble method (d)

The polished sections examined under the ore microscope allowed the determination of chalcopyrite and pyrite surfaces, and the wettability of both chalcopyrite and pyrite were measured in the contact angle measurements. The polished section numbered 1 in Figure 1b, containing both chalcopyrite and pyrite surfaces and having coarse mineral surfaces, was used for contact angle measurements.

## 3. RESULTS AND DISCUSSION

### 3.1 The effect of collector type and amount on the chalcopyrite flotation

Finding the appropriate dosage of collector is a critical parameter in optimizing flotation process, maximizing recovery, and achieving the desired concentrate grade. The results of the flotation experiments conducted with all the collectors are presented in Figures 2a1-a2 for Aerophine 3418A, in Figures 2b1-b2 for MX-515, in Figures 2c1-c2 for HX-231, in Figures 2d1-d2 for sodium isopropyl xanthate (NaIPX) and Figures 2e1-e2 for potassium amyl xanthate (KAX), respectively. The most favorable recovery and grade values were determined at a collector dosage of 50 g/t at all collectors for chalcopyrite. As the collector dosage increased, there was an increase in the recovery while a decrease in the grade of chalcopyrite was observed. This suggests that the collectors tend to preferentially attach themselves to the gangue particles, making them more hydrophobic and more likely to float. In fact, the pyrite grade and recovery were also increased with higher collector dosages. (Figures 2a2-b2-c2-d2-e2). A large amount of the collector attaches to gangue minerals, notably sulfur species like pyrite, which are often abundant in copper deposits, because collectors are frequently not sufficiently selective to the valuable mineral. This decreases the reagent's effectiveness and taints the concentrate since all particles (valuable and unvaluable) covered by collectors become more hydrophobic and are more likely to adhere to the bubbles [8].

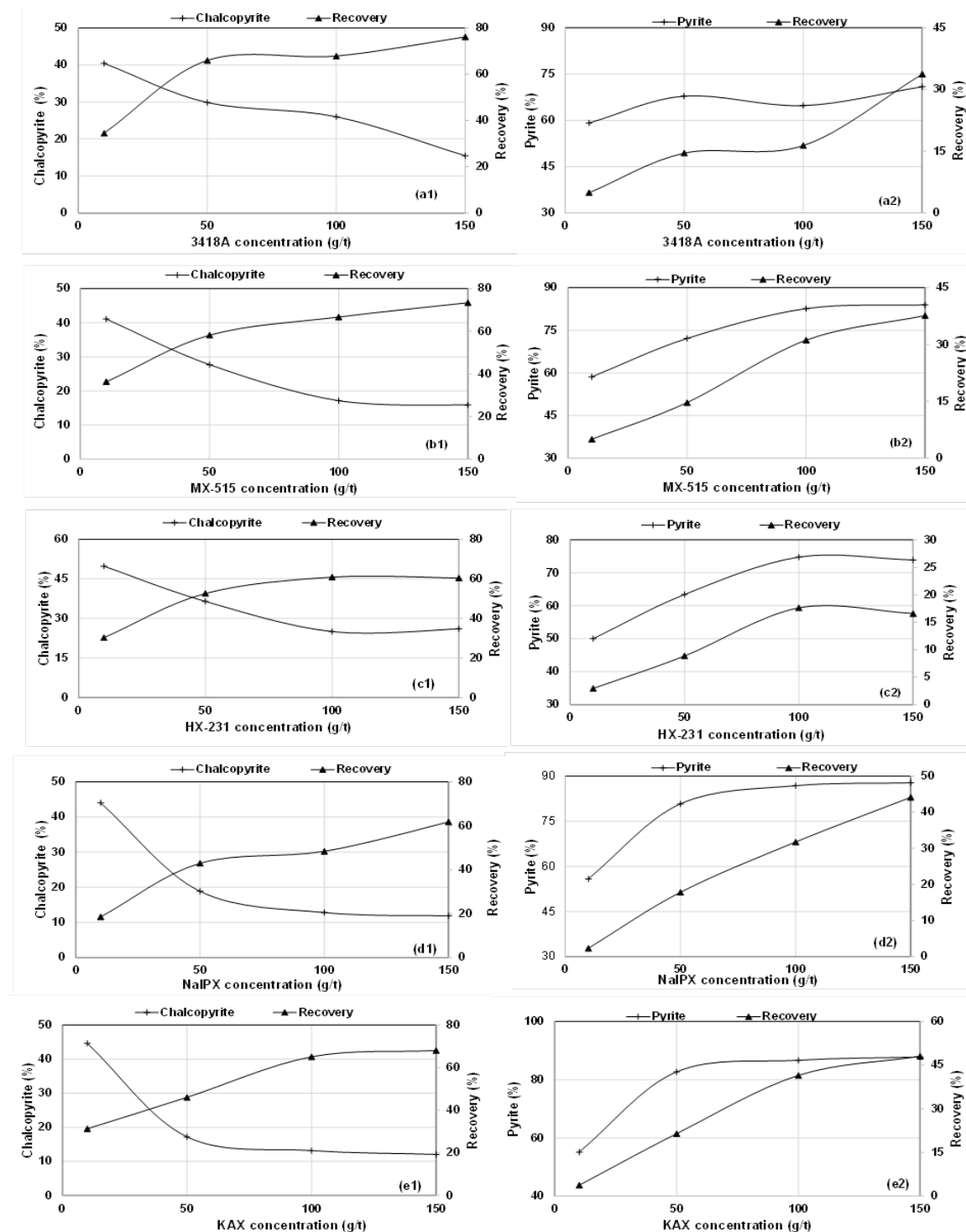


Figure 2 - The effect of concentration of 3418A (a1-chalcopyrite, a2-pyrite), MX-515 (b1-chalcopyrite, b2-pyrite), HX-231 (c1-chalcopyrite, c2-pyrite), NaIPX (d1-chalcopyrite, d2-pyrite) and KAX (e1-chalcopyrite, e2-pyrite) on chalcopyrite grade and recovery

In Figure 3, the effect of collectors at the determined optimum concentrations on chalcopyrite/pyrite grade and recovery was evaluated among each other. The results indicated that 3418A exhibited the best selectivity for chalcopyrite compared to the other collectors.



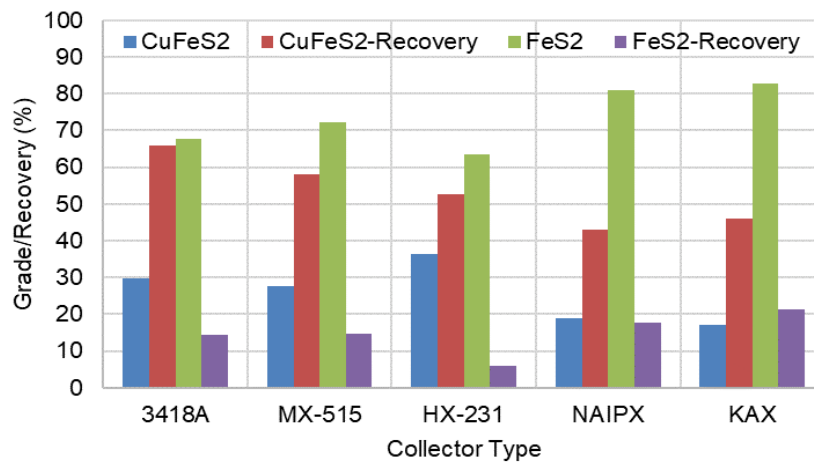


Figure 3 - Flotation results of collectors at 50 g/t concentration

### 3.2 The effect of the collector conditioning time on the chalcopyrite flotation

For 3418A, the effect of collector conditioning time on flotation experiments was investigated at intervals of 1.5, 3, 5, 7, and 9 min. It was found that the most favorable grade and recovery values for chalcopyrite were achieved with 3 min conditioning time. After the 3 min conditioning time, there was not much variation in chalcopyrite recovery, but fluctuations were observed in terms of chalcopyrite grade (Figure 4a). The lowest pyrite grade and recovery were obtained in 3 min conditioning time, after which there were fluctuations (Figure 4b).

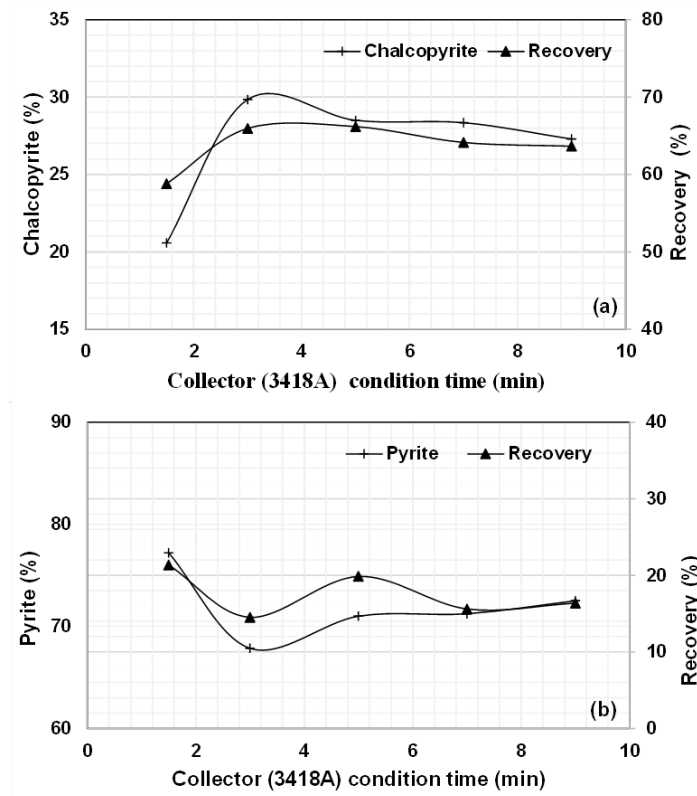


Figure 4 - Effect of the collector (3418A) conditioning time on the chalcopyrite/pyrite grade and recovery

### 3.3 The effect of collector dosage on the contact angle of minerals

The effects of 3418A, which was determined as the optimum collector, on the contact angle were investigated in alkaline medium (pH 10, 11, and 12). For this purpose, 100 mL of distilled water was mixed with 0.01-0.2 g/L of 1% collector solutions, and the mixtures were stirred for 3 min.

As the pH value increased, the contact angle of chalcopyrite generally increased (Figure 5a). 3418A increased the hydrophobicity of the chalcopyrite surface, and the maximum contact angle of 58.4° was obtained at pH 12 with a collector concentration of 0.1 g/L. However, further increases in the collector concentration resulted in a decrease in the contact angle at pH 12. This phenomenon is believed to be due to multilayer adsorption. At alkaline pH values, in the presence of 3418A, the chalcopyrite surface was found to be hydrophobic, and as the pH level decreased, the contact angle of pyrite increased (Figure 5b). For pyrite, at pH 10, the contact angle increased with increasing collector concentration, while at pH 11 and 12, it decreased with increasing concentration.

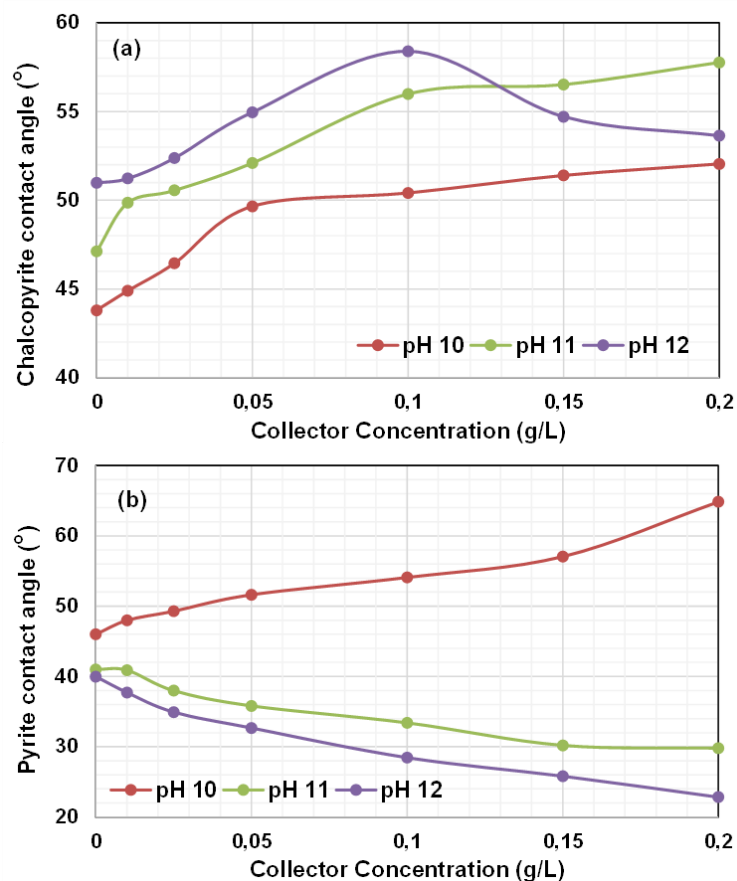


Figure 5 - Effect of 3418A collector on contact angle of chalcopyrite/pyrite minerals

#### 4. CONCLUSION

In this study, the effect of different five collectors on the chalcopyrite flotation were evaluated. In terms of flotation recovery and concentrate grade, optimum conditions were determined using 3418A, 50 g/t collector concentration and conditioning time 3 min. As the collector dosage increased, the chalcopyrite grade decreased, and the chalcopyrite recovery increased. As the pH value increases, the contact angle of chalcopyrite increased. The maximum contact angle (58.4°) was achieved with 3418A at pH 12 with a concentration of 0.1 g/L. However, further increases in the collector concentration resulted in a decrease in the contact angle due to multilayer collector adsorption. At alkaline pH values, in the presence of 3418A, the chalcopyrite surface was become more hydrophobic, and as the pH level decreases, the contact angle of pyrite increased. Pyrite flotation behavior is significantly influenced by the pulp's pH value, and lime is an effective depressant for pyrite. Therefore, for pyrite, the contact angle values increased with increasing collector concentration at pH 10 and decreased at pH 11 and 12.

## ACKNOWLEDGEMENTS

*This study was funded by the Scientific Research Projects Funding Unit of the Selcuk University (Project number 18401029).*

## REFERENCES

- [1] G. Fairthorne, D. Fornasiero, J. Ralston, *Int. J. Miner. Process.*, 49(1-2) (1997) 31-48.
- [2] T. Moimane, Y. Huai, Y. Peng, *Miner. Eng.*, 164 (2021) 106816 1-8.
- [3] A. Hassanzadeh, F. Karakaş, *J. Dispersion Sci. Technol.*, 38(2) (2017) 309-316.
- [4] I. Aarab, M. Derqaoui, A. Abidi, A. Yaacoubi, K. El Amari, A. Etahiri, A. Baçaoui, *Arab. J. Geosci.*, 13 (2020) 1-11.
- [5] I. Aarab, M. Derqaoui, K. El Amari, A. Yaacoubi, A. Abidi, A. Etahiri, A. Baçaoui, *Colloid Surf. A-Physicochem. Eng. Asp.*, 631(2021) 127700 1-11.
- [6] G.P.W. Suyantara, I.N. Rizki, A. Ulmaszoda, H. Miki, K. Sasaki, *J. Environ. Chem. Eng.*, 11(3) (2023) 110006 1-11.
- [7] X. Huang, X. Yuan, H. Yang, R. Zhang, G. Liu, J. Zeng, *Adv. Powder Technol.*, 34(2) (2023) 103935 1-11.
- [8] C.I. Castellón, N. Toro, E. Gálvez, P. Robles, W.H. Leiva, R.I. Jeldres, *Materials*, 15(19) (2022) 6536 1-42.
- [9] X. Qin, J. Liu, Y. Yu, J. Hao, H. Gao, D. Li, L. Dai, *Adv. Powder Technol.*, 34(9) (2023) 104141 1-9.
- [10] H.A. Taner, *The effect of structural properties of clay minerals on flotation performance of metal sulphides*, Doctoral Thesis, Konya Technical University, Konya, 2019, 172.

## A PYRO-HYDROMETALLURGICAL PROCESS FOR THE RECOVERY OF ZINC FROM JAROSITE WASTE

Vesna Conić, Dragana Božić, Miloš Janošević, Ljiljana Avramović,  
Vanja Trifunović, Dejan Bugarin, Ivana Jovanović

Mining and Metallurgy Institute Bor, Zelene Bulevar 35, 19210 Bor, Serbia

### Abstract

*The paper presents a procedure for obtaining Zn from jarosite waste raw material by combining low-temperature roasting at 530°C and leaching in water with its simultaneous separation from Fe. By low-temperature roasting, iron was converted from the  $Fe_2(SO_4)_3$  form into  $Fe_2O_3$ , which is insoluble in water and slightly soluble in acid. As zinc sulfate decomposes at 740°C, the zinc remains in the form of  $ZnSO_4$ , which is easily dissolved in water. In this way, the selectivity of Zn over Fe was achieved. Jarosite is the residue of hot-acid leaching. It is obtained according to the old technology of obtaining zinc. Jarosite with a relatively high content of 4.7% Zn is a technological choice for obtaining products of commercial quality. From the experimental results, by roasting 100g of jarosite for 4 hours at 530°C in electric furnace and leaching the roasted sample in water under the conditions: S:L = 1:5, room temperature, time 1h, the leaching degree of 91.97% and 9.60% were obtained for Zn and Fe respectively. By applying the precipitation, using 1M NaOH, on leaching solution, 99.93% Fe is precipitated to the pH=4. Zinc precipitates at a pH > 5.5, so it completely remains in leach solution. Zn in the form of  $ZnSO_4$  can be further treated by the electrolysis process in order to obtain pure electrolytic Zn, or by precipitation with  $Na_2CO_3$  it can be obtained as  $ZnCO_3$  concentrate of commercial quality.*

**Keywords:** (jarosite, Zn recovery, low temperature roasting, water leaching, metals selectivity)

### 1. INTRODUCTION

In Serbia, Jarosite + Pb–Ag waste sludge has been disposed of for years, which should be the last solution in the hierarchy of waste management, after prevention of waste generation, reuse of waste, recycling and other types of waste utilization in accordance with the principles of circular economy. Jarosite + Pb–Ag sludge, obtained from central Serbia Elixir Factory "Zorka" in Šabac is waste sludge that was obtained from the hot acid leaching process. The product was obtained using traditional refining technology for obtaining zinc, whereby, in addition to Pb–Ag precipitate, jarosite is also obtained. This waste raw material, in addition to zinc, contains copper, lead, silver, gold and indium in quantities that should not be neglected. The processing proposed in this paper may have commercial benefits compared to the processing methods proposed by many authors. There are many studies in which different procedures for the treatment of jarosite raw materials are presented. Some authors presented the procedure of acid leaching as well as brine leaching for the extraction of Zn and Pb [1-3]. Pyrometallurgical processes for the processing of zinc secondary raw materials and waste deposits from zinc hydrometallurgy are very efficient, but they require expensive industrial plants with a large capacity to be economical [4,5]. This work presents a pyro-hydrometallurgical route, for processing jarosite tailing waste with the possibility of separating the present metals and obtaining zinc.

## 2. EXPERIMENTAL

### 2.1 Chemical analysis of jarosite

Chemical analysis of the jarosite sample was performed and presented in Table 1.

Table 1 - Element contents (wt% dry basis) of a jarosite sample

Element	Cu %	Zn %	Fe %
Content	0.7	5.39	30.61

### 2.2 Mineralogical Composition of a Jarosite Sample

The Jarosite XRD pattern is shown in Figure 1. It can be seen that beside jarosite, mineral forms of magnetite and anglesite are present.

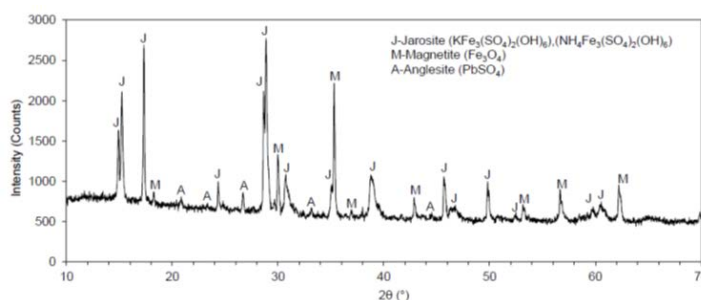


Figure 1 - Diffractogram of a Jarosite tailings waste sample

## 3. RESULTS AND DISCUSSION

### 3.1 Jarosite roasting and water leaching of calcine

The experiment of low-temperature roasting of a 100g sample of jarosite was performed in a stationary electric furnace for 4 hours at 530 °C. The X-ray powder diffraction of the calcine is shown in Figure 2.

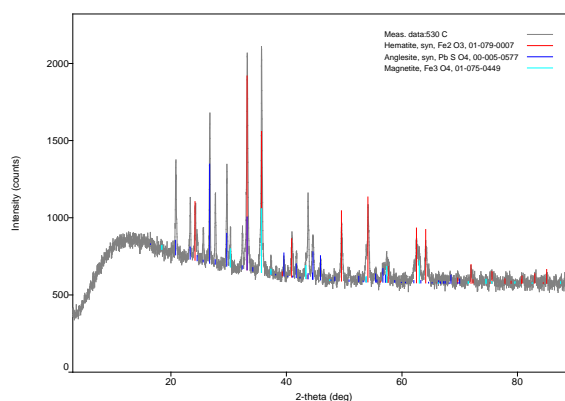


Figure 2 - Diffractogram of calcine obtained by jarosite roasting at "530 °C"

After roasting, the phases present in the calcine were hematite, anglesite and magnetite. After the roasting stage, the calcine is leached in water. Table 2, shows the roasting and leaching conditions for the experiment that showed the best metal recovery.

Table 2 - Conditions of jarosite roasting and leaching with degrees of metal leaching

Roasting time 4h		Leaching with H <sub>2</sub> O (S:L=1:5), t=1h, pH after leaching	Leaching degree			
Sample mass (g)	Temperature roasting (°C)	pH	Zn %	Cu %	Fe %	
1.	100	530	2.25	91.97	91.07	9.60

From the Table 2, can be shows that the metals recovery is 91.97%, 91.07%, and 9.60% for Zn, Cu, and Fe respectively. After leaching, under the conditions of S:L = 1:5, leaching time of 1 h, at room temperature, the measured pH of the leach solution was 2.25. It can be noted that in the experiment, there was enough acid to carry out the leaching process, in other words, no acid needed to be added. The reason for the greater degree of leaching of Zn and Cu is that during the roasting process at low temperatures, they remained in the form of sulfate, which is easily leached in water, while iron was transformed into hematite, which is practically insoluble. By measuring the pH after leaching, it was determined that there is no need to leach in acid. For this reason, we decided to use water for the leaching process. Based on past experience gained through many years of research, it was decided that the S:L ratio should be 1:5, which is a reasonable ratio. The selected leaching time of 1h was sufficient because sulfates are easily soluble in water.

### 3.2 Precipitation of Fe

The leach solution containing Cu, Zn and Fe was treated to separate the present metals. Fe precipitation was done at pH=4 using 1M NaOH. The results show in Table 3 that 100% Zn and 96% Cu remained in the solution after precipitation, while 94% Fe was precipitated from the solution. In this way, Fe was separated in the form of Fe(OH)<sub>3</sub> precipitate, while zinc and copper in the form of sulfates are present in the solution.

Table 3 - Percent metal content in solution after leaching and precipitation

Metals	Zn%	Cu%	Fe%
Leaching degree	91.97	91.07	9.6
The percentage content of metal in the solution after precipitation related to the content in the leach solution	100	96.00	6.3
The percentage content of metals in the solution related to the content of the same in the starting raw material	91.97	87.43	0.61

It can be seen from Table 3, that the percentage metal content of 91.97% zinc and 87.43% copper in the solution in relation to the content of the same in the starting raw material, in fact, represents the utilization of these metals.

### 3.3 Cementation of Cu from solution after Fe precipitation

After the precipitation of iron, in the leach solution, macro components Zn and Cu are present in the form of sulfates as ZnSO<sub>4</sub> and CuSO<sub>4</sub>. In order to achieve selectivity and separation of copper from zinc, copper cementation was carried out at pH=2 with zinc powder, a metal that is more electronegative than copper. The necessary amount of zinc for the cementation process was calculated based on the stoichiometrically required amount with 50% excess.



### 3.4 Precipitation of Zn from solution using Na<sub>2</sub>CO<sub>3</sub>

After copper cementation, the solution was filtered and prepared for obtaining ZnCO<sub>3</sub> from ZnSO<sub>4</sub>. The pH value of the solution was measured, which after Cu cementation was pH=2.84. Precipitation of Zn as ZnCO<sub>3</sub> was carried out up to pH=8 by adding 10% Na<sub>2</sub>CO<sub>3</sub>. The obtained zinc carbonate was washed, dried and submitted to chemical analysis. Zinc carbonate is shown in Figure 3.

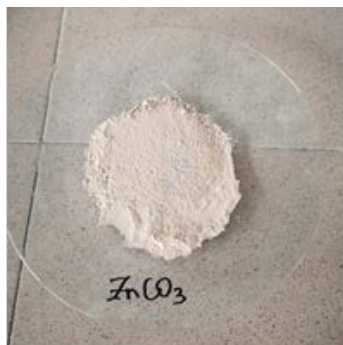


Figure 3 - Zinc – carbonate

The characterization of the obtained zinc carbonate was done and showed the following content: Zn=51%, Cu=0.7% i Fe=0.8%.

### 4. CONCLUSION

Zinc from jarosite tailings waste was obtained through the following main stages of treatment: i) jarosite roasting to convert iron sulfate into insoluble hematite, ii) leaching in water in order to leach Zn, iii) precipitation of Fe from leaching solution with 1MNaOH, iv) cementation of Cu with zinc, v) precipitation of Zn from ZnSO<sub>4</sub> solution with Na<sub>2</sub>CO<sub>3</sub>. This paper shows that the combination of roasting and leaching provides a promising process for obtaining ZnCO<sub>3</sub> concentrate of commercial quality. The total recovery of Zn after leaching, Fe precipitation and carbonate precipitation was 91.97%. The quality of the obtained ZnCO<sub>3</sub> was: Zn=51%, Cu=0.7% and Fe=0.84.

### ACKNOWLEDGMENTS

*This work was financially supported by the Ministry of Education, Science and Technological Development of the Republic of Serbia, Grant No. 451-03-47/2023-01/200052.*

### REFERENCES

- [1] A. Rus, A.S. Sunkar, Y.A. Topkaya, Hydrometallurgy 93 (2008) 45–50.
- [2] M. D. Turan, H. S. Altundoğan, F. Tümen, Hydrometallurgy 75 (2004) 169-176.
- [3] Y. Wang, H. Yang, W. Zhang, R. Song, Jiang, B. Physicochem. Probl. Miner. Process. 54 (2018) 517-526.
- [4] S. Creedy, A. Glinin, R. Matusewics, S. Hughes, M. Reuter, 2013. Outotec Ausmelt Technology for Treating Zinc Residues. World Metall. - ERZMETALL 66, 230–235.
- [5] S. Hughes, M.A. Reuter, R. Baxter, A. Kaye, S. Hughes, 2008. Ausmelt Technology for Lead and Zinc Processing, in: Lead and Zinc. pp. 147–162.

## RESEARCH THE RATE OF CHEMICAL CORROSION OF STEEL 3X14H2 (BDS 3692-78)

Maria Krasteva<sup>1</sup>, Rumen Petkov<sup>2</sup>

University of Chemical Technology and Metallurgy, Sofia, Bulgaria, St. "Kl. Ohridski" №8

### Abstract

*The corrosive stability of steels characterizes their ability to function in chemical (aggressive) environments in the same way they would function in non aggressive environmental conditions. The chromium steels are the most economical in terms of alloying and they are widely used in different branches of technology due to their qualities of stainlessness, corrosion stability and to cauterization. The main application is gas turbines, work and stop blades, repairing details functioning at temperatures higher than 450°C, cutting stainless medical tools. There is no data as to corrosion stability of the most widely used brand of steel 3X14H2 which works in a number of different chemical (aggressive) environments and at various temperatures.*

**Keywords:** steel, corrosion stability, aggressive environment

### 1. INTRODUCTION

Chromium nickel steel of the 3X14H2 type is characterized by high mechanic qualities and high corrosion stability to (environmental conditions and in different chemical (aggressive) environments as a results of the high contents of chromium. Nickel, in quantity not higher than 2% is added to chromium steels in order to improve their tempering and to remove free ferrites. A low quantity of nickel (less than 1%) which gets into blend materials adds a strong enough impact to the critical point of  $\gamma$ - a tempering to the mechanic qualities and the corrosion stability of steel. Adding 2% Ni to 14% chromium steel the quantity of austenite increases at high temperature which leads to the decrease of the critical point of complete tempering and also to increase of the coefficient of corrosion stability [1].

Or order to achieve a homogeneous structure and high level of strength (355 - 400 HB), the 3X14H2 steel when hardened should be heated to 1020 - 1066°C which cooling in oil or in air. The tempering temperature should be in the range of 250 to 400°C. When used for other purposes the 3X14H2 steel is to be hardened on temperatures between 980 and 1020°C and tempering at 540 to 640°C (260-340 HB). The best full tempering takes place at temperatures of 620 to 660°C, holding for 4 to 6 hours and cooling in oil [2].

### 2. EXPERIMENTAL

The aim of the present work is to research the corrosion stability of steel type 3X14H2 at various thermal regimes and different chemical (aggressive) environments.

In order to obtain the 3X14H2 steel blend of 100 kg alloy has been calculated. The charge consists of steel 3, steel 45, low content carbon ferrochromium and nickel. The raw material is dozed in accordance to the balance and is to be charged into the aggregate for the melting of the materials. The melting takes place in a high-frequency induction furnace with acid lining. The blend obtained is cast in ceramic melting model moulds elaborated on the territory of the Buser JSCo in Sofia.

The test bodies of the 3X14H2 steel are cleaned and go through, an additional thermal processing. This additional processing consists of annealing, tempering accompanied by high temperature

tempering, hardening with low temperature tempering and one of the test bodies remains in its cast structural condition [3, 6].

The test bodies of the 3X14H2 steel are cut into equal size pieces with a machine of the MINOSEKAR type with the help of hard discs with diamond coverage at constant water cooling. The area of each body is calculated and its weight is measured on an analytical scale before and after exposing it to a chemical (aggressive) environment for a certain amount of time. Control over the loss of weight is made after both a 24-hour and a 48-hour period of stay in a chemical (aggressive) environment.

The methodology used to determine the corrosion stability of the 3X14H2 steel is a standard one elaborated by the Russian scientist F. Himushin. The chemical (aggressive) environments have been presented by solutions of 2,5% HCl, 5% HCl, 10% HCl, 10% H<sub>2</sub>SO<sub>4</sub>, 10% HNO<sub>3</sub>, 45% H<sub>3</sub>PO<sub>4</sub> and 10 % oxalic acid all of which serve to determine the corrosion stability of 3X14H2 steel [6].

The corrosion stability coefficient is determined as dependent on the difference in the weights of the test bodies before and after their being exposed to the chemical (aggressive) environment as compared to their complete surfaces and the time spent in the solutions [4, 5].

$$K_i = \frac{\Delta m_i}{S_n \cdot t_i}, \text{ g/(cm}^2 \cdot \text{h)}, \text{ where}$$

$K_i$  = corrosion stability coefficient, g/(cm<sup>2</sup>.h);

$S_n$  - complete surface of the tested body, cm<sup>2</sup>;

$T_i$  = time spent by the tested body in the chemical (aggressive) solutions, h;

$\Delta m_i$  = weight difference of the tested body before and after the stay in a chemical (aggressive) environment.

### 3. RESULTS AND DISCUSSION

The alloy obtained is presented for spectrum analysis conducted with a quantum meter at the "M and Ts Hydraulic" Company Kazanlak. In accordance to the Bulgarian State Standard BDS 6738 - 72 the solution obtained enters into the 3X14H2 type of steel with major components as follows: C-0,317%; Cr - 13,4%; Ni - 2,5%; S -0,028%; P - 0,055%; Mn - 0,121 % etc. [6]. Figures 1÷6 present the obtained results from the studies.

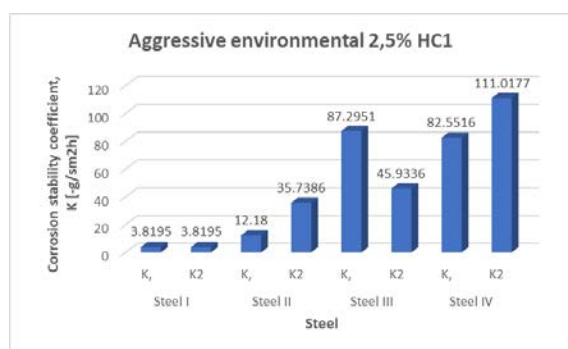


Figure 1 - Dependence of the coefficient of corrosion resistance on an aggressive on an aggressive environment 2,5% HCl

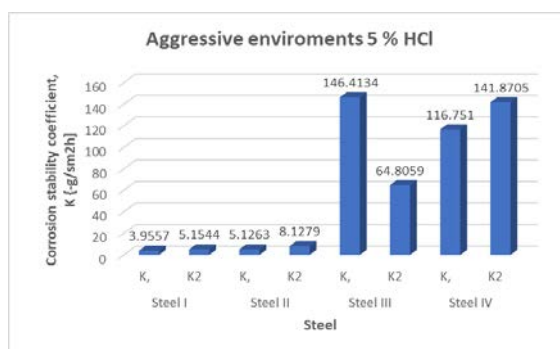


Figure 2 - Dependence of the coefficient of corrosion resistance on an aggressive on an aggressive environment 5% HCl

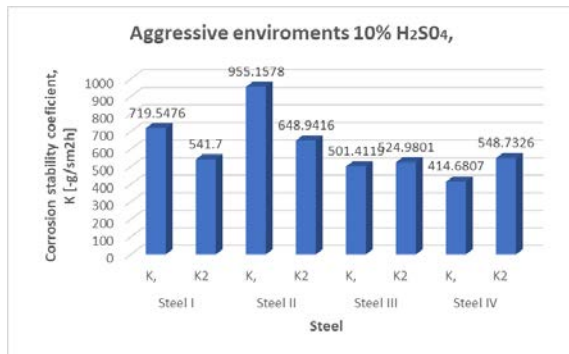


Figure 3 - Dependence of the coefficient of corrosion resistance on an aggressive on an aggressive environment 10% H<sub>2</sub>SO<sub>4</sub>

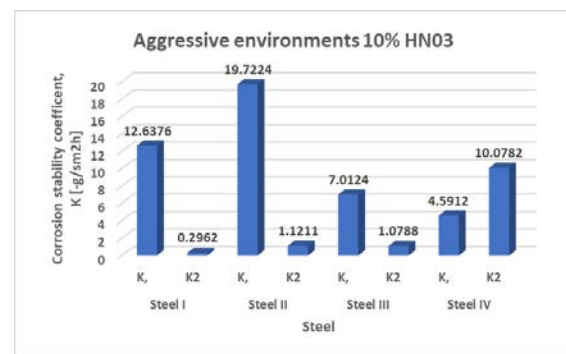


Figure 4 - Dependence of the coefficient of corrosion resistance on an aggressive on an aggressive environment 10% HNO<sub>3</sub>

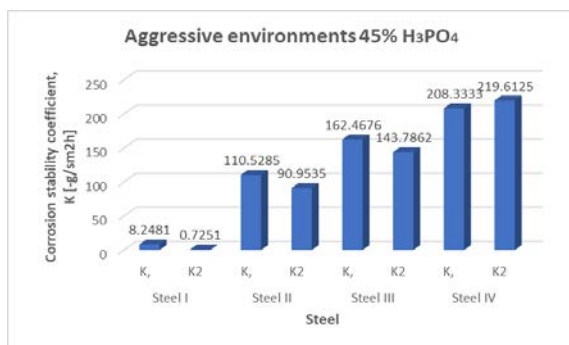


Figure 5 - Dependence of the coefficient of corrosion resistance on an aggressive on an aggressive environment 45% H<sub>3</sub>PO<sub>4</sub>

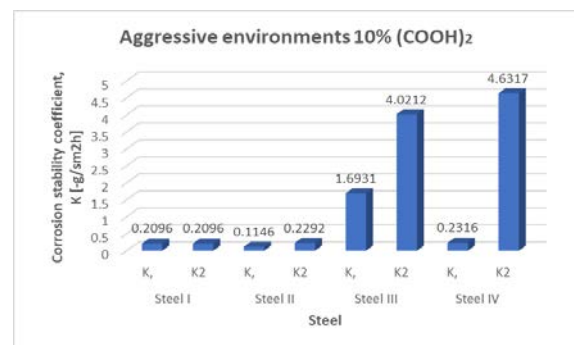


Figure 6 - Dependence of the coefficient of corrosion resistance on an aggressive on an aggressive environment 10% (COOH)<sub>2</sub>

The following conclusion can be made based on the comparative table on corrosion stability coefficient:

- The strongest influence on the corrosion stability coefficient of steel 3X14H2 in all states (found, annealed, hardened/high temperature hardened/low temperature tempered, low temperature tempered) is played by H<sub>2</sub>SO<sub>4</sub> and the weakest one is played by (COOH)<sub>2</sub>.

The comparison graphs on the corrosion stability coefficient of the provisionally labeled Steels of types I, II, II, and IV lead to making the following conclusions:

- The activity of steel 3X14H2 with various structural states (found, annealed, hardened/high temperature, hardened/low temperature) in an aggressive environment of oxalic acid does not greatly impact on the corrosion stability coefficient which means that those details that have been elaborated in steel 3X14H2 can work be employed very successfully in this aggressive environment;
- 45% phosphoric acid, used as aggressive environment for determining the corrosion stability coefficient of the steel 3X14H2 in all researched structural states (found, annealed, hardened/high temperature, hardened/low temperature) has a negative impact on the coefficient of the corrosion stability and an increase of it value can be observed in an increasing order from steel I to steel IV (found → annealed → hardened/high temperature tempered → hardened/low temperature tempered), which means that details of the 3X14H2 steel working under aggressive phosphoric acid environment do not possess high corrosion stability;
- When using 10% nitrogen acid as an aggressive environment to determine the coefficient of corrosion stability of the 3X14H2 steel low values of K<sub>1</sub> and K<sub>2</sub> in the various structural

statuses of the 3X14H2 steel, which leads to the conclusion that the details of the 3X14H2 steel can work well in this environment. The best corrosion stability will be observed with steel 3X14H2 in found and high temperature structure condition. The graphs of the provisionally labeled steels show passive influence of the aggressive environment on the corrosion stability coefficient after the stay of the tested bodies in aggressive environment for a period of 24 hours after the first weight control;

- The influence of the 10% sulfuric acid used for determining the corrosion stability coefficient of the 3X14H2 steel is greatest as compared to the aggressive solutions used which means that the corrosion stability of steel 3X14H2 under the conditions of aggressive environment of sulfuric acid is low, but when compared to other types of steel (unalloyed, low steel alloy) it is still more stable against corrosion. The highest corrosion stability of 3X14H2 steel is to be observed in the aggressive environment of sulfur acid in the condition of hardening and consequent low temperature tempering on the first control for weight loss in 24 hours;
- 5% salt acid used as aggressive environment for the determination of the corrosion stability coefficient of the 3X14H2 steel has a minor impact on the corrosion stability of steel in cast and annealed structural condition, but with tempering followed by high temperature tempering salt acid has a considerably greater impact on the corrosion stability coefficient of the 3X14H2 steel, which means that the details of the 3X14H2 steel will be considerably more resistant working in this environment especially in cast and annealed status;
- 2,5% salt acid used as aggressive environment for the determination of the corrosion stability coefficient of the 3X14H2 steel has a minor impact on the corrosion stability of steel in cast and annealed structural condition during the first loss of weigh control, then the values of the corrosion stability coefficient increase for the remaining structural states, yet the 3X14H2 steel details have satisfactory corrosion stability when employed in such aggressive environment.

#### 4. CONCLUSION

As a conclusion, it can be stated that the resulting corrosion stability coefficients are satisfactory and on the basis of the conclusions we could sum up that the steel 3X14H details shall be capable of working in chemical (aggressive) environments with satisfactory corrosion stability.

#### REFERENCES

- [1] F. Himushin, Nerajdaveiushtie kislotoupornie i jaroprochnie stali, Metalurgizdat, 1945.
- [2] F. Himushin, Nerajdaveiushtie stali, Metalurgizdat, 1963.
- [3] A. Babakov, Nerajdaveiushtie stali, svoistva i himicheskaia stoikost v razlichnih agresivnih sredah, Goshimizdat, 1956.
- [4] Thielsh. Welding Journ., 30, 1951.
- [5] S. Watkins, Metal Progress, 39, 1941, 710 – 714.
- [6] M. Krasteva, R. Petkov, Research on the corrosion stability of steel 3X14H2. 3rd Science Poster Session, UCTM, 19 may, 2006, Sofia, Bulgaria.

## EFFECT OF CASTING SPEED ON TENSILE STRENGTH, ELONGATION AND MICROSTRUCTURE OF CONTINUOUS CAST COPPER WIRE

Srba Mladenović<sup>1</sup>, Bojan Novaković<sup>2</sup>, Ivana Marković<sup>1</sup>, Uroš Stamenković<sup>1</sup>

<sup>1</sup>Technical Faculty Bor, University of Belgrade, V.J. 12, 19210 Bor, Serbia

<sup>2</sup>Metalurg DOO, Pećka bb, 18400 Prokuplje, Serbia

### Abstract

*The present work presents the characterization of oxygen-free copper wire and examines the influence of the casting parameters on its properties. It was found that these parameters could improve the mechanical properties of samples. Also, this investigation showed that there are plenty of possibilities for improving the quality of cast wire cast by UPWARD continuous casting technology..*

**Keywords:** Continuous casting, copper, wire, properties

### 1. INTRODUCTION

The continuous casting technology has been intensively used from the middle of the 20th century, when big volumes of standardized products have to be produced. The main advantages of this technology are: energy saving, mass and a continuous quality production, decreased production costs, simplified production scheduling, more compact production lines.

There is a different variants of this technology regarding mould type, arrangement of mould and furnace, as well as drawing direction. Today, we have a wide variety of mould systems. Special types of casting procedures have been developed, such as the low head casting (LHC) and the electromagnetic casting (EMC) [1,2]. Nonferrous metals and alloys, are often continuous cast using vertical (upward or downward) or horizontal processes to produce round billets for subsequent extrusion, forging or wire drawing.

In 1998 Rautomead introduced an upwards vertical casting process to produce 8mm dia. oxygen-free copper rod (C10200) directly from Grade A copper cathode feedstock (Cu-CATH-1) using a single electrically-heated graphite crucible furnace. This was a novel process when first introduced in the senses that it produced an oxygen-free copper wire rod cast directly at 8mm [3,4].

The aim of this paper is to investigate the impact of the casting parameters on mechanical properties of copper wire casted by Rautomead UPWARD continuous casting technology.

### 2. EXPERIMENTAL

All the measurements and metallographic analysis was performed on samples of Cu-OF copper wire rod obtained by continuous casting. The samples were taken from wire rod obtained on a RS 2200 machine for continuous casting. The machine is basically a single electrically-heated graphite crucible furnace. The graphite crucible is large enough to permit whole cathode sheets to be fed into the melt chamber and to accommodate two separate chambers linked by a submerged bottom transfer port. Rod withdrawal is vertically upwards through water-cooled graphite dies immersed in the liquid copper. The whole rod withdrawal carriage is arranged to move up and down and to maintain a constant immersion depth of the casting dies. On figure 1. the schematic presentation of the machine is presented.

The technical parameters of the machine such as withdrawal temperatures, cooling water temperature at the inlet of the coolers, inlet pressure of the cooling water, outlet pressure were the same trough out the process. Also, the operating parameters of the furnace: temperature, pressure



of shielding gas nitrogen at the inlet, nitrogen pressure in the furnace space and nitrogen flow were constant and have same impact on the final results.

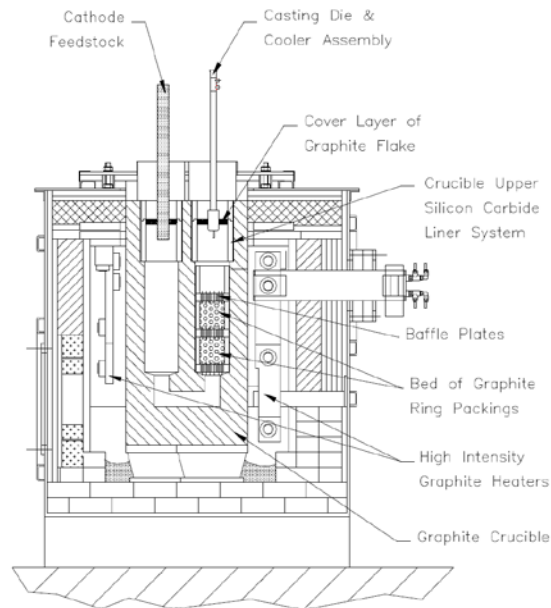


Figure 1 - Section Through Model RS2200 Upwards Vertical Continuous Casting Machine

The main casting parameters that have the influence on microstructure and consequently mechanical properties are:

- Cooling water flow rate.
- Casting speed.
- Pull distance.
- Melt temperature.
- Withdrawal system.
- Continuous casting direction.
- Super cooler size.
- Casting die materials.

In this paper the effect of casting speed was examined. The values of all others parameters are maintained constant during the investigation.

The samples for mechanical testing and for metallographic analysis were prepared according the appropriate standards.

Tensile test was performed on the universal Carl Frank Germany, model 81221 machine where the tensile strength (MPa) of the material as well as ductility in terms of elongation percentage of the copper samples were determined. Samples for microstructural observations were cut with a clean sharp hacksaw. After the sample is sectioned to a convenient size, samples were then ground by using coarse abrasive paper (Grade No. 120) and subsequently 250, 360, 500, 800, 1200, 1500, 2000. Then, the samples were polished on a cloth with a diamond suspension and lubricating solution. In the chemical etching process, nitric acid and distilled water were used. The microstructures were imaged on a Carl Zeiss Jena Epytip 2 metallographic microscope.

### 3. RESULTS AND DISCUSSION

In table 1. the representative copper samples gated by specific casting speed which were analyzed are presented.

Table 1 - OFCu samples tested in this research.

Samples	Rod dia. (mm)	Met. temp (°C)	Water flow rate (l/min.)	Water tem. inlet (°C)	Water tem. outlet (°C)	Casting speed (kg/h)
1.1	12,7	1185	33	32	41,2	100
1.2	12,7	1185	33	32	38,8	80
1.3	12,7	1185	33	32	36,5	60
1.4	12,7	1185	33	32	34,7	40
1.5	12,7	1185	33	32	32,8	20

In this research the casting speed is presented as physical measurement of the as cast rod over the specify time e.g kg/h. Investigation has been performed with five different casting speeds. The results of the mechanical investigations are presented in table 2. and on figure 3. the structure of grains for different samples is presented.

Table 2 - Tensile strength and average elongation percentage

Samples	Rod dia. (mm)	Met. temp (°C)	Water flow rate (l/min.)	Water tem. inlet (°C)	Water tem. outlet (°C)	Casting speed (kg/h)	Ten. st.. N/mm <sup>2</sup>	Aveage elon. %
1.1	12,7	1185	33	32	41,2	100	184,3	42,5
1.2	12,7	1185	33	32	38,8	80	188,2	42,0
1.3	12,7	1185	33	32	36,5	60	191,2	39,5
1.4	12,7	1185	33	32	34,7	40	196,4	38,0
1.5	12,7	1185	33	32	32,8	20	150,8	27,5

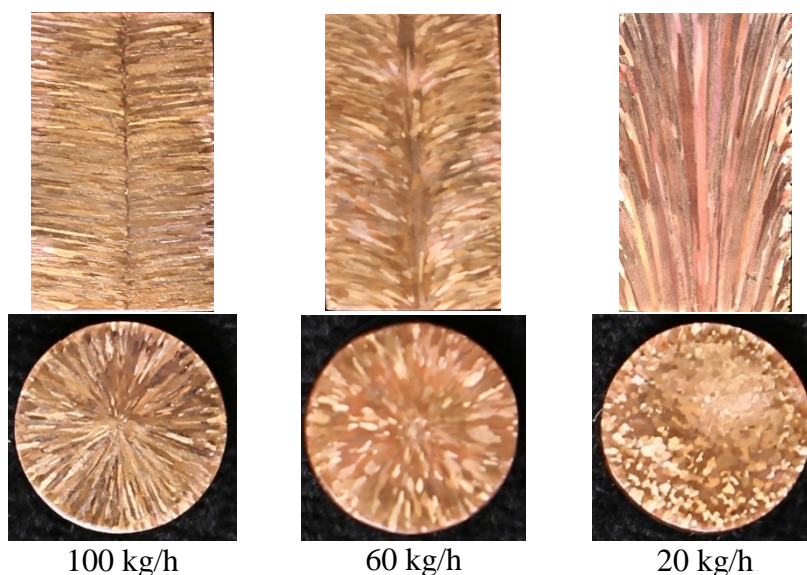


Figure 3 - Grain structure of samples (cross and longitudinal section)

The reason for this improvement of specified mechanical properties is because the casting speed affects the structure formation during solidification. This parameter actually has effect on the cooling condition, which results in making it possible to obtain a structure with finer grains. Figure 3 shows cross and longitudinal sections of continuously cast rods at three different casting speeds. For all samples, except for sample 1.5, an increase in tensile strength was observed with a decrease of casting speed. It was also found that the casting speed could improve the elongation of samples

from 27,5% to 42,5%. The change in tensile strength and elongation with the change in cast speed are shown in figure 4.

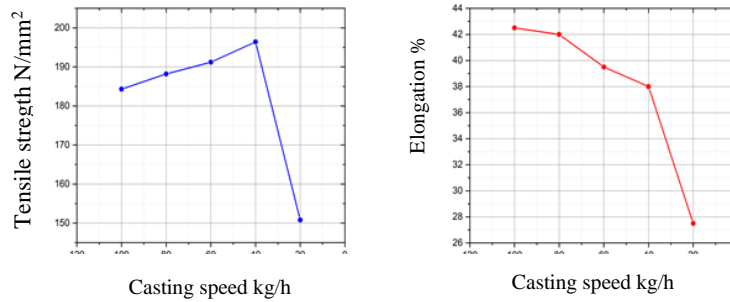


Figure 4 - Tensile strength and elongation percentage of the samples

With maximum casting speeds, the high-temperature liquid metal enters the low-temperature zone at high speed. During the standstill, at the contact of the liquid metal and the inner walls of the graphite mould matrix, a large number of crystallization centers are simultaneously created on the entire contact surface. Most of the heat is dissipated through the walls of the graphite mold. The crystals grow simultaneously parallel to each other and normal to the longitudinal axis, i.e. normal to the casting direction. A very small part of the heat is additionally removed via the already formed wire, which causes a very slight slope of the orientation of the crystal downwards, towards the liquid metal (sample 1.1.). By reducing the casting speed, there are changes in the direction of heat dissipation. The amount of heat that is removed through the walls of the graphite mold decreases, and the heat removal through the hardened copper in the casting direction increases. This causes an even greater change in the angle of inclination and direction of crystal growth (sample 1.3). Most of the heat is dissipated through the wire in the direction of casting, which causes crystal growth parallel to the longitudinal axis of the wire and in the direction opposite to the direction of casting. The picture in Figure 5. illustrates, very nicely, the process of heat dissipation in a concrete case.

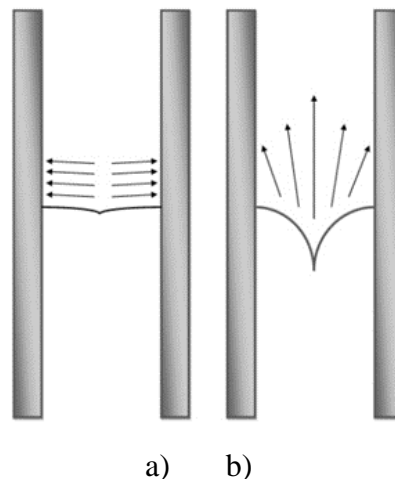


Figure 5 - The scheme of heat dissipation, a) max. cast speed, b) min. cast speed

Also, with an increasing of the casting speed, the grain structure tends to become finer. Smaller grains have greater ratios of surface area to volume, which means a bigger ratio of grain boundaries, which presents a more obstacles for dislocations. The more grain boundaries that occur, the higher the strength of the copper rod samples.

#### 4. CONCLUSION

The effect of casting speed, on the mechanical properties of continuous cast copper wire were investigated. Some important conclusions can be drawn:

- We can influence the quality of the wire with casting speed change.
- With casting speed change the direction of heat dissipation also change.
- The greater casting speed brings more cristalization centers formation, grains are smaller and their orientation are normal to the casting direction. That brings to the increasing of the elongation.
- By reducing the speed, it is possible to obtain a structure with larger crystals whose orientation is parallel to the longitudinal axis of the cast wire, which leads to an increase in tensile strength.

#### REFERENCES

- [1] Antrekowitsch, H., B. Prillhofer. Stranggießen von Aluminium. In: Handbuch Urformen. Ed. by A. Bührig-Polaczek, W. Michaeli, G. Spur. Munich: Carl Hanser Verlag, (2013), 341–347
- [2] Wagstaff, R. B., K. D. Bowles. Practical low head casting (LHC) mold for aluminium ingot casting. In: Light Metals, (1995), 1071–1075
- [3] Wilson, R., A Practical Approach to Continuous Casting of Copper Alloys and Precious Metals, Inst. of Materials, London, (1999), 1-300
- [4] Tyler, D.E., “Copper Continuous Casting”, in Cast Metals, ASM Handbook, (2008), 1019-25

## DEPENDENCE OF COMPRESSIVE STRENGTH OF GEOPOLYMER BASED ON FLY ASH AND ALKALINE ACTIVATOR RATIO

Nadira Bušatlić, Ilhan Bušatlić, Dženana Smajić-Terzić

Faculty of Engineering and Natural Sciences, University in Zenica, Travnička cesta 1, 72 000  
Zenica, Bosnia and Herzegovina

### Abstract

*In this paper, geopolymer samples based on fly ash from the Stanari thermal power plant were tested. Fly ash from the Stanari thermal power plant, 12M NaOH solution and commercial water glass were used as materials. The samples were made with an alkali to fly ash ratio of 1. The  $\text{Na}_2\text{SiO}_3/\text{NaOH}$  ratio ranged from 2; 2.5 and 3. The samples were thermally treated at geopolymerization temperatures of 60, 70 and 80 °C. After that, the compressive strengths of the samples were tested after 2, 7 and 28 days.*

**Keywords:** *geopolymers, environmental pollution, industrial waste, compressive strength, cement*

### 1. INTRODUCTION

In the field of construction, cement is the main ingredient for the production of concrete. However, cement production requires large amounts of raw material. During the production of cement, the burning of limestone causes the emission of carbon dioxide into the atmosphere. There are two sources of carbon dioxide emissions from cement production: the burning of fossil fuels to run the rotary kiln is the largest source, and the other is the chemical process of burning limestone. During the production of 1 ton of cement, approximately 1 ton of CO<sub>2</sub> is emitted into the atmosphere. If we consider that the world production of cement is about 4.18 billion tons, then it can be seen that during the production of cement, the same amount of CO<sub>2</sub> is released into the atmosphere. Of the total global annual CO<sub>2</sub> emissions, 5% is due to cement production. [1,4]

During the last 20 years, geopolymers, which are also known as mineral polymers or inorganic polymers, have attracted a lot of attention as a promising new form of inorganic polymer material that could be used as a replacement for conventional or ordinary Portland cement (OPC), for plastics, and many other mineral-based products. The development of geopolymer cement is an important step towards the production of environmentally friendly cements. [4]

#### 1.1 Materials and methods

The raw materials for preparation of geopolymer can be any natural or unnatural (waste) materials with high content of silicon and aluminum. As natural raw materials most commonly used are different types of clay, and from unnatural raw materials are used fly ash, blast furnace slag and their combinations.

An important role in the geopolymerization process has a raw component that is an activator of the process. Such a raw material component has been called the "alkaline activator" since the reaction takes place in a highly alkaline medium. Various combinations of alkaline solutions can be used.

Palomo et al. (1999) concluded that the type of activator plays an important role in the polymerization process. The reactions take place at a high speed when the alkaline activator contains soluble silicates, either sodium or potassium silicate, compared to the use of only alkaline hydroxides. [3,2,4]

Tempest et al. (2009) state that the sodium silicate activator dissolves rapidly and begins to bond particles of fly ash. Pores are quickly filled with gel as soon as the liquid phase succeeds in reaching ash particles. The liquid phase is important as a fluid transport medium that allows the activator to reach the fly ash particles and reacts with them. [3,2,4]

## 2. EXPERIMENTAL

In this paper, geopolymer samples based on fly ash from the Stanari thermal power plant were tested. Fly ash from the Stanari thermal power plant, 12M NaOH solution and commercial water glass were used as materials. The samples were made with an alkali to fly ash ratio of 1. The Na<sub>2</sub>SiO<sub>3</sub>/NaOH ratio ranged from 2; 2.5 and 3. The samples were thermally treated at geopolymerization temperatures of 60, 70 and 80 °C. After that, the compressive strengths of the samples were tested after 2, 7 and 28 days.

The chemical analysis of the fly ash TPP Stanari is shown in Table 1, and its granulometric composition is shown in Figure 1.

Table 1 - Chemical composition of fly ash from TPP Stanari, B&H[2,4]

Component	SiO <sub>2</sub>	Al <sub>2</sub> O <sub>3</sub>	Fe <sub>2</sub> O <sub>3</sub>	CaO	MgO	MnO	Na <sub>2</sub> O	K <sub>2</sub> O	CO <sub>2</sub>	SO <sub>3</sub>	LOI
Content(%)	48,38	23,49	7,51	11,48	2,76	0,117	0,69	1,79	0,09	2,15	1,543

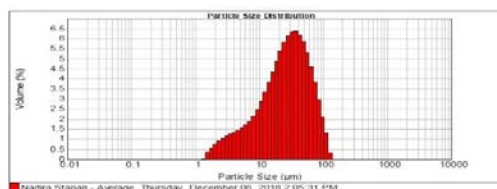


Figure 1 - Granulometric composition of fly ash[2,4]

From Figure 1 it can be seen that particles of fly ash range from 1 to 100 microns. The most of particles is about 50 microns in size. [2,4]

12 M NaOH solution was made in the Laboratory for Analytical Chemistry of the Metallurgical and Technology Faculty in Zenica.

Commercially water glass are used in the examination whose characteristics are shown in Table 2.

Table 2 - Characteristics of commercially water glass

Characteristics	SiO <sub>2</sub> (%)	Na <sub>2</sub> O(%)	Al <sub>2</sub> O <sub>3</sub> + Fe <sub>2</sub> O <sub>3</sub> (%)	Fe (%)	Density (g/cm <sup>3</sup> )	Insoluble substances in water	Module (SiO <sub>2</sub> / Na <sub>2</sub> O)
Values	25,0– 27,5	11,5– 12,5	Max 0,3	Max 0,02	1,40– 1,45	Max 0,15	2,0–2,4

For the preparation of the samples, the ratio AA / FA = 1 was used, while the Na<sub>2</sub>SiO<sub>3</sub>/NaOH ratio was 2; 2,5 and 3. Mixing ratios and designations of fly ash-based geopolymer samples are shown in the table 3. The samples were manually blended and vibrated on a vibrating table for 10 minutes. The binding process is exothermic so the samples must be hermetically closed. After 24 h, the samples were taken out of the mold and wrapped in nylon bags, as shown in Figure 2. The wrapped samples were kept in the oven for 24 hours at activation temperatures of 60, 70 and 80 °C.



Table 3 - Mixing ratios and designations of fly ash-based geopolymer samples

Uzorak	A/FA	VS/NaOH
A	1	2.0
B		2.5
C		3.0



Figure 2 - Prepared of samples[2,4]

### 3. RESULTS AND DISCUSSION

After temperature activation, the samples were taken out from the bags and kept at room temperature. The compressive strength of the samples was tested after 2, 7 and 28 days after thermally treated. The results of the compressive strength are shown in Table 4, and in Figure 3.

Table 4. Compressive strength of the tested samples

Samples	Compressive strength (MPa)		
	2 days	7 days	28 days
A60	19.95	25.45	27.2
A70	22.17	32.1	32.2
A80	22.0	26.69	35.3
B60	24.95	23.5	28.0
B70	24.85	25.3	29.3
B80	33.35	33.75	35.5
C60	19.73	30.25	37.8
C70	25.6	29.05	33.9
C80	22.45	25.75	32.05

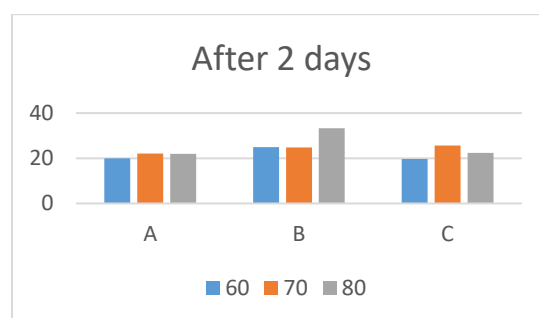


Figure 3 - Dependence of compressive strength after 2 days on temperature and  $\text{Na}_2\text{SiO}_3/\text{NaOH}$  ratio

Figure 3 shows the dependence of the compressive strength after 2 days on the heat treatment temperature and the  $\text{Na}_2\text{SiO}_3/\text{NaOH}$  ratio. It can be seen from the figure that the compressive strength of the samples treated at a temperature of 70°C increases slightly with an increase in the  $\text{Na}_2\text{SiO}_3/\text{NaOH}$  ratio. The compressive strength value after 2 days of 33.35 MPa has a sample treated at a temperature of 80 °C with a ratio of  $\text{Na}_2\text{SiO}_3/\text{NaOH} = 2,5$ .

According to the EN 197-1 standard, the compressive strength of cement after 2 days must be greater than or equal to 10 MPa for cement classes 32.5R and 42.5N, greater than or equal to 20 MPa for cement classes 42.5R and 52.5N and greater than or equal to 30 MPa for cement class 52.5R.

Figure 4 shows the dependence of compressive strength after 7 days on temperature and  $\text{Na}_2\text{SiO}_3/\text{NaOH}$  ratio.

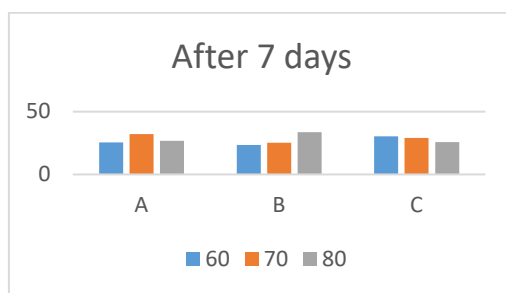


Figure 4 - Dependence of compressive strength after 7 days on temperature and  $\text{Na}_2\text{SiO}_3/\text{NaOH}$  ratio

From Figure 4, it can be seen that the compressive strength after 7 days is the highest in samples with a ratio of  $\text{Na}_2\text{SiO}_3/\text{NaOH} = 2,5$  at temperatures of 80 °C. Samples with  $\text{Na}_2\text{SiO}_3/\text{NaOH} = 2,5$  do not change the compressive strength value after 7 days.

Figure 5 shows the dependence of compressive strength after 28 days on temperature and  $\text{Na}_2\text{SiO}_3/\text{NaOH}$  ratio.

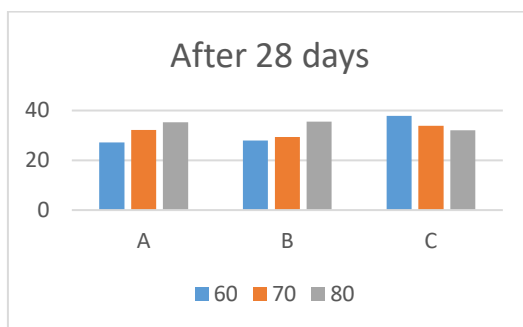


Figure 5 - Dependence of compressive strength after 28 days on temperature and  $\text{Na}_2\text{SiO}_3/\text{NaOH}$  ratio

Figure 5 shows that the compressive strength after 28 days of samples treated at a temperature of 80 °C and at a ratio of  $\text{Na}_2\text{SiO}_3/\text{NaOH} = 2,5$  increases to 35,5 MPa. Also, the compressive strength after 28 days for samples treated at a temperature of 60 °C and at a ratio of  $\text{Na}_2\text{SiO}_3/\text{NaOH} = 3$  increases to 37.7 MPa.

If we compare the compressive strength of the obtained geopolymers and the compressive strength of cement according to EN 197-1, geopolymers prepared with fly ash of the Stanari thermal power plant with a ratio of alkali and fly ash of 1, treated at a temperature of 80 °C with ratios of  $\text{Na}_2\text{SiO}_3/\text{NaOH}$  2.5 would correspond to cement class 32.5N and 32.5R.

## REFERENCES

- [1] Ilhan Bušatlić, Nadira Bušatlić, Cementne sirovine u Bosni i Hercegovini, Štamparija Fojnica d.d. Fojnica, 2018.
- [2] Ilhan Bušatlić, Nadira Bušatlić, THE POSSIBILITY OF USING THE FLY ASH FROM THERMAL POWER PLANT “STANARI” DOBOJ IN THE DEVELOPMENT OF GEOPOLYMERS, XIII International Mineral Processing and Recycling Conference, Belgrade, Serbia, May 2019., pp 141-148.
- [3] M. M. A. Abdullah, K. Hussin, M. Bnhussain, K. N. Ismail, W. M. Ibrahim, IJPAST, 2011.
- [4] N. Bušatlić, I. Bušatlić, Dž. Smajić-Terzić, Geopolymers Based On Fly Ash From The Stanari Thermal Power Plant, 5<sup>th</sup> Metallurgical & Materials Engineering Congress of South-East Europe 2023 – Trebinje, BIH, 2023.

## HYDROCARBON POTENTIAL OF LOWER PALEOZOIC SEDIMENTS IN NE BULGARIA BY GEOCHEMISTRY AND WELL-LOGGING

**Gergana Meracheva, Efrosima Zaneva-Dobranova, Nikolay Hristov,**

University of Mining and Geology “St. Ivan Rilski”, 1700 Sofia, Bulgaria

### **Abstract**

*In NE Bulgaria Lower Paleozoic marine sediments are of interest not only as a source rock but also as a potential unconventional oil and gas reservoir. Several deep wells reached this succession, a small interval was drilled by coring, while most of the section was covered only by logging. Therefore, the knowledge of major parameters of these rocks is obscure. For this reason, in the current study geophysical and geochemical data was integrated to characterize the hydrocarbon (HC) potential of this succession. A main parameter for evaluating the potential of a source rock is total organic carbon (TOC), which in the studied samples varies between 0.5% to 2.61%. This defines the rocks with fair to good potential. The applied method of well-logging allows to identify vertical and lateral distribution of organic matter (OM). A good correlation was observed between the TOC data yielded from the geochemical tests and the well-log calculations. The type of OM and the degree of maturity show mainly gas potential. The combination of the methods allows more detailed and wide-ranging assessment of Lower Paleozoic rocks, and the data received could change the fossil fuels exploration and production strategy.*

**Keywords:** Lower Paleozoic shales, TOC, well-logging

### **1. INTRODUCTION**

The decreasing of HC reserves from the main deposits at accessible depths and territories, as well as still huge dependence on these energy raw materials, cause an increase in interest towards unconventional HC sources of energy. In the last decade in Central and Eastern Europe actively studying the Lower Paleozoic and more specifically the Silurian sediments regarding their potential as unconventional shale reservoirs had been realized [1]. As a result, a sketchy paleogeographic model of the Silurian Basin was created, which shows that basin is scattered along the broad zone trending through Europe with a NW-SE direction. A large part of the Silurian basin of Central and Eastern Europe is located on the Moesian Platform, somewhat isolated from the other basin fragments presently. The distribution of Lower Paleozoic sediments in NE Bulgaria can be concluded from the several wells that have reached these rocks. The section consists of marine sediments – mudstones, dark grey and light grey shales and siltstones with Ordovician age; dark shales, mudstones and siltstones with minor limestones and marls with Silurian–Lower Devonian age, which are up to 2000 m thick. A small interval was drilled by coring, while most of the section was covered only by well-logging. For that reason, the current study combines geophysical and geochemical data approach to characterize the HC potential of the succession. Based on studies on shale gas petroleum plays globally, it was specified that there are several minimal conditions, which should be fulfilled to assess the oil and gas potential of shale sediments [2] - TOC, type, maturity etc. In this research, two different techniques, included geochemical data and geophysical well-logging are integrated to determine TOC content. Next, the comparison of the results allows to evaluate the HC potential of the shales and mudstones in entire examined Lower-Paleozoic succession.

## 2. EXPERIMENTAL

An integrated multidisciplinary approach is needed for an optimal HC potential analysis since in practice data availability (cores, logs, seismic data, geochemistry, geological studies) is limited. One of the key properties for determining the HC potential of shale sediments is TOC content. This parameter is traditionally obtained by laboratory test of core, cuttings and sidewall plugs. This method is relatively effective and accurate; however, it provides non-continuous measurements data only of some parts of the sediment section. Furthermore, it is also costly and time-consuming. To overcome these limitations, different continuous well-logging data can be utilized to estimate TOC along the entire geological section [3,4]. The well-logs used for source rock evaluations and calculation of TOC most commonly include density, sonic, gamma ray, neutron and resistivity by using several methods.

### 2.1 Geochemical analysis

The samples were tested using a model Rock-Eval 6 instrument [5] equipped with the necessary modules to perform the full volume of studies to evaluate the source rock HC potential by pyrolysis. In this study, by using the flame ionization detector (FID), the following set of parameters was measured and subsequently determined:  $S_1$  (thermal distilled free HCs);  $S_2$  (HCs produced by kerogen cracking);  $S_3$  ( $CO_2$  released during the initial phase of the analysis);  $T_{max}$  (temperature of maximum formation of HCs corresponding to maximum  $S_2$ ). With the data obtained from this parameter, the degree of maturity of kerogen in the studied samples was determined. Other diagnostic ratios such as petroleum potential (PP), production index (PI), hydrogen index (HI) and oxygen index (OI) are calculated from the parameters  $S_1$ ,  $S_2$  and  $S_3$ .

### 2.2 Well-log analysis

Identifying source rock is based on the responses of different conventional logs such as gamma-ray, density, resistivity and sonic logs. The physical properties of gamma-ray, sonic, neutron and resistivity logs read high values, while density log reduces. In this study, the method proposed by [3], named  $\Delta\log R$ , is used. It has been observed [3] that a linear relationship exists between  $\Delta\log R$  and TOC content, which is also a function of level of organic maturity (LOM). Hence, using quantified log separation  $\Delta\log R$ , the TOC is calculated by the following equation:

$$TOC = \Delta\log R \log \times 10^{[2,297 - (0.1688 \times LOM)]} \quad (1)$$

When there are scarce sonic log data available, the application of this method, as regards estimation of the distribution of OM in Silurian mudstones and shales, is rather limited. Whereas, some wells were subject to gamma-ray logging, which is suggested [4] as an efficient tool in calculating distribution of OM. In the current study, for the calculation of TOC content from gamma-ray logs, the equation developed by [4] for shales from SE part of Silurian basin is also used. The equation was derived from gamma-ray log data and TOC measurements from several representative wells of the same sediment succession, which unraveled close correlation and can be described by the following equation:

$$TOC = \exp(0,15 \times GR) \times 0,12 \quad (2)$$

## 3. RESULTS AND DISCUSSION

Comparison of TOC and well-log data in gamma-ray, acoustic, density and resistivity logs of the Late Ordovician-Silurian-Early Devonian interval shows good correlation (Figure 1a). It indicates that these curves, especially gamma-ray, can be used for the vertical TOC distribution patterns. This correlation presents a typical response of organic-rich shales in wireline logs according reference values for source rock identification [3], which shows that the 150 API cut-off value chosen to define source potential mudstones and shales in this contribution corresponds to TOC

values of above 1%. The data yielded when measuring TOC from geochemical studies is correlated to the calculated TOC from the logs and the results show a good correlation with a correlation coefficient +0.84 (Figure 1b). The content of TOC in some of the studied samples of well core is over 0.5%, and in one of them the amount reaches 2.61%, which according to the accepted classifications [6] can be considered the rock as a very good source (Figure 1c). The plot of TOC vs. PP reveals that there are data points of the studied samples, which shows TOC content and HC potential indicating fair to good source rocks, this is also as indicated by the calculated from well-logs TOC content.

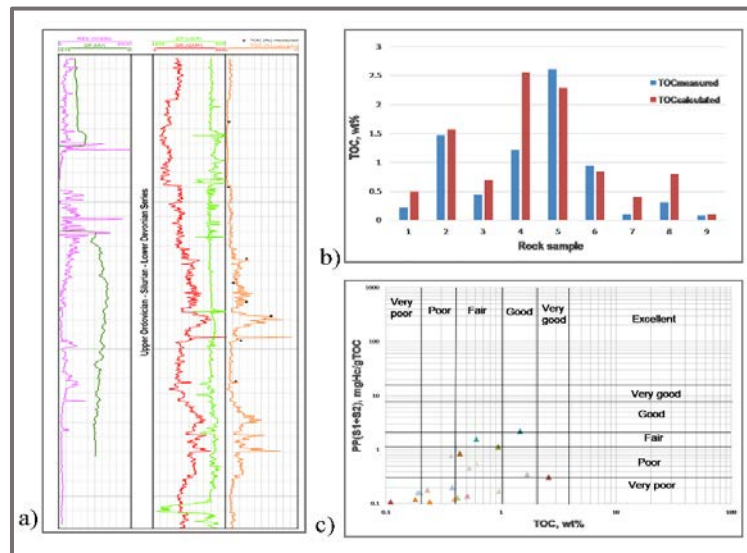


Figure 1 - a) Correlation between well-log curves and TOC estimation by logs (TOC calculated) calibrated by laboratory data (TOC measured); b) Histogram diagram between TOC measured and TOC calculated; c) Diagram presenting HC generation potential

The Rock-Eval pyrolysis data represented by HI vs. OI on the modified Van Krevelen diagram is used to define the main kerogen types based on the atomic ratios between carbon (C), hydrogen (H) and oxygen (O). It can be assumed that in a large part of studied rock intervals, the kerogen is type III, and in the remaining samples it is type II (Figure 2a). The diagram expresses the ration TOC vs. HI (Figure 2b) shows the expected generated HCs from the studied samples as mixed gas and oil, a part of the examined samples shows undefined gas source generation potential, and a few samples are in the zone of fair oil source. Measured  $T_{max}$  from Rock-Eval pyrolysis shows that most of the studied samples are in the immature to mature stage of maturity, but the maturity does not correlate with increasing depth. This is confirmed by the plot of  $T_{max}$  vs. depth (Figure 2c). The plot of  $T_{max}$  vs. HI indicates that the kerogen type of the studied samples in sediments with Late Ordovician-Silurian-Early Devonian ages is type III, which mainly produces gas in case of maturation (Figure 2d).

#### 4. CONCLUSIONS

The applied survey, which combines geophysical and geochemical method for characterization of pelitic sediments with Late Ordovician-Silurian-Early Devonian ages and assessment of their HC potential lead to the following conclusions:

- The comparison between the TOC values measured in geochemical laboratory and those calculated from the well-logs show a good matching between the two types of data;
- The geochemical evaluation of the analyzed samples indicates that the content of TOC is moderate, with the highest values in Silurian mudstones and shales;

- The Lower Paleozoic succession could be characterized by fair to good organic richness, with poor to fair HC potential;
- The OM of the analyzed succession is characterized predominantly by kerogen type III and mixed type II/III in some intervals;
- According to the obtained results, OM is immature to mature in the studied sediments with the capability to expel both oil and some gas HC in case of maturation.

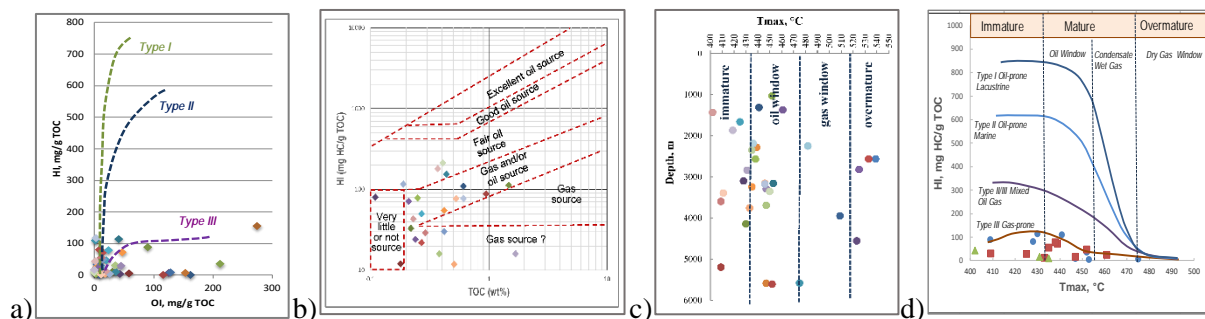


Figure 2. - Diagrams showing a) kerogen type on modified Van Krevelen diagram; b) expected HCs and HC-generation potential; c) relation between thermal maturity ( $T_{max}$ ) and depth of the sample; and d) relation between thermal maturity ( $T_{max}$ ) and HI

The conclusions from the obtained results in this research is made on base of geochemical and geophysical data from a few wells and consideration must be given to the fact that many other factors may affect the correlation. At the same time if the calculated and measured TOC is good correlated in some intervals, then source rock evaluation of such intervals is useful for further analysis and researches. Thus, the integration of the geochemical data with the geophysical survey in the wells, which has been applied in the current research, would significantly be useful to improve the approach of assessing the potential of shale intervals with Early Paleozoic age in NE Bulgaria. The implemented geological, geophysical and geochemical study can be considered as an element for the assessment of the HC potential of shale succession as a source of fossil fuels.

## ACKNOWLEDGEMENTS

*This research is supported by the Bulgarian Ministry of Education and Science under the National Program “Young Scientists and Postdoctoral Students – 2”.*

## REFERENCES

- [1] Tari, G., Poprawa, P., and Krzywiec, P. Silurian Lithofacies and Paleogeography in Central and Eastern Europe: Implications for Shale Gas Exploration. SPE 151606, SPE/EAGE European Unconventional Resources Conference and Exhibition, Vienna (2012) 20-22.
- [2] Zou, C. Unconventional Petroleum Geology, 2nd edition. Elsevier (2017) p. 500.
- [3] Passey, Q. R., Moretti, F. J., Kulla, J. B., Creaney, S., Stroud, J. D. AAPG Bulletin, 74 (12), (1990) 1777–1794.
- [4] Šliaupa, S., Šliaupienė, R., Žaludienė, G., Vaskaboinikava, T., Bibikava, A., Evstratenko, L., Kovkhuto, A. Oil Shale, 33 (4) 2016 357–372, doi: 10.3176/oil.2016.4.04.
- [5] Espitalié, J, G. Deroo, F. Marquis. Revue de L’Institut Francais du petrole 40 (563-579). (1985) 755 – 784
- [6] Peters, K.E. and Cassa, M.R. Applied Source-Rock Geochemistry. In: Magoon, L.B. and Dow, W.G., Eds., The Petroleum System. From Source to Trap, American Association of Petroleum Geologists, Tulsa, (1994) 93-120



## LEACHING OF FLOTATION TAILINGS WITH A SOLUTION OF SULFURIC ACID AND IONIC LIQUID

Dragana Marilovic<sup>1</sup>, Grozdanka Bogdanovic<sup>1</sup>, Sanja Petrovic<sup>2</sup>

<sup>1</sup>University of Belgrade, Technical Faculty Bor, V.J. 12, 19210 Bor, Serbia

<sup>2</sup>Mining and Metallurgy Institute Bor, Zeleni bulevar 35, 19210 Bor, Serbia

### Abstract

*This paper presents the results of leaching flotation tailings containing 0.13% of copper and 4.22 % of iron. The experiments were carried out in a sulfuric acid solution (H<sub>2</sub>SO<sub>4</sub>) and an ionic liquid solution 1-butyl-3-methyl-imidazolium hydrogen sulfate ([bmim]HSO<sub>4</sub>). Concentrations of the reagents of 0.01 mol/dm<sup>3</sup> and 0.05 mol/dm<sup>3</sup> were tested. When leaching with sulfuric acid, the leaching degree of copper was 71.05% at the lower concentration of solution and 76.59% at the higher concentration of solution. When flotation tailings was leached in an ionic liquid solution with the same concentrations, the leaching degree of copper was 72.57% (for 0.01 mol/dm<sup>3</sup>) and 77.10% (for 0.05 mol/dm<sup>3</sup>), respectively. The results showed that the leaching rate of copper increased in the first 5-10 minutes of the reaction due to the presence of oxide minerals and then slightly increased with time. The dissolution of iron was <3% under the tested conditions. These results indicate that the ionic liquid 1-butyl-3-methyl-imidazolium hydrogen sulfate ([bmim]HSO<sub>4</sub>) can be used as agent for the leaching process of flotation tailings.*

**Keywords:** leaching, flotation tailings, sulfuric acid, ionic liquids.

### 1. INTRODUCTION

Flotation tailings are a common solid waste in mining production. Most often, they are disposed of in tailings ponds that occur in nature. In this way, undesirable reactions of atmospheric precipitation with pyrite occur, resulting in acid mine drainage that are potentially hazardous to the environment [1,2,3].

Technologies for recovering useful components from such raw materials are used to obtain copper, but also other elements such as iron, zinc, aluminum, chromium, silver or gold [1]. The old flotation tailings pond in Bor has accumulated about 26 Mt of solid waste during the 70 years of operation of the RTB Bor plant [2]. Considering that the copper content in the processed ores varied from 4% at the beginning of the plant operation to 0.6% at the end of the old flotation plant, the copper content in the tailings also varied from 0.5 to 0.1% [3]. In this way, the flotation tailings became a potential raw material for copper recycling.

Sulfuric acid is used as one of the most common reagents for leaching copper from flotation tailings [2,6,7,8,9]. During the leaching process, sulfuric acid is consumed due to unwanted reactions with oxides and carbonates of alkaline earth metals [10]. Although other leaching agents are used in addition to sulfuric acid, as well as bacterial leaching with microorganisms [11], new environmentally friendly reagents are still being tested. Recently, ionic liquids have begun to be applied in this field to obtain metal ions. Ionic liquids are considered a new branch of chemical compounds and a suitable alternative for organic and inorganic solvents. Ionic liquids are recognized as green reagents due to their characteristics such as viscosity, thermal stability, negligible volatility, non-toxicity and high conductivity [12].

Research has shown that ionic liquids with the sulfate group HSO<sub>4</sub><sup>-</sup> are most often used for copper leaching from chalcopyrite [13, 14, 15, 16], where the leaching degree is up to 75%, but also from waste PCB boards [12], where the leaching degree is almost 100%.

This paper presents the comparative results of flotation tailings leaching with sulfuric acid and the ionic liquid 1-butyl-3-methyl imidazolium hydrogen sulfate ([bmim]HSO<sub>4</sub>).

## 2. EXPERIMENTAL

Flotation tailings taken from the old flotation tailings pond in Bor was used for the experiments. The chemical composition of the initial sample is shown in Table 1.

Table 1 - Chemical composition of the flotation tailings

Element	Cu	Cu <sub>ox</sub>	Fe	Zn	As <sub>ppm</sub>	Pb	S	SiO <sub>2</sub>	Fe <sub>3</sub> O <sub>4</sub>	MgO	CaO
%	0.13	0.09	4.22	0.01	13.24	0.01	4.70	60.02	0.03	0.48	3.50

All experiments were performed in a 600 cm<sup>3</sup> glass reactor with a magnetic stirrer and adjustable speed. Solutions were prepared with analytical grade chemicals and distilled water. After setting the working parameters, 10 g of raw material was taken and added to 200 ml of a solution of a certain concentration. The stirring speed was 400 rpm. At regular time intervals (5, 10, 15, 30, 60, 90 and 120 minutes) 1 ml of the solution was taken and filtered. The diluted solution was analyzed for copper and iron using a UV-VIS spectrophotometer.

## 3. RESULTS AND DISCUSSION

Figure 1 shows the results of flotation tailings leaching at a concentration of 0.01 mol/dm<sup>3</sup> of sulfuric acid and the ionic liquid [bmim]HSO<sub>4</sub> as reagents.

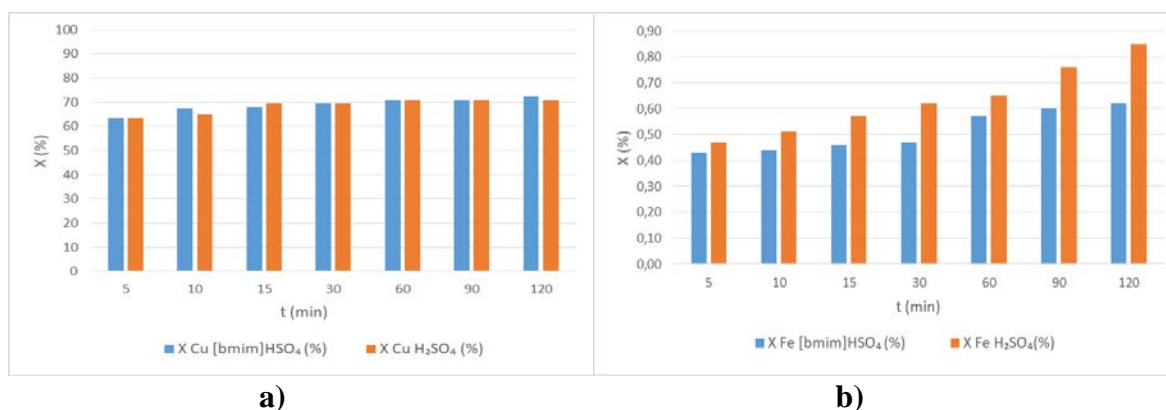


Figure 1 - Leaching degree of copper (a) and iron (b) in 0.01 mol/dm<sup>3</sup> solution of sulfuric acid H<sub>2</sub>SO<sub>4</sub> and 0.01 mol/dm<sup>3</sup> solution of ionic liquid [bmim]HSO<sub>4</sub>

The results show that in the presence of 0.01 mol/dm<sup>3</sup> H<sub>2</sub>SO<sub>4</sub> solution, the leaching degree of copper after 120 minutes was 71.05%, while the leaching of iron was 0.85%. When flotation tailings was leached in [bmim]HSO<sub>4</sub> solution of the same concentration, the copper leaching degree was 72.57%, while the iron leaching degree was lower compared to leaching with a sulfuric acid solution (0.61%).

The leaching degree of copper in the solution of 0.05 mol/dm<sup>3</sup> H<sub>2</sub>SO<sub>4</sub> was 76.59%, while in the solution of 0.05 mol/dm<sup>3</sup> [bmim]HSO<sub>4</sub> it was 77.10% during the leaching time of 120 minutes (Figure 2a). The results obtained clearly demonstrate the rapid leaching kinetics of copper minerals. Approximately 70 % of copper is efficiently leached within the initial 5-10 minutes. This can be attributed to the high presence of copper oxides in the initial sample, which readily undergo leaching. Furthermore, it is evident that under all tested conditions, the dissolution decreases after the initial leaching period.

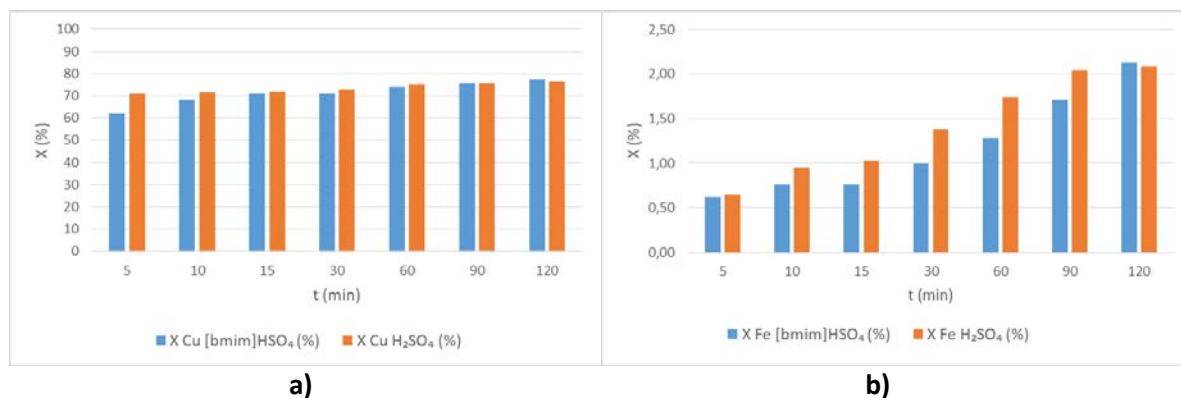


Figure 2 - Leaching degree of copper (a) and iron (b) in 0.05 mol/dm<sup>3</sup> solution of sulfuric acid H<sub>2</sub>SO<sub>4</sub> and 0.05 mol/dm<sup>3</sup> solution of ionic liquid [bmim]HSO<sub>4</sub>

With increasing reagent concentration, the leaching of iron in the sulfuric acid solution was 2.09%, while it was 2.13% in the ionic liquid solution (Figure 2b).

Based on the results, it can be said that [bmim]HSO<sub>4</sub> shows similar behavior as H<sub>2</sub>SO<sub>4</sub> in the leaching of flotation tailings. The dissolution of copper under tested conditions is slightly affected by the concentration of leaching agents, since the difference in the leaching degree at five times higher acid concentration is approximately 5%. However, it can be assumed that a higher concentration of reagents is necessary to enhance the dissolution of copper. It can also be concluded that ionic liquids can replace sulfuric acid as an environmentally friendly reagent and be used in the process of copper leaching from flotation tailings when economically justified.

Similar results were obtained by Carlesi et al. [14]. The authors studied the leaching efficiency of chalcopyrite concentrate with a solution of the ionic liquids [bmim]HSO<sub>4</sub> and [hmim]HSO<sub>4</sub> (1-hexyl-3-methyl imidazolium hydrogen sulphate) and H<sub>2</sub>SO<sub>4</sub> solution at room temperature. The difference in copper concentration in the solution was negligible. Better results were obtained when leaching with [bmim]HSO<sub>4</sub> and [hmim]HSO<sub>4</sub> solutions at a higher temperature (60 °C). This temperature effect may be related to physicochemical properties that affect mass transfer and the rate of chemical reaction. The mechanism of copper dissolution with ionic liquids proposed by authors [17,18] is based on dissociation of hydrogen sulfate anions from the ionic liquid, so that the leaching results are consistent with those obtained when leaching in a sulfuric acid solution.

#### 4. CONCLUSION

In the paper, the leaching of copper and iron in aqueous solutions of sulfuric acid and the ionic liquid [bmim]HSO<sub>4</sub> by the agitation leaching process was studied. Although there is a difference in the copper leaching degree in sulfuric acid solution and in ionic liquid solution, the difference is negligible. At a reagent concentration of 0.01 mol/dm<sup>3</sup>, the copper leaching degree was 71.05 and 72.57% for sulfuric acid and ionic liquid, respectively. At the higher tested concentration of 0.05 mol/dm<sup>3</sup>, the copper leaching degree was 76.59 % for the sulfuric acid solution and 77.10% for the ionic liquid solution. The obtained results suggest that ionic liquids can replace sulfuric acid as an environmentally friendly reagent and can be used in copper leaching from flotation tailings.

#### ACKNOWLEDGMENTS

*The research presented in this paper was done with the financial support of the Ministry of Science, Technological Development and Innovation of the Republic of Serbia, within the funding of the scientific research work at the University of Belgrade, Technical Faculty in Bor, Grant No. 451-*

03-47/2023-01/200131 and Mining and Metallurgy Institute Bor, Grant No. 451-03-47/2023-01/200052.

## REFERENCES

- [1] Guo Z. Q., Pan J., Zhu D. Q., Zhang F., *J. Clean. Prod.*, 2018, 199, 891– 899.
- [2] Jarosikova A., Ettler V., Mihaljevic M., Kribek B., Mapani B., *J. Environ. Manage.*, 2017, 187, 178 – 186.
- [3] Antonijevic M.M., Dimitrijević M.D., Stevanovic Z.O., Serbula.M., Bogdanovic G.D., *J. Hazard. Mater.* 158 (2008) 23–34.
- [4] Taghipour M., Jalali M., *Waste Manag.* 169 (2023) 319–331.
- [5] Stanković V., Milošević V., Milićević D., Gorgievski M., Bogdanović G., (2018), *Chem. Ind. Chem. Eng. Q.* 24 (4) 333–344.
- [6] Z. Mitrović, R. Jovanović, *Seventy Five Years of the RTB Flotation Concentrators*, RTB Bor and Megatrend University, Bor, 2007, 266 (in Serbian).
- [7] Maxim I. Muravyov, Natalya V. Fomchenko, *Miner. Eng.* 122 (2018) 267–276.
- [8] Stevanović Z., PhD Thesis, University of Belgrade, Technical Faculty in Bor, 2012 (in Serbian).
- [9] Stevanović Z., Antonijević M., Bogdanović G., Bugarin M., Trujić V., Marković R., Nedeljković D., *Carpathian J. Earth Environ. Sci.*, 8 (2013) 29.
- [10] Bogdanović G. D., Stanković V. D., Trumić M. S., Antić D. V., Trumić M. Ž., *J. Min. Metal. A*, 52 (1) (2016) 45 – 56.
- [11] Stanković S., Morić I., Pavić A., Vojnović S., Vasiljević B., Cvetković V., *J. Serb. Chem. Soc.*, 80 (3) 391–405 (2015) JSCS–4724.
- [12] Li F., Chen M., 2017, *Environ. Prot. Eng.* 43, 55 – 66.
- [13] Whitehead J.A., J. Zhang, N. Pereira, A. McCluskey, G.A. Lawrance, *Hydrometallurgy* 88 (2007) 109–120.
- [14] Carlesi, C., Cortes, E., Dibernardi, G., Morales, J., Munoz, E., *Hydrometallurgy* 161, (2016) 29 – 33.
- [15] Hu J., Tian G., Zi F, Hu X., *Hydrometallurgy* 169 (2017) 1-8.
- [16] Rodríguez M., Ayala L., Robles P., Sepúlveda R., Torres D., Carrillo-Pedroza F.R., Jeldres R.I., Toro N., *Metals* 10, (2020), 183.
- [17] Whitehead J.A., Lawrence G.A., McCluskey A., *Green Chem.* 6 (7), (2004), 313–315.
- [18] Dong, Y.H.T., Zhang, D.Z.Q., *Hydrometallurgy* 99, (2009), 33–38.

## DETERMINATION OF BOND ROD MILL WORK INDEX OF A VERY LOW-GRADE COPPER ORE

Ivana Jovanović, Vesna Conić, Dragan Milanović, Daniel Kržanović, Tanja Stanković,  
Daniela Urošević, Miloš Janošević

Mining and Metallurgy Institute Bor, Zeleni bulevar 35, 19210 Bor, Serbia

### Abstract

*This paper presents the results obtained by determination of Bond rod mill work index (RWi), on a very low-grade copper ore, containing only 0.13% Cu. The standard Bond rod mill grindability test is performed in this research. RWi depends primarily on the mechanical properties of material conditioned by mineralogical composition and the desired particle size of the ground material. The mineralogical composition of the considered sample included the following metallic ore minerals: pyrite, chalcopyrite, hematite, magnetite, covellite, chalcocite, bornite, sphalerite and rutile. Tailings was presented by quartz, calcite, anhydrite, gypsum and clay minerals. The closing sieve size was 1,18 mm. The obtained value of RWi was 19 kWh/t, and therefore this ore can be classified as hard.*

**Keywords:** Bond rod mill work index, grindability, low-grade copper ore

### 1. INTRODUCTION

Comminution is an essential operation for the mining and mineral processing industry. Accordingly, the liberation of valuable minerals from the gangue is a fundamental requirement for all subsequent separation or extraction operations, and this is achieved through several stages of rock fragmentation, that is, by comminution of the ore [1]. Knowledge of the grindability behavior of solid materials can be considered as an important factor for the design of their grindability systems. Bond work index can be considered as one of the most important affecting factors in the design of grinding systems which indicates the value of energy consumed per ton of the ground ore [2]. The Bond rod mill grindability test is a widely used tool to estimate the response of ores to rod milling. The classical method used to predict the specific energy consumption in grinding ores in rod mills was proposed by Fred Bond and is based on the work index. The Bond rod mill work index (RWi) is measured using Bond's standard rod mill grindability test, which is conducted in locked-cycle mode to emulate the continuous closed-circuit operation. Test procedure typically requires from 5 to 10 cycles for reaching steady-state, and normally requires 8–20 kg of sample with 100% < 12.7 mm, containing less than 50% of material passing the screen selected for the test [3, 4]. RWi depends primarily on the ore mechanical properties (which depend on the mineral composition) and test sieve aperture [1, 2, 5].

### 2. EXPERIMENTAL

#### 2.1 Sample characterization

In this testing a very low-grade copper ore sample was used (Figure 1). Chemical composition of this sample is presented in table 1, where it can be seen that content of copper is only 0.13%. The contents of precious metals are also not high (about 0.1 g/t Au and 1.6 g/t Ag).



Figure 1 – Initial sample of copper ore

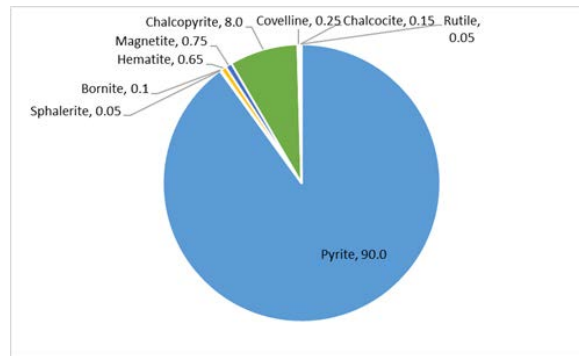


Figure 2 – Distribution of ore minerals in the sample. Values are in percentages per mass.

Table 1 – Chemical composition of copper ore sample

Component	Cu %	S %	Fe %	Au g/t	Ag g/t	Ti %	Al <sub>2</sub> O <sub>3</sub> %	SiO <sub>2</sub> %	CaO %	MgO %	K <sub>2</sub> O %
Value	0.13	6.04	3.92	0.1	1.6	0.23	13.51	58.31	6.10	2.67	2.43

Mineralogical analysis of the ore sample showed the following mineral composition: pyrite, chalcopyrite, hematite, magnetite, covellite, chalcocite, bornite, sphalerite, rutile, tailings minerals (quartz, calcite, anhydrite, gypsum, clay minerals). The tailings mineral content is 80%, while the ore mineral content is 20%. The distribution of ore minerals in percentages is shown in Figure 2.

## 2.2 Experimental procedure

Bond rod mill work index was done according to Bond's standard procedure. This test procedure firstly requires crushing of the representative sample to pass 12.7 mm and its sizing. The test then involves a series of batch grinds in a standard Bond rod mill. A Bond rod mill is 0.305 m by 0.610 m (Figure 3) with wave liners. The grinding media consists of 8 rods weighing a total of 33.38 kg. There are 2 steel rods with 44.45 mm of diameter and 6 rods with 38 mm of diameter.



Figure 3 – Bond rod mill



The mill rotates at 46 rpm on an axis that is positioned horizontally during most of the test, but that is tilted every 10 mill rotations (8 horizontal, one tilted forward 5° and one tilted backward 5°), in order to prevent sample segregation. The test is conducted targeting a 100% circulating load and each cycle finishes with the dry sieving of the entire mill contents with a chosen closing sieve  $P_k$  (in this case  $P_k = 1.18$  mm). When steady-state conditions are reached, the sieve undersize is analyzed and the 80% passing size estimated (P80). The rod mill work index (in kWh/t) is then calculated by standard equation.

The particle size composition was determined by the standard procedure of dry sieving on a series of laboratory sieves.

### 3. RESULTS AND DISCUSSION

Figure 4 shows the particle size composition of the initial sample for the Bond grindability test (–12.7+0 mm), and Figure 5 shows the particle size composition of the undersize of chosen closing sieve.

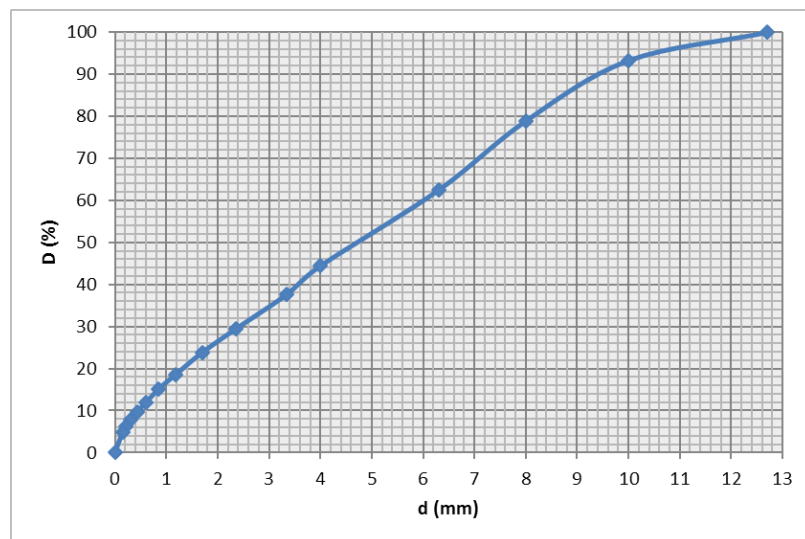


Figure 4 – Particle size composition of the initial sample for the Bond rod mill test, presented by undersize curve (D in %). Corresponding sieve aperture is denoted as d in mm.

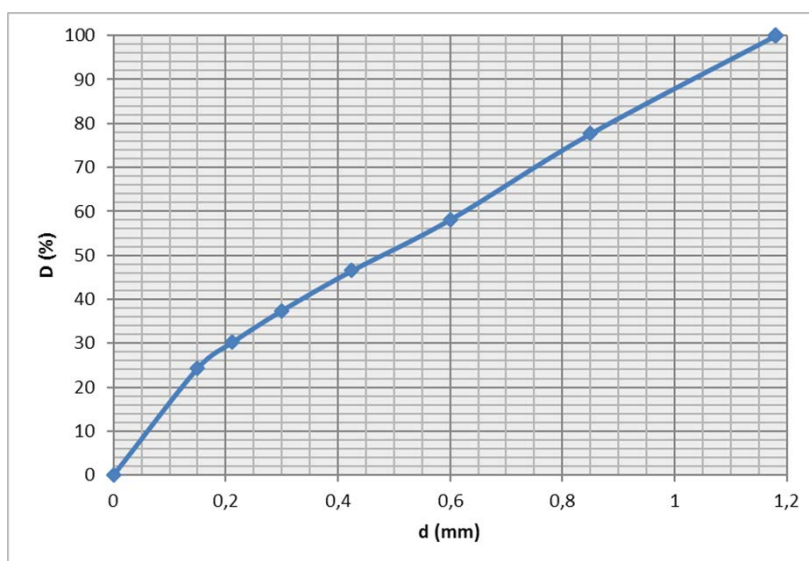


Figure 5 – Particle size composition of the chosen closing sieve undersize. Corresponding sieve aperture is denoted as d in mm.

The rod mill work index (in kWh/t) is then given by the following equation (1):

$$RWi = 1,1 \times \frac{62}{Pk^{0,23} \times G^{0,625} \times \left( \frac{10}{\sqrt{P}} - \frac{10}{\sqrt{F}} \right)} = 18,99 \frac{kWh}{t} \quad (1)$$

Where:

$P_k$  = 1180  $\mu$ m – closing sieve size

$F$  = 8150  $\mu$ m – 80% passing size in the feed

$P$  = 870  $\mu$ m – 80% passing size in the closing sieve undersize

$G$  = 6,10 g/r – the average of the last three net grams of sieve undersize produced per one revolution

Based on the widely accepted classification, where depending on rod mill Bond work index, material can be classified as soft ( $RWi = 7 - 9$ ), medium ( $RWi = 9 - 14$ ), hard ( $RWi = 14 - 20$ ) and very hard ( $RWi > 20$ ), this sample with  $RWi = 18,99$  kWh/t, belongs to hard ores.

#### 4. CONCLUSION

In accordance with the presented research, the following conclusions can be drawn:

- Chemical analysis showed a very low copper content in the tested sample, which is 0.13% Cu.
- Presence of ore minerals in the sample is 20%, and tailings minerals 80%. The most abundant ore mineral is pyrite.
- Bond rod mill work index is 19 kWh/t, which classifies the sample as hard ore.

#### ACKNOWLEDGEMENTS

*This work was financially supported by the Ministry of Education, Science and Technological Development of the Republic of Serbia, Grant No. 451-03-47/2023-01/200052.*

#### REFERENCES

- [1] G.G. García, J. Oliva, E. Guasch, H. Anticoi, A.L. Coello-Velázquez, J.M. Menéndez-Aguado, *Metals* 2021, 11, 970.
- [2] S.A.M.E. Rizk, *JES Assiut University Faculty of Engineering*, 48 (6), (2020), 1106-1118.
- [3] L.M. Tavares, R.M. de Carvalho, J. C. Guerrero, *Miner. Eng.*, 26, (2012), 99-101.
- [4] R. Ahmadi, M. Hashemzadehfini, M. Amiri Parian, *Adv. Powder Technol.* 24, (2013), 441–445.
- [5] G.S. Abdel Hafez, *JES Assiut University*, 40 (1), (2012), 271–280.

## INVESTIGATION OF THE EFFECT OF DEPRESSANT AND COLLECTOR CONDITIONING TIMES ON COBALT RECOVERY BY FLOTATION

Hasan Ali Taner<sup>1</sup>, Ali Aras<sup>1</sup>, Muhammad Hashim Rasa<sup>2</sup>

<sup>1</sup>Department of Mining Engineering, Faculty of Engineering and Natural Sciences, Konya  
Technical University, Konya, Turkey

<sup>2</sup>Graduate Education Institute, Konya Technical University, Konya, Turkey

### Abstract

*Conditioning time in flotation is the time required to establish contact between the mineral surfaces and reagents in the pulp. Conditioning time is a significant parameter affecting selectivity and efficiency in flotation. In this study, effect of conditioning times of reagents used as depressant and collector on the recovery of cobalt by flotation method was investigated through rougher flotation experiments. In the experiments, the tailing of the Küre flotation plant, which was determined to contain 0.17% Co, was used. The experiments were carried out with 50 g/t sodium hexametaphosphate as depressant, 100 g/t X-231 as collector, and conditioning time of 1, 3, 5 and 7 min for both reagents. It was seen from the experimental results that a conditioning time of 3 min was appropriate for both the depressant and the collector in order to obtain cobalt in the concentrate with the highest grade and recovery. In these experimental conditions, cobalt grade and recovery were obtained as 0.46% and 84.15%, respectively.*

**Keywords:** cobalt, collector, depressant, flotation, tailing

### 1. INTRODUCTION

With the development of technology, the importance of metals in our daily lives is increasing. Cobalt, which has a wide range of usage, is used in the production of super alloys, surface coatings, high speed steels and cutting materials with its high melting temperature and high temperature resistance. Moreover, it is also used in the manufacture of rechargeable batteries used in hybrid-electric vehicles and energy storage units [1]. The high demand and price of cobalt reveals the importance of this metal [2].

The decrease of high-grade mineral deposits has turned the attention of the mining industry to the recycling of tailing [3]. Secondary resources such as mine tailing or smelting slags are a potentially important source of cobalt [4]. Cobalt, a metal with a wide range of uses, is obtained from secondary sources in Turkey [5]. Sustainable use of natural resources and protection of the environment is an issue that needs to be taken into consideration.

Flotation is an enrichment method used to separate valuable minerals from gangue minerals by using surface/interface property differences of finely liberated minerals (-0.200 +0.010 mm). The fact that it can be applied to low grade/complex ores that are difficult to enrich with other methods makes this method advantageous. Various reagents are added to the pulp to make the surface properties of the minerals in an ore suitable for flotation [6]. Each of the reagents that enable the flotation process to be highly selective and efficient has a specific function. Collectors are organic substances used to make selected minerals hydrophobic by the adsorption of collector molecules or ions on the mineral surface. Depressants, on the other hand, are reagents that make the gangue minerals hydrophilic and keep them in the pulp.

Conditioning is the process of making the mineral particles in the pulp hydrophobic or hydrophilic by stirring and contacting with reagents. Adsorption of the reagent onto the particle's surface depends on the concentration of reagent, intensity and duration of stirring [7]. Conditioning time

is the time required for the flotation reagents to adsorb onto the mineral surface and modify its hydrophobicity or hydrophilicity. If the conditioning time is too short, the reagents cannot adsorb sufficiently to the particle's surfaces and the recovery decreases, and if it is longer, selectivity decreases. Therefore, the optimum value of conditioning time needs to be determined.

The aim of this study is to investigate the effect of the amount and conditioning times of the depressant and collector on the recovery of cobalt through rougher flotation experiments carried out using the tailing obtained from the Küre flotation plant.

## **2. EXPERIMENTAL**

### **2.1 Material**

The tailing sample used in this study was obtained from the Küre flotation plant in Turkey. The amount of sample was reduced using the coning and quartering method, and then X-ray diffraction analysis was performed. It was determined that the sample contained chalcopyrite, pyrite, quartz, gypsum and chamosite. Chemical analysis was performed using atomic absorption spectroscopy (AAS) and it was determined that the sample contained 0.17% Co, 17.27% Fe, 0.29% Cu and 15.64% S. In the rougher flotation experiments, sodium hexametaphosphate (Tekkim Company), X-231 (thionocarbamate, Clariant Company), Dowfroth 250 (polypropylene glycol methylether, Dow Chemicals) and sulfuric acid (H<sub>2</sub>SO<sub>4</sub>) were used as depressant, collector, frother and pH regulator, respectively. Tap water was used to prepare the pulp and distilled water was used to prepare the reagents.

### **2.2 Method**

Rougher flotation experiments were carried out to investigate the effects of the amounts of depressant and collector and conditioning times on cobalt grade and recovery. The experiments were carried out using a self-aerated Denver type flotation machine at a stirring speed of 1200 rpm. pH was measured using a digital pH meter and all experiments were carried out at pH 6. The experiments were carried out using 20% solids ratio and 1 L cell. To ensure the homogeneity, the pulp was first stirred for 2 min and a pH conditioning time of 7 min was applied. Then, depressant (25, 50, 100 and 250 g/t), collector (10, 25, 50 and 100 g/t) and frother (20 g/t) were added, respectively. The frother conditioning time was 1 min and the flotation time was 3 min. The concentrates were filtered, dried, weighed and chemically analyzed.

## **3. RESULTS AND DISCUSSION**

### **3.1 Effect of depressant amount and conditioning time**

Before determining the effect of depressant conditioning time, the effect of the amount of depressant was investigated and flotation experiments were carried out using 25, 50, 100 and 250 g/t sodium hexametaphosphate and 25 g/t X-231. The experimental results were given in Figure 1a. It was seen from Figure 1a that, the most suitable values in terms of cobalt grade and recovery were obtained at the amount of 50 g/t depressant. While there was not much change in cobalt grade as the amount of depressant increased, cobalt recovery increased up to 50 g/t and then decreased. Therefore, 50 g/t sodium hexametaphosphate was used to determine the effect of depressant conditioning time.

In order to determine the effect of depressant conditioning time, experiments were carried out at 4 different values (1, 3, 5 and 7 min) and the results were given in Figure 1b. According to the experimental results in Figure 1b, the highest values in terms of cobalt grade and recovery were obtained in the 3 min conditioning time. Cobalt grade and recovery increased with the depressant conditioning time and reached the highest value at 3 min. However, when the depressant

conditioning time was 5 and 7 min, there was a decrease in cobalt grade and recovery. It was observed that keeping the depressant conditioning time longer had a negative effect on cobalt recovery. Subsequent experiments were performed with a depressant conditioning time of 3 min.

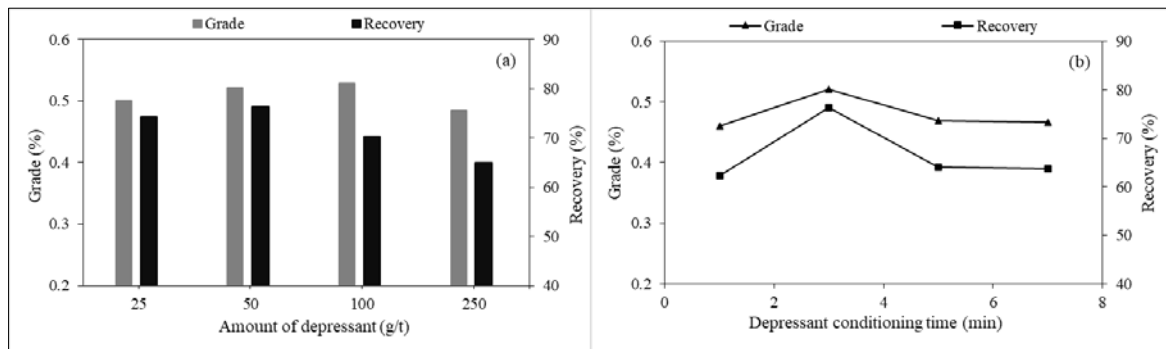


Figure 1 - Effect of depressant amount (a) and depressant conditioning time (b) on cobalt grade and recovery

### 3.2 Effect of the collector amount and conditioning time

Before determining the effect of collector conditioning time, the effect of the collector amount was investigated using 10, 25, 50 and 100 g/t X-231. According to the test results in Figure 2a, while the cobalt grade in the concentrate did not change much for 10 and 25 g/t collector amount, it decreased at 50 and 100 g/t. If an excessive amount of collector is used in flotation, multiple layers occur. Thus, the hydrophobicity of the particles decreases and so the grade decreases [2,8,9,10]. Cobalt recovery increased with the increasing of collector amount. Taking these results into consideration, the most suitable values were obtained at 100 g/t collector amount.

In order to determine the effect of collector conditioning time, experiments were carried out for 4 different values (1, 3, 5 and 7 min) and the results were given in Figure 2b. It was observed that a collector conditioning period of 3 min was appropriate to obtain cobalt in the concentrate with the highest grade and recovery. Since the collector was not sufficiently adsorbed to the mineral surface during the 1 min conditioning time, lower values were obtained compared to 3 min. A slight decrease in cobalt grade and recovery was observed at 5 and 7 min.

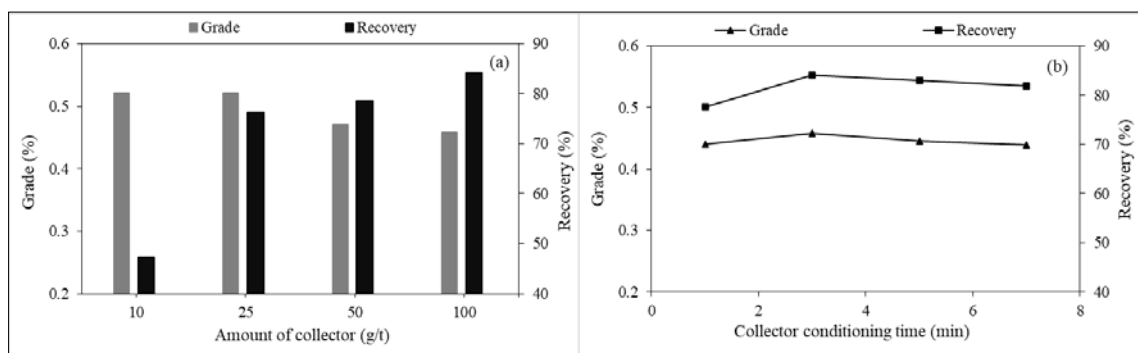


Figure 2 - Effect of collector amount (a) and collector conditioning time (b) on cobalt grade and recovery

It was stated that conditioning increased the flotation recovery of sulphide minerals [11,12]. However, Chen et al. [13] stated that long-term conditioning reduced flotation recovery. In another study, it was reported that in coal flotation, as the collector conditioning time increased, the combustible material recovery decreased, and long-term conditioning caused the coal surface to become more hydrophilic. It was stated that collector desorption occurred on the oxidized coal surface with longer collector conditioning time [14]. Therefore, it is necessary to determine the most appropriate conditioning time for the collector to adsorb to the mineral surface.

#### 4. CONCLUSION

In this paper, flotation experiments were carried out to recover cobalt from Küre flotation plant tailing and the effects of the amount and conditioning times of the depressant and collector were investigated. Using 50 g/t sodium hexametaphosphate as a depressant and a depressant conditioning period of 3 min, 0.52% Co grade and 76.29% concentrate recovery were obtained. The most suitable conditions in which cobalt were obtained as: 50 g/t sodium hexametaphosphate and 100 g/t X-231 as depressant and collector, and a conditioning time of 3 min. It was seen that 84.15% of the cobalt in the sample was recovered with a Co grade of 0.46%. With this study, a valuable metal such as cobalt was recovered from tailing under these conditions.

#### REFERENCES

- [1] USGS, Mineral Commodity Summaries-Cobalt, U.S. Geological Survey, (2017) 52-53.
- [2] M.H. Rasa, Recovery of cobalt from Kure flotation plant tailings, Master's thesis, Konya Technical University, Konya, 2022, p. 48.
- [3] F.K. Crundwell, N.B. Du Preez, B.D.H. Knights, Miner. Eng., 156 (2020) 106450 1-4.
- [4] Q. Dehaine, L.T. Tijsseling, H.J. Glass, T. Törmanen, A.R. Butcher, Miner. Eng., 160 (2021) 106656 1-28.
- [5] B. Yaylalı, Recovery of cobalt from pyritic tailings, Master's thesis, Karadeniz Technical University, Trabzon, 2017, p. 51.
- [6] E.C. Cilek, Mineral flotation, Süleyman Demirel University, Isparta, 2013, p. 157.
- [7] D. Henwood, The effect of conditioning on froth flotation, Master's thesis, University of Cape Town, Rondebosch, 1994, p. 159.
- [8] B.A. Wills, T. Napier-Munn, Mineral Processing Technology 7th Edition, Butterworth-Heinemann, London, 2006, 271-272.
- [9] D.T. Bell, Flotation of cobalt bearing minerals from a mixed copper-cobalt oxidized ore, Dissertation, University of Johannesburg, South Africa, 2011, p. 144.
- [10] S.H. Shahcheraghi, M. Abdollahy, M.R. Khalesi, S.M. Hossein, A study on the effect of some operating parameters on the flotation kinetics of copper sulfide minerals, In Proceedings of the XXVI International Mineral Processing Congress (IMPC), New Delhi, 2012, 24-28.
- [11] M.D. Engel, P.D. Middlebrook, G.J. Jameson, Miner. Eng., 10(1) (1997) 55-68.
- [12] B. Feng, Q. Feng, Y. Lu, P. Lv, Miner. Eng., 39 (2012) 48-50.
- [13] Y. Chen, Q. Shi, Q. Feng, Y. Lu, W. Zhang, Minerals, 7(7) (2017) 125 1-12.
- [14] W.C. Xia, J. Yang, C. Liang, B. Zhu, Energ. Source Part A, 36(1) (2014) 31-37.



## MICROPLASTICS

**Aleksandar Cvetković, Žaklina Tasić, Marija Petrović Mihajlović, Maja Nujkić<sup>1</sup>,  
Milan Radovanović, Ana Simonović**

University of Belgrade, Technical Faculty in Bor, V.J. 12, 19210 Bor, Serbia

### Abstract

*This paper is an illustrated review of the microplastics phenomenon which is caused by human activity and has global reach. Microplastics are insoluble solid particles in the range of sizes between 1 $\mu$ m and 5mm. There can be a further divide into larger macro- and meso- plastics and smaller nanoplastics. Regardless of the size all microplastics can carry adsorbed toxic materials like insoluble organic materials and heavy metals. With these materials microplastics can integrate themselves into the food chain and though it come in contact with the human body where desorption of toxic materials can takes place. It is difficult to recognize the type of microplastics, only with the employment of different recognition methods a sample of microplastics can be correctly identified. The removal of microplastics can be carried out with classic methods or with bioreactors.*

**Keywords:** Microplastics, Adsorption, Toxicity

### 1. INTRODUCTION

Microplastics are materials that originate from a wide number of plastics with their polymers like: polypropylene (PP), polyurethane (PU), polyethylene terephthalate (PET), polyvinyl chloride (PVC), polystyrene (PS) and the most represented type of plastic polymer, polyethylene (PE). These polymers are just the most common types which comprise the majority of microplastics in circulation [1].

### 2. RESULTS AND DISCUSSION

#### 2.1 Plastic degradation and formation of microplastics

A microplastics particle is defined as a particle that isn't soluble and is in the range of sizes between 1 $\mu$ m and 5mm, but in nature the sizes can be smaller than 1 $\mu$ m and bigger than 5mm. Its origins can be divided into primary and secondary microplastics. The first origin is tied to the production of plastic objects or plastic pieces that already to have the range of sizes that would define them as microplastics. The second origin is tied to the degradation of larger plastic parts through the effects of natural and biological factors [2]. Secondary origin of microplastics occurs through the action of abiotic and biotic factors, where abiotic factors are UV radiation, pH values, temperature, salinity, concentration of different compounds and others, while biotic factors depend on the organisms that can emit enzymes and other chemicals that degrade plastics and its polymers [2].

The degradation of plastics to the level of microplastics and beyond begins with the mentioned abiotic factors which prepare the plastic surface for the attack of microorganisms that can degrade the plastic polymer through enzyme use. The impact of microorganisms on plastic can be divided into four stages: biodegradation, biofragmentation, bioassimilation and mineralization. Microplastic particles are being created through the whole process of plastic degradation, starting from the abiotic factors and continuing throughout the stages of biotic factors. UV light in combination with oxygen has the greatest effect on the plastic polymers. By synergetic action oxygen combines to the polymer and creates hydroxylic and carboxylic groups or can cut the polymer into smaller chains. Further synergetic effects come in place after microorganisms begin to degrade the plastic with enzymes [3, 4].

The enzymatic degradation cuts the polymer down to its constituents or to other pieces that require other enzymes to be further degraded. Microorganisms use the products of enzymatic degradation as a carbon source and implement them into their metabolic cycle in the assimilation stage, after which the final result of plastic degradation are carbon-dioxide and water in the mineralization stage [5]. The above discussed origins and creation of microplastics are given on the upper part of Figure 1. below.

## **2.2 Adsorption and desorption of toxic materials on to and from microplastics**

Microplastics have a large specific surface because of their size and numbers, and in combination with the properties of plastic makes them good vectors for a substantial amount of toxic compounds, most commonly insoluble organic species and heavy metals. Adsorption of toxic compounds takes place in different mediums that are contaminated with them. From there microplastics can transport these toxic compounds to uncontaminated environments or organisms and the human body. One of the ways contaminated microplastics can come in contact with the human body is through the food chain, where organisms on the bottom of the chain consume contaminated microplastics and transport them up through food into the human interior. These microplastics differentiate by size and only the smallest particles make it to the organs like the brain. The majority concentrates in the digestive tract where the properties of the medium can desorb the toxic compounds and damage to the tissue can take place [2, 6, 7].

## **2.3 Microplastics type detection and removal from waste water**

Microplastics are difficult to characterize because of their various characteristics and a large amount of polymers that comprise them. A sample of microplastics can contain thousands of microplastic particles. The process of identification can employ the recognition of specific properties that are tied to the polymer like its density, the color of smoke after burning or the melting point. But the best results can be obtained by using laboratory methods that can give a deeper insights in the chemical structure of the polymers in question, and are often used in sequence to get the best insight into the aforementioned structure that indicates different polymers. These methods can be destructive like gas chromatography–mass spectrometry (GC-MS) and thermogravimetric analysis (TGA) or non-destructive like Fourier-transform infrared spectroscopy (FT-IR), which can be most commonly seen in use when it comes to microplastics detection and identification [8 - 10].

## **2.4 Brief segment about removal of microplastics from waste water**

Removal of microplastics from wastewater and water in general is important because it represents one of the primary ways for microplastics dispersion. Likewise microplastics that are contaminated can get into the human body through drinking water. There are several methods that can be utilized for microplastics removal like filtration or sedimentation which are classical water treatment methods. In contrast, bioreactors are relatively newer and utilize bacteria in the process. Namely, in bioreactors microplastics come in contact with bacteria that can create biofilm on their surface which can be sedimented or filtrated [11, 12].

The mentioned processes are given on the bottom part of Figure 1.

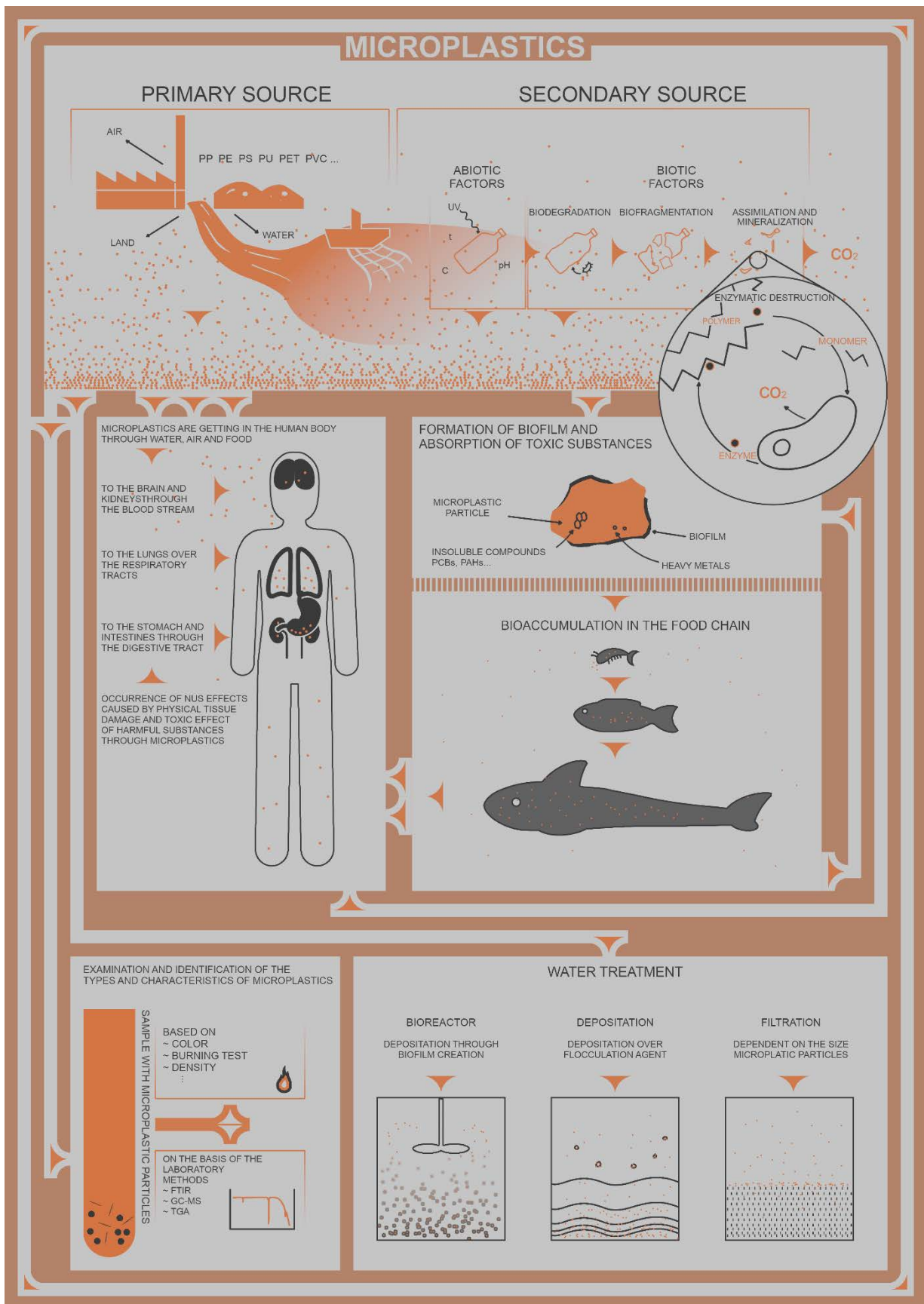


Figure 1 - Illustration of the creation and movement of microplastics based on the work

### 3. CONCLUSION

Microplastics are a diversified field that is in constant flux when it comes to the evolution of the microplastics problem in nature and in industry, as well as in the scientific research on the topic. Only in the coming years the problem can manifest itself as a true burden to humanity or a passing problem.

GNU IMAGE MANIPULATION PROGRAM was used for the illustration of Figure 1.

### ACKNOWLEDGMENTS

*The authors are grateful to the Ministry of Science, Technological Development and Innovation of the Republic of Serbia for financial support according to the contract with the registration number (451-03-47/2023-01/200131).*

### REFERENCES

- [1] S. S. Ali, T. Elsamahy, R. Al-Tohamy, D. Zhu, Y. A.-G. Mahmoud, E. Koutra, M. A. Metwally, M. Kornaros, J. Sun; *Science of the Total Environment* 780 (2021) 146590
- [2] C. Campanale, C. Massarelli, I. Savino, V. Locaputo, V. F. Uricchio; *Int. J. Environ. Res. Public Health* 17 (2020) 1212
- [3] M. Arienzo, L. Ferrara, M. Trifuoggi; *J. Mar. Sci. Eng.* 9 (2021) 433
- [4] B. P. Chang, A. K. Mohanty, M. Misra; *RSC Adv* 10 (2020) 17955
- [5] N. Mohanan, Z. Montazer, P. K. Sharma, D. B. Levin; *Front. Microbiol.* 11 (2020) 580709
- [6] A. W. Verla, C. E. Enyoh, E. N. Verla, K. O. Nwarnorh; *SN Applied Sciences* 1 (2019) 1400
- [7] Y. Deng, Y. Zhang, B. Lemos, Ho. Ren; *Sci. Rep.* 7 (2017) 46687
- [8] M. R. Junga, F. D. Horgena, S. V. Orskib, V. Rodriguez, K. L. Beersb, G. H. Balazsc, T. T. Jonesc, T. M. Workd, K. C. Brignace, S. J. Royerf, K. D. Hyrenbacha, B. A. Jensena, J. M. Lynch; *Marine Pollution Bulletin* 127 (2018) 704–716
- [9] H. A. Nel, A. J. Chetwynd, C. A. Kelly, C. Stark, E. Valsami-Jones, S. Krause, I. Lynch; *Environ. Sci. Technol.* 55 (2021) 8721–8729
- [10] M. N. Sathish, I. Jeyasanta, J. Patterson; *Arch Environ Contam Toxicol.* 79 (2020) 111–121
- [11] W. Liu, J. Zhang, H. Liu, X. Guo, X. Zhang, X. Yao, Z. Cao, T. Zhang; *Environment International* 146 (2021) 106277
- [12] J. Sun, X. Dai, Q. Wang, M. C.M. van Loosdrecht, B. J. Ni; *Water Research* 152 (2019) 21-37

## TAILING MANAGEMENT: TAILINGS FILTERING EQUIPMENT

**Sanja Petrović, Srđana Magdalinović, Ljubiša Obradović, Sandra Milutinović,  
Bojan Drobnjaković, Slađana Krstić**

Mining and Metallurgy Institute Bor, Zeleni bulevar 35, 19210 Bor, Serbia

### Abstract

The implementation of tailings dewatering technologies is essential in minimizing water losses and optimizing water recovery. This issue often has a significant impact on the decision-making process when choosing between high-density slurry, paste, and filtered tailings management approaches. The use of filtered tailings disposal has seen substantial growth in recent years, highlighting the crucial significance of filtering equipment in this process. In that regard, this paper briefly outlines the fundamental equipment used for tailings filtration.

*Keywords: tailings, filtration, water, equipment*

### 1. INTRODUCTION

Managing mineral processing tailings and associated water has become increasingly challenging due to the growing tonnages of minerals processed annually [1]. The challenges associated with tailings storage are increasing. There are two crucial aspects that need to be addressed when it comes to dealing with the tailings from mineral processing plants. First, it is imperative to ensure secure and environmentally sound storage for the tailings. Additionally, it is equally vital to promote the sustainable utilization of water in this process [2]. The choice of the best tailings disposal method depends on several factors. These include the degree of pre-disposal dewatering, which is influenced by the rheology and transportability of the tailings. Furthermore, it is crucial to take into account the chemical and biological reactivity of the tailings, as well as the requirement for return water and the quality of process water for recycling. The site climatic conditions and the topography, the distance and elevation of the selected tailing site facilities relative to the plant impact the selection tailings disposal method as well [3]. There are various options available for disposing of mine tailings, including cross valley or hillside dams, raised embankments, dry stacking of thickened tailings on land, and backfilling into abandoned open pit mines or underground mines [1, 4]. A large number of mines worldwide still use conventional TSFs to disposal tailings. On the other hand, numerous mining companies are adopting a more innovative approach to managing tailings. As an alternative tailings disposal method stands paste disposal (high-density thickened tailings or paste tailings), either as surface deposition or underground backfilling [1, 5]. Using filtered tailings can offer substantial advantages and should be consistently regarded as a viable choice for constructing new tailings storage facilities [5]. In order to minimize water losses and decrease the demand for raw water in the processing plant, it is essential to thickening the tailings before disposal. This allows the possibility of recycling process water directly back into the plant. The tailings continuum simply depicts the nature and behavior of tailings at different thickening degree [6]. Figure 1 shows the tailings continuum concept [7,8].

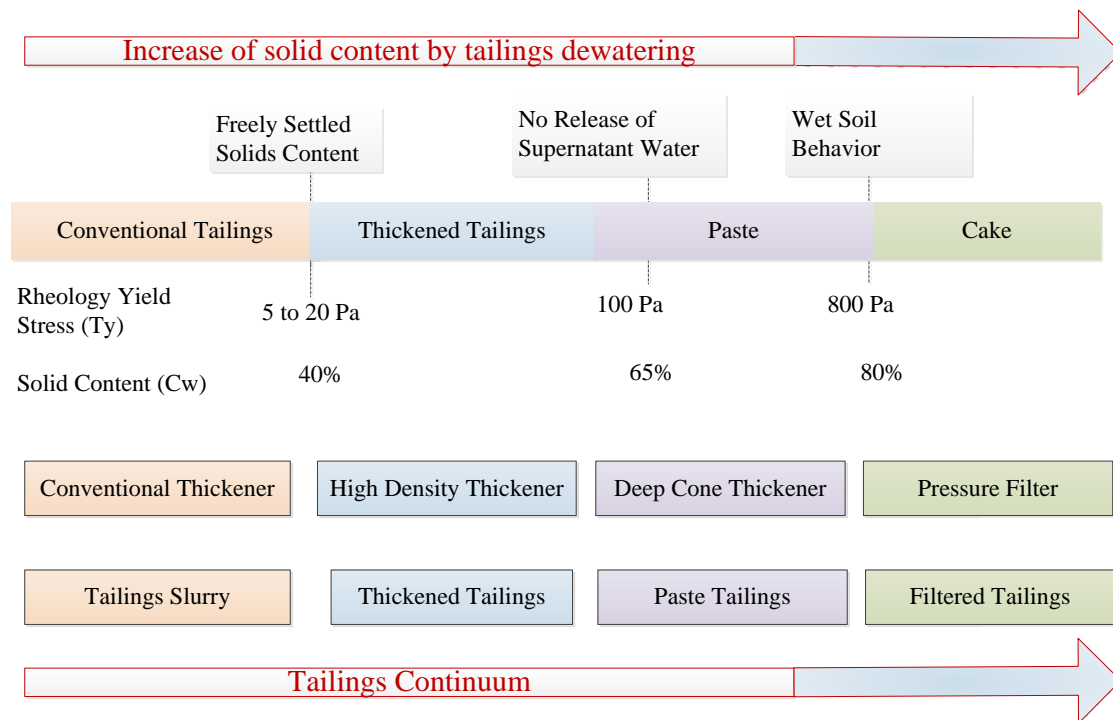


Figure 1 - Dewatering tailings technologies–tailings dewatering continuum [Adapted from Ref. 8]

Dry stack tailings, or filtered tailings, are an innovative and contemporary method for effectively managing tailings. Dry stack tailings, in contrast to traditional wet tailings stored in ponds with water, involve dewatering the tailings to remove excess moisture before methodically stacking them in a controlled manner. This leads to the creation of a stable stack of compact tailings, greatly reducing the persistent risk of tailings dam accidents that have plagued the mining industry for many years [9]. Achieving optimal performance from the thickener is crucial in order to maximize the effectiveness of the filtration equipment.

## 2. TAILINGS FILTERING EQUIPMENT

The nature of the tailings material is critical in the filtration process. High percentages of clay minerals adversely affect the filtration process. It is crucial to define the strength, moisture retention, and hydraulic conductivity of tailings, while considering the corresponding technology employed. The main goal should be to achieve a moisture content that facilitates construction while meeting slope stability requirements [9]. It is generally recommended to target a moisture content that is similar to the standard Proctor optimum moisture content [9].

Table 1 categorizes filtration techniques into two main processes: continuous and batch. In continuous processes, belts or drums are commonly used, while in batch processes, horizontal or vertical pressure filters with a membrane are often employed [10]. The dry matter content that can be obtained is highly dependent on the specific gravity of the material as well as other material characteristics. The numbers in the table 1 are therefore only indicative considering mining default values [10].



Table 1 – Considerations of Filtration Techniques [10]

Type	Process	Heavy duty	*Max. solids content*, %	Electricity consumption	Critical design parameters
Vacuum filtration					
Belt	Continuous	Yes	>75	High	Belt speed, Layer thickness
Disk	Continuous	Limited	>70		Rotation speed, Layer thickness
Drum	Continuous	Limited	>70		Rotation speed, Layer thickness
Pressure filtration					
Chamber	Batch	Yes	>75	Low	Cycle time, Dry matter content
Membrane	Batch	Yes	>85		Cycle time, Dry matter content
Belt	Continuous	Limited	>70		Belt speed, Layer thickness

\* The dry matter content that can be obtained greatly relies on the specific gravity of the material, alongside other material characteristics. Considering default mining values, the numbers in Table 1 are merely indicative [10].

## 2.1 Vacuum Filters

In mineral applications, there are various configurations for vacuum filters, with disc and horizontal belts being the most prevalent ones. Smaller capacity underground backfilling operations often rely on disc filters. Horizontal belt filters are the most common type of vacuum filter used for surface disposal of large tailings throughput [11]. Horizontal belt filters are part of the vacuum filter family and are designed to receive the slurry to be filtered from the top. The Horizontal Vacuum Belt Filter (HVBF) uses filtering fabric as the filter medium, which utilizes the material gravity and vacuum suction to realize the separation of the solid and liquid. The Ceramic Disc Vacuum (CDVF) is an innovative and efficient solid-liquid separation device that emerged in the 1980s, providing remarkable effectiveness and energy conservation [12]. The ceramic filter has a shape and mechanism that closely resembles the working principle of the disc vacuum filter. A pressure difference is responsible for driving the flow of the suspension through the filter medium. This process ultimately results in the capture of particles on the medium's surface and the creation of a filter cake.

## 2.2 Pressure Filters

The Filter Press is an outstanding batch-processing pressure filter that offers remarkable separation efficiency and operates with a simple yet effective mechanism. Over the course of many years, numerous significant improvements have been made to the design of this extensively utilized processing equipment. Significant improvements have been made in automating cake discharge and filter media washing. Filter presses are preferred for dealing with cases where tailings have a fine particle size distribution and high throughput is required. In recent years, Diemme® Filtration has successfully developed and constructed an innovative and groundbreaking "next generation" of colossal filter presses [13]. These pioneering machines boast an impressive throughput capacity, approximately three times greater than the largest filter press currently being used in operation. The GHT5000F Domino stands out as the largest filter press on the market, with an impressive maximum total filtration volume of 71 m<sup>3</sup> and a maximum total filtration area of 2.850 m<sup>2</sup>.

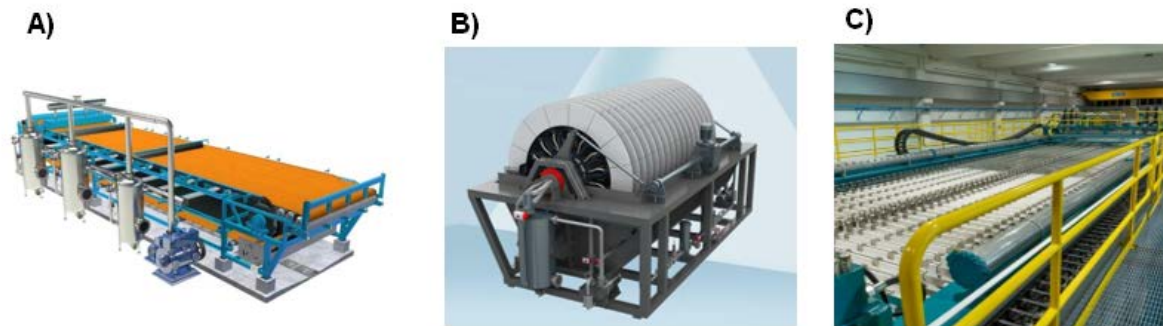


Figure 2 - Tailings filtering equipment (Horizontal Vacuum Belt Filter (A) [14], Ceramic Disk Vacuum Filter (B) [15] and Filter Press (C) [13])

### 3. CONCLUSION

The filtration and dry-stacking of tailings are rapidly gaining popularity as the most preferred method of tailings management. Additionally, the most commonly used dewatering technologies for the filtration of tailings from ore processing are rotary vacuum disc filters, filter presses and belt filters. This technology offers significant benefits that can greatly enhance any project over its lifetime. One of the key advantages is its ability to effectively reduce water supply costs.

### ACKNOWLEDGEMENTS

*The research presented in this paper was done with the financial support of the Ministry of Science, Technological Development and Innovation of the Republic of Serbia, within the funding of the scientific research work at the Mining and Metallurgy Institute Bor, Grant No. 451-03-47/2023-01/200052.*

### REFERENCES

- [1] M. Edraki, T. Baumgartl, E. Manlapig, D. Bradshaw, D. M. Franks, C J. Moran, J. Clean. Prod., 84 (1) (2014) 411-420.
- [2] C. Cacciuttolo, F. Valenzuela, Water, 14 (11) (2022) 1741.
- [3] <https://www.industry.gov.au/sites/default/files/2019-04/lpsdp-tailings-management-handbook-english.pdf>
- [4] N. Araya, Y. Ramírez, L.A. Cisternas, A. Kraslawski, Appl. Energy, 303 (2021) 117626.
- [5] P. Kinnunen, M. Karhu, E. Yli-Rantala, P. Kivikyto-Reponen, Clean. Eng. Technol., 8 (2022) 100499.
- [6] B. Ulrich, Proceedings of the 22nd International Conference on Paste, Thickened and Filtered Tailings, Australian Centre for Geomechanics, Perth, 2019, pp. 71-79.
- [7] C. Cacciuttolo, G.P. Campomanes, Minerals, 12 (2022) 889.
- [8] C. Cacciuttolo, S. Barrera, J. Caldwell, W. Vargas, In Proceedings of the 2nd International Seminar on Tailings Management, Antofagasta, Chile, 2014, pp. 357-370.
- [9] M. Davies, Proceedings Tailings and Mine Waste, Vancouver, BC, 2011.
- [10] A.H. Watson, P.G. Corser, E.E. Garces Padro, T.E. Lopez Christian, J. Vandekeybus, Mine Waste 2010, Perth, Australia, 2010, pp 499-514.
- [11] <https://www.flsmidth.com/>
- [12] <https://cecminingsystems.com/>
- [13] <https://www.diemmefiltration.com/filterpress-for-sludge/filter-press-ght-5000f-domino/>
- [14] <http://www.heshengfilter.com>
- [15] <http://www.longhaimachinery.com>

## XRD ANALYSIS OF CORROSION PRODUCT FORMED IN INDUSTRIAL AGGRESSIVE ENVIRONMENT

Jelena Stefanović, Jelena Đorđević, Sandra Guševac

Mining and Metallurgy Institute Bor, Zelene bulevar 35, 19210 Bor, Serbia

### Abstract

*The aim of this analysis is to improve the control of the corrosion process in order to reduce the impact of corrosion on material degradation and to evaluate the degradation level of mechanical properties of steel due to the corrosion. General corrosion testing was performed on samples after 6 months of exposure to the industrial atmosphere in Bor, at three sites. X-ray diffraction analysis (XRD) was used to identify the mineralogical composition of the corrosion products. The main corrosion product formed was lepidocrocite ( $c\text{-FeOOH}$ ), followed closely by goethite ( $\alpha\text{-FeOOH}$ ). XRD analysis can indicate a relationship between the loss of mechanical characteristics depending on the type of environment in which corrosion develops.*

**Keywords:** (corrosion product, XRD analysis, industrial environment, atmospheric corrosion stations)

### 1. INTRODUCTION (PAPER FORMAT AND MARGINS)

Research on corrosion in the industrially polluted environments is very important, since corrosion is a factor that affects the load-bearing capacity and durability of steel structures, which causes the huge costs for the maintenance of structures. The corrosion process develops the fastest during the winter months due to the increase in concentration of pollutants in the air, such as  $\text{SO}_2$ ,  $\text{CO}_2$ , chloride ions and dust. Various combinations of these factors are typical for the industrial environment. The most important climatic factors that affect the corrosion process are relative humidity, number of sunny hours, air and metal surface temperature, wind speed and duration and frequency of rain, dew and fog. Condensation is considered as an important cause of metal corrosion, especially indoors. Its formation depends on relative humidity and temperature changes.

The subject of this paper research is the loss of physical and mechanical properties of structural steel due to the corrosion propagation caused by the presence of corrosion agents in the industrial environment of RTB Bor. General corrosion testing is performed in the field, in selected atmospheric corrosion stations, near the Sulfuric Acid Plant, Electrolytic Refining Plant (Electrolysis) and next to the automatic air quality monitoring station in Bor. All samples were compared to the standard samples stored in the laboratory conditions. Methods, based on measuring the loss of mass and testing the mechanical properties of samples exposed to the aggressive environments over time, will be used to evaluate the corrosion resistance of metals [1], while XRD analysis will be used to indicate a relationship between the loss of mechanical characteristics depending on the type of environment in which corrosion develops.

### 2. EXPERIMENTAL MATERIAL AND METHODS

Tests were performed on steel tubes of adopted dimensions on the basis of the standard EN 10002-1 (Figure 1).

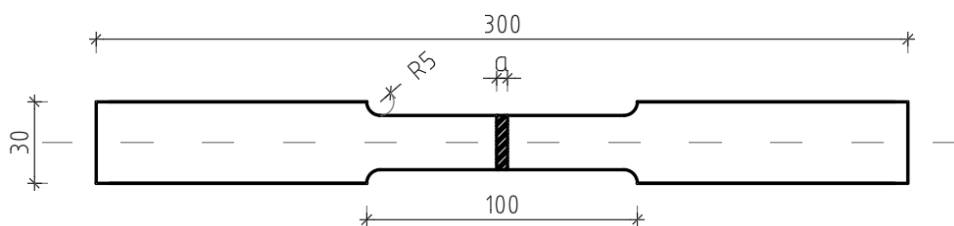


Figure 1 – Schematics of a flat type tensile test specimen (EN 10002-1)

The material used is the commercial steel S235. Chemical composition was tested on a standard measuring, size 30x40x8mm, by the use of optical emission spectrometry [2]. All tested samples, from all places, were previously measured, exposed to the appropriate aggressive environments, cleaned and then measured again. In general, after 6 months of exposure [3], all tubes were 100% covered with corrosion. It is desirable that the corrosion resistance tests are performed in the real operating conditions or on the atmospheric corrosion stations. These are specially selected places, most often with an industrial atmosphere, where samples are exhibited and changes in them and monitored due to corrosion.

This method is used for accelerated testing in the external field conditions, in selected atmospheric corrosion stations. In this experiment, locations near the Sulfuric Acid Plant, Electrolytic Refining Plant (Electrolysis) and next to the automatic air quality monitoring station in Bor were selected. Exposure of samples (steel tubes) lasted 6 months. Samples are placed on a wooden frame so that they rest on it with the smallest surface. They are placed at an angle of 45° to the ground, as a horizontal, and facing south, which in many tests is considered as the position in which the largest surface of sample is affected by corrosion in the longest time interval [4]. The samples were transported to the laboratory and within 24 hours the corrosion products were removed. The deposits from the surface were sampled by scraping with a sterilized spatula.

## 2.1 XRD analysis

The present study assesses the structure and morphology of corrosion product layers formed on mild steel after exposure. Table 1 shows the crystalline phases encountered in the corrosion products formed on S235 steel in the different atmospheres. XRD analysis were performed on powdered rust samples removed from the specimens (Figure 2). A semi-quantitative estimate of each detected phase has been made, expressed as a percentage of the total crystalline products found. It is also interesting to draw attention to the presence of rozenite ( $\text{FeSO}_4(\text{H}_2\text{O})_4$ ) and jarosite ( $\text{KFe}_3(\text{SO}_4)_2(\text{OH})_6$ ) in the industrial atmospheres of Bor, in the corrosion products formed on specimens in the the Electrolytic refining plant.



Figure 2 – Corrosion products prepared for XRD analysis

Table 1 – Crystalline phases of corrosion products of S235 steel formed in the different atmospheres and total sulphate contents (%) from layers of corrosion products.

Atmosphere	$\gamma$ -FeOOH (lepidocrocite)	$\alpha$ -FeOOH (goethite)	FeSO <sub>4</sub> (H <sub>2</sub> O) <sub>4</sub> (rozenite)	KFe <sub>3</sub> (SO <sub>4</sub> ) <sub>2</sub> (OH) <sub>6</sub> (jarosite)	Fe <sub>3</sub> O <sub>4</sub> (magnetite), $\gamma$ -Fe <sub>2</sub> O <sub>3</sub> (maghemite)	Sulfur contents
Near to Sulfuric acid plant in Bor	57	43			Without quantify	0.10
Into the Electrolytic refining plant in Bor		33	20	47	Without quantify	0.31
Next to the automatic air quality monitoring station in Mining and Metallurgy Institute Bor	68	32			Without quantify	0.031

The XRD diagrams (Figs. 2, 3, 4) show that the main corrosion product formed after exposure to the atmosphere is lepidocrocite ( $\gamma$ -FeOOH), followed goethite ( $\alpha$ -FeOOH), which are typical in the case of atmospheric corrosion of carbon steel, as it comes out from other studies.

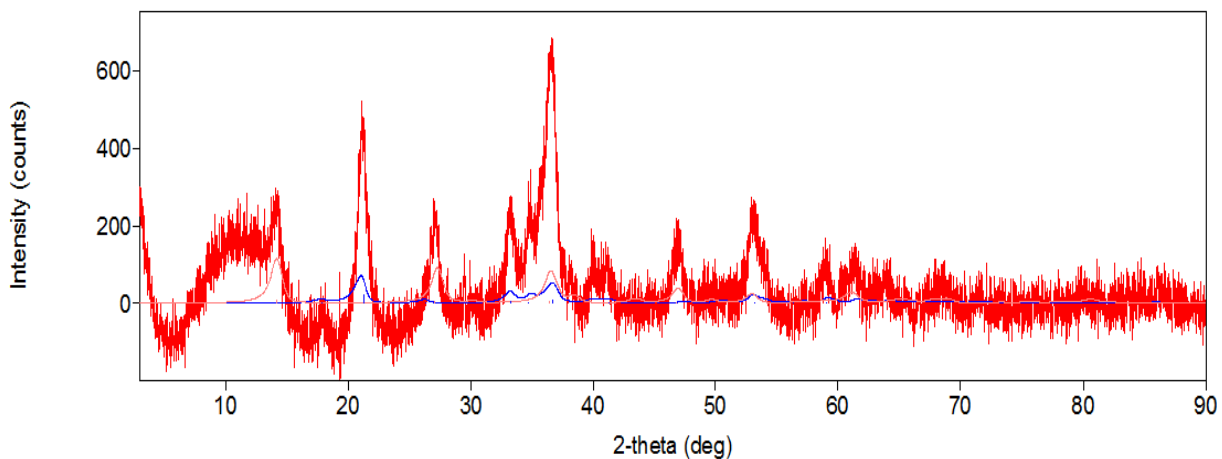


Figure 2 – X-ray diffraction of oxide layer and corrosion products of mild steel after 6 months of exposure near to Sulfuric acid plant in Bor

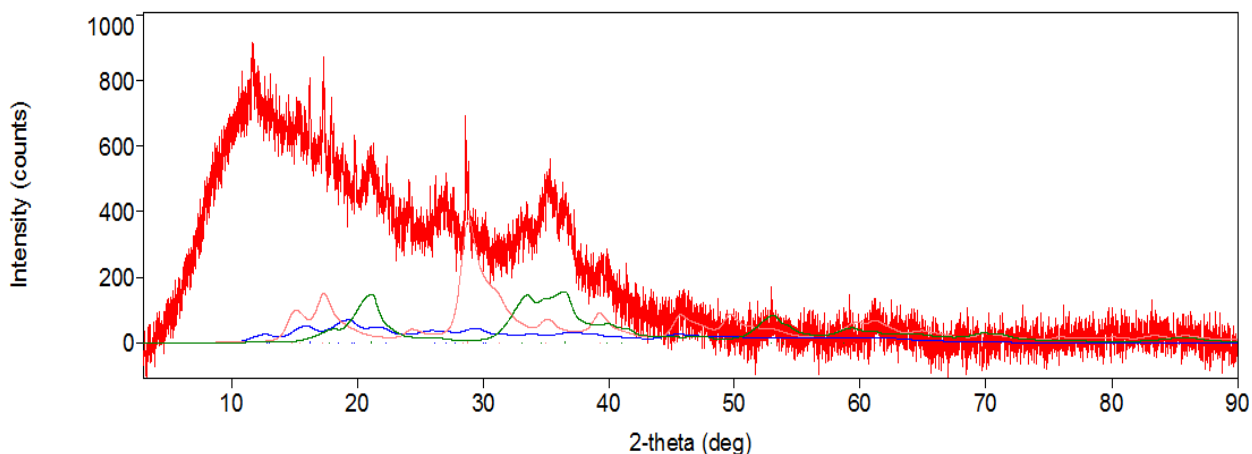


Figure 3 – X-ray diffraction of oxide layer and corrosion products of mild steel after 6 months of exposure into the Electrolytic refining plant in Bor

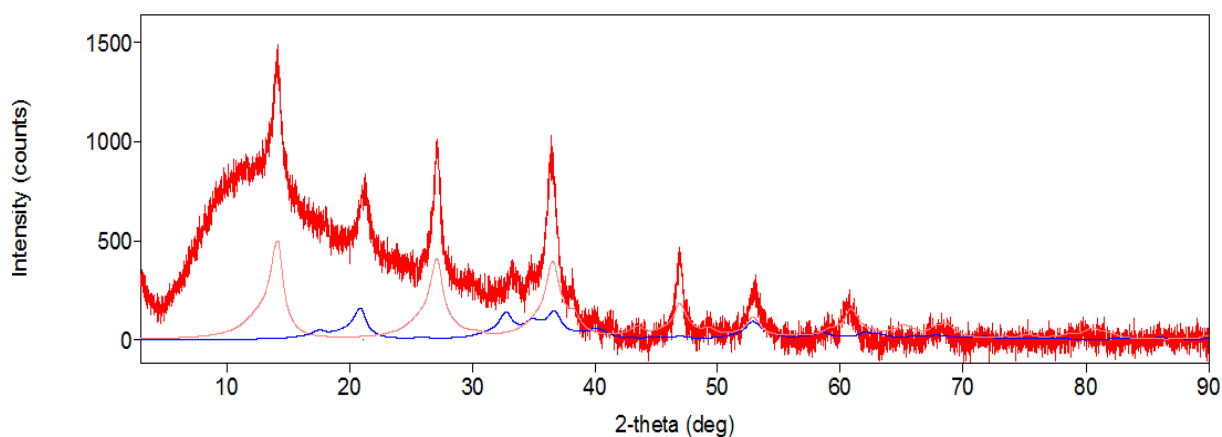


Figure 4 – X-ray diffraction of oxide layer and corrosion products of mild steel after 6 months of exposure next to the automatic air quality monitoring station in Mining and Metallurgy Institute Bor

Table 2 – Monthly average SO<sub>2</sub> deposition (mg/m<sup>3</sup>)

Month	Air quality monitoring station in Mining and Metallurgy Institute Bor	Air quality monitoring station in City park
November 2016	26.41	26.242
December 2016	29.025	26.02
January 2017	54.073	66.766
February 2017	24.691	59.286
March 2017	20.368	43.595
April 2017	15.962	42.262

## 2.2 Atmospheric pollutants

Pollution by SO<sub>2</sub> alone was taken into account in this study because this is the most common and important corrosive agent. The average, monthly values of SO<sub>2</sub> deposition rate for two different test stations, but same exposure conditions, are shown in Table 2. As can be seen in this table, there is a noticeable difference in the SO<sub>2</sub> deposition rate between the two stations in some months.



### 3. RESULTS AND DISCUSSION

The two phases in most cases present are lepidocrocite ( $\gamma$ -FeOOH) and goethite ( $\alpha$ -FeOOH), in this order, in terms of content in the rust. Other phases usually present in the steel corrosion products are magnetite ( $\text{Fe}_3\text{O}_4$ ) or maghemite ( $\gamma$ - $\text{Fe}_2\text{O}_3$ ), which cannot be differentiated by XRD due to their similar crystalline structure. Their preferential location in the lower strata of the rust layer, close to the base steel, explains why they have not been detected in the powder rust samples obtained from the surface of the highly deteriorated steel specimens in the severe industrial atmosphere of Bor.

A certain logical correspondence is also seen between  $\text{SO}_2$  in the atmosphere (Table 2), and the total sulphate contents in the corrosion product layers (Table 1). The highest sulphate contents are found in the corrosion product layers formed into the Electrolytic refining plant in Bor, than near to Sulfuric acid plant in Bor. As expected, the highest sulphate concentrations were found on sheltered specimens. The values obtained only serve to give an idea of the situation at the time when the specimens were withdrawn, since they tend to be strongly dependent on deposition and precipitation conditions in the preceding days and weeks. It is interesting information to know what phases are present in rust according to the type of atmosphere where mild steel has been exposed for long time periods.

### 4. CONCLUSION

The obtained results and data from this work should contribute to the understanding and study of the problem of bearing capacity and durability of steel structures weakened by corrosion in industrial environments, where there are numerous inhibitors of atmospheric corrosion. First of all, it is necessary to check laboratory accelerated corrosion methods in real conditions of exploitation, which would reduce the time required for conducting experiments.

XRD analysis showed that the main corrosion product found was lepidocrocite ( $\gamma$ -FeOOH), followed closely by goethite ( $\alpha$ -FeOOH), which is typical for industrial areas. In accordance with the statements of other authors, transformation of lepidocrocite to goethite is a measure of the corrosion process extend, so that this agrees with the fact that the lowest corrosion is obtain next to the automatic air quality monitoring station in Mining and Metallurgy Institute Bor than near to Sulfuric acid plant in Bor.

### ACKNOWLEDGEMENTS

*The paper presents a part of research that was supported by the Ministry of Science, Technological Development and Innovation of the Republic of Serbia, registration number of the Contract 451-03-47/2023-01/200052.*

### REFERENCES

- [1] J. Stanković, Z. Mišković, M.Pavlović, D. Jevtić, Z. Marković, The Effect of Corrosion Propagation in the Industrially Aggressive Environments and Salt Chamber on the Bearing Capacity of Axially Tensioned Elements, International Conference YuCorr, Tara, Serbia, 2017, 128-133.
- [2] J. Stefanović, S. Dimitrijević, S. Filipović, J. Đorđević, Mining and Metallurgy Engineering Bor, Mining and Metallurgy Institute Bor, Bor, 3-4/2021, 53-60.
- [3] Mendoza, F. Corvo, Corros. Sci. 41 (1999) 75-86
- [4] S. P. Parekh, A. V. Pandya, H. K.Kadiya, Int. J. Chemtech Res., CODEN (USA), 4 (4), (2012), 1700-1774

## INITIATION OF ABNORMAL GRAIN GROWTH IN COLD-ROLLED SHEET OF AA5182 Al-Mg ALLOY: ROLE OF TEXTURE

Muhamad Ghulam Isaq Khan<sup>1</sup>, Filip Rajković<sup>2</sup>, Miljana Popović<sup>1</sup>,  
Dejan Prelević<sup>2</sup>, Aleksandar Ćitić<sup>3</sup>, Tamara Radetić<sup>1</sup>

<sup>1</sup> Faculty of Technology & Metallurgy, University of Belgrade, Karnegijeva 4, 11 120 Belgrade, Serbia

<sup>2</sup> Faculty of Mining & Geology, University of Belgrade, Djušina 7, 11 000 Belgrade, Serbia

<sup>3</sup> Military-Technical Institute, Ratka Resanovića 2, 11 000 Belgrade, Serbia

### Abstract

*In this work, we investigate the role of crystallographic texture on the onset of abnormal grain growth (AGG) in AA5182 alloy. TMP included 65% cold-rolling reduction and isothermal annealing at 480°C at various times. The microstructure characterization by optical microscopy in polarized light revealed that AGG starts after holding for 5 min at 480°C. Further investigation of the sample with incipient abnormal grains was conducted by an SEM equipped with an EBSD detector. The incipient abnormal grains appear to have an orientation of minor texture components, i.e. different cube variants, most likely due to the enhanced grain boundary mobility. However, texture fails to explain the difference in the propensity toward AGG in the region close to the sheet surface and its center, which is likely caused by the non-uniform distribution of the intermetallic particles.*

**Keywords:** Abnormal grain growth, Microtexture, AA5182 alloy

### 1. INTRODUCTION

Recrystallization and grain growth have been subjected to extensive research for over a half of century due to the enormous influence of grain microstructure on the properties of metal materials [1]. However, some fundamental aspects of grain growth, like conditions for the appearance of abnormal grain growth (AGG), are not well understood. Except for a few cases, AGG is undesirable as severely deteriorates mechanical properties of the alloy [1].

The studies of AGG in particle-containing Al-Mg-Mn alloys show that its occurrence depends on the annealing temperature and crystallographic texture of the alloy [2,3]. A high volume fraction of dispersoids can suppress AGG. Hence, the AGG frequently occurs at annealing temperatures close to the solvus when the grain boundary pinning dispersoids coarsen and dissolve [2,3]. However, there are reports of AGG taking place in heavily deformed alloys at annealing temperatures well below solvus [4]. The texture has a major role in low-alloyed Al-alloys with insignificant dispersoid fraction [5,6]. The initiation of AGG is attributed to the size advantage of grains of certain texture components.

In previous work, we reported on observations of AGG in the range of Al-Mg alloys [4,7]. Annealing of the cold-rolled sheets at temperatures >400°C led to AGG and the formation of a microstructure consisting of two bands of abnormal grains enclosing fine-grained material in the center of the cold-rolled sheet. An increase in the content of particle-forming elements, such as Mn and Fe, in the alloy drives the onset of AGG toward higher temperatures [7]. On the other hand, an increase in the cold work lowers the onset temperature [4]. This study aims to examine the role of crystallographic texture in the initiation of abnormal grain growth in AA5182 aluminum alloy.

## 2. EXPERIMENTAL

The material under study was industrially processed - DC cast and hot rolled AA5182 alloy provided by Impol Seval Aluminium Rolling Mill company. The as-received hot band underwent further processing in the laboratory that included cold-rolling with 64% reduction followed by annealing at 480°C for various times ( $\tau = 0-180$  min). The chemical composition of the alloy is given in Table 1.

Table 1 – Chemical composition of the studied alloy (wt%)

Mg	Mn	Si	Fe	Ti	Cu	Zn	Cr	Zn	Other
4.04	0.371	0.0732	0.186	0.0019	0.011	0.0397	0.011	0.0223	0.0082

The microstructure of the alloy, in cold-rolled state and after annealing, was studied by optical microscopy. Longitudinal sections of the cold-rolled sheet, i.e. RD-ND orientation, were mechanically polished and electrolytically etched in Barker's reagent to reveal grain microstructure. The crystallographic texture was characterized in SEM JEOL JSM-6610LV coupled to an EBSD detector Symmetry S3 at the U. of Belgrade, Faculty of Mining and Geology, Depart. for Mineralogy, Crystallography, Petrology and Geochemistry. EBSD data were processed with AZtecCrystal 2.2. From the EBSD data samples orientation distribution functions (ODF) were computed assuming orthotropic symmetry of the cold-rolled sheet, i.e., plane strain. Mechanical polishing was followed by electro-polishing of the specimens for EBSD characterization. Areas,  $\approx 750 \times 500 \mu\text{m}^2$ , were scanned with step size  $1.5-2 \mu\text{m}$ .

## 3. RESULTS AND DISCUSSION

The grain microstructure of the cold-rolled sheet is characterized by elongated, strip-like grains whose thickness and length vary across the cross-section (Figure 1a). Close to the surface, thin grains form within a 600-800  $\mu\text{m}$  thick band. Further toward the center, there is a gradual increase in the grain's thickness and length. Such grain microstructure could be traced to the grain microstructure and size distribution within the hot-band.

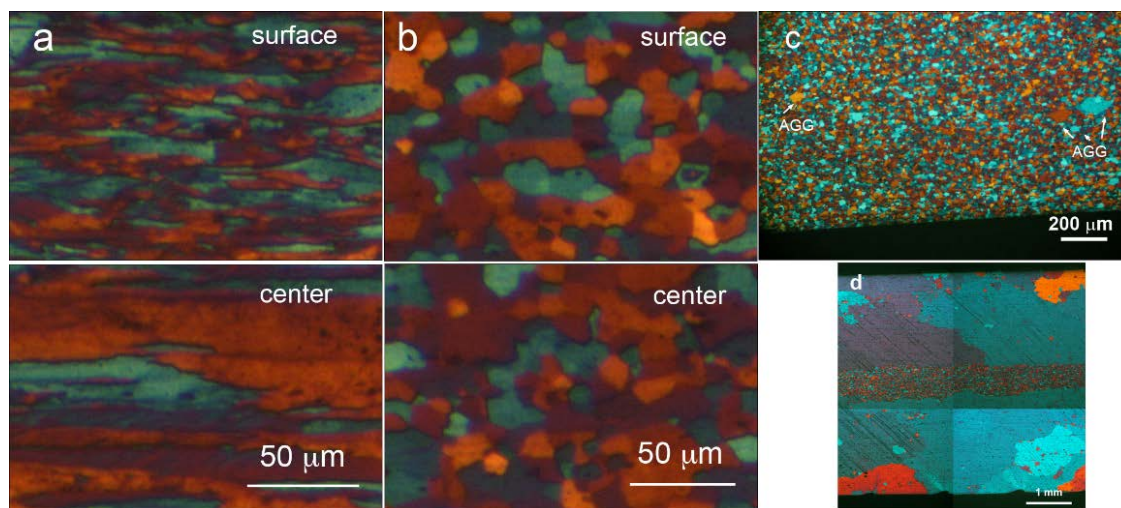


Figure 1 - The grain microstructure of the alloy: (a) cold-rolled state; (b) upon reaching 480°C; (c) annealing for 5 min at 480°C; (d) annealing for 180 min at 480°C.

Recrystallization throughout the cold-rolled sheet occurred during heating up to the annealing temperature (Figure 1b). While there is a gradient in grain size across the sheet thickness, there is no evidence of the presence of enlarged grains that would indicate the onset of the abnormal grain

growth. Annealing for 5 min did not significantly change a mean grain size of  $\approx 9.9 \mu\text{m}$  in the band-region close to the sheet surface. However, enlarged grains (Figure 1c) appeared in the region up to  $700 \mu\text{m}$  from the sheet surface. Longer anneal led to the formation of the bands of abnormal grains. The thickness of the abnormal grains band increased with annealing time, but the strip of fine-grained material in the sheet center was preserved even after annealing for 180 min (Figure 1d). In contrast to excessive grain growth in the outer parts of the sheet, the mean grain size in the plate center increased more slowly from  $14.5$  to  $17.7 \mu\text{m}$ . Annealing at higher temperatures resulted in AGG throughout the plate, with abnormal grains originating also in the center part of the sheet [4].

To evaluate the effect of crystallographic texture and preferential orientation of the grains on AGG, microtexture analysis was conducted in the regions close to the surface and the center of the sheet. The characteristic ODFs of the grains with normal size distribution are shown in Figures 2a and b. The texture is weak, with maximums of  $3.99\times$  and  $3.18\times$  random in the region close to the surface and center, respectively. Although the microstructure shows the morphology of recrystallized grains, the fraction of the cube texture component, which is typical for the recrystallization texture of Al-Mg alloys [1], is at or below the random level. ODF-s show the presence of the  $\beta$ -fiber indicating retained rolling texture. The  $\beta$ -fiber is displaced from the ideal position, and ODF of the central region (Figure 2b) characterizes a larger deviation of Cu and R/S components and weak brass component. While the recrystallization mechanism is unknown, it is likely to adopt a similar path to one proposed for the transformation of S grains into R component [8].

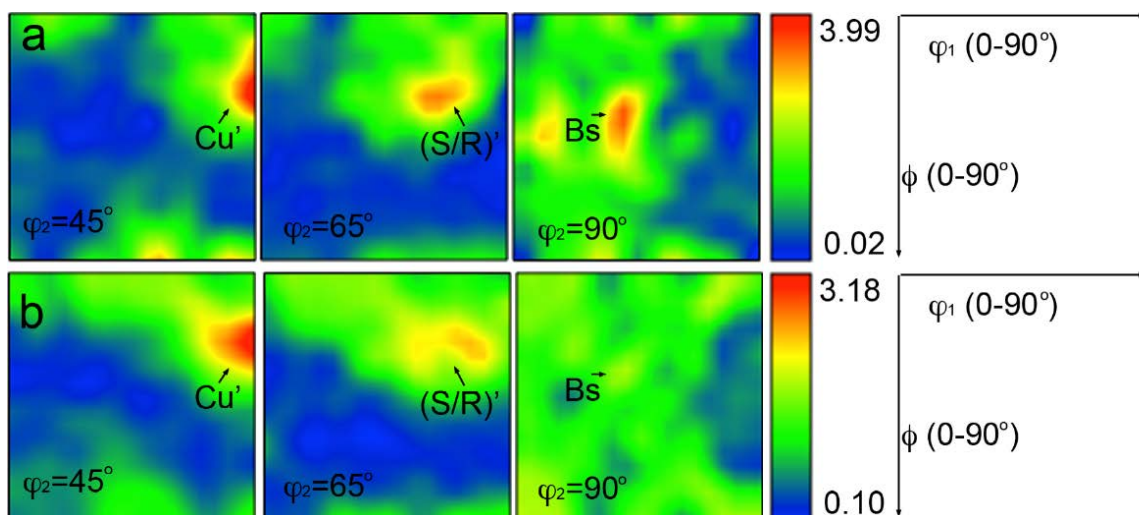


Figure 2 - ODF of the grains having normal size distribution: (a) region close to the sheet surface; (b) region corresponding to the sheet center. Sample was held for 5 min at  $480^\circ\text{C}$ .

A few grains exhibit propensity toward AGG; out of over 5000 grains analyzed, only seven had a size more than  $3\times$  mean grain size. Among them, one had a Brass orientation, while others adopted some cube variants: cube (1), cube ND (1), cube RD (1), and rotation cube (3). Analysis of the grain size distribution did not show any size advantage of these components; actually, their mean grain size was slightly below average. Regardless of the difference in formation mechanism among cube texture variants, the first three being recrystallization and rotation cube shear component, their common feature is low volume fraction. Low volume fraction results in lower interconnectivity of grains with the same texture component. While  $\approx 50\%$  of grains in the dominant texture component, R/S orientation, form clusters of 3 or more grains, less than 15% of grains in one of the cube orientations form groups of 3, if any (Figure 3). Due to the similar orientation of clustered grains, their grain boundaries tend to have limited mobility. Inversely, the grains surrounded by different texture components might have enhanced mobility [9].



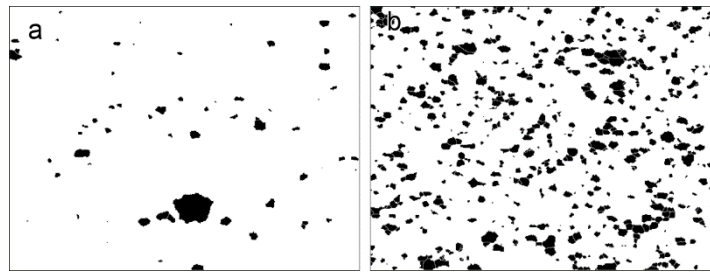


Figure 3 - Distribution of grains of specific texture components: (a) cube; (b) (R/S)'.

However, texture cannot be the sole factor in the AGG initiation. The fact that the surface and central region of the cold-rolled sheet have different propensity toward AGG but are similar in ODF-s points out the other factors. The most likely factor is non-uniform particle distribution, but somewhat larger grain size and broader grain size distribution should not be ruled out.

#### 4. CONCLUSION

The grain morphology of the studied AA5182 alloy indicates the recrystallized microstructure at the onset of abnormal grain growth. However, microtexture analysis shows the absence of the recrystallization texture components and the presence of retained rolling texture; the  $\beta$ -fiber components are displaced from the ideal position. Incipient abnormal grains have an orientation of the different cube variants that are minor texture components and are likely to have higher grain boundary mobility. Due to similarity of ODF from different regions, the crystallographic texture fails to explain the higher propensity toward AGG in the region close to the surface.

#### ACKNOWLEDGEMENT

*This work was supported in part by the Ministry of Science, Technological Development and Innovation of the Republic of Serbia (Contract No. 451-03-47/2023-01/200135). F. R. and D.P. were financed by the Science Fund of the Republic of Serbia through project RECON TETHYS (7744807). We also gratefully acknowledge the help of the Science Fund of the Republic of Serbia in granting the EBSD instrument and software.*

#### REFERENCES

- [1] J. Humphreys, G.S. Rohrer, A. Rollett, Recrystallization and Related Annealing Phenomena, Elsevier, Amsterdam 2017, p. 417.
- [2] I. Samajdar, L. Rabet, B. Verlinden, P. van Houtte, Textures Microstruct., 20 (3-4) (1998), 191-206.
- [3] H.G. Suk, E.J. Shin, M.Y., Solid State Phenom., 116-117 (10) (2006), 316-319.
- [4] T. Radetić, M. Popović, B. Gligorijević, A. Alil, E. Romhanji, Metall. Mater. Eng. 25 (4) (2019) 315-323.
- [5] H-C. Kim, C-G. Kang, M-Y. Huh, O. Engler, Scripta Mater., 57 (4) (2007), 325-327.
- [6] K. Matsumoto, T. Shibayanagi, Y. Umakoshi, Mater.Trans. JIM, 37 (11) (1996), 1659-1664
- [7] T. Radetić, M. Popović, E. Romhanji, Mater. Tech. 54 (1) (2020) 85-90.
- [8] O. Engler, Metal. Mater. Trans. 30 (6) A (1999), 1517-1527.
- [9] O. Engler, Acta Materialia 45 (5) (1998) 1555-1568.

## THE DISSOLVED OXYGEN PREDICTION BASED ON THE MACHINE LEARNING TECHNIQUES

Danijela Voza<sup>1</sup>, Hesam Dehghani<sup>2</sup>, Milica Veličković<sup>1</sup>,

<sup>1</sup>Technical Faculty Bor, University of Belgrade, V.J. 12, 19210 Bor, Serbia

<sup>2</sup>Hamedan University of Technology (HUT), Department of Mining Engineering, Hamedan, Iran

### Abstract

*One of the most reliable indicators of surface water quality is dissolved oxygen (DO). In order to take timely reactions in water pollution prevention and reduction, it is very useful to predict the changes in this parameter. In this study, a comparative analysis of the efficiency of different machine learning models in DO prediction was carried out. The aim was to examine which of the selected techniques indicate the best performance in DO prediction - Decision Tree, Random Forest, Gradient Boost Regression, Support Vector Regression, Multi-Layer Perceptron, and K - Nearest Neighbors Regression (KNN). According to the results, it can be concluded the best-fitted model on the created dataset is KNN.*

**Keywords:** *Dissolved Oxygen, Machine learning, Prediction, Water quality, Tisa River*

### 1. INTRODUCTION

In recent decades, significant efforts towards the renewal and protection of water bodies have been recorded. In order to prevent accidents, it is necessary to recognize and identify all the hydrological variations that could cause negative consequences. The best solution is reflected in developing and improving water quality prediction models as an important step towards reliable water resources management. These models can timely warn about the urgency of undertaking adequate measures.

Water quality modeling is an inevitable activity in water resources engineering. Supportive of that is greater attention being paid to this field by environmental scientists and engineers. Studies related to the prediction of surface water quality parameters by different modern neuro-computing models are increasing. In the example of Laguna Lake among machine learning algorithms such as Naive Bayes (NB), Decision Tree (DT), Random Forest (RF), Gradient Boost (GB), and Deep Learning (DL), the DT achieved the highest accuracy and precision. [1] In comparison with the classical approaches such as the Multi-Layer Perceptron (MLP) and Linear Regression (LR), the DL method was shown to be more reliable in the prediction of water quality parameters, such as pH, dissolved oxygen, turbidity, and chloride. [2] The authors Chen et al. (2020) compared the performances of the seven traditional and the three ensemble learning models for the prediction of water quality by applying a large dataset generated by monitoring the quality of the waters of the main river flows and lakes in China. Their study proved that the DT, the RF, and the Deep Cascade Forest (DCF) were the most efficient. [3]

Despite the proven potential of the machine learning approach in the field of ecological management, there is still an insufficient number of research studies and application of machine learning models in the sphere of water resources management, as well as the comparisons of the performances of different ensemble learning models. [3,4] This methodology, however, is in full swing and an increasingly larger number of studies on their application can be expected in this environmental field.

Dissolved oxygen (DO) is one of the most representative indicators of surface water quality. Therefore, finding the most reliable model for the prediction of the values of this parameter is quite important. This research explores an alternative machine learning method in order to predict water



quality using minimal and easily available water quality parameters. The first step in the model was to determine the significance of each of the selected variables in DO prediction by carrying out variable importance analysis. Additionally, machine-learning algorithms were employed aimed at defining the dataset and the technique whose combination led to the most reliable prediction and the lowest costs of monitoring.

## 2. EXPERIMENTAL

In this study, representative supervised machine learning algorithms were applied for the prediction of the DO value. The modeling processes were conducted using the Rapid Miner Software version 8.9. The methods of Decision Tree, Random Forest, Gradient Boost Regression (GBR), Support Vector Regression (SVR), Multi-Layer Perceptron, and K-nearest neighbors Regression were considered.

### 2.1 Dataset

The study area is the flow of the Tisa River through Serbia, with all the related tributaries. The dataset consists of measurements of water quality parameters from eleven sampling stations. The selection of the parameters analyzed in this paper was made based on the literature review. [1,5,6] The river Temperature (T), Electrical Conductivity (EC), pH, Ammonium Ion (NH<sub>4</sub>-N) and Orthophosphates (PO<sub>4</sub>-P) had most frequently been used in similar studies. Accordingly, the mean monthly values of the mentioned parameters were used as the input data for DO prediction. The physicochemical parameters were retrieved from the water quality monitoring system by the Serbian Environmental Protection Agency (SEPA) that samples river quality monthly, whereas the analysis covered the period from January 2011 to December 2018.

## 3. RESULTS AND DISCUSSION

The initial parameters for examining the efficiency of predicting the DO value were pH, T, EC, NH<sub>4</sub>, and PO<sub>4</sub>. Firstly, the dataset was subjected to a variable importance analysis, which defines the share of each mentioned parameter in DO prediction. In order to obtain the parameters that influence the final result on the same scale, the Z-score standardization of the dataset was first performed. According to the results, it can be concluded that the parameter T has the greatest significance for DO prediction. It is only followed by the parameters: pH, PO<sub>4</sub>, EC, and ultimately NH<sub>4</sub>, as the parameter with the least influence (Figure 1).

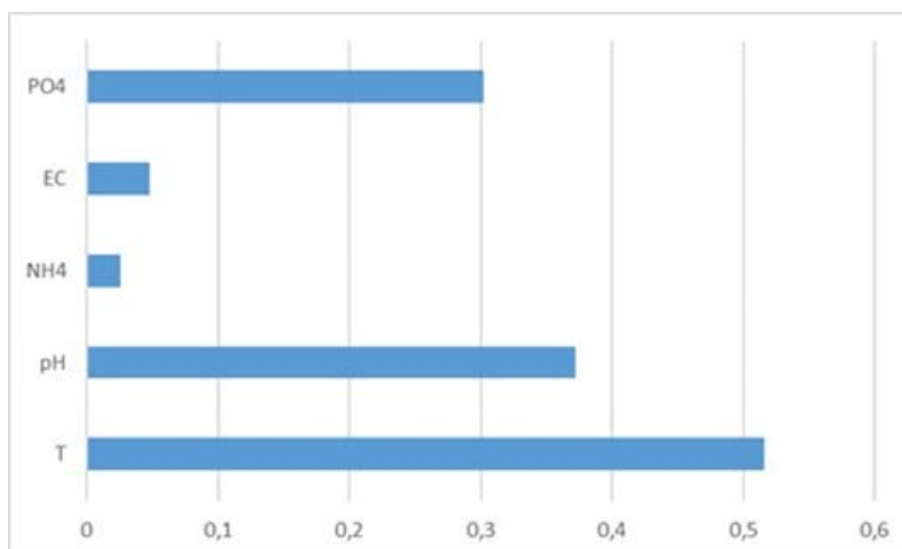


Figure 1 - Variable importance analysis

Further, based on the Model Performance Metrics, a comparison of the predictions with the actual data was made. Correlation Coefficient was used to determine prediction efficiency. It is frequently used to compare models and assess which model provides the best fit to the data. The correlation coefficient (R) is expressed by the values ranging from -1 to +1, where values closer the  $\pm 1$  indicate the greater reliability of a predictive model.

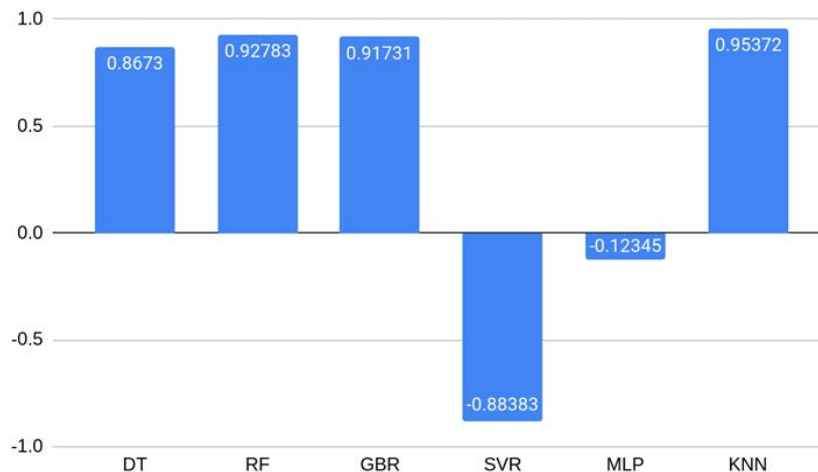


Figure 2. Comparison of model performances

As it can be concluded from Figure 2, the best-fitted model with  $R= 0.95$  is KNN. The KNN model works by the nearest data around the sample. Choosing the number of neighbors (k) is a crucial stage. This method's efficiency depends on selecting samples from the nearest reference database. [7] In this case, the  $K=3$  and the nearest samples are calculated by the distance around the sample.

The main benefits of the KNN method are mathematical simplicity, non-dependence of statistical assumption and the sample space distribution. [8] The KNN method is easy to apply and understand because it doesn't pass through a learning phase. [9] The understandable mechanism and the prediction accuracy of this method make it preferable among the other methods. The obtained results are supported by other studies that proved the advantage of this method in comparison with other machine learning methods. [10,11]

#### 4. CONCLUSION

Surface water quality parameter modeling is regarded as a critical issue that impacts the efficiency and effectiveness of a water resources management system. Finding reliable prediction models and implementing approaches to determine the dominant water quality factors might result in significant cost savings.

The results presented in this paper have indicated that the prediction of the water quality (expressed through the DO values) of the Tisa River on its flow through Serbia can be made with the highest degree of precision by applying the K-Nearest Neighbors Regression, namely in the case when an input dataset consists of the T, pH,  $PO_4$ , and EC values.

The recommendations for future studies relate to the input variables selection and the creation of a hybrid model in which an integration of different machine-supervised techniques would be performed, which would help overcome shortcomings and take advantage of each one of them.

## ACKNOWLEDGEMENTS

*This work was supported by the Ministry of Education, Science and Technological Development of the Republic of Serbia, as part of the financing of scientific research work at the University of Belgrade, Technical Faculty in Bor, according to the contract with registration number 451-03-47/2023-01/200131*

## REFERENCES

- [1] L. J. Leros, V. M. Villarica. *Int. J. Mech. Eng. Robot. Res.* 8(6) (2019)
- [2] A. Solanki, H. Agrawal, K. Khare. *Int. J. Comput. Appl.* 125(9) (2015) 29-34
- [3] K. H. Chen, C. Zhou, Y. Huang, X. Qi, R. Shen, R., F. Liu, M. Zuo, X. Zou, J. Wang, Y. Zhang, D. Chen, X. Chen, Y. Deng, H. Ren. *Water Res.* 171 (2020) 115454
- [4] H. Yajima, J. Derot. *J. Hydroinform.* 20 (2018) 206–220
- [5] S. H. Nemati, M. Fazelifard, O. Terzi, A. M. Ghorbani. *Environ. Earth Sci.* 74 (2015) 4065
- [6] Q. Ren, X. Wang, W. Li, Y. Wei, D. An. *Aquac. Eng.* 90 (2020) 102085
- [7] Ahmed, A.A.M., Jui, S.J.J., Chowdhury, M.A.I. et al. *Environ Sci Pollut Res* 30 (2023) 7851–7873
- [8] W. Luo, S. Huan, H. Fu, G. Wen, H. Cheng, J. Zhou, H. Wu, G. Shen, R. *Food Chem.* 128 (2011) 555–561
- [9] X. C. Nguyen, T. T. H. Nguyen, Q. V. Le, P. C. Le, A. L. Srivastav, Q. B. Pham et al. *J Environ Manage* 301 (2022) 113868
- [10] L. Wang, F. Long, W. Liao, H. Liu *Bioresour Technol* 298 (2020) 122495.
- [11] K. Zidan, S. Sbahi, A. Hejjaj, et al. *Environ Sci Pollut Res* 29 (2022) 75716–75729

## A NOVEL MODEL FOR MINIMIZING MINE CLOSURE COSTS AND THE OPTIMUM FINAL QUARRY BOUNDRY

Hasan Aan, Hasan Ergin

Istanbul Technical University Faculty of Mines, 34469, Maslak/İstanbul

### Abstract

*Mine closure is a very important issue for both the mining industry and other mining-related industries. Planning for mine closure, post-closure land use and closure economics is an imperative task.*

*In this study, a cost estimation model based Excel and VBA-based algorithm was developed to determine the post-mining land use scenario that provide the highest efficiency and to observe the change in the final pit boundary accordingly. With the developed model, mine closure costs can be calculated for different scenarios in a short time. The determined closure costs and post-closure land use revenues were evaluated to decide the optimum mine closure conditions.*

**Keywords:** Mine reclamation; post- mining land-use

### 1. INTRODUCTION

Mine closure is one of the most important issue for the mining industry as well as for the communities that are affected from mining activities. The final goal of mine closure is to provide a safe and stable land configuration for post-mining uses. However, due to the scope of the closure plan and the dynamic nature of the mine plan, mine closure planning is a demanding task. [1]

Post-mining land use planning is an important task for mining sites and it should be performed as early as possible in order to integrate it into the overall mine planning and to keep the restoration costs low. [2] PMLU is the most important element of the mine reclamation plan, and it should be raised and discussed in the primary stage of the mining study. PMLU profoundly affects all mine reclamation activities and their associated costs. [3,4]

A well-established closure planning process should include a closure and reclamation cost ensures investment, development and operating decisions and of deposit. It is made in full recognition of the potential financial impacts for closure in the future. [5]

The impact of mine closure could have a very significant and profound impact on the optimal mine plan and therefore needs to be fully incorporated into the mine planning process. [6]

None of the previous study has covered how the income that can be obtained from the land use form after closure that will affect quarry planning. With the help of the model developed in this study, all the parameters that will constitute income and expense, including mine closure, facility dismantling and post-mining land use, can be evaluated under the same accounting system.

This study aims to present an approach that will enable the determination of the most accurate option by evaluating the economic consequences of different post-mining land use scenarios at the planning stage.

### 2. METHODOLOGY

This study consists of two main stages. In the first stage, mine closure cost model, components and working principles were designed. Calculation tables and formulas are prepared. In the second

stage, an algorithm compatible with this model was created in the Excel environment with the help of Visual basic Application. The aim of this study is to develop an algorithm that will facilitate and speed up cost calculation for the user and enable the evaluation of different alternatives for different scenarios in a short time. While making this calculation, it provides the opportunity to evaluate the economic inputs and outputs for closing and production planning.

Mine closures may require high costs, but second-hand and scrap metal returns, especially as a result of plant dismantling, can provide high economic incomes. Another issue that can generate economic income is the form of land use after mining. It is possible to obtain a one-time or sustainable income with uses such as construction, agriculture, social facilities, which can provide economic income. Sustainable income after this closure may be higher than the income generated by operating the mine. For this reason, it may be possible to change the final quarry limits determined within the scope of open quarry production planning.

### 3. DESCRIPTION OF DEVELOPED MODEL

#### 3.1. General Structure

The general structure of the model was prepared in accordance with Figure 1. First of all, the post-mining land use alternatives are determined. Afterwards, data regarding the entire mine closure phase is collected. These data should cover all income and expense items. Mine closure, rehabilitation, dismantling of facilities and infrastructure units are basic expenses. Revenues are from scrap and second-hand machinery to be obtained from dismantling of the facility and revenues to be obtained from land use after mining constitute. The excavation and filling operations are carried out according to at the post-mining land use scenario. The final quarry limit created according to the operation project are compared. While performing these transactions, Monte Carlo risk analysis and Net Present Value analysis are used. These analyzes are very important for decision-making. If a negative result is obtained, a new post mining land use scenario can be created and the model can be rebuilt from the beginning.

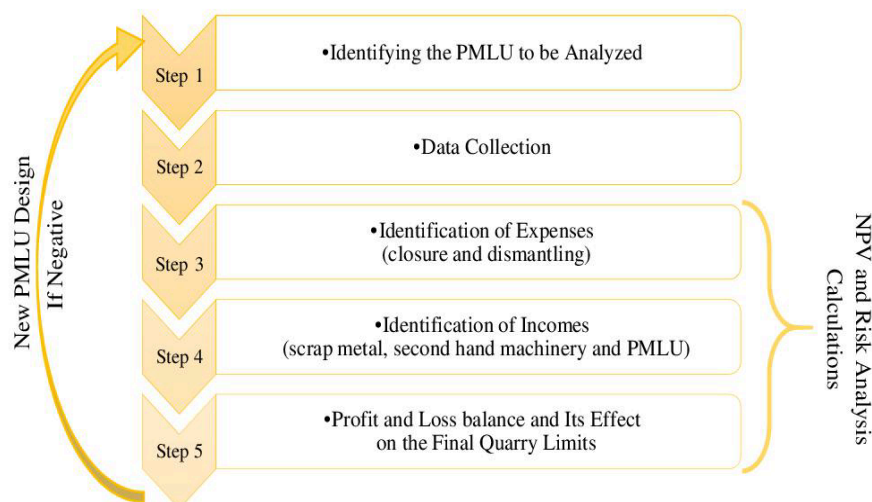


Figure 1 – Structure of Mine Closure Model

#### 3.2. Mine Closure Cost Estimation

Excel was chosen for the creation of the program due to its ease of use and accessibility. The program was created for the calculation of formulas and tables (Figure 2) The program structure consists of modules for data entry.(Figure 3) Also It is possible to analyze the obtained results or cost parameters in the risk analysis and Net Present Value (NPV) modules without the need for

any other software. Using the income and expense data obtained with the help of block model sections previously prepared with integrated mining software. It allows possible changes in the pit limit with the help of the pit limit module. (Figure 4)

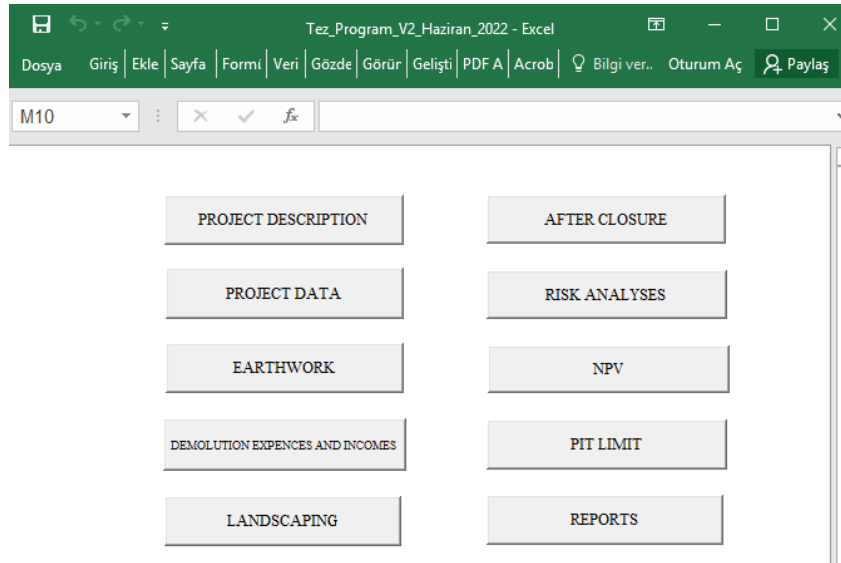


Figure 2– Program Interface

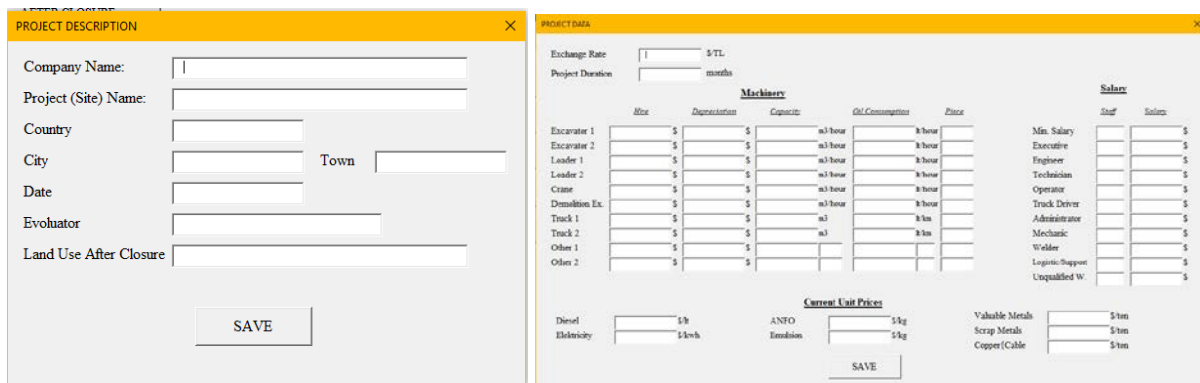


Figure 3 – Data Entry Structure

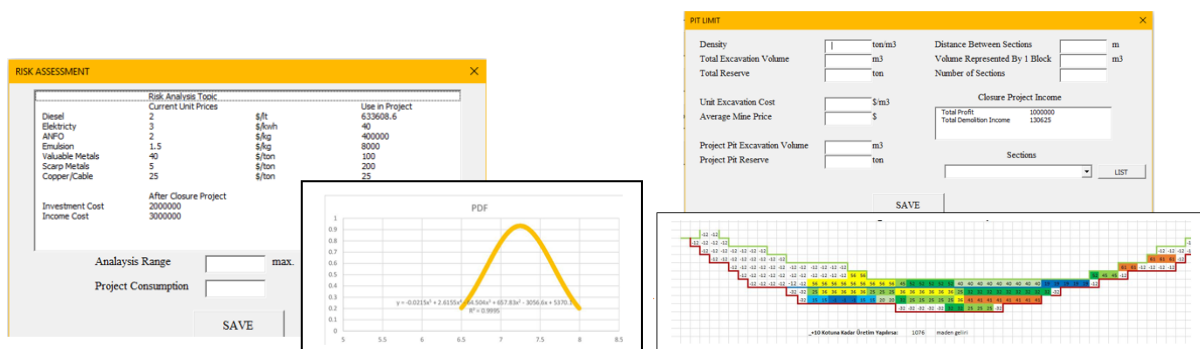


Figure 4 – Risk Analysis and Pit Limit Modules

#### 4. CASE STUDY

A case study was carried out regarding the closure of a cement factory and limestone quarry belonging to a company whose land ownership belongs entirely to itself. First of all, the reserve estimate of the deposit and the final mine pit limits were determined with an integrated mining software. (Figure 5) The situation of terminating production at an elevation where the mine pit



would allow residential buildings was investigated. And it compared to the alternative of producing all the ore by completely deepening the pit. It has been determined that the company could recheck the highest profits.

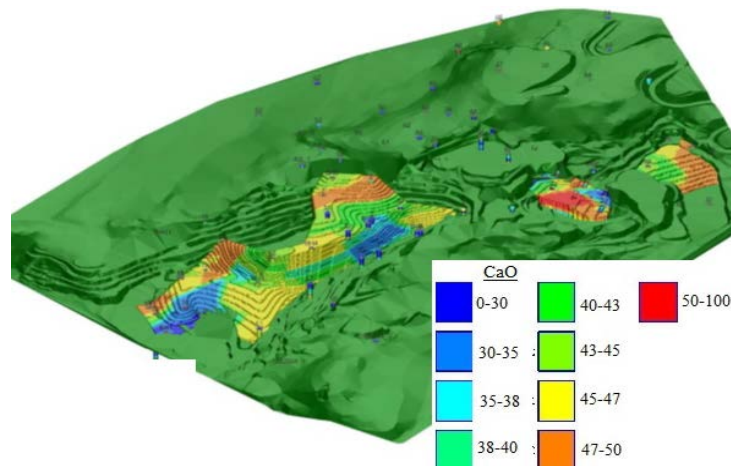


Figure 5 – 3D Topography and Blok Model of Mine Site

## 5. CONCLUSION

It is possible to obtain sustainable economic income from land uses after mining. The economic value of mine land may affect the production of ores with low profitability. More profitability was obtained when optimal and valuable post-mining land use form.

Also dismantling of plant can be turned into a serious economic gain with second-hand machinery and scrap in some countries. With the developed model the cost calculation and comparison can be done easily.

## REFERENCES

- [1] Romero, A. P. Development of a Cost Estimation Model for Mine Closure, Colorado School of Mines (2007)
- [2] K. Broemme, H. Stolpe, C. Jolk, S. Greassidis, A. Borgmann, B. Zindler. Development of methods for post-mining land use planning for coal mines in urban areas in Quang Ninh, Vietnam, Environmental Engineering + Ecology, (2014), Ruhr University Bochum, Bochum, NRW, Germany
- [3] S. Kivinen, Sustain. 9, 10 (2017), 29–33. doi:10.3390/su9101705
- [4] C. Mborah, K.J. Bansah, and M.K. Boateng, Environ. Pollut. 5, 1 (2015), 14. doi:10.5539/ep.v5n1p14
- [5] Slight, M., Lacy, M., JASMR, 4 (2), (2015)
- [6] M. Nehring\*, X. Cheng, J. Clean. Prod. 127 (2016) 228e239. doi.org/10.1016/j.jclepro.2016.03.162

## THE ROLE OF WING TANK IN DMS PROCESS. SUSPENSION VELOCITY THROUGH THE SEAL LEG ORIFICE – CASE STUDY

Ivana Jovanović, Dragan Milanović, Oliver Dimitrijević, Vesna Conić, Igor Svrkota

Mining and Metallurgy Institute Bor, Zeleni bulevar 35, 19210 Bor, Serbia,

### Abstract

*Wing tank represents a specifically designed sump of centrifugal slurry pump, that has a special role in the dense media separation process. The common case is that the mixture of ore and media (suspension) is pumped from the wing tank into the DM cyclone, where the raw material is further separated into heavy and light fractions. This paper provides a brief overview of the function of the wing tank, as well as the calculation of several possible variants of media flowrate and velocity through the seal leg of wing tank. In this way, the potential distribution of material was determined, that is, the amount of medium that will go into the further separation process, or will be separated in the overflow, at a variable height of the overflow threshold.*

**Keywords:** *Dense media separation, wing tank, suspension velocity*

### 1. INTRODUCTION

In heavy-media separation (also called dense media separation, sink-and-float separation), the medium used is a suspension in water of a finely ground heavy mineral (such as magnetite) or technical product (such as ferrosilicon). Such a suspension can simulate a fluid with a higher density than water. When ground ores are fed into the suspension, the gangue particles, having a lower density, tend to float and are removed as tailings, whereas the particles of valuable minerals, having higher density, sink and are also removed. The magnetite or ferrosilicon can be removed from the tailings by magnetic separation and recycled [1, 2]. Separation of materials is performed in devices of different constructions such as: dense media drum separator, separation cone, Daniels dense medium vessel, DM Cyclone, dyna whirlpool, etc. By far, the most widely used centrifugal dense media separator is DM cyclone whose principle of operation is similar to that of the conventional hydrocyclone. The ore is suspended in the medium and introduced tangentially to the DM cyclone, usually by centrifugal slurry pump. The dense material (product in the case of ore) is centrifuged to the cyclone wall and exits at the apex. The light product "floats" to the flow around the axis and exits via the vortex finder [3]. For the proper operation of the DM cyclone, it is necessary that the DM cyclone pump feeds it with material at a constant flow and pressure. This is achieved by the appropriate design of the receiving sump – wing tank, which enables the reception of mineral raw materials and suspension (medium) and can work with a constant liquid level [4].

Wing tank is a tank designed to consistently feed medium and ore to the DMC pump at the desired head to supply sufficient velocity for a sharp separation in the DM cyclone. The wing-side of the wing tank was called this because it is shaped like a wing, running into the side of the tank. Wing tanks are designed to continuously overflow so that head to the pump is kept at a constant level when ore is being delivered to the DM cyclone. When no ore is present, the wing tank will typically operate just below the overflow [5]. The schematic view of the wing tank is given in the Figure 1, and the system wing tank – DMC pump – DM cyclone flowsheet in the Figure 2.

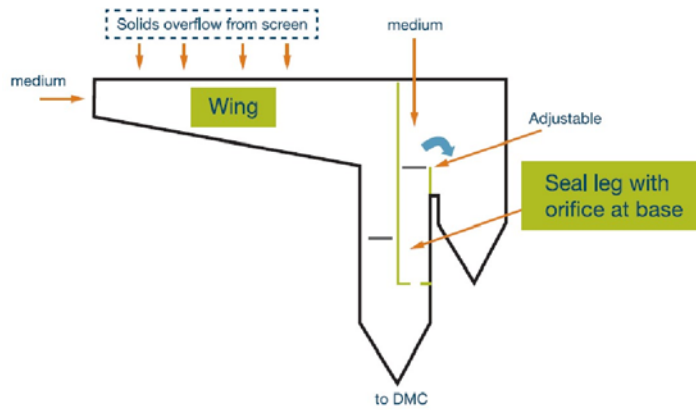


Figure 1 – Wing tank design (adapted from [4])

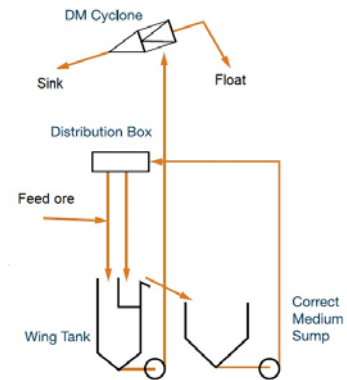


Figure 2 – Typical flowsheet of wing tank – DMC pump – DM cyclone system (adapted from [4])

## 2. THE WING TANK DESIGN AND ROLE

The wing tank is designed to meet two key objectives [4]:

1. To receive the incoming feed solids and medium such that it can operate at a constant level to enable the dense media cyclone to be pump fed at a constant pressure and flowrate. This is achieved by splitting some of the incoming medium directly to an overflow box mounted at the top of the wing tank, from where excess medium overflows to the sump for correct medium.
2. Ensure that all solids that come to the wing tank descend directly to the pump inlet. Due to the buoyancy effect of the medium, coarser, low density particles will tend to ‘raft’ to the surface of the sump; therefore it is critical to ensure that there is a uniform downward velocity of the slurry over the full cross section of the main body of the wing tank. According to literature, this uniform downward flow rate should be about 0.2 m/s in order to counter the tendency for the coarse, light particles to raft to the top.

Wing tank is narrow in shape, with minimal residence time, compared to the normal residence time of many other plant sumps (1–2 minutes). If the downward velocity is insufficient, the coarser, low density grains that raft to the surface will accumulate, displacing volume, and are likely to eventually ‘back up’ the feed particles to block the new feed solids flowing into the wing tank. Rafting and worn orifice plates can also cause the solids carrying over to the correct medium sump, bringing blockages in the bleed valves and trash screens on magnetic separators. Therefore, maintenance procedures in the DMS plant should include a scheduled check on the dimensions of the orifice in the wing tank [4].

Unlike the most other process plant sumps that have residence times ranging from 1 to 2 minutes of pumping, the typical residence time in the wing tanks (for the ore plus medium section, on the wing side, above the orifice level) is about 10 seconds and this normally gives just enough time to de-aerate the slurry while still ensuring a suitable downwards velocity. The flow rate through the orifice is often about 1–2 m/s but this will vary depending on the combination of levels and design flow rates [4].

Cross-sectional schematics presentation of a wing tank with the overflow box, orifice plate and overflow weir for two extreme operating cases is given in Figure 3 and Figure 4. Dense medium circuit is designed for  $Q = 1,000 \text{ m}^3/\text{h}$  slurry flowrate. Considering this, "feed off" case assumes the wing tank is set up such that the medium is just over-flowing into the correct medium sump and there is no solids (ore) in the system. On the other hand, "feed on" case assumes the designed

volume of solids  $Q = 200 \text{ m}^3/\text{h}$  within the same slurry flowrate, considering the plant has been designed for a 4:1 medium:ore ratio [4, 5].

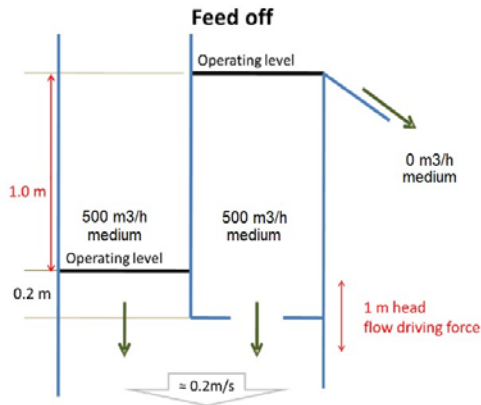


Figure 3 – Schematic of wing tank cross-section for ore feed off; 1,000 m<sup>3</sup>/h medium (adapted from [5])

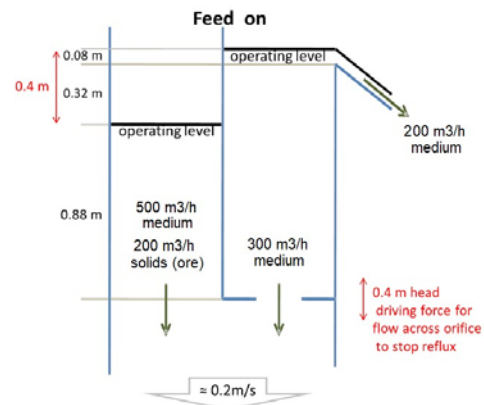


Figure 4 – Schematic of wing tank cross-section for ore feed on; 800 m<sup>3</sup>/h medium + 200 m<sup>3</sup>/h solids (adapted from [5])

### 3. DETERMINATION OF SUSPENSION VELOCITY THROUGH THE SEAL LEG ORIFICE

Given that during the regular operation of each plant there are significant variations in the amount of raw material that reaches the process, the change in the suspension velocity through the seal leg orifice is considered in this paper. The differential head between the ore-side and the seal-side of the wing tank is significant in driving the flows through the orifice plate and therefore determining the orifice velocity. The flow rate of suspension through an orifice is calculated according to equation (1) [4,5]:

$$Q = C \times a \times \sqrt{2gH} \quad (1)$$

Where:  $Q$  is flow rate in m<sup>3</sup>/s;  $H$  is differential head in m;  $a$  is area of orifice opening in m<sup>2</sup> ( $a = d^2\pi/4$ , and  $d$  is orifice diameter);  $g$  is gravity constant ( $g = 9.81 \text{ m/s}^2$ );  $C$  is constant depending on the orifice shape.

From the orifice flowrate, the velocity through the orifice ( $V$ ) can be calculated according to equation (2):

$$V = Q/a \quad (2)$$

During the velocity calculation, the following conditions were applied: (1) total volumetric capacity of the slurry was considered unchanged ( $Q = 800 \text{ m}^3/\text{h}$ ); (2) volumetric flow rate of the ore was variable, and therefore media flow rate through the seal leg was variable; (3) wing tank geometry (height to volume relationship) was not taken into account in the calculation, but considered as normal case; (4) orifice hole diameter is adopted as  $d = 0.25 \text{ m}$  and therefore  $a = d^2\pi/4 = 0,049 \text{ m}^2$ ; (5)  $C = 0.6$  for a submerged square profile circular hole; (6) total flow rate of the suspension that reaches the seal leg is assumed to be  $Q_m = 400 \text{ m}^3/\text{h}$ .

### 4. RESULTS AND DISCUSSION

Table 1 shows the results of calculation of suspension velocity through the seal leg orifice, based on mentioned conditions.

Table 1 – Suspension flow parameters in the seal leg of wing tank

Component	Case I	Case II	Case III	Case IV	Case V
Flow rate of the ore, m <sup>3</sup> /h	0	100	125	150	175
Flow rate through the orifice, m <sup>3</sup> /h	400	300	275	250	225
Suspension overflow, m <sup>3</sup> /h	0	100	125	150	175
Differential head, m	0.72	0.41	0.34	0.28	0.22
Velocity through the orifice, m/h	2.26	1.70	1.56	1.41	1.27

Considering the presented results, it can be seen that in the case of such orifice design (i.e.  $d = 250$  mm), the ore capacity cannot be increased much further, because the velocity of the suspension through the orifice decreases rapidly, and must be greater than 1 m/s. In the same time, differential head tend to reach a very small value, which also is not acceptable. Here, the question arises about the reducing size (diameter) of the seal leg orifice or the change in the overall slurry flow rate, if the process design allows such a modification.

## 5. CONCLUSION

In accordance with the presented research, the following conclusions can be drawn:

- Wing tank is a pump sump of the specific design, which ensures uniform feeding of DM cyclones in DMS plants.
- Wing tank should provide a uniform small downward flow rate of material to the DMC feed pump and disable low density particles to ‘raft’ to the surface of the sump.
- Correct design of the wing tank geometry, as well as the sizing of the seal leg orifice is the crucial for the proper operation of the DMC pump – DM cyclone system.

## ACKNOWLEDGEMENTS

*This work was financially supported by the Ministry of Education, Science and Technological Development of the Republic of Serbia, Grant No. 451-03-47/2023-01/200052.*

## REFERENCES

- [1] W.S. Khan, E. Asmatulu, Md. N. Uddin, R. Asmatulu, Recycling for Sustainable Developments, (2022), 49-68.
- [2] <https://www.britannica.com/technology/heavy-media-separation>
- [3] B. A. Wills, T. Napier-Munn: Dense medium separation (DMS), Chapter 11 in: Wills' mineral processing technology: An introduction to the practical aspects of ore treatment and mineral recovery, seventh edition, Elsevier, Butterworth-Heinemann, (2006), 246-266.
- [4] H. Crowden, B. Atkinson, C. Clarkson, B. Firth, M. O'Brien, D. Wiseman, C. Wood: ACARP Dense Medium Cyclone Handbook, Australian Coal Preparation Society, (2013), 328
- [5] N.J.C. Scott: Dynamic Analysis of Dense Medium Circuits, PhD Thesis, The University of Queensland, Julius Kruttschnitt Mineral Research Centre, (2017), 268

## RISK MANAGEMENT AND MINING MACHINES MAINTENANCE – A BRIEF REVIEW

Dejan Petrović, Jelena Ivaz, Saša Stojadinović, Predrag Stolić, Dragan Zlatanović

Technical Faculty Bor, University of Belgrade, V.J. 12, 19210 Bor, Serbia

### Abstract

*Establishing a risk-based maintenance policy creates a favorable atmosphere for creating a preventive maintenance model. This approach of machine failures enables the excavation process to take place without shutdowns. It is especially important in the case of machines with large capacities, because their failures results in large losses and delays in the production plan. It is crucial to thoroughly evaluate the severity of the consequences caused by the risk event, as well as their potential impact on the continuous operation of the technical system. The importance of the establishing of machine maintenance according to risk of failures is pointed out in this paper.*

**Keywords:** *risk, mining machinery failures, risk assessment, maintenance*

### 1. INTRODUCTION

The economic excavating of deposits with low metal content depends on implementing mass exploitation techniques, such as high-production and high-capacity excavation methods. For this type of production, large-capacity machines are necessary, e.g. trucks with a capacity of over 200 tons. Such machines have a high investment value and their improper maintenance can produce the negative economic influence of the company in whose production system they work. This is especially significant when considering the fact that they typically operate in tandem with other machines within the system.

In general, mining machines represent one of the most complex technical systems in the industry in general. They are distinguished by [1]:

- high investment value,
- they work in complex conditions and expensive technological processes and
- they present a high risk for the working and living environment.

After a certain period of operation of the machines from the time they were introduced into the production system, failures occur, i.e. they stop working. Failure in any form has a direct and detrimental impact on the success of a business. It hampers productivity, prevents meeting set targets, and causes delays in product delivery. Additionally, failure leads to the unfortunate loss of valuable customers. Also, it is very important to point out that machine failures also bring high financial loss to the company.

Apart from the impact on financial operations, failures of complex mining machines have a significant negative impact on the working and living environment. It often happens that workers are physically injured as a result of machine failure. Also, the leakage of hazardous and contaminating substances that reach water and soil additionally increase the severity of the consequences of mechanical system failure.

### 2. RISK MANAGEMENT

Quality and expert risk management provides a clear strategic approach to risk identification, control and reduction of the level of negative effects of a risky event. Such an approach creates the





### 3. DEFINING MAINTENANCE POLICY - MAINTENANCE MANAGEMENT

Operation of mining machines without downtime requires extensive research, analysis and planning of high-quality systematic maintenance in order to provide machines functionality for a long period of time. When one element or part of the system stops working, it usually results in the interruption of the production process. It is known that, in the case of complex technical systems, despite a well-organized system for monitoring work and maintenance, certain elements fail, which can have negative consequences for the machine, employees and the environment. One of the basic requirements for mining machines is reliability in operation, i.e. as few unplanned downtimes as possible.

The maintenance system, i.e. maintenance management of complex technical systems in mining is a very important step in improving the business of a company. The introduction of a maintenance policy in mine systems means the introduction of a procedure for treating failures based on a predetermined procedure. Establishing a high-quality diagnostic system is crucial in this procedure as it allows for the identification of key indicators that signal failures. To ensure effective maintenance practices, it is crucial to develop a comprehensive failure database as part of the maintenance policy. This involves recording every occurrence of failure, allowing us to establish a clear timeline and relationship between severity of failure and operation and down time. By doing so, it can accurately determine the probability of future failures within a specific period. In order to maximize the operating time between two failures, the final stage of the maintenance procedure should include measures aimed at reducing the frequency of failures.

In general, for the reliable operation of machines in mining with the least possible risks, it is necessary to carry out:

- detailed analysis of the technical system using known methods, Figure 2,
- identify weak points,
- predict adverse impacts and their effects,
- define the measures that should be taken in order to keep the system in operational condition for as long as possible and perform the function for which it is intended, without negative consequences for the functional unit it forms as well as the working and living environment.

One example of a detailed decomposition of a technical system necessary for a detailed analysis is shown in Figure 2.

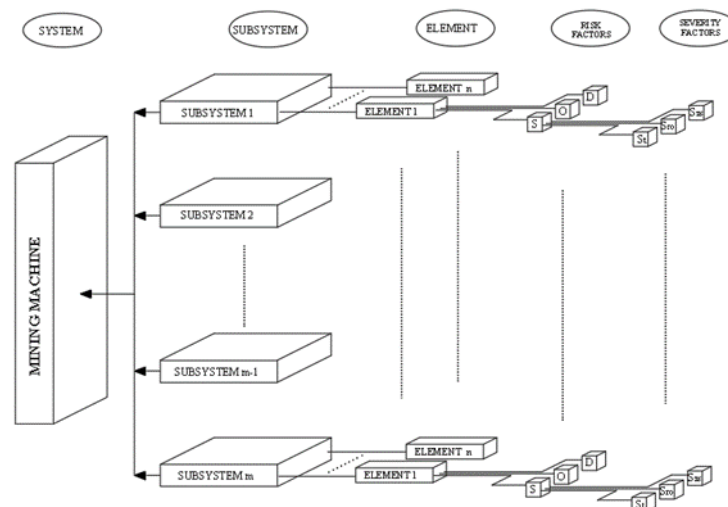


Figure 2 - Decomposition of the technical system [6]

The process of maintenance management is an essential step that must be integrated alongside all other activities within a company. For each activity a company is involved in, it is crucial to establish a comprehensive set of procedures aligned with the relevant industry standards. These procedures form an essential risk management algorithm.

In this sense, mining represents one of the most complex branches of industry considering the complexity of the technology and the machinery used, the costs of unplanned downtime and the working environment.

Constant monitoring and risk management are crucial in the mining industry due to the unique working conditions, the complex relationship between machines and the environment, and the potential impact of unexpected failures on both the machine's functionality and the entire technical system. The application and combination of existing and the development of new risk assessment methods and their implementation in mining technical systems create a favorable atmosphere for reducing of failure and creating maintenance management system.

#### **4. CONCLUSION**

Developing a comprehensive maintenance policy and effectively managing technical systems in the mining industry is crucial for minimizing maintenance costs and ensuring the smooth functioning of a company. Taking action on key points of failure prevention not only avoids production stoppages, but also prevents potential consequences and the need for additional financial resources.

The measures that should be taken in order to reduce the number of failures and the downtime of machines in mining are, first of all, a comprehensive analysis and risk assessment of failure and the reliability of the operation of mining machines and the reorganization of the maintenance system from inert to proactive maintenance according to risk in each of its forms. This approach to machine failures in mining will contribute to increasing the existing capacities of mining and mineral processing and reducing the costs of exploitation, processing and machine maintenance.

#### **ACKNOWLEDGEMENTS**

*This work was supported by the Ministry of Science, Technological Development and Innovation of the Republic of Serbia (Grant No. 451-03-47/2023-01/ 200131, University of Belgrade, Technical Faculty in Bor).*

#### **REFERENCES**

- [1] D. Petrović, Effect of machines failure occurrence on business companies shown in the case of mining machinery. Proceedings of International Symposium Education and social development of Serbia with an emphasis on Bor and eastern Serbia “ 24-25 june, Bor lake, Serbia, (2016), 319 - 330.
- [2] Joy J., Occupational safety risk management in Australian mining. Occupational Medicine 54 (5), (2004), 311–315.
- [3] International standard ISO 31000. (2009) Risk management – Principles and guidelines.
- [4] A. Šijaković, S. Savić, V. Nikolić, J. Taradi, Generički standardi za upravljanje rizicima. 9. Međunarodno savetovanje: Rizik i bezbednosni inženjering, Kopaonik. (2013), 139–145.
- [5] International standard ISO 31010. (2019) Risk management. Risk assessment techniques.
- [6] D. Petrović, Development of algorithm for risk assessment of mining equipment operations based on fuzzy algebra. Doctoral dissertation. University of Belgrade Faculty of Mining and Geology, 2014, Belgrade.

## HISTORY OF SURFACE WATER POLLUTION BY MINING AND METALLURGICAL ACTIVITIES IN BOR, SERBIA

Stefan Đordjević, Dragana Adamović

Mining and Metallurgy Institute Bor, Zeleni Bulevar 35, 19210 Bor, Serbia

### Abstract

*The aim of this paper is to present and compare the monitoring results of wastewater flowing into the Bor River, and the water of Bor River itself from 1931 to 2023 with the purpose of estimating the change in environmental condition and monitoring strategies. The water of Bor River was acidic with a high content of sulfates, iron, and copper since the first record in 1931. However, in 2023 the pH value of Bor River became neutral, and Robule Lake does not exist anymore due to the environmental-friendly mining and metallurgical operations of Serbia Zijin Copper doo.*

**Keywords:** Bor River, Robule Lake, pollution, monitoring, history.

### 1. INTRODUCTION

The degradation of the environment in Bor started after the copper ores were discovered in 1903. The first known complaints of the local community on the pollution caused by mining and smelting activities started already in 1906 [1]. The villagers in the area wanted compensation for the damage to their agricultural fields, pastures, and forests, but they also complained about the water quality of Bor River. In 1931 and 1935, the first results of the chemical analyses of surface waters around Bor were reported [1,2]. Throughout the years, the mining and smelting operations were expanded, and consequently, more contaminants reached the surface waters. In recent years, Bor River was still acidic and had high concentrations of Fe, Cu, As, and other elements due to the inflow of wastewater from the overburden, metallurgical wastewater, and wastewater from Robule Lake [3-6].

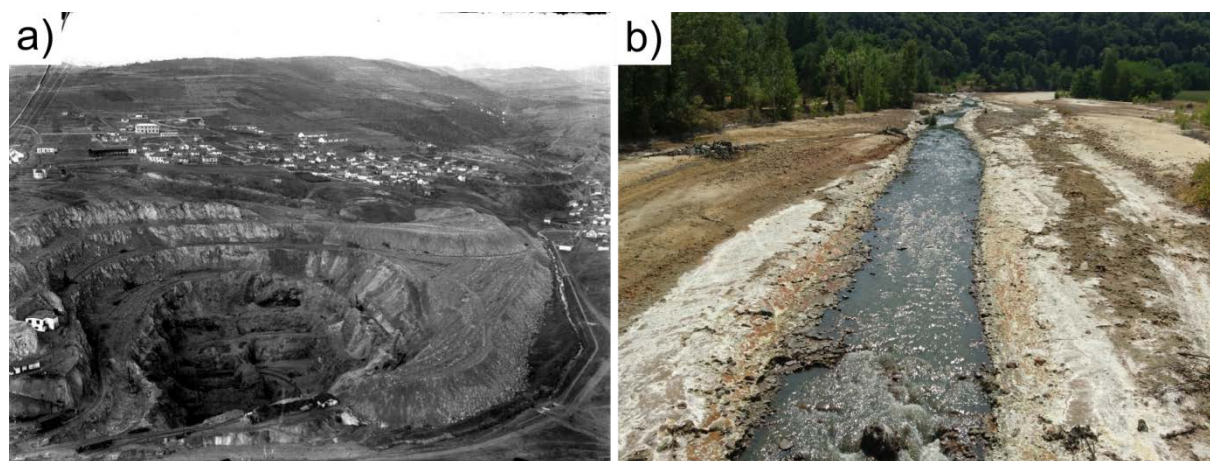


Figure 1 - The photographs of Bor River a) passing by the open pit in Bor in 193? (the year is not exactly known) [7] b) downstream from Slatina Village on 10.08.2017.

### 2. EXPERIMENTAL

The data considered in this paper was obtained from the literature, except the data from September 2021, when the water samples were collected from Robule Lake (N 44.0633, E 22.1365),

Overburden drainage (N 44.0623, E 22.1309), Metallurgical wastewater (N 44.0618, E 22.1314), and Bor River (N 44.0291, E 22.2080) in 50-ml polypropylene bottles, and immediately acidified with 2.5 ml of nitric acid. pH value of water was measured using pH meter model IM-23P. Sulfates were determined using the turbidimeter model WTW-550IR. The content of copper was measured using ICP-MS PerkinElmer NexION 1000, and the content of iron was measured using ICP-OES Spectro Arcos. In 2023 the pH value of the water of Bor River was measured using pH meter Thermo Scientific PC 450.

### 3. RESULTS AND DISCUSSION

One of the first, if not the first results of the chemical analysis of Bor River from 1931 are shown in Table 1 [1]. The sampling and analysis were carried out by the Agricultural Experimental and Control Station in Topčider, Belgrade, the institution from which the contemporary Institute of Soil Science in Belgrade, Serbia was developed. Another set of valuable water quality data was published in 1935, and presented in Table 2 [2]. The analysis was carried out in the laboratory that belonged to the mine in Bor.

Table 1 - Results of the chemical analysis of Bor River from 1931 [1]

Parameter	Unit	Bor River upstream from the mine	Bor River downstream from the mine	Bor River near the Village Slatina
Alkalinity (+) or Acidity (-) as CaCO <sub>3</sub>	mg/L CaCO <sub>3</sub>	+109	-171	-105
Copper, Cu	mg/L	not detected	71	48
Sulfate, SO <sub>4</sub> <sup>2-</sup>	mg/L	35	1463	831
Fe <sub>2</sub> O <sub>3</sub> + Al <sub>2</sub> O <sub>3</sub>	mg/L	not detected	370	78
Precipitate FeO + Fe <sub>2</sub> O <sub>3</sub>	mg/L	not detected	very large quant.	large quantities

Table 2 - Results of the chemical analysis of rivers around Bor mine from 1935 [2]

Parameter	Unit	I	II	III	IV	V	VI	VII
pH	-	7.5	7.1	5.7	7.5	7.7	4.5	4.3
Dry residue	mg/L	557.6	581.6	1766	651.6	1942.7	2152.6	3164.3
SiO <sub>2</sub>	mg/L	13.6	15.9	66.2	33.2	17.9	34	59.2
Al <sub>2</sub> O <sub>3</sub> + Fe <sub>2</sub> O <sub>3</sub>	mg/L	4	17	89	7	8.5	155	396.5
Al <sub>2</sub> O <sub>3</sub>	mg/L	traces	traces	41.1	traces	traces	39.2	149
Fe	mg/L	2.8	11.9	33.5	4.9	5.9	81	173.1
Ca	mg/L	110	127.0	274.2	122.1	453.3	348.2	338.8
Mg	mg/L	20.3	22.1	34.1	37.6	17.7	54	80.3
SO <sub>4</sub> <sup>2-</sup>	mg/L	204.9	267.1	1023.0	198.1	1163.3	1387.2	1884.1
Cl <sup>-</sup>	mg/L	4.6	4.7	12.5	12.8	19.6	18.7	13
Cu	mg/L	0	0	20	0	0	22	17

I Water from Bela River after passing the village of Rgotina

II Water immediately after the junction of the Krivelj River and Bor River

III Water from Bor River after passing the village of Slatina

IV Water from the Bor Stream in Bor, upstream from the flotation

V Water behind the flotation near the barrage

VI Water from Bor River after the junction with Bor Stream

VII Water from Bor River after passing the cementation

Stevanović et al. [5] analyzed the water from Robule Lake, overburden drainage, metallurgical wastewater, and Bor River each month from June 2011 to May 2012 (Table 3). The same parameters at these locations were measured in September 2021 (Table 4).

Table 3 - Minimum and maximum values of water quality parameters from June 2011 to May 2012 [5]

Parameter	Unit	Robule Lake	Overburden drainage	Metallurgical wastewater	Bor River
pH	-	2.56 – 4.20	2.88 – 5.30	1.89 – 3.62	3.26 – 5.99
SO <sub>4</sub> <sup>2-</sup>	mg/L	4604.2–10570.6	3343.4 – 4366.7	1554.2 – 5569.1	110.3 – 1234.0
Cu	mg/L	53.0 – 77.2	11.0 – 29.2	58.5 – 541	1.5 – 27.0
Fe	mg/L	526.4 – 835.6	86.6 – 190.1	214.7 – 4766	1.1 – 130.0

Table 4 - Water quality parameters in September 2021

Parameter	Unit	Robule Lake	Overburden drainage	Metallurgical wastewater	Bor River
pH	-	2.70	4.37	2.54	3.21
SO <sub>4</sub> <sup>2-</sup>	mg/L	10200	3940	6610	1630
Cu	mg/L	56.7	10.5	116.1	12.8
Fe	mg/L	554	188	932	115

The alkalinity of Bor River upstream from the mine in 1931 (Table 1) was 109 mg/L CaCO<sub>3</sub>. However, downstream from the mine, the water of Bor River was acidic, with the acidity of 171 mg/L CaCO<sub>3</sub>. Further from the mine, near the Village of Slatina, the acidity of Bor River decreased to 105 mg/L CaCO<sub>3</sub>, probably due to the dilution and reaction of water with carbonates from the river bed sediment. The acidity of Bor River near the Village of Slatina in 2016 was 842 mg/L CaCO<sub>3</sub> [6], which is about 8 times higher than the acidity in 1931.

The pH value of water of rivers and streams around Bor mine in 1935 ranged from 7.7 in water behind the flotation near the barrage, to 4.3 in water from Bor River after passing the cementation. In 2011 and 2012, the pH range of Bor River extended to more acidic values, from 3.26 to 5.99 [5]. In September 2021, the pH value of the water of Bor River was 3.21. The most recent results from May, June, and July 2023 showed that the pH value of Bor River was near neutral (7.94, 7.33, and 7.08, respectively), which is a significant improvement.

Concentrations of sulfates in Bor River downstream from the mine in 1931 were 1463 mg/L and 831 mg/L, and these values are in the same order of magnitude as the concentrations of sulfates in 1935 (1023.0-1884.1 mg/L), in 2011-2012 (110.3 – 1234.0 mg/L) and in 2021 (1630 mg/L). In contrast, the concentration of sulfates in unpolluted Bor River upstream from the mine in 1931 was 35 mg/L, which was close to the concentrations of sulfates in the unpolluted Ravna River near Bor mine in 2015 (42.2 mg/L) [3]. Therefore, the concentrations of sulfates throughout the years in the polluted and unpolluted rivers are consistent and comparable although the measurement techniques were on different levels of development.

Robule Lake was an accumulation of acid mine drainage at the edge of overburden deposits in Bor. The color of the lake was red due to the presence of dissolved ferric ions (Fe<sup>3+</sup>) and hydrous ferric oxides precipitated on the bottom of the lake (Figure 2 a). The pH value of Robule Lake was very acidic, reaching pH 2.56, and had high concentrations of sulfate (4604.2–10570.6 mg/L), iron (526.4 – 835.6 mg/L), and copper (53.0 – 77.2 mg/L) (Tables 3 and 4) [5]. Wastewater from Robule Lake flowed into the Bor River, contributing to the increase of the contaminants in river water.

However, from the year of 2022, the Robule Lake does not exist anymore because of the remediation activities conducted by Serbia Zijin Copper doo, the current owner of the mine. The place where Robule Lake used to be, as well as the slopes of overburden were covered by soil in 2022 (Figure 2 b).



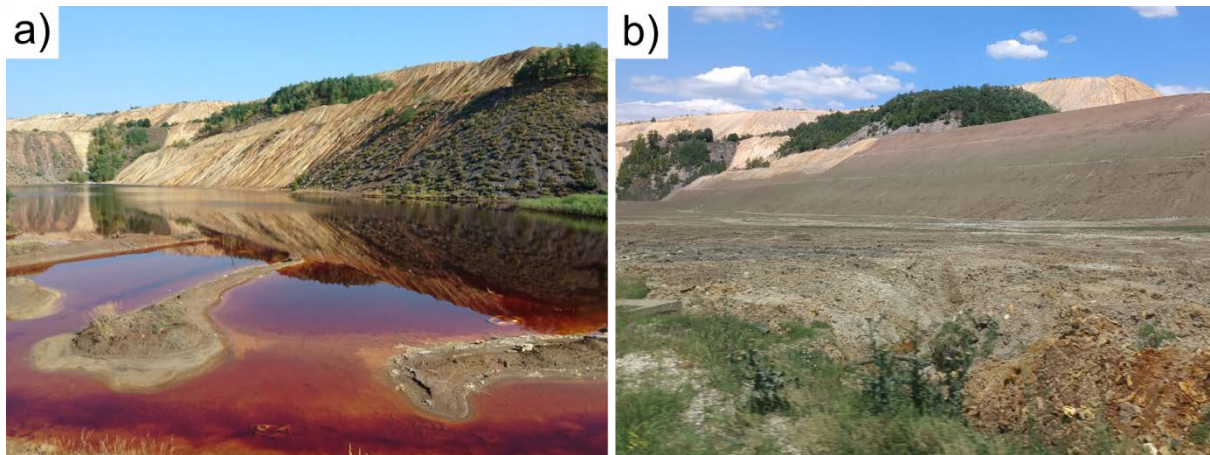


Figure 2 - Robule Lake a) 27.08.2019. b) 19.07.2022.

#### 4. CONCLUSION

The water of Bor River was acidic with increased content of sulfates, iron, and copper since 1931 when it was first recorded, or maybe even earlier, as soon as the copper ore excavation started in 1903. In 2021, the water of Bor River was still acidic, and acid mine drainage from Robule Lake was flowing into the Bor River, contributing to its pollution. However, since 2022 Robule Lake does not exist anymore, and the pH value of Bor River in 2023 was near-neutral thanks to the remediation activities of Serbia Zijin Copper doo.

#### ACKNOWLEDGEMENT

*The authors are grateful to the Ministry of Education, Science and Technological development of the Republic of Serbia for financial support according to the contract with the registration number 451-03-68/2022-14/200052.*

#### REFERENCES

- [1] B. Andrejić, Sulfuric fume from 1908. to 1935. year – archive material, Book XXVIII, Štampa, radio i film, Bor, Serbia (1983), p. 114.
- [2] B. Andrejić, Sulfuric fume from 1935. to 1941. year – archive material, Book XXIX, Štampa, radio i film, Bor, Serbia (1983), p. 161.
- [3] S. Đorđievski, D. Ishiyama, Y. Ogawa, Z. Stevanović, Environ. Sci. Poll. Res. 25 (2018) p. 25005–25019.
- [4] D. Adamovic, D. Ishiyama, S. Đorđievski, et al., Resour. Geol. 71 (2) (2021) 123–143.
- [5] Z. Stevanović, L. Obradović, R. Marković, et al., Mine Waste Water Management in the Bor Municipality in Order to Protect the Bor River Water *in* Waste Water - Treatment Technologies and Recent Analytical Developments, InTech (2013), p. 41–62.
- [6] S. Đorđievski, S. Stanković, Copper 43 (2) (2018), p. 81–90.
- [7] Unknown Author, Panorama of the surface mine in Bor, Available on: <http://www.digitalnizavicaj.org.rs/pics/fotografije/124/pics/img659.jpg>

## Investigation of the properties of Co-Cr-W and Co-Cr-Mo alloys coated with hydroxyapatite for use in dental implants

Olivera Dragutinović<sup>1</sup>, Vaso Manojlović<sup>1</sup>, Đorđe Veljović<sup>1</sup>, Stefan Dikić<sup>1</sup>, Marko Simić<sup>2</sup>

<sup>1</sup> Faculty of Technological Metallurgy, University of Belgrade

<sup>2</sup> Institute of Nuclear Sciences "Vinča" Belgrade

### Abstract

*Metal materials based on Co-Cr are characterized as alloys of base materials that are widely used in various branches of medicine and dentistry. The application of Co-Cr dental alloys is conditioned by their biocompatible, corrosive, and mechanical characteristics. When used as oral implants, they must satisfy stability and non-toxicity in a relatively aggressive environment. According to the physical-mechanical aspect, these alloys are characterized by a high modulus of elasticity, which ensures strength and rigidity, resistance to high temperatures and non-magnetism. The use of metallic biomaterials based on Co-Cr alloys in dentistry is a consequence of their low cost and adequate physical and mechanical properties. The aim of this study is the development of Co-Cr alloys with a layer of hydroxyapatite to improve its properties for use in dentistry. In this work, two Co-Cr alloys will be used, the first alloy is alloyed with W and the second with Mo. Preparation of the sample will involve metallographic preparation in the form of sanding with different paper granulations and polishing using alumina, Al<sub>2</sub>O<sub>3</sub>. The precursor solution of hydroxyapatite (HAp), which consists of particles with a molar ratio of Ca/P of 1.67, doped with magnesium ions (5 mol. %) , zinc (0.4 mol. %) and copper (0.4 mol. %), was hydrothermally synthesized for 3 h at 160 °C. The resulting solution is strained under reduced pressure, and the precipitate obtained is calcined at 1000 °C. X-ray diffraction analysis of hydroxyapatite powder showed that a partial phase transformation of hydroxyapatite into β-tricalcium phosphate (β-TCP) took place. The Co-Cr-Mo and Co-Cr-W alloy samples were polished and ground to a fineness of 3000 mesh, and then a layer of produced HA was applied to them. Scanning electron microscopy showed a uniform distribution of particles on the surface of the samples. The average microhardness values of the Co-Cr-W sample whose surface was polished was 418.7 HV1, and the values the Co-Cr-Mo sample whose surface was sanded with a fineness of 3000 mesh was 476.6 HV1.*

**Key words:** dental materials, Co-Cr-W, Co-Cr-Mo, hydroxyapatite, spray method.

### 1. INTRODUCTION

The choice of material for making implants in dentistry is very important because it must be stable and resistant to bacteriological activity as well as to erosion and wear due to chewing. [1, 2] After the tests, the conclusions were drawn that partial dentures made of metal alloys improve the retention and function of the dentures. [3] Metallic materials can possess oligodynamic and bacteriostatic effects on certain strains of microorganisms. Their potential undesirable effects can be: release of metal ions caused by corrosion, sensitization and causing allergic and immune reactions of the organism. [4, 5] The combination of different metal ions is used to improve mechanical properties (reduced tendency to corrosion and ion elution, increased strength, hardness, and biocompatibility). Co-Cr alloys are characterized by significant strength, biocompatibility, resistance to wear and corrosion, low degree of osseointegration and low price, due to these properties they are used in dental medicine to produce removable covers for partial dentures (crowns, bridges, clasps and partial dentures). [1, 2] The percentage metal content of Co-Cr alloys in the literature is as follows: 30-60% cobalt, 20-30% chromium, 0-20% nickel and less than 4% molybdenum and trace elements such as tungsten. [3] Due to the relatively large amount

of chromium in the alloy, a passive Cr<sub>2</sub>O<sub>3</sub> layer is formed on the surface, which ensures high corrosion resistance. [6]

Deposition of hydroxyapatite (HAp) on metal alloy improves surface bioactivity and corrosion resistance. Coating of the alloy with HAp takes place using several methods: plasma spraying, sputtering process, biomimetic, sol-gel method, and electrochemical deposition. [7] The biosimilarity of HAp to bone tissue can promote osteoblast and osteoclast growth as well as improve osseointegration. Inadequate mechanical properties, poor adhesion and cohesive strength make HAp unsuitable candidates for coating formation. However, these defects can lead to the appearance of cracks and separation of HAp from the surface, which is typical of implant failure. These problems can be overcome by temperature treatments and designing the interface between the HAp coating and the substrate surface. [2, 7] High sintering temperatures can result in the degradation of both the HAp and the metal substrate, leading to the formation of cracks. [2] Designing a composite material with a HAp-based coating achieves better mechanical properties and inhibits the release of metal ions. [2, 7]

## 2. EXPERIMENTAL PART

### Materials:

Commercial samples Co-Cr-W (sample 1) and Co-Cr-Mo (sample 2) were used in this work. The chemical composition of the alloys is shown in Table 1.

*Table 1. Chemical composition of alloys:*

Sample	Si, %	Cr, %	Co, %	W, %	Mo, %	Mn, %	Ni, %	Fe, %	Nb, %	Pb, %
Co-Cr-W	1.34	24.39	60.56	7.79	2.606	0.976	0.159	1.138	1.025	0.022
Co-Cr-Mo	1.10	28.48	64.27	0.080	5.338	0.302	0.230	0.172	0.007	0.020

It can be seen from the table that the samples are multi-component, and the percentage data of base metals and alloying elements of Co-Cr-W and Co-Cr-Mo alloys match the literature data.

### Preparation of samples:

Metallographic sample preparation. The first step involved polishing the samples with alumina Al<sub>2</sub>O<sub>3</sub>. Before the actual polishing process, the surface preparation of the samples followed, which involved processing the surfaces with SiC papers of 1500, 2000, 3000 grit, and then the samples were placed on a rotating device. Alumina was applied to the rotating plate, after which the surface of the samples was placed and polished for half an hour. The second step in metallographic preparation included sanding to remove all surface deformations. The samples were processed using SiC paper of different finenesses 3000, 1200, 500.

Formation of hydroxyapatite suspension and application of coating by spray method. The starting compounds for obtaining hydroxyapatite with a Ca/P molar ratio of 1.67 using the hydrothermal method are: 11.6 g calcium nitrate tetrahydrate, 10.80 g EDTA, 4.68 g sodium dihydrogen phosphate dihydrate, 12 g urea, 0.642 g magnesium - nitrate hexahydrate, 0.0484 g zinc nitrate hexahydrate and 0.0596 g copper nitrate trihydrate. The precursor solution obtained by dissolving the reactants in 1.5 l of deionized water was placed in an autoclave. Hydrothermal synthesis took place at a temperature of 160 °C, for 3 hours. After the expiration of the time, the synthesized solution was cooled for 24 hours. The precipitated powder was then pressed under reduced

pressure and washed with deionized water. The powder thus obtained was dried in an oven at 105 °C for 2 h and then crushed. The synthesized powder was calcined in a furnace at a temperature of 1000 °C, and then used to obtain a suspension. The suspension was obtained by dissolving 0.1 g of calcined powder in 10 ml of 96% alcohol, after which it was subjected to homogenization in an ultrasonic bath for 15 minutes. The homogenous HAp suspension achieved by the spray method was applied to the surface of the samples by applying a layer from a distance of 5 to 6 cm to the surface and waiting a few minutes for it to dry, the procedure was repeated two more times.

#### Characterization methods:

Microhardness-static testing of material properties was carried out on the device Buehler MicroMet Microindentation Hardness Vickers Tester, Model MicroMet 101 with an indenter in the shape of a right pyramid with a square base at an angle of 136° and a load of 500g and 1000g for 10 to 15 seconds.

X-ray diffraction analysis - the phase composition of the calcined hydroxyapatite powder was determined by X-ray diffraction analysis on a Rigaku Smartlab diffractometer using CuK $\alpha$  line radiation in the 2 $\theta$  angle range from 20 to 65 °C with a step of 0.05°.

Scanning Electron Microscopy - The microstructure of samples coated with HAp-based primer was determined by scanning electron microscopy on TESCAN MIRA 3 XMU i and FEI Thermo Scios 2 devices. Sample preparation for SEM analysis involved placing the sample on supports via adhesive graphite tape, and then sputtering with a gold alloy.

### 3. RESULTS

X-ray diffraction analysis of the calcined hydroxyapatite powder with a Ca/P molar ratio of 1.67 showed a biphasic structure in which HAp and  $\beta$ -tricalcium phosphate ( $\beta$ -TCP) were identified as shown in Figure 1.

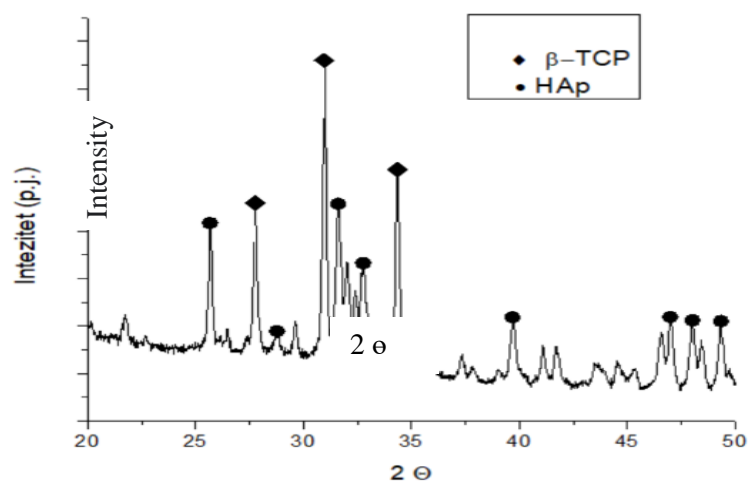


Figure 1 - X-ray diffractogram of calcined hydroxyapatite powder

The located peaks of  $\beta$ -TCP were formed by a partial phase transformation from HAp, where  $\beta$ -TCP is the more dominant phase.

The measurement was performed during multiple repetitions to obtain relevant results. Mean value and standard deviation of samples Co-Cr-Mo (p) (polished), Co-Cr-W (p) (polished), Co-Cr-Mo (3000) (grounded with SiC paper fineness 3000), Co-Cr- W (3000) (ground with SiC paper of fineness 3000) obtained at a load of 1000 g (HV 1) are shown in Table 2. The obtained values were determined according to Vickers.

Table 1 - Presentation of the mean value and standard deviation of the samples:

<i>Sample</i>	<i>HV 1</i>
<i>Co-Cr-Mo (p)</i>	400.5±49
<i>Co-Cr-W (p)</i>	418.7±59.4
<i>Co-Cr-Mo (3000)</i>	467.6±31.4
<i>Co-Cr-W (3000)</i>	388.1±37.7

The microhardness values can be compared, which leads to the conclusion that the highest value is 467.6 HV observed for the Co-Cr-Mo (3000) alloy coated with HAp particles at the load conditions of 1000 g.

The results of scanning electron microscopy of the surface of Co-Cr-Mo and Co-Cr-W samples coated with calcined hydroxyapatite powder are shown in Figure 2.

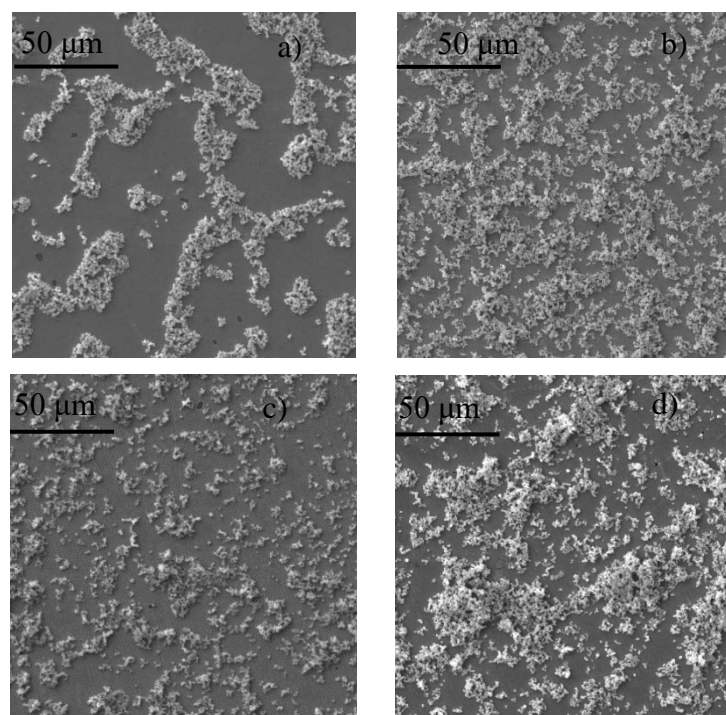


Figure 2 - Micrograph of samples a) polished Co-Cr-Mo sample, b) polished Co-Cr-W sample, c) Co-Cr-Mo sample polished with SiC paper fineness 3000 and d) Co-Cr-W sample polished with SiC 3000 fineness paper

The micrographs indicate a uniform distribution of spherically grouped grain-structured particles on the surface of the samples, with the better coverage being noticeable in both samples sanded with SiC paper with a grain size of 3000, and the best coverage observed in both the polished and sanded Co-Cr-W samples.

#### 4. CONCLUSION

In this study, we examined the microhardness and surface coverage of different Co-Cr alloys obtained in different ways for use in dental medicine. X-ray diffraction analysis of the calcined powder showed the phase transformation of HAp into  $\beta$ -TCP. The values of microhardness in the case of the Co-Cr-W sample increase with the change of sample preparation (400.5 HV1 when the sample was polished, and 467.6 HV1 when the sample was ground with SiC paper of fineness

3000), however, the opposite is true for the Co-Cr-Mo sample, the values decrease with different sample preparations (418.7 HV1 polished sample, 388.1 HV1 if sample prepared by grinding). The micrographs showed a better homogeneous distribution of HAp grains on the surface of the Co-Cr alloyed W samples obtained by both methods.

## REFERENCE

- [1] A. Cerek, L. Slokar Banić, V. Bubalo, Metal Ions Release from Welded Co-Cr Dental Alloys, *Materials*, 16 (9), (2023), 3398.
- [2] M. Rezazadeh Shirdar, I. Sudin, M. Mahdi Taheri, A. Keyvanfar, M. Zamri Mohd Yusop, M. Rafiq Abdul kadir, A novel hydroxyapatite composite reinforced with titanium nanotubes coated on CoCr-based alloy, *Vacuum*, (122), (2015), 82-89.
- [3] A. Carek, Lj. Slokar Benić, D. Buković, M. Šlaj, Investigation of Laser-Welded Co-Cr Dental Alloys by Microscopy and Mechanical Testing, *Metals* (13), (2023), 1323.
- [4] A. Yu. Turkina, I. M. Makeeva, O. N. Dubinin, J. V. Bondareva, D. A. Chernodubov, A. A. Shibalova, A. V. Arzukanyan, A. A. Antoshin, P. S. Timashev, S. A. Evlashin, The Impact of Commercially Available Dry Mouth Products on the Corrosion Resistance of Common Dental Alloys, *Materials*, (16), (2023), 4195.
- [5] B. Grosgeat, A. Vaicelyte, R. Gauthier, Ch. Janssen, Marc Le Borgne, Toxicological Risks of the Cobalt–Chromium Alloys in Dentistry: A Systematic Review, *Materials*, (15), (2022), 5801.
- [6] A. Findrik Balogová, V. Rajt'úková, L'uboš Chromý, A. Somoš, Gabriela Ižaríková, R. Hudák Biomechanical Testing of Two-Unit Bridges and a Comparison of Replacement Retention Depending on a Cementation Medium, Replacement Position, and Gap Size, *Functional biomaterials*, (13), (2022), 286.
- [7] H. Mas Ayu, S. Izman, R. Daud, G. Krishnamurithy, A. Shah, S.H. Tomadi, M.S.Salwanim, Surface Modification on CoCrMo Alloy to Improve the Adhesion Strength of Hydroxyapatite Coating, *Procedia Engineering*, (184), 399-408.



## ABOUT THE “RELATIVE PLASTICITY” BETWEEN STEEL MATRIX AND NON-METALLIC INCLUSIONS

Zoran Karastojković<sup>1</sup>, Dragoslav Gusković<sup>2</sup>, Ognjen Ristić<sup>3</sup>, Zorica Kovačević<sup>3</sup>

<sup>1</sup> Society for ethics and evaluation in culture and science, 11000 Belgrade, Strahinjića bana 27, Serbia

<sup>2</sup> Technical faculty, University of Belgrade, 19210 Bor, Vojske Jugoslavije 12, Serbia

<sup>3</sup> Institute for testing of materials, 11000 Belgrade, blvd. v. Mišića 43, Serbia

### Abstract

*It is clearly established in metallurgy, also in service of machine elements or components, that non-metallic inclusions are not desired into metals, either they are ferrous or nonferrous. One of the main factor for such conclusion is in markably decreasing the plasticity with increasing an amount of the non-metallic content. Non-metallic inclusions were classified according to its nature, shape and dimensions, as many national standards were defined those properties. Sometimes is not simple to make a fully definition of the plasticity, as a property important both for cold or hot deformation processes, because many factors must be involved at the same time. One attempt for judging the plasticity of a steel was made by using a “relatively plasticity”.*

**Keywords:** *elasticity, plasticity, non-metallic inclusions, relatively plasticity of steel*

### 1. INTRODUCTION

Many efforts in mechanics and engineering, over a centuries, were made on defining what are elastic and/or plastic deformations. According to complex composition of many steels, it is not simple task for defining an unique value for plastic behaviour for every steel, and must be done for every steel particularly and for every method of deformation (forging, rolling, drawing, etc.). Such approach is, however, valuable and reliable, but require a huge (experimental) job.

In metallurgy, of course in materials science and engineering, the yield point is defined as the point on a stress-strain curve that indicates the limit of elastic behavior and the beginning of plastic behavior. So, below the yield point, a material will deforms elastically and behind this point the deformation is provided on irreversible manner, it means plastically. It looks like very simple, but in situations when different loads acting, it is not.

On many properties of a metal, including a plasticity, in real circumstances an important role play the content and shape of non-metallic inclusions. The origin of non-metallic inclusions in final metal product is in mineralogical nature of used ore(s) and materials. Great amount of non-metallic inclusions came from the ores, smaller part of them came from the refractory lining from metallurgical furnaces (blast furnace, converters, ladles, used fluxes, etc.),

These non-metallic inclusions practically are not soluble into the metal but show the great influence practically on every property [1-4]. The shape and dimensions of non-metallic inclusions were defined through many national standards [5,6] according to four main groups, and their influence on properties is analyzed and controlled [7,8], but one interesting approach was made when plasticity is considered as a ration between of the true strain of the inclusion and true strain of the steel matrix, and this ratio is called the “relative plasticity” [10].

Here will be analyzed the usiness of such approach.

## 2. ORIGIN, DIMEIONS AND SHAPE OF NON-METALLIC INCLUSIONS IN STEELS

Great amount of non-metallic inclusions came from the ores, smaller part from the refractory lining at metallurgical furnaces (blast furnace, converters, ladles, used fluxes, etc.), used materials during treating of molten metal, as shown in Fig. 1.

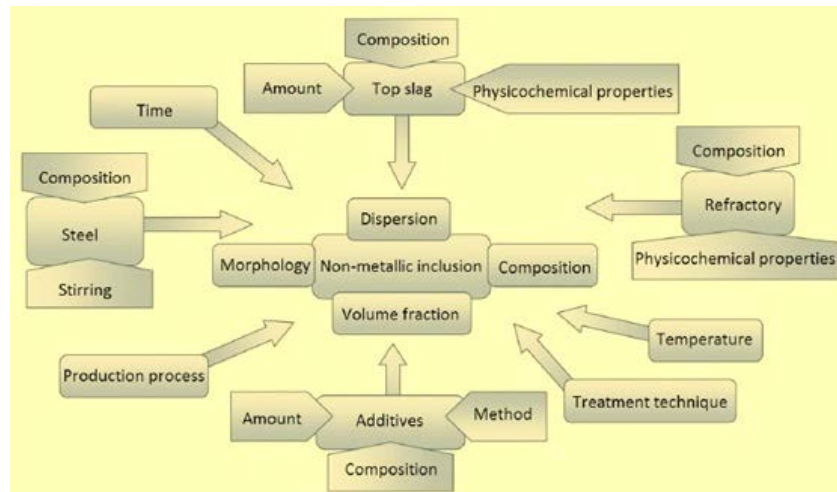


Figure 1 - Scheme of influences on formation of non-metallic inclusions

There is always an intention for removing the non-metallic inclusions from a melt.

In producing&controlling the qualitative steels is well established and wide accepted, through many national standards, the scale for assesment the amount and shapes of non-metallic inclusions, according to four main types (sulphide, globular oxide, silicate and alumina). Non-metallic inclusions are deformed, however, at cold and hot processing. Chemical composition of non-metallic always is complex, one example of their many groups is given in Fig. 2a), as a part of ternery diagram with oxides.

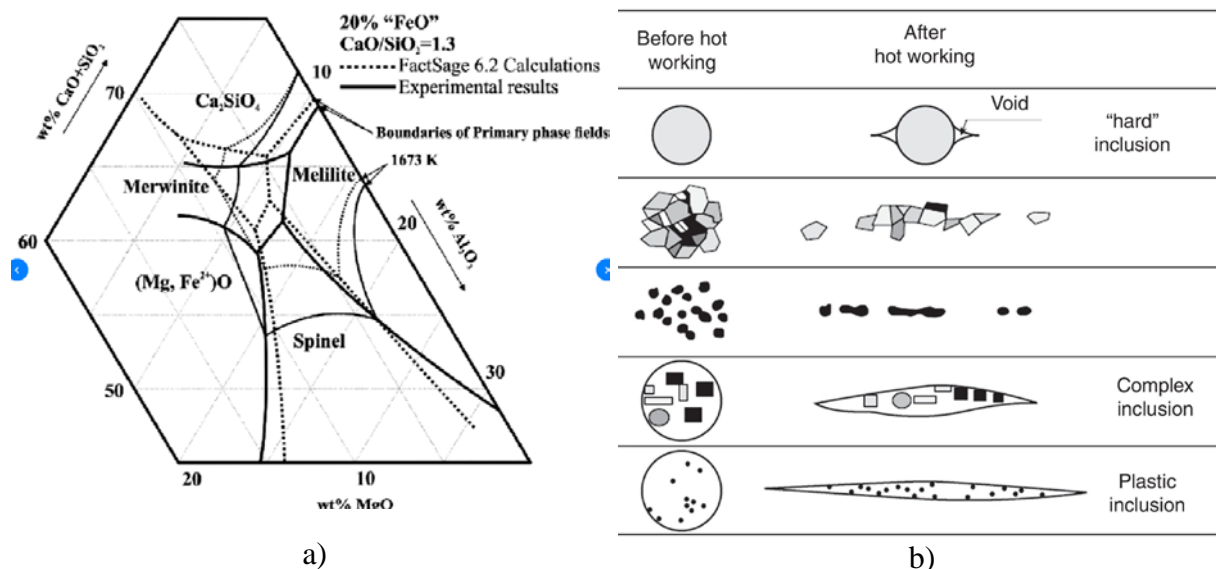


Figure 2 - a) Part of diagram MgO-CaO+SiO<sub>2</sub>-Al<sub>2</sub>O<sub>3</sub> and b) shapes of non-metallic inclusions before and after hot deformation [15]

In reality, the non-metallic inclusions. however, are not limited on oxide types, but on very complex compounds from groups of: silicates, suphates, sulfides, etc. Shapes of non-metallic inclusion before deformation almost are irregular, and after deformation is finished they became

broken, in Fig. 2b) is presented after hot rolling. Non-metallic inclusions also are crushing during cold deformation, no matter the kind of metal working process is applied.

### 3. CONCEPT OF „RELATIVELY PLASTICITY“ IN STEELS

Property of plasticity is pretty complex, depends far away from the circumstances during casting, solidification (dendrite grow) and farther the regime of metal working process. Plasticity [10] „describes the state of stress and strain or strain rate in these bodies under the influence of a given load or deformation”, (underlined by Zoran Karastojković). Well, the load (force) actually has the influence on metal flow/plasticity, but deformation (no matter elastic or plastic) is just the consequence of an acting the load, so the deformation could not be the reason for the appearance the plasticity. The force creates the deformation, i.e. the deformation is self induced it is always from internal stresses or weight of a body.

It is well known that the plasticity of any metal strongly depends from a temperature, but there are other numerous important factors as: composition of an alloy, deformation degree shedule, stress state, strengthening or softening mechanisms, speed of tool moving (in some deformation processes), strain rate, strength of matrix and non-metallic inclusions, and others.

Concept of “relatively plasticity” [10] is established on rather simple manner, eq. 1, and with an improved version as like by eq. 2.

$$v = \varepsilon_i / \varepsilon_m \quad (1)$$

where:  $\varepsilon_i$  is the true strain of the inclusion and  $\varepsilon_m$  is the true strain of the steel matrix

$$v = \frac{\varepsilon_i}{\varepsilon_m} = \frac{(\ln \lambda - \ln \lambda_0) / 2}{\ln \frac{h_0}{h}} \quad (2)$$

where:  $\lambda_0$  and  $\lambda$  are the aspect ratio of an elliptic inclusion before and after rolling.

If inclusions are cylindrical and in the case of plane strain rolling of the steel plate, than the expression from eq. 2. may be used [10]. For applying both equations for cases from crushed non-metallic inclusions given in Fig. 2b), is needed an excese time, always with pretty limited results. At those equations never are included data about strength and/or plasticity of non-metallic inclusions. So, the plasticity, here in steel plate, could not be explained only by geometrical factors about the presence of non-metallic inclusions [16].

The serious analyse in proposed approach needs the constantation that during rolling of (steel) plate exists plane strain, because according, to the rolling theory, in the rolling zone rather exists three stress state.

It should be underlined that temperature dependance of plasticity od any non-metallic inclusions always represents a serious problem. On fatigue strength, also [17]

### 4. CONCLUSIONS

It is clear that the plasticity of metal/alloy is complex in their nature, and in great deal is determined by the presence of non-metallic inclusions in the structure, no matter on the way of applied metal working process, i.e. plastic deformation. The “relative plasticity” here is mentioned in rolling, but the problem of plasticity, however, exists at all methods of deformation.

The plasticity during rolling of steel plate could not be reduced only on the ratio between geometrical dimensions of non-metallic inslusions, as proposed by [10], even the logarithmic deformations are included into account. Crushing of non-metallic inclusions, as like in Fig. 2b), made a proposed manner for calculation the plasticity more problematic and less usable. For all main groups of non-metallic inclusions (sulphide, globular oxide, silicate and/or alumina) such

approach is just unavailable. The main attention must be paid on the metallurgical treatment during refining of molten metal, further for crystallization effects, obtained structure during casting, and related metallurgical factors.

The effects of microalloying were not included in this analyze. so this fact does not represents an advantage, just contrary.

## REFERENCES

- [1] H. Šuman: Metalografija, in Serbian, Belgrade 1965, Zavod za izdavanje udžbenika Srbije, p. 320-330.
- [2] Yu.A. Geller, A.G. Rakhstadt: Science of materials, Moscow 1987, Mir Publ.
- [3] M. I. Vinograd, G.I. Gromova: Vključenija v legirovannih staljah, in Russian, Moscow 1972, Metallurgija
- [4] R. Ćurčić: Identifikacija nemetalnih uključaka u ugljeničnom čeliku za teške otkovke, in Serbian, magistarski rad, Univerzitet u Sarajevu, Metalurški fakultet u Zenici, Zenica 1979.g.
- [5] ASTM E45/2007: Standard test methods for determining the inclusion content of steel
- [6] SRPS CA4.013-1987: Mikroskopska metoda određivanja sadržaja nemetalnih uključaka u čeliku korišćenjem referentnih slika, in Serbian
- [7] O.T. Bruhns in *History of plasticity*, Enciclopedia of Continuum mechanics, p. 1-61.
- [8] C. Mapelli: Non-metallic inclusions and clean steel, La metalurgia italiana, 2008, str. 43-52.
- [9] O.T. Bruhns: History of plasticity, Enciclopedia of Continuum mechanics, p. 1-61.
- [10] T. Malkiewicz, S. Rudnik, J. Iron Steel Inst. 201/1963/, p. 33-38.
- [11] A.L. Vasconcellos da Costa e Silva, J. Mater. Res. Technol., 3/2018, str. 283-299.
- [12] G. Keller, W. Weiss, W. Ranke, R. Schlögl: Bulk and surface phases of iron oxides in oxygen and water atmosphere at low pressure, Physical Chemistry Chemical Physics, 3/2001/1114-1122.
- [13] Z. Karastojković, R. Perić: Nerdjajući čelici, In Serbian, Beograd 2021, Industrijsko društvo za koroziju-Beograd i „Perić&Perić“ Požarevac
- [14] H. Tanei, Y. Kondo: Phase transformation of oxide scale and its control, Nippon steel&Sumitomo metal technical report, No 111, march 2016.
- [15] Ch. Luo: Doctoral Thesis, Royal institute of Technology, Skockholm 2001.
- [16] G.I. Beljčenko, S.I. Gubenko: Osnovi metalografii i plastičeskoj deformaciji stalji, in Russian, Kiev-Donjeck 1987, Višća škola
- [17] T. Lipinski, Appl. Sci. 2022, 12. 9292, <http://doi.org/10.3390/app12189292>

## MODIFIED HYBRID CELLULOSE MEMBRANE FOR NICKEL(II) IONS REMOVAL FROM INDUSTRIAL WASTEWATER

Aleksandar Jovanović<sup>1</sup>, Mladen Bugarčić<sup>1</sup>, Milena Milošević<sup>2</sup>, Marija Vuksanović<sup>3</sup>,  
Muna Abdualatif Abdurahman<sup>4,5</sup>, Miroslav Sokić<sup>1</sup>, Aleksandar Marinković<sup>4</sup>

<sup>1</sup>Institute for Technology of Nuclear and Other Mineral Raw Materials, Boulevard Franš d Eperea 86, 11000 Belgrade, Serbia

<sup>2</sup>University of Belgrade, Institute of Chemistry, Technology, Metallurgy - National Institute of the Republic of Serbia, Njegoševa 12, 11000 Belgrade, Serbia

<sup>3</sup>University of Belgrade, "VINČA" Institute of Nuclear Sciences - National Institute of the Republic of Serbia, Mike Petrovića Alasa 12-14, 11351 Belgrade, Serbia

<sup>4</sup>University of Belgrade, Faculty of Technology and Metallurgy, Karnegijeva 4, 11120 Belgrade, Serbia

<sup>5</sup>University of Sabratha, Department of Biology, Faculty of Science, Sabratha, Libya

### Abstract

Nickel pollution of water induces several problems for the environment. The purpose of this paper was to investigate the adsorption of Ni<sup>2+</sup> ions on fabricated biomembranes. The proposed adsorbent was prepared from epoxy and amino-functionalized waste cellulose fibers, able to participate in cross-linking with amino acid lysine - wCell/Mn-Fe\_LDH. The prepared material underwent preliminary structural characterization by Fourier-transform infrared spectroscopy. In a batch system, the influence of pH, contact time, temperature, and initial concentration on adsorption efficiency was investigated. The effectiveness of the membrane was demonstrated by acceptable adsorption capacities of 40.49 mg g<sup>-1</sup> obtained for Ni<sup>2+</sup> at 45°C. The kinetic study, using the Weber-Morris model, indicates intraparticle diffusion as the rate limiting step. Adsorption mechanism physisorption was proposed based on thermodynamic behaviors. The outcomes demonstrated that environmentally friendly sustainable technology has been successfully developed.

**Keywords:** water treatment, wCell/Mn-Fe\_LDH, adsorption, environmental engineering.

### 1. INTRODUCTION

The total environment, including the air, water, and soil, is widely distributed with a transition element nickel. Nickel might originate from both anthropogenic activity and natural sources. Industries, the use of liquid and solid fuels, as well as municipal and industrial waste, may all contribute to nickel contamination of the environment. Consequently, exposure to nickel can have several adverse effects on people, including allergies, kidney and heart problems [1]. Although it can exist in some oxidative states, the +2 oxidation state (Ni<sup>2+</sup>) is the most prevalent [1]. Water pollution by nickel under the special attention of researchers.

Treatment of wastewaters can be performed by utilizing different processes like photocatalysis [2], adsorption [3], electrochemical oxidation [4] and so on. Among them, adsorption poses the most viable and economical way to solve problems in this area. Various materials are employed during different probes, but hybrid (combination of organic/inorganic) materials show the best results. Due to their numerous uses in catalysis, energy conversion and storage, medicine delivery, environmental cleanup, and carbon dioxide preservation, layered double hydroxides (LDH) are a diverse class of materials [5]. On the other hand, one of nature's most plentiful and eco-friendly polymers is cellulose [6]. Crude cellulose exhibits a poor level of adsorption ability. Because of

this, it has been common practice to chemically or physically modify cellulose to increase its capacity to bind heavy metals [7]. A combination of LDH and cellulose derivates can be the solution for before mentioned issues.

The main objective of the present study was to develop a novel wCell/Mn-Fe\_LDH adsorbent with high affinity toward metal ions (+2 oxidation state). Determination of the ability to remove Ni(II) as a model pollutant by varying process conditions, during adsorption tests, was performed.

## 2. EXPERIMENTAL

### 2.1 Synthesis of biobased membrane

All acquired chemicals for synthesis were p. a. grade without needing further purification (all obtained from Merck). Preparation of membranes was done according to Perendija et al. [1] with deposition of Mn-Fe\_LDH [8] onto the surface of wCells.

### 2.2 Structural characterization

Preliminary structural properties (the presence of organic and inorganic bond in materials) were obtained by Fourier-transform infrared spectroscopy (FTIR). FTIR spectra were collected with a Nicolet™ iS™ 10 FT-IR Spectrometer (Thermo Fisher SCIENTIFIC) with Smart iTR™ Attenuated Total Reflectance (ATR) Sampling accessories. The spectra were recorded in the range 4000-500 cm<sup>-1</sup>, in 20 scans mode, and at a resolution of 4 cm<sup>-1</sup>.

### 2.3 Adsorption experiments

Adsorption tests were carried out by adding 1, 2, 3, 4, 5, 7.5, and 10 mg of adsorbent to an 8 cm<sup>3</sup> vial of standard Ni<sup>2+</sup> solutions with C<sub>i</sub> = 7.55 mg dm<sup>-3</sup>. Adsorptions were conducted at 25, 35, and 45 °C and pH 7. Atomic absorption spectrometry (AAS) was used to determine the amounts of Ni<sup>2+</sup> ions (Perkin Elmer AAnalyst 300). Similar to the equilibrium study, the kinetic study was carried out by altering the contact time: 1, 5, 15, 30, 45, 60, 75, and 90 minutes at 25, 35, and 45 °C.

Using Eq. (1), the adsorption capacity was determined:

$$q = \frac{(C_i - C_f)}{m} V \quad (1)$$

where  $q$  is the adsorption capacity in mg g<sup>-1</sup>,  $C_i$  and  $C_f$  are the initial and final concentrations of ions in the solution in mg dm<sup>-3</sup>,  $V$  is the volume of solution in dm<sup>-3</sup>, and  $m$  is the mass of the adsorbent in g.

## 3. RESULTS AND DISCUSSION

### 3.1 Structural characterization of prepared material

Preliminary structural characterization of fabricated material is presented in Figure 1. ATR-FTIR scans of precursors and finally obtained membrane are depicted together in Figure 1.



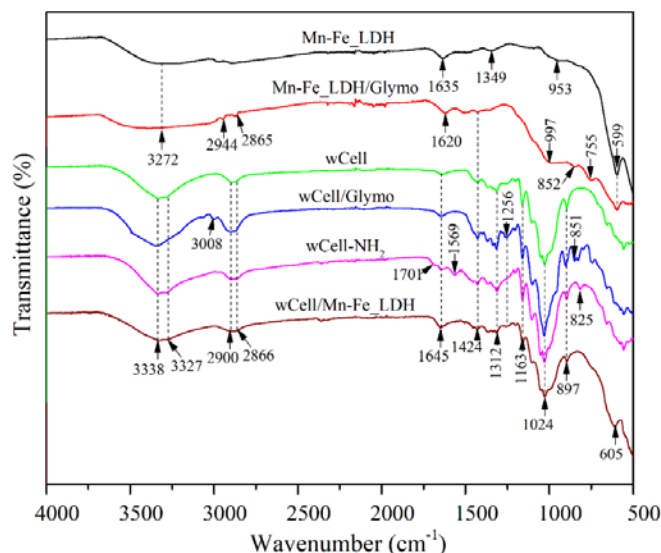


Figure 1 - FTIR spectra of membrane constituents and wCell/Mn-Fe\_LDH membrane

The wCell/Mn-Fe\_LDH membrane's FTIR spectrum shows the existence of all constituent functionalities that were included during cross-linking and Mn-Fe\_LDH deposition. A peak at 605 cm<sup>-1</sup> confirms that Mn-Fe\_LDH successfully covered the surface.

### 3.2 Adsorption results

Removal of Ni<sup>2+</sup> ions from water solution was described by the Langmuir model. Results in Table 2 for Ni<sup>2+</sup> demonstrate that  $q_m$  decreases as temperature rises. The strong connections between the functional groups on the adsorbent surface and the adsorbate were shown by the high values of the Langmuir constant ( $K_L$ ), which measures adsorption affinity.

Table 1 - The results of non-linear fitting using Langmuir isotherm for Ni<sup>2+</sup> adsorption onto wCell/Mn-Fe\_LDH membrane

Langmuir model	$T$ (°C)	$q_m$ (mg g <sup>-1</sup> )	$K_L$ (dm <sup>3</sup> mg <sup>-1</sup> )	$K_L$ (dm <sup>3</sup> mol <sup>-1</sup> )	$R^2$
Ni <sup>2+</sup>	25	42.68±1.45	6.289±0.097	369120.2±5693.2	0.999
	35	41.68±1.54	5.538±0.10	325017.5±5927.5	0.998
	45	40.49±1.64	4.775±0.11	280273.9±6339.2	0.999

Thermodynamic parameters are shown in Table 2.

Table 2 - Calculated thermodynamic parameters for Ni<sup>2+</sup> adsorption onto wCell/Mn-Fe\_LDH membrane

$T$ (K)	$\Delta G^\ominus$ (kJ mol <sup>-1</sup> )			$\Delta H^\ominus$ (kJ mol <sup>-1</sup> )	$\Delta S^\ominus$ (J mol <sup>-1</sup> K <sup>-1</sup> )	$R^2$
	298	308	318			
	-41.73	-42.81	-43.80	-10.85	103.63	0.996

At all temperatures, negative Gibbs free energy ( $\Delta G^\ominus$ ) values demonstrate the spontaneity of adsorption onto wCell/Mn-Fe\_LDH (Table 2). The exothermic nature of the whole process is mirrored by lower energy Ni<sup>2+</sup> electrostatic interactions with surface functions, on the other hand. The increasing randomness of the entire system at the established equilibrium state and the high survivability of the examined processes are both indicated by positive entropy change ( $\Delta S^\ominus$ ).

Table 3 - PSO model parameters and activation energy ( $E_a$ ) for the adsorption of  $Ni^{2+}$  ions onto wCell/Mn-Fe\_LDH membrane at 25, 35, and 45 °C

<i>Ion</i>	<i>T</i> (°C)	$q_e$ (mg g <sup>-1</sup> )	$k_2$ (g (mg min) <sup>-1</sup> )	$R^2$	$E_a$ (kJ mol <sup>-1</sup> )
$Ni^{2+}$	25	52.22±1.34	0.00190±0.00052	0.997	21.26
	35	50.33±1.22	0.00246±0.00048	0.998	
	45	48.59±0.99	0.00325±0.00018	0.999	

The diffusion-controlled processes i.e., ion exchange/complexation are characteristic for the values of  $E_a$  between 8 and 40 kJ mol<sup>-1</sup> [9] and according to the results from Table 3, the diffusion is a rate-controlling step.

#### 4. CONCLUSION

FTIR analysis of obtained composite membrane wCell/Mn-Fe\_LDH showed the presence of functionalities that enable very high adsorption affinity towards cation species. Correlating the equilibrium adsorption results with Langmuir adsorption isotherm model give fine fitting results, and these experiments also showed that adsorption process is exothermic and spontaneous. Kinetics of adsorption process showed that process is in higher order of reaction (third order or higher) which is expected for such kind of materials (composites with complex chemical structure). Performing continuous measurements of adsorption capacity as a function of contact time on different temperatures provided the data needed to determine activation energy of the adsorption process. Obtained value of only 21.26 kJ mol<sup>-1</sup> indicate that adsorption process is very fast due to very low activation energy barrier. In current study we utilized this membrane as an adsorbent of nickel (II) ions and the results we obtained showed that this composite membrane may be perspective choice for cation pollutants diminution.

#### ACKNOWLEDGEMENTS

*This work was funded by the Ministry of Science, Technological Development and Innovation of the Republic of Serbia (Contract No. 451-03-47/2023-01/200023; 451-03-47/2023-01/200026; 451-03-9/2023-14/200017; 451-03-47/2023-01/200135).*

#### REFERENCES

- [1] G. Genchi, A. Carocci, G. Lauria, M.S. Sinicropi, A. Catalano., *Int. J. Environ. Res. Public Health*. 17 (3) (2020) 679.
- [2] A. Jovanović, M. Stevanović, T. Barudžija, I. Cvijetić, S. Lazarević, A. Tomašević, A. Marinković., *Process Saf. Environ. Prot.*, 178 (2023) 423-443.
- [3] M. Bugarčić, Z. Lopičić, T. Šošarić, A. Marinković, J.D. Rusmirovic, D. Milošević, M. Milivojević., *J. Environ. Chem. Eng.*, 9 (2021) 106020.
- [4] P. Brosler, A. V. Girão, R.F. Silva, J. Tedim, F.J. Oliveira., *Environments*, 10 (2) (2023) 15.
- [5] S. Daniel, S. Thomas., *Layered Double Hydroxide Polymer Nanocomposites*, Woodhead Publishing, Duxford, 2020, p. 677.
- [6] J. Perendija, Z.S. Veličković, I. Cvijetić, S. Lević, A.D. Marinković, M. Milošević, A. Onjia., *Process Saf. Environ. Prot.* 147 (2021) 609-625.
- [7] A. Liu, S. He, J. Zhang, J. Liu, W. Shao, *Mater. Chem. Phys.* 296 (2023) 127261.
- [8] M. Abbasi, M.M. Sabzehmeidani, M. Ghaedi, R. Jannesar, A. Shokrollahi., *Appl. Clay Sci.* 203 (2021) 105946.
- [9] V.J. Inglezakis, A.A. Zorpas., *Desalination Water. Treat.* 39 (2012) 149-157.

## STRUCTURAL INVESTIGATION VIA SEM ANALYSIS OF SILICA HYBRID MATERIALS

**Elena Todorova, Nadezhda Kazakova, Georgi Chernev**

University of Chemical Technology and Metallurgy, bul. Kliment Ohridski 8, Sofia, Bulgaria

### **Abstract**

*A new field in the sol-gel technology is the synthesis of hybrid materials simultaneously containing organic and inorganic components. Such kind of materials are subject of intensively investigations because they represent significant interest for the structural chemistry and for studying their physics and chemical properties and possibilities for their applications in electronics, optics, microbiology, medicine, dentistry and pharmacology. In the present work have been described and discussed the research results on sol-gel synthesis and structure of hybrid materials. The structure of obtained hybrid nanomaterials has been studied by SEM.*

**Keywords:** *hybrid materials, sol-gel, low temperature, structure*

### **1. INTRODUCTION**

Synthesis of hybrid materials is a continuous process for development the optimal characteristics, behavior, or structure. The hybrid material combines different raw components into a complex network, as the variation of one of these components or all could lead to products with exceptional properties. Based on our knowledge about hybrid material we can conclude that the most widespread of hybrid materials are with amorphous structure. Another famous fact is that the silica network is the most convenient structure [1-3]. The silica structure is characterized with higher strength and long-term stability, but does not show a huge variety of applications without modification. Our previous work is based on investigation of silica materials, as well as their potential interaction with organic components. Our major purpose is to develop hybrid material with stable and functional/applicable behavior. For this research we decided to investigate the influence of chitosan and methacrylic acid on the silica network. Chitosan in the form of solution is a sensitive organic material, which contains into its structure – free end  $\text{NH}^3^+$  and -OH groups. These groups play a role of free reactive centers, which can easily connect with other components or free molecules/ions. Seong-Bae Park et al. [4] synthesized silica hybrid materials with participation of chitosan. Their main goal is to develop of hybrid membrane, which will be pH sensitive and allows to combine with different drugs forms. Another researcher [5-8] also synthesized hybrid materials – based on silica and chitosan and proved their potential application a adsorbent of pollutants. The modification of the silica network with organic – natural and synthetic organic components allow to vary the structural characteristics and potential application of our hybrids. In this article – we will be presented what is the influence on structure of the type and quantity of chitosan and methacrylic acid on the silica structure and what will be the benefits of the obtained hybrid materials [9].

In this article – we will presented what is the influence on structure (investigated via SEM microscope) of the type and quantity of the chitosan and methacrylic acid on the silica structure and what will be the benefits of the obtained hybrid materials.

## 2. EXPERIMENTAL

### Materials

Tetraethyl orthosilicate (TEOS, 98%, Sigma Aldrich), chitosan (CS, degree of deacetylation 75% - 85%, Fluka), methacrylic acid (MA, Fluka), dH<sub>2</sub>O, HCl (37%, Merck) and acetic acid (99%, Sigma Aldrich) were the initial components for preparation of the innovative silica hybrid materials.

### Synthesis

The silica network – the base of our hybrid materials, as well as the organic incorporated elements are obtained via sol-gel method. The synthesis technique, which is used containing three steps:

- hydrolysis of silica precursor (TEOS) using d H<sub>2</sub>O, and HCl as a catalyst – the goal was to obtain after 1 h stirring on a magnetic stirrer – smooth silica sol. The ratio, which is used for these three components was 1/0.4/0.4

- addition of different organic components to the silica sol:

- chitosan (CS) solution (previously dissolved into 1% acetic acid)
- CS solution and MA
- CS solution and MA and phosphate buffer

The obtained hybrid sols were stirred for another 30 min, after which are poured on the plastic petri dishes. Into the dishes at an ambient condition – the sol is converting into a gel and after that into a monolith hybrid material.

## 3. RESULTS AND DISCUSSION

The samples 1 and 2 are with smooth surface, typical for the silica network. Also, when the sol-gel synthesis method is used with drying at ambient conditions – the good silica structure is easily received. The quantity of organic component in these two samples is low, for that reason holes or circle particles are not visible on the SEM micrographs. With increasing the CS quantity – see Sample 3 and Sample 4 images – a lot of articles are established. These “dots” could be associated with formation of highly reactive organic centers, which transform the silica material into highly reactive hybrid.

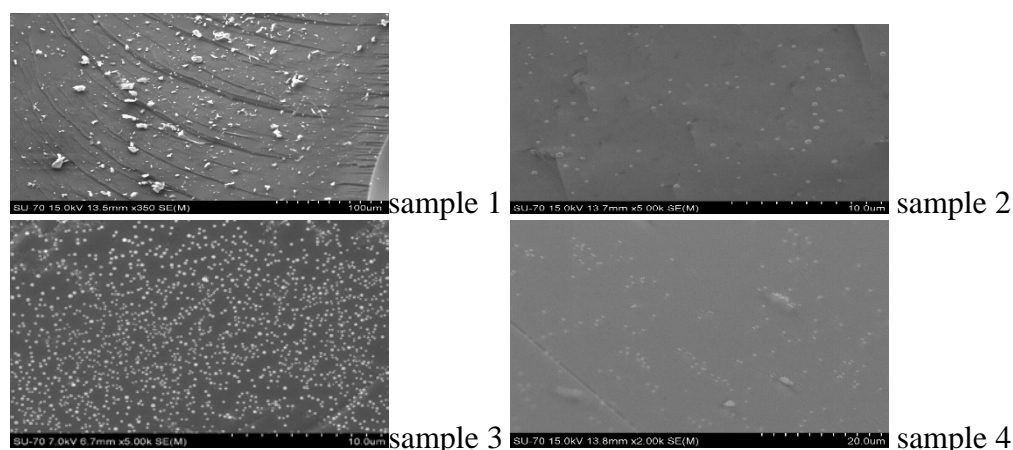


Figure 1 - SEM micrographs of silica-chitosan hybrid materials

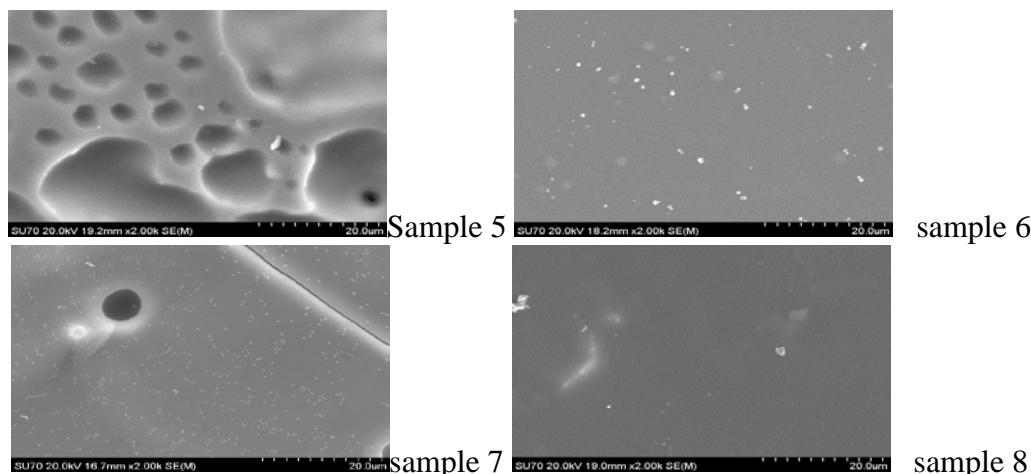


Figure 2 - SEM micrographs of silica-chitosan-MA hybrid materials

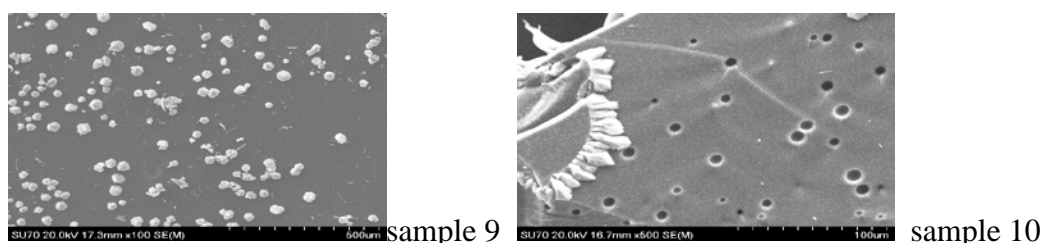


Figure 3 - SEM micrographs of silica-chitosan-MA-phosphate buffer hybrid materials

The micrographs of Sample 4 showed that when the organic and inorganic components are in equal values – nonhomogeneous structure will be formed.

The combination of chitosan + MA + silica led to formation of interesting structures, which are characterized with smooth surface + small particles (the size varies between 1 and over 20  $\mu\text{m}$ ). The SEM micrographs showed that this combination of materials contributes to formation of hybrid with improve contact surface area. The improve “open” area increases possibilities of reactions between the free reactive groups of CS and MA and external ions/molecules.

When is combined silica network with chitosan and MA into one structure in the presence of phosphate buffer interesting structural units are observed on the SEM images. The first three pictures presented “umbrella or mushroom” are visible. Their size varies around 20-40 micrometers, as below than usual (for the previous) holes are also visible. Their size between 1-3  $\mu\text{m}$ . The fourth and the fifth pictures of Sample 10 – showed presence of holes into the hybrid structure, as well as beautiful hills on the surface. This hybrid combination guarantees the structure to absorb and adsorb ions or molecules. Due to highly reactive groups from the CS and MA and the rough structure – the applications of this structure are improved for a variety of areas.

#### 4. CONCLUSIONS

Via sol-gel technique, which is based on a easily combination of different components at ambient conditions are synthesized different hybrid structures. The basic part of the hybrid structures was a silica network obtained via good combination of mixing, distilled water, and acid ratio and TEOS precursor. For improvement of application area into the silica network are incorporated two types of organic components – chitosan and methacrylic acid. The structure of the obtained hybrid materials was investigated via SEM microscope. The images that are made show the huge influence of organic nature. The chitosan materials led to formation of round particles all over the silica smooth network. The combination of chitosan and MA led to the formation of hybrid with

improved contact surface. The SEM images showed that in the correct ratio between inorganic and organic components – highly contact surface area could be obtained. As a future step – the reactivity of the end groups, as well as the potential application of the hybrid materials will be investigated.

## **ACKNOWLEDGEMENTS**

*This study has been supported by the project BG05M2OP001-1.001-0008: National Centre of Mechatronics and Clean Technologies, funded by Operational Programme for Science and Education for Smart Growth at EU Funds.*

## **REFERENCES**

- [1] Simonsen, Morten Enggrob; Søgaaard, Erik Gydesen, J. Solgel. Sci. Technol., 2010.
- [2] A.-M. Siouffi, J. Chromatogr. A, 1000 (2003) 801–818.
- [3] Ayers, Michael R.; Hunt, Arlon J.(2001). Synthesis and properties of Chitosan-silica hybrid aerogels. Lawrence Berkeley National Laboratory. Lawrence Berkeley National Laboratory: Lawrence Berkeley National Laboratory. Retrieved from: <http://escholarship.org/uc/item/2j01k588>.
- [4] Seong-Bae Park, Jin-Oh You, Ham-Yong Park, Seung Joo Haam, Woo-Sik Kim, Biomaterials 22 (2001) 323-330.
- [5] Guillermo J. Copelloa, Andrea M. Meberta, M. Raineria, Mariela P. Pesentia, Luis E. Diaz, J. Hazard. Mater. 186 (2011) 932–939.
- [6] Weitai Wu, Jing Shen, Probal Banerjee, Shuiqin Zhou, Biomaterials 31 (2010) 8371e8381.
- [7] Eveliina Repo, Jolanta K. Warchoł, Amit Bhatnagar, Mika Sillanpa, J. Colloid Interface Sci. 358 (2011) 261–267.
- [8] Yun-Kai Lv, Li-Min Wang, Lei Yang, Chen-Xi Zhao, Han-Wen Sun, J. Chromatogr. A, 1227 (2012) 48– 53.
- [9] Eveliina Repoa, Jolanta K. Warcholc, Tonni Agustiono Kurniawana, Mika E.T. Sillanpa, J. Chem. Eng. 161 (2010) 73–82.



## ATMOSPHERIC BULK DEPOSITION AS ENVIRONMENTAL QUALITY INDICATOR

Tanja Kalinović, Jelena Kalinović, Jelena Milosavljević, Ana Radojević, Snežana Šerbula

University of Belgrade, Technical Faculty in Bor, V.J. 12, 19210 Bor, Serbia

### Abstract

*Atmospheric bulk deposition (ABD) could be used as an environmental quality indicator, not only of the atmospheric but also of the soil and water resources. Contents of ABD, as well as Pb, Cd, As, and Ni in ABD were evaluated for a 10-year period (2013–2022), at four measuring sites in the urban-industrial, urban and industrial zones in the area of the City of Bor, which were under the influence of the polluting substances from the copper mining and smelting operations. The number of the measuring sites at which contents of ABD were above the Maximum Allowable Concentration (MAC) decreased over time, which was in accordance with the general decline of ABD contents, especially at the measuring sites Bolnica and Šumska sekcija. The measuring site Institut was the exception, due to the increasement of contents of the analysed polluting substances in the recent years. This could be the consequence of the wet and dry deposition of the dispersed particulates of the flotation copper concentrate, in the course of handling it and the vicinity of the road and railway transportation routes to the measuring site Institut. The implementation of the flesh smelting technology and continuous reconstructions of the copper smelter facilities have led to the general improvement of the annual air quality in the City of Bor concerning the contents of ABD and the analysed elements in ABD, but it seems that new nonstationary sources of the environmental pollution could change pollution trends in future years.*

**Keywords:** atmospheric bulk deposition, Pb, Cd, As, Ni

### 1. INTRODUCTION

Atmospheric bulk deposition (ABD) represents air polluting substances which were deposited from the atmosphere to the earth's surface through three main mechanisms: wet, dry and occult deposition [1]. Dry deposition of air polluting substances occurs as a result of several processes, but mainly through sedimentation of particulate matter with diameter greater than 10 µm. Wet deposition occurs mainly as a result of inclusion or solution of air polluting substances in raindrops and snowfall [2,3]. Occult deposition manifests through capturing the polluting substances by water droplets in the form of fog, mist, or by cloud interception [1]. Deposition of air pollutants plays a vital role in cleaning the air, but it also brings toxic elements to the receiving terrestrial and aquatic ecosystems. That is the way how deposited pollutants threaten human health through food chains, which is a key part of their biogeochemical cycles [4]. Heavy metals and metalloids in atmospheric bulk deposition are found to exhibit strong correlations with road proximity and traffic volume, as well as with significant effect of the copper smelter and many other anthropogenic sources of inorganic and organic air pollutants [5-9]. Taking this into account, it is possible to use those elements of the ABD as environmental quality indicators for quantification of the contribution of emissions to an area's environmental stress [10,11].

The aim of this study was to evaluate the contents of atmospheric bulk deposition and concentrations of Pb, Cd, As and Ni in ABD, at four measuring sites for the 10-year period (2013–2022), in the area of the City of Bor in which mining and smelting of copper sulphide ores have been performed for more than 100 years.

## 2. EXPERIMENTAL

The main anthropogenic source of the polluting substances, such as SO<sub>2</sub>, and suspended particulate matter (PM<sub>10</sub>) with high content of heavy metals and metalloids, in the study area was copper smelter of sulphide concentrates, as well as flotation tailing ponds located at the edge of the City of Bor and in the vicinity of several rural areas. The City of Bor represents the historical air pollution hotspot in South–Eastern Europe [12,13]. In order to improve production efficiency and environmental quality, the outdated technology of smelting sulphide concentrates was replaced with the flash smelting technology which was in the status of running–in during 2015 [13]. The copper smelter operated at full capacity from the beginning of 2019, while the copper smelter did not operate from April 2022 to the end of 2022, due to the reconstruction. It should be noted that in the recent years a new copper mine and copper ore flotation plant were opened in the area about 5 km in the SSE direction from the City of Bor.

Monitoring of concentrations of air polluting substances in the City of Bor during the analysed period 2013–2022, was performed by the Mining and Metallurgy Institute Bor (MMI). The monthly and annual reports are available for public on the official web site of the City of Bor [14] as well as at the web site of the Serbian Environmental Protection Agency (SEPA) [15]. Contents of atmospheric bulk deposition and concentrations of elements in ABD were determined monthly (30±2 days). The obtained values were expressed as mg/m<sup>2</sup>/day and µg/m<sup>2</sup>/day, for the ABD contents as well concentrations of elements in ABD, respectively.

Contents of atmospheric bulk deposition and Pb, Cd, As and Ni in ABD were determined in the samples from four measuring sites, 3 of which were located in the City of Bor and one near the rural area of Oštrelj. The measuring sites Bolnica and Šumska sekcija were located in the urban–industrial zone, the site Institut in the urban zone, and the site Oštrelj in the industrial zone. The measuring sites were about 1 km (Bolnica and Šumska sekcija), 2 km (Institut) and 4.5 km (Oštrelj) from the copper smelter. The dominant winds in the study area by which the polluting substances were transported from the copper smelter to the measuring sites were: NE for the Bolnica, ENE for the Šumska sekcija, NNE for the Institut and WNW for the Oštrelj measuring site.

## 3. RESULTS AND DISCUSSION

The annual ABD contents at four measuring sites for the 10-years period are given in Figure 1. It should be noted that there were 7 months of measuring (June–December) at the measuring sites Bolnica and Oštrelj during 2015, as well as 11 months of measuring (January–October and December) at the measuring site Šumska sekcija during 2021. In Figure 1, red line represents the maximum allowed concentration (MAC) for ABD (200 mg/m<sup>2</sup>/d), for the averaging period of one calendar year, according to the Regulation of the Republic of Serbia [16].

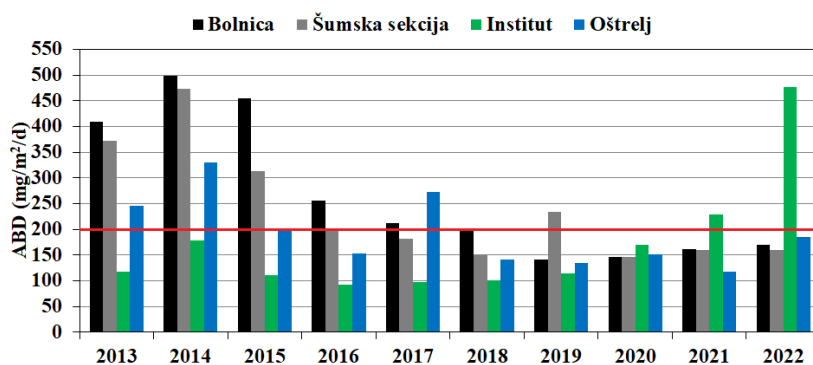


Figure 1 - Annual contents of ABD at four measuring sites during 10-year period

The exceedances of the MAC were noted at three measuring sites (Bolnica, Šumska sekcija, Oštrej) during 2013 and 2014, at two measuring sites during 2015 and 2016 (Bolnica, Šumska sekcija) and 2017 (Bolnica, Oštrej), as well as at one measuring site during: 2019 (Šumska sekcija), 2021 and 2022 (Institut). The contents of ABD at the measuring sites Oštrej (2015) and Bolnica (2018) were below, but close to the MAC (199.3 mg/m<sup>2</sup>/d and 199.5 mg/m<sup>2</sup>/d, respectively). This trend indicated general improvement of the air quality in terms of ABD, from 2013 to 2022. The measuring site Bolnica was the most polluted with ABD during five years (in the period 2013–2016 and in 2018), followed by the measuring site Šumska sekcija (the most polluted during 2019). This could be the consequence of the close vicinity to the copper smelter, and the location of the mentioned measuring sites relative to the prevailing wind directions which bring the pollution from the pollution sources. The measuring site Oštrej was the most polluted with ABD compared to the other measuring sites, during 2017. In the period 2020–2022, the measuring site Institut stood out with the highest pollution with ABD, compared to the other sites, with the noticed trend of increasing ABD contents from 2016 to 2022. The especially interesting data were for the 2022 when copper smelter was not working from April, due to the reconstruction. There has been more intensive mining and copper ore processing in the City of Bor and in the new copper mine and flotation plant, about 5 km from the City, in the recent years. The handling of the copper concentrate obtained in the flotation plant in the City of Bor and newly constructed flotation plant during transportation by railway and roads adjacent to the site Institut probably caused dispersion of very small particulates of copper concentrate, which reached the earth surface by wet and dry deposition. This probably was the main source of the polluting substances determined in the form of ABD at the measuring site Institut.

The average annual concentrations of Pb, Cd, As and Ni in ABD at four measuring sites (Bolnica, Šumska sekcija, Institut and Oštrej), from 2013 to 2022 are given in Figure 2.

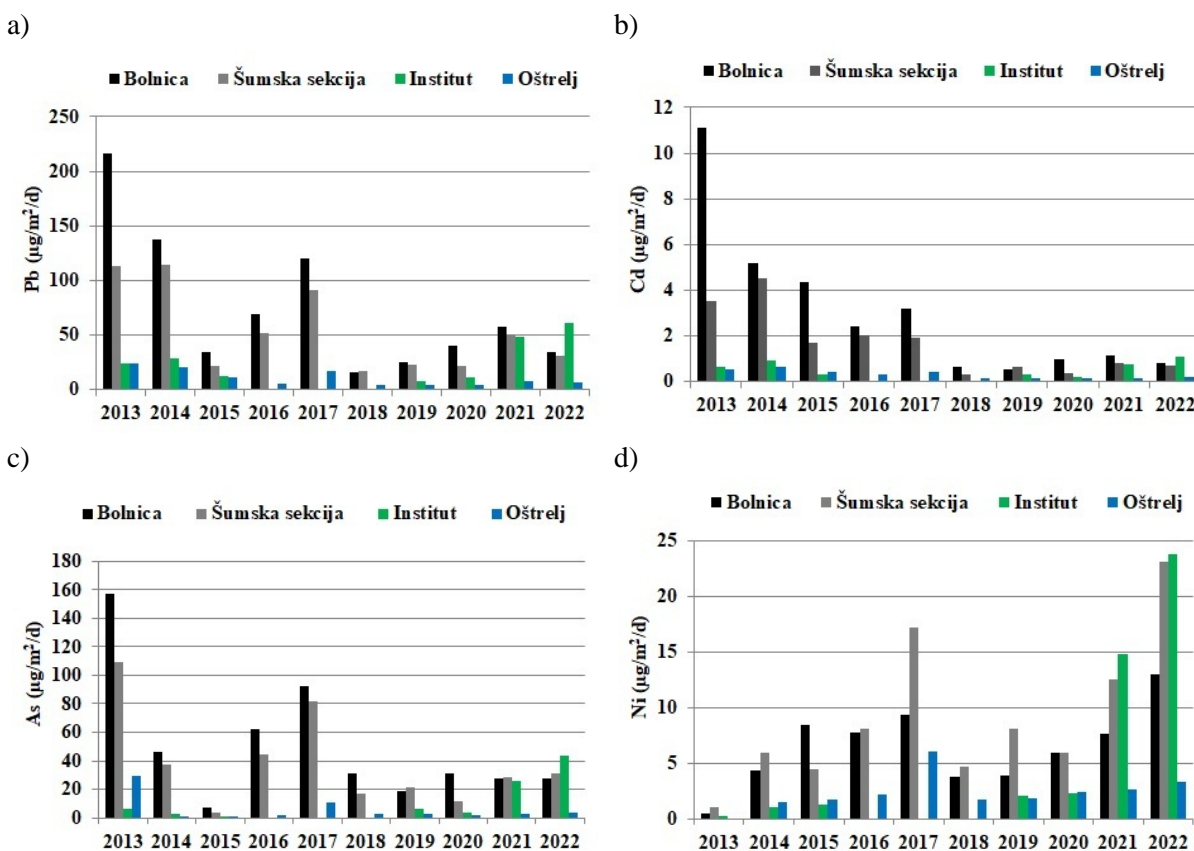


Figure 2 - Average annual contents of a) Pb, b) Cd, c) As and d) Ni in ABD at four measuring sites

The annual concentrations of the analysed elements followed the trend of the annual content of ABD. During the examined period, the measuring sites Bolnica and Šumska sekcija represented the most polluted locations. At the measuring site Bolnica, the concentrations of Pb and Cd were the highest during the examined period, except during 2018 and 2022, and except during 2019 and 2022, respectively. The concentration of As was the highest at the site Bolnica, except in 2019, 2021 and 2022. At the measuring site Šumska sekcija, the most pronounced pollution was with Ni during 6 years (2013, 2014, 2016, 2017, 2018, and 2019). Compared to the other sites, the Oštrej site was less polluted with the analysed elements, except in 2018 when the highest concentration of Pb was observed. As in the case of ABD, at the measuring site Institute the concentrations of Pb, Cd, As and Ni were the highest in 2022 and the concentration of Ni in 2021.

#### 4. CONCLUSION

The annual contents of atmospheric bulk deposition (ABD) as well as Pb, Cd, As, and Ni in ABD, in the urban-industrial, urban and industrial zones which were under the influence of the polluting substances from the copper smelter and flotation tailing ponds, were analysed for 10-year period (2013–2022), in the City of Bor and the surroundings. The number of measuring sites with contents of ABD above the Maximum Allowable Concentration, decreased over the years, which is an indication that the change of copper smelting technology, and the reconstructions of the industrial facilities lead to the general improvement of the air quality in terms of ABD, from 2013 to 2022, in the study area. Contents of ABD and analysed elements increased throughout the years at the measuring site Institut, reaching the maximum during 2022, although the copper smelter did not operate from April, due to the reconstruction. Such trend could be linked to the nonstationary sources of the pollution, such as handling during transportation of the copper concentrate obtained in the flotation plants in the City of Bor and in the newly constructed flotation plant located about 5 km SSE from the City of Bor, by the railway and the roads adjacent to the measuring site Institut.

#### ACKNOWLEDGEMENTS

*The authors are grateful to the Ministry of Education, Technological development and Innovation of the Republic of Serbia for financial support, within the funding of the scientific research at the University of Belgrade, Technical Faculty in Bor (No. 451-03-47/2023-01/200131). Our thanks go to English language teacher Mara Z. Manzalovic from the University of Belgrade, Technical Faculty in Bor, for providing language assistance.*

#### REFERENCES

- [1] F. Brugnone, W. D'Alessandro, F. Parello, *et al.*, Atmosphere, 14 (737) (2023).
- [2] M. Peretti, G. Piñeiro, M. E. Fernández Long, *et al.*, Atmos. Environ., 237 (2020) 117580.
- [3] L. He, S. Wang, M. Liu, *et al.*, The JHM Advances, 9 (2023) 100218.
- [4] Y. Pan, J. Liu, L. Zhang, *et al.*, Atmosphere, 12 (283) (2021).
- [5] M. Tasić, Z. Mijić, S. Rajšić, *et al.*, Journal of Physics: Conference Series 162 (2009) 012018.
- [6] B. S. Davis and G. F. Birch., Water Air Soil Pollut., 214 (2011) 147-162.
- [7] J. Hančulák, T. Špaldon, O. Šestinová, Journal of the Polish Mineral Engineering Society, 1 (43) (2019) 1-8.
- [8] M. Berti, A. Berton, S. Bertini, *et al.*, EQA, 44 (2021) 18-25.
- [9] D. Feng, P. Gong, Y. Li, *et al.*, Heliyon, 9 (2023) e18858.
- [10] I. Hůnová, P. Kurfürst, M. Schreiberová, *et al.*, Atmosphere, 14 (2023) 19
- [11] H. Wang, J. Wu, Z. Tian, Air Qual. Atmos. Health, 16 (2023) 1479-1487/2023.

- [12] S. M. Serbula, J. S. Milosavljevic, A. A. Radojevic, *et al.*, *Sci. Total Environ.*, 586 (2017) 1066-1075
- [13] S. M. Serbula, J. S. Milosavljevic, J. V. Kalinovic, *et al.*, *Sci. Total Environ.*, 777 (2021) 145981.
- [14] MMI, 2014-2023. Mining and Metallurgy Institute Bor, Annual Reports about Quality of Ambient Air in Bor for 2014, 2015, 2016, 2017, 2018, 2019, 2020, 2021, 2022 and 2023. Sector for Measuring and Control of Gaseous and Dust Parametres. Department Chemical–Technical Control, Bor, Serbia (in Serbian). (<https://bor.rs/ekologija/>).
- [15] SEPA, 2016, 2017, 2018. Serbian environmental Protection Agency, Ministry of Environmental Protection, Republic of Serbia, Annual report on the state of air quality in the Republic of Serbia for 2016, 2017 and 2018 (in Serbian).  
<http://www.sepa.gov.rs/index.php?menu=5000&id=1304&akcija=showDocuments&tema=Vazduh&godina&godina=2016>
- [16] Official Gazette of Republic of Serbia, 2013. Regulation on the conditions for monitoring and requirements of the air quality. No 11/10, 75/10, 63/13 (in Serbian).

## DESIGNING BIOCOMPATIBLE HIGH ENTROPY ALLOYS USING MONTE CARLO SIMULATIONS

Gordana Marković<sup>1</sup>, Vaso Manojlović<sup>2</sup>, Miroslav Sokić<sup>1</sup>, Jovana Ružić<sup>3</sup>, Dušan Milojkov<sup>1</sup>

<sup>1</sup> Institute for technology of nuclear and other mineral row materials, 11000 Belgrade, Serbia

<sup>2</sup> Faculty of Technology and Metallurgy, University of Belgrade, 11000 Belgrade, Serbia

<sup>3</sup> “Vinča” Institute of Nuclear Sciences-National Institute of the Republic of Serbia, Department of Materials, University of Belgrade, 11000 Belgrade, Serbia

### Abstract

*This study examines the potential of high-entropy alloys (HEAs) as promising biomaterials, with a specific focus on the development of alloys with a low Young's modulus. Utilizing Monte Carlo simulations coupled with machine learning techniques, the research identifies critical variables that significantly influence the Young's modulus, uncovering a notable correlation between specific heat and the elastic properties of the alloys. The validation of the Extra Trees Regressor as a reliable predictive model in this study, furthermore, facilitates the identification of promising HEAs with tailored properties. These findings provide significant insights that are expected to guide future progresses in the development of HEAs as advanced biomaterials.*

**Keywords:** (HEA, Monte Carlo simulations, Young's modulus)

### 5. INTRODUCTION

Biomaterials made from titanium alloys have been successful for decades as substitutes for hard tissues in the human body [1]. This popularity stems from their exceptional combination of properties: high strength, resistance to corrosion and wear, low Young's modulus, and biocompatibility. Among these titanium alloys, special mention is made of titanium  $\beta$  alloys, which show extremely low values of Young's modulus. These alloys have proven to be advantageous in the field of implantology due to their ability to improve load transfer characteristics, thereby reducing the risk of premature implant failure and preserving the vitality of the surrounding bone tissue. Moreover, the implantation of such materials is associated with significant improvements in bone tissue rehabilitation, affecting cell adhesion and accelerating the healing process [2]. The most traditional alloy used for this purpose, Ti-6Al-4V, has been questioned because of its Young's modulus (>100 GPa), which compared to the Young's modulus of bone (up to 35 GPa) is a big difference. Also, Al and V were declared cytotoxic and emphasis was placed on some other elements such as Ni, Mo, Fe, Zr, whose presence does not leave harmful effects on the human body [3,4].

However, in the last two decades, a new class of biomaterials called high entropy alloys (HEAs) has emerged. This group of materials fundamentally deviates from traditional alloys. In contrast to conventional alloys, in which the desirable properties of a single element predominate, HAE contains at least five primary elements in similar proportions. This unique composition leads to an increase in mixing entropy, resulting in the formation of a single-phase solid solution, predominantly adopting cubic (BCC) and face-centered cubic (FCC) crystal lattices. As a result, these alloys exhibit an extensive range of exceptional properties [2, 5].

Although the potential applications of HEAs in the field of biomaterials are still under active investigation, they promise to be an ideal choice where no compromises need to be made between material properties [5]. This paper presents an innovative approach to the design of HEAs without the presence of cytotoxic elements, with Young's modulus below 70 GPa. The Monte Carlo



simulation and machine learning techniques are used to identify and analyze key variables that significantly affect Young's modulus.

## 6. METHODS

The principle of machine learning was applied to a database of biocompatible titanium alloys with a low value of Young's modulus, precisely defined in the Ref. [6, 7]. Thanks to the ability to decipher complex patterns in the data, it was possible to determine the most important features that affect Young's modulus [8].

Our dataset [6] is divided into a training set (65%) and a test set (35%). The Extra Trees Regressor prediction model was used to display predicted and actual Young's modulus values. In addition, a Monte Carlo simulation was conducted to explore a wide range of random compositions. This simulation involved randomly generating compositions with weighted proportions of alloying elements and impurities within predefined ranges. The aim was to evaluate Young's modulus and different compositions of HEA. This method, and software is given in reference [9].

## 7. RESULTS AND DISCUSSION

The observation that the coefficient of determination ( $R^2$ ) for the test set is  $\sim 0.7$  is a positive indicator of the validity of the model. Figure 1 represents the relationships between actual and predicted values of Young's modulus based on the number of samples tested, provides additional support for the validity of the model. It is possible to see that the largest deviations between the predicted and actual values occurred at the extremes.

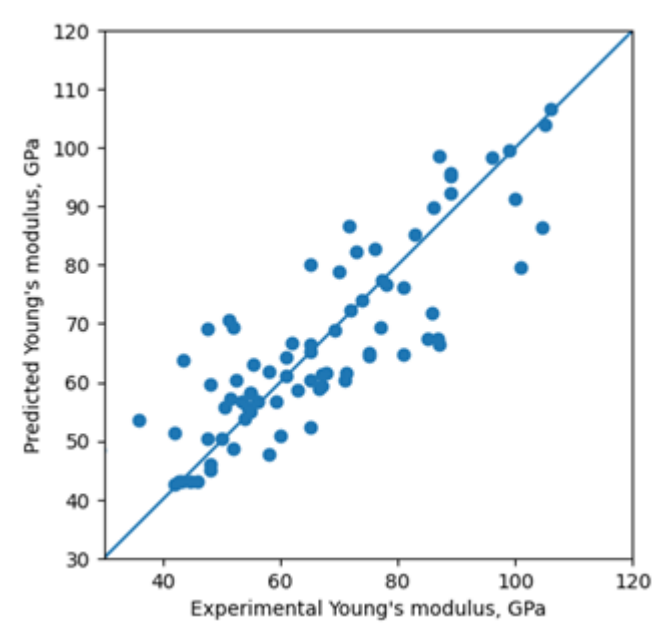


Figure 1- Experimental and predicted value of Young's modulus using machine learning method

The analysis identifies the specific heat as the primary parameter influencing the predictive accuracy of the machine learning model [8, 9]. Theoretical support can be derived from both the Einstein and Debye models, as they provide insights into the quantum mechanical foundations of the changes in molar heat capacity resulting from temperature fluctuations. Consequently, these models establish an important but indirect relationship between specific heat and Young's modulus ( $E$ ). The aforementioned models serve to encapsulate the fundamental nature of atomic vibrations occurring within a given material, which plays an important part in the determination of its elastic properties. Einstein's model provides an initial understanding by making the assumption of independent atomic vibrations. However, the Debye model expands upon this understanding by

considering the collective and interdependent atomic behaviors. V. Pekarek found relation between thermal properties and elastic modulus:

$$c_p \cdot s = \frac{E_a}{1-4 \cdot \sigma^2} \cdot \alpha \quad (1)$$

where  $c_p$  is specific heat at constant pressure per kilogram (J/(kg·K));  $s$  is density (kg/m<sup>3</sup>);  $E_a$  is Young's modulus (GPa);  $\alpha$  is linear coefficient of thermal expansion (1/K), and  $\sigma$  is Poisson's ratio [10].

Monte Carlo simulation was created by ten million alloy samples were under controlled conditions, aiming to achieve HEAs with specific Young's modulus values (70 GPa set as upper value). This approach has led to the discovery of dozens of promising alloys, and Table 1 presents information of these alloys. To maintain consistency with previous research in the literature, we limited the oxygen content to a maximum of 0.78 wt%. The primary elements used in these alloys are titanium, zirconium, tin, manganese, silicon, and niobium. These elements, as well as the other mentioned parameters, proved to be the most influential variables when it comes to predicting Young's modulus. The results obtained from this study, together with the proposed computational methods, can serve as valuable guidelines for future efforts in the design of multicomponent HEA.

Table 1 - Values of various parameters for modeled HEA.

Parameter:	Unit:	Sample ID:		
		2093590	3829568	6719870
<b>Ti</b>	<b>wt.%</b>	15.32	20.62	16.12
<b>O</b>	<b>wt.%</b>	0.26	0.21	0.31
<b>Nb</b>	<b>wt.%</b>	16.02	1.10	11.50
<b>Zr</b>	<b>wt.%</b>	11.72	11.10	6.73
<b>Ta</b>	<b>wt.%</b>	0.17	15.32	12.75
<b>Sn</b>	<b>wt.%</b>	11.72	11.97	11.11
<b>Mn</b>	<b>wt.%</b>	15.38	0.39	10.81
<b>Si</b>	<b>wt.%</b>	26.56	26.65	27.48
<b>Mo</b>	<b>wt.%</b>	2.55	10.46	3.06
<b>Fe</b>	<b>wt.%</b>	0.03	2.17	0.14
<b>Bo-bond order</b>	/	3.27	2.81	3.30
<b>Md-d orbital energy level</b>	/	2.40	1.98	2.40
<b>Specific heat</b>	<b>kgK</b>	408.13	312.50	399.36
<b>Δr</b>	/	-10.05	-6.12	-9.45
<b>Predicted Young's modulus, exp</b>	<b>GPa</b>	<b>66.28</b>	<b>66.34</b>	<b>66.66</b>

Equation 1 establishes a clear and direct relationship between the specific heat capacity and Young's modulus. This relationship is influenced by various additional factors, such as the density of the material and the coefficient of thermal expansion. As depicted in Figure 2, the specific heat values of the alloys shown in Table 1 exhibit a significant decrease, potentially falling below the established thresholds, when compared to the range observed in the extensive database of alloys being investigated. The characteristic necessitates additional investigation, potentially suggesting a new approach in the continuous efforts to improve the structural properties of high-entropy alloys.

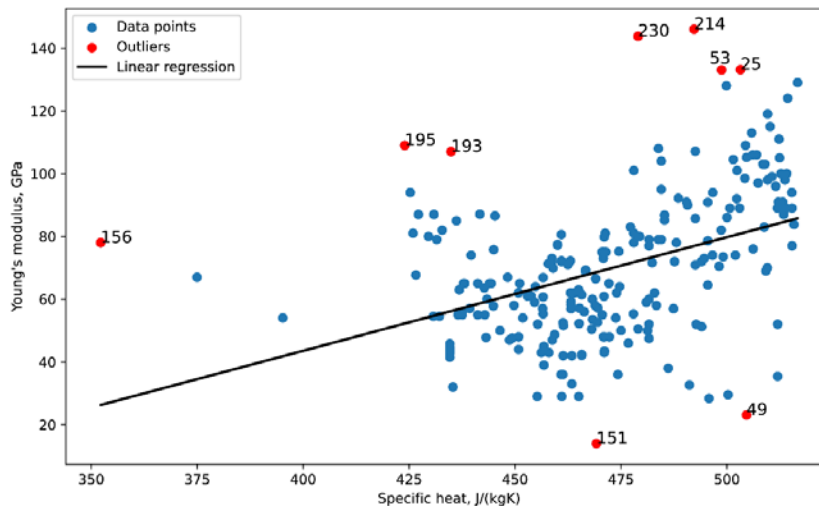


Figure 2- Relation between Young's modulus and specific heat within the Ti-alloys dataset

## 8. CONCLUSION

The present study presents an innovative method for predicting and analyzing the properties of high-entropy alloys (HEAs) through the use of Monte Carlo simulations. This approach is based on the observed strong correlation between the specific heat and Young's modulus, with particular attention given to HEAs that possess a modulus value of approximately 66 GPa. The integration of machine learning with simulations, physical models, and rigorous experimentation could provide a feasible approach to enhance composition design and microstructure control in high-entropy materials. This development holds the potential to redesign the predictive modeling and achievement of advanced high-entropy alloys.

## ACKNOWLEDGEMENTS

*This investigation was financed by the Ministry of Science, Technological Developments and Innovation of the Republic of Serbia (Contract number: 451-03-47/2023-01/200023; 451-03-47/2023-01/200135).*

## REFERENCES

- [1] H. J. Rack, J. I. Qazi., C. Author., *Mat. Sci. Eng.*, 26 (8) C (2006) 1269-1277.
- [2] N. Ma, S. Liu, W. Liu, L. Xie, D. Wei, L. Wang, *Front. Bioeng. Biotechnol.*, 8 (2020) 603522.
- [3] S. Liang., *Adv. Eng. Mater.* 22 (11) (2022) 2000555.
- [4] M. Niinomi, M. Nakai., *Int. J. Biomat.*, (2011).
- [5] G. Popescu, C. A. B. Ghiban, L. Popescu, R. Rosu, I. Truscă, V. S. Carcea, et.al., *IOP Conf. Ser.: Mater. Sci. Eng.* 400 (2018) 022049.
- [6] V. D. Manojlović, G. Marković, *Titanium Alloys Database for Medical Applications* <https://doi.org/10.5281/zenodo.7802694> (accessed 2023-06-25).
- [7] V. D. Manojlović, G. Marković., *Metall. Mater. Data*, 1 (1) (2023) 1–6.
- [8] G. Marković, V. Manojlović, J. Ružić, M. Sokić, *Mat.* 6(19) (2023) 6355; <https://doi.org/10.3390/ma16196355>
- [9] V. D. Manojlović, *Software: Ti-alloys: Prediction of new biocompatible Ti alloys using machine learning methods*, <https://doi.org/10.5281/zenodo.8315020> (accessed 2023-06-25).
- [10] 39. V. Pekárek, *Metals. Mater. Sci. Eng. A.*, 112 (1989) 193–198.

## APPLICATION OF IMAGE ANALYSIS FOR CVITATION EROSION RESISTANCE MONITORING OF SOME ENGINEERING MATERIALS

Tatjana Volkov-Husović<sup>1</sup>, Sanja Martinović<sup>2</sup>, Ana Alil<sup>2</sup>, Milica Vlahović<sup>2</sup>

<sup>1</sup>University of Belgrade, Faculty of Technology and Metallurgy, Belgrade, Serbia;

<sup>2</sup>University of Belgrade, Institute of Chemistry, Technology and Metallurgy-  
National Institute of the Republic of Serbia, Belgrade, Serbia

### Abstract

*Engineering materials are often used in various operating conditions including high temperatures, pressure, aggressive solutions, or cavitation erosion. The phenomenon of cavitation erosion is expected when fluid flow is present, which contains equipment such as turbine blades, high-speed propellers, or pump parts. Cavitation erosion usually causes surface degradation of material with defects that appear in the form of pits and fractures. Such loss of material leads not only to surface degradation but usually also to strength deterioration with the potential risk of failure and therefore also to shortening of material lifetime, thus requiring additional costs for failure analysis, repair, and replacement of parts. This paper will present the results regarding the resistance of various engineering materials to cavitation erosion. As materials, austenitic stainless steel 316L and CuAlNi shape memory alloy are selected and studied. The comparison of the behavior between these two materials in cavitation erosion conditions will be shown based on the results of mass loss and morphology analysis of the pits formed at the surface over time. Image analysis tools will be applied in order to quantify the surface damage level and to analyze selected morphology descriptors.*

**Keywords:** Cavitation erosion, 316L steel, CuAlNi SMA, Image analysis

### 1. INTRODUCTION

The behavior of various engineering materials in different operating conditions is of great interest since the lifetime of the material and/or part of equipment can be monitored and predicted, taking into account material degradation during exposure to temperature, pressure, aggressive solutions, or other conditions over time. One of the parameters that should be studied is cavitation erosion. Hammitt noted in early 1960 that the erosive aggressiveness of cavitating flows can be assessed through a consideration of energy conversion predicting the instantaneous surface impact power of collapsing cavities from the potential energy hypothesis, not on the cavitation type. The cavitation erosion model is based on partly theoretical and partly empirical considerations. The empirical approaches are derived from the knowledge that was achieved in previous studies by various authors, and that continues to this day [1-3].

Through experimental investigations and statistical calculations, an obvious connection between the cavitation structures and cavitation erosion was established. There are four different phases of the cavitation erosion process that ultimately lead to pit formation [1-3]:

- Collapse of the cavitation cloud that causes a shock wave radiating into the fluid;
- The magnitude of the shock wave is attenuated as it travels toward the solid surface;
- Single bubbles present near the solid surface begin to oscillate producing a micro-jet phenomenon if the bubble is close enough to the wall;
- The damage (single pit) is caused by a high-velocity liquid jet impacting the solid surface.

Numerous studies have shown the existence of four different time periods that can be correlated to the different erosion mechanisms [4]:

- I. An incubation period that is characterized by negligible loss of material, elastic or plastic deformation of the material, and the formation of some microcracks;
- II. An accumulation zone is a period of time associated with increasing material loss due to the propagation of cracks in exposed materials;
- III. An attenuation period in which the rate of material loss decreases;
- IV. A stable period or steady-state zone in which the erosion rate is substantially constant.

Image analysis has various tools that offer a simple and reliable quantification of visual information (optical or SEM microphotographs). In this paper, Image Pro Plus, as a software program, will be applied to monitor the levels and characteristics of damages.

Metallic materials such as stainless steel and shape memory alloys (SMAs) are widely used in the fields of electronics, machinery, energy, aerospace, civil engineering, automotive, medicine, and everyday life [4,5].

## 2. EXPERIMENTAL

### 2.1 Samples preparation

**Stainless steel:** Powder of commercial austenitic stainless steel (SURFIT TM 316L) with a diameter from 45 to 90  $\mu\text{m}$  was used. The spherical shape steel powder was obtained by gas atomization with a particle size below 45  $\mu\text{m}$ . The samples were pressed at approximately 150 MPa and then sintered at a temperature of 1200°C for 60 minutes in a vacuum furnace.

**The polycrystalline Cu-12.8Al-4.1Ni (wt.%) SMA** was prepared using pure raw materials of copper, aluminum, and nickel in a vacuum induction furnace at a temperature of 1240°C. Using a vertical continuous casting device connected to a vacuum induction furnace, a solid bar of 8 mm was produced directly from the melt. The bar was continuously cast at a casting speed of 320 mm/min (as-cast state). After the casting, the heat treatment procedure was performed by a solution annealing at 885°C for 60 minutes and then quenching in water [6].

### 2.2 Methods

Cavitation erosion was performed using standard ultrasonic vibratory testing with a stationary sample [8]. Samples were dried between the tests, then measured in order to monitor specimen weight change, and photographed in digital form for further image analysis.

## 3. RESULTS AND DISCUSSION

According to the standard procedure, degradation of the samples exposed to cavitation erosion is monitored using mass loss results. Obtained measurements of mass loss for studied samples are given in Figure 1. Based on the obtained results, it was found that both samples exhibited excellent cavitation resistance. However, the SMA sample showed better results with minimal mass loss after over 7 hours of testing (420 minutes).

The levels of surface degradation for both tested samples, stainless steel and SMAs, are given for different times of exposure. The results for the samples based on steel are given during an exposure time of up to 60 minutes, while the exposure time for the SMA samples time was 420 minutes. Calculated values of surface degradation level and microphotographs of the damaged surfaces presenting the morphology of degradation are given in Figure 2. Based on the total area of formed pits level of degradation was calculated, and the obtained results are presented. The level of degradation for both samples is low, but better values are related to the SMA sample, especially in the case of a very long time of exposure to cavitation erosion (420 minutes).

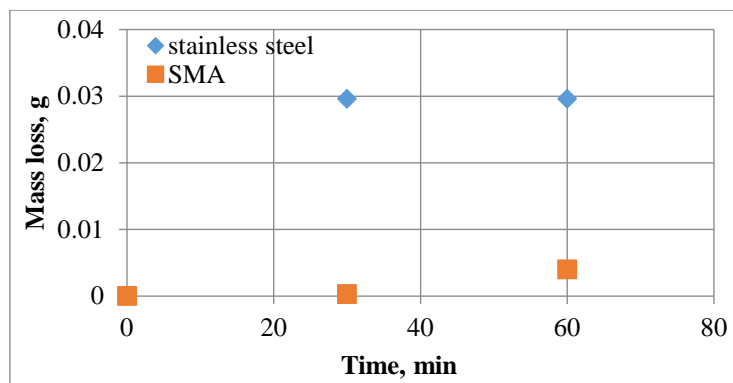


Figure 1 - Mass loss of the samples during cavitation testing

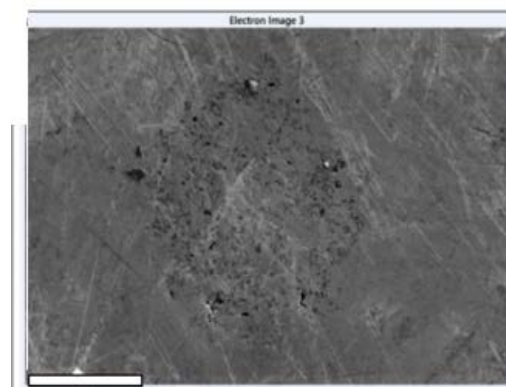
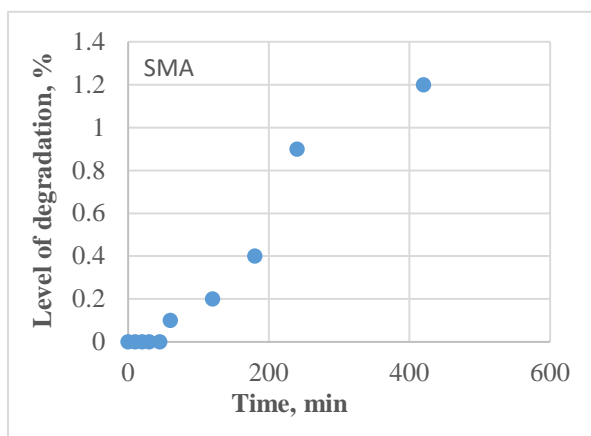
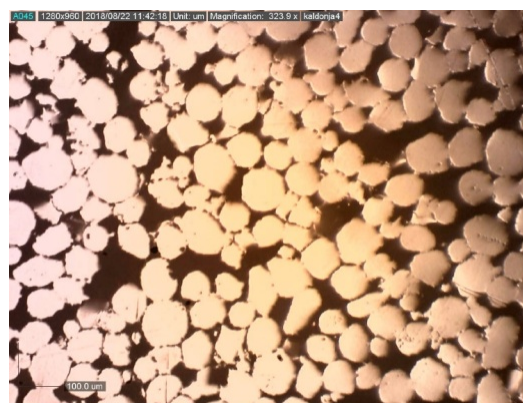
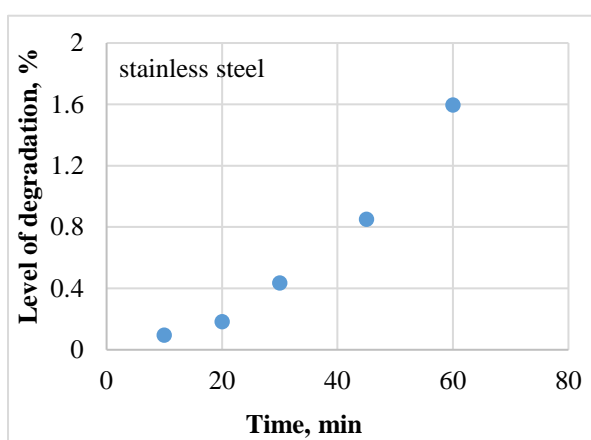


Figure 2 - Level of degradation during testing and microphotographs of the sample surfaces at the end of testing

Besides the above-presented results, the morphology parameters that are characteristic for the formed pits (damages) are also quantified and given for the stainless steel and SMA samples after 60 and 420 minutes, respectively. Selected morphological parameters that best depict the formed pits and therefore used in further image analysis are as follows: *Area*, *Diameter (max)*, *Diameter (mean)*, *Diameter (min)*, *Radius ratio*, and *Roundness*. The average values of measuring selected morphological parameters regarding formed pits are shown in Table 1.



Table 1 - Analysis of morphological parameters for the SMA's and steel 316L.

Parameter	SMA	Steel 316L
	420 minutes	60 minutes
Area, $\mu\text{m}^2$	36.17	1.8
Diameter (max), $\mu\text{m}$	9.55	1.7
Diameter (min), $\mu\text{m}$	3.25	0.8
Diameter (mean), $\mu\text{m}$	6.28	1.2
Radius (min), $\mu\text{m}$	0.72	1.5
Roundness	1.25	1.65

The obtained results confirmed that characteristics of the formed pits related to the SMA samples also exhibited better values considering the time of exposure. However, steel samples also showed very good cavitation erosion resistance.

#### 4. CONCLUSION

The behavior of two metallic engineering materials, stainless steel and SMAs, was analyzed with the aim of monitoring their resistance during exposure to the cavitation resistance. In addition to measuring mass loss over specific time periods of exposure to cavitation erosion, the overall levels of surface degradation were calculated, and characteristic morphological parameters for formed pits and damages were quantified.

The obtained results can point out the following conclusions:

- Results indicated that SMAs exhibited superior resistance to cavitation erosion;
- Stainless steel was quite good, but not as good as in the case of SMAS, as expected.

#### ACKNOWLEDGEMENTS

*This work was supported by the Ministry of Education, Science, and Technological Development and Innovation of the Republic of Serbia (Contract Nos. 451-03-47/2023-01/200135 and 451-03-47/2023-01/200026).*

#### REFERENCES

- [1] F. G. Hammit, Cavitation and multiphase flow phenomena, McGraw-Hill College (1980).
- [2] T.J.C. Van Terwisga, P.A. Fitzsimmons, L. Ziru, E.J. Foeth, Cavitation Erosion – A review of physical mechanisms and erosion risk models, Proceedings of the 7<sup>th</sup> International Symposium on Cavitation CAV2009 – Paper No. 41, Ann Arbor, Michigan, USA, 2009.
- [3] K.L. Tan, S.H. Yeo, Cavitation erosion study in deionized water containing abrasive particles, Proceedings of the 26<sup>th</sup> DAAAM International Symposium, Vienna, Austria, 2016, p.0818- 0824.
- [4] E. Clithy, Sci. Insigt., 33 (3) (2020) 167-174.
- [5] M.H. Wu, L.McD. Schetky, Industrial application for shape memory alloys, Proceedings of the International Conference on Shape Memory and Superelastic Technologies, Pacific Grove, California, P.171-182 (2000).
- [6] T. Volkov Husović, I. Ivanić, S. Kožuh, S. Stevanović, M. Vlahović, S. Martinović, S. Stopić, M. Gojić, Metals 11 (7), 997, 2021.
- [7] S. Martinović, M. Vlahović, M. Dojčinović, M. Pavlović, T. Volkov Husović, Mater. Lett. 220 (2018) 136-139.
- [8] ASTM G32, Standard Test Method for Cavitation erosion using vibratory apparatus.

## CHANGES IN THE STRUCTURE AND DENSITY OF COPPER DURING THE REFINING SMELTING PROCESS

Milan Nedeljković, Srba Mladenović, Jasmina Petrović, Milijana Mitrović

Technical Faculty Bor, University of Belgrade, V.J. 12, 19210 Bor, Serbia

### Abstract

*The technology of pyrometallurgical copper production ends with a fire-refining process. This process, as the first stage of refining blister copper, should reduce the impurity content in blister copper to a level that, in accordance with existing standards, allows for the optimal management of electrolytic refining technology. In terms of mechanism and physical-chemical changes, this process is identical to the refining smelting process and it is increasingly being used as a supporting process in a wide range of processing operations. Both processes go through a series of steps that are different in their mechanism and characteristics and must be monitored throughout the entire process. Effective monitoring of these steps enables the installation of the optimal technology for those processes. In this study, changes in density and microstructure that impact the quality of copper during the fire refining and refining smelting processes were observed.*

**Keywords:** *pyrometallurgy, fire-refining, blister copper*

### 1. INTRODUCTION

Copper, thanks to its properties, is the third most commonly used metal in the world, with a wide range of applications, and demand for it continues to grow. Due to its excellent characteristics, it is used as an alloying element in metallurgy. The processes for obtaining copper can be divided into pyrometallurgical and hydrometallurgical methods. Approximately 90% of copper is obtained through pyrometallurgical processes, while the use of hydrometallurgical methods is limited to copper oxide ores [1].

Copper is required to possess the highest possible electrical conductivity, high plasticity, and, simultaneously, appropriate mechanical properties. The production of copper of this quality is possible by two-stage purification of blister copper. The first phase of purification, known as fire-refining, is important for removing a higher level of impurity constituents from liquid blister copper. The basic impurities present in raw copper are as follows: Fe, Ni, S, O, Pb, Zn, Sn, Bi, As, Sb, Se, Te, Ag, and Au. These impurities, considering their impact on the quality of copper, can be categorized into groups of impurities that significantly affect electrical conductivity, plasticity, mechanical properties, and so on [2]. Blister copper with an average purity of 98.5 - 99% Cu is fire-refined so that the content of impurities in the refined copper is reduced from 0.8 - 2.5% to 0.2 - 0.3%. In this purification stage, nearly all of the contained S, Fe, O, As, Sb, Pb, and Bi are removed [2, 3].

The fire-refining process is applied to both liquid and solid raw copper. Processing liquid charge significantly saves on fuel, shortens the overall operation time, and increases furnace productivity. Through the fire-refining process, the purified copper is cast into anodes, known as anode copper, which is then sent to the electrolytic refining operation [4].

The complete fire-refining process is organized into several phases: the furnace preparation and charging phase, the oxidation phase, the slag removal phase, the reduction (smelting) phase, and the copper casting phase. During each operation, the most sensitive parts of the furnace, casting

machine, and other additional equipment deform or are destroyed. For this reason, it is essential to prepare the furnace and other devices before the start of each operation [4, 5].

The density of copper during the refining process varies at different stages. Before oxidation, and especially during the oxidation phase, copper has the lowest density due to the presence of impurities in the liquid copper, which have a lower density than copper itself [6]. By removing these impurities, the density of copper increases, reaching its highest value at the end of the reduction phase. According to studies, the amount of hydrogen, SO<sub>2</sub>, and other gases in copper impacts its density. The temperature at which the procedure is performed, more precisely the temperature at which a sample is collected, also affects the density of copper during the process. The density of the sample taken during casting is one of the key indicators of copper quality, and it is used to determine the purity of refined copper [7].

## 2. EXPERIMENTAL

The practical part of this study was realized with the previous technology of the Smelter in Bor, by taking samples from the anode furnace. In order to become familiar with all aspects of refining technology and to organize the sample collection, the process of the fire-refining activities was tracked before starting the experiment. The collection of the sample during the operation was the first stage of the experiment. A special spoon was used just for collecting samples. In the first series, the furnace operating regime was recorded, and a specific number of samples of liquid copper were collected from each phase. Samples were collected at 30 minute intervals. The final phase of the experiment was analyzing the process by examining changes in copper density and changes in the microstructure of copper.

## 3. RESULTS AND DISCUSSION

The density of each collected sample was measured to monitor density changes during operations. The determination of density was carried out using a hydrostatic scale. Changes in copper density during the fire-refining process are shown in Figure 1.

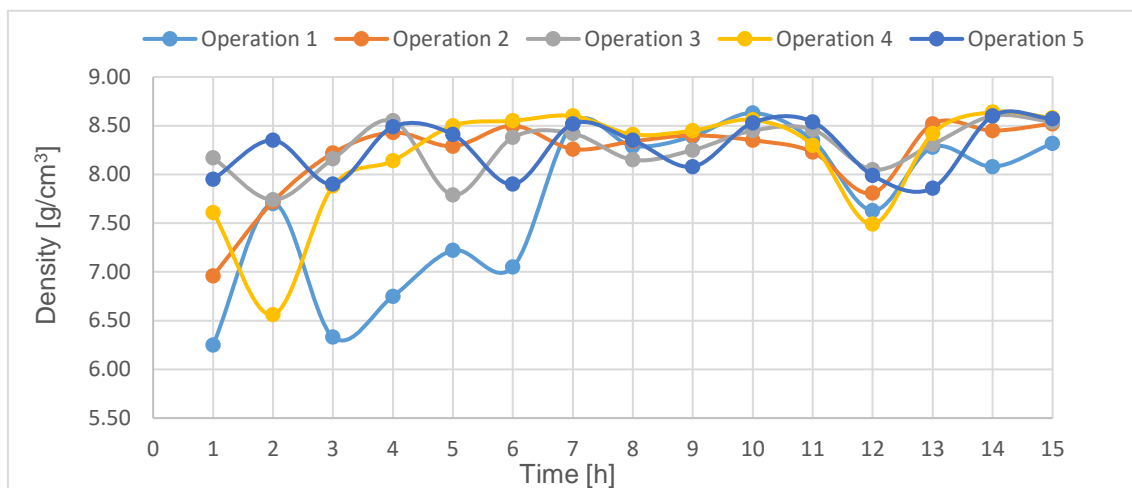


Figure 1 - Change in copper density during fire-refining operations

By analyzing the obtained results, it was determined that the average density of copper consistently rises during the oxidation phase. This increase in density is caused by a reduction in the weight percentage of impurities in the liquid copper system, which has a lower density than copper. In the following stage, which includes the poling and reduction operations, the average density of copper significantly decreases. It's important to mention that the furnace atmosphere also influences on the density of copper samples collected during the fire-refining process.

Studying the changes in microstructure in solidified copper samples obtained during the operations is one way to monitor the fire-refining process. Monitoring was performed by taking samples during the refining operations at specific time intervals, approximately every 25 minutes. The samples were then put through to a complete metallographic study. Microphotographs can be used to determine the oxygen content in the molten metal, specifically the increase or decrease in the oxygen percentage during the refining process. There are numerous methods for determining the amount of  $\text{Cu}_2\text{O}$  or  $\text{O}_2$  in copper throughout the refining process. For samples that have a hypoeutectic composition with a lower  $\text{O}_2$  content, the percentage of oxygen can be determined by comparing the surface of the samples with the GOST standard at the same magnification (200:1). The microstructure of copper with variable oxygen concentration during the fire-refining process is shown in Figure 2.

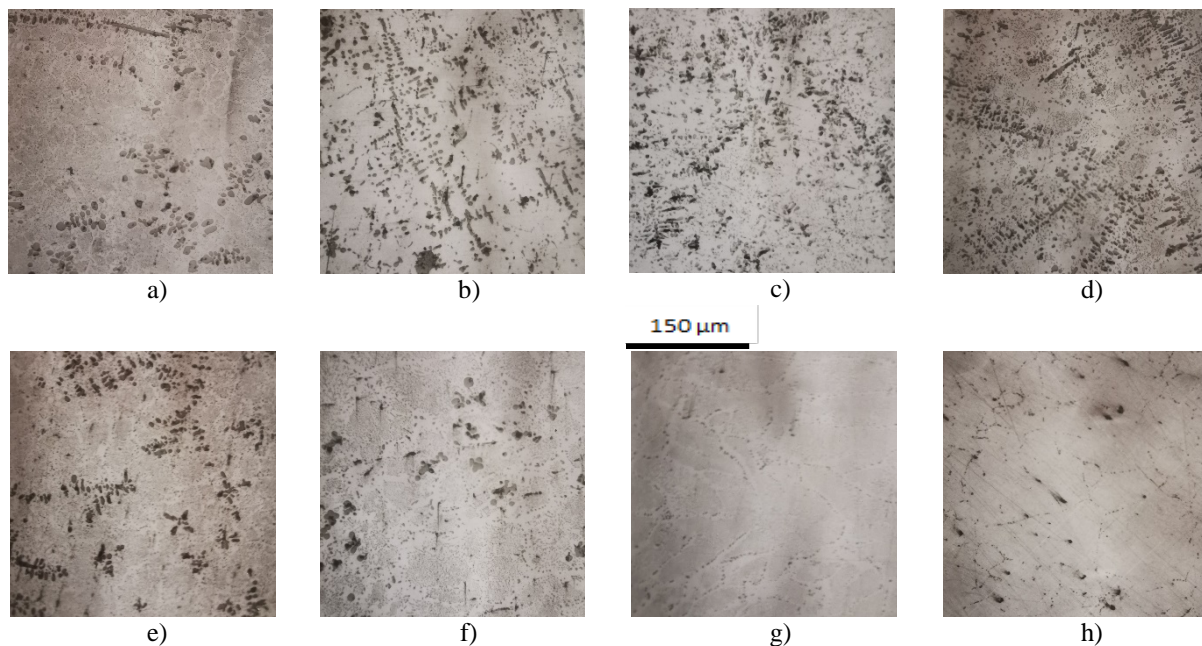


Figure 2 - Microstructure of copper with variable oxygen content during the fire-refining process: (a) 0.77%  $\text{O}_2$ ; (b) 0.91%  $\text{O}_2$ ; (c) 1.1%  $\text{O}_2$ ; (d) 1.34%  $\text{O}_2$ ; (e) 0.82%  $\text{O}_2$ ; (f) 0.52%  $\text{O}_2$ ; (g) 0.39%  $\text{O}_2$ ; (h) 0.01%  $\text{O}_2$

In Figure 2(a), the microstructure of samples from the phase of initial filling of the anode furnace with blister copper is presented.  $\text{Cu}_2\text{O}$  is precipitated in the form of primary dendritic crystals in the eutectic ( $\text{Cu} + \text{Cu}_2\text{O}$ ). Image 2(b) displays the microstructure of a sample taken during the final stage of loading the anode furnace with blister copper. It can be observed that the microstructure has a hypereutectic composition, so in addition to the eutectic ( $\text{Cu} + \text{Cu}_2\text{O}$ ), it also contains primary crystals of  $\text{Cu}_2\text{O}$ , as well as the presence of non-metallic inclusions. The initially formed crystals have a dendritic shape oriented in the direction of cooling. The microstructure of a sample taken during the middle phase of oxidation is presented in Figure 2(c). The amount of primary  $\text{Cu}_2\text{O}$  crystals that have formed in the eutectic is higher than it was in the previous sample. Figure 2(d) shows the sample's microstructure at the end of the oxidation phase. The microstructure of a sample during the slag removal procedure is shown in Figure 2(e).  $\text{Cu}_2\text{O}$  crystals have precipitated in the form of primary crystals within the eutectic ( $\text{Cu} + \text{Cu}_2\text{O}$ ). Figure 2(f) displays the microstructure of copper samples during the reduction phase. The image shows a reduced number of primary  $\text{Cu}_2\text{O}$  crystals precipitated within the eutectic. The microstructure at the end of the reduction phase is shown in Figure 2(g). The percentage of oxygen in copper is very low. The structure of the copper sample at the end of the casting phase is shown in Figure 2(f). From the image, it is evident that the oxygen content in the copper has increased slightly.

Figure 3 shows the change in copper's oxygen content during the fire-refining process. From the image, it can be observed that the oxygen content in copper decreases during the fire-refining process.

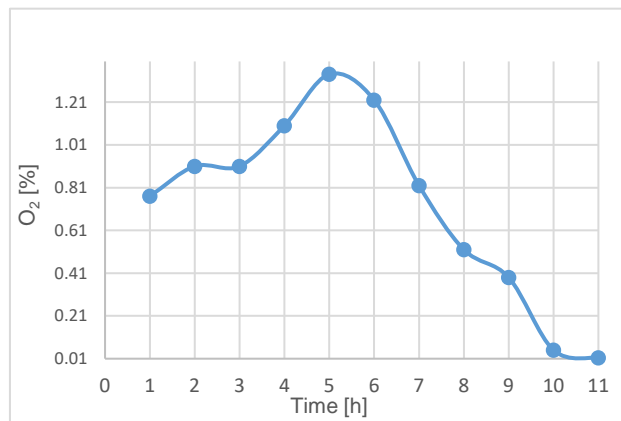


Figure 3 - Change in oxygen content in copper during the fire-refining process

#### 4. CONCLUSION

Through a literature review and based on experimentally obtained results, it is possible to identify the potential for more efficient monitoring of the fire-refining and refining smelting processes. Based on the obtained results, through density measurements and the determination of oxygen content in copper, along with metallographic analysis, it becomes possible to predict and determine the phase of the operation in progress. The density of copper must be understood as a parameter that results from the interplay of various factors crucial for the proper management of the process (temperature, the degree and type of impurities present in copper, oxidation intensity, quality of reducing agents, and so on). The density of the copper samples taken at the end of each observed operation is lower than expected in all cases. Values obtained through such analytical methods must find their place in monitoring the technology of the fire-refining process.

#### ACKNOWLEDGEMENTS

*The research presented in this paper was done with the financial support of the Ministry of Education, Science and Technological Development of the Republic of Serbia, within the funding of the scientific research work at the University of Belgrade, Technical Faculty in Bor, according to the contract with registration number 451-03-47/2023-01/ 200131.*

#### REFERENCES

- [1] J. Davis, *Copper and copper alloys*. ASM International, Ohio, (2001).
- [2] D. Gregurek, J. Schmidl, K. Reinharter, V. Reiter, A. Spanring *JOM* 70(11) (2018) 2428-2434.
- [3] M. Schlesinger, M. King, K. Sole, W. Davenport, *Extractive metallurgy of copper*, Fifth edition, Oxford, UK: Perfamon press an imprint of Elsevier Science, 2011.
- [4] K. Gargul, S. Malecki, W. Marek, Rudy i Metale Nieżelazne, 58(12) (2013) 843-849
- [5] M. Schlesinger, K. Sole, W. Davenport, G. Flores, *Extractive metallurgy of copper*. Elsevier (2021).
- [6] J. Oudiz, *JOM*, 25(12) (1973) 35-38.
- [7] P. Goyal, N. Themelis, W. Zanchuk, *JOM*, 34 (2013) 22-28.



## MICROSTRUCTURE ANALYSIS OF EN AW 6061 ALLOY USING A SEM MICROSCOPE AFTER ARTIFICIAL AGING

Jasmina Petrović, Srba Mladenović, Ivana Marković,  
Milan Nedeljković, Milijana Mitrović

Technical Faculty Bor, University of Belgrade, V.J. 12, 19210 Bor, Serbia

### Abstract

*Aluminium alloys from the Al-Mg-Si system are crucial because they can be used both as cast and plastic-processed states. In this work, the aluminium alloy EN AW 6061 was used for testing. Microstructural changes during the ageing of the alloy were observed. During the ageing process, the samples were heated at different temperatures of 160 °C, 180 °C, 200 °C and 220 °C in different time intervals of 4 h, 5 h, 6 h and 7 h. The alloy has previously been exposed to a specific plastic deformation and heat treatment. The microstructure was studied using a scanning electron microscope, SEM.*

**Keywords:** *microstructure, ageing, plastic deformation, scanning electron microscope*

### 1. INTRODUCTION

The most essential properties that characterize this alloy from other aluminium alloys are its superior strength, outstanding workability through plastic deformation, good surface characteristics after processing, and excellent corrosion resistance in atmospheric and seawater environments [1, 2]. This alloy belongs to the group of aluminium alloys that can be strengthened by cold plastic deformation and heat treatment – ageing (thermal deposition). Plastic deformation is used to increase the number of dislocations, while ageing is a process in which the alloy is reinforced by the production of a very tiny quantity of uniformly distributed secondary phase in the metal base [3]. Particles of the secondary phase are known as precipitates, so this process is also called precipitation strengthening [4]. The process of solution annealing, tempering, and eventually thermal deposition raises the material's mechanical characteristics to the highest possible level.

Magnesium and silicon are the two major alloying components of alloy EN AW 6061. Copper, manganese, chromium, iron, titanium, and zinc can also be found in addition to these main elements. The main alloying elements form the Mg<sub>2</sub>Si phase, which is also the basis for precipitation strengthening. The optimal ratio for the appearance of the Mg<sub>2</sub>Si phase is Mg/Si=1.73, but it is very difficult to obtain this ratio under practical conditions. As a result, most of the alloys include too much silicon or magnesium, which is the basic condition for the occurrence of thermal deposition [5, 6]. The purpose of strengthening by thermal deposition is to create uniformly distributed precipitated particles in the plastic base. The precipitated particles act as barriers to the movement of dislocations, which strengthens the heat-treated alloy through the strengthening process. The mechanism's limitation is that aged alloys can only be used at specific temperatures. At higher temperatures, the formed precipitates begin to grow and, after a period of time, if the temperature is high enough, they dissolve [3].

Controlled thermomechanical treatment can lead to significant improvements in yield stress and hardness in aged aluminium alloys. Micro mechanisms that regulate the fracture characteristics of such alloys depend on the coherence and distribution of precipitates, the size and shape of grains, as well as the presence of other phases that occur due to a certain concentration of impurities [7].



## 2. EXPERIMENTAL

The alloy of the Al-Mg-Si system with the required chemical composition was obtained by melting the technically pure metals of aluminium, silicon and magnesium in an electrical resistance furnace with a reducing atmosphere. The alloy was cast in a steel mould, and the obtained ingot has these measurements: 21×21×85 mm. After that, the casting was homogeneously annealed for 6 hours at 560 °C in a chamber furnace and then cooled in air at room temperature. Then, the casting was cut under a water jet and four samples with dimensions of 10×10×85 mm were obtained for further tests. The next step was cold rolling on a rolling machine that had been calibrated for each sample. After rolling, alloy samples were obtained in the form of a wire with a diameter of 5 mm. The total degree of deformation of the initial samples, achieved by applied cold plastic deformation, was 80.4%. Such a high degree of deformation caused a significant strengthening of the alloy and the impossibility of its further plastic processing. For this reason, recrystallization annealing was performed at a temperature of 520 °C for 15 minutes. Then the process of cold plastic deformation continued on the calibrated rolling mill. The total degree of deformation achieved in this second segment of rolling was 37.6%. A sample was obtained in the form of a wire, square cross-section, dimensions 3.5 × 3.5 mm. Wires with a cross-section of Ø 3.50 mm were obtained by drawing. After that, the samples were solution annealed at 520 °C for 30 minutes before being quenched in cold water. Shortly after that, the samples were artificially aged for 4 h, 5 h, 6 h, and 7 h at temperatures of 160 °C, 180 °C, 200 °C, and 220 °C.

## 3. RESULTS AND DISCUSSION

The chemical composition of the alloy was determined using X-ray fluorescence analysis (XRF) and the NITON XL 3t-950 device. Figure 1 displays the spectrum for the aluminium alloy EN AW 6061, and Table 1 shows the chemical composition of the alloy.

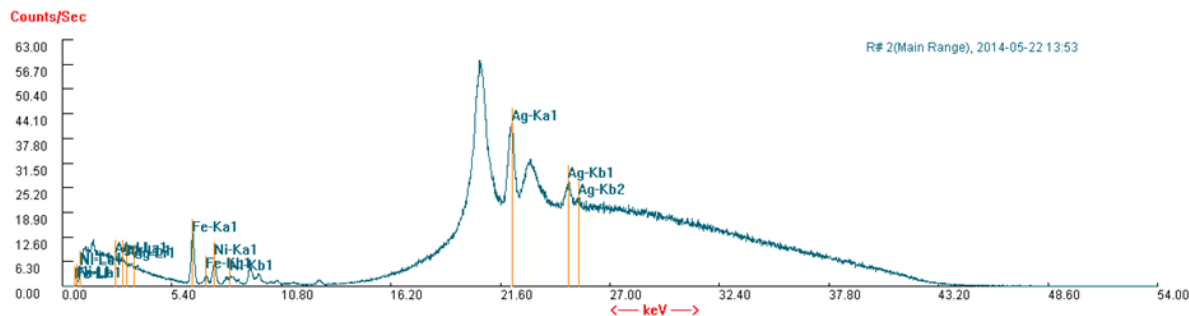
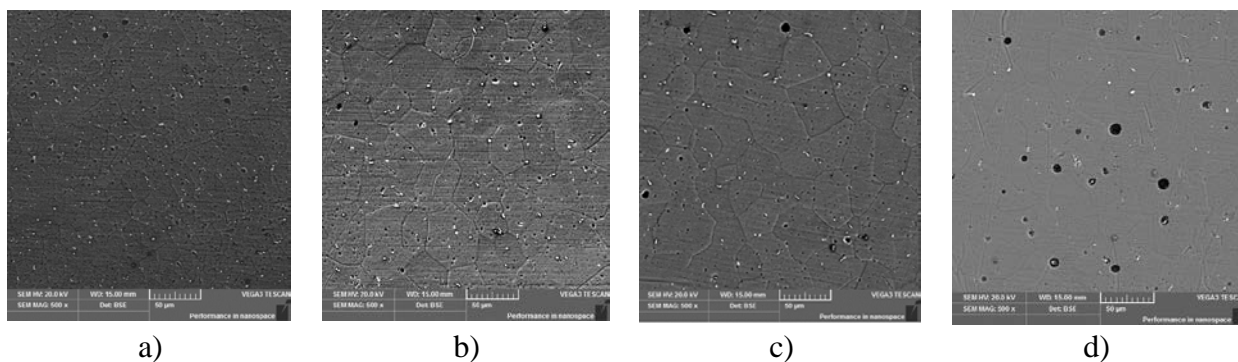


Figure 1 - Spectrograms of EN AW 6061 alloy

Table 1 - Chemical composition of EN AW 6061 alloy

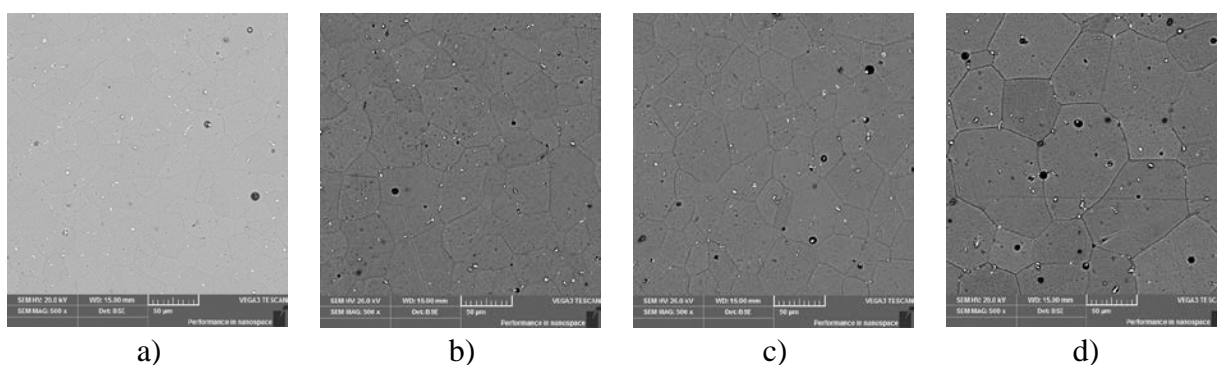
Element	Al	Mg	Si	Cr	Fe
(mas %)	97,54	1,26	0,819	0,231	0,222

Figures from 2 to 5 show the microstructure of the studied samples exposed to various heat treatment cycles. The samples were observed on an SEM with a magnification of 500x.



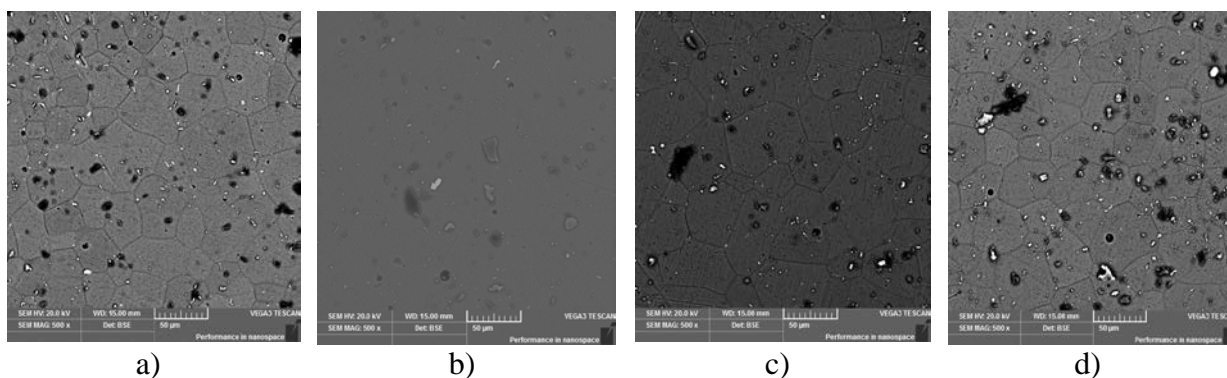
a) b) c) d)  
Figure 2 - Microstructure of EN AW 6061 alloy annealed at 160 °C for a duration of a) 4 h, b) 5 h, c) 6 h, d) 7 h

Studying the microstructures in Figure 2, it is clear that the structure is the finest in the sample that was treated for 4 hours. The boundaries cannot be seen in the case of the 7 hour treated sample.



a) b) c) d)  
Figure 3 - Microstructure of EN AW 6061 alloy annealed at 180 °C for a duration of a) 4 h, b) 5 h, c) 6 h, d) 7 h

In Figure 3, grain boundaries are clearly visible on all microstructures. The sample that was thermally treated for 4 hours has the finest microstructure, but the grain boundaries are also little visible. The biggest grains can be seen in the sample that was treated for 7 h, and the boundaries are most clearly defined.



a) b) c) d)  
Figure 4 - Microstructure of EN AW 6061 alloy annealed at 200 °C for a duration of a) 4 h, b) 5 h, c) 6 h, d) 7 h

Figure 4 shows samples annealed at 200 °C with clearly defined boundaries and a uniform grain size. Only in the case of the sample that was thermally treated for 5 h, it is not possible to observe the grain boundaries. With these samples, it is difficult to determine which sample has the tiniest grains and which has the coarsest grains.

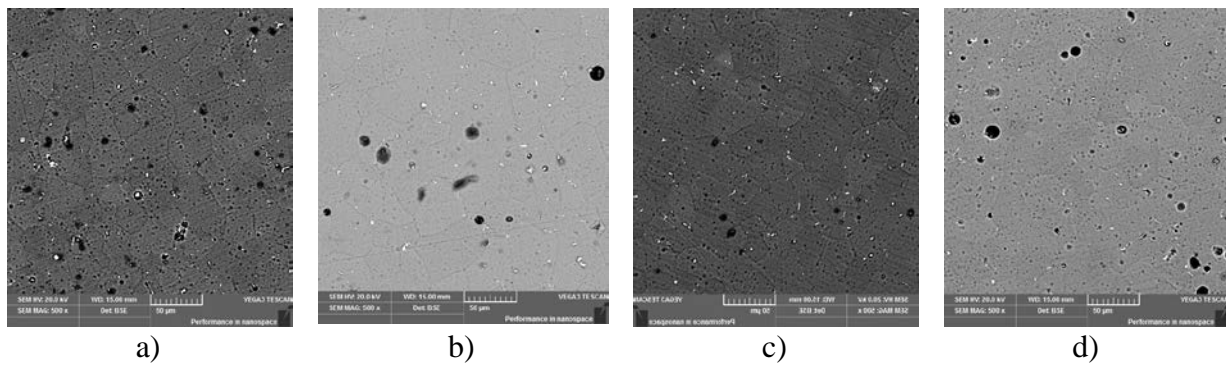


Figure 5 - Microstructure of alloy EN AW 6061 annealed at 220 °C for a duration of  
 a) 4 h, b) 5 h, c) 6 h, d) 7 h

The microstructures of the samples shown in Figure 5 represent the samples annealed at 220 C. It is possible to observe the growth of the grains and that their boundaries are not clearly visible. Similar conclusions can be found in Hossain and Kurny's study on the impact of aging temperature on the structural and mechanical characteristics of the Al-6Si-0.5Mg alloy [7]. For all examined samples, the general conclusion is that during heating, atoms of the precipitate phase are separated from the supersaturated  $\alpha$  solid solution. atoms of the precipitating phase represent nucleation centers, which lead to the formation and growth of precipitates. After a certain time of keeping the alloy at a defined temperature, an equilibrium structure consisting of  $\alpha + \beta$  phase is formed, that is,  $\beta$  phase is obtained which is in the form of uniformly distributed precipitate particles, which is in accordance with the literature [3].

#### 4. CONCLUSION

The basic aspect of the study of the properties of metals and alloys is microstructural characterisation. The microstructure is determined by the methods of obtaining the alloy, metallurgical processing, heat treatment, etc. The term microstructure defines the size and shape of crystal grains, their orientation and distribution of the basic structural phase, as well as other phases present. Metallographic tests of the EN AW 6061 alloy in this paper were performed with the help of SEM microscopy and it was concluded that the  $\beta$  phase is uniformly distributed in the metal base consisting of the  $\alpha$  phase. A comparison of the grain size as a function of annealing time and temperature was also made.

#### ACKNOWLEDGEMENTS

*The research presented in this paper was done with the financial support of the Ministry of Education, Science and Technological Development of the Republic of Serbia, within the funding of the scientific research work at the University of Belgrade, Technical Faculty in Bor, according to the contract with registration number 451-03-47/2023-01/ 200131.*

#### REFERENCES

- [1] S. Shabestari, F. Shahri, J. Mater. Sci., 39 (6) (2004) 2023-2032.
- [2] K. Kumar, The aluminium alloy selection and applications, The Aluminum Association Inc, Washington, 1998.
- [3] S. Ivanov, B. Stojanović, Termička obrada metala, Tehnički fakultet, Bor, 2018.
- [4] S. Pogatscher, H. Antrekowitsch, H. Leitner, T. Ebner, P.J. Uggowitzer, Acta Mater., 59 (2011) 3352-3363.
- [5] L. Zhen, W. D. Fei, S. B. Kang, H. W. Kim, J. Mater. Sci., 32 (1997) 1895-1902.
- [6] M. Yildirim, D. Ozyurek, Mater. Des., 51 (2013) 767-774.
- [7] A. Hossain, A. S. W. Kurny, Universal J. Mater. Sci., 1 (1) (2013) 1-5.

## EFFECTS OF COLD ROLLING AND ANNEALING PROCESSES ON THE MICROSTRUCTURE AND PROPERTIES OF MICRO-ALLOYED COPPER

Milijana Mitrović<sup>1</sup>, Saša Marjanović<sup>1</sup>, Biserka Trumić<sup>2</sup>,  
Jasmina Petrović<sup>1</sup>, Milan Nedeljković<sup>1</sup>,

<sup>1</sup>Technical Faculty Bor, University of Belgrade, V.J. 12, 19210 Bor, Serbia

<sup>2</sup>Mining and Metallurgy Institute Bor, Zeleni bulevar 35, Bor, Serbia

### Abstract

*In this paper, the change of mechanical and structural properties of micro-alloyed copper during the cold rolling and annealing process was monitored. Melting and casting of micro-alloyed copper was carried out in an electrical resistance furnace, with the "up-cast" casting process. The melted and chemically homogenized material was further subjected to the extrusion process, after which cold plastic deformation was performed with deformation degrees of 10, 30, 50 and 75%. Annealing of cold deformed samples was performed at 450°C for 35 min. The cooling of the samples was done in water with alcohol. After each stage of the experiment, the values of hardness, tensile strength and relative elongation were measured. The results showed that the values of hardness and tensile strength of unannealed samples increase with the increase in the deformation degree, while the relative elongation decreases. Deformation degree also affected the final grain size after the annealing process. At the highest deformation degree, the finest grains were obtained.*

**Keywords:** *micro-alloyed copper, extrusion, plastic deformation, microstructure, mechanical properties.*

### 1. INTRODUCTION

Copper has excellent electrical and thermal conductivity, good plasticity, is easy to process, but at the same time has low tensile strength, hardness, wear resistance and fire resistance, i.e. slightly worse mechanical properties [1-4]. One of the procedures that can improve the mechanical and structural properties of copper and copper alloys is cold plastic deformation. Since it is a deformation with complete strengthening, the metal grains are strongly oriented in the direction of the deformation, i.e. in the direction of force action. The higher the deformation force, the more expressed the deformation texture.

Cold plastic deformation improves strength and hardness by changing the crystal structure, but reduces toughness and plasticity, which easily creates residual stress. The subsequent annealing process after cold deformation results in dynamic recrystallization, which can produce the desired grain sizes and properties [5]. The loss of formability and ductility during cold rolling can be recovered during annealing [6].

In this work, the mechanical properties of micro-alloyed copper deformed at different degrees of cold deformation, as well as the change in microstructure after the subsequent annealing process, were investigated.

### 2. EXPERIMENTAL

Deoxidized low-phosphorus copper (DNP-Cu) with a maximum iron content, Fe up to 0.003 wt% and a maximum phosphorus content, P up to 0.014 wt% was used as the starting material. In order to obtain material of this chemical composition, copper cathodes with a purity of 99.99 % Cu were

used, which were melted in an electrical resistance furnace with a protective atmosphere, and then casting was performed using the "up-cast" process. Copper microalloying was performed by adding prealloy CuP6.42 and adding iron in the form of powder. Cast rods of satisfactory chemical composition were subjected to the extrusion process, resulting in strips 90 mm wide and 19.8 mm thick. After obtaining the extruded samples, rolling was followed on a rolling mill with smooth rollers from the manufacturer "FIOA - Italy" with reduction degrees of 10, 30, 50, and 75%, up to the final thickness of the copper plates of 4 mm.

After each phase of the experiment, the hardness measurement was carried out on the device for measuring the hardness of the manufacturer "VEB Leipzig", as well as the measurement of the tensile strength and elongation on the tear machine "OTTO WOLPERTWERKE GmbH".

The metallographic preparation of the samples was carried out on the "METKOM ELOPREP 102" electrolytic polishing and etching device. An aqueous solution of phosphoric acid and alcohol was used as an electrolyte for polishing the samples, and for better structure development, the samples were also etched with a solution of ferric chloride.

Microstructural analysis of the prepared samples as well as statistical grain counting was performed on a "LEICA" microscope equipped with a "Flexcam - C1" digital camera.

### 3. RESULTS AND DISCUSSION

Table 1 shows the results of tensile tests and hardness tests of samples in the unannealed and annealed state. As the degree of deformation increases, hardness and tensile strength increase as a result of deformation strengthening, while relative elongation decreases. During plastic deformation, dislocations react with each other and form immobile dislocations, which are an obstacle to the movement of other dislocations. With the advancement of dislocations, the number of obstacles increases, so it is necessary to apply a higher force in order to continue deformation [7, 8].

Table 1 - Mechanical properties of unannealed and annealed samples at different degrees of deformation

Sample condition	Deformation degree $\varepsilon$ (%)	Hardness (HV)	Tensile strength $R_m$ (MPa)	Relative elongation A (%)
Extruded	0	50,12	207,00	61,50
Deformed, not annealed	10	86,11	258,80	40,00
	30	106,50	336,60	11,25
	50	112,50	372,00	7,50
	75	121,20	381,80	6,25
Deformed, annealed for 35 min. at 450°C	10	45,46	228,50	54,37
	30	47,15	231,60	55,00
	50	48,00	236,50	53,75
	75	49,03	240,40	50,00

The maximum value of hardness and tensile strength was reached at the highest degree of deformation (75%) and for hardness it was 121.20 HV, while the tensile strength was 360 MPa. During the tensile test, the same sample broke with a very small elongation of 6.25%, which is a consequence of the loss of ductility in the cold rolling process.

The subsequent annealing process after cold deformation results in dynamic recrystallization, with a drop in hardness and tensile strength, and an increase in relative elongation.

The level of deformation also affected the final grain size after the annealing process. Figure 1 shows the microstructures of samples with different degrees of deformation after annealing at 450°C for 35 min. It can be concluded that the higher the level of deformation, the finer the grain size after the annealing process, which was confirmed by the statistical analysis of grain counts.



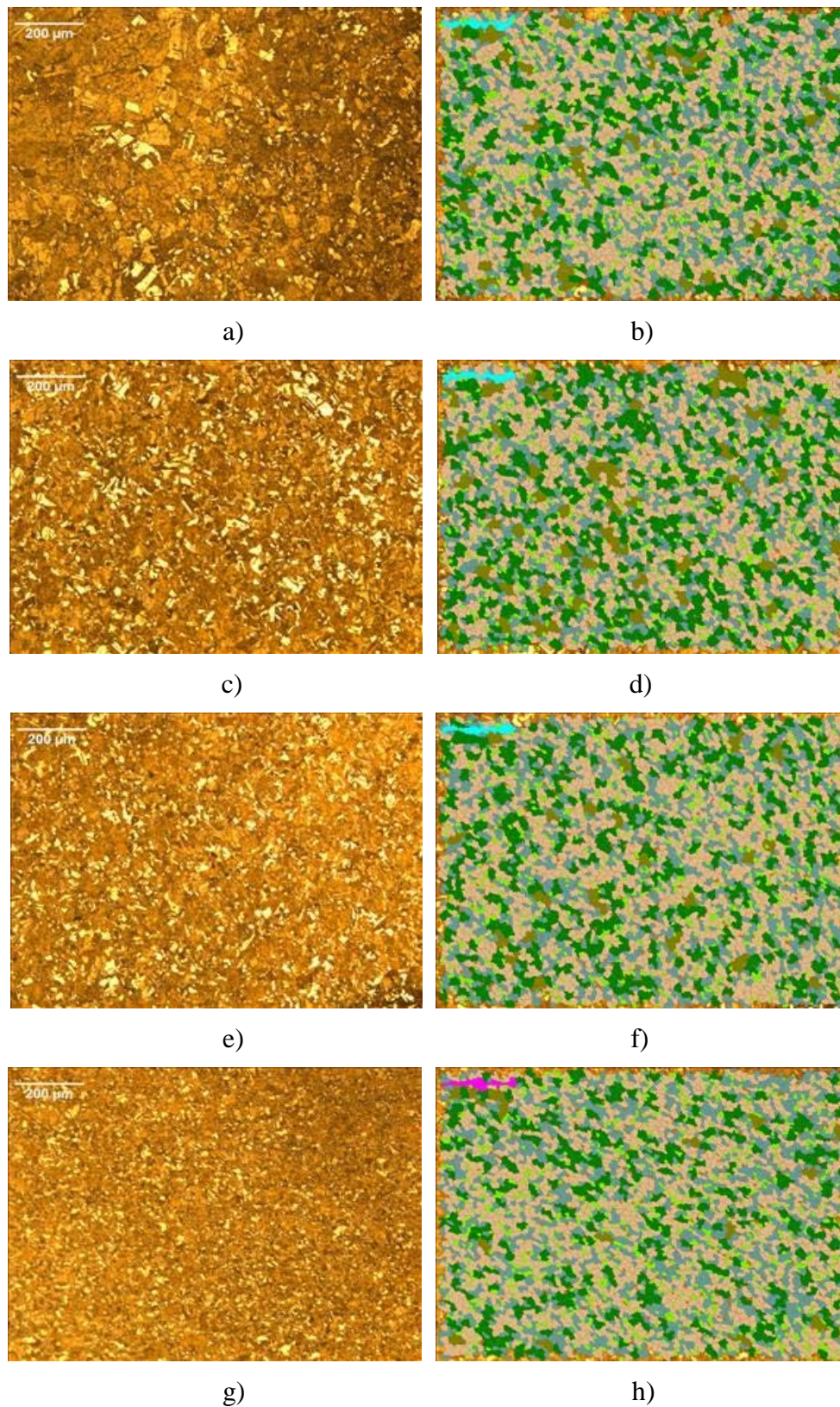


Figure 1 - Optical microphotographs of samples annealed for 35 min. at 450°C with different degrees of deformation: a) deformation degree 10 % with b) grain counting statistics, c) deformation degree 30 % with d) grain counting statistics, e) deformation degree 50 % with f) grain counting statistics, g) deformation degree 75 % with h) grain counting statistics



The deformation process introduces dislocations and texture in the microstructure. Subgrains in between shear bands and twinning may act as nucleation sites for new grains. Therefore, higher deformation leads to higher grain nucleation rate that ends as finer grains after annealing process.

#### 4. CONCLUSION

Based on the conducted research, the following conclusions can be drawn:

- The hardness and tensile strength of microalloyed copper during cold rolling increase with the degree of deformation due to strain hardening, while the relative elongation decreases. The maximum values of hardness and tensile strength were obtained at the highest degree of deformation (75%) and they were 121.20 HV and 360 MPa. Due to the fact that the material lost its ductility in the cold rolling process, the relative elongation of the sample with the highest degree of deformation was only 6.25%.
- During the annealing process at 450°C for 35 min., due to the mechanism of recovery and release from stress, recrystallization and grain growth, there was a decrease in values for hardness and tensile strength, and an increase in relative elongation.
- The degree of deformation also affected the final grain size after the annealing process. As the degree of deformation increased, the structure became finer.

#### ACKNOWLEDGEMENTS

*The research presented in this paper was done with the financial support of the Ministry of Education, Science and Technological Development of the Republic of Serbia, within the funding of the scientific research work at the University of Belgrade, Technical Faculty in Bor, according to the contract with registration number 451-03-47/2023-01/ 200131.*

#### REFERENCES

- [1] C. J. Li, S. Z. Huang, D. M. Zhang, J. Metal heat treatment, 32 (10) (2007) 66-68.
- [2] Liu J. X., Gong S. P., J. Anhui metallurgy, (4) (2004) 51-52.
- [3] Q. R. Luo, J. China Metal Bulletin, 1000 (01) (2020) 34-35.
- [4] I. Goto, S. Aso, K. I. Ohguchi et al., J. Mater. Eng. Perform., 2019.
- [5] S. Nestorovic, J. of Mining and metall. 40 B (2004) 101-109.
- [6] B. T. Sofyan and I. Basori, ARPN J. Eng. App. Sci., 11 (4) (2016) 2741-2745.
- [7] A. G. Guy and J.J. Hren, Elements of Physical Metallurgy, 5th Edition, Addison-Wesley Publishing Company, Los Angeles, 1994.
- [8] E. C. Rollason, Metallurgy for Engineers, 5th Edition, Edward Arnold Publishers, New York, 1996.

## UNLOCKING ENERGY EFFICIENCY: FINANCING PREFERENCES FOR SMES IN THE REPUBLIC OF NORTH MACEDONIA

Makedonka Dimitrova<sup>1</sup>, Jasminka Dimitrova Kapac<sup>2</sup>

<sup>1</sup>University American College Skopje, Treta Makedonska Brigada 60, Skopje, The Republic of North Macedonia

<sup>2</sup>Macedonian Center for Energy Efficiency, Nikola Parapunov 51-2/3a, Skopje, The Republic of North Macedonia

### **Abstract**

*The European strategy emphasises energy efficiency as a critical goal, with SMEs playing a significant role in industrial and commercial energy use. This research aims at identifying financing preferences for energy-saving investments in SMEs, which can enhance competitiveness and sustainability along with barriers to investment activities.*

*The research used semi-structured questionnaire with open ended questions that was administered on fifteen SMEs in the Republic of North Macedonia that have already utilised a loan for energy saving projects. In addition, desk research on the past and current financing schemes was performed, follow by a comparative analysis and case study of the Macedonian market for financial mechanisms for energy efficiency projects. On the parallel five interviews were performed with local banks that offer loans from the existing landing schemes. The approach was done with semi-structured questionnaire with open-ended questions.*

*The research highlights a lack of access to finance, knowledge gap for energy efficiency potential. It reveals that SMEs prefer financial mechanisms with grants for energy efficiency projects. Strengthening corporate financial literacy, knowledge on the benefits of energy saving and conservation project, and on the other hand increasing the offer of innovative designs of financial schemes by the commercial banks could help overcome the current state of the Macedonian industrial SMEs. The Government, on the other hand, could enhance the process of industrial decarbonisation by introducing green bonds or similar financing schemes.*

*The main limitation is the size of the sample and lack of representation of diverse industrial SMEs.*

**Keywords:** *Energy efficiency, SMEs, financing mechanisms, subsidised loans, the Republic of North Macedonia*

### **1. INTRODUCTION**

The European strategy for smart, sustainable, and inclusive growth<sup>3</sup> recognises the importance of energy efficiency (EE) and the role of the industrial sector in developing energy-efficient and decarbonised societies [1].

Small and Medium Enterprises (SMEs) play a significant role in industrial and commercial energy use, but their energy use and saving potential have not been systematically monitored especially in developing countries. While SMEs share similarities with larger enterprises as energy end-users, their capacity for energy considerations and decision-making processes differ. SMEs offer versatile growth and sustainability possibilities, yet they are limited in human and financial capital making them more fragile and risk adverse. Moreover, the energy saving and energy efficiency gap in SMEs persists due to perceived barriers and drivers. Economic incentives, such as cost reductions for past investments and potential energy savings for future investments, serve as key drivers for implementing energy efficiency measures [2]. In addition, limited financial resources often hinder the decision to adopt such measures. Moreover, limited knowledge on saving potential

---

<sup>3</sup> European Commission, "Europe 2020: A strategy for smart, sustainable and inclusive growth," European Commission, 2010.

and return on investment for such projects have been identified as another barrier to growth in SMEs [3].

To be able to stimulate investment decisions for unlocking energy efficiency in the SMEs, the objective of the research is to identify the needs and preferences for green financing mechanisms. The framework will offer a ground for recommending financing schemes to match the current situation among the SMEs for energy saving. These investments can enhance competitiveness, reduce costs per unit, and contribute to carbon footprint reduction and greater sustainability for companies.

Access to finance is crucial for the sustainability of SMEs. It enables market entry, increases entrepreneurial activities, enhances innovation capacity, and improves risk management skills. Financial literacy is identified as a vital knowledge resource for financial decision-making in SMEs, and its impact on sustainability needs further exploration. Difficulty in accessing finance may lead SMEs to seek inappropriate sources of funding, which can negatively impact their sustainability. Therefore, governments worldwide are implementing support policies and programs to finance responsible SMEs and promote clean energy investments. The road to increased investment in the Republic of North Macedonia was paved by the international financial institutions such as European Bank for Reconstruction and Development (EBRD). Two decades now, EBRD implements green financing facilities in the country to help increase the share of renewable energy sources and reduce dependence on coal energy production [4]. However, the past and current financing mechanisms have been of limited scope and there is still a need to implement financing mechanisms that will serve as 'carrot and a stick' to the SMEs by offering subsidised loans or technical support in making backup investments in energy saving.

## **2. EXPERIMENTAL**

### **2.1 Energy Efficiency & Energy Conservation**

The modern economic theory emphasises the role of SMEs in driving economic development, particularly in developing countries. SMEs are gaining importance due to their ability to adapt quickly, work with less capital and lower management costs, resulting in cheaper production. They are also more resilient to economic crises and contribute significantly to job creation and global economic development. SMEs represent around 90% of all enterprises, provide over 50% of global employment, and contribute up to 40% of national income (GDP) in some countries [5].

Access to finance is a significant constraint for the growth of SMEs, particularly in emerging markets and developing countries [6]. This obstacle poses a challenge to the sustainable growth of SMEs. In developed economies like Singapore, 70% of SMEs benefit from business support programs provided by governmental enterprise development agencies and centres [7]. However, countries in the process of development and transition rely on international financial and development organisations to provide support for SMEs.

According to the International Energy Agency energy conservation measures refer to actions taken to reduce energy consumption and improve energy efficiency [8]. As energy conservation and energy efficiency are recognised as drivers of innovation and long-term economic growth green investments as imperative for the SMEs [9]. In this respect, green investments lead to energy saving or clean energy production [10]. In particular, energy efficiency refers to achieving more output with less energy in an economy, and in the industrial sector, it can be measured by the energy required to produce a unit of product [11]. To add, energy conservation measures refer to actions and strategies implemented to reduce energy consumption and improve energy efficiency. These measures are aimed at minimising energy waste, optimising energy use, and reducing the overall environmental impact associated with energy consumption in SMEs. Energy conservation measures can include various approaches such as upgrading heating/ventilation/air-conditioning systems, improving insulation, energy-efficient lighting, utilising renewable energy sources, and optimising energy management practices. The potential benefits of energy conservation measures

are significant. Additionally, energy conservation measures have the potential to enhance the resilience and reliability of micro-grids, leading to improved energy efficiency and cost savings[12]. The evaluation of energy conservation measures involves assessing their economic feasibility, environmental impact, and potential benefits. Cost-benefit analyses are conducted to determine the financial viability of implementing energy conservation measures[13]. Energy efficiency projects encompass various initiatives, including conservation, upgrades, retrofits, and green building improvements. In many SMEs such a projects could help optimise plant and equipment for maximum efficiency not just in energy saving but also in reducing bottlenecks in production, long-term pipeline planning and lead to high operations efficiency. These investments offer savings, short payback periods, and a return on investment (ROI) through reduced energy bills. However, barriers, such as a lack of financing mechanisms and banks' reluctance to fund such projects, hinder their implementation.

Governments prioritise energy efficiency and minimise energy use due to the depletion of natural resources. The economic analysis of climate change policies relies on the interactions between energy use, technological change, and economic growth. Fossil fuels remain essential in modern economies, but reducing greenhouse gas concentrations requires significant reductions in their use, which can impact GDP and economic growth. Moreover, the introduction of energy-efficient technologies can help achieve energy conservation and mitigate the trade-off between energy reduction and economic growth[14]. Therefore, economists emphasise the importance of technological change, improvement, and innovation in climate change, environmental, and energy policies. These policies align economic, environmental, and social development goals for SMEs and take a multidimensional approach.

Energy efficiency is seen as a vital avenue for both developed and developing economies to achieve significant economic and environmental benefits. While developed countries have made strides in this area since the 1970s, there is still untapped potential. The International Energy Agency that the potential benefits of energy efficiency are significant across different types of economies[15]. For industrialised economies, the prospective benefits of energy efficiency are estimated to be as high as 25 to 30%. Transition economies have even greater potential, with estimated benefits of up to 40%. Developing countries fall somewhere in-between, with potential benefits that vary depending on their specific circumstances and level of development[14]. The reason for this is the significant expected increase in energy demand in developing countries and the cost-effectiveness of energy efficiency projects in new constructions or major facility modifications, which are believed to be crucial [16].

## **2.2. Financing energy saving projects**

Global economic shocks, such as the COVID-19 pandemic and the Ukraine conflict, have reshaped energy capital flows and markets, leading to higher energy prices supply chain disruptions, especially in Europe, due to its heavy reliance on energy imports from Russia [17]. At turbulent times, SMEs need external support to overcome the barriers and achieve substantial energy savings to implement projects with modest costs and high energy savings are ideal, shortening the payback period. Yet, a significant funding is required to realise the economic and environmental benefits of energy efficiency where public finance plays a crucial role in the future of energy efficiency. Peng & Zheng assure that green finance serves as an effective tool for environmental regulation and promotes green economic growth [18]. Therefore, market financing tools for energy efficiency projects, such as green bonds<sup>4</sup> and green finance, play may play crucial role in overcoming barriers and promoting investment in energy efficiency[19]. Other financing options, including internal funding and external debt financing, such as loans and leases, are available for energy efficiency investments. Energy performance contracts involving ESCOs can also provide financing for

---

<sup>4</sup> Green bonds, introduced by the World Bank, aim to reduce carbon emissions and mitigate climate change by financing green energy projects

energy-saving projects[20]. Hence, ESCOs have the potential to address these barriers they remain relatively undeveloped in developing countries like the Republic of North Macedonia [21] Banks' hesitation to provide financing options to ESCOs further complicates the issue[16]. Green banks are also a instrument to support energy efficiency investments and economic growth[19] although the development of green finance may be affected by the level of market development, and its impact on energy efficiency may vary depending on the level of marketisation[18]. According to the EBRD and the Energy Community Secretariat, there are various global and centralised EE financing mechanisms, such as (1)Upfront or post-implementation grants, (2)Tax relief, accelerated depreciation, and tax rebate schemes, (3) Direct loans with softened conditions (may be complemented by grants) channeled through an energy efficiency fund, (4) Credit lines for tied loans from commercial banks, (5) Providing financial support via third - parties such as ESCOs to deliver energy savings, (6) Provision of guarantees for loans and (7) On-bill financing with softened conditions[22]. Alike other financing mechanism, the mentioned have advantages and disadvantages given the specific context. Yet, all are designed to reduce the financial burden of implementing energy efficiency measures for SMEs compared to open-market options. Each approach addresses specific market failures that hinder economically beneficial investments. While financial support is essential, it alone cannot address all market failures. A well-designed EE investment plan and policy, considering both internal and external factors, are necessary [22]. Governmental financing is straightforward and progressive but may limit scalability. Financing through energy bills allows scaling but can be regressive and represent a significant portion of expenses. Efforts by governments and international organisations aim to bridge this financing gap[23]. Funding EE projects through donors and international financial institutions (IFIs) is government budget-neutral but may have longer mobilisation times.

In developing economies, the growth of SMEs is hindered by a lack of finance due to factors like an underdeveloped financial sector, limited legal structures for managing SMEs lending risk, high borrowing costs, and rigid interest rates. Energy efficiency, while profitable in the long run, often faces hurdles in SMEs due to high initial investment costs. Many SMEs avoid energy saving investments and renewable energy due to a lack of funding and delivery mechanisms. Soft loans and subsidies can help SMEs transition towards sustainable development through energy efficiency and renewables[24]. On the parallel, the energy efficiency financing gap involving high pre-investment costs, information gaps, and banks view on energy efficiency as a niche could be addressed by the financing facilities to improve the investment pace.

### **3. RESULTS AND DISCUSSION**

#### **3.1 Methodology**

The research applied qualitative research techniques including interview technique and comparative analysis. The research instruments are expected to provide a more comprehensive understanding of which are the preferred financial mechanism/s for the SMEs to overcome the financing gap. We have used secondary data from past energy saving financing programs and official statistical sources for the comparative analysis.

The research goal is to provide recommendations for preferred financial mechanisms in the SME sector and help bridge the financing gap for financing energy saving projects.

The interview guidelines consisted of 5 closed and 10 opened ended questions, for the purpose of collecting primary data. The instrument explored the already implemented energy efficiency measures, if any, the intentions for future investment in energy efficiency, and knowledge on sources of financing and funding awareness. In addition, demographic data of the companies was collected. The interviews were implemented in the months of July and August 2022, both via face-to-face interview method, and scheduled telephone call. The sample anticipated SME selection by the following criteria: production and printing companies, energy intensive processes, and past record of energy saving investment. An engineering expert was consulted in the process of

selection of the companies. Initially 33 SME were contacted while the response rate was less than 50%. The interviews were conducted with appointed technical personnel in medium sized companies or an informed managerial staff in smaller entities. Following the process of data collection, we have categorised the findings and summarised the key words and conclusions.

The first set of questions aimed at acquiring information on the demand for energy efficiency specific financial instruments based on the SMEs. Each question consisted of three sub-questions to understand the dynamics and history of investments in energy efficiency, in particular: implemented (past), planned/potential measures. The second set of questions was developed to explore the attitude towards energy efficiency investments, capacity for energy efficiency investments as well as applicability of the financial mechanisms. The third set of questions aimed at SMEs' preferences for financing mechanisms.

On the parallel, five interviews were performed with local banks that offered loans from the existing lending schemes. The approach was done with semi-structured interview guidelines with 5 closed ended and 11 open-ended questions to explore their lending experiences and market demand for energy saving loans.

Nonetheless, it's important to acknowledge the limitations of this research, including its sample size and limited representation of industrial sectors, primarily focusing on the processing and printing industry.

### **3.2 Research results**

The typical company of the sample was medium sized company, with dominantly male ownership, located in Skopje, operating in two shifts and factory/production facility constructed in the last decade of the 20<sup>th</sup> century. As for the energy mix, electricity use dominates among the companies. The research findings indicate that a significant percentage of companies have already implemented various energy efficiency measures, majority had applied heat distribution measures, followed by process equipment, and compressed air improvements. It was common that one company implemented few measures at the same time or in consecutive investment cycles. Future investments are planned in the refrigeration processes, smart lighting, building envelope and roof refurbishment, refrigeration equipment, and compressed air. We could summarise that 45% of companies were motivated to invest in energy-saving measures due to the proactiveness and push by the informed technical staff employed in the SME. In addition, successfully implemented projects by the top performing SMEs within a specific industry, or free energy audit as part of the financing program stimulated the investments. Few printing companies reported that they were urged to implement energy saving projects since their competitors put pressure on the marginal costs after they have implemented such a project. So, investing in energy saving among the companies from the printing industry became trendy a certain point in time.

Nonetheless, primary factors contributing to energy efficiency investments, as identified by the companies, were grants, followed by plausible interest rates, and loan payback time. Further on, the research revealed that the prevalent source of financing for past energy efficiency investments were programs offering subsidised loans. All companies have pointed out to this program design. Often subsidised loans were combined with company savings, matching European or governmental funds, and bank guarantees. The final investment depended on the financial strength of the company, investment portfolio in a particular bank and the negotiation skills of the top management. For planned/future investments, subsidised loans remained the preferred financing source whereas over 70% of the interviewed companies plan to utilise the loan as sole financing source. Other forms of financing were also identified but they were reported to depend on the overall economic scenery and the current status of the companies' finances.



### 3.2.1 Case Study of Macedonian Energy Saving Finance Mechanisms

The Republic of North Macedonia is an upper middle-income country in which SMEs represent a backbone of the private sector with over 72,000 active enterprises in 2021[25]. The COVID-19 pandemic caused a recession, hitting industries the processing industries at most given their energy intensive operations but also hospitality entities, logistics and services. Energy costs posed challenges to SME growth, requiring immediate action and support, particularly from financial institutions.

According to ECOS Skopje, in 2018, private sector credit in the Republic of North Macedonia amounted to 50.4% of its GDP [26]. Although this figure is lower than what is observed in developed countries, it closely aligns with patterns seen in Western Balkan nations. Banks provided the majority, accounting for up to 48.8% of GDP in total private sector lending, with a smaller portion coming from other financial institutions like savings banks and leasing companies. This differs from some European countries where lending exceeds GDP and Central European countries where lending to companies is twice as substantial as in North Macedonia. These statistics highlight the significant potential for increasing the availability of financial resources for SMEs in the region. Challenges persist due to the rigidity of North Macedonian banks and the absence of a robust lending culture within the SME sector, which hinders local investments in energy-saving and conservation.

Local banks in North Macedonia offer financing options for energy efficiency projects, with similar conditions across the sector. These options include tailored loans for EE investments without incentives but may come with technical assistance, loans without grants but with complimentary technical assistance, and loans with both technical assistance and financial incentives. For SME financing, banks follow strict lending guidelines. Interest rates, typically ranging from 4% to 7%, are determined case by case based on factors like company liquidity, financial history, and growth potential. Some financial institutions set maximum interest rates through mutual agreements. Despite lower interest rates on corporate sector loans, clients prefer products with incentive payments, although they understand these grants are available for a limited time.

The research of the local banks suggests that the existing financial tools for EE are suitable for North Macedonia's current stage of economic development. The post-pandemic recovery and the Ukraine crisis adaptability of the private sector still favour financial incentives accompanied by technical assistance and granting schemes when considering energy saving investments. The banks reported that the companies that invested in EE they come back to the bank to repetitive financing of other energy saving measures, yet the financing schemes are of limited duration and some remain underserved. The 'word of mouth' and continuous education of the decision makers in the companies about the financial and environmental benefits was stressed as crucial in the process of decision making as well.

To facilitate the decarbonisation process and promote energy savings and conservation in the industrial sector, the Republic of North Macedonia has garnered support from various international financial institutions. The EBRD, the World Bank, USAID and the European Union have played an instrumental role in developing the financial markets and the accompanying legal framework to streamline investment processes and provide more financing options. To facilitate investments in energy efficiency and energy conservation, financing facilities accompanied by grant schemes and technical support were introduced in 2008, see Table 1.

The Western Balkans Sustainable Energy Financing Facility presented a new approach to energy efficiency investments in the private sector. WeBSEFF I (2008-2016) was implemented via three local banks, and WeBSEFF II (2014-2019) via two local banks totalling 24 million euro. Green for Growth Programme (2010 – 2020) followed, with 18 mil euro. One of the longest present support programs is the SME Competitiveness Support Programme (2018-), co-funded by the EBRD and European Union Instrument for pre-accession capping 51 million euro. A mechanism

of 6 million euro targeting only women led business was developed by the EBRD, Women in Business I and II, as well. And just in the beginning of 2023, the UNDP GEF/EBRD/IOM financing program for private sector inter alia was announced. The allocation of funds to the private sector is yet to be announced.

Table 1- Energy Saving Financing programs in the Republic of North Macedonia

Financing program name	Implementation period	Value in EURO million	EE Grant max	TA Support	Participating Banks
<b>WEBSEFF 1</b>	2008-2016	12	15%	√	NLB TB Skopje, Halkbank, Ohridska Banka
<b>WEBSEFF 2</b>	2014-2019	12	5%-10%	√	NLB TB Skopje, Ohridska Banka
<b>GGF</b>	2010-2020	18	no	√	Halkbank
<b>SME - CSP</b>	2018-on going	51+	15%	√	Komercijalna Ohridska Sparkasse NLB Prokredit Bank
<b>Women in Business I and II</b>	2015 – 2019	6	5%-15%	√	Ohridska- Societe General Bank and NLB Bank
<b>GFF</b>	2023 - ongoing	30	tbd	√	tbd

*Source: Authors own research*

In general, all financing programs aimed to enhance competitiveness of the SMEs by reducing energy costs per unit, addressing bottlenecks, and improving overall energy management in companies. All programs supported energy efficiency as well as renewable energy projects. These programs, without exception, offered additional stimulations for the SMEs, such as free technical support in a form of 'walk-through' of full size 'energy audits' and/or grants upon successful implementation of the projects of up to 15% of the total loan. These elements served as catalysts for generating interest in energy-saving loans within the industrial sector through a grassroots 'word-of-mouth' approach. However, ultimate goal of the donor community is to gradually reduce the dependence on donor financing schemes on the local market, leaving behind a long-lasting legacy of an investment culture fostered by innovative loans offered by commercial banks and proactive SMEs.

#### 4. CONCLUSION

The findings indicate that subsidised borrowing characterised with grants with technical assistance are preferred financial mechanisms for energy saving investments among the processing and printing SMEs in the Republic of North Macedonia, a finding also confirmed by the commercial banks that have implemented subsidised loans in cooperation with the international financial institutions. The local financial institutions are not yet ready to operate on their own, offering tailor made energy saving financing tools that will be consumable by the SMEs, so the current practice shall continue to stimulate the financial market maturation on the medium run[24].

Only 500 SMEs<sup>5</sup> benefited from the available programs, representing less than 1% from Macedonian SMEs. One of the key challenges is the lack of financing options, particularly for less financially stable SMEs [27] and the absence of technical expertise to effectively manage energy and make informed investment decisions to save on energy and increase the competitiveness of the offerings. Incentives, such as technical support to both technical and non-technical staff as well as investment subsidies, will continue to play a crucial role in encouraging companies to pursue energy-saving projects, given their potential for rapid payback. Also, there is a strong indication that there is a knowledge gap on the return-on-investment potential of energy saving projects both among the SMEs and the banking staff. So, important factors for driving investment in energy efficiency includes access to knowledge within the company, having a culture within the company promoting energy efficiency, and networking within the sector. As for the banks, there is an opportunity for innovation in the financial services by networking with their international counterpart and networks who have been offering such loans for a longer period of time.

At organisational level there is need for improved communication between the technical staff and the management and building risk taking attitude in the company. To add, there is a necessity to increase awareness of energy and economic gains among the managerial staff, being most crucial in making decision while having different scenarios of payback time and similar return on investment indicators.

At Governmental level, the Republic of North Macedonia could introduce market financing tools like green bonds and green finance but also limited time subsidies to support the development of market financing mechanisms, crucial for promoting energy efficiency projects, overcoming obstacles, and driving sustainable economic growth. In particular, support introduction of renewable energy sources to overcome the SMEs dominant reliance on electricity as their primary energy source and support the decarbonisation process of the industry and the country in general. Additionally, the Government could anticipate policy improvements in terms of energy labelling of production equipment, subsidy for energy audits in small- and medium-sized companies, increased taxes to improve the cost-effectiveness of energy efficiency measures to bridge the financing gap that was proven successful in other more developed countries [28].

The future research endeavours could tackle financial literacy among the SMEs, specific knowledge needs of the technical staff to become a catalyst for energy saving investments and product innovation prospects of the financial institutions.

## REFERENCES

- [1] Fresner, J., Krenn, C., Morea, F., Tomasi, F., *J. Clean. Prod.*, 142(4), 2017), p.1650-1660.
- [2] Meath, C., Linnenluecke, M., Griffiths, A., *J. Clean. Prod.*, 112, 2016, 3597-3604.
- [3] Karadağ, H., *EMAJ*, 5(1), 2015, 26-40.
- [4] Sisodia, G., Awad, E., Alkhoja, H., Sergi, B., *BSE*, 29(6), 2020, 2789-2802.
- [5] Keskin, H., Senturk, C., Sungur, O., M. Kiris, H., *The Importance of SMEs in Developing Economies. 2nd International Symposium on Sustainable Development*, 2, 2010.
- [6] The World Bank. n.d. *Small and Medium Enterprises (SMEs) Finance*, 2021.
- [7] Lessidrenska, T., *SMEs and SDGs: challenges and opportunities*. [online] OECD's Development Centre, 2009.
- [8] International Energy Agency (IEA), *Energy Efficiency 2018: Analysis and Outlook to 2040*. Paris: IEA, 2018.
- [9] Chen, T., *Technical and Economic Evaluation of Energy-Saving Measures*, 2022.
- [10] Pavlyk, V., *FMIR*, 4(1), 2020, 117-123.
- [11] Patterson, M.G., *Energy Policy* 24 (5), 1996, 377-90.
- [12] Almarzooq, S. A. A., Al-Shaalan, A. M., Farh, H. M. H., Kandil, T. T. M., *Sustainability*, 14(4), 2022, p.2390.

---

<sup>5</sup> Authors' own calculation based on official statistics from all financial programs implemented in the country

- [13] Shin, J. H., Lee, J., Kim, H., Kim, S., & Cho, Y., *Adv. Civ. Eng.*, 2018, 1-8.
- [14] Smulders, S. and de Nooij, M., *Resour. Energy Econ.*, 25, 2003, 59–79.
- [15] International Energy Agency, *Accelerating energy efficiency: What governments can do now to deliver energy savings*, IEA, Paris, 2022.
- [16] Painuly, J. P., Park, H., Lee, M. K. and Noh, J., *J. Clean. Prod.*, Volume 11, 2003, p.659–665.
- [17] KPMG, *The Economic Impact of the Russia-Ukraine War*, 2023.
- [18] Peng, J., and Zheng Y., *Front. Environ. Sci.* 299, 2021.
- [19] Cherian, J., Sial, M. S., Álvarez-Otero, S., Comite, U., Zia-ud-Din, M., *ESPR*, 30(22), 2022, 61324-61339.
- [20] Energy - European Commission, *Energy Performance Contracting - European Commission*, 2021.
- [21] Stefanovski, Z., *Barriers, lessons learned, and future prospects for ESCOs*, EBRD, 2021.
- [22] European Bank for Reconstruction and Development; Energy Community Secretariat, *Centralised Energy Efficiency Financing Mechanisms: Policy guidelines*, s.l.: European Bank for Reconstruction and Development and the Energy Community Secretariat, 2020.
- [23] Mensah, S., *A Review of SME financing schemes in Ghana*, [online] UNIDO SME Paper, 2004.
- [24] Fleitera, T., Schleich, J., Ravivanpong, P., *Energy Policy*, 51, 2021, 863-875.
- [25] State Statistics Office of the Republic of North Macedonia. *MAKStat Database*, 2022.
- [26] Sustainability Institute ECOS – Skopje, *Yearly Report for the SME Sector for 2021. Agency for promotion of entrepreneurship of the Republic of North Macedonia*, 2022.
- [27] Painuly, J. P., *Int. J. Energy Sect. Manag.*, 3(3), 2009, 293-307.
- [28] Haraldsson, J. and Johansson, M., *Sustainability*, 11(7), 2019, 2043.

## ANALYSIS OF THE EFFECTIVENESS OF DIFFERENT METHODS FOR CUTTING SAMPLES

Zoran Štirbanović, Vesna Vojinović, Jovica Sokolović, Maja Trumić

Technical Faculty Bor, University of Belgrade, V.J. 12, 19210 Bor, Serbia

### Abstract

*In this paper are presented the results of analysis of effectiveness of four different sample cutting methods: quartering, "chessboard" method, Jones riffle splitter and automatic sampler "Vežin". For the analysis of their performance four copper ore samples with different grain size were used. Grain size composition of samples before and after cutting was determined and used for calculating absolute average deviation and real average deviation which were used for determining effectiveness of used methods. According to the obtained results "chessboard" method was the most efficient for cutting all investigated samples, i.e. it provided the samples with highest representativeness.*

**Keywords:** *sampling; sample cutting methods; absolute average deviation; real average deviation.*

### 1. INTRODUCTION

Sampling represents extraction of a smaller portion of material (ore) from a larger mass, according to the precisely established rules so the obtained sample has the same characteristics chemical, physical, mineralogical, etc. like the mass that it was taken from, i.e. it is representative.

In mineral processing, sampling is an operation that is being performed continually along with operating of the process and its main purpose is process control and quality control of final products and by-products as well. Primary samples are usually much larger in quantity than the samples needed for individual experiments or analysis, so it is necessary to cut them, sometimes even in several stages, by using adequate cutting methods. Methods for cutting primary samples that will be applied depend on grain size and quantity of the sample, but some of them can be applied for the same type of samples. The most commonly used methods for cutting samples in laboratory are: quartering, riffle splitters, automatic samplers, composite sampling ("chessboard" method), etc. Their effectiveness can vary depending on their construction and/or materials they are being used [1-3].

Sampling must be undertaken with high precision by applying adequate methodology, because inappropriate sampling can cause technological and economic issues. Sampling errors must be minimized not only during the sampling process but also later when primary samples are being further processed and prepared for analysis and investigation. This is especially important when high value materials are being sampled, i.e. gold containing concentrates [4].

In this paper are presented the results of investigating effectiveness of different methods for cutting samples in terms of their grain size composition before and after cutting.

### 2. EXPERIMENTAL

#### 2.1 Materials

For the investigation, four copper ore samples with different grain sizes:  $-9.50+3.36$ ;  $-2.36+0.71$ ;  $-0.71+0.25$ ;  $-0.25+0.075$  mm, were used. In Table 1 is given grain size composition of the used samples, before cutting

Table 1 – Grain size composition of the samples before cutting

Grain size class (mm)	Sample 1	Sample 2	Sample 3	Sample 4
	Mass (%)			
-9.50+4.75	33.3333	/	/	/
-4.75+3.35	33.3333	/	/	/
-3.35+2.36	33.3333	/	/	/
-2.36+1.70	/	33.3333	/	/
-1.70+1.18	/	33.3333	/	/
-1.18+0.710	/	33.3333	/	/
-0.710+0.425	/	/	33.3333	/
-0,425+0,300	/	/	33.3333	/
-0.300+0.250	/	/	33.3333	/
-0.250+0.150	/	/	/	33.3333
-0.150+0.106	/	/	/	33.3333
-0.106+0.075	/	/	/	33.3333
Σ	100.00	100.00	100.00	100.00

As it can be seen from the Table 1 all four samples were consisted from three different grain size classes with the same mass participation of the each class, 33,3333%.

## 2.2 Methodology

All four samples were cut by applying four methods for cutting samples: quartering, composite sampling, i.e. "chessboard" method, Jones riffle splitter, and automatic sampler "Veziin" (Figure 1). The procedure was repeated five times for each sample and each applied method.



Figure 1 - Applied methods for sample cutting: a) quartering; b) "chessboard" method; c) Jones riffle splitter; d) automatic sampler "Veziin"

After cutting of each sample, secondary samples were measured and they were sieved on the series of sieves depending on their grain size, in order to determine whether the grain size composition was preserved, i.e. whether the secondary samples are representative.

The results obtained from the experimental part of the research were used to calculate absolute average deviation (AAD) which represents average of the absolute deviations from a central point (mean value of the participation of each grain size class). The equation used for this calculation is:

$$AAD = \frac{\sum_{i=1}^n |x - \bar{x}|}{n} \quad (1)$$



where:  $X$  denotes participation of grain size class in secondary sample obtained after cutting,  $\bar{X}$  is a mean value of the participation of the same grain size class in secondary sample obtained from  $n$  number of repetitions.

Besides AAD, real average deviation (RAD), representing average of the deviations from a real (known) value, was also calculated by using following equation:

$$RAD = \frac{\sum_{i=1}^n |X - X_R|}{n} \quad (2)$$

In equation 2,  $X$  represents participation of grain size class in secondary sample obtained after cutting, while  $X_R$  is a real value of the participation of the same grain size class in primary sample.

The main reason why these two deviations were applied was the fact that in this study the hybrid samples, with known participation of each grain size class were used, so the aim was to see whether there are differences between samples before and after their cutting and how big these differences are.

### 3. RESULTS AND DISSCUSIONS

Values for AAD and RAD, calculated for each grain size class of all four investigated samples and for all applied sample cutting methods are given in Figure 2.

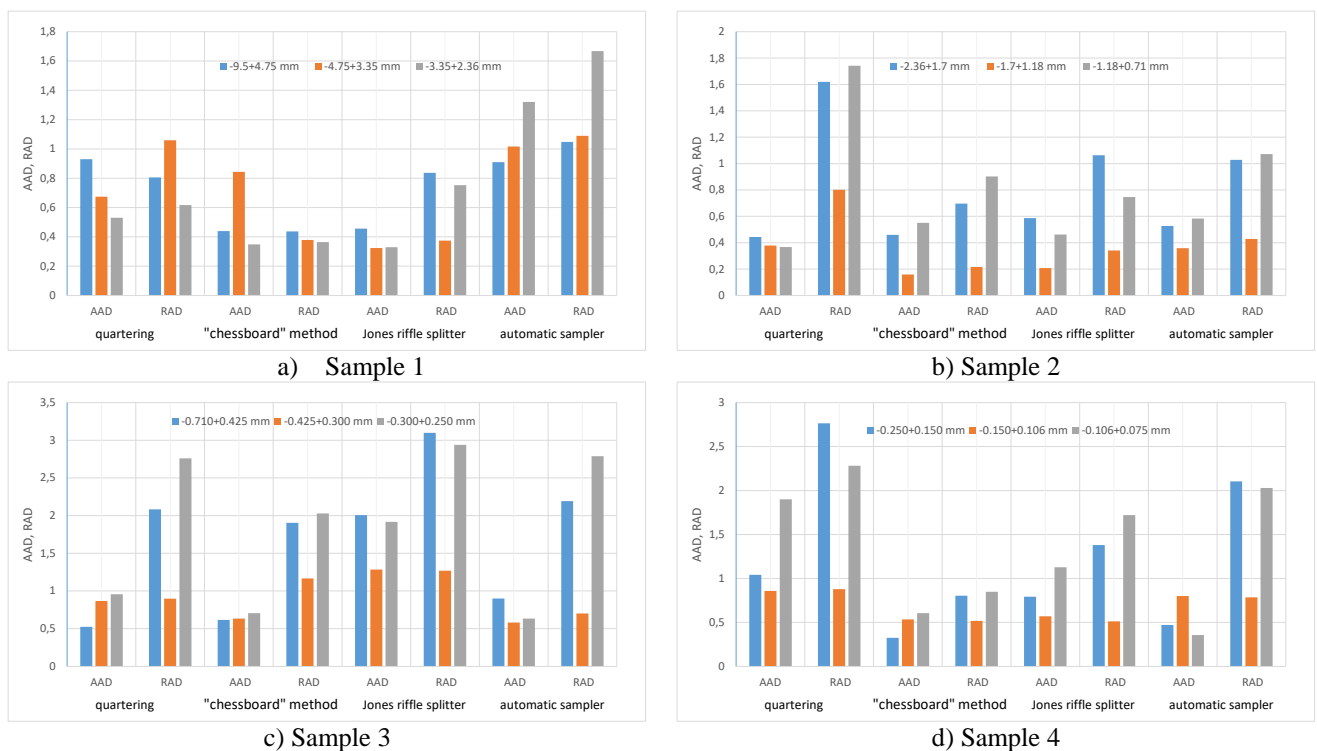


Figure 2 - AAD and RAD for each grain size class of all investigated samples and for all applied sample cutting methods

As it can be seen from Figure 2, the best results, i.e. the lowest values for AAD and RAD for almost each grain class of all four samples were obtained by applying so called "chessboard" method. Therefore it can be said that this method provides the highest representativeness of the samples after cutting.

According to AAD values for quartering were also low, so the conclusion could be that this method also provides representative samples. However, RAD values for this method are high indicating

that there are some, non-negligible differences between grain size compositions of samples before and after cutting. Similar trend can be observed with values for AAD and RAD for Jones riffle splitter and automatic sampler “Veziin”.

The differences between values for AAD and RAD arise due to the way they are being calculated, AAD by using the mean value of grain size participation of the class which can be balanced if similar error occurs more than once and RAD by using the real value of grain size class in primary sample. The good example is grain size class -1.18 + 0.710 mm obtained by using quartering for cutting Sample 2 (Table 2).

Table 2 – Values for  $X$ ,  $\bar{X}$ ,  $X_R$ , AAD, and RAD for grain size class -1.18 + 0.710 mm (Sample 2)

<b>X (%)</b>	34.3321	35.7777	34.9070	35.1745	35.2048
<b><math>\bar{X}</math>(%)</b>	35.0792		<b><math>X_R</math>(%)</b>	33.3333	
<b>AAD</b>	0.3677		<b>RAD</b>	1.7459	

As it can be seen from Table 2, while cutting Sample 2 by applying quartering, all values of grain size class -1.18 + 0.710 mm in secondary samples (after cutting) are more than 1% higher than its real value in primary sample (before cutting), so the mean value is not the best indicator for the representativeness of the sample in this case. However, when dealing with samples from industrial processes the real value is not familiar so it is necessary to perform procedures as precisely as possible.

#### 4. CONCLUSION

Sampling is very important operation especially when it is being used for quality control of final products, therefore it must be performed with extreme caution and by applying defined procedures and methodologies, which also applies for manipulation with primary samples, i.e. their cutting. Results of testing four sample cutting methods on four samples with different grain sizes have shown that "chessboard" method has the highest precision and samples obtained by this method are the most representative. However, other three investigated methods: quartering, Jones riffle splitter, and automatic sampler “Veziin”, can also be applied for cutting samples but their applicability depends on grain size and quantity of the primary sample.

#### ACKNOWLEDGEMENTS

*The authors acknowledge the Ministry of Science, Technological Development and Innovation of the Republic of Serbia for the financial support of scientific research at the University of Belgrade, Technical Faculty in Bor (contract no. 451-03-47/2023-01/ 200131).*

#### REFERENCES

- [1] I.C. Spangenberg, R.C.A. Minnitt, J. South. Afr. Inst. Min. Metall., 114 (2014) 91-102.
- [2] L. Petersen, C. K. Dahl, K. H. Esbensen, Chemometr. Intell. Lab. Syst., 74 (1) (2004) 95-114.
- [3] P.W. Cleary, G.K. Robinson, Chem. Eng. Sci., 66 (11) 2011, 2385-2397.
- [4] S.C. Dominy, Min. Technol., 125 (3) (2016) 129-141,

## LAND TURNOVER INCREASES DUE TO MINING: AN EMPIRICAL ANALYSIS OF BOR, SERBIA, 2013-2022.

Ivica Nikolić, Isidola Milošević, Anđelka Stojanović

Technical Faculty Bor, University of Belgrade, V.J. 12, 19210 Bor, Serbia

### Abstract

*This study examines whether the turnover of land near the mine or land used for the purposes of the mine is increased compared to land outside the mining area. In addition, this paper presents the land turnover after the privatization of RTB Bor by the Chinese company ZiJin Mining Grupe in 2018. For this research, public data from the website of the Geodetic Authority of the Republic of Serbia was used. The study showed that the turnover of land near the mine and for the needs of the mine is several times higher than the turnover obtained outside these areas, except in the area of Lake Bor. In addition, the impact of the increase in traffic and other real estate, especially residential, was observed following the increase in mining activity. This analysis shows the positive impact of mining on land turnover in the city of Bor.*

**Keywords:** land turnover, mining, empirical analysis

### 1. INTRODUCTION

Bor is located in the east of the Republic of Serbia. It consists of the central settlement, which is the seat of the Municipality of Bor, and 13 villages (Gornjane, Tanda, Luka, Krivelj, Bučje, Oštrej, Donja Bela Reka, Brestovac, Slatina, Zlot, Šarbanovac, Topla, Metovnica). The Municipality of Bor consists of 19 cadastral municipalities, with the urban settlement of Bor divided into two cadastral municipalities, Bor I and Bor II and the village of Zlot divided into five cadastral municipalities. Zlot I, Zlot II, Zlot III, Zlot IV and Zlot V. According to the data of 1844 there were 54 houses and 230 inhabitants [1, 2]. The faster development of Bor began in 1903—the year after the discovery and exploitation of copper ore. The copper mine changed hands. From 1903-1940, it was owned by French companies. After that, from 1941 to 1944, it was owned by Germany. After liberation, it became state property, where the Mining and Smelting Basin Bor - RTB-Bor was created. It remains in state ownership until 2018. After signing the contract on the acquisition of 63% of ownership by the Chinese company Zijin Mining Group, Chinese capital takes over the leading position. This change in the ownership structure contributes to the expansion of mining capacity, which is reflected in the need to purchase land to explore and exploit copper ore. In this way, there is a direct increase in land turnover in cadastral municipalities that are suitable for mining, but also an indirect turnover with the aim that former landowners want to buy land in a new location. This paper presents an empirical analysis of the impact of mining on the increase in land turnover in cadastral areas where mining is active, as well as the influence of Chinese capital on the increase in turnover after privatization [3, 4, 5].

### 2. EMPIRICAL ANALYSIS

On the website of the Republic Geodetic Institute of Serbia, every transaction of real estate is recorded for public inspection. Through empirical analysis, in Table 1, data for 19 cadastral municipalities in the city of Bor for ten years were presented, five years before the privatization of the Chinese company ZiJin and five years after the privatization in 2018, that is, from 2013-2022. Also, Figures 1-7 show an atypical real estate transaction caused by the purchase of a Chinese company for mining purposes.

Table 1 - Land turnover by year by cadastral municipality for the period 2013-2022 [2].

Number of turnover per year											
Cadastral municipality / year	2013	2014	2015	2016	2017	2018	2019	2020	2021	2022	Σ
Bor I	11	10	5	10	12	8	8	16	16	24	<b>120</b>
Bor II	5	3	3	1	3	2	2	2	9	19	<b>49</b>
Brestovac	75	44	42	79	72	76	63	82	108	92	<b>733</b>
Bučje	18	6	5	1	2	6	6	9	139	49	<b>241</b>
Gornjane	9	17	6	5	6	12	7	10	7	16	<b>95</b>
Donja Bela Reka	9	15	2	5	23	28	8	35	13	39	<b>177</b>
Zlot I	2	2	4	2	2	0	0	3	7	6	<b>28</b>
Zlot II	6	3	1	6	4	5	4	5	8	12	<b>54</b>
Zlot III	7	3	2	2	5	5	5	9	10	9	<b>57</b>
Zlot IV	10	7	11	2	4	3	7	6	4	10	<b>64</b>
Zlot V	8	10	12	3	4	3	4	8	8	13	<b>73</b>
Krivelj	17	7	1	8	13	12	20	33	75	146	<b>332</b>
Luka	5	1	2	2	3	1	2	2	0	4	<b>22</b>
Metovnica	8	5	4	7	4	13	6	3	4	1	<b>55</b>
Oštrej	18	3	2	5	6	12	9	1	9	6	<b>71</b>
Slatina	5	7	4	6	68	221	39	24	79	127	<b>580</b>
Tanda	5	1	0	3	0	0	0	1	1	0	<b>11</b>
Topla	0	0	0	0	0	1	1	0	0	0	<b>2</b>
Šarbanovac	10	11	11	8	9	10	3	10	14	17	<b>103</b>
Σ	<b>228</b>	<b>155</b>	<b>117</b>	<b>155</b>	<b>240</b>	<b>418</b>	<b>194</b>	<b>259</b>	<b>511</b>	<b>590</b>	<b>2867</b>

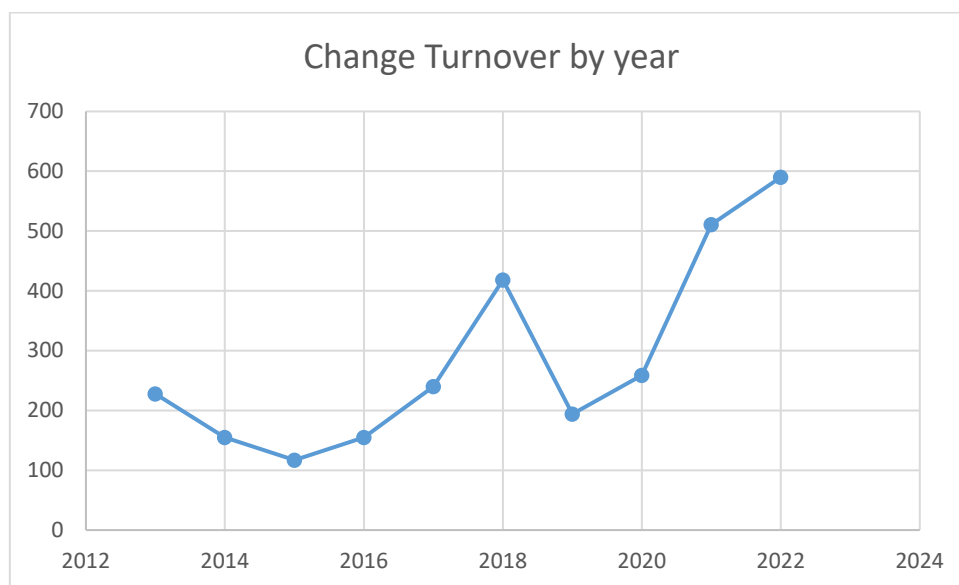


Figure 1 - Land turnover in the period from the beginning of 2013 to the end of 2022 [2].

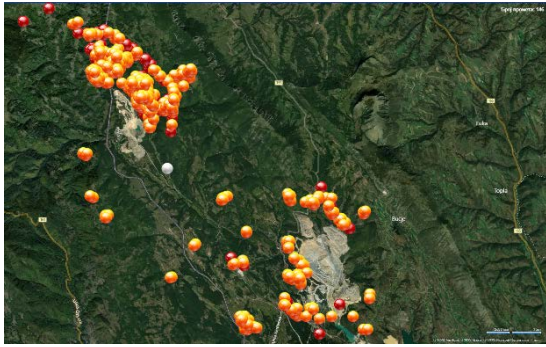


Figure 2. Land turnover in 2022 in the cadastral municipality of Krivelj [2].

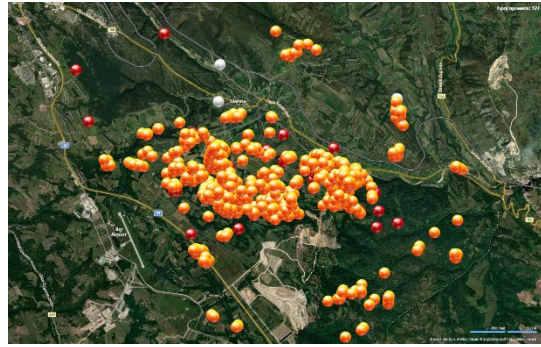


Figure 3. Land turnover in 2022 in the cadastral municipality of Slatina [2].

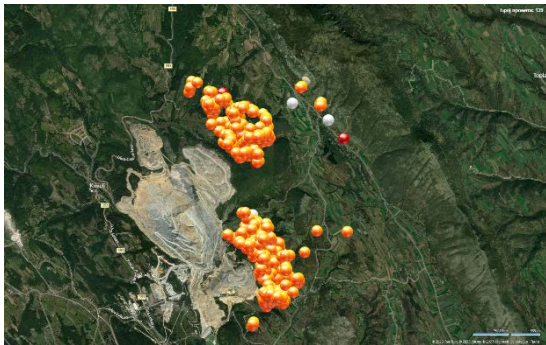


Figure 4 - Land turnover in 2021 in the cadastral municipality of Bučje [2].

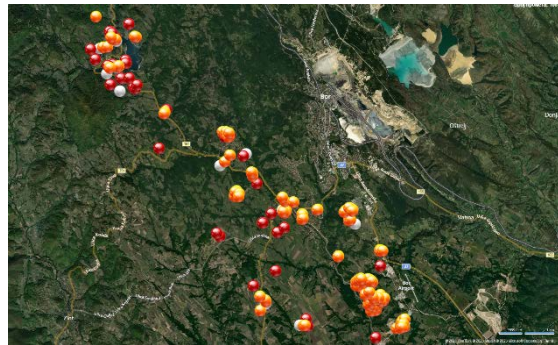


Figure 5 - Land turnover in 2021 in the cadastral municipality of Brestovac [2].

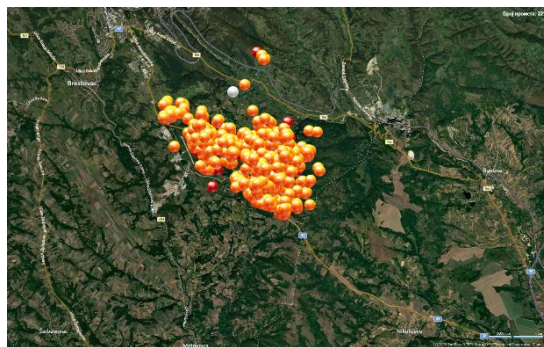


Figure 6 - Land turnover in 2018 in the cadastral municipality of Slatina [2].

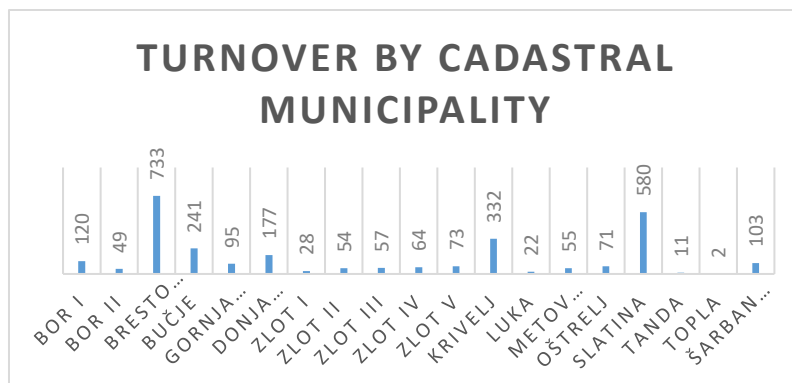


Figure 7 - Land turnover in cadastral municipalities in the period from 2013-2022 [2].



### 3. RESULTS AND DISCUSSION

The research results show that mining activities significantly impact land turnover in the municipality of Bor. Also, after privatization, the number of realized land transactions increased significantly. In the observed period, the most considerable land turnover was realized in 2022, with 590 changes, as seen in Figure 1. The highest turnover was realized in the cadastral municipalities of Krivelj (146 changes) and Slatina (127 changes), with the largest part of the land being purchased for mining. What can be seen in Figure 2 and Figure 3. Also, it is interesting to note that no turnover was achieved in the cadastral municipalities where mining and industry are not represented. The next most represented year in land turnover is 2021, with 511 changes realized, the most in the cadastral municipalities of Bučje (139 changes) and Brestovac (108 changes), which is shown in Figures 4 and 5. In cadastral municipalities Bučje, the largest turnover was achieved by the Chinese company Zijin for mining needs, while in the municipality of Brestovac, the purchase of land from the company was halved. In this cadastral municipality, there is a turnover of land purchases around Lake Bor by individuals. Also, a significantly high turnover was achieved in 2018 in the cadastral municipality of Slatina (221 changes), where the largest share of land acquisition was for mining, which can also be concluded from Figure 6. Figure 7 shows the turnover of land by cadastral municipality. It can be concluded that cadastral municipalities with significant mining activity are significantly ahead in land turnover compared to cadastral municipalities in which mining activity does not exist, such as Topla and Tanda.

### 4. CONCLUSION

Based on the empirical research and the results presented in this paper, it can be concluded that mining activities in the territory of the city of Bor have the most significant impact on land turnover. The highest land turnover was experienced in cadastral municipalities directly affected by mining, such as Slatina, Krivelj, Bučje and Brestovac. The cadastral municipality of Brestovac is in the lead because, in addition to the purchase of land by a Chinese mining company, there is also a significant turnover of land for the construction of houses and cottages near Lake Bor. Also, the privatization of the state company RTB Bor by the Chinese company in 2018 greatly increased the turnover of land in the territory of the city of Bor.

### REFERENCES

- [1] <https://bor.rs/licna-karta-grad/>
- [2] <https://katastar.rgz.gov.rs/eKatastarPublic/publicaccess.aspx>
- [3] <https://zijinbor.com/>
- [4] D. Adamović, D. Ishiyama, H. Kawaraya, Y. Ogawa, Z. Stevanovic, *Groundw. Sustain. Dev.* 16 (2022) 100719.
- [5] E. López-Morales, C. Sanhueza, N. Herrera, S. Espinoza, V. Mosso, *Land Use Policy*, 132 (2023) 106793





# DONORS



**PLATINUM SPONSOR**



**Čukaru Peki – leader of the innovation and first green mine in Serbia**



*Serbia Zijin Mining administrative building*

The company Serbia Zijin Mining is part of the large multinational mining group Zijin Mining, a world-renowned producer of copper, gold, zinc and lithium, and one of the first Chinese mining corporations that, with its activities outside the borders of China, achieved a great impact on global development in accordance with the initiative "Belt and Road".

**Čukaru Peki mine Mineral processing plant and decline**

It has been operating in Serbia since January 2019, when it took over the shares of the Canadian company Nevsun Resources and became the new owner of one of the richest ore deposits, Čukaru Peki. From a research company, it quickly grew into a real mining company. Construction of the main plants and accompanying mining facilities, during which the process technology, industrial equipment and technical performance indicators were set at a high international level, lasted two years, and production began in 2021. Thanks to the design, construction and optimization of the high standard process, production results of the “Čukaru Peki” mine became visible in less than a year and company two years in a row, ranked on a first place on the list of the biggest Serbian exporters.

By choosing the most innovative technological solutions, the most important foundations of green mining were laid, which, along with safety and protection at work, emphasize an ecologically sustainable production process that strives to zero pollution. From the very beginning of work, the

mine has been successively carrying out afforestation and greening. Company plan is implementing of renewable energy sources, by building solar energy plant, as one of the priorities of every ecologically oriented company dedicated to environmental protection. Company is also focused to the building of harmonious relations with the local community and employment of young and professional people, including numerous engineers who graduated from the Technical Faculty in Bor.

### **Unique sustainable green mining circular zero pollution working system**

The company is the owner of the copper and gold ore deposit in Bor and the first green mine in Serbia - Čukaru Peki, which moved the boundaries in mining industry in terms of technologies and standards applied in the ore mining process.

Except modern equipped plants and facilities, the basis of green mining in Čukaru Peki mine was established by unique working system who has introduced new, modern methods of ore mining, by excavating chambers with subsequent filling with a tailings mixture. Company also has unique ventilation system, drainage system for circular use of technical water, without discharge it into nature and closed ore transport system of conveyor belts which prevent the blowing of dust in the air.

As most modern mine, Čukaru Peki has an organized traffic network with light signaling, mobile signal and 4G network, fixed telephony, who enables smooth communication underground. For security reasons whole mining area is covered by video surveillance, monitored from the central dispatch center.

### **High ecological standards**

Čukaru Peki mine has an Upper Zone, where exploitation is carried out and a Lower Zone, where exploration works are ongoing. Since the ore body is deeply positioned shafts and declines were opened and adopted methods of excavation in horizontal bands from the bottom up and of sub-excavation of chambers with subsequent filling. The process of thickening the tailings, which is used for filling of underground chambers, is carried out in the unique Back filling station plant, the only one of its kind in Serbia and Balkan. By using a high percentage of tailings in the backfilling process, the deposition of waste material on the surface is prevented and the soil collapse is prevented. Also, the tailings of copper and pyrite are provided with an impermeable foil and covered with water, in order to prevent the release of harmful substances into the atmosphere. In the mineral processing plant, the internationally advanced "SAB" process and the flotation system developed by the company itself are used for crushing and grinding. The flotation capacity is processing around 10,000 tons of ore per day. In the production process, copper concentrate is obtained as the final product. During processing only electricity is used and no harmful gases are emitted into the air.



*Ecology and safety on a first place*

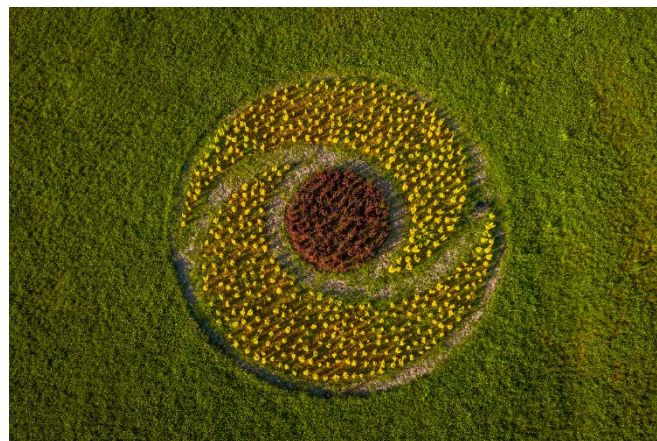


## World class mine

By applying the best practices in mining and the use of modern technologies, the desire is to ensure the long-term successful operation of the company, which will, while respecting established standards, follow quality work, sustainable growth and development. Through a good example of the construction of the "Green Mine", the goal is for Serbia Zijin Mining to become the leading European mining company in terms of: low carbon emissions, green ecology, social responsibility, health, safety and sustainable development, and that investments of 678 million US dollars, continues in the future. According to company strategy, main goal is to build the first "green mine" in Serbia and to reach a leading level around European mining companies, which is also in line with Serbian philosophy of "Green Agenda". To build a "garden-like" green mine, will balance mining development with ecological preservation, strive to achieve zero wastewater discharge and carry out all-round ecological remediation. Aim is to work to foster harmony between mine development and the environment, so as to develop mines with a world-class environment.

## Social responsibility and safety

The motto of the company Serbia Zijin Mining, aimed at the welfare of local communities, citizens, society and the state, is "Mining for a better society". As a leader in innovation in terms of technology, whose function is to preserve and improve the environment, the company Serbia Zijin Mining strives wholeheartedly to contribute to the development of mining in Serbia by moving the framework in the work of the mining industry, and to place the Čukaru Peki mine in the first place among the most successful European and world copper and gold producers. Company is committed to establish and maintain a harmonious relationship of trust with community. Till now, it realized many important projects supporting infrastructural, health, educational, cultural, sport development but also all other fields, providing better life for employees, their families and all citizens of Bor. With the further development of the lower zone of the mine, in which close to 3.8 billion dollars will be invested, it is expected that the company's contribution to the city of Bor and the country of Serbia will be even greater.







**PLATINUM SPONSOR**



SERBIA ZIJIN COPPER DOO is a Chinese-Serbian company that operates as part of the Zijin Mining Group. It was founded on December 18, 2018, when Zijin and the Government of the Republic of Serbia signed the final documents, i.e. the Agreement on the acquisition of 63 percent of ownership of RTB Bor. In this fashion, Zijin became the holder of 63 percent of the company's share in the capital, while the remaining 37 percent belongs to the Republic of Serbia. The planned investment in this Zijin project was 1.26 billion US dollars, and as of August 2023, investments in the amount of 2 billion 283 million dollars were realized.

The company owns four copper mines ("Veliki Krivelj", "Novo Cerovo", "Jama" and "Majdanpek"), a limestone mine, "Kamenolom" Quarry Plant and the Smelter Plant. As of August 2023, the resource reserves of SERBIA ZIJIN COPPER DOO amount to nine million 90 thousand tonnes of copper in ore, with an average grade of 0.392 percent of metal per tonne, and 350 tonnes of gold in the ore, with an average grade of 0.151 grams per tonne. Upon completion of the Project of technical reconstruction, expansion and construction of metallurgical facilities, the Smelter Plant will have the capacity to produce 180 thousand tonnes of cathode copper annually.

By re-industrializing mining and metallurgical capacities, SERBIA ZIJIN COPPER DOO has unequivocally shown its intention to invest in the development and future not only of Bor, Majdanpek and Bor District, but of the whole of Eastern Serbia. The company's aim is for Bor to become a green, low-carbon and sustainable base of non-ferrous metals in Serbia as well as in Europe.

Since taking ownership of the former RTB Bor until the end of August 2023, SERBIA ZIJIN COPPER DOO has paid 421 million US dollars in the name of various taxes and fees and made a cumulative contribution to the social community in Serbia of 787 million dollars. That is why the company ranks among the business entities with largest payments on the basis of taxes and fees. In addition, SERBIA ZIJIN COPPER cooperates with over 1,500 local suppliers, therefore the cumulative value of material procurement reaches one billion 728 million US dollars, indirectly creating over 8,000 jobs.

The total number of employees in SERBIA ZIJIN COPPER DOO at the end of August 2023 was 6,233, of which 6,035 i.e. 96.8 percent are workers with Serbian citizenship, and 198 are of

Chinese nationality. The average monthly net income in August was approximately RSD 125,000, which compared to the net income of 2018 is 87 percent higher. Salaries of employees in SERBIA ZIJIN COPPER DOO far exceed the local level of income per capita, and are 45 percent higher than the average in Serbia. After taking over management, more than 2,700 new, mostly young people got jobs in Bor and Majdanpek, which is the most significant contribution to the economic development of the two cities. Additionally, the large number of newly created jobs for the local population played an important role in maintaining social stability.

Observing the Serbian laws and regulations on production safety and environmental protection, after taking over the management of SERBIA ZIJIN COPPER DOO made a great effort to investigate and eliminate the historical heritage in these areas, thus greatly improving the overall occupational health and safety and environmental conditions. Business activities in the area of production safety is based on the “life comes first” principle and in order to effectively improve the immediate working environment, modern facilities and equipment have been installed. As of August 2023, the accident rate per million business hours was 0.44. On the other hand, 219 million dollars were invested in improving the state of the environment and ecology. Numerous measures have been taken in terms of resolving problems with dust, solid waste, flue gases, waste water and others, which have given notable results. In an effort to build green mines and achieve harmony between mine development and environmental protection, over three million square meters of land were greened and almost half a million seedlings were planted. About 50,000 tonnes of solid and about 2,100 tonnes of hazardous waste were properly disposed of.

As a socially responsible company, SERBIA ZIJIN COPPER DOO pays tremendous attention to the sustainable development of the environment in which it operates and provides assistance to the local governments in Bor and Majdanpek almost every day. It continuously implements a package of plans for the joint construction of social communities and conscientiously fulfils its corporate obligations. It helps numerous cultural, educational, health, tourist and sports institutions and events and directly and concretely shows that it is the engine of development of Timok Valley and Serbia.

SERBIA ZIJIN COPPER DOO made 185 donations by the end of August 2023 and invested 4.5 million US dollars in the improvement of health care, traffic infrastructure, education, sports, traditional art and children entertainment.

In addition to many challenges, we believe that the future will bring progress to all of us in every sense and that by following new technologies, together with hard-working people, we will improve every segment of our business operations. The obligation of the company SERBIA ZIJIN COPPER DOO is to provide the residents with a healthy environment by applying world standards and modern technologies in business and develop mining for the benefit of the whole society.

**PLATINUM SPONSOR**



The Sevojno Copper Mill was founded in 1950 by the decision of the General Directorate of the Government of the Federal People's Republic of Yugoslavia. Production at the Sevojno Copper Mill began in 1952.

From 1950 until privatization, the Sevojno Copper Mill was organized as follows: the Socially Owned Enterprise (SOUR) Copper and Aluminum Mill "Slobodan Penezić Krcun" Sevojno, the Sevojno Copper Mill with a Public Enterprise status, and the Joint Stock Company (DP) Sevojno Copper Mill. Today, the Sevojno Copper Mill is a joint-stock company under the law.

The Sevojno Copper Mill is the largest copper and copper alloy processor in the former Yugoslavia, placing it among the most well-known and giant factories in Europe and the world. The company's headquarters and production facilities are located in Sevojno.

The core activity of the Sevojno Copper Mill involves the processing of copper and copper alloy through rolling, pressing, and drawing into standard semi-finished products, including sheets, strips, foils, waist, rondels, pipes, bars, rods, profiles, and wires. Most of the products are exported to foreign markets (80%), making the Sevojno Copper Mill one of the largest exporters in Serbia, with the main exports going to Western Europe and Central and Eastern Europe.

One-third of the Sevojno Copper Mill's production consists of products used in the defense industry, which is why, in 2018, the Serbian government classified the factory as a company of strategic importance for the country.

The products of the Sevojno Copper Mill find applications in machinery manufacturing, the electrical industry, shipbuilding, petrochemicals, energy, automotive and process industries, construction, and architecture.

The designed capacity of the Sevojno Copper Mill is approximately 50,000 tons per year. The current capacity ranges from 35,000 to 45,000 tons annually, depending primarily on the product range.

In the Sevojno Copper Mill's facilities, various types of pure copper deoxidized with phosphorus and a wide range of copper alloys with zinc are cast and processed through plastic deformation in both cold and hot states, including two-components and three-components alloys (lead brass, special alloys with tin, aluminum, and nickel).

The advantages of the Sevojno Copper Mill over its competitors primarily lie in its production flexibility, characterized by the ability to produce both large quantities and small batch orders, as well as the ability to procure products related to both the Rolling Plant and the Extrusion Plant in one place.

Investing in new equipment, adopting new technologies, developing new products, further improving environmental sustainability, and investing in training and personnel development are strategic priorities and some of the aspects of the business policy for the future of the Sevojno Copper Mill.

Currently, the Sevojno Copper Mill employs approximately 1,100 people.

Address  
Sevojno, industrial area of Uzice, Serbia.  
Prvomajska bb, 31205 Sevojno, Serbia  
Phone: +381 31 531 757;  
Fax: +381 31 532 161;  
office@vbs.co.rs;  
www.vbs.co.rs

**GOLD SPONSOR**



# HBIS SERBIA

HBIS GROUP Serbia is a company established in 2016 and is a part of the HBIS GROUP Corporation. The projected production capacity of the factory is 2.2 million tons of finished products per year. We employ more than 5,000 employees and are among the largest exporters in the Republic of Serbia, making a significant contribution to GDP growth.

HBIS Serbia is a socially responsible company that cares about its employees, the local community and its environment. Over 300 million US dollars were invested in environmental protection projects.

HBIS Serbia production facilities consist of the plant in Smederevo that produces cold and hot rolled flat steel products and the plant in Sabac for the production of tin plate. HBIS Serbia has implemented a quality management system which is applied, maintained and constantly improved.





**GOLD SPONSOR**



Dundee Precious Metals Inc. is an international mining company engaged in the acquisition, development, extraction, and processing of precious metals. Founded in 2004, the DPM company has established a track record of responsible mining practices. In addition to successful mines in Krumovgrad and Chelopech in Bulgaria, Dundee Precious Metals also owns a smelter in Namibia and conducts geological exploration in Bulgaria, Canada, Ecuador, and Serbia. One of the company's key principles is to operate in compliance with local regulations while upholding the same values, ethical standards, and business principles wherever we operate. DPM's goal is to progress and grow in tandem with the local community and support their long-term sustainable development.

DPM Avala d.o.o. is a subsidiary of the international mining company Dundee Precious Metals Inc. based in Canada. DPM Avala d.o.o. is a mineral exploration company focused on exploring and developing gold and copper projects in Serbia. This mining company is dedicated to the successful development of projects based on the highest industry standards and the preservation of local communities, the environment, and long-term benefits for Serbia.



**SILVER SPONSOR**



Trokut Test Serbia has been operating in the market since 2012, offering equipment from renowned global manufacturers in the fields of mechanical testing, quality control, chemical analysis, metrology, metallography, non-destructive testing (ultrasonics, radiography, magnetic testing, penetrant testing), predictive maintenance, and automation systems in production.

The Trokut Test Group consists of 6 local companies located in Croatia (headquarters), Slovenia, Bulgaria, Serbia, Bosnia and Herzegovina, and North Macedonia – our activities span across the entire Balkans and beyond.

Our expert team, along with supplier support, is at your disposal to find suitable solutions for your testing, testing, optimization, and production improvement needs.

Trokut Test Ltd.  
[www.trokuttest.com](http://www.trokuttest.com)  
Milica Antić – Business Associate  
Mobile: +381 60 5557238  
Email: [adminsrb@trokuttest.com](mailto:adminsrb@trokuttest.com)  
Danila Bojovića 18/2  
11010 Belgrade  
Serbia



**EXHIBITION**



<http://www.labtim.rs>

One of the world's leading manufacturers of laboratory equipment, especially in the field of LC and LC/MS chromatography.



<http://www.waters.com>

TA instrument as part of the Waters company is the world leader in Thermal Analysis, Rheology, Microcalorimetry, Biopharmaceuticals, Medical Devices, Elastomers and Rubber.



The First Name In Materials Testing

<http://www.tiniusolsen.com>

Manufacturer and supplier of static tension and/or compression testing machines, designed to measure material's strength and performance.



<http://www.biotage.com>

Biotage is the world's leading supplier of high-performance systems for sample prep, synthesis of organic compounds and synthesis of peptide and variety choice of evaporators.

Daliborka Crnogorac  
Direktor / Managing director  
Email: [daliborka.crnogorac@labtim.rs](mailto:daliborka.crnogorac@labtim.rs)  
Mob:+381 66 5555 200  
Tell:+381 11 770 5550  
Labtim SE d.o.o., Tošin bunar 181a L42, 11070 Beograd, Srbija



**EXHIBITION**



Altium International d.o.o., based in Belgrade, at 120g Milutina Milankovića Street, is an authorized distributor of analytical equipment from Agilent Technologies for the territory of the Republic of Serbia, Montenegro, and North Macedonia.

The company was founded in 1993, and in 1996, it began its distribution partnership with HP, transitioning to Agilent Technologies after 1999.

Our company became a member of the Altium Group in 2022, following which, in May 2023, the business name of DSP Chromatography was changed to Altium International.

Currently, our team consists of 22 individuals.

The company is responsible for equipment sales, delivery to end-users, installation, end-user training, warranty, and post-warranty repairs.

Bojana Vujačić  
Sales Advisor  
M: +381 60 7500 453  
[bojana@dsp-c.co.rs](mailto:bojana@dsp-c.co.rs)  
[www.dsp-c.co.rs](http://www.dsp-c.co.rs)  
Altium International d.o.o.  
120g Milutina Milankovića Boulevard,  
11070 Belgrade, Serbia

## EXHIBITION



MERIS d.o.o., founded in 1992, is a Serbian company dedicated to providing economically viable process solutions with the utilization of cutting-edge technology equipment. They prioritize building enduring business relationships with their clients. The company's core activities encompass representing foreign firms, offering engineering services primarily in the field of measuring and automating processes related to the treatment of potable and wastewater, as well as the regulation and automatic control of technological processes. They also specialize in equipment supply and the maintenance and servicing of measuring instruments.

MERIS d.o.o. proudly serves as the exclusive representative for Serbia and Montenegro for renowned global companies, including ENDRESS+HAUSER, a leading manufacturer of industrial process measurement instruments, XYLEM FLYGT, known for submersible pumps and pump control equipment, and BIOCUBE, offering advanced SBR wastewater treatment systems. Additionally, they partner with AVK and TECOFI for high-quality water and industrial valves, Lutz-Jesco for chlorine dosing systems, SCHNEIDER Armaturen for measuring circuit valves, and CIMBRIA for temperature measurement equipment in silos.

The company ensures that all the equipment they introduce to the market complies with the necessary certifications for public use in the Republic of Serbia, as well as internationally recognized certifications such as PTB, LOYD, and SQS. With a team of twenty employees, including twelve engineers, MERIS d.o.o. is committed to delivering exceptional products and services to meet the diverse needs of its clients. For more information and references, please visit their website at [www.meris.rs](http://www.meris.rs).

Our Vision – MERIS envisions continuous growth in its client and principal base, accompanied by an expansion of its service and product offerings, driven by a team of skilled, satisfied, and ambitious individuals who thrive both professionally and personally. MERIS aims to become a regional leader, always staying one step ahead, with a primary focus on customer satisfaction as a fundamental condition for its existence.

Our Mission – As a socially responsible company and a reliable partner, MERIS empowers its clients to develop production processes in line with the latest technological solutions. In doing so, MERIS promotes increased profitability, energy efficiency, environmental preservation, and enhanced business quality for its customers, thereby creating conditions for retaining talented individuals within the country.

MERIS d.o.o.  
Dunavska 78a  
11060 Belgrade, Serbia  
t: +381 (11) 314 88 00  
f: +381 (11) 314 88 11  
e: [meris@meris.rs](mailto:meris@meris.rs)

## EXHIBITION



Founded in 1969, Measuring Transformers Factory Zajecar (FMT Zajecar) has been a stalwart presence in the electrical equipment market for over five decades.

Throughout its history, FMT Zajecar has consistently enhanced product quality and expanded its offerings, which have demonstrated reliability in diverse operating conditions. Initially specializing in low voltage current measuring transformers and insulators up to 36 kV, the company's capabilities grew with the acquisition of a vacuum casting plant in 1972, enabling the production of various transformer types, both under the SIEMENS AG license and proprietary designs.

Over the years, FMT Zajecar diversified its portfolio to include dry power transformers, inductive reactors, separating transformers, toroidal transformers, and more, catering to a wide range of industrial needs.

They also ventured into industrial electronics, and environmental protection equipment, and embraced cutting-edge insulation materials.

Post privatization in 2005, FMT Zajecar invested heavily in modernization and continues to do so, expanding its product range and reaching customers worldwide, with notable business collaborations in the Balkans, Europe, and across the globe.

Certified with ISO standards and rigorous in-house testing, FMT Zajecar is a trusted name synonymous with quality and innovation in the electrical equipment industry.

BELGRADE  
Timočka 18, 11000 Belgrade,  
Serbia  
+381 (0) 11 283 0000  
[office@fmt.rs](mailto:office@fmt.rs)

ZAJEČAR  
Stražilovska 57, 19000  
Zaječar, Serbia  
+381 (0) 19 3413 111  
+381 (0) 19 3155 554  
+381 (0) 19 3155 555  
+381 (0) 19 3155 556  
[office@fmt.rs](mailto:office@fmt.rs)

## **EXHIBITION**



# REFRATEC

## **ABOUT THE COMPANY**

REFRATEC Sp. z o. o. is a company specializing in the assembly, modernization and overhaul of lining of high-temperature equipment: industrial furnaces, boilers, recuperators, equipment for the steel and non-ferrous metal industries. The company also carries out demolition work and disposal of hazardous materials. We have been operating on the Polish market for over 20 years. For the last 10 years, we have been a member of the Lizmontagens Thermal Technologies group, which is Europe's largest grouping of companies involved in refractory ceramic services. Our association with the LTT group allows us to take advantage of the latest solutions not only in the field of refractory design and technology, but also in the field of work organization and the creation of appropriate working conditions for employees in terms of health and safety.

At present, our company employs more than 140 employees with extensive experience gained from refurbishing and building refractory linings throughout Europe. Among the production staff, in addition to furnace bricklayers, we also employ specialized staff for auxiliary work such as welders, locksmiths, carpenters and formwork fitters.

## **RANGE OF SERVICES OFFERED**

The range of services offered includes design services, supply of refractory materials and, above all, their implementation in new and refurbished power generation equipment. The experience gained during our 2 decades of operation and several decades of the LTT Group, allows us to offer our customers the highest quality services as well as state-of-the-art technological solutions.

REFRATEC Sp. z o.o.  
ul. Księżycowa 3  
01-934 Warszawa  
tel: +48 22 865 72 45  
e-mail: [refratec@refratec.pl](mailto:refratec@refratec.pl)

**EXHIBITION**

**Foundry of non-ferrous metals  
Buntmetall giesserei**



**About the Metalurg Foundry**

Metalurg Foundry Ltd. in Prokuplje specializes in processing non-ferrous metals and alloys through casting. We prioritize quality, cost-efficiency, and customer satisfaction. We adhere to ISO 9001 standards for continuous improvement. With a strong presence in the domestic market, we serve over 200 clients.

**Casting Methods**

We employ various methods:

- Sand casting, Gravity die casting, Centrifugal casting, White metal bearing casting

**Alloys We Work With**

Our alloys include:

- Aluminum Bronze, Tin Bronze, Lead Tin Bronze, Manganese Bronze, White Bronze, Aluminum, Red Brass, Brass, White Metal/Babbitt

**Highlights**

- Sand casting suits complex designs.
- Gravity die casting offers superior quality.
- Centrifugal casting reduces inclusions and porosity.

**Crafting Church Bells**

We excel in crafting church bells for exceptional sound and aesthetics, guided by Russian master calculations.

**Artistic Casting**

We create intricate metal castings, collaborating with renowned sculptors for custom projects.

**Bearing Manufacturing**

With decades of experience, we produce bearings of various sizes using white metal alloys.

**Contact**

Metalurg Foundry Ltd.

Address: Pećka St. bb, 18400 Prokuplje

Phone: +381 27 8429-075

Website: [www.livnica-metalurg.com](http://www.livnica-metalurg.com)

Email: [office@livnica-metalurg.com](mailto:office@livnica-metalurg.com), [metalurgpk@mts.rs](mailto:metalurgpk@mts.rs)

**FRIENDS OF THE CONFERENCE**



Laboratory equipment for quality control and research  
Dedicated for Mining and Metallurgy:

**LECO • [www.leco.com](http://www.leco.com)**

Unique solutions for precise elemental analysis, metallography and thermogravimetry  
CS, CNS, CHN, CHNS, ONH

**BRUKER • [www.bruker.com](http://www.bruker.com)**

Laboratory XRF • Hand held XRF • XRD • Spectroscopy • FT-IR • Raman • NMR

[www.donaulab.rs](http://www.donaulab.rs)



**FRIENDS OF THE CONFERENCE**



Strauss Coffee B.V. entered the Serbian market as part of the Strauss Group through the acquisition of the Doncafé brand in 2003.

The new factory of the Strauss Adriatic business unit was built in 2007 and represents one of the most modern coffee factories in Southeastern Europe, equipped for coffee processing and packaging at the highest standards. Thanks to our dedicated and skilled team, coffee lovers in Serbia and around the world can enjoy the highest quality coffee through our three brands: Doncafé, C kafa, and BeanZ.

Today, Strauss Adriatic employs over 200 people and is one of the leading companies in both retail and the away-from-home segment (AFH), as well as in online sales since 2020.

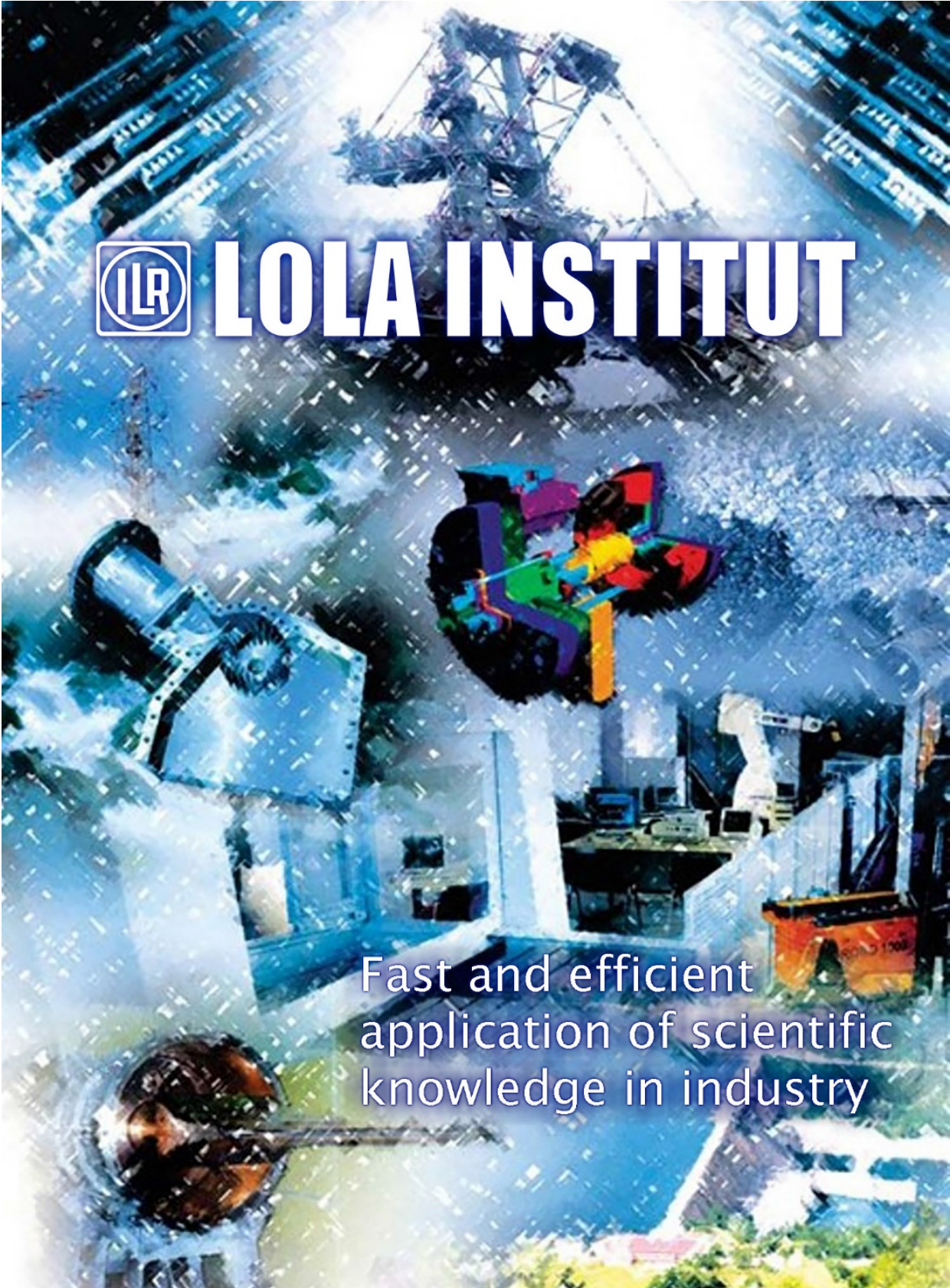
We continuously work on improving our business, guided by the principles of sustainable development because we believe that companies can profit by solving problems rather than creating new ones. Therefore, we are constantly seeking new partners in the FMCG distribution and HoReCa sectors, as well as suppliers with innovative and practical eco-friendly solutions.

You can learn more about our commitments to sustainable development at [sustainability.strauss-group.com](http://sustainability.strauss-group.com)

Contact

Strauss Adriatic  
Miloš Obilića 41  
Šimanovci 22310  
+381 22 408 000

**FRIENDS OF THE CONFERENCE**



**ILR** **LOLA INSTITUT**

Fast and efficient  
application of scientific  
knowledge in industry

**FRIENDS OF THE CONFERENCE**



**THE FOUNDATION  
'B.SC. ENG. BOŠKO INJAC'**  
**Mirjana Injac**  
President

Address: 12/9 Vojvoda Radomir Putnik Street,  
19216 Brestovačka Banja Bor, Serbia  
Phone: + 381 30 77 117, Mobile: + 381 64 265 31 14  
Website: [www.injac.net](http://www.injac.net)

In order to preserve the memory of his father Boško Injac (1946 – 1979), a graduate metallurgical engineer, who was an ambitious and creative student of the Technical Faculty in Bor, and later one of the most promising engineers in the Bor copper mine, attorney Oliver B. Injac, together with other family members, is the patron of the award to the best student of metallurgical engineering study program of the Technical Faculty in Bor, which has been traditionally awarded since 2007.

On this occasion, we should mention all the previous holders of the Charter B.Sc. Eng. Bosko Injac: Dušan Janjić (2007), Milan Georgievski (2008), Slađana Vuleta (2009), Slavko Simov (2010), Vladan Andrejić (2011), Uroš Stamenković (2012), Tatjana Momirović (2013), Ana Angner (2014), Radojica Grekulović (2015), Saša Đorđević (2016), Kristina Božinović (2017), Milko Karanfilovski (2018), Milica Jovkić (2019), Miloš Vuleta (2020), Avram Kovačević (2021), Marina Marković (2022) and Aleksandar Nikolajević (2023).



## AUTHOR INDEX

### A

Abduarahman Muna Abdualatif 514  
Abidi Abdelmoughit 335  
Açan Hasan 489  
Achiței Dragoș 170  
Aćimović Zagorka 357  
Adamović Dragana 501  
Agović Elvis 229  
Akpınar Deniz Eylül 166  
Aksentijević Zoran 216  
Aleksandrova Tatiana 112  
Alil Ana 531  
Alkan Esra 274, 278  
Alkan Murat 274, 278  
Alvarez Eugenio 20  
Amari Khalid El 335  
Amdur Alexey M. 124  
Ananyeva Ludmila 53  
Antonijević Milan 221  
Apostolovski Trujić Tatjana 116, 233  
Aras Ali 464  
Ari Nurdan 274  
Arifović Ana 401  
Arsić Sanela 225  
Avdušinović Hasan 229  
Avramović Ljiljana 128, 145, 154, 158, 233  
Awad Khaola 195

### B

Bacaoui Abdelaziz 335  
Balanović Ljubiša 96, 387  
Basarabić Filip 407  
Beškoski Latinka Slavković 175

Bikić Farzet 195  
Bogdanović Grozdanka 418, 456  
Botić Nenad 23  
Bozić Dragana 128, 145, 154, 158, 233, 435  
Božinović Kristina 301  
Bugarčić Mladen 514  
Bugarin Dejan 145, 435  
Bušatlić Ilhan 448  
Bušatlić Nadira 448

### C

Çelik Ceren 207  
Chernev Georgi 339, 518  
Chicet Daniela Lucia 170  
Cimpoesu Nicanor 170  
Cimpoescu Ramona 170  
Conić Vesna 435, 460, 493  
Cupara Nevena 183  
Cvetković Aleksandar 468

### Ć

Ćitić Aleksandar 481

### D

Damnjanović Zvonko 116  
Darban Ahmad Khodadadi 305  
Davalos Jose Omar 329  
Dehghani Hesam 485  
Denis Ordinartsev 49  
Derqaoui Mohammed 335  
Dikić Stefan 505  
Dilibal Savas 166  
Dimitrijević Jelena 270

Dimitrijević Oliver 493  
Dimitrijević Silvana 128, 145, 211  
Dimitrova Makedonka 547  
Dimitrova Kapac Jasminka 547  
Dojčinović Marina 357  
Dragutinović Olivera 505  
Drobnjaković Bojan 472  
Du Yong 46  
Duraković Mirnes 195  
Dušan Oráč 282

---

## **Đ**

Đokić Jelena 297  
Đokić Nemanja 216  
Đoković Jelena 141  
Đorđević Aleksandar 104, 108  
Đorđević Jelena 76, 476  
Đorđević Nataša 348  
Đorđievski Stefan 501  
Đukanović Duško 216  
Đurđevac Vanja 287, 292  
Đurđevac Ignjatović Lidija 287, 292  
Đurović Dijana 183

---

## **E**

Ercegović Marija 265, 270  
Ergin Hasan 489  
Estemirova Svetlana 49

---

## **F**

Fakić Belma 229  
Fedorov Sergei A. 124  
Fenglai Qi 23  
Filiberto Yaima 20  
Forshev Andrey A. 124

---

## **G**

Gardić Vojka 158, 233  
Gigović-Gekić Almada 229  
Göçmen Müesser 207  
Gorgievski Milan 301, 353, 383, 387, 418  
Grekulović Vesna 301, 353, 383  
Grevtsev Nikolay V. 124  
Guo Jiabao 414  
Gurol Ugur 166, 207  
Gusković Dragoslav 510  
Guševac Sandra 76, 476

---

## **H**

Harbinja Muhamed 357  
Herrera Uzziel Caldiño 329  
Hodić Atif 357  
Holma Marko 325  
Holjevac Grgurić Tamara 424  
Hristov Nikolay 452

---

## **I**

Ignjatović Dragan 287, 292  
Ignjatović Snežana 162  
Ilić Ivana 261, 418  
Ivanov Desislav 325  
Ivaz Jelena 80, 84, 375, 497  
Iveta Vasková 282  
Ivošević Branislav 265

---

## **J**

Jaćimovski Stevo K. 257  
Janković Klara Konc 313  
Janković Marija 92  
Janošević Miloš 435, 460  
Jarmila Trpčevská 282  
Jelić Ivan 76, 379  
Jelić Ivana 92, 348  
Jovanović Aleksandar 514  
Jovanović Ivan 245, 253, 287

Jovanović Ivana 132, 313, 435, 460, 493  
Jovanović Milenko 132, 136, 149, 187  
Jovanović Vladimir 265  
Jovičić Toma 72  
Jović Dalibor 387

## **K**

---

Kalinović Jelena 522  
Kalinović Tanja 522  
Kamenović Vladan 116  
Karakanat Aslihan 278  
Karastojković Zoran 510  
Kašić Vladan 348  
Katarína Pauerová 282  
Kazakova Nadezhda 339, 518  
Khan Muhamad Ghulam Isaq 481  
Koçak Mustafa 207  
Kokkinos E. 88  
Kondratyev Sergey 53  
Koprivica Marija 270  
Korovkin Mikhail 53  
Kostić Slobodan 23  
Kostov Ana 241, 245  
Kostović Milena 203  
Kovačević Avram 407  
Kovačević Sandra 318, 322  
Kovačević Zorica 510  
Krasteva Maria 309, 439  
Krstić Slađana 472  
Krstić Vesna 211  
Kršulja Marko 424  
Kržanović Daniel 132, 149, 187, 191, 199, 460  
Kumrić Ksenija 175

## **L**

---

Lampou A. 88  
Lapčević Veljko 68, 72  
Lazić Dejan 313

Lekić Nikola 379  
Li Kai 46  
Lira Marlenne Alejandra Hernandez 329  
Liu Shuhong 46  
Liverić Lovro 424  
Lu Qiang 46  
Luo Mingshui 4  
Lv Xuewei 4, 370

## **M**

---

Ma Donglai 370  
Magdalinović Srđana 203, 472  
Maksimović Miroslava 136, 149  
Maldybayev Galymzhan 422  
Manasijević Dragan 96, 104, 108, 387  
Manojlović Vaso 505, 527  
Manole Vasile 170  
Marilović Dragana 456  
Marinković Aleksandar 514  
Marinković Vladan 136, 149, 154  
Marjanović Jelisaveta 297  
Marjanović Saša 407, 543  
Marjanović Vesna 233  
Marković Gordana 527  
Marković Ivana 96, 387, 407, 443, 539  
Marković Marija 270  
Marković Marina 301  
Marković Miljan 301, 353, 383, 418  
Marković Radmila 128, 145, 158, 233, 237  
Martina Laubertová 282  
Martinez Manuel Alejandro Lira 329  
Martinović Sanja 531  
Melendez Diego Adan Villordo 329  
Meracheva Gergana 452  
Merchtsaki D. 88  
Merwe Shade Rouxzeta Van Der 343  
Mihajlović Slavica 265, 348  
Mikavica Ivana 366



Mikić Miomir 132, 149, 187, 191, 199, 379  
Milanović Dragan 460, 493  
Milašević Ivana 183  
Miletić Slavica 120, 241  
Milićević Sonja 265  
Milivojević Katarina 287  
Milojkov Dušan 527  
Milojković Nenad 313  
Milosavljević Aleksandra 241, 245  
Milosavljević Jelena 522  
Milosavljević Nenad 361  
Milošević Isidora 100, 225, 560  
Milošević Milena 514  
Milovanović Dobrica 23, 361  
Milutinović Sandra 191, 199, 203, 472, 187  
Minić Duško 104, 108  
Mitovski Aleksandra 353  
Mitrović Milijana 407, 535, 539, 543  
Mladenović Srba 407, 443, 535, 539  
Montenegro Alberto 20  
Mutić Jelena 366

## **N**

---

Nedeljković Milan 535, 539, 543  
Negovanović Milanka 162  
Nešković Jasmina 313  
Nikolaeva Nadezhda 112  
Nikolić Irena 183  
Nikolić Ivica 100, 225, 560  
Nikolić Vladimir 249  
Nourozi Saba 305  
Novaković Bojan 443  
Nujkić Maja 221, 468

## **O**

---

Oabi Omar 335  
Obradović Ljubiša 199, 203, 472  
Obradović Milena 366

Okanigbe Daniel Ogochukwu 343  
Onen Vildan 428  
Orazaliyeva Zhibek 422

## **P**

---

Pačkovski Goran 136  
Patra Satyananda 27  
Pavlović Marko 357  
Pechischeva Nadezhda 49  
Peleka E. 88  
Pešić Batrić 11  
Pešovski Branka 211  
Petkov Rumen 439  
Petrović Ana 237  
Petrović Dejan 64, 80, 84, 375, 497  
Petrović Đorđe 175  
Petrović Jasmina 535, 539, 543  
Petrović Jelena 158, 270  
Petrović Maja 297  
Petrović Sanja 203, 456, 472  
Petrović Mihajlović Marija 221, 468  
Peytcheva Irena 325  
Pirgić Savo 23  
Polavder Svetlana 313  
Polyak Peter 395  
Popa Mihai 170  
Popov Alexandar 339  
Popović Miljana 481  
Potić Branislav 401  
Pourasgharian Fatemeh 305  
Požega Emina 237  
Prčanović Halim 195  
Prelević Dejan 481  
Prochaska C. 88

## **R**

---

Radetić Tamara 481  
Radivojević Daniel 216

Radmilović Velimir R. 3  
Radojević Ana 522  
Radosavljević Mihajlović Ana 348  
Radovanović Milan 211, 221, 468  
Radovanović Mladen 80, 84, 375  
Radović Bojan 116  
Radović Žarko 56, 60  
Radulović Dragan 265, 357  
Rajković Filip 481  
Rajković Radmilo 132, 149, 187, 191, 199  
Rakić Ana 225  
Randelović Dragana 366  
Rasa Muhammad Hashim 464  
Rempel Andrey 49  
Ristić Nevena 116  
Ristić Ognjen 510  
Ristić Tamara 361  
Ružić Jovana 527

## **S**

---

Sarap Nataša 92  
Savinova Olesya 53  
Schmid-Fetzer Rainer 46  
Scripcariu Ana-Maria 170  
Sebastian Mistreanu 170  
Sharipov Rustam 422  
Simeonidis K. 88  
Simić Marija 270  
Simić Marko 505  
Simonović Ana 221, 468  
Simonović Danijela 211  
Sitek Wojciech 424  
Smajić-Terzić Dženana 448  
Smokvina Hanza Sunčana 424  
Sokić Miroslav 514, 527  
Sokolović Jovica 261, 418, 556  
Sretković Branisav 162  
Stakić Branisal 216

Staletović Novica 253  
Stamenković Uroš 96, 387, 407, 443  
Stanić Nikola 379  
Stanić Vojislav 92  
Stanković Katarina 175  
Stanković Suzana 120  
Stanković Tanja 460  
Stanković Velizar 418  
Stanojević Šimšić Zdenka 241, 245  
Stanujkić Dragiša 261  
Stefanović Jelena 76, 476  
Stevanović Zoran 128, 145, 158, 233  
Stjepanović Pavle 313  
Stojadinović Saša 80, 84, 497  
Stojanović Anđelka 100, 225, 560  
Stojanović Jovica 348, 366  
Stojanović Miloš 64, 68  
Stojanović Mirjana 357  
Stojić Anđela 141  
Stojković Pavle 80, 84  
Stolić Predrag 80, 497  
Stoljiljković Miloš 141  
Strainović Gracijan 418  
Suleimenov Essen 422  
Supić Mladen 292  
Sušić Čedomir 23  
Svrkota Igor 493

## **Š**

---

Šabaz Dragan 64  
Šerbula Snežana 522  
Šetrajčić Jovan P. 179, 257  
Šljivić-Ivanović Marija 92  
Špada Vedrana 424  
Štirbanović Zoran 261, 556  
Štrbac Nada 301, 353, 383

## **T**

---

Tadić Milena 183  
Tadić Nebojša 56, 60  
Taner Hasan Ali 428, 464  
Tanikić Dejan 141  
Tasić Viša 116  
Tasić Žaklina 221, 468  
Tašić Dušan 292  
Tilvaldyev Shehret 329  
Todorova Elena 518  
Todorović Dejan 265  
Torbica Slavko 72  
Trifunović Vanja 128, 145, 154, 435  
Trujić Stefan 76, 154  
Trumić Biserka 120, 543  
Trumić Maja 556  
Trumić Milan 249  
Turgut Batuhan 166

---

## U

Ugurluer Dilan 278  
Urošević Daniela 128, 460  
Urošević Tamara 116

---

## V

Vasiljević Ivana 162  
Veličković Milica 485  
Veljović Đorđe 505  
Vlahović Milica 531  
Vojinović Ivica 68  
Vojinović Vesna 556  
Volkov-Husović Tatjana 531  
Vourlias G. 88  
Voza Danijela 485  
Vučenović Siniša M. 179, 257  
Vukadinović Melina 348  
Vuković Milovan 353  
Vuksanović Marija 514  
Wang Jianchuan 46

Wang Jincheng 46

---

## X

Xiang Junyi 4

---

## Y

Yaacoubi Abdelrani 335  
Yamanoglu Ridvan 36  
Yildiz Mehmet Ali 391  
You Yang 4, 370, 414  
You Zhixiong 4, 370, 414  
Yu Jing 4  
Yurak Vera V. 124

---

## Z

Zaneva-Dobranova Efrosima 452  
Zdravković Bojan 383  
Zdravković Milica 301, 353, 383  
Zečević Milena 104, 108  
Zhang Yuhui 46  
Zhao Jianbo 370  
Zhao Xinnan 370  
Zherlitsyn Andrey 53  
Zlatanović Dragan 80, 84, 375, 497  
Zlatičanin Biljana 318, 322  
Zlatković Igor 23  
Zouboulis A. 88

---

## Ž

Živković Bojana 297

**ISBN-978-86-6305-140-9**

